New Series

LANDOLT-BÖRNSTEIN

Numerical Data and Functional Relationships in Science and Technology

GROUP IV

VOLUME 11

Physical Chemistry

Ternary Alloy Systems

Phase Diagrams, Crystallographic and Thermodynamic Data

critically evaluated by MSIT®

SUBVOLUME D

Iron Systems

Part 1

Selected Systems from Al-B-Fe to C-Co-Fe

Springer

Landolt-Börnstein
Numerical Data and Functional Relationships in Science and Technology
New Series / Editor in Chief: W. Martienssen

Group IV: Physical Chemistry
Volume 11D1

Ternary Alloy Systems

Phase Diagrams, Crystallographic and Thermodynamic Data

critically evaluated by MSIT®

Subvolume D
Iron Systems

Part 1
Selected Systems from Al-B-Fe to C-Co-Fe

Editors
G. Effenberg and S. Ilyenko

Authors
Materials Science International Team, MSIT®

ISSN 1615-2018 (Physical Chemistry)

ISBN 978-3-540-69759-6 Springer Berlin Heidelberg New York

Library of Congress Cataloging in Publication Data Zahlenwerte und Funktionen
aus Naturwissenschaften und Technik, Neue Serie Editor in Chief: W.
Martienssen Vol. IV/11D1: Editors: G. Effenberg, S. Ilyenko

At head of title: Landolt-Börnstein. Added t.p.: Numerical data and functional relationships in science and technology. Tables chiefly in English. Intended to supersede the Physikalisch-chemische Tabellen by H. Landolt and R. Börnstein of which the 6th ed. began publication in 1950 under title: Zahlenwerte und Funktionen aus Physik, Chemie, Astronomie, Geophysik und Technik. Vols. published after v. 1 of group I have imprint: Berlin, New York, Springer-Verlag Includes bibliographies.

1. Physics--Tables. 2. Chemistry--Tables. 3. Engineering--Tables.
I. Börnstein, R. (Richard), 1852-1913. II. Landolt, H. (Hans), 1831-1910.
III. Physikalisch-chemische Tabellen. IV. Title: Numerical data and functional relationships in science and technology.
QC61.23 502'.12 62-53136

Springer is a part of Springer Science+Business Media
springeronline.com © Springer-Verlag Berlin
Heidelberg 2008 Printed in Germany

Cover layout: Erich Kirchner, Heidelberg Typesetting: Materials
Science International Services GmbH, Stuttgart Printing and Binding:
AZ Druck, Kempten/Allgäu

SPIN: 1091 6056 63/3020 - 5 4 3 2 1 0 – Printed on acid-free paper

Editors: **Günter Effenberg**
Svitlana Ilyenko
Associate Editor: **Oleksandr Dovbenko**

MSI, Materials Science International Services GmbH
Postfach 800749, D-70507, Stuttgart, Germany
http://www.matport.com

Authors: Materials Science International Team, MSIT®

The present series of books results from collaborative evaluation programs performed by MSI and authored by MSIT®. In this program data and knowledge are contributed by many individuals and accumulated over almost twenty years, now. The content of this volume is a subset of the ongoing MSIT® Evaluation Programs. Authors of this volume are:

Anatoliy Bondar, Kyiv, Ukraine

Gabriele Cacciamani, Genova, Italy

Lesley Cornish, Randburg, South Africa

Jozefien De Keyzer, Heverlee, Belgium

Yong Du, Changsha, China

Olga Fabrichnaya, Stuttgart, Germany

Gautam Ghosh, Evanston, USA

Volodymyr Ivanchenko, Kyiv, Ukraine

Hermann A. Jehn, Stuttgart, Germany

Kostyantyn Korniyenko, Kyiv, Ukraine

Artem Kozlov, Clausthal-Zellerfeld, Germany

Ortrud Kubaschewski, Aachen, Germany

Nathalie Lebrun, Lille, France

Annelies Malfliet, Heverlee, Belgium

Pierre Perrot, Lille, France

Tatiana Pryadko, Kyiv, Ukraine

Peter Rogl, Vienna, Austria

Lazar Rokhlin, Moscow, Russia

Myriam Sacerdote-Peronnet, Lyon, France

Rainer Schmid-Fetzer, Clausthal-Zellerfeld, Germany

Vladislav Sidorko, Kyiv, Ukraine

Vasyl Tomashik, Kyiv, Ukraine

Tamara Velikanova, Kyiv, Ukraine

Andy Watson, Leeds, U.K.

Honghui Xu, Changsha, China

Chao Zhang, Changsha, China

Institutions

The content of this volume is produced by MSI, Materials Science International Services GmbH and the international team of materials scientists, MSIT®. Contributions to this volume have been made from the following institutions:

The Baikov Institute of Metallurgy, Academy of Sciences, Moscow, Russia

Central South University, Research Institute of Powder Metallurgy, State Key Laboratory for Powder Metallurgy, Changsha, China

I.M. Frantsevich Institute for Problems of Materials Science, National Academy of Sciences, Kyiv, Ukraine

Institute for Semiconductor Physics, National Academy of Sciences, Kyiv, Ukraine

G.V. Kurdyumov Institute for Metal Physics, National Academy of Sciences, Kyiv, Ukraine

Katholieke Universiteit Leuven, Department Metaalkunde en Toegepaste Materiaalkunde, Heverlee, Belgium

Laboratoire des Multimateriaux et Interfaces, Université Claude Bernard Lyon I

Max-Planck-Institut für Metallforschung, Institut für Werkstoffwissenschaft, Pulvermetallurgisches Laboratorium, Stuttgart, Germany

School of Chemical and Metallurgical Engineering, The University of the Witwatersrand, DST/NRF Centre of Excellence for Strong Material, South Afrika

Northwestern University, Department of Materials Science and Engineering, Evanston, USA

Technische Universität Clausthal, Metallurgisches Zentrum, Clausthal-Zellerfeld, Germany

Universita di Genova, Dipartimento di Chimica, Genova, Italy

Universite de Lille I, Laboratoire de Metallurgie Physique, Villeneuve d'ASCQ, France

Universität Wien, Institut für Physikalische Chemie, Wien, Austria

University of Leeds, Department of Materials, School of Process, Environmental and Materials Engineering, Leeds, UK

In Memory of Riccardo Ferro

The authors and editors dedicate this volume to the honorable memory of Professor Riccardo Ferro, who was a founding member of MSIT, the Materials Science International Team, the authoring team of this Landolt-Boernstein Series.

Prof. Riccardo Ferro passed away on December 28, 2006 at the age of 80. Born in Genova, Italy, in 1926 he obtained a degree in Industrial Chemistry in 1949. After a few years he became assistant professor at the University of Genova, full professor in 1964 at the University of Cagliari (Sardinia) and then moved to Catania (Sicily). Finally, in 1969, he came back to Genova University where he became the director of the Institute of General and Inorganic Chemistry until it merged to form the current Department of Chemistry and Industrial Chemistry in 1996. In 1974 he was elected Dean of the Science Faculty at Genova University and re-elected a further six times for a total period of more than 20 years. During this time, he was Coordinator of the National Conference of the Deans of the Italian Science Faculties for about 10 years. Finally, he officially retired 6 years ago and, although he stopped teaching, he continued his research work as Professor Emeritus until the end.

He was a member of several scientific societies:

- member of the Italian Chemical Society and director of the Ligurian division
- founding member of MSIT, the Materials Science International Team
- fellow member of the American Chemical Society
- fellow member of the ASM International "in recognition of distinguished contributions to the field of materials science and materials engineering".

During his long academic career he formed, managed and guided a group of 10-12 members working on several subjects related to the chemistry of intermetallic alloys and, in particular, of rare earths and actinides. His main fields of interest were:

- experimental investigation of phase equilibria in binary and ternary systems
- measurement of thermochemical properties, especially enthalpy of formation by direct calorimetry
- crystallochemistry and, in particular, systematic investigation of crystal structures of families of intermetallic compounds
- thermodynamic assessment of phase diagrams

Indeed, his ability as an experimentalist was exceptional. He was very keen in planning measurements and interpreting results but he was also very skilful in planning and building new experimental equipment, often working himself in the workshop of the lab.

His experimental activity led, in particular, to the determination of phase equilibria and/or thermodynamic properties of formation in a huge number of binary and ternary intermetallic systems that have been reported in more than two hundred scientific papers.

Another field of activity was the critical assessment of phase diagrams, crystal structures and thermodynamics. He had been introduced to this work by Prof. O. Kubaschewski who involved him in contributing to a series of books edited by the International Atomic Energy Agency concerning alloys playing a significant role in Nuclear technology.

For over 20 years Riccardo Ferro contributed to the MSIT Ternary Evaluation Program initiated at the Max-Planck-Institute für Metallforschung. In ongoing global cooperations Riccardo Ferro has contributed to 200 of the about 4000 critical evaluations which this team has created so far. We all have greatly benefited from his critical contributions, his tutorial lead and warm hearted friendship.

With him we lost a competent scientist, an enjoyable man and many of us a good friend, who has found his place in materials science and in our memories, forever.

The MSIT authors and editors

Preface

The sub-series *Ternary Alloy Systems* of the *Landolt-Börnstein New Series* provides reliable and comprehensive descriptions of the materials constitution, based on critical intellectual evaluations of all data available at the time and it critically weights the different findings, also with respect to their compatibility with today's edge binary phase diagrams. Selected are ternary systems of importance to alloy development and systems which gained in the recent years otherwise scientific interest. In one ternary materials system, however, one may find alloys for various applications, depending on the chosen composition.

Reliable phase diagrams provide scientists and engineers with basic information of eminent importance for fundamental research and for the development and optimization of materials. So collections of such diagrams are extremely useful, if the data on which they are based have been subjected to critical evaluation, like in these volumes. Critical evaluation means: there where contradictory information is published data and conclusions are being analyzed, broken down to the firm facts and re-interpreted in the light of all present knowledge. Depending on the information available this can be a very difficult task to achieve. Critical evaluations establish descriptions of reliably known phase configurations and related data.

The evaluations are performed by MSIT®, Materials Science International Team, a group of scientists working together since 1984. Within this team skilled expertise is available for a broad range of methods, materials and applications. This joint competence is employed in the critical evaluation of the often conflicting literature data. Particularly helpful in this are targeted thermodynamic and atomistic calculations for individual equilibria, driving forces or complete phase diagram sections.

Conclusions on phase equilibria may be drawn from direct observations *e.g.* by microscope, from monitoring caloric or thermal effects or measuring properties such as electric resistivity, electro-magnetic or mechanical properties. Other examples of useful methods in materials chemistry are mass-spectrometry, thermo-gravimetry, measurement of electro-motive forces, X-ray and microprobe analyses. In each published case the applicability of the chosen method has to be validated, the way of actually performing the experiment or computer modeling has to be validated as well and the interpretation of the results with regard to the material's chemistry has to be verified. Therefore insight in materials constitution and phase reactions is gained from many distinctly different types of experiments, calculation and observations. Intellectual evaluations which interpret all data simultaneously reveal the chemistry of the materials system best.

An additional degree of complexity is introduced by the material itself, as the state of the material under test depends heavily on its history, in particular on the way of homogenization, thermal and mechanical treatments. All this is taken into account in an MSIT® expert evaluation.

To include binary data in the ternary evaluation is mandatory. Each of the three-dimensional ternary phase diagrams has edge binary systems as boundary planes; their data have to match the ternary data smoothly. At the same time each of the edge binary systems A-B is a boundary plane for many other ternary A-B-X systems. Therefore combining systematically binary and ternary evaluations increases confidence and reliability in both ternary and binary phase diagrams. This has started systematically for the first time here, by the MSIT® Evaluation Programs applied to the *Landolt-Börnstein New Series*. The degree of success, however, depends on both the nature of materials and scientists!

The multitude of correlated or inter-dependant data requires special care. Within MSIT® an evaluation routine has been established that proceeds knowledge driven and applies both, human based expertise and electronically formatted data and software tools. MSIT® internal discussions take place in almost all evaluation works and on many different specific questions the competence of a team is added to the work of individual authors. In some cases the authors of earlier published work contributed to the knowledge base by making their original data records available for re-interpretation. All evaluation reports published here have undergone a thorough review process in which the reviewers had access to all the original data.

In publishing we have adopted a standard format that presents the reader with the data for each ternary system in a concise and consistent manner, as applied in the "MSIT® Workplace Phase Diagrams Online". The standard format and special features of the Landolt-Börnstein compendium are explained in the Introduction to the volume.

In spite of the skill and labor that have been put into this volume, it will not be faultless. All criticisms and suggestions that can help us to improve our work are very welcome. Please contact us via effenberg@msiwp.com. We hope that this volume will prove to be as useful for the materials scientist and engineer as the other volumes of *Landolt-Börnstein New Series* and the previous works of MSIT® have been. We hope that the *Landolt Börnstein Sub-series, Ternary Alloy Systems* will be well received by our colleagues in research and industry.

On behalf of the participating authors we want to thank all those who contributed their comments and insight during the evaluation process. In particular we thank the reviewers - Olga Fabrichnaya, Marina Bulanova, Yong Du and Lazar Rokhlin.

We all gratefully acknowledge the dedicated scientific desk editing by Oleksandra Berezhnytska, Oleksandr Rogovtsov and Oleksandra Zaikina.

Günter Effenberg, Svitlana Ilyenko and Oleksandr Dovbenko

Stuttgart, November 2006

Foreword

Can you imagine a world without iron and steel? No? I can't either.

The story of mankind is intimately linked to the discovery and successful use of metals and their alloys. Amongst them iron and steel - we could define steel as 'a generally hard, strong, durable, malleable alloy of iron and carbon, usually containing between 0.2 and 1.5 percent carbon, often with other constituents such as manganese, chromium, nickel, molybdenum, copper, tungsten, cobalt, or silicon, depending on the desired alloy properties, and widely used as a structural material', have shaped our material world.

The story of iron takes us back to the period of the Hittite Empire around 1300 BC, when iron started to replace bronze as the chief metal used for weapons and tools. Until today the story remains uncompleted and the social and economic impact of the iron and steel industry is now beyond imagination. In the year 2005 1.13 billion tons of crude steel were produced. Compared to 2004 this is an increase of 6.8%. That same year the steel production in China increased from 280.5 to almost 350 million tons. Concerning stainless steel: according to the International Stainless Steel Forum (ISSF), the global production forecast for 2006 now stands at 27.8 million metric tons of stainless crude steel, up 14.3% compared to 2005.

An English poem from the 19th century tells us

> Gold is for the mistress
> Silver for the maid
> Copper for the craftsman
> Cunning at his trade
> Good said the baron
> Sitting in his hall
> But iron, cold iron
> Is master of them all

It is still actual and true.

The list of different steel grades and related applications is impressive and still growing: low carbon strip steels for automotive applications, low carbon structural steels, engineering steels, stainless steels, cast irons, and, more recently: dual phase steels, TRIP-steels, TWIP-steels, maraging steels, …

The list of applications seems endless: a wide range of properties from corrosion resistance to high tensile strength is covered. These properties depend on the percentage of carbon, the alloying elements, and increasingly on the thermo-mechanical treatments that aim at optimizing the microstructure.

Yet many potential improvements remain unexplored, also due to the increasing complexity of the new steel grades. For instance, a recently patent protected new die steel for hot deformation has the following composition specifications: C 0.46 – 0.58; Si 0.18 – 0.40; Mn 0.45 – 0.75, Cr 0.80 – 1.20; Ni 1.30 – 1.70; Mo 0.35 – 0.65; V 0.18 – 0.25; Al 0.01 – 0.04; Ti 0.002 – 0.04; B 0.001 – 0.003; Zr 0.02 – 0.04; Fe remaining.

Although many properties of steel are directly related to non-equilibrium states, it remains a fact that the equilibrium state creates the reference frame for all changes that might occur in any material - and consequently would effect its properties in use - that is actually not in its thermodynamic equilibrium state. This is what these volumes in the Landolt-Börnstein series stand for: they have collected the most reliable data on the possible phase equilibria in ternary iron based alloys. Therefore this first volume of data, as well as the other ones in a series of four to appear, is of immeasurable value for metallurgists and materials engineers that improve the properties of existing steels and develop new and more complex steel grades. It is about materials, it is about quality of life.

The well-recognized quality label of MSIT®, the Materials Science International Team, also applies to the present volume of the Landolt-Börnstein series. It should be available for every materials engineer, scientist and student.

Prof. Dr. ir. Patrick Wollants
Chairman - Department of Metallurgy and Materials Engineering
Katholieke Universiteit Leuven
Belgium

Contents

IV/11D1 Ternary Alloy Systems
Phase Diagrams, Crystallographic and Thermodynamic Data

Subvolume D Iron Systems

Part 1 Selected Systems from Al-B-Fe to C-Co-Fe

Introduction

Data Covered ... XI
General ... XI
Structure of a System Report ... XI
Introduction ... XI
Binary Systems ... XI
Solid Phases ... XII
Quasibinary Systems ... XIII
Invariant Equilibria ... XIII
Liquidus, Solidus, Solvus Surfaces ... XIII
Isothermal Sections ... XIII
Temperature – Composition Sections ... XIII
Thermodynamics ... XIII
Notes on Materials Properties and Applications ... XIII
Miscellaneous ... XIII
References ... XVI
General References ... XVII

Ternary Systems

Al – B – Fe (Aluminium – Boron – Iron) ... 1
Al – C – Fe (Aluminium – Carbon – Iron) ... 11
Al – Cr – Fe (Aluminium – Chromium – Iron) ... 30
Al – Fe – H (Aluminium – Iron – Hydrogen) ... 67
Al – Fe – Mo (Aluminium – Iron – Molybdenum) ... 74
Al – Fe – N (Aluminium – Iron – Nitrogen) ... 89
Al – Fe – O (Aluminium – Iron – Oxygen) ... 96
Al – Fe – P (Aluminium – Iron – Phosphorus) ... 136
Al – Fe – Si (Aluminium – Iron – Silicon) ... 147
Al – Fe – Ta (Aluminium – Iron – Tantalum) ... 213
Al – Fe – Ti (Aluminium – Iron – Titanium) ... 223
Al – Fe – Zn (Aluminium – Iron – Zinc) ... 258
B – C – Fe (Boron – Carbon – Iron) ... 279
B – Co – Fe (Boron – Cobalt – Iron) ... 302
B – Cr – Fe (Boron – Chromium – Iron) ... 320

B – Fe – Mn (Boron – Iron – Manganese) 344
B – Fe – Mo (Boron – Iron – Molybdenum) 354
B – Fe – N (Boron – Iron – Nitrogen) 368
B – Fe – Nb (Boron – Iron – Niobium) 379
B – Fe – Nd (Boron – Iron – Neodymium) 388
B – Fe – Ni (Boron – Iron – Nickel) 416
B – Fe – P (Boron – Iron – Phosphorus) 434
B – Fe – Ti (Boron – Iron – Titanium) 444
B – Fe – W (Boron – Iron – Tungsten) 455
Ba – Fe – O (Barium – Iron – Oxygen) 464
C – Co – Fe (Carbon – Cobalt – Iron) 482

Introduction

Data Covered

The series focuses on light metal ternary systems and includes phase equilibria of importance for alloy development, processing or application, reporting on selected ternary systems of importance to industrial light alloy development and systems which gained otherwise scientific interest in the recent years.

General

The series provides consistent phase diagram descriptions for individual ternary systems. The representation of the equilibria of ternary systems as a function of temperature results in spacial diagrams whose sections and projections are generally published in the literature. Phase equilibria are described in terms of liquidus, solidus and solvus projections, isothermal and quasibinary sections; data on invariant equilibria are generally given in the form of tables.
The world literature is thoroughly and systematically searched back to the year 1900. Then, the published data are critically evaluated by experts in materials science and reviewed. Conflicting information is commented upon and errors and inconsistencies removed wherever possible. It considers those, and only those data, which are firmly established, comments on questionable findings and justifies re-interpretations made by the authors of the evaluation reports.
In general, the approach used to discuss the phase relationships is to consider changes in state and phase reactions which occur with decreasing temperature. This has influenced the terminology employed and is reflected in the tables and the reaction schemes presented.
The system reports present concise descriptions and hence do not repeat in the text facts which can clearly be read from the diagrams. For most purposes the use of the compendium is expected to be self-sufficient. However, a detailed bibliography of all cited references is given to enable original sources of information to be studied if required.

Structure of a System Report

The constitutional description of an alloy system consists of text and a table/diagram section which are separated by the bibliography referring to the original literature (see Fig. 1). The tables and diagrams carry the essential constitutional information and are commented on in the text if necessary.
Where published data allow, the following sections are provided in each report:

Introduction

The opening text reviews briefly the status of knowledge published on the system and outlines the experimental methods that have been applied. Furthermore, attention may be drawn to questions which are still open or to cases where conclusions from the evaluation work modified the published phase diagram.

Binary Systems

Where binary systems are accepted from standard compilations reference is made to these compilations. In other cases the accepted binary phase diagrams are reproduced for the convenience of the reader. The selection of the binary systems used as a basis for the evaluation of the ternary system was at the discretion of the assessor.

Solid Phases

The tabular listing of solid phases incorporates knowledge of the phases which is necessary or helpful for understanding the text and diagrams. Throughout a system report a unique phase name and abbreviation is allocated to each phase.

DOI: 10.1007/978-3-540-69761-9_1

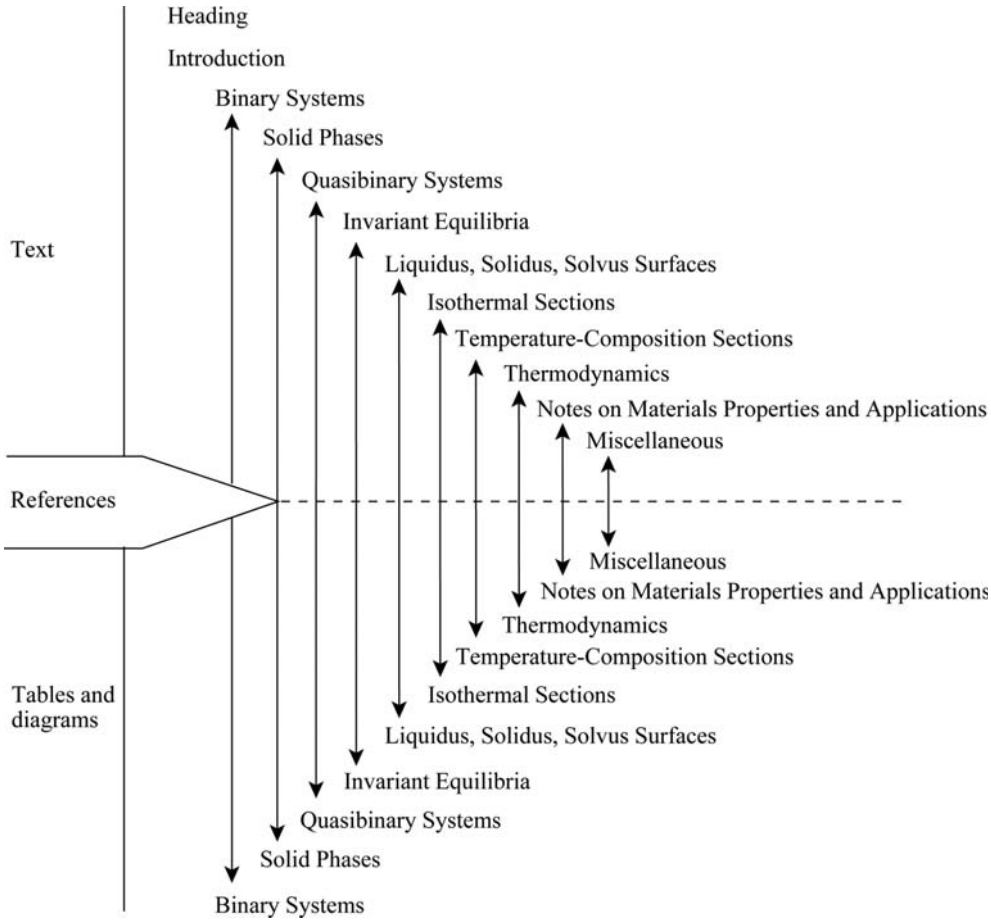

Fig. 1. Structure of a system report

Phases with the same formulae but different space lattices (e.g. allotropic transformation) are distinguished by:

- small letters (h), high temperature modification ($h_2 > h_1$)
  (r), room temperature modification
  (l), low temperature modification ($l_1 > l_2$)
- Greek letters, *e.g.*, ε, ε'
- Roman numerals, *e.g.*, (I) and (II) for different pressure modifications.

In the table "Solid Phases" ternary phases are denoted by * and different phases are separated by horizontal lines.

Quasibinary Systems

Quasibinary (pseudobinary) sections describe equilibria and can be read in the same way as binary diagrams. The notation used in quasibinary systems is the same as that of vertical sections, which are reported under "Temperature – Composition Sections".

Invariant Equilibria

The invariant equilibria of a system are listed in the table "Invariant Equilibria" and, where possible, are described by a constitutional "Reaction Scheme" (Fig. 2).

DOI: 10.1007/978-3-540-69761-9_1

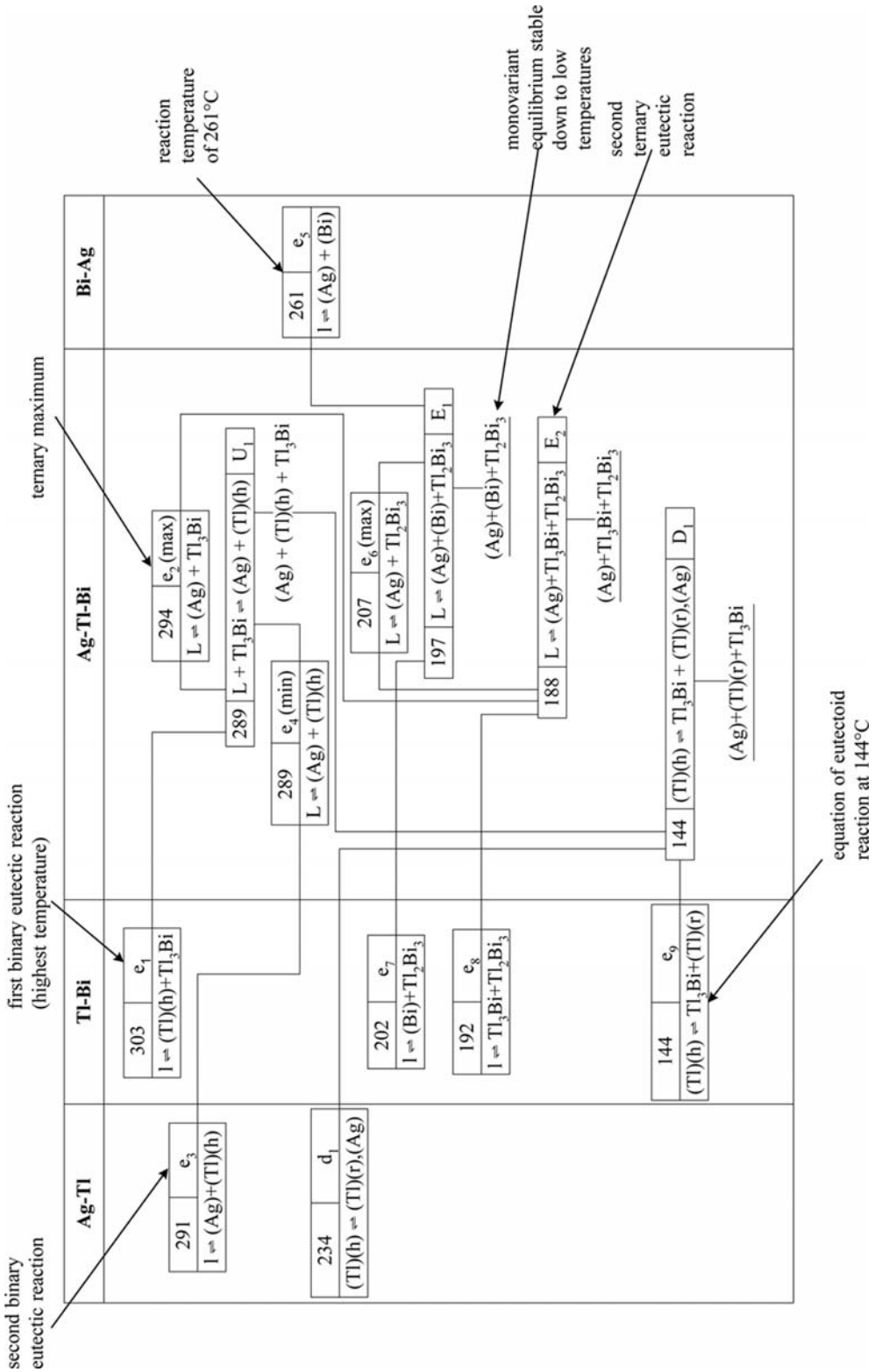

Fig. 2. Typical reaction scheme

DOI: 10.1007/978-3-540-69761-9_1

The sequential numbering of invariant equilibria increases with decreasing temperature, one numbering for all binaries together and one for the ternary system.
Equilibria notations are used to indicate the reactions by which phases will be

- decomposed (e- and E-type reactions)
- formed (p- and P-type reactions)
- transformed (U-type reactions)

For transition reactions the letter U (Übergangsreaktion) is used in order to reserve the letter *T* to denote temperature. The letters d and D indicate degenerate equilibria which do not allow a distinction according to the above classes.

Liquidus, Solidus, Solvus Surfaces

The phase equilibria are commonly shown in triangular coordinates which allow a reading of the concentration of the constituents in at.%. In some cases mass% scaling is used for better data readability (see Figs. 3 and 4).
In the polythermal projection of the liquidus surface, monovariant liquidus grooves separate phase regions of primary crystallization and, where available, isothermal lines contour the liquidus surface (see Fig. 3).

Isothermal Sections

Phase equilibria at constant temperatures are plotted in the form of isothermal sections (see Fig. 4).

Temperature – Composition Sections

Non-quasibinary *T-x* sections (or vertical sections, isopleths, polythermal sections) show the phase fields where generally the tie lines are not in the same plane as the section. The notation employed for the latter (see Fig. 5) is the same as that used for binary and quasibinary phase diagrams.

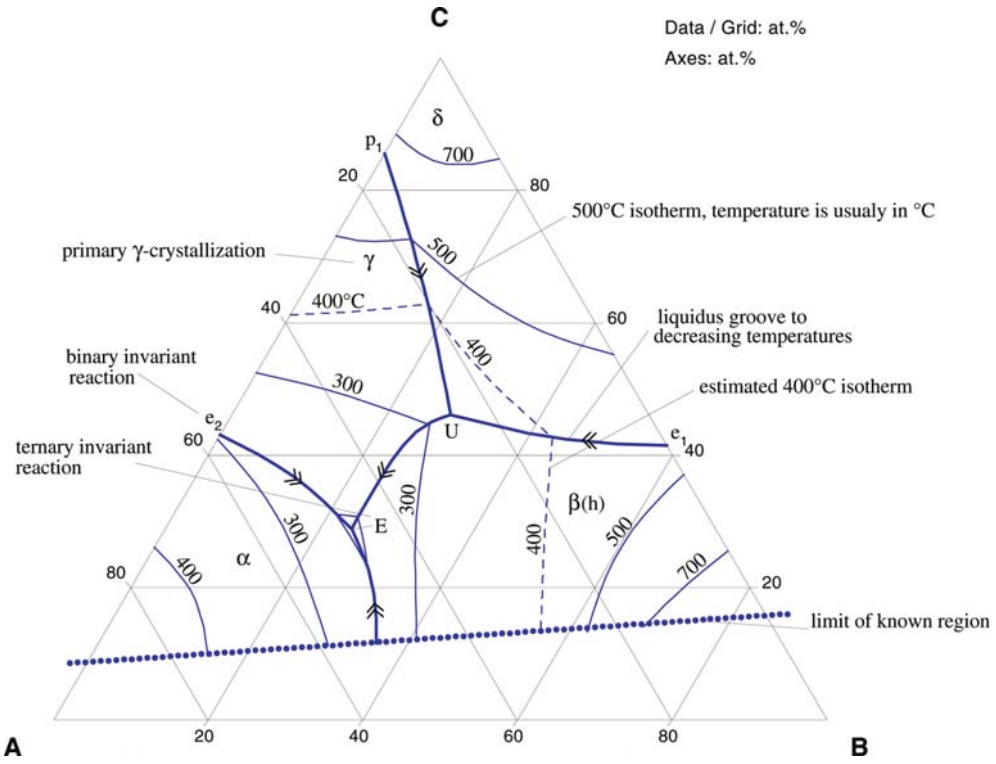

Fig. 3. Hypothetical liquidus surface showing notation employed

DOI: 10.1007/978-3-540-69761-9_1

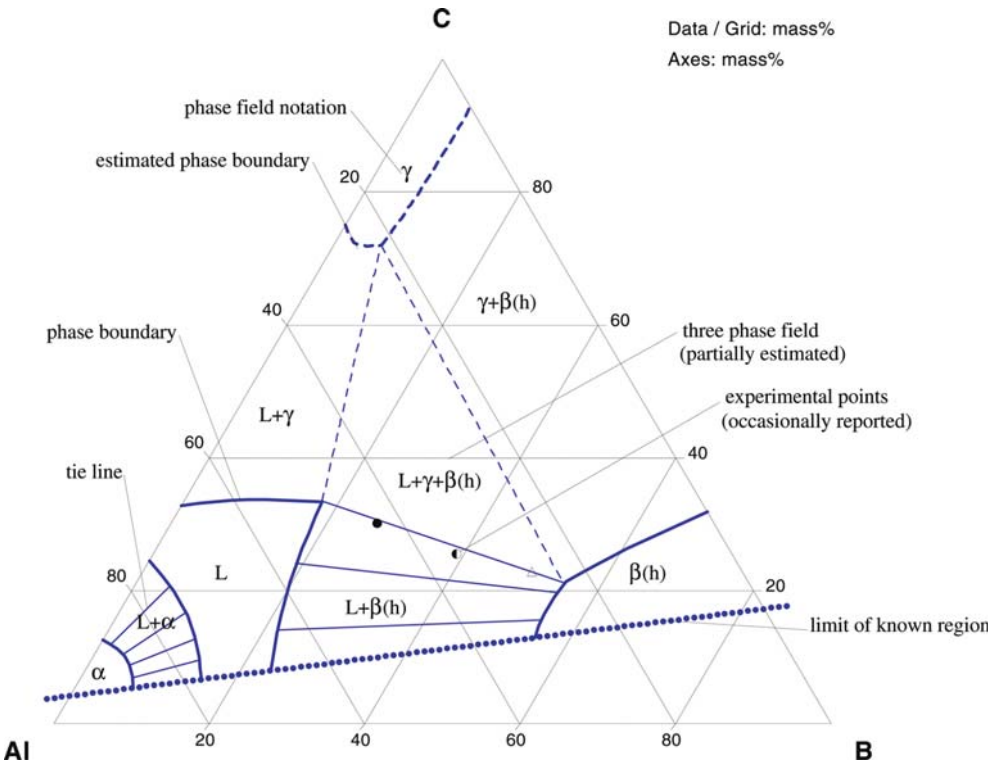

Fig. 4. Hypothetical isothermal section showing notation employed

Thermodynamics

Experimental ternary data are reported in some system reports and reference to thermodynamic modeling is made.

Notes on Materials Properties and Applications

Noteworthy physical and chemical materials properties and application areas are briefly reported if they were given in the original constitutional and phase diagram literature.

Miscellaneous

In this section noteworthy features are reported which are not described in preceding paragraphs. These include graphical data not covered by the general report format, such as lattice spacing – composition data, *p-T-x* diagrams, *etc.*

References

The publications which form the bases of the assessments are listed in the following manner:
[1974Hay] Hayashi, M., Azakami, T., Kamed, M., "Effects of Third Elements on the Activity of Lead in Liquid Copper Base Alloys" (in Japanese), *Nippon Kogyo Kaishi*, **90**, 51–56 (1974) (Experimental, Thermodyn., 16)
This paper, for example, whose title is given in English, is actually written in Japanese. It was published in 1974 on pages 51–56, volume 90 of Nippon Kogyo Kaishi, the Journal of the Mining and Metallurgical Institute of Japan. It reports on experimental work that leads to thermodynamic data and it refers to 16 cross-references.

DOI: 10.1007/978-3-540-69761-9_1

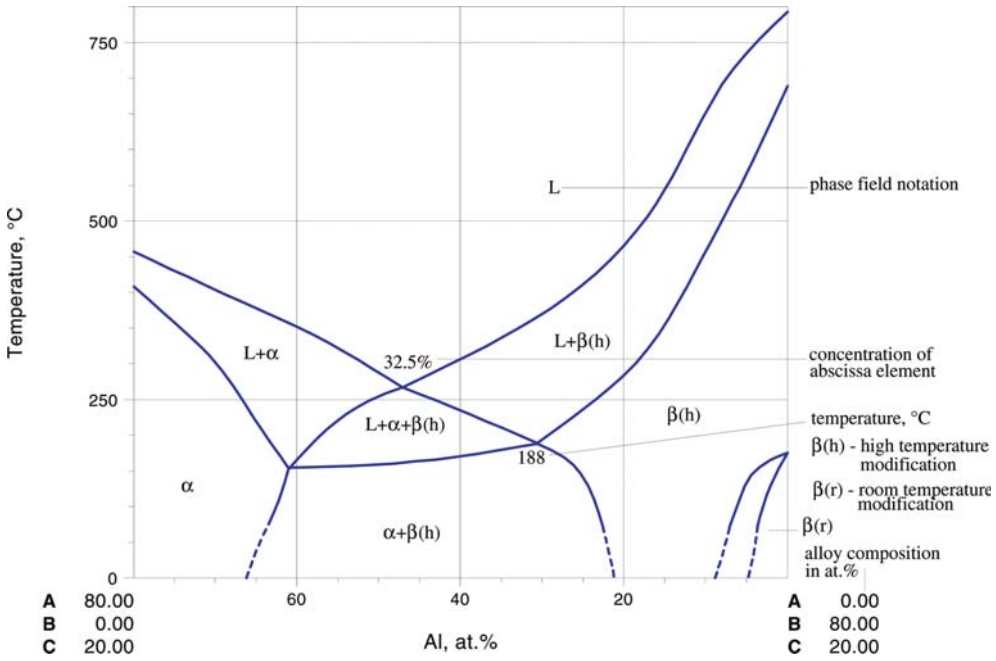

Fig. 5. Hypothetical vertical section showing notation employed

Additional conventions used in citing are:

to indicate the source of accepted phase diagrams

* to indicate key papers that significantly contributed to the understanding of the system.

Standard reference works given in the list "General References" are cited using their abbreviations and are not included in the reference list of each individual system.

General References

[C.A.] *Chemical Abstracts* - pathways to published research in the world's journal and patent literature - *http://www.cas.org/*

[Curr. Cont.] *Current Contents* - bibliographic multidisciplinary current awareness Web resource - *http://www.isinet.com/products/cap/ccc/*

[E] Elliott, R.P., *Constitution of Binary Alloys, First Supplement*, McGraw-Hill, New York (1965)

[G] Gmelin *Handbook of Inorganic Chemistry*, 8th ed., Springer-Verlag, Berlin

[H] Hansen, M. and Anderko, K., *Constitution of Binary Alloys*, McGraw-Hill, New York (1958)

[L-B] Landolt-Boernstein, *Numerical Data and Functional Relationships in Science and Technology (New Series). Group 3 (Crystal and Solid State Physics)*, Vol. 6, Eckerlin, P., Kandler, H. and Stegherr, A., *Structure Data of Elements and Intermetallic Phases* (1971); Vol. 7, Pies, W. and Weiss, A., *Crystal Structure of Inorganic Compounds*, Part c, Key Elements: N, P, As, Sb, Bi, C (1979); Group 4: *Macroscopic and Technical Properties of Matter*, Vol. 5, Predel, B., *Phase Equilibria, Crystallographic and Thermodynamic Data of Binary Alloys*, Subvol. a: Ac-Au ... Au-Zr (1991); Springer-Verlag, Berlin.

[Mas] Massalski, T.B. (Ed.), *Binary Alloy Phase Diagrams*, ASM, Metals Park, Ohio (1986)

[Mas2] Massalski, T.B. (Ed.), *Binary Alloy Phase Diagrams*, 2nd edition, ASM International, Metals Park, Ohio (1990)

[P] Pearson, W.B., *A Handbook of Lattice Spacings and Structures of Metals and Alloys*, Pergamon Press, New York, Vol. 1 (1958), Vol. 2 (1967)

[S] Shunk, F.A., *Constitution of Binary Alloys, Second Supplement*, McGraw-Hill, New York (1969)

DOI: 10.1007/978-3-540-69761-9_1

[V-C] Villars, P. and Calvert, L.D., *Pearson's Handbook of Crystallographic Data for Intermetallic Phases*, ASM, Metals Park, Ohio (1985)

[V-C2] Villars, P. and Calvert, L.D., *Pearson's Handbook of Crystallographic Data for Intermetallic Phases*, 2nd edition, ASM, Metals Park, Ohio (1991)

DOI: 10.1007/978-3-540-69761-9_1

Index of alloy systems

Index of Ternary Iron Alloy Systems Al-B-Fe to C-Co-Fe

Al – B – Fe (Aluminium – Boron – Iron)
Al – C – Fe (Aluminium – Carbon – Iron)
Al – Cr – Fe (Aluminium – Chromium – Iron)
Al – Fe – H (Aluminium – Iron – Hydrogen)
Al – Fe – Mo (Aluminium – Iron – Molybdenum)
Al – Fe – N (Aluminium – Iron – Nitrogen)
Al – Fe – O (Aluminium – Iron – Oxygen)
Al – Fe – P (Aluminium – Iron – Phosphorus)
Al – Fe – Si (Aluminium – Iron – Silicon)
Al – Fe – Ta (Aluminium – Iron – Tantalum)
Al – Fe – Ti (Aluminium – Iron – Titanium)
Al – Fe – Zn (Aluminium – Iron – Zinc)
B – C – Fe (Boron – Carbon – Iron)
B – Co – Fe (Boron – Cobalt – Iron)
B – Cr – Fe (Boron – Chromium – Iron)
B – Fe – Mn (Boron – Iron – Manganese)
B – Fe – Mo (Boron – Iron – Molybdenum)
B – Fe – N (Boron – Iron – Nitrogen)
B – Fe – Nb (Boron – Iron – Niobium)
B – Fe – Nd (Boron – Iron – Neodymium)
B – Fe – Ni (Boron – Iron – Nickel)
B – Fe – P (Boron – Iron – Phosphorus)
B – Fe – Ti (Boron – Iron – Titanium)
B – Fe – W (Boron – Iron – Tungsten)
Ba – Fe – O (Barium – Iron – Oxygen)
C – Co – Fe (Carbon – Cobalt – Iron)

DOI: 10.1007/978-3-540-69761-9_2

Aluminium – Boron – Iron

Peter Rogl

Introduction

Information on the constitution of the Al-B-Fe system is still scarce. Phase relations within the isothermal section at 800°C have been determined by [1966Sta] and were later reviewed by [1974Cha, 1990Kuz] and [1989Gho]. Phase relations at 800°C reveal the existence of only one ternary compound, the composition of which was first located by [1966Sta] at about "Fe_3AlB_3", but from X-ray crystal structure determination was found to be at Fe_2AlB_2 [1969Jei, 1969Kuz]. The experimental activities related to the constitution of the ternary Al-B-Fe system are summarized in Table 1.

Binary Systems

The accepted Al-Fe phase diagram [2006MSIT] is mainly based on the assessment by [1993Kat], except for the Fe rich region, where the ordering equilibria between the (αFe), FeAl and Fe_3Al solid solutions have been recently investigated by [2001Ike]. The Al-B phase diagram is taken in the version of [2004Gry]. The B-Fe system is from [Mas2]. Crystallographic and melting data of the phases pertinent to the Al-B-Fe system are listed in Table 2.

Solid Phases

Mutual solid solubilities of binary borides and aluminides were shown to be rather small except for the solubility of Al in BFe_2. Stadelmaier [1966Sta] reported a solubility of about 11 at.% Al in Fe_2B at 800°C under strong expansion of the unit cell (see Table 2). The direction of the homogeneity region was originally shown for the line BFe_2-Al [1966Sta] with a small reduction of the B-content $(Fe_{1-x}Al_x)_2B_{1-y}$, however, Fe/Al substitution seems to be more likely than simultaneous B/Al substitution. Thus a metal substitution mechanism is assumed in terms of $(Fe_{1-x}Al_x)_2B$. No significant homogeneity region was reported for the (stoichiometric) ternary compound Fe_2AlB_2 [1969Jei, 1969Kuz], which originally was believed to be located at about "AlB_3Fe_3" [1966Sta]. From Z-contrast imaging and electron energy loss spectroscopy a new tetragonal precipitate Fe_8Al_7B has been identified in Al-Fe alloys with small B, C additions; the structure was said to be a superlattice of ordered vacancies on Al-sites; it was described to contain 16 blocks of CsCl type ($a = 4a_{FeAl}$, $c = a_{FeAl}$), 14 out of which appear as distorted FeAl units, the other two are diamond like Fe arrangements with interstitial B atoms. The phase was only observed in B containing Al-Fe alloys and exhibits an orientation relationship with FeAl according to $[100]_{Fe8Al7B}//[100]_{FeAl}$ and $(001)_{Fe8Al7B}//(001)_{FeAl}$. For details see [2000Chi] and references therein.

Liquidus, Solidus and Solvus Surfaces

No information is available on liquidus, solidus or solvus surfaces. The ternary phase "Fe_3AlB_3" (later found to be Fe_2AlB_2 [1969Jei, 1969Kuz]) was said to melt incongruently in the primary field of BFe with a eutectic matrix of Fe_4Al_{13} [1966Sta].

Isothermal Sections

Phase equilibria have been established in an isothermal section at 800°C [1966Sta], however, in view of the assessed binary boundary diagrams a few minor adaptations were made in order to comply with the phase relations accepted. Furthermore small solid solubilities of Fe and Al in (βB) were taken into account (see Fig. 1). The region Fe_2AlB_2 - AlB_2 - (βB) was not investigated by [1966Sta]; phase relations for this region are estimated in Fig. 1.

DOI: 10.1007/978-3-540-69761-9_3

Thermodynamics

No experimental thermodynamic data are presently available for the ternary system. Calculations of mixing enthalpy and mismatch entropy were made to understand the ability to form amorphous material in Al-B-Fe alloys [2000Tak].

Miscellaneous

To understand the beneficial hardening effect of small boron additions to AlFe and 40Al-Fe was the subject of extensive studies [2006Kel, 2005Ric, 2004Cad, 2003Jor, 2000Pik, 1998Bak, 1997Dee, 1996Li, 1996Kim, 1995Sch, 1995Mun, 1994Kle, 1991Liu]. Intergranular boron segregation in 40-46Al-Fe alloys was studied by [1999Gay] and in B-doped 25mass%Al-150ppmB-Fe alloys by [1995Kob]. [2002Bru] investigated the positive influence of micro-alloying elements such as B (Ti, Nb) on microstructure, re-crystallization texture and mechanical properties of Al-Fe light weight steels; similar investigations were carried out defining the influence of B (Nb, Cr, Mo) additions to 38Al-Fe alloys [1998Kwa] as well as on 25Al-Fe alloys [1997Han, 1997Kwa]. The morphology of the iron boride phase in a cast iron-aluminide matrix composite (B1-Al25-Fe alloy) containing 15 vol.% iron borides was determined by [1996Suw]. The effect of deformation processing and resulting microstructure in this alloy was discussed by [1997Suw]. DFT calculations for B in AlFe alloys (CsCl type) indicated Al/B-substitution except for sufficient Al content where B enters interstitially [2002Bes]. Hot-corrosion resistance measurements of sprayed and atomized 40Al-Fe+0.1B+10Al_2O_3 (in at.%) intermetallics in $NaVO_3$ at 625 to 700°C [2001Esp, 2005Are] or in Na_2SO_4 at 900 to 1000°C [2005Are] were interpreted in terms of an electrochemical model; less corrosion resistance was obtained for the alloy with 0.4 at.% B [2005Are]. Mössbauer studies of melt spun $Fe_{60}Al_{28}B_{12}$ identified an amorphous ferromagnet [1987McC, 1991McC]. Magnetic properties (magnetization, coercivity, magnetostriction) of rapidly quenched alloys [1980Lub], $Fe_{100-x-y}Al_xB_y$ ($0 \le x \le 28.3$, $0 \le y \le 20.4$) [1988Sat] and ($0 \le x \le 10$, $15 \le y \le 25$) [1980Ara] showed relatively soft magnetic properties near the $Fe_{75}Al_{25}$ composition. An amorphous structure was achieved in the range $12 \le y \le 25$ and best soft magnetic properties (Hc = 1.6 A/m, Bs = 1.1 T, mum = 1.4105, ρ = 160 μΩ · cm) were obtained around the composition $Fe_{60}Al_{20}B_{20}$ [1988Sat]. Iron aluminide composites containing up to 30-90 vol.% borides or carbides can be processed to near full density via conventional liquid-phase sintering or pressureless melt infiltration [1997Sub].

Table 1. Experimental Investigations of the Al-B-Fe Phase Relations, Structures and Thermodynamics

Reference	Method/Experimental Technique	Temperature/Composition/Phase Range Studied
[1966Sta]	Metallographic and XRD inspection on about 40 ternary alloys prepared by melting in sintered alumina crucibles under argon. Starting materials: 99.99 mass% Al, 99.5% electrolyte Fe, 98.5–98.9% crystallized B-powder. Heat treatment at 800°C in vacuum-sealed Vycor capsules for 300 h; water quench.	Phase equilibria in an isothermal section at 800°C. The region AlB_2-Fe_2AlB_2-B was not studied.
[1969Jei]	Single crystals from an induction melted alloy (alumina crucible, argon) by dissolving the Al-matrix in dilute HCl.	Determination of the crystal structure of AlB_2Fe_2 from X-ray single crystal photographic film data.

(*continued*)

DOI: 10.1007/978-3-540-69761-9_3

Reference	Method/Experimental Technique	Temperature/Composition/Phase Range Studied
[1969Kuz]	Alloys prepared by arc melting powder compacts in argon. Heat treatment at 800°C in evacuated quartz capsules 240 h.	Determination of the crystal structure of Fe_2AlB_2 from X-ray single crystal photographic film data.
[2000Chi]	Extrusion at 1000°C of vacuum-induction melted ingot of Fe-Al-B-C (area reduction 16:1; chemical composition Fe-40at.%Al-0.53B-0.7C); heat treatment at 1150°C for 30 min, then air cooled to RT. For TEM jet-polishing in a 20% HNO_3/methanol al –26°C, 15 V plus short time ion milling with 1 kV Ar.	Determination of atomic structure of τ_2, Fe_8Al_7B from Z-contrast in scanning transition microscope at 300 kV. High-spatial-resolution EELS was used to define the composition and bonding.

Table 2. Crystallographic Data of Solid Phases

Phase/ Temperature Range [°C]	Pearson Symbol/ Space Group/ Prototype	Lattice Parameters [pm]	Comments/References
(Al) < 660.452	*cF*4 $Fm\bar{3}m$ Cu	a = 404.96	[Mas2]
(βB) < 2092	*hR*333 $R\bar{3}m$ βB	a = 1093.30 c = 2382.52	[Mas2, 1993Wer]
		a = 1096.5 c = 2386.8	at AlB_{31} [V-C2]
		a = 1095.14 c = 2386.1	at $FeB_{\sim 49}$ [V-C2]
		a = 1097.18 c = 2387.05	at $FeB_{\sim 20}$ [V-C2]
(γFe) 1394 - 912	*cF*4 $Fm\bar{3}m$ Cu	a = 364.67 a = 357.3	[Mas2] at 25°C [V-C2]
(αδFe) (αFe)(r) ≤ 912	*cI*2 $Im\bar{3}m$ W	a = 286.65	pure Fe at 25°C [Mas2]
(δFe)(h_2) 1538 - 1394		a = 293.15	pure Fe at 1480°C [Mas2]
$Fe_{1-x}B_x$		a = 286.0	at x = 0.09 [V-C2]
Al_2B_3 < 525	*hR** Al_2B_3 (?)	a = 1840 c = 896	at 60 at.% B [1992Var] metastable?

(*continued*)

DOI: 10.1007/978-3-540-69761-9_3

Phase/ Temperature Range [°C]	Pearson Symbol/ Space Group/ Prototype	Lattice Parameters [pm]	Comments/References
AlB_2 < 956 ± 5	*hP*3 *P*6/*mmm* AlB_2	*a* = 300.6 *c* = 325.2	[1994Dus], temperature from [2000Hal]
		a = 300.67 ± 0.01 *c* = 325.36 ± 0.02	[2002Zhe]
		a = 300.43 ± 0.03 *c* = 325.19 ± 0.06	[1999Bur] for $Al_{0.9}B_2$
αAlB_{12} < 2050	*tP*216 $P4_12_12$ αAlB_{12}	*a* = 1015.8 *c* = 1427.0	[1994Dus] $\rho_{exp.}$ = 2.65·Mgm^{-3}
		a = 1018 *c* = 1434.3	[1991Pri]
εAlB_{12}	*oP*384 $P2_12_12_1$ εAlB_{12}	*a* = 1014.4 *b* = 1657.3 *c* = 1751.0	[1983Hig, 1994Dus, 2000Hig] metastable phase or ternary product stabilized by small amounts of impurity metals present in Al-flux grown material $\rho_{exp.}$ = 2.56·Mgm^{-3}
		a = 1019.5 *b* = 1666 *c* = 1769	[1991Pri]
FeB <1588	*oP*8 *Pnma* FeB	*a* = 550.6 *b* = 295.2 *c* = 406.1	[1992Rog]
Fe_2B <1407	*tI*12 *I*4/*mcm* $CuAl_2$	*a* = 510.9 *c* = 424.9	[1992Rog]
$(Fe_{1-x}Al_x)_2B$		*a* = 510.95 *c* = 424.92	0 < *x* < 0.11 at 800°C at *x* = 0 [1966Sta]
		a = 512.05 *c* = 425.80	at *x* = 0.11 [1966Sta] from three-phase alloy
$Fe_3B(h_1)$ ~1250 - ~ 1150	*tI*32 $I\bar{4}$ Fe_3P	*a* = 865.5 *c* = 429.7	metastable [1992Rog]
$Fe_3B(h_2)$ ~1220 - ~ 1140	*tP*32 $P4_2/n$ Ti_3P	*a* = 864.8 *c* = 431.4	metastable [1992Rog]
Fe_3B < 1214	*oP*16 *Pnma* Fe_3C	*a* = 542.8 *b* = 666.9 *c* = 443.9	metastable, [1992Rog]

(*continued*)

DOI: 10.1007/978-3-540-69761-9_3

Phase/ Temperature Range [°C]	Pearson Symbol/ Space Group/ Prototype	Lattice Parameters [pm]	Comments/References
$Fe_{23}B_6$ ~800 - ~ 650	*cF*116 *Fm*3*m* $Cr_{23}C_6$	*a* = 1076	[1991Kha] metastable
Fe_4Al_{13} < 1160	*mC*102 *C*2/*m* Fe_4Al_{13}	*a* = 1552.7 to 1548.7 *b* = 803.5 to 808.4 *c* = 1244.9 to 1248.8 β = 107.7 to 107.99°	74.16-76.70 at.%Al [1986Gri] Sometimes called $FeAl_3$ in literature
		a = 1549.2 *b* = 807.8 *c* = 1247.1 β = 107.69°	at 76.0.% Al [1994Gri]
Fe_2Al_5 < 1169	*oC*24 *Cmcm*	*a* = 765.59 *b* = 641.54 *c* = 421.84	70-73 at.%Al at 71.5 at.% Al [1994Bur]
$FeAl_2$ < 1156	*aP*18 *P*1 $FeAl_2$	*a* = 487.8 *b* = 646.1 *c* = 880.0 α = 91.75° β = 73.27° γ = 96.89°	at 66.9 at.% Al [1993Kat]
ε 1232 - 1102	*cI*16?	*a* = 598.0	at 58 - 65 at.% Al [Mas2]
FeAl < 1310	*cP*2 $Pm\bar{3}m$ CsCl	*a* = 289.48 to 290.5	34.5 - 47.5 at.% Al [1961Lih]
		a = 289.53 to 290.9	36.2 - 50.0 at.% Al [1958Tay]
		a = 289.81 to 291.01	39.7 - 50.9 at.% Al [1997Kog]
		a = 289.76 to 190.78	Quenched from 500°C in water room temperature
Fe_3Al < 547	*cF*16 $Fm\bar{3}m$ BiF_3	*a* = 579.30 to 578.86	~24- ~37 at.% Al [2001Ike] 23.1-35.0 at.% Al [1958Tay]
		a = 579.30 to 578.92	24.7-31.7 at.% Al [1961Lih]
Fe_2Al_9	*mP*22 $P2_1/c$ Co_2Al_9	*a* = 869 *b* = 635 *c* = 632 β = 93.4°	metastable 81.8 at.% Al [1993Kat]

(*continued*)

DOI: 10.1007/978-3-540-69761-9_3

Phase/ Temperature Range [°C]	Pearson Symbol/ Space Group/ Prototype	Lattice Parameters [pm]	Comments/References
$FeAl_6$	*oC*28 $P\bar{3}m1$ Cu_3P	*a* = 744.0 *b* = 646.3 *c* = 877.0	metastable 85.7 at.% Al [1993Kat]
		a = 744 *b* = 649 *c* = 879	[1998Ali]
$FeAl_{4+x}$	*t***	*a* = 884 *c* = 2160	(0 < *x* < 0.4) metastable [1998Ali]
*τ_1, AlB_2Fe_2	*oC*10 *Cmmm* Al_2BMn_2	*a* = 292.33 *b* = 1103.37 *c* = 287.03	[1969Jei] R_F = 0.084
		a = 292.23 *b* = 1104.6 *c* = 287.5	[1969Kuz]
*τ_2, Al_7BFe_8 $\lesssim$ 700°C	*t*** ? superstructure of FeAl	*a* = 1156 *c* = 289	[2000Chi]

DOI: 10.1007/978-3-540-69761-9_3

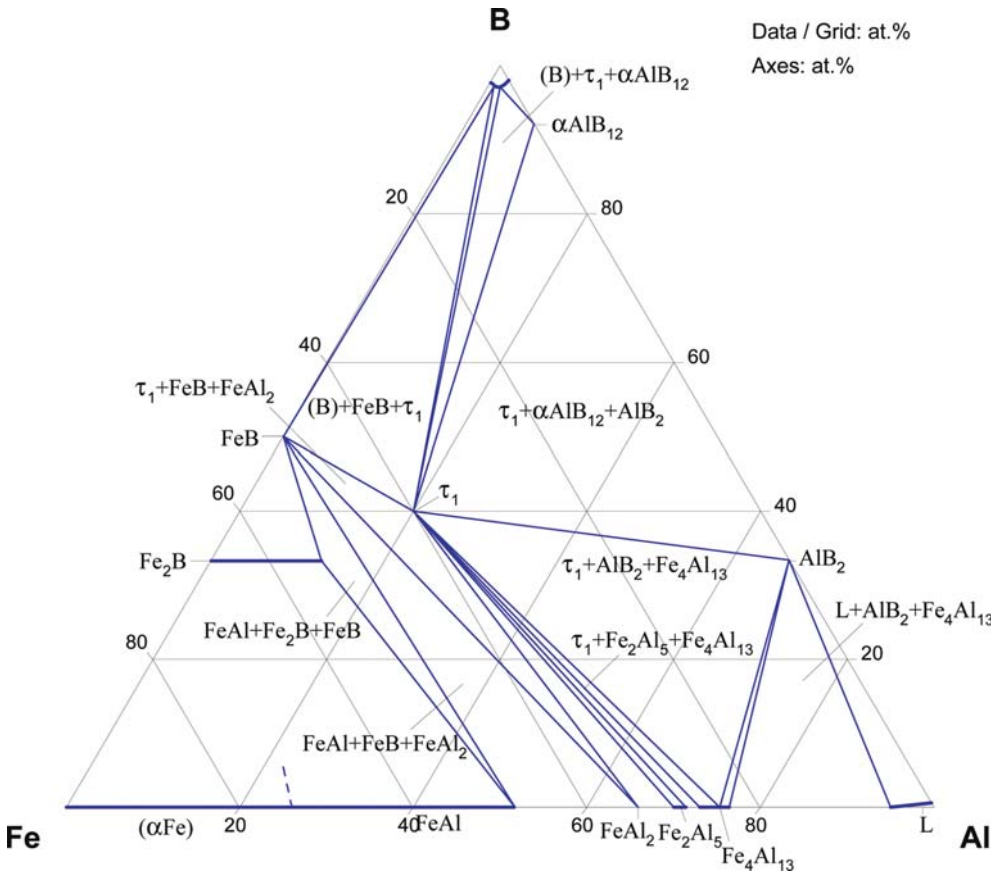

Fig. 1. Al-B-Fe. Isothermal section at 800°C

DOI: 10.1007/978-3-540-69761-9_3

References

[1958Tay] Taylor, A., Jones, R.M., "Constitution and Magnetic Properties of Iron-Rich Iron-Aluminium Alloys", *J. Phys. Chem. Solids*, **6**, 16–37 (1958) (Crys. Structure, Experimental, 49)

[1961Lih] Lihl, F., Ebel, H., "X-Ray Examination of the Constitution of Iron-Rich Alloys of the Iron-Aluminium System" (in German), *Arch. Eisenhuettenw.*, **32**, 483–487 (1961) (Crys. Structure, Experimental, 12)

[1966Sta] Stadelmaier, H.H., Burgess, R.E., Davis, H.H., "The Ternary System Fe-Al-B" (in German), *Metall*, **20**(3), 225–226 (1966) (Experimental, Crys. Structure, Phase Diagram, Phase Relations, 14)

[1969Jei] Jeitschko, W., "The Crystal Structure of Fe_2AlB_2", *Acta Crysallogr.*, **25B**, 163–165 (1969) (Experimental, Crys. Structure, 10)

[1969Kuz] Kuz'ma, Yu.B., Chaban, N.F., "Crystal Structure of the Compound Fe_2AlB_2", *Inorg. Mater. (Engl. Trans.)*, **5**(2), 321–322 (1969), translated from *Izv. Akad. Nauk SSSR, Neorg. Mater.*, **5**(2), 384–385 (1969) (Experimental, Crys. Structure, 2)

[1974Cha] Chaban, N.F., Kuz'ma, Y.B., "Metallides in the Period IV Transition Metal-Aluminum (Gallium) - Boron Ternary System" (in Russian), *Stroenie Svoistva i Primenenie Metall.*, Nauka, 102–107 (1974) (Experimental, Crys. Structure, Review, Phase Diagram, Phase Relations, 18)

[1980Ara] Arai, S., Nagakura, M., "Magnetic Properties of Fe-Al-B System Amorphous Alloy" (in Japanese), *Research Reports of the Faculty of Engineering*, Meiji University, Japan, **40**, 25–29 (1980) (Experimental, Magn. Prop., 11)

[1980Lub] Luborsky, F.E., Walter, J.L., Wohlfarth, E.P., "The Saturation Magnetisation, Curie Temperature and Size Effect of Amorphous Iron Alloys", *J. Phys. F (Metal Physics)*, **10**(5), 959–966 (1980) (Experimental, Magn. Prop., 20)

[1983Hig] Higashi, I., "Aluminum Distribution in the Boron Framework of (γ-AlB_{12}", *J. Solid State Chem.*, **47**, 333–349 (1983) (Crys. Structure, 17)

[1986Gri] Griger, A., Syefaniay, V., Turmezey, T., "Crystallographic Data and Chemical Compositions of Aluminum-Rich Al-Fe Intermetallic Phases", *Z. Metallkd.*, **77**, 30–35 (1986) (Phase Diagram, Phase Relations, Crys. Structure, Experimental, 23)

[1987McC] McCally, R.L., Moorjani, K., Kistenmacher, T.J., "A Möessbauer Investigation of Melt-Spun $Fe_{60}Al_{28}B_{12}$", *J. Appl. Phys.*, **61/8-IIA**, 3655–3657 (1987) (Crys. Structure, Experimental, 5)

[1988Sat] Sato, F., Ishio, S., Miyazaki, T., "Soft Magnetic Properties of Rapidly Quenched Fe-Al-M (M = Si, B, Ge) Alloys", *Physica Status Solidi*, **A107**(1), 355–363 (1988) (Experimental, Magn. Prop., 14)

[1989Gho] Ghosh, G., "The Al-B-Fe (Aluminum-Boron-Iron) System", *Bull. Alloy Phase Diagrams*, **10**(6), 667–668 (1989) (Review, Phase Diagram, Phase Relations, 6)

[1990Kuz] Kuz'ma, Y.B., Chaban, N.F., "System Al-B-Fe", in "*Ternary Metal Boron Systems*" (in Russian), Metallurgia, Moscow, 66–67 (1990) (Review, Phase Diagram, Phase Relations, 4)

[1991Kha] Khan, Y., Wibbeke, H., "Formation of the τ-Phase in the Fe-B Alloys", *Z. Metallkd.*, **82**(9), 703–705 (1991) (Experimental, Crys. Structure, 6)

[1991Liu] Liu, C.T., George, E.P., "Effect of Aluminum Concentration and Boron Dopant on Environmental Embrittlement in FeAl Aluminides", *Mater. Res. Soc. Symp. Proc.: High-Temp. Ordered Intermetallic Alloys IV*, **213**, 527–532 (1991) (Experimental, Phys. Prop., 28)

[1991McC] McCally, R.L., "Magnetism in Amorphous Iron-Based Alloys: the Iron-Phosphorus and Iron-Aluminum-Boron Systems", *Diss. Abstr. Int.*, **52**(6), 180 (1991) (Abstract, Magn. Prop., 0)

[1991Pri] Prikhina, T.A., Kisly, P.S., "Aluminium Borides and Carboborides", in "*Boron-Rich Solids*", AIP Conf. Proc. 231, Emin, D. et al. (Eds.), Albuquerque, USA, 1990, AIP, New York, 590–593 (1991) (Experimental, 11)

[1992Rog] Rogl, P., Schuster, J.C., "System Iron-Boron-Nitrogen", in "*Ternary Boronnitrides and Siliconnitrides*", ASM, Materials Park, OH, 1–128 (1992) (Phase Diagram, Phase Relations, Review)

[1992Var] Vardiman, R.G., "Microstructures in Aluminium, Ion Implanted with Boron and Heat Treated", *Acta Metall. Mater.*, **40**, 1029–1035 (1992) (Crys. Structure, Experimental, 7)

DOI: 10.1007/978-3-540-69761-9_3

[1993Kat] Kattner, U.R., Burton, B.P., "Al-Fe (Aluminum-Iron)", in "*Phase Diagrams of Binary Iron Alloys*", Okamoto, H. (Ed.), ASM Intl., Metals Park, OH, 12–28 (1993) (Review, Phase Diagram, Phase Relations, 99)

[1993Wer] Werheit, H., Kuhlmann, U., Laux, M., Lundström, T., "Structural and Electronic Properties of Carbon-Doped β-Rhombohedral Boron", *Phys. Status Solidi*, **B179**, 489–511 (1993) (Crys. Structure, Phys. Prop., Experimental, 51)

[1994Bur] Burkhardt, U., Grin, J., Ellner, M., Peters, K., "Structure Refinement of the Iron-Aluminium Phase with the Approximate Composition Fe_2Al_5", *Acta Crystallogr., Sect. B: Struct. Crystallogr. Crys. Chem.*, **B50**, 313–316 (1994) (Crys. Structure, Experimental, 9)

[1994Dus] Duschanek, H., Rogl, P., "The System Al-B", *J. Phase Equilib.*, **15**(5), 543–52 (1994) (Crys. Structure, Phase Diagram, Experimental, #, 78) see also *ibid*, **16**(1), 6 (1995) (Experimental, Review, 78)

[1994Gri] Grin, J., Burkhardt, U., Ellner, M., Peters, K., "Refinement of the Fe_4Al_{13}Structure and its Relationship to Quasihomological Homotypical Structures", *Z. Kristallogr.*, **209**, 479–487 (1994) (Crys. Structure, Experimental, 39)

[1994Kle] Klein, O., Baker, I., "The Effect of Boron on the Temperature Dependence of the Flow and Fracture of Fe-45Al", *Scr. Metall. Mater.*, **30**(11), 1413–1417 (1994) (Experimental, Mechan. Prop., 15)

[1995Kob] Kobylanski, G., LeCoze, J., "Boron Heterogeneities in As-cast FeAl Intermetallics", *J. Phys. IV*, **5**(C7), 205–209 (1995) (Experimental, Mechan. Prop., 3)

[1995Mun] Munroe, P.R., Baker, I., "Dislocations in Fe-45 at.% Al+B after High-Temperature Deformation", *Philos. Mag. A (Physics of Condensed Matter, Defects and Mechanical Properties)*, **72**(5), 1301–1310 (1995) (Experimental, Mechan. Prop., Crys. Structure, 26)

[1995Sch] Scheff, S.A., Stout, J.J., Crimp, M.A., "Effect of Extrusion Texture on the Compressive Behavior of *B*2 Fe-Al Alloys", *Scr. Metall. Mater.*, **32**(7), 975–980 (1995) (Experimental, Mechan. Prop., 15)

[1996Kim] Kim, M.H., Kwun, S.I., "Tensile Properties of Cast and Mechanically Alloyed FeAl With High Boron Content", *Scr. Mater.*, **35**(3), 317–322 (1996) (Experimental, Mechan. Prop., Morphology, 17)

[1996Li] Li, X., Baker, I., "The Effect of Boron on the Hall-Petch Behavior of Fe-45Al", *Scr. Mater.*, **34**(8), 1219–1223 (1996) (Experimental, Mechan. Prop., 47)

[1996Suw] Suwas, S., Bhargava, S., Sangal, S., "Morphology of the Boride Phase in a Cast Iron-Aluminide Matrix Composite", *J. Mater. Sci. Lett.*, **15**(14), 1216–1218 (1996) (Experimental, Mechan. Prop., Crys. Structure, 11)

[1997Dee] Deevi, S.C., Sikka, V.K., Inkson, B.J., Cahn, R.W., "Effect of Boron on the Vacancy Hardening of FeAl", *Scr. Mater.*, **36**(8), 899–904 (1997) (Experimental, Mechan. Prop., 16)

[1997Han] Han-Cheol, Choe, Dap-Chun, Choi, "Effects of Cr, Mo, Nb and B on the Intergranular Corrosion Behaviour of Fe-25 at.% Al Intermetallic Compounds" (in Korean), *J. Korean Inst. Met. Mater.*, **35**(4), 468–476 (1997) (Experimental, Mechan. Prop., 16)

[1997Kog] Kogachi, M., Haraguchi, T., "Quenched-in Vacancies in *B*2-Structured Intermetallic Compound FeAl", *Mater. Sci. Eng. A*, **A230**, 124–131 (1997) (Crys. Structure, Experimental, 23)

[1997Kwa] Kwang-Il, Park, Sung-Min, Joo, Dap-Chun, Choi, "Effects of Cr, Mo, Nb and B Additions on the Microstructure and Mechanical Properties in Fe-25at.%Al Alloy" (in Korean), *J. Korean Inst. Met. Mater.*, **35**(3), 305–311 (1997) (Experimental, Mechan. Prop., 17)

[1997Sub] Subramanian, R., Schneibel, J.H., "Processing Iron-Aluminide Composites Containing Carbides or Borides", *J. Min. Met. Mater. Soc.*, **49**(8), 50 (1997) (Experimental, Mechan. Prop., 41)

[1997Suw] Suwas, S., Bhargava, S., Sangal, S., "The Effect of Deformation Processing on Microstructural Evolution in a Boron Containing Fe-25Al Intermetallic Alloy", *High Temp. Mater. Proc.*, **16**(1), 29–38 (1997) (Experimental, Mechan. Prop., 13)

[1998Ali] Aliravci, C.A., Pekgueleryuez, M.O., "Calculation of Phase Diagrams for the Metastable Al-Fe Phases Forming in Direct-chill (DC)-Cast Aluminium Alloy Ingots", *Calphad*, **22**, 147–155 (1998) (Calculation, Phase Diagram, Phase Relations, 20)

DOI: 10.1007/978-3-540-69761-9_3

[1998Bak] Baker, I., Li, X., Xiao, H., Carleton, R., George, E.P., "The Room Temperature Strengthening Effect of Boron as a Function of Aluminium Concentration in FeAl", *Intermetallics*, **6**(3), 177–183 (1998) (Experimental, Mechan. Prop., 27)

[1998Kwa] Kwang-Il, Park, Sung-Min, Joe, Han-Cheol, Choe, Dap-Chun, Choi, "Effects of Cr, Mo, Nb and B Additions on Microstructure and Mechanical Properties in Fe-38at.% Al Alloys" (in Korean), *J. Kor. Inst. Met. Mater.*, **36**(3), 377–384 (1998) (Experimental, Mechan. Prop., 18)

[1999Bur] Burkhardt, U., Grin, Y., "Refinement of the Aluminium Diboride Crystal Structure", in "*Borides and Related Compounds*", Abst. 13th Int. Symp. on Boron, Dinar (France), 13pp., (1999) (Crys. Structure, 3)

[1999Gay] Gay, A.S., Fraczkiewicz, A., Biscondi, M., "Mechanisms of the Intergranular Segregation of Boron in (*B*2) FeAl Alloys", *Integranlar and Interphase Boundaries in Materials*, IIB98, **294**(2), 453–456 (1999) (Experimental, Mechan. Prop., 10)

[2000Chi] Chisholm, M.F., Duscher, G., Pang, L.X., Kumar, K.S., "$Fe_{16}Al_{14}B_2$ Phase in Fe-Al Alloys", *Philos. Mag. A (Physics of Condensed Matter, Defects and Mechanical Properties)*, **80**(11), 2737–2745 (2000) (Experimental, Crys. Structure, Phase Relations, Mechan. Prop., 17)

[2000Hal] Hall, A., Economy, J., "The $Al_{(L)}+AlB_{12}\rightarrow AlB_2$ Peritectic Transformation and Its Role in the Formation of High Aspect Ratio AlB_2 Flakes", *J. Phase Equilib.*,**21**(1), 63–69 (2000) (Phase Diagram, Phase Relations, Experimental, 21)

[2000Hig] Higashi, I., "Crystal Chemistry of α-AlB_{12} and (γ-AlB_{12}", *J. Solid State Chem.*, **154**, 168–176 (2000) (Crys. Structure, Experimental, 18)

[2000Pik] Pike, L.M., Liu, C.T., "The Effect of Vacancies on the Environmental Yield Strength Dependence of Boron-free and Boron-doped Fe-40Al", *Intermetallics*, **8**(12), 1413–1416 (2000) (Experimental, Mechan. Prop., 23)

[2000Tak] Takeuchi, A., Inoue, A., "Calculations of Mixing Enthalpy and Mismatch Entropy for Ternary Amorphous Alloys", *Mater. Trans. JIM.*, **41**(11), 1372–1378 (2000) (Thermodyn., Experimental, 10)

[2001Esp] Espinosa-Medina, M.A., Casales, M., Martinez-Villafane, A., Porcayo-Calderon, J., Martinez, L., Gonzalez-Rodriguez, J.G., "Hot Corrosion of Atomized Iron Aluminides Doped With Boron and Reinforced With Alumina", *Mater. Sci. Eng. A*, **A300**(1–2), 183–189 (2001) (Experimental, Mechan. Prop., Morphology, 18)

[2001Ike] Ikeda, O., Ohnuma, I., Kainuma, R., Ishida, K., "Phase Equilibria and Stability of Ordered BCC Phases in the Fe-Rich Portion of the Fe-Al System", *Intermetallics*, **9**, 755–761 (2001) (Thermodyn., Experimental, 18)

[2002Bes] Besson, R., Legris, A., Morillo, J., "Comprehensive ab Initio Thermodynamic Treatment of Impurities in Ordered Alloys: Application to Boron in *B*2 Fe-Al", *Phys. Rev. Lett.*, **89**(22), 225502 (2002) (Calculation, Crys. Structure, Magn. Prop., Thermodyn., 25)

[2002Bru] Bruex, U., Frommeyer, G., Jimenez, J., "Light-Weight Steels Based on Iron-Aluminum-Influence of Micro Alloying Elements (B, Ti, Nb) on Microstructures, Textures and Mechanical Properties", *Steel Res.*, **73**(12), 543–548 (2002) (Experimental, Mechan. Prop., 10)

[2002Zhe] Zheltov, P., Grytsiv, A., Rogl, P., Velikanova, T.Ya., Research at Univ. Wien (unpublished) (2002) (Phase Diagram, Phase Relations, Crys. Structure)

[2003Jor] Jordan, J.L., Deevi, S.C., "Vacancy Formation and Effects in FeAl", *Intermetallics*, **11**(6), 507–528 (2003) (Experimental, Crys. Structure, Mechan. Prop., 73)

[2004Cad] Cadel, E., Fraczkiewicz, A., Blavette, D., "Suzuki Effect on {001} Stacking Faults in Boron-doped FeAl Intermetallics", *Scr. Mater.*, **51**(5), 437–441 (2004) (Crys. Structure, Experimental, Morphology, 13)

[2004Gry] Grytsiv, A., Rogl, P., "Aluminium-Boron-Carbon", MSIT Ternary Evaluation Program, in *MSIT Workplace*, Effenberg, G. (Ed.), MSI, Materials Science International Services GmbH, Stuttgart; Document ID: 10.12170.3.20, also published in "*Landolt-Boernstein, Numerical Data and Functional Relationships in Science and Technology (New Series). Group IV: Physical Chemistry*", Martiensen, W. (Ed.), "*Ternary Alloy Systems. Phase Diagrams, Crystallographic and Thermodynamic Data*", Vol. 11A1, Effenberg, G., Ilyenko, S. (Eds.),

DOI: 10.1007/978-3-540-69761-9_3

Springer-Verlag, Berlin, Heidelberg, 29–51 (2004) (Phase Diagram, Phase Relations, Crys. Structure, Assessment, 118)

[2005Are] Arenas, O.L., Porcayo-Calderon, J., Salinas-Bravo, V.M., Martinez-Villafane, A., Gonzalez-Rodriguez, J.G., "Effect of Boron on the Hot Corrosion Resistance of Sprayed $Fe_{40}Al$ Intermetallics", *High Temp. Mater. Proc.*, **24**(2), 93–100 (2005) (Experimental, Electrochem. Prop., Morphology, 23)

[2005Ric] Rico, M.M., Greneche, J.M., Alcazar, G.A.P., "Effect of Boron on Structural and Magnetic Properties of the $Fe_{60}Al_{40}$ System Prepared by Mechanical Alloying", *J. Alloys Compd.*, **398** (1–2), 26–32 (2005) (Crys. Structure, Experimental, Magn. Prop., Optical Prop., 19)

[2006Kel] Kellou, A., Grosdidier, T., Aourag, H., "Comparative Behavior of Vacancy and C, B, N, O Atoms Single Defect on Hardening the *B*2-FeAl Structure: An Atomistic Study", *Intermetallics*, **14**(2), 142–148 (2006) (Calculation, Crys. Structure, Electronic Structure, 43)

[2006MSIT] "Al-Fe (Aluminum-Iron)", Diagrams as Published, in MSIT Workplace, Effenberg, G. (Ed.), Materials Science International Services, GmbH, Stuttgart; Document ID: 30.10236.1.20, (2006) (Crys. Structure, Phase Diagram, Phase Relations, 11)

[Mas2] Massalski, T.B. (Ed.), *Binary Alloy Phase Diagrams*, 2nd edition, ASM International, Metals Park, Ohio (1990)

[V-C2] Villars, P. and Calvert, L.D., *Pearson's Handbook of Crystallographic Data for Intermetallic Phases*, 2nd edition, ASM, Metals Park, Ohio (1991)

DOI: 10.1007/978-3-540-69761-9_3

Aluminium – Carbon – Iron

Gautam Ghosh

Introduction

A summary of experimental studies of phase equilibria is given in Table 1. Initial studies of phase equilibria of Fe corner were carried out by [1930Kei, 1931Soe, 1934Mor, 1936Vog] and [1938Loe]. These results were reviewed by [1953Cas]. Subsequently, the system was reinvestigated later by [1968Nis, 1969Loe, 1980Gor1] and [1980Gor2]. for studying the Fe rich side [1968Nis] prepared 24 ternary alloys using electrolytic Fe, graphite (99.8% C) and Al (99.99%) in an argon atmosphere. As C does not dissolve in liquid Al-Fe alloys [1936Vog, 1938Loe] and [1968Nis], the ternary alloys were always prepared by adding Al to liquid C-Fe alloys. They were isothermally annealed between 1000 and 1250°C over a period of 1.5 to 6 h in an argon atmosphere. Then the samples were quenched in iced brine and examined by means of X-ray diffraction, metallography and hardness measurements. Using thermodynamic data from [1987Yok] liquidus curves were calculated which agree fairly well with the values measured at 1600°C [1955Chi, 1963Mor]. [1986Sch] investigated the iron rich part of the liquidus surface by isothermal saturation of melts and by thermal analysis. [1987Sch] calculated the surfaces of primary crystallization of (αFe), (γFe) and graphite.
[1989Ode] investigated the ternary system in the temperature range of 1500 to 2300°C. He reported isothermal sections of the entire system and also the solubility of C in two Al-Fe liquid alloys. Using 99.99 mass% Fe, [1989Ode] prepared several binary Al-Fe alloys, which were equilibrated in graphite crucibles, heated in a graphite resistance furnace above atmospheric pressure of high purity Ar. Isothermal sections were constructed from the chemical analyses and metallographic observations.
These results were assessed by [1987Rag], [1990Gho] and [1993Rag].
Recently, [1995Pal] reinvestigated the phase equilibria of the Fe corner and reported the liquidus surface, three isothermal sections and three temperature-composition sections. [1995Pal] used 99.99% Al, 99.97% Fe and graphite. They prepared 50 ternary alloys by arc melting. The alloys were equilibrated at 1200 (24 or 2 h), 1000 (50 h) and 800°C (240 h) and water quenched. The microstructure and phases were characterized by EPMA, SEM and XRD.
The effect of pressure on the phase equilibria has been studied by [1978Kam, 1992Put]. [1996Koc] presented a review of the effect of pressure on the Al-C-Fe phase equilibria. [1978Kam] determined the liquid/solid equilibria of Fe rich alloys up to 10 GPa. [1992Put] quenched ternary alloys from 1527 to 25°C at a pressure of 6 GPa. They determined the solid-state phase equilibria using metallography, microprobe and XRD techniques.
These results were further assessed by [2002Rag] and [2005Gho].

Binary Systems

The Al-C binary is accepted from [2004Per]. Both liquid and solid solubilities of C in (Al) are very limited and the only reported compound in this system is Al_4C_3. The Al-Fe binary is accepted from [2006MSIT1]. The C-Fe binary is adopted from [2006MSIT2]. Since Al is a graphite stabilizer the stable form (graphite) of the C-Fe diagram is accepted here.

Solid Phases

The crystallographic data of solid phases are listed in Table 2. So far only one ternary phase Fe_3AlC_x(6) has been reported [1934Mor, 1938Loe, 1958Hue, 1961Hen, 1962Mas, 1964Bae, 1964Pal, 1968Nis, 1971Kuc, 1973Nud, 1975Ver, 1976Pog]. Structurally, Fe and Al form an $AuCu_3$ type superlattice in which C atoms occupy interstitial positions. The x in the formula Fe_3AlC_x can vary from 0.5 to 1.0. [1985Cho] reported the variation of lattice parameter as a function of x: a (in pm) = 366.26 ± 0.33 + 0.59x. However, to account

DOI: 10.1007/978-3-540-69761-9_4

for the atom distributions and deviation from stoichiometry the formula $Fe_{4-y}Al_yC_x$ has been suggested [1985And] for the κ phase. [1985And] did not report the ranges for x and y. Adopting this formula, [1995Pal] reported the composition dependence of lattice parameter of κ as: a = 362.5+0.14 (at.% Al) +0.72 (at.% C), in pm. This empirical relationship is valid in the composition range between $Fe_{3.2}Al_{0.8}C_{0.71}$ and $Fe_{2.8}Al_{1.2}C_{0.42}$. The data of [1983Lys] also confirm the increase in lattice with C content in κ phase.

Invariant Equilibria

Figure 1 shows the partial reaction scheme based on the experimental results of [1995Pal]. The temperatures of invariant reactions U_1, U_2 and U_3 reported by [1995Pal] differ by less than 20°C compared with earlier results [1938Loe, 1969Loe, 1985Gor, 1986Sch]. Within the composition range studied by [1969Loe], the solidification was not complete, and the solidification path starting from the U_2 reaction is not known. The temperature of the U_4 reaction is 825°C [1995Pal] which is much higher than 780°C reported by [1980Gor2]. The temperature of the three-phase peritectic reaction p_2 is 1410°C [1995Pal], and the temperature of the three-phase eutectic reaction e_1 is 1335°C [1995Pal], the latter is much lower than 1410°C suggested by [1986Sch]. The compositions of the phases [1995Pal] participating in the invariant reactions are listed in Table 3.
The predicted invariant temperatures [1991Kum], based on calphad modeling, for U_1, U_2, U_3 and U_4 reactions agree within 5°C of the experimental values reported by [1995Pal]. On the other hand, those predicted by [2004Oht], also based on calphad modeling, differ by as much as 27°C. While the experimental data is available only for the Fe corner, calphad modeling [1991Kum] predicts that the reaction scheme of the entire system consists of nine U type and two E type invariant reactions.

Liquidus Surface

Figure 2 shows the liquidus surface and the extent of the fields of primary crystallization of the phases α, γ, κ and graphite [1995Pal]. They observed significant differences in compositions of phases participating in the invariant equilibria, particularly α, γ, and κ, compared with earlier results [1938Loe, 1969Loe, 1980Gor1]. The liquidus surfaces of both [1936Vog, 1980Gor1] were rejected. [1936Vog] assumed that the double carbide reported by [1934Mor] was a ternary solid solution of the high temperature ε phase of the Al-Fe system. [1980Gor1] presented the liquidus surface as Al-C-Fe containing both graphite and cementite. However, here we accept the stable form of the C-Fe diagram. With the addition of Al to the binary C-Fe alloys, the temperature of the graphite eutectic reaction increases [1930Kei, 1931Soe, 1938Loe, 1977Car, 1988Mag] and the eutectic carbon content decreases up to the addition of about 10 mass% Al.
The liquidus surface has also been calculated by calphad method [1991Kum, 2004Oht], both essentially agree with the experimental data.

Isothermal Sections

Figures 3, 4, 5 show isothermal sections of the Al-C-Fe system at 2000°C, 1850°C and 1700°C respectively after [1989Ode]. Isothermal sections of the Fe rich corner have been investigated several times [1934Mor, 1936Vog, 1938Loe, 1959Vyk, 1968Nis] and [1995Pal]. Three isotherms at 1200, 1000, and 800°C reported by [1995Pal] are shown in Figs. 6, 7 and 8, respectively. [1968Nis] reported isothermal sections at 1250, 1200, 1100 and 1000°C. The results of [1968Nis] and [1995Pal] essentially agree very well in terms of the topology of the phase fields. However, the main differences between these two sets of results are that [1995Pal] reported higher Al solubility in γ, higher C solubility in α, and larger homogeneity range of the κ phase. The isothermal section determined by [1934Mor] is essentially the same as [1968Nis] except for the extents of the (α+κ), (α+κ+graphite) and (α+γ+κ) regions. As aluminum is a graphitizing element, the fraction of graphite formation increases with the addition of aluminum, giving a maximum at about 4 mass% Al and then decreases to about zero at 10 mass% Al. The double carbide Fe_3AlC_x appears in the composition range of about 10-17 mass% Al. Beyond 17 mass% Al, graphite again dominates the phase equilibria. As shown in Figs. 6, 7 and 8 with increasing temperature the homogeneity range of κ increases. In addition to experimental isothermal sections, several calculated isothermal sections have also been reported. Using previously reported thermodynamic data, [1987Yok] calculated isothermal sections at 2027

DOI: 10.1007/978-3-540-69761-9_4

and 1600°C. [1991Kum] calculated the eight isothermal sections at 2000, 1850, 1700, 1300, 1200, 1100 and 800°C, while [2004Oht] calculated three isothermal sections at 800, 1000 and 1200°C using calphad method. The latter three isothermal sections show a good agreement with the experimental data of [1995Pal].

Temperature – Composition Sections

[1936Vog] determined several isopleths at 2, 7, 10, 13 and 20 mass% Al and at 0.5, 1.0, 1.4, 2.0 and 2.7 mass% C. [1938Loe] reported the vertical sections at 0.5, 7, 10 and 15 mass% Al and 0.4, 0.7, 1.1 and 2.2 mass% C. [1967Ken] determined a vertical section at 0.3 mass% C.
[1995Pal] reported three vertical sections at 5, 10.5 and 23 at.% C. These are shown in Figs. 9, 10 and 11, respectively.
Using single crystals, [1995Pal] investigated the effect of C on the order-disorder transition temperature involving (αFe) and *B*2 phases. Their results are shown in Fig. 12. It is obvious that at a constant Al content, C increases the order-disorder temperature. This was attributed to the fact that in *B*2 structure six Fe atoms create favorable sites for the C atoms. In addition, ab initio calculations show that C atoms prefer to occupy the Fe sublattice in *B*2-FeAl leading to an increase in cohesion [2006Kel].

Thermodynamics

Thermodynamic data of ternary Al-C-Fe alloys have been reported several times [1955Chi, 1963Mor, 1973Rim, 1974Sig, 1977Cho, 1983Jan, 1983Vre, 1987Yok] and [1991Kum]. Among these, the thermodynamic modeling of [1991Kum] is the most comprehensive. Aluminum increases the activity of C in liquid iron. [1978Zhu, 1979Zhu] provided the thermodynamic explanations of the composition dependence of the graphitizing power of Al in ternary alloys.
Calphad modeling has been performed by [1991Kum] and [2004Oht]. [1991Kum] treated the κ phase as a stoichiometric phase ($Fe_3AlC_{0.565}$), while [2004Oht] allowed a homogeneity range. The ab initio calculated formation energies of Fe_3AlC (κ) are –25.7 (non-magnetic) –27.9 (ferromagnetic) kJ·mol^{-1} of atoms [2004Oht].

Notes on Materials Properties and Applications

A summary of experimental investigation of properties is given in Table 4.
The atomic and magnetic structures of the 6 phase have been discussed by several authors [1985And, 1994Mor, 1994Oda, 1995Fuj, 1998Iva]. The latter authors found that the stoichiometric Fe_3AlC is paramagnetic while non-stoichiometric $Fe_3AlC_{0.64}$ is ferromagnetic with T_c = 210°C. The magnetic moment of Fe is determined primarily by the nearest neighbor C atoms. Quantum-mechanical calculations show that the transition from para to ferromagnetic state, with increasing Al content, is caused by the charge transfer and *p-d* hybridization [1994Mor]. The coercivity and remenance of κ phase was reported by [1985Bri].
The mechanical properties of Fe rich alloys containing κ and/or graphite phase have been investigated in detail [2001Rad, 2004Bal1, 2004Bal2, 2004Min, 2004Mor, 2004Sch, 2005Min, 2005Sch1, 2005Sch2]. [2005Pal, 2005Sch1] reported that in (αFe + κ) alloys, in general the yield strength increases with increasing C content, but at higher temperatures the strengthening efficiency is rather poor. [2004Mor] showed that fine scale stable carbides are beneficial for creep resistance only up to 500-600°C. The strength, ductility and creep resistance of Fe_3AlC_x based alloys have also been investigated [1989Jun, 1997San]. The strength and ductility were sensitive to microstructure. [1989Jun] found that the creep exponent is 4.4 ± 1.1, and activation energy is 355 kJ·mol^{-1} for single phase κ, 365 kJ·mol^{-1} for κ+graphite microstructure, 244 kJ·mol^{-1} for κ +(αFe) microstructure, and 365 kJ·mol^{-1} for κ+(αFe)+graphite microstructure. On the other hand, [1997San] reported that in Fe_3AlC_x ($0.3 \leq x \leq 0.8$) alloys the stress exponent for creep is 3 and activation energy lies between 250 to 320 kJ·mol^{-1}.
The hardening, softening, tensile and compressive properties of *B*2 alloys [2001Mun, 2001Oca, 2001Rad, 2002Bal. The hardening and softening of the *B*2 phase have been attributed to the precipitation of $Fe_3AlC_{0.5}$ and graphite, respectively.
The oxidation kinetics [2003Rao, 2004Rao] and corrosion behavior [2005Rao] of Fe rich alloys containing κ phase have been studied in detail. While carbide containing two-phase iron aluminides have beneficial effects with regard to high-temperature strength and resistance to hydrogen embrittlement, the effect of

DOI: 10.1007/978-3-540-69761-9_4

carbides on the oxidation resistance is rather complicated due to an inversion temperature below which the oxidation resistance of Al-C-Fe alloys is poorer than binary Al-Fe alloys [2004Rao].
[1991Jia] investigated the shape memory behavior in an Fe-7Al-2C (at.%) alloy. They found that the shape memory effect is restricted by the alloy brittleness and precipitation of carbide. The precipitation of κ phase during aging of martensite has also been reported by [1982Suy] and [1983Lys].

Miscellaneous

[1989Ode] reported the solubility of C in liquid Fe-12.5Al (at.%) and Fe-25.0Al (at.%) alloys over an extended temperature range. The C solubility can be expressed as:
In Fe-12.5 at.% Al:

$$C = -0.55067 + 0.01112 \cdot T \text{ (in °C)}$$

In Fe-25.0 at.% Al:

$$C = -8.46728 + 0.01373 \cdot T \text{ (in °C)}$$

The solid solubility of C in Al-Fe ferrite has been measured by [1966Jae1]. Whose results, in the temperature range of 548 to 723°C and up to 2.1 mass% Al, can be described by the empirical equation:

$$\log (\text{mass\% C}) = -2200/T + 0.0675 (\text{mass\% Al}) + 0.52,$$

where T is in K.
The effect of high pressure on the diamond crystallization from liquid alloys has been studied several times [1978Kam, 1992Put, 2002Tur]. Under high pressure the primary crystallization products of liquid Fe rich ternary alloys may be austenite, graphite, cementite and diamond.
Figure 13 shows the 25°C isothermal section at pressure of 6 GPa. An important feature to be noted that in addition to the binary phases at ambient pressure, it is noted that high pressure phases $FeAl_6$, Fe_7C_3 and diamond.
[1991Sar] investigated the microstructure of Fe-(8 to 10) mass% Al-(1.8 to 2.4) mass% C alloys by melt spinning and levitation melting. They found the melt spun alloys yielded γ+γ′($L1_2$) microstructure while levitation melting always yielded α+γ+Fe_3C microstructure.
Iron rich alloys containing Al and C undergo martensitic transformation [1986And]. One particular feature of Al-C-Fe martensite that has receive numerous attention is the abnormally high tetragonality [1972Lys, 1980Dra, 1980Lys, 1981Koz, 1981Lys, 1986Lys, 1986Pro1, 1986Pro2, 1992Ueh]. The abnormal tetragonality has been attributed to the presence of short-range order, nanoscale fcc ordered ($L1_2$) domains and the elastic strain fields around them.

Table 1. Investigations of the Al-C-Fe Phase Relations, Structures and Thermodynamics

Reference	Method/Experimental Technique	Temperature/Composition/Phase Range Studied
[1930Kei]	Metallography, thermal analysis	Fe rich alloys; 700–1600°C
[1931Soe]	Metallography, thermal analysis, dilatometry	Fe rich alloys
[1934Mor]	Metallography, XRD	Fe rich alloys; 1000°C
[1936Vog]	Metallography, thermal analysis	Fe rich alloys; 750–1500°C and several vertical sections
[1938Loe]	Metallography, thermal analysis	Fe rich alloys; 700–1525°C
[1955Chi]	Chemical analysis	Fe rich alloys; activity of Al at 1600°C

(*continued*)

DOI: 10.1007/978-3-540-69761-9_4

Reference	Method/Experimental Technique	Temperature/Composition/Phase Range Studied
[1958Hue]	Metallography, XRD	Fe rich alloys
[1968Nis]	Metallography, thermal analysis	Fe rich alloys; 1000–1200°C
[1969Loe]	Metallography, thermal analysis	Fe rich alloys; liquidus surface
[1977Cho]	Mass spectrometry	Al-Fe alloys saturated with C; 1600°C; activity of C
[1989Ode]	Metallography, chemical analysis	Fe rich alloys; 1550-2300°C isothermal sections
[1992Put]	Metallography, SEM, EPMA,XRD	Fe rich alloys; 1527°C and 6 GPa
[1995Pal]	EPMA, metallography, SEM,XRD	Fe rich alloys; liquidus surface; 800-200°C isothermal sections; three vertical sections
[2002Tur]	Metallography	Fe rich alloys; 1447-1647°C and 6.5 GPa

Table 2. Crystallographic Data of Solid Phases

Phase/ Temperature Range [°C]	Pearson Symbol/ Space Group/ Prototype	Lattice Parameters [pm]	Comments/References
(Al) < 660.452	cF4 $Fm\bar{3}m$ Cu	a = 408.57	at 25°C [Mas2]
(C)gr < 3827 (subl.)	hP4 $P6_3/mmc$ C (graphite)	a = 246.4 c = 671.1	at 25°C [Mas2]
(C)d	$cF8$ $Fd\bar{3}m$ C (diamond)	a = 356.69	at 25°C, 60 GPa [Mas2]
(αδFe) (αFe)(r) ≤ 912	$cI2$ $Im\bar{3}m$ W	a = 286.65	pure Fe at 25°C [Mas2]
(δFe)(h_2) 1538 - 1394		a = 293.15	pure Fe at 1480°C [Mas2]
γ, (γFe)(h_1) 1394 - 912	$cF4$ $Fm\bar{3}m$ Cu	a = 364.67	pure Fe at 915°C [V-C2, Mas2]
Al_4C_3 < 2156	$hR21$ $R\bar{3}m$ Al_4C_3	a = 330.70 c = 2490.6	[2004Per]

(*continued*)

DOI: 10.1007/978-3-540-69761-9_4

Phase/ Temperature Range [°C]	Pearson Symbol/ Space Group/ Prototype	Lattice Parameters [pm]	Comments/References
α_1, Fe_3Al ≤ 547	*cF*16 $Fm\bar{3}m$ BiF_3	*a* = 578.86 to 579.3	solid solubility ranges from ~25 to ~37 at.% Al [2006MSIT1] [2006MSIT1]
α_2, FeAl ≤ 1310	*cP*2 $Im\bar{3}m$ CsCl	*a* = 289.76 to 290.78	[2006MSIT1], at room temperature solid solubility ranges from ~24 to ~55 at.% Al
ε, Fe_2Al_3 1232 - 1102	*cI*16?	*a* = 598.0	[2006MSIT1], solid solubility ranges from 58 to 65 at.% Al at 61 at.% Al [V-C2]
ζ, $FeAl_2$ ≤ 1154	*aP*18 *P*1 $FeAl_2$	*a* = 487.8 *b* = 646.1 *c* = 880.0 α = 91.75° β = 73.27° γ = 96.89°	at 66.9 at.% Al [V-C2] solid solubility ranges from ~66 to ~67 at.% Al [2006MSIT1]
η, Fe_2Al_5 ≤ 1169	*oC*24 *Cmcm*	*a* = 765.59 *b* = 641.54 *c* = 421.84	[2006MSIT1], at 71.5 at.% Al solid solubility ranges from ~70 to ~73 at.% Al
θ, Fe_4Al_{13} ≤ 1160	*mC*102 *C*2/*m* Fe_4Al_{13}	*a* = 1552.7 to 1548.7 *b* = 803.5 to 808.4 *c* = 1244.9 to 1248.8 β = 107.7 to 107.99°	[2006MSIT1], 74.16 to 76.7 at.% Al solid solubility ranges from 74.5 to 75.5 at.% Al Also denoted $FeAl_3$ or Fe_2Al_7
* κ, Fe_3AlC_x	*cP*5 $Pm\bar{3}m$ $CaTiO_3$	*a* = 366.6 to 366.8 *a* = 375.8	0.5 ≤ *x* ≤ 1.0 Solid solubility is up to 14 at.% C and 21 at.% Al [V-C2]

Table 3. Invariant Equilibria

Reaction	T [°C]	Type	Phase	Composition (at.%)		
				Al	C	Fe
L + (C) ⇌ κ	1410	p_2	L	~22.7*	~11.3	~66.0
L ⇌ α + κ	1335	e_1	L	~26.4*	~6.6	~67
L + α ⇌ γ + κ	1315	U_1	L	20.2	7.9	71.9
			α	27.0	0.7	72.3
			γ	24.5	4.0	71.5
			κ	24.0	8.5	67.7
L + κ ⇌ α + (C)	1295	U_2	L	34.2	5.4	60.4
			κ	27.3	8.7	64.0
			α	33.7	0.7	65.6
			(C)	0.0	100.0	0.0

(*continued*)

DOI: 10.1007/978-3-540-69761-9_4

Reaction	T [°C]	Type	Phase	Composition (at.%)		
				Al	C	Fe
L + κ ⇌ γ + (C)	1282	U_3	L	13.4	12.4	74.2
			κ	19.0	13.0	68.0
			γ	16.5	4.5	79.0
			(C)	0.0	100.0	0.0
γ + κ ⇌ α + (C)	825	U_4	γ	8.5	4.7	86.7
			κ	17.6	14.6	67.8
			α	9.3	0.7	90.0
			(C)	0.0	100.0	0.0

* Compositions of p_2 and e_1 reactions are estimated from Fig. 2

Table 4. Investigations of the Al-C-Fe Materials Properties

Reference	Method/Experimental Technique	Type of Property
[1966Jae1]	Internal friction	Damping behavior
[1966Jae2]	Internal friction, magnetometry	Damping behavior and coercivity
[1985Bri]	Magnetometry	Coercivity and remenance of κ phase
[1989Jun]	Mechanical tests	Hardness; compression and creep (900-1250°C)
[1991Jia]	Mechanical tests	Shape memory properties
[1997San]	Mechanical tests	Flow stress, creep, ductility and toughness of κ phase (RT-1200°C)
[2001Mun]	Mechanical tests	Hardness, yield stress, fracture stress and strain at fracture
[2001Rad]	Mechanical tests	Yield stress and elongation at RT
[2002Bal]	Mechanical tests	Hardness; yield stress, ultimate tensile stress and elongation (RT-600°C)
[2003Rao]	Oxidation tests	Oxidation kinetics
[2004Bal1, 2004Bal2]	Mechanical tests	Hardness; yield stress, ultimate tensile stress, elongation and creep (RT-600°C)
[2004Min]	Mechanical tests	Compressive strength (RT-700°C)
[2004Mor]	Mechanical tests	Creep
[2005Min]	Mechanical tests	Compressive strength (RT-700°C)
[2005Rao]	Electrochemical tests	Oxidation and corrosion kinetics
[2005Sch1]	Mechanical tests	Yield and ductility (up to 800°C)

DOI: 10.1007/978-3-540-69761-9_4

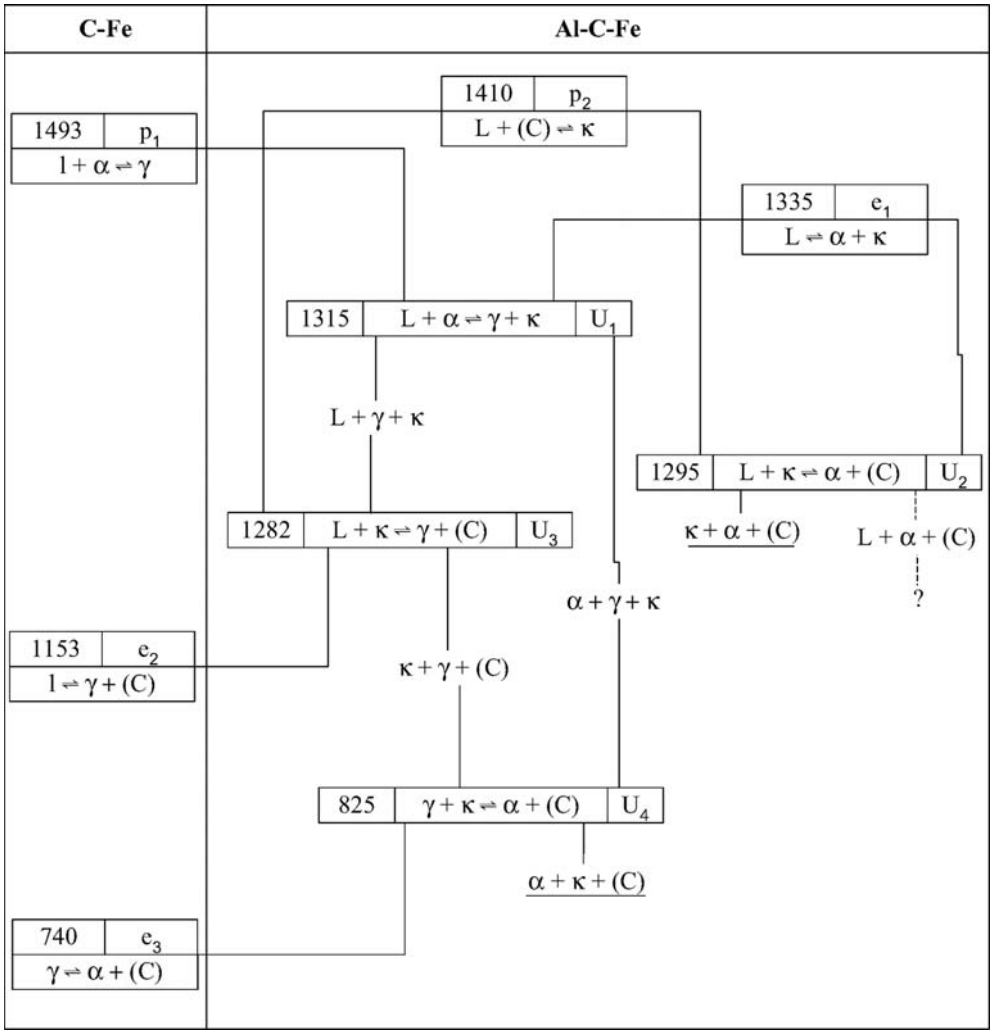

Fig. 1. Al-C-Fe. Reaction scheme

DOI: 10.1007/978-3-540-69761-9_4

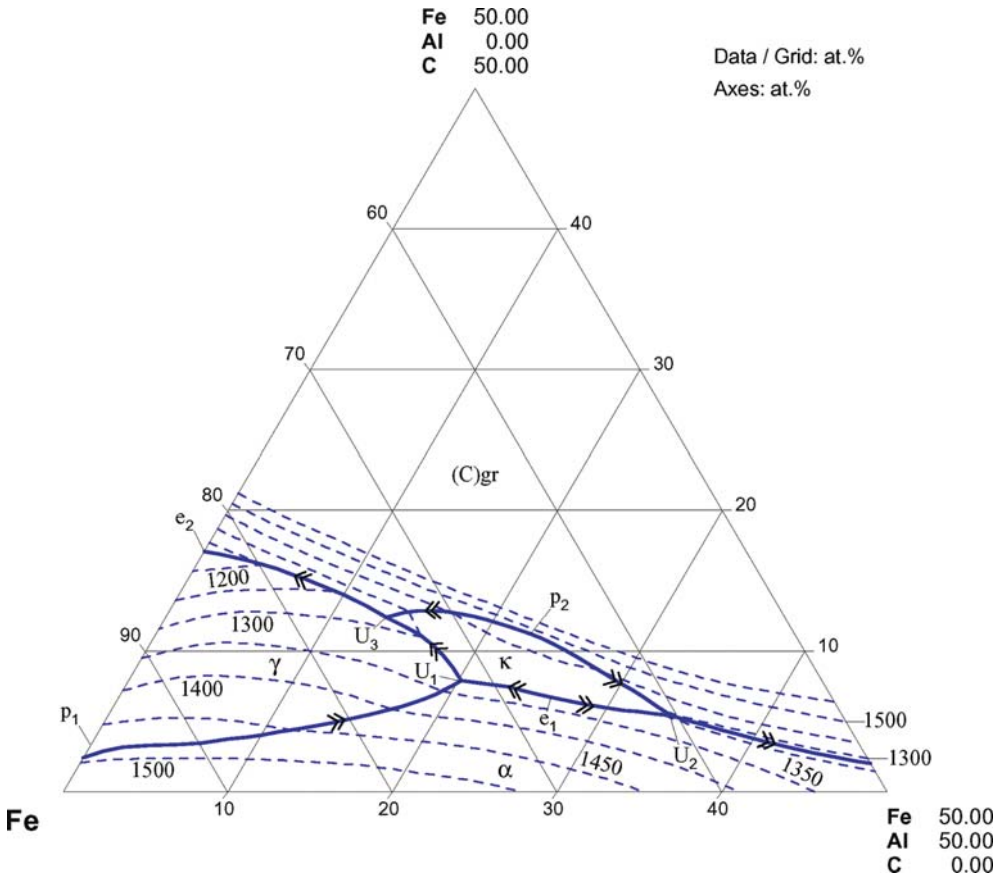

Fig. 2. Al-C-Fe. Liquidus surface projection

DOI: 10.1007/978-3-540-69761-9_4

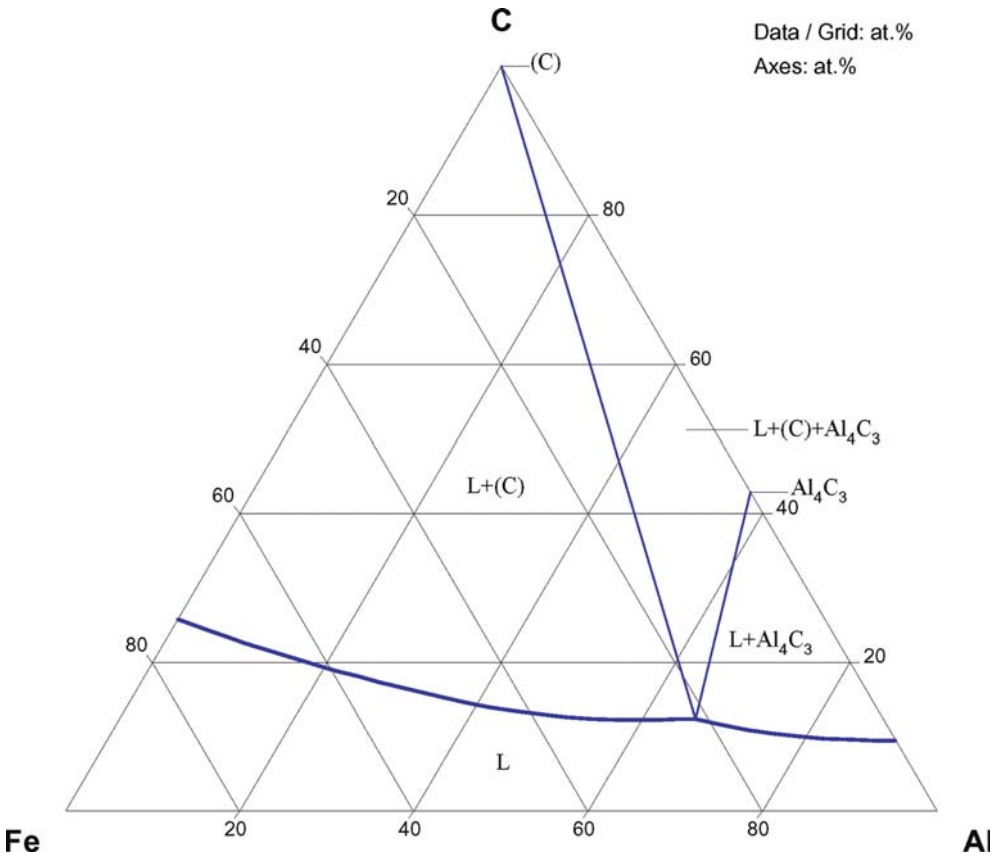

Fig. 3. Al-C-Fe. Isothermal section at 2000°C

DOI: 10.1007/978-3-540-69761-9_4

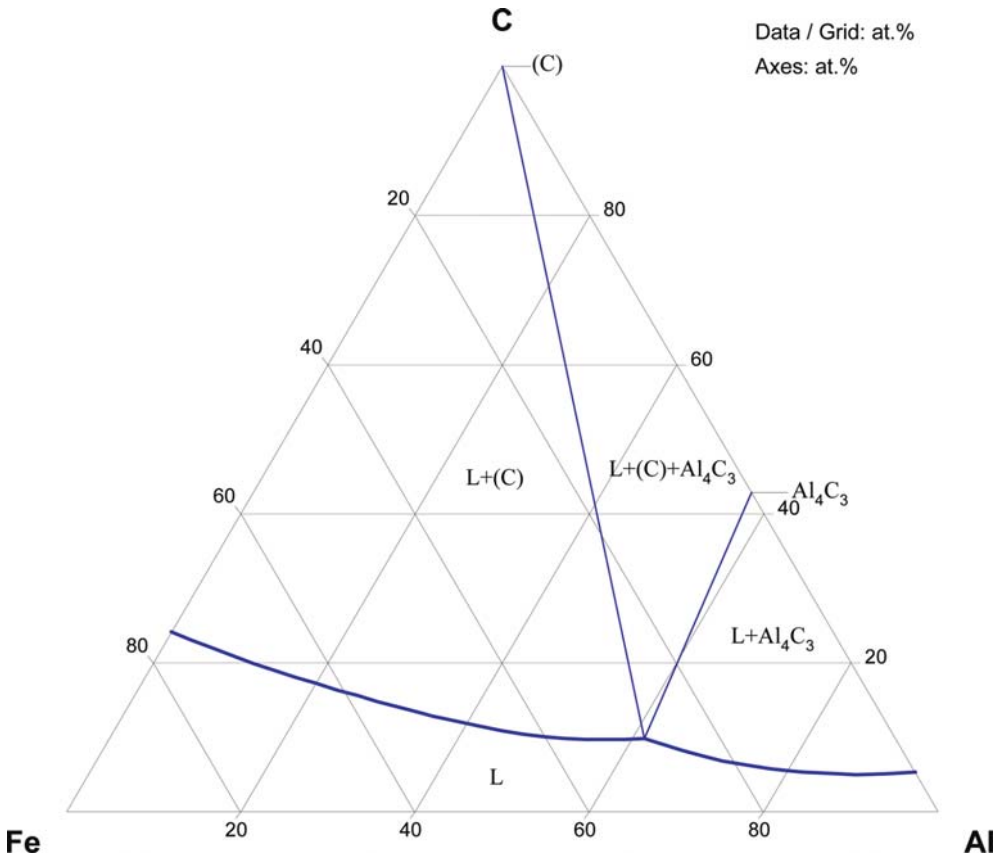

Fig. 4. Al-C-Fe. Isothermal section at 1850°C

DOI: 10.1007/978-3-540-69761-9_4

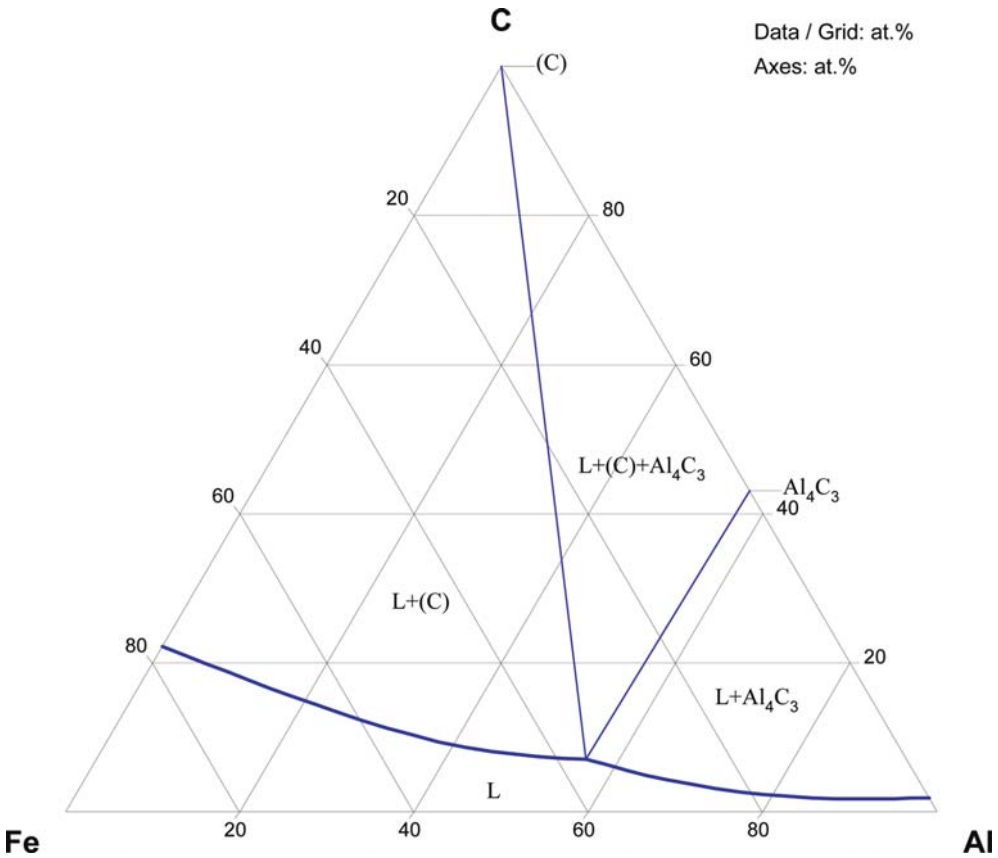

Fig. 5. Al-C-Fe. Isothermal section at 1700°C

DOI: 10.1007/978-3-540-69761-9_4

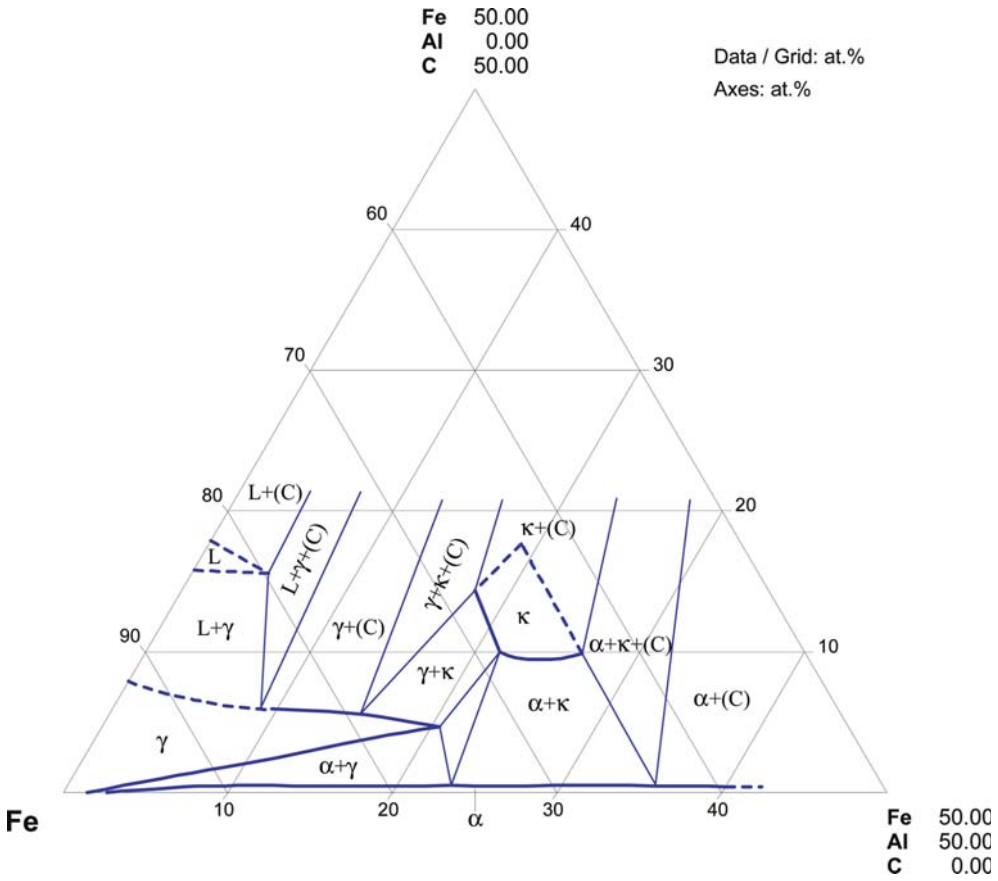

Fig. 6. Al-C-Fe. The isothermal section at 1200°C

DOI: 10.1007/978-3-540-69761-9_4

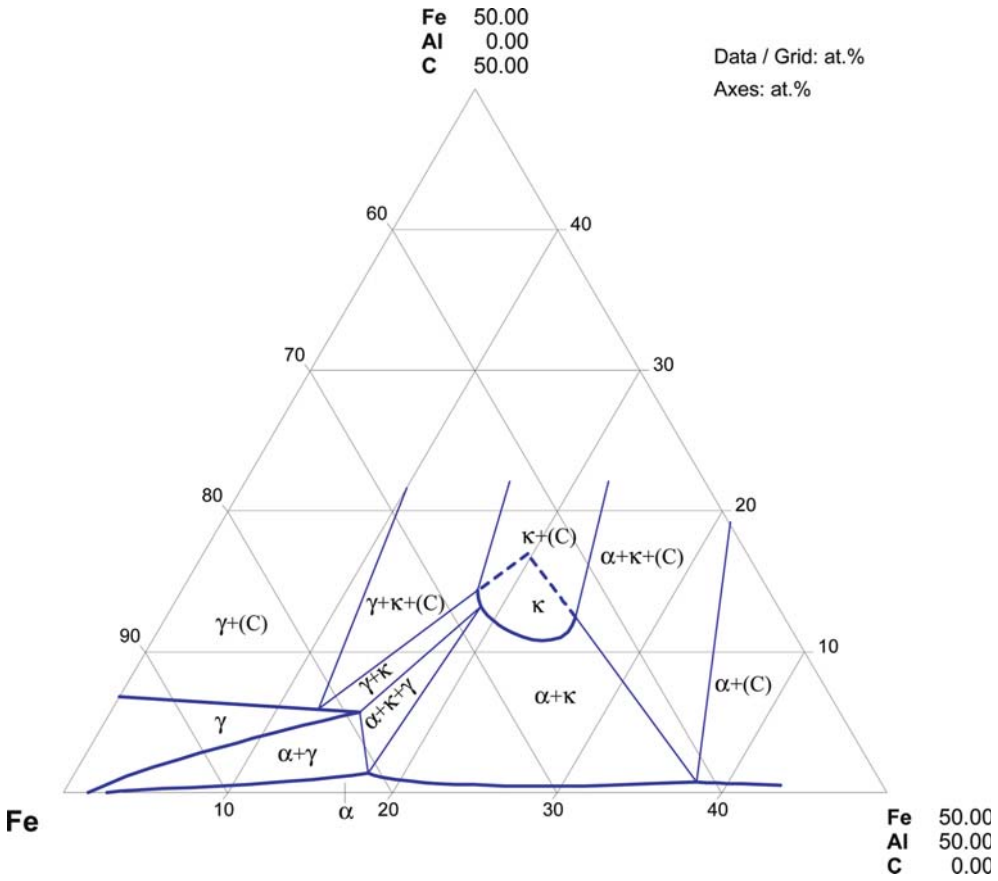

Fig. 7. Al-C-Fe. The isothermal section at 1000°C

DOI: 10.1007/978-3-540-69761-9_4

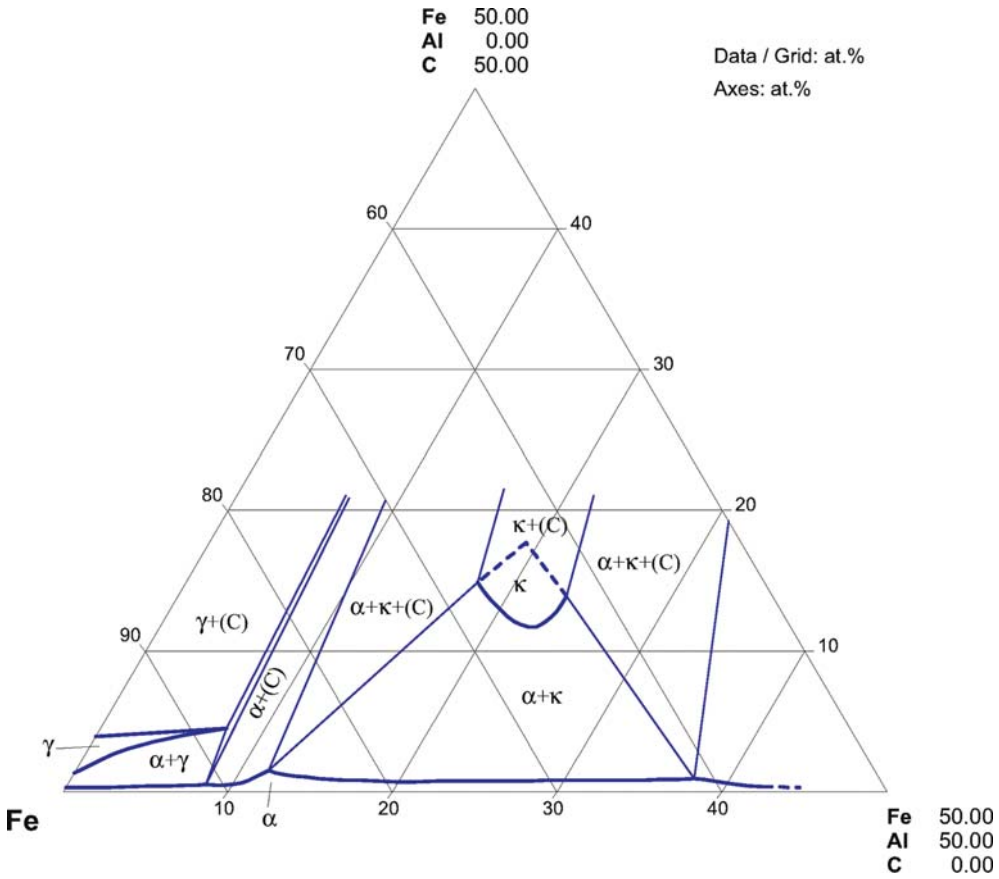

Fig. 8. Al-C-Fe. The isothermal section at 800°C

DOI: 10.1007/978-3-540-69761-9_4

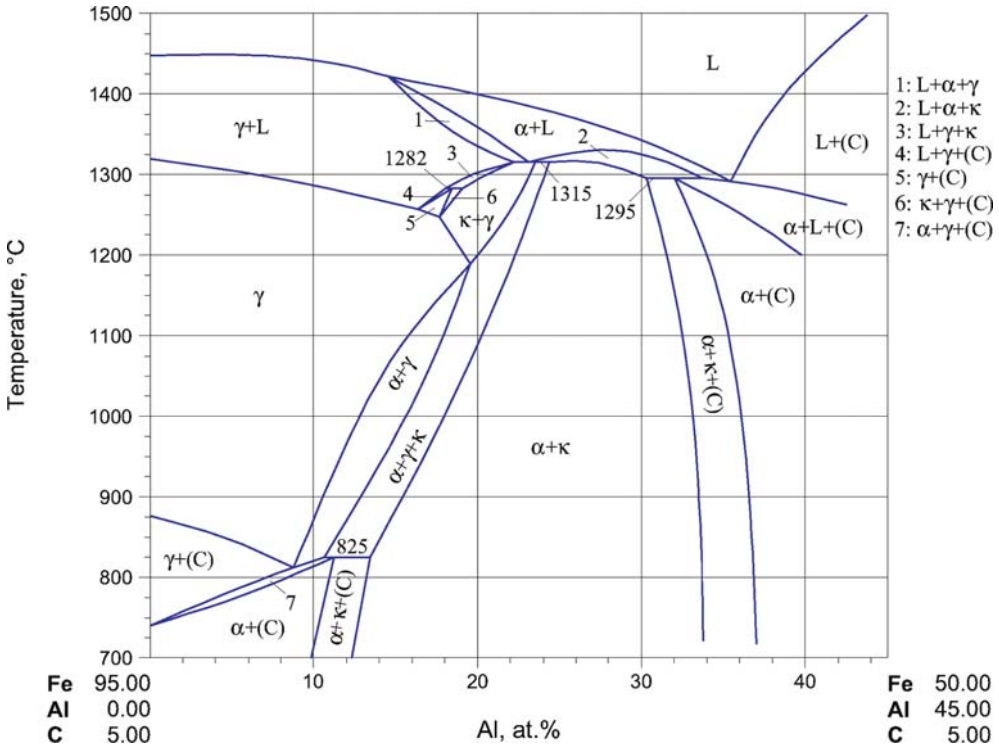

Fig. 9. Al-C-Fe. The vertical section at a constant C content of 5.0 at.%

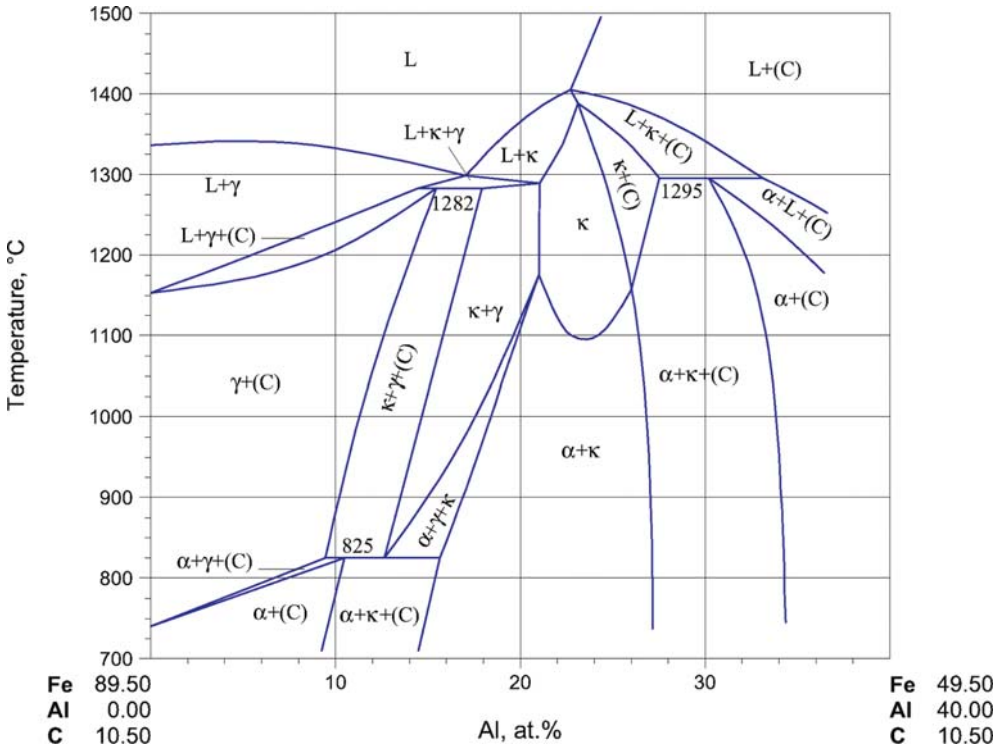

Fig. 10. Al-C-Fe. The vertical section at a constant C content of 10.5 at.%

DOI: 10.1007/978-3-540-69761-9_4

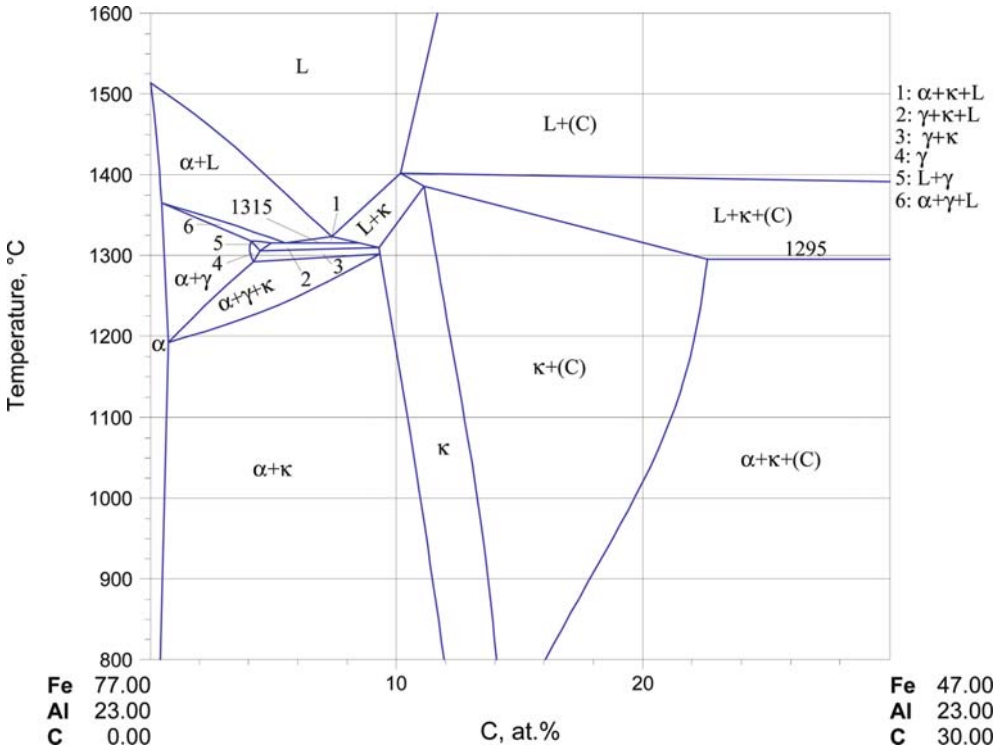

Fig. 11. Al-C-Fe. The vertical section at a constant Al content of 23.0 at.%

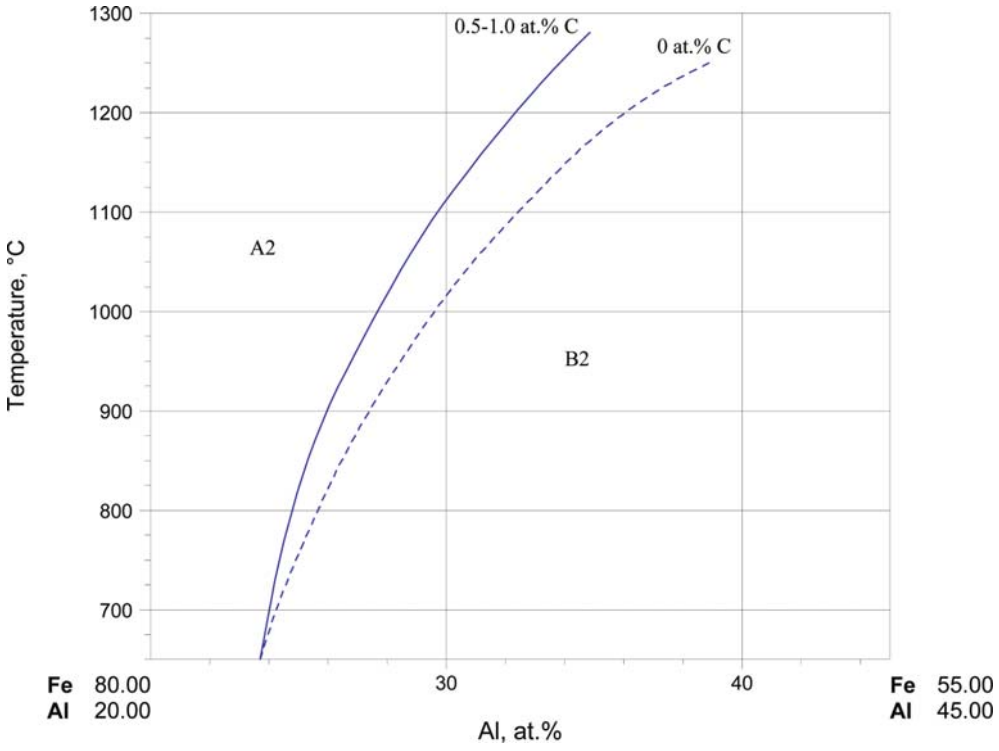

Fig. 12. Al-C-Fe. The effect of C on the order-disorder temperature of Al-Fe alloys

DOI: 10.1007/978-3-540-69761-9_4

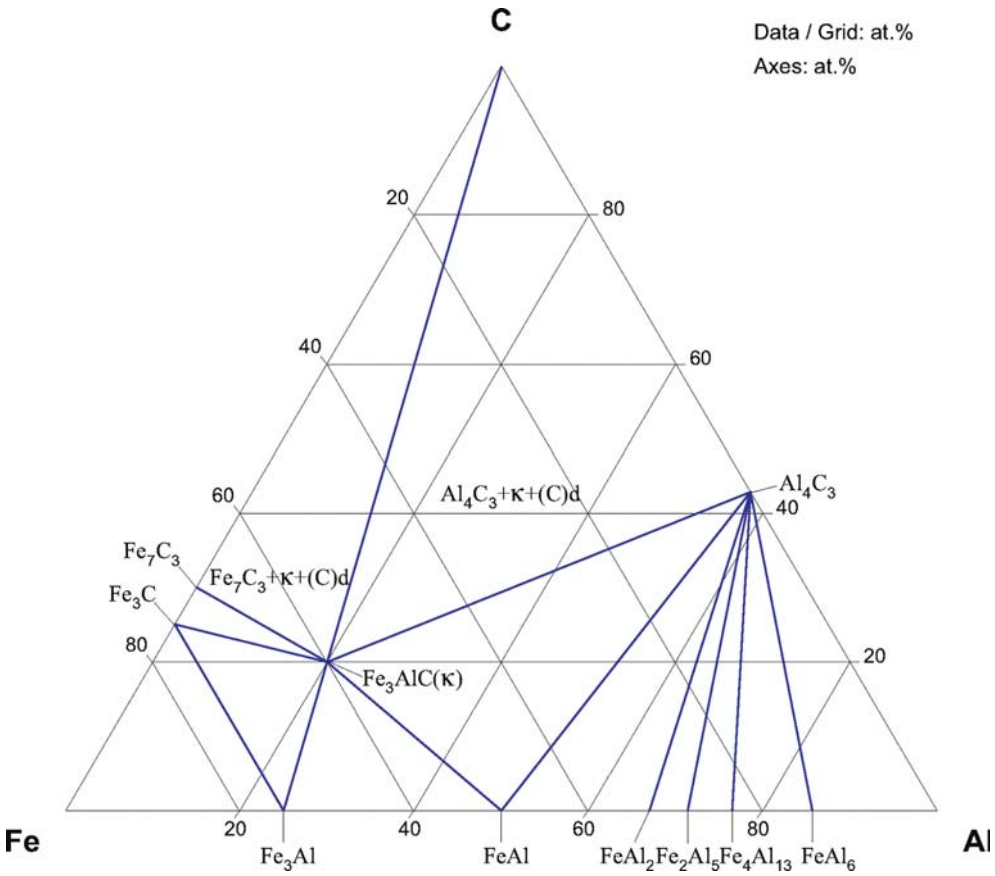

Fig. 13. Al-C-Fe. The isothermal section at a pressure of 6 GPa and at 25°C

DOI: 10.1007/978-3-540-69761-9_4

References

[1930Kei] Keil, O.V., Jungwirth, O., "Contribution to the Knowledge of Fe-Al-C Alloys" (in German), *Arch. Eissenhuettenwes*., **4**, 221–224 (1930) (Phase Relations, Phase Diagram, Experimental, 8)

[1931Soe] Soehnenchen, E., Piwowarsky, E., "The Influence of the Alloy Elements Ni, Si, Al and P on the Solubility of C in Liquid and Solid Fe" (in German), *Arch. Eissenhuettenwes*., **5**, 111–120 (1931) (Experimental, 49)

[1934Mor] Morral, F.R., "The Constitution of Iron-Rich Iron-Aluminium-Carbon Alloys", *J. Iron Steel Inst*., London, **130**, 419–428 (1934) (Phase Diagram, Experimental, #, *, 45)

[1936Vog] Vogel, R., Mäder, H., "The Fe-Al-C System" (in German), *Arch. Eissenhuettenwes*., **9**, 333–340 (1936) (Experimental, Phase Relations, Phase Diagram, 6)

[1938Loe] Loehberg, K., Schmidt, W., "The Fe Corner of the Fe-Al-C System" (in German), *Arch. Eissenhuettenwes*., **11**, 607–614 (1938) (Phase Diagram, Experimental, #, *, 16)

[1953Cas] Case, S.L., Van Horn, K.R., "The Consitution of Binary and Complex Iron-Aluminum Alloys" in "*Aluminum in Iron and Steel*", JohnWiley & Sons, Inc., New York, Chapman & Hall, Ltd., London., 607–614 (1953) (Phase Relations, Phase Diagram, Review, 2)

[1955Chi] Chipman, J., Floridis, T.P., "Activity of Al in Liquid Ag-Al, Fe-Al, Fe-Al-C and Fe-Al-C-Si Alloys", *Acta Metall*., **3**, 267–269 (1955) (Experimental, Thermodyn., 8)

[1958Hue] Huetter, L.J., Stadelmaier, H.H., "Ternary Carbides of Transition Metals with Aluminium and Magnesium", *Acta Metall*., **6**, 367–370 (1958) (Crys. Structure, Review, 6)

[1959Vyk] Vyklicky, M., Tuma, H., "Crystallization of Commercial Fe-Al-C Alloys in the Region of α Solid Solution" (in Czech), *Hutn. Listy*, **14**, 118–127 (1959) (Phase Relations, Phase Diagram, Experimental, #, 20)

[1961Hen] Henry, J.M., Baker, J.M., Bellot, J., Bogot, R., Herzog, E., "The Formation of Aluminium Carbides in Alloy Steels and Their Effects on the Mechanical Properties", *Mem. Sci. Rev. Met*., **58**, 117–128 (1961) (Experimental, Mechan. Prop., 12)

[1962Mas] Maslenkov, S.B., Molotilov, V., "Micro X-Ray Diffraction Analysis of Fe-Al-C Alloys", *Fiz. Metall. Metalloved*., **14**, 633–635 (1962) (Experimental, Mechan. Prop., 12)

[1963Mor] Mori, T., Fujimura, K., Kanoshima, H., "Effects of Aluminium, Sulphur and Vanadium on the Solubility of Graphite in Liquid Iron", *Mem. Fac. Eng. Kyoto Imp. Univ*., **25**, 83–105 (1963) (Experimental, 22)

[1964Bae] Bäcker, L., "Contribution on the Study of the Distribution of Alloy Constituents Between Cementite and Ferrite in Steels", *Mem. Sci. Rev. Metall.*, **61**, 865–892 (1964) (Morphology, Experimental, 35)

[1964Pal] Palatnik, L.S., Tananko, I.A., Bobro, Yu.G., "On the Nature of the γ Phase in the Fe-Al-C Alloys", *Sov. Phys.-Crystallogr., (Engl. Transl.)*, **9**, 163–165 (1964), translated from *Krystallografiya*, **9**, 209–212 (1964) (Crys. Structure, Experimental, 9)

[1966Jae1] Jaeniche, W., Brauner, J., Heller, W., "Effect of Aluminium on the Damping Curve and Solubility of Carbon in α Iron", *Arch. Eissenhuettenwes*., **37**, 719–728 (1966) (Phase Relations)

[1966Jae2] Jaeniche, W., Heller, W., Brauner, J., "Effect of Aluminium on the Precipitation of C in α Iron", *Arch. Eissenhuettenwes*., **37**, 821–828 (1966) (Experimental, 33)

[1967Ken] Kenford, A.S., Rance, V.E., Turner, S., "Constitution, T-T-T Characteristics and Hardenability of a 0.3% Steel with Al Additions up to 2.45%", *J. Iron Steel Inst*., London, **205**, 665–667 (1967) (Experimental, #, 11)

[1968Nis] Nishida, K., "A Study of Fe-Al-C Alloys" (in Japanese), *Hokkaido Daigaku Kogakubu Kenkyu Hokoku*, (48), 71–108 (1968) (Phase Relations, Phase Diagram, Experimental, #, 8)

[1969Loe] Loehberg, K., Ueberschaer, A., "On the Additional Transition Reaction in the Fe Corner of the Fe-C-Al System" (in German), *Giessereiforschung*, **21**, 171–173 (1969) (Phase Relations, Phase Diagram, Experimental, #, *, 6)

DOI: 10.1007/978-3-540-69761-9_4

[1971Kuc] Kuchly, J.P., Rimlinger, L., "Iron-Aluminium Mixed Carbide Formed in Fe-Al Alloys Containing ≤6.43% C" (in French), *Compt. Rend. Acad. Sci. Paris, Ser. C*, **272C**, 898–901 (1971) (Crys. Structure, Experimental, 10)

[1972Lys] Lysak, L.I., Drachinskaya, A.G., Storchak, N.A., "Influence of Austenite Ordering on the Martensitic Transformation in Iron-Aluminium-Carbon Alloys", *Fiz. Met. Metalloved.*, **34**(2), 107–114 (1972) (Crys. Structure, Experimental, 20)

[1973Nud] Nude, L.A., Talismanova, A.A., "Phase Analysis of Iron-Aluminium Alloys", *Zavod. Lab.*, **39**, 150 (1973) (Experimental)

[1973Rim] Rimkus, H.J., "Contribution to theThermodynamics of C in Fe-C as well as in Fe-Rich Three- and Multicomponent Systems" (in German), *Thesis*, Tech. Univ. Clausthal, (1973) (Experimental, 40)

[1974Sig] Sigworth, G.K., Elliot, J.F., "Thermodynamics of Liquid Dilute Iron Alloys", *Met. Sci.*, **8**, 298–310 (1974) (Thermodyn., 249)

[1975Ver] Vereshchak, M.F., Zhetbaev, A.K., Kaipov, D.K.,"Study of the Phase Changes in Binary Iron-Aluminium andTernary Iron-Aluminium-Carbon Alloys by Use of the Mössbauer Effect" (in Russian), *Proc. 5th Int. Conf. Mössbauer Spectroscopy*, 1973, Hucl, M., Zemcik, T. (Eds.), Nuclear Int. Centre, Prague, 314–317 (1975) (Crys.Structure, Experimental, 7)

[1976Pog] Pogrebnyak, A.I., Emlin, B.I., "Phase Composition of Iron-Aluminium-Carbon Alloys" (in Russian), *Metall. Koksokhimiya Resp. Mezhaved. Nauk.-Tekhn. Sb.*, **49**, 24–28 (1976) (Experimental, 1)

[1977Car] Carlberg, T., Fredriksson, H., "Influence of Silicon and Aluminium on the Solidification of Cast Iron", *Int. Conf. Solidification Casting*, Sheffield, **Vol. 1**, Metals Society, London, 115–124 (1977) (Experimental, #, 19)

[1977Cho] Choudary, U.V., Belton, G.R., "Activities of Carbon- Saturated in Fe-Al Alloys and Stability of Al_4C_3 at 1873 K", *Metall. Trans. B*, **8B**, 531–534 (1977) (Experimental, Thermodyn., 23)

[1978Kam] Kamenetskaya, D.S., Korsunskaya, I.A., Litvin, Y.A., "The Effect of Graphitizing Elements on the Equilibria with the Melt in the Iron-Carbon System under High Pressure", *Phys. Met. Metallogr.*, **45**, 101–111 (1979), translated from *Fiz. Metall. Metalloved.*, **45**, 569–579 (1978) (Phase Relations, Phase Diagram, Experimental, Thermodyn. *, 27)

[1978Zhu] Zhukov, A.A., "The Geometric Thermodynamics of Iron-Carbon Alloys Alloyed with Graphitizing Elements", *Izv. Akad. Nauk SSSR, Met.*, (5), 210–218 (1978) (Thermodyn., 8)

[1979Zhu] Zhukov, A.A., "Thermodynamics of Structure Formation in Cast Iron Alloyed with Graphitizing Elements", *Met. Forum*, **2**, 127–136 (1979) (Experimental, Thermodyn., 13)

[1980Dra] Drachinskaya, A.G., Lysak, L.I., Storchak, N.A., "Role of Mn and Al in Alterning the Crystalline Structure of Martensite Heated in the Low-Temperature Range", *Phys. Met. Metallogr.*, **47**, 80–86 (1980) (Crys. Structure, Experimental, 22)

[1980Gor1] Gorev, K.V., Gurinovich, V.I., "The Diagram of State of Fe-Al-C Alloys with a Low Content of Aluminium", *Vest. Akad. Navuk BSSR (Fiz.-Tekh.) Navuk*, (4), 26–30 (1980) (Phase Relations, Phase Diagram, Experimental, 7)

[1980Gor2] Gorev, K.V., Gurinovich, V.I., Topalov, Yu.F., "Phase Composition and Structure of Iron Alloys with Carbon and Aluminium Adjacent to the Iron Corner", *Vest. Akad. Navuk BSSR (Fiz.-Tekh.) Navuk*, **3**, 27–34 (1980) (Experimental, Phase Relations, Crys. Structure, 7)

[1980Lys] Lysak, L.I., Drachinskaya, A.G., Andryushchenko, V.A., "On the Nature of the Abnormally High Tetragonality of the Martensite Lattice of Fe-Al-C Alloys", *Russ. Metall.*, **6**, 166–167 (1980) (Crys. Structure, Experimental, 12)

[1981Koz] Kozlova, O.S., Makarov, V.A., "Mössbauer Study of the Austenite of Alloy Fe-Al-C", *Phys. Met. Metallogr.*, **48**, 63–67 (1981) (Crys. Structure, Experimental, 17)

[1981Lys] Lysak, L.I., Drachinskaya, A.G., Andryushchenko, V.A., Bogaichuk, I.L., "The Role of Aluminium and Carbon in the Formation of the Anomalous Tetragonality of the α-Martensite of Fe-Al-C" (in Russian), *Fiz. Met. Metalloved.*, **52**(5), 1068–1073 (1981) (Crys. Structure, Experimental, 13)

DOI: 10.1007/978-3-540-69761-9_4

[1982Suy] Suyazov A.V., Usikov, M.P., "Structure Transformations of High-Carbon Aluminium Steels During Tempering", *Phys. Met. Metallogr.*, **54**(1), 109–117 (1982) (Crys. Structure, Experimental, 21)

[1983Jan] Janas, M., Mamro, M., Ludinikowski S., Jowsa, J., "Carbon Solubility in Fe-C_{max}-Al, Fe-C_{max}-Co, Fe-C_{max}-Cu Alloys", *Metal. Odlew.*, **9**, 99–118 (1983) (Experimental, 10)

[1983Lys] Lysak, L.I., Drachinskaya, A.G., Andryushchenko, V.A., "Influence of the Chemical Composition of Alloy Fe-Al-C on Formation of an Ordered Carbide Phase", *Phys. Met. Metallogr.*, **56**(3), 183–185 (1983) (Experimental, 5)

[1983Vre] Vrestal, J., Pokorna, A., "Effects of Aluminium on the Thermodynamic Activity of Carbon in Iron" (in Czech), *Kovove Mater.*, **21**, 223–227 (1983) (Experimental, Thermodyn., 11)

[1985And] Andryushchenko, V.A., Gavrilyuk, V.G., Nadutov, V.M., "Atomic and Magnetic Ordering in the 6-Phase of Fe-Al-C Alloys", *Phys. Met. Metallogr.*, **60**(4), 50–55 (1985) (Crys. Structure, Experimental, 13)

[1985Bri] Briggs, I., Russel, G.J., Clegg, A.G., "Some Structural and Magnetic Properties of Fe-Al-C and Fe-Mn-Al-C Alloys", *J. Mater. Sci.*, **20**, 668–673 (1985) (Magn. Prop., 10)

[1985Cho] Cho, W.K., Han, K.H., "Phase Constitution and Lattice Parameter Relationships in Rapidly Solidified $(Fe_{0.65}Mn_{0.35})_{0.83}Al_{0.17-x}C$ and $Fe_3Al_{1-x}C$ Pseudobinary Alloys", *Metall. Trans. A*, **16A**, 5–10 (1985) (Crys. Structure, Experimental, *, 14)

[1985Gor] Gorev, K.V., Gurinovich, V.I., "The Stable Phase Diagram of Fe-C-Al Alloys in the Iron-Rich Region" (in Russian), in "*Stable and Metastable Phase Equilibria in Metallic Systems*", Nauka, Moscow, 119–124 (1985) (Phase Relations, Phase Diagram, Experimental, #, 6)

[1986And] Andrushchenko, V.A., Lysak, L.I., "Two Stage Kinetics of the Martensitic Transformation in Alloy Fe-Al-C", *Phys. Met. Metallogr.*, **61**(1), 92–97 (1986) (Crys. Structure, Experimental, 9)

[1986Lys] Lysak, L.I., Drachinskaya, A.G., Andryushchenko, V.A., "Influence of Atomic Ordering on the Phase and Structural Changes in High-Carbon Alloys of the Fe-Al-C System", *Met. Sci. Heat Treat*. (USSR), (7), 485–487 (1986), translated from *Metalloved. Term. Obrab. Met*., (7), 20–21 (1986) (Crys. Structure, Experimental, 6)

[1986Pro1] Prokoshkin, S.D., Kaputkina, L.M., Bernshtein, M.L., Moszhukhin, V.E., Andreeva, S.A., "The Structure of Martensite During Cluster Formation and Two-Phase Decomposition", *Acta Metall*., **34**(1), 177–186 (1986) (Crys. Structure, Experimental, 29)

[1986Pro2] Prokoshkin, S.D., Kaputkina, L.M., Bernshtein, M.L., "The Mechanism of Low-Temperature Lattice Changes of Martensite with Abnormal Tetragonality. Part 2. Martensite with Abnormally High Tetragonality", *Scr. Metall*., **20**, 299–304 (1986) (Crys. Structure, Experimental, 20)

[1986Sch] Schürmann, E., Schweinichen, J.V., "Investigation of the Liquidus Equilibria of Iron Rich Carbon Containing Ternary Systems Fe-C-X with X = Al, Cu, Ni and Cr" (in German), *Giessereiforsch.*, **38**, 125–132 (1986) (Review, Phase Relations, Phase Diagram, Experimental, 63)

[1987Rag] Raghavan, V., "The Al-C-Fe (Aluminium-Carbon-Iron) System" in "*Phase Diagrams of Ternary Iron Alloys. PartI"*, ASM International, Metals Park, OH, 89–97 (1987) (Phase Relations, Phase Diagram, Review, 30)

[1987Sch] Schürmann, E., Schweinichen, J.V., Völker R., Fischer, H., "Calculation of the α/δ resp. γ Liquidus Surfaces of Iron and the Liquidus Surface of Carbon as Well as the Lines of Double Saturation in Iron Rich Carbon Containing Ternary and Higher Systems Fe-C-X_1-X_2" (in German), *Giessereiforsch.*, **39**, 104–113 (1987) (Review, Phase Relations, Phase Diagram, Thermodyn., 19)

[1987Yok] Yokokawa, H., Fujishige, M., Ujie, S., Dakiya, M., "Phase Relations Associated with the Aluminum Blast Furnace: Aluminum Oxycarbide Melts and Al-C-X (X = Fe,Si) Liquid Alloys", *Metall. Trans. B*, **18B**, 433–444 (1987) (Review, Thermodyn., 74)

DOI: 10.1007/978-3-540-69761-9_4

[1988Mag] Magnin, P., Kurz, W., "Stable and Metastable Eutectic Temperatures of Fe-C with Small Additions of a Third Element", *Z. Metallkd.*, **79**, 282–284 (1988) (Experimental, Phase Relations, 5)

[1989Jun] Jung, I., Sauthoff, G., "High-Temperature Deformation Behavior of the Perovskite-type Phases Fe_3AlC and Ni_3AlC", *Z. Metallkd.*, **80**, 490–496 (1989) (Experimental, Mechan. Prop., 45)

[1989Ode] Oden, L.L., "Phase Equilibria in the Al-Fe-C System: Isothermal Sections 1500°C to 2300° C", *Metall. Trans. A*, **20A**, 2703–2706 (1989) (Experimental, Phase Relations, Phase Diagram, #, *, 12)

[1990Gho] Ghosh, G., "Al-C-Fe(Aluminium-Carbon-Iron)", MSIT Ternary Evaluation Program, in*MSIT Workplace*, Effenberg, G.(Ed.), MSI, Materials Science International Services GmbH, Stuttgart;Document ID: 10.13509.1.20 (1990) (Phase Relations, Phase Diagram, Assessment, 40)

[1991Jia] Jian, L., Wayman, C.M., "Assessment Fe-7Al-2C as a Shape Memory Alloy", *Scr. Metall. Mater.*, **25**(11), 2435–2440 (1991) (Experimental, 13)

[1991Kum] Kumar, K.C.H., Raghavan, V., "A Thermodynamic Analysis of the Al-C-Fe System", *J. Phase Equilib.*, **12**(3), 275–286 (1991) (Phase Relations, Phase Diagram, Calculation, Assessment, *, 32)

[1991Sar] Sarreal, J.A., Koch, C.C., "Metastable Microstructures of Rapidly Solidified and Undercooled Fe-Al-C and Fe-(Ni, Mn)-Al-C Alloys", *Mater. Sci. Eng. A*, **136**, 141–149 (1991) (Crys. Structure, Phase Relations, Phase Diagram, Experimental, 12)

[1992Put] Putyatin, A.A., Davydov, V.E., Nesterenko, S.N., "High Temperature Interactions in the Fe-Al-C System at 6 GPa Pressure", *J. Alloy. Compd.*, **179**(1–2), 165–175 (1992) (Phase Relations, Phase Diagram, Experimental, #, *, 16)

[1992Ueh] Uehara, S., Kajiwara, S., Kikuchi, T., "Origin of Abnormally Large Tetragonality of Martensite in High Carbon Iron Alloys Containing Aluminum", *Mater. Trans., JIM*, **33**(3), 220–228 (1992) (Crys. Structure, Experimental, 34)

[1993Rag] Raghavan, V., "Al-C-Fe (Aluminum-Carbon-Iron)", *J. Phase Equilib.*, **14**(5), 615–616 (1993) (Phase Relations, Phase Diagram, Review, 10)

[1994Mor] Moravetski, V.I., Andryushchenko, V.A., Sheludchenko, L.M., "Computer Simulation of the Electronic Structure of the $Fe_{(4-y)}Al_{(y)}C$ Carbide Phase in its Para- and Ferromagnetic States", *J. Phys. Chem. Solids*, **55**(2), 195–200 (1994) (Crys. Structure, Theory, 9)

[1994Oda] Oda, K., Fujimura, H., Ino, H., "Local Interactions in Carbon-Carbon and Carbon-M (M: Al, Mn, Ni) Atomic Pairs in FCC γ-Iron", *J. Phys., Condens. Matter*, **6**, 679–692 (1994) (Experimental, 32)

[1995Fuj] Fujimura, H., Ino, H., "Ordering of γ-Phase and Formation of κ-Phase in Melt-Quenched Fe-Al-C Alloys and Treir Magnetic Structures" (in Japanese), *J. Jpn. Inst. Met.*, **59**(7), 686–693 (1995) (Crys. Structure, Phase Relations, Phase Diagram, 29)

[1995Pal] Palm, M., Inden, G., "Experimental Determination of Phase Equilibria in the Fe-Al-C System", *Intermetallics*, **3**, 443–454 (1995) (Phase Relations, Phase Diagram, Experimental, #, *, 33)

[1996Koc] Kocherzhinski, Yu.A., Kulik, O.G., "Equilibrium Phase Diagrams and Manufacture of Synthetic Diamond", *Powder Metall. Met. Ceram.*, **35**(7–8), 470–483 (1996) (Phase Relations, Phase Diagram, Experimental, 37)

[1997San] Sanders, W., Sauthoff, G., "Deformation Behaviour of Perovskite-type Phases in the System Fe-Ni-Al-C. I: Strength and Ductility of Ni_3AlC_x and Fe_3AlC_x Alloys with Various Microstructures", *Intermetallics*, **5**, 361–375 (1997) (Phase Relations, Phase Diagram, Experimental, 57)

[1998Iva] Ivanovskii, A.L., Sabiryanov, R.F., Skazkin, A.N., "Band Structure and Magnetic Properties of $M_3M'C$ Antiperovskites (M = Mn, Fe; M′= Zn, Al, Ga, Sn)", *Phys. Solid State*, **40**(9), 1516–1519 (40) (Calculation, Electronic Structure, Magn. Prop., 16)

DOI: 10.1007/978-3-540-69761-9_4

[2001Mun] Munitz, A., Fields, R.J., "Mechanical Properties of Hot Isostatically Pressed Nanograin Iron and Iron Alloy Powder", *Powder Met.*, **44**(2), 139–147 (2001) (Crys. Structure, Experimental, Mechan. Prop., 14)

[2001Oca] Oca, C.G., Morris, D.G., Munoz-Morris, M.A., "The Role of Carbon and Vacancies in the Quench Hardning and Age Softening of a Fe-40Al-C Alloy", *Scr. Mater.*, **44**(4), 561–568 (2001) (Experimental, Mechan. Prop., 14)

[2001Rad] Radhakrishna, A., Baligidad, R.G., Sarma, D.S., "Effect of Carbon on Structure and Properties of FeAl Based Intermetallic Alloy", *Scr. Mater.*, **45**(9), 1077–1082 (2001) (Crys. Structure, Experimental, Mechan. Prop., 18)

[2002Bal] Baligidad, R.G., Radhakrishna, A., "Effect of B, Zr, Ce and Nb Addition on Structure and Mechanical Properties of High Carbon Fe-10.5 wt.% Al Alloy", *J. Mater. Sci. Lett.*, **21**(16), 1231–1235 (2002) (Experimental, Mechan. Prop., 17)

[2002Rag] Raghavan, V., "Al-C-Fe (Aluminum-Carbon-Iron)", *J. Phase Equilib.*, **23**(6), 508–510 (2002) (Phase Relations, Phase Diagram, Review, 6)

[2002Tur] Turkevich, V., Okada, T., Utsumi, W., Garan, A., "Kinetics of Diamond Spontaneous Crystallization from the Melt of the Fe-Al-C System at 6.5 GPa", *Diamond and Related Mater.*, **11**(10), 1769–1773 (2002) (Experimental, Kinetics, 18)

[2003Rao] Rao, V.S., "The Influence of Temperature on the Oxidation Behaviour of Fe_3Al-$Fe_3AlC_{0.69}$ and FeAl-$Fe_3AlC_{0.69}$ Intermetallics", *Intermetallics*, **11**(7), 713–719 (2003) (Experimental, Interface Phenomena, Kinetics, Phase Relations, 29)

[2004Bal1] Baligidad, R.G., Radhakrishna, A., "Effect of Zirconium on Structure and Properties of High Carbon Fe-10.5 wt. %Al Alloy", *Mater. Sci. Technol.*, **20**(1), 111–116 (2004) (Experimental, Mechan. Prop., Morphology, Phase Relations, 27)

[2004Bal2] Baligidad, R.G., "Effect of Niobium on Microstructure and Mechanical Properties of High Carbon Fe-10.5 wt.% Al Alloys", *Mater. Sci. Eng. A*, **368**(1–2), 131–138 (2004) (Crystal Structure, Experimental, Mechanical Properties, Morphology, Phase Relations, 24)

[2004Min] Minamino, Y., Koizumi, Y., Tsuji, N., Hirohata, N., Mizuuchi, K., Ohkanda, Y., "Microstructures and Mechanical Properties of Bulk Nanocrystalline Fe-Al-C Alloys Made by Mechanically Alloying with Subsequent Spark Plasma Sintering", *Sci. Technol. Adv. Mater.*, **5**, 133–143 (2004) (Mechan. Prop., Morphology, Experimental, 17)

[2004Mor] Morris, D.G., Munoz-Morris, M.A., Chao, J., "Development of High Strength, High Ductility and High Creep Resistant Iron Aluminide", *Intermetallics*, **12**(7–9), 821–826 (2004) (Interface Phenomena, Mechan. Prop., Morphology, Phase Relations, Review, 52)

[2004Oht] Ohtani, H., Yamano, M., Hasebe, M., "Thermodynamic Analysis of the Fe-Al-C Ternary System by Incorporating ab initio Energetic Calculations into the CALPHAD Approach", *ISIJ Int.*, **10**, 1738–1747 (2004) (Calculation, Phase Relations, Phase Diagram, Thermodyn., 34)

[2004Per] Perrot, P., "Al - C (Aluminium - Carbon)", MSIT Binary Evaluation Program, in *MSIT Workplace*, Effenberg, G. (Ed.), MSI, Materials Science International Services GmbH, Stuttgart, Document ID: 20.15738.1.20, (2004) (Phase Relations, Phase Diagram, Assessment, 19)

[2004Rao] Rao, V.S., "High Temperature Oxidation Behaviour of Fe-Al-C Alloys: an Overview", *Mater. Sci. Eng. A*, **364**(1–2), 232–239 (2004) (Review, Interface Phenomena, Kinetics, Transport Phenomena, 33)

[2004Sch] Schneider, A., Sauthoff, G., "Iron Aluminium Alloys with Strengthening Carbides and Intermetallic Phases for High-Temperature Applications", *Steel Res. Int.*, **75**, 55–61 (2004) (Review, 72)

[2005Gho] Ghosh, G., "Aluminium-Carbon-Iron", in *Landolt-Börnstein: Numerical Data and Functional Relationship in Science and Technology, New Series.* Group IV: Physical Chemistry. Ed. W. Martiensen, "*Ternary Alloy Systems. Phase Diagrams, Crystallographic and*

DOI: 10.1007/978-3-540-69761-9_4

Thermodynamic Data", Vol. 11A1, Eds. G. Effenberg, S. Ilyenko, Springer-Verlag, Berlin, Heidelberg, 123–138 (2005) (Phase Relations, Phase Diagram, Review, 76)

[2005Min] Minamino, Y., Koizumi, Y., Tsuji, N., Hirohata, N., Mizuuchi, K., Ohkanda, Y., "Bulk Fe-Al-C Nanoalloys Made by Mechanically Alloying with Subsequent Spark Plasma Sintering and Their Mechanical Properties", *Diffus. Defect Data. Part B (Solid State Phenomena)*, **101–102**, 103–110 (2005) (Experimental, Mechan. Prop., 12)

[2005Pal] Palm, M., "Concepts Derived from Phase Diagram Studies for the Strengthening of Fe-Al-Based Alloys", *Intermetallics*, **13**(12), 1286–1295 (2005) (Phase Relations, Review, 81)

[2005Rao] Rao, V.S., Raja, V.S., "Correlation Between High-Temperature Oxidation and Electrochemical Corrosion Behavior in Sulfuric Acid of Fe-Al-C Alloys: an Insight", *Corrosion*, **61**(8), 751–756 (2005) (Experimental, Interface Phenomena, Electrochem. Prop., 36)

[2005Sch1] Schneider, A., Falat, L., Sauthoff, G., Frommeyer, G., "Microstructures and Mechanical Properties of Fe_3Al-Based Fe-Al-C Alloys", *Intermetallics*, **13**(12), 1322–1331 (2005) (Crys. Structure, Experimental, Mechan. Prop., Morphology, Phase Relations, 47)

[2005Sch2] Schneider, A., Zhang, J., "Orientation Relationship Between a Ferritic Matrix and κ-Phase (Fe_3AlC_x) Precipitates Formed During Metal Dusting of Fe-15Al", *Intermetallics*, **13**(12), 1332–1336 (2005) (Crys. Structure, Experimental, Kinetics, Morphology, Phase Relations, 31)

[2006Kel] Kellou, A., Grosdidier, T., Aourag, H., "Comparative Behavior of Vacancy and C, B, N, O Atoms Single Defect on Hardening the *B*2-FeAl Structure: An Atomistic Study", *Intermetallics*, **14**(2), 142–148 (2006) (Calculation, Crys. Structure, Electronic Structure, 43)

[2006MSIT1] "Al-Fe (Aluminum-Iron)", Diagrams as Published, in *MSIT Workplace*,Effenberg, G. (Ed.), Materials Science International Services, GmbH, Stuttgart; Document ID: 30.10236.1.20, (2006) (Crys. Structure, PhaseDiagram, Phase Relations, 11)

[2006MSIT2] "C-Fe (Iron-Carbon)", Diagrams as Published, in *MSIT Workplace*, Effenberg, G. (Ed.), Materials ScienceInternational Services, GmbH, Stuttgart; Document ID: 30.13598.1.20 (2006) (Crys. Structure, Phase Diagram, Phase Relations, 2)

[Mas2] Massalski, T.B. (Ed.), *Binary Alloy Phase Diagrams*, 2nd edition, ASM International, Metals Park, Ohio (1990)

[V-C2] Villars, P. and Calvert, L.D., *Pearson's Handbook of Crystallographic Data for Intermetallic Phases*, 2nd edition, ASM, Metals Park, Ohio (1991)

DOI: 10.1007/978-3-540-69761-9_4

Aluminium – Chromium – Iron

Gautam Ghosh, Kostyantyn Korniyenko, Tamara Velikanova, Vladislav Sidorko

Introduction

There is a number of reasons for the scientific interest in the phase relations in the Al-Cr-Fe system, particularly as alloys of this system are employed as new lightweight materials for structural applications. The existence of quasicrystal approximants is also an interesting peculiarity of the Al-Cr-Fe system. Although this system has undergone many investigations, the Al-Cr-Fe equilibrium diagram has not been determined across the whole composition range. The liquidus surface has been constructed through experimental studies by [1932Tai1, 1932Tai2, 1940Kor1, 1940Kor2, 1943Mon, 1945Kor, 1946Kor, 1951Pra, 1954Chi, 1960Zol1, 1960Zol2]. The results of experimental investigations of phase relations at different temperatures along with isothermal sections have been presented by [1945Kor, 1946Kor, 1951Pra, 1961Phi, 1955Tag, 1958Chu, 1958Tag, 1968Bul, 1969Bul1, 1969Bul2, 1995Sta, 1995Zia, 1997Pal]. Data concerned with temperature-composition sections have been reported by [1946Kor, 1969Bul1, 1991Tre]. Crystal structure data are presented in [1954Chi, 1955Tag, 1958Tag, 1968Bul, 1969Bul1, 1969Bul2, 1969Kal, 1969Sel, 1970Koz3, 1972Kaj, 1974Niz, 1975Lit, 1976Vla, 1977Tys, 1982Nao, 1982Yea, 1983Bus, 1988Man, 1988Sch, 1989Law1, 1989Law2, 1989Man, 1990Ioa, 1992Don, 1995Li, 1995Sta, 1995Sui, 1995Zia, 1997Sat, 1997Sui, 1998Lia, 1998Sun, 1999Mek, 1999Sui, 1999Wit, 2000Dem, 2000Mo1, 2000Mo2, 2000Spi, 2001Alo, 2001Dem, 2001Rod, 2002Dem1, 2002Dem2, 2002Zho, 2003Zou, 2004Wu, 2005Dem, 2006Dem]. Experimentally determined thermodynamic properties have been presented by [1970Koz2, 1977Ost, 1992Hil, 1997Rud]. The experimental methods used by the above as well as the temperature and composition ranges studied are presented in Table 1. Reviews of the literature data concerning phase equilibria have been conducted by [1943Mon, 1961Phi, 1973Wil, 1976Mon, 2003Rag]; critical assessments of the available data by [1970Koz1, 1970Koz2, 1980Riv, 1987Sau, 1991Gho, 2004Gho]. Thermodynamic calculations of phase equilibria have been carried out by [1975Kau, 1987Sau, 1988Hoc, 2000Sub, 2001Sch].

Binary Systems

The Al-Cr and Al-Fe systems are accepted from [2006Cor] and [2006MSIT], respectively. Data concerning the Cr-Fe system are from [Mas2, 1982Kub].

Solid Phases

Crystallographic data on the known unary and binary phases as well as recently reported ternary ones are listed in Table 1. Seven ternary phases with crystal structures different from those of the binary intermetallics are reported in the ternary Al rich alloys solidified and consequently (directly or after homogenization) cooled at conventional rate. One of them, ν $Cr_{11}Fe_8Al_{81}$, can be believed to be a stable ternary compound at high temperature. This hexagonal phase investigated by [2000Mo1, 2000Mo2, 2003Zou] was found in the $CrFe_2Al_{12}$ alloy by [1999Sui] as the main phase together with orthorhombic "O-CrFeAl" and monoclinic "M-CrFeAl". [2003Zou] produced a three-dimensional (3D) reconstruction of the ν phase using electron crystallography. In their opinion, this technique offers the new possibility of *ab initio* structure determination of inorganic compounds existing only with very small crystal sizes. There is no limit in terms of the number of unique atoms in a structure that can be solved by 3D reconstruction. Body centered orthorhombic phase, labelled as "O-CrFeAl" was observed in Al rich as-cast alloys (prepared by arc melting) by [1995Sui, 1996Ros, 1997Sui, 1998Lia] and also by [2000Dem]. Found together with O phase, C-centered monoclinic ternary phase "M-CrFeAl" has a structure which is considered a superstructure of "O-CrFeAl". The lattice correspondence between the lattice parameters of the M- and O-phases are as follows:
$\boldsymbol{a}_m = \boldsymbol{c}_o - \boldsymbol{b}_o$ ($\boldsymbol{a}_m = \boldsymbol{c}_o / \sin\beta$),
$\boldsymbol{b}_m = \boldsymbol{a}_o$
$\boldsymbol{c}_m = 2\boldsymbol{b}_o$

DOI: 10.1007/978-3-540-69761-9_5

The interconnection of icosahedral clusters in the ν phase is similar to the orthorhombic structure of the Al_4(Cr,Ni) phase described by [2002Den]. Three orthorhombic phases "O-CrFeAl", "O_1-CrFeAl" and "$C_{3.1}$-CrFeAl" additionally to (Al) solid solution were found by [2000Dem] in as-cast alloy of $Cr_{11}Fe_8Al_{81}$ nominal composition, prepared by levitation melting. Phases with the same crystal structure as the two latter ones, O_1- and the $O_{3.1}$-, earlier were observed in Al-Cr-Cu-Fe by [1992Don], as well as in Al-Mn-Ni and Al-Pd-Ru systems by [1988Ten] and [1995Zha], respectively. A new "O_2-CrFeAl" phase together with orthorhombic phases "O-CrFeAl", "O_1-CrFeAl" as well as Al_8Cr_5, which is isostructural with γ-brass, were obtained by [2001Dem] in alloys of the compositions (at.%): Cr-6.0Fe-77.5Al (O+O_1+hexagonal phase γ type), Cr-8.0Fe-72.5Al O+O_2+hexagonal γ type), Cr-6.0Fe-72.5Al (O_1+O), as well as Cr-9.1Fe-67.6Al (hexagonal γ type). The alloys after induction melting were annealed in the range 900 to 1050°C for 20 h. The O_2-phase is for the first time observed in this system, but a phase with the same structure was identified before in Al-Cr-Cu-Fe by [1992Don, 1995Li]. The orthorhombic O_1 and O_2 phases were observed by [2002Dem1, 2002Dem2] in the alloy of Cr-6.0Fe-77.5Al (at.%) composition, prepared by induction melting, subsequently crushed and pressed in a graphite mold and then sintered at 980 and 1060°C. In the alloy of the same composition which was annealed at 900 to 1050°C for 20 h directly after melting the O_1- and O-phases coexist. Both [2002Dem1] and [2002Dem2] found a γ-brass-like phase in the Cr-7Fe-65Al (at.%) alloy as single phase with somewhat shorter lattice parameters. The last fact, which is in agreement with data of [1997Pal] for 1000°C, demonstrates the high solubility of Fe in the Cr_8Al_5(r) phase, and supports the results concerning orthorhombic phases. As one can see, most of the investigated alloys were not in an equilibrium state. Quenching experiments were not made. Except for the ν, $Cr_{11}Fe_8Al_{81}$, the compositions of the reported ternary phases are unknown. The latter may be either ternary compounds or stable or unstable polymorphous modifications of the binary intermetallics because of their close structural relationship to each other. [2005Dem] have identified the ζ_1 and γ_2 phases in as-cast alloys of the $Cr_{23.3}Fe_{9.1}Al_{67.6}$ and $Cr_{19.5}Fe_8Al_{72.5}$ compositions. It was noted that the structures of these phases are closely related to each other and can co-exist in the same alloys together with quasicrystal approximants. There is a resemblance between the atomic structure of these phases and the "O_1-CrFeAl" approximant. The hypothesis is that the γ-brass structure embodies a specific type of quasicrystal approximant.

There is a body centred cubic continuous solid solution α(Fe,Cr,Al) in the system and a wide field of ordered phases α_2 (FeAl) and α_1 (Fe_3Al) based on the bcc lattice. FeAl dissolves more than 30 at.% Cr at 600°C at the equiatomic Al/Fe ratio according to [1991Tre, 1997Pal]. Fe_3Al can dissolve a considerable amount of Cr (more than 26%) [1968Bul, 1969Bul1] and [1969Bul2], which leads to some increase in both $Fe_3Al \rightleftharpoons$ FeAl and FeAl $\rightleftharpoons$ (αFe) transition temperatures [1969Bul2] and [1969Sel]. [1972Kaj] suggested that at certain compositions Fe occupies one sublattice while Cr and Al occupy the other. [1993Kni] found that the alloys on the basis of Fe_3Al with 2 and 5 mass% Cr (about 1.3 and 3.3 at.% Cr, respectively) have an equilibrium structure of the BiF_3 type (*cF*16) at low temperatures which transforms to the CsCl type structure (*cP*2) above 500°C. The crystal structures of alloys in a similar range of compositions were investigated also by [1999Wit]. The experimental results of [1998Sun] identified the site occupation of the substitutional element chromium (content up to 5 at.%) in the Fe_3Al phase. An ordering treatment was conducted at 500°C for 13 days. It was established that all of the Cr atoms occupy the next nearest neighbor positions of the Al atoms. The energetic and structural characteristics of atomic ordering processes in $Fe_{0.5}(Cr_nAl_{1-n})_{0.5}$ have been analyzed qualitatively by [1999Mek] on the basis of the statistico-thermodynamic theory of ordering utilizing a quasi-chemical method combined with electronic theory in the pseudo-potential approximation. The effect of the chromium impurity on the order-disorder α_2 phase transformation temperature and the characteristics of the atomic short-range order were studied. It was suggested that Cr atoms substitute mainly on Al sublattice sites. The same conclusion was arrived at by [2002Boz] who employed calculations based of the Bozzolo-Ferrante-Smith (BFS) method. [1976Vla] studied the decomposition behavior of a Cr-68.3Fe-10.4Al (at.%) alloy after quenching from 750°C and subsequent annealing at 490°C for up to 200 h. Though no ternary phase was detected upon annealing, the authors observed phase separation into two isomorphous solid solutions which were depleted or enriched in Cr, respectively. The location of the ((γFe) + (αFe))/(αFe) surface of the (γFe)-loop in the Al-Cr-Fe system is given in Table 3 based on the experimental results obtained on eight ternary alloys that had been heat treated between 800 and 1300°C [1946Kor]. [2001Rod] obtained a nanocomposite with an amorphous

DOI: 10.1007/978-3-540-69761-9_5

matrix containing metallic nanocrystals through the controlled crystallization of an amorphous Cr-5Fe-90Al (at.%) alloy. Milling of this alloy for 60 h resulted in the formation of amorphous and nanocrystalline regions and the crystallization temperatures for the primary and intermetallic phases occurred within 50°C. All binary intermetallics of the ternary system dissolve the third component. Cr_2Al is reported by [1969Kal] to dissolve Fe up to $x = 0.25$ replacing Cr atoms in the lattice. Data on the lattice parameters of $(Cr_{1-x}Fe_x)_2Al$ as a function of x are listed in Table 2. [1951Pra] reported that the extracted crystals of Cr_2Al_{13} and Cr_2Al_{11} (from alloys cooled slowly to room temperature from the liquid phase) dissolved iron. The observed compositions of Cr_2Al_{13} and Cr_2Al_{11} at maximum Fe solubilities were Cr-5.49Fe-75.05Al (mass%) (Cr-3.02Fe-85.48Al (at.%)) and Cr-13.47Fe-67.96Al (mass%) (Cr-7.73Fe-80.81Al (at.%)), respectively. [1960Zol1] and [1960Zol2] also analyzed Cr_2Al_{13} crystals from alloys with various Fe contents. The solid solubility data of [1960Zol1] and [1960Zol2] showed a lower Fe solubility in Cr_2Al_{13} of 2.66 mass% (1.3 at.%) Fe, but it was not certain to be a maximum value. The data of [1951Pra] show that the replacement of Cr for Fe deviates from a simple one-to-one atomic substitution scheme, but that in [1960Zol1] and [1960Zol2] is somewhat closer to one-to-one atomic replacement. Solution of Fe in Cr_2Al_{13} is reported to cause a reduction in the lattice parameter of the Cr_2Al_{13} phase [1960Zol1, 1960Zol2]. Fe_4Al_{13} is reported to dissolve some Cr, and the Fe_4Al_{13} composition, according to chemical analysis data, is Cr-39.89Fe-56.17Al (mass%) (Cr-24.87Fe-72.49Al (at.%)) [1951Pra]. But the value 2.64 at.% for Cr solubility in Fe_4Al_{13} can not be accepted as maximal, because according to [1997Pal], the solid solubility of Cr in Fe_4Al_{13} at 1000°C is considerably higher - about 6.4 at.% (Table 2). All Al-rich phases that are in a solid state at 1000°C (based on Fe_4Al_{13}, Fe_2Al_5, $FeAl_2$, Cr_4Al_9 and Cr_5Al_8) extend deep into the ternary system. The maximum solubilities of the third component at 1000°C are observed for the Cr_5Al_8 and Cr_4Al_9 phases - 32.5 and 9.6 at.% Fe, respectively (Table 2). The lattice parameters of the, Cr_5Al_8 (r) (γ_2) phase versus Fe content are presented in Figs. 1a, 1b. [1990Ioa] found that the rapidly solidified alloy Cr-1Fe-95Al (mass%) (Cr-0.5Fe-97.37Al (at.%)) exhibits a mixed microstructure composed of featureless and cellular morphologies. According to X-ray data, the equilibrium Cr_2Al_{13} phase coexists in the alloy with the aluminium matrix and an unknown phase. Taking into account the data of [1995Zia] and [1995Sta], the latter could be a ternary quasicrystalline phase with an icosahedral symmetry, see Table 2. [1995Zia] found the *i* phase, named Q by him, in the $Cr_3Fe_zAl_x$ (z = 0, 1 or 3 at.%) alloys, using X-ray diffraction. The accepted composition of the phase $Cr_{12\pm1}Fe_{12\pm1}Al_{75\pm0.5}$, was established using chemical microanalysis. During the "low" temperature sequences of the rapidly solidified alloys, the Q phase reacts with the Al matrix giving rise to the non-equilibrium and equilibrium phases: (Al)+Q → $FeAl_6$+Cr_2Al_{13}+ Fe_4Al_{13}. At higher temperatures (450 to 550°C), the quasicrystal transforms directly into the stable phases, by-passing the step of the metastable $FeAl_6$ phase formation. At the quasicrystal/matrix interface the orthorhombic phase was observed. According to EDX analysis, the ratio (Al)/(Cr+Fe) is equal to 3.1 ± 0.1 and the content of Cr << 1 at.%. [1995Zia] concludes that this phase is the allotropic variant of Fe_4Al_{13}, which is monoclinic in the binary system. The structure of the *i* phase, found in a melt spun alloy of $Cr_8Fe_6Al_{86}$ (at.%) composition, is reported by [1995Sta] as simple icosahedral type with the value of the six-dimensional hypercubic lattice constant a_{6D} = 654.2 ± 0.02 pm. In a rapidly solidified alloy, the *i* phase coexisted with the (Al) solid solution. This mixture transformed to a mixture of stable phases Cr_2Al_{13}+Fe_4Al_{13} after 5 min heating at 580 or 635°C. Earlier a metastable icosahedral ternary phase was also reported by [1987Wou, 1988Man, 1989Man, 1988Sch, 1989Law1, 1989Law2, 1989Man].

Invariant Equilibria

Figure 2 gives the tentative invariant equilibria for the Al rich corner. The equilibrium L+Cr_2Al_{11}+Fe_4Al_{13} within the ternary is not known, while equilibrium L+Cr_2Al_{13}+Fe_4Al_{13} is unquestioned because the existence of the three-phase equilibrium Cr_2Al_{13}+Fe_4Al_{13}+(Al) is established well at temperatures close to the solidus: 500°C [1995Zia] and 635°C [1995Sta]. [1943Mon] suggested that the invariant U_1 reaction takes place at Cr-4.2Fe-93.7Al (mass%), but the temperature was not given. Careful thermal analysis data of [1932Tai1] and [1932Tai2] show the presence of a ternary eutectic E at Cr-2Fe-97Al (mass%). On the other hand, [1943Mon] and [1976Mon] suggested that E takes place at Cr-1.70Fe-97.95Al (mass%), to which there is no experimental evidence. It remains inconclusive whether the ternary eutectic reaction E

DOI: 10.1007/978-3-540-69761-9_5

exists or not. Thermodynamic calculations of the Al-rich corner of the Al-Cr-Fe system by Saunders [1987Sau] suggest that the reaction E is unlikely and instead he predicted a ternary transition U_1 reaction $L+Cr_2Al_{11} \rightleftharpoons Cr_2Al_{13}+Fe_4Al_{13}$ at 709°C (0.63 mass% (0.33 at.%) Cr, 3.09 mass% (1.52 at.%) Fe) followed by the ternary transition U_2 reaction $L+Cr_2Al_{13} \rightleftharpoons (Al)+Fe_4Al_{13}$ at 654.5°C (0.19 mass% (0.10 at.%) Cr, 2.02 mass% (0.99 at.%) Fe). The latter shows a good agreement with the findings of [1960Zol2] and [1973Wil] showing no ternary eutectic reaction at 640°C, but a transition reaction at 655°C. Because of this uncertainty, alternative paths for E and U are given by broken lines in Fig. 2.

Liquidus Surface

Figures 3 and 4 show two versions for the liquidus surface of the Al corner. Fig. 3 is presented after experimental data [1932Tai1, 1932Tai2] and [1943Mon]. The melting troughs separate 4 different areas of primary crystallization. Ternary alloys from 100 to about 94 at.% Al have been investigated by different authors [1932Tai1, 1932Tai2, 1951Pra, 1954Chi, 1960Zol1, 1960Zol2], and no ternary compound has been reported by them in this composition range. The presence of the ternary eutectic E is concluded from thermal analysis data of [1932Tai1] and [1932Tai2], even though limited thermal analysis results of [1960Zol1] and [1960Zol2] failed to confirm it. Figure 4 is the calculated liquidus surface of the Al corner after [1987Sau], showing the presence of the transition invariant reaction U_2 instead of a ternary eutectic reaction. [1951Pra] failed to observe the ρ, Cr_2Al_{11} phase in binary and ternary alloys either slowly cooled or quenched from 730 to 765°C. In accordance with the old version of the Al-Cr binary phase diagram adopted by [1951Pra], in which a reaction $L + \rho \rightleftharpoons \theta$ takes place at 755°C instead of 790°C in the presently accepted binary phase diagram, the obtained result seems to reject the existence of the stable Cr_2Al_{11} compound. Nevertheless, these data are in good agreement with the Al-Cr phase diagram accepted in this assessment. But there is no confidence that the equilibrium $L+\rho+Fe_4Al_{13}$ exists. It can be prevented by possible formation of high-temperature incongruently melting ternary compounds with aluminium content less than 94 at.%. Therefore the monovariant curves in the vicinity of U_1 are dotted. The liquidus surface in Fig. 5, after [1945Kor], shows a melting trough defining the primary crystallization field of (Cr,αFe). Approximate isotherms at 50 K intervals are also shown. [1935Gru] reported the melting point of a Cr-64.6Fe-5.3Al (mass%) Cr-59.86Fe-10.17Al (at.%)) alloy which agrees reasonably well with Fig. 5. [1970Koz1] and [1970Koz2] compared the calculated and experimental results for liquidus points for compositions from the Cr corner to about 70 mass% Fe and 40 mass% Al. The experimental values were always 30 to 40 K lower than the calculated ones, which was attributed to undercooling. Nevertheless, the isotherms between 1500 and 1800°C agree well with those of [1945Kor]. [1974Vya] used the "simplex lattice method" to construct the liquidus and solidus surfaces and reported a good agreement with data of [1970Koz1]. The original publications [1940Kor1, 1940Kor2, 1945Kor, 1946Kor] show the liquidus surface of (Cr,αFe) as terminated by the uninterrupted monovariant curve p_1p_2, corresponding to the equilibrium of liquid with the (Cr,αFe) phase and assumed continuous solid solution of the binary γ_1 and ε phases. There is reason to believe that the γ_1 phase has a cubic structure. If the cubic γ phase is isomorphous with γ_1, the continuous cubic solid solution in the ternary system is possible at high temperatures. But until now the existence of a (γ,ε) continuous series has not been established.

Isothermal Sections

Figure 6 shows the isothermal section at 1150°C based on data of [1945Kor, 1946Kor] and [1991Tre, 1997Pal]. In the original paper [1946Kor], the two-phase "$\alpha_3+\varepsilon_3$" field is not very clear. Even though "α_3" is the ternary (Cr,αFe) solid solution and ε_3 is the ε or γ phase, the authors made very little investigation of the "ε_3" phase and they interpreted it as a continuous solid solution between ε (Fe_2Al_3) and γ_1 (Cr_5Al_8)(h) [1946Kor]. Since the crystal structure of ε is unknown, better evidence for the existence of a continuous solid solution between ε (Fe_2Al_3) and γ_1 (Cr_5Al_8)(h) is required. On the other hand, [1997Pal] established a large extension of γ_2 into the ternary system - up to 32.5 at.% Fe at about 48 at.% Al at 1000°C. The α_2/α transition of the second order is shown according to the binary Al-Fe system and data of [1991Tre] on an FeAl-Cr polythermal section. Figures 7, 8, 9, 10, and 11 show isotherms

DOI: 10.1007/978-3-540-69761-9_5

at 900, 750, 700, 650, and 600°C, respectively, after [1958Chu], with correction in the range of the ordering of the α phase according to the experimental data of [1991Tre]. Phase equilibria between the γ-brass type phases are assumed by taking into account the data of [1997Pal] for 1000°C. Phase equilibria in the Al corner are presented after data of [1951Pra, 1961Phi, 1995Zia, 1995Sta]. Annealing times for different alloys used by [1958Chu] are listed in Table 4. More than 50 ternary alloys were studied by [1958Chu], most of them near the region of σ phase formation. As one can see in the isothermal sections at 750, 700, 650, and 600°C, the extent of the σ phase field decreases with increasing Al content. This is in agreement with the results of [1945Kor]. Even though the η phase (Cr_2Al) is stable up to 911°C according to the accepted Al-Cr binary phase diagram, this phase does not appear in the isothermal section at 900°C shown in Fig. 7. Such a difference of 11 K is not unreasonable when comparing data from different sources [1980Riv]. In his original paper, Chubb [1958Chu] presented a wide two-phase α_2+α field in all isothermal sections of a the ternary system, as well as two three-phase (αFe)+$FeAl\alpha_2$+Cr_2Al(η) and $FeAl\alpha_2$+Cr_2Al(η)+Cr_4Al_9(ζ) ones, the latter two being contiguous, which is not likely. The existence of the wide α_2+α field, because of a very narrow (to 1 or 2 at.% Cr) α_2 region shown by [1958Chu], is rather doubtful when the data of [1991Tre] and [1997Pal] are taken into account. FeAl dissolves at 1000°C about 30 at.% Cr at 45 at.% Al after [1997Pal]. In agreement with the above mentioned data, [1991Tre] showed that the extension of α_2 in the FeAl-Cr section increases with decreasing temperature down to about 28 at.% Cr at 36 at.% Al at 1000°C. The phase transition α/α_2 of the second order in the Al-Fe binary at high temperatures becomes first order below 665°C [1993Oka, 2006MSIT]. A rise in the α/α_1 temperature with increasing Cr content is reported by [1968Bul, 1969Bul1] and [1969Bul2]. The influence of Cr on the type of the ordering transition $\alpha/\alpha_2/\alpha_1$ in ternary solid solution has not been studied in detail. In the isothermal sections at 900, 750, 700, 650 and 600°C, α phase ordering is presented based on the Al-Fe binary as well as on the compared data of [1991Tre, 1997Pal]. There is some contradiction between the results of [1958Chu] and those of [1955Tag] and [1958Tag] as far as the formation of the σ phase in the ternary alloys is concerned. Based on the purity of the material, heat treatment regime and number of alloys used, the results of [1955Tag] and [1958Tag] seem to be more reliable than those of [1958Chu]. The results of [1955Tag] and [1958Tag] on σ phase formation in alloys containing up to 32 mass% Al are in accordance with those of [1958Chu], but they disagree with [1958Chu] for ternary alloys containing 35 mass% Cr. It should be emphasized that the formation of the σ phase is reported to be sensitive to non-equilibrium factors arising from impurities in ternary alloys [1955Tag, 1969Mue]. Phase equilibria above 50 at.% Al proposed in Figs. 7 to 11 are based on a significant solubility of Fe in γ (ζ) phases at 1000°C found by [1997Pal]. A very strong temperature dependence of the solubility of Fe in γ and ζ phases can be assumed taking into account the low thermodynamic stability of the binary ε phase, which coexists in equilibrium with γ and is stable only within close limits of the equilibrium parameters at high temperature. It is seen in the isothermal sections. The isothermal section at 1000°C for Al content greater than 50 at.% is presented in Fig. 12 according to [1997Pal]. The data presented by [1997Pal] for the ternary alloys fit well to those for Al-Fe [Mas2] and Al-Cr [1995Aud], respectively, as accepted in the [2006Cor] assessment of Al-Cr. The Al solubility within the ternary Fe based solid solutions is near to that for 1150°C but higher than reported for 900°C by [1958Chu]. While no ternary intermetallic phases have been found at 1000°C in this work, in contradiction to the above mentioned observation of the ternary phases, the solubility of the third component in the Al-Cr and Al-Fe binary phases in some cases is very high. Solubility of Fe in the γ_2 phase reaches about 30 at.% at 10 at.% Cr and 60 at.% Al. Fe stabilizes the γ_2 structure so that at a content higher than about 13 at.% Fe only the γ_2 phase (but not γ_1) is reported to participate in phase equilibria at temperatures under investigation. The solubility of Cr in the Al-Fe binary phases is less than that of Fe in the binary Al-Cr phases as seen in Table 2. When the aluminium content exceeds 80 at.%, the liquid and liquid-solid regions appear. Figure 13 shows the partial isothermal section for the Al corner at 600°C, according to the data of [1951Pra, 1961Phi]. [1951Pra] reported that undercooling suppresses the reaction $L + Cr_2Al_{11} \rightleftharpoons Cr_2Al_{13}$ in both binary and ternary alloys. In the composition range shown in Fig. 13, no ternary phase has been reported and the phase fields remain the same at 425°C with a small shift in the phase boundaries

DOI: 10.1007/978-3-540-69761-9_5

[1951Pra]. Saunders [1987Sau] calculated the isothermal sections of the Al-rich corner at 600 and 425°C. The agreement between the calculated (presented by dashed line in Fig. 13) and the experimental (Al) +Cr_2Al_{13}/(Al)+Cr_2Al_{13}+Fe_4Al_{13} phase boundary accepted by [1951Pra] was reported to be very good, whereas that for the (Al)+Fe_4Al_{13}/(Al)+Cr_2Al_{13}+Fe_4Al_{13} boundary was less satisfactory. After [1995Zia, [1995Sta], in ternary alloys at Al contents greater than 94 at.% at 635°C and below, only (Al), Cr_2Al_{13} and Fe_4Al_{13} phases coexist in equilibrium, in agreement with [1951Pra, 1961Phi] and [1987Sau]. The sections through the surface ((γFe)+(αFe))/(αFe) of the γ-loop in the ternary system are given in Fig. 14. Further work is necessary to clarify the phase equilibria in the Al corner of the system.

Temperature – Composition Sections

Figure 15 shows the polythermal FeAl-Cr section of the phase diagram according to [1991Tre]. The alloys containing up to 70 at.% Cr were prepared by arc melting from aluminium (99.5 mass% purity), electrolytic chromium and carbonyl iron. The annealings were carried out at 1200°C and 1300°C for 70 h each. As can be seen in Fig. 15, the temperature of the $\alpha \rightleftharpoons \alpha_2$ transformation decreases with increasing chromium content. The α_2 field extends to about 28 at.% Cr at 1000°C. Fig. 16 shows the variation in the order-disorder reaction temperature as a function of the Cr content along the Fe_3Al-$CrFe_3$ section. In the Fe_3Al-$CrFe_3$ isopleth taken from [1969Bul1], additional dashed boundaries are given approximately according to the phase transformations in $Fe_{75}Al_{25}$ (at.%) by [1993Oka]. The partial isopleth along Fe_3Al-Cr_3Al [1969Bul1] is in poor agreement with the general data set discussed above and is not considered here.
[1946Kor] gave four isopleths at constant mass ratios Cr/Fe. These diagrams partially contradict the isothermal sections shown in Figs. 6, 7, 8, 9, 10, 11, 12 and therefore are not reproduced here.

Thermodynamics

Information on thermodynamic properties of the Al-Cr-Fe alloys is incomplete. [1975Kau] used a simple thermodynamic model to calculate the phase boundaries between liquid and (Cr,αFe) at 1747, 1647, 1547 and 1527°C. In general, there is a substantial disagreement between the calculated [1975Kau] and the experimental phase boundaries [1970Koz2]. Thermodynamic calculations of the phase equilibria in the Al rich corner (96-100 at.% Al) was carried out by [1987Sau]. Applying a defect model, [1988Hoc] calculated the activity of Cr in FeAl, assuming that FeAl is either a compound or a solid solution. The calculated results do not show a significant discrepancy and both cases suggest complete solid solubility between Cr and FeAl. [1977Ost] studied the heats of dissolution of aluminium in a melt of $Fe_{70}Cr_{30}$ (at.%) at temperatures between 1550 and 1600°C. The experimental results were in a good agreement with calculations based on the application of the subregular model that are available in the literature. [1992Hil] studied the vaporization of the alloy Cr-75.4Fe-4.8Al (mass%) (Cr-70.72Fe-9.32Al (at.%)) using Knudsen effusion mass spectrometry in the temperature range 1313-1556 K. This composition virtually agrees with those of the commercial Aluchrom and MA956 alloys. The obtained thermodynamic data are presented in Tables 5 and 6. The heat capacities of the Fe_3Al-based compound with a Cr content of 5 at.% have been measured in the temperature range from 20 to 700°C by [1997Rud]. The results of the $C_p(T)$ measurement are shown in Fig. 17. [2000Sub] have reported a thermodynamic assessment of the Al-Cr-Fe system, which was performed applying the standard CALPHAD method. There the old version of the Al-Cr phase diagram [Mas2] was accepted, and no ternary phases have been assumed. A four-sublattice model for the γ-brass type phases was developed. [2001Sch] calculated isopotential curves of the thermodynamic forces for ternary diffusion as a function of composition for the Al-Cr-Fe system at 1073 and 1273 K.

Notes on Materials Properties and Applications

Al-Cr-Fe alloys are of interest as new lightweight alloys for structural applications, in particular, for the production of protective coatings formed by alumina scales from alloys of compositions that lie in the Al-rich corner of the system. Al-Cr-Fe quasicrystal approximants are also potential candidates for new applications because of their specific properties. Alternatively, the addition of chromium to Fe_3Al- and FeAl-based alloys produces excellent candidates for moderate and high temperature applications. [2005Pal] showed that

DOI: 10.1007/978-3-540-69761-9_5

strengthening of Al-Fe-based alloys at high temperatures can be achieved through solid-solution hardening, precipitation of incoherent or coherent particles and by ordering. However, in the Al-Cr-Fe ternary system, within a large composition region (up to 50 at.% Al) strengthening of the alloys can be achieved only through solid solution hardening. At higher Al contents the possibility of precipitating a second phase, *e.g.* γ_1 phase, exists.

Investigations regarding materials properties of the Al-Cr-Fe system are listed in Table 7. Mechanical properties of the Al-Cr-Fe alloys were investigated by [1955Tag, 1958Tag, 1982Nao, 1991Pra, 1991Sik1, 1993Kni, 1996Jim, 1998Su, 1998Sun, 2000Spi, 2002Zho] and [2004Hua]. In particular, [1955Tag, 1958Tag] studied the hardness of Al-Cr-Fe alloys containing 20 to 30 at.% Cr, 0 to 4 at.% Al after aging for 720 h at temperatures of 500, 600, 700, 800 and 900°C. It was established that alloys with about 35 at.% Cr have the highest hardness of all the alloys. Aging at 500°C makes alloys much harder than at other temperatures. This is referred to as the "475°C embrittlement".

[1982Nao] obtained the ductile supersaturated ferrite solid solution with high hardness and strength by the rapid quenching technique. The range of its formation is limited to less than about 35 at.% Cr and 23 at.% Al. The hardness, yield strength and tensile fracture strength increase with increasing amounts of chromium and aluminium. [1991Pra] studied mechanical properties of ordered alloys in the composition range 50 to 80 at.% Fe, 0 to 20 at.% Cr, that were rapidly solidified by melt spinning. An increasing preponderance of cleavage fracture with increasing ternary substitution for iron was observed. Mechanical properties of Fe_3Al-based alloys were investigated by [1991Sik1, 1993Kni, 1998Sun, 2004Hua]. According to [1991Sik1], room-temperature tensile ductility of the samples with 2 to 5 mass% Cr (1.3 and 3.3 at.%, respectively), prepared using the melting process described in [1991Sik2], approach 20%, which should be acceptable for many practical applications, and [1993Kni] established that increasing the Cr content from 2 to 5 mass% has a small effect on the ductility of the alloys based on Fe_3Al.

[1998Sun] established that chromium significantly affected the room temperature tensile properties in vacuum. In comparison with binary Fe_3Al, in the $Cr_{5.38}Fe_{70.42}Al_{24.20}$ (at.%) alloy (arc melted, then forged at 1000°C, rolled into plates with thickness of 1.0-1.2 mm within the temperature range between 950 and 600°C; the plates were then annealed at 750°C for 1 h, followed by ordering treatment at 500°C for 13 d) a decrease in yield strength from 841 to 695 MPa, increase in elongation from 5.18 to 9.1% and ultimate tensile strength from 990 to 1084 MPa take place. Two large ingots weighing 269 or 104 kg, with approximate composition of 5.5Cr-78.6Fe-15.9Al (at.%) and the presence (according to the conventional chemical analysis) of small amounts of C, Si, Mn, P and S, were prepared by [2004Hua] using vacuum induction melting and top cast. They had a satisfying surface appearance and no crack was detected. Conventional thermomechanical processes were used to produce bars, sheets and seamless tubes. By controlling the thermomechanical treatment, a room temperature ductility with a value of more than 10% was achieved. The creep lifetime at 600°C and 200 MPa was more than 2000 h after annealing.

The tensile properties of the Cr-65Fe-30Al (at.%) alloy in air and in vacuum were investigated by [1998Su]. The yield strength of the Fe_3Al alloy was reduced by the addition of 5 at.% Cr, indicating a softening with the addition of chromium, but the ultimate tensile strength (UTS) was increased slightly. [1996Jim] studied the creep behavior of several Al-Cr-Fe alloys ranging in aluminium from 21.7 to 48 at.% and established that the ternary alloys exhibit an improvement in strength under high temperature compressive creep.

The microstructure of four Al-Cr-Fe alloys containing 9.3 to 18.0 at.% Cr and 7.6 to 25.5 at.% Al was investigated by [2000Spi] using TEM after different heat treatments and different degrees of compressive deformation. The maximum of the work-hardening curves is found to be shifted to higher strains with increasing aluminium concentration. At a deformation temperature of 400°C dynamic strain aging occurs. [1976Vla] investigated three alloys (mass%): Cr-7Fe-92Al, Cr-7.0Fe-92.5Al and Cr-7.0Fe-91.5Al (in at.%: Cr-3.5Fe-95.9Al, Cr-3.5Fe-96.2Al and Cr-3.5Fe-95.7Al) designed to be used at elevated temperatures. Extrusion bars were made from powders. The as-extruded and annealed at 482°C alloys, investigated by optical microscopy, TEM and XRD, had a microstructure consisting of equiaxed grains of aluminium matrix and two types of precipitates, namely (Cr,Fe) Al_3 and a metastable (Cr,Fe) Al_6 phase.

Data on the magnetic behavior of the Al-Cr-Fe alloys were obtained by [1969Kal, 1974Niz, 1975Lit, 1983Bus, 1985Okp, 1995Sta, 1997Sat, 2004Wu]. [1969Kal] studied the antiferromagnetic behavior

DOI: 10.1007/978-3-540-69761-9_5

and Neel temperature of ternary alloys based on the η (Cr_2Al) phase. [1974Niz] and [1975Lit] reported the magnetic atomic moment, Curie temperature, temperature dependence of magnetic coercivity and susceptibility in the temperature range from 627 to –196°C. [1983Bus] obtained the values of Curie temperature, saturation moment at 4.2 K and Kerr rotation angle for the $CrFe_2Al$ alloy annealed at 800 K (527°C) for 11 d. [1985Okp] studied the ferromagnetism of ternary alloys based on FeAl, with Cr contents up to 50 at.%, quenched from 830°C. Ferromagnetism was observed in alloys with Cr contents no less than 35 at.%. [1995Sta] investigated magnetic susceptibility of the $Cr_8Fe_6Al_{86}$ (at.%) alloy solidified by melt spinning, of the phase content i+θ+Fe_4Al_{13}+(Al). The icosahedral symmetry was concluded not to produce any magnetic properties in the studied alloy. [1997Sat] determined the magnetic moment of chromium in Fe_3Al-based alloys with chromium content up to 15 at.% in the temperature range 10 to 300 K. The overall moment was found to be small and that of neighboring iron atoms was reduced by about 0.1μ_B per Cr atom. [1982Nao] reported that the room temperature electric resistivity of the alloys with less than about 35 at.% Cr and less than 23 at.% Al increases with increasing chromium and aluminium contents and reaches a maximum value for the $Cr_{30}Fe_{50}Al_{20}$ (at.%) alloy. The temperature coefficient of resistivity in the temperature range between room temperature and 500°C decreases with increasing chromium and aluminium contents and becomes zero in the vicinity of 20 to 30 at.% Cr and 15 at.% Al. [2004Wu] studied strain-induced ferromagnetism in a ternary FeAl-based single crystal with a composition of $Cr_3Fe_{57}Al_{40}$ (at.%). It was grown in an alumina crucible under an argon atmosphere using a modified Bridgman technique, annealed at 1200°C for 10 h, then cooled slowly in the furnace and annealed at 400°C for 5 d in order to minimize the concentration of thermal vacancies. After deformation to similar rolling strains along the same orientation, the saturation magnetization, M_S, was found to be similar to that of the $Fe_{57}Al_{43}$ (at.%) alloy. This behavior can be explained by the site preferences of the Cr atoms on the Al sublattices, which change the probability of a Fe atom having like nearest-neighbors in the anti-phase boundary (APB) tubes, affecting the energy of the anti-phase boundaries. Calculation of M_S at 0 K of the rolled specimen, based on APB tube density and considerations of the APB tube size and geometry, was found to be in reasonable agreement with the experimentally determined value. The effect of heat treatment and grain size on the damping capacity of the Cr-70Fe-5Al (mass%) (Cr-63.4Fe-12.3Al (at.%)) has been investigated by [2002Zho]. It has been shown that annealing temperature and grain size have a significant influence on the damping capacity and strain amplitude dependence of this alloy. It has a rather low damping capacity after being water quenched or cold worked due to a high internal stress in the structure. [2002Dem2] studied the optical conductivity of the ternary phases and interpreted the obtained data on the basis of a tunneling transition. Good agreement between the obtained results and a theoretical approach developed for aperiodic intermetallics assuming an anomalous diffusion of the electron wavepacket was found.

Miscellaneous

[1970Koz3] reported the solubility of C in liquid Al-Cr-Fe alloys at different temperatures. The formation and growth characteristics of iron-based aluminide diffusion layers at the Al-Fe interface have been analyzed by [1998Akd] in terms of interfacial interaction potentials based on the statistico-thermodynamical theory of multicomponent alloys combined with electronic theory in the pseudopotential approximation. The pairwise interatomic interaction potentials and partial ordering energies have been calculated to predict the effect of various alloying additions, in particular, of chromium, on the activity coefficient of Al atoms in $\alpha Fe_{0.95}(Al_{1-n}Cr_n)_{0.05}$ alloys and considered up to 1 at.%. The results of calculation show that chromium decreases the activity coefficient of Al atoms in (αFe). So as to reduce the thickness of the Al-Fe intermetallic diffusion layer. The influence of aluminium on the kinetics of σ phase formation in alloys at the equiatomic Cr/Fe ratio with fine- and coarse-grained structures was studied by [2000Bla] using ^{57}Fe Mössbauer spectroscopy. It was found that the addition of 0.2 at.% Al slightly accelerated the kinetics in the coarse-grained samples, and practically did not affect in the fine-grained samples. On the other hand, doping with 1 at.% Al resulted in a significant retardation of the σ phase formation both in the fine-grained samples as well as in the coarse-grained samples.

DOI: 10.1007/978-3-540-69761-9_5

Table 1. Investigations of the Al-Cr-Fe Phase Relations, Structures and Thermodynamics

Reference	Method/Experimental Technique	Temperature/Composition/Phase Range Studied
[1932Tai1]	Thermal analysis	94-100 at.% Al
[1932Tai2]	Thermal analysis	94-100 at.% Al
[1935Gru]	Thermal analysis	$Cr_{29.97}Fe_{59.86}Al_{10.17}$
[1940Kor1]	Thermal analysis	Whole range of compositions
[1940Kor2]	Thermal analysis	Whole range of compositions
[1945Kor]	Thermal analysis	Whole range of compositions
[1946Kor]	Optical microscopy, thermal analysis	800-1300°C, whole range of compositions
[1951Pra]	Optical microscopy, X-ray diffraction, thermal analysis, chemical analysis	425, 600°C, the Al rich corner
[1953Cas]	Optical microscopy, thermal analysis	0-50 at.% Al
[1954Chi]	Thermal analysis, optical microscopy	0-50 at.% Al
[1955Tag]	X-ray diffraction, optical microscopy, thermal analysis	500-1000°C; 20-35 at.% Cr, 0-4 at.% Al
[1958Chu]	X-ray diffraction, optical microscopy, thermal analysis	600-1000°C, whole range of compositions
[1958Tag]	X-ray diffraction, optical microscopy, thermal analysis	500-1000°C; 20-35 at.% Cr, 0-4 at.% Al
[1960Zol1] [1960Zol2]	X-ray diffraction, optical microscopy, thermal analysis	Al rich corner
[1968Bul] [1969Bul1] [1969Bul2]	X-ray diffraction, dilatometry	≤ 1000°C; 0-25 at.% Cr, 50-100 at.% Fe
[1969Kal]	Neutron diffraction	700-1000°C, $Cr_{2-x}Fe_xAl$ (x = 0 to 0.25)
[1969Sel]	High-temperature X-ray diffraction	≤ 1000°C; 0-25 at.% Cr, 50-100 at.% Fe
[1970Koz1] [1970Koz2] [1970Koz3]	Optical microscopy, thermal analysis, X-ray diffraction	0-70 mass% Fe, 0-40 mass% Al
[1972Kaj]	X-ray diffraction, neutron diffraction	25 at.% Al
[1974Niz]	X-ray diffraction, neutron diffraction	25 at.% Al
[1975Lit]	X-ray diffraction, neutron diffraction	25 at.% Al
[1976Vla]	X-ray diffraction, optical microscopy	490°C, $Cr_{21.3}Fe_{68.3}Al_{10.4}$
[1977Ost]	Solution calorimetry	1550-1600°C; aluminium solutions in $Fe_{70}Cr_{30}$ (at.%) melt

(*continued*)

DOI: 10.1007/978-3-540-69761-9_5

Reference	Method/Experimental Technique	Temperature/Composition/Phase Range Studied
[1977Tys]	X-ray diffraction, neutron diffraction	25 at.% Al
[1982Yea]	X-ray diffraction, optical microscopy	400°C, Al rich corner
[1983Bus]	X-ray diffraction	800°C, $CrFe_2Al$
[1988Man]	X-ray diffraction	850-900°C, ≥ 92 at.% Al
[1988Sch]	Angular dispensive X-ray diffraction (ADXD), TEM, energy dispersive X-ray diffraction (EDXD)	50 at.% Al
[1989Law1]	X-ray diffraction, DTA, TEM, electron diffraction	86 at.% Al
[1989Law2]	X-ray diffraction, DTA	86 at.% Al
[1989Man]	X-ray diffraction	≥ 80 at.% Al
[1990Ioa]	X-ray diffraction, optical microscopy	$Cr_{2.13}Fe_{0.5}Al_{97.37}$
[1991Tre]	X-ray diffraction, optical microscopy, DTA	≤ 1800°C, Cr-FeAl section
[1992Hil]	Knudsen effusion mass spectrometry	1040-1283°C, $Cr_{19.96}Fe_{70.72}Al_{9.32}$
[1995Sta]	X-ray diffraction, DTA, EDX	$Cr_8Fe_6Al_{86}$
[1995Sui]	X-ray diffraction, TEM	$CrFe_2Al_{12}$
[1997Pal]	Metallography, EMPA, X-ray diffraction studies	1000°C, 40-100 at.% Al
[1997Rud]	DSC, EMPA	20-700°C, Fe_3Al - 5 at.% Cr
[1997Sat]	X-ray diffraction, neutron diffraction, Mössbauer studies	10-300 K, $Cr_xFe_{3-x}Al$
[1997Sui]	X-ray diffraction, HREM	$CrFe_2Al_{12}$
[1998Lia]	Electron diffraction, HREM	$CrFe_2Al_{12}$
[1998Sun]	Neutron diffractometry, X-ray diffraction, TEM	500°C, Fe_3Al + 5 at.% Cr
[1999Sui]	Electron diffraction, TEM	$CrFe_2Al_{12}$, Cr_2FeAl_{12}
[1999Wit]	TEM, EDX, atomic force microscopy (AFM), lateral force microscopy (LFM)	0-18 at.% Cr, 7-25 at.% Al
[2000Bla]	EMPA, Mössbauer spectroscopy	1200°C, ≤ 1 at.% Al
[2000Dem]	DTA, TEM, SEM, EMPA	$Cr_{11}Fe_8Al_{81}$
[2000Mo1]	High-resolution transmission electron microscopy, X-ray diffraction	$Cr_{10.71}Fe_{8.68}Al_{80.61}$
[2000Mo2]	TEM, HREM, X-ray diffraction	$CrFe_2Al_{12}$
[2000Spi]	X-ray diffraction, TEM	9.3-18 at.% Cr, 7.6-25.5 at.% Al

(*continued*)

DOI: 10.1007/978-3-540-69761-9_5

Reference	Method/Experimental Technique	Temperature/Composition/Phase Range Studied
[2001Alo]	X-ray diffraction, Mössbauer spectroscopy	830°C, $Cr_xFe_{0.7-x}Al_{0.3}$ ($x \leq 0.35$)
[2001Dem]	DTA, TEM, SEM, EMPA	$Cr_{11}Fe_8Al_{81}$
[2001Rod]	X-ray diffraction, SEM, TEM, DSC	$Cr_5Fe_5Al_{90}$
[2002Dem1]	X-ray diffraction, TEM	900-1050°C, $Cr_{19.5}Fe_8Al_{72.5}$, $Cr_{21.5}Fe_6Al_{72.5}$, $Cr_{23.7}Fe_{9.1}Al_{67.6}$
[2002Dem2]	X-ray diffraction, TEM	980°C, 1060°C, $Cr_{16.5}Fe_6Al_{77.5}$, $Cr_{28}Fe_7Al_{65}$
[2003Zou]	High-resolution transmission electron microscopy, electron diffraction	$CrFe_2Al_{12}$
[2004Wu]	X-ray Laue back reflection technique	400°C, $Cr_3Fe_{57}Al_{40}$
[2005Dem]	X-ray diffraction, TEM, high resolution microscopy	$Cr_{23.3}Fe_{9.1}Al_{67.6}$, $Cr_{19.5}Fe_8Al_{72.5}$
[2006Dem]	TEM, electron diffraction	65-81 at.% Al

Table 2. Crystallographic Data of Solid Phases

Phase/Temperature Range [°C]	Pearson Symbol/ Space Group/ Prototype	Lattice Parameters [pm]	Comments/References
(Al) ≤ 660.452	*cF*4 $Fm\bar{3}m$ Cu	a = 404.88	pure Al, T = 24°C [V-C]
$Cr_xFe_yAl_{1-x-y}$			x = 0 to 0.00375 [2006Cor] y = 0 to 0.004 [2006MSIT]
α, (Cr,αδFe) (Cr) ≤ 1863	*cI2* $Im\bar{3}m$ W	a = 288.4	pure Cr, T = 27°C [V-C] x = 0 to 0.46 [V-C2]
(αFe)(r) ≤ 912		a = 286.65 a = 286.60	pure Fe, T = 27°C [V-C] pure Fe, room temperature [1961Lih, 1993Oka]
(δFe)(h_2) 1538 - 1394		a = 293.80	[1993Oka]
$Cr_xFe_{1-x-y}Al_y$		a = 287.67 a = 288.55 a = 289.2	x = 0, y = 0 to 0.46 [1980Sch] x = 0, y = 0.06 [1961Lih, 1993Oka] x = 0, y = 0.105 [1961Lih, 1993Oka]

(*continued*)

DOI: 10.1007/978-3-540-69761-9_5

Phase/Temperature Range [°C]	Pearson Symbol/ Space Group/ Prototype	Lattice Parameters [pm]	Comments/References
		a = 289.99	x = 0, y = 0.155 [1961Lih, 1993Oka]
			x = 0, y = 0.19 [1961Lih, 1993Oka]
			Quenched from 250°C [1958Tay, 1993Oka]:
		a = 288.13	x = 0, y = 0.0985
		a = 288.96	x = 0, y = 0.141
		a = 289.43	x = 0, y = 0.177
		a = 289.59	x = 0, y = 0.188
			Quenched from 1000°C (100 h) [1997Pal]:
		a = 2912.0	x = 0.028, y = 0.444
		a = 2971.4	x = 0.556, y = 0.444
γ, (γFe)(h_1)	*cF*4	a = 366.60	pure Fe, T = 1167°C [1993Oka]
1394 - 912	$Fm\bar{3}m$	a = 364.67	T = 915°C [Mas2]
	Cu		
$Fe_{1-x}Al_x$			x = 0 to 0.013 [1993Oka]
Cr_yFe_{1-y}			y = 0 to 0.119 [Mas2]
$Cr_xFe_{1-x-y}Al_y$			y = ~0.04 at x = 0.083, T = 1200°C [1946Kor]
			y = 0.06 at x = 0.083, T = 1100°C [1946Kor]
			y = 0.077 at x = 0.082, T = 1000°C [1946Kor]
α_2, FeAl	*cP*8		x = 0.22 at T = 600°C to x = 0.545 at
≤ 1310	$Pm\bar{3}m$		T = 1102°C [1993Oka]
$Fe_{1-x}Al_x$	CsCl	a = 289.48	x = 0.345 [1961Lih, 1993Oka]
		a = 289.60	x = 0.389 [1961Lih, 1993Oka]
		a = 289.86	x = 0.422 [1961Lih, 1993Oka]
		a = 290.50	x = 0.475 [1961Lih, 1993Oka]
		a = 290.9	x = 0.5 [1958Tay, 1993Oka]
			Quenched from T = 500°C [1997Kog]:
		a = 289.81	x = 0.397
		a = 291.01	x = 0.509
			Quenched from T = 250°C [1958Tay]:
		a = 289.53	x = 0.362
		a = 289.66	x = 0.383
		a = 289.77	x = 0.409
		a = 290.17	x = 0.438
$(Fe,Cr,Al)_1(Al,Cr,Fe)_1$		a = 291.9	30 at.% Cr, 40 at.% Fe [2001Alo]
		a = 291.7	35 at.% Cr, 35 at.% Fe [2001Alo]

(*continued*)

DOI: 10.1007/978-3-540-69761-9_5

Phase/Temperature Range [°C]	Pearson Symbol/ Space Group/ Prototype	Lattice Parameters [pm]	Comments/References
α_1, Fe_3Al	*cF*16		x = 0.225 to 0.365 [V-C]
≤ 547	$Fm\bar{3}m$	a = 579.23	x = 0.25 [V-C]
$Fe_{1-x}Al_x$	BiF_3	a = 579.30	x = 0.247 [1961Lih, 1993Oka]
		a = 579.28	x = 0.263 [1961Lih, 1993Oka]
		a = 579.30	x = 0.28 [1961Lih, 1993Oka]
		a = 579.24	x = 0.307 [1961Lih, 1993Oka]
		a = 578.92	x = 0.317 [1961Lih, 1993Oka]
			Quenched from T = 250°C [1958Tay, 1993Oka]:
		a = 579.30	x = 0.231
		a = 579.28	x = 0.237
		a = 579.18	x = 0.243
		a = 579.30	x = 0.254
		a = 579.32	x = 0.261
		a = 579.38	x = 0.272
		a = 579.32	x = 0.283
		a = 579.06	x = 0.295
		a = 578.94	x = 0.315
		a = 578.96	x = 0.34
		a = 578.86	x = 0.35
$(Fe,Cr,Al)_3(Al,Cr,Fe)_1$			$CrFe_2Al$ alloy, annealed at T = 527°C
		a = 578.86	[1983Bus]
ε, Fe_2Al_3	*cI*16 (?)		x ≈ 0.58 to 0.65 [1993Oka]
1232 - 1102	-		
$Fe_{1-x}Al_x$		a = 598.0	x = 0.61 [1934Osa]
$FeAl_2$	*aP*18		x = 0.655 to 0.670 [V-C]
≤ 1156	*P*1	a = 488	T = 900°C [V-C]
$Fe_{1-x}Al_x$	$FeAl_2$	b = 646	
		c = 880	
		α = 91.70°	
		β = 73.3°	
		γ = 96.90°	
		a = 487.8	x = 0.669; ρ = 4200 kg·m^{-3}
		b = 646.1	[1973Cor]
		c = 880.0	
		α = 91.75°	
		β = 73.27°	
		γ = 96.89°	
	A-base-centred pseudomono-clinic	a = 759.4	[1978Bas]
		b = 1688.6	
		c = 486.2	
		α = 89.55°	
		β = 122.62°	
		γ = 90.43°	

(*continued*)

DOI: 10.1007/978-3-540-69761-9_5

Phase/Temperature Range [°C]	Pearson Symbol/ Space Group/ Prototype	Lattice Parameters [pm]	Comments/References
	Triclinic	a = 487.8	x = 0.666, quenched from T = 1000°C
	$P1$	b = 646.1	(100 h) [1997Pal]
		c = 880.0	
		α = 91.75	
		β = 73.27	
		γ = 96.89	
$(Cr_yFe_{1-y})Al_2$	Triclinic		y = 0 to 0.045, T = 1000°C [1997Pal]
	$P1$	a = 486.3	y = 0.045, quenched from T = 1000°C
		b = 645.4	(100 h) [1997Pal]
		c = 880.1	
		α = 91.92	
		β = 72.95	
		γ = 96.87	
Fe_2Al_5	$oC24$		x = 0.70 to 0.73 [1993Oka]
≤ 1169	$Cmcm$	a = 767.5	x = 0.72 [1953Sch]
$Fe_{1-x}Al_x$		b = 640.3	
		c = 420.3	
		a = 765.73	x = 0.7145 [1986Gri]
		b = 640.87	
		c = 422.65	
		a = 765.59	x = 0.715 [1994Bur]
		b = 641.54	
		c = 421.84	
		a = 767.5	x = 0.7145, quenched from T = 1000°C
		b = 640.3	(100 h) [1997Pal]
		c = 420.3	
		a = 769.4	y = 0 to 0.062, T = 1000°C [1997Pal]
$(Cr_yFe_{1-y})_2Al_5$		b = 644.3	y = 0.062, quenched from T = 1000°C
		c = 422.7	(100 h) [1997Pal]
Fe_4Al_{13}	$mC102$		x = 0.745 to 0.766 [1993Oka]
≤ 1160	$C2/m$		Sometimes called $FeAl_3$ in the literature
$Fe_{1-x}Al_x$			x = 0.767 [1986Gri]
		a = 1548.7	
		b = 808.4	
		c = 1248.8	
		β = 107.99°	x = 0.7665 [1986Gri]
		a = 1548.3	
		b = 807.9	
		c = 1250.9	
		β = 108.11°	x = 0.766, single crystal
		a = 1548.9	[1955Bla1, 1955Bla2]
		b = 808.31	
		c = 1247.6	

(*continued*)

DOI: 10.1007/978-3-540-69761-9_5

Phase/Temperature Range [°C]	Pearson Symbol/ Space Group/ Prototype	Lattice Parameters [pm]	Comments/References
		β = 107.72° *a* = 1550.4 *b* = 807.0 *c* = 1247.2	*x* = 0.7602 [1986Gri]
		β = 107.71° *a* = 1549.2 *b* = 807.8 *c* = 1247.1	*x* = 0.76 [1994Gri]
		β = 107.69° *a* = 1550.9 *b* = 806.3 *c* = 1247.7	*x* = 0.7594 [1986Gri]
		β = 107.74° *a* = 1551.3 *b* = 805.1 *c* = 1248.6	*x* = 0.7463 [1986Gri]
		β = 107.80° *a* = 1552.7 *b* = 803.5 *c* = 1244.9	*x* = 0.7416 [1986Gri]
		β = 107.70° *a* = 1548.9 *b* = 808.3 *c* = 1247.6	*x* = 0.75, quenched from *T* = 1000°C (100 h) [1997Pal]
		β = 107.72°	From 0 to 3 at.% Cr, at 600°C [1951Pra] From 0 to 6.4 at.% Cr, from 22 to 25 at.% Fe, at 1000°C [1997Pal]
$(Fe,Cr,Al)_1(Al,Cr,Fe)_3$		*a* = 1554.3 *b* = 802.9 *c* = 1245.0	6.4 at.% Cr, 21.1 at.% Fe, quenched from 1000°C (100 h) [1997Pal]
	orthorhombic, *A*2*mm* or *Amm*2 or $A_{2/m}A_{2/m}A_{2/m}$	β = 107.47° *a* = 640 *b* = 840 *c* = 620	<< 1 at.% Cr at 23.3 at.% Fe; in the alloys (at.%) Cr_3Al_{97}, Cr_3FeAl_{96} and $Cr_3Fe_3Al_{94}$ prepared by hot extrusion of rapidly solidified powder, followed annealing at 400°C [1995Zia]
Fe_2Al_9	*mP*22 $P2_1/c$ Co_2Al_9	*a* = 869 *b* = 635 *c* = 632 β = 93.4°	Metastable 81.8 at.% Al [1977Sim, 1993Oka]
$FeAl_6$	*oC*28 $Cmc2_1$ $FeAl_6$	*a* = 744.0 *b* = 646.3 *c* = 877.0 *a* = 744 *b* = 649 *c* = 879	Metastable 85.7 at.% Al [1993Oka] [1998Ali]

(*continued*)

DOI: 10.1007/978-3-540-69761-9_5

Phase/Temperature Range [°C]	Pearson Symbol/ Space Group/ Prototype	Lattice Parameters [pm]	Comments/References
$FeAl_{4+x}$	*t***		Metastable, $0 < x < 0.4$
		$a = 884$ $c = 2160$	[1998Ali]
θ, Cr_2Al_{13} ≤ 791	*mC*104 *C2/m* V_7Al_{45}	$a = 2519.6$ $b = 757.4$ $c = 1094.9$ $\beta = 128.7°$	Room temperature, 13.5 at.% Cr [1975Ohn, 1995Aud, 2006Cor] Sometimes called $CrAl_7$ in the literature
$(Cr,Fe,Al)_2(Al,Cr,Fe)_{13}$			From 0 to 3.2 at.% Fe; 11.5 at.% Cr at 3.2 at.% Fe; cooled slowly from the liquid state [1951Pra]
ρ, Cr_2Al_{11} ≤ 941	*oC*584 *Cmcm*		16.9 to 19.2 at.% Cr [1995Aud, 2000Mah, 2006Cor] Sometimes called $CrAl_5$ in the literature
		$a = 1240$ $b = 3460$ $c = 2020$	Quenched from 920°C, 16.9 to 19.2 at.% Cr [1995Aud, 2000Mah, 2006Cor] "ϵ$CrAl_4$" [1992Wen]
$(Cr,Fe,Al)_2(Al,Cr,Fe)_{11}$		$a = 1260$ $b = 3460$ $c = 2000$	From 0 to 7.74 at.% Fe; 11.45 at.% Cr at 7.74 at.% Fe; cooled slowly from the liquid state, in equilibrium with Fe_4Al_{13} [1951Pra]
μ, $CrAl_4$ ≤ 1031 $Cr_{1-x}Al_x$	*hP*574 $P6_3/mmc$ μ$MnAl_4$		$x = 0.78$ to 0.80 [2006Cor] $y = 0.788$ to 0.794, at 800°C [1995Aud] $x = 0.791 \pm 0.003$
		$a = 1998$ $c = 2467$	[1995Aud, 2000Mah, 2006Cor] $y = 0.777 \pm 0.001$, quenched from 1000°C [2000Mah, 2006Cor]
$(Cr,Fe,Al)_1(Al,Cr,Fe)_4$		$a = 2010$ $c = 2480$ $a = 2146.9$ $c = 1634$ $a = 2165.1$ $c = 1644.9$	From 0 to 11.9 at.% Fe, $T = 1000$°C [1997Pal] at 10.9 at.% Fe, 19.1 at.% Cr, quenched from 1000°C (100 h) [1997Pal] The $Cr_{19.9}Fe_{75.0}Al_{5.1}$ sample quenched from 1000°C (100 h) [1997Pal]
i, $CrAl_4$ (or $CrAl_5$)	icosahedral	-	In melt spun alloys Al-Cr at 8 to 13 at.% Cr; by decomposition of amorphous of 20 at.% Cr, metastable [1998Mur]
ζ_1, Cr_4Al_9 (h) $Cr_{1-x}Al_x$	*cI*52 $I\bar{4}3m$ Cu_4Al_9	$a = 912.3$	$x \approx 0.55$ to 0.69 [Mas2] $x = 0.71$ at Al rich border, quenched from $T = 920$°C [1995Aud]

(*continued*)

DOI: 10.1007/978-3-540-69761-9_5

Phase/Temperature Range [°C]	Pearson Symbol/ Space Group/ Prototype	Lattice Parameters [pm]	Comments/References
ζ_2, Cr_4Al_9 (r) $Cr_{1-x}Al_x$	*hR*156 $R\bar{3}m$ Cr_4Al_9		x = 0.650 to 0.672 [Mas2]
		a = 1291 c = 1567.7	In the alloy $Cr_{15}Fe_{15}Al_{70}$ quenched from 1000°C (100 h) [1997Pal]
$(Cr,Fe,Al)_4(Al,Cr,Fe)_9$			From 29 to 39 at.% Cr, from 0 to 9.6 at.% Fe (or to 12.5 at.% Fe estimated), T = 1000°C [1997Pal]
		a = 1284.7 c = 1545.9	29 at.% Cr, 9.6 at.% Fe, quenched from 1000°C (100 h) [1997Pal]
γ_1, Cr_5Al_8(h) ≥ 1100 (?)	*cI*52 $I\bar{4}3m$ Cu_5Zn_8	a = 904.7 to 910.4	30.0 to 42.0 at.% Cr, quenched from liquid [1989Ell]
γ_2, Cr_5Al_8(r) ≤ 1100 (?) $Cr_{1-x}Al_x$	*hR*78 $R\bar{3}m$ Cr_5Al_8	a = 1271.9 c = 793.6	[1994ICD], No. 29-15
		a = 1276.5 to 1271.5 c = 795.4 to 782.8	x = 0.58 to 0.65 [1989Ell]
		a = 1272.8 c = 794.2	[1977Bra]
$(Cr,Fe,Al)_5(Al,Cr,Fe)_8$			37 to 40 Cr, 0 to 32.5 Fe (at.%) T = 1000°C [1997Pal]
		a = 1267.0 c = 790.0	6 at.% Fe, quenched from 1000°C (100 h) [1997Pal]
		a = 1258.4 c = 785.0	18.5 at.% Fe, quenched from 1000°C (100 h) [1997Pal]
		a = 1255.4 c = 783.0	24 at.% Fe,quenched from 1000°C (100 h) [1997Pal]
		a = 1254.0 c = 782.0	25.5 at.% Fe, quenched from 1000°C (100 h) [1997Pal]
		a = 1253.0 c = 779.0	5 at.% Fe, quenched from 1000°C (100 h) [1997Pal]
η, Cr_2Al < 910 $(Cr_{1-x}Fe_x)_2Al$	*tI*6 *I*4/*mmm* $MoSi_2$		~65.5 to 71.4 at.% Cr [1998Mur]
		a = 300.45 c = 864.77	[1937Bra, 1998Mur]
		a = 300.5 ± 0.1 c = 864.9 ± 0.1	[1989Ell]
		a = 300.1 to 299.0 c = 864.7 to 865.9	$0 \le x \le 0.25$, annealed at 700 to 1000°C [1969Kal]
		a = 299.5 c = 865.8	x = 0.025

(*continued*)

DOI: 10.1007/978-3-540-69761-9_5

Phase/Temperature Range [°C]	Pearson Symbol/ Space Group/ Prototype	Lattice Parameters [pm]	Comments/References
		a = 298.8 c = 867.1 a = 298.4 c = 867.5 a = 298.0 c = 867.6 a = 297.7 c = 868.0	x = 0.045 x = 0.075 x = 0.085 x = 0.120
X ≤ 400	Cr_5Al_3 or Cr_3Al superlattice	-	Possibly metastable [1998Mur] ~75 to ~80 at.% Cr [1981Bro, 1981Ten]
T	-	-	In quenched alloys Al-Cr at 60 to 100 at.% Cr [2000Sha1, 2000Sha2]
σ, CrFe 830 - 440	*tP*30 $P4_2/mnm$ CrFe	a = 879.95 c = 454.42	44.5 to 50.0 at.% Cr [V-C]
* ν	$P6_3/m$	a = 4068.0 ± 0.07 c = 1254.6 ± 0.01 atoms/cell = 1184.56 a = 4000 c = 1240	$Cr_{10.71}Fe_{8.68}Al_{80.61}$ single crystal, elicited from ingot after inductive melting followed cooling in sand bath [2000Mo2]. Sometimes called "H-CrFeAl". $Cr_{11}Fe_8Al_{81}$ together with κ-CrFeAl in as-cast $CrFe_2Al_{12}$ alloy [1999Sui]
* "κ-CrFeAl"	hexagonal, κ-$Cr_{18}Ni_6Al_{76}$	-	In as-cast $CrFe_2Al_{12}$ alloy together with ν [1999Sui]
* "O-CrFeAl"	orthorhombic body-centered	a = 1230 b = 1240 c = 3070	In as-cast $Cr_{11}Fe_8Al_{81}$ alloy together with O_1-CrFeAl and $C_{3.1}$-CrFeAl [2000Dem]. In as-cast Cr_2FeAl_{12} alloy together with H-CrFeAl and M-CrFeAl [1997Sui, 1999Sui] In as-cast $CrFe_2Al_{12}$ alloy [1998Lia]
* "O_1-CrFeAl"	orthorhombic base-centered or primitive	a = 3250 b = 1220 c = 2360	In as-cast $Cr_{11}Fe_8Al_{81}$, $Cr_{16.5}Fe_6Al_{77.5}$ and $Cr_{21.5}Fe_6Al_{72.5}$ alloys together with O-CrFeAl and $C_{3.1}$-CrFeAl [2000Dem, 2001Dem]
* "O_2-CrFeAl"	orthorhombic	a = 1990 b = 1240 c = 2320	In as-cast $Cr_{19.5}Fe_8Al_{72.5}$ alloy together with O-CrFeAl [2001Dem]

(*continued*)

DOI: 10.1007/978-3-540-69761-9_5

Phase/Temperature Range [°C]	Pearson Symbol/ Space Group/ Prototype	Lattice Parameters [pm]	Comments/References
* "$C_{3.1}$-CrFeAl"	orthorhombic primitive [1988Ten]	a = 3270 b = 1250 c = 2380	In as-cast $Cr_{11}Fe_8Al_{81}$ alloy together with O_1-CrFeAl [2000Dem]
* "M-CrFeAl"	monoclinic	a = 3310 b = 1230 c = 2480 β = 112°	In as-cast $CrFeAl_{12}$ alloy [1998Lia]
		-	In as-cast alloy Cr_2FeAl_{12} together with O-CrFeAl and H-CrFeAl [1997Sui, 1999Sui]
* *i*, $Cr_{12\pm1}Fe_{12\pm1}Al_{75\pm0.5}$	simple icosahedral-type	-	rapid solidification by centrifugal atomization followed extrusion at 340°C [1995Zia]
		a_{6D}= 654.2 ± 0.2	In $Cr_8Fe_6Al_{86}$, rapid solidification by melt spinning [1995Sta]

Table 3. Coordinates of the ((γFe)+αFe))/(αFe) Surface of the γ-loop [1946Kor, 1991Gho]

Temperature [°C]	Al		Cr	
	(mass%)	(at.%)	(mass%)	(at.%)
1200	1.7	3.4	4.0	4.2
1100	2.2	4.4	4.0	4.2
	3.0	6.0	8.0	8.3
1000	2.9	5.8	4.0	4.2
	3.9	7.7	8.0	8.2
	1.9	3.8	12.0	12.5
	3.8	7.5	4.0	4.1

Table 4. Heat Treatment Schedule for Different Alloys by [1958Chu]

Alloys with > 50 mass% Fe		Alloys with > 10 mass% Al	
Temperature [°C]	Time [h]	Temperature [°C]	Time [h]
750	720	900	100
700	1000	750	200
650	720	700	500
600	720	650	250
500	2000	600	250
480	2200	500	1200

DOI: 10.1007/978-3-540-69761-9_5

Table 5. Partial Pressures of Cr, Fe and Al over the Alloy Cr-75.4Fe-4.8Al (mass%) and Temperature Range of the Measurements ΔT [1992Hil]. Errors of A and B Values are Standard Deviations. Errors of p_i Values are Probable Overall Errors

Gaseousspecies i	p_i [Pa]at 1500 K	ΔT [K]	$\ln p_i = -A \cdot 10^4/T+B$	
			A	B
Cr	$1.6 \cdot 10^{-2} \pm 14$ %	1313-1556	4.298 ± 0.015	24.51 ± 0.05
Fe	$7.5 \cdot 10^{-3} \pm 15$ %	1313-1556	4.622 ± 0.022	25.92 ± 0.12
Al	$4.5 \cdot 10^{-3} \pm 43$ %	1313-1556	4.501 ± 0.071	24.50 ± 0.56

Table 6. Chemical Activities a_i, Excess Chemical Potentials μ_i^E, and Partial Excess Enthalpies H_i^E of the Components in the Alloy Cr-75.4Fe-4.8Al (mass%) for a Temperature of 1500 K [1992Hil]. Errors are Probable Overall Errors

Alloy Component i	a_i (at 1500 K)	μ_i^E (at 1500 K) [kJ·mol^{-1}]	H_i^E (at 1450 K) [kJ·mol^{-1}]
Cr	0.28 ± 0.04	4.3 ± 1.9	27.6 ± 8.8
Fe	0.50 ± 0.07	–4.4 ± 2.0	13.7 ± 7.5
Al	$(3.3 \pm 1.4) \cdot 10^{-3}$	–42.0 ± 7.0	–66.0 ± 8.6

Table 7. Investigations of the Al-Cr-Fe Materials Properties

Reference	Method/Experimental Technique	Type of Property
[1940Kor2]	Electrical resistivity measurements	Electrical resistivity
[1946Kor]	Hardness, electrical resistivity measurements, dilatometry	Hardness, electrical resistivity, elongation
[1955Tag] [1958Tag]	Rockwell hardness test	Hardness
[1969Kal]	Magnetic measurements	Antiferromagnetic behaviour, Neel temperature
[1974Niz] [1975Lit]	Magnetic measurements	Magnetic atomic moment, Curie temperature, magnetic coercivity, magnetic susceptibility
[1982Nao]	Mechanical properties studies	Hardness, yield strength, tensile fracture stress
[1983Bus]	Magneto-optical Kerr rotation, magnetic measurements (PAR vibrating sample magnetometer)	Kerr rotation angle, Curie temperature, saturation magnetization
[1985Okp]	Magnetic measurements (PAR vibrating sample magnetometer)	Ferromagnetic behavior
[1991Pra]	Mechanical properties studies	Microhardness, tensile properties
[1991Sik1]	Tensile and creep tests	Tensile ductility, yield strength, ultimate tensile strength, elongation, creep-rupture strength

(*continued*)

DOI: 10.1007/978-3-540-69761-9_5

Reference	Method/Experimental Technique	Type of Property
[1993Kni]	Mechanical properties studies	Ductility
[1995Sta]	Magnetic measurements (Faraday technique)	Magnetic susceptibility
[1996Jim]	Mechanical properties studies	Creep behavior
[1997Sat]	Magnetic measurements (magnetic balance)	Magnetization, magnetic moments
[1998Su]	Mechanical properties studies	Yield strength, ultimate tensile strength
[1998Sun]	Tensile tests (Gleeble-1500 machine), SEM, TEM, neutron diffraction, magnetic measrements	Yield strength, magnetic moment of Fe atoms
[2000Spi]	TEM, deformation tests	Compressive deformation
[2002Dem2]	Optical measurements (on spectrometers)	Reflectivity, refraction index, optical conductivity
[2002Zho]	Optical microscopy, TEM	Internal friction, damping capacity
[2004Hua]	Tensile, creep rupture tests	Yield strength, creep properties (creep rupture lifetime, grain size, ductility)
[2004Wu]	Vibrating sample magnetometer studies	Magnetization

DOI: 10.1007/978-3-540-69761-9_5

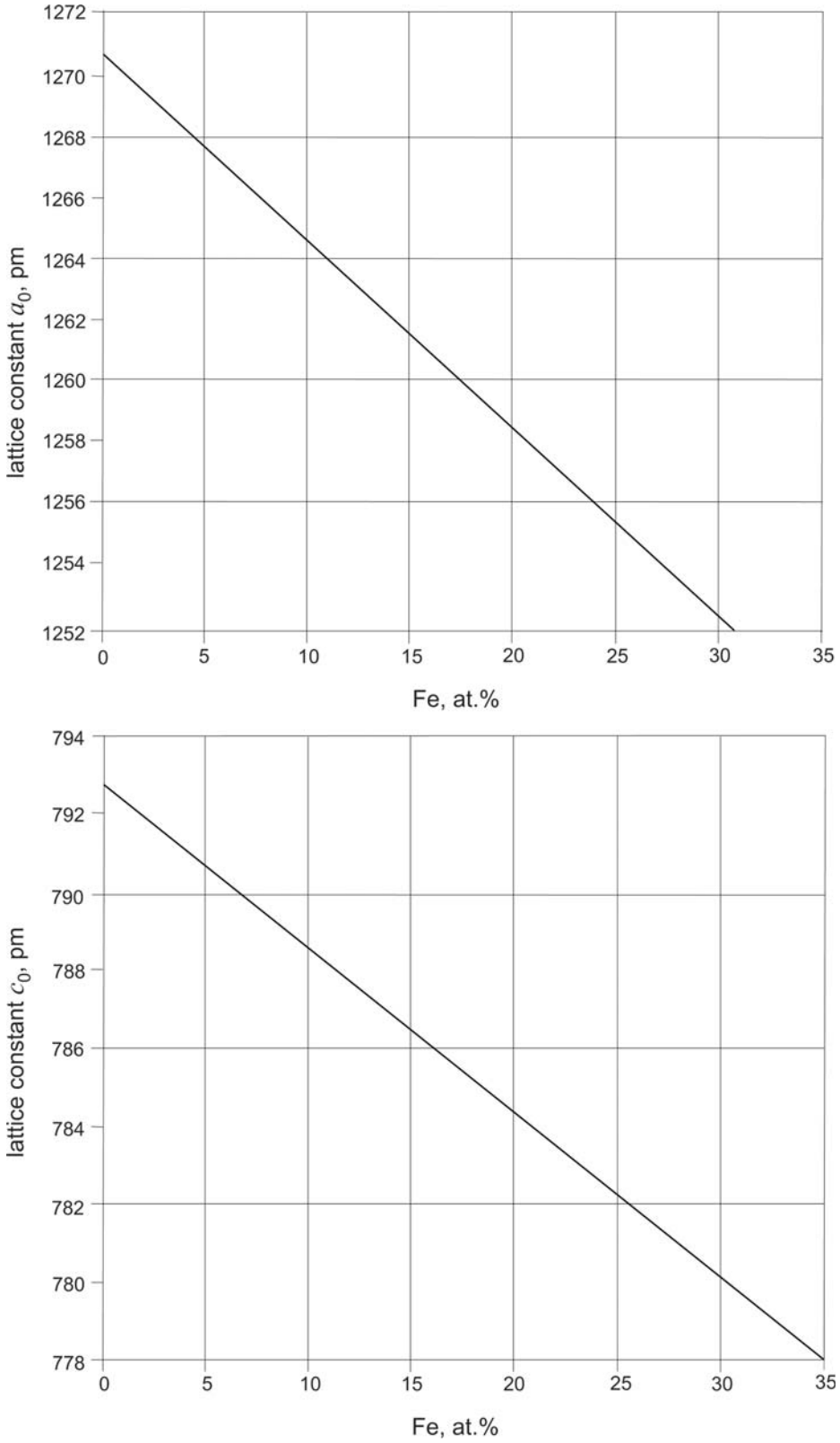

Fig. 1. Al-Cr-Fe. (a) Lattice constant a_0 of the Cr_5Al_8(r) phase *vs* Fe content. Al content is 55 to 58 at.%. (b) Lattice constant c_0 of the Cr_5Al_8(r) phase *vs* Fe content. Al content is 55 to 58 at.%

DOI: 10.1007/978-3-540-69761-9_5

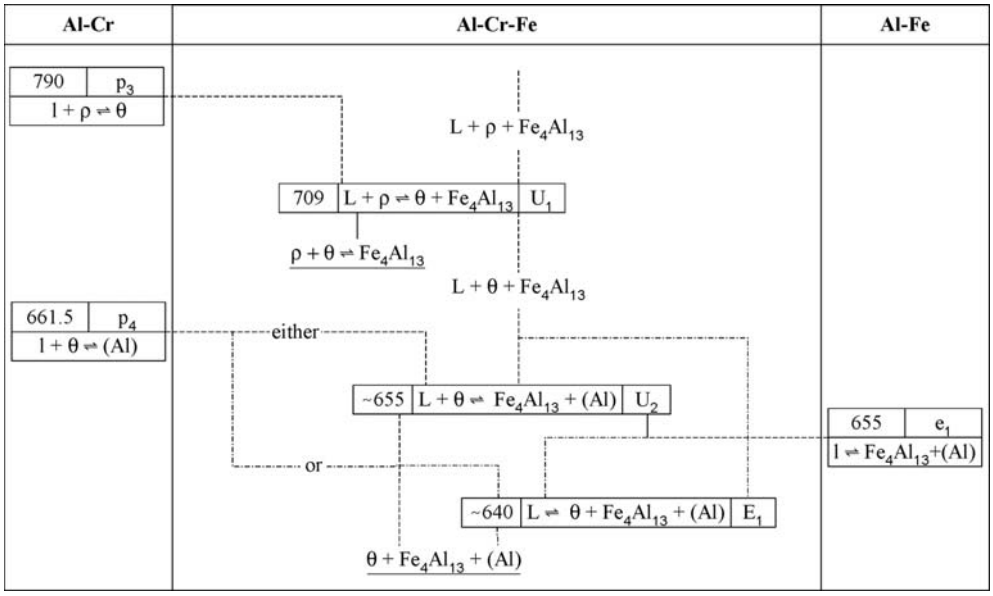

Fig. 2. Al-Cr-Fe. Partial reaction scheme of the Al rich alloys

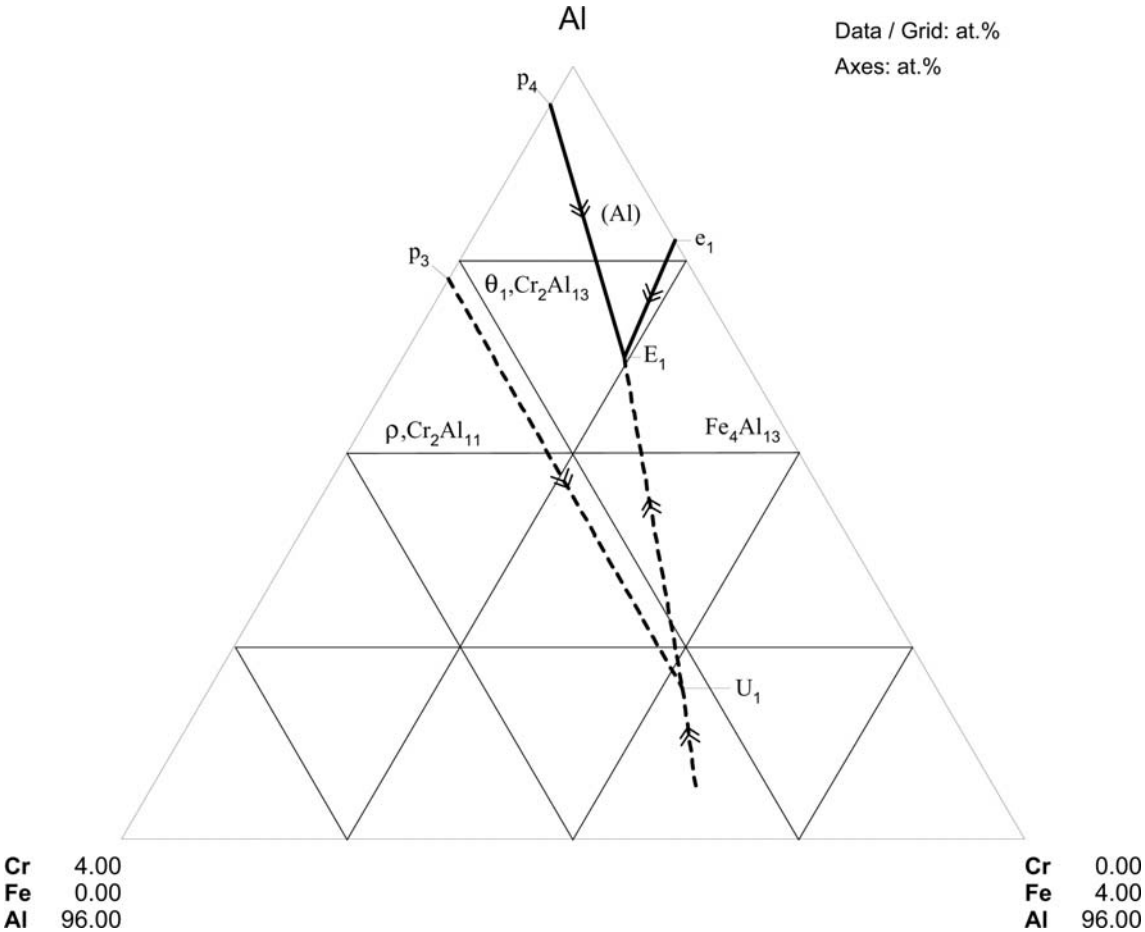

Fig. 3. Al-Cr-Fe. Liquidus surface projection of the Al corner

DOI: 10.1007/978-3-540-69761-9_5

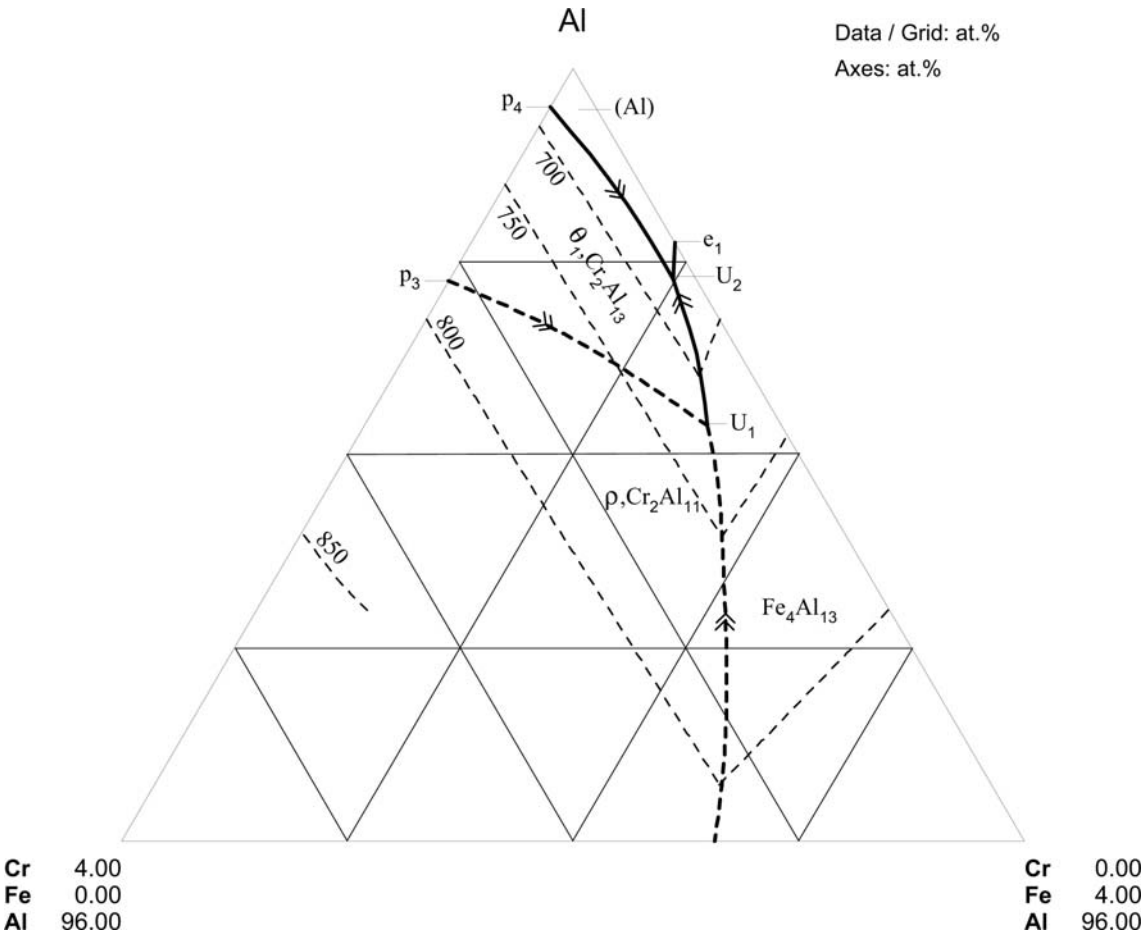

Fig. 4. Al-Cr-Fe. Calculated liquidus surface projection of the Al corner

DOI: 10.1007/978-3-540-69761-9_5

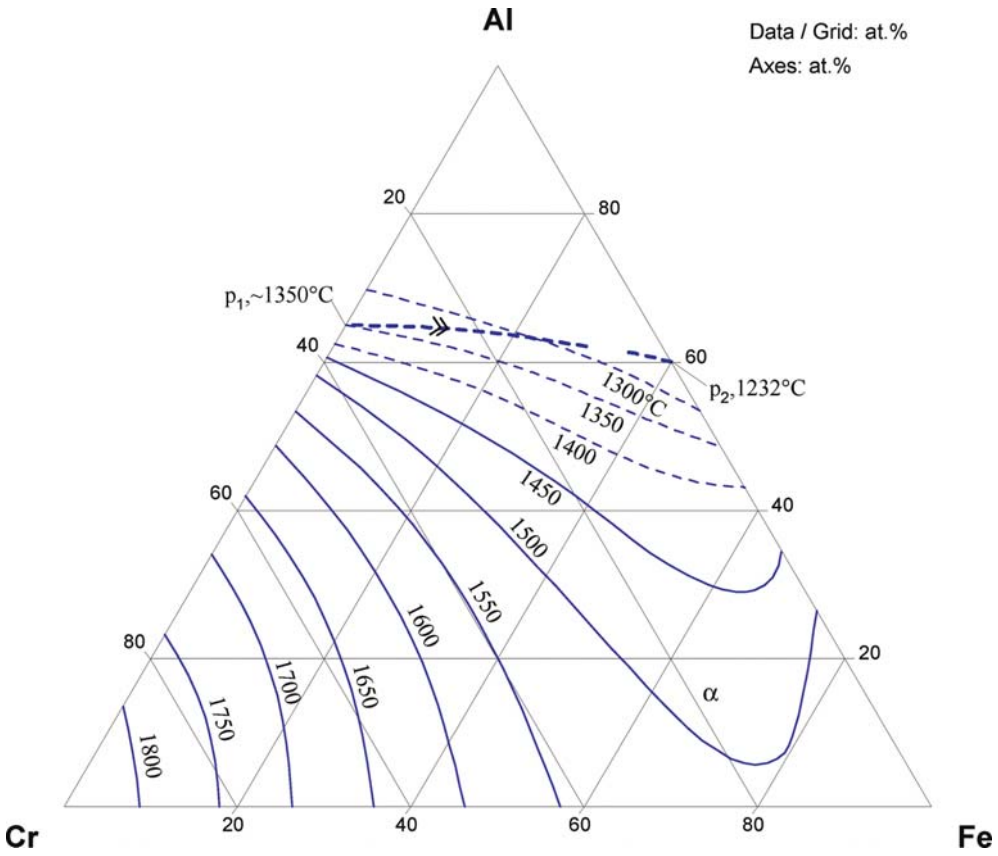

Fig. 5. Al-Cr-Fe. Partial liquidus surface projection

DOI: 10.1007/978-3-540-69761-9_5

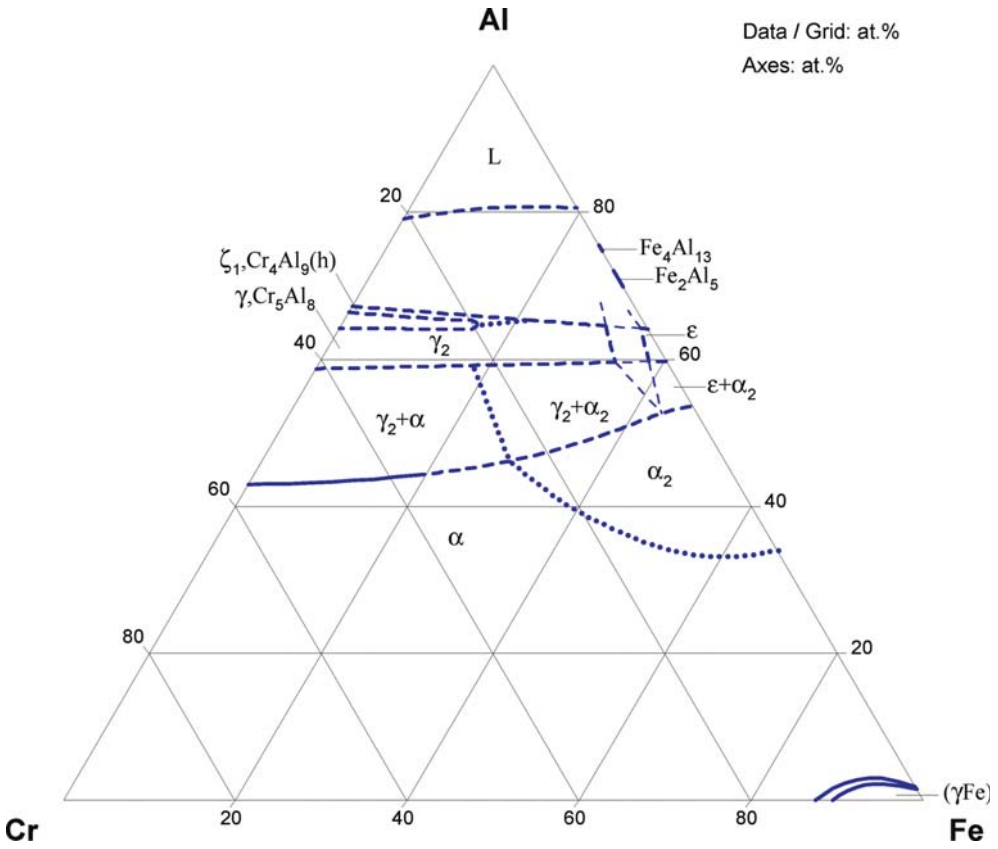

Fig. 6. Al-Cr-Fe. Isothermal section at 1150°C

DOI: 10.1007/978-3-540-69761-9_5

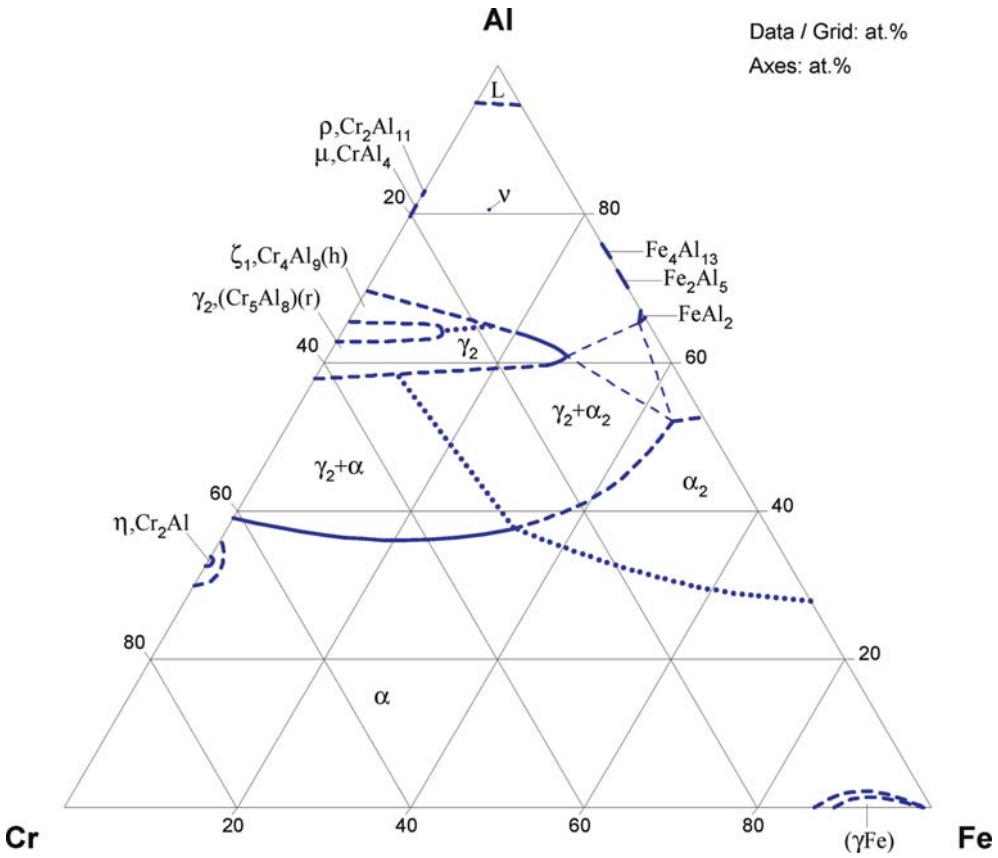

Fig. 7. Al-Cr-Fe. Isothermal section at 900°C

DOI: 10.1007/978-3-540-69761-9_5

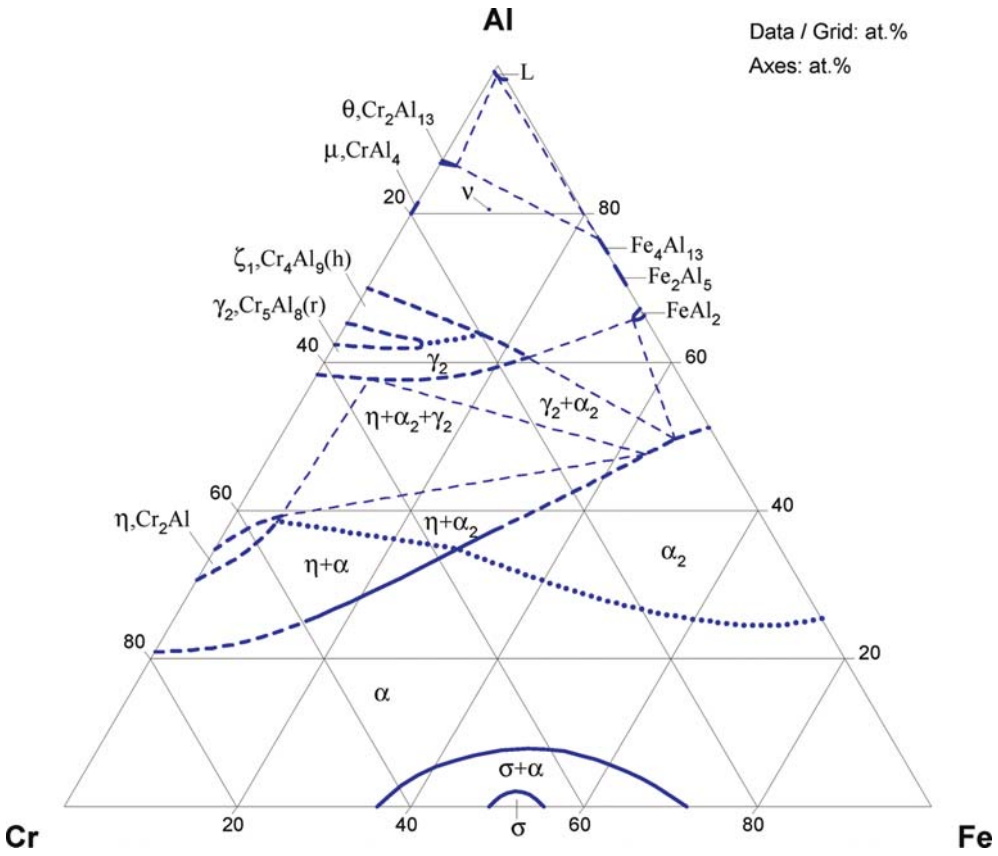

Fig. 8. Al-Cr-Fe. Isothermal section at 750°C

DOI: 10.1007/978-3-540-69761-9_5

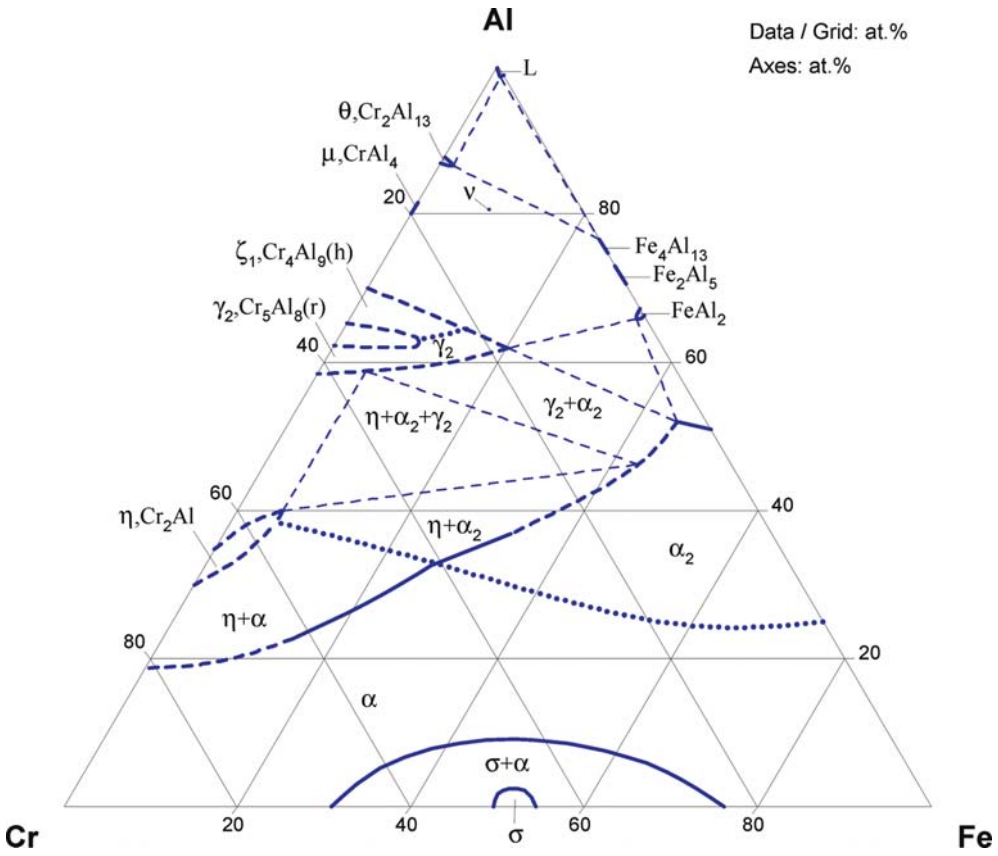

Fig. 9. Al-Cr-Fe. Isothermal section at 700°C

DOI: 10.1007/978-3-540-69761-9_5

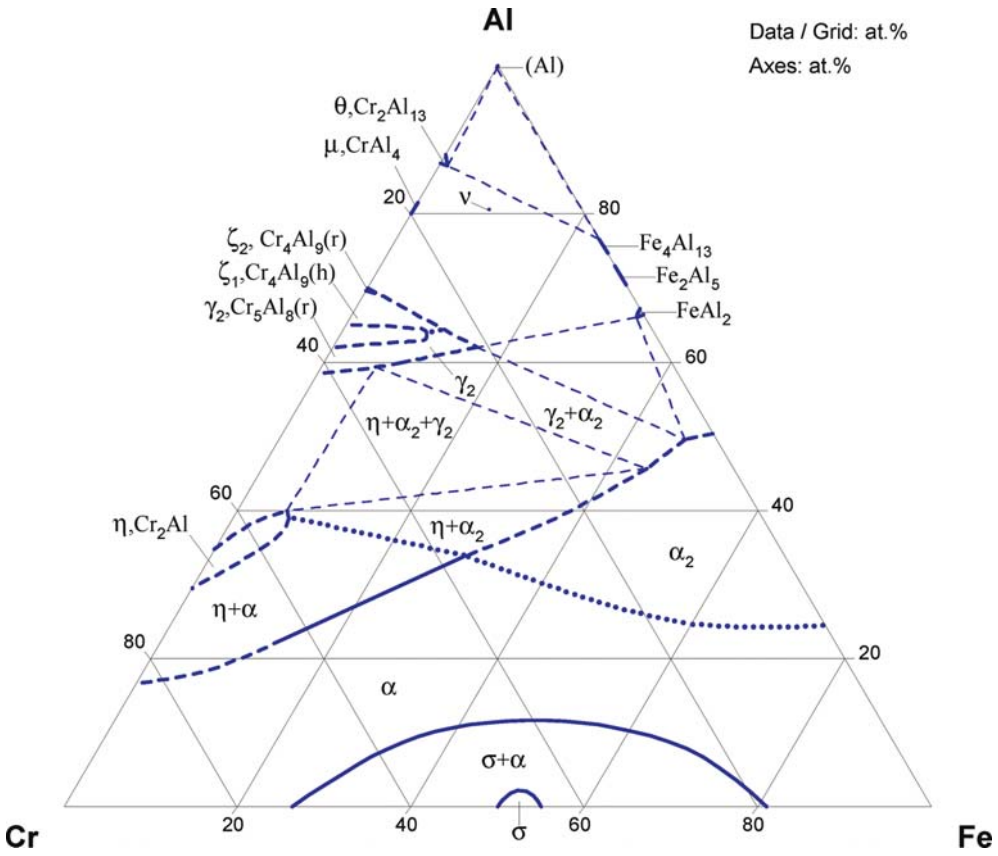

Fig. 10. Al-Cr-Fe. Isothermal section at 650°C

DOI: 10.1007/978-3-540-69761-9_5

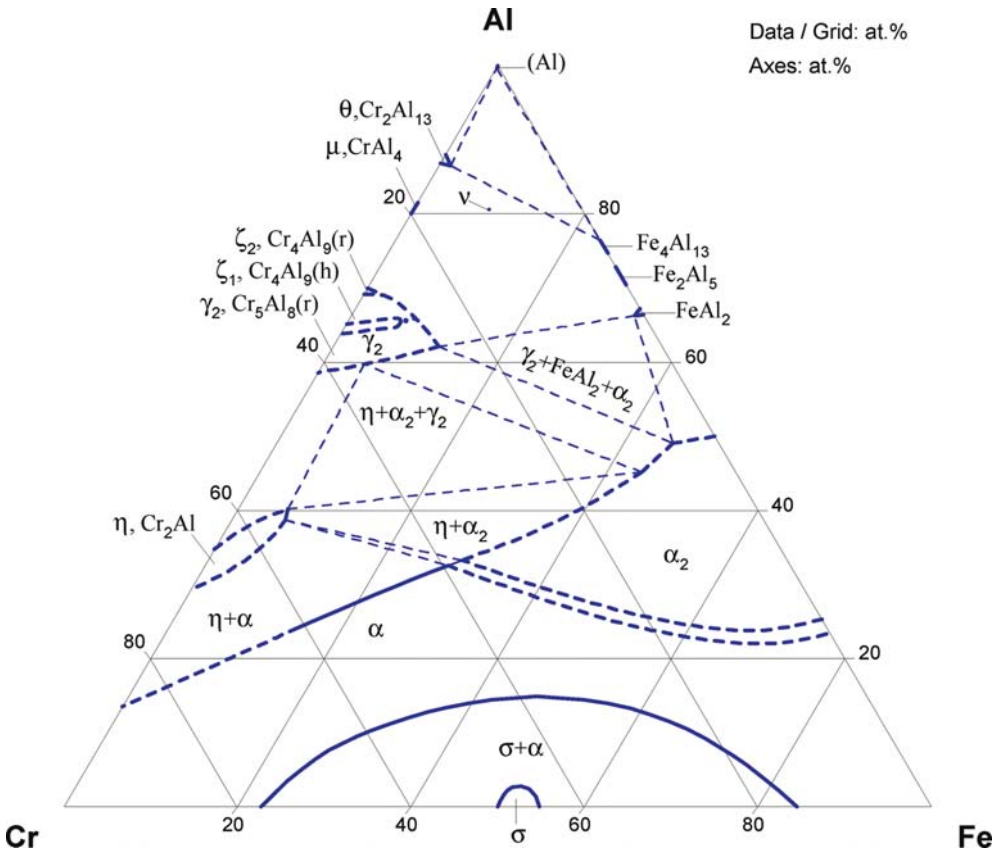

Fig. 11. Al-Cr-Fe. Isothermal section at 600°C

DOI: 10.1007/978-3-540-69761-9_5

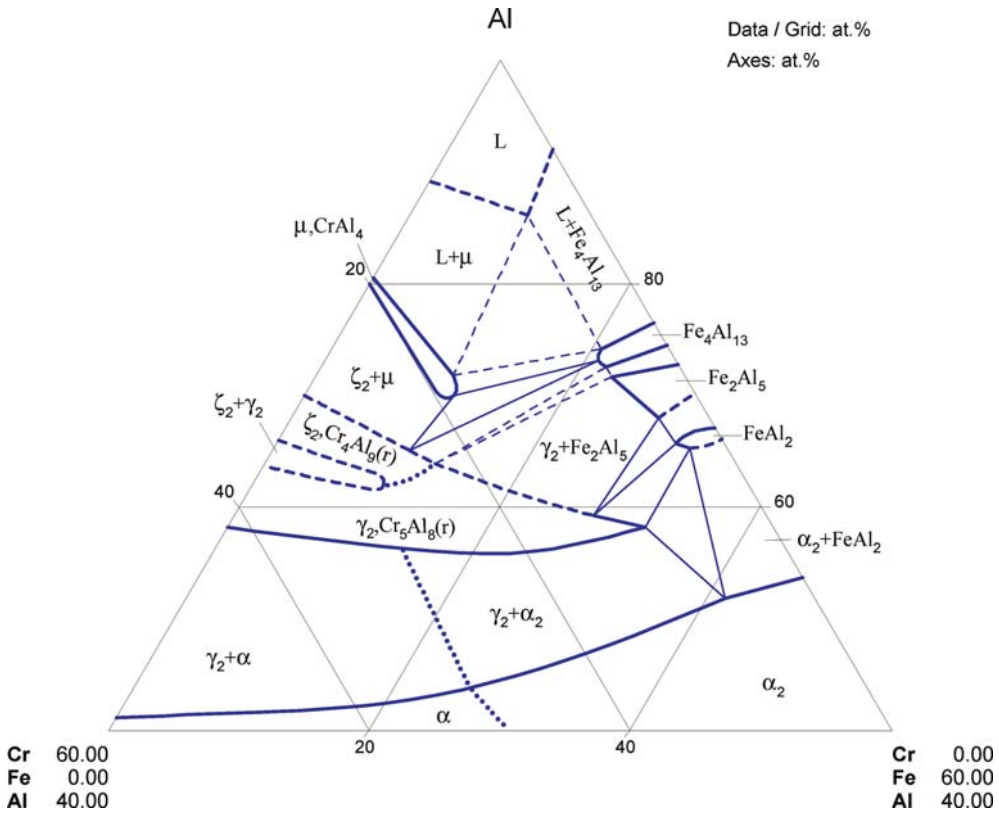

Fig. 12. Al-Cr-Fe. Partial isothermal section at 1000°C

DOI: 10.1007/978-3-540-69761-9_5

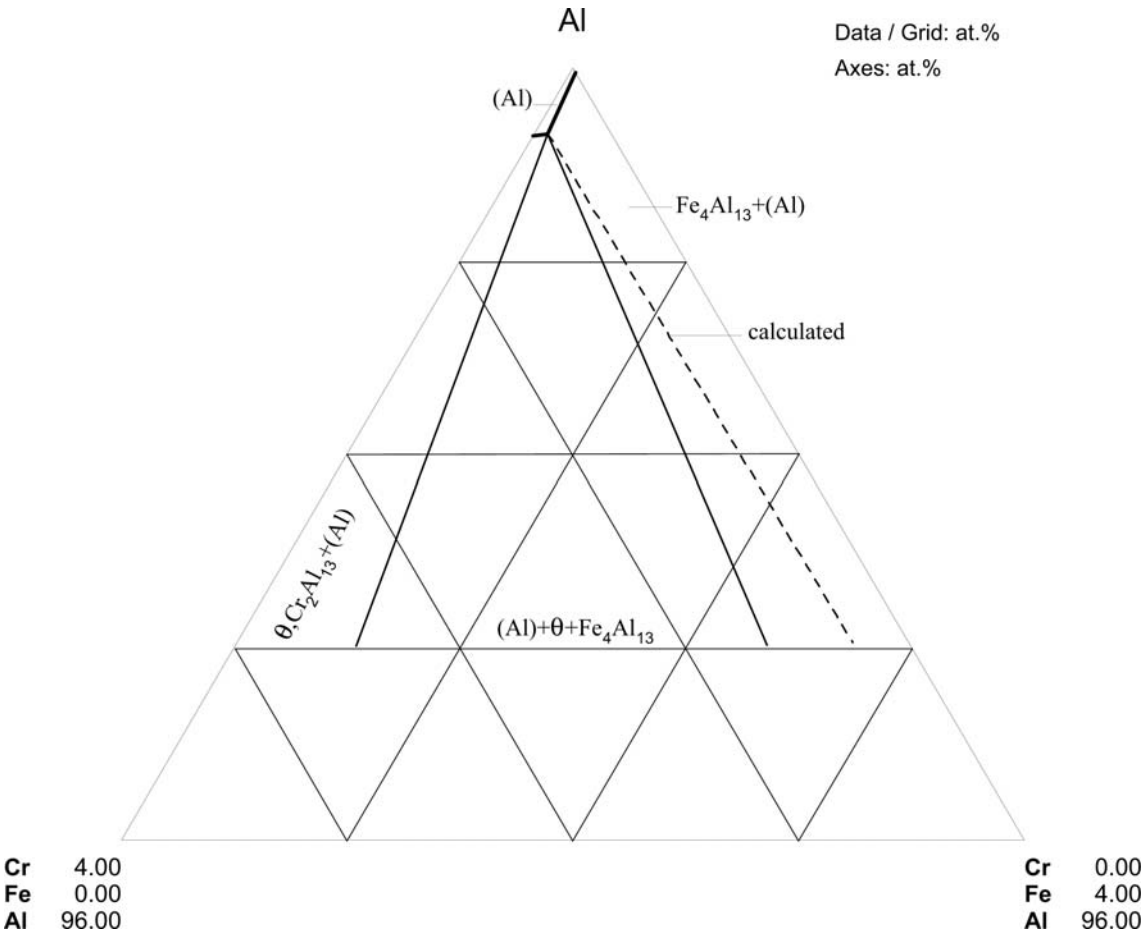

Fig. 13. Al-Cr-Fe. Partial isothermal section of the Al corner at 600°C

DOI: 10.1007/978-3-540-69761-9_5

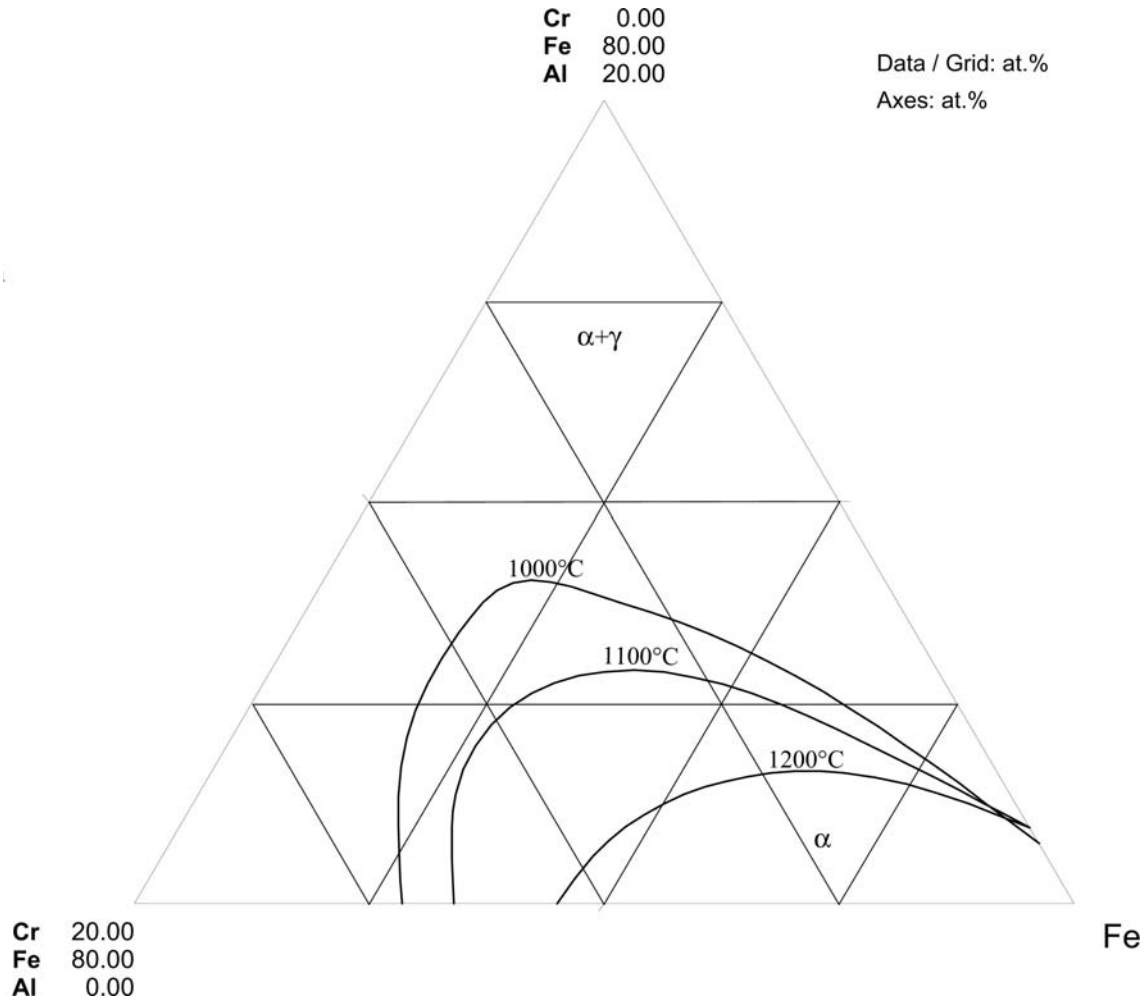

Fig. 14. Al-Cr-Fe. Isotherms of the surface ((γFe)+(αFe))/(αFe) of the γ-loop in the ternary system

DOI: 10.1007/978-3-540-69761-9_5

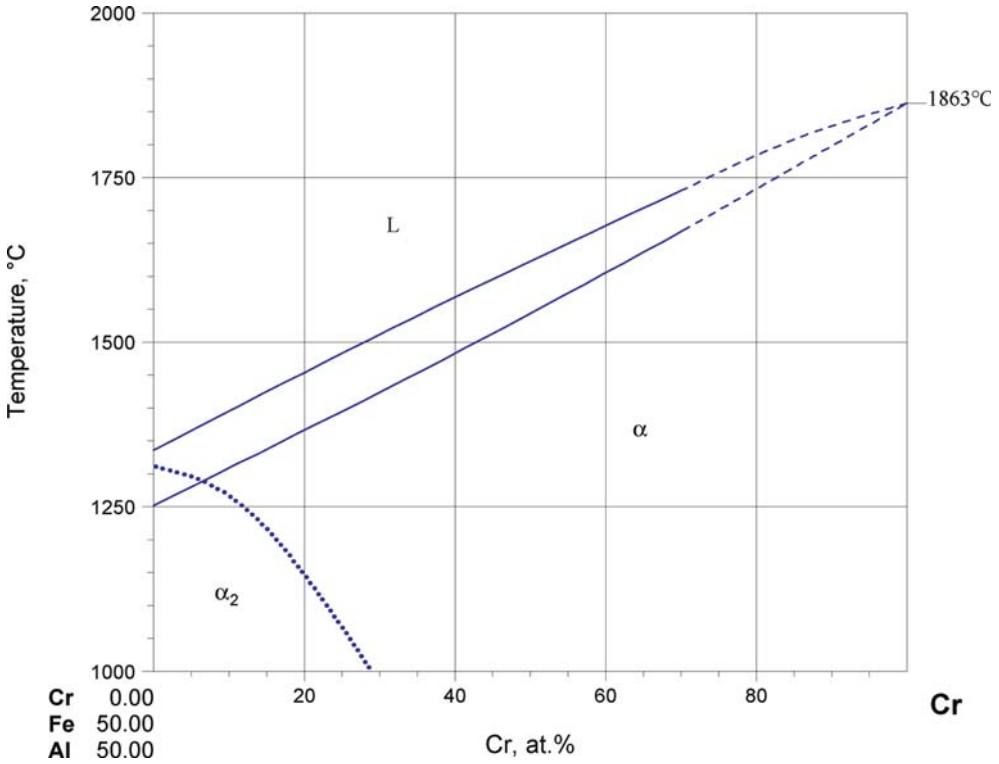

Fig. 15. Al-Cr-Fe. Polythermal section FeAl - Cr

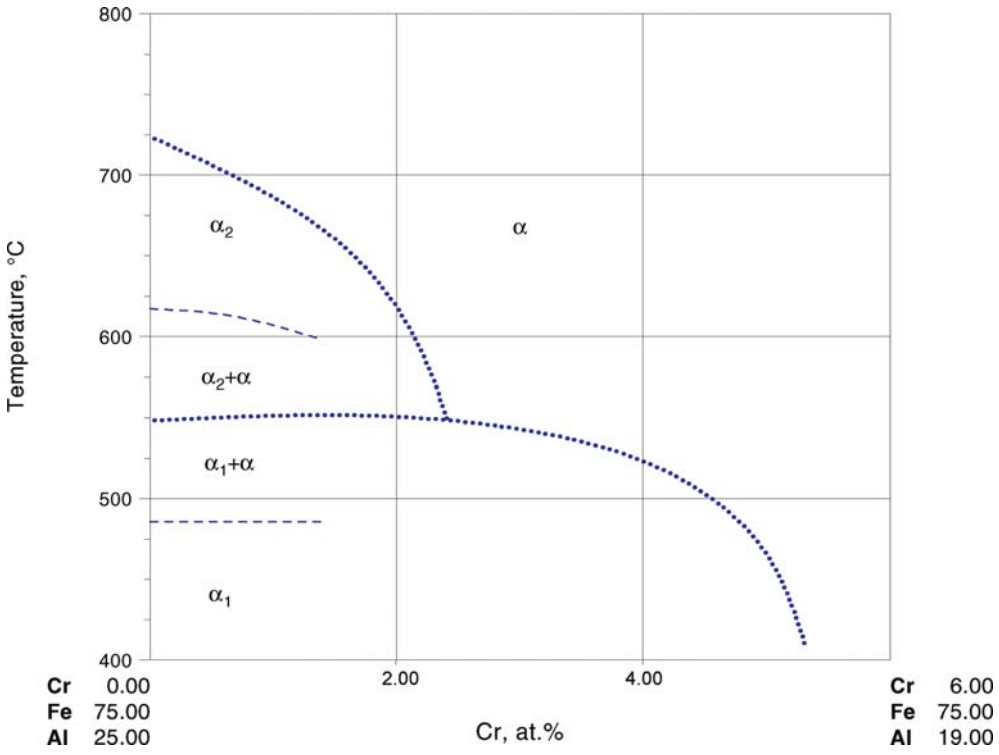

Fig. 16. Al-Cr-Fe. Variation of order-disorder reaction temperature as a function of the Cr content along the Fe_3Al-$CrFe_3$ section

DOI: 10.1007/978-3-540-69761-9_5

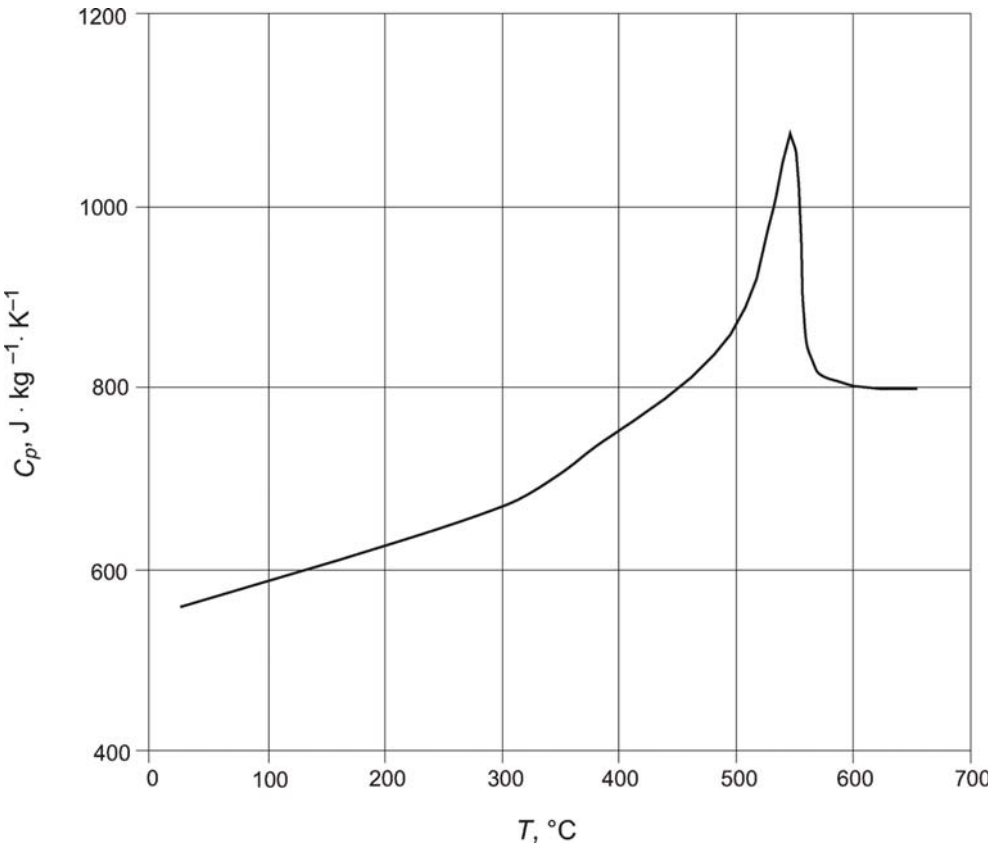

Fig. 17. Al-Cr-Fe. Temperature dependence of the heat capacity C_p of the Fe_4Al_{13}-based compound with chromium content 5 at.%

DOI: 10.1007/978-3-540-69761-9_5

References

[1932Tai1] Taillandier, M.Ch., "Contribution to Al-Fe-Cr Alloys, Part I" (in French), *Rev. Metal.*, **29**, 315–325 (1932) (Phase Diagram, Experimental, #, *, 8)

[1932Tai2] Taillandier, M.Ch., "Contribution to Al-Fe-Cr Alloys, Part II" (in French), *Rev. Metall.*, **29**, 348–356 (1932) (Experimental, 19)

[1934Osa] Osawa, A., "X-Ray Analysis of Fe-Al Alloys. The 2nd Report", *Metals & Alloys*, **5**, 154 (1934) (Crys. Structure, Review)

[1935Gru] Grunert, A., Hesselbruch, W., Schistal, K., "On the High Heat-Resistant Cr-Al-Fe Alloys with and without Cobalt" (in German), *Electrowaerme*, **5**, 131–132 (1935) (Experimental, 2)

[1937Bra] Bradley, A.J., Lu, S.S., "An X-Ray Study of the Chromium-Aluminium Equilibrium Diagram", *J. Inst. Met.*, **60**, 319–337 (1937) (Phase Diagram, Crys. Structure, Experimental, 8)

[1940Kor1] Kornilov, I.I., Mikheev, V.S., Konenko-Gracheva, O.K., "Equilibrium Diagram of the Ternary Fe-Cr-Al System (Preliminary Communication)" (in Russian), *Stal'*, (5/6), 57–59 (1940) (Phase Diagram, Experimental, #, *, 3)

[1940Kor2] Kornilov, I.I., "New Heat-Resistant Fe-Cr-Al Alloys with High Electrical Resistance" (in Russian), *Izv. Akad. Nauk SSSR, Ser. Khim.*, (5), 751–757 (1940) (Experimental, 15)

[1943Mon] Mondolfo, L.F., "Al-Cr-Fe", in "*Metallography of Aluminium Alloys*", John Wiley & Sons Inc., New York, 70–71 (1943) (Phase Diagram, Review, #, *, 1)

[1945Kor] Kornilov, I.I., "Alloys of Fe-Cr-Al" in "*Iron Alloys*" (in Russian), **Vol. 1**, Akad. Nauk SSSR, Leningrad, Moscow (1945) (Phase Diagram, Experimental, #)

[1946Kor] Kornilov, I.I., Mikheeva, V.S., Konenko-Gracheva, O.K., Mints, R.S., "Equilibrium Diagram of the Ternary System Fe-Cr-Al" (in Russian), *Izv. Sekt. Fiz.-Khim. Anal.*, **16**, 100–115 (1946) (Phase Diagram, Experimental, #, *, 48)

[1951Pra] Pratt, J.N., Raynor, G.V., "The Al-Rich Alloys of the System Al-Cr-Fe", *J. Inst. Met.*, **80**, 449–458 (1951) (Phase Diagram, Experimental, #, *, 15)

[1953Cas] Case, S.L., van Horn, K.R., "The Constitution of Binary and Complex Iron-Aluminium Alloys", in "*Aluminium in Iron and Steel*", John Wiley & Sons Inc., New York, 265–278 (1953) (Phase Diagram, Review, #, 19)

[1953Sch] Schubert, K., Roesler, U., Kluge, M., Anderko, K., Haerle, L., "Crystallographic Results on Phases with Penetration Bonding" (in German), *Naturwissenschaften*, **40**, 437 (1953) (Crys. Structure, Experimental)

[1954Chi] Chinetti, J., "Research on the Formation of Coarse Precipitates in Light Alloys Containing Cr" (in French), *Metaux*, **29**, 151–161 (1954) (Crys. Structure, Morphology, Experimental, 8)

[1955Bla1] Black, P.J., "The Structure of $FeAl_3$.I", *Acta Crystallogr.*, **8**, 43–48 (1955) (Crys. Structure, Experimental, 17)

[1955Bla2] Black, P.J., "The Structure of $FeAl_3$.I", *Acta Crystallogr.*, **8**, 175–182 (1955) (Crys. Structure, Experimental, 24)

[1955Tag] Tagaya, M., Nenno, S., "The Effect of Al on the σ Formation in Fe-Cr System", *Technol. Repts., Osaka Univ.*, (5), 149–152 (1955) (Crys. Structure, Morphology, Mechan. Prop., Experimental, 4)

[1958Chu] Chubb, W., Alfant, S., Bauer, A.A., Jablonowski, E.J., Schober, F.R., Dickenson, R.F., "Constitution, Metallurgy and Oxidation Resistance of Fe-Cr-Al Alloys", *Batelle Memorial Institute*, Columbus (1958) (Phase Diagram, Experimental, #, *, 66)

[1958Tag] Tagaya, M., Nenno, S., Kawamoto, M., "Effect of Al on σ Formation in the Fe-Cr System" (in Japanese), *Nippon Kinzoku Gakkai Shi*, **22**, 387–389 (1958) (Crys. Structure, Morphology, Mechan. Prop., Experimental, 4)

[1958Tay] Taylor, A., Jones, R.M., "Constitution and Magnetic Properties of Iron-Rich Iron-Aluminium Alloys", *J. Phys. Chem. Solids*, **6**, 16–37 (1958) (Crys. Structure, Experimental, Magn. Prop.) as quoted in [1993Oka]

DOI: 10.1007/978-3-540-69761-9_5

[1960Zol1] Zoller, H., "The Influence of Zn, Mg, Si, Cu, Fe, Mn, Ti on the Primary Crystallisation of Al_7Cr. Part 1–5" (in German), *Schweiz. Arch. Angew. Wiss. Techn.*, **26**, 437–448 (1960) (Experimental, Phase Diagram, 20)

[1960Zol2] Zoller, H., "The Influence of Zn, Mg, Si, Cu, Fe, Mn, Ti on the Primary Crystallisation of Al_7Cr. Part 6–12" (in German), *Schweiz. Arch. Angew. Wiss. Techn.*, **26**, 478–491 (1960) (Phase Diagram, Experimental, 33)

[1961Lih] Lihl, F., Ebel, H., "X-Ray Examination of the Constitution of Iron-Rich Alloys of the Iron-Aluminium Systems" (in German), *Arch. Eisenhuettenwes.*, **32**, 483–487 (1961) (Crys. Structure, Experimental, 33) as quoted in [1993Oka]

[1961Phi] Phillips, H.W.L., "Al-Cr-Fe", in "*Equilibrium Diagrams of Aluminium Alloy Systems. Information Bulletin 25*", Aluminium Development Association, London, 1–78 (1961) (Phase Diagram, Review, 1)

[1968Bul] Bulycheva, Z.N., Tolochko, M.N., Svezhova, S.I., Kondrat'ev, V.K., "Influence of Cr on the Ordering of Fe-Al Alloys" (in Russian), *Akad. Nauk Ukr. SSR, Metallofiz.*, **20**, 120–124 (1968) (Crys. Structure, Experimental, 9)

[1969Bul1] Bulycheva, Z.N., Tolochko, M.N., Svezhova, S.I., Kondrat'ev, V.K., "Change in the Ordering Temperature of Fe_3Al on Adding a Third Element" (in Russian), *Ukrain. Fiz. Zh.*, **14** (10), 1706–1708 (1969) (Crys. Structure, Phase Diagram, Experimental, #, *, 5)

[1969Bul2] Bulycheva, Z.N., Kondrat'ev, V.K., Pogosov, V.Z., Svezhova, S.I., Tolochko, M.N., "The Effect of Cr and Co on the Structure and Properties of Ordered Fe-Al Alloys" (in Russian), *Sb. Tr. T. N.- Inst. Chern. Met. (Moscow)*, **71**, 55–62 (1969) (Crys. Structure, Phase Diagram, Experimental, #, *, 7)

[1969Kal] Kallel, A., "Antiferromagnetic Order in the Alloys $AlCr_{2-x}Fe_x$" (in French), *Compt. Rend. Acad. Sci., Paris*, **268B**, 455–458 (1969) (Crys. Structure, Experimental, Magn. Prop., 8)

[1969Mue] Müller, F., Kubaschewski, O., "The Thermodynamic Properties and Equilibrium Diagram of the System Cr-Fe", *High Temp.-High Pres.*, **1**, 543–551 (1969) (Phase Diagram, Review, Thermodyn., 34)

[1969Sel] Selissky, Ya.P., Tolochko, M.N., "High-Temperature X-Ray Diffraction Study of Fe-Al-Cr, Fe-Al-Mo and Fe-Al-W Alloys" (in Russian), *Ukr. Fiz. Zhurn.*, **14**(10), 1692–1694 (1969) (Crys. Structure, Phase Diagram, Experimental, #, *, 7)

[1970Koz1] Kozheurov, V.A., Ryss, M.A., Pigasov, S.E., Antonenko, V.I., Kuznetsov, Yu.S., Mikhailov, G.G., Pashkeev, I.Yu., "The Fe-Cr-Al Phase Diagram" (in Russian), *Sb. Nauchn. Tr. Chel. Polit. Inst.*, **78**, 3–15 (1970) (Phase Diagram, Experimental, Review, #, *, 2)

[1970Koz2] Kozheurov, V.A., Ryss, M.A., Pigasov, S.E., Antonenko, V.I., Kuznetsov, Yu.S., Mikhailov, G.G., Pashkeev, I.Yu., "The Phase Diagram of Fe-Cr-Al in the Region of Crystallisation of the Solid Solution from the Melt" (in Russian), *Sb. Trud. Chelyab. Elektromet. Kombinata*, **2**, 69–79 (1970) (Phase Diagram, Experimental, Review, #)

[1970Koz3] Kozheurov, V.A., Ryss, M.A., Pigasov, S.E., Antonenko, V.I., "Solubility of Carbon in Melts of Fe-Cr-Al System" (in Russian), *Sb. Trud. Chelyab. Elektromet. Kombinata*, **2**, 62–68 (1970) (Crys. Structure, Phase Relations, Experimental, 9)

[1972Kaj] Kajzar, F., Lesniewska, B., Niziol, S., Oles, A., Pacyna, A., Tucharz, Z., "Neutron Diffraction Study of Ordered Arrangement of Fe-Cr-Al Alloys", *Inst. Tech. Jad.*, AGH Rep., No. 22/PS, Institute of Nuclear Physics, Cracow (1972) (Crys. Structure, Experimental)

[1973Cor] Corby, R.N., Black, P.J., "The Structure of $FeAl_2$ by Anomalous Dispersion Methods", *Acta Cryst. B*, **29**, 2669–2677 (1973) (Crys. Structure, Experimental, 31)

[1973Wil] Willey, L.A., "Al-Cr-Fe Aluminum-Chromium-Iron)" in "*Metal Handbook*", 8th Edition, ASM, Metals Park, OH, 382 (1973) (Phase Diagram, Review, *, 3)

[1974Niz] Niziol, S., Oles, A., Tucharz, Z., Tyszko, Z., "Crystallographic Ordering and Magnetic Properties of Alloys" (in Russian), *Trans. Internat. Conf. on Magnetism*, 1973, **2**, Nauka, Moscow, 227–231 (1974) (Experimental, Crys. Structure, Magn. Prop., 10)

DOI: 10.1007/978-3-540-69761-9_5

[1974Vya] Vyatkin, G.P., Mishchenko, V.Ya., Povolotskii, D.Ya., "Using the Simplex-Lattice Method for Calculating the Equilibrium Diagram of the Fe-Cr-Al System" (in Russian), *Izv. Vyssh. Ucheb. Zaved. Chern. Metall.*, (8), 9–12 (1974) (Phase Diagram, Calculation, 4)

[1975Kau] Kaufman, L., Nesor, H., "Calculation of Superalloy Phase Diagrams: Part IV", *Met. Trans.*, **6A**, 2123–2131 (1975) (Phase Diagram, Calculation, Thermodyn., Theory, 38)

[1975Lit] Litinska, L., Niziol, S., "Crystallographic Structure and Magnetic Properties of $(FeCr)_3Al$ Type Phases in Iron-Chromium-Aluminium ($Fe_{0.67}Cr_{0.08}Al_{0.23}$) Alloys", *Inst. Tech. Jad.*, AGH Rep., No. 70/PS, Institute of Nuclear Physics, Cracow (1975) (Crys. Structure, Magn. Prop., Experimental)

[1975Ohn] Ohnishi, T., Nakatani, Y., Okabayashi, K., *Bull. Univ. Osaka Prefect.*, **24**, 183–191 (1975) (Phase Diagram, Crys. Structure, Experimental)

[1976Mon] Mondolfo, L.F., "*Aluminium Alloys: Structure and Properties*", Butterworths, London, 480–481 (1976) (Phase Diagram, Review, *, 38)

[1976Vla] Vlasova, E.N., Prokoshin, A.F., "Formation of $L2_1$ Superstructure and Stratification in Solid Fe-Cr Solutions Doped with Al and V" (in Russian), *Dokl. Akad. Nauk SSSR*, **231**, 599–602 (1976) (Crys. Structure, Morphology, Experimental, 2)

[1977Bra] Brandon, J.K., Pearson, W.B., Riley, P.W., Chieh, C., Stokhuyzen, R., "γ-Brasses with R Cells", *Acta Crystallogr.*, **3B**, 1088–1095 (1977) (Crys. Structure, Experimental, 16)

[1977Ost] Ostrovskii, O.I., Stomakhin, A.Ya., Ditrikh, E., Grigoryan, V.A., "Heats of Dissolution of Aluminium, Silicon and Titanium in the Melts Iron-Chromium and Nickel-Chromium" (in Russian), *Seventh International Conference on Calorimetry*, (Broadened Abstracts), I-HOP, Chernogolovka (Russia), 59–63 (1977) (Thermodyn., Experimental, 11)

[1977Sim] Simensen, C.J., Vellasamy, R., "Determination of Phases Present in Cast Material on an Al-0.5wt.%Fe-0.2wt.%Si", *Z. Metallkd.*, **68**, 428–431 (1977) (Crys. Structure, Experimental) as quoted in [1993Oka]

[1977Tys] Tyszko, Z., Oles, A., Niziol, Z., "Structure and Physical Properties of Fe-Cr-Al Alloys" (in French), *Cercle d'Etudes de Metaux*, **13**, 473–492 (1977) (Experimental, Crys. Structure, Phys. Prop., 20)

[1978Bas] Bastin, G.F., Van Loo F.J.J., Vrolijik, J.W.G.A., Wolf, L.R., "Crystallography of Aligned Fe-Al Eutectoid", *J. Crys. Growth*, **43**, 745–751 (1978) (Crys. Structure, Experimental)

[1980Riv] Rivlin, V.G., Raynor, G.V., "Critical Evaluation of Constitution of Al-Cr-Fe System", *Int. Met. Rev.*, **25**, 139–157 (1980) (Phase Diagram, Assessment, Review, #, *, 45)

[1980Sch] Schuermann, E., Kaiser, H.-P., "Contribution to the Melting Equilibria of Iron-Aluminium and Iron-Phosphorous Alloys" (in German), *Arch. Eisenhuettenwes.*, **51**, 325–327 (1980) (Phase Diagram, Experimental)

[1981Bro] den Broeder, F.J.A., van Tendeloo, G., Amelinckx, S., Hornstra, J., de Ridder, R., van Landgut, J., van Daal, H.J., "Microstructure of $Cr_{100-x}Al_x$ Alloys (10 at.% < x < 33 at.%) Studied by Means of Transmission Electron Microscopy and Diffraction. II. Discovery of a New Phase", *Phys. Status Solidi A*, **67**, 233–248 (1981) (Phase Diagram, Morphology, Experimental, 2)

[1981Ten] van Tendeloo, G., van den Broeder, F.J.A., Amelinckx, S., de Ridder, R., van Landuyt, J., van Daal, H.J., "Microstructure of $Cr_{100-x}Al_x$ Alloys (10 at.% < x < 33 at.%) Studied by Means of Transmission Electron Microscopy and Diffraction. I. Microstructure of the β-Phase", *Phys. Status Solidi A*, **67**, 217–232 (1981) (Phase Diagram, Morphology, Experimental, 10)

[1982Kub] Kubaschewski, O., "Fe-Al" and "Fe-Cr", in "*Binary Iron Phase Diagrams*", Springer Verlag, Berlin, 5–9 and 31–34 (1982) (Phase Diagram, Crys. Structure, Review, #, *, 26, 22)

[1982Nao] Naohara, T., Inoue, A., Minemure, T., Masumoto, T., Kumada, K., "Microstructure, Mechanical Properties and Electrical Properties of Rapidly Quenched Fe-Cr-Al Alloys", *Metall. Trans. A*, **13A**, 337–343 (1982) (Experimental, Morphology, Electr. Prop., Mechan. Prop., 10)

DOI: 10.1007/978-3-540-69761-9_5

[1982Yea] Yearim, R., Shechtman, D., "The Structure of Rapidly Solidified Al-Fe-Cr Alloys", *Metall. Trans. A.*, **13A**, 1891–1898 (1982) (Crys. Structure, Experimental, 14)

[1983Bus] Buschow, K.H.J., van Engen, P.G., Jongebreur, R., "Magneto-Optical Properties of Metallic Ferromagnetic Materials", *J. Magn. Magn. Mater.*, **38**, 1–22 (1983) (Crys. Structure, Magn. Prop., Optical Prop., 23)

[1985Okp] Okpalugo, D.E., Booth J.G., Faunce, C.A., "Onset of Ferromagnetism in 3d-Substituted FeAl Alloys. I: Ti, V and Cr Substituents", *J. Phys. F, Met. Phys.*, **15**, 681–692 (1985) (Experimental, Morphology, Magn. Prop., 19)

[1986Gri] Griger, A., Stefaniay, V., Tumezey, T., "Crystallographic Data and Chemical Compositions of Aluminium-Rich Al-Fe Intermetallic Phases", *Z. Metallkd*., **77**, 30–35 (1986) (Phase Diagram, Crys. Structure, Experimental, 23)

[1987Sau] Saunders, N., Rivlin, V.G., "A Critical Review and Thermodynamic Calculations for the Al-Rich Portion of the Al-Cr-Fe Phase Diagram", *Z. Metallkd.*, **78**, 795–801 (1987) (Phase Diagram, Phase Relations, Assessment, Calculation, Thermodyn., 36)

[1987Wou] van der Woude, F., Schurer, P.J., "A Study of Quasi-Crystalline Al-Fe Alloys by Mössbauer Spectroscopy and Diffraction Techniques", *Canad. J. Phys.*, **65**(10), 1301–1308 (1987) (Crys. Structure, Experimental, Moesbauer, 39)

[1988Hoc] Hoch, M., "Thermodynamic Behavior of Very Stable Binary Compounds with a Wide Homogeneity Range: Their Influence in the Liquid Phase and in the Ternary and Higher Component Systems in the Solid State", *Z. Metallkd.*, **79**, 426–434 (1988) (Phase Relations, Theory, Thermodyn., Calculation, 34)

[1988Man] Manaila, R., Florescu, V., Jianu, A., Badescu, A., "Icosahedral Phases in the Al-Fe-Cr Alloys System", *Phys. Status Solidi A*, **109**, 61–66 (1988) (Crys. Structure, Experimental, 15)

[1988Sch] Schurer, P.J., Koopmans, B., van der Woude, F., "Structure of Icosahedral Al-($M_{1-x}Fe_x$) Alloys (M = Cr, Mn, or Fe)", *Phys. Rev. B.*, **37**(1), 507–510 (1988) (Crys. Structure, Experimental, 25)

[1988Ten] van Tendeloo, G., van Landgut, J., Amelinckx, S., Ranganathan, S., "Quasi-Crystals and their Crystalline Homologues in the $Al_{60}Mn_{11}Ni_{14}$ Ternary Alloys", *J. Microscopy*, **149**, 1 (1988) (Exeperimental, Crys. Structure, 22)

[1989Ell] Ellner, M., Braun, J., Predel, B., "X-Ray Study on Cr-Al Phases of the W-Family", *Z. Metallkd.*, **80**(5), 374–383 (1989) (Crys. Structure, Phase Diagram, Experimental, 38)

[1989Law1] Lawther, D.W., Dunlap, R.A., Lloyd, D.J., McHenry, M.E., "Structure and Stability of Rapidly Quenched $Al_{86}Cr_{14-x}Fe_x$ Alloys", *J. Mater. Sci.*, **24**, 3076–3080 (1989) (Crys. Structure, Phase Diagram, Experimental, 18)

[1989Law2] Lawther, D.W., Dunlap, R.A., Srivinas, V., "On the Question of Stability and Disorder in Icosahedral Aluminium - Transition Metal Alloys", *Canad. J. Phys.*, **67**, 463–467 (1989) (Crys. Structure, Phase Diagram, Experimental, 17)

[1989Man] Manaila, R., Florescu, V., Jianu, A., Radulescu, O., "On the Transition Metal Quasisublattice in Icosahedral Al-Cr-Fe Phases", *Phil. Mag.*, **B60**(5), 589–599 (1989) (Crys. Structure, Experimental, 33)

[1990Ioa] Ioannidis, E.K, Sheppard, T., "Powder Metallurgy Aluminium Alloys: Characteristics of an Al-Cr-Fe Rapidly Solidified Alloys", *J. Mater. Science*, **25**, 3965–3975 (1990) (Crys. Structure, Morphology, Experimental, 15)

[1991Gho] Ghosh, G., "Aluminium-Chromium-Iron", MSIT Ternary Evaluation Program, in *MSIT Workplace*, Effenberg, G. (Ed.), MSI, Materials Science International Services GmbH, Stuttgart; Document ID: 10.14873.1.20 (1991) (Crys. Structure, Phase Diagram, Assessment, 45)

[1991Pra] Prakash, U., Buckley, R.A., Jones, H., "Mechanical Properties of Ordered Fe-Al-X Alloys", *Mater. Res. Soc. Symp. Proc.: High-Temp. Ordered Intermetallic Alloys IV*, **213**, 691–696 (1991) (Morphology, Crys. Structure, Mechan. Prop., 19)

DOI: 10.1007/978-3-540-69761-9_5

[1991Sik1] Sikka, V.K., Baldwin, R.H., Reinshagen, J.H, Knibloe, J.R., Wright, R.N., "Powder Processing of Fe_3Al-Based Iron-Aluminide Alloys", *Mater. Res. Soc. Symp. Proc.: High-Temp. Ordered Intermetallic Alloys IV*, **213**, 901–906 (1991) (Crys. Structure, Experimental, Phys. Prop., 4)

[1991Sik2] Sikka, V.K., "Production of Fe_3Al-Based Intermetallic Alloys", *Mater. Res. Soc. Symp. Proc.: High-Temp. Ordered Intermetallic Alloys IV*, **213**, 907–912 (1991) (Experimental, 2)

[1991Tre] Tret'yachenko, L.A., Prima, S.B., Petyukh, V.M., "The Polythermal Cr-FeAl Section of the Phase Diagram of the Ternary System Cr-Fe-Al" (in Russian), *Diagramy Sostoyaniya v Materialovedenii*, Akad. Nauk Ukr. SSR. Nauch. Sov. Akad. Nauk Ukr. SSR po Probl. Khim. Termodin. i Term. Anal., Kiev, 143–146 (1991) (Assessment, Phase Relations, Phase Diagram, #, *, 4)

[1992Don] Dong, C., Dubois, J.M., Kang, S.S., Audier, M., "The Orthorhombic Approximant Phases of the Decagonal Phase", *Philos. Mag., B*, **65**(1), 107–126 (1992) (Crys. Structure, Experimental, 29)

[1992Hil] Hilpert, K., Miller, M., "Study of the Vaporization of Ni-Cr-Al and Fe-Cr-Al Base Alloys by Knudsen Effusion Mass Spectrometry", *Z. Metallkd.*, **83**(10), 739–743 (1992) (Experimental, Thermodyn., 15)

[1992Wen] Wen, K.Y., Chen, Y.L., Kuo, K.H., "Crystallographic Relationships of the Al_4Cr Crystalline and Quasicrystalline Phases", *Metall. Trans. A*, **23A**, 2437–2445 (1992) (Crys. Structure, Experimental, 36)

[1993Kni] Knibloe, J.R., Wricht, R.N., Trybus, C.L., Sikka, V.K., "Microstructure and Mechanical Properties of Fe_3Al Alloys with Chromium", *J. Mater. Sci.*, **28**, 2040–2048 (1993) (Crys. Structure, Mechan. Prop., Experimental, 8)

[1993Oka] Okamoto, H., *Phase Diagrams of Binary Iron Alloys*, Materials Park OH, ASM, 1-475 (1993) (Phase Diagram, Crys. Structure, Review)

[1994Bur] Burkhardt, U., Grin, J., Ellner, M., Peters, K., "Structure Refinement of the Iron-Aluminium Phase with the Approximate Composition Fe_2Al_5", *Acta Cryst. B: Struct.Crystallogr. Crys. Chem.*, **B50**, 313–316 (1994) (Crys. Structure, Experimental, 9)

[1994Gri] Grin, J., Burkhardt, U., Ellner, M., Peters, K., "Refinement of the Fe_4Al_{13} Structure and its Relationship to the Quasidecagonal Homotypical Structures", *Z. Krist.*, **209**, 479–487 (1994) (Crys. Structure, Experimental)

[1994ICD] ICDD Powder Diffraction File. International Centre for Diffraction Data, Newtown Square, Pa (1994) (Crys. Structure, Experimental)

[1995Aud] Audier, M., Durand-Charre, M., Laclau, E., Klein, H., "Phase Equilibria in the Al-Cr System", *J. Alloys Compd.*, **220**, 225–230 (1995) (Crys. Structure, Experimental, *, 17)

[1995Li] Li, X.Z., Dong, C., Dubois, J.M., "Structural Study of Crystalline Approximants of the Al-Cu-Fe-Cr Decagonal Quasicrystal", *J. Appl. Crystallogr.*, **28**(2), 96–104 (1995) (Crys. Structure, Experimental, 16)

[1995Sta] Stadnik, Z.M., Mueller, F., "Thermal, Structural and Magnetic Properties of Icosahedral $Al_{86}Cr_8Fe_6$ Alloy", *Philos. Mag. B*, **71**(2), 221–238 (1995) (Crys. Structure, Magn. Prop., Experimental, 67)

[1995Sui] Sui, H.X., Liao, X.Z., Kuo, K.H., "A Non-Fibonacci Type of Orthorhombic Decagonal Approximant", *Philos. Mag. Lett.*, **71**, 139 (1995) (Crys. Structure, Experimental, 18)

[1995Zha] Zhang, B., Gramlich, V., Steurer, W., "$Al_{13-x}(Co_{1-y}Ni_y)_4$, a New Approximant of the Decagonal Quasicrystal in the Al-Co-Ni System", *Z. Krist.*, **210**, 498–503 (1995) (Crys. Structure, Experimental, 24)

[1995Zia] Ziani, A., Michot, G., Pianelli, A., Redjaimia, A., Zahra, C.Y., Zahra, A.M., "Transformation of the Quasicrystalline Phase Al-Cr-Fe Induced by Rapid Solidification", *J. Mater. Sci.*, **30**, 2921–2929 (1995) (Crys. Structure, Phase Diagram, Experimental, 27)

[1996Jim] Jimenez, J.A., Frommeyer, G., "Creep Behavior of Intermetallic Fe-Al and Fe-Al-Cr Alloys", *Mater. Sci. Eng. A*, **A220**, 93–99 (1996) (Experimental, Morphology, Mechan. Prop., 18)

DOI: 10.1007/978-3-540-69761-9_5

[1996Ros] Rosell-Laclau E., Durand-Charre, Audier, M, "Liquid-Solid Equilibria in the Aluminium-Rich Corner of the Al-Cr-Ni System", *J. Alloys Compd.*, **233**, 246–263 (1996) (Crys. Structure, Phase Diagram, Experimental, 37)

[1997Kog] Kogachi, M., Haraguchi, T., "Ordered In Vacancies in *B*2-Structured Intermetallic Compound Feal", *Mater. Sci. Eng. A*, **A230**, 124–131 (1997) (Crys. Structure, Experimental, 231)

[1997Pal] Palm, M., "The Al-Cr-Fe System - Phases and Phase Equilibria in the Al-Rich Corner", *J. Alloys Compd*., **252**, 192–200 (1997) (Phase Diagram, Phase Relations, Crys. Structure, Experimental, 41)

[1997Rud] Rudajevova, A., Shima, V., "Thermal Properties of the Fe_3Al_5 at.% Cr Intermetallic Compound and Thermal Diffusivity Anomaly in $D0_3$ Phase", *Mater. Res. Bull.*, **32**(4), 441–449 (1997) (Experimental, Thermodyn., 15)

[1997Sat] Satula, D., Dobrzynski, L., Waliszewski, J., Szymanski, K., Recko, K., Malinowski, A., Brueckel, Th., Schaerpf, O., Blonowski, K., "Structural and Magnetic Properties of Fe-Cr-Al Alloys with *D*03-Type Structure", *J. Magn. Magn. Mater.*, **169**, 240–252 (1997) (Crys. Structure, Experimental, Magn. Prop., 29)

[1997Sui] Sui, H.X., Liao, X.Z., Kuo, K.H., Zou, X., Hovmoeller, S., "Structural Model of the Orthorhombic Non-Fibonacci Approximant in the $Al_{12}Fe_2Cr$ Alloy", *Acta Crystallogr., Sect. B: Struct. Crystallogr. Crys. Chem.*, **B53**, 587–595 (1997) (Crys. Structure, Experimental, 41)

[1998Akd] Akdeniz, M.V., Mekhrabov, A.O., "The Effect of Substitutional Impurities on the Evolution of Fe-Al Diffusion Layer", *Acta Mater.*, **46**(4), 1185–1192 (1998) (Morphology, Calculation, Experimental, Interface Phenomena, 55)

[1998Ali] Aliravci, C.A., Pekgueleryuez, M.O., "Calculation of Phase Diagrams for the Metastable Al-Fe Phases Forming in Direct-Chill (Dc)-Cast Aluminium Alloy Ingots", *Calphad*, **22**, 147–155 (1998) (Crys. Strucutre, Calculation, Phase Diagram, 20)

[1998Lia] Liao, X.Z., Sui, H.X., Kuo, K.H., "A New Monoclinic Approximant of the Decagonal Quasicrystal in Al-Co-Cu-W and Al-Fe-Cr Alloys", *Philos. Mag. A*,**78**(1), 143–156 (1998) (Crys. Structure, Experimental, 19)

[1998Mur] Murray, J.L., "The Al-Cr (Aluminium-Chromium) System", *J. Phase Equilib.*, **19**(4), 368–375 (1998) (Crys. Structure, Phase Diagram, Assessment, Calculation, Review, #, *, 43)

[1998Su] Su, J.-Q., Gao, S.-J., Hu, Zh.-Q., "The Influence of Chromium and Boron on Mechanical Properties of Fe-30Al Alloy", *J. Mater. Sci. Lett.*, **17**, 2021–2023 (1998) (Mechan. Prop., Experimental, 12)

[1998Sun] Sun, Z.Q., Yang, W.Y., Shen, L.Z., Huang, Y.D., Zhang, B.S., Yang, J.L., "Neutron Diffraction Study on Site Occupation of Substitutional Elements at Sub Lattices in Fe-Al Intermetallics", *Mater. Sci. Eng. A*, **258**, 69–74 (1998) (Crys. Structure, Morphology, Experimental, Mechan. Prop., 19)

[1999Mek] Mekhrabov, A.O., Akdeniz, M.V., "Effect of Ternary Alloying Elements Addition on Atomic Ordering Characterisctics of Fe-Al Intermetallics", *Acta Mater.*, **47**(7), 2067–2075 (1999) (Crys. Structure, Calculation, Theory, Electronic Structure, 63)

[1999Sui] Sui, H.X., Li, X.Z., Kuo, K.H., "Hexagonal $Al_{81}Fe_8Cr_{11}$ with a = 4.00 nm and c = 1.24 nm", *Philos. Mag. Lett.*, **79**(4), 181–185 (1999) (Crys. Structure, Experimental, 10)

[1999Wit] Wittmann, R., Spindler, S., Fischer, B., Wagner, H. Gerthsen, D., Lange, J., Brede, M., Kloewer, J., Schunk, P., Schimmel, T., "Transmission Electron Microscopic Investigation of the Microstructure of Fe-Cr-Al Alloys", *J. Mater. Sci.*, **34**, 1791–1798 (1999) (Phase Diagram, Experimental, Morphology, Phase Relations, Crys. Structure, 26)

[2000Bla] Blachowski, A., Dubiel, S.M., Zukrowski, J., Cieslak, J., Sepiol, B., "On the Kinetics of the σ-α Phase Transformation in an Al-Doped Fe-Cr Alloy", *J. Alloys Compd.*, **313**, 182–187 (2000) (Phase Relations, Experimental, Kinetics, 15)

[2000Dem] Demange, V., Wu, J.S., Brien, V., Machizaud, F., Dubois, J.M., "New Approximant Phases in Al-Cr-Fe", *Mater. Sci. Eng. A*, **294–296**, 79–81 (2000) (Crys. Structure, Experimental, 13)

DOI: 10.1007/978-3-540-69761-9_5

[2000Mah] Mahdouk, K., Gachon, J.-C., "Thermodynamic Investigation of the Aluminium-Chromium System", *J. Phase Equilib.*, **21**(2), 157–166 (2000) (Phase Diagram, Thermodyn., Experimental, *, 26)

[2000Mo1] Mo, Z.M., Kuo, K.H., "A Family of Hexagonal Approximants of Decagonal Quasicrystals", *Mater. Sci. Eng. A*, **294–296**, 242–245 (2000) (Crys. Structure, Experimental, 14)

[2000Mo2] Mo, Z.M., Zhou, H.Y., Kuo, K.H., "Structure of ν-$Al_{80.61}Cr_{10.71}Fe_{8.68}$, a Giant Hexagonal Approximant of a Quasicrystal Determined by a Combination of Electron Microscopy and X-Ray Diffraction", *Acta Crystallogr., Sect. B: Struct. Crystallogr. Crys. Chem.*, **56**, 392–401 (2000) (Crys. Structure, Experimental, 16)

[2000Sha1] Shao, G., Tsakiropoulos, P., "On the ω Phase Formation in Cr-Al And Ti-Al-Cr Alloys", *Acta Mater.*, **48**, 3671–3685 (2000) (Crys. Structure, Experimental, 39)

[2000Sha2] Shao, G., Nguyen-Manh, D., Pettifor, D.G., Tsakiropoulos, P., "ω-Phase Formation in a Rapidly Solidified Cr-40 at.% Al Alloy", *Philos. Mag. Lett.*, **80**(11), 703–710 (2000) (Crys. Structure, Thermodyn., Experimental, 22)

[2000Spi] Spindler, S., Wittmann, R., Gerthsen, D., Lange, J., Brede, M., Kloewer, J., "Dislocation Properties of Polycrystalline Fe-Cr-Al Alloys and their Correlation with Mechanical Properties", *Mater. Sci. Eng. A*, **A289**, 151–161 (2000) (Crys. Structure, Experimental, 27)

[2000Sub] Subasic, N., Sundman, B., "Thermodynamic Assessment of the Al-Cr-Fe System and Reassessment of the Al-Cr System", *Proc. Disc. Meet. Thermodyn. Alloys*, 42 (2000) (Thermodyn., Abstract, 0)

[2001Alo] Al-Omari, I.A., "Structural and Mössbauer Spectroscopic Studies of $Fe_{0.7-x}Cr_xAl_{0,3}$ Alloys", *J. Magn. Magn. Mater.*, **225**, 346–350 (2001) (Crys. Structure, Experimental, 21)

[2001Dem] Demange, V., Anderegg, J.W., Ghanbaja, J., Machizaud, F., Sordelet, D.J., Besser, M., Thiel, P.A., Dubois, J.M., "Surface Oxidation of Al-Cr-Fe Alloys Characterized by X-Ray Photoelectron Spectroscopy", *Appl. Surf. Sci.*, **173**, 327–338 (2001) (Crys. Structure, Experimental, 30)

[2001Rod] Rodriguez, C.A.D., Botta, F.W.J., "High-Energy Ball Milling of Al-Based Alloys", *Key Eng. Mater.*, **189–191**, 573–578 (2001) (Crys. Structure, Experimental, 10)

[2001Sch] Schoen, C.G., "Order-Disorder Transformation and Diffusion in Ternary bcc Alloys: the Role of Second-Order Boundaries", *J. Phase Equilib.*, **22**(3), 287–290 (2001) (Calculation, Phase Diagram, Thermodyn., 9)

[2002Boz] Bozzolo, G.H., Noebe, R.D., Amador, C., "Site Occupancy of Ternary Additions to *B*2 Alloys", *Intermetallics*, **10**, 149–159 (2002) (Crys. Structure, Calculation, Review, Theory, 27)

[2002Dem1] Demange, V., Machizaud, F., Dubois, J.M., Anderegg, J.W., Thiel P.A., Sordelet, D.J., "New Approximants in the Al-Cr-Fe System and their Oxidation Resistance", *J. Alloys Compd.*, **342**, 24–29 (2002) (Crys. Structure, Experimental, 20)

[2002Dem2] Demange, V., Milandri, A., Weerd, M.C., Machizaud, F., Jeandel, G., Dubois, J.M., "Optical Conductivity of Al-Cr-Fe Approximant Compounds", *Phys. Rev. B*, **65**, 144205–1 -144205–11 (2002) (Calculation, Crys. Structure, Experimental, Optical Prop., 39)

[2002Den] Deng, D.W., Kuo, K.H., "Crystal Structure of the b.c.o. Al_4(Cr,Ni) Decagonal Approximant", *J. Alloys Compd.*, **342**(1–2), 101–104 (2002) (Crys. Structure, Calculation, Experimental, 18)

[2002Zho] Zhou, Z.C., Wie, J.N., Han, F.S., "Influences of Heat Treatment and Grain Size on the Damping Capacity of an Fe-Cr-Al Alloy", *Phys. Status Solidi A*, **191**(1), 89–96 (2002) (Experimental, Mechan. Prop., Phys. Prop., 14)

[2003Rag] Raghavan, V., "Al-Cr-Fe (Aluminum-Cromium-Iron)", *J. Phase Equilib.*, **24**(3), 257–258 (2003) (Crys. Structure, Phase Diagram, Phase Relations, Review, 19)

[2003Zou] Zou, X.D., Mo, Z.M., Hovmoeller, S., Li, X.Z., Kuo, K.H., "Three-Dimensional Reconstruction of the ν-AlCrFe Phase by Electron Crystallography", *Acta Crystallogr., Sect. A: Found. Crystallogr.*, **59**, 526–539 (2003) (Crys. Structure, Electronic Structure, Experimental, 24)

DOI: 10.1007/978-3-540-69761-9_5

[2004Gho] Ghosh, G., Velikanova, T., Korniyenko, K., Sidorko, V., "Aluminium - Chromium - Iron", in *"Landolt-Boernstein, Numerical Data and Functional Relationships in Science and Technology (New Series). Group IV: Physical Chemistry"*, Ed. W. Martiensen, *"Ternary Alloy Systems. Phase Diagrams, Crystallographic and Thermodynamic Data"*, Vol. 11A1, Effenberg, G., Ilyenko, S., (Eds.) Springer-Verlag, Berlin, Heidelberg, 320–350 (2004) (Crys. Structure, Phase Diagram, Thermodyn., Assessment, Phys. Prop., 118)

[2004Hua] Huang, Y.D., Yang, W.Y., Sun, Z.Q., Froyen, L., "Preparation and Mechanical Properties of Large-Ingot Fe_3Al-Based Alloys", *J. Mat. Proc. Tech.*, **146**(2), 175–180 (2004) (Morphology, Experimental, Mechan. Prop., 23)

[2004Wu] Wu, D., Baker, I., Munroe, P.R., "The Effect of Substitutional Elements on the Strain-Induced Ferromagnetism in *B*2-Structured Fe-Al Single Crystals", *Intermetallics*, **12**(7–9), 851–858 (2004) (Crys. Structure, Morphology, Calculation, Experimental, Magn. Prop., 19)

[2005Dem] Demange, V., Ghanbaja, J., Machizaud, F., Dubois, J.M., "About γ-Brass Phases in the Al-Cr-Fe System and their Relationships to Quasicrystals and Approximants", *Philos. Mag.*, **85**(12), 1261–1272 (2005) (Crys. Structure, Experimental, 36)

[2005Pal] Palm, M., "Concepts Derived from Phase Diagram Studies for the Strengthening of Fe-Al-Based Alloys", *Intermetallics*, **13**(12), 1286–1295 (2005) (Phase Diagram, Review, Mechan. Prop., 81)

[2006Cor] Cornish, L., Saltykov, P., Cacciamani, G., Velikanova, T., "Al-Cr (Aluminum - Chromium)", MSIT Binary Evaluation Program, in *MSIT Workplace*, Effenberg, G. (Ed.), MSI, Materials Science International Services GmbH, Stuttgart, to be published, (2006) (Phase Diagram, Assessment, 51)

[2006Dem] Demange, V., Ghanbaja, J., Dubois, J.M., "Electron Microscopy Study of Approximant Phases in the Al-Cr-Fe System", *Philos. Mag. A.*, **86**(3–5), 469–474 (2006) (Crys. Structure, Experimental, Theory, 19)

[2006MSIT] "Al-Fe (Aluminum-Iron)", Diagrams as Published, in *MSIT Workplace*, Effenberg, G. (Ed.), Materials Science International Services, GmbH, Stuttgart; Document ID: 30.10236.1.20, (2006) (Crys. Structure, Phase Diagram, Phase Relations, 11)

[Mas2] Massalski, T.B. (Ed.), *Binary Alloy Phase Diagrams*, 2nd edition, ASM International, Metals Park, Ohio (1990)

[V-C] Villars, P. and Calvert, L.D., *Pearson's Handbook of Crystallographic Data for Intermetallic Phases*, ASM, Metals Park, Ohio (1985)

[V-C2] Villars, P. and Calvert, L.D., *Pearson's Handbook of Crystallographic Data for Intermetallic Phases*, 2nd edition, ASM, Metals Park, Ohio (1991)

DOI: 10.1007/978-3-540-69761-9_5

Aluminium – Iron – Hydrogen

Pierre Perrot

Introduction

Al-Fe alloys, in presence of H do not form hydrides, but interstitial solid solutions which play an important role in steelmaking because of undesirable effects in the embrittlement of steel products. Most of the investigations have been directed towards the solubility of H in Al-Fe melts, solid alloys and on the effect of hydrogen in mechanical properties of Al-Fe alloys. The main experimental results are gathered in Table 1.

Binary Systems

The Al-Fe and Al-H systems are accepted from [2006MSIT] and [2002Per], respectively. The Fe-H system under 0.1 MPa of hydrogen pressure is accepted from [1990San]. The Fe-H system has been carefully investigated by [2003Fuk] up to 10 GPa of hydrogen pressure and 1500°C. The hydrogen pressure- temperature diagram, shown in Fig. 1 presents a drastic lowering of the melting point down to 800°C at 3 GPa. The triple point α-γ-ε of iron is shifted from 8.4 GPa and 430°C for pure iron to 5 GPa and 260°C for the Fe-H system. The hydrogen solubility under high pressure has been investigated by [2005Hir] in the γ region. Under 2.5 GPa, the hydrogen solubility increases with the temperature (from H/Fe = 0.12 at 700°C to H/Fe = 0.2 at 1000°C; under 4 GPa, H/Fe = 0.4 between 400 and 1000°C; under 6 GPa, the hydrogen solubility decreases when the temperature increases (from H/Fe = 0.7 at 700°C to H/Fe = 0.6 at 1000°C).

Solid Phases

Crystallogrphic data of solid phases are given in Table 2. No ternary compounds are known. The H solubility in ferrite containing up to 50 at.% Al determined by direct chemical analysis of alloys equilibrated in gaseous hydrogen at 500, 600 and 700°C was presented by [1957Sie] with a maximum around 5 at.% Al. However, the H solubility in pure αFe used by these authors was too low and the maximum disappears by using the expression proposed by [1982Kub] for the H solubility in pure αFe (Fig. 1). [1957Sie] did not recognize the structural variants of the α ferrite in the range 0 to 50 at.% Al as given by [1982Kub, 2006MSIT]. From the temperature dependence of these data the H_2 dissolution entropy into Al-Fe alloy was evaluated (–70 to –78 $J \cdot K^{-1}$ per mol of H) [1957Lie], in agreement with the hypothesis of hydrogen atoms in interstitial position.

Liquidus, Solidus and Solvus Surfaces

A number of investigations on the solubility of H in liquid Al-Fe alloys are reported. [1961Mae], using a sampling method, reported first order Wagner interaction parameters to be slightly negative (e_H^{Al} = –0.006 at 1600°C), indicating that Al decreases the activity coefficient of H in the melt and increases its solubility at a given H_2 pressure. This behavior is in agreement with earlier investigations [1957Lie] but was not confirmed by most recent investigations. On the contrary, [1963Wei, 1965Bur, 1974Ban1, 1974Ban2], using a Sieverts' method, [1970Fuk] by a sampling method, and [1974Boo, 1974Lev] with a constant volume (drop pressure) technique (also confirmed by more recent work of [1981Sch]) found a decrease of the H solubility with the Al content of the liquid. The solubility of hydrogen in liquid Al decreases also with the iron content [1999Din]. At 1600°C, the minimum of solubility is observed at 0.095 at.% H in a liquid melt containing 44.2 at.% Al.

DOI: 10.1007/978-3-540-69761-9_6

The isobaric H solubility in Al-Fe melts can be represented by the following equation where x_{Al} is the mole fraction of Al:

$$\ln(S/\text{at.\% H}) = 0.5\ln(p_H/\text{Pa}) + A + B\,x_{Al} + C\,x^2_{Al}.$$

The experimental results of [1974Lev] and the accepted values for the H solubility in pure liquid iron ($x_{Al} = 0$) and in pure liquid Al ($x_{Al} = 1$) are well-fitted by the following parameters:

$A = -5.4986 - 4190.7 / T$
$B = -4.4513 + 5189.8 / T$
$C = 6.4972 - 8612.8 / T.$

According to the preceding equations, above 1000°C, iron decreases the solubility of hydrogen into aluminium, and the tendency would be reversed below 1000°C. This is confirmed by the work of [1982Sig] related to the kinetics of hydrogen removal in Al alloys, which accepts an interaction parameter $e_H^{Fe} \approx 0$ at 800-900°C, which means that iron does not modify the solubility of hydrogen in aluminium.

Isothermal Sections

The hydrogen solubility in α(Fe,Al) alloys at 500, 600 and 700°C is shown in Fig 2; the hydrogen solubility in liquid (Fe,Al) alloys at 1600, 1700 and 1800°C is shown in Fig 3.

Thermodynamics

The entropy of dissolution of H_2 gas into α(Fe,Al) alloy at 600°C, evaluated from the hydrogen solubility measurements [1957Lie, 1957Wit] varies from –160 $J \cdot K^{-1}$ per mole of H_2 for pure αFe to –140 $J \cdot K^{-1}$ per mol of H_2 for the α($Fe_{0.5}Al_{0.5}$) alloy.
The value of the Wagner first order interaction parameter deduced from the accepted solubility of hydrogen in the liquid alloy ($e_H^{Al} = +0.012$ at 1600°C) is confirmed by the following experimental determinations: 0.013 [1963Wei], 0.0092 [1970Fuk], 0.011 [1974Ban1] and 0.0116 [1974Boo].
Experimental data are well-fitted with a statistical model developed by [1984Fro] in order to calculate the hydrogen solubility in the whole concentration range from the solubility in pure metals and the first order Wagner interaction parameters (Fig. 3).
From the solubility measurements of hydrogen in Al-Fe alloys (28 at.% Al), [1997Xu] calculates an enthalpy of dissolution of H atoms varying from –159.7 kJ per mole of H between 125 and 550°C, stability domain of the ordered α_1 solid solution to –144.0 kJ per mole of H between 550 and 770°C, stability domain of the ordered α_2 solid solution and –132.1 kJ per mole of H between 770 and 1100°C, stability domain of the disordered α solid solution.

Notes on Materials Properties and Applications

Hydrogen plays an important role in environmental embrittlement of Al-Fe alloys, even for hydrogen contents as low as 0.42 ppm in Fe_3Al [2001Pri]. Aluminium of the alloy reacts with moisture of the air producing atomic hydrogen which enters in the metal in the vicinity of the crack tips. When the embrittlement mechanism is suppressed, for instance in dry oxygen, the ductility of the alloy is found to increase as much as 17-18% [1991Liu]. The embrittlement mechanism was further investigated by [1991She, 1997Su] which observed the fracture path by Scanning Electron Microscopy and draw the same conclusions. For Fe_3Al and disordered α(Fe,Al) alloys, fractures are transgranular in all environment, including in high vacuum; for FeAl and ordered alloys, fractures are intergranular in vacuum and of the mixed mode in air or after hydrogen charging. The *B*2 α_2(FeAl) ordered alloys are thus more subject to environmental embrittlement than the $D0_3$ α_1(FeAl) ordered alloys which exhibits mainly transgranular cleavage fractures [1997Su]. Tensile stress measurements carried out under high vacuum [1989Els] showed that degassing under high vacuum at 350°C leads to an improvement of the ductility at low strain rate; at high strain rate (0.05 s^{-1}), no effect of degassing is observed. These results are explained by the interactions of dislocations with hydrogen atoms. The hot rolled aluminides offer better tensile strength and ductility in comparison with the as-cast iron aluminide [2001Luu]. Due to the fact that hydrogen transport mechanism in Fe_3Al is mainly lattice diffusion, the cleavage strength is decreased significantly by hydrogen.

DOI: 10.1007/978-3-540-69761-9_6

Miscellaneous

The diffusivity of hydrogen in (αFe) is lowered by alloying with Al [1992Hag], which is caused by interstitial sites around the substitutional Al atoms acting as trapping sites. Ordering of the α(Fe,Al) solid solution decreases the diffusivity and permeation rate of hydrogen [2000Luu]. α disordered iron aluminides have higher hydrogen diffusivity and permeation rates than *B*2 (or α_2,FeAl) ordered alloys.

Table 1. Investigations of the Al-Fe-H Thermodynamics

Reference	Method/Experimental Technique	Temperature/Composition/Phase Range Studied
[1957Sie, 1957Wit]	Hydrogen solubility measurement by the Sievert's method	500-700°C, 0.1 MPa H_2, 0 to 50 at.% Al
[1961Mae]	Hydrogen solubility measurement by the sampling method	1600°C, 0.1 MPa, liquid (Fe,Al) alloy (< 6 mass% Al)
[1963Wei]	Hydrogen solubility measurement by the Sievert's method	1530-1750°C, 0.1 MPa, liquid alloy (< 10 mass% Al)
[1970Fuk]	Hydrogen solubility measurement by the sampling method	1550-1650°C, < 0.1 MPa, liquid (Fe,Al) alloy (< 6 mass% Al)
[1974Ban1, 1974Ban2]	Hydrogen solubility measurement by the Sievert's method	1548-1672°C, 0.1 MPa, liquid (Fe,Al) alloy (< 10 mass% Al)
[1974Boo]	Hydrogen solubility measurement by a constant volume technique	1600°C, 0.1 MPa, liquid (Fe,Al) alloy (< 10 mass% Al)
[1974Lev]	Hydrogen solubility measurement by the Sievert's method	1480-1600°C, 0.1 MPa, liquid alloy (< 30 mass% Al + pure Al)
[1997Xu]	Hydrogen solubility measurement by hydrogen extraction	250-1100°C, 0.1 MPa, 28 at.% Al

Table 2. Crystallographic Data of Solid Phases

Phase/ Temperature Range [°C]	Pearson Symbol/ Space Group/ Prototype	Lattice Parameters [pm]	Comments/References
(Al) < 660.452	*cF*4 $Fm\bar{3}m$ Cu	a = 404.88	pure Al at 24°C [Mas2, V-C2]
δ, (δFe) 1538 - 1394	*cI*2 $Im\bar{3}m$ W	a = 293.15	[Mas2]
α, (αFe) < 912°C	*cI*2 $Im\bar{3}m$ W	a = 286.65	pure Fe at 20°C [Mas2, V-C2] (*A*2 structure). Dissolves up to 50 at.% Al at 1102°C

(*continued*)

DOI: 10.1007/978-3-540-69761-9_6

Phase/ Temperature Range [°C]	Pearson Symbol/ Space Group/ Prototype	Lattice Parameters [pm]	Comments/References
γ, (γFe) 1394 - 912	*cF*4 $Fm\bar{3}m$ Cu	a = 293.16	at 915°C [Mas2, V-C2] dissolves up to 1.2 at.% Al at 1170°C
α_1, Fe_3Al < 552.5	*cF*16 $Fm\bar{3}m$ BiF_3	a = 578.86 to 579.3	[2006MSIT] composition range from 22.5 to 36.5 at.% Al ($D0_3$ structure)[a)]
α_2, FeAl < 1310	*cP*2 $Pm\bar{3}m$ CsCl	a = 289.76 to 290.78	[2006MSIT] Composition range from 22.0 to 50.0 at.% Al (*B*2 structure)[a)]
ε, Fe_2Al_3 1232 - 1102	*cI*16	a = 598.0	[2006MSIT] composition range from 54.5 to 62.5 at.% Al
ζ, $FeAl_2$ < 1156	*aP*8 *P*1 $FeAl_2$	a = 487.8 b = 646.1 c = 880.0 α = 91.756° β = 73.27° γ = 96.89°	at 66.9 at.% Al [2006MSIT] composition range from 65.5 to 67.0 at.% Al
θ, Fe_2Al_5 < 1169	*oC*24 *Cmcm*	a = 765.59 b = 641.54 c = 421.84	at 71.5 at.% Al [2006MSIT] composition range from 71.0 to 72.5 at.% Al
η, Fe_4Al_{13}	*mC*102 *C2/m* Fe_4Al_{13}	a = 1552.7 to 1548.7 b = 803.5 to 808.4 c = 1244.9 to 1248.8	from 74.16 to 76.7 at.% Al [2006MSIT] sometimes labelled $FeAl_3$

a) $\alpha_1(Fe_3Al)$ ($D0_3$ structure) and α_2(FeAl) (*B*2 structure) are ordered structures of the α(Fe,Al) (*A*2 structure) solid solution whose stability range extends up to 50 at.% Al

DOI: 10.1007/978-3-540-69761-9_6

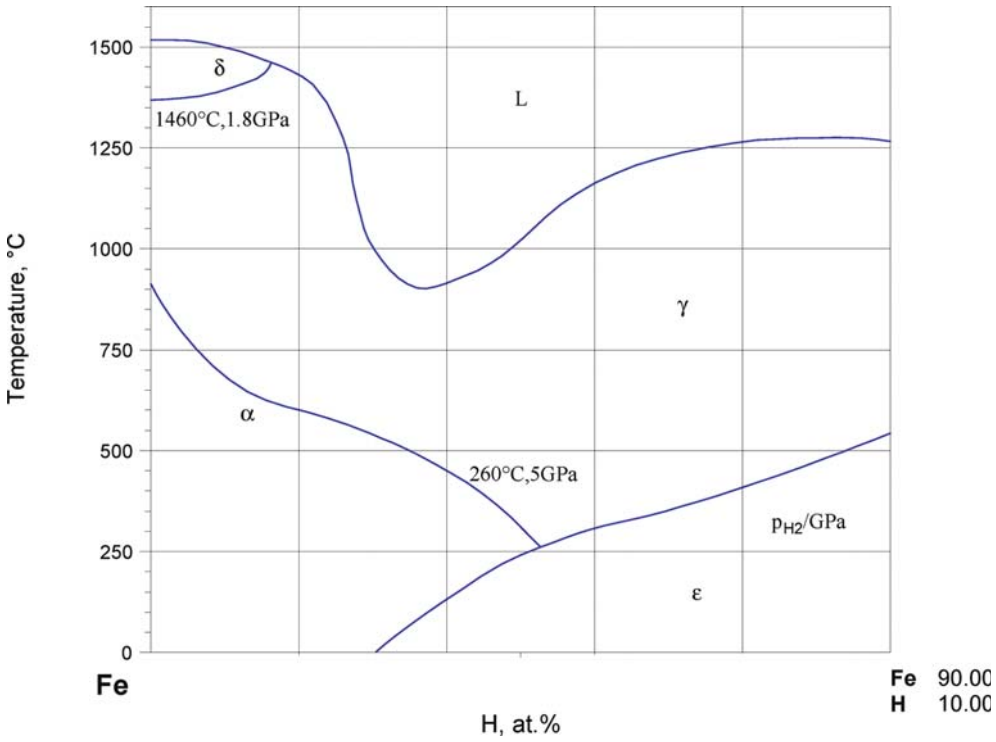

Fig. 1. Al-Fe-H. The Fe-H binary system under high pressures

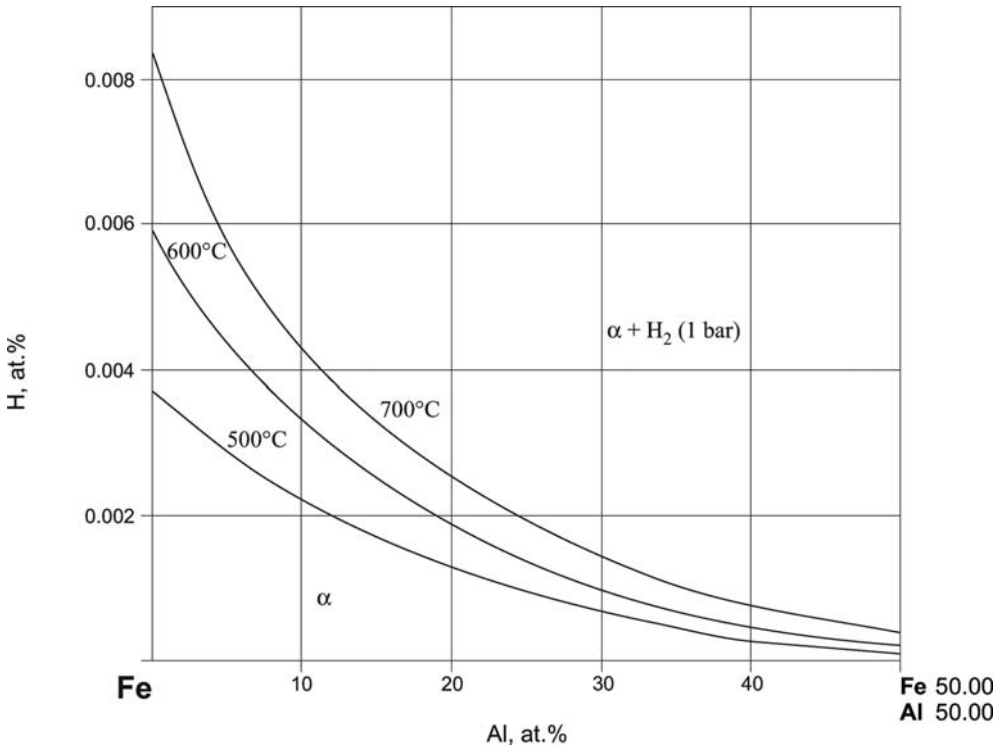

Fig. 2. Al-Fe-H. The hydrogen solubility in α(Fe,Al) alloys at 500, 600 and 700°C

DOI: 10.1007/978-3-540-69761-9_6

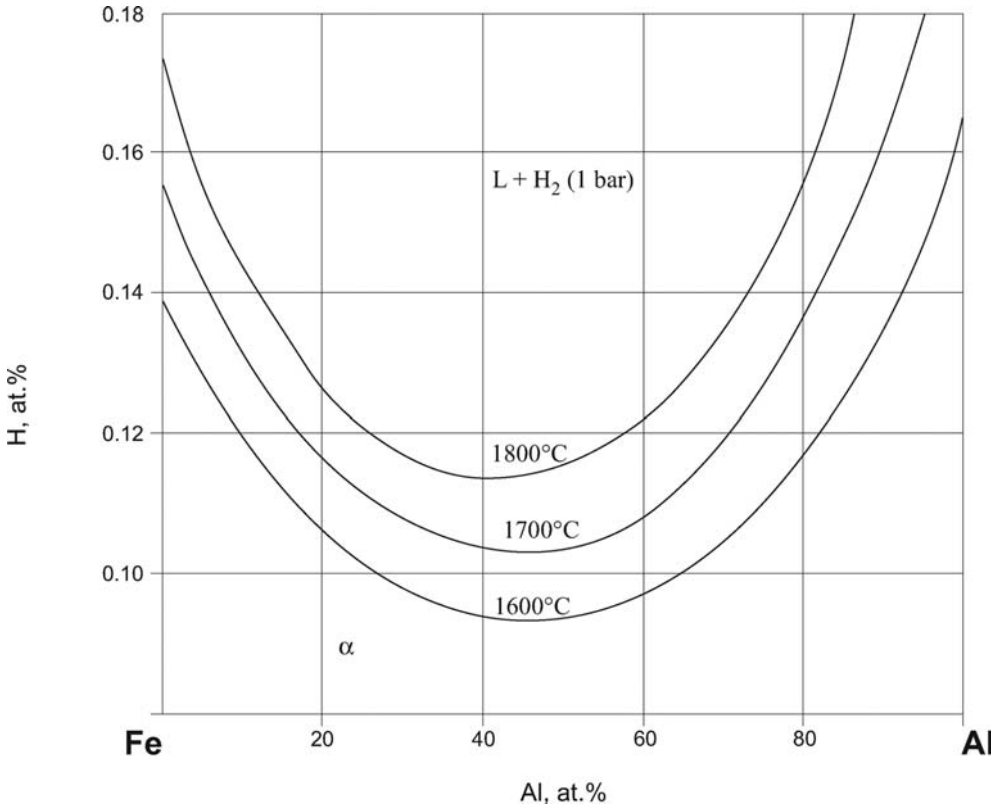

Fig. 3. Al-Fe-H. The hydrogen solubility in liquid (Fe,Al) alloys at 1600, 1700 and 1800°C

DOI: 10.1007/978-3-540-69761-9_6

References

[1957Lie] Lieser, K.H., Witte, H., "Solubility of Hydrogen in Alloys. IV. Discussion" (in German), *Z. Elektrochem.*, **61**(3), 367–376 (1957) (Phase Relation, Calculation, Review, 29)

[1957Sie] Siegelin, W., Lieser, K.H., Witte, H., "Hydrogen Solubility in Alloys. III. Investigations on the Ternary Systems $MgCu_2$-$MgAl_2$, $MgCu_2$-$MgSi_2$, $MgNi_2$-$MgCu_2$ and Binary Systems Ag-Cd, Cu-Be, Ag-Mg, Cu-Mg, Ni-Al, Ni-Si, Co-Al, Fe-Al" (in German), *Z. Elektrochem.*, **61**(3), 359–366 (1957) (Experimental, Phase Diagram, 28)

[1957Wit] Witte, H., "Solubility of Hydrogen in Alloys" (in German), *Neue Huette*, **2**(12), 749–756 (1956) (Experimental, Thermodyn., 24)

[1961Mae] Maekawa, S., Nakagawa, Y., "The Effect of Some Alloying Elements on the Solubility of Hydrogen in Liquid Iron" (in Japanese), *Nippon Kinzoku Gakkai-shi*, **25**(9), 577–580 (1961) (Experimental, Phase Relations, Thermodyn., 6)

[1963Wei] Weinstein, M., Elliott, J.F., "Solubility of Hydrogen in Liquid Iron Alloys", *Trans. Met. Soc. AIME*, **227**, 382–393 (1963) (Calculation, Experimental, Thermodyn., 27)

[1965Bur] Burylev, B.P., "Solubility of Hydrogen in Liquid Iron Alloys" (in Russian), *Izv. Vyss. Uchebn. Zaved., Chern. Metall.*, **8**(2), 17–22 (1965) (Phase Relations, Thermodyn., Review, 13)

[1970Fuk] Fukuda, S., Sugiyama, T., Furukawa, T., Kato, E., "Solubility of Hydrogen in Liquid Iron Alloys", *Rep. Casting Research Lab./Waseda Univ.*, (21), 35–46 (1970) (Calculation, Experimental, Phase Relations, Thermodyn., 22)

[1974Ban1] Ban-ya, S., Fuwa, T., "Solubility of Hydrogen in Liquid Iron Alloys", *Tech. Rep. Tohoku Imp. Univ.*, **39**(1), 209–227 (1974) (Experimental, Phase Relations, Thermodyn., 22)

[1974Ban2] Ban-ya, S., Fuwa, T., "The Effect of Al, B, Ge, Ta, Sn and Zr on the Solubility of Hydrogen in Liquid Iron" (in Japanese), *Tetsu to Hagane (J. Iron Steel Inst. Jpn.)*, **60**, 1299–1309 (1974) (Experimental, Phase Relations, Thermodyn., 12)

[1974Boo] Boorstein, W.M., Pehlke, R.D., "Measurements of Hydrogen Solubility in Liquid Iron Alloys Employing a Constant Volume Technique", *Metall. Trans.*, **5**, 300–405 (1974) (Experimental, Phase Relations, Thermodyn., 29)

[1974Lev] Levin, E.S., Kostina, T.K., Petrushevsky, M.S., Gel'd, P.V., Kurochkin, K.T., "Solubility of Hydrogen in Iron-Aluminium Melts", *Russ. Metall.*, (2), 30–33 (1974) translated from *Izv. Akad. Nauk SSSR, Met.*, (2), 43–47, (1974) (Experimental, Phase Relations, Thermodyn., 17)

[1981Sch] Schuermann, E., Kaettlitz, W., "Equivalent Effect of the Alloying Elements on the Concentration- and Temperature-Dependent Hydrogen Solubility in Iron-Rich Ternary and Multicomponent Melts" (in German), *Arch. Eisenhuettenwes.*, **52**(8), 295–301 (1981) (Calculation, Phase Diagram, Review, 20)

[1982Kub] Kubaschewski, O., "Iron-Hydrogen" in "*Iron Binary Phase Diagrams*", Springer-Verlag, Berlin, 46–48 (1982) (Phase Diagram, Review, 15)

[1982Sig] Sigworth, G.K., Engh, T.A., "Chemical and Kinetics Factors Related to Hydrogen Removal from Aluminum", *Metall. Trans. B*, **13B**, 447–460 (1982) (Calculation, Kinetics, Theory, Thermodyn., Transport Phenomena, 45)

[1984Fro] Frohberg, M.G., Anik S., "The Prediction of Hydrogen Solubility in Binary Iron Melts" (in German), *Arch. Eisenhuettenwes.*, **55**(2), 45–48 (1984) (Calculation, Experimental, Phase Relations, Thermodyn., 20)

[1989Els] Elstrom, J.C., Andrieu, E., Pineau, A., "Hydrogen Effect on High Temperature Ductility of a Powder Metallurgy Fe-Al Alloy", *Scr. Metall.*, **23**(8), 1397–1400 (1989) (Experimental, Mechan. Prop., 12)

[1990San] San Martin, A., Manchester, F.D., "The Fe-H (Iron-Hydrogen) System", *Bull. Alloys Phase Diagrams*, **11**(2), 173–184 (1990) (Phase Diagram, Review, Thermodyn., 86)

[1991Liu] Liu, C.T., Fu, C.L., George, E.P., Painter, G.S., "Environmental Embrittlement in Fe-Al Aluminides", *ISIJ International*, **31**(10), 1192–1200 (1991) (Experimental, Mechan. Prop., 41)

[1991She] Shea, M., Castanga, A., Stoloff, N.S., "Hydrogen Embrittlement of FeAl and Fe_3Al", *Mater. Res. Soc. Symp. Proc.: High-Temp. Ordered Intermetallic Alloys IV*, **213**, 609–616 (1991) (Experimental, Mechan. Prop., 3)

DOI: 10.1007/978-3-540-69761-9_6

[1992Hag] Hagi, H., "Effect of Substitutional Alloying Elements (Al, Si, V, Cr, Mn, Co, Ni, Mo) on Diffusion Coefficient of Hydrogen in αFe", *Mater. Trans., JIM*, **33**(5), 472–479 (1992), translated from *J. Jpn. Inst. Met.*, **55**(12), 1283–1290 (1991) (Experimental, Mechan. Prop., Transport Phenomena, 35)

[1997Su] Su, J.Q., Gao, S.J., Zhang, S.S., Guo, J.T., Hu, Z.Q., "The Effect of Atomic Order on Environmental Embrittlement of an Fe_3Al Based Alloy", *Mater. Letters*, **31**(3–6), 227–231 (1997) (Experimental, Mechan. Prop., 27)

[1997Xu] Xu, Z.R., McLellan, R.B., "The Solubility of Hydrogen in Fe_3Al-Intermetallics", *J. Phys. Chem. Solids*, **58**(12), 2127–2129 (1997) (Experimental, Phase Relations, 26)

[1999Din] Ding, X., Fan, P., Wang, W., "Thermodynamic Calculations for Alloy Systems", *Met. Mat. Trans., B*, **30B**(2), 271–277 (1999) (Thermodyn., Calculation, Review, 17)

[2000Luu] Luu, W.C., Wu, J.K., "Hydrogen Transport and Environmental Embrittlement Effects in Iron Aluminides", *J. Mater. Sci.*, **35**(16), 4121–4127 (2000) (Experimental, Transport Phenomena, Mechan. Prop., 24)

[2001Luu] Luu, W.C., Wu, J.K., "Moisture and Hydrogen Embrittlement of Fe_3Al Alloy", *Mater. Chem. Phys. Sci.*, **35**(16), 4121–4127 (2000) (Experimental, Transport Phenomena, Mechan. Prop., 24)

[2001Pri] Priyadarshi, A., Balasubramaniam, R., "On Critical Hydrogen Concentration for Hydrogen Embrittlement of Fe_3Al", *Bull. Mater. Sci.*, **24**(5), 559–562 (2001) (Experimental, Mechan. Prop., 20)

[2002Per] Perrot, P., "Al-H (Aluminium - Hydrogen), "MSIT Binary Evaluation Program, in *MSIT Workplace*, Effenberg, G. (Ed.), MSI, Material Science International Service GmbH, Stuttgart; Document ID: 20.14832.20, (2002) (Phase Diagram, Phase Relations, Assessment, Crys. Structure, 21)

[2003Fuk] Fukai, Y., Mori, K., Shinomiya, H., "The Phase Diagram and Superabundant Vacancy Formation in Fe-H Alloys under High Hydrogen Pressures", *J. Alloy Compd.*, **348**, 105–109 (2003) (Phase Diagram, Experimental, 42)

[2005Hir] Hiroi, T., Fukai, Y., Mori, K., "The Phase Diagram and Superabundant Vacancy Formation in the Fe-H Alloy Revisited", *J. Alloys Compd.*, **404/406**, 252–255 (2005) (Phase Diagram, Experimental, 42)

[2006MSIT] "Al-Fe (Aluminum-Iron)", Diagrams as Published, in *MSIT Workplace*, Effenberg, G. (Ed.), Materials Science International Services, GmbH, Stuttgart; Document ID: 30.10236.1.20, (2006) (Crys. Structure, Phase Diagram, Phase Relations, 11)

[Mas2] Massalski, T.B. (Ed.), *Binary Alloy Phase Diagrams*, 2nd edition, ASM International, Metals Park, Ohio (1990)

[V-C2] Villars, P. and Calvert, L.D., *Pearson's Handbook of Crystallographic Data for Intermetallic Phases*, 2nd edition, ASM, Metals Park, Ohio (1991)

DOI: 10.1007/978-3-540-69761-9_6

Aluminium – Iron – Molybdenum

Gautam Ghosh

Introduction

A summary of experimental studies of phase equilibria is given in Table 1. While most of these studies have investigated the effect of Mo on the order-disorder transitions has been investigated in Fe rich alloys [1968Bir, 1969Bir, 1969Sel, 1984Kra, 1985Men, 1987Die, 1987For, 1989McK, 1991Pra1, 1991Pra2, 1991Pra3, 1991Pra4, 1993Pra, 1995Ant, 1998Nis, 1998Sun, 2004Nis], others have investigated the phase equilibria of Al corner [1970Mar, 1987Sok, 1988Che]. Only recently, a complete isothermal section at 1000°C has been reported [2004Eum1, 2004Eum2]. The experimental results have been reviewed from time to time [1980Fer, 1990Kum, 1992Gho, 1992Rag, 2005Rag].

[1970Mar] investigated the phase equilibria at 800 and 1050°C in alloys containing up to about 46 at.% Fe and 60 at.% Mo, and reported two partial isotherms. They prepared 75 ternary alloys using elements of the following purity: 99.97% Al, 99.95% Fe, 99.95% Mo. The alloys were prepared in an electric furnace under an argon atmosphere and subsequently annealed in vacuum at 1050°C for 8 h and 800°C for 800 h. The phases were identified by X-ray diffraction and microstructural observations. [1987Sok] reported two polythermal sections along Fe:Mo = 3:1 (at.%) and $FeAl_3$-$MoAl_{12}$. They prepared a number of ternary alloys in an arc furnace under Ar atmosphere. The alloys were annealed at 550°C in evacuated silica capsules and subsequently quenched in ice water. The phase analysis was carried out by means of DTA, X-ray diffraction and microstructural techniques. [1988Che] studied the phases formed after rapid solidification (by melt-spinning technique) of six ternary alloys containing up to about 6 at.% Fe and 2 at.% Mo and also their decomposition behavior after annealing at 250, 350 and 450°C for 25 h. These alloys were prepared by arc melting using metals of the following purity: 99.999 mass% Al, 99.95 mass% Fe and 99.999 mass% Mo. DTA, microstructural and X-ray diffraction techniques were used to determine the phases.

Very recently, [2004Eum1, 2004Eum2] reported an isothermal section at 1000°C. They prepared 25 ternary alloys by levitation melting and using elements of following purity: 99.999% Al, 99.95% Fe, 99.95% Mo. The alloys were annealed at 1000°C for 200 h followed by quenching in iced brine. The alloys were characterized by conventional metallography, electron probe microanalysis and X-ray diffraction.

Binary Systems

The Al-Fe system is accepted from [2006MSIT]. The Al-Mo system is accepted from [2005Sch] which is based on the experimental data of [1971Rex] in the composition range Mo-Mo_3Al_8 and [1991Sch] in the composition range Al-Mo_3Al_8. The Fe-Mo binary phase diagram is accepted from [1982Kub].

Solid Phases

The maximum equilibrium solid solubilities of Fe and Mo in (Al) are about 0.5 at.% at 652°C [1982Kub] and 0.05 at.% at 660.35°C [Mas], respectively. However, by rapid solidification the corresponding solid solubilities can be increased up to about 4.4 at.% Fe and 2.5 at.% Mo [1976Mon]. The lattice parameter of supersaturated (Al) containing about 4.4 at.% Fe is about 401.2 pm [1976Mon]. Fe_3Al is reported to dissolve at least 20 at.% Mo [2004Nis] with a concomitant increase in $D0_3$ (α_1) → B_2 (α_2) temperature [1968Bir, 1969Bir, 1969Sel, 1984Kra, 1985Men, 1987Die, 1987For, 1989McK, 1991Pra1, 1991Pra2, 1991Pra3, 1991Pra4, 1993Pra, 1995Ant, 1998Nis, 2004Nis]. The lattice parameter of $B2$ (α_2) also increases with increasing Mo content. The μ phase, $Mo_2(Fe,Al)_3$, dissolves about 16 at.% Al at 1000°C [2004Eum1, 2004Eum2].

So far, four ternary phases, τ_1, τ_2, τ_3 and τ_4, have been reported, and their compositions are designated as $MoFe_{0.28}Al_{2.72}$, $Mo_5Fe_{35}Al_{60}$, $Mo_9Fe_{4.75}Al_{0.25}$ and $Mo_3Fe_8Al_9$, respectively. The τ_1 phase is stable above

DOI: 10.1007/978-3-540-69761-9_7

900°C, and the τ_2 phase is stable between 1050 and 1000°C [1970Mar]. However, [2004Eum1, 2004Eum2] observed only τ_1 at 1000°C. The structure of τ_2 is unknown [1970Mar]. [1999Ste] obtained τ_3 phase accidentally during heating of Al-Fe-U alloys in a molybdenum tube at 1650°C. The composition of needle-shaped single crystals was confirmed by EDAX in SEM. [2004Eum2] observed τ_4 phase in as-cast alloys with compositions Fe-(36.9-39.5) at.% Al-(12.4-22.8) at.% Mo, and it is reported to be stable above 1000° C. During heat treatment at 1000°C, τ_4 decomposes to form Mo_3Al [2004Eum2]. The structure of τ_4 is unknown.

[1983Bus] reported the Heusler phase $MoFe_2Al$ with a lattice parameter a = 591.8 pm in the as-cast alloy, but it was not confirmed in subsequent investigations. Therefore, it is not considered as an equilibrium phase. [1991Bi] observed a grain boundary phase, in rapidly solidified Al-2.2 at.% Mo-(0.1-0.5) at.% Fe alloys that were annealed at 400-450°C, with a bcc structure and a lattice parameter a = 1272 pm.

Rapid solidification of an Al-8 mass% Fe-2 mass% Mo alloy gives rise to (Al) and T' phases [1986Fie]. The latter phase has a five-fold diffraction symmetry, but it is different from that of an icosahedral phase. On the other hand, rapid solidification of $Mo_9Fe_{11}Al_{80}$ gives rise to a quasicrystal with icosahedral symmetry [1988Men, 1989Sri, 1993Kel], and it has a quasilattice constant of a = 460.3 pm [1989Sri].

The details of the crystal structures and lattice parameters of the solid phases are listed in Table 2.

Order-Disorder Phase Transitions

The effect of Mo additions on the order-disorder transition temperatures of Fe_3Al has been studied extensively [1968Bir, 1969Bir, 1969Sel, 1984Kra, 1985Men, 1987Die, 1987For, 1989McK, 1991Pra1, 1991Pra2, 1991Pra3, 1991Pra4, 1993Pra, 1995Ant, 1998Nis, 2004Nis] employing various experimental techniques, such as X-ray diffraction, electrical resistivity, hardness, dilatometry, transmission electron microscopy and calorimetry. Along the section Fe_3Al-Mo_3Al, addition of Mo to Fe_3Al increases the temperature of both the Fe_3Al ($D0_3$ or α_1) → FeAl ($B2$ or α_2) and FeAl (α_2) → (αFe) transitions [1968Bir, 1969Bir, 1969Sel, 1984Kra, 1985Men, 1987Die, 1987For, 1989McK, 1991Pra1, 1991Pra2, 1991Pra3, 1991Pra4, 1993Pra, 1995Ant, 1998Nis, 2004Nis]. Along the section Fe_3Al-$MoFe_3$, addition of Mo to Fe_3Al increases the Fe_3Al ($D0_3$ or α_1) → FeAl ($B2$ or α_2) transition temperature whereas that of FeAl ($B2$ or α_2) → (αFe) decreases [1968Bir, 1969Sel]. With the addition of more than 3.5 at.% Mo, Fe_3Al is likely to transform directly into the (αFe) phase [1968Bir]. The composition and temperature limits of the ternary ordered phases based on Fe_3Al and FeAl are shown in Fig. 1 [1993Pra, 1995Ant] and Fig. 2 [1969Sel].

X-ray diffraction data show that Mo atom occupies predominantly the 4 (b) Wyckoff sites (1/2, 1/2, 1/2) in $D0_3$ structure [1987For, 1993Pra, 1995Ant, 1998Sun]. Different arguments have been proposed about the relation between the site occupancy of Mo in $D0_3$ and its effect on the $D0_3$ → $B2$ transition temperature. [1987For] have pointed out that the increase in $D0_3$ → $B2$ is related to the increase in ordering energy of the $D0_3$ structure. Consequently, the stabilization of $D0_3$ phase should be attributed to the site preference of the substituted atom. Based on a systematic study involving several early transition elements, [1995Ant] argued that the site preference of Mo has no strong correlation with atomic size, rather it is better correlated to its position in the periodic table, and hence the character of its valence electrons. However, they showed that the increase in $D0_3$ → $B2$ transition temperature is related to the difference in metallic radius of the Mo atom and an Al atom, specifically $(r_{Al} - r_{Mo})^2$, or the elastic energy associated with the atom size mismatch. On the other hand, [1998Nis] proposed that the increase in transition temperature may be related to the variation in average electron concentration.

A theoretical analysis of order-disorder ($A2$/$B2$) transition temperature and short-range ordering characteristics of $Fe_{0.5}(Al_{1-x}Mo_x)_{0.5}$ alloys were carried out by [1999Mek]. They applied a combination of statistico-thermodynamical theory of ordering within quasi-chemical framework, and predicted that Mo preferentially substitutes Fe sublattice sites in $Fe_{0.5}(Al_{1-x}Mo_x)_{0.5}$. Also, based on the calculated partial ordering energies they predicted an increase in $B2$ → $A2$ temperature for $Fe_{0.5}(Al_{1-x}Mo_x)_{0.5}$ alloys. While there is no experimental data of such alloys, available data along Fe_3Al-$MoFe_3$ section (Fig. 1) does show an increase in $B2$ → $A2$ temperature. Using a linear muffin-tin orbital method, [2002Boz] calculated the formation energies of $(Fe,Mo)_{0.5}Al_{0.5}$ and $Fe_{0.5}(Al,Mo)_{0.5}$ alloys with $B2$ structure. They predicted that in both cases Mo atoms prefer to occupy the Al sublattice. Also, the calculated formation energies are predicted to be more positive compared to binary $Fe_{0.5}Al_{0.5}$.

DOI: 10.1007/978-3-540-69761-9_7

Isothermal Sections

Figures 3, 4 and 5 shows a partial isothermal section at 1050°C [1970Mar], an isothermal section at 1000°C [2004Eum1, 2004Eum2] and a partial isothermal section at 800°C [1970Mar], respectively. [1980Bre] reported that $MoAl_3$ is metastable and it transforms to the stable $MoAl_5$ phase; however, in the accepted Al-Mo diagram $MoAl_3$ is stable between 818 and 1222°C. [1970Mar] did not report the solubility of Fe in Al-Mo intermetallics. In this assessment it is assumed that the Fe solubilities at 1050°C are similar to those at 1000°C, as reported by [2004Eum1, 2004Eum2], and at 800°C they are negligible. Minor adjustments have been made to comply with the binary phase diagrams accepted here. In Fig. 4, the phase boundaries involving Mo_4Al_{17} are shown dotted as this phase was not considered by [2004Eum1, 2004Eum2]. Table 3 summarizes the phases present in six alloys in the as-melt-spun condition, and also after annealing at 250, 300 and 450°C for 25 h [1988Che]. It should be noted that $MoAl_3$ and $FeAl_6$ are metastable phases, but they exist even after annealing at 450°C for 25 h. From the data presented in Table 3, it is concluded that, except for the alloy containing 6 at.% Fe and 2 at.% Mo, which was annealed at 450°C for 25 h, equilibrium is not achieved [1988Che]. In the ternary composition range investigated by [1988Che], after annealing the conventionally cast alloys, the isothermal section at 550°C was reported to contain a large (Al)+Fe_4Al_{13}+$MoAl_{12}$ three-phase field surrounded by small two-phase fields (Al)+Fe_4Al_{13} and (Al)+$MoAl_{12}$.

Temperature – Composition Sections

Figures 6 and 7 show the polythermal sections along Fe:Mo = 3:1 (at.%) and Fe_4Al_{13}-$MoAl_{12}$, respectively, after [1987Sok]. In Fig. 6, the liquidus consists of two branches and they correspond to the regions of primary crystallization of (Al) and Fe_4Al_{13}. The solidus in Fig. 6 is represented by a horizontal line at 605°C. In Fig. 7, the liquidus consists of eight branches that correspond to the regions of primary crystallization of Fe_4Al_{13}, Mo_3Al_8, $Mo_{1-x}Al_{3+x}$, $MoAl_4$, Mo_4Al_{17}, Mo_5Al_{22}, $MoAl_5$, and $MoAl_{12}$ phases. Along this section, a quasibinary eutectic reaction L ⇌ Fe_4Al_{13}+$MoAl_{12}$ occurs at about 89.5 at.% Al and 660°C. Here the solidus is represented by a horizontal line at 660°C.

Notes on Materials Properties and Applications

A summary of experimental investigation of properties is given in Table 4. In particular, the microstructural stability [1988Che, 1990Nam, 1991Nam, 1993Mil, 1993Bar, 1995Lou, 1996Yam] and mechanical properties [1988Ots, 1989Cho, 1990Cho, 1991Nam, 1993Bar, 1996Yam] of rapidly solidified Al-rich alloys have received considerable interests. Rapid solidification of Fe rich alloys leads to novel microstructures [1991Pra2, 1991Pra3, 1991Pra4]. The effect of order-disorder transition on the mechanical properties of Fe rich alloys have also been reported [1987Die, 1989McK, 1991Pra1, 1997Nis, 1998Nis, 1998Sun, 2004Nis]. [2004Eum1] reported the hardness, compressive yield stress (25-1000°C) and ductile-brittle transition temperature of 13 ternary alloys with composition Fe-(3.2-10) at.% Al-(4-50) at.% Mo. While many of them contain μ phase, alloys containing 10-20 at.% Al and 16.1-23.4 at.% Mo show a metastable R phase in the as-cast condition. After annealing at 1000°C for 200 h, the R phase transforms to the equilibrium μ phase. They found that both R and μ phases impart similar hardness and strength in these alloys. [2004Eum2] reported the hardness and compressive yield stress (25-1000°C) of 12 ternary alloys with composition Fe-(28-41.4) at.% Al-(3-22.8) at.% Mo. These alloys have either *B*2 or $D0_3$ matrix, and are strengthened by either Mo_3Al or τ_4 as precipitates. However, the phase τ_4 is observed only in as-cast alloys, and it transforms to Mo_3Al during annealing at 1000°C. Strength levels up to 1.6 GPa have been achieved in these alloys, although they are brittle.

An icosahedral phase has been obtained by rapid solidification of $Mo_9Fe_{11}Al_{80}$ alloy [1988Men, 1989Sri]. At a heating rate of 10°C·min^{-1}, the icosahedral phase undergoes decomposition around 598°C to form three equilibrium phases Fe_4Al_{13}, $MoAl_5$ and $MoAl_{12}$ [1988Men]. Magnetization data of the icosahedral phase show that the alloy exhibits Curie paramagnetism at low temperature (< 100 K) and Pauli paramagnetism at higher temperatures. The icosahedral phase exhibits a localized Fe moment of 0.19 μ_B [1989Sri]. The magnetic moment of as-cast $MoFe_2Al$ ($L2_1$) is reported to be 0.36 μ_B per formula unit [1983Bus].

The influence of atomic structure on the magnetic properties of Fe rich ternary alloys has been presented based on the experimental data [1984Zak] and calculated results [2005Gon]. The results of Mössbauer

DOI: 10.1007/978-3-540-69761-9_7

spectroscopy in Fe-29Al-1.5Mo (at.%) alloy show that the model of highly localized exchange interaction is applicable, and also the influence of nearest-neighbor is dominant in the magnetic polarization [1984Zak]. [2005Gon] calculated the local magnetic moment of Fe in several bcc-based ordered ternary phases employing first-principles technique. They also found that the localized magnetic moment of Fe is sensitive to the nearest-neighbor environment.

The oxidation and corrosion resistance, up to 1000°C, of ternary alloys have been investigated several times [1954Fon, 1991Ge, 1993Kai, 2000Che, 2004Eum1, 2004Eum2]. The short term oxidation resistance of Al-Fe alloys is not significantly impaired due to the addition of Mo [2004Eum1, 2004Eum2].

Table 1. Investigations of the Al-Fe-Mo Phase Relations, Structures and Thermodynamics

Reference	Method/Experimental Technique	Temperature/Composition/Phase Range Studied
[1968Bir]	Dilatometry, XRD	20-25 at.% Al, 0.5-5 at.% Mo, Fe = bal.; 100-900°C; $D0_3 \rightleftharpoons B2$ order-disorder transition
[1969Bir]	Dilatometry, resistivity, XRD	20-25 at.% Al, 1-5 at.% Mo, Fe = bal.; up to 900°C; $D0_3 \rightleftharpoons B2$ order-disorder transition
[1969Sel]	XRD	20-25 at.% Al, 1-5 at.% Mo, Fe = bal.; up to 800°C; $D0_3 \rightleftharpoons B2$ order-disorder transition
[1970Mar]	Metallography, XRD	Up to 46% Fe and 60% Mo, 1-5 at.% Mo, Al = bal.; 1050-800°C
[1983Bus]	XRD	$MoFe_2Al$
[1984Kra]	Calorimetry, XRD	$Mo_{0.005}Fe_3Al_{0.995}$; up to 900°C
[1985Men]	TEM	3-6 at.% Mo, 25 at.% Al, Fe = bal.; $D0_3 \rightleftharpoons B2$ order-disorder transition
[1986Fie]	TEM	2 mass% Mo, 8 mass% Fe, Al = bal.
[1987For]	High-temperature XRD	1.5-1.7 at.% Mo, 25.3-27.2 at.% Al, Fe = bal.; $D0_3 \rightleftharpoons B2$ order-disorder transition
[1987Sok]	DTA, metallography, XRD	$FeAl_3$-$MoAl_{12}$ section, 90.5-96 at.% Fe with Fe/Mo ratio of 3:1
[1988Che]	DTA, metallography, XRD	0.15-2 at.% Mo, 0.35-6 at.% Fe, Al = bal.; 250-550°C
[1988Men]	TEM, XRD, DSC	$Mo_9Fe_{11}Al_{80}$
[1989McK]	DSC, resistivity	0.42 - 6.88 at.% Mo, 26.67-30.7 at.% Al, Fe = bal.; up to 800°C
[1989Sri]	XRD	$Mo_9Fe_{11}Al_{80}$
[1991Pra1]	XRD	Up to 15 at.% Mo, 20-60 at.% Al, Fe = bal.; 250-550°C
[1991Pra2]	TEM	15 at.% Mo, 37 at.% Al, Fe = bal.
[1994Che]	XRD	36.7 at.% Mo, 9.5 at.% Al, Fe = bal.
[1995Ant]	DTA, XRD	$Mo_2Fe_{72}Al_{26}$, $Mo_4Fe_{70}Al_{26}$; $D0_3 \rightleftharpoons B2$ order-disorder transition

(*continued*)

DOI: 10.1007/978-3-540-69761-9_7

Reference	Method/Experimental Technique	Temperature/Composition/Phase Range Studied
[1997Nis]	Hardness, XRD	$(Fe_{1-x}Mo_x)_3Al$; up to 920°C and $D0_3 \rightleftharpoons B2$ order-disorder transition
[1998Nis]	Hardness, TEM, resistivity	$(Fe_{1-x}Mo_x)_3Al$ with $0 \le x \le 0.1$; $D0_3 \rightleftharpoons B2$ order-disorder transition
[1998Sun]	SEM, TEM, neutron diffraction, XRD	5.75 at.% Mo, 25.08 at.% Al, Fe = bal.; 1000 and 500°C
[2004Eum1, 2004Eum2]	Metallography, SEM, XRD	5.75 at.% Mo, 25.08 at.% Al, Fe = bal.; 1000°C
[2004Nis]	Resistivity, XRD	$(Fe_{1-x}Mo_x)_3Al$ with $0 \le x \le 0.2$; up to 800°C and $D0_3 \rightleftharpoons B2$ order-disorder transition

Table 2. Crystallographic Data of Solid Phases

Phase/ Temperature Range [°C]	Pearson Symbol/ Space Group/ Prototype	Lattice Parameters [pm]	Comments/References
(Al) ≤ 660.452	*cF*4 $Fm\bar{3}m$ Cu	a = 404.88	pure Al at 25°C [Mas2]
(αδFe) (αFe)(r) ≤ 912	*cI*2 $Im\bar{3}m$ W	a = 286.65	pure Fe at 25°C [Mas2]
(δFe)(h_2) 1538 - 1394		a = 293.15	pure Fe at 1480°C [Mas2]
γ, (γFe)(h_1) 1394 - 912	*cF*4 $Fm\bar{3}m$ Cu	a = 364.67	pure Fe at 915°C [Mas2]
(Mo) ≤ 2623	*cI*2 $Im\bar{3}m$ W	a = 314.7	pure Mo at 25°C [Mas2]
α_1, Fe_3Al ≤ 547 $(Fe_{1-x},Mo_x)_3Al$	*cF*16 $Fm\bar{3}m$ BiF_3	 a = 578.86 to 579.3 a = 580.13 a = 581.26 a = 581.79 a = 581.99	solid solubility ranges from ~25 to ~37 at.% Al [2006MSIT] [2006MSIT] x = 0.05 at 25°C [1997Nis] x = 0.15 at 25°C [1997Nis] x = 0.15 at 25°C [1997Nis] x = 0.20 at 25°C [1997Nis]
α_2, FeAl ≤ 1310 (Fe_{1-x},Mo_x) Al	*cP*2 $Pm\bar{3}m$ CsCl	a = 289.76 to 290.78	[2006MSIT], at room temperature solid solubility ranges from ~24 to ~55 at.% Al

(*continued*)

DOI: 10.1007/978-3-540-69761-9_7

Phase/ Temperature Range [°C]	Pearson Symbol/ Space Group/ Prototype	Lattice Parameters [pm]	Comments/References
ε, Fe_2Al_3 1232 - 1102	*cI*16? $FeAl_2$	 *a* = 598.0	[2006MSIT], solid solubility ranges from 58 to 65 at.% Al at 61 at.% Al [V-C2]
$FeAl_2$ ≤ 1156	*aP*18 *P*1 $FeAl_2$	*a* = 487.8 *b* = 646.1 *c* = 880.0 α = 91.75° β = 73.27° γ = 96.89°	at 66.9 at.% Al [V-C2] solid solubility ranges from ~66 to ~67 at.% Al [2006MSIT]
η, Fe_2Al_5 ≤ 1169	*oC*24 *Cmcm*	*a* = 765.59 *b* = 641.54 *c* = 421.84	[2006MSIT], at 71.5 at.% Al solid solubility ranges from ~70 to ~73 at.% Al
Fe_4Al_{13} ≤ 1160	*mC*102 *C*2/*m* Fe_4Al_{13}	*a* = 1552.7 to 1548.7 *b* = 803.5 to 808.4 *c* = 1244.9 to 1248.8 β= 107.7 to 107.99° *a* = 1549.2 *b* = 807.8 *c* = 1247.1 β = 107.69°	[2006MSIT], 74.16 to 76.7 at.% Al solid solubility ranges from 74.5 to 75.5 at.% Al [2006MSIT], at 76.0 at.% Al. Also denoted $FeAl_3$ or Fe_2Al_7
$MoAl_{12}$ <712	*cI*26 $Im\bar{3}m$ WAl_3	 *a* = 758.3 *a* = 758.15	92.4 at.% Al [1991Sch] [1954Ada] [1980Fer]
$MoAl_5$ (h_2) 846 to 800-750	*hP*12 $P6_3$ WAl_5	*a* = 491.2 *c* = 886.0 *a* = 489.0 *c* = 880.0	83.8 at.% Al [1991Sch] [1980Fer]
$MoAl_5$ (h_1) 800 - 750 to ~648	*hP*60 $P\bar{3}$ $MoAl_5$ (h_1)	*a* = 489.0 *c* = 880.0	at 83.3 at.% Al [1991Sch]
$MoAl_5$ (r) < 648	*hP*36 $R\bar{3}c$ $MoAl_5$ (r)	*a* = 495.1 *c* = 2623	at 83.8 at.% Al [1991Sch]
Mo_5Al_{22} 964 - 831	*oF*216 *Fdd*2 Mo_5Al_{22}	 *a* = 7382 ± 3 *b* = 916.1 ± 0.3 *c* = 493.2 ± 0.2	81.7 at.% Al [1991Sch] [1995Gri]
Mo_4Al_{17} < 1034	*mC*84 *C*2 Mo_4Al_{17}	 *a* = 915.8 ± 0.1 *b* = 493.23 ± 0.08 *c* = 2893.5 ± 0.5 β = 96.71 ± 0.01°	80.9 at.% Al [1991Sch] [1995Gri]

(*continued*)

DOI: 10.1007/978-3-540-69761-9_7

Phase/ Temperature Range [°C]	Pearson Symbol/ Space Group/ Prototype	Lattice Parameters [pm]	Comments/References
$MoAl_4$ 942 - 117	*mC*30 *Cm* WAl_4	 *a* = 525.5 ± 0.5 *b* = 1776.8 ± 0.5 *c* = 522.5 ± 0.5 β = 100.88 ± 0.06° *a* = 525.5 *b* = 1176.8 *c* = 522.5 β = 100.7°	79 to 80 at.% Al [1991Sch] [1964Lea] [1991Sch]
$Mo_{1-x}Al_{3+x}$ 1154 - 126	*cP*8 $Pm\bar{3}m$ Cr_3Si	 *a* = 494.5 ± 0.1	76 to 79 at.% Al [1991Sch] [1991Sch]
$MoAl_3$ 1222 - ~818	*mC*32 *C*2/*m* $MoAl_3$	*a* = 1639.6 ± 0.1 *b* = 359.4 ± 0.1 *c* = 838.6 ± 0.4 β = 101.88 ± 0.07°	at 75 at.% Al [1991Sch]
Mo_3Al_8 < 1555 ± 10	*mC*22 *Cm* Mo_3Al_8	 *a* = 920.8 ± 0.3 *b* = 363.78 ± 0.03 *c* = 1006.5 ± 0.3	72 to 75 at.% Al [Mas2] [1962For]
Mo_2Al_3 1570 - 1490	-	β = 101.78 ± 0.05°	Called "ζ_1" (h) [1971Rex]
MoAl 1750 - 1470	*cP*2 $Pm\bar{3}m$ CsCl	 *a* = 309.8 *a* = 309.8 to 309.9	46 to 51.7 at.% Al [Mas2] Called "ζ_2" (h) [1971Rex] [1971Rex] [1980Fer]
Mo_3Al < 2150	*cP*8 $Pm\bar{3}n$ Cr_3Si	*a* = 495	22 to 27 at.% Al [Mas2] [1958Woo]
σ, MoFe 1540 - 1235	*tP*30 $P4_2/mnm$ CrFe	 *a* = 921.8 *c* = 481.3	42 to 55 at.% Mo [1982Kub] [V-C2]
μ, Mo_2Fe_3 < 1370	*hR*39 $R\bar{3}m$ W_6Fe_7	 *a* = 475.46 *c* = 2571.6 *a* = 476.0 *c* = 2576.4	40 to 42.5 at.% Mo [1982Kub] [V-C2] Fe-8.7Al-38.8Mo (at.%) [1994Che]
R, Mo_3Fe_5 1488 - 1200	*hR*159 $R\bar{3}$ $Co_5Cr_2Mo_3$	 *a* = 1091.0 *c* = 1935.4	35.1 to 37.4 at.% Mo [1982Kub] [V-C2]

(*continued*)

DOI: 10.1007/978-3-540-69761-9_7

Phase/ Temperature Range [°C]	Pearson Symbol/ Space Group/ Prototype	Lattice Parameters [pm]	Comments/References
λ, $MoFe_2$ < 950	*hP*12 *P*6$_3$/*mmc* $MgZn_2$	*a* = 474.5 *c* = 773.4	33.5 to 34.5 at.% Mo [1982Kub] [V-C2]
* τ_1, $MoFe_{0.28}Al_{2.72}$ < 900	*tI*8 *I*4/*mmm* $TiAl_3$	*a* = 376.7 *c* = 843.3	[1970Mar]
* τ_2, $Mo_5Fe_{35}Al_{60}$ 1050 - 1000	-	-	[1970Mar]
* τ_3, $Mo_9Fe_{4.75}Al_{0.25}$	*tI*56 *I*4/*mcm* Nb_9Co_4Ge	*a* = 1268.3 *c* = 4838.0	[1999Ste]
* τ_4, $Mo_3Fe_8Al_9$	-	-	[2004Eum2]

Table 3. Phases Present in as-Melt-Spun Condition and After Annealing Treatments

Composition (at.%)			As-Melt-Spun	After Annealing for 25 h, at	
Al	Fe	Mo		250 or 300°C	450°C
99.5	0.35	0.15	(Al)	(Al)+$MoAl_3$+$FeAl_6$	(Al)+$MoAl_3$+$FeAl_6$
99.0	0.75	0.25	(Al)	(Al)+$MoAl_3$+$FeAl_6$	(Al)+$MoAl_3$+$FeAl_6$
97.0	2.30	0.70	(Al)+$MoAl_3$+$FeAl_6$	(Al)+$MoAl_3$+$FeAl_6$	(Al)+$MoAl_3$+$FeAl_6$ +$MoAl_{12}$+Fe_4Al_{13}
94.67	3.59	1.74	(Al)+$MoAl_3$+$FeAl_6$	(Al)+$MoAl_3$+$FeAl_6$	(Al)+$MoAl_3$+$FeAl_6$ +$MoAl_{12}$+Fe_4Al_{13}
93.5	5.0	1.50	(Al)+$MoAl_3$+$FeAl_6$	(Al)+$MoAl_3$+$FeAl_6$	(Al)+$MoAl_3$+$FeAl_6$ +$MoAl_{12}$+Fe_4Al_{13}
92.0	6.00	2.00	(Al)+$MoAl_3$+$FeAl_6$	(Al)+$MoAl_3$+$FeAl_6$	(Al)+$MoAl_{12}$+Fe_4Al_{13}

Table 4. Investigations of the Al-Fe-Mo Materials Properties

Reference	Method/Experimental Technique	Type of Property
[1954Fon]	Electrochemical and mechanical tests	Corrosion and creep at 650°C
[1983Bus]	Magneto-optical test	Magnetic moment, Magneto-optical Kerr rotation
[1988Ots]	Mechanical tests	Creep
[1989Sri]	Magnetometry	Magnetization and Curie temperature
[1989Cho]	Mechanical tests	Tensile properties
[1990Cho]	Mechanical tests	Tensile properties and formability
[1991Ge]	Corrosion tests	Sulfidation kinetics

(*continued*)

DOI: 10.1007/978-3-540-69761-9_7

Reference	Method/Experimental Technique	Type of Property
[1991Nam]	Mechanical tests	Tensile properties
[1991Pra1]	Mechanical tests	Hardness and tensile properties
[1993Bar]	Mechanical and electrochemical tests	Tensile, creep, fracture and corrosion
[1993Kai]	Corrosion tests	Oxidation and sulfidation kinetics
[1998Nis]	Mechanical tests	High-temperature hardness
[1996Yam]	Mechanical tests	Creep rupture
[2000Che]	Corrosion tests	Oxidation kinetics
[2004Eum1]	Mechanical and oxidation tests	Compressive yield strength, hardness, oxidation rate, ductile-brittle transition temperature
[2004Eum2]	Mechanical and oxidation tests	Compressive yield strength, hardness, oxidation rate
[2004Nis]	Mechanical tests	Compressive stress-strain relations up to 1000°C

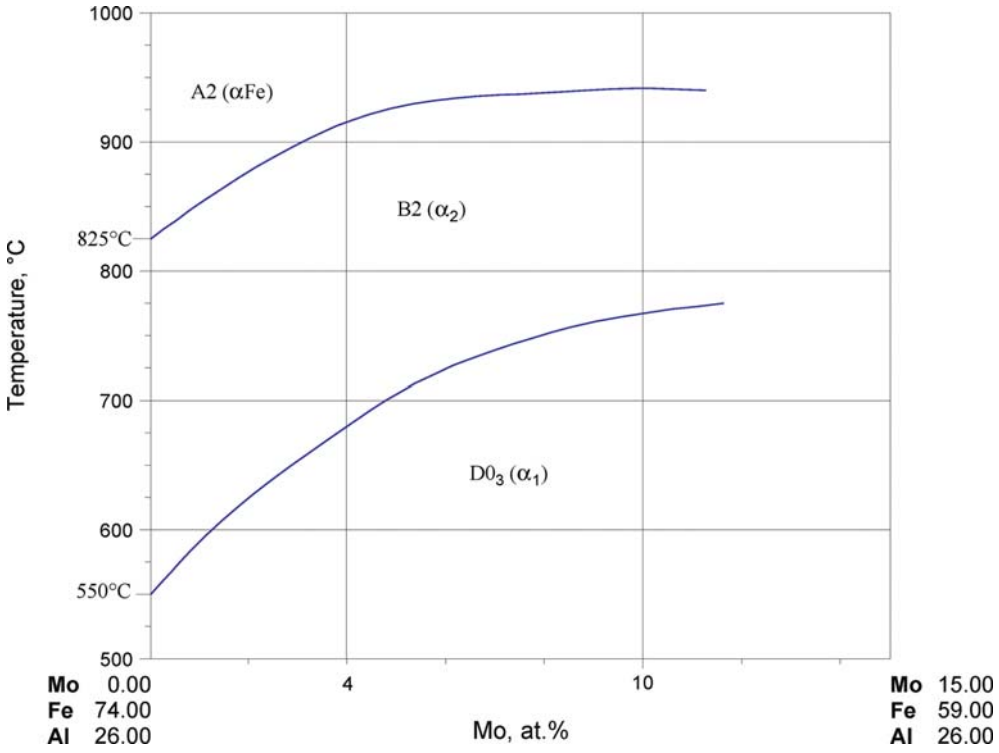

Fig. 1. Al-Fe-Mo. Variation of order-disorder temperature of $Fe_{74}Al_{26}$ as a function of Mo content along the $Fe_{74}Al_{26}$-$Mo_{74}Al_{26}$ section

DOI: 10.1007/978-3-540-69761-9_7

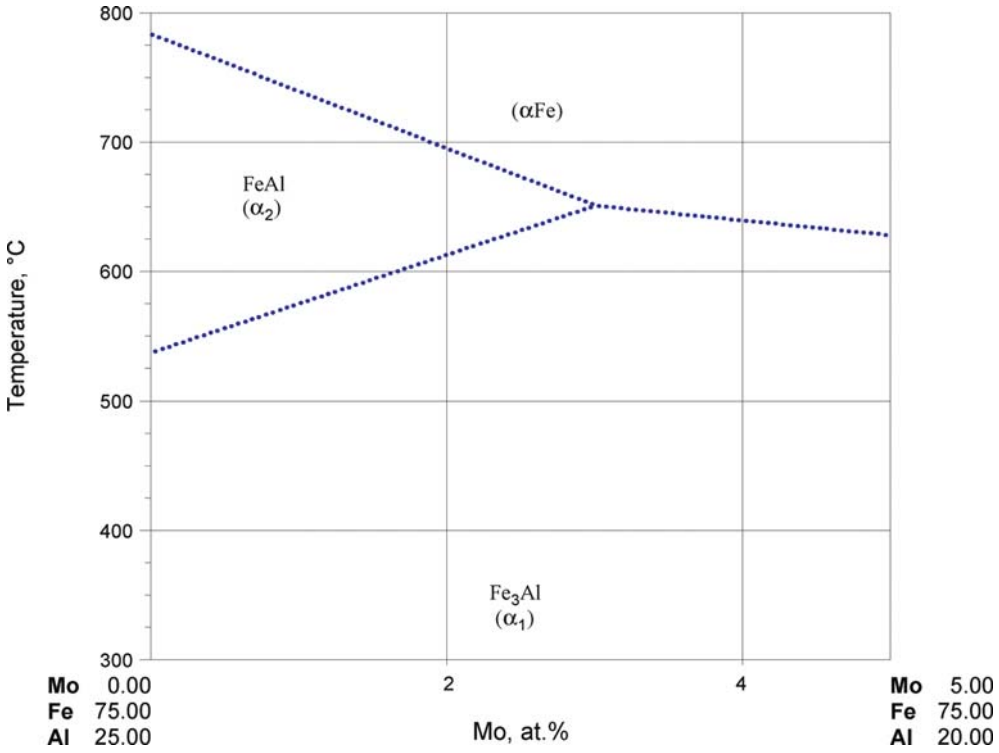

Fig. 2. Al-Fe-Mo. Variation of order-disorder temperature of Fe_3Al as a function of Mo content along the Fe_3Al-$MoFe_3$ section

DOI: 10.1007/978-3-540-69761-9_7

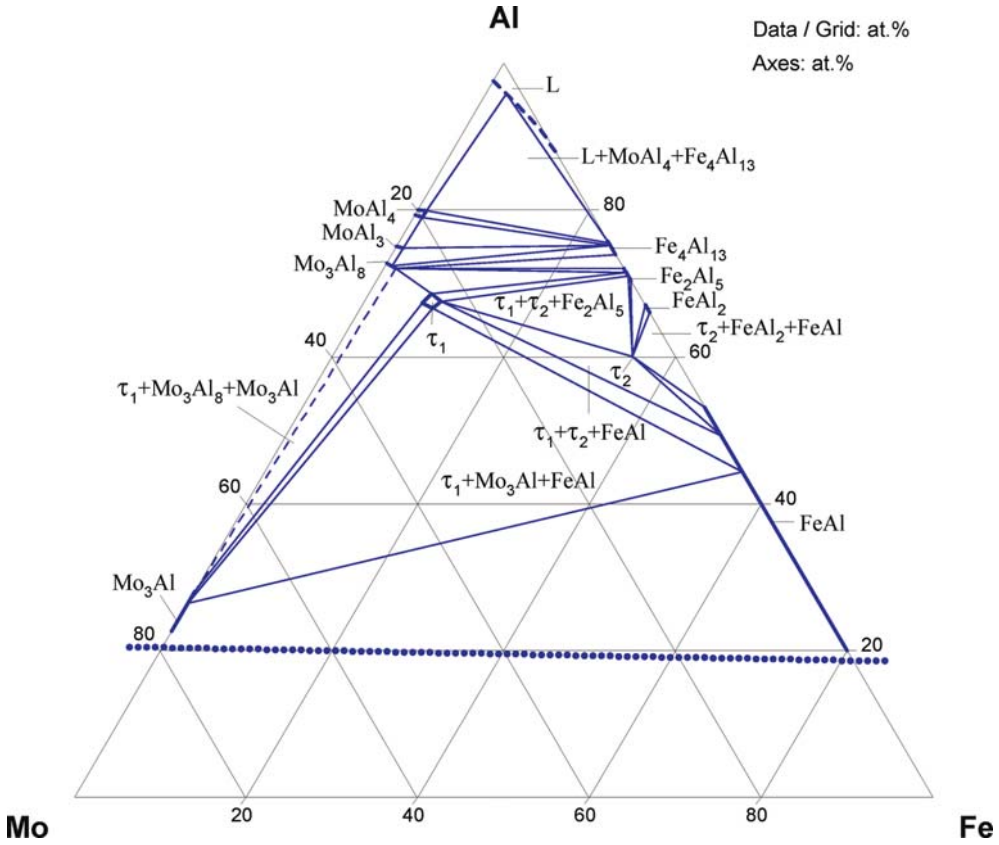

Fig. 3. Al-Fe-Mo. Partial isothermal section at 1050°C

DOI: 10.1007/978-3-540-69761-9_7

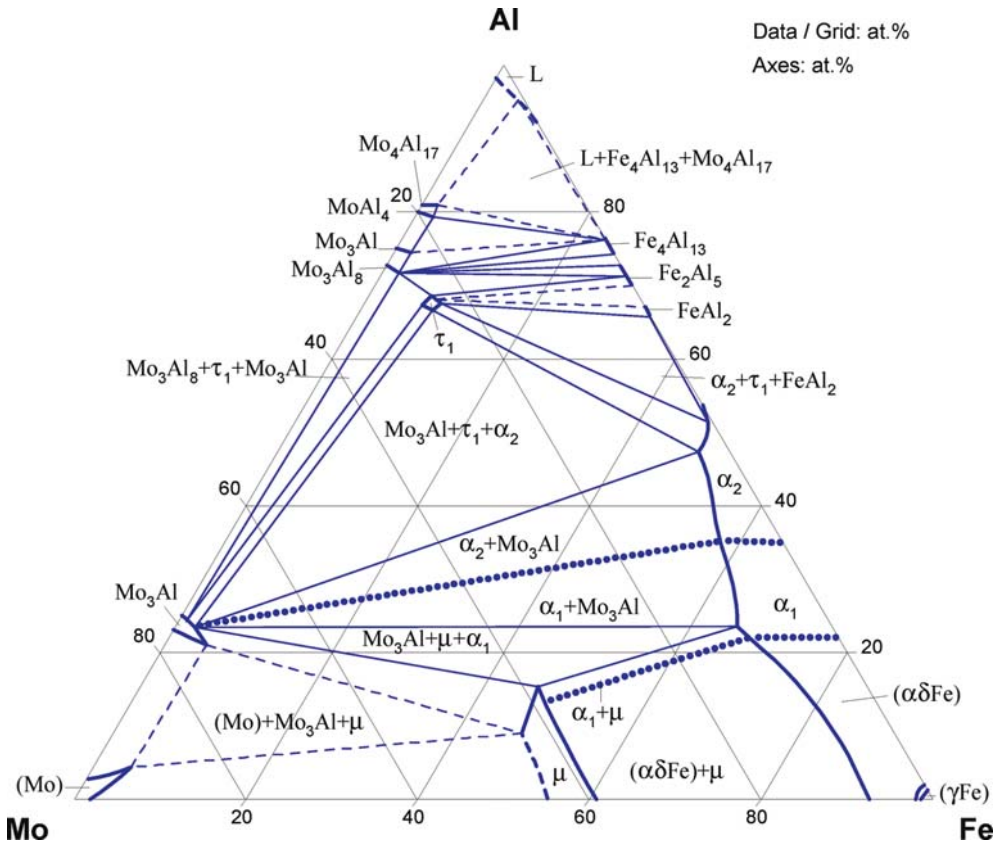

Fig. 4. Al-Fe-Mo. Isothermal section at 1000°C

DOI: 10.1007/978-3-540-69761-9_7

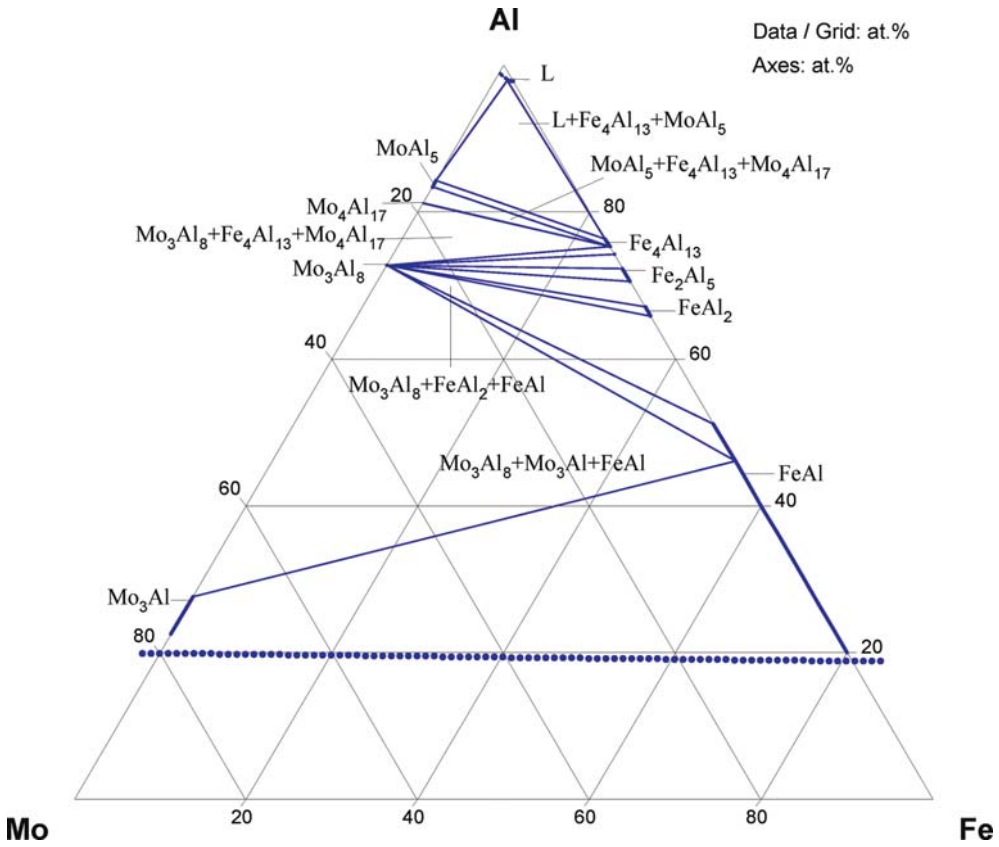

Fig. 5. Al-Fe-Mo. Partial isothermal section at 800°C

DOI: 10.1007/978-3-540-69761-9_7

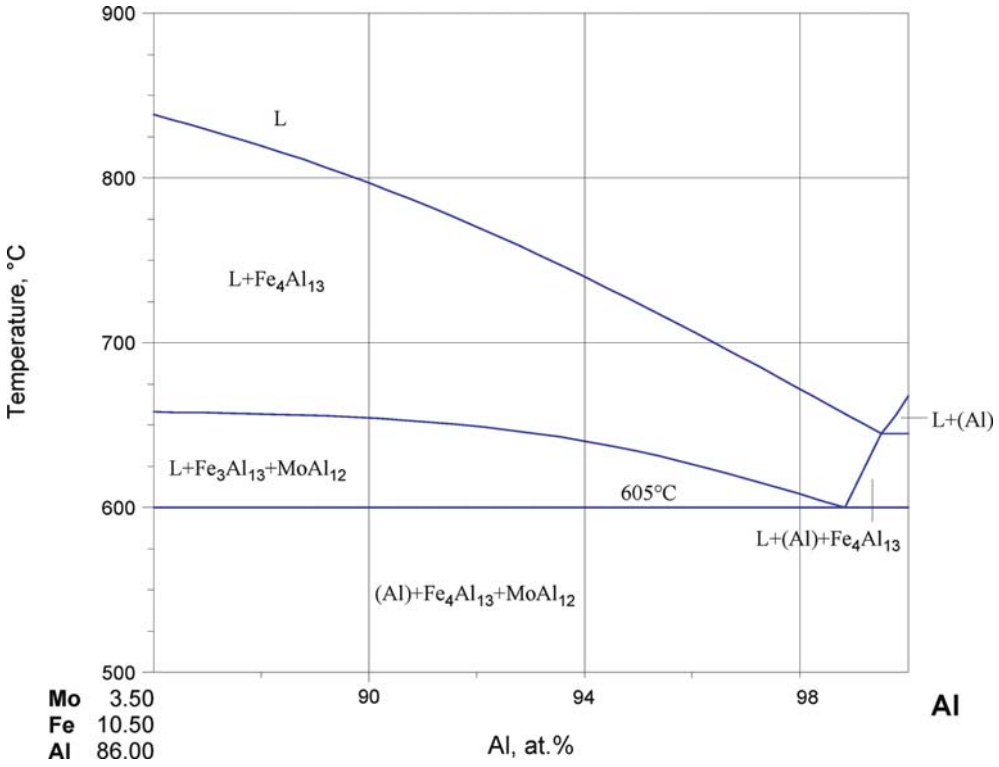

Fig. 6. Al-Fe-Mo. Polythermal section of the Al corner along Fe:Mo=3:1(at.%)

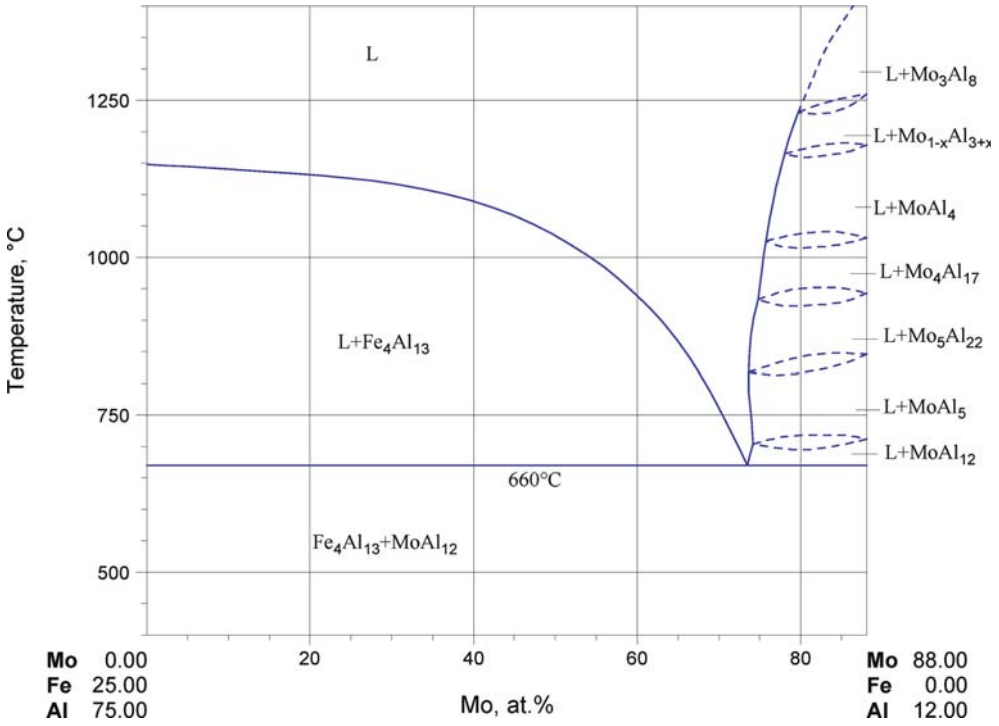

Fig. 7. Al-Fe-Mo. Polythermal section along $FeAl_3$-$MoAl_{12}$

DOI: 10.1007/978-3-540-69761-9_7

References

[1954Ada] Adam, J., Rich, J.B., "The Crystal Structure of WAl_5", *Acta Crystallogr.*, **7**, 813–816 (1954) (Crys. Structure, Experimental, 14)

[1954Fon] Fontana, M.G., "Corrosion Al-Fe and New Al-Mo-Fe Alloys Show Excellent Oxidation Resistance and Low Corrosion by Some Aqueous Solutions", *Indust. Eng. Chem.*, **46**(5), A85–A90 (1954) (Experimental, Interface Phenomena, 1)

[1958Woo] Wood, E.A., Compton, V.B., Matthias, B.T., Corenzwit, E., "β-Wolfram Structure of Compounds Between Transition Elements and Aluminium, Gallium and Antimony", *Acta Crystallogr.*, **11**, 604–606 (1958) (Crys. Structure, Experimental, 13)

[1962For] Forsyth, J.B., Gran, G., "The Structure of Intermetallic Phase γ (Mo-Al)-Mo_3Al_8", *Acta Crystallogr.*, **15**, 100–104 (1962) (Experimental, Crys. Structure, 13)

[1964Lea] Leake, J.A., "The Refinement of the Crystal Structure of Intermetallic Phase Al_4Mo", *Acta Crystallogr.*, **17**, 918–924 (1964) (Crys. Structure, Experimental, 38)

[1968Bir] Birun, N.A., Selissky, Ya.P., "Influence of Mo on Ordering in an Fe_3Al Alloy" (in Russian), *Akad. Nauk Ukr. SSR, Metallofizika*, (20), 96–99 (1968) (Experimental, Phase Relations, #, *, 3)

[1969Bir] Birun, N.A., Selissky, Ya.P., "Effect of Mo on a Transformation in an Fe-Al Ordering Alloy (Fe_3Al)", *Phys. Met. Metallogr.*, **27**(6), 104–110 (1969) (Experimental, #, *, 11)

[1969Sel] Selissky, Ya.P., Tolochko, M.N., "High-Temperature X-Ray Diffraction Study of Fe-Al-Cr, Fe-Al-Mo and Fe-Al-W Alloys" (in Russian), *Ukr. Fiz. Zh.*, **14**(10), 1692–1694 (1969) (Phase Relations, Phase Diagram, Experimental, #, *, 7)

[1970Mar] Markiv, V.Ya., Burnashova, V.V., Ryabov, V.R., "Study of the Al-rich Part of the Phase Diagram of the Mo-Fe-Al System" (in Ukrainian), *Dopov. Akad. Nauk Ukr. RSR.*, (A), (1), 69–72 (1970) (Phase Relations, Phase Diagram, Experimental, #, *, 6)

[1971Rex] Rexer, J., "Phase Equilibria in the Aluminum-Molybdenum at Temperature Above 1400°C" (in German), *Z. Metallkd.*, **62**, 844–848 (1971) (Crys. Structure, Phase Diagram, Experimental, 23)

[1976Mon] Mondolfo, L.F., "Aluminum-Iron Systems" in "*Aluminum Alloys: Structure and Properties*", Butterworths, London, 282–289 (1976) (Phase Relations, Phase Diagram, Review, 171)

[1980Bre] Brewer, L., Lamereaux, R.H., "The Al-Mo (Aluminium-Molybdenum) System", *Bull. Alloy Phase Diagrams*, **1**, 71–75 (1976) (Phase Diagram, Review, #, *, 32)

[1980Fer] Ferro, R., Marazza, R., "Crystal Structure and Density Data, Molybdenum Alloys and Compounds other than Hallides and Chalcogenides", *Atomic Energy Rev.: Spec. Iss.*, **7**, 359–507 (1980) (Crys. Structure, Review, 961)

[1982Kub] Kubaschewski, O., "Iron-Molybdenum" in *"Iron-Binary Phase Diagrams"*, Springer-Verlag, Berlin, 64–67 (1982) (Phase Relations, Phase Diagram, Review, 13)

[1983Bus] Buschow, K.H.J., van Engen, P.G., Jongebreur, R., "Magneto-Optical Properties of Metallis Ferromagnetic Materials", *J. Magn. Magn. Mater.*, **38**, 1–22 (1983) (Magn. Prop., Optical Prop., 23)

[1984Kra] Krantsova, O.A., Kubalova, L.M., Viting, L.M., Troshkina, V.A., Kaloev, N.I., "Calorimetric Study of the Compound Fe_3Al Alloyed with 0.5 at.% Molybdenum" (in Russian), *Vestn. Mosk. Univ., Khim.*, **25**(2), 179–181 (1984) (Experimental, Thermodyn., 8)

[1984Zak] Zak, T., "Atomic Structure and Magnetic Polarization of Fe-Al-Mo Alloy Sheets", *J. Magn. Magnetic Mater.*, **41**(1–3), 47–48 (1984) (Experimental, Magn. Prop., 4)

[1985Men] Mendiratta, M.G., Lipsitt, H.A., "$D0_3$-Domain Structures in Fe_3Al-X Alloys", *Mater. Res. Soc. Symp. Proc.: High-Temp. Ordered Intermetallic Alloys II*, **81**, 155–162 (1991) (Experimental, Phase Relations, *, 4)

[1986Fie] Field, R.D., Zindel, J.W., Fraser, H.L., "The Intercellular Phase in Rapidly Solidified Alloys Based on the Al-Fe System", *Scr. Metall.*, **20**, 415–418 (1986) (Crys. Structure, Experimental, 8)

[1987Die] Diehm, R.S., Mikkola, D.E., "Effects of Mo and Ti Additions on the High Temperature Compressive Properties of Iron Aluminides Near Fe_3Al", *Mater. Res. Soc. Symp. Proc.: High-Temp. Ordered Intermetallic Alloys II*, **81**, 329–334 (1991) (Experimental, Phase Relations, Mechan. Prop., 8)

DOI: 10.1007/978-3-540-69761-9_7

[1987For] Fortnum, R.T., Mikkola, D.E., "Effects of Molybdenum, Titatnium and Silicon Additions on the $D0_3 = B2$ Transition Temperature for Alloys near Fe_3Al", *Mater. Sci. Eng.*, **91**, 223–231 (1987) (Experimental, Phase Relations, *, 36)

[1987Sok] Sokolovskaya, E.M., Chel'dieva, G.M., Kazakova, E.V., Kaloev, N.I., "Investigation of Alloys of the Al-Al_3Fe-$MoAl_{12}$ System" (in Russian), *Vestn. Mosk. Univ., Khim.*, **28**(5), 511–512 (1987) (Phase Relations, Phase Diagram, Experimental, #, *, 3)

[1988Che] Chel'dieva, G.M., Kazakova, E.F., Sokolovskaya, E.M., Borovikova, C.I., Romanova, V.S., "Effect of Heat Treatment on the Phase Composition of Rapidly Quenched Al-Fe-Mo Alloys" (in Russian), *Izv. Akad. Nauk SSSR, Met.*, (3), 119–121 (1988) (Experimental, *, 5)

[1988Men] Mengjun, H., Xishen, C., "Formation and Crystallization of Metastable Al-Fe-Mo-(Mn) Quasicrystals", *Solid State Comm.*, **68**(9), 813–816 (1988) (Crys. Structure, Experimental, 4)

[1988Ots] Otsuka, M., Inoue, M., Hirano, T., Horiuchi, R., "High Temperature Creep of a P/M Al-8Fe-2Mo Alloy", Strength of Metals and Alloys (ICSMA 8) Proceedings of the 8th International Conference, Pergamon, Oxford, UK, **Vol. 3**, 1463–1468 (1988) (Experimental, 10)

[1989McK] McKamey, C.G., Horton, J.A., "The Effect of Molybdenum Addition on Properties of Iron Aluminides", *Metall. Trans. A.*, **20A**, 751–757 (1989) (Experimental, Phase Relations, Mechan. Prop., 16)

[1989Cho] Chowdhury, A.J.S., Sheppard, T., "Characteristics of an Al-7Fe-2Mo Alloy Prepared from RS Powders", *Key Eng. Mater.*, **38–39**, 263–276 (1989) (Experimental, Mechan. Prop., 15)

[1989Sri] Srinivas, V., McHenry, M.E., Dunlap, R.A., "Magnetic Properties of Icosahedral Al-Fe-Mo and Al-Ta-Fe Alloys", *Phys. Rev. B.*, **40**(15), 9590–9594 (1989) (Crys. Structure, Experimental, Magn. Prop., 25)

[1990Cho] Chowdhury, A.J.S., Sheppard, T., "Processing and Properties of High Temperature Application Al-Fe-Mo Based Alloys Prepared from Rapidly Solidified Powder", *Mater. Sci. Tech.*, **6**(6), 535–542 (1990) (Experimental, Mechan. Prop., 24)

[1990Kum] Kumar, K.S., "Ternary Intermetallics in Aluminium-Refractory Metal-X-Systems (X = V, Cr, Mn, Fe, Co, Ni, Cu, Zn)", *Int. Met. Rev.*, **35**, 293–327 (1990) (Crys. Structure, Phase Relations, Phase Diagram, Review, 158)

[1990Nam] Nam, I.B., Sung, K.H., Hyung, Y.R., "Effects of Alloying Elements on the Thermal Stability of Rapidly Solidified Al-Fe Based Alloys", *J. Korean Inst. Met.*, **28**(2), 170–178 (1990) (Experimental, Mechan. Prop., 12)

[1991Bi] Bi, Y.J., Loretto, M.H., "The Influence of Iron on Precipitation from Supersaturated Al-Mo Solid Solutions", *Mater. Sci. Eng. A*, **A134**, 1188–1192, (1991) (Crys. Structure, Experimental, 9)

[1991Ge] Ge, W., Douglass D.L., Gesmundo, F., "High-Temperature Sulfidation of Fe-30Mo Alloys Containing Ternary Additions of Al", *Oxidation Met.*, **35**(5–6), 349–373 (1991) (Experimental, Kinetics, 30).

[1991Nam] Nam, I.B., Sung, K.H., Hyung, Y.R., "Microstructure and Mechanical Properties of Rapidly Solidified Al-Fe-(Mo,Si) Alloy Powder-Extrudates", *J. Korean Inst. Met.*, **29**(8), 847–852 (1991) (Experimental, Mechan. Prop., 12).

[1991Pra1] Prakash, U., Buckley, R.A., Jones, H., "Mechanical Properties of Ordered Fe-Al-X Alloys", *Mater. Res. Soc. Symp. Proc.: High-Temp. Ordered Intermetallic Alloys IV*, **213**, 691–696 (1991) (Experimental, Mechan. Prop., 19)

[1991Pra2] Prakash, U., Buckley, R.A., Jones, H., "Novel Faulted Structures in Rapidly Solidified Fe-37 at.% Al-15 at.% Mo Alloy", *Acta Metall. Mat.*, **39**(7), 1677–1682 (1991) (Experimental, Morphology, 23)

[1991Pra3] Prakash, U., Buckley, R.A., Jones, H., Sellars, C.M., "On Strain Contrast from B2 Antiphase Domain Boundaries in Rapidly Solidified Fe-32 at.% Al-15 at.% Mo Alloy", *Scripta Metall. Mat.*, **25**(10), 2249–2253 (1991) (Experimental, Morphology, 16)

[1991Pra4] Prakash, U., Buckley, R.A., Jones, H., "Effect of Molybdenum Substitution on B2 Antiphase Domain Formation in Rapidly Solidified Fe-Al-Mo Alloys", *Mater. Sci. Eng.*, **A133**, 588–591 (1991) (Experimental, Morphology, 18)

DOI: 10.1007/978-3-540-69761-9_7

[1991Sch] Schuster, J.C., Ipser, H., "The Al-Al_8Mo_3 Section of the Binary System Aluminum-Molybdenum", *Metall. Trans. A*, **22A**, 1729–1736 (1991) (Crys. Structure, Phase Diagram, Experimental, 20)

[1992Gho] Ghosh, G., "Aluminium-Iron-Molybdenum", in "*Ternary Alloys. A Comprehensive Compedium of Evaluated Constitutional Data and Phase Diagrams*", G. Petzow, G. Effenberg (Eds.), VCH, Weinheim, Germany, **Vol. 5**, 265–274 (1992) (Phase Diagram, Phase Relations, Crys. Structure, Assessment, 13)

[1992Rag] Raghavan, V., "The Al-Fe-Mo (Aluminium-Iron-Molybdenum) System", in "*Phase Diagrams of Ternary Iron Alloys*", Indian Institute of Metals, Calcutta, India, **Part 6A**, 135–141 (1992) (Phase Diagram, Review, 9)

[1993Kel] Kelton, K.F., "Quasicrystals: Structure and Stability", *Int. Mater. Rev.*, **38**(3), 105–137 (1993) (Crys. Structure, Review, 424)

[1993Bar] Barbaux, Y., Pons, G., "New Rapidly Solidified Aluminium Alloys for Elevated Temperature Applications on Aerospace Structures", *J. Phys. IV*, **3(C7)**, 191–196 (1993) (Experimental, Mechan. Prop., 6)

[1993Kai] Kai, W., Douglass, D.L., "The High-Temperature Corrosion Behavior of Fe-Mo-Al Alloys in $H_2/H_2O/H_2S$ Mixed-Gas Environments", *Oxidation Met.*, **39**(3–4), 281–316 (1993) (Experimental, Interface Phenomena, 17)

[1993Mil] Miller, D.J., Fraser, H.L., "Enhanced Decomposition of Rapidly Solidified Microstructures in Al-Fe-Mo and Ti-Al-Er Alloys by Plastic Deformation and Applied Stress", *Acta Metall. Mater.*, **41**(1), 73–83 (1993) (Experimental, Mechan. Prop., 6)

[1993Pra] Prakash, U., Buckley, R.A., Jones, H., "Effect of Molybdenum Substitution on Crystal Structure of Ordered Fe-Al Alloys", *Mater. Sci. Technol.*, **9**, 16–20 (1993) (Crys. Structure, Experimental, Phase Diagram, #, *, 8)

[1994Che] Chen, Y., "Phase Identification of Two Intermetallic Compounds in Fe-Mo-Al and Fe-Mo-Al-Mn Alloys", *J. Mater. Sci. Lett.*, **13**, 1114–1117 (1994) (Crys. Structure, Experimental, 6)

[1995Ant] Anthony, L., Fultz, B., "Effects of Early Transition Metal Solutes on the $D0_3$-$B2$ Critical Temperature of Fe_3Al", *Acta Metall. Mater.*, **43**(10), 3885–3891 (1995) (Experimental, Phase Relations, *, 35)

[1995Gri] Grin, Y.N., Ellner, M., Peters, K., Schuster, J.C., "The Crystal Structures of Mo_4Al_{17} and Mo_5Al_{22}", *Z. Kristallogr.*, **210**, 96–99 (1995) (Crys. Structure, Experimental, 11)

[1995Lou] Loucif, K., Vigier, G., Merle, P., "Microstructural Stability of Rapidly Quenched Al-Fe-Mo Alloys", *Mater. Sci. Eng. A*, **A190**(1–2), 187–192 (1995) (Crys. Structure, Experimental, 11)

[1996Yam] Yamada, S., Kato, Y., "Effect of Cooling Rate of Rapid Solidification on Softening Behaviour of Al-8%Fe-2%Mo Alloy", *J. Jap. Inst. Light Met.*, **46**(1), 21–26 (1996) (Experimental, Mechan. Prop., 7)

[1997Nis] Nishino, Y., Asano, S., Ogawa, T., "Phase Stability and Mechanical Properties of Fe_3Al with Addition of Transition Elements", *Mater. Sci. Eng. A*, **A234-A236**, 271–274 (1997) (Experimental, Phase Relations, Mechan. Prop., 18)

[1998Nis] Nishino, Y., Inkson, B.J., Ogawa, T., Humphreys, C.J., "Effect of Molybdenum Substitution on Phase Stability and High-Temperature Strength of Fe_3Al Alloys", *Phil. Mag. Lett.*, **78**(2), 97–103 (1998) (Experimental, Phase Relations, 20)

[1998Sun] Sun, Z.Q., Yang, W.Y., Shen, L.Z., Huang, Y.D., Zhang, B.S., Yang, J.L., "Neutron Diffraction Study on Site Occupation of Substitution Elements at Sub Lattices in Fe-Al Intermetallics", *Mater. Sci. Eng. A*, **258**, 69–74 (1998) (Crys. Structure, Experimental, Magn. Prop., Mechan. Prop., 19)

[1999Mek] Mekhrabov, A.O., Akdeniz, M.V., "Effect of Ternary Alloying Elements Addition on Atomic Ordering Characteristics of Fe-Al Intermetallics", *Acta Mater.*, **47**(7), 2067–2075 (1999) (Calculation, Theory, Thermodyn., 63)

[1999Ste] Stepien-Damm, J., Salamakha, P., Wochowski, K., Suski, W., "Crystal Structure of $Mo_9Fe_{4.75}Al_{0.25}$", *J. Alloys Compd.*, **282**(1–2), 182–183 (1999) (Crys. Structure, Experimental, 5)

DOI: 10.1007/978-3-540-69761-9_7

[2002Boz] Bozzolo, G.H., Noebe, R.D., Amador, C., "Site Occupancy of Ternary Additions to *B*2 Alloys", *Intermetallics*, **10**, 149–159 (2002) (Crys. Structure, Theory, Review, 27)

[2000Che] Chen, R.Y., Young, D.J., Blairs, S., "The Corrosion Behavior of Sulfidation-Resistant Fe-Mo-Al Alloys in H_2/H_2S Atmospheres at 900°C", *Oxidation Met.*, **54**(1–2), 103–120 (2000) (Experimental, Interface Phenomena, Kinetics, 42)

[2004Eum1] Eumann, M., Palm, M., Sauthoff, G., "Iron-Rich Iron-Aluminium-Molybdenum Alloys with Strengthening Intermetallic mu Phase and R Phase Precipitates", *Steel Res.*, **75**(1), 62–73 (2004) (Experimental, Mechan. Prop., Phase Diagram, #, *, 48)

[2004Eum2] Eumann, M., Palm, M., Sauthoff, G., "Alloys Based on Fe_3Al or FeAl with Strengthening Mo_3Al Precipitates", *Intermetallics*, **12**(6), 625–633 (2004) (Crys. Structure, Experimental, Interface Phenomena, Kinetics, Mechan. Prop., Morphology, #, *, 39)

[2004Nis] Nishino, Y., Tanahashi, T., "Effect of Molybdenum Substitution on the Yield Stress Anomaly in Fe_3Al-Based Alloys", *Mater. Sci. Eng. A*, **A387–A389**, 973–976 (2004) (Experimental, Phase Relations, Mechan. Prop., #, *, 20)

[2005Gon] Gonzales-Ormeno, P.G., Nogueira, R.N., Schon, C.G., Petrilli, H.M., "Magnetic Behavior of Fe Sites in Fe-Mo-Al Alloys: The Role of the First Neighborhood", *Calphad*, **29**(3), 222–229 (2005) (Calculation, Theory, 36)

[2005Rag] Raghavan, V., "Al-Fe-Mo (Aluminum-Iron-Molybdenum)", *J. Phase Equilib. Diffus.*, **26**(1), 68–69 (2005) (Phase Diagram, Review, 8)

[2005Sch] Schuster, J.C., "Al-Mo (Aluminum-Molybdenum)", MSIT Binary Evaluation Program, in *MSIT Workplace*, Effenberg, G. (Ed.), MSI, Materials Science International Services, GmbH, Stuttgart; Document ID: 30.12123.1.20, (2005) (Crys. Structure, Phase Diagram, Assessment, 61)

[2006MSIT] "Al-Fe (Aluminum-Iron)", Diagrams as Published, in *MSIT Workplace*, Effenberg, G. (Ed.), Materials Science International Services, GmbH, Stuttgart; Document ID: 30.10236.1.20, (2006) (Crys. Structure, Phase Diagram, Phase Relations, 11)

[Mas] Massalski, T.B. (Ed.), *Binary Alloy Phase Diagrams*, ASM, Metals Park, Ohio (1986)

[Mas2] Massalski, T.B. (Ed.), *Binary Alloy Phase Diagrams*, 2nd edition, ASM International, Metals Park, Ohio (1990)

[V-C2] Villars, P. and Calvert, L.D., *Pearson's Handbook of Crystallographic Data for Intermetallic Phases*, 2nd edition, ASM, Metals Park, Ohio (1991)

DOI: 10.1007/978-3-540-69761-9_7

Aluminium – Iron – Nitrogen

Hermann A. Jehn and Pierre Perrot, updated by Pierre Perrot

Introduction

Al-Fe alloys, in the presence of N, form aluminium nitride which plays an important role in steelmaking because of grain refining and texture development. Most of the investigations have been directed at the solubility of N in Al-Fe melts [1960Peh, 1963Mor, 1978Wad, 1979Wad, 1982Ish] and phase boundaries in the liquid state [1963Mor, 1964Eva, 1968Isa] and in austenite [1951Dar, 1961Isa] represented by the solubility product of AlN [1984Rag, 1987Rag]. [1961Sta] nitrided four ternary alloys at 600°C for 20 h and analyzed the resulting phases. A review of the Al-Fe-N system has been presented by [1987Rag] and updated by [1993Rag]. A Calphad assessment of the Al-Fe-N system has been reported by [1992Hil]. Kinetics of precipitation of AlN in steels has been investigated by [1972Oga, 1988Lan, 1995Big]. Since the years 1980, no more experimental determinations of the solubilities of nitrogen in Al-Fe alloys are available. The actual trend is to use the accepted results to calculate the solubility of nitrogen in more complex alloys, then to check the calculated solubilities with experimental observations.
This evaluation incorporates and continues the critical evaluation made by [1992Jeh] considering new published data.

Binary Systems

The binaries Al-Fe, Al-N and Fe-N are taken from [2006MSIT], [2003Fer] and [2003Per], respectively.
N is practically insoluble in Al(s). The solubility of N in liquid Al under 0.1 MPa is given by [1986Wri]:

$$\log_{10}(\text{at.\% N}) = 2.633 - 1157/T.$$

The only stable phase, AlN, melts at 2800 ± 50°C under nitrogen pressure of 10 to 50 MPa. AlN sublimates congruently, the decomposition pressure being 0.1 MPa at 2435°C. Metastable AlN_9 is also reported [1986Wri].
All Fe modifications dissolve more or less N [1976Kru, 1982Fro, 1987Wri]. The (γFe) phase is stabilized to lower temperatures and then decomposes eutectoidally into (αFe) and γ′Fe_4N at 590°C and 8.75 at.% N. (Fe_4N, stable up to 670°C transforms into ε, hexagonal nitride with a wide homogeneity range γFe_2N (orthorhombic) is stable up to 500°C [H, 1976Kru]. For the Fe-rich part of the Fe-N phase diagram, including *T-c* isobars, see [1976Kru]. A Calphad assessment of the Fe-N diagram has been carried out by [1987Fri] and an extensive review presented by [1987Wri]. The solubility of nitrogen in pure liquid iron had been determined between 1580 and 2000°C under 0.1 MPa by [1960Mae, 1960Peh, 1964Eva, 1978Wad, 1982Ish] and [1986Wad].

Solid Phases

No ternary compounds are known. According to [1961Sta], considerable amount of Al is dissolved in the (γ′ and ε iron nitrides (Fig. 1). The lattice parameter of ε nitride containing 57 at.% Fe, 19 at.% Al and 24 at.% N (79 mass% Fe, 12.7 mass% Al, 8.3 mass% N) is slightly increased compared to binary iron nitride of the same N content (see Table 1). The N solubility in austenite containing Al was determined by direct chemical analysis of alloys equilibrated in gaseous nitrogen [1951Dar]. At low Al content, the N solubility is independent of the Al content and given by the relation ((%N) in mass%, *T* in K): (%N) = $0.0404 - 1.2.10^{-5}T$. At higher Al content, the precipitation of AlN is observed. The solubility product of AlN in γFe is represented by the equations:

$\log_{10}((\%\text{Al})(\%\text{N})) = 1.95 - 7400/T$ ((%) in mass%, *T* in K) [1976Kru]
$\log_{10}(c_{Al}c_N) = 2.866 - 7400/T$ (*c* in at.%, *T* in K).

DOI: 10.1007/978-3-540-69761-9_8

Phase boundaries calculated from the above equations are shown in Fig. 2. Few data exist on the solubility of N in (αFe)-Al alloys. They have been obtained when studying the precipitation kinetics of AlN in ferrite containing 0.19 at.% Al and 0.04 at.% N [1972Oga] or 2 at.% Al and 0.02 at.% N, the maximum amount of nitrogen dissolved in the ferrite matrix at 575°C [1988Lan]. An appreciable rate of precipitation was found between 450 and 620°C; the rate was greater in cold-worked samples than in as-quenched ones.

Liquidus Surface

After early measurements by [1939Ekl], a number of investigations on the solubility of N in liquid Al-Fe alloys were undertaken in the 1960's. [1960Mae, 1960Peh, 1964Eva] and [1982Ish] report first order interaction coefficients to be slightly positive indicating that Al increases the activity coefficient of N in the melt and decreases its solubility at a given N_2 pressure. On the contrary, [1963Mor, 1968Isa], confirmed by more recent work of [1978Wad], found an increase of the N solubility with the Al content of the liquid. According to [1978Wad], the isobaric N solubility in Al-Fe melts obeys Sieverts' law ($c_N \sim p(N_2)^{1/2}$) and can be represented by the equation:

$$\log c_N = 0.5 \log p(N_2) + A + B c_{Al} + C c^2_{Al}$$

Numerical data for A, B and C are given in Table 2. These results were confirmed by the model of an ideally associated mixture proposed by [2000Yag]. The solubility product of AlN in Al-Fe melts, is given at 1580°C by [1961Isa], at 1580°C and 1675°C by [1963Mor, 1968Isa] and [1973Mok]. [1978Wad] proposed the following equation (T in K, (%) in mass%, c in a.%):

$$\log_{10}((\%\,Al)(\%\,N)) = 6.10 + 5.88 \cdot 10^{-2}(\%Al) - 14000/T$$
$$\log_{10}(c_{Al} \cdot cN) = 7.016 + 2.84 \cdot 10^{-2} c_{Al} - 14000/T$$

Figure 3 gives the liquidus isotherms under 0.1 MPa N_2 and between 1550 and 1700°C according to [1978Wad]. The solubility of N_2 in liquid Al-Fe alloys calculated by [1992Hil] under 0.1 MPa pressure at 1900 K is shown in Fig. 4. A reasonable agreement is observed with experimental solubilities measured by [1978Wad] in the iron-rich part of the diagram.
The first order interaction parameter of nitrogen for the Al-Fe liquid alloys was experimentally determined by [1979Wad] between 1600 and 1700 K and may be represented by the following expression:

$$e_N^{(Al)} = \mathrm{d}(\log_{10} f_N / \mathrm{d}(\%Al)) = -0,81 + (1426/T) \text{ with } f_N = (\%N)_{\text{pure Fe}} \Big/ (\%N)_{\text{Fe,Al alloy}}.$$

(%Al) or (%N) in the above formula represent mass%. In the liquid alloys, $e_N^{(Al)} < 0$, which means that the solubility of N in liquid alloys increases with the Al content of the alloy. As shown in Fig. 3, once the solubility product of AlN obtained, the solubility of N in liquid alloy does not increase any more, but decreases because of the precipitation of AlN. [1982Ish] measures a positive first order interaction parameter, which implies a decrease of the nitrogen solubility due to aluminium, result which contradicts the well established experimental observations.

Isothermal Sections

From the phases found by [1961Sta] in four ternary alloys, a partial isothermal section at 600°C is constructed. It is given in Fig. 1, including the composition of the four alloys and the phases observed.
[1978Tro, 1985Sch] show that the mixture AlN+Fe is thermodynamically stable at 1950°C under a N_2 atmosphere, it decomposes above 1750°C under an Ar atmosphere with formation of a FeAl alloy.

Miscellaneous

[1995Big] investigated the kinetics of precipitation of AlN on internal nitriding the Fe-2 at.% Al alloy in the temperature range 530 - 580°C. The precipitation of AlN is associated with a Gibbs energy barrier for the formation of a precipitate of critical size and thus is controlled by nucleation and growth.
Multilayered thin films Fe-N/Al-N are currently receiving increasing attention [1991Bar, 2001Liu] due to their excellent soft magnetic properties with large saturation magnetization of 19 kG and a high relative permeability of 4300 at high frequency [1991Kub]. These layers are prepared by ion sputtering under a

DOI: 10.1007/978-3-540-69761-9_8

mixture of Ar and N_2 introduced under the sputtering ion source. The layers are generally oversaturated and the thinnest (less than 12 nm) exhibits an essentially amorphous structure.

Table 1. Crystallographic Data of Solid Phases

Phase/ Temperature Range [°C]	Pearson Symbol/ Space Group/ Prototype	Lattice Parameters [pm]	Comments/References
(γFe) 1394 - 912	*cF*4 $Fm\bar{3}m$ Cu	a = 364.67	at 915°C [V-C2, Mas2] dissolves 0.1 at.% N at 912°C, 0.1 MPa
(αδFe)	*cI*2 $Im\bar{3}m$ W		dissolves 0.0166 at.% N at 912°C, 0.1 MPa; dissolves up to 54.0 at.% Al at 1102°C
(δFe) 1538 - 1394		a = 293.15	pure Fe at 1480°C [Mas2]
(δFe) < 912		a = 286.65	pure Fe at 25°C [Mas2]
(Al) ≤ 660.452	*cF*4 $Fm\bar{3}m$ Cu	a = 404.96	at 25°C, [Mas2]
γ′, Fe_4N ≤ 680	*cP*5 $Pm\bar{3}m$ Fe_4N	a = 378.7	[1987Rag] 19.3 to 20.0 at.% N
ε, $Fe_3N_{1\pm x}$	*hP*3 $P6_3/mmc$ $Fe_3N_{1\pm x}$	a = 272.9 c = 439.2	~ 15 to ~ 33 at.% 23 at.% N
		a = 272.9 c = 440.4	30 at.% N
$(Fe,Al)_3N_{1\pm x}$		a = 276 c = 442	$Fe_{57}Al_{19}N_{24}$ [1961Sta]
Fe_2N ≤ 500	*oP*12 *Pbcn* Fe_2N	a = 551.2 b = 482.0 c = 441.6	33.7 at.% N, [1984Rag]
AlN < 2437.4	*hP*4 $P6_3mc$ ZnS- wurtzite	a = 311.14 c = 497.92	at 25°C, [1986Wri]

Table 2. Isobaric Nitrogen Solubility in Al-Fe Melts [1978Wad] $\log_{10}c_N=0.5\log_{10}p_{N2}+A+Bc_{Al}+Cc^2_{Al}$ (c_N, c_{Al} in at.%, P_{N2} in Pa)

T [°C]	A	B	C
1550	– 3.859	$+ 1.25\cdot10^{-2}$	$+ 9.8\cdot10^{-3}$
1600	– 3.856	$+ 2.34\cdot10^{-2}$	$+ 8.2\cdot10^{-3}$
1650	– 3.852	$+ 3.37\cdot10^{-2}$	$+ 6.9\cdot10^{-3}$
1700	– 3.849	$+ 4.34\cdot10^{-2}$	$+ 5.7\cdot10^{-3}$

DOI: 10.1007/978-3-540-69761-9_8

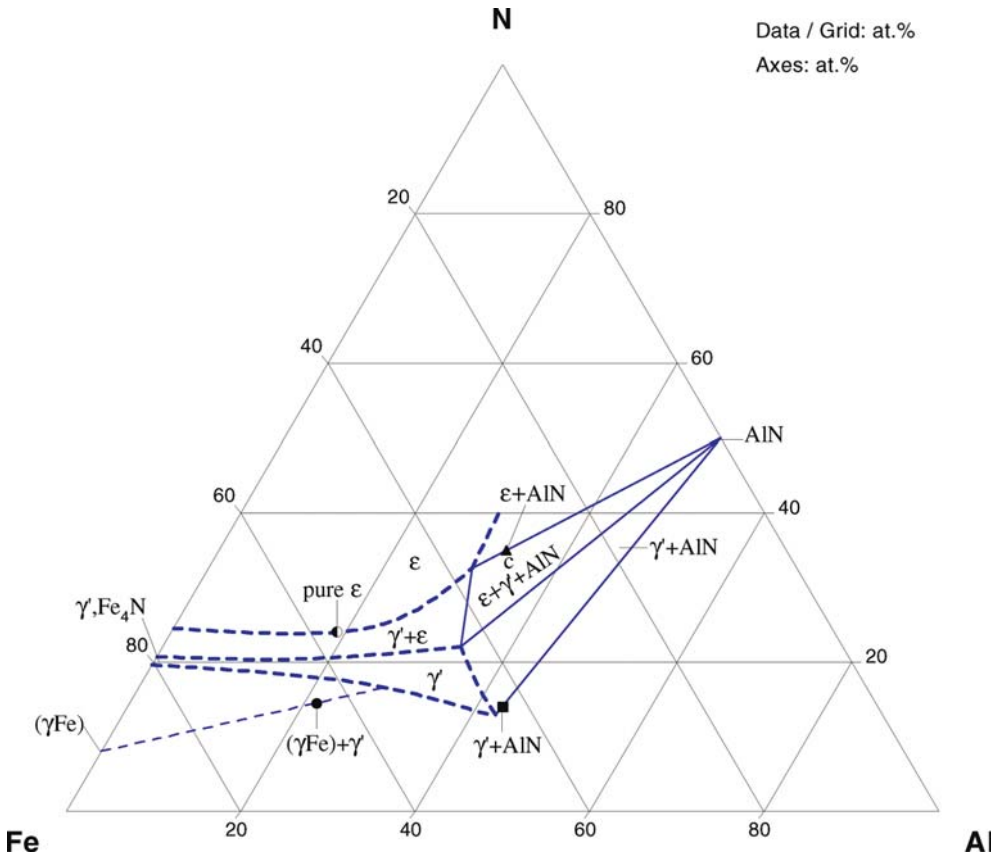

Fig. 1. Al-Fe-N. Partial isothermal section at 600°C

DOI: 10.1007/978-3-540-69761-9_8

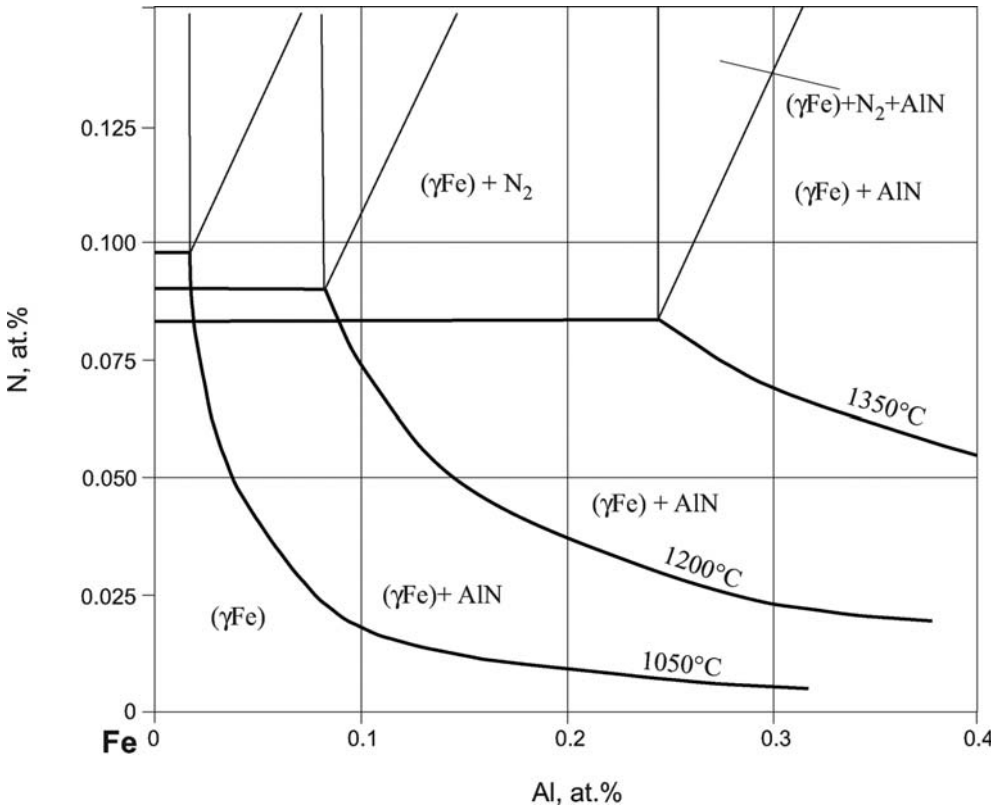

Fig. 2. Al-Fe-N. Solubility limits in the (γFe) phase

DOI: 10.1007/978-3-540-69761-9_8

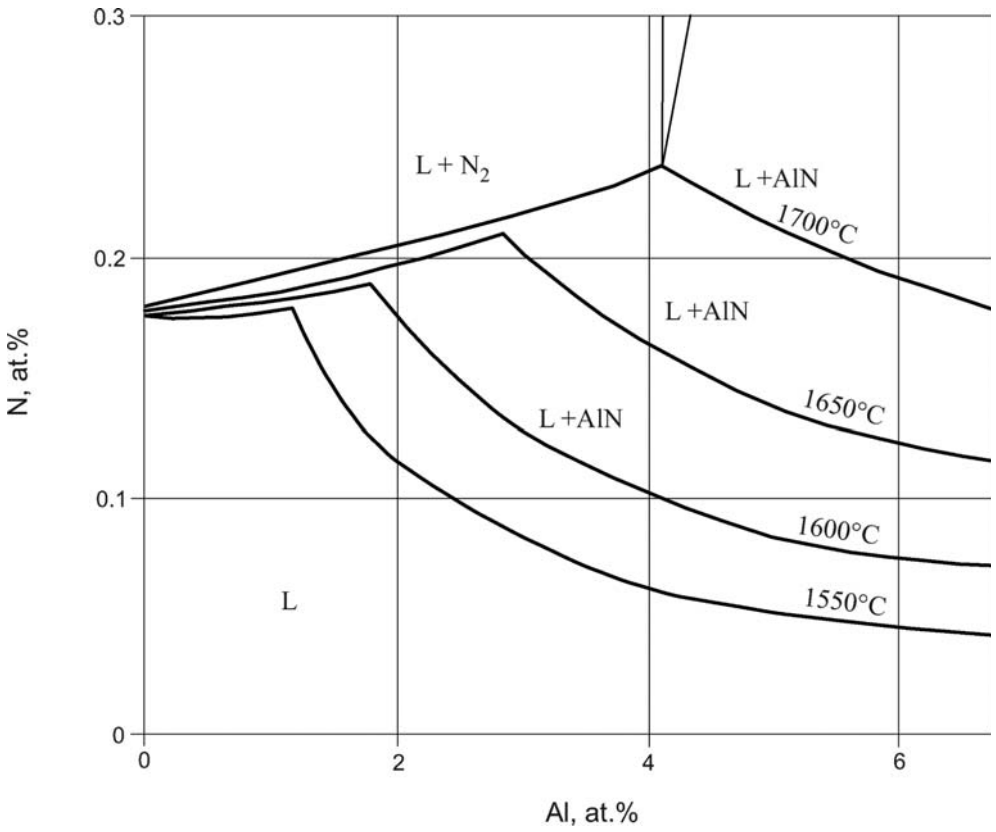

Fig. 3. Al-Fe-N. Solubility limits in the liquid phase

DOI: 10.1007/978-3-540-69761-9_8

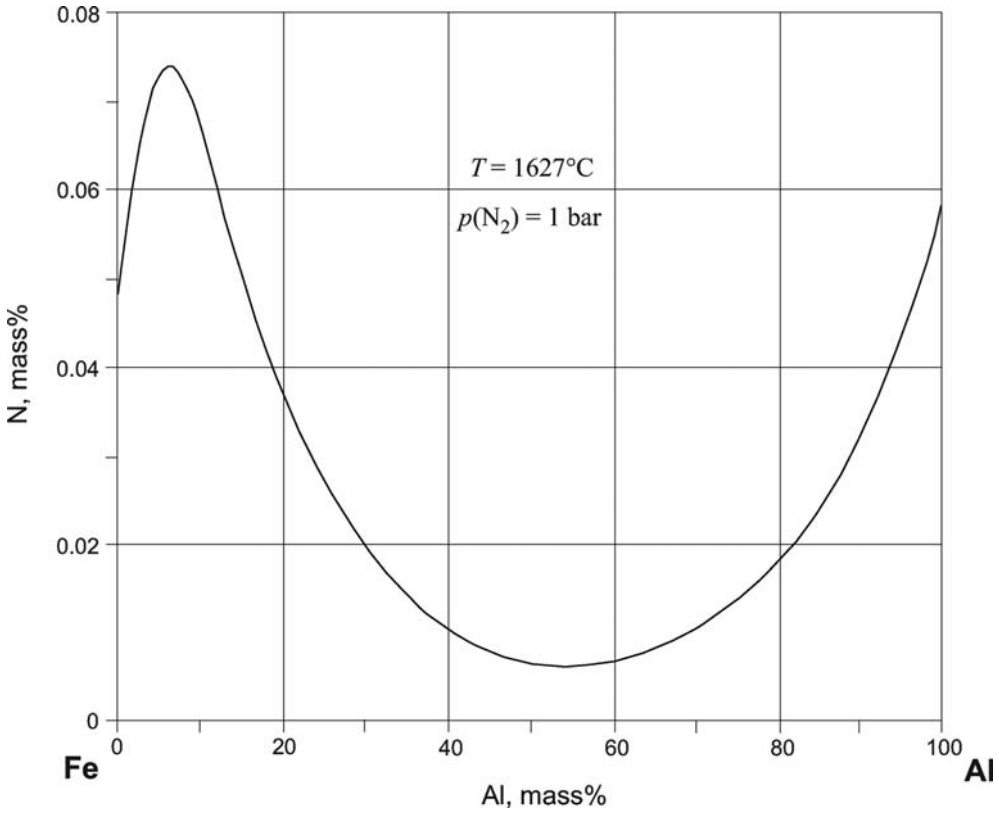

Fig. 4. Al-Fe-N. Solubility of N_2 in Al-Fe liquid alloys at 1627°C under 1 bar N_2

DOI: 10.1007/978-3-540-69761-9_8

References

[1939Ekl] Eklund, L., "The Solubility of Nitrogen in Steel" (in Swedish), *Jernkontorets Ann.*, **123**, 545–556 (1939) (Phase Diagram, Phase Relations, Experimental, 13)

[1951Dar] Darken, L.S., Smith, R.P., Filer, E.W., "Solubility of Gaseous Nitrogen in γ Iron and the Effect of Alloying Constituents - Aluminium Nitride Precipitation", *Trans. Metall. Soc. AIME*, **191**, 1174–1179 (1951) (Phase Diagram, Phase Relations, Experimental, *, 12)

[1960Mae] Maekawa, S., Nagakawa, Y., "Effect of Titanium, Aluminium and Oxygen on the Solubility of Nitrogen in Liquid Iron" (in Japanese), *Tetsu to Hagane*, **46**, 1438–1441 (1960) (Phase Diagram, Phase Relations, Thermodyn., Experimental, 8)

[1960Peh] Pehlke, R.D., Elliott, J.F., "Solubility of Nitrogen in Liquid Iron Alloys-I-Thermodynamics", *Trans. Metall. Soc. AIME*, **218**, 1088–1101 (1960) (Phase Diagram, Phase Relations, Experimental, Thermodyn., *, 32)

[1961Isa] Isaev, V.F., Morozov, A.N., "Conditions of Formation of AlN in Liquid Fe" (in Russian), *Sb. Nauchn.-Tehn. Trud., Nauchno-Issled. Inst. Met. Chelyab. Sovnarkhoz*, (4), 12–18 (1961) (Thermodyn., Experimental, 8)

[1961Sta] Stadelmaier, H.H., Yun, T.S., "Alloys of Nitrogen and the Transition Metals Mn, Fe, Co and Ni with Mg, Al, Zn and Cd", *Z. Metallkd.*, **52**, 477–480 (1961) (Crys. Structure, Phase Diagram, Phase Relations, Experimental, *, 22)

[1963Mor] Morozov, A.N., Isaev, V.F., Korolev, L.G., "Conditions of Nitride Formation and Solubility of N in Alloys of Fe with Al, Ti and V" (in Russian), *Izv. Akad. Nauk SSSR, Metall. i Gorn. Delo*, (4), 141–144 (1963) (Phase Diagram, Phase Relations, Experimental, 6)

[1964Eva] Evans, D.B., Pehlke, R.D., "The Aluminium Nitrogen Equilibrium in Liquid Iron", *Trans. Metall. Soc. AIME*, **230**, 1651–1656 (1964) (Phase Diagram, Phase Relations, Experimental, 12)

[1968Isa] Isaev, V.F., Danilovich, Yu.A., Morozov, A.N., "Solubility of Nitrogen for the Formation of Nitrides in Molten Alloys Based on Iron and Nickel" (in Russian), *Fiz-Khim. Osn. Pro. Stali. Publ. Nauka*, Samarin, A.M. (Ed.), Nauka, Moscow, 296–301 (1968) (Phase Diagram, Phase Relations, Thermodyn., Experimental, 11)

[1972Oga] Ogawa, R., Fukutsuwa, T., Yagi, Y., "Precipitation of AlN in Cold Worked High Purity Fe-Al-N Alloys" (in Japanese), *Tetsu to Hagane*, **58**, 872–884 (1972) (Phase Diagram, Phase Relations, Experimental, 21)

[1973Mok] Mokrov, I.A., Aleshchenko, G.M., Stomakhin, A.Ya., "Thermodynamic Evaluation of Oxides and Nitrides in Metallic Melts", (in Russian), *Izv. Vyss. Uchebn. Zaved., Chern. Metall.*, (7), 63–67 (1973) (Phase Diagram, Phase Relations, Thermodyn., 9)

[1976Kru] Krueger, J., Kunze, H.D., Schuermann, E., "Eisen" (in German), in "*Gases and Carbon in Metals*", Fromm, E., Gebhardt, E, (Eds.), Springer, Berlin, 578–613 (1976) (Phase Diagram, Phase Relations, Review, *, 241)

[1978Tro] Trontelj, M., Kolar, D., "Reactions of AlN with the Iron Group Elements", *Vestn. Sloven. Kem. Drus.*, **25**(2), 165–172 (1978) (Thermodyn., Eperimental, 8)

[1978Wad] Wada, H., Pehlke, R.D., "Nitrogen Solubility and Aluminium Nitride Precipitation in Liquid Fe, Fe-Cr, Fe-Cr-Ni, and Fe-Cr-Ni-Mo Alloys", *Metall. Trans. B*, **9B**, 441–448 (1978) (Phase Diagram, Phase Relations, Thermodyn., Experimental, *, 12)

[1979Wad] Wada, H., Pehlke, R.D., "Nitrogen Solubility and Aluminium Nitride Precipitation in Liquid Iron Alloys containing Nickel and Aluminum", *Metall. Trans. B*, **10B**, 409–412 (1979) (Phase Diagram, Phase Relations, Thermodyn., Experimental, *, 4)

[1982Fro] Fromm, E., Jehn, H., Hehn, W., Speck, H., Hörz, G., "Gases and Carbon in Metals, Pt XV, Ferrous Metals (3), Iron - Nitrogen", *Phys. Data*, Fachinformationszentrum Energie, Physik, Mathematik, Karlsruhe, **85**, 5–17 (1982) (Phase Diagram, Phase Relations, Review, 40)

[1982Ish] Ishii, F., Ban'ya, B., Fuwa, T., "Effect of C, Al, Si, P, Mn and Ni on the Solubility of Nitrogen in Liquid Iron Alloys" (in Japanese), *Tetsu to Hagane*, **68**, 1551–1559 (1982) (Phase Diagram, Phase Relations, Experimental, Thermodyn., 43)

DOI: 10.1007/978-3-540-69761-9_8

[1984Rag] Raghavan, V., "The Al-Fe-N System", *Trans. Indian Inst. Met.*, **37**, 411–415 (1984) (Phase Diagram, Phase Relations, Review, 16)

[1985Sch] Schuster, J.C., Bauer, J., Nowotny, "Applications to Materials Science of Phase Diagrams and Crystal Structures in the Ternary Systems Transition Metal-Aluminum-Nitrogen", *Rev. Chim. Miner.*, **22**(4), 546–554 (1985) (Phase Diagram, Phase Relations, Review, #, 20)

[1986Wad] Wada, H., Lee, S.W., Pehlke, R.D., "Nitrogen Solubility in Liquid Fe and Mn-Fe Alloys", *Metall. Trans. B*, **17B**, 238–239 (1986) (Experimental, 17)

[1986Wri] Wriedt, H.A., "The Al-N (Aluminium-Nitrogen) System", *Bull. Alloy Phase Diagrams*, **7**, 329–333 (1986) (Phase Diagram, Phase Relations, Review, #, 54)

[1987Fri] Frisk, K., "A New Assessment of the Fe-N Phase Diagram", *Calphad*,**11**, 127–134 (1987) (Phase Diagram, Phase Relations, Thermodyn., Theory, 34)

[1987Rag] Raghavan, V., "The Al-Fe-N System", in "*Phase Diagrams of Ternary Iron Alloys, Part I*", ASM International, **1**, 145–147 (1987) (Phase Diagram, Phase Relations, Review, 13)

[1987Wri] Wriedt, H.A., Gokcen, N.A., Nafziger, R.H., "The Fe-N (Iron-Nitrogen) System", *Bull. Alloy Phase Diagrams*, **8**(4), 355–377 (1987) (Phase Diagram, Phase Relations, Thermodyn., Review, #, 126)

[1988Lan] Lankreijer, L.M., Somers, M.A.J., Mittemeijer, E.T., "Kinetics and Nitride Precipitation in Fe-Al and Fe-Si Alloys on Nitriding", *Proc. Internat. Conf. High Nitrogen Steels, Lille*, Edited 1989 by the Institute of Metals, London, 108–111 (1988) (Phase Diagram, Phase Relations, Experimental, 17)

[1991Bar] Barnard, J.A., Tan, M., Waknis, A., Haftek, E., "Magnetic Properties and Structure of Al/Fe-N Periodic Multilayer Thin Films", *J. Appl. Phys.*, **69**(8), 5298–5300 (1991) (Crys. Structure, Magn. Prop., 8)

[1991Kub] Kubota, K., Naoe, M., "Magnetic Properties of Fe-N/Al-N Multilayerd Films Prepared by Ar Ion-Assist Sputtering", *J. Appl. Phys.*, **70**(10), 6430–6432 (1991) (Crys. Structure, Magn. Prop., 2)

[1992Jeh] Jehn, H.A., Perrot, P., "Aluminium - Iron - Nitrogen", MSIT Ternary Evaluation Program, in *MSIT Workplace*, Effenberg, G. (Ed.), MSI, Materials Science International Services GmbH, Stuttgart; Document ID: 10.14876.1.20, (1992) (Crys. Structure, Phase Diagram, Phase Relations, Assessment, 23)

[1992Hil] Hillert, M., Jonsson, S., "An Assessment of the Al-Fe-N System", *Metall. Trans. A*, **23A** (11), 3141–3149 (1992) (Phase Diagram, Phase Relations, Thermodyn., Assessment, #, 27)

[1993Rag] Raghavan, V., "Al-Fe-N (Aluminum-Iron-Nitrogen)", *J. Phase Equilib.*, **14** (5), 617–618 (1993) (Phase Diagram, Phase Relations, Review, 7)

[1995Big] Biglari, M.H., Brakman, C.M., Mittemeijer, E.J., Zwaag, S.V.D., "The Kinetics of the Internal Nitriding of Fe-2 at.% Al Alloy", *Metall. Mater. Trans. A*, **26A**, 765–776 (1995) (Calculation, Experimental, Kinetics, Thermodyn., 41)

[2000Yag] Yaghmaee, M.S., Kaptay, G., Janosfy, G., "Equilibria in the Ternary Fe-Al-N System", *Mater. Sci. Forum*, **329-330**, 519–524 (2000) (Phase Diagram, Phase Relations, Theory, 9)

[2001Liu] Liu, Y.-K., Harris, V.G., Kryder, M.H., "Evolutions of Magnetic and Structural Properties of FeAlN Thin Films via N Doping", *IEEE Trans. Magn.*, **37**(4), 1779–1782 (2001) (Experimental, Magn. Prop., 8)

[2003Fer] Ferro, R., Bochvar, N., Sheftel, E., Ding, J.J., "Al-N (Aluminum-Nitrogen)", MSIT Evaluation Program, in *MSIT Workplace*, Effenberg, G. (Ed.), MSI, Materials Science International Services GmbH, Stuttgart; submitted for publication, (2003) (Phase Diagram, Phase Relations, Crys. Structure, Assessment, 33)

[2003Per] Perrot, P., "Fe-N (Iron-Nitrogen)", MSIT Binary Evaluation Program, in *MSIT Workplace*, Effenberg, G. (Ed.), MSI, Materials Science International Services GmbH, Stuttgart; submitted for publication, (2003) (Crys. Structure, Phase Diagram, Phase Relations, 35)

[2006MSIT] "Al-Fe (Aluminum-Iron)", Diagrams as Published, in *MSIT Workplace*, Effenberg, G. (Ed.), Materials Science International Services, GmbH, Stuttgart; Document ID: 30.10236.1.20, (2006) (Crys. Structure, Phase Diagram, Phase Relations, 11)

DOI: 10.1007/978-3-540-69761-9_8

[H] Hansen, M. and Anderko, K., *Constitution of Binary Alloys*, McGraw-Hill, New York (1958)
[Mas2] Massalski, T.B. (Ed.), *Binary Alloy Phase Diagrams*, 2nd edition, ASM International, Metals Park, Ohio (1990)
[V-C2] Villars, P. and Calvert, L.D., *Pearson's Handbook of Crystallographic Data for Intermetallic Phases*, 2nd edition, ASM, Metals Park, Ohio (1991)

DOI: 10.1007/978-3-540-69761-9_8

Aluminium – Iron – Oxygen

Ortrud Kubaschewski, Rainer Schmid-Fetzer, updated by Lazar Rokhlin, Lesley Cornish, Olga Fabrichnaya

Introduction

The system is important because alumina is used to reduce iron oxides in steelmaking, and knowledge of the slag properties, especially the effects of metal-slag reactions is essential for greater control in steelmaking [1953Gok, 1961Kuz, 1966Nov, 1975Kim, 1979Kay]. No complete phase diagram has been reported for the Al-Fe-O system, although specific reactions of mainly industrial interest have been investigated, especially the deoxidation of steel with Al and the sub-solidus reactions in the partial systems FeO-Al_2O_3-Fe_2O_3 and Al-Al_2O_3-Fe_2O_3-Fe [1954Ric, 1961Tur, 1962Tur, 1966Nov, 1980Mey, 1989Rag1]. The complex phase relationships in the Al-Fe-O system are partly due to the ratio of ferrous to ferric oxide at equilibrium, which itself is dependent on both temperature and oxygen pressure. This survey therefore describes the system by isothermal and polybaric projections. Among the many published contributions on the clarification and description of the phase relationships, only selected reports are given in the References section. The relation between deoxidation data and the phase equilibria is essential for understanding of discrepancies in this system, and will be elucidated in the Miscellaneous section. Table 1 summarizes the work done since 1994.

Binary Systems

The binary Al-O phase diagrams accepted from [1992Tay] are presented in Figs. 1a, 1b. Crystallographic data for solid phases are from [1985Wri]. The phase diagram of Al-Fe is accepted from the thermodynamic assessment of [1993Kat], combined with experimental data of [2001Ike] for phase relations between bcc phases with *A*2, *B*2 and $D0_3$ structures. The derived phase diagram of the Al-Fe system is presented in Fig. 2 [2006MSIT]. The phase diagrams of the Fe-O system are from the thermodynamic assessment of [1991Sun], while crystallographic data for high pressure and metastable/low temperature phases are from [Mas2], [V-C2], [V-C] and [1982Kub]. The phase diagrams for the Fe-O system are presented in Figs. 3a, 3b.

Solid Phases

Data on the solid phases are given in Table 2. One ternary high temperature compound $FeAlO_3$ (τ), stable between 1318°C and about 1500°C, depending on the oxygen pressure was reported by [1956Mua, 1958Mua], although [2005Fee] synthesized the $FeAlO_3$ phase by heating a γAl_2O_3 + αFe_2O_3 mixture at 1300°C. Based on experimental data, formation of the $Fe_{2-x}Al_xO_3$ was suggested at 1150°C [2001Lad]. $FeAl_2O_4$ (hercynite) and Fe_3O_4 (magnetite) form a continuous series of solid solutions at temperatures above 860°C [1962Tur]. At temperatures below 860°C, spinel has miscibility gap forming Fe rich (σ″) and Al rich (σ″) solid solutions.

Several studies (see section Quasibinary Systems and [2005Fee]) indicated restricted mutual solubility between αAl_2O_3 (corundum) and αFe_2O_3 (hematite). [1979Rou, 1991Skl], together with more recent investigations [2005Fee, 2005Liu], indicated formation of metastable γ spinel solid solutions in the system Al_2O_3-Fe_2O_3 system in the Al rich composition range. However, here γAl_2O_3 and γFe_2O_3 are considered as different phases, because there is no evidence of complete mutual solubility. It was shown in [2005Liu] that iron oxide doping reduced the γ to αAl_2O_3 transformation temperature.

Mechanical milling of mixtures consisting of various combinations of (Al), Fe_3O_4, Fe_2O_3 and Al_2O_3 extended the homogeneity ranges of some of the phases [2001Sur, 2003Bot, 2004Cot]. According to [2001Sur], during mechanical milling, Al_2O_3 dissolved up to 25 mol% Fe_2O_3.

DOI: 10.1007/978-3-540-69761-9_9

Quasibinary Systems

The section FeO-Al_2O_3 was established as a quasibinary using DTA, X-ray, microscopy and petrographic analysis. A new version of the quasibinary system FeO-Al_2O_3 was proposed by [1974Ros]. However, it should be noted that the system is not strictly quasibinary because Fe occurs in different states of oxidation in varying amounts, even in oxide phases in contact with metallic Fe, and the "melting point" of FeO actually corresponds to a eutectic. The results are shown in Fig. 4 which summarizes findings of [1974Ros] and previous studies [1955Oel, 1956Fis] and [1957Gal], and is in agreement with [1965Nov, 1966Nov]. The congruent melting point of $FeAl_2O_4$, reported by [1957Gal] as 1800°C, was accepted in Fig. 4 (1820, 1800 and 1820°C are given by [1956Fis, 1957Gal] and [1963Nov], respectively. X-ray diffraction and petrographic analysis of the samples from simultaneous sintering of iron aluminate and corundum at 1700°C showed that there is negligible miscibility between $FeAl_2O_4$ and Al_2O_3 in the solid phase [1965Nov], which was later confirmed by [1974Ros]. According to earlier studies [1956Fis, 1956Mua, 1958Atl, 1964Roi], a measurable solution of Al_2O_3 in $FeAl_2O_4$ occurs above 1350°C.

The Fe_3O_4-$FeAl_2O_4$ and Fe_2O_3-Al_2O_3 sections are also quasibinary, at least at temperatures below the solidus and high enough pressure to prevent oxide decomposition. [1962Tur] carried out experiments defining the limits of the spinel solid solution of the Fe_3O_4 (magnetite) - $FeAl_2O_4$ (hercynite) system. The buffered hydrothermal technique and lattice parameter measurements were used to find the solvus. A method of "bracketing" was developed, *i.e.* approaching the equilibria from both directions, the exsolution and solid solution. To induce solid solubility, samples were held for 2 d at 800°C, 12 d at 700°C and 1 month at 600°C, under a total pressure of 2 kbar. Equilibrium at 500°C was not obtained. The results are plotted in Fig. 5.

The Fe_2O_3-Al_2O_3 section below 1000°C was studied by [1962Tur] using their own data established by the hydrothermal method and X-ray analysis, combined with results published by [1956Mua, 1958Atl] to construct the diagram in Fig. 6. Measurements by [1956Mua] were found to contain about 5 mass% less Al_2O_3 than those reported by [1958Atl] and extrapolated by [1962Tur].

More recent investigations by [1983Boj] indicate a lower solid solubility of Al_2O_3 in Fe_2O_3 (Fig. 6). The solubility at lower temperatures has been determined by [1980Kli]. The $FeAlO_3$ compound appears at the upper limit of Fig. 6. Some "quasibinary" sections were calculated with a simple regular solution-type model as a basis for calculations in multicomponent oxide systems [1978Kau].

Invariant Equilibria

The reaction scheme for the Fe-Fe_2O_3-Al_2O_3-Al partial system, constructed by [1989Rag1], was corrected as described in the next section and is presented in Fig. 7. It includes the invariant points of the liquidus surface and incorporates the sub-solidus invariant reactions based on results published as isothermal sections. The reaction p_1 at about 1700°C, $L'' + Al_2O_3 \rightleftharpoons Fe_2O_3$, may also be of the eutectic type, $L'' \rightleftharpoons Al_2O_3 + Fe_2O_3$. This reaction must not be confused with the peritectic at about 1730°C shown later in the section Fe_2O_3-Al_2O_3 (Fig. 21) at 0.21 bar. This peritectic cannot appear in Fig. 7 since the entire reaction scheme is given under sufficient pressure to exclude the gas phase. An extrapolation of the Fe_2O_3 solvus and the Al_2O_3 liquidus in Fig. 21 does not lead to a clear conclusion concerning the type of the reaction p_1. The formation and decomposition of τ is also viewed differently compared to [1989Rag1]. The formation must occur above 1495°C as shown by the series Figs. 20, 21 and 22, extrapolated to higher pressures. It is shown as P_1 in Fig. 7, an almost degenerated reaction with τ located almost on the tie-line Fe_2O_3-Al_2O_3. An alternative formation reaction in a three-phase maximum $Fe_2O_3 + Al_2O_3 \rightleftharpoons \tau$ is rather unlikely since it would require a larger O solubility range in Fe_2O_3 and Al_2O_3 than in τ. Thus, the three-phase invariant reactions given in [1989Rag1] at 1450 and 1318°C cannot be accepted. The decomposition of τ in E_3 at 1318°C (Fig. 7) is also almost degenerated and virtually identical to the 1318°C reaction in the Fe_2O_3-Al_2O_3 system at fixed oxygen partial pressure 0.21 and 1 bar, emphasizing the non-quasibinary character of these sections. Data on the invariant reactions at 1 bar total pressure involving Fe rich liquids are compiled in Table 3 [1972Ell].

Liquidus Surface

[1989Rag1] proposed a schematic liquidus surface which may be mostly accepted. However, the liquid miscibility gap of the Al-O system had not been taken into account, suggesting that liquid Fe and liquid

DOI: 10.1007/978-3-540-69761-9_9

Al_2O_3 form a continuous solution, which is extremely unlikely. Another proposition, given in Fig. 6, accepts a continuous band of the miscibility gap between liquid metals (L′) and liquid oxides (L″). As a consequence of this, the eutectic type reaction E_1'-E_1'' and also a maximum e_2'-e_2'' must occur. A critical point, given as c_1 and confused with the congruent melting point of $FeAl_2O_4$ by [1989Rag1], does not appear. Figure 8 incorporates the results of [1972Ell, 1979Ell]. The reactions e_3 and e_9 belong to the quasibinary system FeO-Al_2O_3 (Fig. 4). The invariant reactions U_6 to E_5 virtually coincide with the Al-Fe binary system. Quantitative data are available for liquidus surfaces in the Fe corner [1972Ell, 1979Ell] and Fig. 9 shows a projection. The Al_2O_3 liquidus surface has been studied by [1953Gok, 1954Ric, 1961Kuz, 1963Ent, 1965McL, 1967Swi, 1969Buz, 1969Nov, 1970Fru, 1971Roh, 1976Jan, 1981She, 1982Lia], the early solubility data of [1939Wen] are much too high (probably due to insufficient time being allowed for equilibrium) and have been disregarded.

Figure 10 gives isotherms of the Al_2O_3 liquidus surface from the results reported by [1963Ent] for 1740 and 1910°C, [1967Swi] for 1580°C and [1981She] for 1600°C. The 1580°C and 1600°C isotherms also reflect the scatter of the data; the actual slope of the Al_2O_3 liquidus surface is considered to be smooth in the 1590°C to 1910°C temperature range. [1963Ent, 1967Swi] investigated the Al and O contents of liquid Fe in equilibrium with Al_2O_3. [1963Ent] applied the gravimetric (Al_2O_3) and [1967Swi] the vacuum fusion method for the determination of the O concentration. As indicated by [1963Ent], the vacuum fusion method is susceptible to grave errors at high Al contents due to the absorption of gas by the Al distilled from the sample and the vaporization of Al_2O, which would account for the low oxygen contents at high Al concentrations in the 1580°C isotherm. The results of [1967Swi] appear to be inconsistent with other data, and thus, this may arise from his method of oxygen analysis. The findings agree that the solubility of O in Al-Fe melts decreases with increasing Al content to a minimum and then increases rapidly as shown in Fig. 10, 0.39 mass% Al decreases the solubility of oxygen in liquid Fe to a minimum of 8 ppm (0.0008 mass% O) at 1600°C.

The 0.01 to 100 mass% Al range at 1600°C was studied by [1981She] who also discussed earlier work by [1961Kuz]. The initial materials were hydrogen-refined carbonyl-iron and high purity Al. The solubility of oxygen was examined by the phase equilibrium method [1981She, 1970Nov]. The curve has two minima and one maximum. The first minimum is in good agreement with published data [1961Kuz, 1963Ent, 1967Swi, 1971Roh]. There are no other reported data on the position of the second minimum. The maximum approaches the experimental findings by [1963Ent] and [1970Fru].

Oxygen concentration in liquid iron being equilibrated with Al_2O_3 and $FeAl_2O_4$ was determined in experiments of [1966McL, 1975Kim] at temperatures 1550-1750°C. Oxygen solubility results obtained by [1969Nov] at 1600°C by calculation and the vacuum fusion method are higher than those reported by [1981She]. Values at the minimum are 0.0035 mass% O [1969Nov] and 0.0008 mass% O [1981She], respectively.

It should be mentioned that the isotherm at 1600°C in Fig. 10 has been moved down within the experimental uncertainty, because the curve from the original work [1981She] intersected with the isotherm at 1740°C and it was far away from the isothrem at 1580°C while the temperature difference was only 20°C.

Isothermal Sections

[1961Tur, 1962Tur] studied Fe spinels by controlled synthesis from chemical mixtures in the temperature range 500 to 900°C and used X-ray measurements for the determination of solid solutions. Silver, which is not miscible with Fe at the temperature involved, was used as container material. Reaction rates were slow and experiments lasted up to 40 d. The isothermal sections displayed in Figs. 11 to 15 summarize the experimental results by [1961Tur, 1962Tur, 1980Mey] and [1983Elr], as well as findings from a review published by [1989Rag1] for the partial systems Fe-Fe_2O_3-Al_2O_3-Al and FeO-Fe_2O_3-Al_2O_3. The isothermal sections must be seen in conjunction with the oxygen pressure (stability) diagrams, given under Miscellaneous, where the techniques used by [1980Mey] and [1983Elr] are also described.

Potential Diagrams

[1980Mey] determined the composition limits for the spinel solid solution $\sigma = (Fe,Al)_3O_4$ experimentally as a function of oxygen pressure at 1280, 1380 and 1500°C using lattice parameter measurements. The results were combined with information from the literature [1946Dar, 1956Fis, 1956Mua, 1958Atl,

DOI: 10.1007/978-3-540-69761-9_9

1958Phi, 1964Roi, 1976Sti, 1976Pol] to develop self-consistent stability diagrams (Figs. 16 to 18), which show $p(O_2)$ versus cation (metal) fraction at constant temperatures for the Al-Fe-O system. In these diagrams, the left and right vertical axes constitute the binary Fe-O and Al-O systems, respectively. The complete spinel solid solution does not exist at any specific oxygen pressure. The spinels with higher Al content are only stable at lower oxygen pressure. The metallic Al-Fe phases would only appear below the pressure range of Figs. 16 to 18. [1983Elr] determined the equilibrium oxygen pressures of the univariant ternary equilibria of Fe_2O_3+σ+Al_2O_3, metal+FeO+σ and metal+σ+Al_2O_3, where the metal is essentially pure Fe. They used data derived from solid state electrochemical cell experiments in the temperature range 850°C to 1150°C in combination with published data [1956Mua, 1958Mua, 1958Atl, 1962Tur, 1964Roi, 1981Pet] to construct oxygen pressure diagrams at 1000°C, 900°C and 800°C, as shown in Figs. 19 to 21, where the boundaries for the Al- or Fe-rich spinel are schematic. The spinel miscibility gap (σ′+σ″) appears at 800°C in Fig. 21 and in Fig. 5. The σ′+σ″ boundaries are virtually independent of pressure. The composition of the spinel phase in equilibrium with Al_2O_3 at 900°C and $p(O_2) = 10^{-12}$, 10^{-13} and 10^{-14} bar was reported by [1962Tur]. FeO dissolves up to 0.55 mol% Al_2O_3. Alumina (Al_2O_3) was found to dissolve approximately 1.1 at.% Fe in the temperature region 1000°C to 1300°C, whereas the Al content in the Al-Fe alloys was extremely small: 0.1 mass% Al above $p(O_2)$ ~10 to 30 bar. The data of the Fe_3O_4/FeO equilibrium were taken from [1946Dar, 1969Bry]. [1984Sch] produced a projection of the aluminium and oxygen contents for $Fe_{1-x}O$-Al_2O_3, as well as a polythermal deoxidation diagram of aluminium. However, these diagrams are not presented here, because they are inconsistent with the diagram of the FeO-Al_2O_3 system accepted in the present work. In a study of diffusion coatings, [2001Jha] plotted the relationship of oxygen potential and (low) Al content.

The effect of oxygen partial pressure on grain boundary migration in $95Al_2O_3 \cdot 5Fe_2O_3$ was studied by [1996Lee]. High oxygen partial pressure caused fast dissolution of the spinel, agreeing with earlier work described above, with migration of the Al_2O_3 solid solution grain boundaries. The Al_2O_3 was enriched in Fe_2O_3 after the boundary had passed. Low oxygen partial pressures gave grain boundary migration without spinel precipitation.

Temperature – Composition Sections

The Al_2O_3-Fe_2O_3 section was investigated at temperatures above 1000°C with different oxygen pressures by [1956Mua, 1958Mua]. They applied the "quenching method" and microscopy, as well as lattice parameter measurements for identification of different phases. $FeAlO_3$ (τ) exists in stable equilibrium only at temperatures above 1318°C and a partial pressure of O_2 above 0.03 bar. The upper decomposition temperature of τ is pressure dependent. The phase relationships are illustrated in Figs. 22 to 24 for decreasing oxygen pressure [1958Mua]. These vertical sections appear to be quasibinary diagrams, although this cannot be true at higher temperatures. The decomposition when heating pure Fe_2O_3 at 1390°C in Fig. 23 corresponds to the three-phase reaction: $6Fe_2O_3 \rightleftharpoons 4Fe_3O_4 + O_2$. The resulting phase Fe_3O_4 (σ) is no longer located on the section Fe_2O_3-Al_2O_3 and this shift is balanced by substantial amounts of O_2 (gas), which is the meaning of the designation "+O_2" in the upper phase fields. A slight inconsistency concerns the reported solubility limits of the Fe_2O_3+σ equilibrium. According to [1958Mua] (Figs. 22 to 24) the solubility of Al_2O_3 in σ is larger than in Fe_2O_3. This is reversed in Figs. 17 to 21, however, where the solubility differences are small. [1992Tru] calculated the oxygen concentration in (γFe) with αAl_2O_3, $FeAl_2O_4$ and $Fe_{1-x}O$ (denoted 'FeO') as shown in Fig. 25.

Thermodynamics

In the literature, there is a great number of publications about equilibria in the Fe rich composition range. The data were obtained for the equilibrium between liquid iron and solid Al_2O_3 according to the reaction:

$$Al_2O_3(s) = 2\{\text{mass\% Al}\} + 3\{\text{mass\% O}\} \quad (1)$$

using the equilibration method with gas mixtures [1953Gok, 1961Kuz, 1963Ent, 1966Nov, 1967Swi, 1970Nov, 1970Sch, 1973Buz, 1981She, 1998Seo] and from emf measurements [1970Fru, 1976Jan, 1979Kay, 1992Hol, 1995Dim]. The Gibbs energy of reaction (1) is given in Table 4 according to the recommendation of [2000Jan], based on analysis of experimental data on phase equilibria and emf

DOI: 10.1007/978-3-540-69761-9_9

measurements. The same methods were used to study equilibrium of iron liquid with $FeAl_2O_4$ (σ) and solid Al_2O_3 according to the reaction (2):

$$FeAl_2O_4(s) = Fe_L + Al_2O_3(s) + 1\{mass\%\,O\} \quad (2)$$

The Gibbs energy of reaction (2) was obtained by the equilibration technique [1960Pil, 1966McL, 1966Nov, 1975Kim] and emf [1963Rez, 1973Cha, 1973Jac, 1978Apt, 1978Sto, 1979Kay]. The results of [1978Apt] are in a good agreement with other data and they are recommended here (Table 4). The experimental data for the spinel + solid Al_2O_3 + (γFe) equilibrium was obtained by equilibration with a gas mixture and emf and analyzed by [1992Tru] and the Gibbs energy for the reaction:

$$(\gamma Fe) + 1/2O_2(gas) + Al_2O_3(s) = FeAl_2O_4(\sigma) \quad (3)$$

are recommended. The expression of Gibbs energy is presented in Table 4.

The results of experimental studies of the reaction (1) were thermodynamically treated and equilibrium constants and mixing parameters of liquid were derived. The oxygen and aluminum solubility in liquid were described by Wagner's model with first-order parameters by [1953Gok, 1961Kuz, 1963Ent, 1965Nov, 1967Buz, 1968Pie, 1970Fru, 1974Fel, 1976Jan], and with higher order parameters by [1974Sig, 1986Gho, 1992Hol, 1995Dim, 1995Jow, 1997Ito]. [1980Gus] presented two equations involving first order and higher order interaction parameters. The thermodynamic descriptions with first order parameters reproduce experimental data only for compositions up to 0.3 mass% Al. Involving higher order parameters makes it possible to reproduce experimental data up to 2 mass% Al. However, at higher concentrations of Al, the calculated oxygen content drastically decreases, which was not confirmed by experimental data. [1968Pie] suggested that taking the formation of the AlO cluster into account should improve fit to experimental data. In the calculation of the liquidus isotherms, [1982Lia] used the thermodynamic model based on Wagner's solvation-shell approach, which required data only from the binary edge systems. His predictions for the ternary Al-Fe-O liquid alloys are in good agreement with the experimental data and Fig. 10 up to about 3 mass% Al, while at 10 mass%, the calculated solubility at 1627°C to 1727°C is approximately 0.1 mass% O, about 10 times higher than the data of [1981She] at 1600°C. [1981She] investigated Al-Fe alloys from 0.01 to 100 mass% Al, and indicated two minima (at 0.39 and 19.9 mass% Al) and one maximum (at 7.7 mass% Al) on oxygen solubility curve, using two different equations to describe his data in different composition ranges. It should be mentioned that similar shape of oxygen solubility was observed for Cr-Fe alloys [1968Pie]. In addition, [1982Lia] clearly demonstrated that previous calculations using interaction parameters are not suitable above 0.3 mass% Al. At higher Al contents, the first order interaction parameter calculation gives a too strong increase in O solubility. The calculation with both first and second order parameters also gives a maximum qualitatively similar to the one at 1600°C in Fig. 10, but at a much lower Al content of about 1 mass% Al and then the O solubility drops to unrealistic low values with only a slight increase of Al content. It can be also concluded that the interaction parameter type calculation must fail at higher Al contents since it is in principle restricted to "infinite" dilution of both O and Al, while the solvation-shell approach is in principle valid over the entire Al-Fe composition range. This calculation should be redone using the new experimental Al-O data of [1981She].

The solubility curves of $FeAl_2O_4$ have also been calculated by [1982Lia], and from the intersection with the Al_2O_3 liquidus isotherms it was concluded that $FeAl_2O_4$ is the most stable oxide precipitate in the liquid below $0.2\cdot10^{-4}$ mass% Al at 1627°C and $2.5\cdot10^{-4}$ mass% Al at 1827°C. The oxygen solubilities at the L+Al_2O_3+$FeAl_2O_4$ three-phase equilibrium are 0.053, 0.074, 0.1 and 0.134 mass% O at 1550°C, 1600°C, 1650°C and 1700°C, respectively, and are in agreement with experimental data [1966McL, 1975Kim].

The associate model for metallic liquid was used by [1988Was, 1995Bou]. [1988Was] considered Fe_3Al, FeAl, $FeAl_3$, FeO, $FeAl_2O_4$, Al_2O_3 and Al_2O as associates. The shape of oxygen solubility curve obtained by [1988Was] was characterized by the presence of two minima in O content and in Al content. However, there is no experimental evidence of a minimum in Al content at low oxygen concentrations. [1995Bou] optimized thermodynamic parameters using three models: Wagner's formalism with high-order mixing parameters, an associate model accounting only for AlO species, and an associate model with both species AlO and Al_2O. [1995Bou] showed that the maximum in the oxygen solubility was apparently due to a large positive second order parameter in Wagner's formalism. The large and negative first-order interaction parameter indicates strong short-range interaction between oxygen and aluminum. When the AlO clusters were introduced into

DOI: 10.1007/978-3-540-69761-9_9

the model by [1995Bou], a good agreement between experimental and calculated values was obtained. The introduction of Al_2O species as well as AlO also reproduced experimental data satisfactorily. In the latter model, the liquid phase was virtually ideal; *i.e.* the excess Gibbs energy of solution is small.

The obtained thermodynamic data for reaction (2) in combination with other thermodynamic data makes it possible to calculate the enthalpy and entropy of formation of $FeAl_2O_4$ from solid Al_2O_3 and Fe [1992Tru]. There is a large scatter in both enthalpy of formation from elements and standard entropy values for the $FeAl_2O_4$ at 298.15 K [1988Ber, 1995Bar, 1993Kub, 1993Sax, 1990Hol, 1997Got, 2004Fab]. Some of these data [1990Hol, 1993Sax, 1997Got, 2004Fab] are results of optimizations based on high-pressure mineral reactions. The reason for inconsistencies can be the different degrees of cation disordering between octahedral and tetrahedral sites in the $FeAl_2O_4$. The degree of inversion was recently determined from neutron diffraction, and the results were treated by thermodynamic models [1998Har]. Recently, new adiabatic calorimetry measurements from 3 to 400 K have provided heat capacity data and a standard entropy value at room temperature [2003Kle], which are given in Table 5. The new entropy value is 7.6 $J\cdot(mol\cdot K)^{-1}$, which is higher than the previous adiabatic calorimetry result of [1956Kin], although the latter did not take the magnetic contribution to the entropy into account.

Activity measurements were conducted in oxygen-rich liquids in the Fe_3O_4-$FeAl_2O_4$ system [1969Sch, 1981Pet] and FeO-Al_2O_3 systems [1980Ban, 2004Fre], using a gas equilibrium technique. The activity in the Fe_3O_4-$FeAl_2O_4$ system was investigated at 900°C and compositions up to 65 mol% Fe_3O_4 by [1969Sch], and at 1300°C and compositions up to 80 mol% Fe_3O_4 by [1981Pet]. In both studies, negative deviations from ideal behavior were indicated, although at high temperatures, deviation from ideality decreased. The experimental activities in the Fe_3O_4-$FeAl_2O_4$ system at 900°C and 1300°C are shown in Figs. 26 and 27. The activity of FeO was studied at 1400°C at compositions up to 8.9 at.% Al_2O_3 by [1980Ban], while in [2004Fre], data were obtained at 1550°C and 1600°C and compositions up to 14 at.% Al_2O_3. Both investigations demonstrated negative deviations from ideal behavior. It should be mentioned that the experimental data on activity in the FeO-Al_2O_3 system [2004Fre] demonstrate quite large scatter. The experimental data of [1980Ban, 2004Fre] were fitted using a liquid model from [2000Bjo] and interaction parameters were assessed. The fitted data on the FeO activity for the FeO-Al_2O_3 system at 1400 and 1600°C from [2004Fre] are presented in Fig. 28. Authors of [2004Fre] also made calculations of activities (a_{FeO} and a_{Al2O3}) in the FeO-Al_2O_3 system using an ionic liquid model and a modified quasi-chemical model of liquid and thermodynamic data available in Thermo-Calc and Fact-sage databanks, respectively. Activity values in the FeO-Al_2O_3 liquid were also calculated by [2000Bjo] from experimental data of [1980Ban], using a model for liquid phase described in [2000Bjo]. As a demonstration, [2002Dav] calculated an isopleth between Fe_2O_3 and Al_2O_3 in air.

The enthalpy of formation of the Fe_2O_3-Al_2O_3 solid solution was determined by drop-solution calorimetry by [2002Maj]. The temperature dependent mixing parameter was assessed in [2002Maj] to reproduce solvus data. The more complicated asymmetric model with temperature dependent parameters was applied by [2005Fee] to describe excess Gibbs energy of the Fe_2O_3-Al_2O_3 solid solutions using available data on miscibility gap and calorimetric data of [2002Maj]. The enthalpy of mixing is presented in Fig. 29. For the $FeAlO_3$ compound, the enthalpy of formation from oxides and heat capacity were determined by drop-solution calorimetry, and by differential scanning calorimetry by [2002Maj], with the data presented in Table 4-Table 5. The standard entropy of the $FeAlO_3$ was calculated by [2002Maj] taking into account vibrational, magnetic, dilatational and configurational contributions due to disordering contributions as 98.9 $J\cdot(mol\cdot K)^{-1}$.

An assessment of thermodynamic functions was presented by [1978Kau]. The calculated phase diagrams of Fe_3O_4-Al_2O_3, FeO-Al_2O_3, Fe_2O_3-Al_2O_3 are in a reasonable agreement with experimental data. The phase diagram of the FeO-Al_2O_3 system was calculated using thermodynamic data of [1984Sch, 1993Eri]. The diagram of [1993Eri] was calculated using a quasi-chemical model for liquid. It should be mentioned that the character of $FeAl_2O_4$ (σ) melting is peritectic and this contradicts experimental data of [1956Fis, 1966Nov, 1974Ros], *i.e.* the peritectic melting of the $FeAl_2O_4$ indicated by [1955Oel] was not confirmed by later studies. The activities of FeO and $AlO_{1.5}$ in the liquid phase were calculated at 1900°C and 2200°C by [1993Eri], with positive deviations from ideal behavior at both temperatures. Since experimental data did not show strong temperature dependence, it is likely that the description of [1993Eri] is in contradiction with the FeO experimental activity data of [1980Ban, 2004Fre]. The 3-D potential diagram of the Al-Fe-O system, based on thermodynamic calculations of [1999Yok], is presented in Fig. 30, with the

DOI: 10.1007/978-3-540-69761-9_9

formation of the Fe_3O_4-$FeAl_2O_4$ spinel solid solution taken into account (calculations without this consideration is shown by a dashed line).

Notes on Materials Properties and Applications

The alloys of the Al-Fe-O system are interesting as materials in applications requiring high resistance to oxidation and sulfidation. The alloys consist of an Fe-40 at.% Al matrix with embedded Al_2O_3 particles, where the Al_2O_3 particles improve the high temperature strength of the alloys (composites) [1997Sub, 2003Lan, 2003Mun]. One of the ways to prepare such alloys is a pre-oxidation of the Fe-40 at.% Al alloy in air, where the gas corrosion resistant layer of the Al-Fe-O alloy is formed on a designated surface [2003Lan]. In [2001Mas], microstructure and oxidation behavior of Fe-40 at.% Al layers deposited on iron plate by low-pressure plasma spraying method were studied and good resistance to oxidation of the layers at high temperatures was confirmed. Al-Fe-O alloys also have interesting magnetic and thermopower properties [2002Gra, 2003Xue]. In [2002Gra], tunneling thermopower in the Al-Fe-O alloys was studied. In nanocomposite Al_2O_3-Fe_2O_3, the phenomenon of superparamagnetism was revealed by [2005Liu].
[1985Tay] presented characteristics of thermal expansion of $FeAl_2O_4$ (hercynite). [1983Yam] investigated vacancy diffusion in the Fe_3O_4-$FeAl_2O_4$ solid solution. [1971Iml] measured microhardness of the spinel Fe_3O_4-$FeAl_2O_4$ solid solution, showing a linear relationship between 675 for magnetite to 1550 for hercynite. [2004Vil] measured the magnetic susceptibility of $Fe_{2-x}Al_xO_3$ compound.

Miscellaneous

The Al-Fe-O phase diagram is applied widely in the analysis and understanding of various metallurgical processes, such as the deoxidation of molten steel by addition of Al. During deoxidizing, Al_2O_3 particles are formed in the melt and tend to escape. In [2000Jan, 2001Sas], the behavior of the Al_2O_3 particles in the deoxidizing steel during continuous casting was investigated, by considering the phase equilibria in the Al-Fe-O system. [1991Nak, 2003Kap] studied wettability of Al_2O_3 by liquid iron with different oxygen contents. [2002Was] applied thermodynamic analysis to study Al_2O_3 formation in deoxidized iron. [1985Meh] used interaction data between molten Fe and solid Al_2O_3 for the development of a model to predict the interfacial behavior in ceramic-molten metal systems with varying partial pressure of oxygen. In [1999Mei], the Al-Fe-O phase diagram was used for analysis of the wide-spread thermite reaction between Fe_2O_3 and Al.
[2002Bot, 2003Bot] studied the reaction in a Al-Fe_3O_4 mixture activated by ball milling. The reaction was ended by formation of the (αFe), $FeAl_2O_4$ and Al_2O_3 phases, which conformed to the equilibrium Al-Fe-O phase diagram. The particular phases formed after the reaction depended on the ratio between components in the mixture Al-Fe_3O_4 [2001Sur].
[2002Tak] reported attempts to prepare magnetic nano-composites consisting of Fe and Al_2O_3 phases by mechanically induced self-propagating reactions in the Fe_3O_4-Al mixture. However, the product obtained after combustion contained significant contents of $FeAl_2O_4$, as well as the targeted Fe and Al_2O_3 phases. Similar results were obtained by [2002Tak], when hematite Fe_2O_3 was reduced with Al by the same method of mechanically induced self-propagating combustion.
Experiments by [1999Fuj] on the deoxidation equilibrium for aluminum in liquid iron and an Fe-36%Ni alloy under pressure controlled by H_2/H_2O gas at 1700°C resulted in the interaction parameters between Al and O in liquid iron and the Fe-36%Ni alloy. [1990Kuz] studied the effect of alloying with Zr, Al-Zr, Hf and Al-Hf on oxygen activity in Co-Cu-Fe-Ni alloys at 1600°C.
[1999Yok] discussed features of generalized chemical potential diagrams and their application to interface reactions between materials having different chemical bonds, such as alloys and ceramics. The calculated stability diagram of the Al-Fe-O system as a function of chemical potentials was presented as an example of a system including solid solutions. A stability diagram for the Al-Cr-Fe system as function of oxygen and sulfur partial pressure at 982°C was calculated by [1979Gor] and utilized to estimate corrosion resistance of alloys used in natural gas production. [1993Tyu] presented thermodynamic descriptions of systems involving an Fe-containing alloy, oxide solid solutions and oxide-sulfide melt.
[2002Gos] reported hematite (Fe_2O_3) produced via oxinate precursors by combustion at 700°C in an air flow to incorporate up to 10 at.% Al. Oxidation of an alloy Fe-2 mass% Al was accompanied by formation

DOI: 10.1007/978-3-540-69761-9_9

of a thin Al_2O_3 film on its surface if the oxygen pressure was less than 10^{-7} torr, and by the Fe_3O_4 film on the surface with the layer of Al_2O_3 underneath, if the oxygen pressure was higher than 10^{-7} torr [1980Aki]. [1979Nec] studied the solubility of Fe in (Al), and materials with high density of dislocations stabilized by Al_2O_3 by Mössbauer spectroscopy. [1984Mac] synthesized the ternary compound $FeAlO_3$ ($Fe_{2-x}Al_xO_3$) at 1370°C, and studied its room-temperature Mössbauer spectrum. Analysis of the spectrum suggested that Fe^{3+} ions occupied both tetrahedral and octahedral sites in the compound lattice. [1998Cos] reviewed and conducted their own study on the Mössbauer spectra of maghemite (γFe_2O_3) and aluminium-substituted maghemite ($\gamma(Fe_{1-y}Al_y)_2O_3$). The dependence of the Mössbauer spectra of the compounds on formation conditions and the possible sites of the ions in their lattices were discussed.
[1990Tsu] studied the solid solution formation between Fe_2O_3 and Al_2O_3 during annealing of mixtures of goethite (αFeOOH) with various hydrated aluminas. Preliminary grinding of the mixtures was established to accelerate the reactions. [1991Yao] investigated the behavior of spinel $FeAl_2O_4$ during annealing at 1200°C under low oxygen partial pressure ($7.1 \cdot 10^{-11}$ - $1.4 \cdot 10^{-8}$ Pa). With increasing annealing time, the spinel decomposed partially forming metallic Fe and αAl_2O_3. Decreasing oxygen partial pressure accelerated the decomposition. X-ray investigations indicated a decrease in the $FeAl_2O_4$ lattice parameter after partial decomposition, which was explained by vacancy formation in lattice sites of the escaped Fe ions. Mössbauer spectra indicated that the ratio of the Fe ions in the tetrahedral sites compared to the total number of Fe ions in the $FeAl_2O_4$ lattice decreased in the decomposition process.
Al is the strongest deoxidiser commonly used in steelmaking. The extent to which it removes dissolved oxygen has been the subject of many investigations. After the work of [1953Gok], it is known that the "deoxidation constant" is extremely small. The equilibrium constant for the reaction $Al_2O_3(s) \rightleftharpoons 2\{Al\}_{Fe} + 3\{O\}_{Fe}$ can be calculated. However, it disagrees with the bulk of the deoxidation constants observed in practice [1979Kub]. The reason for this discrepancy appears to be the following: firstly, when the Al shot is added to undeoxidized liquid steel, the reaction of the solid Al particle with {O} in the immediate surroundings to form Al_2O_3, proceeds at a higher rate than that at which Al dissolves and diffuses through the Fe. Secondly, the resultant Al_2O_3 particle in a deoxidized area is transmitted to an undeoxidized region by turbulences. Oxygen in the undeoxidized area comes out of solution to form FeO, which in turn combines with the Al_2O_3 particle to form the spinel $FeO \cdot Al_2O_3$ ($FeAl_2O_4$). This would result in a high FeO content, as well as a larger deoxidation constant [1957Fit]. Careful experiments over longer time periods proved that the deoxidation constant varies with time. [1967Rep, 1973Iye] demonstrated that projecting the path of reactions with the aid of the phase diagram, allows the metastable or non-equilibrium conditions to be predicted.
The change of Mössbauer spectra, magnetic properties and reduction rate of magnetite-based solid solutions were studied as function of impurity additions of Al, Ca and Mg [1976Mal].
The "quasibinary" system FeO_4-Al_2O_3 has been calculated by [1984Sch] in stable, as well as metastable versions, in which the formation of $FeAl_2O_4$ is suppressed. The results of the calculation are in agreement with the experiments of [1955Oel, 1956Fis].

Table 1. Investigations of the Al-Fe-O Phase Relations, Structures and Thermodynamics

Reference	Method/Experimental Technique	Temperature/Composition/Phase Range Studied
[1995Bou]	Modeling/thermodynamic calculation	1600-1866°C/Alumina solubility in liquid Fe
[1995Dim]	EMF technique/thermodynamic calculation	1600°C/up to 1 mass% Al, 10^{-5}-0.02 mass% O
[1995Esc]	X-ray diffraction, Fourie-transform infrared and diffuse reflectance ultraviolet-visible spectroscopy	400-900°C/Fe_2O_3-Al_2O_3

(*continued*)

DOI: 10.1007/978-3-540-69761-9_9

Reference	Method/Experimental Technique	Temperature/Composition/Phase Range Studied
[1995Jow]	Thermodynamic calculation	~1600°C/10^{-4}-~2 mass% Al, $1.8\cdot10^{-4}$-0.2 mass% O
[1996Bou]	Neutron diffraction/high resolution diffractometer	Room temperature and 30 K/$FeAlO_3$
[1996Lee]	X-ray diffraction/EDS	Annealed at 1500°C/Al_2O_3-Fe_2O_3
[1997Ito]	Thermodynamic calculation	1500-1900°C/10^{-4}-10^{2} mass% Al, 10^{-5}-$2\cdot10^{2}$ mass% O
[1997Li]	Electrochemical measurements/EMF technique	1600°C/$2.5\cdot10^{-4}$-0.3 mass% Al, $4\cdot10^{-4}$-$7\cdot10^{-2}$ mass% O
[1998Cos]	Mössbauer spectroscopy, XRD	8-475 K/$(Fe_{1-y}Al_y)_2O_3$ with y = 0-0.66
[1998Har]	Neutron powder diffraction	25-1150°C $FeAl_2O_4(\sigma)$
[1998Seo]	Thermodynamic assessment/chemical analysis for determination of equilibrium composition	1600°C/$2\cdot10^{-4}$-0.99 mass% Al, $1.1\cdot10^{-3}$-0.011 mass% O
[1999Ma]	Thermodynamic calculation	1600°C/10^{-4}-0.05 mass% Al
[1999Mei]	Chemical reaction between powders/DTA, SEM, XRD	20-1060°C/Al-Fe_2Al_3
[1999Was1]	Computer simulation / Thermodynamic calculation	1600°C/0.01-0.1 mass% Al, 0.005-0.025 mass% O
[1999Was2]	Alloys prepared by heating mixtures of components/Selective chemical analysis, XRD	1600°C/Fe-$FeAl_2O_4$
[1999Yok]	Phase diagram calculation	1300°C 3-D potential diagram
[2000Ban]	EPMA, EDS	700°C, Fe-5 mass% Al oxidizing environment
[2000Bjo]	Thermodynamic calculation	1400°C, FeO-Al_2O_3 system, $x(Al_2O_3)$ = 0-0.1
[2001Jha]	Phase diagram calculation MTDATA, NPL database	1000°C, Fe-Al 0-100 mass% $p(O_2)$=10^{-20}-1
[2001Lad]	XRD, Mössbauer spectroscopy	1150°C synthesis, 25°C measurements
[2001Mas]	XRD, SEM-EDX	700-1000° Fe-40 at.% Al in air
[2002Bot]	Mechanical milling/XRD, magnetic properties, TA, SEM	room temperature/ Al-Al_2O_3-$FeAl_2O_4$-Fe_3O_4-Fe
[2002Gos]	XRD, thermal analysis, FTIR spectroscopy, optical reflection analysis, TEM, Mössbauer spectra	80, 298 K Fe_2O_3-Al_2O_3 system up to 10% Al_2O_3

(*continued*)

DOI: 10.1007/978-3-540-69761-9_9

Reference	Method/Experimental Technique	Temperature/Composition/Phase Range Studied
[2002Dav]	Phase diagram calculation MTDATA, NPL database	900-2100°C Fe_2O_3-Al_2O_3 system in air
[2002Maj]	HT oxide-melt drop calorimetry, DS calorimetry, Rietveld refinement of XRD, Mössbauer spectroscopy, calculation	200-1550 K, $FeAlO_3$, C_p; 25, 602°C Fe_2O_3-Al_2O_3 system, $\Delta H°_f$,oxides; 25°C, $FeAlO_3$, $S°$
[2002Was]	Modelling of process/Thermodynamic calculation	1600°C/Fe-Al_2O_3
[2003Bot]	Mechanical milling/XRD, Mössbauer spectroscopy, DTA	room temperature/x(Al) + y(Fe_3O_4) at x:y = 2.67:1
[2003Kap]	Contact angle measurement by X-ray sessile-drop method	1550-1600°C Fe-Al_2O_3 system p(O_2 in Ar) ≤10-14 Pa 1550°C $p(O_2)$=$9.9\cdot10^{-4}$, $3\cdot10^{-3}$ Pa(CO/CO_2+Ar)
[2003Kle]	Adiabatic calorimetry	3-400 K; $FeAl_2O_4$(σ)
[2004Cot]	Mechanical milling / XRD, Mössbauer spectroscopy	room temperature/$(\alpha Fe_2O_3)_x(\alpha Al_2O_3)_{1-x}$ with $0.10 \le x \le 0.50$
[2004Fre]	Slag-metal equilibrium technique/ Chemical analysis, thermodynamic modelling	1400-1600°C/FeO-Al_2O_3
[2004Vil]	XRD, density measurement by picknometry	25°C, $Fe_{2-x}Al_xO_3$, $0.9 \le x \le 1.08$
[2005Fee]	Synthesis of materials by sintering powders / EMPA	800-1300°C/ Al_2O_3-Fe_2O_3
[2005Liu]	Preparation of Fe_2O_3-Al_2O_3 nanocomposites by sol-gel means/XRD, Mössbauer spectroscopy	500-1100°C/ Fe_2O_3-Al_2O_3

Table 2. Crystallographic Data of Solid Phases

Phase/Temperature Range [°C]	Pearson Symbol/ Space Group/ Prototype	Lattice Parameters [pm]	Comments/References
(αAl) < 660.452	*cF*4 $Fm\bar{3}m$ Cu	a = 404.96	at 25°C [Mas2]
(βAl)	*hP*2 $P6_3/mmc$ Mg	a = 269.3 c = 439.8	25°C, 20.5 GPa [Mas2]

(*continued*)

DOI: 10.1007/978-3-540-69761-9_9

Phase/Temperature Range [°C]	Pearson Symbol/ Space Group/ Prototype	Lattice Parameters [pm]	Comments/References
α, (αδFe) (αFe)(r) ≤ 912	*cI*2 $Im\bar{3}m$ W	a = 286.65 a = 293.15	pure Fe at 25°C [Mas2] pure Fe at 1480°C [Mas2]
(δFe)(h_2) 1538 - 1394			
(γFe)(h_1) 1394 - 912	*cF*4 $Fm\bar{3}m$ Cu	a = 364.67	at 915°C [V-C2, Mas2]
(εFe)	*hP*2 $P6_3/mmc$ Mg	a = 246.8 c = 396.0	at 25°C, 13 GPa [Mas2]
$Fe_{1-x}O$ < 912	*cF*8 $Fm\bar{3}m$ NaCl	a = 431.0 a = 429.3	x = 0.05, x = 0.12 [V-C2] wustite, 51.15 to 54.6 at.% O
σ, $Fe_{3-x}Al_xO_4$(r) Fe_3O_4 < 1597	*cF*56 $Fd\bar{3}m$ $MgAl_2O_4$	 a = 839.6 a = 854.5	0 ≤ x ≤ 2 above 860°C spinel at 25°C, x = 0, at 1000°C, x =0 magnetite, 57.14 to 58.3 at.% O
$FeAl_2O_4$ < 1800		a = 815	at x = 2, hercynite, [1962Tur]
Fe_3O_4 (l)	*oP*56 *Pbcm* Fe_3O_4(LT)	a = 1186.8 b = 1185.1 c = 1675.2	at 10 K [V-C2]
Fe_3O_4(HP)	*m**14		Stable at pressures >25GPa [Mas2]
α$Fe_{2-x}Al_{2x}O_3$ (r)	*hR*30 $R\bar{3}c$ Al_2O_3	 a = 503.42 c = 1374.83	0 ≤ x ≤ 0.3 at T~1300°C [V-C], hematite at x = 0, peritectoid formation at 1457°C, 1.013 bar p_{O2}
εFe_2O_3 (l)	*m**100	a = 1297 b = 1021 c = 844 β = 95.32°	[V-C], [1989Rag2] low temperature or metastable
βFe_2O_3 (l)	*cI*80 $Ia\bar{3}$ Mn_2O_3	a = 939.3	[V-C2], low temperature or metastable

(*continued*)

DOI: 10.1007/978-3-540-69761-9_9

Phase/Temperature Range [°C]	Pearson Symbol/ Space Group/ Prototype	Lattice Parameters [pm]	Comments/References
γFe_2O_3	*cF*56 $Fd\bar{3}m$ $MgAl_2O_4$	a = 834	low temperature or metastable [1989Rag2]
$\alpha Al_{2-x}Fe_{2x}O_3$ < 2054	*hR*30 $R\bar{3}c$ Al_2O_3	a = 475.4 c = 1299	$0 \le x \le 0.3$ at T~1300°C x = 0 [V-C], corundum, congruent melting 2054°C [Mas2]
$\gamma Al_{2-x}Fe_{2x}O_3$	*cF*56 $Fd\bar{3}m$ $MgAl_2O_4$	a = 794.7	x = 0 [V-C2] metastable phase [Mas2]
Fe_3Al < 547	*cF*16 $Fm\bar{3}m$ BiF_3	a = 578.86 to 579.3	solid solubility ranges from ~25 to ~37 at.% Al [2006MSIT]
FeAl < 1310	*cP*2 $Pm\bar{3}m$ CsCl	a = 289.76 to 290.78	solid solubility ranges from ~24 to ~55 at.% Al [2006MSIT], at room temperature
ε, Fe_2Al_3 1232 - 1102	*cI*16	a = 598.0	[2006MSIT], solid solubility ranges from 58 to 65 at.% Al at 61 at.% Al [V-C2]
$FeAl_2$ < 1156	*aP*18 *P*1 $FeAl_2$	a = 487.8 b = 646.1 c = 880.0 α = 91.75° β = 73.27° γ= 96.89°	solid solubility ranges from ~66 to ~67 at.% Al [2006MSIT] at 66.9 at.% Al [V-C2]
Fe_2Al_5 < 1169	*oC*24 *Cmcm* Co_2Al_5	a = 76.35.59 b = 641.54 c = 421.84	[2006MSIT], at 71.5 at.% Al solid solubility ranges from ~70 to ~73 at.% Al
Fe_4Al_{13} < 1160	*mC*102 *C*2/*m* Fe_4Al_{13}	a = 1552.7 to 1548.7 b = 803.5 to 808.4 c = 1244.9 to 1248.8 β = 107.7 to 107.99° a = 1549.2 b = 807.8 c = 1247.1 β = 107.69°	[2006MSIT], 74.16 to 76.7 at.% Al solid solubility ranges from 74.5 to 75.5 at.% Al [2006MSIT], at 76.0 at.% Al. Also denoted $FeAl_3$ or Fe_2Al_7

(*continued*)

DOI: 10.1007/978-3-540-69761-9_9

Phase/Temperature Range [°C]	Pearson Symbol/ Space Group/ Prototype	Lattice Parameters [pm]	Comments/References
Fe_4Al_{13}(h)	*oB~50* *Bmmm*	a = 775.10 ± 0.09 b = 403.36 ± 0.05 c = 2377.1 ± 0.3	high temperature modification by splat cooling, metastable? [1995Ell]
Fe_2Al_9	*mP*22 $P2_1/C$ Co_2Al_9	a = 869 b = 635 c = 632 β = 93.4°C	metastable, at 81.8 at.% Al [1993Kat]
$FeAl_6$	*oC*28 $Cmc2_1$	a = 744 b = 649 c = 879	metastable [1998Ali]
$FeAl_{4+x}$	tetragonal	a = 884 c = 2160	$0 < x < 0.4$ metastable [1998Ali]
* τ, $Fe_{2-x}Al_xO_3$ 1410 - 1318	*oP*40 $Pna2_1$ $FeGaO_3$	a = 856.61 b = 924.91 c = 498.92	$0.9 \le x \le 1.08$ [1958Mua, 1980Mey, 1996Bou, 2004Vil]

Table 3. Invariant Equilibria

Reaction	T [°C]	Type	Phase	Composition (at.%)		
				Al	Fe	O
L′ ⇌ (αδFe) + Al_2O_3	1537.6	e_5	L′	$1.03 \cdot 10^{-2}$	99.98	$1.12 \cdot 10^{-3}$
L′ + Al_2O_3 ⇌ (αδFe) + σ	1535.5	U_1	L′	$8.48 \cdot 10^{-6}$	99.87	0.1255
L′ + σ ⇌ L″ + (αδFe)	1528.5	U_2	L′	$8.05 \cdot 10^{-7}$	99.52	0.48

Table 4. Thermodynamic Data of Reaction or Transformation

Reaction or Transformation	Temperature [°C]	Quantity, per mol of atoms [kJ, mol, K]	Comments
1/7 {Fe(γ) + 1/2 O_2(gas) + Al_2O_3(α) → $FeAl_2O_4$(σ)}	750 - 1536	$\Delta G = -292.800 + 0.0687T$	emf [1973Cha]
1/7{$FeAl_2O_4$(σ) → Fe_L + $\{O\}_{Fe\_L}$ + Al_2O_3(α)}	1550 - 1600	$\Delta G = 28.01 - 0.01184T$	[1978Apt] emf
1/2Fe_2O_3+1/2Al_2O_3(α) → $FeAlO_3$(τ)	25	$\Delta H = 5.58$	Drop solution calorimetry [2002Maj]
1/5{Al_2O_3(α) → 2$\{Al\}_{Fe_L}$+3$\{O\}_{Fe_L}$}	1550 - 1750	$\Delta G = 245.051 - 0.078761T$	[2000Jan] analysis of phase equilibria and emf data

DOI: 10.1007/978-3-540-69761-9_9

Table 5. Thermodynamic Properties of Single Phases

Phase	Temperature Range [°C]	Property, per mole of atoms [J, mol, K]	Comment
$FeAl_2O_4$ (σ)	25	$S°$ = 16.2714	Adiabatic calorimetry [2003Kle]
$FeAl_2O_4$ (σ)	25 26.85 46.85 66.85 86.85 106.85 130.67	C_p = 17.7714 C_p = 17.8286 C_p = 18.5286 C_p = 19.1571 C_p = 19.7 C_p = 20.2 C_p = 20.7143	Adiabatic calorimetry [2003Kle]
$FeAlO_3$ (τ)	25 - 1277	$C_p = 35.16–0.0004944 \cdot T–3.916 \cdot 10^5/T^2 –183.46/T^{0.5}+1.5092 \cdot 10^{-6} \cdot T^2$	Differential scanning calorimetry [2002Maj]

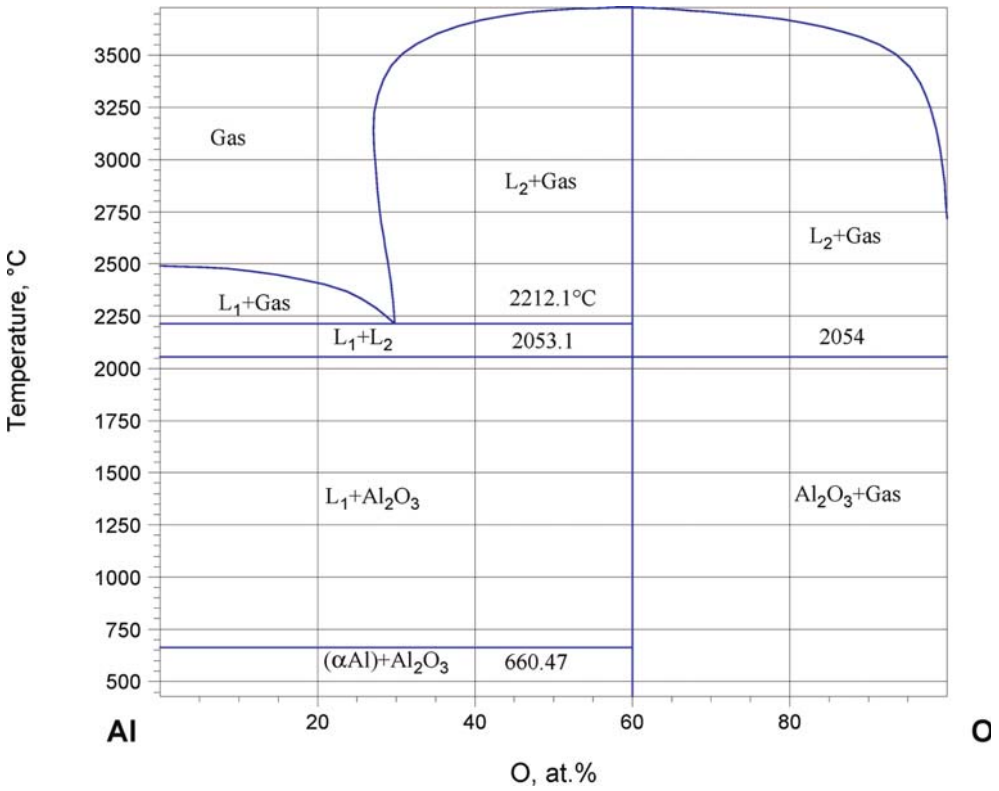

Fig. 1a. Al-Fe-O. Temperature - composition phase diagram of the Al-O system

DOI: 10.1007/978-3-540-69761-9_9

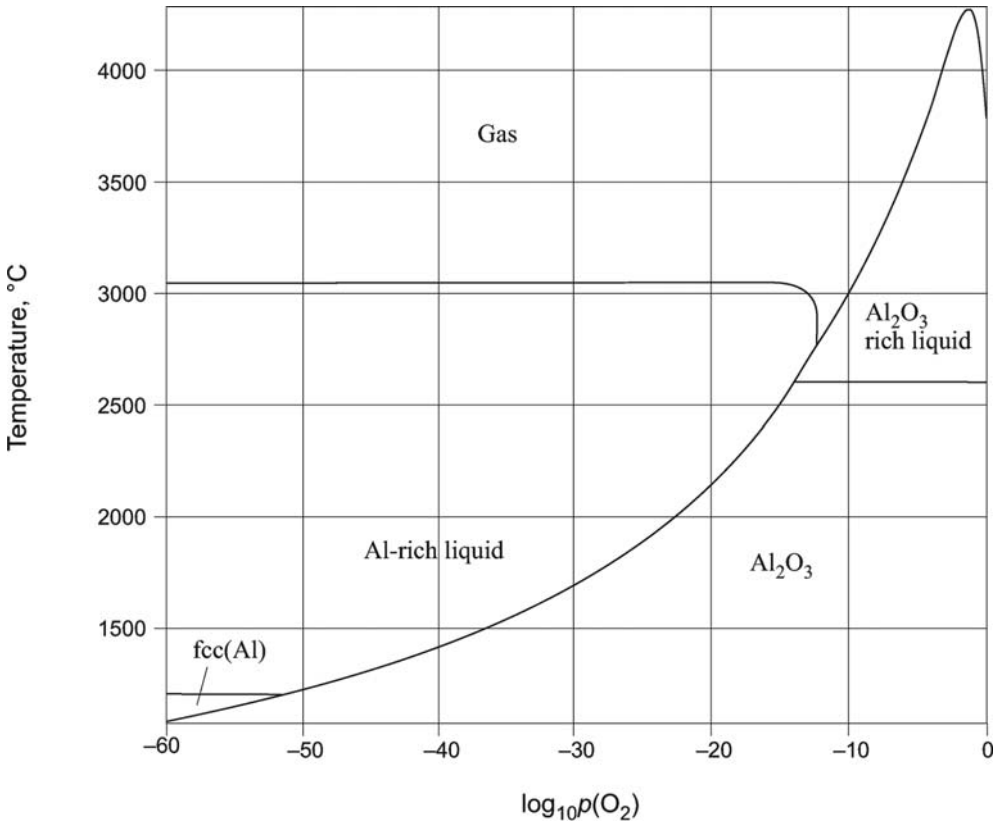

Fig. 1b. Al-Fe-O. Temperature - $p(O_2)$ phase diagram of the Al-O system

DOI: 10.1007/978-3-540-69761-9_9

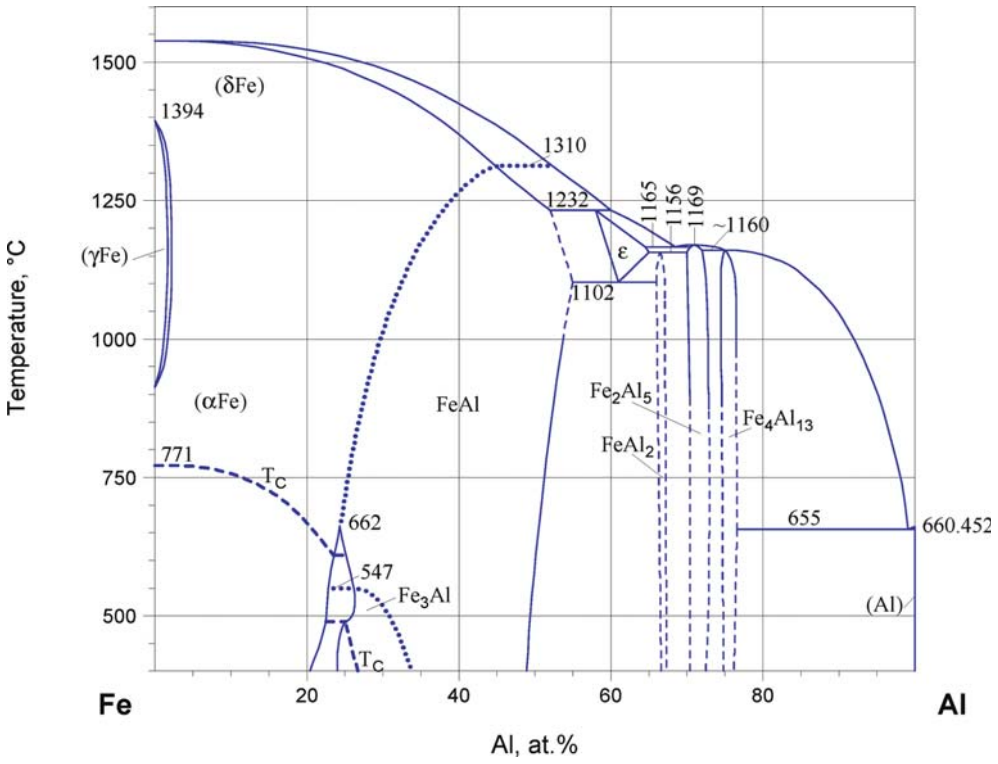

Fig. 2. Al-Fe-O. Phase diagram of the Al-Fe system

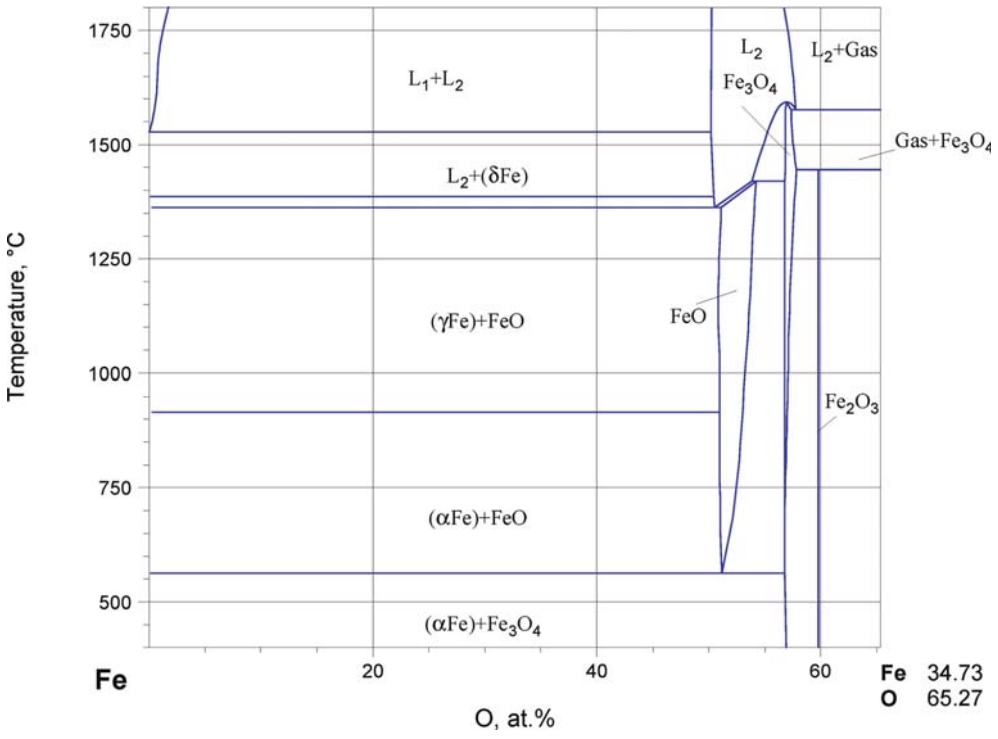

Fig. 3a. Al-Fe-O. Temperature - composition phase diagram of the Fe-O system

DOI: 10.1007/978-3-540-69761-9_9

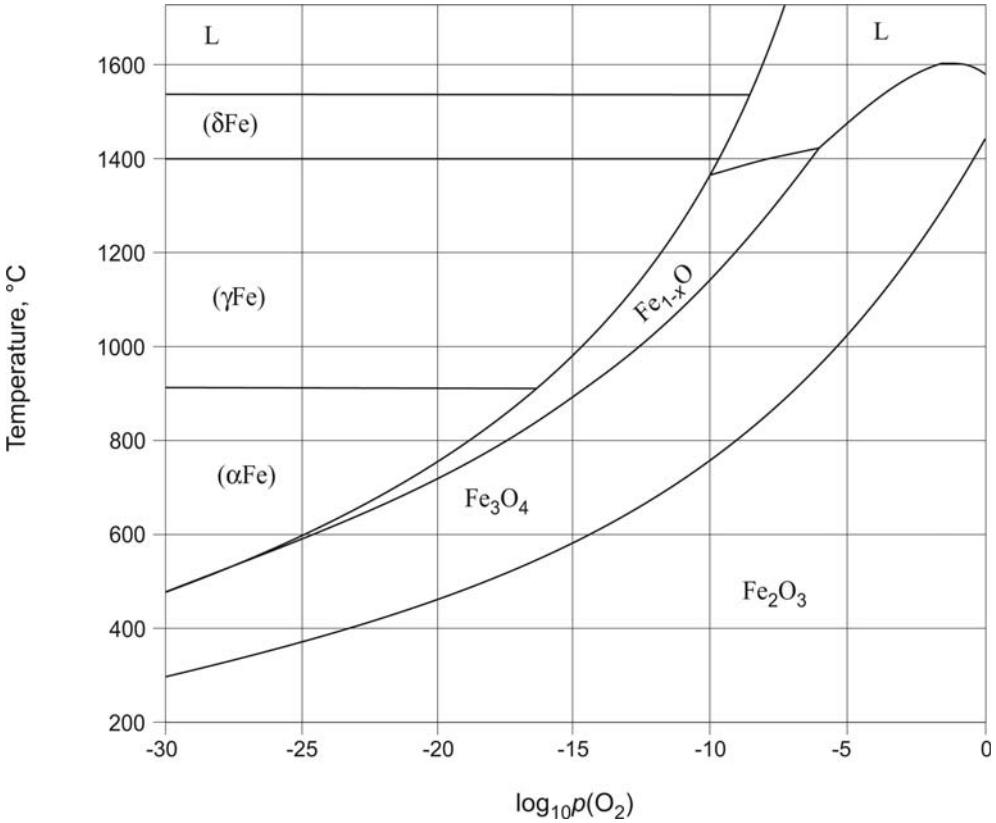

Fig. 3b. Al-Fe-O. Temperature - $p(O_2)$ phase diagram of the Fe-O system

DOI: 10.1007/978-3-540-69761-9_9

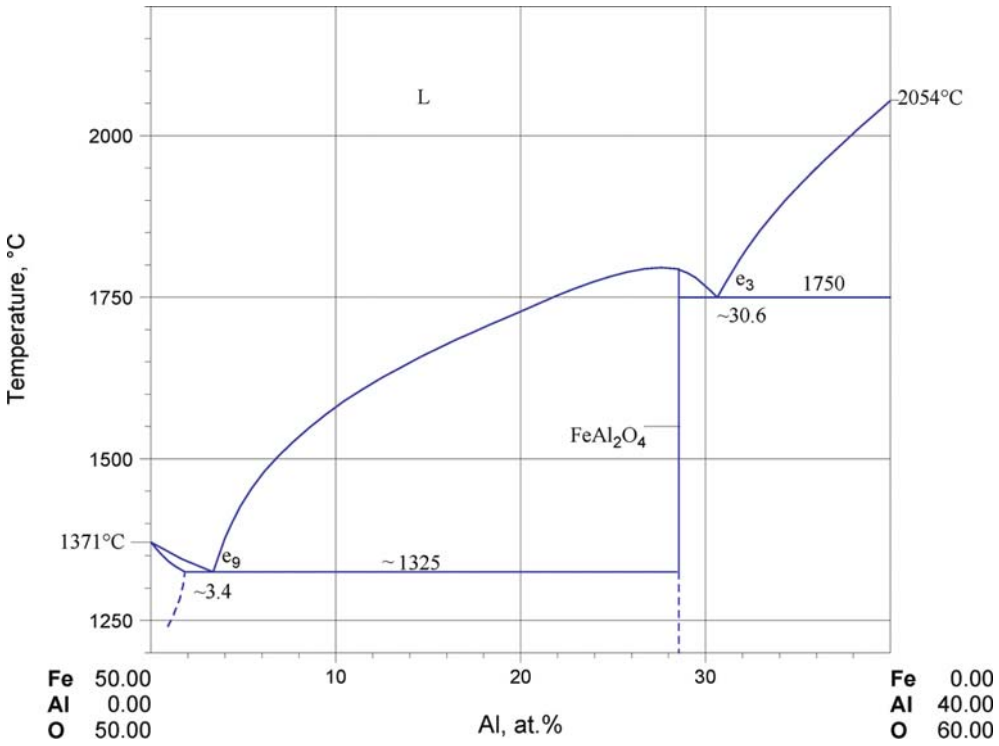

Fig. 4. Al-Fe-O. Quasibinary system FeO-Al_2O_3

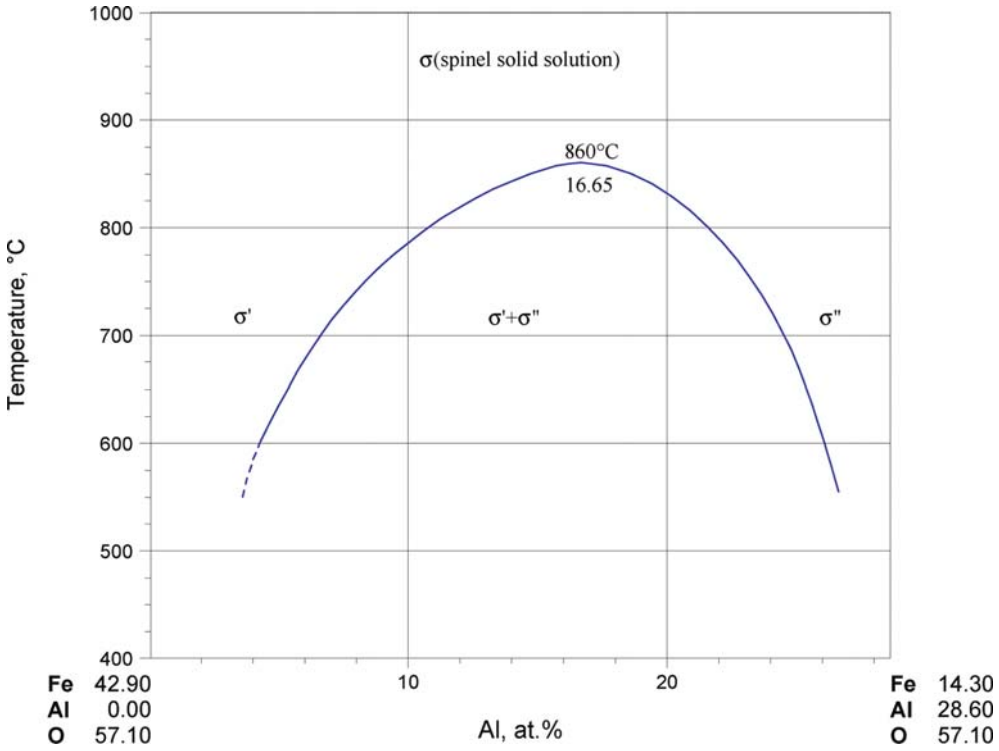

Fig. 5. Al-Fe-O. Subsolidus quasibinary section Fe_3O_4-$FeAl_2O_4$ under pressure 2 kbar

DOI: 10.1007/978-3-540-69761-9_9

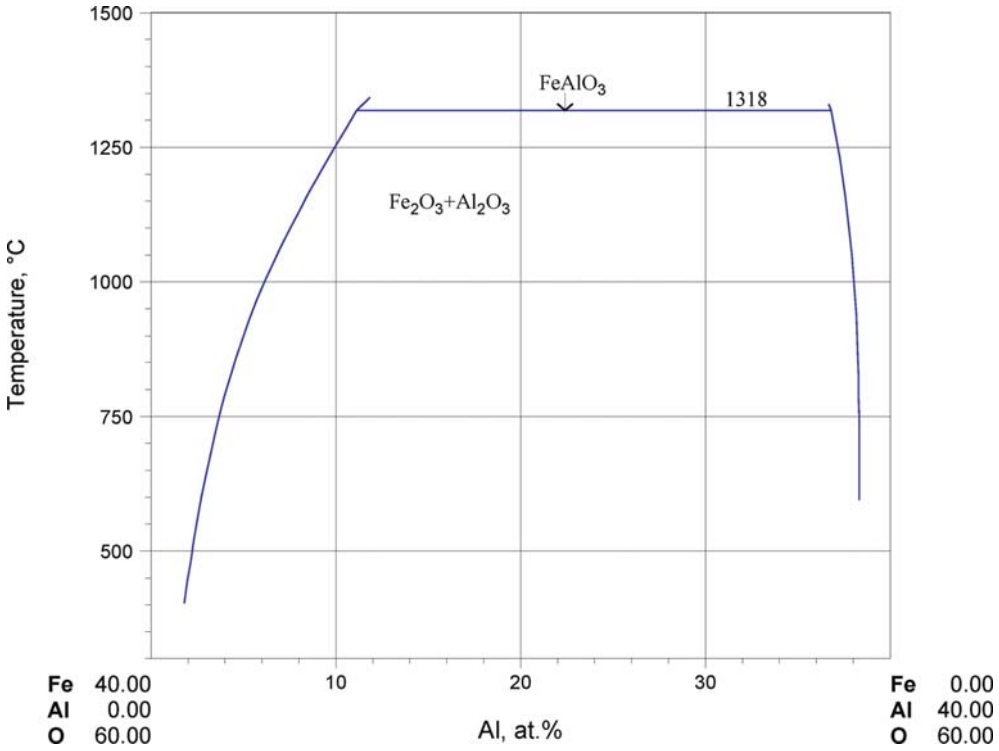

Fig. 6. Al-Fe-O. Subsolidus quasibinary part of the section Fe_2O_3-Al_2O_3 below 1350°C (1.013 bar)

DOI: 10.1007/978-3-540-69761-9_9

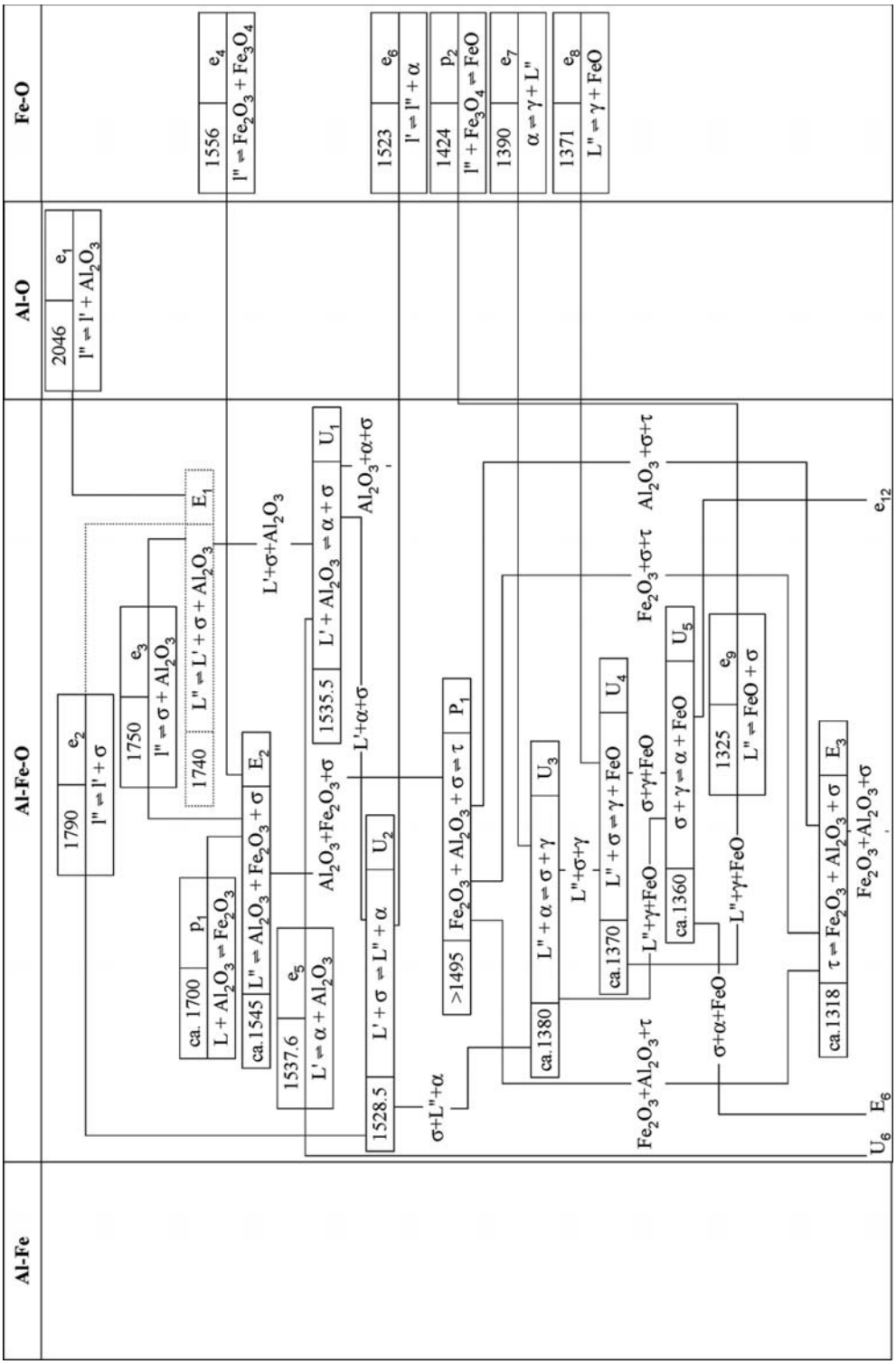

Fig. 7a. Al-Fe-O. Reaction scheme, part 1

DOI: 10.1007/978-3-540-69761-9_9

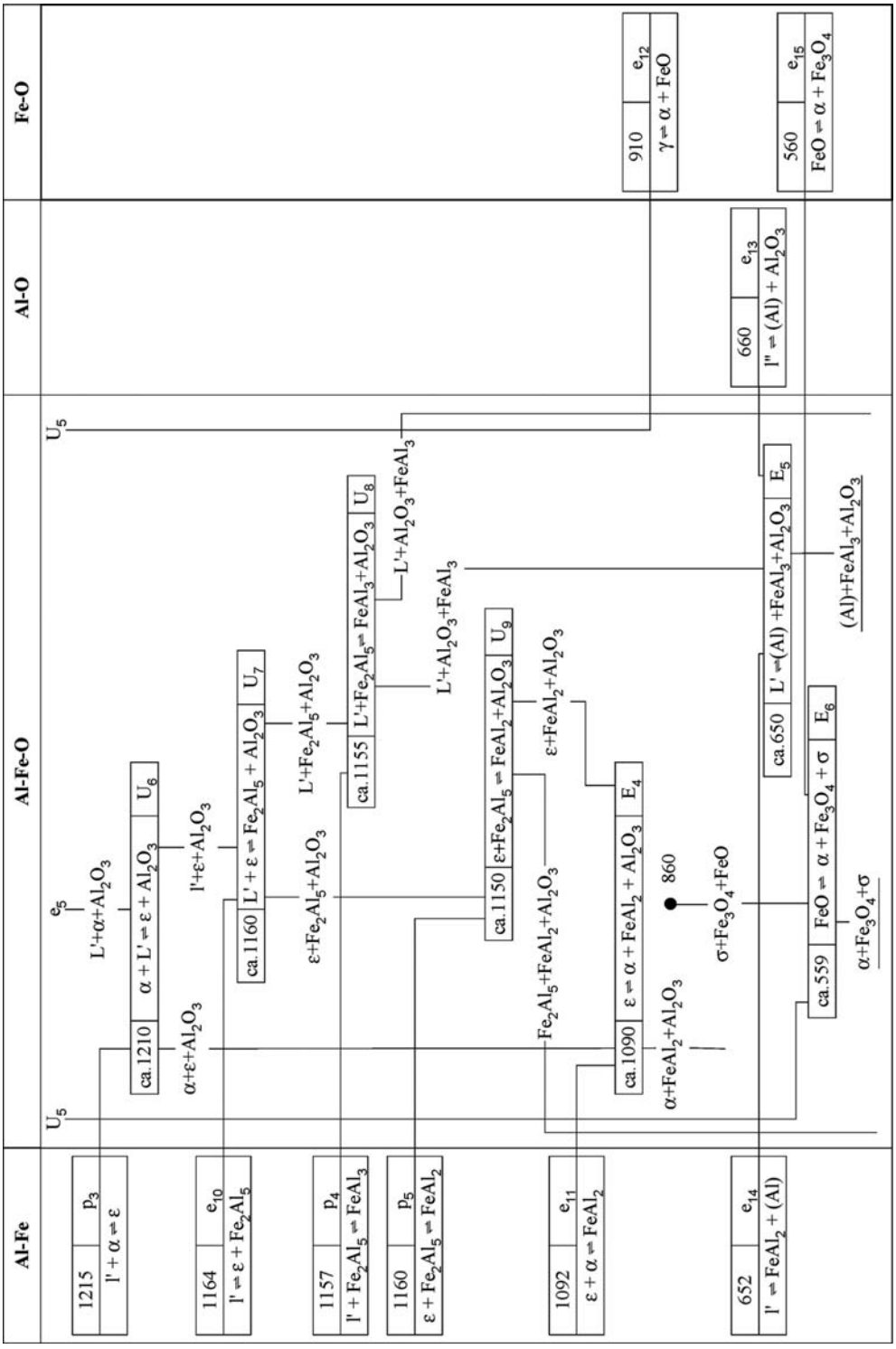

Fig. 7b. Al-Fe-O. Reaction scheme, part 2

DOI: 10.1007/978-3-540-69761-9_9

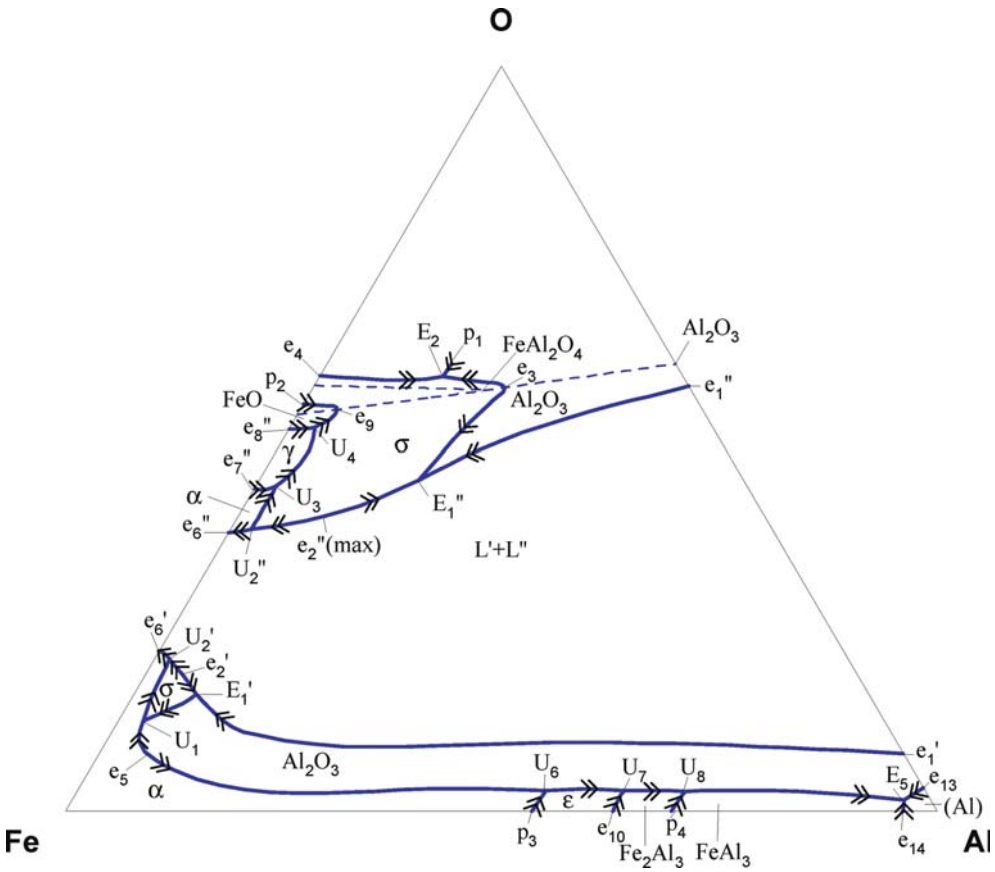

Fig. 8. Al-Fe-O. Schematic liquidus surface of Fe-Fe_2O_3-Al_2O_3-Al region under pressure, no gas equilibria

DOI: 10.1007/978-3-540-69761-9_9

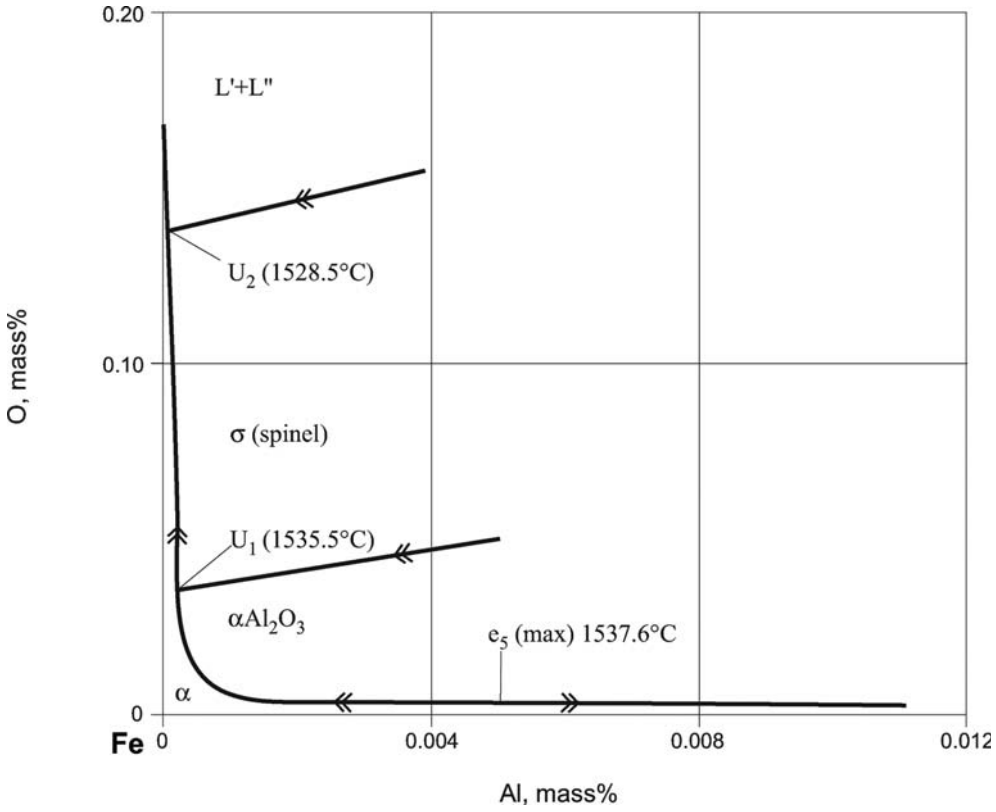

Fig. 9. Al-Fe-O. Liquidus surface of the Fe corner

DOI: 10.1007/978-3-540-69761-9_9

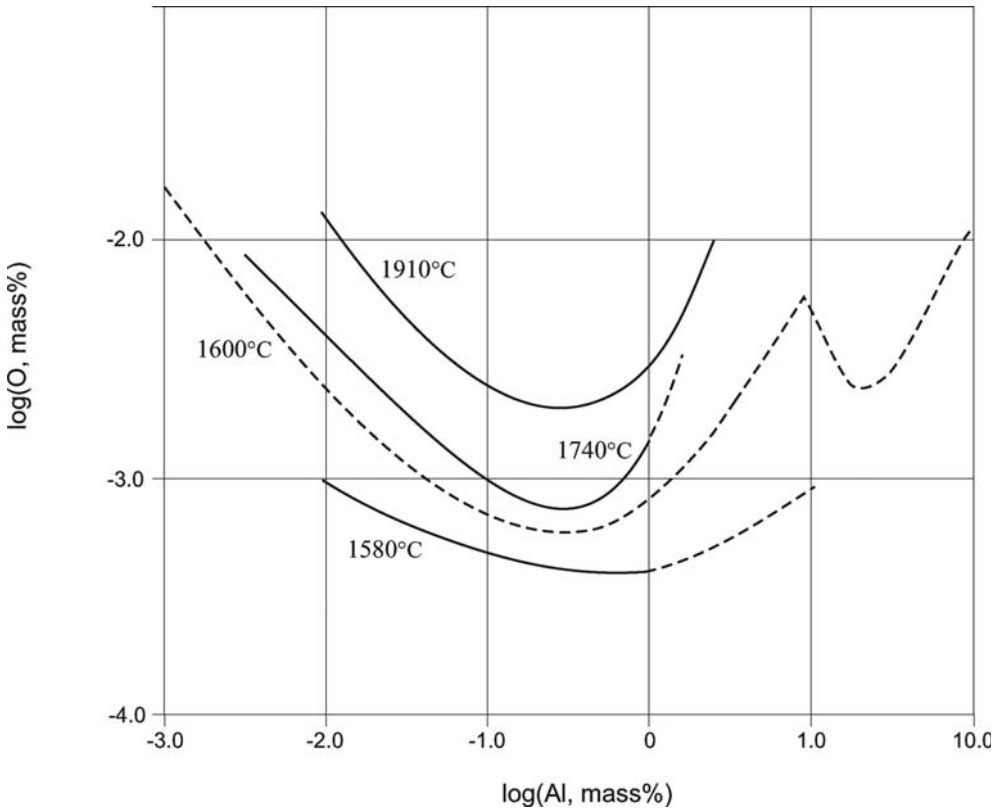

Fig. 10. Al-Fe-O. Isotherms of liquidus surface of $A1_2O_3$ in the Fe corner (deoxidation equilibrium, log scale); 1740, 1910°C [1963Ent], 1600°C [1981She], 1580°C [1967Swi]

DOI: 10.1007/978-3-540-69761-9_9

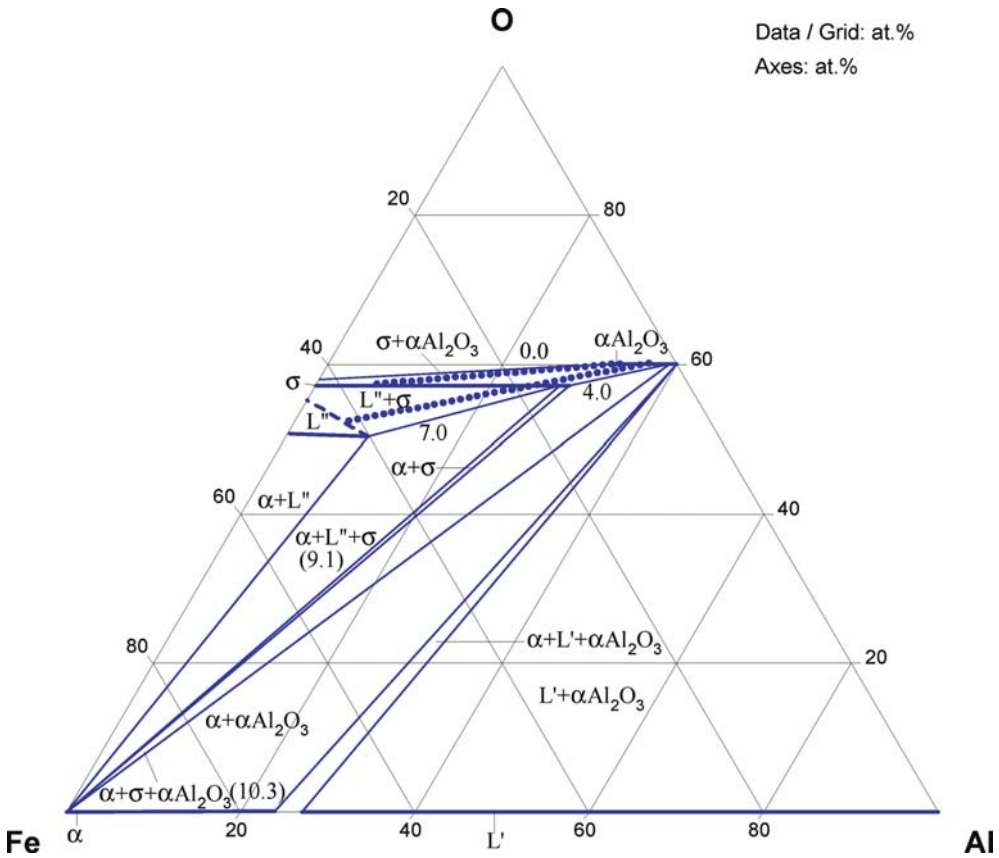

Fig. 11. Al-Fe-O. Isothermal section at 1500°C. Numbers in tie-triangles and on tie-lines are values of $-\log p(O_2)$(bar)

DOI: 10.1007/978-3-540-69761-9_9

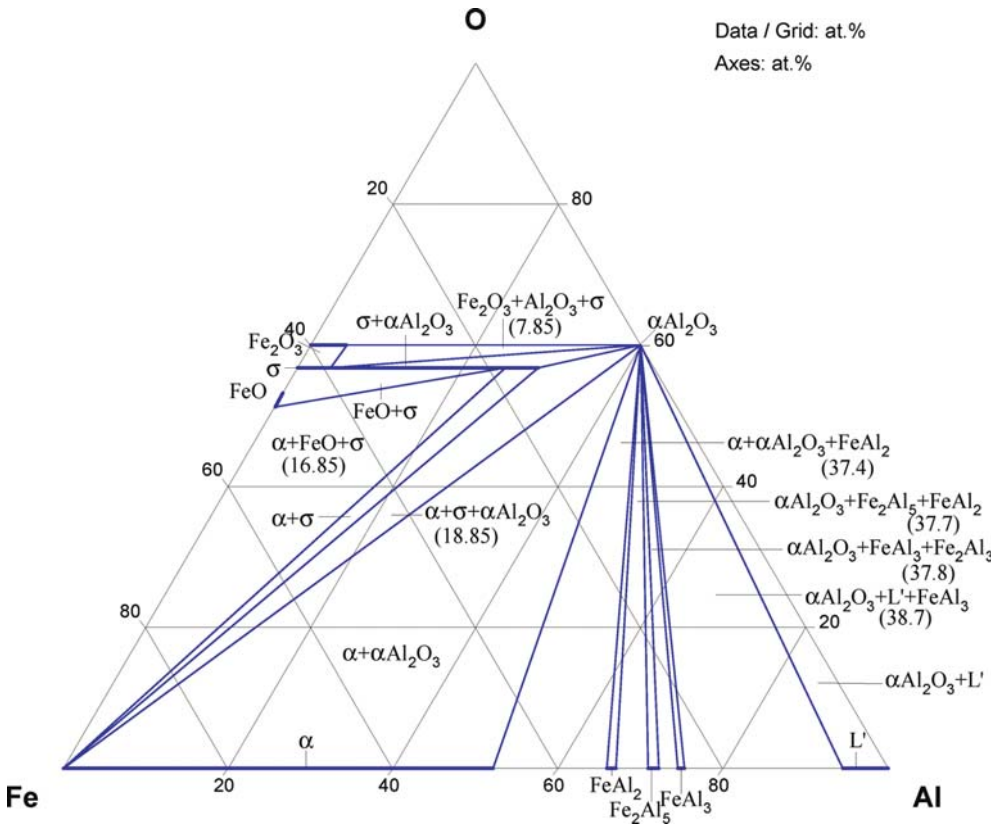

Fig. 12. Al-Fe-O. Isothermal section at 900°C. Numbers in tie-triangles and on tie-lines are values of $-\log p(O_2)$(bar)

DOI: 10.1007/978-3-540-69761-9_9

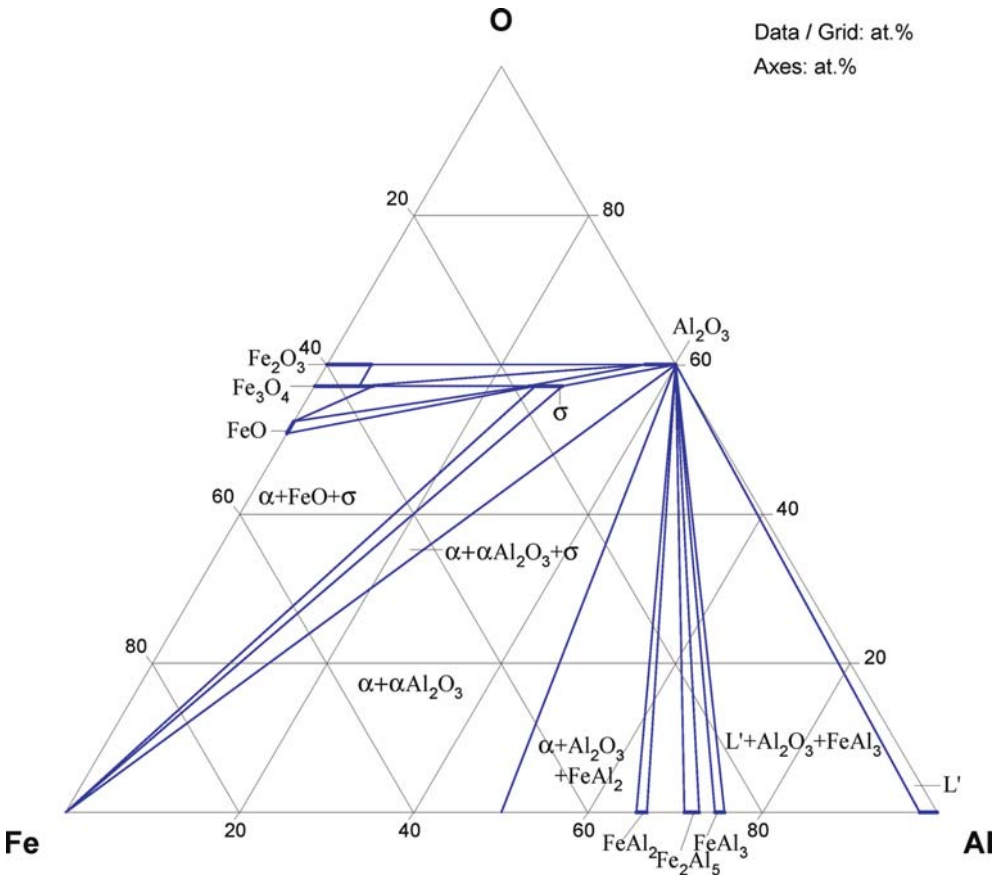

Fig. 13a. Al-Fe-O. Isothermal section at 700°C

DOI: 10.1007/978-3-540-69761-9_9

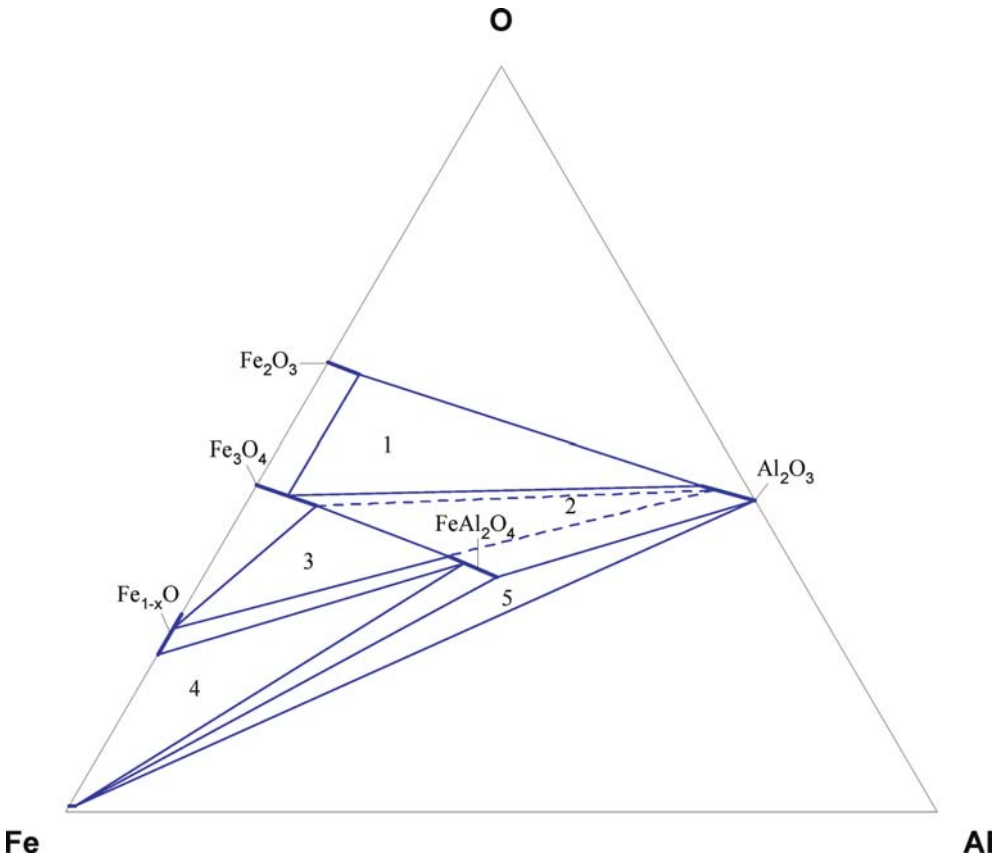

Fig. 13b. Al-Fe-O. Schematic sketch at 700°C, the five three-phase solid state fields of the Fe-Al_2O_3-Fe_2O_3- regions are numbered from 1 to 5

DOI: 10.1007/978-3-540-69761-9_9

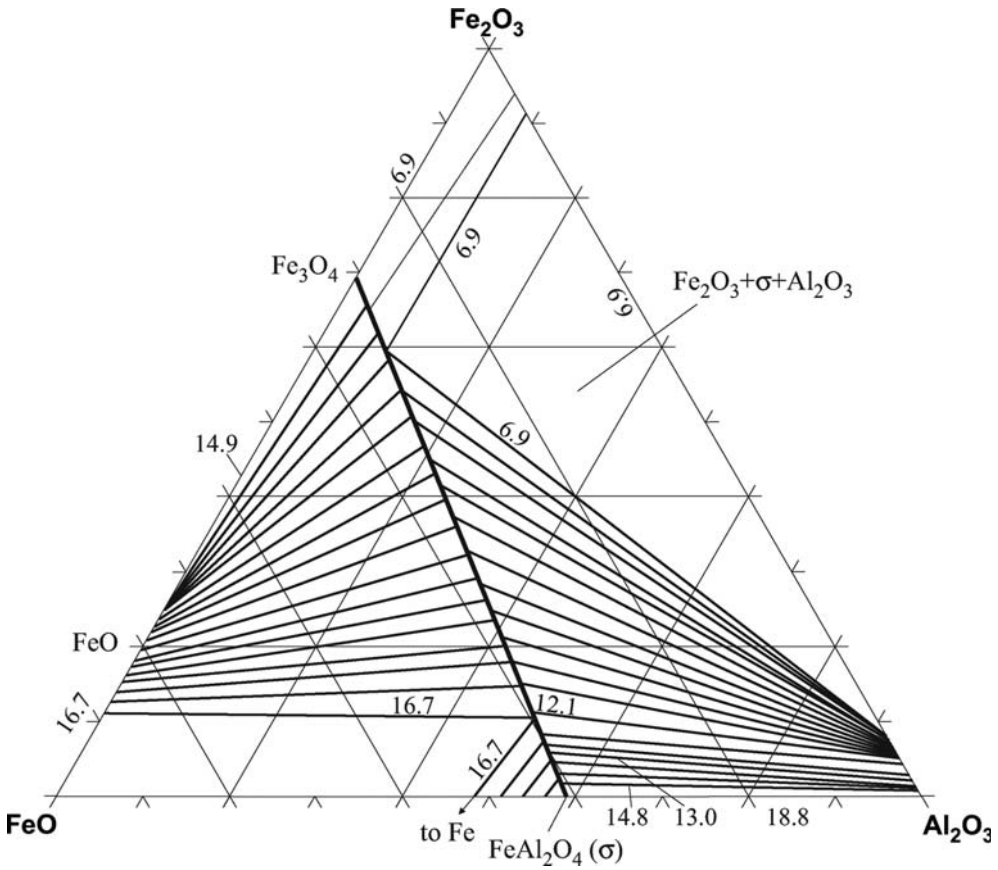

Fig. 14. Al-Fe-O. Isothermal section of the partial system FeO-Fe_2O_3-Al_2O_3 at 900°C, oxygen gas in equilibrium with condensed phases at given numbers is –log $p(O_2)$

DOI: 10.1007/978-3-540-69761-9_9

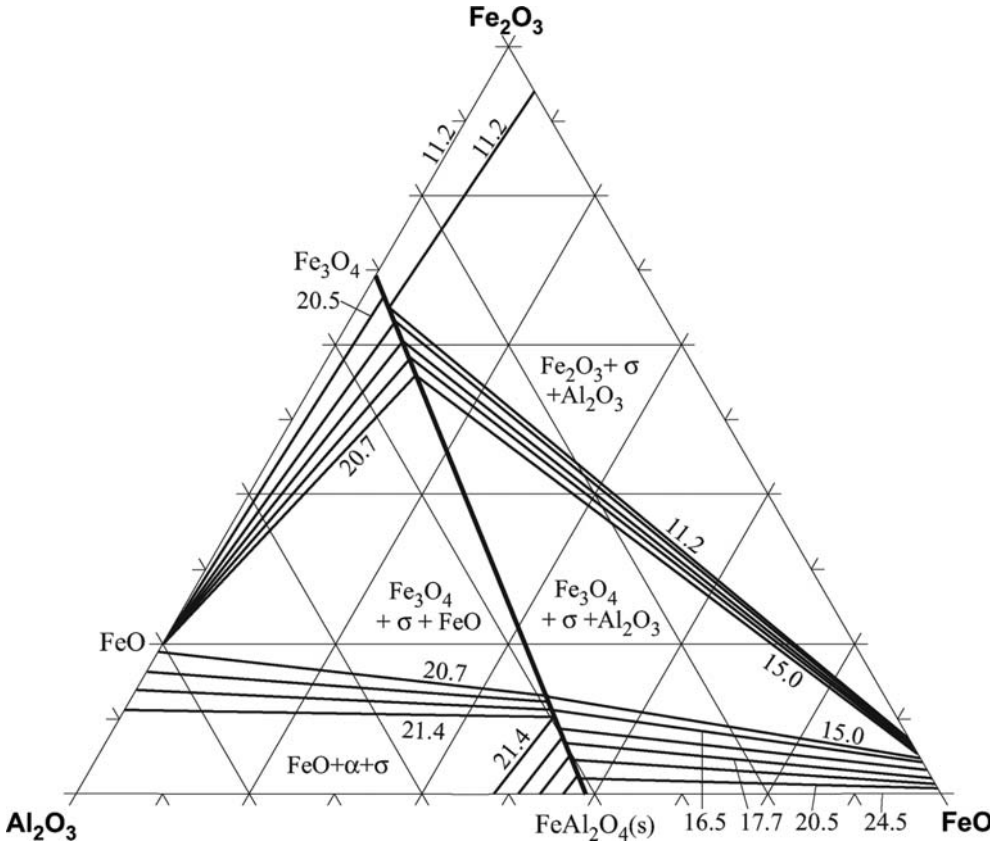

Fig. 15. Al-Fe-O. Isothermal section of the partial system FeO-Fe_2O_3-Al_2O_3 at 700°C, values on the tie lines show –log $p(O_2)$

DOI: 10.1007/978-3-540-69761-9_9

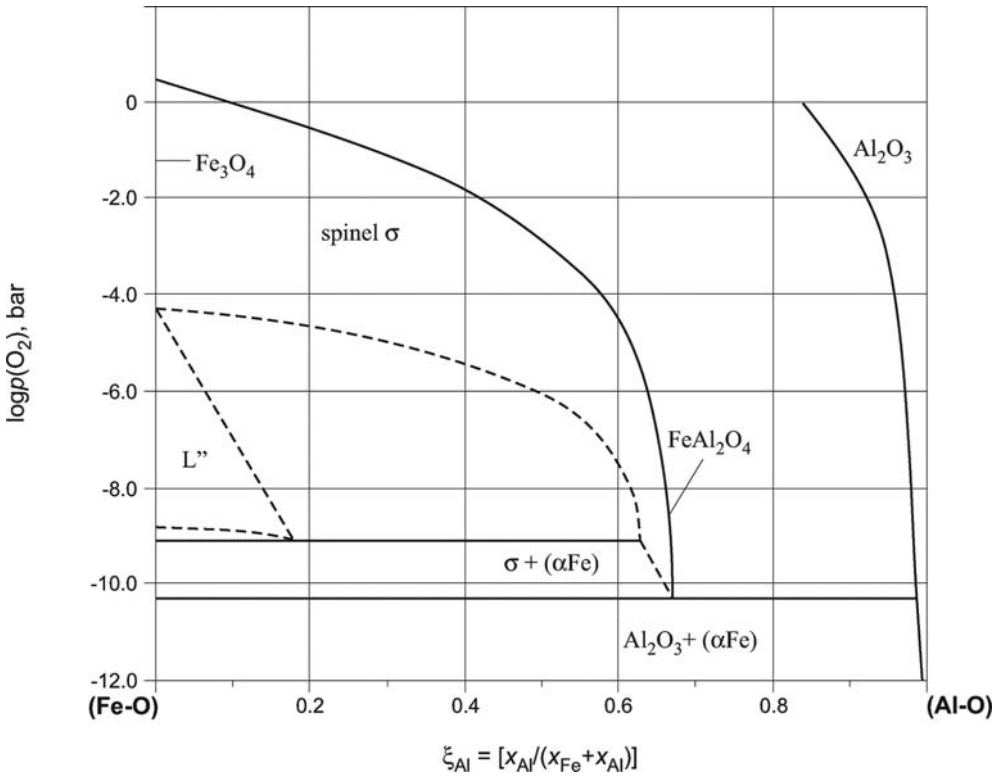

Fig. 16. Al-Fe-O. Equilibrium oxygen pressure diagram at 1500°C

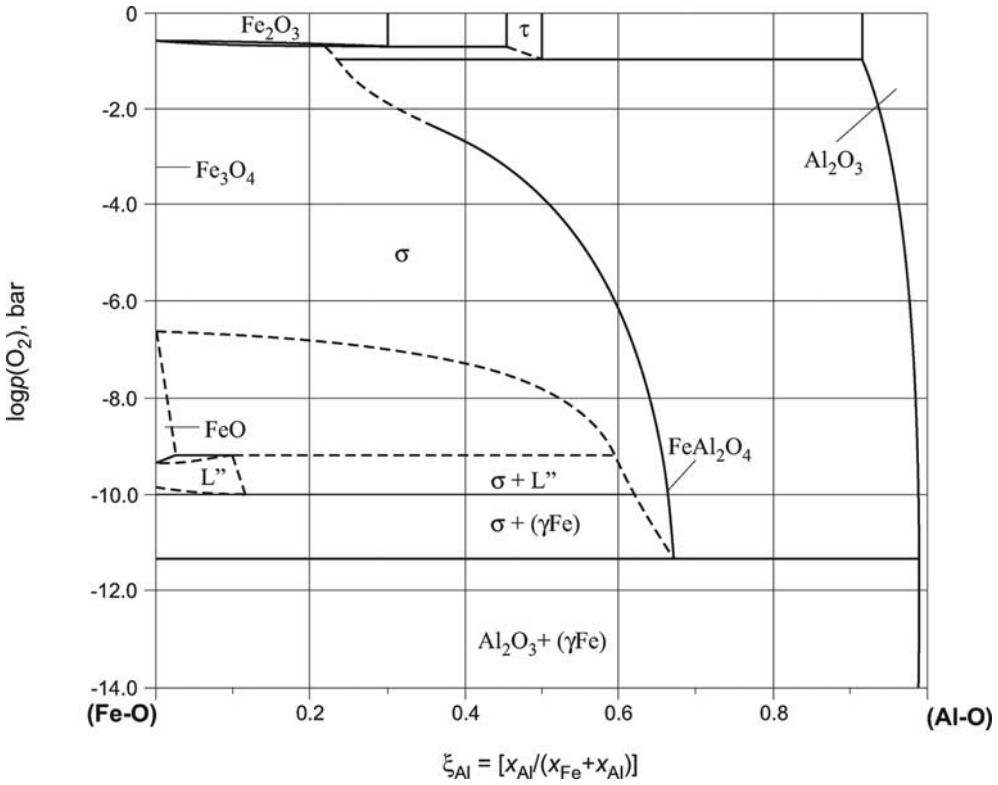

Fig. 17. Al-Fe-O. Equilibrium oxygen pressure diagram at 1380°C

DOI: 10.1007/978-3-540-69761-9_9

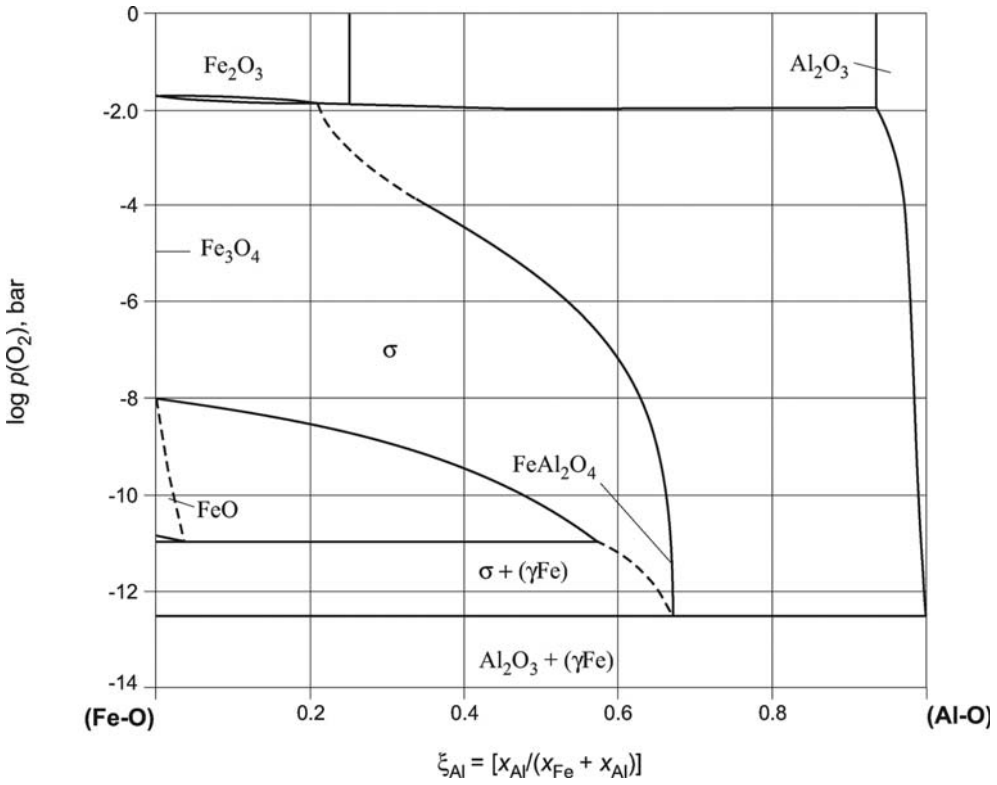

Fig. 18. Al-Fe-O. Equilibrium oxygen pressure diagram at 1280°C

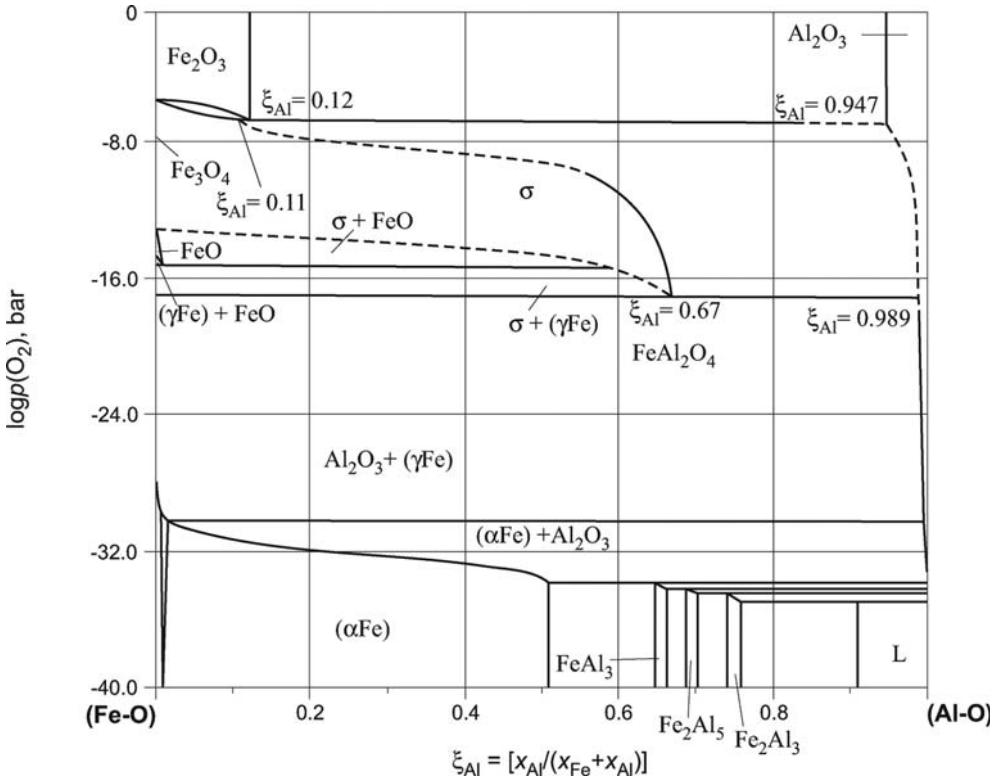

Fig. 19. Al-Fe-O. Equilibrium oxygen pressure diagram at 1000°C

DOI: 10.1007/978-3-540-69761-9_9

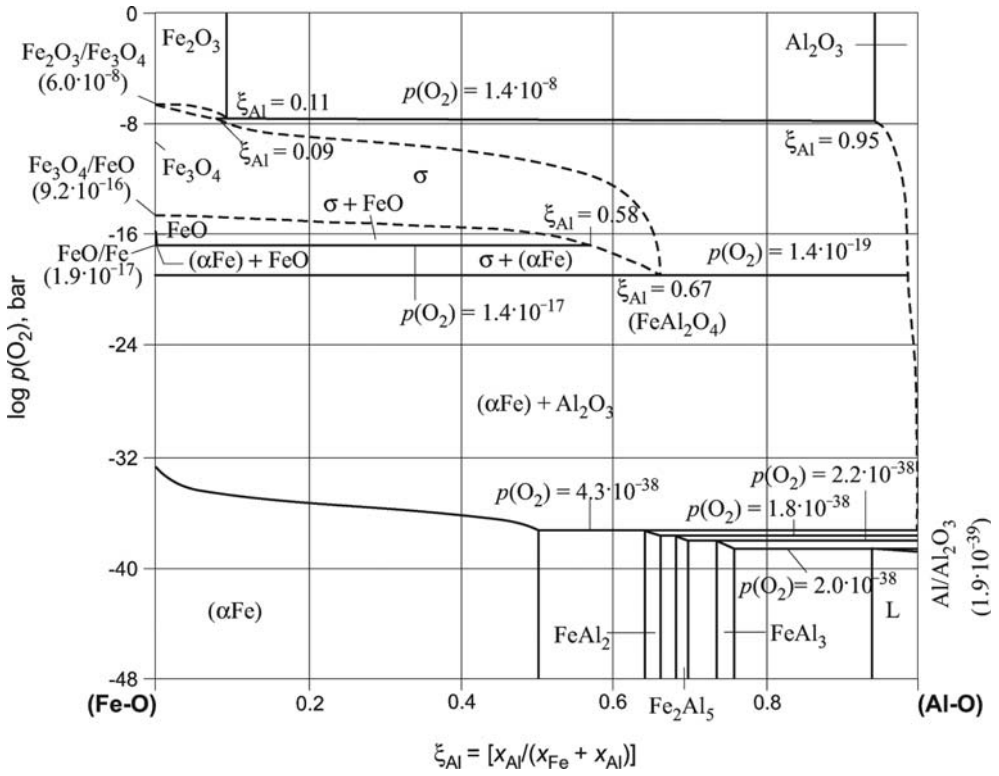

Fig. 20. Al-Fe-O. Equilibrium oxygen pressure diagram at 900°C

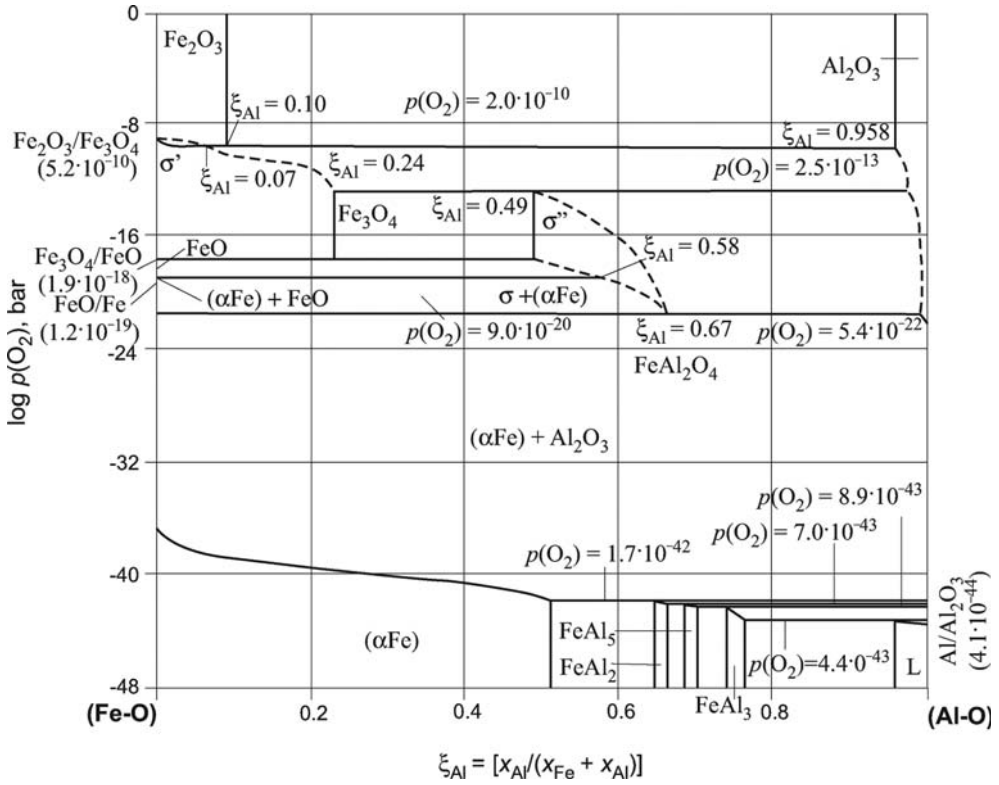

Fig. 21. Al-Fe-O. Equilibrium oxygen pressure diagram at 800°C

DOI: 10.1007/978-3-540-69761-9_9

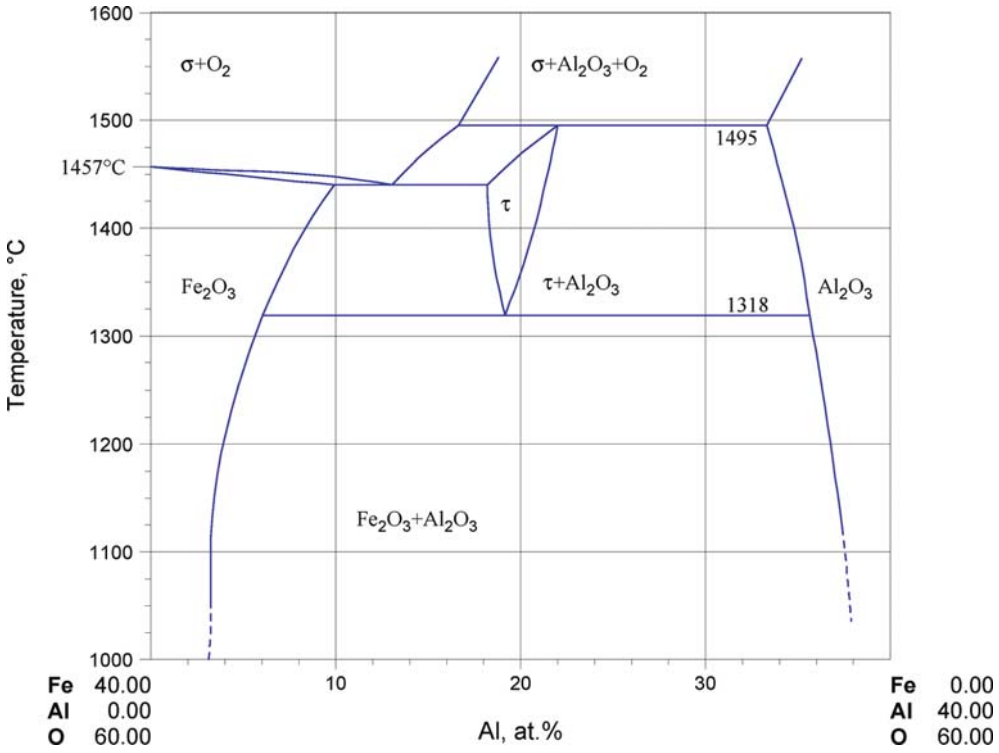

Fig. 22. Al-Fe-O. Vertical section Fe_2O_3-$A1_2O_3$ at $p(O_2)$ = 1 bar

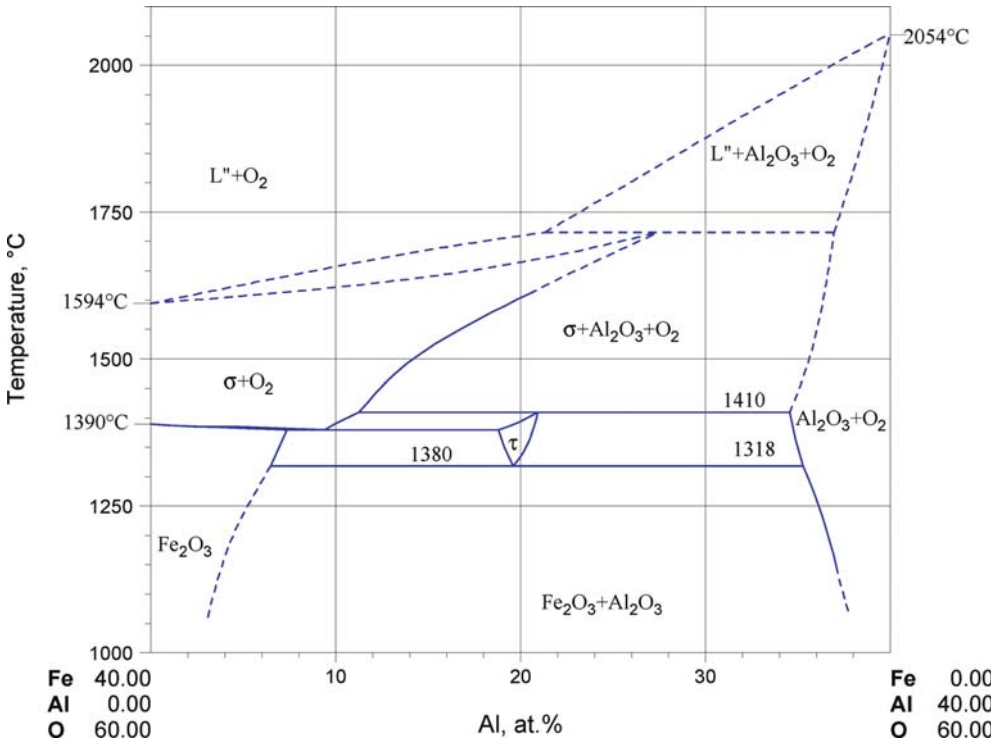

Fig. 23. Al-Fe-O. Vertical section Fe_2O_3-$A1_2O_3$ at $p(O_2)$ = 0.21 bar

DOI: 10.1007/978-3-540-69761-9_9

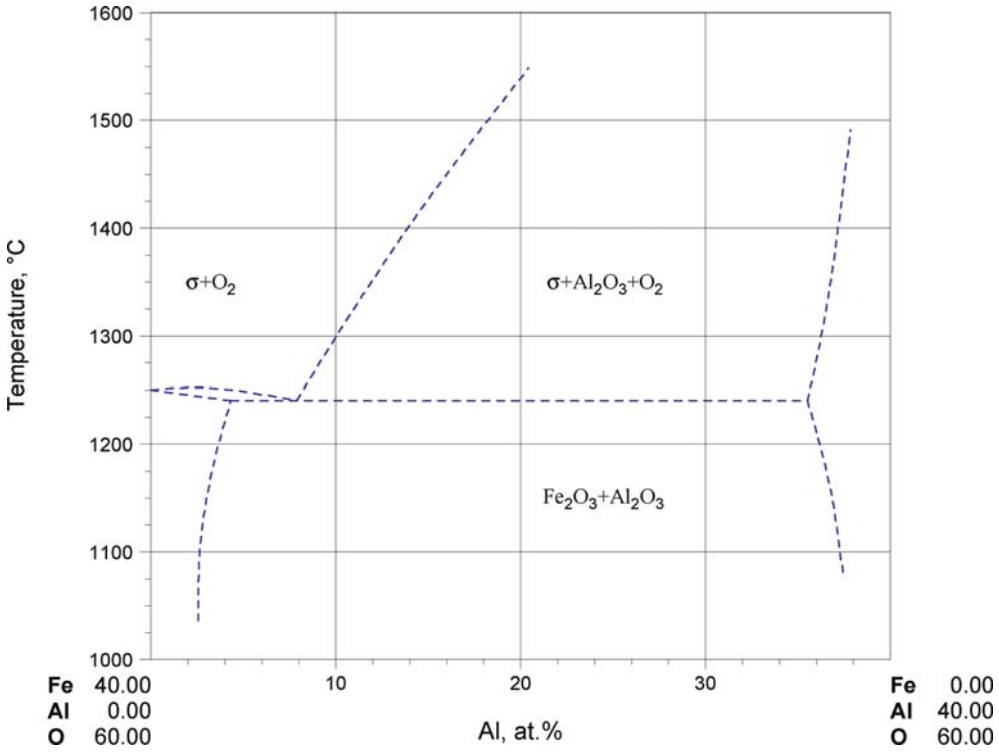

Fig. 24. Al-Fe-O. Vertical section Fe_2O_3-$A1_2O_3$ at $p(O_2) < 0.03$ bar

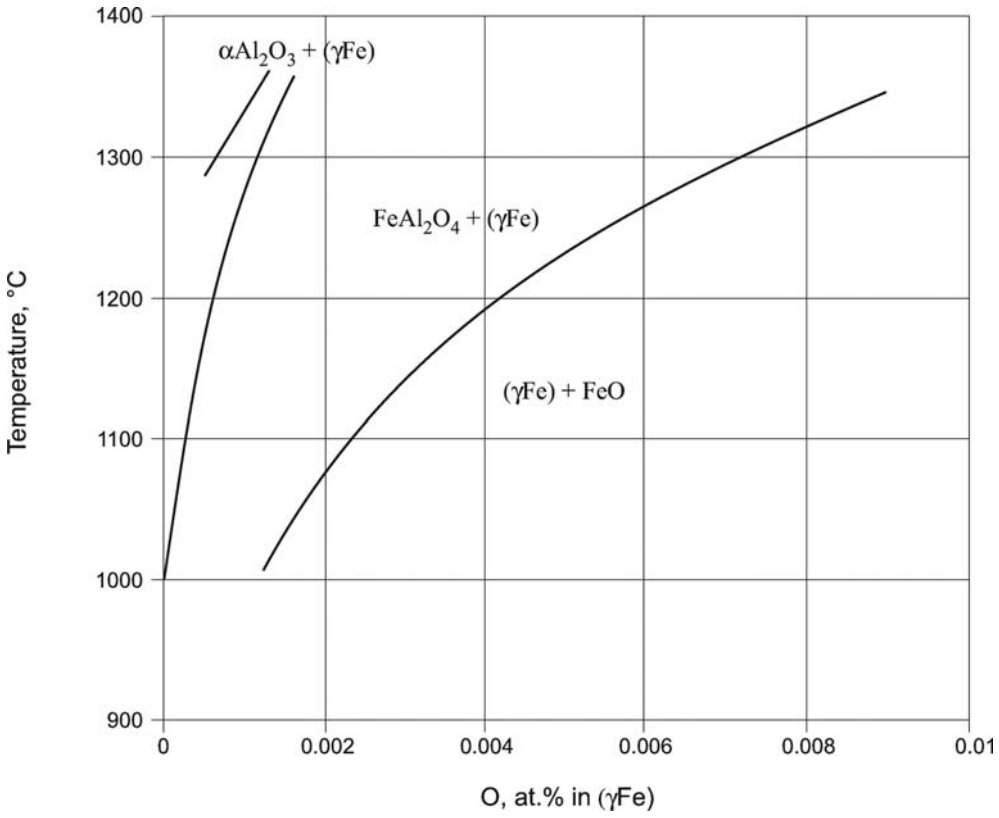

Fig. 25. Al-Fe-O. Stability diagram. Oxygen content in (γFe) in equlibrium with $\alpha A1_2O_3$, $FeA1_2O_4$ (σ) and FeO

DOI: 10.1007/978-3-540-69761-9_9

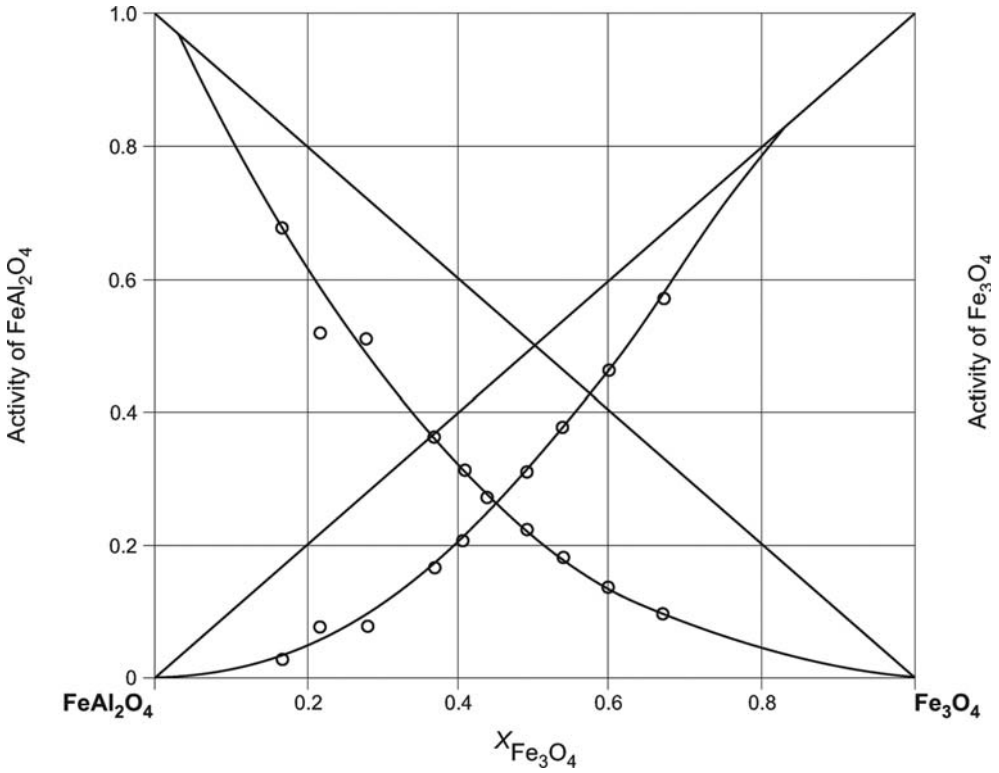

Fig. 26. Al-Fe-O. Activities of Fe_3O_4 and $FeAl_2O_4$ in the Fe_3O_4-$FeA1_2O_4$ system at 900°C

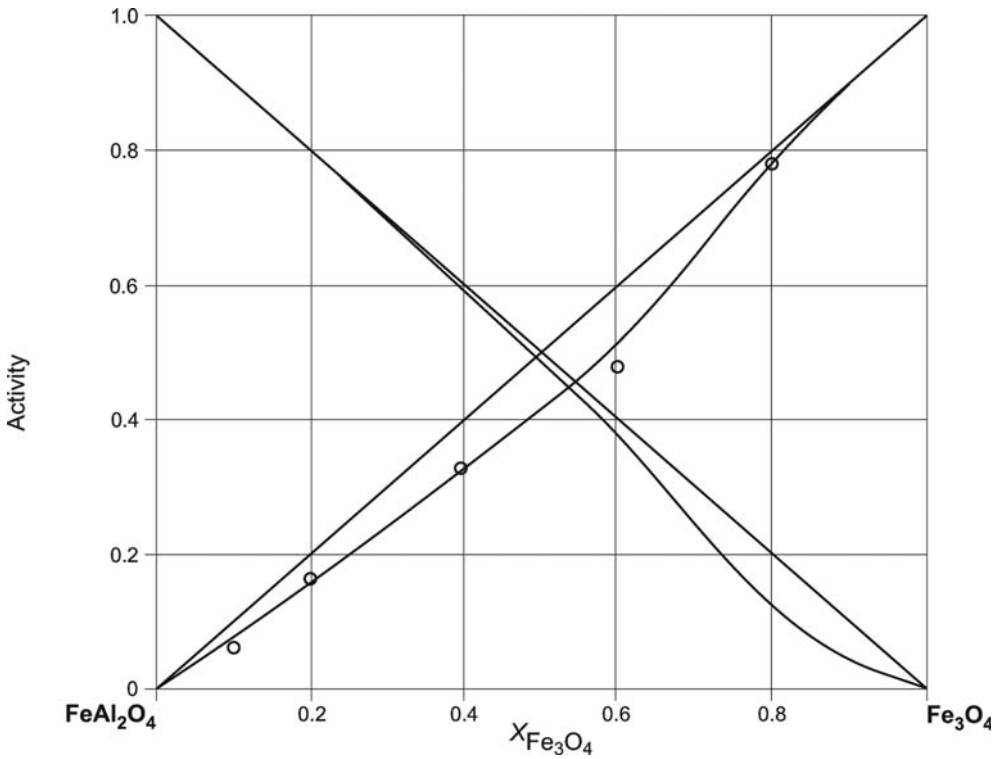

Fig. 27. Al-Fe-O. Activities of Fe_3O_4 (experimental) and $FeA1_2O_4$ (calculated) in the Fe_3O_4-$FeA1_2O_4$ system at 1300°C

DOI: 10.1007/978-3-540-69761-9_9

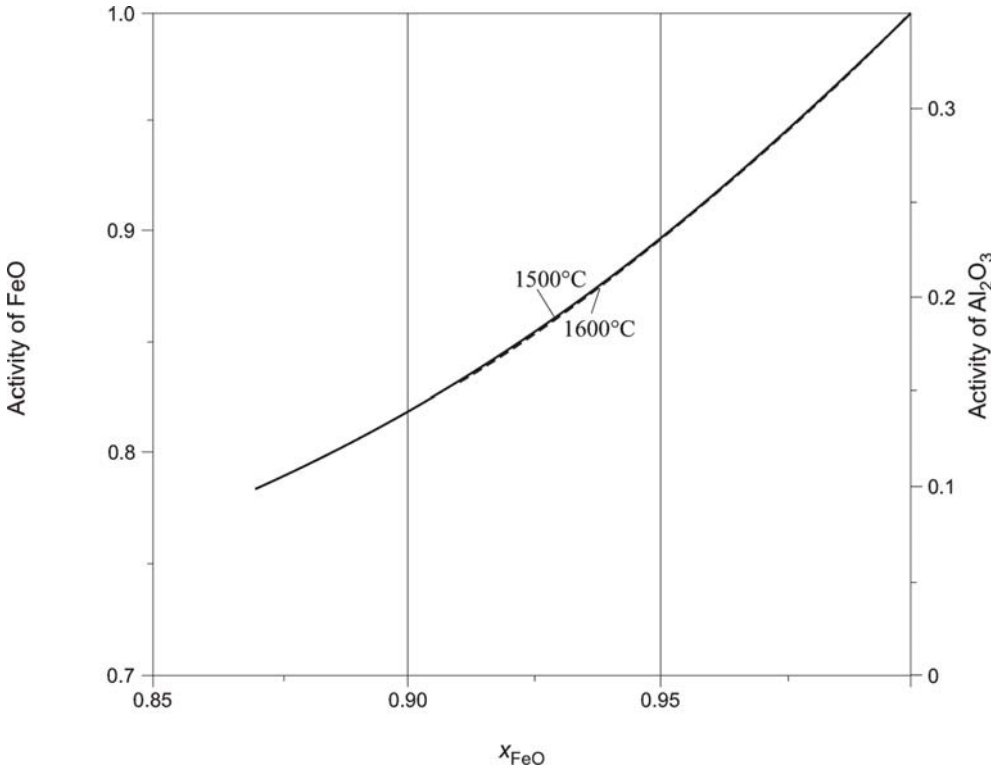

Fig. 28. Al-Fe-O. Activity of FeO in the FeO-$A1_2O_3$ liquid phase

DOI: 10.1007/978-3-540-69761-9_9

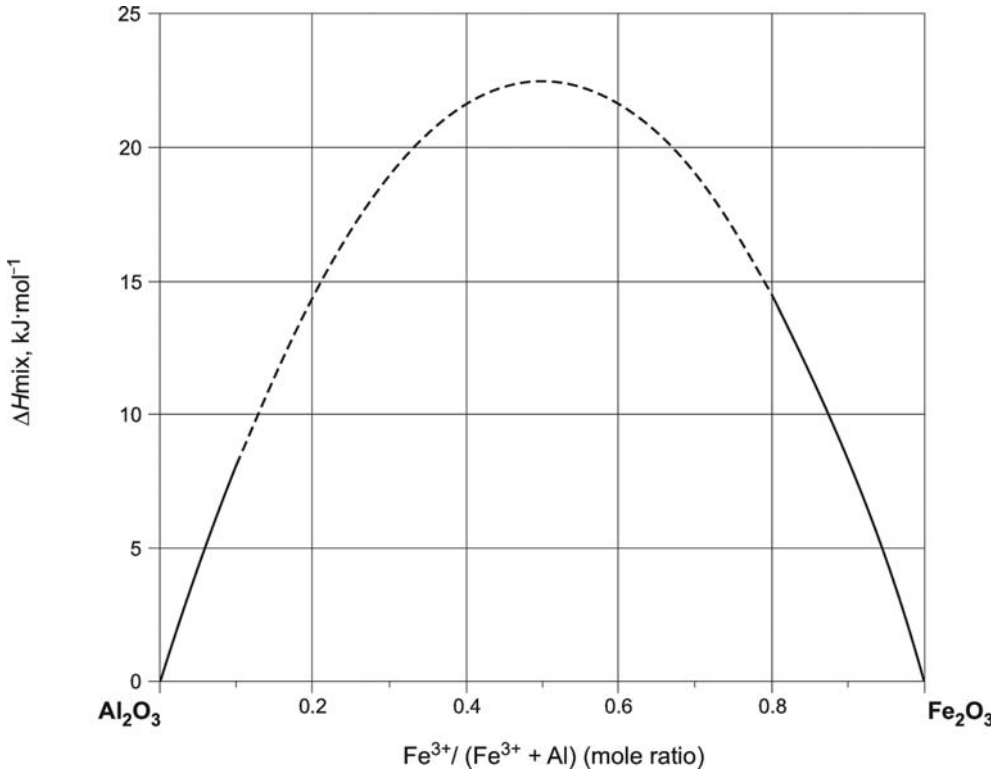

Fig. 29. Al-Fe-O. Enthalpy of mixing in the Fe_2O_3-$A1_2O_3$ solid solution. The dashed line is enthalpy of mixing within the miscibility gap

DOI: 10.1007/978-3-540-69761-9_9

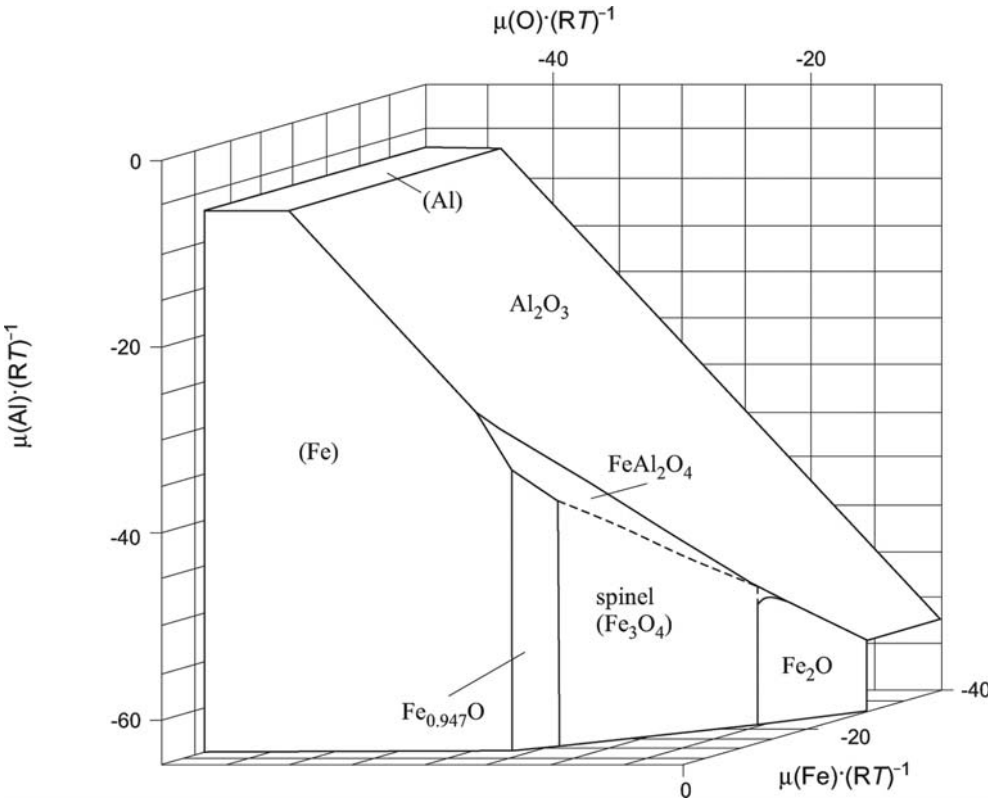

Fig. 30. Al-Fe-O. Chemical potential phase diagram at 1300°C. The spinel phase is treated as ideal solution. The case when Fe_3O_4 and $FeAl_2O_4$ are treated as different phases is shown by a dashed line

DOI: 10.1007/978-3-540-69761-9_9

References

[1939Wen] Wentrup, H., Hieber, G., "Reactions Between Al and O in Iron Melts", *Arch. Eisenhuettenwes*., **13**, 15 (1939) (Phase Relations, Experimental, 10)

[1946Dar] Darken, L.S., Gurry, R.W., "The System Iron-Oxygen: II", *J. Am. Chem. Soc*., **68**, 798–816 (1946) (Phase Relations, Phase Diagram, Experimental, Thermodyn., 24)

[1953Gok] Gokcen, N.A., Chipman, J., "Aluminium-Oxygen Equilibrium in Liquid Iron", *Trans. AIME*., 173–178 (1953) (Phase Relations, Phase Diagram, Experimental, Thermodyn., 12)

[1954Ric] Richards, R.G., White, J., "Phase Relationships of Iron-Oxide-Containing Spinels. Part I. Relationships in the System Fe-Al-O", *Trans. Brit. Ceram. Soc.*, **53**, 233–270 (1954) (Experimental, Phase Diagram, Phase Relations, 26)

[1955Oel] Oelsen, W., Heynert, G., "The Reaction Between Iron-Manganese Melts and Melting of their Aluminate" (in German), *Arch. Eisenhuettenwes.*, **26**(10), 567–575 (1955) (Phase Relations, Phase Diagram, Experimental, 12)

[1956Fis] Fischer, W.A., Hoffmann, A., "The Phase Diagram Ferrous Oxide - Aluminium Oxide" (in German), *Arch. Eisenhuettenwes.*, **27**(5), 343–346 (1956) (Experimental, Phase Diagram, 15)

[1956Kin] King, E.G., "Heat Capacities at Low Temperatures and Entropies of Five Spinel Minerals", *J. Phys. Chem*., **60**, 410–412 (1956) (Experimental, Thermodyn., 17)

[1956Mua] Muan, A., Gee, C.L., "Phase Equilibrium Studies in the System Iron Oxide-Alumina in Air and at One Atmosphere Oxygen Pressure", *J. Am. Ceram. Soc.*, **39**, 207–214 (1956) (Experimental, Phase Diagram, Phase Relations, 17)

[1957Fit] Fitterer, G.R., "The Physical Chemistry of Steelmaking - A Tribute to Dr. C. H. Herty, Jr.", *Proc. 40th Nat. Open Hearth Steel Comm. Iron Steel Division, AIME*, Pittsburgh, 40, 281–303 (1957) (Experimental, Phase Relations, Phys. Prop., 40)

[1957Gal] Galakhov, F.Ya., "Alumina Regions of Ternary Aluminosilicate Systems. Communication 1. The Systems FeO-Al_2O_3-SiO_2 and MnO-Al_2O_3-SiO_2" (in Russian), *Izv. Akad. Nauk SSSR, Otd. Khim. Nauk*, **5**, 525–531 (1957) (Phase Relations, Phase Diagram, Experimental, 16)

[1958Atl] Atlas, L.M., Sumida, W.K., "Solidus, Subsolidus and Subdissociation Phase Equilibria in the System Fe-Al-O", *J. Am. Ceram. Soc.*, **41**(5), 150–160 (1958) (Experimental, Phase Diagram, Phase Relations, 23)

[1958Mua] Muan, A., "On the Stability of the Phase $Fe_2O_3.Al_2O_3$", *Amer. J. Sci*., **256**, 413–422 (1958) (Phase Relations, Phase Diagram, Experimental, #, *, 8)

[1958Phi] Phillips, B., Muan, A., "Phase Equilibria in the System CaO - Iron Oxide in Air and at 1 Atm. O_2 Pressure", *J. Am. Ceram. Soc.*, **41**(11), 445–454 (1958) (Experimental, Phase Diagram, Phase Relations, 16)

[1958Tay] Taylor, A., Jones, R.M., "Constitution and Magnetic Properties of Iron-Rich Iron-Aluminium Alloys", *J. Phys. Chem. Solids*, **6**, 16–37 (1958) (Crys. Structure, Experimental, Magn. Prop., Phase Diagram, 49)

[1960Pil] Pillay, T.C.M., D'Entremont, J., Chipman J., "Stability of Hercynite at High Temperature", *J. Amer. Ceram. Soc*., **43**, 583–585 (1960) (Experimental, Thermodyn., 9)

[1961Kuz] Kuznetsov, V.M., Samarin, A.M., "Deoxidation Capacity of Al in Liquid Iron" (in Russian), *Physiochemical Fundamentals of Steelmaking*, Izd. AN SSSR, Moscow 11–17 (1961) (Thermodyn., Phase Relations, Phase Diagram, Experimental, 8)

[1961Tur] Turnock, A.C., Lindsley, D.H., "Fe-Al and Fe-Ti Spinels and Related Oxides", Carnegie Inst., Washington, Yearbook, **60**, 152–157 (1961) (Phase Relations, Phase Diagram, Experimental, #, *, 3)

[1962Tur] Turnock, A.C., Eugster, H.P., "Fe-Al Oxides: Phase Relationships Below 1000°C", *J. Petrology*, **3**(3), 533–565 (1962) (Experimental, Phase Diagram, 35)

[1963Ent] d'Entremont, J.C., Guernsey, D.L., Chipman, J., "Aluminium - Oxygen Interaction in Liquid Iron", *Trans. Met. Soc. AIME*, **227**, 14–17 (1963) (Experimental, Phase Relations, 13)

[1963Nov] Novokhatskii, I.A., Lenov, L.M., *Izv. Akad. Nauk SSSR, Metall. i Gorn. Delo*., (6), 47 (1963) as quoted by [1965Nov]

DOI: 10.1007/978-3-540-69761-9_9

[1963Rez] Rezukhina, T.N., Levitskii, V.A., Ozhegov, P., "Thermodynamic Properties of Iron Aluminate", *Russ. J. Phys. Chem.*, **37**, 358 (1963) (Experimental, Thermodyn., 11)

[1964Roi] Roiter, B.D., "Phase Equilibria in the Spinel Region of the System FeO-Fe_2O_3-Al_2O_3", *J. Am. Ceram. Soc.*, **47**(10), 509–511 (1964) (Experimental, Phase Diagram, Phase Relations, 9)

[1965McL] McLean, A., Bell, H.B., "Experimental Study of the Reaction $Al_2O_3+H_2=3H_2O+2Al$", *J. Iron Steel Inst.*, **203**, 123–130 (1965) (Experimental, Phase Relations, 33)

[1965Nov] Novokhatskii, I.A., Belov, B.F., Gorokh, A.V., Savinskaya, A.A., "The Phase Diagram for the System Ferrous Oxide-Alumina", *Russ. J. Phys. Chem.*, **39**(11), 1498–1499 (1965) (Phase Relations, Phase Diagram, Experimental, 9)

[1965Nov] Vachet, V., Desre, P., Bonnier, E., "Thermodynamics of the Liquid Systems (Fe, Al, O), (Co, Al, O), (Ni, Al, O) in the Fe, Co or Ni-Rich Regions at 1600°C" (in French), *Compt. Rend. Acad. Sci. Paris*, **260**(7), 1943–1946 (1965) (Experimental, 4)

[1966McL] McLean, A., Ward, R.G., "Thermodynamics of Hercynite Formation", *J. Iron Steel Inst.*, **204**, 8–11 (1966) (Experimental, Thermodyn., 36)

[1966Nov] Novokhatsky, I.A., Belov, B.F., "Phase Equilibria and Distribution of Elements in the Fe-O-Al System" (in Russian), *Izv. Akad. Nauk SSSR, Met.*, (1) 38–48 (1966) (Phase Relations, Phase Diagram, Experimental, 18)

[1967Buz] Buzek, Z., Schindlerova, V., Macoszek, M., "The Influence of Cr, Mn, V, Si, Ti, Al, Zr, Ce and Ca on the Activity and Solubility of Oxygen in Liquid Iron", *Sb. Ved. Pr. Vys. Sk. Ban. Ost., Rada Hutn.*, **13**(2–3), 175–193 (1967) (Experimental, 26)

[1967Rep] Repetylo, O., Olette, M., Kozakevitch, P., "Deoxidation of Liquid Steel with Aluminum and Elimination of the Resulting Alumina", *J. Metals*, 45–49 (1967) (Experimental, 24)

[1967Swi] Swisher, J.H., "Note on the Aluminum-Oxygen Interaction in Liquid Iron", *Trans. Met. Soc. AIME*, **239**, 123–124 (1967) (Experimental, #,, 8)

[1968Pie] Pierre, G.R.St., Blackburn, R.D., "The Relationship Between First-Order Interactions and Oxide Solubilities in Liquid Iron", *Trans. Metall. Soc. AIME*, **242**, 2–4 (1968) (Experimental, Theory, 18)

[1969Bry] Bryant, P.E.C., Smeltzer, W.W., "The Dissociation Pressure of Hematite", *J. Electrochem. Soc.*, **116**, 1409–1410 (1969) (Experimental, 4)

[1969Buz] Buzek, Z., Hutla, A., "The Influence of the Aluminium, Titanium, Zirconium Dissolved in Liquid Iron on the Activity and Solubility of Oxygen" (in German), *Freib. Forsch. B*, *Metall. Werkstofftech.*, **B117**, 59–73 (1969) (Experimental, Phase Relations, Phase Diagram, 20)

[1969Nov] Novokhatsky, I.A., Belov, B.F., "Concentration Dependence of the Solubility of Oxygen in Alloys" (in Russian), *Izv. Akad. Nauk SSSR, Met.*, (3) 15–26 (1969) (Phase Relations, Phase Diagram, Experimental, Thermodyn., 29)

[1969Sch] Schmahl, G., Dillenburg, H., "Equilibrium Studies of Iron Oxid Containing Solid Solutions in the Ternary Systems Fe-Al-O, Fe-Cr-O and Fe-V-O" (in German), *Z. Phys. Chem.*, **65**, 119–138 (1969) (Experimental, Phase Diagram, 70)

[1970Fru] Fruehan, R.J., "Activities in Liquid Fe-Al-O and Fe-Ti-O Alloys", *Metall. Trans.*, **1**, 3403–3410 (1970) (Phase Relations, Phase Diagram, Experimental, Thermodyn., 28)

[1970Nov] Novokhatskii, I.A., Belov, B.F., "Method for the Investigation of Reduction Processes of Metallic Melts", *Russ. J. Phys. Chem.*, **44**(8), 1138–1140 (1970), translated from *Zh. Fiz. Khim.*, **44**(8), 2013–2017, 1970 (Experimental, 18)

[1970Sch] Schenck, H., Steinmet, E., Mehta, K.K., "Equilibrium and Kinetics of Precipitation of Alumina in System Iron-Oxygen-Aluminium at 1600°C" (in German), *Arch. Eisenhuettenwes.*, **41**(2), 131–138 (1970) (Experimental, Phase Relations, Thermodyn., 51)

[1971Iml] Imlach, J.A., Glasser, F.P., "Sub-Solidus Phase Relations in the System CaO-Al_2O_3-Fe-Fe_2O_3", *Trans. J. Br. Ceram. Soc.*, **70**, 227–234 (1971) (Experimental, Phase Diagram, Mechan. Prop., 7)

[1971Roh] Rohde, L.E., Choudhury, A., Wahlster, M., "New Investigation into the Aluminium-Oxygen Equilibrium in Iron Melts" (in German), *Arch. Eisenhuettenwes.*, **B42**(3), 165–174 (1971) (Phase Relations, Phase Diagram, Experimental, 50)

DOI: 10.1007/978-3-540-69761-9_9

[1972Ell] Elliott, J.F., Wright, J.K., "Equilibrium Phase Relations During Solidification of Fe-O-C-X Alloys. System Fe-Al-O. Projected Equilibria Involving Iron Between 1500 and 1538°C at One Atmosphere", *Canad. Metall. Quart.*, **11**(4), 573–584 (1972) (Phase Relations, Phase Diagram, Experimental, #, *, 17)

[1973Buz] Buzek, Z., "Effect of Alloying Elements on the Solubility and Activity of Oxygen and Sulphur in Liquid Iron at 1600°C", *Int. Symp. Metall. Chem. - Appl. Ferrous Metall.*, Sheffield, July 1971, Iron and Steel Inst, London 173-177 (1973) (Crys. Structure, Experimental, Review, 8)

[1973Cha] Chan, J.C., Alcock, C.B., Jacob, K.T., "Electrochemical Measurement of the Oxygen Potential of the System Iron-Alumina-Hercynite in the Temperature Rang 750 to 1600°C", *Can. Metall. Quart.*, **12**(4), 439–443 (1973) (Experimental, Themodyn., 15)

[1973Iye] Iyengar, R.K., Philbrook, W.O., "Application of Phase Diagrams to Predict Phases Formed During Deoxidation of Steel", *Metall. Trans.*, **4**(9), 2189–2193 (1973) (Phase Relations, Phase Diagram, Experimental, 20)

[1973Jac] Jacquemot, A., Gatellier, C., Olette, M., "Study of Aluminium-Oxygen Equilibrium in Molten Iron at 1600°C with Help of Battery Having Solid Electrolyte ThO_2-Y_2O_3" (in French), *Compt. Rend. Acad. Sci. Paris, Ser. C*, **277**(6), C271–C273 (1973) (Experimental, Thermodyn., 10)

[1974Fel] Feldman, S.E., Kirkaldy, J.S., "On the Solubility Minimum in Ternary Oxide-Metal Equilibria", *Canad. Metall. Quart.*, **13**(4), 625–630 (1974) (Theory, Phase Relations, 20)

[1974Ros] Rosenbach, K., Schmitz, J.A., "Investigations in the Ternary System Iron(II)-Oxide-Chromium(III)-Oxide-Alumina" (in German), *Arch. Eisenhuettenwes.*, **45**(12), 843–847 (1974) (Phase Relations, Phase Diagram, Experimental, #, 13)

[1974Sig] Sigworth, G.K., Elliott, J.F., "The Thermodynamics of Liquid Dilute Iron Alloys", *Met. Sci.*, **8**, 298–309 (1974) (Review, Thermodyn., 249)

[1975Kim] Kim, C.K., McLean, A., "Hercynite Formation in Molten Iron Alloys", in "*Metal-Slag-Gas Reactions and Processes*", Foroulis, Z.A., Smeltzer, W.W., (Eds.), Electrochem. Soc., Princeton, New Jersey 284–295 (1975) (Phase Relations, Phase Diagram, Thermodyn., Experimental, 12)

[1976Jan] Janke, D., Fischer, W.A., "Deoxidation Equilibria of Ti, Al and Zr in Fe Melts at 1600°C" (in German), *Arch. Eisenhuettenwes.*, **47**(4), 195–198 (1976) (Experimental, Phase Relations, Phase Diagram, 30)

[1976Mal] Malysheva, T.Ya., Lyadova, V.Ya., Ostroskaya, I.V., Model, M.S., Davidyuk, A.A., "Nature of the Ferrite Phases in the Blast-Furnace Charge" (in Russian), *I. P. Bardin Razvit. Metall. SSSR*, Savitskii, E.M., (Ed.), Nauka, Moscow 39-58 (1976) (Experimental, 32)

[1976Pol] Pollak, T.M., "High Temperature Electrical Conductivity and Defect Chemistry of Iron-Doped Alumina", *Thesis*, Massachusets Inst. Technology, 81pp. (1976) (Electr. Prop., Experimental, 29)

[1976Sti] Sticher, J., Schmalzried, H., Schmalzried, C.-Z., "Geometrical Representation of Thermodynamic State Variables in the Ternary System Iron-Titanium-Oxygen in the Temperature Range Between 1300 and 1600°C" (in German), *Arch. Eisenhuettenwes.*, **47**(5), 261–266 (1976) (Theory, Thermodyn., Phase Relations, Phase Diagram, Experimental, 54)

[1978Apt] Apte, P., Stournaras, C., Kay, D.A.R., "Steelmaking Thermodynamics and Oxygen Concentration Cells", *Conf. Steelmaking Proc.*, Chicago, Ill, 16–20 Apr. 1978, Amer. Inst. Min., Met. Petroleum Engin., **61**, 555–560 (1978) (Experimental, Phase Relations, 18)

[1978Kau] Kaufman, L., Nesor, H., "Calculation of Quasibinary and Quasiternary Oxide Systems - I", *Calphad*, **2**, 35–53 (1978) (Thermodyn., Phase Relations, Phase Diagram, Theory, 30)

[1978Sto] Stournaras, C.J., "Thermodynamic Studies in Liquid Fe-Nb-O, Fe-Al-O, Fe-Al-Mn-O Systems Using Solid Electrolytes", *Diss. Absr. Int. B*, **38**(7), 3351 (1978) (Experimental, Thermodyn., 0)

[1979Ell] Elliott, J.F., "Chemical Equilibria and Phase Equilibria", *TMS / AIME, Conf. Calcul. Phase Diagrams hermochem. Allloy Phases*, Milwaukee, Wis, 17-18 Sept., 1979, Warrendale, Pa., 185–196 (1979) (Experimental, Phase Diagram, Phase Relations, 19)

DOI: 10.1007/978-3-540-69761-9_9

[1979Gor] Gordon, B.A., Worrell, W., Nagarajan, V., "Thermodynamic Predictions of the Behavior of Fe-Cr-Al Alloys in Coal Gasifier Environments", *Oxid. Met.*, **13**(1), 13–23 (1979) (Calculation, Experimental, Interface Phenomena, Phase Diagram, Thermodyn., 9)

[1979Kay] Kay, D.A.R., "Thermodynamic Data from Oxygen Concentration Cells at 1500–1600°C", *Rev. Int. Hautes Temp. Refract.*, **16**(1), 21–32 (1979) (Experimental, Thermodyn., 43)

[1979Kub] Kubaschewski, O., Alcock, C.B., "Metallurgical Thermochemistry", 5th Edition, *Int. Ser. Mat Sci. Technol.*, Pergamon Press, Vol. **24**, 238–239 (1979) (Review, Theory)

[1979Nec] Nechaev, Yu.S., Edigarov, V.S., Pustov, Yu.A., "Investigation of Iron Solubility in Aluminium and in Materials of SAP Type by Mössbauer Spectroscopy" (in Russian), *Izv. Vyss. Uchebn. Zaved., Chern. Metall.*, **5**, 92–97 (1979) (Experimental, Phase Relations, 14)

[1979Rou] Rousset, A., Paris, J., Chassagneux, F., "Importance of Reactivity of the Finely Divided Solids for the Synthesis of New Phases" (in French), *Ann. Chim. Fr.*, **4**, 115–122 (1979) (Experimental, Phase Relations, Thermodyn., 20)

[1980Aki] Akimov, A.G., Kazanskiy, L.P., "Oxidizing and Composition of the Surface of an Al-Fe Alloy" (in Russian), *Izv. Akad. Nauk SSSR, Otd. Khim. Nauk*, **10**, 2201–2205 (1980) (Experimental, Phase Diagram, 12)

[1980Ban] Ban-Ya, S., Chiba, A., Hikosaka, A., "Thermodynamics of Fe(t)O-M(x)O(y) (M(x)O(y) = CaO, SiO_2, TiO_2 and Al_2O_3) Binary Melts Saturated With Solid Iron", *Austral.-Jap. Extractive Metall. Symp.*, Sydney, Australia 16–18 July 1980, Australian Inst. Min. Metall., **23**, 457–467 (1980) (Experimental, Thermodyn., 22)

[1980Gus] Gustafsson, S., Mellberg, P.O., "On The Free Energy Interaction between some Strong Deoxidizers, Especially Calcium, Aluminum and Oxygen in Liquid Iron", in *Scaninject II, Injection Metal.*, *Proc. Conf.*, Lulea, Sweden, **20**(23), 1–19 (1980) (Thermodyn., 7)

[1980Kli] Klissurski, D.G., Mitov, I.G., Petrov, K.P., "A Study of the Preparation of Solid Solutions in the System αFe_2O_3-Al_2O_3", *Thermochim. Acta*, **41**(2), 181–186 (1980) (Crys. Structure, Experimental, Phase Diagram, 17)

[1980Mey] Meyers, C.E., Mason, T.O., Petuskey, W.T., Halloran, J.W., Bowen, H.K., "Phase Equilibria in the System Fe-Al-O", *J. Am. Ceram. Soc.*, **63**(11–12), 659–663 (1980) (Experimental, Phase Diagram, #, *, 20)

[1981Pet] Petric, A., Jacob, K.T., Alcock, C.B., "Thermodynamic Properties of Fe_3O_4-$FeAl_2O_4$ Spinel Solid Solutions", *J. Am. Ceram. Soc.*, **64**(11), 632–639 (1981) (Thermodyn., Experimental, 28)

[1981She] Shevtsov, V.E., "Thermodynamics of Oxygen Solutions in the Fe-Al System", *Russ. Metall. (Engl. Transl.)*, (1) 52–57 (1981) (Phase Relations, Phase Diagram, Experimental, Thermodyn., #, 16)

[1982Kub] Kubaschewski, O., "Iron - Binary Phase Diagrams", Springer Verlag, Berlin, Verlag Stahl Eisen, Düsseldorf, 5–9 and 79–82 (1982) (Phase Relations, Phase Diagram, Review, #, 32)

[1982Lia] Liang, W.W., "Prediction of Solubility of Oxides in Liquid Fe-Al-O, Co-Al-O, Ni-Al-O and Cu-Al-O Alloy", *Z. Metallkd.*, **73**(6), 369–375 (1982) (Thermodyn., Phase Relations, Phase Diagram, Theory, #, *, 31)

[1983Boj] Bojarski, Z., Isakow, Z., "Investigations of Al^{3+} and Ga^{2+} Solid Solutions in αFe_2O_3 Oxide" (in Polish), *Archiw. Nauki Mater.*, **4**(1), 3–20 (1983) (Experimental, #, 23)

[1983Elr] Elrefaie, F.A., Smeltzer, W.W., "Thermodynamics of the System Iron-Aluminium-Oxygen Between 1073 K and 1573 K", *Metall. Trans. B*, **14B**, 85–93 (1983) (Phase Relations, Phase Diagram, Experimental, Thermodyn., #, 31)

[1983Yam] Yamauchi, S., Nakamura, A., Shimizu, T., Fueki, K., "Vacancy Diffusion in Magnetite-Hercynite Solid Solution", *J. Solid State Chem.*, **50**, 20–32 (1983) (Experimental, Theory, Thermodyn., 21)

[1984Mac] Mackenzi, K.J.D., Brown, I.W.M., "The Mössbauer Spectrum and Structure of Iron(III) Aluminium Oxide, $FeAlO_3$", *J. Mater. Sci. Lett.*, **3**, 159–161 (1984) (Crys. Structure, Experimental, 8)

DOI: 10.1007/978-3-540-69761-9_9

[1984Sch] Schuermann, E., Bannenberg, N., "Metal-Slag Equilibria in the System Iron-Aluminium-Oxygen as a Basis of Aluminium Deoxidation of Steel Melts" (in German), *Arch. Eisenhuettenwes.*, **55**(9), 409–414 (1984) (Phase Relations, Phase Diagram, Experimental, Thermodyn., #, 27)

[1985Meh] Mehrotra, S.P., Chaklader, A.C.D., "Interfacial Phenomena between Molten Metals and Sapphire Substrate", *Metall. Trans. B*, **16B**, 567–575 (1985) (Experimental, 43)

[1985Tay] Taylor, D., "Thermal Expansion Data. VI. Complex Oxides, AB_2O_4, the Spinels", *British Ceram. Transact. J.*, **84**(4), 121–127 (1985) (Calculation, Crys. Structure, Review, 99)

[1985Wri] Wriedt, H.A., "The Al-O (Aluminium-Oxygen) System", *Bull. Alloy Phase Diagrams*, **6**(6), 548–553 (1985) (Phase Relations, Phase Diagram, Review, #, 46)

[1986Gho] Ghosh, A., Murthy, G.V.R., "An Assessment of Thermodynamic Parameters for Deoxidation of Molten Iron by Cr, V, Al, Zr and Ti", *Trans. Iron Steel Inst. Jpn.*, **26**(7), 629–637 (1986) (Assessment, Phase Diagram, Thermodyn., 41)

[1988Ber] Berman, R.G., "Internally-Consistent Thermodynamic Data for Minerals in the System Na_2O-K_2O-CaO-MgO-FeO-Fe_2O_3-Al_2O_3-SiO_2-TiO_2-H_2O-CO_2", *J. Petrol.*, **29**, 445–552 (1988) (Review, Thermodyn., 419)

[1988Was] Wasai, K., Mukai, K., "Thermodynamic Analysis of Fe-Al-O Liquid Alloy Equilibrated with α-Al_2O_3(s) by an Associated Solution Model", *J. Japan Inst. Metals*, **52**(11), 1088–1097 (1988) (Thermodyn., 30)

[1989Rag1] Raghavan, V., "The Al-Fe-O System", in "*Phase Diagrams of Ternary Iron Alloys, Part 5*", Indian Inst. of Metals, Calcutta, **5**, 10–28 (1989) (Phase Relations, Phase Diagram, Review, #, 29)

[1989Rag2] Raghavan, V., "The Fe-O System", in "*Phase Diagrams of Ternary Iron Alloys, Part 5*", Indian Inst. of Metals, Calcutta, **5**, 5–8 (1989) (Phase Diagram, Crys. Structure, Review, 3)

[1990Hol] Holland, T.J.B., Powell R., "An Enlarged and Updated Internally Consistent Thermodynamic Dataset with Uncertainties and Correlations - the System K_2O-Na_2O-CaO-MgO-MnO-FeO-Fe_2O_3-Al_2O_3-TiO_2-SiO_2-C-H_2-O_2", *J. Metamorphic Geol.*, **8**, 89–124 (1990) (Review, Thermodyn., 267)

[1990Kuz] Kuznetsov, V.M., Kulikov, I.S., "The Solubility and Activity of Oxygen in Fe-Co-Ni-Cu Alloys Containing Zr, Hf, and Al", *Russ. Metall.*, (2), 19-22 (1990), translated from Izv. *Akad. Nauk SSSR, Met.*, 2, 1922 (1990)(Thermodyn., Experimental, 9)

[1990Tsu] Tsuchida, T., Sugimoto, K., "Effect of Grinding of Mixtures of Goethite and Hydrated Alumina on the Formation of Fe_2O_3-Al_2O_3 Solid Solutions", *Thermochim. Acta*, **170**, 41–50 (1990) (Experimental, 50)

[1991Nak] Nakashima, K., Takihira, K., Mori, K., Shinozaki, N., "Wettability of Al_2O_3 Substrate by Liquid Iron - Effects of Oxygen in Liquid Iron and Purity of Al_2O_3 Substrate" (in Japanese), *J. Jpn. Inst. Met.*, **55**(11), 1199–1206 (1991) (Experimental, Interface Phenomena, Phase Relations, 28)

[1991Skl] Sklad, P.S., McHargue, C.J., Romana, L., White, C.W., McCallum, J.C., "The Effect of Post-Implantation Annealing on the Microstructure of Al_2O_3 Implanted with Iron at 185°C", *Nucl. Instrum. Methods Phys. Res./B*, **B59–B60**(II), 1187–1194 (1991) (Morphology, Abstract, 7)

[1991Sun] Sundman, B., "An Assessment of the Fe-O System", *J. Phase Equilib.*, **12**(1), 127–140 (1991) (Phase Relations, Assessment, 53)

[1991Yao] Yao, T., Maki, J., Jinno, H., "Decomposition of Iron Spinel Under Low Oxygen Partial Pressure" (in Japanese), *J. Ceram. Soc. Jpn.*, **99**(7), 639–641 (1991) (Crys. Structure, Experimental, 13)

[1992Hol] Holcomb, G.R., Pierre, G.R.St., "The Solubility of Alumina in Liquid Iron", *Metall. Trans. B*, **23B**, 789–790 (1992) (Thermodyn., Experimental, 12)

[1992Sui] Suito, H., Inoue, R., Nagatani, A., "Mullite as an Electrochemical Probe for the Determination of Low Oxygen Activity in Liquid Iron", *Steel Res.*, **63**(10), 419–425 (1992) (Experimental, Thermodyn., 20)

DOI: 10.1007/978-3-540-69761-9_9

[1992Tay] Taylor, J.R., Dinsdale, A.T., Hillert, M., Selleby, M., "A Critical Assessment of Thermodynamic and Phase Diagram Data for the Al-O System", *Calphad*, **16**(2), 173–179 (1992) (Calculation, Phase Diagram, Thermodyn., 22)

[1992Tru] Trumble, K.P., "Thermodynamic Analysis of Aluminate Formation at Fe/Al_2O_3 and Cu/Al_2O_3 Interfaces", *Acta Metall. Mat., Suppl.*, **40**, S105-S110 (1992) (Thermodyn., 30)

[1993Eri] Eriksson, G., Wu, P., Pelton, A.D., "Critical Evaluation and Optimization of the Thermodynamic Properties and Phase Diagrams of the MgO-Al_2O_3, MnO-Al_2O_3, FeO-Al_2O_3 and K_2O-Al_2O_3 Systems", *Calphad*, **17**(2), 189–205 (1993) (Phase Diagram, Review, 74)

[1993Kat] Kattner, U.R., Burton, B.P., "Al-Fe (Aluminum-Iron)", in "Phase Diagrams of Binary Iron Alloys", Okamoto, H., (Ed.), ASM Int., Mater. Park, OH, 12–28 (1993) (Crys. Structure, Electr. Prop., Magn. Prop., Phase Diagram, Review, Thermodyn., 99)

[1993Kub] Kubaschewski, O., Alcock, C.B., Spencer, P.J., "*Materials Termochemistry*", Pergamon Press, Oxford (1993)

[1993Sax] Saxena, S.K., Chatterjee, N., Fei, Y., Shen, G., "*Thermodynamic Data on Oxides and Silicates*", Springer Verlag (1993)

[1993Tyu] Tyurin, A.G., "Thermodynamics of Molecular and Ionic Solutions", *Russ. Metall. (Engl. Transl.)*, (2), 39–47 (1993), translated from *Izv. RAN, Met*., (2), 48-56 (1993) (Theory, Thermodyn., 35)

[1995Bar] Barin, I., "Thermochemical Data for Pure Substances", Wiley-VCH, New-York (1995) (Thermodyn., Review)

[1995Bou] Bouchard, D., Bale, C.W., "Thermochemical Properties of Iron-Rich Liquid Solutions Containing Oxygen and Aluminium", *J. Phase Equilib.*, **16**(1), 16–23 (1995) (Thermodyn., 29)

[1995Dim] Dimitrov, S., Weyl, A., Janke, D., "Control of the Aluminum-Oxygen Reaction in Pure Melts", *Steel Res.*, **66**(1), 3–7 (1995) (Experimental, Phase Relations, Thermodyn., 29)

[1995Ell] Ellner, M., "Polymorphic Phase Transformation of Fe_4Al_{13} Causing Multiple Twinning with Decagonal Pseudo-Symmetry", *Acta Crystallogr.*, **B51**, 31–36 (1995) (Crys. Structure, Experimental, 28)

[1995Esc] Escribano, V.S., Amores, J.M.G., Finocchio, E., Daturi, M., Busca, G., "Characterization of α-$(Fe,Al)_2O_3$ Solid-Solution Powders', *J. Mater. Chem.*, **5**(11), 1943–1951 (1995) (Crys. Structure, Experimental, 44)

[1995Jow] Jowsa, J., "Phase Equilibrium of Fe-O-I Systems (I = Ca, Al) Used for Steelmaking", *Hutnik-Wiadomosci Hutnicze*, **8**, 301–304 (1995) (Phase Relations, Phase Diagram, Thermodyn., Calculation, 13)

[1996Bou] Bouree, F., Baudour, J.L., Elbadraoui, E., Musso, J., Laurent, C., Rousset, A., "Crystal and Magnetic Structure of Piezoelectric, Ferrimagnetic and Magnetoelectric Aluminium Iron Oxide $FeAlO_3$ from Neutron Powder Diffraction', *Acta Crystallogr., Sect. B: Struct. Crystallogr. Crys. Chem.*, **B52**(2), 217–222 (1996) (Crys. Structure, Experimental, 10)

[1996Lee] Lee, H.Y., Rhee, Y.W., Kang, S.J.L., "Discontinuous Dissolution and Grain-Boundary Migration in Al_2O_3-Fe_2O_3 by Oxygen Partial Pressure Change", *J. Am. Ceram. Soc.*, **79**(6), 1659–1663 (1996) (Experimental, Morphology, Phase Diagram, Phase Relations, 24)

[1997Ito] Itoh, H., Hino, M., Banya, S., "Assessment of Al Deoxidation Equilibrium in Liquid Iron", *J. Iron Steel Inst. Jpn.*, **83**(12), 773–778 (1997) (Experimental, Thermodyn., 17)

[1997Got] Gottschalk, M., "Internally Consistent Thermodynamic Data for Rock-Forming Minerals in the System SiO_2-TiO_2-Al_2O_3-Fe_2O_3-CaO-MgO-FeO-K_2O-Na_2O-H_2O-CO_2", *Eur. J. Mineral.*, **9**, 175–223 (Review, Thermodyn., Calculation, 246)

[1997Li] Li, G.Q., Suito, H., "Electrochemical Measurement of Critical Supersaturation in Fe-O-M (M = Al, Si, and Zr) and Fe-O-Al-M (M = C, Mn, Cr, Si, and Ti) Melts by Solid Electrolyte Galvanic Cell", *ISIJ Int.*, **37**(8), 762–769 (1997) (Experimental, Phase Relations, 26)

[1997Sub] Subramanian, R., McKamey, C.G., Buck, L.R., Schneibel, J.H., "Synthesis of Iron Aluminide-Al_2O_3 Composites by In-situ Displacement Reactions", *Mater. Sci. Eng. A*, **239–240**, 640–646 (1997) (Experimental, Mechan. Prop., Morphology, Phase Diagram, Phase Relations, 23)

DOI: 10.1007/978-3-540-69761-9_9

[1998Cos] Da Costa, G.M., De Grave, E., Vandenberghe, R.E., "Mössbauer Studies of Magnetite and Al-Substituted Maghemites", *Hyperfine Interact.*, **117**, 207–243 (1998) (Crys. Structure, Experimental, 77)

[1998Ali] Aliravci, C.A., Pekgueleryuez, M.O., "Calculation of Phase Diagrams for the Metastable Al-Fe Phases Forming in Direct-Chill (DC)-Cast Aluminum Alloy Ingots", *Calphad*, **22**, 147–155 (1998) (Calculation, Phase Relations, 20)

[1998Har] Harrison, R.J., Redfern, S.A.T., O'Neill, H.S.C., "The Temperature Dependence of the Cation Distribution in Synthetic Hercynite ($FeAl_2O_4$) from in-situ Neutron Structure Refinements", *Am. Mineral.*, **83**, 1092–1099 (1998) (Experimental, Theory, 35)

[1998Seo] Seo, J.-D., Kim, S.-H., Lee, K.-R., "Thermodynamic Assessment of the Al Deoxidation Reaction in Liquid Iron", *Steel Res.*, **69**(2), 49–53 (1998) (Experimental, Thermodyn., 16)

[1999Fuj] Fujiwara, H., Hattori, A., Ichise, E., "Equilibrium Between Aluminum and Oxygen in Fe-36%Ni Alloy and Liquid Iron at 1973K" (in Japanese), *J. Iron Steel Inst. Jpn.*, **85**(3), 201–207 (1999) (Experimental, Thermodyn., 14)

[1999Ma] Ma, Z., Janke, D., "Oxygen and Nitrogen Reactions in Fe-X and Fe-Cr-Ni-X Melts", *Steel Res.*, **70**(10), 395–402 (1999) (Calculation, Thermodyn., 69)

[1999Mei] Mei, J., Halldearn, R.D., Xiao, P., "Mechanisms of the Aluminium-iron Oxide Thermite Reaction", *Scr. Mater.*, **41**(5), 541–548 (1999) (Crys. Structure, Experimental, Morphology, Phase Diagram, Phase Relations, 8)

[1999Was1] Wasai, K., Mukai, K., "Thermodynamics of Nucleation and Supersaturation for the Aluminum-deoxidation Reaction in Liquid Iron", *Metall. Mater. Trans. B*, **30**(6), 1065–1074 (1999) (Calculation, Thermodyn., 17)

[1999Was2] Wasai, K., Mukai, K., Fuchiwaki, H., Yoshida, A., "Determination of Aluminum and Oxygen Contents in Liquid Iron in Equilibrium With α-Alumina and Hercynite", *ISIJ Int.*, **39**(8), 760–766 (1999) (Experimental, Morphology, Phase Relations, 17)

[1999Yok] Yokokawa, H., "Generalized Chemical Potential Diagram and Its Applications to Chemical Reactions at Interfaces between Dissimilar Materials", *J. Phase Equilib.*, **20**(3), 258–287 (1999) (Phase Relations, Review, 93)

[2000Ban] Banovic, S.W., Dupont, J.N., Marder, A.R., "The Use of Ternary Phase Diagrams in the Study of High Temperature Corrosion Products Formed on Fe-5wt% Al Alloys in Reducing and Oxidizing Environments", *Acta Mater.*, **48**(11), 2815–2822 (2000) (Experimental, Interface Phenomena, Morphology, Phase Diagram, Phase Relations, 34)

[2000Bjo] Bjoerkvall, J., Sichen, D., Seetharaman, S., "Thermodynamic Description of Al_2O_3-CaO-MnO and Al_2O_3-FeO-MnO Melts - a Model Approach", *Calphad*, **24**(3), 353–376 (2000) (Assessment, Calculation, Phase Relations, Thermodyn., 18)

[2000Jan] Janke, D., Ma, Z.T., Valentin, P., Heinen, A., "Improvement of Castability and Anality of Continuously Cast Steel", *ISIJ Int.*, **40**(1), 31–39 (2000) (Theory, Thermodyn., 46)

[2001Ike] Ikeda, O., Ohnuma, I., Kainuma, R., Ishida, K., "Phase Equilibria and Stability of Ordered BCC Phases in the Fe-rich Portion of the Fe-Al System", *Intermetallics*, **9**, 755–761 (2001) (Experimental, Mechan. Prop., Phase Relations, 18)

[2001Jha] Jha, R., Haworth, C.W., Argent, B.B., "The Formation of Diffusion Coating on Some Low-Alloy Steels and Their High Temperature Oxidation Behaviour: P_2 Oxidation Studies", *Calphad*, **25**(4), 667–689 (2001) (Calculation, Phase Relations, 35)

[2001Lad] Ladavos, A.K., Bakas, T.V., "The Al_2O_3-Fe_2O_3 Mixed Oxidic System, I. Preparation and Characterization", *React. Kinet. Catal. Lett.*, **73**(2), 223–228 (2001) (Crys. Structure, Experimental, Phase Relations, 10)

[2001Mas] Masahashi, N., Watanabe, S., Hanada, Sh., "Microstructure and Oxidation Behaviour of Low Pressure Plasma Sprayed Iron Aluminides", *ISIJ Int.*, **41**(9), 1010–1017 (2001) (Crys. Structure, Experimental, Mechan. Prop., 16)

[2001Sas] Sasai, K., Mizukami, Y., "Mechanism of Alumina Adhesion to Continuous Caster Nozzle With Reoxidation of Molten Steel", *ISIJ Int.*, **41**(11), 1331–1339 (2001) (Experimental, Interface Phenomena, Morphology, 22)

DOI: 10.1007/978-3-540-69761-9_9

[2001Sur] Suryanarayana, C., "Mechanical Alloying and Milling", *Prog. Mater. Sci.*, **46**(1–2), 1–184 (2001) (Crys. Structure, Experimental, Kinetics, Phase Relations, Review, Thermodyn., 932)

[2002Bot] Botta, P.M., Bercoff, P.G., Aglietti, E.F., Bertorello, H.R., Lopez, J.M.P., "Magnetic and Structural Study of Mechanochemical Reactions in the Al-Fe_3O_4 System", *J. Mater. Sci.*, **37**(12), 2563–2568 (2002) (Crys. Structure, Experimental, Magn. Prop., Morphology, Phase Relations, 25)

[2002Dav] Davies, R.H., Dinsdale, A.T., Gisby, J.A., Robinson, J.A.J., Martin, S.M., "MTDATA - Thermodynamic and Phase Equilibrium Software from the National Physical Laboratory", *Calphad*, **26**(2), 229–271 (2002) (Calculation, Phase Relations, Thermodyn., 29)

[2002Gos] Da Gosta, G.M., Van San, E., De Grave, E., Vanderberghe, R.E., Barron, V., Datas, L., "Al Hematites Prepared by Homogeneous Precipitation of Oxinates: Material Characterization and Determination of the Morin Transition", *Phys. Chem. Miner.*, **29**, 122–131 (2002) (Crys. Structure, Experimental, Magn. Prop., 24)

[2002Gra] Granovskii, A., Sato, H., Aoki, Y., Yurasov, A., "Tunneling Thermopower in Magnetic Granular Alloys", *Phys. Solid State*, **44**(11), 2095–2097 (2002) (Calculation, Magn. Prop., Theory, 10)

[2002Maj] Majzlan, J., Navrotsky, A., Evans, B.J., "Thermodynamics ans Crystal Chemistry of the Hamatite-Corundum Solid Solution and the $FeAlO_3$ Phase", *Phys. Chem. Miner.*, **29**(8), 515–526 (2002) (Thermodyn., Crys. Structure, Experimental, Phase Relations, 43)

[2002Tak] Takacs, L., "Self-Sustaining Reactions Induced by Ball Milling", *Prog. Mater. Sci.*, **47**, 355–414 (2002) (Experimental, Kinetics, Mechan. Prop., Review, Theory, Thermodyn., 192)

[2002Was] Wasai, K., Mukai, K., "Thermodynamic Analysis on Metastable Alumina Formation in Aluminum Deoxidized Iron Based on Ostwalds Step Rule and Classical Homogeneous Nucleation Theories", *ISIJ Int.*, **42**(5), 467–473 (2002) (Calculation, Thermodyn., 20)

[2003Bot] Botta, P.M., Mercader, R.C., Aglietti, E.F., Lopez, J.M.P., "Synthesis of Fe-$FeAl_2O_4$-Al_2O_3 by High-Energy Ball Milling of Al-Fe_3O_4 Mixtures", *Scr. Mater.*, **48**(8), 1093–1098 (2003) (Crys. Structure, Experimental, Phase Relations, 16)

[2003Kap] Kapilashrami, E., Jakobsson, A., Lahiri, A.K., Seetharaman, S., "Studies of the Wetting Chracteristics of Liquid Iron on Dense Alumina by X-Ray Sessile Drop Techhique", *Metall. Mater. Trans. B*, **34B**(2), 193–199 (2003) (Phase Diagram, Thermodyn., 18)

[2003Kle] Klemme, S., van Miltenburg, J.C., "Thermodynamic Properties of Hercynite ($FeAl_2O_4$) Based on Adiabatic Calorimetry at Low Temperatures", *Am. Mineral.*, **88**, 68–72 (2003) (Experimental, Thermodyn., 42)

[2003Lan] Lang, F., Yu, Zh., Gedevanishvili, Sh., Deevi, S.C., Narita, T., "Effect of Pre-Oxidation on the Corrosion Behaviour of Fe-40Al Sheet in a N_2-11.2O_2-7.5CO_2-500 ppm SO_2 Atmosphere at 1273 K", *Intermetallics*, **11**(2), 129–134 (2003) (Experimental, Interface Phenomena, 24)

[2003Mun] Munoz-Morris, M.A., Garcia Oca, C., Morris, D.G., "Microstructure and Room Temperature Strength of Fe-40Al Containing Nanocrystalline Oxide Particles", *Acta Mater.*, **51**(17), 5187–5197 (2003) (Experimental, Mechan. Prop., Morphology, 32)

[2003Xue] Xue, D.S., Huang, Y.L., Ma, Y., Zhou, P.H., Niu, Z.P., Li, F.S., Job, R., Fahrner, W.R., "Magnetic Properties of Pure Fe-Al_2O_3 Nanocomposites", *J. Mater. Sci. Lett.*, **22**(24), 1817–1820 (2003) (Experimental, Magn. Prop., Morphology, 17)

[2004Cot] Cotica, L.F., Zanatta, S.C., de Medeiros, S.N., dos Santos, I.A., Paesano, A., da Cunha, J.B.M., "Mechanical Milling of the $(\alpha\text{-}Fe_2O_3)_{(x)}(\alpha\text{-}Al_2O_3)_{(1-x)}$ System: an X-ray Diffraction and Mössbauer Spectral Study", *Solid State Ionics*, **171**(3-4), 283–288 (2004) (Crys. Structure, Electronic Structure, Experimental, 27)

[2004Fab] Fabrichnaya, O.B., Saxena, S.K., Richet, P., Westrum, E.F., "*Thermodynamic Data, Models and Phase Diagrams in Multicomponent Oxide Systems*", Springer-Verlag, Berlin, Heidelberg (2004) (Review, Thermodyn.)

DOI: 10.1007/978-3-540-69761-9_9

[2004Fre] Fredriksson P., Seetharaman, S., "Thermodynamics Activities of FeO in some Binary FeO-Containing Slags", *Steel Res.*, **75**, 240–246 (2004) (Calculation, Experimental, Thermodyn., 23)

[2004Vil] Villafuerte-Castrejon, M.E., Castillo-Pereyra, E., Tartaj, J., Fuentes, L., Bueno-Baques, D., Gonzalez, G., Matutes-Aquino, J.A., "Synthesis and AC Magnetic Susceptibility Measurements of $Fe_{2-x}Al_xO_3$ Compounds", *J. Magn. Magn. Mater.*, **272–276**(2), 837–839 (2004) (Crys. Structure, Experimental, Magn. Prop., Phys. Prop., 7)

[2005Fee] Feenstra, A., Saemann, S., Wunder, B., "An Experimental Study of Fe-Al Solubility in the System Corundum-Hematite up to 40 kbar and 1300°C", *J. Petrology*, **46**(9), 1881–1892 (2005) (Crys. Structure, Experimental, Phase Relations, Thermodyn., 36)

[2005Liu] Liu, M., Li, H.B., Xiao, L., Yu, W.X., Lu, Y., Zhao, Z.D., "XRD and Mössbauer Spectroscopy Investigation of Fe_2O_3-Al_2O_3 Nano-composite", *J. Magn. Magn. Mater.*, **294**(3), 294–297 (2005) (Crys. Structure, Experimental, 8)

[2006MSIT] "Al-Fe (Aluminum-Iron)", Diagrams as Published, in *MSIT Workplace*, Effenberg, G. (Ed.), Materials Science International Services, GmbH, Stuttgart; Document ID: 30.10236.1.20, (2006) (Crys. Structure, Phase Diagram, Phase Relations, 11)

[V-C] Villars, P. and Calvert, L.D., *Pearson's Handbook of Crystallographic Data for Intermetallic Phases*, ASM, Metals Park, Ohio (1985)

[V-C2] Villars, P. and Calvert, L.D., *Pearson's Handbook of Crystallographic Data for Intermetallic Phases*, 2nd edition, ASM, Metals Park, Ohio (1991)

[Mas] Massalski, T.B. (Ed.), *Binary Alloy Phase Diagrams*, ASM, Metals Park, Ohio (1986)

[Mas2] Massalski, T.B. (Ed.), *Binary Alloy Phase Diagrams*, 2nd edition, ASM International, Metals Park, Ohio (1990)

DOI: 10.1007/978-3-540-69761-9_9

Aluminium – Iron – Phosphorus

Rainer Schmid-Fetzer, Vasyl Tomashik

Introduction

Critical assessments of the Al-Fe-P ternary system have been published by [1988Rag] and [1989Rag], where only three works ([1952Vog, 1965Kan1, 1965Kan2]) were included.
Information on Al-Fe-P phase relations appeared for the first time in the work of [1952Vog], where the phase equilibria of the Fe-Fe_2P-AlP-$Fe_{50}Al_{50}$ subsystem were studied. There was found that the AlP-Fe_2P and AlP-Fe_2Al_5 sections are the quasibinaries of the simple eutectic type and the $Fe_{50}Al_{50}(\alpha_2)$-AlP section is almost quasibinary eutectic (a quasibinary section exists between AlP and the α_2 (FeAl) phase saturated with Al and P). The liquidus surface, isothermal section and some temperature-compositions sections of the investigated part of this ternary system were constructed also by [1952Vog]. The data of [1952Vog] agree with those of [1965Kan1].
The solubility of P in (αFe) containing Al was investigated by [1965Kan2].
Some thermodynamic properties of the Al-Fe-P alloys were investigated by [1979Yam, 1983Yam, 1993Din] and amorphous phase formation in this system was discussed in [1983Ino].
Investigations of the system are listed in Table 1.

Binary Systems

Binary systems Al-P and Fe-P are accepted from [Mas2]. Al-Fe boundary system is taken from 2006MSIT].

Solid Phases

No ternary compounds were found in the Al-Fe-P system. All unary and binary phases are listed in Table 2. Solubility of P in (αFe), containing 1 at.% Al, increases linearly from about 0.7 at.% at 650°C to about 4 at.% at 1050°C and decreases from 4.4 at.% in pure (αFe) to 2.1 at.% at 7.9 at.% Al at 1000°C [1965Kan2].

Quasibinary Systems

The AlP-Fe_2P section belongs to the simple eutectic quasibinary systems, the eutectic at 1225°C is given as e_1(max) in Table 3. The AlP-Fe_2Al_5 section also constitutes a simple eutectic system [1952Vog].

Invariant Equilibria

The quantitatively determined invariant equilibria of [1952Vog] (Table 3) and the accepted binaries have been used to construct the reaction scheme of the Al-Fe-Fe_2P-AlP subsystem in Fig. 1. In addition to the four-phase reactions U_4 and E_2 [1952Vog] and the degenerated ternary eutectic D_3 in the Al corner six additional four-phase reactions (U_1, U_2, U_3, D_1, D_2 and E_1) have been estimated and shown in Fig. 1. These reactions are quantitatively fixed by the observed $Fe_{50}Al_{50}(\alpha_2)$-AlP equilibrium, which ensures the equilibria of AlP with the other Al-Fe phases and the extension of the AlP liquidus surface. The ordered phase Fe_3Al and the second order transition α/α_2 (αFe/FeAl) of the Al-Fe system have been omitted in Fig. 1. This reaction scheme differs from the one suggested by [1988Rag, 1989Rag] mainly by the incorporation of a liquidus of $FeAl_2$, which should emerge from the eutectic line e_2 in the vicinity of the peritectoid formation temperature of $FeAl_2$ at p_4. The estimated invariant temperatures are also different from those of [1988Rag, 1989Rag].

Liquidus Surfaces

The liquidus surface of the Fe-Fe_2P-AlP-Al subsystem is given in Fig. 2. The Al rich part, shown dashed, is estimated using the binaries and the ternary phase equilibria. The P solubilities in this part might be somewhat exaggerated.

DOI: 10.1007/978-3-540-69761-9_10

Isothermal Sections

The isothermal section of the Fe-Fe_2P-AlP-P subsystem at room temperature shown in Fig. 3 is redrawn from [1952Vog].

Temperature – Composition Sections

The vertical section AlP-$Fe_{50}Al_{50}$, which is between AlP and the α_2(FeAl) phase saturated with Al and P, is given in Fig. 4. The vertical sections at 6 and 9 mass% P and at 10 and 25 mass% Al are shown in Figs. 5 and 6, respectively (the Al-Fe solid phases in Figs. 5a, 5b and 6a have been collectively designated as α [1952Vog]).

Thermodynamics

Aluminium was found to increase the activity of P in liquid Fe at 1600°C, the interaction coefficients being $\varepsilon^{Al}_P = 4.6 \pm 0.7$ and $e^{Al}_P = 0.037$ [1979Yam, 1983Yam] (according to the thermodynamic calculation the value of this coefficients is equal $\varepsilon^{Al}_P = 8.78$ [1993Din]).

Miscellaneous

It was found that Al has a weak tendency to combine with P in steel because any phosphide phases except Fe_3P were not found in the Al-Fe-P ternary system [1965Kan1].

Amorphous phase formation with good ductility has been found in this ternary system by using a melt-spinning technique [1983Ino]. Formation of a completely amorphous phase was achieved for a wide range of compositions as shown in Fig. 7 (0 to 18 at.% Al and 13 to 21 at.% P). Crystallization temperature and Vickers hardness increase with increasing Al and P content and maximum values are attained at 448°C and 640 diamond pyramid number for $Fe_{66}Al_{16}P_{18}$ alloy. Their fracture strengths are about 2000 MPa. The activation energy for amorphous phase crystallization is estimated to be about 315 $kJ \cdot mol^{-1}$ for $Fe_{78}Al_4P_{18}$ and 340 $kJ \cdot mol^{-1}$ for $Al_8Fe_{74}P_{18}$ [1983Ino].

Treatments of a pure Al melt at 800°C with the equivalent of 200 to 800 mass ppm P by means of an Al-Fe-P addition prior to casting results in a distribution of polyhedral AlP particles of medium size ~6 to 9 mkm with some tendency of cluster at the higher levels of addition [2001Kyf].

Table 1. Investigations of the Al-Fe-P Phase Relations, Structures and Thermodynamics

Reference	Method/Experimental Technique	Temperature/Composition/Phase Range Studied
[1952Vog]	DTA, metallography	up to 1500°C / Fe-Fe_2P-AlP-Al
[1965Kan1]	XRD, chemical analysis	800°C / 3.78 at.% Al + 91.75 at.% Fe + 4.47 at.% P and 7.51 at.% Al + 88.23 at.% Fe + 4.26 at.% P
[1965Kan2]	DTA, XRD	650 - 1050°C
[1979Yam], [1983Yam]	Knudsen cell mass spectrometry	1600°C
[1983Ino]	DTA, DSC, XRD, TEM, Vickers microhardness testing	up to 500°C / Al-Fe-P
[1993Din]	Calculation	1600°C / Al-Fe-P
[2001Kyf]	SEM with EDS	800°C / Al-Fe-P

DOI: 10.1007/978-3-540-69761-9_10

Table 2. Crystallographic Data of Solid Phases

Phase/Temperature Range [°C]	Pearson Symbol/ Space Group/ Prototype	Lattice Parameters [pm]	Comments/References
(αAl) < 660.452	*cF*4 $Fm\bar{3}m$ Cu	*a* = 404.96	at 25°C [Mas2]
δ, (δFe) 1538 - 1394	*cI*2 $Im\bar{3}m$ W	*a* = 293.15	[Mas2]
γ, (γFe) 1394 - 912	*cF*4 $Fm\bar{3}m$ Cu	*a* = 364.67	at 915°C [V-C2, Mas2]
α, (αFe) < 912	*cI*2 $Im\bar{3}m$ W	*a* = 286.65	at 25°C [Mas2]
(P) (red) < 417	*c**66	 *a* = 1131	sublimation at 1 bar triple point at 576°C, >36.3 bar; triple point at 589.6 at 1 atm [Mas2] [V-C2]
(P) (white) < 44.14	*c*** ? P (white)	*a* = 718	at 25°C [Mas2] common form of elemental P, probably less stable than P (red) at 25°C [Mas2]
(P) (black)	*oC*8 *Cmca* P (black)	*a* = 31.36 *b* = 1047.8 *c* = 437.63	at 25°C [Mas2]
AlP < 2530 ± 50	*cF*8 $F\bar{4}3m$ ZnS	*a* = 546.25 ± 0.05	[V-C2, Mas2]
α_2, $FeAl_x$ < 1310	*cP*2 $Pm\bar{3}m$ CsCl	*a* = 290.80	23.3 to ~55 at.% Al [V-C2, Mas2]
Fe_3Al < 550	*cF*16 $Fm\bar{3}m$ BiF_3	*a* = 579.1	~23 to ~34 at.% Al [V-C2, Mas2]
ε, Fe_2Al_3 1232 - 1102	*cI*16? ? ?	-	~58 to ~65 at.% Al [V-C2, Mas2]
$FeAl_2$ < 1153	*aP*18 *P*1 $FeAl_2$	*a* = 487.8 ± 0.1 *b* = 646.1 ± 0.2 *c* = 880.0 ± 0.3 α = 91.75° β = 73.27°	66 to 66.9 at.% Al [V-C2, Mas2]

(*continued*)

DOI: 10.1007/978-3-540-69761-9_10

Phase/Temperature Range [°C]	Pearson Symbol/ Space Group/ Prototype	Lattice Parameters [pm]	Comments/References
		$\gamma = 96.89°$	
Fe_2Al_5 < 1169	*oC*16 *Cmcm* Fe_2Al_5	*a* = 764.4 *b* = 641.1 *c* = 422.0	70 to 73 at.% Al [V-C2, Mas2]
$FeAl_3$. 1160	*mC*102 *C2/m* $FeAl_3$	*a* = 1550.9 ± 0.3 *b* = 806.6 ± 0.2 *c* = 1246.9 ± 0.2 $\beta = 107.72 \pm 0.02°$	74.5 to 76.6 at.% Al [V-C2, Mas2]
Fe_2Al_9	*mP*22 $P2_1/c$ Co_2Al_9	-	metastable phase [Mas2]
$FeAl_6$	*oC*28 $Cmc2_1$ $MnAl_6$	a = 743.7 b = 649.2 c = 422.0	metastable phase [V-C2, Mas2]
Fe_3P < 1166	*tI*32 $I\bar{4}$ Ni_3P	*a* = 910.0 *c* = 445.92 *a* = 913.7 *c* = 450.62 *a* = 917.4 *c* = 452.99	at 22°C; at 414°C; at 678°C, mineral Schreibersite [V-C2, Mas2]
Fe_2P < 1370	*hP*9 $P\bar{6}2m$ Fe_2P	*a* = 586.75 ± 0.02 *c* = 345.81 ± 0.02	33.3 to 34 at.% P, mineral Barringerite [V-C2, Mas2]
Fe_2P	*oP*12 *Pnma* Co_2Si	*a* = 577.5 *b* = 357.1 *c* = 664.1	high-pressure phase [V-C2, Mas2]
FeP	*oP*8 *Pmna* MnP	*a* = 519.10 *b* = 309.83 *c* = 579.09	[V-C2, Mas2]
FeP_2	*oP*6 *Pnnm* FeS_2	*a* = 497.29 ± 0.07 *b* = 565.68 ± 0.08 *c* = 272.30 ± 0.04	66 to 67 at.% P [V-C2, Mas2]

(*continued*)

DOI: 10.1007/978-3-540-69761-9_10

Phase/Temperature Range [°C]	Pearson Symbol/ Space Group/ Prototype	Lattice Parameters [pm]	Comments/References
FeP_4	*mP*30 $P2_1c$ FeP_4	a = 461.9 ± 0.1 b = 1367.0 ± 0.2 c = 700.2 ± 0.1 β = 101.48°	[V-C2, Mas2]
	or		
	*mC*40 *C*2/*c* FeP_4	a = 505.43 ± 0.07 b = 1040.7 ± 0.2 c = 1106.9 ± 0.2 β = 91.14 ± 0.01°	at 20°C [V-C2, Mas2]
FeP_4(HP)	*oC*12 $C222_1$ FeP_4	a = 500.5 ± 0.1 b = 1021.3 ± 0.3 c = 553.0 ± 0.1	high-pressure phase [V-C2, Mas2]

Table 3. Invariant Equilibria

Reaction	T [°C]	Type	Phase	Composition (at.%)		
				Al	Fe	P
$L + Fe_3P \rightleftharpoons \alpha + Fe_2P$	1020	U_4	L	14.01	67.68	18.31
			Fe_3P	0	75	25
			α	25.0	73.14	1.86
			Fe_2P	0	67	33
$L \rightleftharpoons \alpha_2 + AlP + Fe_2P$	995	E_2	L	27.53	55.54	16.93
			α_2	45.48	52.88	1.64
			AlP	50	0	50
			Fe_2P	0	67	33
$L \rightleftharpoons Fe_2P + AlP$	1225	e_1(max)	L	5.09	60.2	34.71
			Fe_2P	0	67	33
			AlP	50	0	50
$L \rightleftharpoons \alpha_2 + AlP$	1125	e_3(max)	L	50.84	41.19	7.97
			α_2	50.89	47.49	1.62
			AlP	50	0	50

MSIT®
DOI: 10.1007/978-3-540-69761-9_10

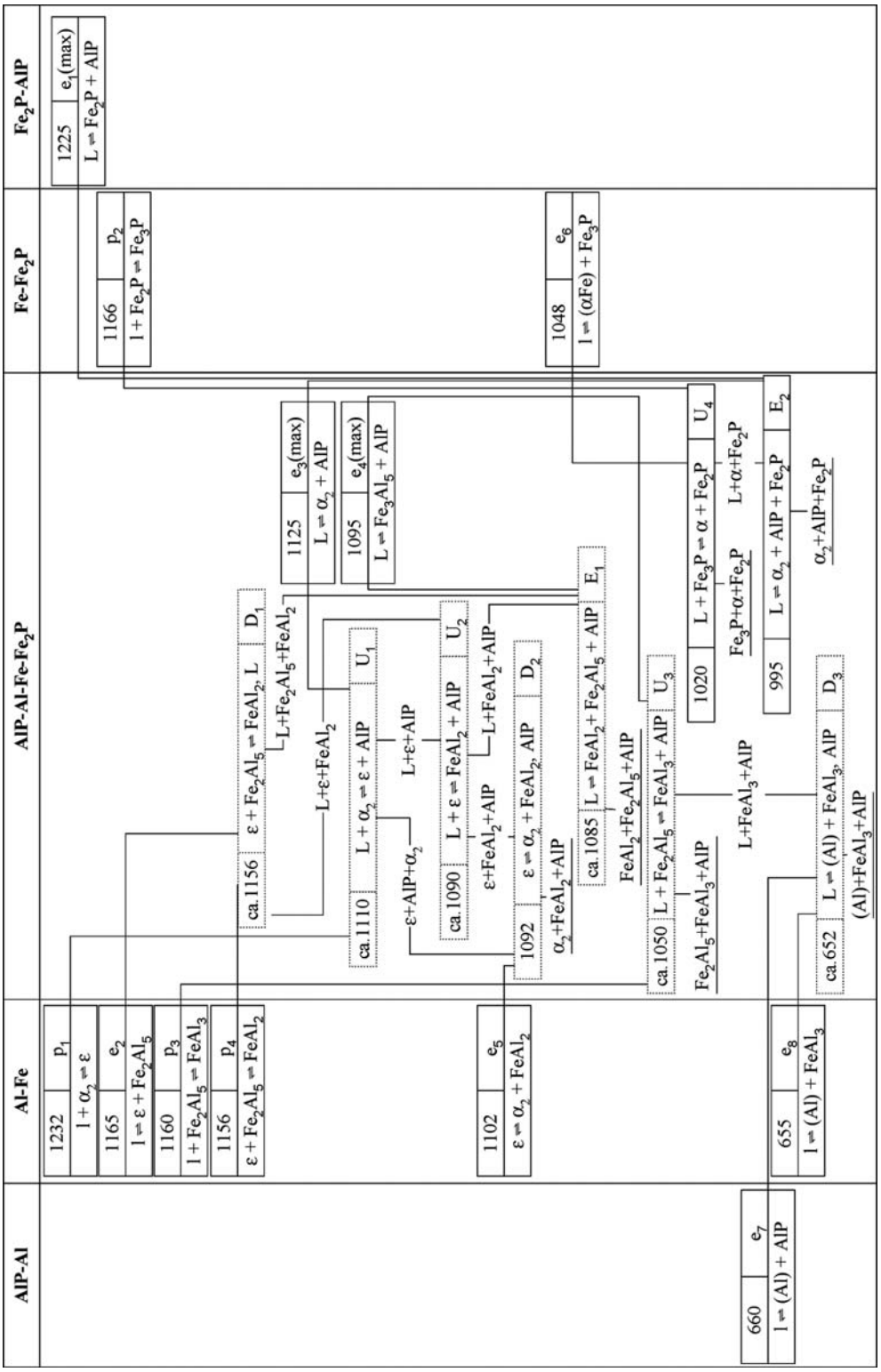

Fig. 1. Al-Fe-P. Reaction scheme

DOI: 10.1007/978-3-540-69761-9_10

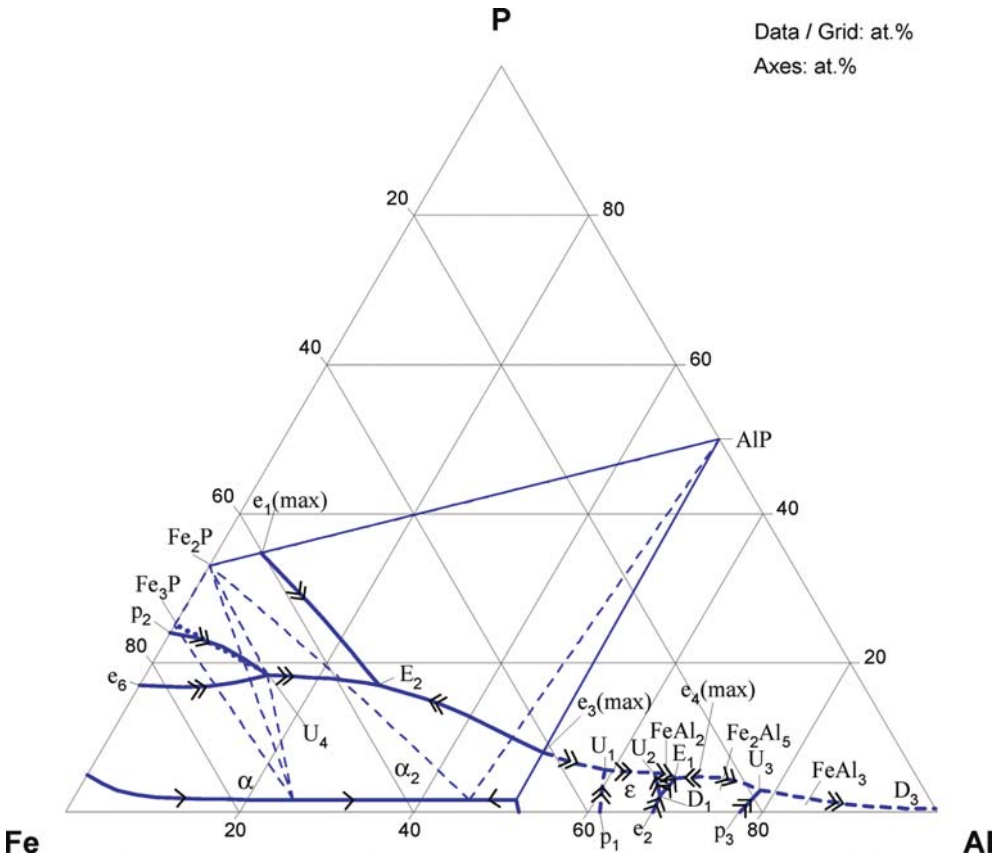

Fig. 2. Al-Fe-P. Liquidus surface of the Fe-Fe_2P-AlP-P subsystem

DOI: 10.1007/978-3-540-69761-9_10

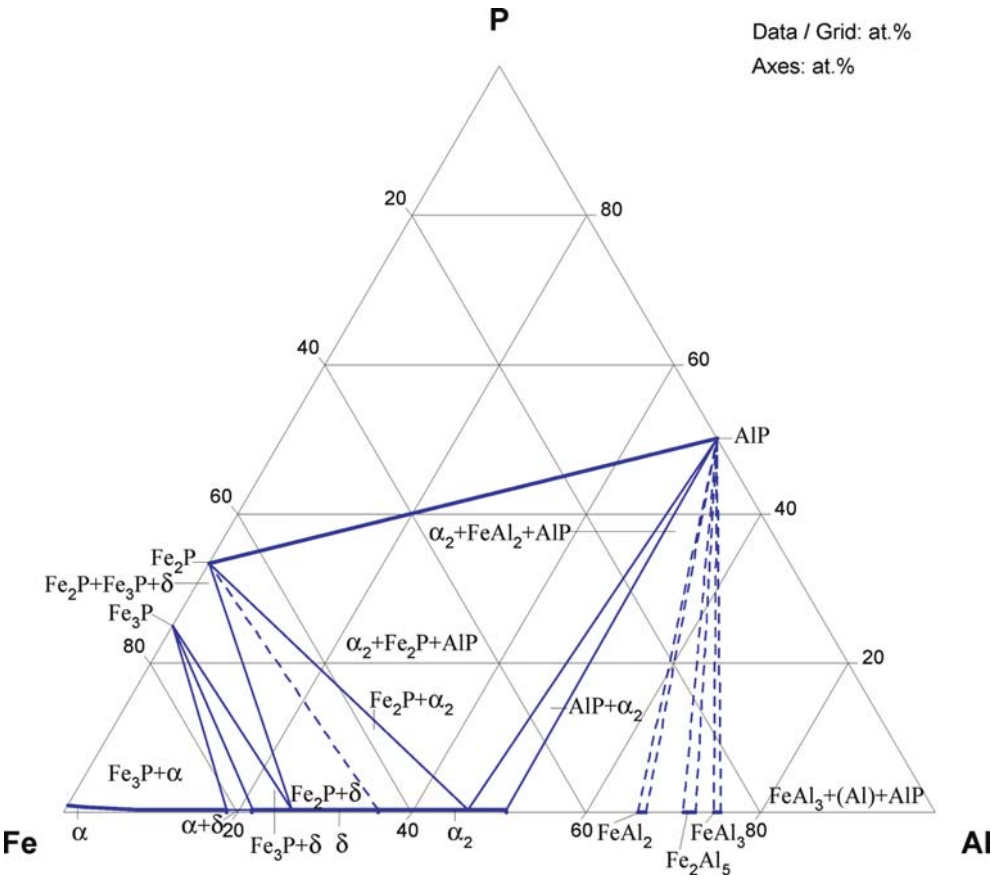

Fig. 3. Al-Fe-P. Isothermal section of the Fe-Fe$_2$P-AlP-P subsystem at room temperature

DOI: 10.1007/978-3-540-69761-9_10

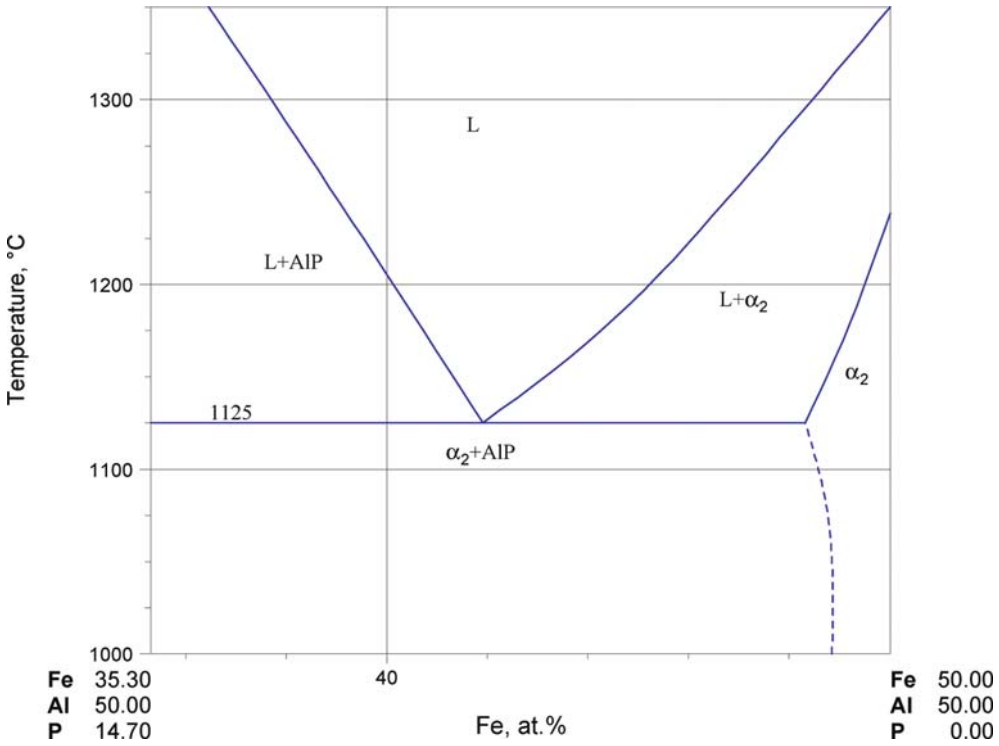

Fig. 4. Al-Fe-P. Partial vertical section AlP-$Fe_{50}Al_{50}$

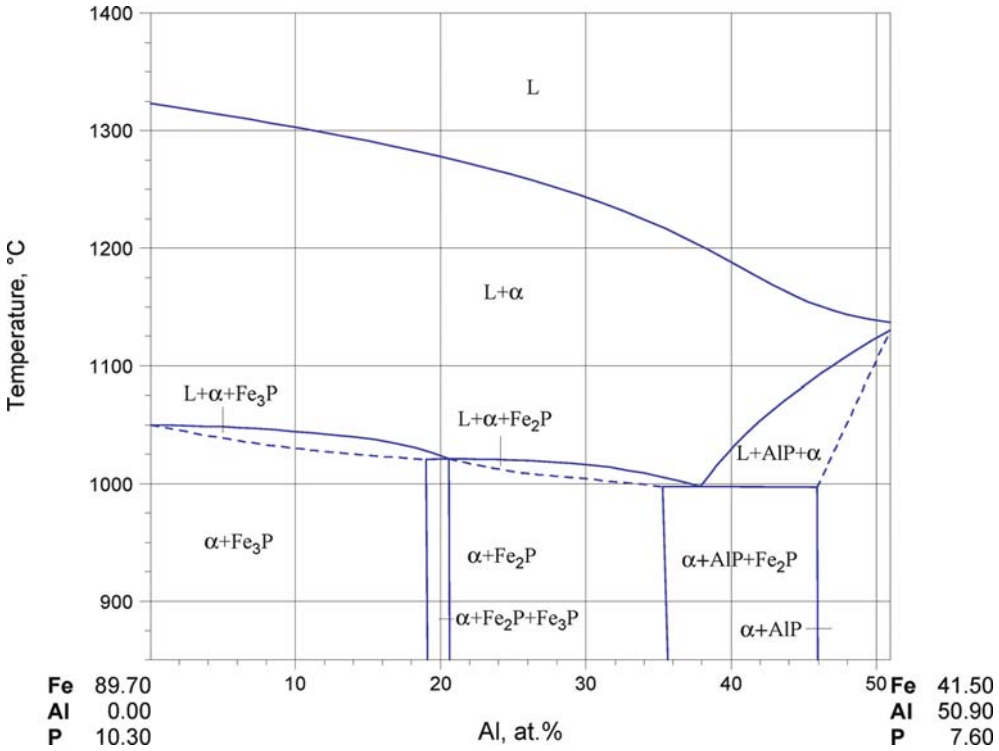

Fig. 5a. Al-Fe-P. Partial vertical section at 6 mass% P

DOI: 10.1007/978-3-540-69761-9_10

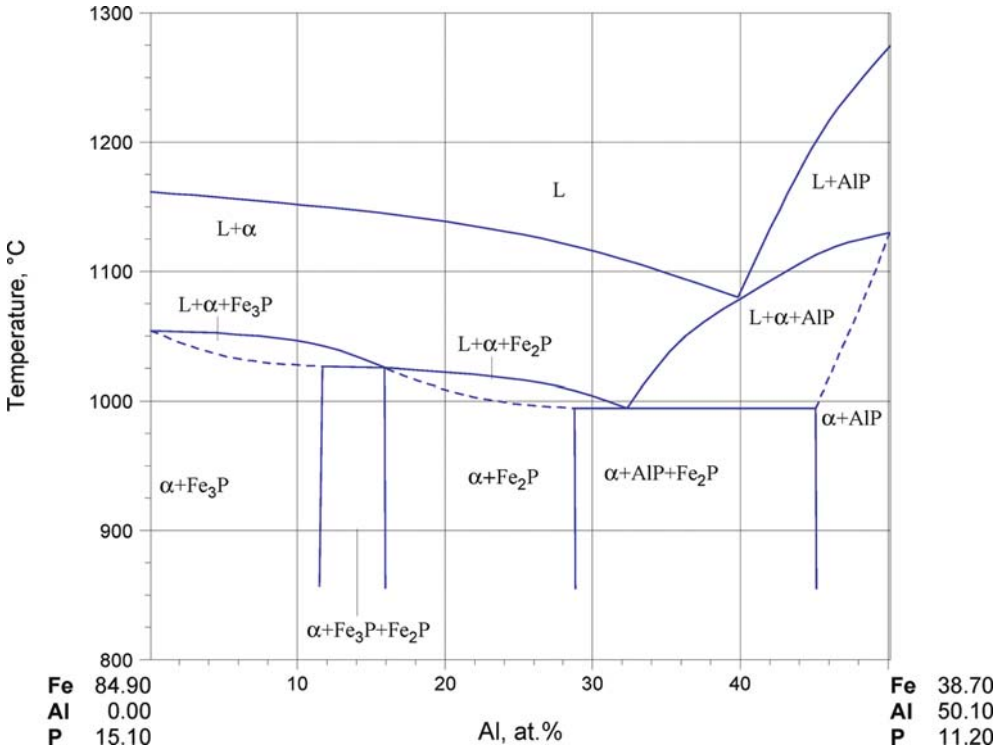

Fig. 5b. Al-Fe-P. Partial vertical section at 9 mass% P

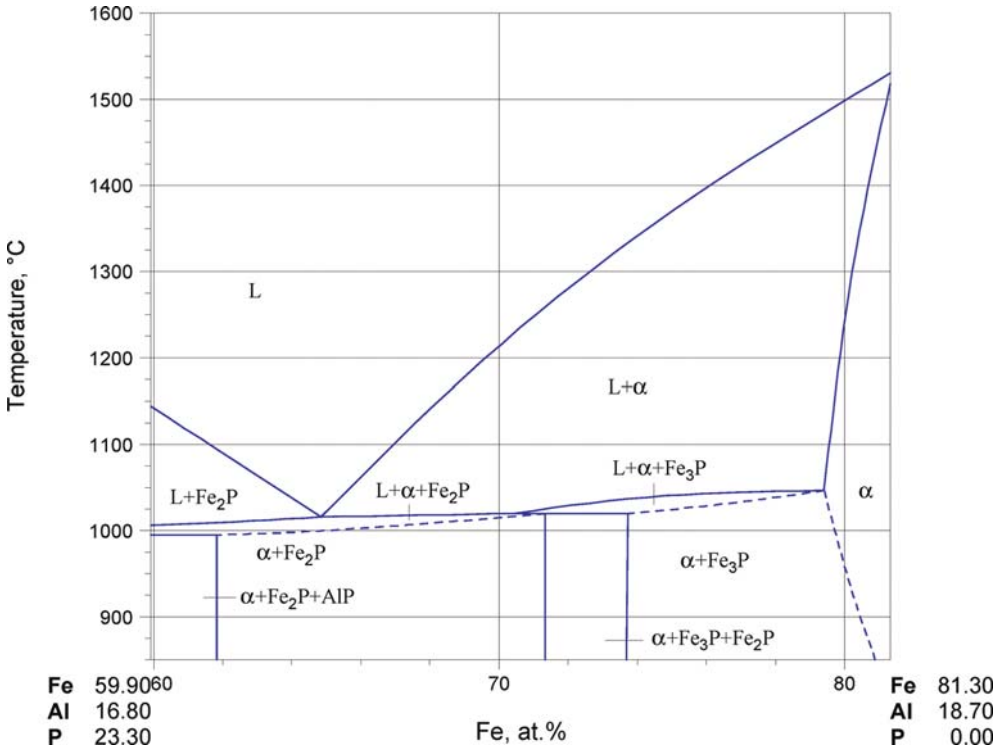

Fig. 6a. Al-Fe-P. Partial vertical section at 10 mass% Al

DOI: 10.1007/978-3-540-69761-9_10

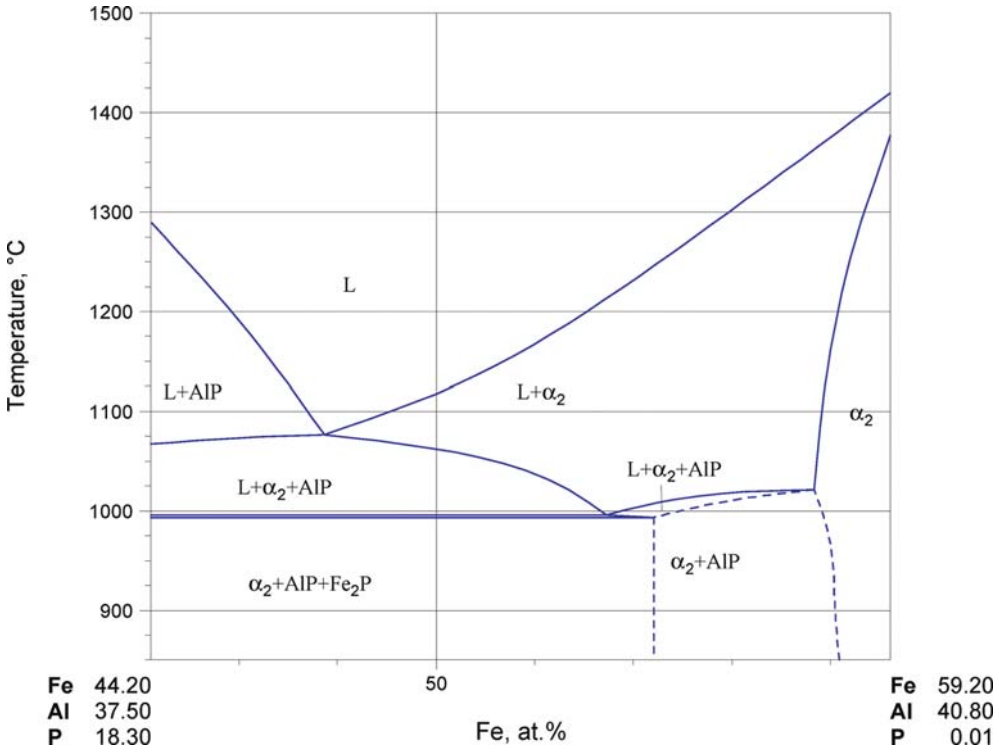

Fig. 6b. Al-Fe-P. Partial vertical section at 25 mass% Al

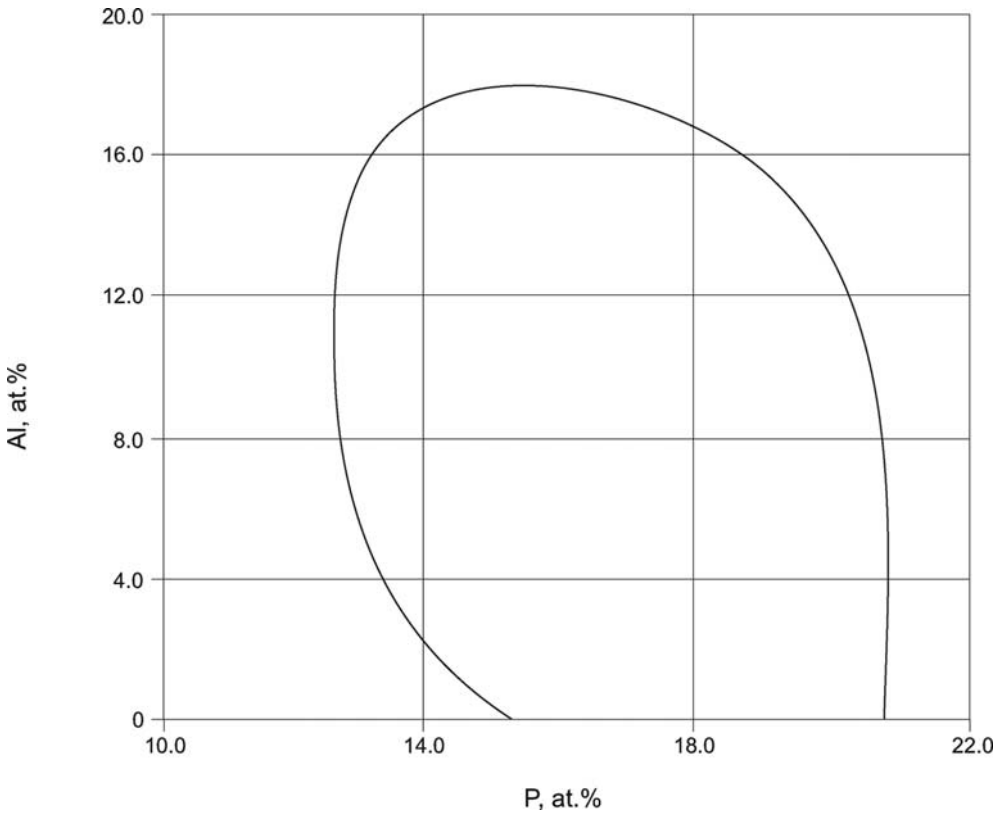

Fig. 7. Al-Fe-P. Range of glass state

DOI: 10.1007/978-3-540-69761-9_10

References

[1952Vog] Vogel, R., Klose, H., "The Iron-Iron Phosphide-Aluminium Phosphide-Aluminium Phase Diagram" (in German), *Arch. Eisenhuettenwes.*, **23**(7–8), 287–291 (1952) (Experimental, Morphology, Phase Diagram, #, *, 4)

[1965Kan1] Kaneko, H., Nishizawa, T., Tamaki, K., "Phosphide-Phases in Ternary Alloys of Iron, Phosphorus and Other Elements" (in Japanese), *Nippon Kinzoku Gakkai-shi*, **29**(2), 159–165 (1965) (Experimental, Morphology, Phase Diagram, Phase Relations, 24)

[1965Kan2] Kaneko, H., Nishizawa, T., Tamaki, K., Tanifuji, A., "Solubility of Phosphorus in α and γ Iron" (in Japanese), *Nippon Kinzoku Gakkai Shi*, **29**(2), 166–170 (1965) (Experimental, Phase Relations, 20)

[1979Yam] Yamada, K., Kato, E., "Mass Spectrometric Determination of Activities of Phosphorus in Liquid Fe-P-Si, Al, Ti, V, Cr, Co, Ni, Nb and Mo Alloys" (in Japanese), *Tetsu-to-Hagane (J. Iron Steel Inst. Jap.)*, **65**(2), 273–280 (1979) (Experimental, Thermodyn., 40)

[1983Ino] Inoue, A., Kitamura, A., Masumoto, T., "The Effect of Aluminium on Mechanical Properties and Thermal Stability of (Fe,Ni)-Al-P Ternary Amorphous Alloys", *J. Mater. Sci.*, **18**, 753–758 (1983) (Experimental, Phase Relations, Mechan. Prop., Thermodyn., #, 11)

[1983Yam] Yamada, K., Kato, E., "Effect of Dilute Concentrations of Si, Al, Ti, V, Cr, Co, Ni, Nb and Mo on the Activity Coefficient of P in Liquid Iron", *Trans. Iron Steel Inst. Jap.*, **23**(1), 51–55 (1983) (Experimental, Thermodyn., 16)

[1988Rag] Raghavan, V., "The Al-Fe-P (Aluminium-Iron-Phosphorus) System", in "*Phase Diagrams of Ternary Iron Alloys*", **3**, 9–16 (1988) (Review, Crys. Structure, Phase Diagram, Phase Relations, 5)

[1989Rag] Raghavan, V., "The Al-Fe-P System (Aluminium-Iron-Phosphorus)", *J. Alloy Phase Diagrams*, **5**(1), 32–39 (1989) (Review, Crys. Structure, Phase Diagram, Phase Relations, 5)

[1993Din] Ding, X., Wang, W., Han, Q., "Thermodynamic Calculation of Fe-P-j System Melt" (in Chinese), *Acta Metall. Sin. (China)*, **29**(12), B527-B532 (1993) (Calculation, Theory, Thermodyn., 7)

[2001Kyf] Kyffin, W.J., Rainforth, W.M., Jones, H., "The Formation of Aluminum Phosphide in Aluminum Melt Treated with an Al-Fe-P Inoculant Addition", *Z. Metallkd.*, **92**(4), 396–398 (2001) (Experimental, Morphology, 14)

[2006MSIT] "Al-Fe (Aluminum-Iron)", Diagrams as Published, in *MSIT Workplace*, Effenberg, G. (Ed.), Materials Science International Services, GmbH, Stuttgart; Document ID: 30.10236.1.20, (2006) (Crys. Structure, Phase Diagram, Phase Relations, 11)

[V-C2] Villars, P. and Calvert, L.D., *Pearson's Handbook of Crystallographic Data for Intermetallic Phases*, 2nd edition, ASM, Metals Park, Ohio (1991)

[Mas2] Massalski, T.B. (Ed.), *Binary Alloy Phase Diagrams*, 2nd edition, ASM International, Metals Park, Ohio (1990)

DOI: 10.1007/978-3-540-69761-9_10

Aluminium – Iron – Silicon

Gautam Ghosh

Introduction

The ternary system contains, and also forms the basis for, many alloys in engineering applications, such as cast aluminium alloys, foil and sheet products for food packaging, capacitors, lithographic printing sheets, soft magnetic alloys for transformers. In addition, iron and silicon originating from bauxite ore and anode material are present in nearly all industrial Al alloys, and the metallurgical grade silicon contains, among others, aluminum and iron as impurities.

Iron has a strong influence on the porosity, mechanical properties and extrusion characteristics of Al-Si castings, which are governed by the amount and morphology of Fe containing intermetallics. Furthermore, the morphology and stability of intermetallics in commercial Al-Si castings are affected by other transition metals such as cobalt, chromium, manganese and strontium that may be present either as impurities or as intentional additions. It is generally agreed that the elimination of plate-shaped and Chinese-script intermetallic phases results in an improvement of mechanical properties of Al-Si castings.

Due to these reasons, there have been numerous experimental studies on the characterization of intermetallics (morphology, composition and crystal structure) and phase equilibria of the ternary system. A summary of experimental studies of phase equilibria is given in Table 1. The experimental results have been reviewed from time to time [1934Fus, 1937Ser, 1943Mon, 1950Gme, 1952Han, 1959Phi, 1968Dri, 1979Mor, 1981Riv, 1981Wat, 1985Riv, 1987Pri, 1988Ray, 1992Gho, 1992Zak, 1994Rag, 2002Rag, 2005Gho].

The system is characterized by a large number of ternary phases, both stable and metastable, and at least twenty ternary invariant reactions during solidification which impart difficulties in establishing the phase equilibria of the system. The difficulties are further augmented by the effects of metastability, impurity elements, incomplete reactions, undercooling, and many solid-state reactions which are not well understood.

Many earlier works by [1923Dix, 1923Han, 1923Wet, 1924Fus, 1934Roe, 1941Pan] reported primarily the microstructures of Al rich alloys. [1951Ran] determined the phase boundaries of the Al corner at 475°C by diffusional anneal technique. Due to extensive investigations [1927Gwy, 1933Nis, 1936Jae, 1937Ura, 1943Phi, 1951Hol, 1951Now, 1967Mun, 1987Gri1, 1987Ste], the phase equilibria of Al corner are well established.

The first comprehensive study of phase equilibria of the entire system was performed by [1940Tak]. They used electrolytic iron, pure aluminium and metallic silicon (unspecified purity). Over 150 ternary alloys were prepared using master alloys of selected compositions in an arc furnace, under hydrogen atmosphere with NaCl as flux on the molten surface of the alloys, followed by cooling at a rate of 2 to 3°C per 5 to 10 sec. In some cases, in order to confirm and identify solid-state reactions, the cooling curves were supplemented by heating runs. [1940Tak] employed metallography, thermal, X-ray, magnetic and dilatometric analyses to establish the phase equilibria. They reported six ternary phases which form by peritectic reactions. They also presented several vertical sections from 500°C up to the liquidus temperature. Based on these results, [1981Riv, 1988Ray] constructed a probable isothermal section at 1000°C.

[1968Lih] studied the Fe corner up to 50 at.% Al and 35 at.% Si using DTA, magnetometry, microhardness and X-ray diffraction techniques. The phase equilibria involving ordered and disordered phases in Fe rich alloys were determined by [1982Miy] and [1986Miy] in the temperature range of 450 to 700°C using transmission electron microscopy.

Due to their importance in commercial Al alloys, there have been renewed interests on the phase equilibria of Al corner. [1987Gri1] and [1987Ste] studied the phase equilibria of Al corner, using alloys up to 14 at.% Si and 35 at.% Fe, by means of thermal analysis, X-ray diffraction and electron probe microanalysis techniques. They reported a partial liquidus surface, and partial isothermal sections at 570 and 600°C. However,

DOI: 10.1007/978-3-540-69761-9_11

the latter results were slightly modified by [1987Pri] to make them consistent with thermodynamic rules of phase diagram construction.
[1981Zar] reported ten ternary phases, and an isothermal section at 600°C. [2001Kre] determined a partial isothermal section at 550°C. About 100 alloys, containing up to 50 at.% Fe and 50 at.% Si, were used [2001Kre]. The phase relations were established by means of optical metallography, EDS analysis of the phases, and X-ray diffraction methods. [2002Gup, 2002Mai] performed diffusion couple (between pure Fe and Al-Si alloy) experiments in the temperature range of 600 to 1100°C, followed by quenching the specimens. They reported five isothermal sections based on the microstructural observations and composition analysis (by EPMA) of phases in as-quenched specimens.
Thermodynamic properties of ternary alloys were measured by emf method [1970Mit, 1973Nag, 1980Sud, 1984Ber, 1989Bon, 2004Kan] and calorimetry [1937Koe, 1937Oel, 1997Vyb, 2000Li1, 2000Li2, 2003Kan]. In addition, thermodynamic datasets of the ternary system were also assessed within calphad formalism [1994Ang, 1998Kol, 1999Liu].

Binary Systems

The Al-Si binary phase diagram is accepted from [2004Luk]; the Al-Fe binary phase diagram is accepted from [2006MSIT]; and the Fe-Si binary phase diagram is accepted from [1982Kub]. However, the Al-Fe phase diagram has undergone slight modification due to recently established congruent melting behavior of the Fe_4Al_{13} phase [1960Lee, 1986Len].

Solid Phases

As far as the binary intermetallics are concerned, here we consider only those are present in the accepted phase diagrams. For example, direct chill-cast of commercially pure Al alloys are reported to contain Al-Fe intermediate phases that are not present in the equilibrium phase diagram [1977Sim, 1982Wes, 1985Don2, 1986Liu1, 1986Liu2, 1987Cha, 1987Skj1, 1987Skj2, 1987Ste, 1988Cha, 1988Liu2]. Therefore, they are not considered in constructing the ternary phase diagrams.
At 550°C, the solubility of Fe and Si in (Al) is less than 1 at.% [2001Kre], and that of Fe and Al in (Si) is extremely small.
The Fe_4Al_{13} phase is reported to dissolve 0.8 mass% Si [1955Arm], 0.2 mass% Si [1967Sun], 1.0 mass% Si [1984Don], 2.9 mass% Si [1987Skj1], up to 6.0 mass% Si at 600°C [1987Ste], 4 at.% Si at 550°C [2001Kre], and 5 to 6 at.% Si in the temperature range of 800 to 1115°C [2002Mai]. This is associated with an increase in the *a*-lattice parameter and a decrease in the *b*-lattice parameter; whereas no significant changes in the *c*-lattice parameter and β were detected [1987Ste]. The composition dependence of *a*- and *b*-lattice parameters in Fe_4Al_{13} is expressed by [1987Ste] as

$$a\ (\text{in pm}) = 1505.0 + 1.14 \cdot W_{Fe} - 0.41 \cdot W_{Si}$$

$$b\ (\text{in pm}) = 862.8 - 1.41 \cdot W_{Fe} - 1.3 \cdot W_{Si}$$

where W_{Fe} and W_{Si} are the mass% of Fe and Si, respectively. A detailed crystallographic analysis of the Fe_4Al_{13}, by means of convergent beam electron diffraction and high resolution electron microscopy, has been performed by [1987Skj3]. Lattice images revealed that the Fe_4Al_{13} crystals are divided into tiny domains (few thousand pm) which are separated by lattice displacements such as stacking faults [1987Skj2, 1987Skj3].
Available data indicate that the solid solubility of Si in Fe_2Al_5 decreases from about 4.5 at.% at 1020°C to about 1.5 at.% at 600°C [2002Gup, 2002Mai]. Fe_2Al_3 may dissolve up to 11 at.% Si at 1115°C [2002Gup]. At 550°C, $FeAl_2$ dissolves about 1 at.% Si, and Fe_2Al_5 dissolves about 2 at.% Si [2001Kre].
Initial studies showed that the $FeSi_2$(h) phase dissolves up to about 0.5 mass% Al [1961Sab, 1965Sab, 1965Skr, 1968Sab1, 1968Sab2] which is accompanied by a small increase in both the *a*- and *c*-lattice parameters. However, later it was found that $FeSi_2$ dissolves up to 10 at.% Al [1994Ang, 1995Gue3]. The FeSi phase also dissolves substantial amount of Al [1996Szy, 1998Dit], and at 550°C it is about 10 at.%

DOI: 10.1007/978-3-540-69761-9_11

with Al substituting Si [2001Kre]. The ambient temperature lattice parameters of FeSi, $FeSi_2$(h) and $FeSi_2$(r) as functions of Al content were reported by [1996Szy]:

For FeSi: a (in pm) $= 448.1 + 5.4x_{Al}$

For $FeSi_2$(h): a (in pm) $= 269.1 + 179x_{Al}$

c (in pm) $= 515.7 + 30.2x_{Al}$

For $FeSi_2$(r): a (in pm) $= 986.6 + 7.3x_{Al}$

b (in pm) $= 778.7 + 10.3x_{Al}$

c (in pm) $= 782.1 + 27.6x_{Al}$

where x_{Al} is the atomic fraction of Al.

The Fe_3Al and Fe_3Si phases form a continuous solid solution. The lattice parameter of the alloys along Fe_3Al-Fe_3Si and $Fe_{73}Al_{27}$-$Fe_{73}Si_{27}$ sections and also for the commercial SENDUST and ALSIFER 32 alloys were determined systematically and accurately by [1979Cow]. The composition dependence of the lattice parameter can be expressed as:

Along the Fe_3Al-Fe_3Si section

$$a \text{ (in pm)} = 565.54 + 12.846 \cdot W + 1.896 \cdot W^2 - 0.7245 \cdot W^3$$
$$= 565.54 + 12.776 \cdot C + 1.9522 \cdot C^2 - 0.7094 \cdot C^3$$

where W = mass fraction of Fe_3Al and C = mole fraction of Fe_3Al.

Along the $Fe_{73}Al_{27}$-$Fe_{73}Si_{27}$ section

$$a \text{ (in pm)} = 564.462 + 11.964 \cdot W + 5.3929 \cdot W^2 - 2.5 \cdot W^3$$
$$= 564.462 + 11.915 \cdot C + 5.3183 \cdot C^2 - 2.321 \cdot C^3$$

where W = mass fraction of $Fe_{73}Al_{27}$ and C = mole fraction of $Fe_{73}Al_{27}$.

[1979Cow] attributed small, but consistent, deviations from the linear dependence on composition, along both sections, to the incomplete ordering as Al is replaced by Si. [1979Bur] also reported limited lattice parameter data along Fe_3Al-Fe_3Si section which are in reasonable agreement with those of [1979Cow], but [1979Bur] assumed a linear dependence of lattice parameter on composition (see also [1977Nic1], [1977Nic2]). [1968Lih] reported lattice parameters of ternary alloys up to 30 at.% Si and 47 at.% Al at 20, 500, 600 and 900°C. [1946Sel] also measured the lattice parameter of ternary alloys up to 18 mass% Si and 13 mass% Al. The lattice parameter of Fe_3(Al,Si) containing about 10 mass% Al and 5 mass% Si is reported to be 570 ± 3 pm [1978Xu]. The lattice parameter of an Fe-5.5 mass% Al-9.7 mass% Si alloy is reported to be 568.4 pm after water quenching and 568.54 pm after annealing for 24 h at 600°C.

The complexity of phase equilibria of the Al-Fe-Si system is primarily due to the occurrence of many ternary phases, and the associated metallurgical reactions during solidification, and also in the solid state. While some of these ternary phases are stable, some are metastable. In recent years, the detailed crystallographic characterization of stable phases have been performed; however, the current crystallographic data of many metastable ternary phases are far from being complete. The difficulties of complete crystallographic characterization of these phases are due to (i) the occurrence of several phases over a relatively narrow composition range in the Al corner, (ii) their complex crystal structures along with the presence of high density of planar defects, (iii) the order-disorder reactions in the Fe corner, (iv) many invariant reactions which under normal experimental conditions (both during solidification and during heat treatments) do not undergo completion, and (v) the effect of heterogeneous nucleation on the phase selection during solidification. In the past decades a large number of ternary phases in the Al-Fe-Si system have been reported. A chronological survey of these ternary phases is given in Table 2, where it may be noted that some of the results are still controversial.

Nine ternary phases are accepted for the construction of phase diagrams. These are labeled as τ_1/τ_9 to τ_{10}. Among these, [1940Tak] reported six ternary phases (τ_1/τ_9 to τ_6), four of which (τ_2, τ_4, τ_5 and τ_6) could be identified without much difficulty. Their investigation was mainly based on thermal analysis and microstructural examination, supplemented by limited X-ray diffraction. The details of the crystal structures and lattice parameters of stable solid phases are listed in Table 3. The composition ranges of the equilibrium

DOI: 10.1007/978-3-540-69761-9_11

ternary phases reported by different authors are plotted in Fig. 1. It may be noted that while most of the composition ranges are isolated from each other, there are overlapping composition ranges among τ_2, τ_3, τ_4 and τ_{10} phases.

The τ_1 phase has a triclinic structure, and its composition is represented nominally as $Fe_3Al_2Si_3$ [1996Yan]. A careful analysis of X-ray diffraction data established that the previously assigned τ_1 and τ_9 [1992Gho] are actually the same phase [2001Kre], thus designated as τ_1/τ_9 in this assessment. The τ_1 phase corresponds to the K_1 phase of [1940Tak] and the E phase of [1981Zar], while τ_9 [1992Gho] corresponds to the D phase of [1981Zar]. [2001Kre] also confirmed the triclinic structure [1996Yan] of τ_1/τ_9. At 550°C, τ_1/τ_9 coexists with Fe_2Al_5, Fe_4Al_{13}, α_2, FeSi, τ_2, τ_3, τ_7, τ_{10}, and possibly τ_8 [2001Kre].

The τ_2 phase (often designated as (γ-AlFeSi) corresponds to the K_2 phase of [1940Tak] and the K phase of [1981Zar]. [1981Zar] represented its homogeneity range as $Fe_{22}Al_{52\text{-}63}Si_{15\text{-}26}$, while [2001Kre] represented as $Fe(Al_{1-x}Si_x)_7$, with $0.2 \le x \le 0.33$. As seen in Table 3, three crystal structures of τ_2 have been reported. [2001Kre] indexed the X-ray diffraction pattern of τ_2 using the monoclinic unit cell proposed by [1967Mun]. At 550°C, τ_2 coexists with Fe_4Al_{13}, τ_1/τ_9, τ_3, τ_4, τ_5, τ_6 and τ_7 [2001Kre].

The τ_3 phase corresponds to the K_3 phase of [1940Tak] and the G phase of [1981Zar]. It has a negligible homogeneity range [2001Kre]. The composition of τ_3 is represented as $FeAl_2Si$ [1981Zar], but the EDX analysis of [2001Kre] gave $Fe_{25}Al_{56\pm1}Si_{19\pm1}$, or $Fe(Al_{1-x}Si_x)_3$, with $x = 0.25$. On the other hand, [1989Ger2] reported its composition as $Fe(Al_{1-x}Si_x)_3$, with $x = 0.33$ based on XRD analysis. [2001Kre] suggested that it is impossible to detect such a small difference in Al/Si-ratio based on XRD analysis. Its structure has been confirmed to be orthorhombic [1974Mur, 1981Zar, 1989Ger2, 2001Kre]; however, there is a scatter in the lattice parameter values. At 550°C, τ_3 coexists with Fe_4Al_{13}, τ_1/τ_9, τ_2 and τ_{10} [2001Kre].

The τ_4 phase (often designated as δ-AlFeSi) corresponds to the K_4 phase of [1940Tak] and the A phase of [1981Zar]. It is single phase at the composition $Fe(Al_{0.6}Si_{0.4})_5$ [2001Kre]. The tetragonal structure of the τ_4 phase was first reported by [1936Jae], and subsequently confirmed by several others [1950Phr, 1969Pan, 1974Mur, 2001Kre, 2006Kra]. Convergent beam electron diffraction of perfect crystals confirmed its space group as *I*4/*mcm*; however, the space group reduces to *P*4/*mcm* due to the presence of defects [2006Kra]. At 550°C, τ_4 coexists with (Si), τ_2, τ_6 and τ_7 [2001Kre].

The τ_5 phase (often designated as α-AlFeSi) corresponds to the K_5 phase of [1940Tak] and the M phase of [1981Zar]. Its stoichiometry may be described as $Fe_{46}(Al_{0.875}Si_{0.125})_{200-x}$, with $x \approx 7$ [2001Kre]. The hexagonal structure of the τ_5 phase was first reported by [1953Rob], and subsequently confirmed by [1967Mun, 1975Bar, 1977Cor, 1977Hoi, 1987Gri2, 1997Vyb, 2001Kre]. In the earlier studies [1950Phr, 1952Arm, 1955Arm, 1967Coo] a cubic structure of τ_5 was reported, but later it was claimed that the cubic structure might have been stabilized by the traces (~0.3 mass%) of dissolved transition metals such as Mn or Cu [1967Sun, 1967Mun]. At 550°C, τ_5 coexists with (Al), Fe_4Al_{13}, τ_2, and τ_6 [2001Kre].

The τ_6 phase (often designated as β-AlFeSi) corresponds to the K_6 phase of [1940Tak] and the L phase of [1981Zar]. Its nominal stoichiometry is $FeAl_{4.5}Si$. Despite numerous studies, the crystal structure of τ_6 is still controversial. While X-ray diffraction studies reported its structure to be monoclinic [1950Phr, 1954Spi, 1955Obi, 1975Bar, 1994Mur, 1994Rom, 1996Mur, 1997Vyb, 2001Kre], convergent beam electron diffraction studies found that τ_6 is orthorhombic [1993Car, 2000Zhe]. In fact, [2000Zhe] did not find any monoclinic phase in their electron microscopic investigation. They concluded that the misinterpretation of X-ray diffraction data, indexed by a monoclinic cell, may be due to intergrowth of different phases and a high density of planar defects. At 550°C, τ_6 coexists with (Al), (Si), τ_2, τ_4 and τ_5 [2001Kre]. A three-dimensional reconstruction of a group of τ_6 platelets suggests that they form an interclocking network [2005Din].

[1951Pra1] correlated the formation of τ_5 and τ_6 with the electron-to-atom ratio. [1979Mor] analyzed the composition of the intermetallic phases by electron microprobe technique and grouped them into two categories based on the size and Fe/Si ratios which can be matched with the τ_5 and τ_6 phases. However, [1979Mor] reported 'indeterminate' particles having intermediate size and Fe/Si ratios between 2.75 and 2.25. [1977Igl] postulated that the τ_5 phase is metastable and can replace the τ_6 phase at cooling rates greater than 200 K·min^{-1}. [1985Suz] and [1987Nag] reported Mössbauer spectra of the τ_5 and τ_6 phases, the former gave a relatively complex spectrum, and the latter gave a simpler one.

The τ_7 phase corresponds to the B phase of [1981Zar], and it has a negligible homogeneity range [2001Kre]. Based on the EDX data, the stoichiometry of τ_7 is $Fe_{25}Al_{45}Si_{30}$, or $Fe(Al_{1-x}Si_x)_3$, with $x = 0.4$

DOI: 10.1007/978-3-540-69761-9_11

[2001Kre]. On the other hand, based on XRD data [1995Gue2] proposed the stoichiometry of τ_7 as $Fe_2Al_3Si_3$, or $Fe(Al_{1-x}Si_x)_3$, with $x = 0.5$. This reflects a discrepancy in Al/Si ratio. Nonetheless, the monoclinic structure of τ_7 reported by [1995Gue2] was also confirmed by [2001Kre]. The phase designated as $Fe_5Al_8Si_7$ [1994Ang] most likely corresponds to τ_7 [2001Kre], based on the assumption of a composition shift similar to τ_1, even though [1994Ang] did not report its crystal structure. At 550°C, τ_7 coexists with (Si), τ_1/τ_9, τ_2, τ_4 and τ_8 [2001Kre].

The τ_8 phase corresponds to the C phase of [1981Zar]. Its composition may be designated as $Fe(Al_{1-x}Si_x)_2$, with x ranging from 0.5 [1981Zar] to 0.67 [1996Yan]. It has an orthorhombic structure [1996Yan, 2001Kre]. The phase designated as $Fe_5Al_5Si_6$ [1994Ang] most likely corresponds to τ_8 [2001Kre], based on the assumption of a composition shift similar to τ_1, even though [1994Ang] did not report its crystal structure.

The τ_{10} phase corresponds to the F phase of [1981Zar] with a nominal stoichiometry of $Fe_{25}Al_{60}Si_{15}$. [1981Zar] reported that its structure in as-cast alloy is different from annealed condition, which was later confirmed by [1987Ste]. The hexagonal structure of τ_{10} is prototypical of either Co_2Al_5 or Mn_3Al_{10}. [1989Ger1] reported Mn_3Al_{10} type structure of τ_{10} annealed at 600°C, while [2001Kre] reported the same structure in an as-cast alloy. At 550°C, τ_{10} coexists with Fe_4Al_{13}, τ_1/τ_9 and τ_3 [2001Kre].

The atomic coordinates (Wyckoff positions) in the ternary intermetallics have been determined by X-ray diffraction (also in some cases by synchrotron radiation) and using single crystals: τ_1/τ_9 [1996Yan], τ_3 [1989Ger2], τ_4 [1995Gue1], τ_5 [1977Cor], τ_6 [1994Rom, 1998Han], τ_7 [1995Gue2], τ_8 [1996Yan], τ_{10} [1989Ger1].

Recent investigations of precipitates in commercial Al alloys, by means of TEM/STEM, EDAX, and high resolution electron microscopy, have revealed a wide variety of precipitate crystal structures, lattice parameters and compositions [1982Wes, 1984Don, 1985Don1, 1985Don2, 1985Gri, 1985Liu, 1986Liu1, 1986Liu2, 1987Cha, 1987Czi, 1987Skj1, 1987Ste, 1987Tur, 1988Ben2, 1988Cha] which can not be grouped together (for details see Table 2). In this assessment, these phases are considered to be metastable. In the absence of detailed crystallographic data, a classification of these metastable phases based on the crystal system is proposed in Table 4.

[1987Nag] and [1987Tur] found that the compositions of intermediate phases and the phase transformations that take place during high temperature annealing depend on the Fe/Si ratio in the alloys. [1986Liu2] reported three different kinds of precipitates, in dilute Al-Fe-Si alloys, formation of which is reported to be a function of Fe/Si ratio, alloy purity, solidification rate and heat treatment. These factors probably explain the occurrence of so many ternary phases as reported by different authors. The principles governing the substitution of Al by Si in the ternary intermetallics have been described by [1989Tib].

The composition ranges of the metastable phases are plotted in Fig. 2. Compared to the stable phases in Fig. 1, the scenario here is much more complex. Virtually all metastable phases have overlapping composition range between 25 to 35 mass% Fe and 0 to 11 mass% Si. Besides crystalline metastable phases, amorphous phases in a number of Al-Fe-Si alloys have also been reported [1986Dun, 1987Ben, 1988Ben1].

Order – Disorder Phase Transitions

There have been extensive studies of order-disorder transitions of Fe rich ternary alloys, both experimentally and theoretically. Mutual solid solubility between Fe_3Al and Fe_3Si is well-established. The solid solubility and the magnetic behavior of $Fe_3(Al, Si)$ were correlated with the electron-atom ratio [1977Nic1] and [1977Nic2]. The ordered phases α_1 (Fe_3Al and Fe_3Si which have $D0_3$ or BiF_3 type order) and α_2 (FeAl and FeSi which have $B2$ or CsCl type order) along the Fe_3Al-Fe_3Si section were studied by means of high temperature X-ray diffraction and recording the disappearance of $D0_3$ superlattice reflections as a function of temperature and composition [1969Pol, 1973Kat]. [1946Sel] measured the lattice parameter of alloys up to 13 mass% Al and 18 mass% Si, and observed an inflection point in the lattice parameter versus composition curve which was attributed to the ordering transition and the formation of $Fe_3(Al,Si)$ having $D0_3$ superstructure. This was further supported by the specific heat measurements as a function of Si/Al ratio by [1951Sat], who found the transformation is accompanied by a small change in Gibbs energy suggestive of second-order type. However, with the addition of Si in Fe_3Al the ordering energies increase monotonically [1973Kat]. The order-disorder transitions along Fe_3Al-Fe_3Si was further studied

DOI: 10.1007/978-3-540-69761-9_11

by transmission electron microscopy (TEM) [1982Cha] and by magnetic method [1986Tak]. Despite these results, there is still some controversy regarding the sequence of ordering transitions along this section. Previous studies by [1969Pol] and [1973Kat] indicate that the sequence of ordering transition (on cooling) is always (αFe) $\rightleftharpoons$ α_2 $\rightleftharpoons$ α_1 along the entire Fe_3Al-Fe_3Si section. However, recent studies by [1982Cha] and [1986Tak] indicate that substitution of more than 50% of the Al atoms by Si atoms (αFe) transforms directly into $D0_3$ structure (α_1).

The results of [1969Pol] and [1973Kat] indicate that an addition of Si in Fe_3Al increases $\alpha_1 \rightleftharpoons \alpha_2$ transition temperature while that of $\alpha_2 \rightleftharpoons$ (αFe) increases with up to about 12.5 at.% Si, beyond which it levels off. The initial increase in ordering temperatures is consistent with the observation of [1977Nic1], and also confirmed by [1987For]. A recent study of magnetic measurements [1986Tak] indicate that the (αFe) $\rightleftharpoons$ α_2 and $\alpha_2 \rightleftharpoons \alpha_1$ transition temperatures vary non-monotonically with increasing Si content as shown in Fig. 3. Here, a few minor adjustments have been made to comply with the accepted Al-Fe binary phase diagram, and also by taking into account the results of [1982Cha] that the (αFe) $\rightleftharpoons$ α_1 ordering temperature of $Fe_3(Al_{0.392}Si_{0.608})$ is greater than 1050°C. Even though the effect of Si on the ordering induced phase separation around Fe_3Al has not been investigated in detail, it is important to note that [1996Mor] observed (αFe) + α_1 microstructure in an Fe-17Al-1Si (at.%) alloy in the temperature range of 400 to 600°C. It is expected that the topology of phase boundaries involving α_1, α_2 and (αFe) near Fe_3Al will follow the general features of phase diagrams associated with multicritical points [1982All]. Due to these reasons, several amendments are proposed in Fig. 3, shown by dashed lines, in the vicinity of Fe_3Al.

Even though the nucleation and growth of α_1 domain in α_2 domain is easier than in (αFe) matrix, the direct (αFe) $\rightleftharpoons$ α_1 transformation in certain composition range has been attributed to the lowering of atomic potential energy when Al atoms are substituted by Si atoms. This causes the formation of different types of anti phase boundaries and the corresponding changes in dislocation configuration leads to double dissociation of superlattice dislocations [1982Cha]. Depending on the composition of an alloy, the nucleation of ordered phases may also take place in the melt. TEM and Mössbauer spectroscopy study [1983Gle] of an Fe-5.4Al-9.6Si (mass%) alloy revealed that the $B2$ type of ordering takes place directly in the melt which subsequently undergoes $D0_3$ ordering. However, [1969Pol] observed that the $D0_3$ superlattice reflections persist up to the melting point in an alloy of Fe_3Al + 12 at.% Si. A similar conclusion was also made by [1954Gar] who investigated the order-disorder transition, after quenching from different temperatures, in an Fe-9.7Si-5.5Al (mass%) alloy. By rapid quenching an Fe-5.4Al-9.6Si (mass%) alloy, [1983Gle] observed that excess vacancies are introduced which occupy ordered sublattice positions, giving rise to a new crystallographic superstructure of the $D0_3$ type. Such type of vacancy-induced long range ordering has also been observed at another composition [1988Liu1].

Mössbauer spectroscopy study of $Fe_{73}Al_{11}Si_{16}$ (ALSIFER27) and $Fe_{68}Al_{22}Si_{10}$ (ALSIFER32), by [1977Suw], revealed that excess diamagnetic atoms (Al and Si) preferentially occupy the Fe site at (0, 0, 0) in the $D0_3$ lattice. They argued that powder methods used in X-ray diffraction may not represent the ordering reactions in the bulk materials. Later, measurements of on-site magnetic moment by neutron diffraction, and also the Mössbauer spectroscopy data suggest that the excess Al and Si atoms occupy the Fe-site at (1/4, 1/4, 1/4) in the $D0_3$ lattice [1987Dob]. A theoretical study of ordering process in $Fe_{0.5}(Al_{1-x}Si_x)_{0.5}$ [1999Mek] predicts an increase in order-disorder temperature. Furthermore, they predicted that Si preferentially substitute Fe in $Fe_{0.5}(Al_{1-x}Si_x)_{0.5}$. Mössbauer spectroscopy results indicate that 'order-annealing' treatment is accompanied by a separation of Fe_3Al and Fe_3Si types of local surroundings [1983Sch]. However, this has only weak influence on the physical properties, and the predominant factor being the composition of the alloy. The long-range order parameter of ball-milled and annealed alloy of $Fe_{75}Si_{15}Al_{10}$ ($D0_3$) has been reported by [2004Zuo].

Figures 4, 5, 6 and 7 show the topology of ordered (α_1, α_2) and disordered (αFe) phase fields in the partial isothermal sections at 700, 650, 550 and 450°C, respectively. These results are adopted from [1982Miy] and [1986Miy] who studied about 20 ternary alloys, containing up to 40 at.% solute atoms (Al + Si), by means of transmission electron microscopy. They reported two types of phase separation $\alpha_1(D0_3)$ + $\alpha_2(B2)$ and (αFe) + $\alpha_1(D0_3)$ in the ternary alloys connecting Fe-10 to 14 at.% Si with Fe-20 to 25 at.% Al and also near Fe-30Si (at.%) alloy. [1984Mat] also observed two kinds of ordering processes leading to phase separation, $\alpha_2 \rightleftharpoons$ (αFe + α_1) and $\alpha_1 \rightleftharpoons$ (αFe + α_1), in an Fe-6Fe-9Si (at.%) alloy that was investigated by means of X-ray diffraction and transmission electron microscopy. Single phase α_1 and α_2 structures were retained

DOI: 10.1007/978-3-540-69761-9_11

by quenching the alloy from 700 and 900°C, respectively. X-ray diffraction data and TEM observations of [1971Gle] concerning various order-disorder reaction in the ternary alloys qualitatively agree with those of [1982Miy, 1986Miy].
[1996Mor] studied the kinetics of ordering and phase separation in an Fe-17Al-1Si (at.%) alloy in the temperature range of 400 to 600°C, where they monitored the evolution of $\alpha + \alpha_1$ microstructure. They found that partial substitution of Al by Si improves microstructural stability against coarsening, most probably due to decrease diffusivity and a reduction in misfit strain.
Theoretical analysis of phase separation involving the ordered (α_1, α_2) and disordered (αFe) phases was carried out by [1991Fuk, 1994Koz]. The free energy of ternary alloys was described by a statistical model that uses pair-wise interaction up to second nearest neighbor. Both chemical and magnetic interactions based on Bragg-Williams-Gorsky model were used. The calculated phase diagrams are found to be consistent with the experimental ones. These theoretical studies underscore the influence of ferromagnetic ordering on phase separation.

Quasibinary Systems

[1931Fus] and [1934Fus] proposed a quasibinary section Si-Fe_4Al_{13} with a peritectic reaction $l + Fe_4Al_{13} \rightleftharpoons Fe_2Al_6Si_3$ at about 920°C and a eutectic reaction between (Si) and $Fe_2Al_6Si_3$ at 850°C and 32 mass% Si. However, later works failed to confirm the presence of such a quasibinary section and consequently it is disregarded.

Invariant Equilibria

Figure 8 shows the assessed reaction scheme, based on both experimental results [1940Tak] and thermodynamic calculations [1998Kol, 1999Liu]. At least twenty invariant equilibria take place during solidification of Al-Fe-Si alloys. The assessed compositions of the liquid phase, after [1927Gwy, 1936Jae, 1937Ura, 1940Tak, 1951Now, 1960Spe], for the ternary invariant reactions are listed in Table 5. [1940Tak] proposed nineteen ternary invariant reactions for the solidification of the Al-Fe-Si alloys. However, they reported that some of these reactions take place in a very narrow range of temperature, thus, difficult to resolve by thermal analysis. For example, [1940Tak] proposed the following two reactions:
$L + \varepsilon \rightleftharpoons \alpha_2 + FeAl_2$ at 1120°C
$L + FeAl_2 \rightleftharpoons \alpha_2 + Fe_2Al_5$ at 1115°C
According to [1940Tak], these two reactions could not be distinguished clearly and a temperature interval of 5°C was assumed. Nonetheless, thermodynamic modelling predicted both invariant reactions [1998Kol, 1999Liu].
Ignoring the solubility of Si in $FeAl_2$ and Fe_2Al_5, thermodynamic datasets [1998Kol, 1999Liu] give following three reactions:
$\varepsilon + Fe_2Al_5 \rightleftharpoons FeAl_2$, L (degenerate binary reaction)
$L + \varepsilon \rightleftharpoons \alpha_2 + FeAl_2$ at 1125°C [1998Kol], at 1127°C [1999Liu]
$L + FeAl_2 \rightleftharpoons \alpha_2 + Fe_2Al_5$ at 1062°C [1998Kol], at 1073°C [1999Liu]
Among these, the first reaction was not explicitly mentioned by [1999Liu]. Since the solubility of Si in $FeAl_2$ and Fe_2Al_5 phases are not considered in thermodynamic modeling, the temperature of the three-phase equilibrium $\varepsilon + Fe_2Al_5 + FeAl_2$ in the ternary is connected with the Si content of epsilon by a "generalized Raoult's law". In the Al-Fe system, the eutectic temperature of $L \rightleftharpoons \varepsilon + Fe_2Al_5$ is very closely above the temperature of $\varepsilon + Fe_2Al_5 \rightleftharpoons FeAl_2$. For the three-phase equilibria going down from these temperatures into the ternary a "generalized Raoult's law" is valid, due to which the two three-phase equilibria meet and form the above mentioned four-phase equilibrium. This meeting happens very near to the binary Al-Fe system. The amount of liquid participating in the four phase equilibrium roughly corresponds to the ratio of Si solubility in ε and liquid phases.
In previous assessments, [1981Riv, 1988Ray] did not consider the participation of $L \rightleftharpoons \subsetneq \alpha_2 + Fe_2Si$ binary invariant reaction in the solidification process of ternary alloys. Also, they did not consider Fe_2Si to be a primary crystallization product in the ternary regime. To alleviate these drawbacks, an invariant reaction with highest temperature must be assumed near the Fe-Si side and it is labelled as U_1. In the absence

DOI: 10.1007/978-3-540-69761-9_11

of any experimental information it was assumed that U_1 takes place around 1150°C [1992Gho]; however, recent thermodynamic modelling [1998Kol, 1999Liu] predicted the reaction temperature around 1175°C:

$$L + Fe_2Si \rightleftharpoons \alpha_2 + FeSi$$

Thermodynamic modeling also confirmed the existence of following invariant reactions: P_1, U_2, U_3, U_4, U_5, U_6, P_2, U_8, U_9, P_5, U_{11}, U_{12}, U_{13} and E_1.

It should be noted that Fig. 8 represents only a partial reaction scheme. It considers the participation of only six ternary phases, τ_1, τ_2, τ_3, τ_4, τ_5 and τ_6, during solidification. The reaction scheme does not account for the experimental observation of several three-phase fields, such as $\tau_2 + \tau_5 + \tau_6$ at 600°C [1987Ste] and at 550°C [2001Kre], $\tau_2 + \tau_4 + \tau_6$ at 550°C [2001Kre], $\tau_2 + \tau_4 + \tau_7$ at 550°C [2001Kre]. These may originate from additional invariant reactions such as $L + \tau_2 \rightleftharpoons \tau_5 + \tau_6$ around 650°C [1952Arm, 1967Mun], $L + \tau_2 + \tau_4 \rightleftharpoons \tau_6$ around 700°C [1927Gwy, 1940Tak], and $L + \tau_7 \rightleftharpoons \tau_2 + \tau_4$, respectively. However, to account for all observed three-phase fields at 600 [1992Gho] and 550°C [2001Kre], including those involving τ_8 and τ_{10}, it is necessary to introduce too many speculative invariant reactions. Therefore, no attempt was made to propose a complete reaction scheme. Further careful experiments are needed to establish the invariant reactions both during solidification and solid state aging.

Liquidus Surface

Figure 9 shows the liquidus surface of the Al corner calculated by the thermodynamic dataset of [1999Liu], which reproduces the experimental results of [1927Gwy, 1943Phi, 1946Phi1] very well. The general form of the liquidus surface has been confirmed by other investigators [1933Nis, 1936Jae, 1937Ura, 1951Now, 1967Mun, 1987Gri1, 1988Zak, 2003Kha]. However, some disagreement exists over the temperature contours. [1967Mun] reported that the cooling rate is an important factor. On the other hand, using a variety of cooling rates [1967Sun] confirmed the results of [1927Gwy] and [1943Phi], and proposed that the nucleation is the decisive factor. [1977Igl] claimed a marked sensitivity of cooling rate not only on the temperature arrest, but also on the final product. In this assessment, the data of [1927Gwy] and [1943Phi] are considered to be representative of normal equilibrium condition and more complete compared to those reported by others [1933Nis, 1937Ura, 1951Now].

Figure 10 shows the liquidus surface of the whole Al-Fe-Si system [1940Tak], depicting the melting grooves separating 17 different areas of primary crystallization. The calculated liquidus surfaces [1998Kol, 1999Liu] gave similar results, except in the Al corner where they differ by several at.% in composition and up to 30°C in temperature compared to that of [1940Tak]. The liquidus surface of Al corner reported by [1937Ura] agrees reasonably well with the results of [1940Tak]. The liquidus temperatures of [1936Jae] are few tens of degrees higher than [1940Tak], and could be due to inadequate experimental arrangements.

Approximate isotherms at 50°C interval are superimposed in Fig. 10. In both Al-Fe and Fe-Si binary systems, depending on the alloy composition, either (αFe) or α_2 may be the primary crystallization product. In the ternary system, as an approximation, the composition domains of (αFe) and α_2 as primary crystallization products are delineated by the linear extrapolation between the composition limits of two binary edges. This is shown by a dashed line in Fig. 10. In the Fe-Si system, α_1 is the primary crystallization product during solidification of alloys containing 27.5 to 32 at.% Si. However, the extension of this composition range into the ternary system is not known.

Isothermal Sections

Figures 11 and 12 show the isothermal sections at 1100 and 1020°C [2002Gup], respectively. [2002Gup] constructed these two isothermal sections based on the microstructural characterization in diffusion couples that were quenched from the respective temperature. They also utilized the vertical sections of [1940Tak]. However, several amendments are done to comply with the accepted binary phase diagrams, and also the reaction scheme in Fig. 8. According to our accepted binary phase diagrams, Fe_2Al_3 (ε) is stable up to 1102°C while Fe_2Si is stable between 1040 and 1212°C. Consequently, all two- and three-phase fields involving Fe_2Al_3 (ε), originally proposed by [2002Gup], are not accepted. Also, three three-phase

DOI: 10.1007/978-3-540-69761-9_11

fields that should be present, but were not shown by [2002Gup], are added (as dashed) in Fig. 11. These are α_1 + FeSi + Fe_2Si (from U_1), L + α_1 + $FeAl_2$ (from U_2), L + $FeAl_2$ + η (from D_1).
Two amendments are made in the isothermal section at 1020°C in Fig. 12. [2002Gup] showed two three-phase fields L + $FeSi_2$ + τ_1 and FeSi + $FeSi_2$ + τ_1, but they are incompatible with the reaction scheme in Fig. 8. To be consistent, these are replaced by two three-phase fields: L + FeSi + $FeSi_2$ (from e_1) and L + FeSi + τ_1 (from P_1). Figure 13 shows the isothermal section at 1000°C adopted from [1981Riv, 1988Ray], who constructed it utilizing the results of the polythermal sections of [1940Tak]. Unlike the isothermal section at 1020°C in Fig. 11, the three-phase field FeSi + $FeSi_2$ + τ_1 (originating from U_6) is stable at 1000°C.
Figures 14 and 15 show the isothermal sections at 900 and 800°C [2002Mai], respectively. Once again, these isothermal sections are based on their microstructural characterization in diffusion couples that were quenched from the respective temperature, and also utilizing the vertical sections of [1940Tak]. Two amendments are made in Fig. 14. [2002Mai] showed two three-phase fields L + $FeSi_2$(r) + τ_3 and $FeSi_2$(r) + τ_1 + τ_3 at 900°C that are incompatible with the reaction scheme in Fig. 8. They are replaced by the expected three-phase fields: L + $FeSi_2$(r) + τ_1 and L + τ_1 + τ_3. It should be noted that according to the reaction scheme in Fig. 8, the phase field $FeSi_2$(r) + τ_1 + τ_3 is stable at temperatures ≤ 885°C. In Figs. 11 to 15, the (αFe)/α_2 boundary is shown by a dotted line that is extrapolated from the Fe-Al edge to the Fe-Si edge. However, the α_2/α_1 boundary originating from the Fe-Si edge is expected to turn around as is the case, for example, in Fig. 4, and its locus can not be ascertained from the available data. Therefore, the α_2/α_1 boundary is tentatively shown up to 20 at.% Al in Figs. 11 to 15. A question mark in the doubtful region indicates the need for further experimental data.
[2004Pon] reported a partial isothermal section of the Al corner at 727°C showing three three-phase fields. Among them, the presence of L + Fe_4Al_{13} + τ_5 and L + τ_2 + τ_5 phase fields that are consistent with the reaction scheme in Fig. 8. However, [2004Pon] also showed the presence of a three-phase field, L + τ_2 + τ_4, which can not be rationalized with the reaction scheme in Fig. 8.
Figure 16 shows the isothermal section of the Al corner at 640°C [1959Phi]. [1987Ste] reported the phase equilibria in a set of commercial Al based alloy after heat treating the as-cast samples for one month between 570 and 600°C. The heat treated state was referred to as 'quasi-equilibrium' condition [1987Ste]. The phase equilibria of the Al corner at 600°C are shown in Fig. 17, after [1987Pri] who amended the isothermal section reported by [1987Gri1] and [1987Ste]. It is to be noted that the (Al) + τ_6 and (Al) + τ_6 + (Si) phase fields were derived from the measurements on samples annealed at 570°C. So the existence of these phase fields is consistent with the reaction scheme in Fig. 8, giving the temperature for E_1 as 573°C. Also, [1987Ste] reported that three ternary intermetallics α-FeAlSi (τ_5), β-FeAlSi (τ_6) and α-FeAlSi (τ_2), the details of which are given in Table 3, crystallize from the liquid. This is consistent with the proposed reaction scheme in Fig. 8. During heat treatment of as-cast samples, the Fe_4Al_{13}, τ_5 and (Si) phases react to form τ_6 phase, but this reaction does not go to completion [1987Ste].
Figure 18 shows the assessed isothermal section at 600°C. The Fe corner involving the ordered phases is taken from [1982Miy, 1986Miy], but in certain composition ranges the ordered phase regions are still doubtful, and they are shown as dashed. The isothermal section at 600°C reported by [1981Zar] has undergone several amendments. Previously reported τ_1 and τ_9 phases [1992Gho] are treated as one phase [2001Kre]. The composition of τ_8 is accepted from [1996Yan]. Two three-phase fields, τ_2 + τ_4 + τ_5 and τ_2 + τ_5 + τ_6, are unaccounted for in the reaction scheme in Fig. 8, but these may originate from a solid state reaction τ_4 + τ_5 ⇌ τ_2 + τ_6 ocurring above 600°C.
Figure 19 shows the partial isothermal section at 550°C [2001Kre]. There are important differences between Figs. 18 and 19, even though the temperature difference is only 50°C. For example, Fig. 18 shows the presence of (Al) + (Si) + τ_4 phase field which is unaccounted for by the reaction scheme in Fig. 8, while Fig. 19 shows the presence of (Al) + (Si) + τ_6 phase field which is consistent with the reaction scheme in Fig. 8. Figure 18 shows the presence of τ_{10} + Fe_2Al_5 (η) + Fe_4Al_{13} phase field, while Fig. 19 shows the presence of τ_1/τ_9 + Fe_2Al_5 + Fe_4Al_{13} phase field. In Fig. 19, several phase boundaries involving τ_8 are uncertain. [2001Kre] reported that the tie-triangles involving τ_8 would depend on its composition, which was not determined. As a results, some of the phase boundaries in τ_8 are shown dotted.
Figure 20 shows the partial isothermal section at 500°C proposed by [1984Don] in which the phase boundaries have shifted to the right, compared to [1943Phi, 1946Phi1, 1946Phi2], in order to

DOI: 10.1007/978-3-540-69761-9_11

account for the observation of various phases as well as the amount of Si in solid solution in the (Al) matrix in industrially pure Al.

Temperature – Composition Sections

Figures 21, 22 and 23 show the polythermal sections at 0.7 mass% Fe [1949Cru, 1959Phi], 4.0 mass% Fe [1959Phi] and 8.0 mass% Si [1959Phi], respectively. There are no published data for the solidus projection of the entire system, even though a number of polythermal projections are available [1927Gwy, 1932Nis, 1933Nis, 1940Tak, 1946Phi1]. The solidus projection of the Fe corner was reported [1968Lih], but their results differ substantially along the Al-Fe binary edge, so they are not accepted here. Figure 24 shows the solidus and solvus surfaces of the Al corner calculated using the thermodynamic dataset of [1999Liu]. These results are in good agreement with reported by [1961Phi].

Thermodynamics

Thermodynamic properties of ternary alloys have been investigated a number of times by measuring the heat of formation of solid alloys [1937Koe, 1937Oel], activity measurements in liquid alloys [1969Bed, 1970Mit, 1973Nag, 1973Per, 1980Sud, 1984Ber, 1985Cao, 1989Bon, 2004Kan], heat of mixing of liquid alloys [2003Kan], and the standard heat of formation of ternary intermetallics [1997Vyb, 2000Li1, 2000Li2].

[1969Bed] determined the activity coefficients at several constant mole fraction ratios (x_{Si}/x_{Fe}) at 1627°C. The Al activities in the temperature range of 800 to 1100°C were reported by [1973Nag], and at 900°C by [1973Per]. [1980Sud] reported Al activity in an 1Al-Fe-1Si (mass%) alloy at 1485 and 1546°C. Further experiments were carried out by [1984Ber] and [1989Bon]. The latter authors measured the chemical potential of Al in alloys containing up to 11.8 at.% Fe and 23.7 at.% Si by the concentration cell method in the temperature range of 577 to 1027°C. The activities of Al show a negative deviation from the ideal behavior. The results of [1984Ber] also show a similar trend. The activity of Al in $Fe_x(Al_{0.879}Si_{0.121})_{1-x}$, $0.0249 \le x \le 0.0512$, show a transition from positive to negative deviation from the ideal behavior at $x = 0.035$ [2004Kan].

Recently, [2003Kan] measured the heat of mixing of liquid alloys at 1477°C using a high-temperature isoperibolic calorimeter. Some selected data is listed in Table 6, while several isoenthalpy (mixing) contours are plotted in Fig. 25.

The heat of mixing of solid alloys was measured by pouring liquid Al-Si alloy and liquid Fe into a water calorimeter [1937Koe, 1937Oel]. However, the state of equilibrium in these experiments is uncertain [1999Liu]. The standard heat of formation of ternary intermetallics, except τ_7, has been determined by solution calorimetry by [1997Vyb], [2000Li1] and [2000Li2]. These results are summarized in Table 7. [1997Vyb] used 99.99% Al, 99.9% Fe and 99.99% Si to prepare single phase τ_5 and τ_6 samples by annealing cast ingots either at 550°C (τ_5) or at 600°C (τ_6) for 1 month. They used an aluminum bath at 1070°C for solution calorimetry. Li *et al* [2000Li1, 2000Li2] used 99.99% Al, 99.999% Fe and 99.999% Si to prepare the intermetallics. Levitation melting followed by annealing, the conditions of which varied, were employed to obtain single phase alloys of τ_1/τ_9, τ_5 and τ_{10} [2000Li1], and τ_2, τ_3, τ_4, τ_6, and τ_8 [2000Li2]. Unlike [1997Vyb], Li *et al* used an aluminum bath at a lower temperature of 800°C for solution calorimetry. There are differences between the results of [1997Vyb] and [2000Li1, 2000Li2]. For example, [1997Vyb] reported that the standard heat of formation of τ_5 ($Fe_{19.2}Al_{71.2}Si_{9.6}$) and τ_6 ($Fe_{15.4}Al_{69.2}Si_{15.4}$) are –34.3 ± 2 and –24.5 ± 2 kJ·(g-at)$^{-1}$, respectively. The corresponding values reported by Li *et al* are –24.44 ± 1.387 kJ·(g-at)$^{-1}$ for τ_5 at $Fe_{18}Al_{72}Si_{10}$ [2000Li1] and –20.209 ± 0.926 kJ·(g-at)$^{-1}$ for τ_6 at $Fe_{15}Al_{70}Si_{15}$ [2000Li2]. Even though the τ_5 and τ_6 compositions of [1997Vyb] and [2000Li1, 2000Li2] are not identical, large differences in heat of formation are unexpected. Apparently, Li *et al* [2000Li1, 2000Li2] were unaware of the results of [1997Vyb], and they did not discuss this discrepancy. Nonetheless, it is not clear if a higher bath temperature (causing oxidation) and relatively impure starting materials used by [1997Vyb] compared to Li *et al* have contributed to more negative heat of formation. Comparing the standard heat of formation of ternary intermetallics and heat of mixing of liquid alloys at approximately similar compositions, [2003Kan] concluded that the ternary interaction term in liquid phase is almost negligible.

[1994Ang] determined the enthalpy of fusion of $FeAl_3Si_2$ (τ_4) and $Fe_5Al_8Si_7$ (τ_7).

DOI: 10.1007/978-3-540-69761-9_11

Thermodynamic modeling of the ternary system has also been carried out by the CALculation of Phase Diagram (CALPHAD) method [1994Ang, 1995Gue3, 1998Kol, 1999Liu], where the Gibbs energies of the relevant phases are described by simple analytical functions. [1949Cru] reported calculated solubility isotherms of Fe and Si in solid (Al). They suggested the formation of a ternary compound Fe_2Al_7Si which is close to the τ_5 phase at low Si content. On the other hand their calculation seems to suggest the ternary phase $FeAl_5Si$ which is close to the τ_6 phase [1981Riv]. Calculation of the liquidus surface from a purely thermodynamic approach [1946Phi2] seems to produce good result near the binary edges. However, their approach can neither predict the composition of the precipitating phase nor calculate the solidus curves.
[1994Ang] employed the CALPHAD technique and calculated two vertical sections corresponding to x_{Al}/x_{Si}=3/1 and at x_{Si} = 0.85. [1995Gue3] calculated two partial isothermal sections at 600 and 900°C, and a vertical section at x_{Si} = 0.78 by the CALPHAD method. They considered only two ternary phases: $FeAl_3Si_2$ (τ_4) and $Fe_2Al_9Si_2$ (τ_6).
[1998Kol] and [1999Liu] carried out detailed thermodynamic assessments of the ternary system by the CALPHAD method. According to our classification, [1998Kol] considered six ternary phases τ_1/τ_9, τ_2, τ_3, τ_4, τ_5 and τ_6, whereas [1999Liu] considered seven ternary phases: τ_1/τ_9, τ_2, τ_3, τ_4, τ_5, τ_6, and τ_7, which were labelled as τ_1, γ, τ_{23}, δ, α, β, τ, respectively. [1999Liu] argued that τ_2 and τ_3 have very similar Fe contents, and wondered, if they are the same phase with a small homogeneity range. This view was also accepted by [2002Rag]. However, as summarized in Table 2, τ_2 and τ_3 have different crystal structures. [1999Liu] computed the liquidus surface, isothermal sections at 600 and 1000°C, and vertical sections at 1.3, 2, 5, 10 mass% Fe and 2 mass% Si.

Notes on Materials Properties and Applications

A summary of experimental investigation of properties is given in Table 8. [1951Oga1, 1951Oga2, 1983Sch] reported the ferromagnetic behavior of Fe_3Al-Fe_3Si alloys. [1968Aru1, 1968Aru2, 1970Aru] reported that the occupation of ordered sites by all three Al, Fe and Si atoms accompanied with a minimum in electrical resistivity at $Fe_{75}Al_{18}Si_7$ and Fe_6(Al,Si). [1996Szy] reported that dissolved Al in $FeSi_2$(r) increases its magnetic susceptibility, and both FeSi and $FeSi_2$(r) exhibit Van Vleck paramagnetism even at very low temperature (up to 4.2 K). [1996Fri] and [1998Dit] studied the metal-insulator transition in Al doped FeSi. [1998Dit] reported lattice constant, thermoelectric effect, Hall effect, electrical conductivity, magnetic susceptibility, specific heat and magnetoresistance in $FeSi_{1-x}Al_x$, with $0 \le x \le 0.08$. All these properties confirm a metal to insulator transition of FeSi, which is otherwise a Kondo insulator. [1999Oht] has reported that doping of $FeSi_2I$ with 3 at.% Al improves its thermoelectric figure of merit. The magnetic properties of ternary alloys have been discussed in detail by [1986Tak] and [1988Dor].
[1993Sch] investigated the plastic deformation of single-crystal $Al_{20}Fe_{75}Si_5$ alloy as a function of temperature. The critical resolved shear stress exhibits a non-monotonic behavior with a maximum around 530°C. The non-monotonic behavior was correlated with the temperature-dependent dislocation mobility rather than a decrease in $D0_3$ long-range order parameter. [1996Cho, 2001Cho] reported the microstructure, hardness and tensile properties of Al-5 mass% Fe-16 mass% Si alloy, processed by powder metallurgy, up to 520°C.
[2003Cie] observed Portevin-Le Chatelier Effect in biaxially strained Al-Fe-Si foils. This effect is attributed to the diffusion of Si rather than Fe, as the latter has much slower diffusivity and low solubility in (Al). [2003Mur] reported the hardness and indentation fracture toughness of τ_2 and τ_5 phases, both have hardness much higher than binary aluminides and they have very similar indentation fracture toughness.
[1948Jen] demonstrated a relationship between the constitutional diagram and the susceptibility to cracking of the Al-Fe-Si alloys. A key factor in determining the corrosion behavior of Al rich alloys is the Fe/Si ratio. Low Fe/Si ratio in ternary alloys exhibit better corrosion resistance in both industrial and marine environment [2000Bha].

Miscellaneous

In recent years, the solidification of Al rich ternary alloys has been investigated rather extensively [1983Per, 1991Don, 1991Lan, 1995Bel, 1995Gue3, 1996All, 1997All, 1997Sto, 1997Can, 1999Cho, 1999Tay, 2000Dut, 2001Hsu, 2001Sha, 2002Dut, 2002Mer, 2004Kha, 2005Kha].

DOI: 10.1007/978-3-540-69761-9_11

[1983Per] discussed the effect of metastable liquid miscibility gaps, metastable eutectic and metastable peritectic on the rapid solidification processing and alloy design. Addition of up to 0.11 mass% Fe in an Al-0.5Si (mass%) alloy is reported to favor the formation of the metastable phase $FeAl_6$ [1978Suz].
[1995Bel] proposed a non-equilibrium solidification method to analyze the cast microstructure of ternary alloys. This method utilizes equilibrium phase diagram, but assumes that the peritectic reactions are suppressed and the eutectic reactions occur according to the equilibrium phase diagram. The role of heterogeneous nucleation on phase selection, solidification, and grain refinement of Al has been investigated in detail [1996All, 1997All, 1997Can, 2004Kha]. In particular, [2004Kha] investigated the nucleation potency of Al on the surface of MgO, TiB_2, TiC, α-Al_2O_3 and SiC inclusions. They showed that in dilute hypoeutectic alloys (Al+Fe less than 1.5 mass%) these inclusions act as efficient grain refiner caused by a decrease in liquid/inclusion interfacial energy due to the segregation of Si. [2005Kha] investigated heterogeneous nucleation of ternary intermetallics (τ_4, τ_5, τ_6, μ_3) on the surface of CaO, MgO, TiB_2, TiC, Al_4C_3, α-Al_2O_3, γ-Al_2O_3 and SiC inclusions. They found that reactive inclusion such as CaO and SiC are potent nucleants for the intragranular ternary intermetallics. Also, the potent nucleants for the primary phase, (Al), such as γ-Al_2O_3 exhibit poor potency for the nucleation of ternary phases. [2002Dut] reported the effect of cooling rate on the amount of ternary eutectic, and also the effect of Fe/Si ratio on the morphology of intermetallics in cast Al alloys.
[1997Sto] studied the effect of cooling rate and solidification velocity on the microstructure selection of Al-3.5Fe-(1 to 8.5) Si (mass%) alloys by wedge chill casting and Bridgman directional solidification techniques. In the latter case, the front growth velocity was in the range of 0.01 to 2 $mm \cdot s^{-1}$ under a temperature gradient of $15°C \cdot mm^{-1}$. Also, at front velocities greater than 1 $mm \cdot s^{-1}$, the primary intermetallics were suppressed. The results of Al-3.5Fe-8.5Si (mass%) were summarized in terms of a kinetically based solidification microstructure selection diagram.
[1999Tay] applied Scheil equation to predict the defect-onset (porosity) during solidification of Al rich alloys as a function of Fe and Si contents. The effect of Fe and other elements on the porosity of hypoeutectic Al-Si castings has also been discussed by [2005Lu]. [1999Tay] found that a defect-free casting can be obtained if the solidification proceeds directly to the invariant reaction E_1 ($L \rightleftharpoons \tau_6 + (Al) + (Si)$), whereas poor casting may result when the solidification proceeds via the (Al)-τ_6 eutectic valley. The critical Fe content at which the porosity is minimized is a function of Si content in the alloy. [2001Sha] also carried out Bridgman directional solidification of a model 6xxx alloy (Al-0.3Fe-0.6Si-0.8Mg (mass%)), and obtained solidification front velocity in the range of 5 to 120 $mm \cdot min^{-1}$. They observed two ternary phases, α-FeAlSi (τ_5) and β-FeAlSi (τ_6), of which the latter is metastable. At low front velocity, such as 30 to 60 $mm \cdot min^{-1}$, β-FeAlSi dominate the microstructure, while at high front velocity, such as 120 $mm \cdot min^{-1}$, β-FeAlSi dominates the phase selection.
Figure 26 shows the surface of secondary crystallization of the Al corner after [1943Phi]. It should be noted that the data relate to slowly-cooled alloys in a non-equilibrium state.
Since both Al-Fe and Fe-Si binary systems form γ loops, a ternary γ loop is expected. [1931Wev] reported the coordinates of the phase boundaries of the ternary γ loop which are listed in Table 9. [1960Voz] reported the effect of impurities on the solid solubility of Al alloys by means of electrical resistivity. [1972Ere] studied the dissolution kinetics of Fe in Al-Si melts at 700, 750 and 800°C, the kinetics of which was correlated with the formation of various intermediate phases.
[2000Sri] reported synthesis of bulk ternary intermetallics using elemental powder mixture by self-propagating high temperature synthesis. They used cold compacted powder mixtures that were heated to 650°C in a vacuum furnace. Both stable (τ_2, τ_5 and τ_6) and metastable phases were obtained in this process. They also reported hardness of the intermetallics.
[1998Akd] proposed that the value of activity coefficient of Al in α-(Fe,Al,Si) alloys has a strong influence on the formation and growth kinetics of interfacial diffusion layer. [1999Oht] has discussed the sintering mechanism of Al-Fe-Si alloys, particularly the role of liquid phase, in the context of fabricating an Al doped $FeSi_2I$ phase. [2001Jha] has discussed the diffusion path of Al in ternary bcc alloys.

DOI: 10.1007/978-3-540-69761-9_11

Table 1. Investigations of the Al-Fe-Si Phase Relations, Structures and Thermodynamics

Reference	Method/Experimental Technique	Temperature/Composition/Phase Range Studied
[1927Gwy]	Metallography, thermal analysis	Al rich alloys; liquidus surface
[1928Dix]	Metallography, thermal analysis	25 Al rich alloys; Fe ≤ 11 mass%, Si ≤ 29 mass%, Al = bal.; 560°C
[1931Fin]	Metallography, XRD	11 Al rich alloys; Fe: 7.29-36 mass%, Si: 1.85-13.36 mass%; 560-600°C
[1931Fus]	Metallography, thermal analysis	About 50 Al rich alloys; liquidus surface of Al corner
[1932Nis, 1933Nis]	Metallography, thermal analysis	Al rich alloys; liquidus surface of Al corner
[1937Koe, 1937Oel]	Calorimetry	Heat of formation of liquid alloys
[1937Ura]	Metallography, thermal analysis	Alloys up to 68 mass% Fe; liquidus surface of Al corner
[1937Ser]	Chemical analysis; XRD	Al rich alloys
[1940Tak]	Dilatometry, magnetometry, metallography, thermal analysis, XRD	About 150 alloys; entire composition range
[1943Phi]	Metallography, XRD	Al rich alloys.; Fe ≤ 12 mass%, Si ≤ 6mass%, Al = bal.; liquidus surface of Al-corner
[1946Phi1, 1946Phi2]	Metallography, XRD	Al rich alloys.; liquidus surface of Al-corner
[1949Cru]	Thermoelectric power	3 Al rich alloys; Fe ≤ 0.51 mass%, Si ≤ 0.35 mass%, Al = bal.; 420-640°C
[1950Phr]	Metallography, XRD	Al rich alloys; liquidus surface of Al corner
[1951Oga1, 1951Oga2]	Metallography, thermal analysis	Al rich alloys; liquidus surface of Al corner
[1951Pra1]	Metallography, chemical analysis, XRD	11 Al rich alloys; liquidus surface of Al corner
[1951Pra2]	Metallography, chemical analysis, XRD	11 Al rich alloys; liquidus surface of Al corner
[1952Arm]	Thermal analysis, chemical analysis	Al rich alloys; liquidus surface of Al-corner
[1967Mun]	EPMA, TEM, XRD	Al rich alloys; (Fe + Si) ≤ 22 mass%, Al = bal.
[1967Sun]	Chemical analysis, XRD	Al rich alloys
[1968Lih]	DTA, magnetometry, microhardness, XRD	Fe corner; Al ≤ 50 at.%, Si ≤ 35 at.%, Fe = bal.; up to solidus temperature (≈1500°C)

(*continued*)

DOI: 10.1007/978-3-540-69761-9_11

Reference	Method/Experimental Technique	Temperature/Composition/Phase Range Studied
[1969Pol]	High-temperature XRD, resistivity	15 Fe rich alloys; $Fe_3(Al_xSi_{1-x})$, $0 \le x \le 1$; order-disorder transition
[1970Mit, 1973Nag]	Galvanic cell	35 Al rich alloys with Fe/Si ratio (in mass%) 0.133, 0.338, 0.561, 1, 1.667, 3.04, 6.94; activity of Al in liquid alloys; 785-1100°C
[1973Kat]	High-temperature XRD	15 Fe rich alloys; $Fe_3(Al_xSi_{1-x})$, $0 \le x \le 1$; order-disorder transition, up to 1325°C
[1977Nic1, 1977Nic2]	NMR, magnetometry, XRD	$Fe_3(Al_xSi_{1-x})$, x = 0, 0.04, 0.08, 0.15, 0.25; α_1 phase
[1977Suw]	Mössbauer spectroscopy	$Fe_{73}Al_{11}Si_{16}$ and $Fe_{68}Al_{22}Si_{10}$; α_1 phase
[1979Cow]	XRD	16 alloys of $Fe_3(Al_xSi_{1-x})$, $0 \le x \le 1$; α_1 phase
[1980Sud]	Galvanic cell	Activity of Al in an Fe-1 mass% Al-1 mass% Si alloy
[1982Cha]	TEM	$Fe_3(Al_xSi_{1-x})$, x = 0.392; order-disorder transitions
[1982Miy]	TEM	20 Fe rich alloys; Al = 0.5-33 at.%, Si = 2.8-15.1 at.%, Fe = bal.; 450-700°C; order-disorder transitions
[1983Gle]	TEM, Mössbauer spectroscopy	Fe-5.4Al-9.6Si (mass%); order-disorder transitions
[1983Sch]	Mössbauer spectroscopy	8 alloys along Fe_3Al-Fe_3Si; α_1 phase
[1984Ber]	Galvanic cell	Al-2.5Fe-6Si (mass%) alloy; activity of Al; 660-900°C
[1984Don]	TEM	3 Al rich alloys; Fe = 0.21-0.6 mass%, Si = 0.14-0.59 mass%, Al = bal.; 400-600°C
[1986Tak]	Magnetometry	$Fe_3(Al_xSi_{1-x})$ alloys; order-disorder transitions
[1986Miy]	Hardness, TEM	20 Fe rich alloys; Al = 0.5-33 at.%, Si = 2.8-15.1 at.%, Fe = bal.; 450-700°C; order-disorder transitions
[1987Dob]	Neutron diffraction, Mössbauer spectroscopy	$Fe_{73.6}Al_{2.9}Si_{23.5}$, $Fe_{70.8}Al_{5.8}Si_{23.4}$ and $Fe_{69.4}Al_{7.2}Si_{23.4}$; α_1 phase
[1987Gri1]	DTA, EPMA, XRD	Al rich alloys; Fe = 18-35 mass%, Si = 4-12 mass%, Al = bal.; 600°C
[1987Ste]	SEM, EPMA, XRD	9 Al rich alloys; Fe = 17.8-34.9 mass%, Si = 3.9-14.1 mass%, Al = bal.; 570-600°C
[1988Zak]	DTA, XRD	15 Al rich alloys; Fe = 1-3 mass%, Si = 10-14 mass%, Al = bal.; Al corner liquidus surface and vertical sections

(*continued*)

DOI: 10.1007/978-3-540-69761-9_11

Reference	Method/Experimental Technique	Temperature/Composition/Phase Range Studied
[1989Bon]	Galvanic cell	Al rich alloys; Fe = 3.6-11.8 at.%, Si = 6.9-23.7 at.% Si, Al = bal.; activity of Al in liquid alloys
[1996Mor]	DSC, TEM	$Fe_{82}Al_{17}Si_1$; TEM; order-disorder transitions
[1997Vyb]	Calorimetry	Heat of formation of τ_5 and τ_6
[2000Li1, 2000Li2]	Calorimetry	Heat of formation of τ_1/τ_9, τ_2, τ_3, τ_4, τ_5, τ_6, τ_8, and τ_{10}
[2002Gup]	EPMA	Diffusion couples; 1020-1115°C
[2002Mai]	EPMA	Diffusion couples; 600-900°C
[2003Kan]	Calorimetry	Heat of mixing of liquid alloys at 1477°C
[2004Kan]	Galvanic cell	$Fe_x(Al_{0.879}Si_{0.121})_{1-x}$, $0.0249 \leq x_{Fe} \leq 0.0512$; activity of Al in liquid alloys

Table 2. A Chronological Survey of Ternary Phases in the Al-Fe-Si System

Author	Phase Designation	Composition (mass%)			Comments
		Fe	Al	Si	
[1927Gwy]	χ, β, δ, ζ	-	-	-	Ternary alloys up to about 20 mass% Fe and 30 mass % Si were studied. The ζ phase reported to be solid solution of Fe, Al and Si.
[1928Dix]	α(Fe-Si) β(Fe-Si)	30.0 27.0	62.0 68.0	8.0 15.0	Ternary alloys up to 41 mass% Fe and 29 mass% Si were studied using pure Al (99.95%). The alloys were annealed for 1-5 weeks at 560°C. These two crystal species were reported to be ternary solid solutions rather than ternary compounds. They reported to form a part-section with $FeAl_3$ and β(Fe-Si).
[1931Fin]	α(Fe-Si) β(Fe-Si)	30.3 27.3	61.4 57.7	8.3 15.0	Alloys and heat treatments were same as [1928Dix]. They assumed α(Fe-Si) was a solid solution of Si in $FeAl_3$.
[1931Fus]	$Fe_2Al_6Si_3$	31.3	45.2	23.5	$Fe_2Al_6Si_3$ formed by a peritectic reaction.

(*continued*)

DOI: 10.1007/978-3-540-69761-9_11

Author	Phase Designation	Composition (mass%)			Comments
		Fe	Al	Si	
[1932Nis], [1933Nis]	$Fe_2Al_3Si_2$	44.9	32.5	22.6	$Fe_2Al_3Si_2$ was reported to occur around the composition Al-32 mass% Fe-30 mass% Si. The χ phase was not studied further.
	χ	-	-	-	
[1935Bos]	$Fe_2Al_6Si_3$	-	-	-	Formed in diffusion couples between Al-Fe and Al-Si alloys at 550°C
[1936Jae]	$FeAl_4Si_2$	27.2	47.6	25.2	X-ray diffraction, goniometric and dilatometric measurements were carried out in ternary alloys up to 40 mass% Fe and 30 mass% Si. The chemical compositions of the hexagonal (a=836 pm, c=1458 pm), orthorhombic (a=609 pm, b=996 pm, c=374 pm) and triclinic (a=688 pm, b=593 pm, c=432 pm, α=104.75°, β=130.67°, γ=68.4°) phases were not given. $FeAl_4Si_2$ has tetragonal structure (a=615 pm, c=947 pm).
	Hexagonal	-	-	-	
	Orthorhombic	-	-	-	
	Triclinic	-	-	-	
[1937Ser]	$FeAl_nSi$				Microscopic and X-ray diffraction were carried out in alloys up to 10 mass% Fe and 25 mass% Si. The densities of $FeAl_5Si$ and $FeAl_4Si_2$ were reported to be 3.35 and 3.30 $g \cdot cm^{-3}$, respectively. $FeAl_4Si_2$ was found to have cubic crystal structure.
	$n = 4$	29.1	56.3	14.6	
	$n = 5$	25.6	61.6	12.8	
	$FeAl_4Si_2$	25.4	49.1	25.5	
[1937Ura]	β	-	-	-	According to these authors β and γ are formed by peritectic reaction, they have no definite composition, and are solid solutions.
	γ	-	-	-	
[1940Tak]	K_1:$Fe_3Al_3Si_2$	55.0	26.6	18.4	These authors reported six ternary phases (K_1 to K_6)
	K_2:$Fe_6Al_{12}Si_5$	41.9	40.5	17.6	

(*continued*)

DOI: 10.1007/978-3-540-69761-9_11

Author	Phase Designation	Composition (mass%)			Comments
		Fe	Al	Si	
	K_3:$Fe_5Al_9Si_5$	42.2	36.7	21.1	formed by peritectic reactions.
	K_4:$FeAl_3Si_2$	28.9	41.9	29.2	
	K_5:$Fe_6Al_{15}Si_5$	38.1	46.0	15.9	
	K_6:$FeAl_4Si$	29.1	56.3	14.6	
[1943Phi]	α(Fe-Si)	-	-	-	They investigated ternary alloys up to 12 mass% Fe and 6 mass% Si.
	β(Fe-Si)	-	-	-	
[1950Phr]	*c*-FeAlSi	31.9	62.5	5.6	Alloys up to 42 mass% Fe and 30 mass% Si were studied. *c*-FeAlSi has cubic (*a*=1254.83 pm), *m*-FeAlSi has monoclinic (*a*=*b*=612.23 pm, *c*=4148.36 pm, β= 91°) and *t*-FeAlSi has tetragonal (*a*=612.23 pm, *c*=947.91 pm) crystal structure.
	m-FeAlSi	27.2-27.8	59.3-58.2	13.5-14.0	
	t-FeAlSi	-	-	-	
[1951Pra2]	α(Fe-Si)	32.1-32.7	59.5-57.0	8.4-10.3	Chemical analysis and X-ray diffraction were carried out on extracted crystals. The crystal structure of α(Fe-Si) was reported to be the same as Fe_4Al_{13} and β(Fe-Si) represents a distinct ternary compound.
	β-(Fe-Si)	26.7-27.3	59.5-57.8	13.8-14.9	
[1951Now]	α(Fe-Si)	30.6	59.1	10.3	150 ternary alloys up to 45 mass% Fe and 30 mass% Si were investigated by thermo- analytical, microscopic and X-ray diffraction methods. Homogeneity ranges of these phases were reported to be small. Approximate stoichiometries of α(Fe-Si), β(Fe-Si) and γ(Fe-Si) can be represented as $Fe_{1.5}Al_6Si$, $FeAl_{4.5}Si$ and $Fe_{0.5}Al_{1.5}Si$, respectively. The latter has tetragonal structure (*a*=495.0 pm, *c*=707.0 pm).
	β(Fe-Si)	27.2	59.1	13.7	
	γ(Fe-Si)	28.9	41.9	29.2	
	δ(Fe-Si)	-	-	-	
[1952Arm], [1955Arm]	α_1	27.3	65.7	7.0	Alloys up to 20 mass% Fe and 50 mass% Si were
	α_2	29.2	59.5	11.3	

(*continued*)

DOI: 10.1007/978-3-540-69761-9_11

Author	Phase Designation	Composition (mass%)			Comments
		Fe	Al	Si	
	α_3	35.3	51.9	12.8	studied. Microscopic, X-ray diffraction and density measurements were performed to characterize the phases in as-cast alloys. The crystal structures of α_1, α_2 and α_3 were reported to be cubic (a=1254.83 pm), hexagonal (a=496 pm, c=702.11 pm) or orthorhombic (a=4360 pm, b=4960 pm, c = 7080 pm) and cubic (a=1603.23 pm), respectively. The densities were 3.50, 3.58 and 3.65 g·cm^{-3}, respectively.
[1953Rob]	α-FeAlSi	32.5	58.8	8.7	Single crystals of α-FeAlSi, prepared by [1951Pra1] and [1951Pra2] were studied by X-ray diffraction. The crystal structure and density were reported to be hexagonal (with $P6_3/mmc$ symmetry and a=1230 pm, c=2620 pm) and 3.62±0.02 g·cm^{-3} respectively.
[1954Spi]	*c*-FeAlSi *t*-FeAlSi *m*-FeAlSi	- - -	- - -	- - -	The crystal structures of c-FeAlSi, t-FeAlSi and m-FeAlSi were reported to be cubic (a=1254.23 pm), tetragonal (a=612.23 pm, c=948.94 pm) and monoclinic (a=b=612.23 pm, c=4148.36 pm, β=91°), respectively. They correspond to α(Fe-Si), β(Fe-Si) of [1943Phi] and γ of [1927Gwy], respectively.
[1955Bla]	$Fe_2Al_9Si_2$	27.2	59.1	13.7	X-ray diffraction was carried out on the extracted crystals of [1951Pra1]. The crystal structure and

(*continued*)

DOI: 10.1007/978-3-540-69761-9_11

Author	Phase Designation	Composition (mass%)			Comments
		Fe	Al	Si	
					density were reported to be tetragonal (with 4/*m* symmetry and *a*=618±6 pm, *c*=4250±50 pm) and 3.50±0.1 g·cm^{-1}, respectively.
[1955Obi]	α(Fe-Si)	30.2-32.8	58.1-60.0	11.2-7.2	α(Fe-Si) was obtained in Al-5 mass% Fe-(3 to 7) mass% Si which were water quenched after annealing at 615 to 620°C for 1 h, and β(Fe-Si) was obtained in Al-4Fe-(9 to 13) Si (mass%) alloys which were f/c cooled after the same heat treatment. These crystals were extracted from alloys after subjecting to different heat treatments and were studied by X-ray diffraction. The powder patterns obtained from these two phases were almost the same as *c*-FeAlSi and *m*-FeAlSi of [1950Phr]. The lattice parameters of α(Fe-Si) and β(Fe-Si) were *a*=1254.8 pm; and *a*=*b*=612.2 pm, *c*=4148.4 pm, and β=91°, respectively.
	β(Fe-Si)	23.4-25.8	57.6-58.5	19.0-15.7	
[1956Spe]	α(Mn,Fe) AlSi	-	-	-	Found in wrought commercial 2024 alloy.
[1964Lai]	$FeAl_5Si$	-	-	-	Formed in an Al-1.5 mass % Si alloy plated with Fe and annealed at 500°C. The ternary phase was identified by X-ray and electron diffraction techniques.
[1967Coo]	α-FeAlSi	31.9	61.7	6.4	X-ray diffraction study of these crystals yielded cubic structure with *a*=1256 pm, 138 atoms/unit cell and

(*continued*)

DOI: 10.1007/978-3-540-69761-9_11

Author	Phase Designation	Composition (mass%)			Comments
		Fe	Al	Si	
					*Im*3 symmetry. The composition of the crystals was close to $Fe_5Al_{20}Si_2$ and the density was ~3.59 ±0.06 g·cm^{-3}.
[1967Mun]	α-CrFeAlSi	-	-	-	Alloys containing up to 22 mass% (Fe+Si) were cooled at 0.75°C/min. The phases were analyzed by X-ray and electron diffraction. The crystal structures of α-CrFeAlSi, α-FeAlSi and γ-FeAlSi were reported to be cubic (*a*=1250 to 1270 pm), hexagonal (*a*=230 pm, *c* =2620 pm) and C-face-centered monoclinic (*a*=1780±10 pm, *b*=1025 ±5 pm, *c*=890±5 pm, β=132°), respectively. The "cubic" (*a*=1603 pm) pattern of α_3 of [1955Arm] was indexed on the basis of this monoclinic cell. δ-FeAlSi was reported to be the same as α_2 of [1952Arm].
	α-FeAlSi	-	-	-	
	β-FeAlSi	-	-	-	
	γ-FeAlSi	33.0-38.0	54.0-43.5	13.0-18.5	
	δ-FeAlSi	-	-	-	
[1967Sun]	α_1(FeAlSi)	31.1	60.8	8.1	50 different ternary and quaternary alloys were analyzed by chemical and X-ray diffraction. The α_1 crystals were reported to contain 1.05 mass% Mn. The crystal structures of α_1 and α_2 were reported to be cubic (*a*=1250±10 pm) and hexagonal, respectively.
	α_2(Fe_2Al_8Si)	30.0-33.0	62.6-56.0	7.4-11.0	
	α_3($FeAl_3Si$)	34.0-35.2	50.4-47.7	15.6-17.1	
	β($FeAl_5Si$)	25.5-26.5	62.4-58.9	12.1-14.6	
	δ($FeAl_4Si_2$)	25.0-26.0	49.0-47.0	26.0-27.0	
[1969Pan]	$FeAl_3Si_2$	28.9	41.9	29.2	The alloy was annealed at 800°C for 14 h and water quenched, and was analyzed by X-ray diffraction. The crystal structure was reported to be tetragonal (*a*=607 pm, *c*=950 pm) of $PdGa_5$-type,

(*continued*)

DOI: 10.1007/978-3-540-69761-9_11

Author	Phase Designation	Composition (mass%)			Comments
		Fe	Al	Si	
[1973Kow]	$Fe_2Al_9Si_2$	-	-	-	Found in Al-11.17 mass% Si-0.4 mass% Fe-0.49mass %Mg-9.8mass% Si and Al-0.1Fe-0.4Mg-7.5Si-0.1Ti (mass%) alloys. The extracted crystals were analyzed by X-ray diffraction and microprobe analysis. The composition of the precipitate as given by the authors does not add up to 100.
[1974Mur], [1981Zar]	A: $Fe_{15}Al_{57-47}Si_{28-38}$	26.5-27.5	40.0-48.6	33.5-24.9	The crystal structures of $Fe_{25}Al_{50}Si_{25}$, $Fe_{25}Al_{60}Si_{15}$ and $Fe_{22}Al_{63-52}Si_{15-36}$ were reported to be orthorhombic (a=768 pm, b=1530 pm, c=1600 pm), hexagonal (a=752.6 pm, c=763.2 pm) and monoclinic (a=420 pm, b=760 pm, c=1533 pm, β=89°), respectively. The crystal structures of other phases were not reported. The A phase has hexagonal crystal structure with lattice parameters varying from a=630±0.5 pm, c=941±0.7 pm at $Fe_{15}Al_{57}Si_{28}$ to a=612±0.5 pm, c=953±0.7 pm at $Fe_{15}Al_{47}Si_{38}$. In the as-cast samples, the F phase has hexagonal structure, but its structure is different after annealing at 600°C.
	B: $Fe_{22}Al_{40}Si_{38}$	36.4	32.0	31.6	
	C: $Fe_{32}Al_{38}Si_{30}$	48.9	28.1	23.0	
	D: $Fe_{36}Al_{36}Si_{28}$	53.3	25.8	20.9	
	E: $Fe_{40}Al_{40}Si_{20}$	57.7	27.8	14.5	
	F: $Fe_{25}Al_{60}Si_{15}$	40.5	39.1	20.4	
	G: $Fe_{25}Al_{50}Si_{25}$	40.6	47.1	12.3	
	K: $Fe_{22}Al_{63-52}Si_{15-36}$	36.7-36.6	50.7-41.7	12.6-21.7	
	L: $Fe_{15}Al_{70}Si_{15}$	26.6	60.0	13.4	
	M: $Fe_{17}Al_{72}Si_{11}$	29.7	60.7	9.6	
[1975Bar]	$FeAl_5Si$	25.0	62.0	13.0	These two phases were found in Al-Fe-Mn-Mg-Si alloys. The crystal structures of $FeAl_5Si$ and Fe_2Al_8Si were reported to be monoclinic (a=b=612 pm, c=4150 pm, β=91°) and hexagonal
	Fe_2Al_8Si	31.0	61.0	8.0	

(*continued*)

DOI: 10.1007/978-3-540-69761-9_11

Author	Phase Designation	Composition (mass%)			Comments
		Fe	Al	Si	
					(with $P6_3/mmc$ symmetry and a=1230 pm, c=2630 pm), respectively.
[1977Cor]	α-(FeAlSi)	32.5	58.8	8.7	The extracted crystals of [1951Pra2] were analyzed by X-ray diffraction using Mo-K_α, Fe-K_α and Cu-K_α radiations. The crystal structure was reported to be hexagonal (a=1240.4 ± 0.1 pm, c=2623.4 ± 0.2 pm) with 44.9 atoms of Fe, 167.8 atoms of Al and 23.9 atoms of Si and the density was reported to be 3.665 g·cm^{-3}.
[1977Hoi]	β-FeAlSi α'-FeAlSi	- -	- -	- -	Found in an Al-0.2Fe-0.55Mg-0.6Si (mass%) alloy. β-FeAlSi was present in as-cast alloy and it transforms to α'-FeAlSi upon annealing at 580°C for 1 h. The crystal structures of β-FeAlSi and α'-FeAlSi were reported to be monoclinic (a=b=618 pm, c=2080 pm, β = 91°) and hexagonal (a=1230 pm, c=2630 pm), respectively.
[1977Sim]	α'-$Fe_5Al_{20}Si_2$ α-Fe_2Al_8Si Unknown phase	- - 34.1	- - 65.5	- - <0.5	Found in strip cast Al-0.5Fe-0.2Si (mass%) alloy. The precipitates were characterized by TEM with EDAX analyzer. The crystal structures of α′-$Fe_5Al_{20}Si_2$, α-Fe_2Al_8Si and the unknown phases were cubic (a=1260 pm), hexagonal and monoclinic (a=869±6 pm, b=635±2 pm, c=632±6 pm, β=93.4 ±0.5°, isomorphous with Al_9Co_2), respectively.
[1979Mor]	α_2-FeAlSi	30.0-33.0	64.0-55.0	6.0-12.0	About 80 extracted particles from the

(*continued*)

DOI: 10.1007/978-3-540-69761-9_11

Author	Phase Designation	Composition (mass%)			Comments
		Fe	Al	Si	
	β-FeAlSi	25.0-30.0	63.0-55.0	12.0-15.0	homogenized commercial 6063 aluminium alloy were analyzed by EDAX. The size and Fe/Si ratio in α_2-FeAlSi were found to be 3 μm and 2.75 to 5.5, respectively. Similar figures for the β-FeAlSi were 8 μm and 1.6 to 2.25.
[1982Wes]	β′-FeAlSi α″-FeAlSi	- -	- -	- -	Found in direct-chilled cast commercial purity Al-Fe-Si alloys. The precipitates were characterized by TEM/STEM and EDAX analyzer. The crystal structures of β'-FeAlSi and α″-FeAlSi were found to be monoclinic (*a*=890 pm, *b*=490 pm, *c*=160 pm, β=92°) and tetragonal (*a* =1260 pm, *c* =3720 pm), respectively. The Fe/Si ratio in β' was almost unity and that in α″ was between 7 and 9.
[1984Don]	α_v-FeAlSi $Fe_3Al_{12.4\text{-}14.6}Si_{1.0\text{-}2.1}$	31.6-27.0	63.1-63.5	5.3-9.5	Found in direct-chill cast as well as heat treated (400 to 600°C) three industrial cast alloys. Electrical resistivity and TEM/EDAX were performed to characterize the phases. The crystal structure was reported to be monoclinic (*a*=847 pm, *b*=635 pm, *c*=610 pm, β=93.4°).
[1985Don1]	α_T-FeAlSi ($Fe_3Al_{13}Si_{1.0\text{-}1.5}$) α-FeAlSi ($Fe_3Al_{13}Si_{1.0\text{-}2.0}$)	30.6-29.9 29.2-30.7	64.2-62.6 61.0-64.2	5.2-7.5 9.8-5.1	Found in both strip cast and direct-chill cast of 10 commercial Al-alloys which were heat treated between 400 to 600°C. The precipitates were analyzed by TEM and the crystal structures of α_T-FeAlSi and α-FeAlSi reported to be c-centered

(*continued*)

DOI: 10.1007/978-3-540-69761-9_11

Author	Phase Designation	Composition (mass%)			Comments
		Fe	Al	Si	
					monoclinic (a=2810 pm, b=3080 pm, c=2080 pm, β=97.74°) and bcc (a=1250 pm).
[1985Don2]	α-FeAlSi α′-FeAlSi β-FeAlSi α_v-FeAlSi α_T-FeAlSi	- - - - -	- - - - -	- - - - -	Found in a number of strip cast alloys in the range of Al-(0.21 to 2.98) Fe-(0.06 to 1.16) Si (mass%), and also after heat treatment at 450°C for 1 week.
[1985Gri]	-	31.5	60.7	7.8	Found in as-cast and heat treated Al-(17 to 35) mass % Fe (4 to 14) mass% Si alloy. The precipitates were characterized by X-ray diffraction and EDAX analysis.
[1985Liu], [1986Liu1], [1986Liu2], [1987Liu], [1988Liu1], [1988Liu2]	α-FeAlSi θ_1-FeAlSi θ_2-FeAlSi	25.0 25.8 27.8	69.7 70.5 68.8	5.3 3.7 3.4	Dilute Al-Fe-Si alloys with Fe/Si mass ratios of 2 and 4 were studied. Formation of the precipitates was reported to be a function of Fe/Si ratio, alloy purity, solidification rate and alloy heat treatment. The composition and the crystal structures of the phases were analyzed by EDAX and STEM. The crystal structures of α-FeAlSi, θ_1-FeAlSi and θ_2-FeAlSi were found to be bcc (a=1256 pm), c-centered orthorhombic (with *Cmmm* symmetry and a=1270 pm, b=3620 pm, c=1270 pm) and monoclinic (with *Pm* symmetry and a=1250 pm, b=1230 pm, c=1930 pm, β=109°), respectively. In the commercial alloy with Fe/Si ratio of 2, θ_1-FeAlSi transformed to θ_2-FeAlSi upon annealing at 600°C. But in a high purity alloy

(*continued*)

DOI: 10.1007/978-3-540-69761-9_11

Author	Phase Designation	Composition (mass%)			Comments
		Fe	Al	Si	
					with Fe/Si ratio of 2, neither θ_1 nor θ_2-FeAlSi formed, and α-FeAlSi persisted even after prolonged annealing at 600°C.
[1985Suz]	α-FeAlSi β-FeAlSi	32.0 27.0	60.0 59.0	8.0 14.0	The α and β crystals were extracted from Al-4 mass % Fe-5 mass% Si and Al-4 mass% Fe-10 mass% Si ingots, respectively, which were heat treated at 590 to 640°C for 1 h. The precipitates were characterized by EPMA, X-ray diffraction and Mössbauer spectroscopy.
[1986Dun]	α-FeAlSi β-FeAlSi	- -	- -	- -	The α and β phases were observed after complete crystallization of an $Fe_{14}Al_{74}Si_{12}$ amorphous alloy obtained by melt-spinning (cooling rate: $1.5 \cdot 10^6$ °C·s^{-1}).
[1987Cha], [1988Cha]	-	27.0-19.0	73.0-78.0	0.0-3.0	Found in Al-6Fe (mass%) alloy which was atomized and extruded at 400°C. The crystal structure of the metastable phase was reported to be rhombohedral (with $R3c$ or $R\bar{3}c$ symmetry, a=890 pm, α=111.8°) or hexagonal (a=1470 pm, c=780 pm). The above phase was not present after a heat treatment at 450°C for 54 h.
[1987Czi]	α-FeAlSi α′-FeAlSi β-FeAlSi	- - -	- - -	- - -	Investigated microstructures of direct-chill cast and heat treated alloys: Al-0.58Fe-0.28Si (mass%) and Al-0.54Fe-0.95Si (mass%). The as-cast microstructure of first alloy

(*continued*)

DOI: 10.1007/978-3-540-69761-9_11

Author	Phase Designation	Composition (mass%)			Comments
		Fe	Al	Si	
					contains α- and α′-AlFeSi precipitates having hexagonal and cubic structure, respectively. The as-cast microstructure of first alloy contains β-AlFeSi precipitates. Isothermal heat treatment at 350, 400, 450, 530 and 600°C resulted in the formation of Fe_4Al_{13} and $FeAl_6$ precipitates.
[1987Gri2]	α_H-FeAlSi	33.5	58.5	8.0	Alloys close to the composition of Fe_2Al_8Si were prepared and annealed at 600°C for 1 month. X-ray powder diffraction and EPMA were used to characterize the phase. The hexagonal structure (a=1240.56±0.7 pm, c=2623.6±0.2 pm and $P6_c/mmc$ symmetry) was confirmed. The details of the powder diffraction data were also presented.
[1987Nag]	α_C-FeAlSi α_H-FeAlSi	- -	- -	- -	A number of ternary alloys in direct-chill cast state and heat treated (450 to 620°C) were investigated by means of X-ray diffraction, EPMA and Mössbauer spectroscopy. α_C-FeAlSi was reported to be metastable and decomposes into Fe_4Al_{13} and Si, which in turn react to form α_H-FeAlSi.
[1987Skj1]	α″-FeAlSi	30.9-32.5	65.4-63.3	3.7-4.2	Found in direct-chill casting of Al-0.25Fe-0.13Si (mass%) alloy. The precipitates were analyzed by EDAX, TEM and HREM. The crystal structure was

(*continued*)

DOI: 10.1007/978-3-540-69761-9_11

Author	Phase Designation	Composition (mass%)			Comments
		Fe	Al	Si	
					reported to be c-centered orthorhombic (a=1300 pm, b=3600 pm, c=1260 pm).
[1987Ste]	α-FeAlSi	28.0-36.0	66.0-51.0	6.0-13.0	Alloys up to 20 to 35 mass % Fe and 4 to 14 mass% Si were investigated. As-cast alloys were reported to contain some non-equilibrium phases. The compositions of the ternary phases were found to depend on the heat treatment. The precipitates were analyzed by means of X-ray diffraction and electron probe microanalysis.
	β-FeAlSi	25.0-28.0	62.0-56.0	13.0-16.0	
	γ-FeAlSi	31.0-37.0	60.0-45.0	9.0-18.0	
	α_2-FeAlSi	40.0-42.0	48.0-42.0	12.0-16.0	
[1987Tur]	β-FeAlSi	-	-	-	β-FeAlSi (having cubic structure) formed in an Al-0.5Fe-1Si (mass%) alloy, whereas α_C-FeAlSi, hexagonal and rhombohedral phases formed in an Al-0.5Fe-0.2Si (mass%) alloy. The lattice parameters of latter three phases were a=1256 pm; a=1776 pm, c=1088 pm; a=2082 pm and α=95.2°, respectively.
	α_C-FeAlSi	-	-	-	
	Hexagonal	-	-	-	
	Rhombohedral	-	-	-	
[1988Ben2]	α-FeAlSi	-	-	-	Decomposition of rapidly solidified Al-(10 to 14) Fe-2Si (mass%) alloys were investigated by TEM. α-FeAlSi forms from an amorphous phase at 380°C and was reported to be metastable and decomposes into α′-FeAlSi and α″-FeAlSi superlattices above 430°C. The crystal structures of α-FeAlSi, α′-FeAlSi and α″-FeAlSi were reported to be cubic (a=1250 pm), rhombohedral (with $R3$
	α'-FeAlSi	-	-	-	
	α''-FeAlSi				

(*continued*)

DOI: 10.1007/978-3-540-69761-9_11

Author	Phase Designation	Composition (mass%)			Comments
		Fe	Al	Si	
					symmetry and a=2080 pm, α=95.2°) or c-hexagonal (a=2080 pm, c=3260 pm) and trigonal (with $P\bar{3}$ symmetry and a=1776 pm, c=1088 pm), respectively.
[1988Zak]	β-$FeAl_5Si$	25.9-26.6	61.3-60.1	12.8-13.3	β-$FeAl_5Si$ has monoclinic structure and δ-Fe_4Si_2 has tetragonal structures and their densities are 3.61 and 3.36 g·cm^{-3}, respectively.
	δ-$FeAl_4Si_2$	25.9-27.8	48.8-45.8	25.3-26.4	
[1993Car]	β-$Fe_3Al_{10}Si_2$	-	-	-	β-$Fe_3Al_{10}Si_2$ has B-face centered orthorhombic structure with lattice parameters a=618.4 pm, b=625 pm, c=2069 pm. The approximate composition corresponds to the EDS data. However, based on the density data of [1950Phr] and measured unit cell volume, the proposed formula is Fe_2Al_5Si.
[1994Mur] [1996Mur]	β-$FeAl_5Si$	19.5-26.8	57.3-67.9	12.5-15.8	Observed in Al-7Si-0.3Mg-0.6Fe (mass%), Al-7Si-0.3Mg-0.8Fe (mass%), Al-7Si-0.3Mg-0.64Fe-0.27Be (mass%) and Al-7Si-0.3Mg-1Fe-0.26Be (mass%) alloys. The density of β phase is 3.29 g·cm^{-3}.
[1994Rom] [1998Han]	β-$FeAl_{4.5}Si$				β-$FeAl_{4.5}Si$ crystals were grown from the melt. A combination of electron and X-ray (including synchrotron radiation) diffraction were used for crystallographic characterization. X-ray diffraction gave a=616.61, b=616.76, c=2081.3, β=90.41°.

(*continued*)

DOI: 10.1007/978-3-540-69761-9_11

Author	Phase Designation	Composition (mass%)			Comments
		Fe	Al	Si	
[1996Mul]	α-Fe_2Al_8Si β-$FeAl_5Si$	31.7 25.1	60.0 61.9	8.3 13.0	The α and β phases were observed in an Al-0.29Fe-0.58Si-0.58Mg (mass%) alloy. α-Fe_2Al_8Si forms by L ⇌ (Al) + α-Fe_2Al_8Si, and β-$FeAl_5Si$ forms by L + α-Fe_2Al_8Si ⇌ (Al) + β-$FeAl_5Si$. α-Fe_2Al_8Si is cubic with a=1250 pm, and β-$FeAl_5Si$ is monoclinic with lattice parameters a=b=612 pm, c=4150 pm and β=91°.
[1999Cho]	δ-$FeAl_4Si_2$	-	-	-	Observed in Al-8Fe-20Si and Al-5Fe-30Si (mass%) alloys, cooled at about 10° C·min^{-1}. δ-$FeAl_4Si_2$ has tetragonal structure, and it transforms to equilibrium $Fe_2Al_9Si_2$ phase at 500°C.
[2000Sri]	α-Fe_2Al_8Si α'-(Fe,Al,Si) β-$FeAl_5Si$ γ-$FeAl_3Si$ δ-$FeAl_9Si_3$ $FeAl_4Si_2$	31.6 32.1 27.2 33.0- 38.0 15.0 25.4	60.6 52.9 59.3 44.0- 54.0 65.0 49.1	7.8 8.7 13.3 13.0- 18.0 20.0 25.5	Bulk intermetallics prepared from elemental powders by self-propagating high temperature synthesis. However, only α-Fe_2Al_8Si and $FeAl_4Si_2$ were single phase.
[2000Zhe]	β-(Fe-Al-Si)	-	-	-	Observed in Al-7Si-0.3Mg-0.6Fe (mass%) alloy prepared by [1996Mur]. They found that β-$FeAl_5Si$ is actually a multiphase composite. An A-centered orthorhombic phase (space group *Cmcm*, #63) with a=618 pm, b=620 pm and c=2080 pm was observed.
[2001Hsu]	α_C-FeAlSi	-	-	-	Observed in a model 6xxx alloy containing 0.3 mass % Fe, 0.6 mass% Si and 0.8 mass% Mg. Cubic α_C-FeAlSi may form by L+Fe_4Al_{13}⇌(Al)+ α_C-

(*continued*)

DOI: 10.1007/978-3-540-69761-9_11

Author	Phase Designation	Composition (mass%)			Comments
		Fe	Al	Si	
					FeAlSi and L⇌(Al)+α_C-FeAlSi. The atomic ratio Al:Fe:Si in α_C-FeAlSi may vary from 7:4:1 to 9:5:1.
[2001Kre]	τ_1/τ_9: $Fe_3(Al_{0.4}Si_{0.6})_5$	-	-	-	All ternary phases exist at 550°C. Previously reported τ_1 and τ_9 [1992Gho] are established as one phase with large homogeneity range.
	τ_2: $Fe_2(Al_{1-x}Si_x)_7$ $0.2x<0.33$	-	-	-	
	τ_3: $FeAl_{2.25}Si_{0.75}$				
	τ_4: $FeAl_3Si_2$	-	-	-	
	τ_5: $Fe_2Al_{7.4}Si$	-	-	-	
	τ_6: $FeAl_{4.5}Si$	-	-	-	
	τ_7: $FeAl_{1.5}Si_{1.5}$	-	-	-	
	τ_8: $FeAl_{0.67}Si_{1.33}$	-	-	-	
	τ_{10}: $Fe_5Al_{12}Si_3$	-	-	-	
[2001Sha]	α-FeAlSi	-	-	-	Observed in a model 6xxx alloy containing 0.3 mass % Fe, 0.6 mass% Si and 0.8 mass% Mg. α-FeAlSi may be simple cubic with a=1252 pm, or bcc with a=1256 pm. β-FeAlSi is monoclinic. They may form by the following reactions: L+Fe_4Al_{13}⇌(Al)+α-FeAlSi, L⇌(Al)+α-FeAlSi, and L+α-FeAlSi⇌(Al)+β-FeAlSi. β-FeAlSi is metastable.
	β-FeAlSi	-	-	-	
[2002Gup]	τ_1: $Fe_{36-39}Al_{41}Si_{20-23}$	-	-	-	Observed in diffusion couples (Fe/(Al-Si) eutectic) that were annealed at 1115°C (4 h), 1100°C (1 h), and 1020°C (4 h) followed by either water quenching or furnace cooling. All solid phases were identified by EDX analysis only in an electron probe microanalyzer.
	τ_2: $Fe_{23}Al_{55-56}Si_{21-22}$	-	-	-	
	τ_3: $Fe_{32}Al_{44}Si_{24}$	-	-	-	
	τ_4: $Fe_{15}Al_{59}Si_{26}$	-	-	-	
	τ_5: $Fe_{20}Al_{69}Si_{11}$	-	-	-	
	τ_6: $Fe_{15-16}Al_{66-67}Si_{18}$	-	-	-	
	τ_7: $Fe_{25}Al_{36}Si_{39}$	-	-	-	
	τ_9: $Fe_{36}Al_{36}Si_{28-29}$	-	-	-	
	τ_{10}: $Fe_{24-27}Al_{59-62}Si_{13-14}$	-	-	-	
[2002Mai]	τ_1: $Fe_{35-36}Al_{38-41}Si_{23-27}$	-	-	-	Observed in diffusion couples (Fe/(Al-Si) eutectic) that were annealed at 900°C (25 h),
	τ_2: $Fe_{19-23}Al_{57-63}Si_{18-22}$				
	τ_4: $Fe_{15}Al_{56}Si_{29}$	-	-	-	
	τ_5: $Fe_{18-19}Al_{69-70}Si_{11-13}$				

(*continued*)

DOI: 10.1007/978-3-540-69761-9_11

Author	Phase Designation	Composition (mass%)			Comments
		Fe	Al	Si	
	τ_6: $Fe_{16-17}Al_{67-69}Si_{14-18}$	-	-	-	800°C (36 h), and 600°C (36 h) followed by either water quenching or furnace cooling. All solid phases were identified by EDX analysis only in an electron probe microanalyzer.
		-	-	-	
		-	-	-	
[2003Kha]	α: $Fe_2Al_{8.1-9.1}Si_{0.87-1.25}$ (hexagonal)	-	-	-	Solidification process in six ternary alloys, in the composition range Al-(0.23-1.03) mass% Fe-(0.35-6.32) mass% Si, were studied by thermal analysis. The alloys were cooled at various rates between 0.16 to 14.7 °C·s^{-1}. The intermetallics were characterized by metallography, SEM and EPMA (EDX/WDX).
	α: $Fe_2Al_{10.42-11.67}Si_{1.08-1.25}$(cubic)	-	-	-	
	β: $FeAl_{4.25-4.98}Si_{0.98-1.14}$				
	δ: $FeAl_4Si_2$	-	-	-	
	q_1: $FeAl_{13.2-14.9}Si_{0.66-0.79}$	-	-	-	
		-	-	-	
[2003Wen]	α-Al_8Fe_2Si	63.7	28.6	5.7	Observed in commercial A356 alloy thixoformed at 578°C. The intermetallics were characterized by metallography and TEM.
	β-$FeAl_{4.5}Si$	58.2	24.5	17.3	
[2004Kra]	α-$(Fe,Mn)_5Al_{19}Si_2$	-	-	-	Observed in as-cast Al-11.7 mass% Si-0.16 mass % Fe-0.16 mass% Mn alloy. The intermetallics were characterized by SEM/EDX and EBSD (EDX/WDX).The α phase has cubic symmetry with a=1256 pm, and the β phase has tetragonal symmetry with a=607 pm and c=950 pm.
	β-(Fe,Mn) Al_3Si_2	-	-	-	
[2004Pon]	α-$Fe_2Al_{7.4}Si$	bal.	31-33.5	8.6-10.9	Eighteen Al rich alloys in the composition range of Al-(3-42) Si-8Fe (at.%) were investigated by means of metallography, SEM, XRD, and EPMA
	δ-$FeAl_3Si_2$	bal.	26.5-29.5	27-33	
	γ-$FeAl_3Si$		33-36	13-22	

(*continued*)

DOI: 10.1007/978-3-540-69761-9_11

Author	Phase Designation	Composition (mass%)			Comments
		Fe	Al	Si	
					techniques. The alloys were equilibrated at 727°C for 72 h.
[2004Sug]	λ-$Fe_{20.9}Al_{63}Si_{16.1}$	-	-	-	Observed in an $Al_{74}Fe_{18.5}Si_{7.5}$ alloy that was melted in an induction furnace and then cooled at 10°C·h^{-1}. X-ray diffraction of single crystals established rhombohedral structure with a=882.08 pm and α=70.82° (original data was given in hexagonal setting with a=1022.2 pm and c=1966.8 pm)
[2005Kra]	α-$(Fe,Mn)_5Al_{19}Si_2$ δ-(Fe,Mn) Al_3Si_2	- -	- -	- -	Observed in an as-cast Al-11.7 mass% Si- 0.16 mass% Fe-0.13 mass% Mn alloy. A combination of SEM/EDX, EBSD, TEM, and CBED techniques were employed for structural characterization of intermetallics. The α phase was established to be cubic with a = 1256 pm, and the δ phase is tetragonal with a=607 pm and c=950 pm.
[2006Kra]	α-FeAlSi δ-$FeAl_3Si_2$ β-$Fe_9Al_2Si_2$	- 65.8 61.2	- 11.12 16.6	- 20.2 19.7	Observed in an as-cast Al-11.7 mass% Si- 0.16 mass% Fe-0.13Mn alloy. A combination of SEM/EDX, TEM, and CBED techniques were employed for structural characterization of intermetallics. The α phase was established to be cubic with a=1256 pm, and the δ phase is reported to have the space group *I*4/*mcm* as reported by [1969Pan]

DOI: 10.1007/978-3-540-69761-9_11

Table 3. Crystallographic Data of Solid Phases

Phase/ Temperature Range [°C]	Pearson Symbol/ Space Group/ Prototype	Lattice Parameters [pm]	Comments/References
(Al) ≤ 660.452	*cF*4 $Fm\bar{3}m$ Cu	*a* = 404.88	pure Al at 24°C [Mas2].
(αδFe) (αFe)(r) ≤ 912	*cI*2 $Im\bar{3}m$ W	*a* = 286.65	pure Fe at 25°C [Mas2]
(δFe)(h_2) 1538 - 1394		*a* = 293.15	pure Fe at 1480°C [Mas2]
γ(Fe)(h_1) 1394 - 912	*cF*4 $Fm\bar{3}m$ Cu	*a* = 364.67	pure Fe at 915°C [Mas2]
(Si) ≤ 1414	*cF*8 $Fm\bar{3}m$ C-diamond	*a* = 543.088 *a* = 542.86	at 20°C and 99.999 at.% purity [V-C] at 20°C and 99.97 at.% purity [V-C].
α_1, Fe_3Al ≤552.5	*cF*16 $Fm\bar{3}m$ BiF_3	*a* = 578.86 to 579.3	solid solubility ranges from ~25 to ~37 at.% Al [2006MSIT]
Fe_3Si ≤ 1235		*a* = 565.54	[V-C]; 11.0 to 30.5 at.% Si [Mas].
α_2, FeAl ≤ 1310	*cP*2 $Pm\bar{3}m$ CsCl	*a* = 289.76 to 290.78	[2006MSIT], at room temperature solid solubility ranges from ~24 to ~55 at.% Al
FeSi ≤ 1280		-	10.0 to 23.5 at.% Si [Mas].
ε, Fe_2Al_3 1232 - 1102	*cI*16?	 *a* = 598.0	[2006MSIT], solid solubility ranges from 58 to 65 at.% Al at 61 at.% Al [V-C2]
$FeAl_2$ ≤ 1156	*aP*18 *P*1 $FeAl_2$	*a* = 487.8 *b* = 646.1 *c* = 880.0 α = 91.75° β = 73.27° γ = 96.89°	[2006MSIT], at 71.5 at.% Al. Solid solubility ranges from ~70 to ~73 at.% Al
η, Fe_2Al_5 ≤ 1169	*oC*24 *Cmcm*	*a* = 765.59 *b* = 641.54 *c* = 421.84	[2006MSIT], at 71.5 at.% Al. Solid solubility ranges from 71.0 to 72.5 at.% Al.

(*continued*)

DOI: 10.1007/978-3-540-69761-9_11

Phase/ Temperature Range [°C]	Pearson Symbol/ Space Group/ Prototype	Lattice Parameters [pm]	Comments/References
Fe_4Al_{13} ≤ 1160	*mC*102 *C*2/*m* Fe_4Al_{13}	*a* = 1552.7 to 1548.7 *b* = 803.5 to 808.4 *c* = 1244.9 to 1248.8 β = 107.7 to 107.99°	[2006MSIT], 74.16 to 76.7 at.% Al solid solubility ranges from 74.5 to 75.5 at.% Al
		a = 1549.2 *b* = 807.8 *c* = 1247.1 β = 107.69°	[2006MSIT], at 76.0 at.% Al. Also denoted $FeAl_3$ or Fe_2Al_7
Fe_2Si 1212 - 1040	*hP*6 $P6_3/mmc$ Fe_2Si	*a* = 405.2 *c* = 508.55	[V-C]; 33.0 to 34.5 at.% Si [Mas].
Fe_5Si_3 1060 - 825	*hP*16 $P6_3/mmc$ Mn_5Si_3	*a* = 675.52 *c* = 471.74	[V-C].
FeSi ≤1410	*cP*8 $P2_13$ FeSi	*a* = 448.91	[V-C]; 49.0 to 51.0 at.% Si [Mas].
$FeSi_2$(h) 1220 - 937	*tP*3 *P*4/*mmm* $FeSi_2$	*a* = 269.5 *c* = 509.0	[V-C]; 69.5 to 73.0 at.% Si [Mas].
$FeSi_2$(r) ≤ 982	*oC*48 - $FeSi_2$	*a* = 986.3 *b* = 779.1 *c* = 783.3	[V-C].
* τ_1/τ_9, $Fe_3Al_2Si_3$			K_1 of [1940Tak]. Most likely the E phase of [1974Mur] and [1981Zar]. Also, D phase of [1981Zar] and τ_9 of [1992Gho].
	*aP*16 $P\bar{1}$ $Fe_3Al_2Si_3$	*a* = 465.1 *b* = 632.6 *c* = 749.9 α = 101.37° β = 105.92° γ = 101.23°	[1996Yan], $Fe_3Al_2Si_3$ annealed at 600°C.
		a = 462.3 *b* = 637.4 *c* = 759.9 α = 102.81° β = 105.6° γ = 100.85°	[2001Kre], at $Fe_{38.2}Al_{29}Si_{32.8}$, in equilibrium with τ_2 and τ_7 at 550°C.
		a = 469.1 *b* = 632.5 *c* = 751.1	[2001Kre], at $Fe_{38}Al_{35}Si_{27}$, in equilibrium with τ_3 and τ_{10} at 550°C.

(*continued*)

DOI: 10.1007/978-3-540-69761-9_11

Phase/ Temperature Range [°C]	Pearson Symbol/ Space Group/ Prototype	Lattice Parameters [pm]	Comments/References
		α = 100.6° β = 105.5° γ = 101.78° *a* = 468.7 *b* = 633.1 *c* = 751.9 α = 100.43° β = 105.44° γ = 101.63°	[2001Kre], at $Fe_{37}Al_{41}Si_{22}$, in equilibrium with α_2 and Fe_2Al_5 at 550°C.
* τ_2,γ-AlFeSi, $Fe_2Al_5Si_2$	- *c***	- *a* = 1603.23	K_2 of [1940Tak] at $Fe_6Al_{12}Si_6$. [1952Arm, 1955Arm], in an Al-35.3Fe-12.8Si (mass%) alloy.
	*mC**	*a* = 890.0 *b* = 1025.0 *c* = 1780.0 β = 132.0°	[1967Mun], $Fe_{19.4\text{-}23}Al_{59\text{-}61.4}Si_{27.6\text{-}15.6}$ and most likely the K phase of [1974Mur] and [1981Zar].
		a = 889.3 *b* = 1018.8 *c* = 1766.9 β = 132.18°	[2001Kre], at $Fe_{22}Al_{60}Si_{18}$, in equilibrium with Fe_2Al_{13}.
	*m***	*a* = 420.0 *b* = 760.0 *c* = 1533.0 β = 89.0°	[1974Mur, 1981Zar]. K phase at $Fe_{22}Al_{63\text{-}52}Si_{15\text{-}26}$. Annealed at 600°C.
* τ_3, $Fe_5Al_9Si_5$, $FeAl_2Si$	*oC*128 *Cmma* $FeAl_2Si$		K_3 of [1940Tak].
		a = 768.0 *b* = 1530.0 *c* = 1600.0	[1974Mur, 1981Zar], G phase at $FeAl_2Si$. Annealed at 600°C.
		a = 799.5 *b* = 1516.2 *c* = 1522.0	[1989Ger2] at $Fe_{25}Al_{50}Si_{25}$. Annealed at 600°C.
		a = 726.2 *b* = 1551.2 *c* = 1550.6	[2001Kre], at $Fe_{25}Al_{55}Si_{20}$, in equilibrium with τ_1/ τ_9 and τ_{10} at 550°C.
		a = 795.8 *b* = 1517.8 *c* = 1523.7	[2001Kre], at $Fe_{25}Al_{50}Si_{25}$, in equilibrium with τ_{10} and Fe_4Al_{13} at 550°C.
* τ_4, δ-AlFeSi, $FeAl_3Si_2$	*tI*24 *I4/mcm* $PdGa_5$		K_4 of [1940Tak] at $FeAl_3Si$.
		a = 607.0 *c* = 950.0	[1969Pan], annealed at 800°C for 14 h and water quenched.
		a = 615.0 *c* = 947.0	[1936Jae], at $FeAl_4Si_2$. In an Al-27.04Fe-25.0Si (mass%) alloy.
		a = 612.23 *c* = 947.91	[1950Phr], in an Al-15Fe-20Si (mass%) alloy.
		a = 612.23 *c* = 948.91	[1954Spi].

(*continued*)

DOI: 10.1007/978-3-540-69761-9_11

Phase/ Temperature Range [°C]	Pearson Symbol/ Space Group/ Prototype	Lattice Parameters [pm]	Comments/References
		a = 612.0 c = 953.0	[1974Mur, 1981Zar], A phase at $FeAl_{2.76}Si_{2.24}$. Annealed at 600°C.
		a = 630.0 c = 941.0	[1974Mur, 1981Zar], A phase at $FeAl_{3.35}Si_{1.65}$. Annealed at 600°C.
		a = 606.1 c = 952.5	[1995Gue1].
		a = 608.74 c = 951.36	[2001Kre], at $Fe_{16.9}Al_{49.5}Si_{33.3}$. Single phase at 700°C.
		a = 608.87 c = 950.39	[2001Kre], at $Fe_{17}Al_{50}Si_{33}$, in equilibrium with τ_7 at 550°C.
		a = 611.25 c = 949.16	[2001Kre], at $Fe_{17}Al_{53}Si_{30}$, in equilibrium with τ_2 at 550°C.
		a = 607.0 c = 950.0	[2004Kra, 2005Kra], in as-cast Al-11.7Si-0.16Fe-0.16Mn (mass%) alloy.
* τ_5, α-AlFeSi, $Fe_2Al_{7.4}Si$ $Fe_{46}(Al_{0.875}Si_{0.125})_{200-x}$ $x \neq 7$	*hP*245 $P6_3/mmc$ $Fe_2Al_{7.4}Si$		K_5 of [1940Tak] at $Fe_6Al_{15}Si_5$.
		a = 1240.4 c = 2623.4	[1977Cor], at $Fe_{1.9}Al_{7.1}Si$. Most likely the M phase of [1974Mur] and [1981Zar].
		a = 1240.56 c = 2623.6	[1987Gri2], at $Fe_{2.1}Al_{7.6}Si$. Annealed at 600°C for a month.
		a = 1239.4 c = 2621.0	[1987Gri2], 9.5 ± 5 mass% Si in τ_5. Annealed at 600°C for a month.
		a = 1239.2 c = 2619.3	[1987Gri2], 9.0 ± 5 mass% Si in τ_5. Annealed at 600°C for a month.
		a = 1241.0 c = 2626.4	[1987Gri2], 7.0 ± 4 mass% Si in τ_5. Annealed at 600°C for a month.
		a = 1230.0 c = 2630.0	[1975Bar], at $Fe_{1.95}Al_{7.93}Si$.
		a = 1230.0 c = 2630.0	[1953Rob].
		a = 1230.0 c = 2620.0	[1967Mun].
		a = 1230.0 c = 2630.0	[1977Hoi].
		a = 1240.06 c = 2622.41	[1997Vyb], at $Fe_{19.2}Al_{71.2}Si_{9.6}$.
		a = 1238.9 c = 2625.5	[2001Kre], at $Fe_{19}Al_{69}Si_{12}$, in equilibrium with τ_6 and (Al) at 550°C.
		a = 1239.86 c = 2621.9	[2001Kre], at $Fe_{18}Al_{71}Si_{11}$, in equilibrium with Fe_4Al_{13} at 550°C.
* τ_6, β-AlFeSi $Fe_2Al_9Si_2$	*C*2/*c* *mC*52 $Fe_2Al_9Si_2$		K_6 of [1940Tak] at $FeAl_4Si$.
		$a = b$ = 612.23 c = 4148.36	[1950Phr], at $Fe_2Al_9Si_2$. Composition may vary from 27.2 to 27.4 mass% Fe and 13.5 to 13.6

(*continued*)

DOI: 10.1007/978-3-540-69761-9_11

Phase/ Temperature Range [°C]	Pearson Symbol/ Space Group/ Prototype	Lattice Parameters [pm]	Comments/References
		β = 91.0°	mass% Si. Most likely the L phase of [1974Mur] and [1981Zar].
		a = *b* = 612.23 *c* = 4148.36 β = 91.0°	[1954Spi].
		a = *b* = 612.2 *c* = 4148.4 β = 91.0°	[1955Obi].
		a = *b* = 612.0 *c* = 4150.0 β = 91.0°	[1975Bar], at $Fe_2Al_{10.26}Si_{2.06}$.
		a = 616.1 *b* = 617.5 *c* = 2081.3 β = 90.42°	[1994Rom, 1998Han], X-ray diffraction.
		a = 616.76 *b* = 616.61 *c* = 2080.93 β = 91°	[1998Han, 2003Gjo], synchrotron radiation.
		a = 612 *b* = 612 *c* = 4150 β = 91°	[1996Mul], at $Fe_{14}Al_{71.6}Si_{14.4}$.
		a = 579.2 *b* = 1227.3 *c* = 431.3 β = 98.9°	[1994Mur, 1996Mur].
		a = 615.59 to 620.89 *b* = 616.87 to 619.78 *c* = 2076.7 to 2081.2 β = 90.1° to 90.6°	[1997Vyb].
		a = 615.9 *b* = 618.2 *c* = 2076.5 β = 90.11°	[2001Kre], at $Fe_{15}Al_{68.5}Si_{16.5}$, in equilibrium with τ_5 and (Al) at 550°C.
		a = 616.6 *b* = 617.1 *c* = 2082.7 β = 90.28°	[2001Kre], at $Fe_{15}Al_{69}Si_{16}$, in equilibrium with (Al) at 550°C.
	oC? *Cmcm*	*a* = 618.4 *b* = 625.0 *c* = 2069.0	[1993Car].
		a = 618.0 *b* = 620.0 *c* = 2080.0	[2000Zhe].
			[1955Bla], at $Fe_2Al_{8.98}Si_2$.

(*continued*)

DOI: 10.1007/978-3-540-69761-9_11

Phase/ Temperature Range [°C]	Pearson Symbol/ Space Group/ Prototype	Lattice Parameters [pm]	Comments/References
	*t***	*a* = 618.0	
	-	*c* = 4250.0	
* τ_7,	$P2_1/c$		[1974Mur, 1981Zar], B phase.
$Fe_{22}Al_{40}Si_{38}$	*mP*64		Annealed at 600°C.
$Fe(Al_{0.5}Si_{0.5})_3$	$Fe_2Al_3Si_3$	*a* = 717.9	[1995Gue2], annealed at 800°C.
		b = 835.4	
		c = 1445.5	
		β = 93.8°	
		a = 718.9	[2001Kre] at $Fe_{25.3}Al_{45}Si_{29.7}$, in equi-
		b = 831.7	librium with τ_1/τ_9 and τ_2 at 550°C.
		c = 1454.2	
		β = 93.48°	
* τ_8,	*oC*36	-	[1974Mur, 1981Zar], C phase at
$Fe_3Al_2Si_4$,	*Cmcm*		$Fe_{32}Al_{38}Si_{30}$. Annealed at 600°C.
$Fe(Al_{0.33}Si_{0.67})_2$	$Fe_3Al_2Si_4$	*a* = 366.8	[1996Yan], at $Fe_3Al_2Si_4$ annealed at
		b = 1238.5	500°C.
		c = 1014.7	
		a = 366.7	[2001Kre]
		b = 1236.2	
		c = 1014.0	
* τ_{10},	*hP*26 or	*a* = 752.6	[1974Mur, 1981Zar], F phase in the
$Fe_5Al_{12}Si_3$	*hP*28	*c* = 763.2	as-cast sample. The crystal structure
$Fe(Al_{0.8}Si_{0.2})_3$	$P6_3/mmc$		of F phase after annealing at 600°C is
	Mn_3Al_{10} or		different from that in the as-cast
	Co_2Al_5		samples.
		a = 750.9	[1989Ger1], at $Fe_{1.7}Al_4Si$.
		c = 759.4	
		a = 1551.8	[2001Kre], single phase at $Fe_{25}Al_{60}Si_{15}$.
		c = 729.7	

Table 4. A Classification of Metastable Phases Based on the Crystal System

Phase Designation	Crystal System	Composition (mass%)			Lattice Parameters [pm]	References
		Fe	Al	Si		
μ_1	Cubic	25.4	49.1	25.5	-	[1937Ser]
		31.9	62.5	5.6	*a* = 1254.83	[1950Phr]
		27.3	65.7	7.0	*a* = 1254.83	[1952Arm, 1955Arm]
		-	-	-	*a* = 1254.53	[1954Spi]
		30.2-	58.1-	7.2-11.7	*a* = 1254.8	[1955Obi]
		32.8	60.0	6.4	*a* = 1256	[1967Coo]
		31.9	61.7	-	*a* = 1250 to 1270	[1967Mun]
		-	-	8.1	*a* = 1250 ± 10	[1967Sun]
		31.1	60.8	-	*a* = 1260.0	[1977Sim]

(*continued*)

DOI: 10.1007/978-3-540-69761-9_11

Phase Designation	Crystal System	Composition (mass%)			Lattice Parameters [pm]	References
		Fe	Al	Si		
		-	-	5.1-9.8	a = 1250	[1985Don1]
		29.2-30.7	61.0-64.2	5.3	a = 1256	1986Liu1, 1986Liu2, 1987Liu]
		25.0	69.7			
				-	a = 1256	[1987Tur]
				-	a = 1250	[1988Ben2]
		-	-		a = 1250	[1996Mul]
		-	-		a = 1256	[2004Kra, 2005Kra, 2006Kra]
μ_2	Tetragonal	-	-	-	a = 495.0	[1951Now]
		-	-	-	c = 707.0	
					a = 1260.0	[1982Wes]
					c = 3720.0	
μ_3	Orthorhombic	-	-	-	a = 609.0	[1936Jae]
					b = 996.0	
					c = 374.0	
		29.2	59.5	11.3	a = 4360.0	[1952Arm, 1955Arm, 1967Mun]
					b = 4960.0	
					c = 7080.0	
		25.8	70.5	3.7	a = 1270.0	[1986Liu1, 1986Liu2, 1987Liu]
					b = 3620.0	
					c = 1270.0	
		30.9-32.5	63.3-65.4	3.7- 4.2	a = 1300.0	[1987Skj1]
					b = 3600.0	
					c = 1260.0	
μ_4	Rhombohedral	27.0-19.0	73.0-78.0	0.0-3.0	a = 890.0	[1987Cha, 1988Cha]
					α = 111.8°	
		-		-	a = 2082.0	[1987Tur]
			-		α = 95.2°	
		-		-	a = 2080.0	[1988Ben2]
			-		α = 95.2°	
					a = 882.08	[2004Sug]
					α = 70.82°	
μ_5	Hexagonal	-	-	-	a = 836.0	[1936Jae]
					c = 1458.0	
		29.2	59.5	11.3	a = 496.0	[1952Arm, 1955Arm, 1967Mun]
					c = 702.1	
		27.0-19.0	73.0-78.0	0.0-3.0	a = 1470.0	[1987Cha, 1988Cha]
					c = 780.0	
				-	a = 1776.0	[1987Tur]
		-	-		c = 1088.0	
				-	a = 1776.0	[1988Ben2]
		-	-		c = 1088.0	

(*continued*)

DOI: 10.1007/978-3-540-69761-9_11

Phase Designation	Crystal System	Composition (mass%)			Lattice Parameters [pm]	References
		Fe	Al	Si		
μ_6	Monoclinic	32.1-32.7	57.0-59.5	8.4-10.3	-	[1951Pra2]
		-	-	-	a = 618.0 b = 618.0 c = 2080.0 β = 91.0°	[1977Hoi]
		34.1	65.5	<0.5	a = 869.0 ± 6 b = 635.0 ± 2 c = 632.0 ± 6 β = 93.4 ± 0.5°	[1977Sim]
		-	-	-	a = 890.0 b = 490.0 c = 4160.0 β = 90.0°	[1982Wes]
		27.0-31.6	63.1-63.5	5.3-9.5	a = 847.0 b = 635.0 c = 610.0 β = 93.4°	[1984Don]
		29.9-30.6	62.6-64.2	5.2-7.5	a = 2810.0 b = 3080.0 c = 2080.0 β = 97.74°	[1985Don1]
		27.8	68.8	3.4	a = 1250.0 b = 1230.0 c = 1930.0 β = 109.0°	[1986Liu1, 1986Liu2, 1987Liu]
μ_7	Triclinic	-	-	-	a = 688.0 b = 593.0 c = 432.0 α = 104.75° β = 130.67° γ = 68.4°	[1936Jae]

Table 5. Invariant Equilibria

Reaction	T [°C]	Type	Phase	Composition, mass% (at.%)		
				Fe	Al	Si
L + Fe_2Si ⇌ α_1 + FeSi	ca. 1175	U_1	L	~78.0 (64.02)	~1.0 (1.70)	~21.0 (34.28)
Fe_2Al_3+Fe_2Al_5⇌$FeAl_2$, L	ca. 1160	D_1	L	~49.0 (31.71)	~50.8 (68.03)	~0.2 (0.26)
L + ε ⇌ α_2 + Fe_2Al_5	ca. 1125	U_2	L ε, Fe_2Al_3 α_2 Fe_2Al_5	51.0 (33.51) 56.5 (38.57) 58.0 (40.34) 45.0 (28.37)	46.0 (62.57) 43.0 (60.75) 28.0 (40.30) 52.0 (67.86)	3.0 (3.92) 0.5 (0.68) 14.0 (19.36) 3.0 (3.76)

(*continued*)

DOI: 10.1007/978-3-540-69761-9_11

Reaction	T [°C]	Type	Phase	Composition, mass% (at.%)		
				Fe	Al	Si
$L + FeAl_2 \rightleftharpoons \alpha_2 + Fe_2Al_5$	ca. 1095	U_3	L	~51.0 (33.59)	~42.0 (57.25)	~7.0 (9.16)
$L + \alpha_1 + FeSi \rightleftharpoons \tau_1$	1050	P_1	L	50.0 (32.91)	31.0 (42.23)	19.0 (24.86)
			α_1	63.0 (45.43)	26.0 (38.80)	11.0 (15.77)
			FeSi	66.3 (49.72)	0.4 (0.62)	33.3 (49.66)
			τ_1	55.0 (37.51)	26.6 (37.54)	18.4 (24.95)
$L + \alpha_2 \rightleftharpoons Fe_2Al_5 + \tau_1$	1030	U_4	L	48.5 (31.50)	37.5 (50.42)	14.0 (18.08)
			α_2	65.0 (47.57)	25.0 (37.87)	10.0 (14.56)
			Fe_2Al_5	45.0 (28.37)	52.5 (68.50)	2.5 (3.13)
			τ_1	55.0 (37.51)	26.6 (37.54)	18.4 (24.95)
$L + Fe_2Al_5 \rightleftharpoons Fe_4Al_{13} + \tau_1$	1020	U_5	L	48.0 (31.07)	38.0 (50.91)	14.0 (18.02)
			Fe_2Al_5	45.0 (28.37)	52.5 (68.50)	2.5 (3.13)
			Fe_4Al_{13}	39.2 (23.76)	60.0 (75.28)	0.8 (0.96)
			τ_1	55.0 (37.51)	26.6 (37.54)	18.4 (24.95)
$L + FeSi \rightleftharpoons FeSi_2(h) + \tau_1$	1000	U_6	L	42.0 (26.34)	26.0 (33.75)	32.0 (39.91)
			FeSi	66.3 (49.72)	0.4 (0.62)	33.3 (49.66)
			$FeSi_2(h)$	44.8 (28.98)	0.5 (0.67)	54.7 (70.35)
			τ_1	55.0 (37.51)	26.6 (37.54)	18.4 (24.95)
$L + Fe_4Al_{13} + \tau_1 \rightleftharpoons \tau_2$	940	P_2	L	40.0 (24.59)	41.0 (52.18)	19.0 (23.23)
			Fe_4Al_{13}	39.2 (23.76)	60.0 (75.28)	0.8 (0.96)
			τ_1	55.0 (37.51)	26.6 (37.54)	18.4 (24.95)
			τ_2	41.9 (26.07)	40.5 (52.16)	17.6 (21.77)
$L + \tau_1 + \tau_2 \rightleftharpoons \tau_3$	935	P_3	L	39.0 (23.86)	39.0 (49.38)	22.0 (26.76)
			τ_1	55.0 (37.51)	26.6 (37.54)	18.4 (24.95)
			τ_2	41.9 (26.07)	40.5 (52.16)	17.6 (21.77)
			τ_3	42.2 (26.36)	36.7 (47.44)	21.1 (26.20)
$L + \tau_1 \rightleftharpoons FeSi_2(?) + \tau_3$	885	U_7	L	28.0 (16.08)	36.0 (42.80)	36.0 (41.12)
			τ_1	55.0 (37.51)	26.6 (37.54)	18.4 (24.95)
			$FeSi_2(?)$	49.7 (33.19)	0.5 (0.69)	49.8 (66.12)
			τ_3	42.2 (26.36)	36.7 (47.44)	21.1 (26.20)
$L + FeSi_2(?) \rightleftharpoons \tau_3 + (Si)$	880	U_8	L	26.0 (14.75)	38.0 (44.63)	36.0 (40.62)
			$FeSi_2(?)$	49.7 (33.19)	0.5 (0.69)	49.8 (66.12)
			τ_3	42.2 (26.36)	36.7 (47.44)	21.1 (26.20)
			(Si)	0.01 (0.01)	0.013 (0.01)	99.977 (99.98)
$L + \tau_3 + (Si) \rightleftharpoons \tau_4$	865	P_4	L	23.0 (12.79)	45.0 (51.81)	32.0 (35.40)
			τ_3	42.2 (26.36)	36.7 (47.44)	21.1 (26.20)
			(Si)	0.01 (0.01)	0.013 (0.01)	99.977 (99.98)
			τ_4	28.9 (16.64)	41.9 (49.93)	29.2 (33.43)
$L + Fe_4Al_{13} + \tau_2 \rightleftharpoons \tau_5$	855	P_5	L	25.0 (13.98)	58.0 (67.12)	17.0 (18.90)
			Fe_4Al_{13}	39.2 (23.76)	60.0 (75.28)	0.8 (0.96)
			τ_2	41.9 (26.07)	40.5 (52.16)	17.6 (21.77)
			τ_5	38.1 (23.10)	46.0 (57.73)	15.9 (19.17)

(*continued*)

DOI: 10.1007/978-3-540-69761-9_11

Reaction	T [°C]	Type	Phase	Composition, mass% (at.%)		
				Fe	Al	Si
$L + \tau_3 \rightleftharpoons \tau_2 + \tau_4$	835	U_9	L	22.0 (12.11)	56.0 (63.81)	22.0 (24.08)
			τ_3	42.2 (26.36)	36.7 (47.44)	21.1 (26.20)
			τ_2	41.9 (26.07)	40.5 (52.16)	17.6 (21.77)
			τ_4	28.9 (16.64)	41.9 (49.93)	29.2 (33.43)
$L + \tau_2 \rightleftharpoons \tau_4 + \tau_5$	790	U_{10}	L	18.0 (9.67)	61.0 (67.88)	21.0 (22.45)
			τ_2	41.9 (26.07)	40.5 (52.16)	17.6 (21.77)
			τ_4	28.9 (16.64)	41.9 (49.93)	29.2 (33.43)
			τ_5	38.1 (23.10)	46.0 (57.73)	15.9 (19.17)
$L + \tau_4 + \tau_5 \rightleftharpoons \tau_6$	700	P_6	L	7.2 (3.63)	78.8 (82.32)	14.0 (14.05)
			τ_4	28.9 (16.64)	41.9 (49.93)	29.2 (33.43)
			τ_5	38.1 (23.10)	46.0 (57.73)	15.9 (19.17)
			τ_6	29.1 (16.66)	56.3 (66.72)	14.6 (16.62)
$L + Fe_4Al_{13} \rightleftharpoons (Al) + \tau_5$	632	U_{11}	L	2.0 (0.98)	93.8 (94.94)	4.2 (4.08)
			Fe_4Al_{13}	39.2 (23.76)	60.0 (75.28)	0.8 (0.96)
			(Al)	0.05 (0.02)	99.31 (99.36)	0.64 (0.62)
			τ_5	38.1 (23.10)	46.0 (57.73)	15.9 (19.17)
$L + \tau_5 \rightleftharpoons (Al) + \tau_6$	613	U_{12}	L	1.8 (0.88)	92.0 (93.09)	6.2 (6.03)
			τ_5	38.1 (23.10)	46.0 (57.73)	15.9 (19.17)
			(Al)	0.04 (0.02)	98.96 (99.02)	1.0 (0.96)
			τ_6	29.1 (16.66)	56.3 (66.72)	14.6 (16.62)
$L + \tau_4 \rightleftharpoons \tau_6 + (Si)$	600	U_{13}	L	1.5 (0.73)	84.2 (85.35)	14.3 (13.92)
			τ_4	28.9 (16.64)	41.9 (49.93)	29.2 (33.43)
			τ_6	29.1 (16.66)	56.3 (66.72)	14.6 (16.62)
			(Si)	0.01 (0.01)	0.012 (0.01)	99.978 (99.98)
$L \rightleftharpoons \tau_6 + (Al) + (Si)$	573	E_1	L	0.5 (0.24)	87.8 (88.44)	11.7 (11.32)
			τ_6	29.1 (16.66)	56.3 (66.72)	14.6 (16.62)
			(Al)	0.01 (0.00)	98.34 (98.41)	1.65 (1.59)
			(Si)	0.01 (0.01)	0.01 (0.01)	99.98 (99.98)

Table 6. Selected Data of Heat of Mixing of Liquid Alloys

Reaction	Temperature [°C]	$\Delta_{mix}H$ [kJ·(g-at)$^{-1}$]	Comments
$xFe(l) + yAl(l) + zSi(l) \rightleftharpoons Fe_xAl_ySi_z(l)$	1477	–29.4	$x = 0.36$, $y = 0.36$, $z = 0.28$
		–27.9	$x = 0.32$, $y = 0.38$, $z = 0.30$
		–28.9	$x = 0.40$, $y = 0.40$, $z = 0.20$
		–28.3	$x = 0.39$, $y = 0.42$, $z = 0.19$
		–17.3	$x = 0.15$, $y = 48$, $z = 0.37$
		–23.3	$x = 0.25$, $y = 0.50$, $z = 0.25$
		–17.2	$x = 0.154$, $y = 0.538$, $z = 0.308$
		–20.6	$x = 0.22$, $y = 0.58$, $z = 0.20$
		–19.3	$x = 0.20$, $y = 0.60$, $z = 0.20$

(*continued*)

DOI: 10.1007/978-3-540-69761-9_11

Reaction	Temperature [°C]	$\Delta_{mix}H$ [kJ·(g-at)$^{-1}$]	Comments
		–21.5	$x = 0.25$, $y = 0.60$, $z = 0.15$
		–14.9	$x = 0.15$, $y = 0.70$, $z = 0.15$
		–16.2	$x = 0.18$, $y = 0.72$, $z = 0.10$
			High-temperature isoperibolic calorimeter [2003Kan]

Table 7. The Standard Heat of Formation of Ternary Intermetallics

Reaction	Temperature [°C]	$\Delta_f H^{298.15}$ [kJ·(g-at)$^{-1}$]	Comments
$xFe(s) + yAl(s) + zSi(s) \rightleftharpoons Fe_xAl_ySi_z(s)$	298.15	–34.3 ± 2	$x = 2$, $y = 7.4$, $z = 1$ (τ_5)
		–24.5 ± 2	$x = 2$, $y = 9$, $z = 2$ (τ_6)
			Isoperibolic high-temperature solution calorimeter [1997Vyb]
$xFe(s) + yAl(s) + zSi(s) \rightleftharpoons Fe_xAl_ySi_z(s)$	298.15	–35.731 ± 1.381	$x = 0.39$, $y = 0.42$, $z = 0.19$ (τ_1/τ_9)
		–34.176 ± 1.570	$x = 0.40$, $y = 40$, $z = 0.20$ (τ_1/τ_9)
		–36.704 ± 1.860	$x = 0.36$, $y = 0.36$, $z = 0.28$ (τ_1/τ_9)
		–24.440 ± 1.387	$x = 0.18$, $y = 0.72$, $z = 0.10$ (τ_5)
		–30.384 ± 1.869	$x = 0.25$, $y = 0.60$, $z = 0.15$ (τ_{10})
			Setaram microcalorimeter of the Tian-Calvet type [2000Li1]
$xFe(s) + yAl(s) + zSi(s) \rightleftharpoons Fe_xAl_ySi_z(s)$	298.15	–25.273 ± 1.556	$x = 0.20$, $y = 0.60$, $z = 0.20$ (τ_2)
		–28.392 α1.891	$x = 0.22$, $y = 0.58$, $z = 0.20$ (τ_2)
		–20.475 ± 1.208	$x = 0.154$, $y = 0.538$, $z = 0.308$ (τ_4)
		–19.222 ± 1.253	$x = 0.15$, $y = 0.48$, $z = 0.37$ (τ_4)
		–29.634 ± 0.929	$x = 0.25$, $y = 0.50$, $z = 0.25$ (τ_3)
		–20.209 ± 0.926	$x = 0.15$, $y = 0.70$, $z = 0.15$ (τ_6)
		–35.845 ± 1.760	$x = 0.32$, $y = 0.38$, $z = 0.30$ (τ_8)
			Setaram microcalorimeter of the Tian-Calvet type [2000Li2]

Table 8. Investigations of the Al-Fe-Si Materials Properties

Reference	Method/Experimental Technique	Type of Property
[1968Aru1, 1968Aru2, 1970Aru]	Resistivity measurements	Electrical resistivity
[1968Lih]	Magnetometry	Curie temperature
[1977Nic2]	Magnetometry	Saturation magnetization
[1983Sch]	Magnetometry	Saturation magnetization

(*continued*)

DOI: 10.1007/978-3-540-69761-9_11

Reference	Method/Experimental Technique	Type of Property
[1986Tak, 1987Tak1, 1987Tak2]	Magnetometry	Magnetostriction, magnetocrystalline anisotropy
[1988Dor]	Magnetometry	Magnetic permeability
[1993Sch]	Mechanical tests	Critical resolved shear stress up to 720°C
[1996Fri]	Electrical tests	Metal/insulator transition
[1996Szy]	Magnetometry	Magnetic susceptibility
[1998Dit]	Electrical and magnetic	Electrical conductivity, Hall effect, magneto-resistance, magnetic susceptibility
[1999Oht]	Electrical tests	Thermoelectric power
[2000Bha]	Electrochemical tests	Corrosion
[2001Cho]	Mechanical tests	Hardness, strength, and elongation up to 520°C
[2003Cie]	Mechanical tests	Dynamic strain aging
[2003Mur]	Mechanical tests	Hardness and indentation fracture toughness

Table 9. Coordinates of the γ/(α+γ) and (α+γ)/α Phase Boundaries in the Al-Fe-Si System

Composition (mass%)		Temperature [°C] of the	
Al	Si	γ/(α+γ) boundary	(α +γ)/α boundary
0.16	0.25	905	1385
0.19	0.58	952	1351
0.31	0.93	1014	1300
0.44	0.19	935	1350
0.44	0.53	976	1326
0.48	0.13	948	1347
0.64	0.23	1030	1275
0.71	0.65	1048	1270
0.74	0.24	1000	1303

DOI: 10.1007/978-3-540-69761-9_11

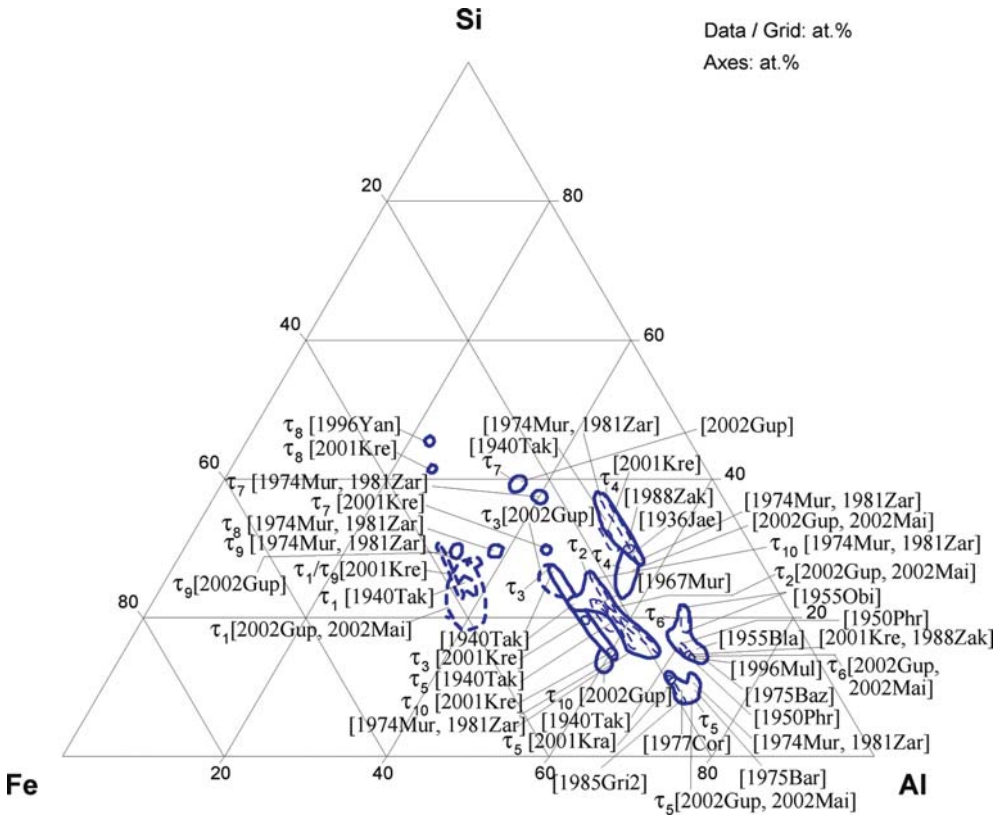

Fig. 1. Al-Fe-Si. Distribution of the equilibrium ternary phases, as reported by different authors

DOI: 10.1007/978-3-540-69761-9_11

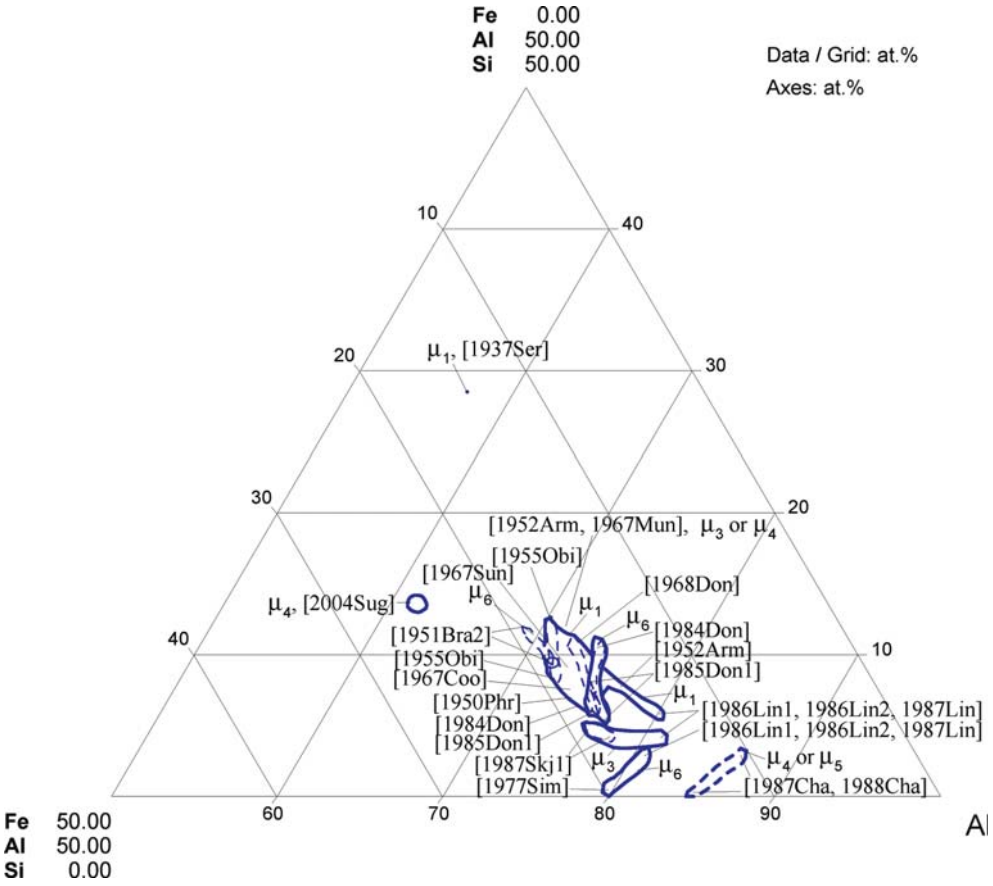

Fig. 2. Al-Fe-Si. Distribution of the metastable ternary phases, as reported by different authors

DOI: 10.1007/978-3-540-69761-9_11

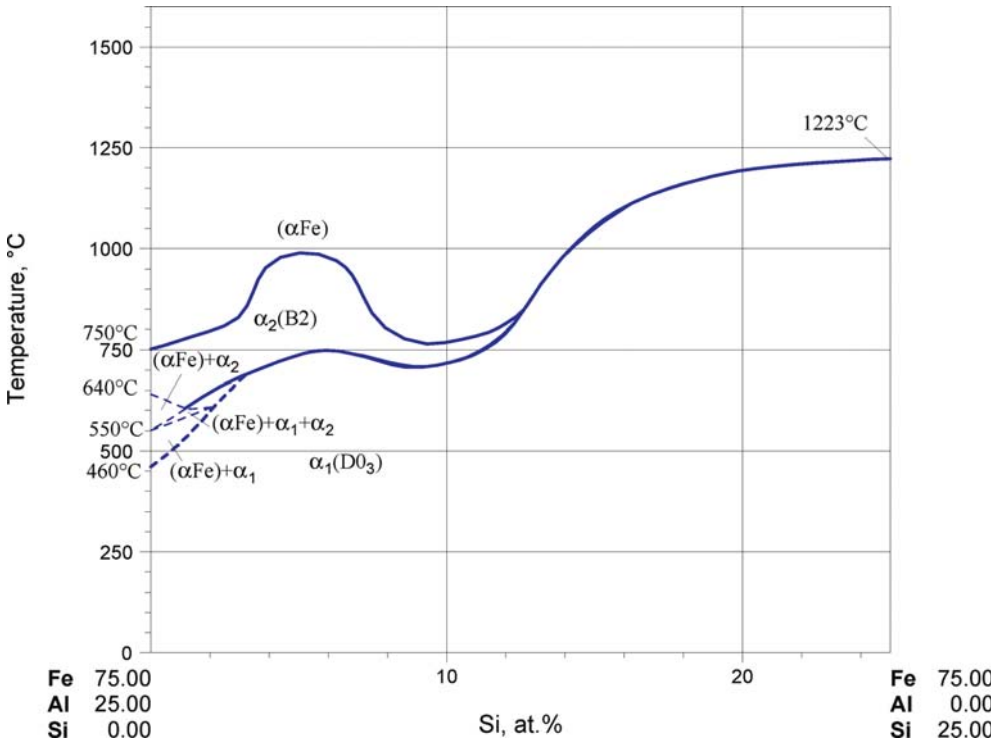

Fig. 3. Al-Fe-Si. The Fe_3Al-Fe_3Si sections showing the boundaries of α_1 ($D0_3$), α_2 ($B2$) and (αFe) (disordered bcc) phases

DOI: 10.1007/978-3-540-69761-9_11

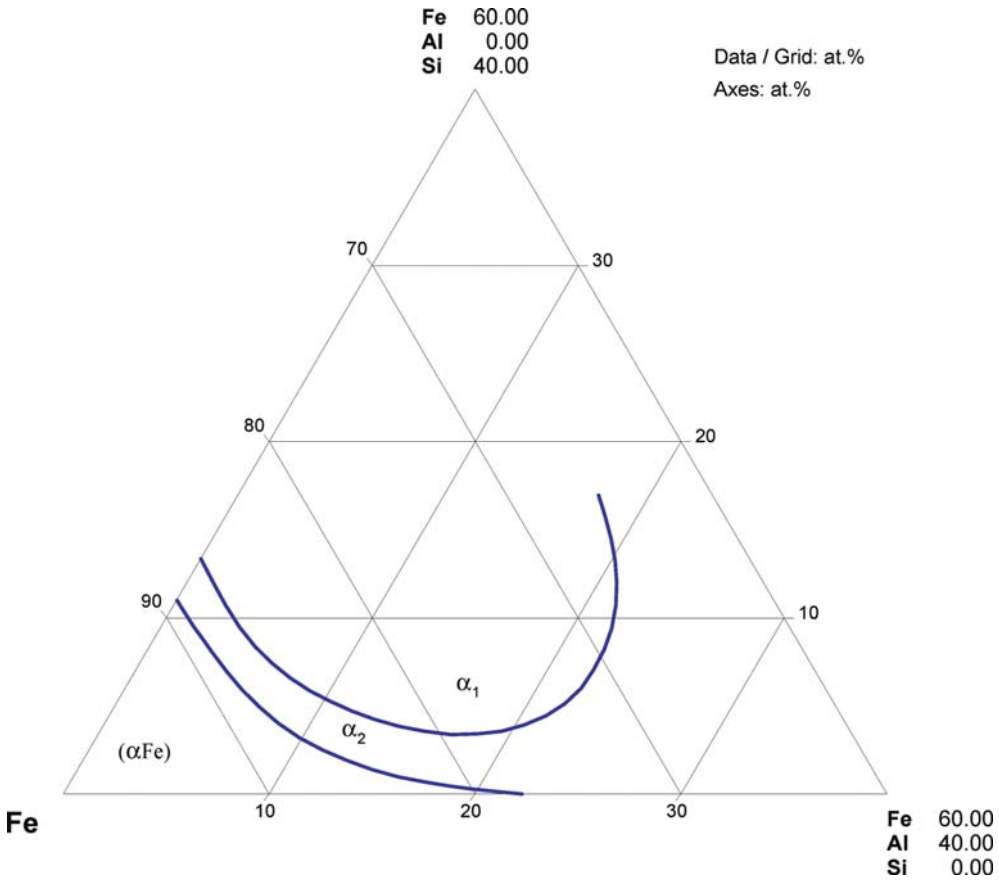

Fig. 4. Al-Fe-Si. Isothermal section of the Fe corner at 700°C with ordered (α_1 and α_2) and disordered (αFe) phases

DOI: 10.1007/978-3-540-69761-9_11

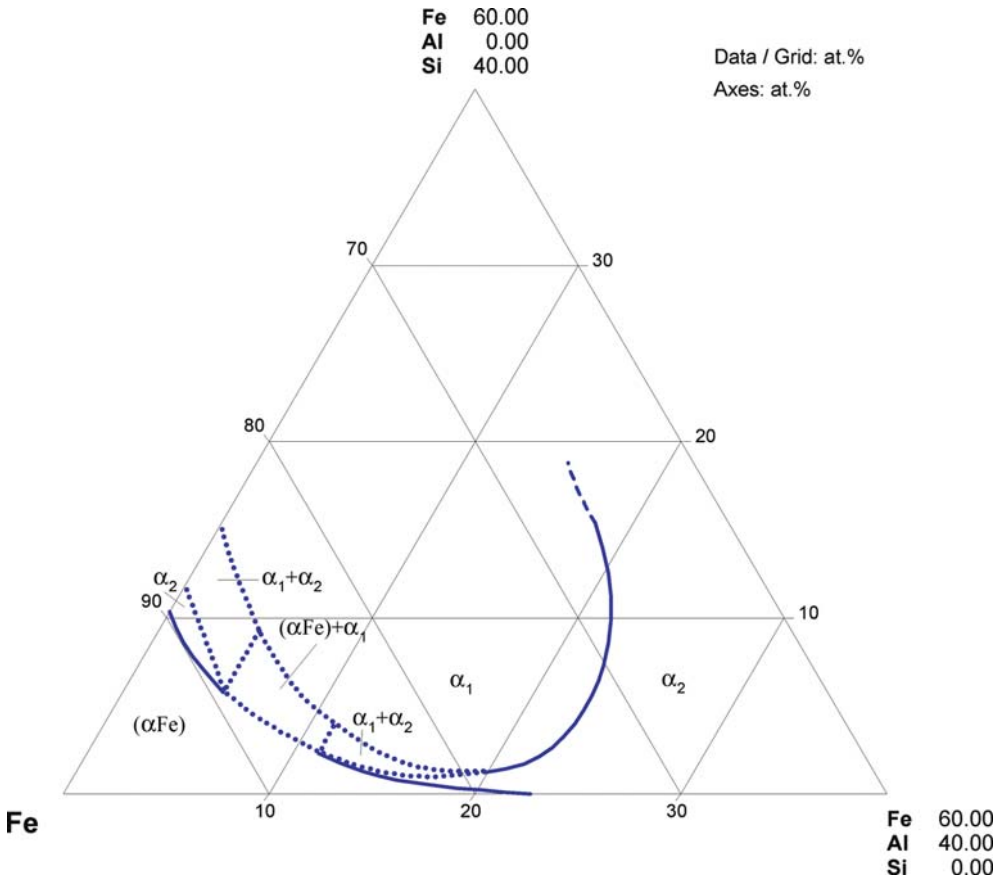

Fig. 5. Al-Fe-Si. Isothermal section of the Fe corner at 650°C with ordered (α_1 and α_2) and disordered (αFe) phases

DOI: 10.1007/978-3-540-69761-9_11

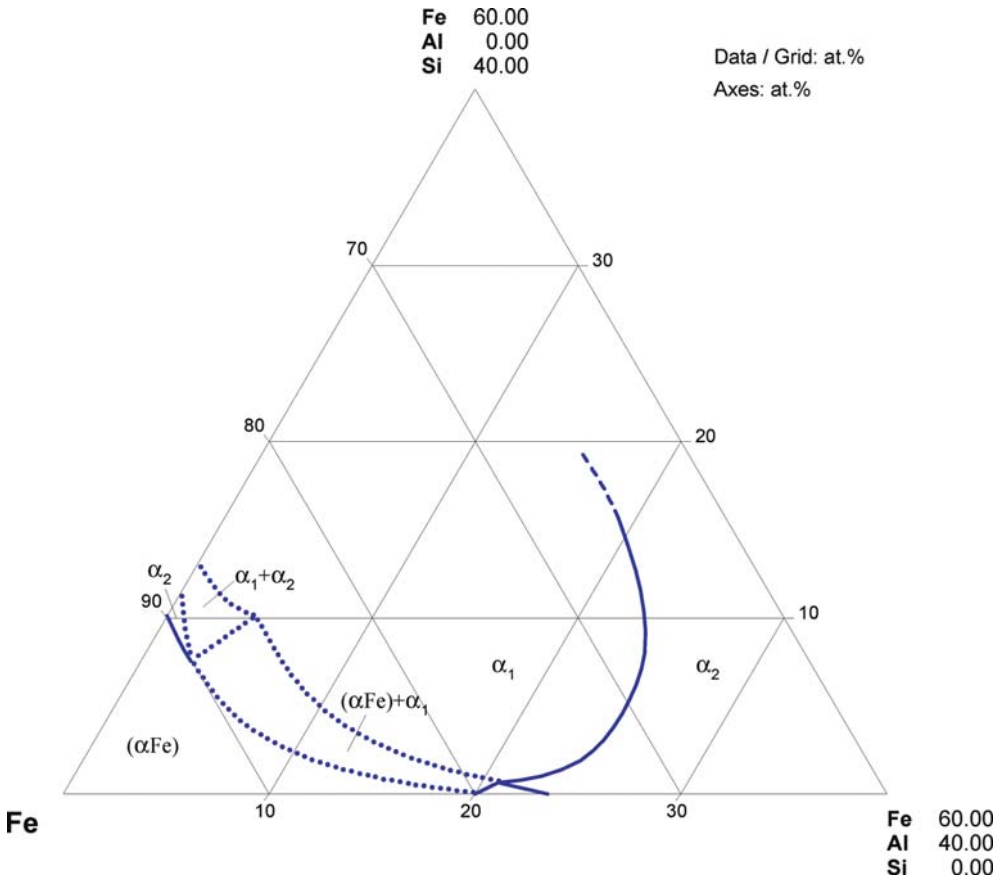

Fig. 6. Al-Fe-Si. Isothermal section of the Fe corner at 550°C with ordered (α_1 and α_2) and disordered (αFe) phases

DOI: 10.1007/978-3-540-69761-9_11

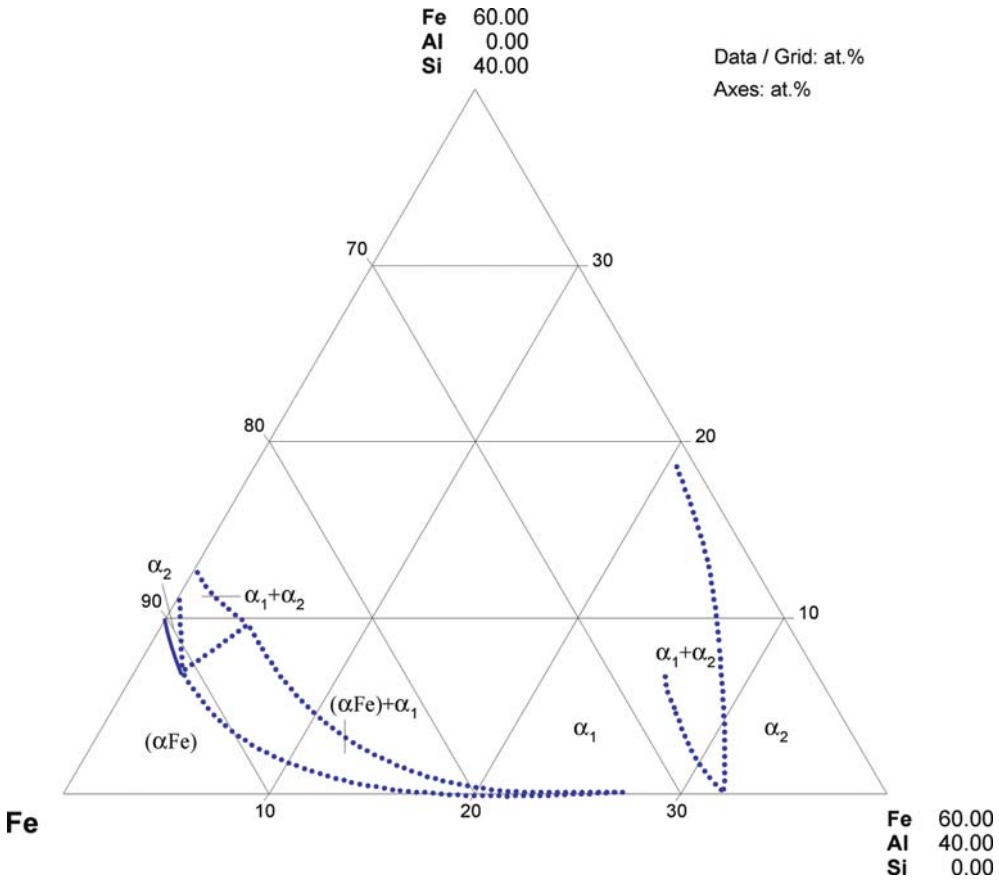

Fig. 7. Al-Fe-Si. Isothermal section of the Fe corner at 450°C with ordered (α_1 and α_2) and disordered (αFe) phases

DOI: 10.1007/978-3-540-69761-9_11

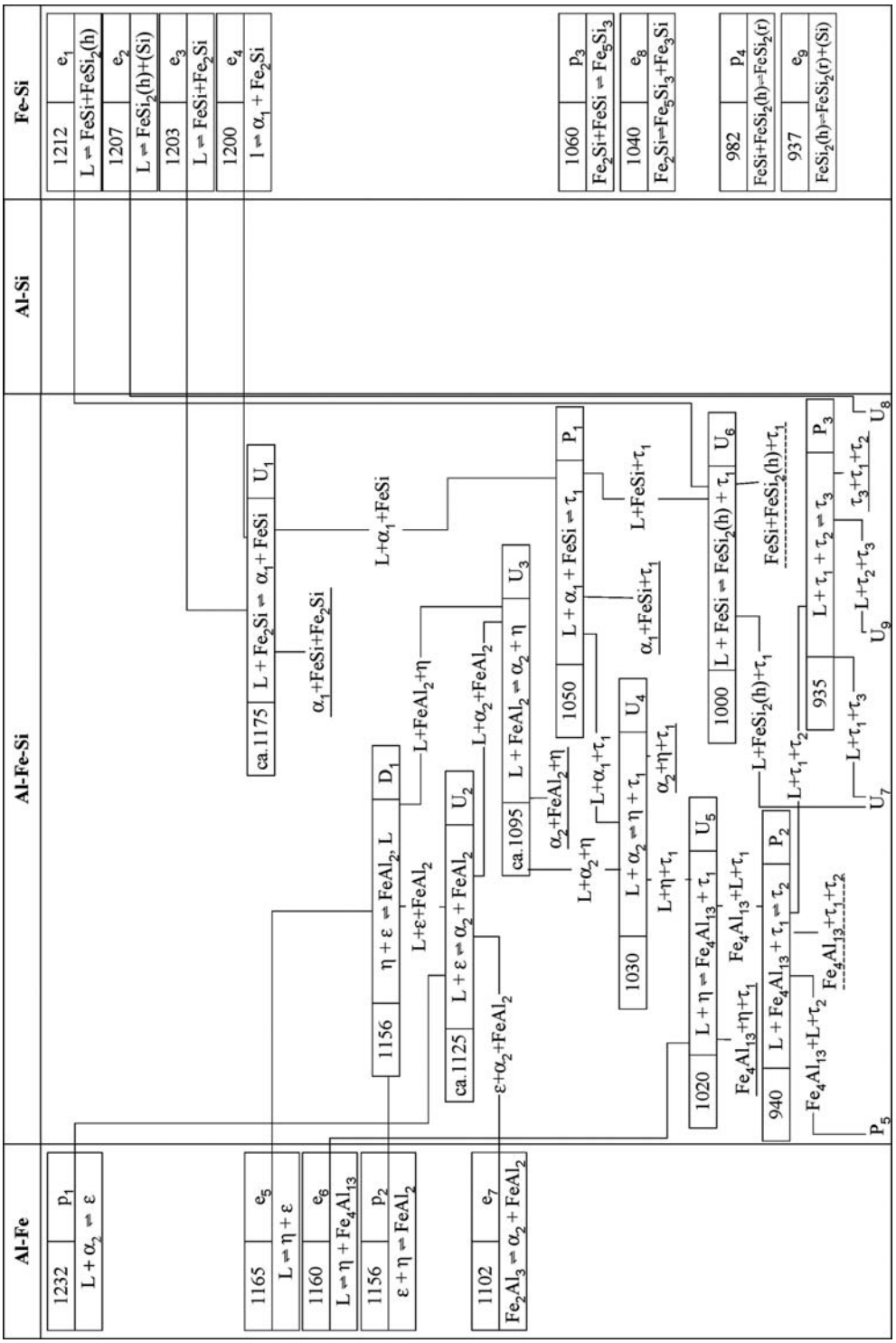

Fig. 8a. Al-Fe-Si. Reaction scheme, part 1

DOI: 10.1007/978-3-540-69761-9_11

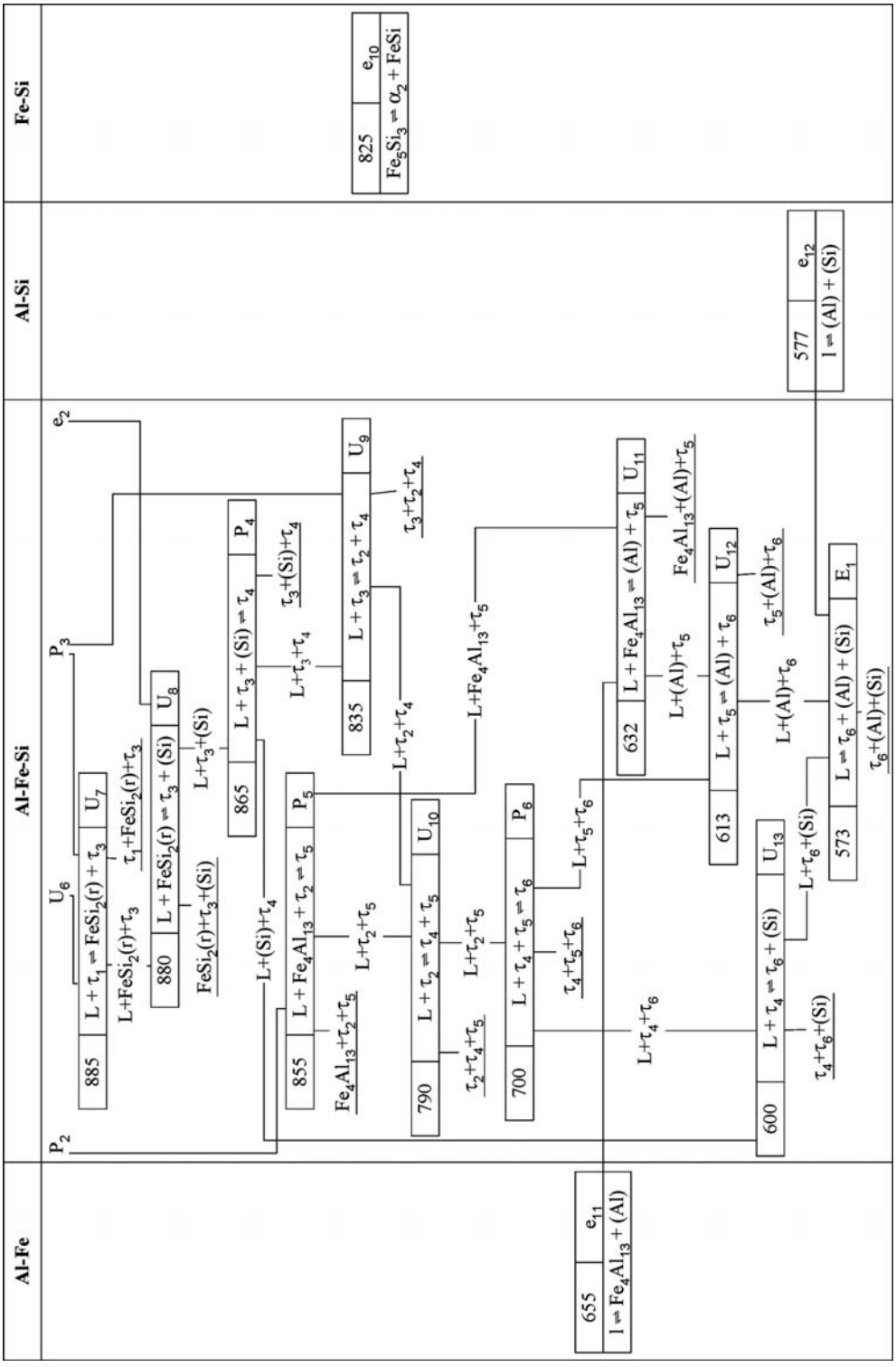

Fig. 8b. Al-Fe-Si. Reaction scheme, part 2

DOI: 10.1007/978-3-540-69761-9_11

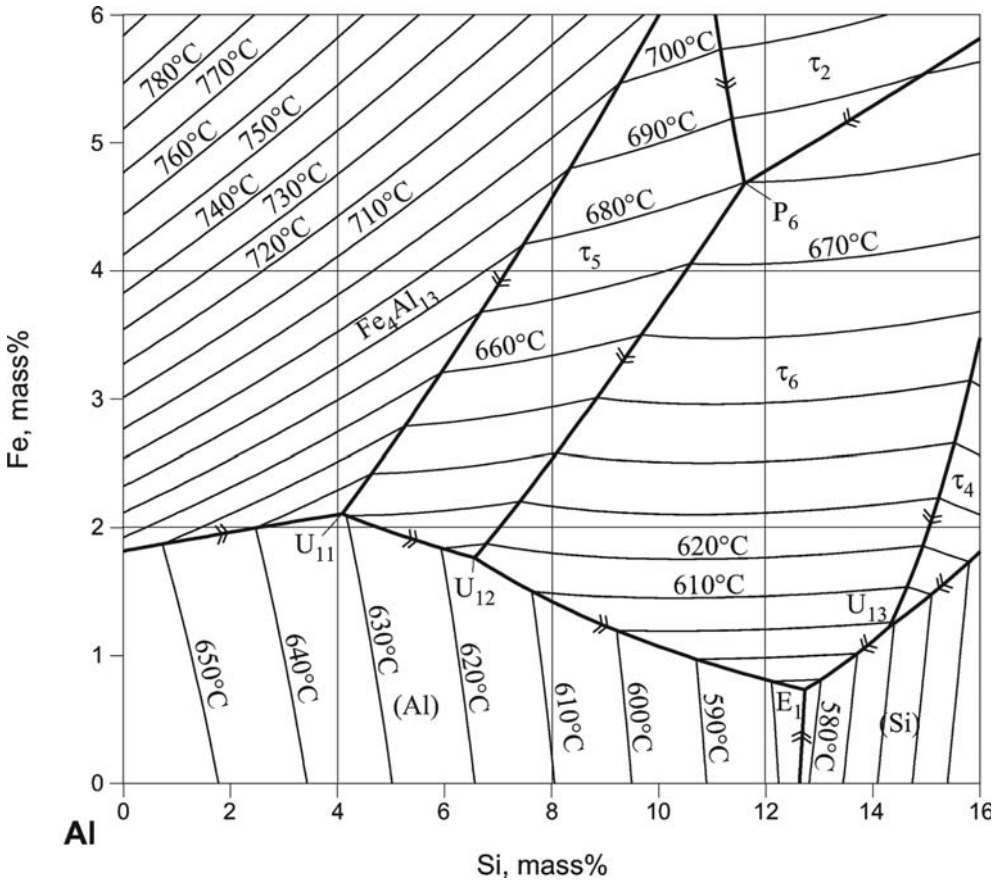

Fig. 9. Al-Fe-Si. Calculated liquidus surface of the Al corner

DOI: 10.1007/978-3-540-69761-9_11

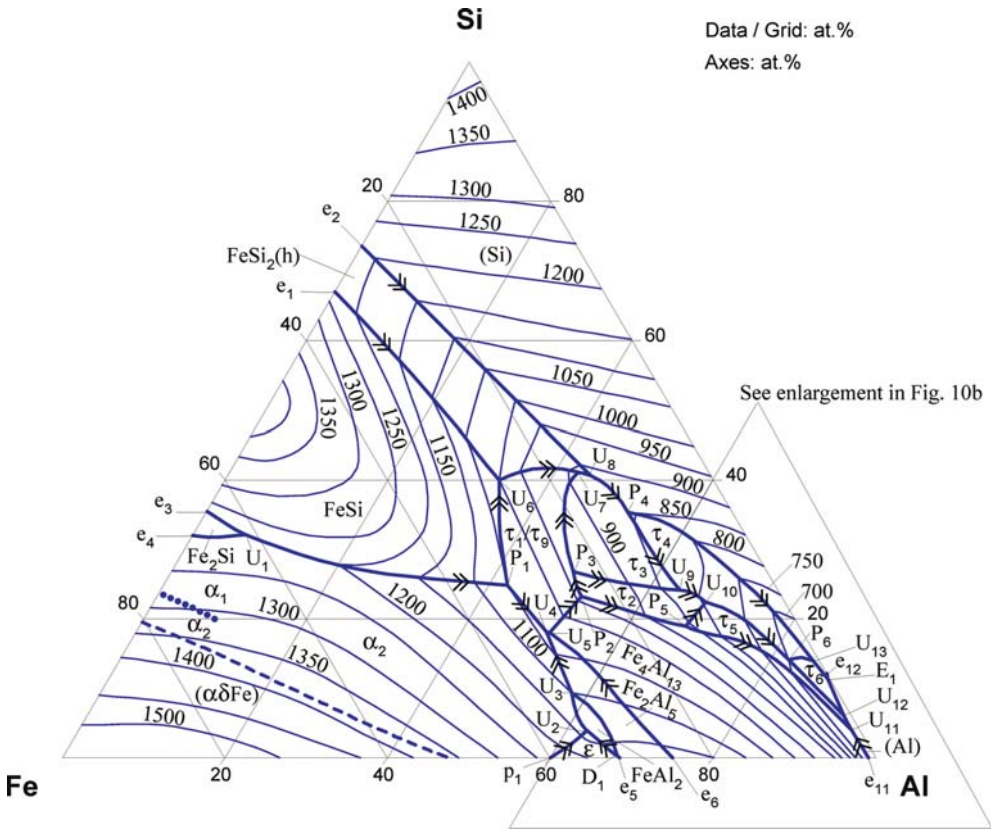

Fig. 10a. Al-Fe-Si. Liquidus surface

DOI: 10.1007/978-3-540-69761-9_11

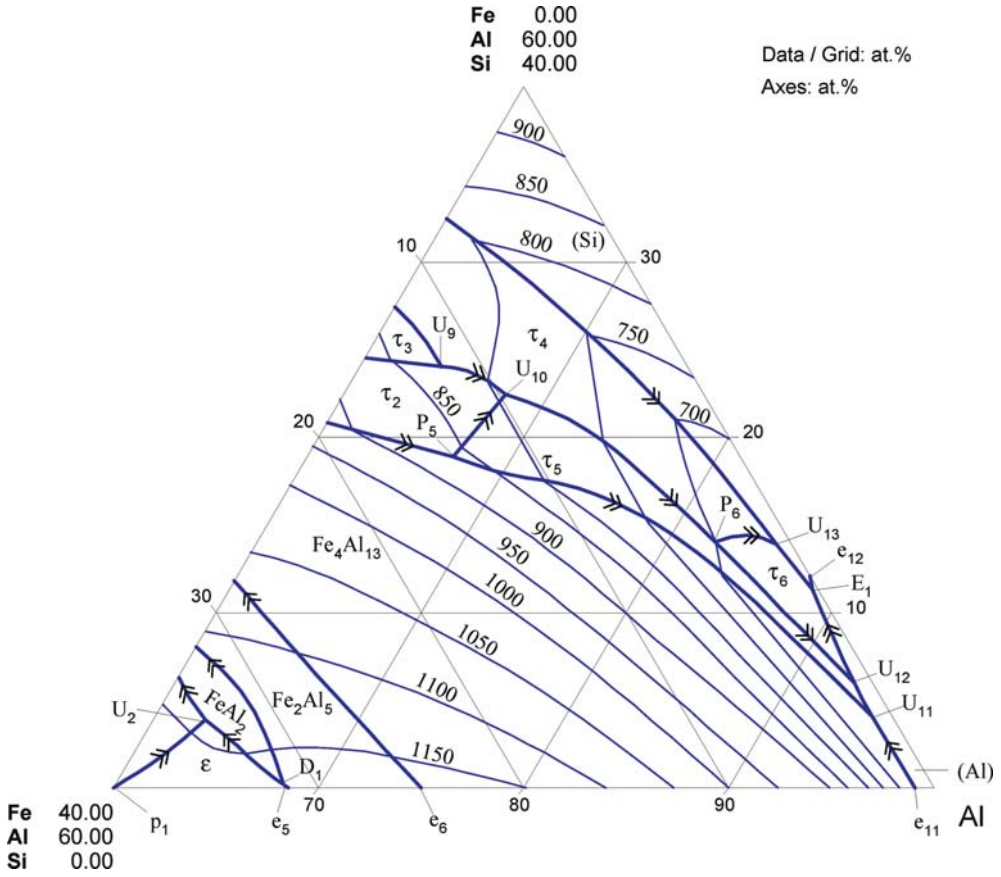

Fig. 10b. Al-Fe-Si. Liquidus surface in the Al corner (enlargement of Fig. 10a)

DOI: 10.1007/978-3-540-69761-9_11

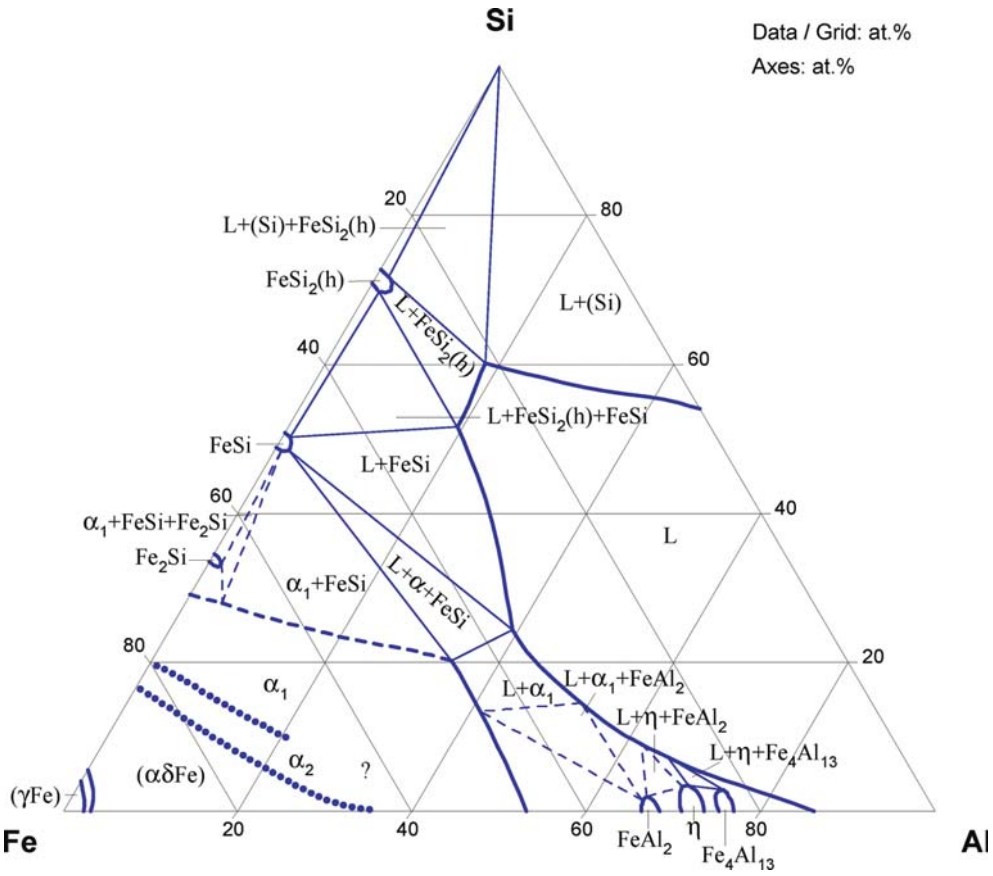

Fig. 11. Al-Fe-Si. Isothermal section at 1100°C

DOI: 10.1007/978-3-540-69761-9_11

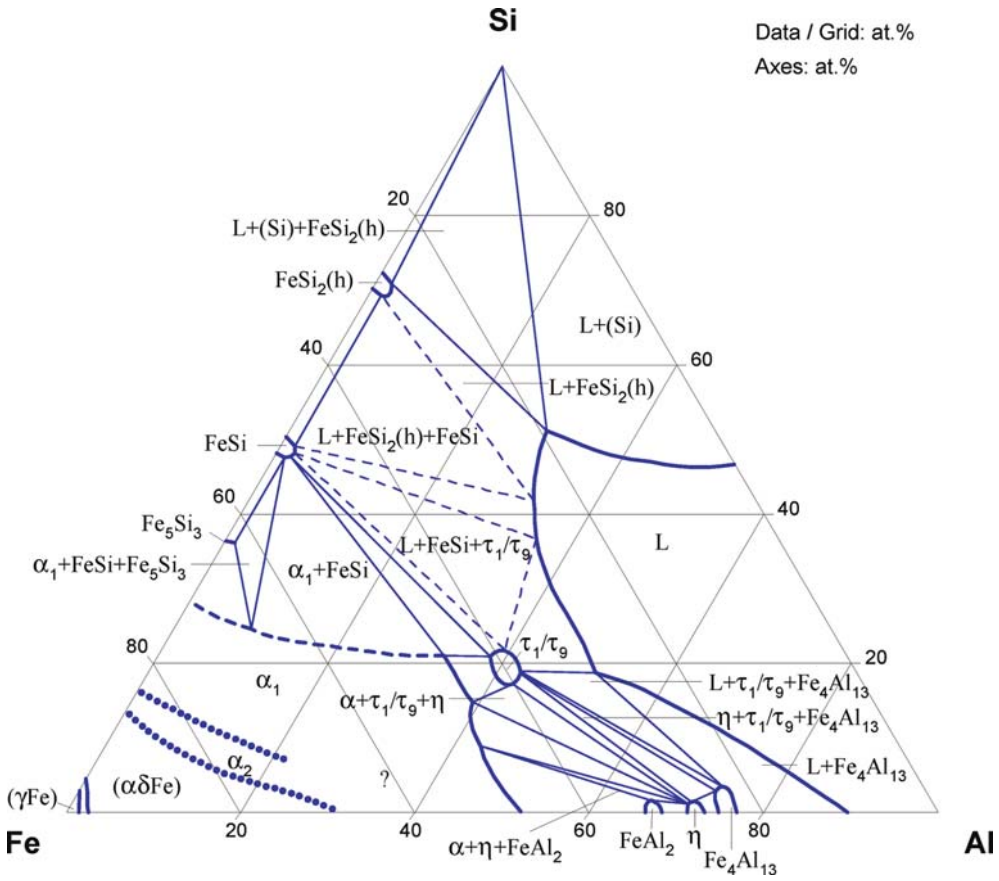

Fig. 12. Al-Fe-Si. Isothermal section at 1020°C

DOI: 10.1007/978-3-540-69761-9_11

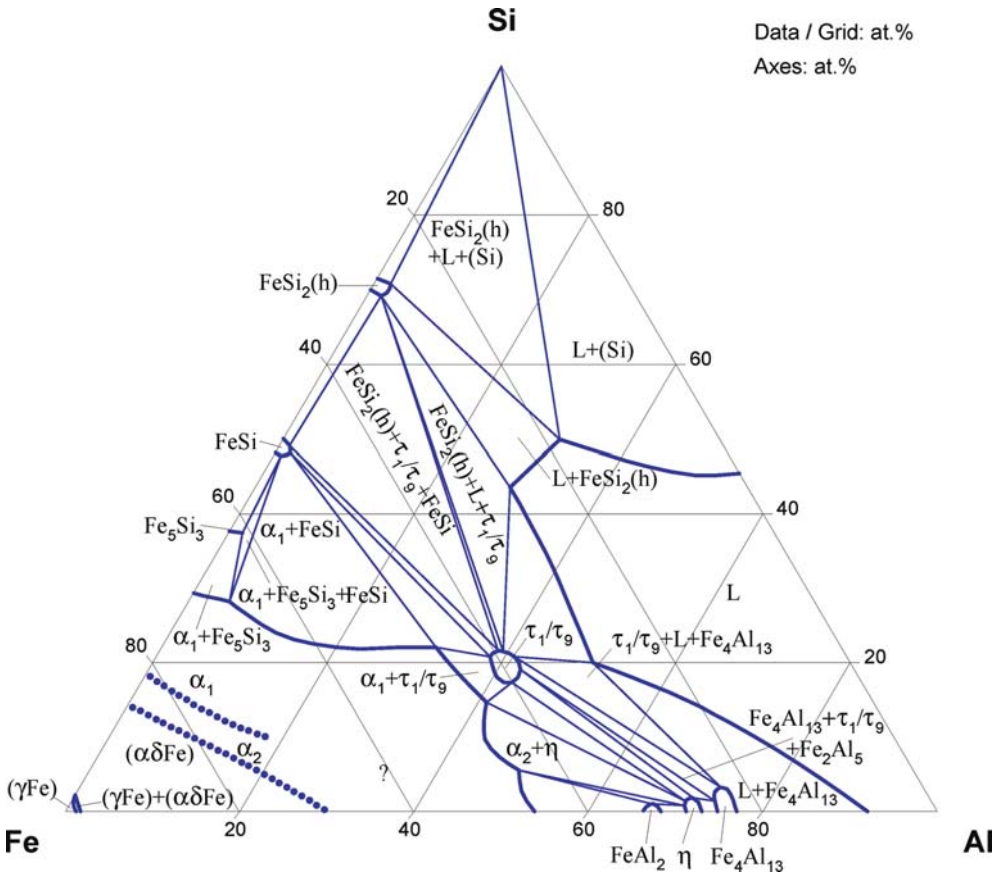

Fig. 13. Al-Fe-Si. Isothermal section at 1000°C

DOI: 10.1007/978-3-540-69761-9_11

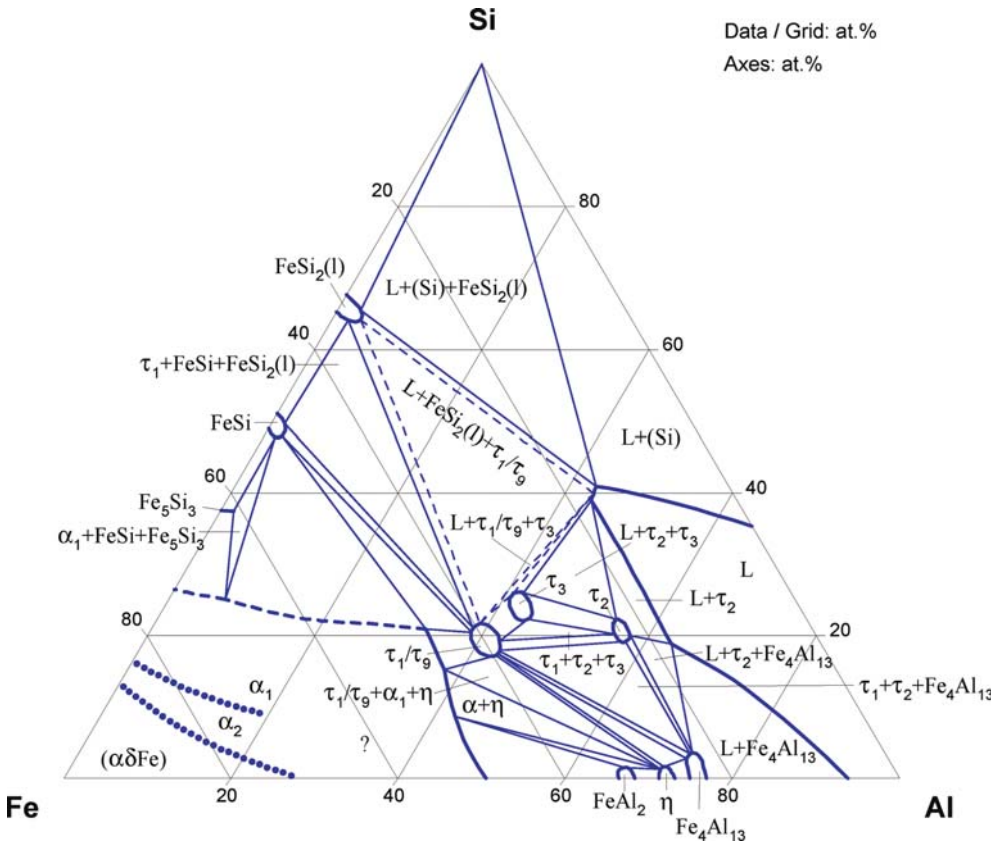

Fig. 14. Al-Fe-Si. Isothermal section of the Fe corner at 900°C

DOI: 10.1007/978-3-540-69761-9_11

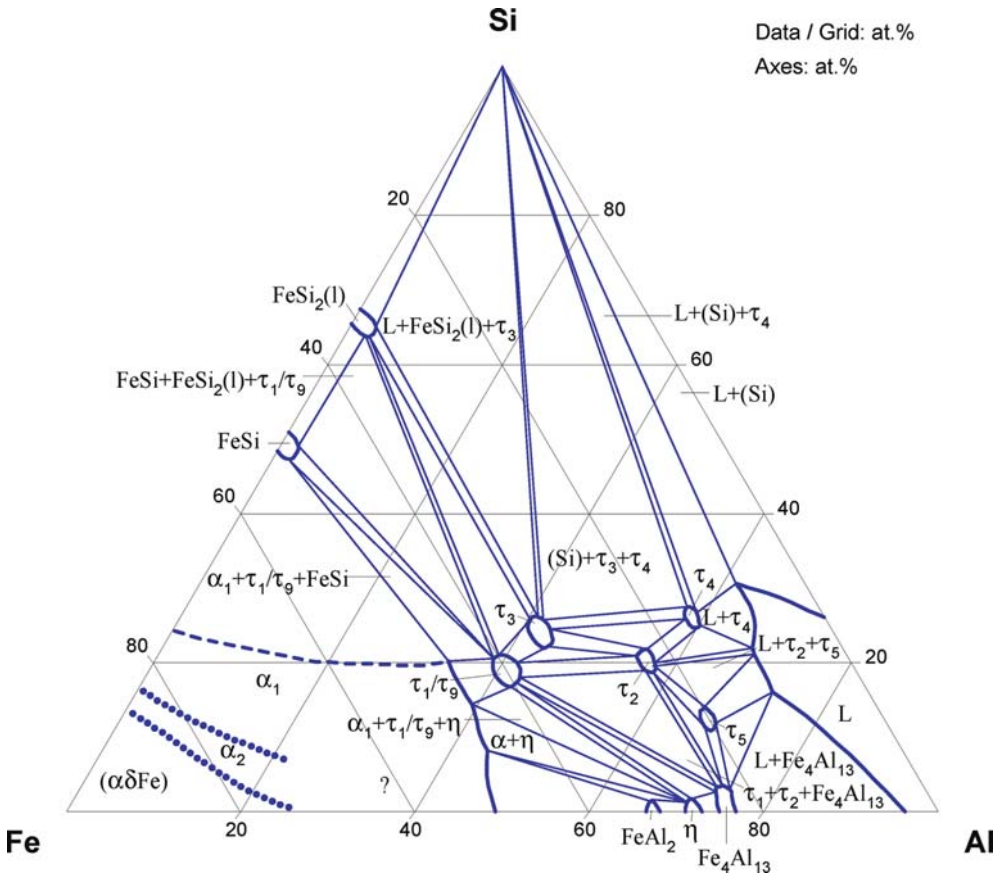

Fig. 15. Al-Fe-Si. Isothermal section at 800°C

DOI: 10.1007/978-3-540-69761-9_11

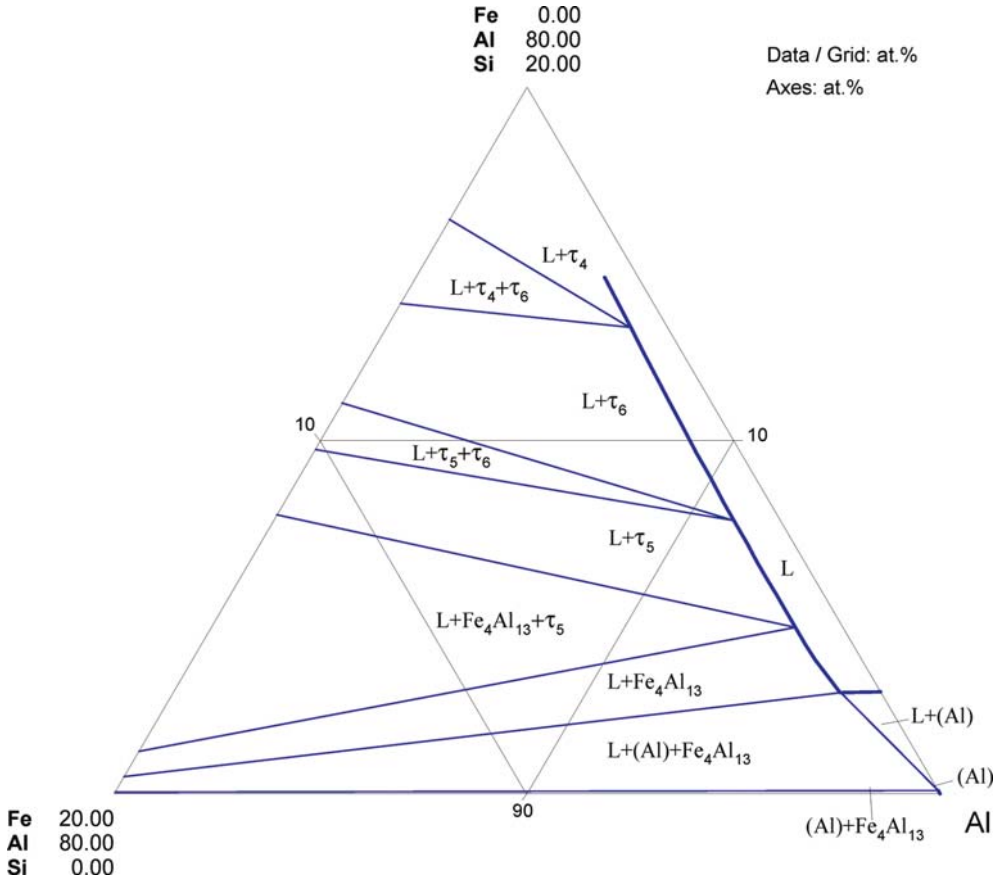

Fig. 16. Al-Fe-Si. Isothermal section of the Al corner at 640°C

DOI: 10.1007/978-3-540-69761-9_11

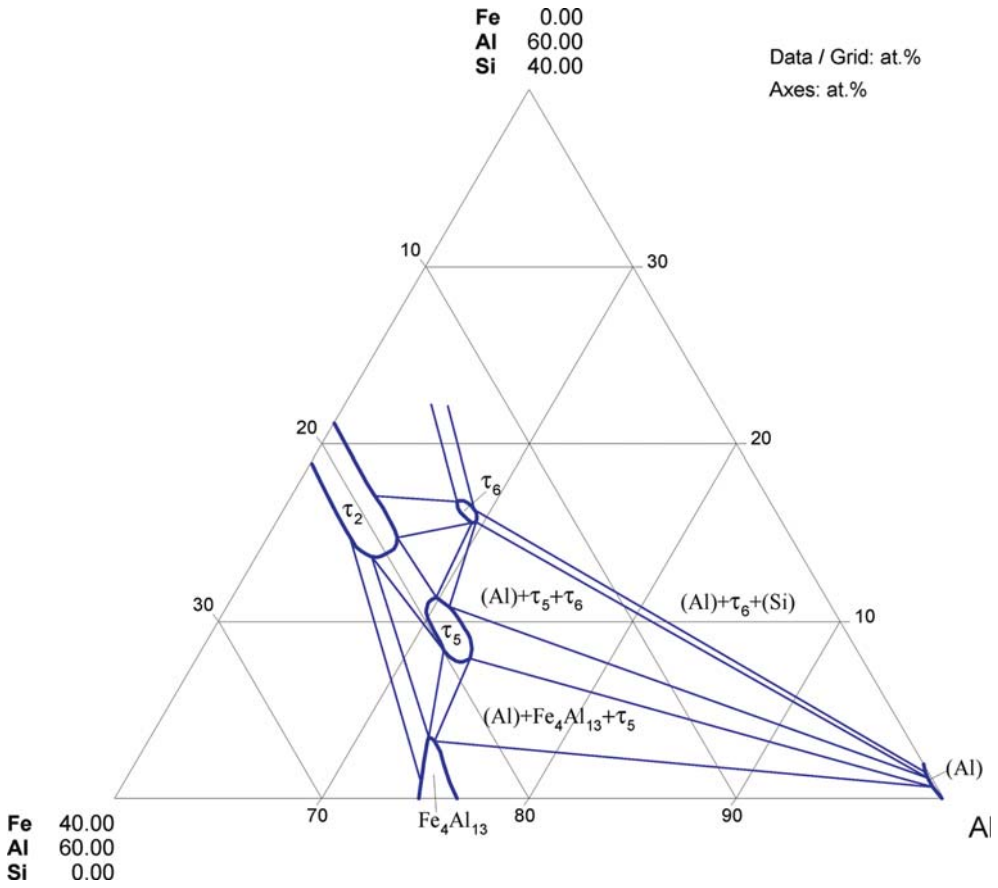

Fig. 17. Al-Fe-Si. Isothermal section of the Al corner at 570/600°C

DOI: 10.1007/978-3-540-69761-9_11

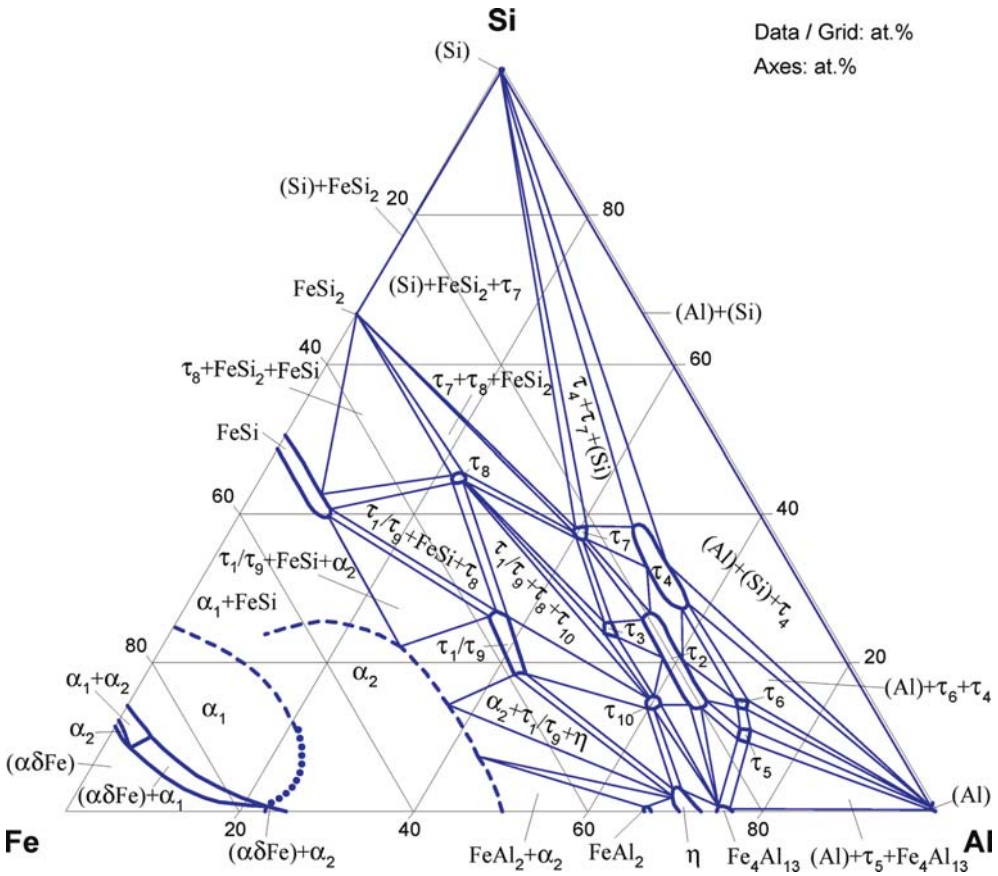

Fig. 18. Al-Fe-Si. Isothermal section at 600°C

DOI: 10.1007/978-3-540-69761-9_11

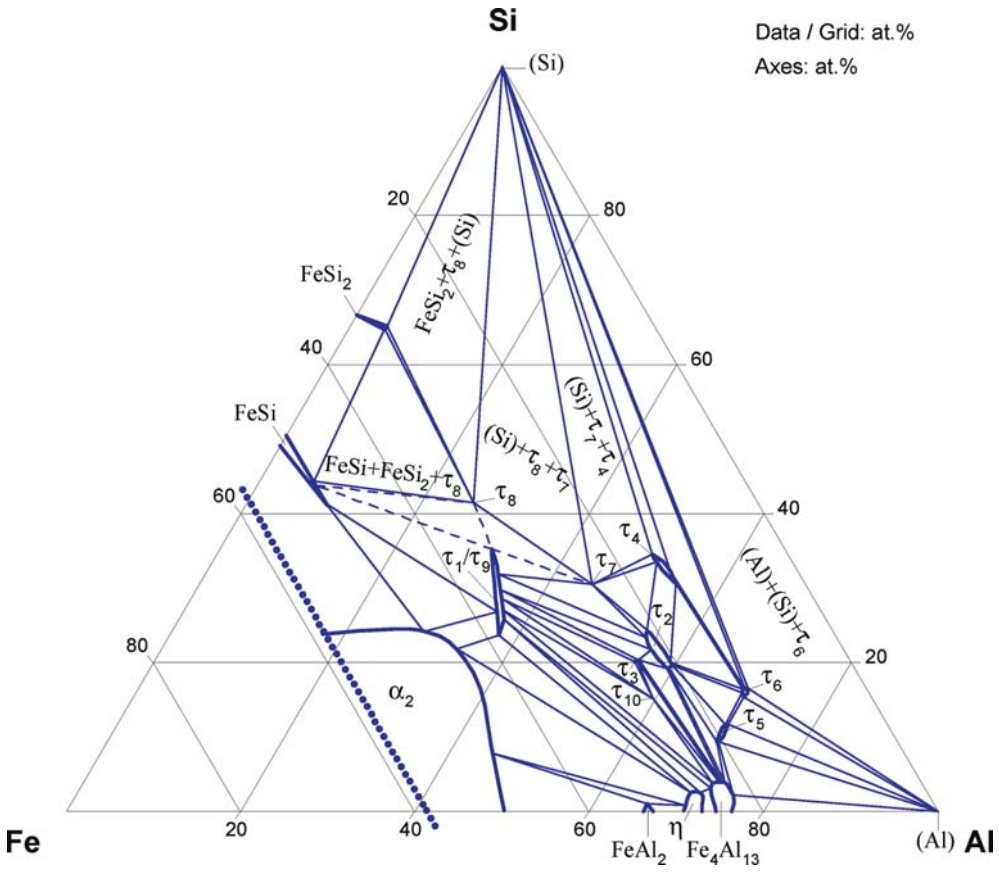

Fig. 19. Al-Fe-Si. Partial isothermal section at 550°C

DOI: 10.1007/978-3-540-69761-9_11

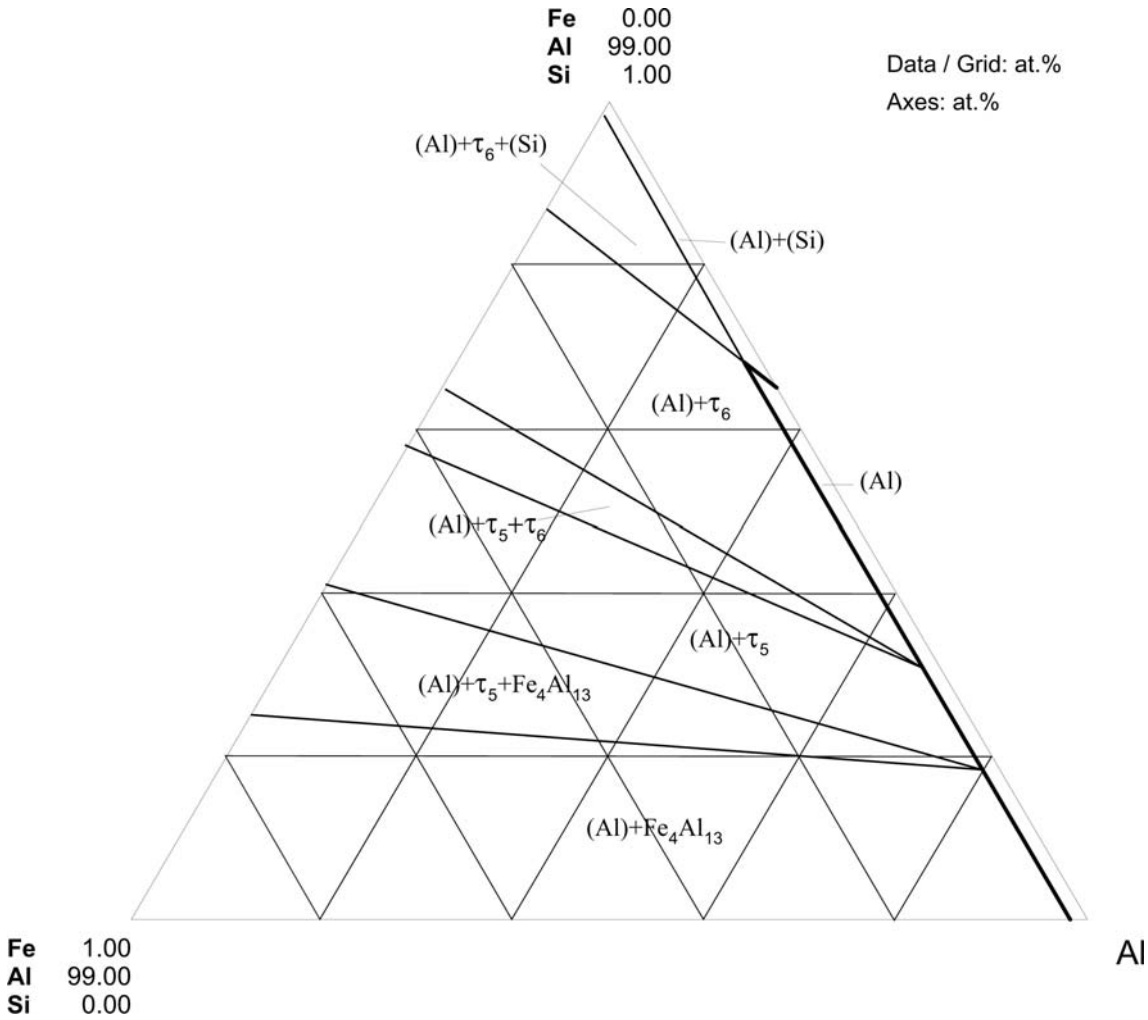

Fig. 20. Al-Fe-Si. Isothermal section of the Al corner at 500°C

DOI: 10.1007/978-3-540-69761-9_11

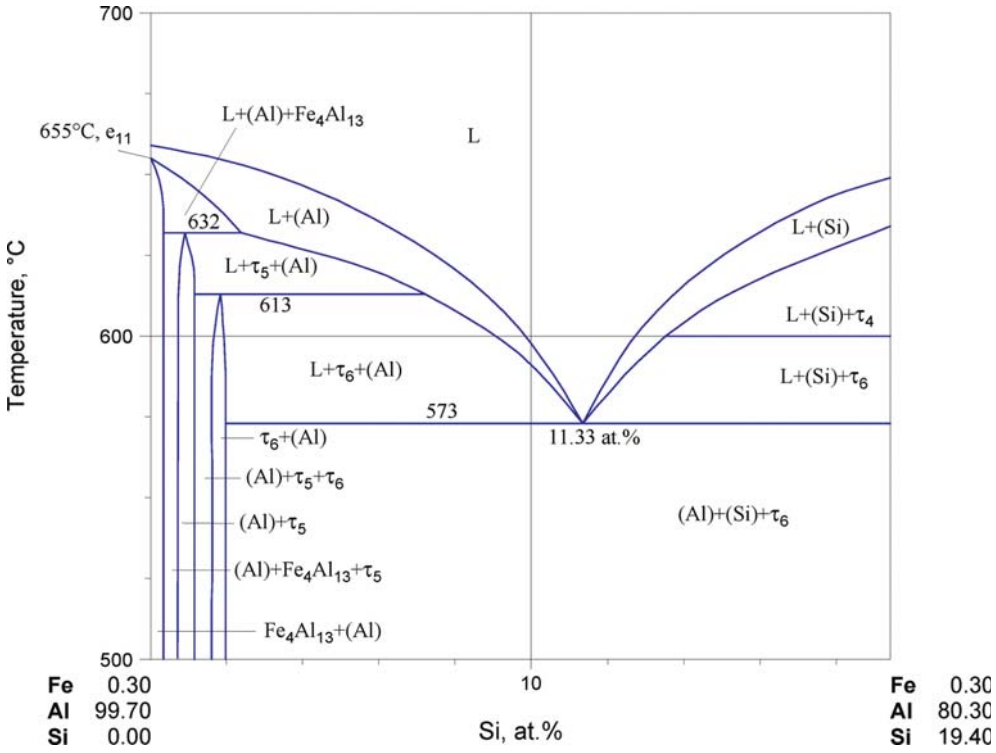

Fig. 21. Al-Fe-Si. Polythermal section at a constant Fe content of 0.7 mass%

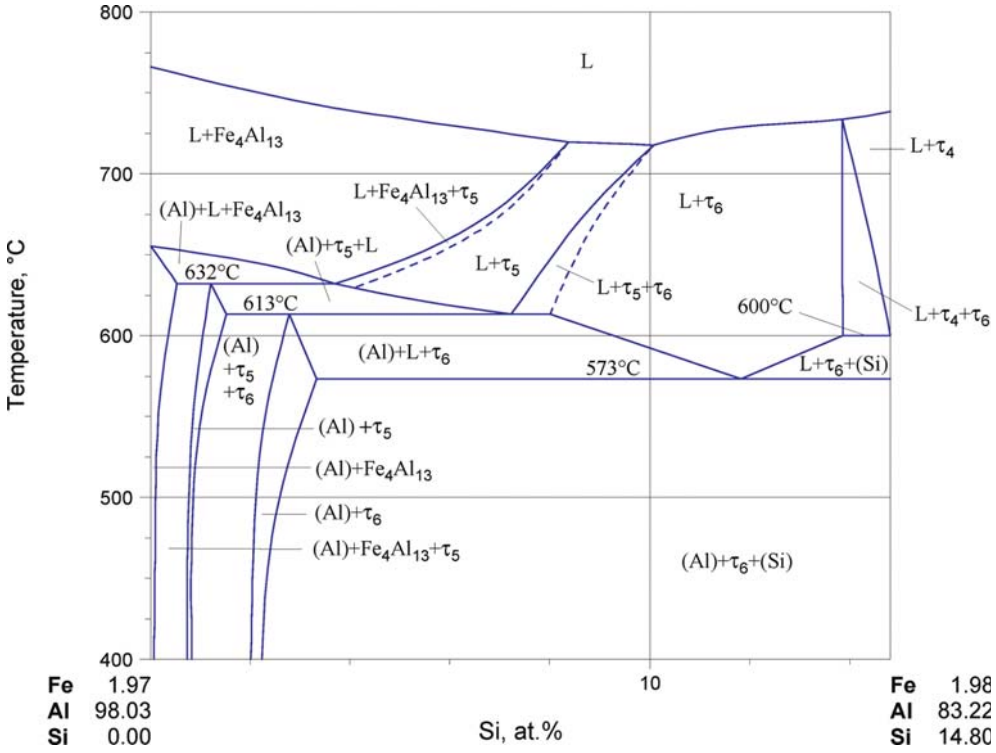

Fig. 22. Al-Fe-Si. Polythermal section at a constant Fe content of 4 mass%

DOI: 10.1007/978-3-540-69761-9_11

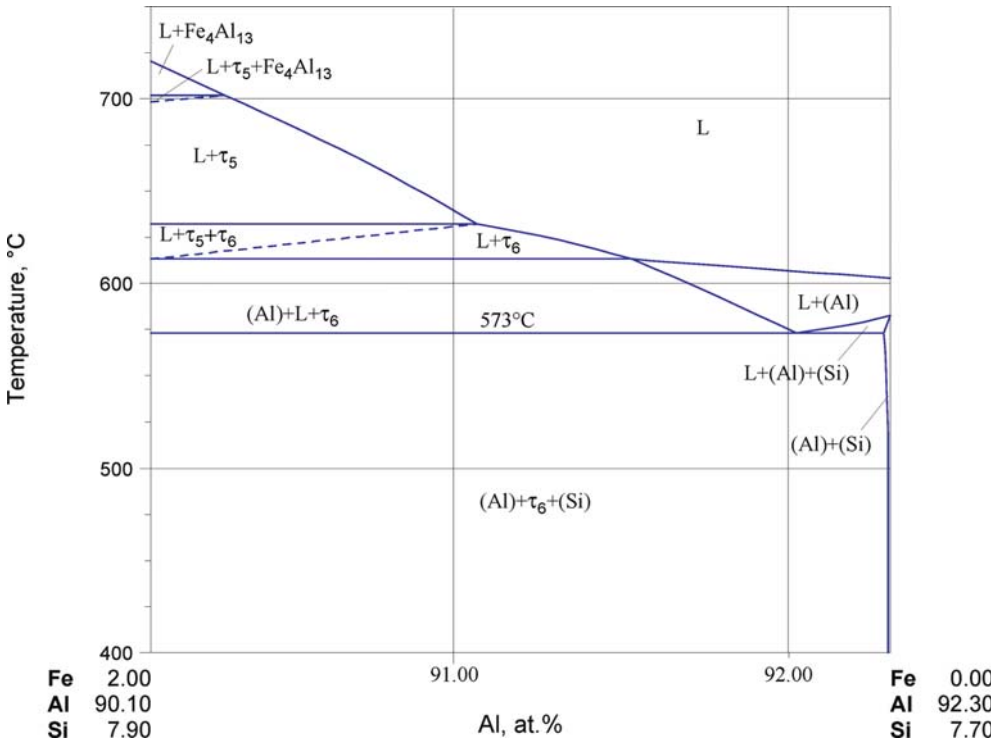

Fig. 23. Al-Fe-Si. Polythermal section at a constant Si content of 8 mass%

DOI: 10.1007/978-3-540-69761-9_11

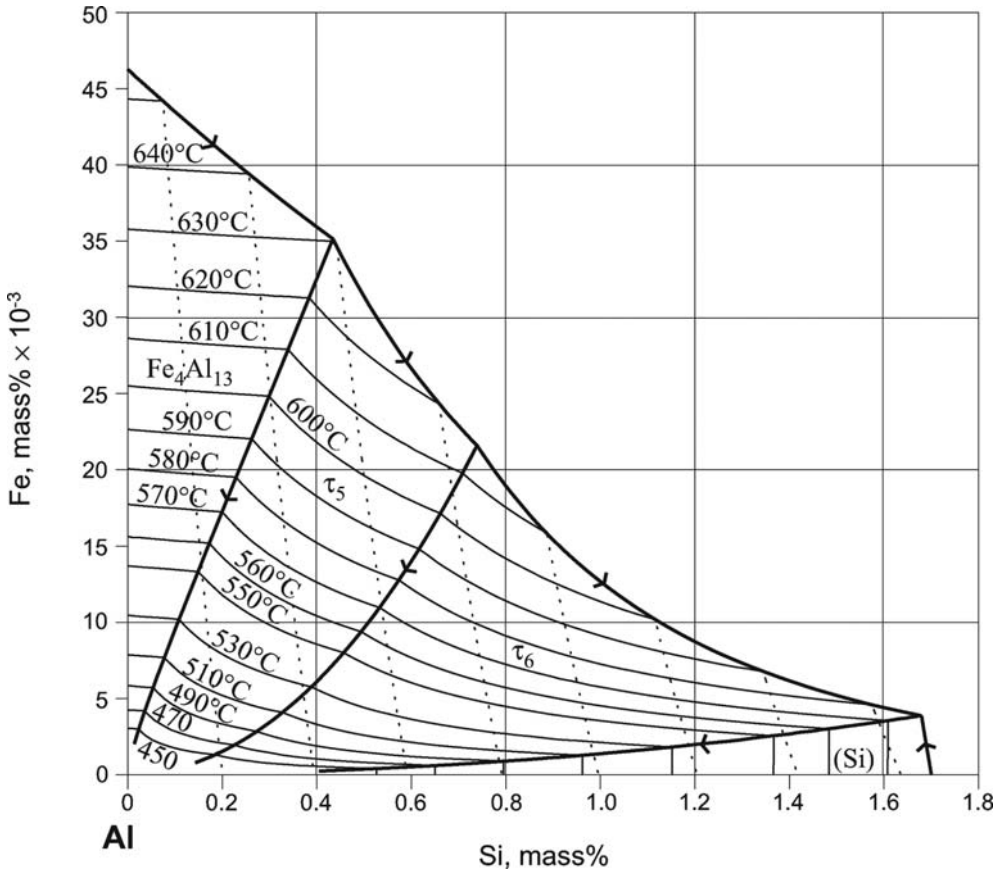

Fig. 24. Al-Fe-Si. Calculated (Al)-solidus (dash lines) and -solvus (solid lines) surfaces

DOI: 10.1007/978-3-540-69761-9_11

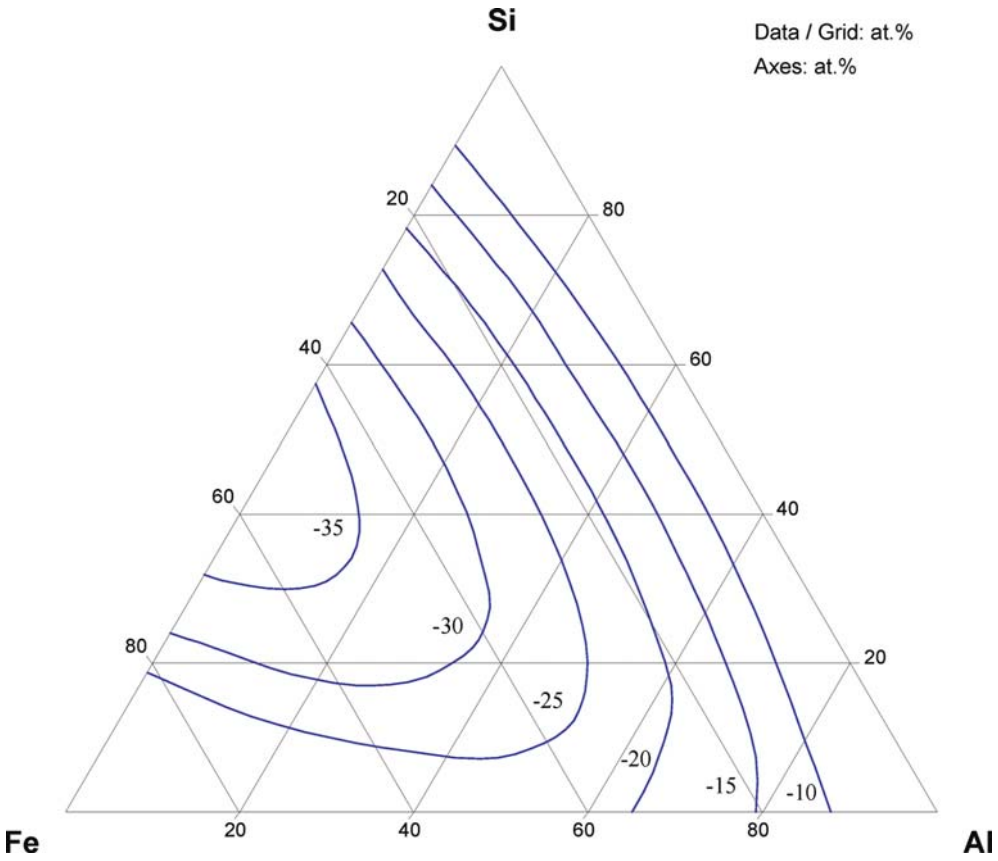

Fig. 25. Al-Fe-Si. Integral enthalpy of mixing of liquid alloys at 1477°C, in kJ·mol^{-1} of atoms

DOI: 10.1007/978-3-540-69761-9_11

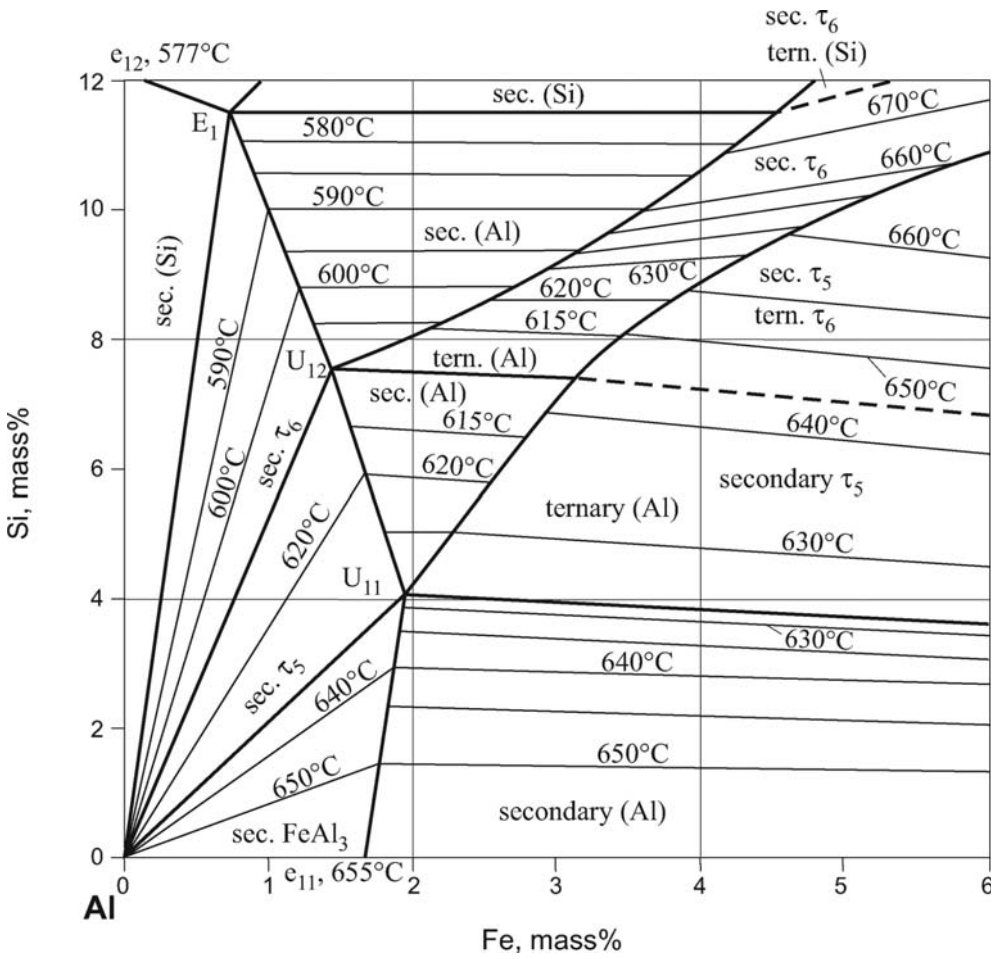

Fig. 26. Al-Fe-Si. Surface of secondary crystallization in the Al corner

DOI: 10.1007/978-3-540-69761-9_11

References

[1923Dix] Dix, Jr., E.H., "Observations on the Occurrence of Iron- and Silicon in Aluminium", *Trans. AIME*, **69**, 957–971 (1923) (Experimental, 12)

[1923Han] Hanson, D., Gayler, M.L.V., "The Heat-treatment and Mechanical Properties of Alloys of Aluminium with Small Percentages of Copper", *J. Inst. Met.*, **29**, 491–506 (1923) (Experimental, 1)

[1923Wet] Wetzel, E., "Advances in Aluminium Research" (in German), *Die Metallboerse*, **13**, 737–738 (1923) (Phase Diagram, Experimental, 6)

[1924Fus] Fuss, V., "On the Constitution of Ternary Al Alloys" (in German), *Z. Metallkd.*, **16**, 24–25 (1924) (Experimental, 3)

[1927Gwy] Gwyer, A.G.C., Phillips, H.W.L., "The Ternary System: Aluminium-Silicon-Iron" in "The Constitution of Alloys with Silicon and Iron", *J. Inst. Met.*, **38**, 44–83 (1927) (Phase Diagram, Experimental, #, *, 9)

[1928Dix] Dix Jr., E.H., Heath Jr., A.C., "Equilibrium Relations in Aluminium-Silicon and Aluminium-Iron-Silicon Alloys of High Purity", *Trans. AIME, Inst. Met. Div.*, **93**, 164–197 (1928) (Phase Diagram, Experimental, #, *, 39)

[1931Fin] Fink, W.L., Van Horn, K.R., "Constituents of Aluminium-Iron-Silicon Alloys", *Trans. AIME, Inst. Met. Div.*, 383–394 (1931) (Phase Diagram, Experimental, #, *, 12)

[1931Fus] Fuss, V., "The Constitution of Aluminium rich Al-Fe-Si Alloys" (in German), *Z. Metallkd.*, **23**, 231–236 (1931) (Phase Diagram, Experimental, 6)

[1931Wev] Wever, F., Heinzel, A., "Two Examples of Ternary Iron Systems with Closed γ-Loop" (in German), *Mitt. K.-W.-Inst. Eisenforschung*, **13**, 193–197 (1931) (Phase Diagram, Experimental, #, *, 14)

[1932Nis] Nishimura, H., "An Investigation of Al rich Al-Fe-Si Alloys" (in Japanese), *Tetsu to Hagane*, **18**, 849–860 (1932) (Phase Diagram, Experimental, #, *, 40)

[1933Nis] Nishimura, H., "Investigation of Ternary Aluminium Alloy Systems: Al Rich Al-Fe-Si System", *Mem. Coll. Eng. Kyoto Univ.*, **7**, 285–303 (1933) (Phase Diagram, Experimental, #, *, 13)

[1934Fus] Fuess, V., "Aluminium-Iron-Silicon" in "*Metallography of Aluminium and Its Alloys*" (in German), Berlin, 109–117 (1934) (Phase Diagram, Experimental, 6)

[1934Roe] Roehrig, H., Kopernick, E., "On Spherically Precipitated Aluminium-Iron-Silicon Eutectic in Pure Aluminium" (in German), *Metallwirtschaft*, **13**, 591–593 (1934) (Experimental, 2)

[1935Bos] Bosshard, M., "Diffusional Research as a Means for the Simple Micrographic Detection of Compound Formation Between Alloy Constituents in Ternary and Multicomponent Systems" (in German), *Aluminium*, **17**, 477–481 (1935) (Experimental)

[1936Jae] Jaeniche, W., "On the System Aluminium-Iron-Silicon" (in German), *Alum. Arch.*, (5), 1–21 (1936) (Crys. Structure, Phase Diagram, Experimental, #, *, 28)

[1937Koe] Koerber, F., Oelsen, W., Lichtenberg, H., "On the Thermochemistry of Alloys. II. Direct Determination of the Heat of Formation of Ternary Alloys of the System Iron-Nickel-Aluminium-Silicon, as well as Certain Alloys of the Copper-Manganese-Aluminium System" (in German), *Mitt. K.-W.-Inst. Eisenforschung*, **19**, 131–159 (1937) (Experimental, Thermodyn., 50)

[1937Oel] Oelsen, W., "The Heats of Formation of Binary and Ternary Alloys and Their Importance in Metallurgical Reactions" (in German), *Z. Electrochem.*, **43**, 530–535 (1937) (Experimental, Thermodyn., 15)

[1937Ser] Sergeev, L.N., Rimmer, B.I, "Constitution of the System Aluminium-Iron-Silicon" (in Russian), *Metallurg.*, (9/10), 112–125 (1937) (Crys. Structure, Phase Diagram, Review)

[1937Ura] Urasov, G.G., Shashin, A.V., "Constitution of the (Ternary) Aluminium Alloys with Silicon and Iron" (in Russian), *Metallurg.*, (4), 27–41 (1937) (Phase Diagram, Experimental)

[1940Tak] Takeda, H.P., Mutuzaki, K., "The Equilibrium Diagram of the Iron-Aluminium-Silicon System" (in Japanese), *Tetsu to Hagane*, **26**, 335–361 (1940) (Phase Diagram, Experimental, #, *, 27)

DOI: 10.1007/978-3-540-69761-9_11

[1941Pan] Panseri, C., Guastalla, B., "Investigations on the Permanent Modification of Eutectic Aluminium-Silicon Alloys. I.-Influence of Titanium Additions as the Third Component" (in Italian), *Alluminio*, **10**(5), 202–227 (1941) (Phase Diagram, Experimental, Review, 161)

[1943Mon] Mondolfo, L.F., "Aluminum-Iron-Silicon", in "*Metallography of Aluminum Alloys*", John Wiley & Sons, Inc., New York, 95–97 (1943) (Phase Diagram, Review, #, 27)

[1943Phi] Phillips, H.W.L., Varley, P.C., "Constitution of Alloys of Aluminium with Magnesium, Silicon and Iron", *J. Inst. Met.*, **69**, 317–350 (1943) (Phase Diagram, Experimental, #, *, 11)

[1946Phi1] Phillips, H.W.L., "The Constitution of Alloys of Aluminium with Magnesium, Silicon and Iron", *J. Inst. Met.*, **72**, 151–227 (1946) (Phase Diagram, Experimental, #, *, 86)

[1946Phi2] Phillips, H.W.L., "The Application of Some Thermodynamic Principles to the Liquidus Surfaces of Alloys of Aluminium with Magnesium, Silicon and Iron", *J. Inst. Met.*, **72**, 229–242 (1946) (Theory, Thermodyn., #, *, 21)

[1946Sel] Selisski, Ya.P., "The Lattice Spacing of Solid Solutions of Fe, Si and Al Rich in Fe" (in Russian), *Zh. Fiz. Khim.*, **20**, 597–604 (1946) (Crys. Structure, Experimental, *, 15)

[1948Jen] Jennings, P.H., Pumphrey, W.L., "A Consideration of the Constitution of Aluminium-Iron-Silicon Alloys and Its Relation to Cracking Above the Solidus", *J. Inst. Met.*, **74**, 249–258 (1948) (Experimental, 14)

[1949Cru] Crussard, C., Aubertin, F., "Study of Thermo-electric and Thermodynamic Properties of Aluminium base Alloys Containing Mg, Si, Fe or Ti" (in French), *Rev. Metall.*, **46**, 661–675 (1949) (Phase Diagram, Experimental, #, *, 12)

[1950Gme] *Gmelins Handbook of Inorganic Chemistry*, "Aluminium-Iron-Silicon Alloys. The Al-Fe-Si Phase Diagram" (in German), **A**(8), System No. 35, Verlag Chemie GmbH, Weinheim, 1334–1370 (1950) (Phase Diagram, Review, #, *, 15)

[1950Phr] Phragmen, G., "On the Phase Occurring in Alloys of Aluminium with Copper, Magnesium, Manganese, Iron and Silicon", *J. Inst. Met.*, **77**, 489–552 (1950) (Phase Relations, Experimental, #, *, 67)

[1951Hol] Holik, L., Nowotny, H., Thury, W., "Investigation of the Microstructure in the Al corner of the System Aluminium-Iron-Silicon" (in German), *Berg- und Huettenmn. Monatsh. Hochsch. Loeben*, **96**, 181–184 (1951) (Phase Diagram, Experimental, #, *, 12)

[1951Now] Nowotny, H., Komerek, K., Kromer, J., "An Investigation of the Ternary System: Aluminium-Iron-Silicon" (in German), *Berg- und Huettenmn. Monatsh. Hochsch. Loeben*, **96**, 161–169 (1951) (Crys. Structure, Phase Diagram, Experimental, *, 31)

[1951Oga1] Ogawa, S., Matsuzaki, Y., "Study of the Supperlattices in Ternary Iron-Aluminium-Silicon Alloys by X-rays", *Nippon Kinzoku Gakkaishi*, **15**, 242–244 (1951) (Crys. Structure, Experimental, *, 9)

[1951Oga2] Ogawa, S., Matsuzaki, Y., "Study on the Superlattice of Ternary Alloys by X-rays", *Sci. Rep. Research Inst. Tohoku University*, **3A**, 50–54 (1951) (Crys. Structure, Experimental, *, 9)

[1951Pra1] Pratt, J.N., Raynor, G.V., "Intermetallic Compounds in Ternary Aluminium Rich Alloys Containing Transitional Metals", *Proc. Royal Soc.*, **A205**, 103–118 (1951) (Theory, 14)

[1951Pra2] Pratt, J.N., Raynor, G.V., "The Intermetallic Compounds in the Alloys of Aluminium and Silicon with Chromium, Manganese, Iron, Cobalt and Nickel", *J. Inst. Met.*, **79**, 211–232 (1951) (Crys. Structure, Phase Relations, Phase Diagram, Experimental, #, *, 32)

[1951Ran] Ransley, C.E., "Determination of Phase Boundaries in Solid Alloy Systems by a Diffusion Technique", *Nature*, **167**, 814 (1951) (Experimental, 1)

[1951Sat] Sato, H., Yamamoto, H., "The Behaviours of Fe-Al, Fe-Si and Fe-Al-Si Alloys Considered from the Standpoint of Ferromagnetic Supperlattice", *J. Phys. Soc. Jpn.*, **6**, 65–66 (1951) (Experimental, *, 2)

[1952Arm] Armand, M., "On the Phases in the Ternary System Aluminium-Iron-Silicon" (in French), *C.R. Seances Acad. Sci.*, 235, 1506–1508 (1952) (Crys. Structure, Experimental, *, 9)

[1952Han] Hanemann, H., Schrader, A., in "*Ternary Alloys of Aluminium*" (in German), Verlag Stahleisen, Duesseldorf, 109–115 (1952) (Phase Diagram, Review, #, 12)

DOI: 10.1007/978-3-540-69761-9_11

[1953Rob] Robson, K., Black, P.J., "An X-ray Examination of an α-(Al-Fe-Si) Ternary Compound", *Philos. Mag*., **44**, 1392–1397 (1953) (Crys. Structure, Experimental, *, 10)

[1954Gar] Garrod, R.I., Hogan, L.M., "The Superlattice in Sendust", *Acta Metall*., **2**, 887–888 (1954) (Crys. Structure, Experimental, *, 5)

[1954Spi] Spiegelberg, A.P.W., Danielsson, S.L.A., Astroem, H., "The Crystal Structure of Some Phases Occurring in Alloys of Aluminium, Iron and Silicon and Their Relationship to Other Phases", *Acta Crystallogr.*, **7**, 634 (1954) (Crys. Structure, Experimental, *, 4)

[1955Arm] Armand, M., "Liquation and Equilibrium Diagram: Applications to the Diagram of Aluminium-Iron-Silicon Alloys" (in French), in *Congress International de l'Aluminium, Revue de l'Aluminium*, **1**, 305–327 (1955) (Crys. Structure, Experimental, *, 9)

[1955Bla] Black, P.J., "Brillouin Zones of Some Intermetallic Compounds", *Philos. Mag.*, **46**, 401–409 (1955) (Crys. Structure, Experimental, *, 23)

[1955Obi] Obinata, I., Komatsu, N., "On the Phases occuring in Alloys of Aluminium with Iron and Silicon" (in Japanese), *Nippon Kinzoku Gakkaishi*, **19**, 197–201 (1955) (Crys. Structure, Experimental, 30)

[1956Spe] Sperry, P.R., "The Intermetallic Phases in 2024 Aluminum Alloys", *Trans. ASM*, **48**, 904–918 (1956) (Experimental, 11)

[1959Phi] Phillips, H.W.L., in "*Annoted Equilibrium Diagrams of Some Al Alloy Systems*", Monograph, Inst. Of Met., London, (25), 57–65 (1959) (Phase Diagram, Review, #, *, 18)

[1960Lee] Lee, J.R., "Liquidus - Solidus Relations in the System Iron-Aluminum", *J. Iron Steel Inst. Met.*, **194**, 222–224 (1960) (Phase Diagram, Experimental, 5)

[1960Spe] Spengler, H., "The Importance of Research on Eutectics and its Application to Ternary Eutectic Aluminium Alloys" (in German), *Metall*, **14**, 201–206 (1960) (Experimental)

[1960Voz] Vozdvizhenskiy, V.M., "The Effect on the Saturation of Solid Solution in Some Al Alloys" (in Russian), *Izv. Vyss. Uchebn. Zaved. Tsvetn. Metall*., (5), 116–120 (1960) (Phase Diagram, Experimental, 19)

[1961Phi] Phillips, H.W.L., "Al-Fe-Si" in "*Equilibrium Diagrams of Aluminium Alloy Systems*", The Aluminium Development Association, London, 91–96 (1961) (Phase Diagram, Experimental, #, *)

[1961Sab] Sabirzyanev, A.V., Shumilov, M.A., Gel´d, P.V., Ozhogikhina, G.V., "Solubility of Al in α-Leoboite", *Phys. Met. Metallogr.*, **12**(5), 81–87 (1961), translated from *Fiz. Met. Metalloved*., **12**, 714–721 (1961) (Crys. Structure, Experimental, 14)

[1964Lai] Lainer, D.A., Kurakin, A.K., "Mechanism of the Influence of Silicon in Aluminium on the Reaction Diffusion of Iron", *Phys. Met. Metallogr*., **18**, 134–137 (1964), translated from *Fiz. Metall. Metalloved*., **18**, 145–148 (1964) (Crys. Structure, Experimental, 13)

[1965Sab] Sabirzyanev, A.V., Shumilov, M.A., "The Solubility of Al and P in Constituents of High-Si Ferrosilicon" (in Russian), *Tr. Ural'sk Politekhn. Inst*., (144), 35–40 (1965) (Experimental, 14)

[1965Skr] Skripova, E.A., Letun, G.M., "The Solubility of Al in α-Leboite" (in Russian), *Tr. Ural'sk Politekhn. Inst*., (144), 67–70 (1965) (Crys. Structure, Experimental, 4)

[1967Coo] Cooper, M., "The Crystal Structure of the Ternary Alloys S-AlFeSi", *Acta Crystallogr.*, **23**, 1106–1107 (1967) (Crys. Structure, Experimental, *, 5)

[1967Mun] Munson, D., "A Clarification of the Phases Occuring in Aluminium Rich Aluminium-Iron-Silicon Alloys with Particular Reference to the Ternary Phase α-AlFeSi", *J. Inst. Met*., **95**, 217–219 (1967) (Crys. Structure, Phase Diagram, Experimental, *, 12)

[1967Sun] Sun, C.Y., Mondolfo, L.F., "A Clarification of the Phases Occuring in Al Rich Al-Fe-Si Alloys", *J. Inst. Met*., **95**, 384 (1967) (Crys. Structure, Experimental, *, 2)

[1968Aru1] Arutyunyan, S.V., Selissky, Ya.P., "The Question of Superstructure in Fe-Si-Al Alloys" (in Russian), *Izv. Akad. Nauk. Arm. SSR, Fiz*., **3**, 8–11 (1968) (Crys. Structure, Experimental, 5)

DOI: 10.1007/978-3-540-69761-9_11

[1968Aru2] Arutyunyan, S.V., "Some Features of Atomic Ordering in Ternary Fe-Si-Al Alloys" (in Russian), *Izv. Akad. Nauk Arm. SSR, Fiz.*, **3**, 294–297 (1968) (Crys. Structure, Experimental, 2)

[1968Dri] Drits, M.E., Kadaner, E.S., Turkina, N.I., "The System Al-Fe-Si" in "*Diagrammy Sostoyaniya Metallich. Sistem*" (in Russian), Publ. Nauka, Moscow, **XIV**, 109 (1968) (Phase Diagram, Review, 1)

[1968Lih] Lihl, F., Burger, R., Sturm, F., Ebel, H., "Constitution of Fe Rich Ternary Al-Fe-Si Alloys" (in German), *Arch. Eisenhuettenwes.*, **39**, 877–880 (1968) (Phase Diagram, Experimental, *, 22)

[1968Sab1] Sabirzyanev, A.V., Gel´d, V.P., "Some Features of the Peritectoid Transformation in β-Leboite ($FeSi_2$) Alloys Alloyed with Al, Ca and P" (in Russian), *Tr. Ural'sk Politekhn. Inst.*, (167), 75–80 (1968) (Experimental, 6)

[1968Sab2] Sabirzyanev, A.V., Gel´d, V.P., "Nature of Solid Solutions of Aluminium and Phosphorus in Iron Monosilicide" (in Russian), *Izv. Vyss. Uchebn. Zaved. Chern. Metall.*, **11**, 21–26 (1968) (Experimental, 3)

[1969Bed] Bedon., P., Ansara, I., Desre, P., "Isothermal Sections at 1900 K of the Silver - Aluminium - Iron - Silicon and Silver - Aluminium - Nickel - Silicon Metallic Systems; Activity of Aluminium in Molten Aluminium - Iron - Silver - Silicon and Aluminium - Nickel - Silver Alloys" (in French), *Mem. Sci. Rev. Metall.*, **66**, 907–913 (1969) (Experimental, Thermodyn., 5)

[1969Pan] Panday, P.K., Schubert, K., "Structure Studies in Some Alloys $T\text{-}B^3\text{-}B^4$ (T = Mn, Fe, Co, Ir, Ni, Pd; B^4 = Si, Ge)" (in German), *J. Less-Common Met.*, **18**, 175–202 (1969) (Crys. Structure, Experimental, *, 32)

[1969Pol] Polishchuk, V.E., Selissky, YA.P., "High-Temperature Study of the Structure and Electrical Properties of the Fe-Si-Al System" (in Russian), *Ukrain. Fiz. Zhur.*, **14**, 1722–1724 (1969) (Phase Diagram, Experimental, #, *, 9)

[1970Aru] Arutyunyan, S.V., "Transition from Atomic Ordering to Disordering in $Fe_3(Al,Si)$ Alloys Related to the Formation of the K-Effect" (in Russian), *Izv. Akad. Nauk Arm. SSR, Ser. Tekh. Nauk*, **32**, 36–42 (1970) (Experimental, 4)

[1970Mit] Mitani, H., Nagai, H., Ohtani, T., "Dry Refining of Aluminium. IV. Activity Measurements of the Ternary Liquid Al-Fe-Si System by the EMF Method" (in Japanese), *Nippon Kinzoku Gakkaishi*, **34**, 165–170 (1970) (Experimental, Thermodyn., 16)

[1971Gle] Glezer, A.M., Molotilov, B.V., Polishchuk, V.Ye., Selissky, Ya.P., "X-ray and Electron Microscopic Analysis of the Fine Structure of Ordering High-Fe-Al-Si Alloys", *Phys. Met. Metallogr.*, **32**(4), 39–47 (1971), translated from *Fiz. Met. Metalloved.*, **32**, 713–722 (1971) (Experimental, 19)

[1972Ere] Eremenko, V.N., Natanzon, Ya.V., Ryabov, V.R., Dzykovich, I.Ya., "Interaction of Al-Si Melts with Steel" (in Russian), *Liteinoe Proizod.*, (2), 21–22 (1972) (Experimental)

[1973Kat] Katsnel´son, A.A., Polishchuk, V.Ye., "Energy Characteristics of Atomic Ordering in Alloys of Iron with Aluminium and Silicon", *Phys. Met. Metallogr.*, **36**(2), 86–90 (1972), translated from *Fiz. Met. Metalloved.*, **36**, 321–325 (1973) (Phase Diagram, Experimental, #, *, 10)

[1973Kow] Kowatschewa, R., Dafinowa, R., Kamenowa, Z., Momtschilov, E., "Metallographic Determination of Intermetallic Compounds in Aluminium Alloys", *Metallography*, **10**, 131–143 (1973) (Crys. Structure, Experimental, 9)

[1973Nag] Nagai, H., Mitani, H., "Activity Measurements of the Ternary Liquid Al-Si-Fe System by the EMF Method", *Trans. Jpn. Inst. Met.*, **14**, 130–134 (1973) (Experimental, Thermodyn., 9)

[1973Per] Perkins, J., Desre, P., "Determination of Activities in the Al-Fe-Si System by a EMF Method" (in French), *Rev. Int. Hautes Temp. Refract.*, **10**, 79–84 (1973) (Experimental, Thermodyn., 13)

[1974Mur] Murav´eve, A.A., German, N.V., Zarechnyuk, O.S., Gladyshevskii, E.I., "Ternary Compounds of the Fe-Al-Si System" (in Russian), *Proc. Second All-Union Conf. Crystal Chem. Intermet. Compd.*, L'vov, October, 35–36 (1974) (Crys. Structure, Experimental, *)

DOI: 10.1007/978-3-540-69761-9_11

[1975Bar] Barlock, J.G., Mondolfo, L.F., "Structure of Some Aluminum-Iron-Magnesium-Silicon Alloys", *Z. Metallkd.*, **66**, 605–611 (1975) (Crys. Structure, Phase Diagram, Experimental, *, 7)

[1977Cor] Corby, R.N., Black, P.J., "The Structure of α-AlFeSi by Anomalous Dispersion Method", *Acta Crystallogr. B*, **33B**, 3468–3475 (1977) (Crys. Structure, Experimental, *, 18)

[1977Hoi] Hoeier, R., Lohne, O., Moertvedt, S.T., "AlFeSi-Particles in an Al-Mg-Si-Fe Alloy", *Scand. J. Metall.*, **6**, 36–37 (1977) (Crys. Structure, Experimental, *, 3)

[1977Igl] Iglessis, J., Frantz, C., Gantois, M., "Conditions for the Formation of the Iron Phases in Commercial Purity Aluminium-Silicon Alloys" (in French), *Mem. Sci. Rev. Metall.*, **74**, 237–242 (1977) (Experimental, *, 14)

[1977Nic1] Niculescu, V., Raj, K., Burch, T., Budnick, J.J., "Hyperfine Interactions and Structural Disorder of $Fe_2Si_{1-x}Al_x$ Alloys", *J. Phys. F, Met. Phys.*, **7**, L73-L76 (1977) (Experimental, 7)

[1977Nic2] Niculescu, V., Budnick, J.J., "Limits of Solubility, Magnetic Properties and Electron Concentration in $Fe_{3-x}T_xSi$ System", *Solid State Commun.*, **24**, 631–634 (1977) (Theory, 17)

[1977Sim] Simensen, C.J., Vellasamy, R., "Determination of Phases Present in Cast Material of an Al-0.5 wt.% Fe-0.2 wt.% Si Alloy", *Z. Metallkd.*, **68**, 428–431 (1977) (Crys. Structure, Experimental, 10)

[1977Suw] Suwalski, J., Drabowski, L., Piekoszewski, J., Tucholski, Z., "Study of Order-Disorder Transformation in Fe-Al-Si Alloys by Mössbauer Spectroscopy", *Phys. Status Sol.(a),* **41**, 191–195 (1977) (Experimental, Crys. Structure, Phase Relations, 15)

[1978Suz] Suzuki, H., Kanno, M., Tanabe, H., Itoi, K., "The Effect of Si or Mg Addition on the Metastable to Stable Phase Changes in an Al-0.5% Fe Alloy" (in Japanese), *J. Jpn. Inst. Light Met.*, **28**, 558–565 (1978) (Crys. Structure, Experimental, 7)

[1978Xu] Xu, W.-C., Su, X.-J., "An Investigation on the Structure of Fe-Si-Al Alloy" (in Chinese), *Acta Phys. Sin.*, **27**, 576–582 (1978) (Crys. Structure, Experimental, *, 9)

[1979Bur] Burch, T.J., Raj, K., Jena, P., Budnick, J.I., Niculescu, V., Muir, W.B., "Hyperfine-field Distribution in $Fe_3Si_{1-x}Al_x$ Alloys and a Theoretical Interpretation", *Phys. Rev. B: Solid State*, **19**, 2933–2938 (1979) (Experimental, Theory, 17)

[1979Cow] Cowdery, J.S., Kayser, F.X., "Lattice Parameters of Ferromagnetic $D0_3$-Structured Iron-Aluminium-Silicon Alloys", *Mater. Res. Bull.*, **14**, 91–99 (1979) (Crys. Structure, Experimental, *, 24)

[1979Mor] Mora, R., "The Determination of the Al-Fe-Si Phase in Homogenized Aluminium Alloy 6063" (in Spanish), *Rev. Metall.*, **15**, 91–95 (1979) (Crys. Structure, Experimental, *, 15)

[1980Sud] Sudavsova, V.S., Batalin, G.I., "Aluminium Activity in Liquid Iron Alloys" (in Russian), *Ukr. Khim. Zh.*, **46**, 268–270 (1980) (Experimental, Thermodyn., 8)

[1981Riv] Rivlin, V.G., Raynor, G.V., "Phase Equilibria in Iron Ternary Alloys 4: Critical Evaluation of Constitution of Aluminium-Iron-Silicon System", *Int. Met. Rev.*, **26**, 133–152 (1981) (Phase Diagram, Review, #, *, 56)

[1981Wat] Watanabe, H., Sato, E., "Phase Diagram in Aluminium Alloys" (in Japanese), *J. Jpn. Inst. Light Met.*, **31**, 64–79 (1981) (Phase Diagram, Review, #, *, 22)

[1981Zar] Zarechnyuk, O.S., German, N.V., Yanson, T.I., Rykhal, R.M., Murav'eva, A.A., "Some Phase Diagrams of Aluminium with Transition Metals, Rare Earth Metals and Silicon" (in Russian), *Faz. Ravnoves. Metall. Splav.*, Nauka, Moscow, 1981, 69–71 (1981) (Crys. Structure, Phase Diagram, Experimental, #, *, 5)

[1982All] Allen, S.M., Cahn, J.W., "Phase Diagram Features Associated with Multicritical Points in Alloy Systems", *Bull. Alloy Phase Diagrams*, **3**(3), 287–295 (1982) (Theory, Phase Relations, 25)

[1982Cha] Chang, Y.J., "An Electron Microscopic Investigation of Order-Disorder Transformation in a Fe-Si-Al (SENDUST) Alloy and Its Dislocation Configurations", *Acta Metall.*, **30**, 1185–1192 (1982) (Crys. Structure, Experimental, 17)

[1982Kub] Kubaschewski, O., "Iron-Aluminium" and "Iron-Silicon" in "Iron-binary Phase Diagrams", Springer Verlag, Berlin, 5–9 and 136-139 (1982) (Phase Diagram, Review, #, *, 26, 23)

DOI: 10.1007/978-3-540-69761-9_11

[1982Miy] Miyazaki, T., Tsuzuki, T., Kozakai, T., Fujimoto, Y., "Phase Separation of Fe-Si-Al Ordering Alloys" (in Japanese), *Nippon Kinzoku Gakkai-Si*, **46**, 1111–1119 (1982) (Crys. Structure, Experimental, 37)

[1982Wes] Westgren, H., "Formation of Intermetallic Compounds During DC Casting of Commercial Purity Al-Fe-Si Alloy", *Z. Metallkd.*, **73**, 361–368 (1982) (Crys. Structure, Experimental, 24)

[1983Gle] Glezer, A.M., Molotilov, B.V., Prokoshin, A.F., Sosnin, V.V., "Structural Features of a SENDUST (Fe-Si-Al) Alloy Obtained by Quenching from the Melt. I. The Study of Atomic Ordering Properties", *Phys. Met. Metallogr.*, **56**(4), 110–117 (1983), translated from *Fiz. Met. Metalloved.*, **56**, 750–757 (1983) (Crys. Structure, Experimental, *, 12)

[1983Per] Perepezko, J.H., Boettinger, J.W., "Use of Metastable Phase Diagrams in Rapid Solidification", in *Alloy Phase Diagrams*, Proc. Mater. Soc. Symp., **19**, 223–240 (1983) (Review, Theory, 52)

[1983Sch] Schneeweiss, O., Zemcik, T., Zak, T., Mager, S., "Atomic Structure and Magnetic Properties of the Pseudobinary Alloys Fe_3(Al,Si)", *Phys. Status Solidi (a)*, **79**, 125–129 (1983) (Experimental, 10)

[1984Ber] Berecz, E., Bader, I., Weberner, Kovacs, E., Hovath, J., Szina, G., "Thermodynamic Examination of Aluminium Alloys by the Electrochemical Method", (in Hungarian), *Banyasz. Kohasz. Lapok*, **117**, 413–417 (1984) (Experimental, Thermodyn., 10)

[1984Don] Dons, A.L., "AlFeSi-Particles in Commercial Pure Aluminium", *Z. Metallkd.*, **75**, 170–174 (1984) (Phase Diagram, Experimental, #, *, 10)

[1984Mat] Matsumura, S., Sonobe, A, Oki, K., Eguchi, T., "Ordering with Phase Separation in an Fe-Al-Si Alloy", in *Phase Transformations in Solids*, Proc. Conf. Materials Research Society, Elsevier, Amsterdam, Vol. **21**, 269–274 (1984) (Crys. Structure, Experimental, 12)

[1985Cao] Cao, R., Li, G., Wu, X., "Some Thermodynamic Properties in Process of Thermal Reduction of Magnesium with High Aluminium Alloy" (in Chinese), *Acta Metall. Sin.*, **21**, A471-A476 (1985) (Experimental, Thermodyn., 9)

[1985Don1] Dons, A.L., "Superstructure in α-Al(MnFeCrSi)", *Z. Metallkd.*, **76**, 151–153 (1985) (Crys. Structure, Experimental, *, 11)

[1985Don2] Dons, A.L., "AlFeSi-Particles in Industrially Cast Aluminium Alloys", *Z. Metallkd.*, **76**, 609–612 (1985) (Experimental, 14)

[1985Gri] Griger, A., Stefaniay, V., Turmezey, T., "Analysis of Ternary Al-Fe-Si Phases on High Purity Base", in *High Purity Materials in Science and Technology*, Proc. 6th Int. Symp. Supplement, Dresden, GDR, 6–10 May, 187–188 (1985) (Experimental)

[1985Liu] Lui, P., Thorvaldsson, L., Dunlop, G.L., "The Formation of Intermetallic Compounds during Solidification of Dilute Al-Fe-Si Alloys", *Ultramicroscopy*, **17**, 178 (1985) (Crys. Structure, Experimental)

[1985Riv] Rivlin, V.G., "Assessment of Phase Equilibria in Ternary Alloys of Iron", *J. Less-Common Met.*, **114**, 111–121 (1985) (Phase Diagram, Review, #, *, 4)

[1985Suz] Suzuki, H., Arai, K., Shiga, M., Nakamura, Y., "Mössbauer Effect of Al-Fe-Si Intermetallic Compounds", *Metall. Trans. A*, **16A**, 1937–1942 (1985) (Experimental, 22)

[1986Dun] Dunlap, R.A., Dini, K., "Amorphization of Rapidly Quenched Quasicrystalline Al Transition Metal Alloys by the Addition of Si", *J. Mater. Res.*, **1**, 415–419 (1986) (Crys. Structure, Experimental, 19)

[1986Len] Lendvai, A., "Phase Diagram of the Al-Fe System up to 45 mass% Iron", *J. Mater. Sci. Lett.*, **5**, 1219–1220 (1986) (Phase Diagram, Experimental, 7)

[1986Liu1] Liu, P., Dunlop, G.L., "Constituent Formed during Solidification of Al-Fe-Si Alloys", *Proc. Conf. Aluminium Alloys: Their Physical and Mechanical Properties*, **I**, Chalottesville, Virginia, USA, 15–20 (1986) (Crys. Structure, Experimental, *, 20)

[1986Liu2] Lui, P., Thorvaldsson, L., Dunlop, G.L., "Formation of Intermetallic Compounds During Solidification of Dilute Al-Fe-Si Alloys", *Mater. Sci. Technol.*, **2**, 1009–1018 (1986) (Crys. Structure, Experimental, *, 26)

DOI: 10.1007/978-3-540-69761-9_11

[1986Miy] Miyazaki, T., Kozaki, T., Tsuzuki, T., "Phase Decomposition of Fe-Si-Al Ordered Alloys", *J. Mater. Sci.*, **21**, 2557–2564 (1986) (Phase Diagram, Experimental, #, *, 26)

[1986Tak] Takahashi, M., Arai, H., Tanaka, T, Wakiyama, T., "Magnetocrystalline Anisotropy for Fe-Al-Si (SENDUST) Single-Crystals with $D0_3$ Ordered Structure", *IEEE Trans. Magnetics*, **22**, 638–640 (1986) (Experimental, 7)

[1987Ben] Bendersky, L.A., Biancaniello, F.S., Schaefer, R.J., "Amorphous Phase Formation in $Al_{70}Si_{17}Fe_{13}$ Alloys", *J. Mater. Res.*, **2**, 427–430 (1987) (Experimental, 21)

[1987Cha] Chandrasekaran, M., Liu, Y.P., Vincent, R., Staniek, G., "On a Metastable Rhombohedral Al-Fe-Si Intermetallic Phase", *Proc. Electron Microscopy Analysis Group Meeting*, Manchester, Sept. (1987), 63–65 (1988) (Crys. Structure, Experimental, 5)

[1987Czi] Cziraki, A., Fogarassy, B., Oszko, A., Szabo, I., Teravaginov, A., Reibold, M., "Effect of Heat Treatment on the Microstructure of Cast Al-Fe-Si Alloys", *Mater. Sci. Forum*, **13-14**, 343–350 (1987) (Crys. Structure, Experimental, 5)

[1987Dob] Dobrzynski, L., Giebultowicz, T., Kopcewicz, M., Piotrowski, M., Szymanski, K., "Neutron and Mössbauer Studies of $Fe_{3-x}Al_xSi$ Alloys", *Phys. Status Solidi (A)*, **101**, 567–575 (1987) (Crys. Structure, Experimental, 24)

[1987For] Fortnum, R.T., Mikkola, D.E., "Effects of Molybdenum, Titanium and Silicon Additions on The $D0_3$ Reversible $B2$ Transition-Temperature for Alloys Near Fe_3Al", *Mater. Sci. Eng.*, **91**, 223–231 (1987) (Crys. Structure, Experimental, 37)

[1987Gri1] Griger, A., Lendrai, A., Stefaniay, V., Turmezey, T., "On the Phase Diagrams of the Al-Fe and Al-Fe-Si Systems", *Mater. Sci. Forum*, **13/14**, 331–336 (1987) (Phase Diagram, Experimental, 9)

[1987Gri2] Griger, A., "Powder Data for the α_H Intermetallic Phases with Slight Variation in Composition in the System Al-Fe-Si", *Powder Diffr.*, **2**, 31–35 (1987) (Crys. Structure, Experimental, *, 21)

[1987Liu] Liu, P., Dunlop, G.L., "Determination of the Crystal Symmetry of Two Al-Fe-Si Phases by Convergent-beam Electron Diffraction", *J. Appl. Crystallogr.*, **20**, 425–427 (1987) (Crys. Structure, Experimental, 13)

[1987Nag] Nagy, S., Homonnay, Z., Vertes, A., Murgas, L., "Mössbauer Investigation of Iron in Aluminium. II. Al-Fe-Si Samples", *Acta Metall.*, **35**, 741–746 (1987) (Experimental, 2)

[1987Pri] Prince, A., "Comment on Intermetallic Phases in the Al-side of the AlFeSi-Alloy System", *J. Mater. Sci. Lett.*, **6**, 1364 (1987) (Phase Diagram, Theory, #, 1)

[1987Skj1] Skjerpe, P., "Intermetallic Phases Formed During DC-Casting of an Al-0.25 wt% Fe-0.13 wt% Si Alloy", *Metall. Trans. A*, **18A**, 189–200 (1987) (Crys. Structure, Experimental, 35)

[1987Skj2] Skjerpe, P., Gjonnes, J., "Solidification Structure and Primary Al-Fe-Si Particles in Direct-Chilled-Cast Aluminum Alloys", *Ultramicroscopy*, **22**, 239–250 (1987) (Crys. Structure, Experimental, 21)

[1987Skj3] Skjerpe, P., "An Electron Microscopy Study on the Phase Al_3Fe", *J. Microscopy*, **148**, 33–50 (1987) (Crys. Structure, Experimental, Theory, 12)

[1987Ste] Stefaniay, V., Griger, A., Turmezey, T., "Intermetallic Phases in the Aluminium-side Corner of the AlFeSi-alloy System", *J. Mater. Sci.*, **22**, 539–546 (1987) (Crys. Structure, Phase Diagram, Experimental, #, *, 13)

[1987Tak1] Takahashi, M., Arai, H., Wakiyama, T., "Magnetostriction of Fe-Al-Si Sputtered Thin-Films", *IEEE Trans. Magnetics*, **23**, 3068–3070 (1987) (Experimental, 9)

[1987Tak2] Takahashi, M., Arai, H., Wakiyama, T., "Magnetostriction Constants for Fe-Al-Si (SENDUST) Single-Crystals with $D0_3$ Ordered Structure", *IEEE Trans. Magnetics*, **23**, 3523–3525 (1987) (Experimental, Magn. Prop., 5)

[1987Tur] Turmezey, T., "AlFe and AlFeSi Intermetallic Phases in Aluminium Alloys", *Mater. Sci. Forum*, **13/14**, 121–132 (1987) (Crys. Structure, Experimental, 12)

[1988Ben1] Bendersky, L., "Rapidly Solidified Al-Fe-Si Alloys", *Mater. Sci. Eng.*, **98**, 213–216 (1988) (Crys. Structure, Experimental, 9)

DOI: 10.1007/978-3-540-69761-9_11

[1988Ben2] Bendersky, L.A., McAlisetr, A.J., Biancaniello, F.S., "Phase Transformation during Annealing of Rapidly Solidified Al rich Al-Fe-Si Alloys", *Metall. Trans. A*, **19A**, 2893–2900 (1988) (Crys. Structure, Experimental, 29)

[1988Cha] Chandrasekaran, M., Lin, Y.P., Vincent, R., Staniek, G., "The Structure and Stability of Some Intermetallic Phases in Rapidly Solidified Al-Fe", *Scr. Metall.*, **22**, 797–802 (1988) (Crys. Structure, Experimental, 9)

[1988Dor] Dorofeyeva, Ye.A., Sasnin, Y.V., Stolokotniy, V.L., "Cross-Relaxation of Magnetic Permeability in Alloy FeSiAl", *Phys. Met. Metallogr.*, **65**(3), 172–174 (1988) (Experimental, 2).

[1988Liu1] Liu, P., Dunlop, G.L., "Long-range Ordering of Vacancies of BCC α-AlFeSi", *J. Mater. Sci.*, **23**, 1419–1424 (1988) (Crys. Structure, Experimental, 20)

[1988Liu2] Liu, P., Dunlop, G.L., "Crystallographic Orientation Relationships for Al-Fe and Al-Fe-Si Precipitates in Aluminium", *Acta Metall.,***36**, 1481–1489 (1988) (Crys. Structure, Experimental, 20)

[1988Ray] Raynor, G.V., Rivlin, V.G., "Al-Fe-Si", in "*Phase Equilibria in Iron Ternary Alloys*", Institute of Metals, London, 122–139 (1988) (Phase Diagram, Review, #, 39)

[1988Zak] Zakharov, A.M., Gul´man, I.T., Arnol´d, A.A., Matsenko, Yu.A., "Phase Diagram of the Aluminium-Silicon-Iron System in the Concentration Range of 10-14% Si and 0-3% Fe", *Russ. Metall.*, (3), 177–180 (1988), translated from *Izv. Akad. Nauk SSSR, Met.*, (3), 178–181 (1988) (Phase Diagram, Experimental, #, *, 8)

[1989Bon] Bonnet, M., Rogez, J., Castanet, R., "EMF Investigation of Al-Si, Al-Fe-Si and Al-Ni-Si Liquid Alloys", *Thermochim. Acta*, **155**, 39–56 (1989) (Experimental, Thermodyn., 15)

[1989Tib] Tibballs, J.E., "Al-Si Substitution in Al(Fe,Mn)Si Phases", Unpublished work (1989) (Crys. Structure, Experimental, 23)

[1989Ger1] German, N.V., Bel`skii, V.K., Yanson, T.I., Zarechnyuk, O.S., "Crystal Structure of the Compound $Fe_{1.7}Al_4Si$", *Sov. Phys. Crystallogr.*, **34**(3), 437–438 (1989) (Crys. Structure, Experimental, 5)

[1989Ger2] German, N.V., Zavodnik, V.E., Yanson, T.I., Zarechnyuk, O.S., "Crystal Structure of $FeAl_2Si$", *Sov. Phys. Crystallogr.*, **34**(3), 439–440 (1989) (Crys. Structure, Experimental, 5)

[1991Don] Dons, A.L., "Simulation of Solidification a Short Cut to a Better Phase Diagram Al-Mg-Fe-Si Alloys?", *Z. Metallkd.*, **82**(9), 684–688 (1991) (Calculation, Phase Diagram, Experimental, Thermodyn., 17)

[1991Fuk] Fukaya, M., Miyazaki, T., Kozakai, T., "Phase Diagrams Calculated for Fe Rich Fe-Si-Co and Fe-Si-Al Ordering Systems", *J. Mater. Sci.*, **26**(2), 5420–5426 (1991) (Calculation, Phase Relations, 42)

[1991Lan] Langsrud, Y., "The Use of Phase Diagrams for Calculating Solidification Paths", in *User Aspects of Phase Diagrams*, Proceedings Conf.; Hayes, F.H., (Ed.), Inst. of Metals, London, 90–100 (1991) (Theory, 7)

[1992Gho] Ghosh, G., "Aluminium-Iron-Silicon", MSIT Ternary Evaluation Program, in *MSIT Workplace*, Effenberg, G. (Ed.), MSI, Materials Science International Services GmbH, Stuttgart; Document ID: 10.14596.1.20, (1992) (Crys. Structure, Phase Relations, Phase Diagram, Assessment, 134)

[1992Zak] Zakharov, A.M., Guldin, I.T., Arnold, A.A., Matsenko, Yu.A., "Phase Equilibria in Multicomponent Aluminum Systems with Copper, Iron, Silicon, Manganese and Titanium" (in Russian), *Metalloved. Obrab. Tsvetn. Splavov: To 90th Anniversary of Academician A.A. Bochvar Birthday. RAN. Inst. Metallurg., Moscow*, 6–17 (1992) (Phase Diagram, Experimental, 14)

[1993Car] Carpenter, G.J.C., Le Page, Y., "Revised Cell Data for the β-FeSiAl Phase in Aluminum Alloys", *Scr. Metall. Mater.*, **28**, 733–736 (1993) (Crys. Structure, Experimental, 6)

[1993Sch] Schroeer, W., Hartig, C., Mecking, H., "Plasticity of $D0_3$-ordered Fe-Al and Fe-Al-Si Single-Crystals", *Z. Metallkd.*, **84**(5), 294–300 (1993) (Phase Relations, Experimental, 30)

[1994Ang] Anglezio, J.C., Servant, C., Ansara, I., "Contribution to the Experimental and Thermodynamic Assessment of the Al-Ca-Fe-Si System - I. Al-Ca-Fe, Al-Ca-Si, Al-Fe-Si and

DOI: 10.1007/978-3-540-69761-9_11

Ca-Fe-Si Systems", *Calphad*, **18**(3), 273–309 (1994) (Calculation, Phase Diagram, Phase Relations, Thermodyn., 71)

[1994Koz] Kozakai, T., Miyazaki, T., "Experimental And Theoretical Investigations on Phase Diagrams of Fe Base Ternary Ordering Alloys", *ISIJ Int.*, **34**(5), 373–383 (1994) (Calculation, Phase Diagram, Magn. Prop., 18)

[1994Mur] Murali, S., Guru Row, T.N., Sastry, D.H., Raman, K.S., Murthy, K.S.S., "Crystal Structure of β-$FeSiAl_5$ and (Be-Fe)-$BeSiFe_2Al_8$ Phases.", *Scr. Metall. Mater.*, **31**(3), 267–271 (1994) (Experimental, Crys. Structure, 13)

[1994Rag] Raghavan, V., "The Al-Fe-Si System", *J. Phase Equilib.*, **15**(4), 414–416 (1994) (Phase Diagram, Review, 27)

[1994Rom] Romming, Chr., Hansen, V., Gjonnes, J., "Crystal Structure of β-$Al_{4.5}FeSi$", *Acta Crystallogr., Sect. B: Struct. Crystallogr. Crys. Chem.*, **B50**(3), 307–312 (1994) (Crys. Structure, Experimental, 10)

[1995Bel] Belov, N.A., "Analysis of Nonequilibrium Solidification of Subeutectic Sillumines Using Multicomponent Phase Diagrams", *Russ. Metall. (Engl. Transl.)*, **(1)**, 41–47 (1995) (Phase Relations, Experimental, 5)

[1995Gue1] Gueneau, C., "$FeAl_3Si_2$", *Acta Crystallogr., Sect. C: Cryst. Struct. Commun.*, **C51**, 177–179 (1995) (Crys. Structure, Experimental, 9)

[1995Gue2] Gueneau, C., Servant, C., "$Fe_2Al_3Si_3$", *Acta Crystallogr., Sect. C: Cryst. Struct. Commun.*, **C51**, 2461–2464 (1995) (Crys. Structure, Experimental, 8)

[1995Gue3] Gueneau, C., Servant, C., Ansara, I., "Experimental and Thermodynamic Assessments of Substitutions in the AlFeSi, FeMnSi, FeSiZr and AlCaFeSi Systems", *Appl. Thermodyn. Synth. Procee. Mater., Proc. Symp.*, Nash, P., Sundman, B., (Eds.), The Minerals, Metals and Materials Society, Warrendale, Pa, 303–317 (1995) (Experimental, Theory, 19)

[1996All] Allen, C.M., O'Reilly, K.A.Q., Cantor, B., Evans, P.V., "Nucleation of Phases in Al-Fe-Si Alloys", *Mater. Sci. Forum*, **217-222**, 679–684 (1996) (Calculation, Phase Relations, 14)

[1996Cho] Choi, Y., Ra, H., "Microstructure of Gas Atomized Al-Fe-Si Alloy Powders" (in Korean), *J. Korean Inst. Met.*, **34**(2), 230–235 (1996) (Experimental, 11)

[1996Fri] Friemelt, K., Ditusa, J.F., Bucher, E., Aeppli, G., "Coulomb Interactions in Al Doped FeSi at Low Temperatures", *Ann. Physik-Leipzig*, **5**(2), 175–183 (1996) (Crys. Structure, Experimental, 25)

[1996Mor] Morris, D.G., Gunther, S., "Order-Disorder Changes in Fe_3Al Based Alloys and the Development of an Iron-Base α-α`` Superalloy", *Acta Mater.*, **44**(7), 2847–2859 (1996) (Crys. Structure, Phase Relations, Experimental, 23)

[1996Mul] Mulazimoglu, M.H., Zaluska, A., Gruzleski, J.E., Parray, F., "Electron Microscopy Study of Al-Fe-Si Intermetallics in 6021 Aluminum Alloys", *Metall. Mater. Trans. A*, **27A**, 929–936 (1996) (Crys. Structure, Experimental, 48)

[1996Mur] Murali, S., Raman, K.S., Murthy, K.S.S., "Al-7Si-0.3Mg Cast Alloy: Formation and Crystal Structure of β-$FeSiAl_5$ and (Be-Fe)-$BeSiFe_2Al_8$ Phases", *Mater. Sci. Forum*, **217-222**, 207–212 (1996) (Crys. Structure, Experimental, 8)

[1996Szy] Szymanski, K., Baas, J., Dobrzynski, L., Satula, D., "Magnetic and Moessbauer Investigation of $FeSi_{2-x}Al_x$", *Physica B (Amsterdam)*, **225**, 111–120 (1996) (Crys. Structure, Experimental, 20)

[1996Yan] Yanson, T.I., Manyako, M.B., Bodak, O.I., German, N.V., Zarechnyuk, O.S., Cerny, R., Pacheko, J.V., Yvon, K., "Triclinic $Fe_3Al_2Si_3$ and Orthorhombic $Fe_3Al_2Si_4$ with New Structure Types", *Acta Crystallogr., Sect. C: Cryst. Struct. Commun.*, **C52**, 2964–2967 (1996) (Crys. Structure, Experimental, 15)

[1997All] Allen, C.M., O`Reilly, K.A.Q., Cantor, B., Evans, P.V., "Heterogeneous Nucleation of Solidification of Equilibrium and Metastable Phases in Melt-Spun Al-Fe-Si Alloys", *Mater. Sci. Eng. A*, **A226-228**, 784–788 (1997) (Experimental, Phys. Prop., 10)

DOI: 10.1007/978-3-540-69761-9_11

[1997Can] Cantor, B., "Impurity Effects on Heterogenous Nucleation", *Mater. Sci. Eng. A*, **A226-228**, 151–156 (1997) (Crys. Structure, Experimental, 38)

[1997Sto] Stone, I.C., Jones, H., "Effect of Cooling Rate and Front Velosity on Solidification Microstructure Selection in Al-3.5wt.%Fe-0 to 8.5wt.%Si Alloys", *Mater. Sci. Eng. A*, **A226-228**, 33–37 (1997) (Phase Relations, Experimental, 10)

[1997Vyb] Vybornov, M., Rogl, P., Sommer, F., "The Thermodynamic Stability and Solid Solution Behavior of the Phases τ_5-$Fe_2Al_{7.4}Si$ and τ_6-$Fe_2Al_9Si_2$", *J. Alloys Compd.*, **247**, 154–157 (1997) (Crys. Structure, Phase Relations, Experimental, 7)

[1998Akd] Akdeniz, M.V., Mekhrabon, A.O., "The Effect of Substitutional Impurities on the Evolution of Fe-Al Diffusion Layer", *Acta Mater.*, **46**(4), 1185–1192 (1998) (Calculation, Thermodyn., 55)

[1998Dit] Ditusa, J.F., Friemelt, K., Bucher, E., Aeppli, G., Ramirez, A.P., "Heavy Fermion Metal-Kondo Insulator Transition in $FeSi_{1-x}Al_x$", *Phys. Rev. B*, **58**(16), 10288–10301 (1998) (Crys. Structure, Experimental)

[1998Kol] Kolby, P., "System Al-Fe-Si" in "*COST 507, Thermochemical Database for Light Metal Alloys*", **Vol. 2**, Ansara, I., Dinsdale, A.T., Rand, M.H. (Eds.), Office for official publications of the European Communities, Luxembourg, 1998, ISBN 92-828-3902-8, 319–321 (Assessment, Thermodyn.)

[1998Han] Hansen, V., Hauback, B., Sundberg, M., Romming, Ch., Gjonnes, J., "A Combined Synchrotron Powder Diffraction, Electron Diffraction, High-Resolution Electron Microscopy and Single-Crystal X-ray Diffraction Study of a Faulted Structure", *Acta Crystallogr.*, **54B**, 351–357 (1998) (Crys. Structure, Experimental, 7)

[1999Cho] Choi, Y.S., Lee, L.S., Kim, W.T., Ra, H.Y., "Solidification Behavior of Al-Si-Fe Alloys and Phase Transformation of Metastable Intermetallic Compound by Heat Treatment", *J. Mater. Sci.*, **34**, 2163–2168 (1999) (Phase Relations, Experimental, 14)

[1999Liu] Liu, Z.-K., Chang, A., "Thermodynamic Assessment of the Al-Fe-Si System", *Metall. Mater. Trans.A.*, **30A**(7), 1081–1095 (1999) (Calculation, Thermodyn., 56)

[1999Mek] Mekhrabov, A.O., Akdeniz, M.V., "Effect of Ternary Alloying Elements Addition on Atomic Ordering Characteristics of Fe-Al Intermetallics", *Acta Mater.*, **47**(7), 2067–2075 (1999) (Calculation, Theory, Thermodyn., 63)

[1999Oht] Ohta, Y., Miura, S., Mishima, Y., "Thermoelectric Semiconductor Iron Disilicides Produced by Sintering Elemental Powders", *Intermetallics*, **7**, 1203–1210 (1999) (Phase Relations, Experimental, Transport Phenomena, 19)

[1999Tay] Taylor, J.A., Schaffer, G.B., St. John, D.H., "The Role of Iron in the Formation of Porosity in Al-Si-Cu-Based Casting Alloys: Part II. A Phase-Diagram Approach", *Metall. Mater. Trans. A*, **30A**, 1651–1655 (1999) (Calculation, Crys. Structure, Experimental, 12)

[2000Bha] Bhattamishra, A.K., Chattoraj, I., Basu, D.K., De, P.K., "Study on the Influence of the Si/Fe Ratio on the Corrosion Behavior of Some Al-Fe-Si Alloys", *Z. Metallkd.*, **91**(5), 393–396 (2000) (Interface Phenomena, Experimental, 23)

[2000Dut] Dutta, B., Rettnmayr, M., "Effect of Coolig Rate on the Solidification Behavior of Al-Fe-Si Alloys", *Mater. Sci. Eng. A*, **A283**, 218–224 (2000) (Phase Relations, Experimental, 23)

[2000Li1] Li, Y., Ochin, P., Quivy, A., Telolahy, P., Legendre, B., "Enthalpy of Formation of Al-Fe-Si Alloys (τ_5, τ_{10}, τ_1, τ_9)", *J. Alloys Compd.*, **298**, 198–202 (2000) (Experimental, Thermodyn., 20)

[2000Li2] Li, Y., Legendre, B., "Enthalpy of Formation of Al-Fe-Si Alloys II (τ_6, τ_2, τ_3, τ_8, τ_4)", *J. Alloys Compd.*, **302**, 187–191 (2000) (Experimental, Thermodyn., 21)

[2000Sri] Sritharan, T., Murali, S., Hing, P., "Synthesis of Aluminium-Iron-Silicon Intermetallics by Reaction of Elemental Powders", *Mater. Sci. Eng. A*, **A286**, 209–217 (2000) (Crys. Structure, Experimental, 18)

[2000Zhe] Zheng, J.G., Vincent, R., Steeds, J.W., "Crystal Structure of an Orthorhombic Phase in β-(Al-Fe-Si) Precipitates Determined by Convergent-Beam Electron Diffraction", *Philos. Mag. A*, **80**(2), 493–500 (2000) (Crys. Structure, Experimental, 11)

DOI: 10.1007/978-3-540-69761-9_11

[2001Cho] Cho, H.S., Kim, K.S., Jeong, H.G., Yamagata, H., "Microstructure and Mechanical Properties of Extruded Rapidly Solidified Al-16Si-5Fe Based Alloys", *Key Eng. Mater.*, **189-191**, 479–483 (2001) (Experimental, Mechan. Prop., 5)

[2001Hsu] Hsu, G., O´Reilly, K.A.Q., Cantor, B., Hamerton, R., "Non-Equilibrium Reactions in 6xxx Series Al Alloys", *Mater. Sci. Eng. A*, **304-306**, 119–124 (2001) (Phase Relations, Experimental, 14)

[2001Jha] Jha, R., Haworth, C.W., Argent, B.B., "The Formation of Diffusian Coatings on Some Low-Alloy Steels and Their High Temperature Oxidation Behavior: Part 1 Diffusion Coatings", *Calphad*, **25**(4), 651–665 (2001) (Calculation, Phase Diagram, Phase Relations, 9)

[2001Kre] Krendelsberger, N., "Constitution of the Systems Aluminium-Manganese-Silicon, Aluminium-Iron-Silicon, und Aluminium-Iron-Manganese-Silicon", *Thesis*, Inst. of Physical Chemistry, University of Vienna, 2001 (Crys. Structure, Phase Diagram, Experimental, #, *, 83)

[2001Sha] Sha, G., O´Reilly, K., Cantor, B., Worth, J., Hamerton, R., "Growth Related Metastable Phase Selection in a 6xxx Series Wrought Al Alloy", *Mater. Sci. Eng. A*, **304-306**, 612–616 (2001) (Crys. Structure, Phase Relations, Experimental, 9)

[2002Dut] Dutta, B., Rettenmayr, M., "Microsegregation and Its Effects on Quantity and Morphology of Secondary Phases During Solidification of Al-Fe-Si Alloys", *Mater. Sci. Technol.*, **18**, 1428–434 (2002) (Calculation, Experimental, Morphology, Phase Relations, 22

[2002Gup] Gupta, S.P., "Intermetallic Compound Formation in Fe-Al-Si Ternary System: Part I", *Mater. Charact.*, **49**, 269–291 (2002) (Experimental, Phase Diagram, #, *, 22).

[2002Mai] Maitra, T., Gupta, S.P., "Intermetallic Compound Formation in Fe-Al-Si Ternary System: Part II", *Mater. Charact.*, **49**, 293–311 (2002) (Experimental, Phase Diagram, #, *, 30)

[2002Mer] Meredith, M.W., Worth, J., Hamerton, R.G., "Intermetallic Phase Selection During Solidification of Al-Fe-Si(-Mg) Alloys", *Mater. Sci. Forum*, **396-402**, 107–112 (2002) (Phase Relations, Experimental, 9)

[2002Rag] Raghavan, V., "Al-Fe-Si (Aluminium-Iron-Silicon)", *J. Phase Equilib.*, **25**(4), 107–112 (2002) (Phase Diagram, Review, 24)

[2003Cie] Cieslar, M. C., Fressengeas, C., Karimi, A., Martin, J.L., "Portevin-Le Chatelier Effect in Biaxially Strained Al-Fe-Si Foils", *Scr. Mater.*, **48**, 1105–1110 (2003) (Experimental, Mechan. Prop., 19)

[2003Gjo] Gjonnes, J., Hansen, V., Andersen, S.J., Marioara, C.D., Li, X.Z., "Electron Crystallography of Aluminum Alloy Phases", *Z. Kristallogr.*, **218**, 293–307 (2003) (Crys. Structure, Review, 73)

[2003Kan] Kanibolotsky, D.S., Bieloborodova, O.A., Kotova, N.V., Lisnyak, V.V., "Enthalpy of Mixing in Liquid Al-Fe-Si Alloys at 1750 K", *Thermochim. Acta*, **408**(1-2), 1–7 (2003) (Experimental, Thermodyn., *, 20)

[2003Kha] Khalifa, W., Samuel, F.H., Gruzleski, "Iron Intermetallic Phases in the Al Corner of the Al-Si-Fe System", *Metall. Mater. Trans. A*, **34A**, 807–825 (2003) (Experimental, Phase Diagram, #, *, 50)

[2003Mur] Murali, S., Sritharan, T., Hing, P., "Self-Propagating High Temperature Synthesis of AlFeSi Intermetallic Compound", *Intermetallics*, **11**(3), 279–281 (2003) (Experimental, Kinetics, Phase Relations, 10)

[2003Wen] Wen, K. Y., Hu, W., Gottstein, G., "Intermetallic Compounds in Thixoformed Aluminium Alloy A356", *Mater. Sci. Tech.*, **19**(6), 762–768 (2003) (Crys. Structure, Experimental, Morphology, 28)

[2004Kan] Kanibolotsky, D.S., Stukalo, V.S., Lisnyak, V.V., "Thermodynamic Properties of Eutectic Silumins Doped by Transition Metals", *Z. Naturforschung A.*, **59**, 288–290 (2004) (Experimental, Thermodyn., 9)

[2004Kha] Khalifa, W., Samuel, F.H., Gruzleski, J.E., "Nucleation of Solid Aluminum on Inclusion Particles Injected into Al-Si-Fe Alloys", *Metall. Mater. Trans. A*, **35A**, 3233–3250 (2004) (Experimental, Morphology, 57)

DOI: 10.1007/978-3-540-69761-9_11

[2004Kra] Kral, M.V., McIntyre, H.R., Smillie, M.J., "Identification of Intermetallic Phases in a Eutectic Al–Si Casting Alloy Using Electron Backscatter Diffraction Pattern Analysis", *Scr. Mater.*, **51**, 215–219 (2004) (Experimental, Crys. Structure, Morphology, 41)

[2004Luk] Lukas, L, "Al-Si (Aluminum-Silicon)", MSIT Ternary Evaluation Program, in *MSIT Workplace,* Effenberg, G. (Ed.), MSI, Materials Science International Services, GmbH, Stuttgart; Document ID: 20.14887.1.20, (2004) (Crys. Structure, Phase Diagram, Assessment, 29)

[2004Pon] Pontevichi, S., Bosselet, F., Barbeau, F., Peronnet, M., Viala, J.C., "Solid-Liquid Phase Equilibria in the Al-Fe-Si System at 727°C", *J. Phase Equilib. Diffus.*, **25**(6), 528–537 (2004) (Crys. Structure, Experimental, Morphology, Phase Diagram, Phase Relations, #, *, 34)

[2004Sug] Sugiyama, K., Kaji, N., Hiraga, K., "Crystal Structure of Rhombohedral γ-AlFeSi", *J. Alloys Compd.*, **368**(1-2), 251–255 (2004) (Crys. Structure, Experimental, Morphology, 26)

[2004Zuo] Zuo, B., Saraswati, N., Sritharan, T., Hng, H.H., "Production and Annealing of Nanocrystalline Fe-Si and Fe-Si-Al Alloy Powders", *Mater. Sci. Eng. A*, **371**(1-2), 210–216 (2004) (Crys. Structure, Experimental, Kinetics, Morphology, Phase Relations, 25)

[2005Din] Dinnis, C.M., Taylor, J.A., Dahle, A.K., "As-cast Morphology of Iron-Intermetallics in Al-Si Foundry Alloys", *Scr. Mater.*, **53**, 955–958 (2005) (Experimental, Morphology, 23)

[2005Gho] Ghosh, G., "Aluminium-Iron-Silicon", in "*Landolt-Boernstein, Numerical Data and Functional Relationships in Science and Technology (New Series). Group IV: Physical Chemistry*", Martiensen, W. (Ed.), "*Ternary Alloy Systems. Phase Diagrams, Crystallographic and Thermodynamic Data*", Vol. 11A2, Effenberg, G., Ilyenko, S. (Eds.), Springer-Verlag, Berlin, Heidelberg, 369–409 (2005) (Phase Diagram, Phase Relations, Assessment, Crys. Structure, 196)

[2005Kha] Khalifa, W., Samuel, F.H., Gruzleski, J.E., Doty, H.W., Valtierra, S., "Nucleation of Fe-Intermetallic Phases in the Al-Si-Fe Alloys", *Metall. Mater. Trans. A*, **36A**(4), 1017–1032 (2005) (Experimental, Morphology, Phase Relations, 40)

[2005Kra] Kral, M.V., "A Crystallographic Identification of Intermetallic Phases in Al–Si Alloys", *Scr. Mater.*, **59**, 2271–2276 (2005) (Crys. Structure, Experimental, Morphology, 39)

[2005Lu] Lu, L., Dahle, A.K., "Iron rich Intermetallic Phases and Their Role in Casting Defect Formation in Hypoeutectic Al-Si Alloys", *Metall. Mater. Trans. A*, **36A**(3), 819–835 (2005) (Crys. Structure, Experimental, Morphology, Phase Relations, 29)

[2006Kra] Kral, M.V., Nakashima, P.N.H., Mitchell, D.R.G., "Electron Microscope Studies of Al-Fe-Si Intermetallics in an Al-11% Si Alloy", *Metall. Mater. Trans A*, **37A**, 1987–1997 (2006) (Crys. Structure, Experimental, Morphology, 54)

[2006MSIT] "Al-Fe (Aluminum-Iron)", Diagrams as Published, in *MSIT Workplace*, Effenberg, G. (Ed.), Materials Science International Services, GmbH, Stuttgart; Document ID: 30.10236.1.20, (2006) (Crys. Structure, Phase Diagram, Phase Relations, 11)

[Mas] Massalski, T.B. (Ed.), *Binary Alloy Phase Diagrams*, ASM, Metals Park, Ohio (1986)

[Mas2] Massalski, T.B. (Ed.), *Binary Alloy Phase Diagrams*, 2nd edition, ASM International, Metals Park, Ohio (1990)

[V-C] Villars, P. and Calvert, L.D., *Pearson's Handbook of Crystallographic Data for Intermetallic Phases*, ASM, Metals Park, Ohio (1985)

[V-C2] Villars, P. and Calvert, L.D., *Pearson's Handbook of Crystallographic Data for Intermetallic Phases*, 2nd edition, ASM, Metals Park, Ohio (1991)

DOI: 10.1007/978-3-540-69761-9_11

Aluminium – Iron – Tantalum

Gautam Ghosh

Introduction

A summary of experimental studies of phase equilibria is given in Table 1. [1965Gan] reported the *C*14 type Laves phase, in the Ta($Fe_{1-x}Al_x$)$_2$ ternary regime. [1968Hun] reported a partial isothermal section at 1000°C showing equilibria involving the μ (TaFe), σ (Ta_2Al) and μ′ (~$Ta_{50}Fe_{20}Al_{30}$) phases. Five ternary alloys were prepared in an arc furnace under argon atmosphere using Ta (99.9 mass%), Al (99.999 mass%) and Fe (99.99 mass%). The alloys were annealed in evacuated silica tubes at 1000°C for 168 h. The phases were identified by X-ray diffraction. These experimental results were reviewed earlier [1990Kum, [1992Gho, [1992Rag].
Recent experimental studies are focussed on Fe rich alloys [1989Bla, 1995Ant, 1997Rev, 1998Kei, 2005Ris1, 2005Ris2]. In particular, the effect of Ta on the order-disorder transitions in Fe_3Al [1995Ant, 2005Ris1], and the phase equilibria between λ (*C*14-$TaFe_2$) and (Fe) [1997Rev, 1998Kei, 2005Ris1, 2005Ris2] have received significant interests. [1995Ant] measured $D0_3 \rightarrow B2$ transition temperature in three $(Fe,Ta)_{74}Al_{26}$ alloys. [1998Kei] prepared 12 Fe rich alloys, containing 6-20 at.% Al and 7-16 at.% Ta, annealed them at 1200°C for 6 h, and measured the tie-lines compositions between (Fe) and Ta$(Fe,Al)_2$ phases. [2005Ris1, 2005Ris2] prepared 8 ternary alloys using 99.9% Al, 99.98% Fe and 99.999% Ta, and annealed them at 800°C for 1000 h and at 1000°C for 200 h. In addition to experimental studies, several isothermal sections have been calculated using CALculation of PHAse Diagram (CALPHAD) method [1991Kau].

Binary Systems

The Al-Fe system is accepted from [2006MSIT]. The Al-Ta system is accepted from the thermodynamic modeling by [1996Du]. The Fe-Ta phase diagram is accepted from [1982Kub].

Solid Phases

The crystal structures and lattice parameters of the solid phases are listed in Table 2.
The *C*14 type Laves phase (λ-$TaFe_2$) dissolves about 25 at.% Al [1998Kei, [2005Ris1] causing an increase of both *a* and *c* lattice parameters [1998Kei]. [1985Tro, 1989Bla] reported the lattice parameter of single-phase *C*14-($Ta_{1-x}Al_x$)Fe_2 alloys, with $0.1 \leq x \leq 0.5$. However, available phase relations data [997Rev, 1998Kei, 2005Ris1] show that these alloys lie in the two-phase field (Fe) + λ, perhaps except for ($Ta_{0.9}Al_{0.1}$)Fe_2. Therefore, lattice parameter data of [1985Tro, 1989Bla] are not considered. The μ phase (TaFe) is reported to dissolve up to 23 at.% Al and the σ phase (Ta_2Al) can dissolve up to about 8.5 at.% Fe [1968Hun].
Both λ and μ phases, originating from the Ta-Fe binary system, reappear in the ternary regime. As a result, they are not considered as true ternary phases. The λ-phase reappears in the ternary regime around equiatomic composition [1965Gan, 1996Mac, 2005Ris1], and it is labeled as λ′-TaFeAl. Similarly, the μ phase reappears in the ternary regime. It is labeled as μ′, and its composition varies from $Ta_{46}Fe_{19}Al_{35}$ to $Ta_{54}Fe_{23}Al_{23}$ [1968Hun].
Rapid solidification of $Ta_{10}Fe_{20}Al_{70}$ gives rise to a quasicrystal phase with icosahedral symmetry [1988Tsa, 1989Sri, 1993Kel], and it has a quasilattice constant of $a = 460$ pm [1989Sri].

Order – Disorder Phase Transitions

[1995Ant] studied the effect of Ta additions on the order-disorder transition temperatures of $(Fe,Ta)_{74}Al_{26}$ alloys by means of X-ray diffraction and calorimetry techniques. Their results show that Ta increases $D0_3 \rightarrow B2$ transition temperature. Also, X-ray diffraction data show that Ta atom occupies predominantly the 4(*b*) Wyckoff sites (1/2, 1/2, 1/2) in $D0_3$ structure. Based on a systematic study involving several early transition elements, [1995Ant] argued that the site preference of Ta has no strong correlation with atomic

DOI: 10.1007/978-3-540-69761-9_12

size, rather it is better correlated to its position in the periodic table, and hence the character of its valence electrons. However, they showed that the increase in $D0_3 \rightarrow B2$ transition temperature is related to the difference in metallic radius of the Ta atom and an Al atom, specifically $(r_{Al} - r_{Ta})^2$ [1995Ant], or the elastic energy associated with the atom size mismatch.
A theoretical analysis of order-disorder ($A2/B2$) transition temperature and short-range ordering characteristics of $Fe_{0.5}(Al_{1-x}Ta_x)_{0.5}$ alloys were carried out by [1999Mek]. They applied statistical thermodynamics of ordering within quasi-chemical framework, and predicted that Ta preferentially substitutes Fe sublattice sites in $Fe_{0.5}(Al_{1-x}Ta_x)_{0.5}$. Also, based on the calculated partial ordering energies they predicted an increase in $B2 \rightarrow A2$ temperature for $Fe_{0.5}(Al_{1-x}Ta_x)_{0.5}$ alloys. While there is no experimental data of such alloys, available data along $Fe_{74}Al_{26}$-$Ta_{26}Fe_{74}$ section [1995Ant] do support such a prediction. Using a linear muffin-tin orbital method, [2002Boz] calculated the formation energies of $(Fe,Ta)_{0.5}Al_{0.5}$ and $Fe_{0.5}(Al,Ta)_{0.5}$ alloys with $B2$ structure. They predicted that in both cases Ta atoms prefer to occupy the Al sublattice. Also, the calculated formation energies are predicted to be more positive compared to binary $Fe_{0.5}Al_{0.5}$.

Isothermal Sections

[1991Kau] reported calculated isothermal sections at 2327, 1927, 1527, 1427, 1227 and 1000°C. At least two approximations were made in the calculation of isothermal sections. First, the chemical ordering in (αFe) was not considered. Second, except for the σ-Ta_2Al phase, all intermetallics were considered as line compounds within the binary limits. However, the solubilities of Fe in σ-Ta_2Al, and Al in λ-$TaFe_2$ and μ-FeTa phases were considered. The phase $Ta_{31}Al_{69}$ in Table 2 was designated as $TaAl_2$ by [1991Kau]. There are other differences as well between the calculated [1991Kau] binary phase diagrams and those accepted in this assessment. Despite the approximations, the calculated phase diagrams help to identify the composition range and key experiments to investigate the phase equilibria. Figures 1, 2, 3 and 4 show the calculated isothermal section at 1927, 1527, 1427, 1227°C, respectively.
Figure 5 shows the partial isothermal section at 1000°C, based on the experimental data of [1968Hun, 2005Ris1]. The following information was used to tentatively draw α_1/α_2 boundaries in the ternary regime: (i) [1997Rev] reported that the microstructure of Fe rich alloys with 7-8 at.% Al and 7-11 at.% Ta consists of $C14$ phase in (αFe) matrix, (ii) [1998Kei] reported that the microstructure of Fe rich alloys with 16-19 at.% Al and 12-16 at.% Ta consists of $C14$ phase in $D0_3$ matrix, and (iii) [2005Ris1] reported that the microstructure of Fe rich alloys with 16-45 at.% Al and 2-6 at.% Ta consists of $C14$ phase in either $D0_3$ or $B2$ matrix. In addition, a few amendments have been made in Fig. 5 to comply with the binary phase diagrams accepted here. Unlike Al-Fe system, the Fe-Ta system does not exhibit a γ-loop and at 1000°C the Fe corner show (γFe) + λ-$TaFe_2$ phase field. As a result, there should be a narrow two-phase field, (γFe) + λ-$TaFe_2$, and a narrow three-phase field, (αFe) + (γFe) + λ-$TaFe_2$, very close to the Fe-Ta edge. Figure 6 shows the calculated isothermal section at 1000°C. The three-phase field (αFe) + (γFe) + λ-$TaFe_2$, yet to be experimentally detected, is revealed in the calculated isothermal section. However, the calculated phase diagram underestimates the solubility of Al in λ and μ phases.

Thermodynamics

There are no experimental thermodynamic data for ternary alloys. [1991Kau] reported thermodynamic model parameters of several phases within CALPHAD formalism. Thermodynamic model parameters were obtained by primarily matching the available experimental phase equilibria.

Notes on Materials Properties and Applications

A summary of experimental investigations of properties is given in Table 3.
[1962Min] studied the effect of additions of Ta on the properties of Fe_3Al. It increases hardness, electrical resistivity and also improves the high temperature properties of Fe_3Al.
The temperature dependence (25 to 1350°C) of yield stress of λ′-TaFeAl ($C14$ type) has been reported by [1990Sau, 1996Mac]. [2005Ris1, 2005Ris2] reported the temperature dependence of yield stress and the ductile-brittle transition temperature of Fe rich two-phase alloys. These alloys, containing 16-45 at.% Al

DOI: 10.1007/978-3-540-69761-9_12

and 2-6 at.% Ta, have either $D0_3$ or $B2$ matrix and they are strengthened by λ-Ta(Fe,Al)$_2$ phase. They found that in general as-cast alloys have higher yield stress than those heat treated at 1000°C. The short term oxidation resistance of Al-Fe alloys is not significantly impaired due to the addition of Ta [2005Ris1, 2005Ris2].

An icosahedral phase has been obtained by rapid solidification of $Ta_{10}Fe_{20}Al_{70}$ alloy [1988Tsa, 1989Sri]. At a heating rate of 40°C·min^{-1}, the icosahedral phase undergoes decomposition around 577°C with a heat of transformation 102 kJ·mol^{-1} [1988Tsa]. Magnetization data of the icosahedral phase show that the alloy exhibits Curie paramagnetism at low temperature (<100 K) and Pauli paramagnetism at higher temperatures. The icosahedral phase exhibits a localized Fe moment of 0.48 μ_B [1989Sri].

Miscellaneous

The melting point of λ phase gradually decreases with increasing Al content, from 1800°C in $Ta_{0.348}Fe_{0.608}Al_{0.044}$ to 1725°C in $Ta_{0.306}Fe_{0.341}Al_{0.353}$.

Table 1. Investigations of the Al-Fe-Mo Phase Relations, Structures and Thermodynamics

Reference	Method/Experimental Technique	Temperature/Composition/Phase Range Studied
[1965Gan]	XRD	TaFeAl (λ′)
[1968Hun]	XRD	19-27 at.% Fe, 23-35 at.% Al, Ta = bal.; 1000°C
[1985Tro]	XRD	$(Ta_{0.8}Al_{0.2})Fe_2$
[1988Tsa]	TEM, XRD, electrical resistivity, DSC	$Ta_{10}Fe_{20}Al_{70}$
[1989Bla]	XRD	$(Ta_{1-x}Al_x)Fe_2$ with $0 \le x \le 0.5$; 900-1200°C
[1989Sri]	XRD	$Ta_{10}Fe_{20}Al_{70}$
[1995Ant]	DTA, XRD	$Ta_1Fe_{73}Al_{26}$, $Ta_2Fe_{72}Al_{26}$, $Ta_4Fe_{70}Al_{26}$; $D0_3 \rightarrow B2$ order-disorder transition
[1996Mac]	Metallography, SEM, EDX, XRD	$Ta_{0.334}Fe_{0.334}Al_{0.332}$
[1997Rev]	SEM, EDX	7-8 at.% Al, 7-11 at.% Ta, Fe = bal.
[1998Kei]	Metallography, EPMA, XRD	0-35.3 at.% Al, 30.6-34.8 at.% Ta, Fe = bal; 1200°C
[2005Ris1, 2005Ris2]	DTA, metallography, XRD	16-45 at.% Al, 2-6 at.% Ta, Fe = bal.; 800 and 1000°C

Table 2. Crystallographic Data of Solid Phases

Phase/ Temperature Range [°C]	Pearson Symbol/ Space Group/ Prototype	Lattice Parameters [pm]	Comments/References
(Al) ≤ 660.452	*cF*4 $Fm\bar{3}m$ Cu	a = 404.88	pure Al at 24°C [Mas2]

(*continued*)

DOI: 10.1007/978-3-540-69761-9_12

Phase/ Temperature Range [°C]	Pearson Symbol/ Space Group/ Prototype	Lattice Parameters [pm]	Comments/References
(αδFe) (αFe)(r) ≤ 912	*cI*2 $Im\bar{3}m$ W	*a* = 286.65	pure Fe at 25°C [Mas2]
(δFe)(h_2) 1538 - 1394		*a* = 293.15	pure Fe at 1480°C [Mas2]
(γFe)(h_1) 1394 - 912	*cF*4 $Fm\bar{3}m$ Cu	*a* = 364.67	pure Fe at 915°C [Mas2]
(Ta) ≤ 2623	*cI*2 $Im\bar{3}m$ W	*a* = 330.65	pure Ta at 25°C [Mas2]
α_1, Fe_3Al ≤552.5	*cF*16 $Fm\bar{3}m$ BiF_3	*a* = 578.86 to 579.3	solid solubility ranges from ~25 to ~37 at.% Al [2006MSIT]
α_2, FeAl ≤ 1310	*cP*2 $Pm\bar{3}m$ CsCl	*a* = 289.76 to 290.78	[2006MSIT], at room temperature solid solubility ranges from ~24 to ~55 at.% Al
Fe_2Al_3 1232 - 1102	*cI*16?	 *a* = 598.0	[2006MSIT], solid solubility ranges from 58 to 65 at.% Al at 61 at.% Al [V-C2]
$FeAl_2$ ≤ 1156	*aP*18 *P*1 $FeAl_2$	*a* = 487.8 *b* = 646.1 *c* = 880.0 α = 91.75° β = 73.27° γ = 96.89°	[2006MSIT], at 71.5 at.% Al. Solid solubility ranges from ~70 to ~73 at.% Al
Fe_2Al_5 ≤ 1169	*oC*24 *Cmcm*	*a* = 765.59 *b* = 641.54 *c* = 421.84	[2006MSIT], at 71.5 at.% Al. Solid solubility ranges from 71.0 to 72.5 at.% Al
Fe_4Al_{13} ≤ 1160	*mC*102 *C*2/*m* Fe_4Al_{13}	*a* = 1552.7 to 1548.7 *b* = 803.5 to 808.4 *c* = 1244.9 to 1248.8 β = 107.7 to 107.99° *a* = 1549.2 *b* = 807.8 *c* = 1247.1 β = 107.69°	[2006MSIT], 74.16 to 76.7 at.% Al. Solid solubility ranges from 74.5 to 75.5 at.% Al [2006MSIT], at 76.0 at.% Al. Also denoted $FeAl_3$ or Fe_2Al_7
σ, Ta_2Al < 2061	*tP*30 $P4_2/mnm$ CrFe	*a* = 982.9 to 995.0 *c* = 519.4 to 524.09	25 to 50 at.% Al [V-C2]

(*continued*)

DOI: 10.1007/978-3-540-69761-9_12

Phase/ Temperature Range [°C]	Pearson Symbol/ Space Group/ Prototype	Lattice Parameters [pm]	Comments/References
TaAl < 1446	*mP**	-	[1996Du]
Ta_5Al_7 < 1345	*hP**	-	[1996Du]
Ta_2Al_3 ≤ 1226	*cF**	-	[1996Du]
$Ta_{31}Al_{69}$ 1548 - 1183	*cF*432 $F\bar{4}3m$ -	-	[1996Du] designated as $TaAl_2$ by [1991Kau]
$TaAl_3$ ≤ 1608	*tI*8 *I*4/*mmm* $TiAl_3$	*a* = 384.1 *c* = 858.0	[V-C2]
μ, $Ta_6(Fe_{1-x}Al_x)_7$ TaFe < 1875	*hR*39 $R\bar{3}m$ W_6Fe_7	 *a* = 491.9 *c* = 2700.0 *a* = 500.5 *c* = 2722.0	0 ≤ *x* ≤ 0.45 49 to 54 at.% Ta in Fe-Ta [1982Kub] Ta_2FeAl, [1968Hun]
λ, $TaFe_2$ ≤ 1775 $Ta(Fe_{1-x}Al_x)_2$	*hP*12 *P*6$_3$/*mmc* $MgZn_2$	 *a* = 482.7 *c* = 787.8 *a* = 493.2 *c* = 803.3 *a* = 494.7 *c* = 804.7 *a* = 481.4 *c* = 781.8 *a* = 486.3 *c* = 793.3 *a* = 488.4 *c* = 795.4 *a* = 491.9 *c* = 800.8 *a* = 495.8 *c* = 807.5	28.0 to 36.0 at.% Ta [1982Kub] $Ta_{0.336}Fe_{0.667}$ [1998Kei] TaFeAl, [1965Gan] TaFeAl, [1996Mac] $Ta_{0.348}Fe_{0.608}Al_{0.044}$ [1998Kei] $Ta_{0.333}Fe_{0.587}Al_{0.083}$ [1998Kei] $Ta_{0.306}Fe_{0.516}Al_{0.176}$ [1998Kei] $Ta_{0.324}Fe_{0.428}Al_{0.246}$ [1998Kei] $Ta_{0.306}Fe_{0.341}Al_{0.353}$ [1998Kei]

Table 3. Investigations of the Al-Fe-Ta Materials Properties

Reference	Method/Experimental Technique	Type of Property
[1962Min]	Mechanical tests	Hardness, resistivity
[1989Sri]	Magnetometry	Magnetization and Curie temperature
[1990Sau]	Mechanical tests	Yield stress of TaFeAl (λ')

(*continued*)

DOI: 10.1007/978-3-540-69761-9_12

Reference	Method/Experimental Technique	Type of Property
[1996Mac]	Mechanical tests	Yield stress and hardness of TaFeAl (λ')
[2005Ris1, 2005Ris2]	Mechanical and oxidation tests	Compressive yield stress of two-phase alloys, ductile-brittle transition temperature, oxidation kinetics

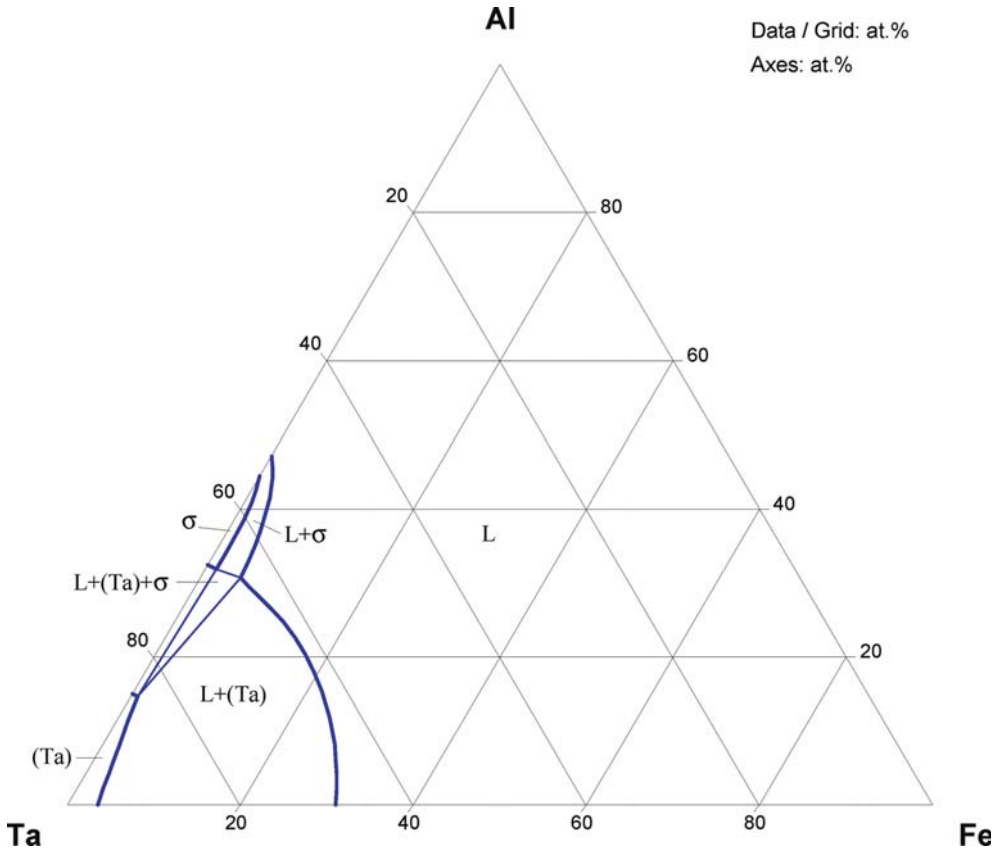

Fig. 1. Al-Fe-Ta. Calculated isothermal section at 1927°C

DOI: 10.1007/978-3-540-69761-9_12

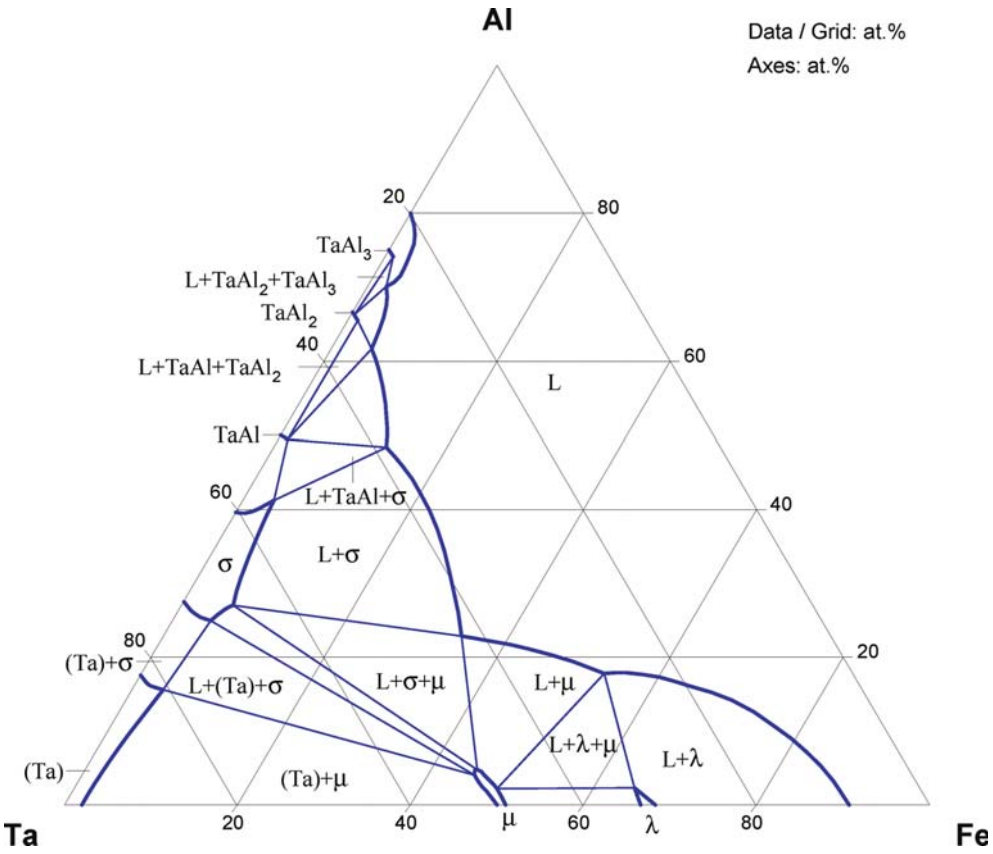

Fig. 2. Al-Fe-Ta. Calculated isothermal section at 1527°C

DOI: 10.1007/978-3-540-69761-9_12

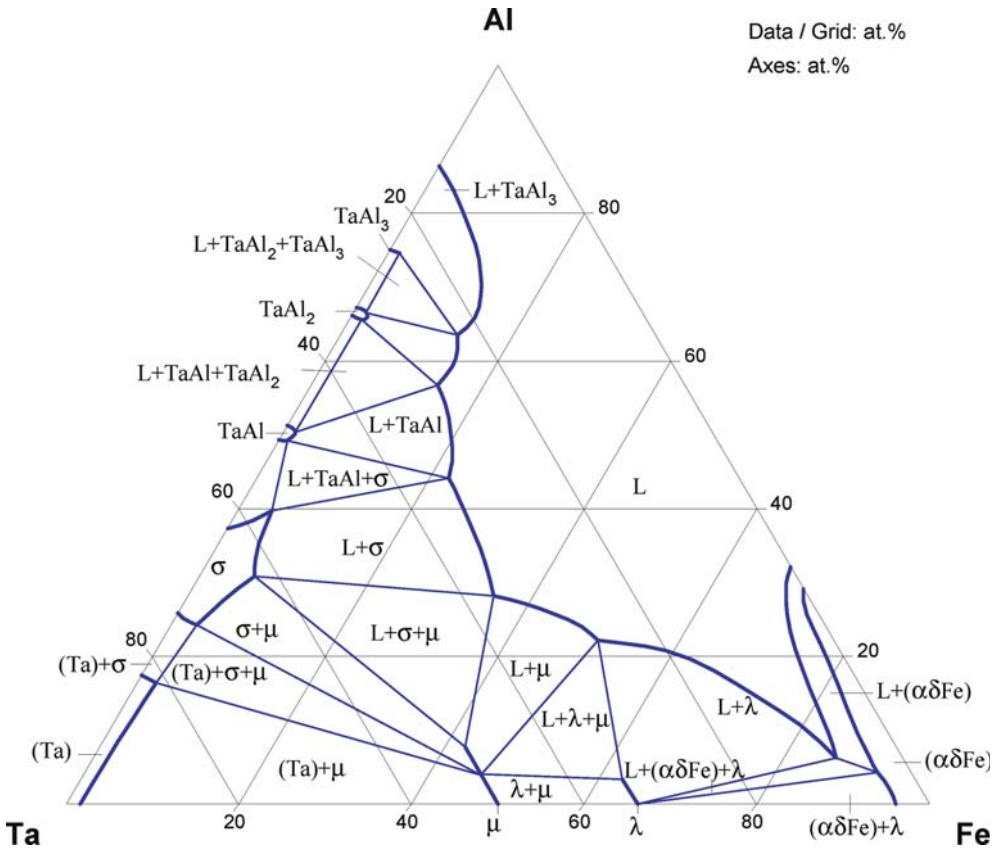

Fig. 3. Al-Fe-Ta. Calculated isothermal section at 1427°C

DOI: 10.1007/978-3-540-69761-9_12

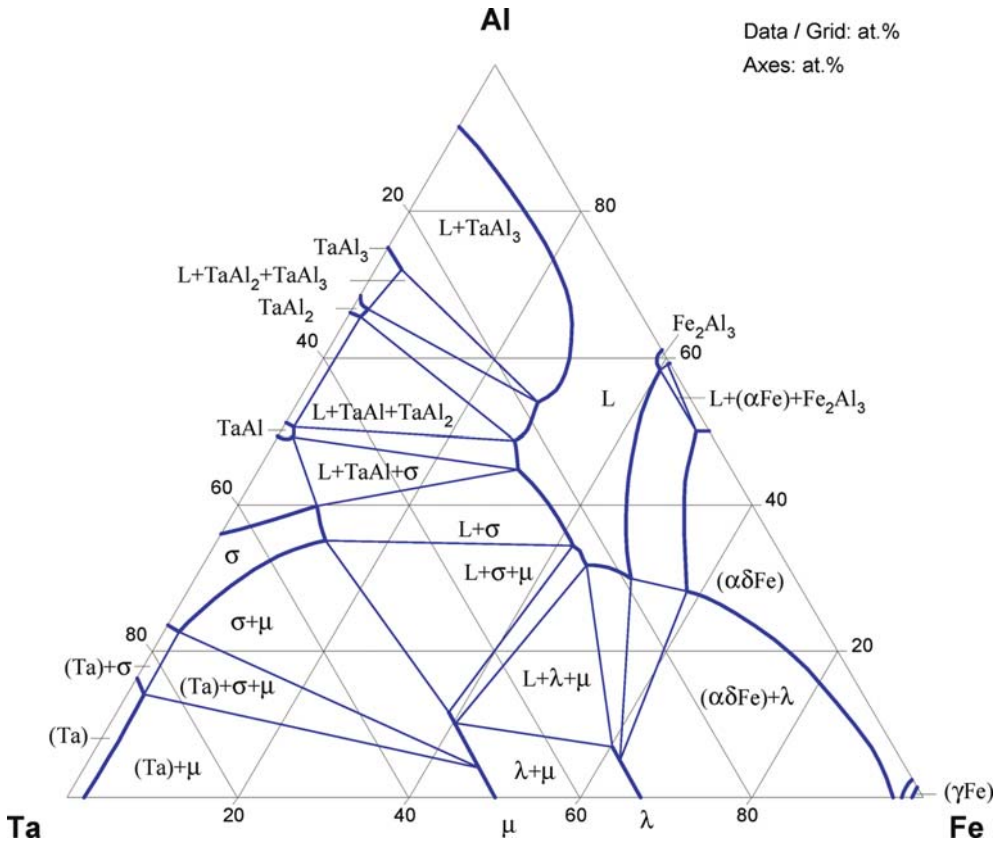

Fig. 4. Al-Fe-Ta. Calculated isothermal section at 1227°C

DOI: 10.1007/978-3-540-69761-9_12

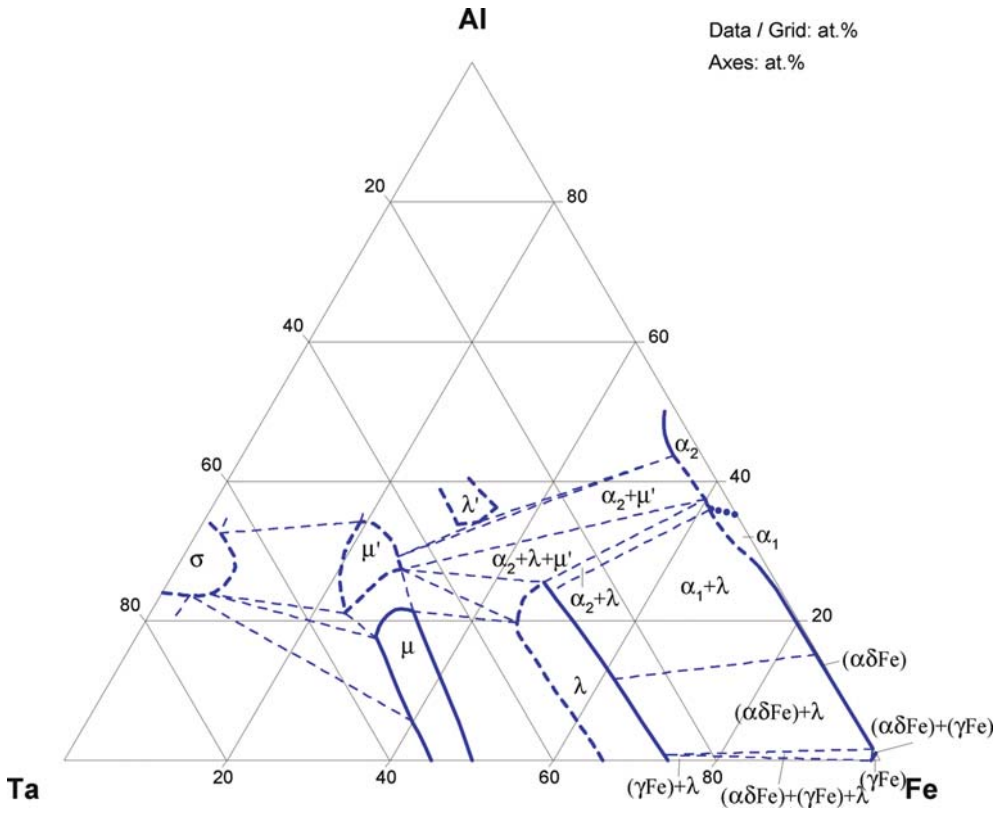

Fig. 5. Al-Fe-Ta. Partial isothermal section at 1000°C

DOI: 10.1007/978-3-540-69761-9_12

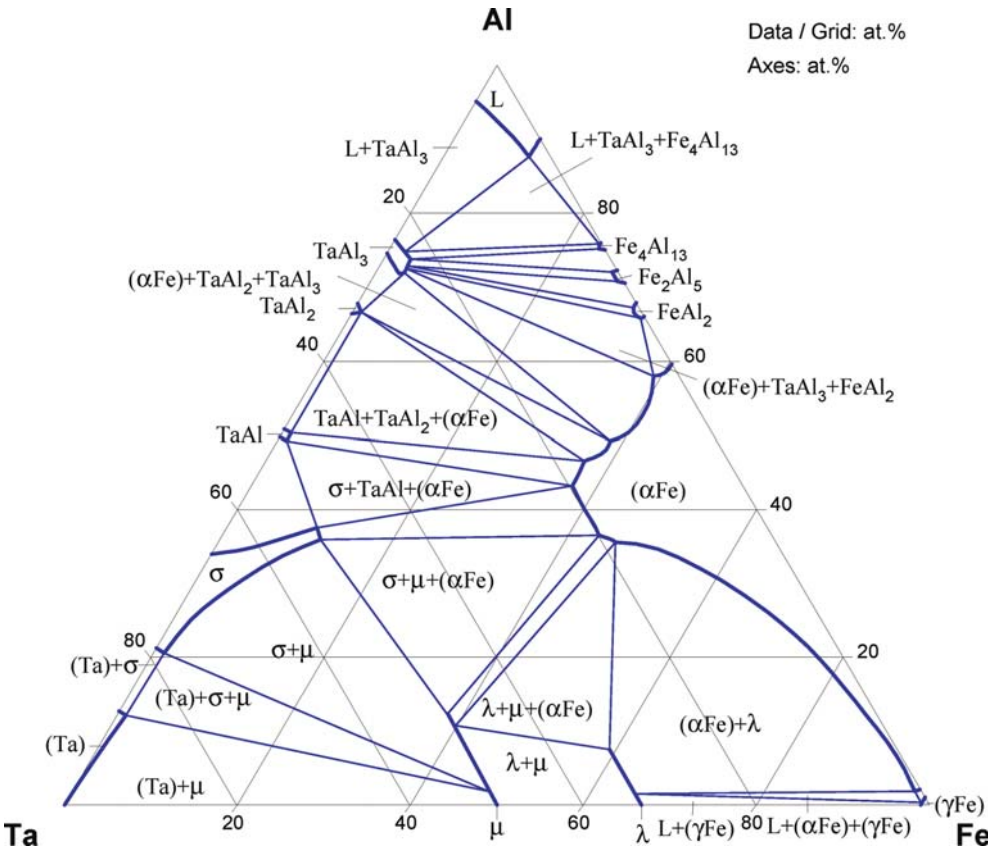

Fig. 6. Al-Fe-Ta. Calculated isothermal section at 1000°C

DOI: 10.1007/978-3-540-69761-9_12

References

[1962Min] Mints, R.S., Samsonova, N.N., Malkov, Yu.S., "The Effects of Elements of Group V in the Periodic System (V,Nb,Ta) on the Properties of Fe_3Al" (in Russian), *Dokl. Akad. Nauk SSSR*, **144**, 1324–1327 (1962) (Experimental, 6)

[1965Gan] Ganglberger, E., Nowotny, H., Benesovsky, F., "Ternary Phases with $MgZn_2$ Structure" (in German), *Monatsh. Chem.*, **96**, 1658–1659 (1965) (Crys. Structure, Experimental, 3)

[1968Hun] Hunt, C.R., Raman, A., "Alloy Chemistry of σ (βU)-Related Phases. I. Extension of μ- and Occurrence of μ′-Phases in the Ternary Systems Nb(Ta)-X-Al (X = Fe, Co, Ni, Cu, Cr, Mo)", *Z. Metallkd.*, **59**, 701–707 (1968) (Experimental, Phase Diagram, Phase Relations, #, *, 14)

[1982Kub] Kubaschewski, O., "Iron-Aluminium" and "Iron-Tantalum" in "*Iron Binary Phase Diagrams*", Springer Verlag, Berlin, 5–9 and 143–146 (1982) (Review, Phase Diagram, #, 26, 14)

[1985Tro] Trojko, R., Blazina, Z., "Metal-Metalloid Exchange in Some Friauf-Laves Phases Containing Two Transition Metals", *J. Less-Common Met.*, **106**, 293–300 (1985) (Crys. Structure, Experimental, 13)

[1988Tsa] Tsai, A.-P., Inoue, A., Masumoto, T., "A New Icosahedral Al-Fe-Ta Alloy Prepared by Rapid Solidification", *Jpn. J. Appl. Phys.*, **27**(1), L5–L8 (1988) (Experimental, 18)

[1989Bla] Blazina, Z., Pavkovic, S., "On Friauf-Laves Phases in the $Ta_{1-x}Al_xT_2$ and $Ta_{1-x}Si_xT_2$ (T = Cr, Mn, Fe, Co, Ni) Systems", *J. Less-Common Met.*, **155**, 247–253 (1985) (Crys. Structure, Experimental, 9)

[1989Sri] Srinivas, V., McHenry, M.E., Dunlap, R.A., "Magnetic Properties of Icosahedral Al-Mo-Fe and Al-Ta-Fe Alloys", *Phys. Rev. B*, **40**(14), 9590–9594 (1989) (Experimental, Magn. Prop., 25)

[1990Kum] Kumar, K.S., "Ternary Intermetallics in Aluminium-Refractory Metal-X Systems (X = V, Cr, Mn, Fe, Co, Ni, Cu, Zn)", *Int. Mater. Rev.*, **35**(6), 293–327 (1990) (Crys. Structure, Phase Diagram, Review, 158)

[1990Sau] Sauthoff, G., "Intermetallic Alloys – Overview on New Materials Developments for Structural Applications in West Germany", *Z. Metallkd.*, **81**(12), 855–861 (1990) (Experimental, Mechan. Prop., 36)

[1991Kau] Kaufman, L., "Calculation of the Multicomponent Tantalum Based Phase Diagrams", *Calphad*, **15**(3), 261–282 (1991) (Calculation, Phase Diagram, 15)

[1992Gho] Ghosh, G., "Aluminium-Iron-Tantalum", MSIT Ternary Evaluation Program, in *MSIT Workplace*, Effenberg, G. (Ed.), MSI, Materials Science International Services GmbH, Stuttgart; Document ID: 10.16122.1.20, (1992) (Crys. Structure, Phase Relations, Phase Diagram, Assessment, 5)

[1992Rag] Raghavan, V., "The Al-Fe-Ta (Aluminium-Iron-Tantalum) System", in "*Phase Diagrams of Ternary Iron Alloys*", Indian Institute of Metals, Calcutta, India, **Part 6A**, 187–190 (1992) (Phase Diagram, Review, 6)

[1993Kel] Kelton, K.F., "Quasicrystals: Structure and Stability", *Int. Mater. Rev.*, **38**(3), 105–137 (1993) (Crys. Structure, Review, 424)

[1995Ant] Anthony, L., Fultz, B., "Effects of Early Transition Metal Solutes on the $D0_3$-$B2$ Critical Temperature of Fe_3Al", *Acta Metall. Mater.*, **43**(10), 3885–3891 (1995) (Experimental, Crys. Structure, *, 35)

[1996Du] Du, Y., Schmid-Fetzer, R., "Thermodynamic Modeling of the Al-Ta System", *J. Phase Equilib.*, **17**, 311–324 (1996) (Phase Diagram, Phase Relations, Thermodyn., Calculation, 55)

[1996Mac] Machon, L., Sauthoff, G., "Deformation Behaviour of Al-Containing $C14$ Laves Phases Alloys", *Intermetallics*, **4**, 469–481 (1996) (Experimental, Phase Relations, 41)

[1997Rev] Reviere, R., Sauthoff, G., Johnson, D.R., Oliver, B.F., "Microstructure of Directionally Solidified Eutectic Based Fe(Al,Ta)/Fe_2Ta(Al) Alloys as a Function of Processing Conditions", *Intermetallics*, **5**(3), 161–172 (1997) (Experimental, Morphology, Phase Diagram, Phase Relations, 10)

DOI: 10.1007/978-3-540-69761-9_12

[1998Kei] Von Keitz, A., Sauthoff, G., Neumann, P., "Laves Phases for High Temperatures-Structure, Stability and Constitution", *Z. Metallkd.*, **89**(12), 803–810 (1998) (Crys. Structure, Experimental, Phase Relations, 20)

[1999Mek] Mekhrabov, A.O., Akdeniz, M.V., "Effect of Ternary Alloying Elements Addition on Atomic Ordering Characteristics of Fe-Al Intermetallics", *Acta Mater.*, **47**(7), 2067–2075 (1999) (Calculation, Theory, Thermodyn., 63)

[2002Boz] Bozzolo, G.H., Noebe, R.D., Amador, C., "Site Occupancy of Ternary Additions to *B*2 Alloys", *Intermetallics*, **10**, 149–159 (2002) (Crys. Structure, Review, 27)

[2005Ris1] Risanti, D.D., Sauthoff, G., "Strengthening of Iron Aluminide Alloys by Atomic Ordering and Laves Phase Precipitation for High-temperature Applications", *Intermetallics*, **13**(12), 1313–1321 (2005) (Crys. Structure, Experimental, Mechan. Prop., Morphology, Phase Diagram, Phase Relations, #, *, 37)

[2005Ris2] Risanti, D.D., Sauthoff, G., "Iron-Aluminium-base Alloys With Strengthening Laves Phase for Structural Applications at High Temperatures", *Mat. Sci. Forum*, **475-479**(1), 865–868 (2005) (Experimental, Mechan. Prop., Morphology, 13)

[2006MSIT] "Al-Fe (Aluminum-Iron)", Diagrams as Published, in *MSIT Workplace*, Effenberg, G. (Ed.), Materials Science International Services, GmbH, Stuttgart; Document ID: 30.10236.1.20, (2006) (Crys. Structure, Phase Diagram, Phase Relations, 11)

[V-C2] Villars, P. and Calvert, L.D., *Pearson's Handbook of Crystallographic Data for Intermetallic Phases*, 2nd edition, ASM, Metals Park, Ohio (1991)

[Mas2] Massalski, T.B. (Ed.), *Binary Alloy Phase Diagrams*, 2nd edition, ASM International, Metals Park, Ohio (1990)

DOI: 10.1007/978-3-540-69761-9_12

Aluminium – Iron – Titanium

Gautam Ghosh

Introduction

The ternary system is of significant interest for design and development of engineering alloys in many diverse applications, such as light structural alloys (both Al based and Ti based) at elevated temperatures, development of ductile intermetallics, Ti rich alloys for surgical implants, grain refinement of Al based alloys, and *C*14-Ti$(Fe_{1-x}Al_x)_2$ and *B*2-$TiFe_{1-x}Al_x$ intermetallics for hydrogen storage. As a result a large number of experimental studies have been carried out to determine the phase equilibria. Earlier investigations are due to [1940Nis, 1954Sto, 1958Bok, 1958Kor, 1963Luz, 1969Vol, 1970Vol, 1971Vol, 1973Mar] and [1981Sei]. [1969Vol] used electrolytic Fe, "iodide" Ti and AV-000 grade Al. The alloys were annealed at 800°C (200-400 h), 700°C (300 h) and 500-600°C (1000 h). After annealing they were water quenched. Thermal analysis and phase analysis by X-ray diffraction and microstructural observation were performed. Volkova *et al*. presented isothermal sections at 1100, 800 and 550°C [1970Vol, 1971Vol, and also several temperature-composition sections [1969Vol]. [1981Sei] used electrolytic Fe, Ti sponge and 99.99% purity Al. First, the Fe-Ti alloys were prepared by electron-beam melting and then the ternary alloys were made in an arc furnace using an argon atmosphere. [1981Sei] presented a liquidus surface, a complete isothermal section at 800°C, and a partial isothermal section at room temperature. A critical assessment of these results along with several amendments of liquidus surface of [1981Sei] were presented by [1987Rag]. [1990Kum] presented only a brief review of the phase equilibria.

[1987Men] studied order-disorder transitions involving (αFe), *B*2-FeAl (α_2) and $D0_3$-Fe_3Al (α_1) phases using five ternary alloys of Fe-(17.3 to 25.2) at.% Al-(4.4 to 5.2) at.% Ti. They carried out the transmission electron microscopic investigations to establish phase relations in the temperature range of 400 to 1000°C. [1989Maz] produced 50 to 100 g ingots of nine ternary alloys in the composition range of Al-(16.6 to 34.1) at.% Ti-(1.6 to 17.8) at.% Fe. The alloys were prepared by arc melting in vacuum. Some alloys were annealed at 1200°C for 500 h in Ar atmosphere, some were annealed subsequently at 800°C for 300 h. It was reported that the O and N impurity levels remained below 500 ppm by mass. [1991Nwo] determined the (αTi) + (βTi) two-phase field at 700 and 800°C by annealing alloys for 10 h at 800°C and 30 h at 700°C. The alloys were prepared using elements of following purity: Ti 99.5%, Al 99.99% and Fe 99.9%. The phases were identified by X-ray diffraction, SEM and TEM and quantitatively analyzed by EDAX. All these results were reviewed by [1992Gho]. [1993Rag] presented an update of phase equilibria based on experimental results published between 1985 and 1992.

In a significant contribution, [1995Pal] determined two complete isothermal sections at 800 and 1000°C. They prepared 59 ternary alloys in a crucible-free levitation furnace and cast into a copper mold. They used elements of following purity: 99.99% Al, 99.97% Fe and 99.77% Ti. The alloys were heat treated at 1000 and 800°C for 100 and 500 h, respectively, followed by quenching in brine solution. In addition, they also performed six diffusion couple experiments at 1000°C.

[1995Yan1] investigated the phase equilibria at 800°C using nine ternary alloys in the composition range of Al-(0.5 to 8) at.% Fe-(25 to 35) at.% Ti. They used elements of purity of 99.999% Al, 99% Fe and 99% Ti. The final heat treatment was at 800°C for 10 days. [1998Ohn] studied the order-disorder transitions in Fe rich alloys, and reported three temperature-composition sections, and two isothermal sections of Fe corner at 800 and 900°C. They prepared 24 ternary alloys and several diffusion couples to study order-disorder transitions, and to determine the phase equilibria. [1999Gor] investigated the phase equilibria in ten ternary alloys that were heat treated at 1000°C for 96 h. Supplementing the results of [1995Pal], [1999Gor] presented an updated isothermal section at 1000°C. [1999Li] studied the effect of 1 at.% Fe on the Ti_3Al-TiAl phase boundaries between 1000 and 1250°C.

The phase equilibria of Ti rich alloys were investigated by [2000Kai1] and [2000Kai2]. [2000Kai1] prepared alloys in the composition range of Ti-(35 to 47) at.% Al-(0.5 to 12) at.% Fe using 99.99% Al, 99.99% Fe and 99.7% Ti. The final heat treatments were at 1000°C for either 168 or 504 h, at 1200°C

DOI: 10.1007/978-3-540-69761-9_13

for 168 h, and at 1300°C for 24 h. [2000Kai2] investigated the order-disorder transitions ($A2 \rightleftharpoons B2$), and also determined tie-line compositions involving (αTi), (βTi) and FeTi phases in Ti rich area at 1000°C. They used ternary alloys in the composition range of Ti-(11 to 27) at.% Al-(3 to 25) at.% Fe. In addition, the tie-line compositions involving the phases present in diffusion couples equilibrated at 1000°C were determined.
[2000Mab] also investigated the phase equilibria of Al rich alloys in the composition range of Al-(2 to 14) at.% Fe-(25 to 40) at.% Ti. They produced samples as sintered compacts and ingots. For sintered compacts the starting powders of 99.9% Al, 99.9% Fe and 99.5% Ti were used, and for ingots elements of purity of 99.99% Al, 99.9% Fe and 99.7% Ti were used. The final heat treatments for the sintered compacts were at 1150°C for 24 h and at 1000°C for 48 h, while the ingots were heat treated at 1150°C for 48 h and at 1000°C for 144 h. [2002Rag] presented a further update of phase equilibria based on the experimental results published between 1981 and 2000.
[2001Pra] reported the phase compositions of eight as-cast ternary alloys. They found that except for two alloys lying in the $Fe_2Ti + L2_1$ field, the phase compositions agree with the previously reported 800°C isothermal section due to Palm *et al.* [1995Pal]. In a more recent significant work, Ducher *et al.* [2003Duc] re-investigated the liquidus surface using 38 alloys selected from those used by Palm *et al.* [1995Pal]. [2003Duc] used DTA, metallography, SEM/EDX and XRD to identify the reactions during solidification. Based on their extensive results, a reaction scheme was proposed. These recent results have also been reviewed [2005Gho, 2005Ste, 2006Pal].
A summary of experimental studies on phase relations is given in Table 1.

Binary Systems

The Al-Fe, Al-Ti and Fe-Ti binary phase diagrams are accepted from [2006MSIT], [2004Sch] and [1982Kub], respectively.
The Al-Fe phase diagram has undergone slight modification due to recently established congruent melting behavior of the Fe_4Al_{13} phase [1986Len]. The Al-Ti binary phase diagram is accepted from the recent review of [2004Sch]. The system is characterized by the presence of five intermediate phases and eight invariant reactions. [2004Sch] accepted the invariant temperatures based on a CALPHAD modeling of the phase equilibria. However, in this assessment the temperature of the peritectoid reaction $TiAl + Ti_2Al_5 \rightleftharpoons\subsetneq TiAl_2$ is taken as 1205°C [1991Mis] rather than 1199°C [2004Sch] for the reasons discussed in "Invariant Equilibria".

Solid Phases

The Fe_3Al (α_1) phase dissolves a significant amount of Ti [1973Mar, 1977Ath]. Besides increasing $D0_3 \rightarrow B2$ transition temperature, the addition of Ti also increases Curie temperature [1994Sel] and lattice parameter of Fe_3Al [1996Pra, 1997Nis2]. The details of substitution of Fe by Ti have been studied using X-ray diffraction, transmission electron microscopy and Mössbauer spectroscopy [1977Ath, 1995Mah]. The Mössbauer spectroscopic data show that Ti replaces Fe at a specific lattice site with 8 nearest Fe atoms rather than a site with 4 Fe and 4 Al nearest atoms [1977Ath, 1995Mah]. This implies that $TiFe_2Al$ is a Heusler phase ($L2_1$) [1985Okp, 1995Mah] and not $D0_3$-$(Fe,Ti)_3Al$.
The FeAl (α_2) phase also dissolves a significant amount of Ti [1995Pal, 1998Ohn, 1999Gor, 2002Aze] leading to an increase in lattice parameter. For example, the lattice parameter of $Ti_xFe_{0.7-x}Al_{0.3}$ can be expressed as:
a (in pm) = 291.0 + 9.2 x; [2002Aze].
The site occupancy of Ti in FeAl (α_2) has been investigated theoretically [1996Fu, 2002Ban, 2002Boz] and experimentally [1993Li, 1994Kon, 1997And, 1998Sun]. [1996Fu] employed FLAPW-LDA (Full Potential Linearized Augmented Plane Wave - Local Density Approximation) method, and calculated the heat of formation associated with substitution of Ti in $B2$-FeAl. Based on the trends of calculated heat of formation associated with the substitution of Ti in Al and Fe sublattices, [1996Fu] concluded that Ti atoms prefer to occupy Al sublattice in both Al rich and Fe rich compositions. [2002Ban] calculated the ordering tie lines at 627°C in $B2$-$Ti_{10}Fe_{50}Al_{40}$ alloy using binary interaction parameters, and reported that about 62% of Ti atoms occupy the Al sublattice while the rest of Ti atoms occupy the Fe sublattice. Using a linear muffin-tin orbital method, [2002Boz] calculated the formation energies associated with dilute additions of

DOI: 10.1007/978-3-540-69761-9_13

Ti in *B*2-FeAl and Al in *B*2-TiFe. They predicted that in the dilute limit, Ti atoms prefer to occupy the Al sublattice in both $Fe_{0.5}(Al,Ti)_{0.5}$ and $(Fe,Ti)_{0.5}Al_{0.5}$. Also, in the dilute limit of Ti in $Fe_{0.5}(Al,Ti)_{0.5}$ the calculated formation energy is predicted to be more negative compared to binary $Fe_{0.5}Al_{0.5}$. On the other hand, it was predicted that in the dilute limit, Al atoms prefer to occupy the Ti sublattice in $Fe_{0.5}(Al,Ti)_{0.5}$ and the Fe sublattice in $(Fe,Al)_{0.5}Ti_{0.5}$.

[1993Li] used Mössbauer spectroscopy to determine the site occupancy of Ti in $Ti_1Fe_{50}Al_{40}$, $Ti_5Fe_{55}Al_{40}$, and $Ti_{10}Fe_{50}Al_{40}$ alloys having *B*2 (α_2) structure. They found that Ti atoms occupy primarily the Fe sublattice.

[1994Kon] employed ALCHEMI (Atom Location by CHanneling Enhanced MIcroanalysis) technique in TEM, and also found that Ti atoms occupy the Fe sublattice in an $Ti_1Fe_{49}Al_{50}$ (α_2) alloy. [1997And] also determined the site occupancy of Ti in $Ti_5Fe_{50}Al_{45}$ and $Ti_3Fe_{52}Al_{45}$ (α_2) alloys by ALCHEMI, and found that about 85% of the Al site is occupied by Ti. The residual Fe site occupancy is attributed to the kinetics of site-equilibrium mechanism.

The Fe_4Al_{13}, Fe_2Al_5 and $FeAl_2$ phases can dissolve up to 6.5, 2.5 and 1.8 at.% Ti, respectively [1995Pal]. At room temperature, Fe_4Al_{13} can dissolve about 2.5 at.% Ti [1981Zhu].

The TiFe (*B*2) phase dissolves a substantial amount of Al [1980Dew, 1981Sei, 1995Pal, 1999Gor]. The maximum solubilities at 800, 900 and 1000°C are 13, 24 and 33 at.% Al, respectively [1995Pal, 1999Gor]. The substitution of Al in TiFe causes a linear increase in lattice parameter [1980Dew, 1995Pal, 1999Lee]. For example, the lattice parameter (*a*) of Ti(Fe,Al) can be expressed as:

a (in pm) = 297.0 + 5.07 (50 – x_{Fe}); [1995Pal],

where x_{Fe} is the Fe content in at.%. The lattice parameter data of [1995Pal] is in good accord with those reported by [1980Dew].

The *C*14 Laves phase $TiFe_2$ also dissolves a substantial amount of Al [1967Mar, 1973Mar, 1974Dwi, 1980Dew, 1995Pal, 1999Gor, 2006Yan]. The data of [1973Mar] show a linear increase of both *a* and *c* lattice contents as Al replaces Fe in $TiFe_2$. However, recent measurements by [1995Pal, 2006Yan] also show a linear increase of the *a* lattice constant but a non-linear increase of the *c* lattice constant of $Ti(Fe,Al)_2$. A least-square fit of experimental data of [2006Yan] gives

a (in pm) = 479.41 + 0.0502 x_{Al}

c (in pm) = 781.97 + 0.0568 x_{Al} – $4.27 \cdot 10^{-4} x_{Al}^2$

where x_{Al} is the Al content in at.%. This gives a minimum in *c/a* around 30 at.% Al [2006Yan].

Among the Al-Ti intermetallics, $TiAl_3$, Ti_2Al_5, $TiAl_2$, TiAl and Ti_3Al can dissolve up to 1.2, 0.8, 2.5, 2.5 and 1.5 at.% Fe at 1000°C, respectively [1995Pal]. [2001Sun] obtained 1.92 at.% Fe in the TiAl phase in a $Ti_{52}Fe_2Al_{46}$ alloy that was heat treated at 900°C for 8 h. [1985Pas] reported 0.5 at.% Fe in TiAl at 550 to 600°C. All these results clearly demonstrate that the solubility of Fe in TiAl increases with temperature. Furthermore, results of ALCHEMI experiments in TEM show that Fe atoms reside primarily on the Al sublattice in TiAl [1999Hao, 2000Yan]. Due to low solubility, the site occupancy of Fe in Ti_3Al could not be determined conclusively [1999Hao].

[2003Duc] observed a phase with composition $Ti_{0.065}Fe_{0.33}Al_{0.605}$, in an as-cast $Ti_{0.077}Fe_{0.314}Al_{0.609}$ alloy, with lattice parameter a = 1268 pm and c = 790 pm. They proposed that it has Al_8Cr_5 type of structure, but not a ternary phase.

Two ternary phases are accepted in this assessment: τ_2 ($TiFeAl_2$) and τ_3 ($Ti_8Fe_3Al_{22}$). The τ_2 phase was first reported by [1967Mar], and subsequently confirmed by [1980Dew] and [1981Sei]. It forms by a peritectic reaction at about 1225°C [2003Duc]. [1973Mar] reported that the homogeneity range of τ_2 at 800°C is from 40 to 50 at.% Al at 24 at.% Fe, and that reported by [1981Sei] is from 53 to 55.5 at.% Al and 21 to 24 at.% Fe. [1980Dew] reported that the homogeneity range of τ_2 at 1000°C is from 28 to 52 at.% Al at 25 at.% Fe. Recent results of [1995Pal] show that the τ_2 phase split into two islands at 1000°C, one with homogeneity range of 30 to 39 at.% Al, and the other with a homogeneity range of 44.5 to 54.5 at.% Al. So far, a two-phase field has not been observed. Also, [1995Pal] reported that the ambient crystal symmetry of τ_2 changes from cubic, when the Ti content is in the range of 30.8 to 50.9 at.%, to tetragonal-τ_2' when the Ti content is less than 24 at.%. [1999Lev] observed both cubic and tetragonal phases in an Al-49.6 at.% Ti-1.9 at.% Fe alloy that was heat treated at 1400 and 1300°C for 40 min and 90 min, respectively, and then either water quenched or furnace cooled. Based on these experiments, [1999Lev] concluded that the tetragonal-τ_2' is a metastable phase, and it forms from Ti(Fe,Al) by a massive transformation. In a similar study, [1999Lev, 2001Tok] characterized the phases present in a Ti-1.9 at.% Fe-46.9 at.% Al alloy that

DOI: 10.1007/978-3-540-69761-9_13

was heat treated at 1200°C for 8 h, and then either water quenched or furnace cooled. They found the cubic-τ_2 ($Ti_{38}Fe_{23}Al_{39}$) in furnace cooled specimen while the tetragonal-τ_2' ($Ti_{52}Fe_{10}Al_{38}$) in water quenched specimen.

In an effort to resolve the differences and the nature of phase transformation involving τ_2 and τ_2', [2003Gry, 2006Gry] carried out systematic studies using both X-ray and neutron diffraction techniques. Specifically, [2006Gry] used two alloys, $Ti_{22}Fe_{23}Al_{55}$ and $Ti_{43}Fe_{24}Al_{33}$, that were annealed at 900°C for 240-670 h, and then water quenched. A careful analysis of X-ray and neutron diffraction data show that $Ti_{22}Fe_{23}Al_{55}$ (τ_2') has a centrosymmetric space group of $Fm\bar{3}m$ (filled variant of Th_6Mn_{23} type) in both as-cast and annealed states, while $Ti_{43}Fe_{24}Al_{33}$ (τ_2) has a non-centrosymmetric space group of $F\bar{4}3m$ [2006Gry]. In the absence of a two-phase field and based on the space group theory arguments, they suggested that the transition from centrosymmetric to non-centrosymmetric space group is possibly a second-order type [2006Gry]. In light of all these results, both τ_2 and τ_2' are accepted to have cubic symmetry.

The τ_3 phase was first reported by [1973Mar], and subsequently confirmed by others [1980Dew, 1981Sei, 1990Nic, 1991Nic]. Besides conventional processing, the τ_3 phase also forms during mechanical alloying of elemental powders [2004Nay]. [1981Sei] designated the composition of τ_3 as $Ti_{24}Fe_9Al_{66}$, while [1989Maz] reported $Ti_{28}Fe_8Al_{64}$. All subsequent investigations also confirmed a homogeneity range [1992Dur1, 1992Win, 1993Nak, 1995Pal, 1995Yan1, 1999Yam, 2000Mab], which increases with temperature. For example, at 800°C the homogeneity range is about 5 at.% Fe [1995Pal, 1995Yan1], and at 1200°C it is about 7 at.% Fe [1989Maz]. Notwithstanding this homogeneity range, both $TiAl_2$ and $TiAl_3$ phases have been observed in τ_3 compositions that are expected to be single phase. For example, [1991Wu] observed both $TiAl_2$ and TiAl in single crystals of $Ti_{27.4}Fe_{5.8}Al_{66.8}$. [1992Mor] also observed $TiAl_2$ in $Ti_{28}Fe_8Al_{64}$ and $Ti_{29}Fe_8Al_{63}$ alloys that were heat treated between 600 and 1150°C. [1994Yan] observed the precipitation of $TiAl_2$ phase in a $Ti_{28}Fe_8Al_{64}$ alloy which corresponds to the geometric centre of τ_3's composition range. The alloy was prepared using 99.999% Al, 99% Fe and 99% Ti, and heat treated at 1200°C for 50 h. Furthermore, [1994Yan] observed three types of $TiAl_2$: $TiAl_2^{I}$ ($ZrGa_2$-type), $TiAl_2^{II}$ ($HfGa_2$-type) and $TiAl_2^{III}$. The latter is similar to the other two, but with different stacking sequence. It is believed to be stabilized by Fe, and has never been observed in binary Al-Ti alloys.

Based on a geometric approach [1991Dur] and an electron-concentration approach [1992Dur2], Durlu *et al.* argued that τ_3 should be considered as $TiAl_2$-based rather than $TiAl_3$-based $L1_2$ phase. Furthermore, [1992Dur2] proposed that Fe should replace Ti in stabilizing $L1_2$ structure. However, an electronic-level ab initio calculations [1990Car, 1991Car] showed that replacement of Al by Fe in $TiAl_3$ energetically favors the cubic $L1_2$ structure over the tetragonal $D0_{22}$ structure. Indeed, ALCHEMI results show that in a $Ti_{23.1}Fe_{11.9}Al_{63.5}$ alloy about 77% of Fe atoms reside on the Al sublattice and 23% of Fe atoms reside on the Ti sublattice [1992Ma]. X-ray diffraction has been used to determine the long-range order parameter of τ_3 [1992Kog, 1992Mor, 1992Win]. In a $Ti_{27.7}Fe_{9.7}Al_{62.6}$ alloy annealed at 800°C, the long-range order parameter lies between 0.45 and 0.53 [1992Win].

[1973Mar] also reported another compound $Ti_6Fe_{25}Al_{69}$, but later at the same composition [1981Sei] found a two-phase mixture of Fe_2Al_5 and τ_3. On the other hand, [1995Pal] reported that this composition represents a ternary extension of the binary phase Fe_4Al_{13}. [1981Sei] reported the ternary phase τ_1 ($TiFe_2Al$) having cubic structure with lattice parameter a = 414.0 pm; however, a subsequent investigation failed to confirm the existence of this phase [1995Pal]. A cubic phase at $TiFe_2Al$ (Heusler-type) also reported by [1983Bus], but with lattice parameter very different from [1981Sei].

The details of the crystal structures and lattice parameters of all the unary, binary and ternary solid phases are listed in Table 2.

Order-Disorder Phase Transitions

The effect of Ti additions on the order-disorder transition temperatures of Fe_3Al (α_1) has been studied extensively [1985Men, 1987Die, 1987For, 1987Men, 1994Sel, 1995Ant, 1996Pra, 1997Nis1, 1997Nis2, 1998Ohn, 2003Ste] employing various experimental techniques, such as X-ray diffraction, electrical resistivity, hardness, dilatometry, transmission electron microscopy and calorimetry. All studies confirm an increase in $D0_3 \rightarrow B2$ temperature in $(Ti_xFe_{1-x})_3Al$ alloys. For example, in $Ti_xFe_{74-x}Al_{26}$ alloys, the transition temperature increases linearly from 550°C at $Fe_{74}Al_{26}$ to 775°C at $Ti_4Fe_{70}Al_{26}$ [1995Ant]. However, a

DOI: 10.1007/978-3-540-69761-9_13

deviation from the linear behavior has been observed in $(Ti_xFe_{1-x})_3Al$ alloys where the reported transition temperatures are 783, 951 and 1037°C at $x = 0.05$, $x = 0.1$, and $x = 0.15$, respectively [1997Nis2]. Positron annihilation study [2003Pan] shows that the addition of Ti in $Fe_{70}Al_{30}$ alloy accelerates the $B2 \rightarrow D0_3$ kinetics.

Figures 1 and 2 show the vertical sections at constant Al content of 25 and 23 at.%, respectively [1998Ohn]. In addition to (αFe) + α_2 phase field as in the case of Al-Fe system, the presence of $\alpha_1 + \alpha_2$ phase field in the ternary system may be seen in Figs. 1 and 2. As discussed by [1998Ohn], the topology of the phase boundaries involving ordered (α_1, α_2) and disordered phases (αFe) are consistent with the general features of phase diagrams associated with multicritical points [1982All].

An addition of about 5 at.% Ti is reported to shift the (αFe) + α_1 phase field to higher temperature and to lower Al contents compared to Al-Fe alloys [1987Men]. [1998Ohn] also re-investigated the vertical of Fe-5 at.% Ti-*x*Al, and found good agreement with the results of [1987Men]. Their results are summarized in Fig. 3.

The effects of substitution of Fe by Ti in Fe_3Al (α_1) and the substitution of Al by Ti in FeAl (α_2) on the order-disorder transitions are summarized in Fig. 4. This conjoined vertical section was originally published by [1998Ohn], but the Fe_3Al-side has been significantly modified to make it consistent with the Figs. 1 and 3. It is seen that $TiFe_2Al$ ($L2_1$) undergoes a second-order phase transition to *B*2 at about 1220°C. However, the ideal transition temperature is predicted to be about 500°C higher [2002Ish]. In Figs. 1, 2 and 4, minor adjustments have been made to comply with the accepted Al-Fe phase diagram.

[1998Ohn] carried out theoretical studies of order-disorder phase transitions and the bcc phase equilibria, in the composition range Fe-FeAl-TiFe, employing cluster variation method using the irregular tetrahedron method. They considered first- and second-nearest neighbor as well as tetrahedron interactions. They found an excellent agreement between the calculated and experimental results. A theoretical analysis of order-disorder (*A*2/*B*2) transition temperature and short-range ordering characteristics of $Fe_{0.5}(Al_{1-x}Ti_x)_{0.5}$ alloys was also carried out by [1999Mek]. They applied statistico-thermodynamical theory of ordering within quasi-chemical framework, and found that Ti preferentially substitutes Fe sublattice sites in $Fe_{0.5}(Al_{1-x}Ti_x)_{0.5}$, with $0 \le x \le 0.01$. Also, based on the calculated partial ordering energies they predicted an increase in $B2 \rightarrow A2$ temperature for $Fe_{0.5}(Al_{0.99}Ti_{0.01})_{0.5}$ alloy, and a decrease in alloys containing less than 0.5 at.% Ti. However, there is no experimental data to verify such theoretical predictions. The transient states associated with *A*2/*B*2 transition have been discussed elsewhere [2000Ni].

The additions of Fe and Al in (βTi) lead to *B*2 ordering [2000Kai2], and it is claimed to be a second-order phase transition. Accordingly, [2000Kai2] employed Bragg-Williams-Gorsky approximation to model *A*2/*B*2 transition in Ti rich ternary alloys. By extrapolating the ternary results to Al-Ti system, they predicted that a Ti-23.5 at.% Al alloys undergoes metastable *A*2/*B*2 transition at 1000°C.

[1987Kal] performed theoretical studies of the effect of Fe on the $D0_{19}$-type ordering of Ti_3Al. They found that Fe increases the ordering temperature.

Invariant Equilibria

Figure 5 shows the reaction scheme, mostly adopted from the works of [1995Pal] and [2003Duc]. No distinction is made between disordered (αFe) and its ordered forms *B*2 and $D0_3$; similarly, no distinction is made between disordered (βTi) and ordered (βTi); τ_2 is the Ti rich variant and τ_2' is the Al rich variant. The study of [1995Pal] has contributed significantly to our knowledge of solid-solid phase equilibria. The systematic study of [2003Duc] by DTA followed by careful characterization of as-solidified microstructures have led to a number of changes in the reaction scheme compared to that first proposed by [1981Sei]. However, the reaction scheme proposed by [2003Duc] suffers from at least four drawbacks, which have been rectified in this assessment.

First, [2003Duc] did not consider the primary crystallization of Ti_2Al_5. To account for this, we have introduced two ternary invariant reactions, P_1 ($L + TiAl + Ti_2Al_5 \rightleftharpoons \tau_3$) and U_1 ($L + Ti_2Al_5 \rightleftharpoons TiAl_3 + \tau_3$), tentatively occurring around 1380 and 1370°C, respectively. Second, [2003Duc] considered four binary invariant reactions, labelled c_1, pd_1, pd_2 and pd_3, originating from Al-Ti system that are incompatible with the presently accepted Al-Ti phase diagram. Accordingly, these and the associated ternary invariant reactions are not considered in Fig. 5. Third, [2003Duc] proposed the invariant reaction U_6 around 1150°C:

DOI: 10.1007/978-3-540-69761-9_13

(αTi) + (βTi) $\rightleftharpoons$ Ti_3Al + TiAl. However, this is inconsistent with the observation of the three-phase field (αTi) + (βTi) + Ti_3Al in 1100, 1000, 900 and 800°C isothermal sections [1995Pal, 1999Gor]. To be consistent with these experimental observations, we have rewritten the invariant reaction as (αTi) + TiAl $\rightleftharpoons$ (βTi) + Ti_3Al. In addition, two more corrections in the reaction scheme of [2003Duc] are made in this assessment. The monovariant and invariant equilibria E_3 and U_{10} of [2003Duc], respectively, are correctly written as L $\rightleftharpoons$ Fe_4Al_{13}+τ_3 and L+τ_3 $\rightleftharpoons$ Fe_4Al_{13}+τ_2'. Fourth, [2003Duc] proposed the invariant reaction U_{20} around 900°C: TiAl+Fe_2Ti $\rightleftharpoons$ τ_2'+τ_2. Once again, the consequences of this reaction contradict the experimental observations. For example, the τ_2 phase splits into two islands, τ_2 and τ_2' above 1000°C [1995Pal]. A further serious drawback is that none of the experimental isothermal sections at 1000, 900 and 800°C shows τ_2'+τ_2+Fe_2Ti and/or τ_2'+τ_2+TiAl phase fields. Therefore, this invariant reaction is not considered in Fig. 5. [2002Rag] proposed a reaction scheme in which the invariant reaction L+Ti_2Al_5 $\rightleftharpoons$ TiAl+$TiAl_3$ (U_2 in [2002Rag]) takes place around 1340°C, and this gives rise to the three-phase field Ti_2Al_5+TiAl+$TiAl_3$ that persists until about 1200°C. However, in the presence of ternary phase τ_3, in the vicinity of $TiAl_2$ and $TiAl_3$, the existence of Ti_2Al_5+TiAl+$TiAl_3$ phase field is very unlikely. Ducher *et al.* [2003Duc] have discussed other major differences between their reaction scheme and that proposed by [2002Rag].
[1989Maz] observed $TiAl_2$ phase in ternary alloys heat treated at 1200°C. Accordingly, three-phase fields such as $TiAl_3$+$TiAl_2$+τ_3, $TiAl_2$+TiAl+τ_3 are expected at this temperature as they have been observed at 1150°C [2000Mab]. To account for these three-phase fields at 1200°C, the binary invariant reaction TiAl + Ti_2Al_5 $\rightleftharpoons$ $TiAl_2$ is considered to take place at 1205°C [1991Mis] instead of 1199°C [2004Sch]. The proposed reaction scheme in Fig. 5 is consistent with the observed phase fields in 1300 [2000Kai1], 1200 [2000Kai1], 1150 [2000Mab], 1100 [1970Vol], 1000 [1995Pal, 2000Mab], 900 [1999Gor] and 800°C [1970Vol, 1973Mar, 1995Pal] isothermal sections, and also the vertical sections reported by other investigators [1969Vol, 1973Vol, 1987Men, 1998Ohn].

Liquidus Surface

[1940Nis] and [1958Bok] reported the liquidus surface of Al corner only. A comprehensive report of the liquidus surface was first given by [1981Sei], and subsequently modified by [2003Duc]. Figure 6 shows the liquidus surface and the melting grooves separating 13 different areas of primary crystallization. To incorporate the primary crystallization of Ti_2Al_5, a slight modification has been made. The doubtful regions of the liquidus surface are shown by dotted lines. Using the melting temperature data of [2003Duc], approximate isotherms at 100°C intervals from 1600 to 1000°C are also shown in Fig. 6.

Isothermal Sections

The early works of [1940Nis, 1954Sto] and [1958Bok] were focused on to the Al corner. [1958Bok] reported two isotherms at 640 and 600°C with up to 2.2 at.% Fe and 1.1 at.% Ti. [1958Kor] reported the isothermal sections at 1100, 1000, 800 and 550°C with up to 30 mass% (Fe+Al). Recent significant results are the following: (i) the complete isothermal sections at 1000, 900 and 800°C [1995Pal, 1999Gor], (ii) isothermal sections of the Al corner at 1150 [2000Mab], 1000 [2000Mab] and 800°C [1995Yan1], (iii) isothermal sections of Fe corner at 900 and 800°C [1998Ohn], and (iv) isothermal sections of the Ti corner at 1300 and 1200°C [2000Kai1].
Figures 7 and 8 show the isothermal sections of the Ti corner depicting phase equilibria involving (αTi), (βTi) and TiAl at 1300 and 1200°C. The phase equilibria of the Al corner at 1200 [1989Maz], and 1150°C [2000Mab] are shown in Figs. 9 and 10, respectively. The original phase diagram reported by [2000Mab] had to be modified to comply with the Al-Fe and Al-Ti binary phase diagrams. In particular, the liquid phase should be present in the Al rich side at 1150°C, but this was not considered by [2000Mab]. The phase boundaries involving the liquid phase are shown dotted as their exact locations are not known.
Figure 11 shows a partial isothermal section in the region Ti-TiAl-TiFe at 1100°C, based on the work of [1970Vol]. Figures 12, 13 and 14 show complete isothermal sections at 1000, 900 and 800°C adopted from the works of [1995Pal], [1999Gor] and [2000Kai2]. It has been proposed that (βTi) in Al-Ti system

DOI: 10.1007/978-3-540-69761-9_13

undergoes a second-order transition to form *B*2 structure [2000Ohn], therefore a similar behavior is expected in ternary alloys as well. [2000Kai2] established the phase boundaries at 1000°C associated with the second-order transition in Ti rich alloys. Accordingly, the (βTi) field in Fig. 13 is divided into *A*2 and *B*2 regions by a second-order line. Figure 15 shows the isothermal section at 550°C after [1970Vol] in the region of Ti-TiAl-TiFe. Below 550°C, the phase fields remain unchanged down to room temperature as has been confirmed by [1981Sei]. Several minor adjustments have been made in the isothermal sections to comply with the accepted binary phase diagrams.

Temperature – Composition Sections

[1969Vol] determined three vertical sections at constant Al/Fe mass ratios 3:1, 1:1 and 1:3 and (Al+Fe) was varied from 0 to 30 mass%. [1973Vol] determined four vertical sections of the Ti rich alloys at 5, 10, 12 and 16 mass% Al. [1969Vol] reported three vertical sections in the Ti corner at constant Al/Fe ratios of 3:1, 1:1, and 1:3 with a (Al+Fe) content up to 30 mass%, and [1991Nwo] gave the β transus and α solubility for sections with 2 and 4 mass% Al up to 16 mass% Fe.

Thermodynamics

[1994Bro] measured the heat content of a few Ti rich alloys using a high-temperature Calvet calorimeter.
[2006Yan] measured the partial enthalpy of dissolution of TiFeAl in liquid Al at 1136°C using isoperibolic drop calorimetry. The measure value is reported to be –0.66 ± 1.14 kJ·mol^{-1} of atom. This result along with the knowledge of enthalpy of dissolution pure elements in liquid Al, [2006Yan] reported that the standard heat of formation of TiFeAl is –31.38 ± 1.47 kJ·mol^{-1} of atom. [2006Yan] also reported the results of ab initio (using Projector-Agmented-Wave pseudopotentials) calculation of heat of formation of quasi-binary alloys $TiFe_2$-$TiAl_2$ with *C*14 structure using a supercell method. Both spin-polarized and non-spinpolarized calculations were performed. The spin-polarized state was predicted to be more stable. The calculated heat of formation of TiFeAl was reported to be –32.6 and –38.7 kJ·mol^{-1} of atom for the non-spinpolarized and spin-polarized state, respectively. The former value agrees very well with their calorimetric value of –31.38 ± 1.47 kJ·mol^{-1} of atom.
[1990Car] studied the effect of Fe on the relative stability of cubic $L1_2$ and tetragonal $D0_{22}$ structures of $TiAl_3$ phase using *ab initio* (Augmented-Spherical-Wave method) electronic band structure calculations. They found that 4.5 at.% Fe is sufficient to stabilize the $L1_2$ structure which is in reasonable agreement with the experimental homogeneity range of τ_3. Using FLAPW method, [2003Kel] reported that the formation energy of $L2_1$-$TiFe_2Al$ is –47.952 kJ·mol^{-1} of atom.
[1979Dew, 1979Kau1] and [1979Kau2] calculated the isothermal section at 1000°C. However, they did not consider the ternary phases, because the Gibbs energies of formation of these phases are not known. The calculated ternary (αFe) / (αFe) + (γFe) and (αFe) + (γFe) / (γFe) phase boundaries have also been reported [1986Gho, 1988Kum].

Notes on Materials Properties and Applications

A summary of experimental investigation of properties is given in Table 3. [1983Bus] reported the magneto-optical Kerr rotation effect of the Heusler phase $TiFe_2Al$. [1994Sel] studied the magnetic and electrical properties of $Fe_{0.73}Al_{0.27-x}Ti_x$ ($0 < x < 0.16$) alloys. [1979Sup] studied the magnetic susceptibility of the τ_2 phase.
The magnetic properties of *C*14-$Ti(Fe_{1-x}Al_x)_2$ alloys were investigated using magnetization and NMR measurements [1998Yam]. It was found that antiferromagnetism in $TiFe_2$ is suppressed by the Al substitution for $x < 0.1$, while ferromagnetism appears for $0.1 < x < 0.5$. Neutron diffraction study of $Ti_5Fe_{70}Al_{25}$ ($D0_3$) showed that the magnetic moment of Fe atom at α_1 and α_2 sites is 1.49 μ_B while at β site is 2.10 μ_B [1998Sun].
[2003Ter] determined the diffusion coefficient of ^{59}Fe in single crystal γ-TiAl in directions parallel and perpendicular to [001]. They observed an anisotropy in ^{59}Fe diffusion coefficient which is in contrast with the self-diffusion of ^{44}Ti, and suggested that the anisotropy is related to the site occupancy of Fe in γ-TiAl.

DOI: 10.1007/978-3-540-69761-9_13

[2005Gol] studied ^{59}Fe radiotracer diffusion in $Fe_{74}Al_{26}$, $Ti_2Fe_{72}Al_{26}$ and $Ti_4Fe_{70}Al_{26}$ alloys in the temperature range of 675-849°C. The results showed that radiotracer diffusion proceeds with similar rates in all three alloys, suggesting that minor effect of the alloying elements on the vacancy concentration in these alloys.
[1999Lee] studied the hydrogen absorption-desorption behavior of $TiFe_{1-x}Al_x$ alloys at 50°C. Addition of Al causes an increase in lattice parameter of TiFe, and also inhibits the formation of γ-hydride. The latter was attributed to different sizes of octahedral sites, and preferential site occupation of hydrogen atoms. [2001Ish] also studied hydrogen absorption-desorption of $Ti_{75-x}Fe_xAl_{25}$ ($0 \le x \le 25$) alloys. At $x = 15$, the desorption temperature is about 510°C which is about the same as binary Ti_3Al; however, the hydrogen absorption is significantly reduced.
[2004Her, 2005Pal] have discussed the strengthening mechanisms in Al-Fe based alloys, such as solid solution, ordering, and precipitation by incoherent ($C14$ Laves phase) or coherent ($B2$ or $L2_1$) particles. Mechanical properties of Fe_3Al based alloys containing Ti have been investigated by several authors [1996Mac, 1996Pra, 1997Nis2, 2000Sha, 2000Sun, 2000Zhu, 2001Pra, 2001Zhu, 2003Ino]. The hardness, density, temperature dependence of Young's modulus and yield stress, and creep properties of $Ti_{33.1}Fe_{33.9}Al_{33}$ were reported by [1996Mac]. [2000Sha] demonstrated superplastic deformation of Fe-28 at.% Al-2 at.% Ti and Fe-28 at.% Al-4 at.% Ti alloys in the temperature range of 600 to 750°C. The compressive creep behavior, in the temperature range of 600 to 800°C, of Fe rich two- and three-phase alloys is reported to exhibit power-law behavior with the exponent varying from 3 to 6, and the activation energy varying from 400 to 600 $kJ \cdot mol^{-1}$ [2001Pra]. The order-disorder transitions in Al-Fe and Al-Fe-Ti alloys lead to non-monotonic behavior of temperature-dependent mechanical properties, which have been discussed in detail by [1997Nis2, 2000Zhu, 2001Zhu, 2003Ste].
Rapid solidification of Al rich alloys gives fine scale dispersion of crystalline [2002Su], quasi-crystalline [2003Ino] and amorphous [2003Ino] particles in (Al) matrix. Addition of Ti in Fe_3Al lowers the wear rate and slightly decreases the coefficient of friction [2004Gua].
The mechanical properties of the ternary phase τ_3 have been studied extensively. [1991Nic] reported the hardness and Young's modulus of τ_3 at $Ti_8Fe_3Al_{22}$. [1991Wu] reported the deformation behavior of single crystal $Ti_{27.4}Fe_{5.8}Al_{66.8}$ (τ_3) as a function orientation and temperature dependence of yield stress of up to 1200°C. The compressive yield stress as a function of temperature has been reported by [1991Ino] for τ_3 at $Ti_{25}Fe_{7.5}Al_{67.5}$ and by [1991Kum] for τ_3 at $Ti_8Fe_3Al_{22}$. The hardness and cracking load of $Ti_{28}Fe_8Al_{64}$ and $Ti_{29}Fe_8Al_{63}$ alloys were reported by [1992Mor]. [1993Win] determined the temperature dependence of yield stress of $Ti_{27.7}Fe_{9.7}Al_{62.6}$ alloy in the range of –200°C to 900°C. The ambient yield and fracture properties of $Ti_{30}Fe_4Al_{66}$ and $Ti_{26}Fe_8Al_{66}$ were reported by [2002Bra].
[2004Pal] reported mechanical properties (compressive yield strength (0.2%) and creep) and oxidation behavior of Fe-(10-43.5) at.% Al-(10-33) at.% Ti alloys in the temperature range of 20 to 1100°C. The microstructure of these alloys after heat treatment at 800, 900 and 1000°C were either single phase ($L2_1$ or $C14$) or two-phase ($L2_1$ + $C14$ or $B2$ + τ_2 ($Mn_{23}Th_6$)). The ductile to brittle transition temperature (DBTT) falls between 675 and 900°C. Oxidation behavior of some alloys at 900C exhibits parabolic behavior.
A Ti-5 mass% Al-2.5 mass% Fe is reported to be biocompatible, thus, a candidate implant material for hip prothesis [1986Zwi]. This alloy, with (αTi)+(βTi) microstructure, exhibits superplasticity at 850°C. Furthermore, powder metallurgy processing of this alloy reduces the Young's modulus from about 111 GPa to 10 GPa which is very close to that of bone (5 to 9 GPa) [1986Zwi]. The stress-induced $\alpha \rightarrow \beta$ transformation and associated superplasticity in the temperature range of 777 to 927°C in a Ti-5.5 mass% Al-1 mass% Fe alloy has been discussed by [2000Koi].

Miscellaneous

The β transus temperature increases with increasing Al content [1991Nwo]. [1973Kol] investigated the solubility of Ti in liquid (Al) in the temperature range of 700° to 850°C for Al - 0.7 mass% Ti and Al - 0.46 mass% Fe - 0.7 mass% Ti alloys. They found that the presence of Fe up to 0.5 mass% does not affect the solubility of Ti in (Al) in the above temperature range.

DOI: 10.1007/978-3-540-69761-9_13

[1998Akd] proposed that the value of activity coefficient of Al in α-(Fe,Al,Ti) alloys has a strong influence on the formation and growth kinetics of interfacial diffusion layer.
[1998Leo] synthesized nanocrystalline single-phase alloys of different structures in $Ti_xFe_{50-x}Al_{50}$ ($10 \le x \le 40$) by mechanical alloying. Along the composition $Ti_{50}Al_{50}$-$Ti_{50}Fe_{50}$, they observed a number of phase transformations during mechanical alloying in the sequence $A3$ (hcp) → $C14$ (hcp) → $D8_a$ (fcc) → $B2$(bcc) → $A2$ (bcc). During continuous heating, they also found that the nanocrystalline state is preserved until about 500°C.
[2000Izu] studied the sulfidation of TiAl-2 at.% Fe alloy at 900°C using a gas mixture of H_2-H_2S. The multilayer sulfide-scale was reported to consist of Ti- and Al-sulfides. They discussed the results in terms of diffusion paths.

Table 1. Investigations of the Al-Fe-Ti Phase Relations, Structures and Thermodynamics

Reference	Method/Experimental Technique	Temperature/Composition/ Phase Range Studied
[1940Nis]	Metallography, thermal analysis	Al rich alloys; liquidus surface
[1958Bok]	Metallography, thermal analysis	Al rich alloys; liquidus surface
[1958Kor]	Metallography, XRD	About 30 Ti rich alloys; 550, 800, 1000, and 1100°C
[1970Vol]	Metallography, XRD	About 80 Ti rich 80 alloys; 550, 800, and 1100°C
[1971Vol]	Metallography, XRD	About 75 Ti rich alloys; 550°C
[1973Mar]	Metallography, XRD	About 100 alloys covering the entire composition range; 800°C
[1980Dew]	EPMA, metallography, XRD	About 25 FeTi based alloys; 1000°C
[1981Sei]	Metallography, thermal analysis, XRD	About 65 Ti rich alloys; liquidus surface and 800°C
[1985Men]	TEM	$Fe_{0.75-x}Ti_xAl_{0.25}$ with $0 \le x \le 0.05$; $D0_3 \rightleftharpoons B2$ order-disorder transition
[1987Die]	TEM	$Fe_{0.699}Ti_{0.043}Al_{0.258}$; $D0_3 \rightleftharpoons B2$ order-disorder transition
[1987For]	High-temperature XRD	Fe rich alloys.; $D0_3 \rightleftharpoons B2$ order-disorder transition
[1989Maz]	EPMA, metallography, SEM, TEM, XRD	About 10 Al rich alloys; phase equilibria involving τ_3 phase at 1200°C
[1991Nwo]	EPMA, metallography, SEM, TEM	7 Ti rich alloys; phase equilibria involving (αTi) and (βTi) phases at 700 and 800°C
[1995Ant]	DSC, XRD	$Fe_{0.74-x}Ti_xAl_{0.26}$ with $0 \le x \le 0.04$; $D0_3 \rightleftharpoons B2$ order-disorder transition
[1995Pal]	EPMA, metallography, SEM, XRD	About 65 ternary alloys; full isothermal sections at 800 and 1000°C
[1995Yan1]	EPMA, SEM, TEM	12 Al rich alloys; 800°C
[1997Nis2]	Hardness, XRD	$Fe_{0.75-x}Ti_xAl_{0.25}$ with $0 \le x \le 0.15$; $D0_3 \rightleftharpoons B2$ order-disorder transition

(*continued*)

DOI: 10.1007/978-3-540-69761-9_13

Reference	Method/Experimental Technique	Temperature/Composition/ Phase Range Studied
[1998Ohn]	DSC, EPPA, SEM, TEM	Fe rich alloys, diffusion couples; vertical section involving order and disordered phases
[1998Sun]	SEM, TEM, neutron diffraction, XRD	$Fe_{0.70}Ti_{0.05}Al_{0.25}$; $D0_3 \rightleftharpoons B2$ order-disorder transition
[1999Gor]	EPMA, metallography, XRD	10 ternary alloys; 1000°C
[2000Hao]	TEM, XRD	13 ternary alloys; phase relations involving Ti_3Al and TiAl at 900°C
[2000Kai1]	EPMA, metallography	5 Ti rich alloys; 1000, 1200 and 1300°C
[2000Kai2]	EPMA, metallography, TEM	14 Ti rich alloys and diffusion couples; 1000°C
[2000Mab]	EPMA, metallography, SEM, TEM, XRD	About 35 Al rich alloys; phase equilibria involving τ_3 phase at 1000 and 1150°C
[2001Tok]	SEM, TEM, XRD	$Ti_{48.5}Fe_{1.9}Al_{49.6}$; 700-1300°C
[2006Gry]	Neutron diffraction and XRD	$Ti_{22}Fe_{23}Al_{55}$ and $Ti_{43}Fe_{24}Al_{33}$; 900°C

Table 2. Crystallographic Data of Solid Phases

Phase/ Temperature Range [°C]	Pearson Symbol/ Space Group/ Prototype	Lattice Parameters [pm]	Comments/References
(Al) < 660.452	*cF*4 $Fm\bar{3}m$ Cu	a = 404.96	at 25°C [Mas2]
(αδFe) (αFe)(r) ≤ 912	*cI*2 $Im\bar{3}m$ W	a = 286.65	pure Fe at 25°C [Mas2]
(δFe)(h_2) 1538 - 1394		a = 293.15	pure Fe at 1480°C [Mas2]
(γFe)(h_1) 1394 - 912	*cF*4 $Fm\bar{3}m$ Cu	a = 364.67	pure Fe at 915°C [Mas2]
(βTi)(h) 1670 - 882	*cI*2 $Im\bar{3}m$ W	a = 330.65	[Mas2]
(αTi)(r) < 882	*hP*2 $P6_3/mmc$ Mg	a = 295.06 c = 468.25	pure Ti at 25°C [Mas2]

(*continued*)

DOI: 10.1007/978-3-540-69761-9_13

Phase/ Temperature Range [°C]	Pearson Symbol/ Space Group/ Prototype	Lattice Parameters [pm]	Comments/References
$TiAl_3$ ≤ 1393	*tI*8 *I*4/*mmm* $TiAl_3$	*a* = 384.9 *c* = 860.9	[2004Sch]
		a = 384.8 *c* = 859.6	[2000Mab], at Al-25 at.% Ti
		a = 384.7 *c* = 860.2	[1995Pal], contains 1.2 at.% Fe
Ti_2Al_5 1416 - 990	*tP*28 *P*4/*mmm* Ti_2Al_5	*a* = 390.53 *c* = 2919.63	[2004Sch]
		a = 387.5 *c* = 3348.4	[1995Pal]
		a = 392.0 *c* = 2919.4	[2000Mab], Al-28.5 at.% Ti. Heat treated at 1150°C for 24 h followed by water quench
$TiAl_2$ ≤ 1205	*tI*24 $I4_1/amd$ $HfGa_2$	*a* = 397.0 *c* = 2497.0	[2004Sch]
		a = 397.1 *c* = 2432.0	[2000Mab], at Al-35 at.% Ti. Heat treated at 1000°C for 48 h followed by water quench. Single phase alloy.
TiAl ≤ 1463	*tP*4 *P*4/*mmm* AuCu	*a* = 400.0 *c* = 407.5	[2004Sch], at 50 at.% Ti. Solid solubility ranges from 33.5 to 53.3 at.% Ti [2004Sch].
		a = 398.4 *c* = 406.0	[2004Sch], at 38 at.% Ti.
		a = 399.5 *c* = 408.0	[2000Mab], at Al-47 at.% Ti. Heat treated at 1000C for 48 h followed by water quench
		a = 399.6 *c* = 407.7	[1999Gor], at $Ti_{50.4}Fe_{1.71}Al_{47.9}$
		a = 400.7 *c* = 404.9	[1999Gor], at $Ti_{51.8}Fe_{2.2}Al_{46}$
		a = 400.5 *c* = 404.7	[1999Gor], at $Ti_{53.1}Fe_{1.3}Al_{45.6}$
Ti_3Al ≤ 1164	*hP*8 $P6_3/mmc$ Ni_3Sn	*a* = 580.6 *c* = 465.5	[2004Sch], at 78 at.% Ti. Solid solubility ranges from 61.8 to 80 at.% Ti [2004Sch].
		a = 574.6 *c* = 462.4	[2004Sch], at 62 at.% Ti.
		a = 576.1 *c* = 462.4	[1999Gor], at $Ti_{62.8}Fe_{0.93}Al_{36.3}$
α_1, Fe_3Al ≤ 552.5	*cF*16 $Fm\bar{3}m$ BiF_3	*a* = 578.86 to 579.3	[2006MSIT], solid solubility ranges from 22.5 to 36.5 at.% Al. Labelled as $D0_3$ ($L2_1$) in isothermal sections.

(*continued*)

DOI: 10.1007/978-3-540-69761-9_13

Phase/ Temperature Range [°C]	Pearson Symbol/ Space Group/ Prototype	Lattice Parameters [pm]	Comments/References
		a = 579.82	[1997Nis1, at $(Fe_{0.95}Ti_{0.05})_3Al$
		a = 580.59	[1997Nis1, at $(Fe_{0.90}Ti_{0.10})_3Al$
		a = 581.34	[1997Nis1, at $(Fe_{0.85}Ti_{0.15})_3Al$
		a = 582.35	[1997Nis1, at $(Fe_{0.80}Ti_{0.20})_3Al$
		a = 583.80	[1997Nis1, at $(Fe_{0.75}Ti_{0.25})_3Al$
		a = 581.71	[1998Sun], at $(Fe_{0.933}Ti_{0.067})_3Al$
		a = 579.75	[2001Zhu], at $Fe_{71.25}Ti_{3.75}Al_{25}$
		a = 580.64	[2001Zhu], at $Fe_{67.5}Ti_{7.5}Al_{25}$
		a = 581.46	[2001Zhu], at $Fe_{63.75}Ti_{11.25}Al_{25}$
		a = 582.42	[2001Zhu], at $Fe_{60}Ti_{15}Al_{25}$
		a = 583.91	[2001Zhu], at $Fe_{56.2}Ti_{18.8}Al_{25}$
α_2, FeAl ≤ 1310	*cP*2 $Pm\bar{3}m$ CsCl	a = 289.76 to 290.78	[2006MSIT], at room temperature solid solubility ranges from 22.0 to 54.5 at.% Al. Labelled as *B*2 in isothermal sections.
		a = 318.5	[1999Gor], at $Al_{33.5}Fe_{5.6}Ti_{60.9}$
		a = 318.5	[1999Gor], at $Al_{33.1}Fe_{9.5}Ti_{57.4}$
ε, Fe_2Al_3 1232 - 1102	*cI*16?	a = 598.0	[2006MSIT], solid solubility ranges from 54.5 to 62.5 at.% Al
$FeAl_2$ ≤ 1156	*aP*18 *P*1 $FeAl_2$	a = 487.8 b = 646.1 c = 880.0 α = 91.75° β = 73.27° γ = 96.89°	[2006MSIT], at 66.9 at.% Al solid solubility ranges from 65.5 to 67.0 at.% Al
		a = 487.2 b = 645.9 c = 879.4 α = 91.76° β = 73.35 γ = 96.89°	[1995Pal, contains about 1.8 at.% Ti
η, Fe_2Al_5 ≤ 1169	*oC*24 *Cmcm* Fe_2Al_5	a = 765.59 b = 641.54 c = 421.84	[2006MSIT], at 71.5 at.% Al Solid solubility ranges from 71.0 to 72.5 at.% Al.
		a = 766.5 b = 640.9 c = 422.1	[1995Pal], contains 1.5 at.% Ti
		a = 765.6 b = 646.3 c = 422.9	[1995Pal], contains 2.5 at.% Ti

(*continued*)

DOI: 10.1007/978-3-540-69761-9_13

Phase/ Temperature Range [°C]	Pearson Symbol/ Space Group/ Prototype	Lattice Parameters [pm]	Comments/References
Fe_4Al_{13} ≤ 1160	*mC*102 *C*2/*m* Fe_4Al_{13}	*a* = 1552.7 to 1548.7 *b* = 803.5 to 808.4 *c* = 1244.9 to 1248.8 β = 107.7 to107.99°	[2006MSIT], 74.16 to 76.7 at.% Al solid solubility ranges from 74.5 to 75.5 at.% Al
		a = 1549.2 *b* = 807.8 *c* = 1247.1 β = 107.69	[2006MSIT], at 76.0 at.% Al
		a = 1548.9 *b* = 808.3 *c* = 1247.6 β = 107.72	[1995Pal], contains about 6.5 at.% Ti with Al being replaced
		a = 1565.3 *b* = 805.2 *c* = 1243.0 β = 107.58	[1995Yan2], at $Fe_4Ti_{0.93}Al_{12.07}$
$TiFe_2$ ≤ 1427	*hP*12 $P6_3/mmc$ $MgZn_2$	*a* = 478.7 *c* = 781.5	solid solubility ranges from 24.0 to 36.0 at.% Ti [V-C]
		a = 495.6 *c* = 803.2	[1996Mac], at $Ti_{33.1}Fe_{33.9}Al_{33}$
		a = 479.29 *c* = 782.34	[2006Yan], $Ti_{33.3}Fe_{66.7}$ annealed at 900°C
		a = 483.65 *c* = 786.72	[2006Yan], $Ti_{34}Fe_{58}Al_8$ annealed at 900°C
		a = 487.41 *c* = 791.70	[2006Yan], as-cast $Ti_{33.3}Fe_{50}Al_{16.7}$
		a = 491.64 *c* = 798.47	[2006Yan], $Ti_{33.3}Fe_{41.7}Al_{25}$ annealed at 900°C
		a = 494.95 *c* = 803.64	[2006Yan], $Ti_{34}Fe_{36}Al_{30}$ annealed at 900°C
		a = 496.49 *c* = 805.93	[2006Yan], $Ti_{33.3}Fe_{33.3}Al_{33.4}$ annealed at 1000°C
		a = 496.49 *c* = 805.93	[2006Yan], $Ti_{33.3}Fe_{33.3}Al_{33.4}$ annealed at 1000°C

(*continued*)

DOI: 10.1007/978-3-540-69761-9_13

Phase/ Temperature Range [°C]	Pearson Symbol/ Space Group/ Prototype	Lattice Parameters [pm]	Comments/References
		a = 496.61 c = 806.28	[2006Yan], $Ti_{33.3}Fe_{33.3}Al_{33.4}$ annealed at 1000°C
		a = 503.66 c = 819.71	[2006Yan], as-cast $Ti_{34}Fe_{17}Al_{49}$
TiFe ≤ 1317	*cP*2 $Pm\bar{3}m$ CsCl	a = 297.6	solid solubility ranges from 49.8 to 51.8 at.% Ti [V-C]
* τ_1, $TiFe_2Al$	*cF*16 $Fm\bar{3}m$ Cu_2AlMn	a = 587.9	[1983Bus], annealed at 900°C for 14 days
* τ_2	*cF** $F\bar{4}3m$	a = 1211.0	[1995Pal], at $Ti_{50.9}Fe_{24.5}Al_{24.6}$
		a = 1209.59	[2006Gry], $Ti_{43}Fe_{24}Al_{33}$ annealed at 900°C; both X-ray and neutron diffraction data
* τ_2'	*cF*116 $Fm\bar{3}m$ Th_6Mn_{23}	a = 1199.0 a = 1182.0 a = 1203.8 a = 1207.6 a = 1209.9 a = 1211.0 a = 1189.0	[1967Mar, 2000Mab] [1981Sei] [1995Pal], at $Ti_{30.8}Fe_{21.4}Al_{47.8}$ [1999Gor], at $Ti_{38.4}Fe_{23}Al_{38.6}$ [1999Gor], at $Ti_{42.2}Fe_{23.1}Al_{34.7}$ [1999Lev] [2003Gry] at $Ti_{20.3}Fe_{23.7}Al_{56}$
	filled Th_6Mn_{23}	a = 1209.2	[2003Gry] at $Ti_{42}Fe_{23.3}Al_{34.7}$
	filled Th_6Mn_{23}	a = 1199.44	[2006Gry], $Ti_{22}Fe_{23}Al_{55}$ annealed at 900°C; neutron diffraction data
* τ_3, $Ti_8Fe_3Al_{22}$	*cP*4 $Pm\bar{3}m$ $AuCu_3$	a = 394.2 a = 394.3 a = 394.16 a = 392.7 a = 394.3 a = 394.44 a = 393.5	[1990Nic], at $Ti_8Fe_3Al_{22}$ [1991Nic], at $Ti_8Fe_3Al_{22}$ [1992Kog], at $Ti_{22}Fe_9Al_{66}$ [1992Win], at $Ti_{27.7}Fe_{9.7}Al_{62.6}$ [1995Pal], at $Ti_{28.6}Fe_{7.5}Al_{63.9}$ [1995Pal], at $Ti_{25.8}Fe_{7.6}Al_{66.6}$ [2000Mab], at $Ti_{28}Fe_8Al_{64}$

Table 3. Investigations of the Al-Fe-Ti Materials Properties

Reference	Method/Experimental Technique	Type of Property
[1983Bus]	Magnetometry	Curie temperature and saturation magnetization of $TiFe_2Al$ at 25°C
[1991Ino]	Mechanical tests	Temperature dependence of yield stress

(*continued*)

DOI: 10.1007/978-3-540-69761-9_13

Reference	Method/Experimental Technique	Type of Property
[1991Kum]	Mechnical tests	Temperature dependence of yield stress
[1991Wu]	Mechnical tests	Temperature dependence of yield stress and critical resolved shear stress
[1994Sel]	Magnetometry	Magnetization data at 25 and −196°C
[1996Mac]	Mechanical tests	Temperature dependence of yield stress
[1997Nis2]	Mechanical tests	Temperature dependence of hardness
[1999Gor]	Mechanical tests	Temperature dependence of yield stress and steady state creep rate
[2000Koi]	Mechanical tests	Stress-induced phase transformation and superplasticity
[2000Sha]	Mechanical tests	Superplasticity
[2000Sun]	Mechanical tests	Hot hardness and creep
[2000Zhu]	Mechanical tests	Compressive deformation and hot workability
[2001Ish]	Physico-chemical tests	Hydrogen absorption-desorption
[2001Pra]	Mechanical tests	Ambient and high-temperature Young's modulus, yield stress, and steady state creep rate
[2002Bra]	Mechanical tests	Stress and strain to failure under three-point bend test
[2003Ino]	Mechanical tests	Tensile and fracture strengths
[2003Ste]	Mechanical tests	Temperature dependence of compressive flow stress
[2004Gua]	Mechanical tests	Dry sliding wear rate
[2004Her]	Mechanical tests	Hardness and yield strength
[2004Pal]	Mechanical tests	Hardness, compressive yield stress, ductile-to-brittle transition temperature, steady state creep rate, and oxidation kinetics

DOI: 10.1007/978-3-540-69761-9_13

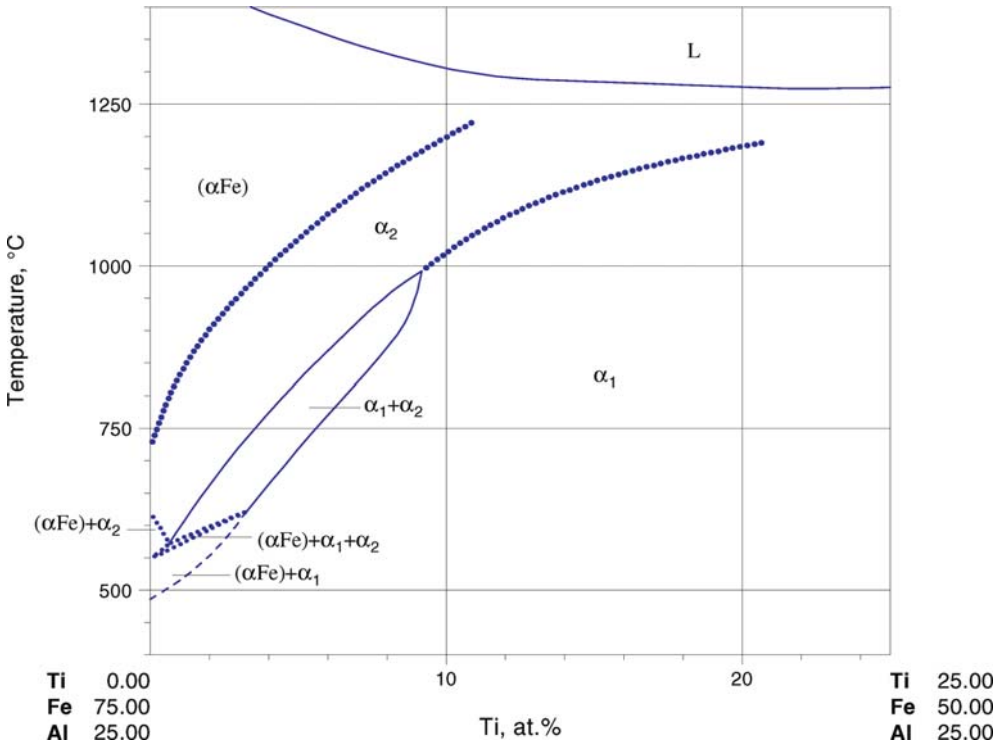

Fig. 1. Al-Fe-Ti. Vertical section at a constant Al content of 25 at.%

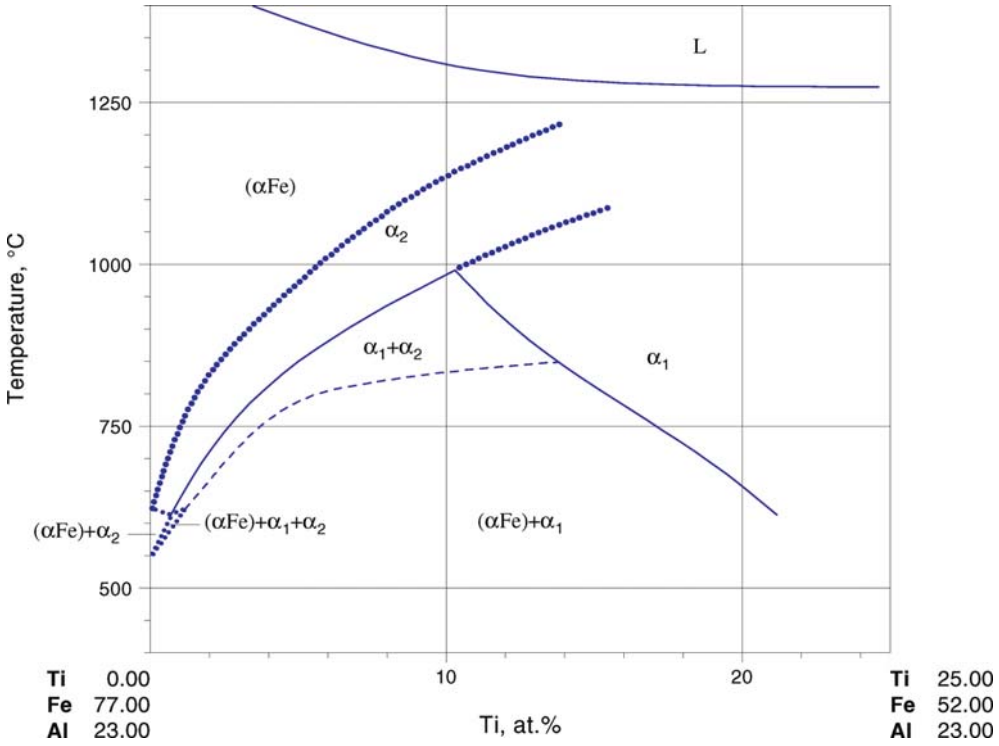

Fig. 2. Al-Fe-Ti. Vertical section at a constant Al content of 23 at.%

DOI: 10.1007/978-3-540-69761-9_13

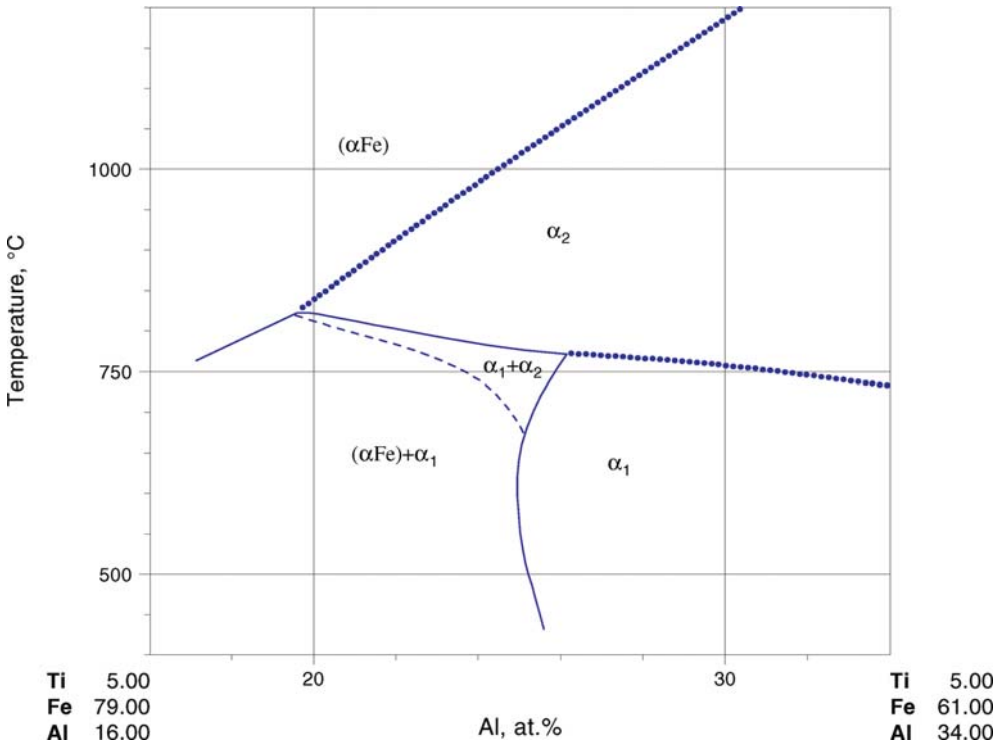

Fig. 3. Al-Fe-Ti. Vertical section at a constant Ti content of 5 at.%

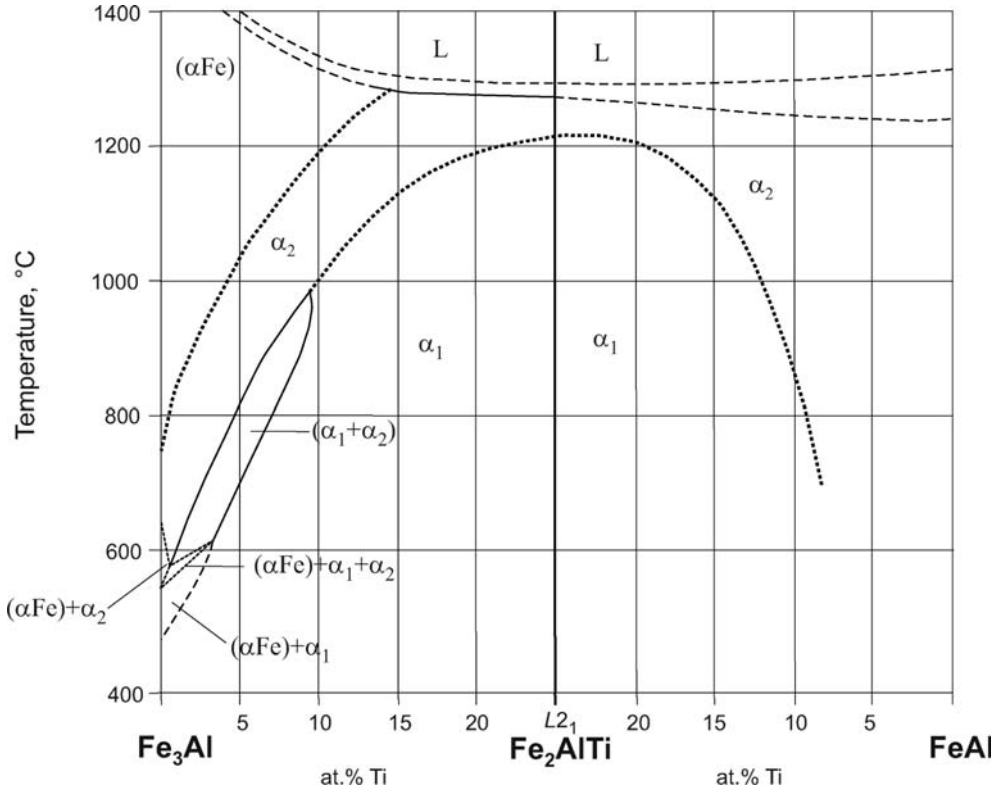

Fig. 4. Al-Fe-Ti. Conjoined vertical sections along Fe_3Al-Fe_2TiAl and Fe_2TiAl-FeAl

DOI: 10.1007/978-3-540-69761-9_13

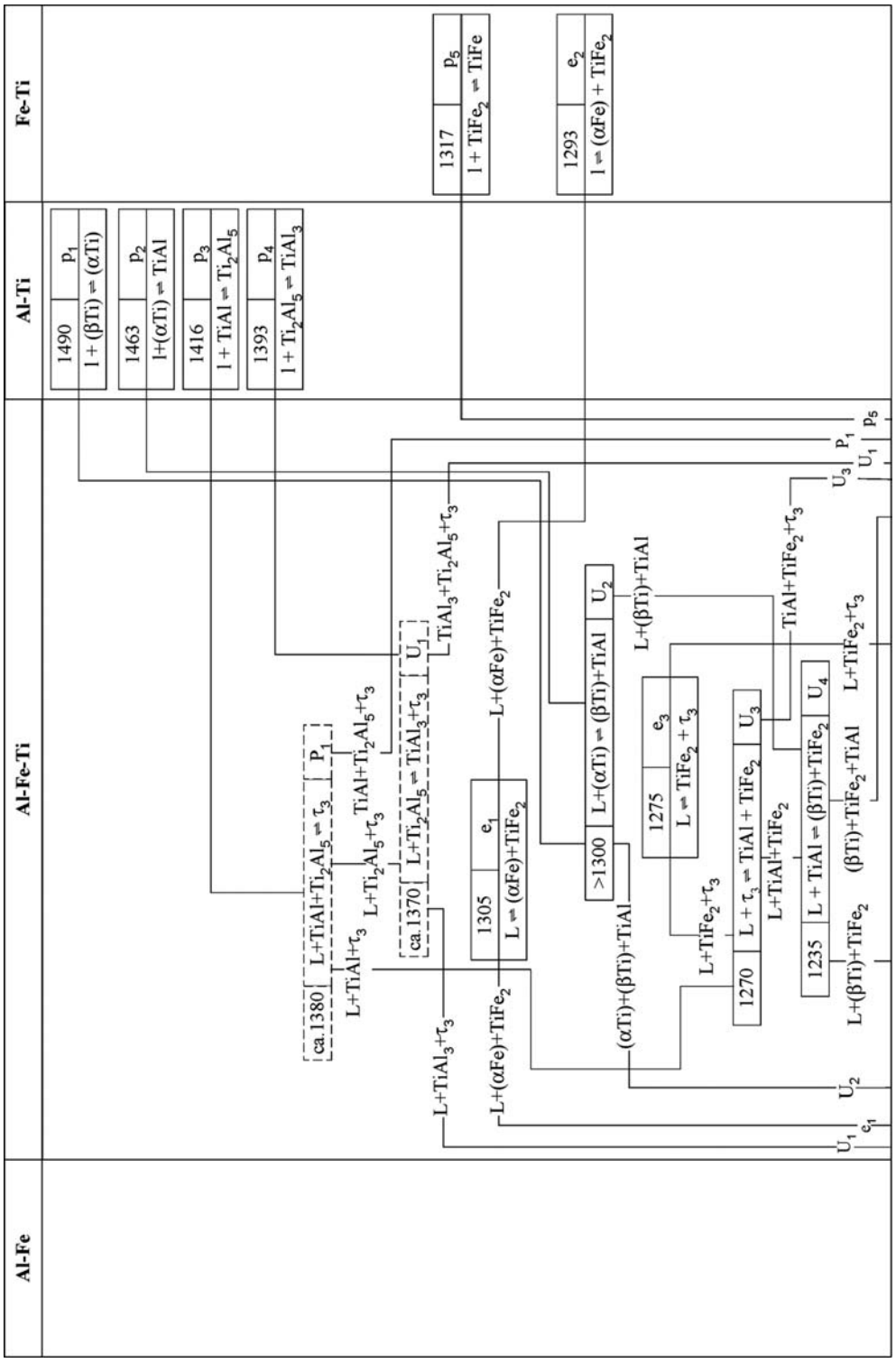

Fig. 5a. Al-Fe-Ti. Reaction scheme, part 1

DOI: 10.1007/978-3-540-69761-9_13

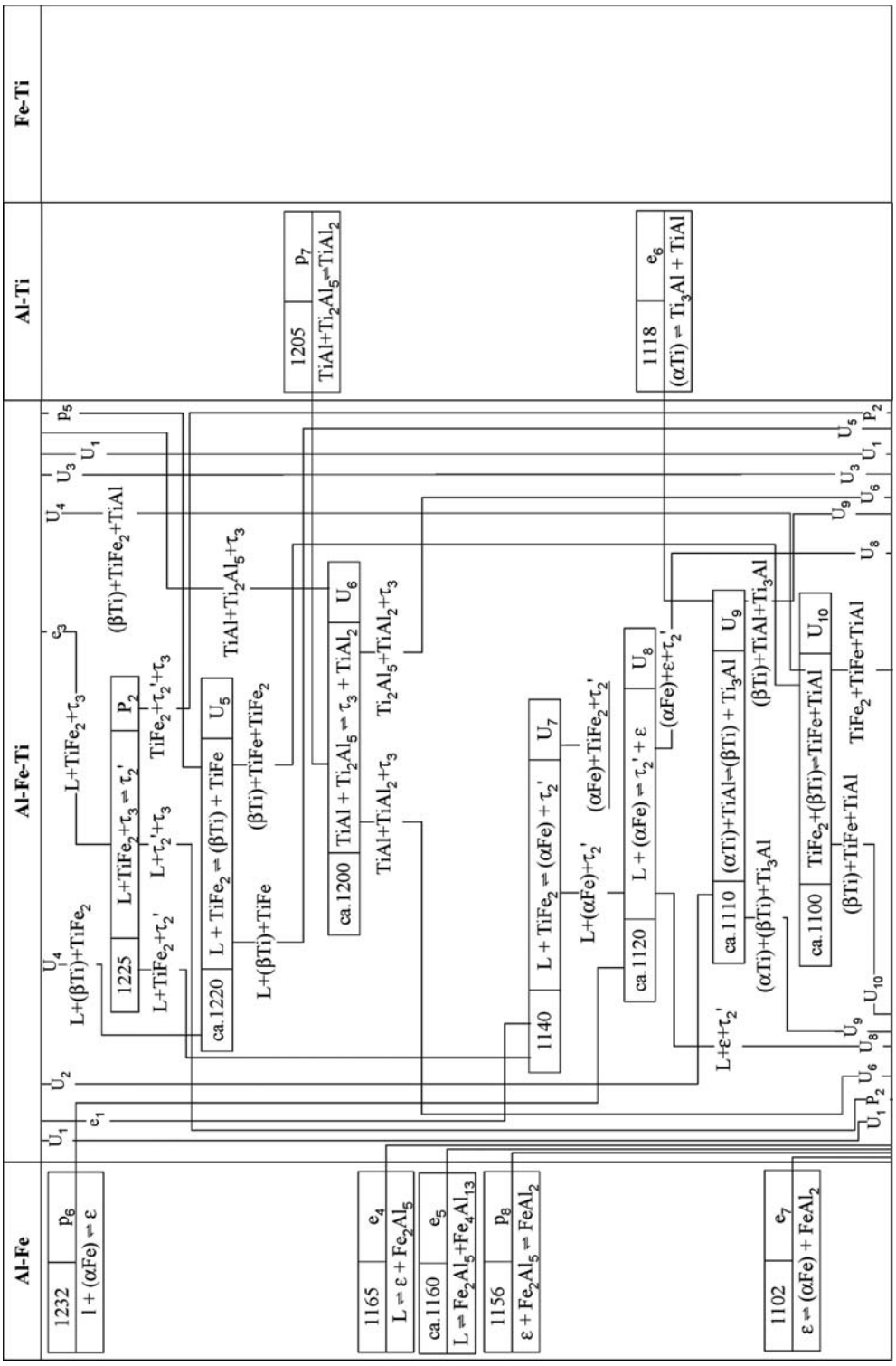

Fig. 5b. Al-Fe-Ti. Reaction scheme, part 2

DOI: 10.1007/978-3-540-69761-9_13

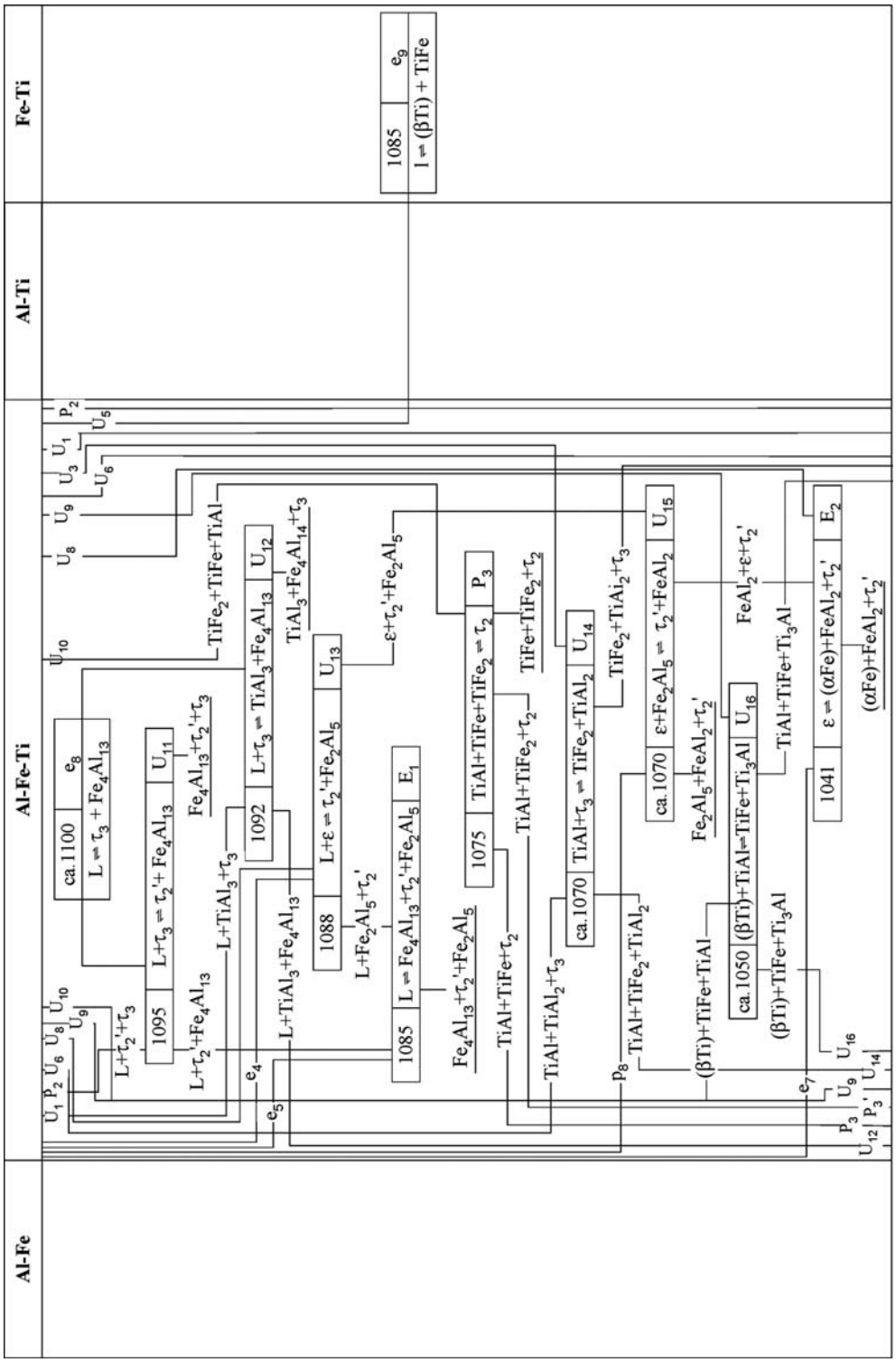

Fig. 5c. Al-Fe-Ti. Reaction scheme, part 3

DOI: 10.1007/978-3-540-69761-9_13

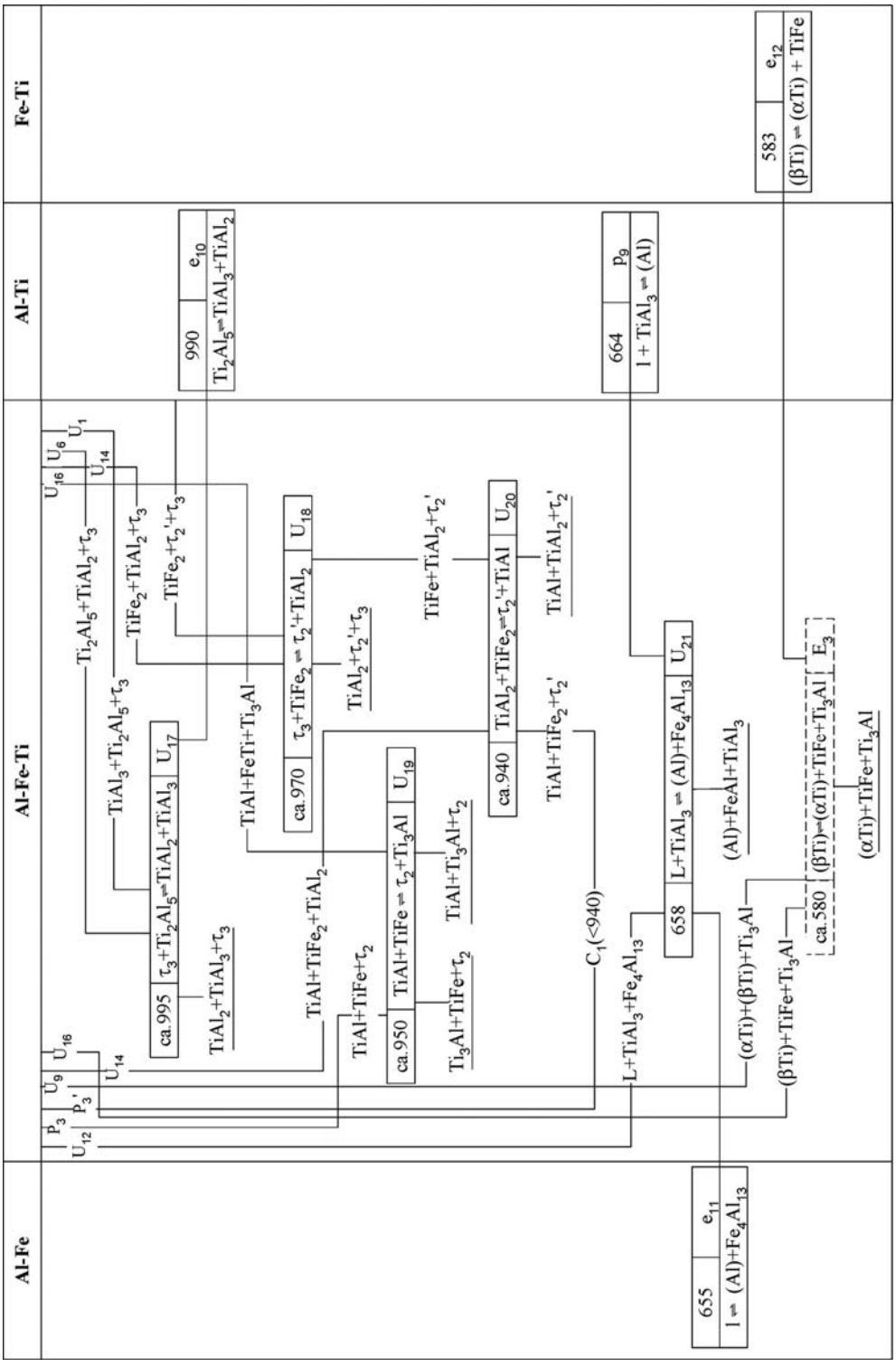

Fig. 5d. Al-Fe-Ti. Reaction scheme, part 4

DOI: 10.1007/978-3-540-69761-9_13

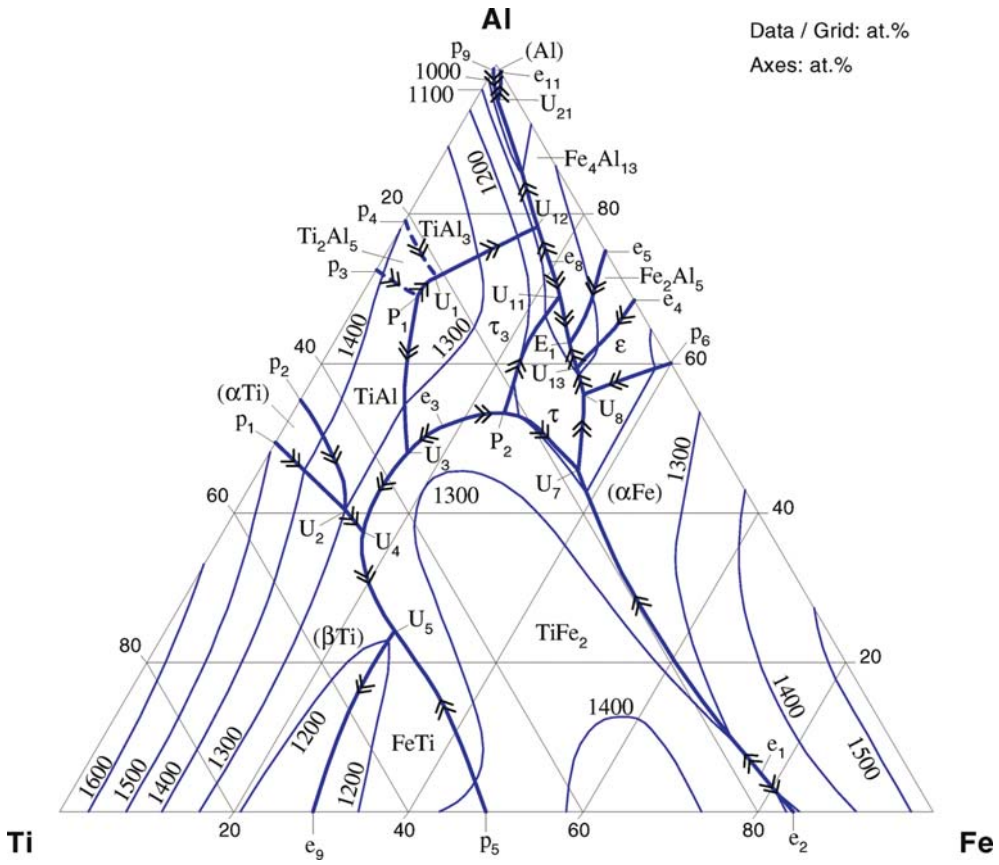

Fig. 6. Al-Fe-Ti. The liquidus surface projection

DOI: 10.1007/978-3-540-69761-9_13

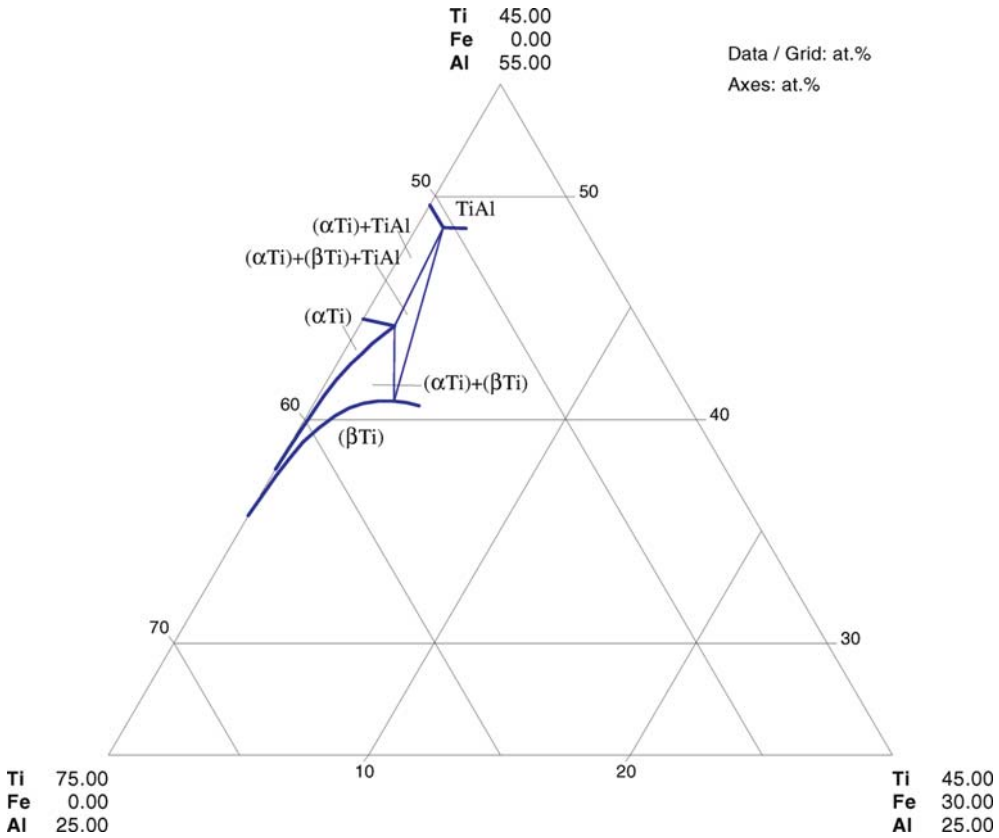

Fig. 7. Al-Fe-Ti. Partial isothermal section at 1300°C

DOI: 10.1007/978-3-540-69761-9_13

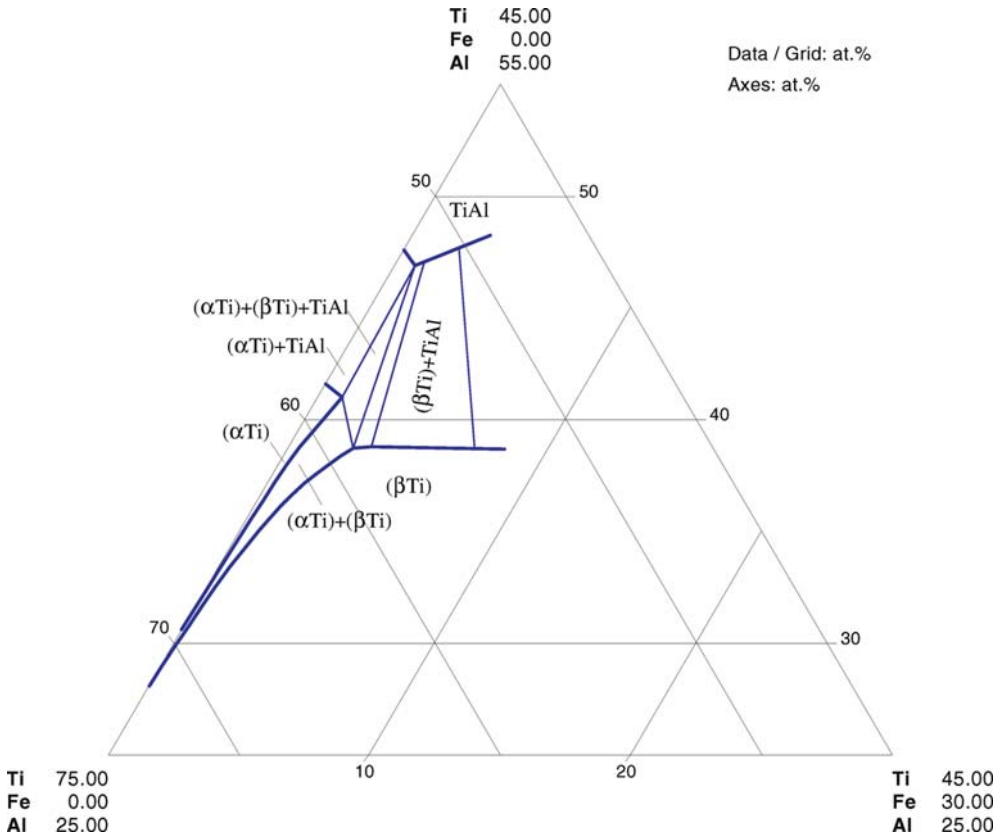

Fig. 8. Al-Fe-Ti. Partial isothermal section of Ti corner at 1200°C

DOI: 10.1007/978-3-540-69761-9_13

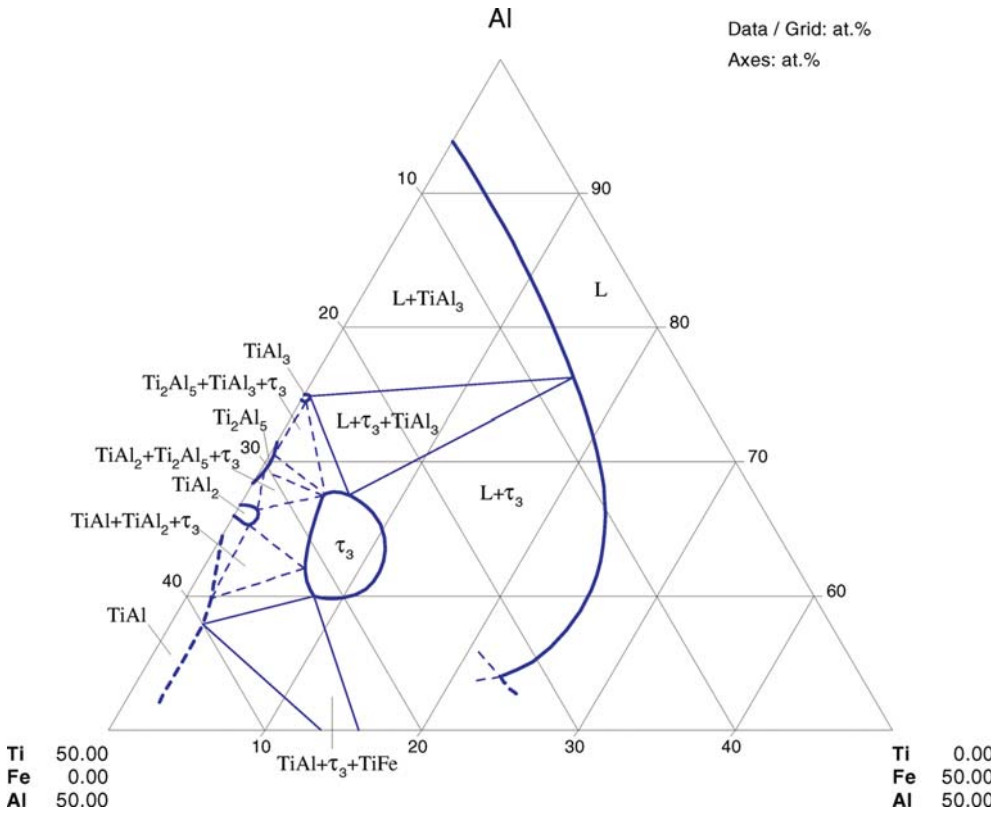

Fig. 9. Al-Fe-Ti. Partial isothermal of Al corner section at 1200°C

DOI: 10.1007/978-3-540-69761-9_13

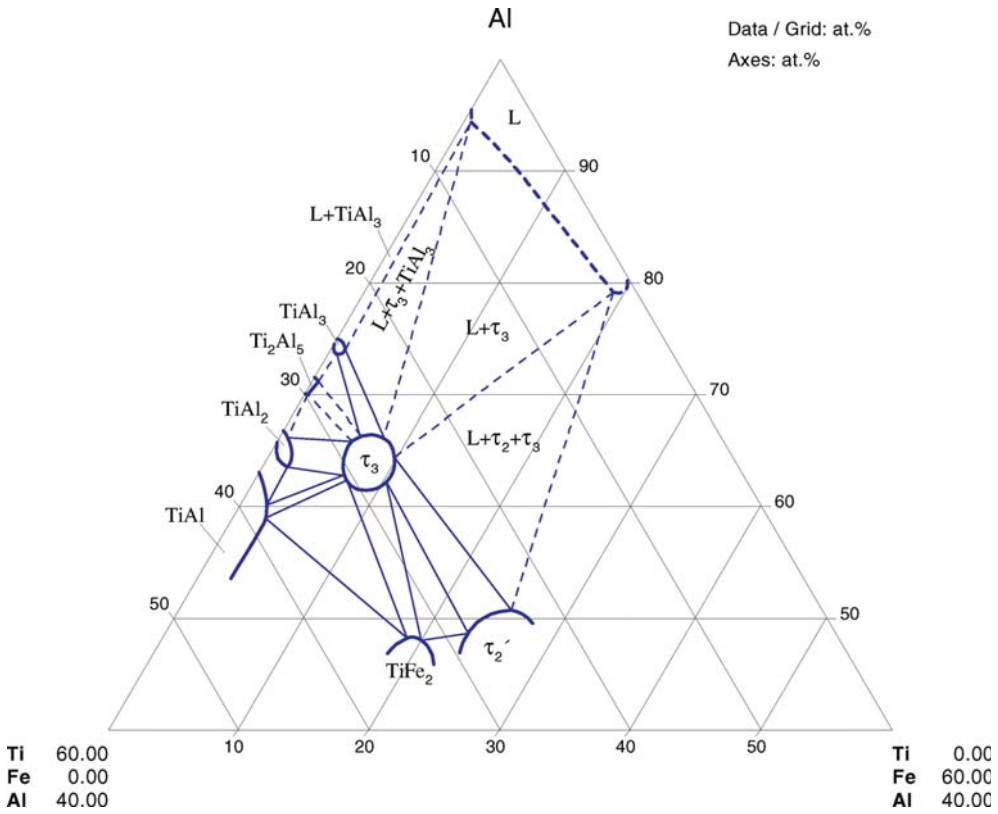

Fig. 10. Al-Fe-Ti. Partial isothermal section at 1150°C

DOI: 10.1007/978-3-540-69761-9_13

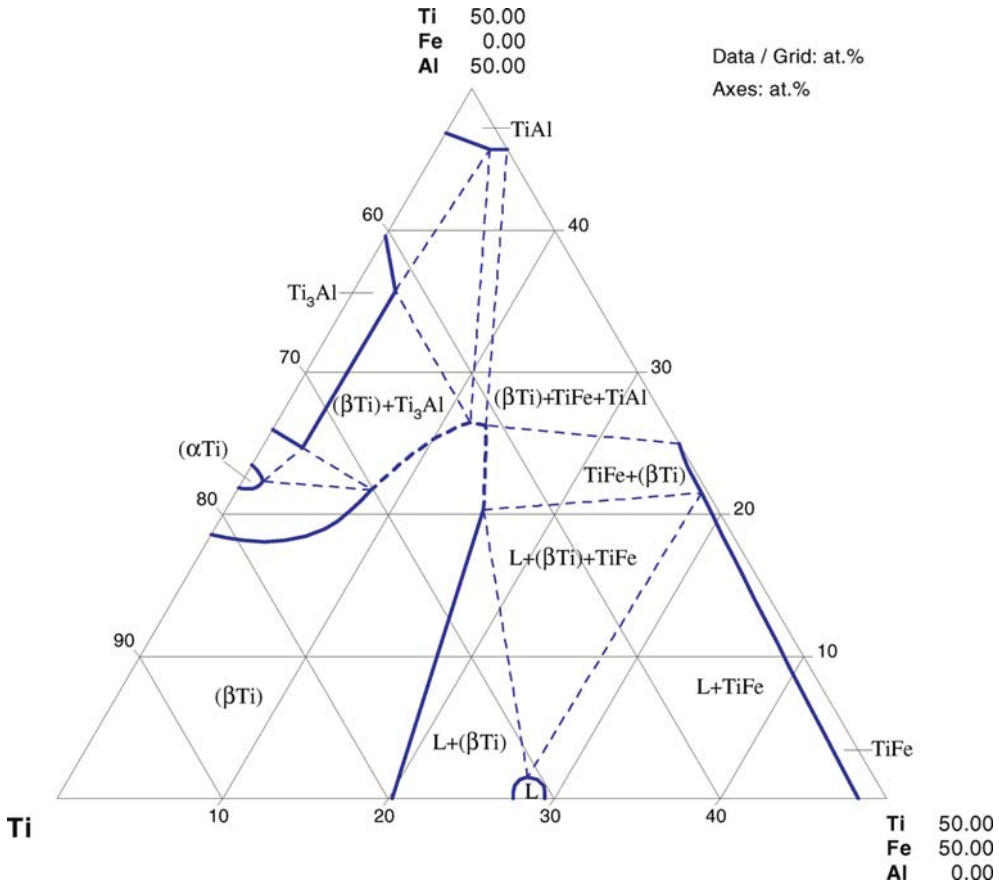

Fig. 11. Al-Fe-Ti. Partial isothermal section at 1100°C

DOI: 10.1007/978-3-540-69761-9_13

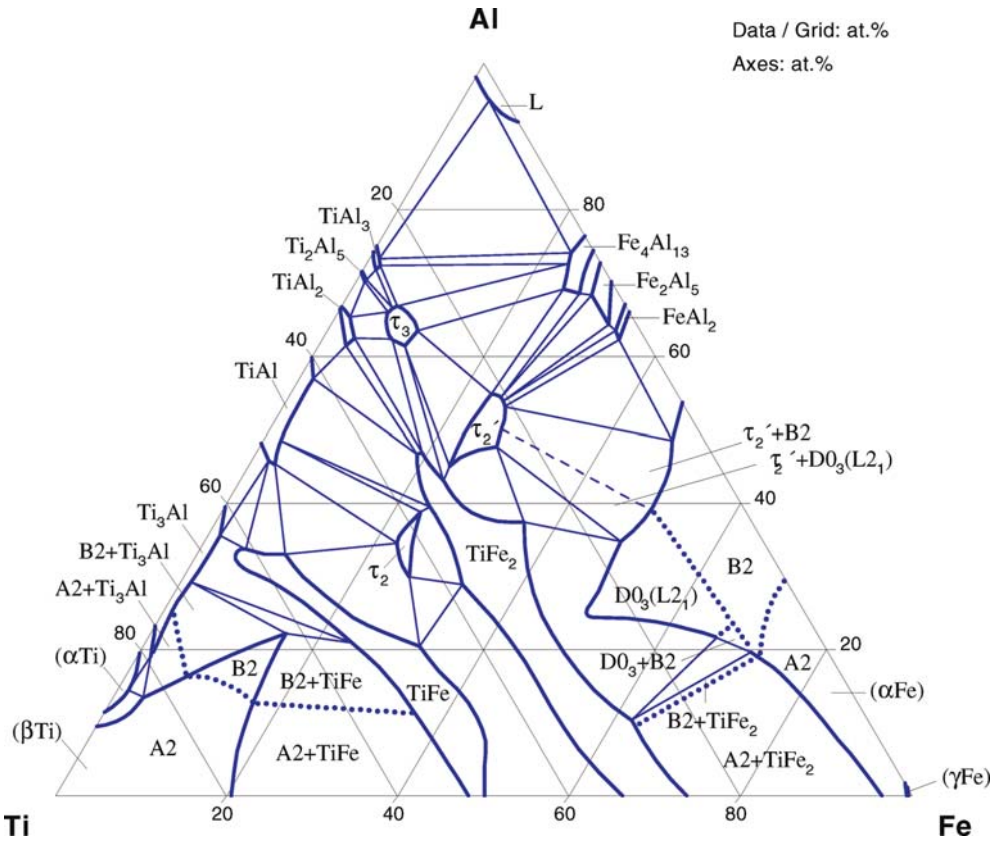

Fig. 12. Al-Fe-Ti. Isothermal section at 1000°C

DOI: 10.1007/978-3-540-69761-9_13

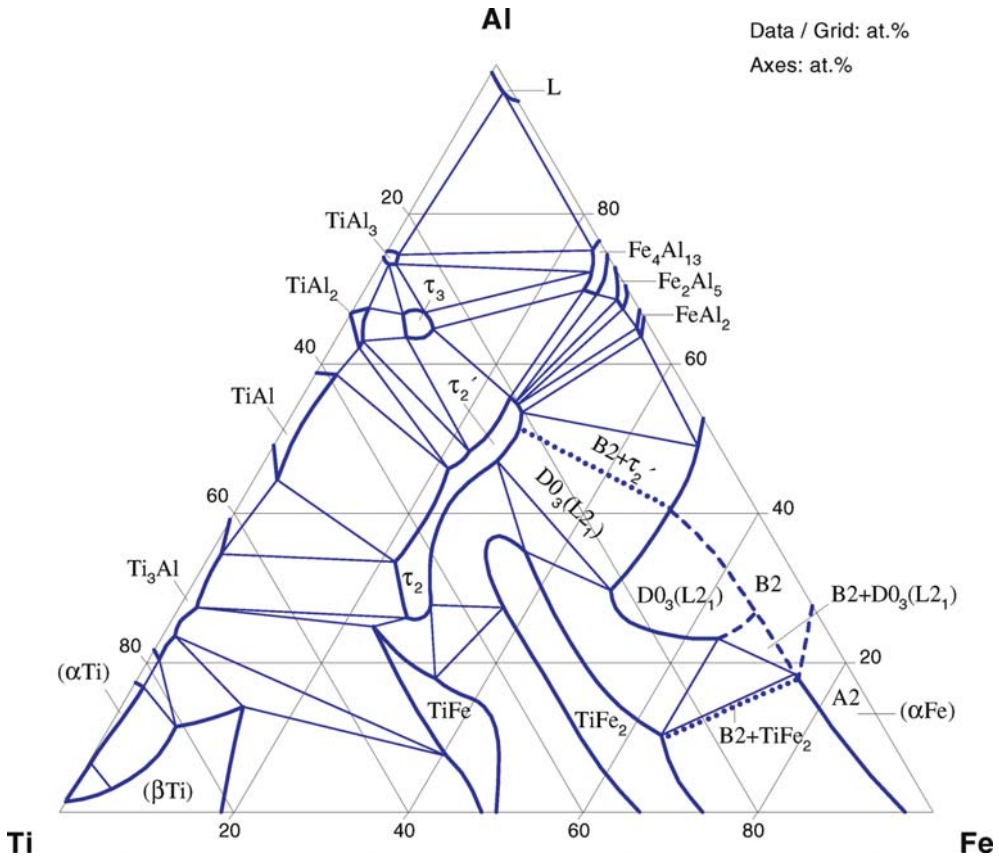

Fig. 13. Al-Fe-Ti. Isothermal section at 900°C

DOI: 10.1007/978-3-540-69761-9_13

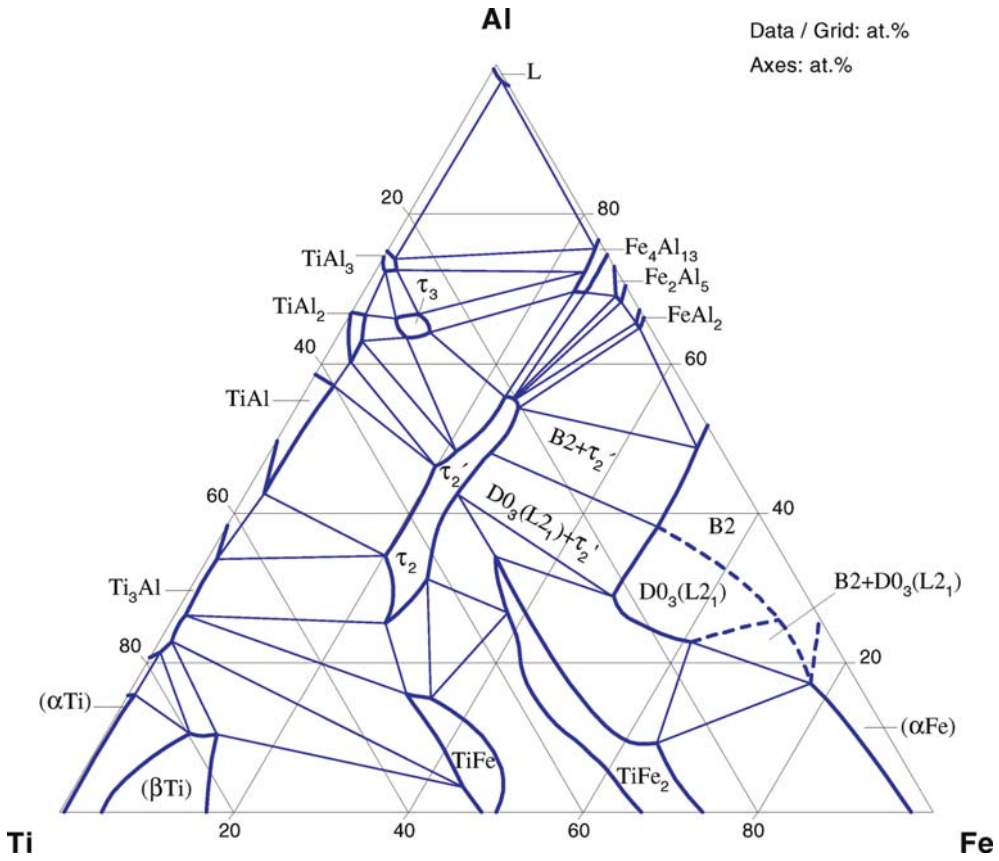

Fig. 14. Al-Fe-Ti. Isothermal section at 800°C

DOI: 10.1007/978-3-540-69761-9_13

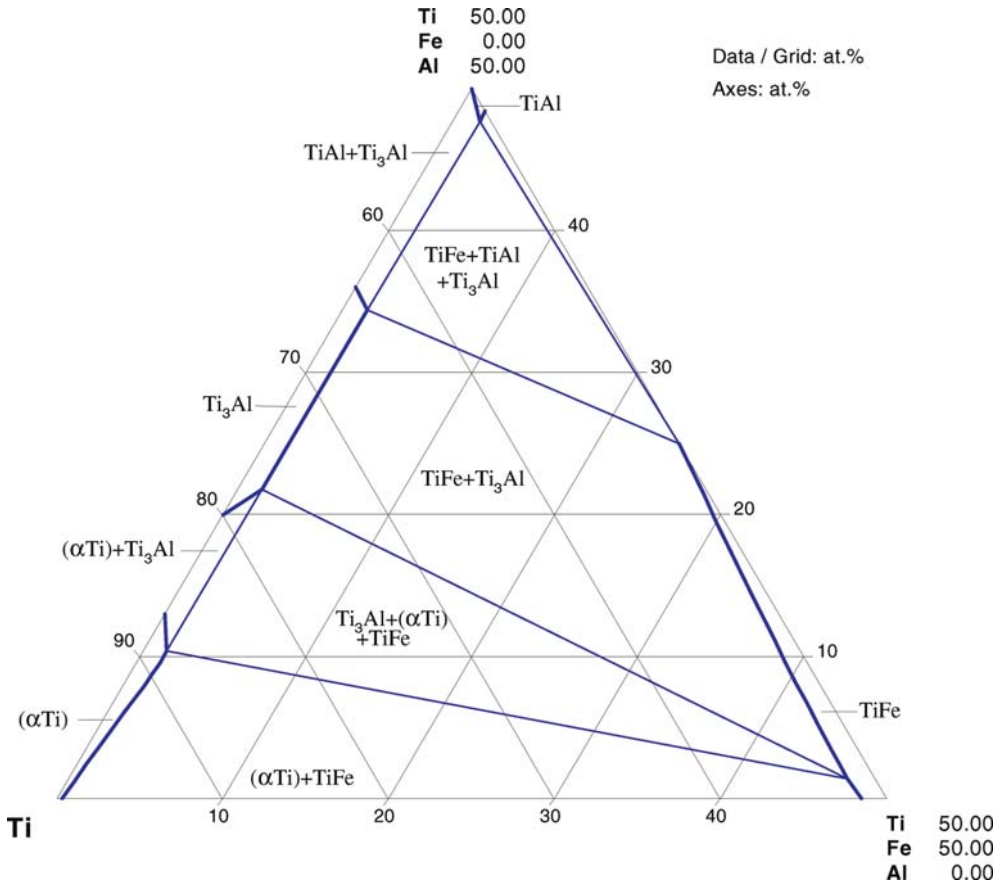

Fig. 15. Al-Fe-Ti. Partial isothermal section at 550°C

DOI: 10.1007/978-3-540-69761-9_13

References

[1940Nis] Nishimura, H., Matsumoto, E., "The Equilibrium Diagram of the Al-Fe-Ti System and the Segregation of Fe and Ti" (in Japanese), *Nippon Kinzoku Gakkaishi*, **10**, 339–343 (1940) (Phase Diagram, Phase Relations, Experimental, #, *, 5)

[1954Sto] Stone, L., Margolin, H., "The Ti-V-Fe and Ti-Al-Fe Systems", U.S. Atomic Energy Commission Publication, AD-43730, 1–72 (1954) (Phase Diagram, Phase Relations, Experimental, #, *)

[1958Bok] Bok, Y.V., Mal'tsev, M.V., "Investigation of the Equilibrium Diagram of the Al-Fe-Ti System" (in Russian), *Izv. Vyss. Uchebn. Zaved. Tsvetn. Metall.*, **3**, 110–114 (1958) (Phase Diagram, Phase Relations, Experimental, #, *, 2)

[1958Kor] Kornilov, I.I., Pylaeva, E.N., Volkova, M.A., "An Investigation into the Equilibrium of the Ternary System Ti-Al-Fe" (in Russian), *Zh. Neorg. Khim.*, **3**, 1391–1397 (1958) (Phase Diagram, Phase Relations, Experimental, #, *, 13)

[1963Luz] Luzhinov, L.P., Novikova, V.M., Marsev, A.P., "Solubility of β-Stabilizers in α-Ti" (in Russian), *Metalloved. Term. Obrab. Met.*, **2**, 13–16 (1963) (Experimental, Phase Relations,4)

[1967Mar] Markiv, V.Ya., Kripyakevich, P.I., "Compounds of the Type $R(X',X'')_2$ in the Systems with R = Ti, Zr, Hf; X′ = Fe, Co, Ni, Cu and X″ = Al, Ga and Their Crystal Structures", *Sov. Phys. Crystallogr.*, **11**, 733–738 (1967) (Crys. Structure, Experimental, 25)

[1969Vol] Volkova, M.A., Kornilov, I.I., "Investigation of the Phase Transformation in Ti-rich Ti-Al-Fe Alloys" (in Russian), *Izv. Akad. Nauk SSSR, Met.*, **4**, 236–240 (1969) (Phase Diagram, Phase Relations, Experimental, #, *, 7)

[1970Vol] Volkova, M.A., Kornilov, I.I., "Phase Equilibria in Ti rich Ti-Al-Fe Alloys" (in Russian), *Izv. Akad. Nauk SSSR, Met.*, **3**, 187–193 (1970) (Phase Diagram, Phase Relations, Experimental, #, *, 6)

[1971Vol] Volkova, M.A., Kornilov, I.I., "Phase Equilibriums and Some Mechanical Properties of the Ti-Al-Fe and Ti-Al-V Alloys" (in Russian), *Izv. Akad. Nauk SSSR, Met.*, **1**, 200–205 (1971) (Phase Diagram, Phase Relations, Experimental, #, *, 13)

[1973Kol] Kolpachev, A.A., Medvedeva, N.D., Samoilov, Yu.A., Titova, I.A., "Effect of Iron on Titanium Solubility in Aluminium and Aluminium-Magnesium Alloys" (in Russian), *Tekhnol. Legk. Splavov, Nauchno-Tekh. Byull., Vses. Inst. Splavov*, **8**, 15–17 (1973) (Experimental, 3)

[1973Mar] Markiv, V.Ya., Burnashova, V.V., Rybov, V.P., "The Systems Titanium-Iron-Aluminium, Titanium-Nickel-Aluminium and Titanium-Copper-Aluminium" (in Russian), *Akad. Nauk Ukr. SSR*, *Metallofizika.,***46**, 103–110 (1973) (Phase Diagram, Phase Relations, Experimental, #, *, 24)

[1973Vol] Volkova, M.A., Kornilov, I.I., "Study on the Phase Constitution of Alloys of the Ternary Titanium-Aluminium-Iron System" (in Russian), *Khim. Met. Splav.*, **1**, 77–80 (1973) (Phase Diagram, Phase Relations, Experimental, #, *, 9)

[1974Dwi] Dwight, A.E., "Alloying Behavior of Zr, Hf and Actinides in Several Series of Isostructural Compounds", *J. Less-Common Met.*, **34**, 279–284 (1974) (Crys. Structure, Experimental, 6)

[1977Ath] Athanassiadis, F., La Caer, G., Foct, J., Rimlinger, L., "Study of Ternary Ordered Solid Solutions Derived from Fe_3Al by Substitution", *Phys. Status Solidi (a)*, **40**, 425–435 (1977) (Crys. Structure, Experimental, 20)

[1979Dew] Dew-Hughes, D., Kaufman, L., "Ternary Phase Diagrams of the Manganese-Titanium-Iron and Aluminium-Titanium-Iron Systems: a Comparison of Computer Calculations with Experiment", *Calphad*, **3**, 175–203 (1979) (Thermodyn., Phase Relations, Phase Diagram, Theory, #, *, 23)

[1979Kau1] Kaufman, L., Dew-Hughes, D., "Illustration of Ternary Diagram Synthesis: Manganese-Titanium-Iron and Aluminium-Titanium-Iron", in *"Calculation of Phase Diagrams and Thermochemistry of Alloy Phases*", Y.A. Chang and J.F. Smith (Eds.), The Metallurgical Society of AIME, Warrendale, PA, 46–71 (1979) (Thermodyn., Theory, #, *,23)

DOI: 10.1007/978-3-540-69761-9_13

[1979Kau2] Kaufman, L., Dew-Hughes, D., "Illustration of Ternary Diagram Synthesis: Manganese-Titanium-Iron and Aluminium-Titanium-Iron", *Energy Res. Rep.*, **4**(19), 1–21 (1979) (Thermodyn., Theory, #, *, 23)

[1979Sup] Suprunenko, P.A., Markiv, V.Ya., Storozhenko, A.L., "Magnetic Susceptibility of Intermetallides with the Th_6Mn_{23} Structure in the Systems Ti-Fe, Co, Ni-Al, Ga", *Ukr. Fiz. Zh.*, **24**, 114–116 (1979) (Experimental, 8)

[1980Dew] Dew-Hughes, D., "The Addition of Manganese and Aluminium to the Hydriding Compound Iron-Titanium (Fe-Ti): Range of Homogeneity and Lattice Parameters", *Metall. Trans. A*, **11A**, 1219–1225 (1980) (Experimental, #, *, 14)

[1981Sei] Seibold, A., "Phase Equilibria in the Ternary Systems Ti-Fe-O and Ti-Al-Fe" (in German), *Z. Metallkd.*, **72**, 712–719 (1981) (Phase Diagram, Phase Relations, Experimental, #, *, 25)

[1981Zhu] Zhuang, Y.-H., Liu, J.-Q., Cheng, C.S., "A Room-Temperature Section of the Phase Diagram of $TiAl_3$-VAl_3-MAl_3 of the Quaternary System Alloys of Al-Ti-V-M (M = Ni, Fe)" (in Chinese), *Acta Phys. Sin.*, **30**, 972–975 (1981) (Phase Diagram, Phase Relations, Experimental, *, 9)

[1982All] Allen, S.M., Cahn, J.W., "Phase Diagram Features Associated with Multicritical Points in Alloy Systems", *Bull. Alloy Phase Diagrams*, **3**(3), 287–295 (1982) (Theory, Phase Relations, 25)

[1982Kub] Kubaschewski, O., "Iron-Titanium" in *Iron-Binary Phase Diagrams*, Springer Verlag, Berlin, 152–156 (1982) (Phase Diagram, Phase Relations, Review, #, *, 26)

[1983Bus] Buschow, K.H.J., van Engen, P.G., Jongebreur, R., "Magneto-Optical Properties of Metallis Ferromagnetic Materials", *J. Magn. Magn. Mater.*, **38**, 1–22 (1983) (Magn. Prop., Optical Prop., 23)

[1985Men] Mendiratta, M.G., Lipsitt, H.A., "$D0_3$-Domain Structures in Fe_3Al-X Alloys", *Mater. Res. Soc. Symp. Proc.: High-Temp. Ordered Intermetallic Alloys*, **39**, 155–162 (1985) (Experimental, Crys. Structure, Phase Relations, *, 4)

[1985Okp] Okpalugo, D.E., Booth, J.G., Faunce, C.A., "Onset of Ferromagnetism in 3*d*-Substituted Fe-Al Alloys. I: Ti, V and Cr Substitutions", *J. Phys. F, Met. Phys.*, **15**, 681–692 (1985) (Crys. Structure, Experimental, 21)

[1985Pas] Pastushenko, S.N., "Mössbauer Spectroscopic Study of Phase Equilibria in the Ti-Al-Fe Ternary System" (in Russian), *Raschety Eksp. Metody Postroeniya Diagramm Sostoyaniya.*, Ageev, N.N., (Ed.) Nauka, Moscow, 148–151 (1985) (Experimental, 10)

[1986Gho] Ghosh, G., Raghavan, V., "The Austenite Phase Boundaries in Four Fe-Ti-X System" in *Prog. Metall. Res.: Fundam. Appl. Aspects*, *Proc. Int. Conf.*, Mehrotra, S.P., Ramachandran, T.R., (Eds.), Tata McGraw-Hill, New Delhi, 403–408 (1986) (Review, Thermodyn., 11)

[1986Len] Lendval, A., "Phase Diagram of the Al-Fe System up to 45 mass% Iron", *J. Mater. Sci. Lett.*, **5**, 1219–1220 (1986) (Phase Diagram, Phase Relations, Experimental, 7)

[1986Zwi] Zwicker, U., "Investigations on the $TiAl_5Fe_{2.5}$ Alloy as Implant Material" (in German), *Z. Metallkd.*, **77**, 714–720 (1986) (Experimental, 26)

[1987Die] Diehm, R.S., Mikkola, D.E., "Effects of Mo and Ti Additions on the High Temperature Compressive Properties of Iron Aluminides Near Fe_3Al", *Mater. Res. Soc. Symp. Proc.: High-Temp. Ordered Intermetallic Alloys II*, **81**, 329–334 (1987) (Experimental, Crys. Structure, Phase Relations, Mechan. Prop., 8)

[1987For] Fortnum, R.T., Mikkola, D.E., "Effects of Molybdenum, Titanium and Silicon Additions on The $D0_3$ Reversible $B2$ Transition-Temperature for Alloys Near Fe_3Al", *Mater. Sci. Eng.*, **91**, 223–231 (1987) (Crys. Structure, Experimental, 37)

[1987Kal] Kaluzhnyi, V.V., Matysina, Z.A., Milyan, M.I., "Ordering of Atoms in Ternary Alloys with Hexagonal Close-Packed Structure of $D0_{19}$ Type" (in Russian), *Izv. V.U.Z. Fiz.*, **30**(3), 70–77 (1987) (Crys. Structure, Theory, 17)

[1987Men] Mendiratta, M.G., Ehlers, S.K., Lipsitt, H.A., "$D0_3$-$B2$-α Phase Relations in Fe-Al-Ti Alloys", *Metall. Trans. A*, **18A**, 509–518 (1987) (Phase Diagram, Phase Relations, Experimental, #, *, 12)

DOI: 10.1007/978-3-540-69761-9_13

[1987Rag] Raghavan, V., "The Al-Fe-Ti (Aluminum-Iron-Titanium) System" in "*Phase Diagrams of Ternary Iron Alloys*", Part I, ASM International and the Indian Inst. Metals, 9–21 (1987) (Phase Diagram, Phase Relations, Review, #, *, 23)

[1988Kum] Kumar, K.C.H., Raghavan, V., "BCC-FCC Equilibrium in Ternary Iron Alloys", *J. Alloy Phase Equilibria*, **4**(1), 53–71 (1988) (Phase Diagram, Phase Relations, Thermodyn., Review, 27)

[1989Maz] Mazdiyasni, S., Miracle, D.B., Dimiduk, D.M., Mendiratta, M.G., Subramanian, P.R., "High Temperature Phase Equilibria of the $L1_2$ Composition in the Al-Ti-Ni, Al-Ti-Fe and Al-Ti-Cu Systems", *Scr. Metall.*, **23**, 327–331 (1989) (Phase Diagram, Phase Relations, Experimental, #, 10)

[1990Car] Carlsson, A.E., Meschter, P.J., "Relative Stabilities of $L1_2$ and $D0_{22}$ Structures in Ternary MAl_3-Base Aluminides", *J. Mater. Res.*, **5**, 2813–2818 (1990) (Phase Diagram, Phase Relations, Theory, 15)

[1990Kum] Kumar, K.S., "Ternary Intermetallics in Aluminium-Refractory Metal-X Systems (X = V, Cr, Mn, Fe, Co, Ni, Cu, Zn)", *Int. Mat. Rev.*, **35**, 293–327 (1990) (Phase Diagram, Phase Relations, Review, 158)

[1990Nic] Nic, J.P., Zhang, S., Mikkola, D.E., "Obervations on the Systematic Alloying of Al_3Ti with Fourth Period Elements to Yield Cubic Phases", *Scripta Metall. Mater.*, **24**, 1099–1104 (1990) (Crys. Structure, Experimental, 15)

[1991Car] Carlsson, A.E., Meschter, P.J., "Ab Initio Calculations of Structural Energetics of Transitional-Metal Aluminides and Silicides", *Mater. Res. Soc. Symp. Proc.: High-Temp. Ordered Intermetallic Alloys IV*, **213**, 19–23 (1991) (Calculation, Thermodyn., 10)

[1991Dur] Durlu, N., Inal, O.T., Yost, F.G., "$L1_2$-Type Ternary Titanium Aluminides of the Composition $Ti_{25}X_8Al_{67}$: $TiAl_3$-Based or $TiAl_3$-Based?", *Scr. Metall. Mater.*, **25**(11), 2475–2479 (1991) (Crys. Structure, Review, 30)

[1991Ino] Inoue, H.R., Cooper, C.V, Favrow, L.H., Hamada, Y., Wayman, C.M., "Mechanical Properties of Fe-Modified $L1_2$-Type Al_3Ti", *Mater. Res. Soc. Symp. Proc.: High-Temp. Ordered Intermetallic Alloys IV*, **213**, 493–498 (1991) (Experimental, Mechan. Prop., 10)

[1991Kum] Kumar, K.S., Dipietro, M.S., Whittenberger, J.D., "Compession Studies on Particulate Composites of Ternary Al-Ti-Fe, and Quaternary Al-Ti-Fe-Nb and Al-Ti-Fe-Mn $L1_2$ Compounds", *Mater. Res. Soc. Symp. Proc.: High-Temp. Ordered Intermetallic Alloys IV*, **213**, 1039–1044 (1991) (Experimental, 11)

[1991Mis] Mishurda, J.C., Perepezko, J.H., "Phase Equilibria in Ti-Al Alloys", *Microstructure-Property Relationships in Titanium Aluminides and Alloys*, Kim. Y.W., Boyer, R.R., (Eds.), 3–30 (1991) (Phase Diagram, Phase Relations, #, *, 75)

[1991Nic] Nic, J.P., Zhang, S., Mikkola, D.E., "Alloying of Al_3Ti with Mn and Cr to Form Cubic $L1_2$ Phases", in *Mater. Res. Soc. Symp. Proc.: High-Temp. Ordered Intermetallic Alloys IV*, **213**, 697–702 (1991) (Crys. Structure, Phase Diagram, Phase Relations, Experimental, Mechan. Prop., 12)

[1991Nwo] Nwobu, A., Maeda, T., Flower, H.M., West, D.R.F., "The Constitution of Ti Rich Alloys of the Ti-V-Fe-Al System", in "*Proceedings of User Aspects of Phase Diagrams*", Institute ofMetals, London, 102–111 (1991) (Experimental, Phase Diagram, Phase Relations, #, *, 15)

[1991Wu] Wu, Z.L., Pope, D.P., Vitek, V., "Mechanical Behavior of Single Crystalline $Al_{66.8}Ti_{27.4}Fe_{5.8}$", *Mater. Res. Soc. Symp. Proc.: High-Temp. Ordered Intermetallic Alloys IV*, **213**, 487–492 (1991) (Crys. Structure, Experimental, Mechan. Prop., 9)

[1992Dur1] Durlu, N., Inal, O.T., "Phase Relations in $TiAl_2$-Based Ternary Titanium Aluminides of Iron or Nickel", *Mater. Sci. Eng. A*, **152**(1/2), 67–75 (1992) (Crys. Structure, Morphology, Mechan. Prop., Phase Relations, Experimental)

[1992Dur2] Durlu, N., Inal, O.T., "$L1_2$-Type Ternary Titanium Aluminides as Electron Concentration Phases", *J. Mater. Sci.*, **27**(12), 3225–3230 (1992) (Assessment, Electronic Structure, Crys. Structure, 41)

DOI: 10.1007/978-3-540-69761-9_13

[1992Gho] Ghosh, G., "Aluminium-Iron-Titanium",", MSIT Ternary Evaluation Program, in *MSIT Workplace*, Effenberg, G. (Ed.), MSI, Materials Science International Services GmbH, Stuttgart; Document ID: 10.16711.1.20, (1992) (Crys. Structure, Phase Diagram, Phase Relations, Assessment, 31)

[1992Kog] Kogachi, M., Minamigawa, S., Kakahigashi, K., "Long-Range Order in $L1_2$ Ternary Intermetallic Compound Al_3Ti-X (X = Fe, Ni, Cu, Ag)", *Scripta Metall. Mater.*, **27**, 407–412 (1992) (Crys. Structure, Phase Relations, Experimental, 10)

[1992Ma] Ma, Y., Gjonnes, J., "Ternary Atom Location in $L1_2$-Structured Intermetallic Phases: $Al_{62.5+x}Ti_{25-y}$(Fe, Ni or Cu)$_{12.5-z}$ Using ALCHEMI", *J. Mater. Res.*, **7**(8), 2049–2058 (1992) (Calculation, Crys. Structure, Experimental, 30)

[1992Mor] Morris, D.G., Gunter, S., "Ordering Ternary Atom Location and Ageing in $L1_2$ Trialuminide Alloys", *Acta Metall. Mat.*, **40**(11), 3065–3073 (1992) (Experimental, Crys. Structure, Phase Relations, 23)

[1992Win] Winnicka, M.B., Varin, R.A., "Microstructure and Ordering of $L1_2$ Titanium Trialuminides", *Metall. Trans. A*, **23A**(11), 2963–2972 (1992) (Crys. Structure, Morphology, Experimental, 24)

[1993Li] Li, D., Li, P., Sun, D., Lin, D, "Mössbauer Study on $B2$ Intermetallic Compound Fe-40Al and its Mn or Ti Containing Alloys", *Mater. Res. Soc. Symp. Proc.: High-Temp. Ordered Intermetallic Alloys*, **288**, 281–286 (1993) (Crys. Structure, Experimental, 10)

[1993Nak] Nakayama, Y., Mabuchi, H., "Formation of Ternary $L1_2$ Compounds in Al_3Ti-Base Alloys", *Intermetallics*, **1**, 41–48 (1993) (Crys. Structure, Phase Diagram, Phase Relations, Experimental, Mechan. Prop., 40)

[1993Rag] Raghavan, V., "Al-Fe-Ti (Aluminum-Iron-Titanium)", *J. Phase Equilib.*, **14**(5), 618–619 (1993) (Phase Diagram, Phase Relations, Review, 8)

[1993Win] Winnicka, M.B., Varin, R.A., "Microhardness and Compressive Mechanical Behavior of $L1_2$ Tittanium Trialuminides", *Metall. Trans. A*, **24A**, 935–946 (1993) (Crys. Structure, Experimental, Mechan. Prop., 24)

[1994Bro] Bros, J.P., Michel, M.L., Castanet, R., "Enthalpy and Heat Capacity of Titanium Based Alloys", *J. Thermal Analysis*, **41**, 7–24 (1994) (Experimental, Thermodyn., 6)

[1994Kon] Kong, C.H., Munroe, P.R., "The Effect of Ternary Additions on the Vacancy Hardening of FeAl", *Scripta Metall. Mater.*, **30**, 1079–1083 (1994) (Crys. Structure, Experimental, 15)

[1994Sel] Sellers, C.H., Hyde, T.A., O'Brien, T.K., Wright, R.N., "Phase Transformations in Fe_3Al +Ti Alloys", *J. Phys. Chem. Solids*, **55**(6), 505–515 (1994) (Experimental, 30)

[1994Yan] Yang, T.Y., Goo, E., "Al_2Ti Precipitation in $Al_{64}Fe_8Ti_{28}$ Alloy", *Metall. Trans. A*, **25A**(4), 715–721 (1994)

[1995Ant] Anthony, L., Fultz, B., "Effects of Early Transition Metal Solutes in the $D0_3$-$B2$ Critical Temperature of Fe_3Al", *Acta Metall. Mater.*, **43**, 3885–3891 (1995) (Crys. Structure, Experimental, 35)

[1995Mah] Mahmood, S.H., Gharaibeh, M.A., Saleh, A.S., "Moessbauer and Structural Studies of $FeAl_{1-x}Ti_x$", *Solid State Commun.*, **95**(4), 263–266 (1995) (Crys. Structure, Experimental, 10)

[1995Pal] Palm, M., Inden, G., Thomas, N., "The Fe-Al-Ti System", *J. Phase Equilib.*, **16**(3), 209–222 (1995) (Crys. Structure, Phase Diagram, Phase Relations, Experimental, #, *, 34)

[1995Yan1] Yang, T.Y, Goo, E., "Phase Stability and Microstructure of Al-Ti-Fe near Al_3Ti", *Metall. Mater. Trans. A*, **26A**(5), 1029–1033 (1995) (Phase Diagram, Phase Relations, Experimental, 26)

[1995Yan2] Yanson, T.I., Manyako, N.B., Bodak, O.I., Cerny, R., Gladyshevskii, R.E., "Crystal Structure of $Fe_4Ti_{0.93}Al_{12.07}$, a Substitutional Variant of the Fe_4Al_{13} Structure Type", *J. Alloys Compd.*, **219**, 135–138 (1995) (Crys. Structure, Experimental, 8)

[1996Fu] Fu, C.L., Zou, J., "Site Preference of Ternary Alloying Additions in FeAl and NiAl by First-principles Calculations", *Acta Mater.*, **44**, 1471–1478 (1996) (Calculations, Theory, 18)

DOI: 10.1007/978-3-540-69761-9_13

[1996Mac] Machon, L., Sauthoff, G., "Deformation Behaviour of Al-Containing *C*14 Laves Phaes Alloys", *Intermetallics*, **4**, 469–481 (1996) (Phase Diagram, Phase Relations, Experimental,41)

[1996Pra] Prakash, U., Muraleedharan, K., "Effect of Titanium Substitution on the Structure and Properties of Fe_3Al-Based Intermetallic Alloys", *J. Mater. Sci.*, **31**, 1569–1573 (1996) (Crys. Structure, Experimental, 9)

[1997And] Anderson, I.M., "Alchemi Study of Site Distributions of 3*d*-Transition Metals in *B*2-Ordered Iron Aluminides", *Acta Mater.*, **45**(9), 3897–3909 (1997) (Calculation, Crys. Structure, Experimental, Theory, 26)

[1997Nis1] Nishino, Y., Kumada, C., Asano, S., "Phase Stability of Fe_3Al with Addition of 3d Transition Elements", *Scripta Mater.*, **36**, 461–466 (1997) (Crys. Structure, Phase Diagram, Phase Relations, Experimental, 26)

[1997Nis2] Nishino, Y., Asano, S., Ogawa, T., "Phase Stability and Mechanical Properties of Fe_3Al with Addition of Transition Elemnets", *Mater. Sci. Eng. A*, **A234-236**, 271–274 (1997) (Crys. Structure, Phase Diagram, Phase Relations, Experimental, 18)

[1998Akd] Akdeniz, M.V., Mekhrabon, A.O., "The Effect of Substitutional Impurities on the Evolution of Fe-Al Diffusion Layer", *Acta Mater.*, **46**(4), 1185–1192 (1998) (Theory, Thermodyn., Transport Phenomena, 55)

[1998Leo] Leonov, A.V., Fadeeva, V.I., Gladilina, O.E., Matyja, H., "Structure of $Al_{50}Ti_{50-x}Fe_x$ Alloys Prepared by Mechanical Alloying and Subsequent Annealing", *J.Alloys Compd.*, **281**, 275–279 (1998) (Crys. Structure, Phase Diagram, Phase Relations, Experimental, 13)

[1998Ohn] Ohnuma, I., Schoen, C.G., Kainuma, R., Inden, G., Ishida, K., "Ordering and Phase Separation in the b.c.c. Phase of the Fe-Al-Ti System", *Acta Mater.*, **46**(6), 2983–2094 (1998) (Calculation, Crys. Structure, Phase Diagram, Phase Relations, Experimental, Thermodyn., #, *, 22)

[1998Sun] Sun, Z.Q., Yang, W.Y., Shen, L.Z., Huang, Y.D., Zhang, B.S., Yang, J.L., "Neutron Diffraction Study on Site Occupation of Substitution Elements at Sub Lattices in Fe-Al Intermetallics", *Mater. Sci. Eng. A*, **258**, 69–74 (1998) (Crys. Structure, Experimental, Magn. Prop., Mechan. Prop., 19)

[1998Yam] Yamada, Y., Kuroda, K., Sakata, A., Murakami, T., "Magnetic Properties of $Ti(Fe_{1-x}Al_x)_2$", *J. Magn. Magn. Mater.*, **177-181**, 1397–1398 (1998) (Experimental, Magn. Prop., 6)

[1999Gor] Gorzel, A., Palm, M., Sauthoff, G., "Constitution-based Alloy Selection for the Screening of Intermetallic Ti-Fe-Al Alloys", *Z. Metallkd.*, **90**(1), 64–70 (1999) (Crys. Structure, Phase Diagram, Phase Relations, Experimental, #, *, 36)

[1999Hao] Hao, Y.L., Xu, D.S., Cui, Y.Y., Yang, R., Li, D., "The Site Occupancies of Alloying Elements in TiAl and Ti_3Al Alloys", *Acta Mater.*, **47**(4), 1129–1139 (1999) (Crys. Structure, Experimental, 41)

[1999Lee] Lee, S.M., Perng, T.P., "Correlation of Substitutional Solid Solution with Hydrogenation Properties of $TiFe_{1-x}M_x$ (M = Ni, Co, Al) Alloys", *J. Alloys Compd.*, **291**, 254–261 (1999) (Crys. Structure, Phase Diagram, Phase Relations, Experimental, 18)

[1999Lev] Levin, L., Tokar, A., Talianker, M., Evangelista, E., "Non-Equilibrium Microstructures in TiAl-2Fe Alloy", *Intermetallics*, **7**, 1317–1322 (1999) (Crys. Structure, Morphology, Experimental, 14)

[1999Li] Li, J., Zong, Y., Hao, S.H., "Effects of Alloy Elements (C, B, Fe, Si) on the Ti-Al Binary Phase Diagram", *J. Mater. Sci. Technol.*, **15**(1), 58–62 (1999) (Phase Diagram, Phase Relations, Experimental, *, 13)

[1999Mek] Mekhrabov, A.O., Akdeniz, M.V., "Effect of Ternary Alloying Elements Addition on Atomic Ordering Characteristics of Fe-Al Intermetallics", *Acta Mater.*, **47**(7), 2067–2075 (1999) (Calculation, Theory, Thermodyn., 63)

[1999Yam] Yamamoto, Y., Hashimoto, K., Kimura, T., Nobuki, M., Kohno, N., "$L1_2$ Single Phase Region in Al-Ti Base Ternary and Quaternary Systems at 1450K" (in Japanese), *J. Jpn. Inst. Met.*, **63** (10), 1317–1326 (1999) (Crys. Structure, Phase Diagram, Phase Relations, Experimental, 15)

DOI: 10.1007/978-3-540-69761-9_13

[2000Hao] Hao, Y.L., Yang, R., Cui, Y.Y., Li, D., "The Influence of Alloying on the $\alpha_2/(\alpha_2+\gamma)/\gamma$ Phase Boundaries in TiAl Based Systems", **48**, 1313–1324 (2000) (Experimental, Phase Relations, 41)

[2000Kai1] Kainuma, R., Fujita, Y., Mitsui, H., Ishida, K., "Phase Equilibria Among α (hcp), β (bcc) and γ ($L1_o$) Phases in Ti-Al Base Ternary Alloys", *Intermetallics*, **8**, 855–867 (2000) (Crys. Structure, Phase Diagram, Phase Relations, Experimental, #, *, 29)

[2000Kai2] Kainuma, R., Ohnuma, I., Ishukawa, K., Ishida, K., "Stability of *B*2 Ordered Phase in the Ti-Rich Portion of Ti-Al-Cr and Ti-Al-Fe Ternary Systems", *Intermetallics*, **8**, 869–875 (2000) (Crys. Structure, Phase Diagram, Phase Relations, Experimental, #, *, 19)

[2000Koi] Koike, J., Shimoyama, Y., Ohnuma, I., Okamura, T., Kainuma, R., Ishida, K., Maruyama, K., "Stress-Induced Phase Transformation During Superplastic Deformation in Two-Phase Ti-Al-Fe", *Acta Mater.*, **48**, 2059–2069 (2000) (Calculation, Crys. Structure, Phase Diagram, Phase Relations, Experimental, Thermodyn., 26)

[2000Mab] Mabuchi, H., Nagayama, H., Tsuda, H., Matsui, T., Mori, K., "Formation of Ternary $L1_2$ Intermetallic Compound and Phase Relation in the Al-Ti-Fe System", *Mater. Trans., JIM*, **41**(6), 733–738 (2000) (Crys. Structure, Phase Diagram, Phase Relations, Experimental, #, *, 50)

[2000Ni] Ni, J., Ashino, T., Iwata, S., "Kinetics of Ordering and Disordering in the Fe–Al–Ti Ternary Alloy", *Acta Mater.*, **48**, 3193–3199 (2000) (Theory, Crys. Structure, Phase Relations, Kinetics, 21)

[2000Ohn] Ohnuma, I., Fujita, Y., Mitsui, H., Ishikawa, K., Kainuma, R., Ishida, K., "Phase Equilibria in the Ti-Al Binary System", *Acta Mater.*, **48**, 3113–3123 (2000) (Calculation, Phase Diagram, Phase Relations, Experimental, Thermodyn., #, *, 37)

[2000Sha] Shan, A., Lin, D., "Low Temperature Superplasticity in Fe_3Al Alloy", *Key Eng. Mater.*, **171-174**, 349–354 (2000) (Experimental, Mechan. Prop., 11)

[2000Sun] Sundar, R.S., Kutty, T.R.G., Sastry, D.H., "Hot Hardness and Creep of Fe_3Al-based Alloys", *Intermetallics*, **8**, 427–437 (2000) (Experimental, Mechan.Prop., 50)

[2000Yan] Yang, R., Hao, Y., Song, Y., Guo, Z.X., "Site Occupancy of Alloying Additions in Titanium Aluminides and its Application to Phase Equilibrium Evaluation", *Z. Metallkd.*, **91**(4), 296–301 (2000) (Crys. Structure, Phase Diagram, Phase Relations, Review, 38)

[2000Zhu] Zhu, S.-M., Sakamoto, K., Tamura, M., Iwasaki, K., "A Comparative Study of the High Temperature Deformation Behavior of Fe-25Al and Fe-25Al-10Ti Alloys", *Scripta Mater.*, **42**, 905–910 (2000) (Experimental, Mechan.Prop., 15)

[2001Ish] Ishikawa, K., Hashi, K., Suzuki, K., Aoki, K., "Effect of Substitutional Elements on the Hydrogen Absorption-Desorption Properties of Ti_3Al Compounds", *J. Alloys Compd.*, **314**, 257–261 (2001) (Phase Diagram, Phase Relations, Experimental, 9)

[2000Izu] Izumi, T., Yoshioka, T., Hayashi, S., Narita, T., "Sulfidation Properties of TiAl-2 at.% X (X = V, Fe, Co, Cu, Nb, Mo, Ag and W) Alloys at 1173 K and 1.3 Pa Sulfur Pressure in an H_2S-H_2 Gas Mixture", *Intermetallics*, **8**, 891–901 (2000) (Crys. Structure, Experimental, 42)

[2001Pra] Prakash, U., Sauthoff, G., "Structure and Properties of Fe-Al-Ti Intermetallics Alloys", *Intermetallics*, **9**, 107–112 (2001) (Crys. Structure, Phase Diagram, Phase Relations, Experimental, Mechan. Prop., 7)

[2001Sun] Sun, F.-S., Cao, C.-X., Kim, S.-E., Lee, Y.-T., Yan, M.-G., "Alloying Mechanism of β Stabilizers in a TiAl Alloy", *Metall. Mater. Trans. A*, **32A**, 1573–1589 (2001) (Crys. Structure, Phase Diagram, Phase Relations, Experimental, Mechan. Prop., 37)

[2001Tok] Tokar, A., Berner, A., Levin, L, "The Origin of a New Phase Observed During Quenching of a TiAl-2Fe Alloy", *Mater. Sci. Eng. A*, **308**, 13–18 (2001) (Crys. Structure, Phase Diagram, Phase Relations, Experimental, 22)

[2001Zhu] Zhu, S.M., Sakamoto K, Tamura M, Iwasaki K, "Effects of Titanium Addition on the Microstructure and Mechanical Behavior of Iron Aluminide of Fe_3Al", *Mater. Trans. JIM*, **42**, 484–490 (2001) (Crystal Structure, Experimental, Mechan. Prop., 22)

DOI: 10.1007/978-3-540-69761-9_13

[2002Aze] Azez, K.A., AlL-Omari, I.A., Shobaki, J., Hasan, M.K., Al-Zoubi, G.M., Hamdeh, H.H., "Mössbauer Spectroscopic and Crystal Structure Investigation of the $Fe_{0.7-x}TixAl_{0.3}$ Alloy System", *Physica B*, **321**(1-4), 178–182 (2002) (Crys. Structure, Experimental, 16)

[2002Ban] Banerjee, R., Amancherla S., Banerjee, S., Fraser, H. L., "Modeling of Site Occupancies in *B*2 FeAl and NiAl Alloys with Ternary Additions", *Acta Mater.*, **50**, 633–641 (2002) (Theory, Crys. Structure, 21)

[2002Boz] Bozzolo, G.H., Noebe, R.D., Amador, C., "Site Occupancy of Ternary Additions to *B*2 Alloys", *Intermetallics*, **10**, 149–159 (2002) (Crys. Structure, Theory, 27)

[2002Bra] Brandt, C., Inal, O.T., "Mechanical Properties of Cr, Mn, Fe, Co, and Ni Modified Titanium Trialuminides", *J. Mater. Sci.*, **37**(20), 4399–4403 (2002) (Crys. Structure, Experimental, Mechan. Prop., 17)

[2002Ish] Ishikawa, K., Kainuma, R., Ohnuma, I., Aoki, K., Ishida, K., "Phase Stability of the X_2AlTi (X: Fe, Co, Ni and Cu) Heusler and *B*2-Type Intermetallic Compounds", *Acta Mater.*, **50**, 2233–2243 (2002) (Calculation, Phase Diagram, Phase Relations, Experimental, Thermodyn., 12)

[2002Rag] Raghavan, V., "Al-Fe-Ti (Alimunum-Iron-Titanium)", *J. Phase Equilib.*, **23**(4), 367–374 (2002) (Phase Diagram, Phase Relations, Review, *, 20)

[2002Su] Su, Y., Chen, Y.Q., Cao, Q.P., Ding, H.F., "Evolution of Rapidly Solidified Al-Ti-Fe System Alloys" (in Chinese), *Rare Met. Mater. Eng.*, **31**, 423–426 (2002) (Experimental, 4)

[2003Duc] Ducher, R., Stein, F., Viguier, B., Palm, M., Lacaze, J., "A Re-examination of the Liquidus Surface of the Al-Fe-Ti System", *Z. Metallkd.*, **94**(4), 396–410 (2003) (Phase Diagram, Phase Relations, Experimental, #, *, 34)

[2003Gry] Grytsiv, A., Ding, J.J., Rogl, P., Weill, F., Chevalier, B., Etourneau, J., Andre, G., Bouree, F., Noel, H., Hundegger, P., Wiesinger, G., "Crystal Chemistry of the G-phases in the Systems Ti-{Fe,Co,Ni}-Al with a Novel Filled Variant of the Th_6Mn_{23}-type", *Intermetallics,* **11**, 351–359 (2003) (Experimental, Crys. Structure, 26)

[2003Ino] Inoue, A., Kimura, H., Yamaura, S., "Production and Mechanical Properties of Aluminum Alloys with Dispersed Nanoscale Quasicrystalline and Amorphous Particles", *Met. Mater. Int.*, **9**, 527–536 (2003) (Crys. Structure, Experimental, Mechan. Prop., 31)

[2003Kel] Kellou, A., Fenineche, N.E., Grosdidier, T., Aourag, H., Coddet, C., "Structural Stability and Magnetic Properties in X_2AlX' (X = Fe, Co, Ni; X'= Ti, Cr) Heusler Alloys from Quantum Mechanical Calculations", *J. Appl. Phys.*, **94**, 3292–3298 (2003) (Calculation, Crys. Structure, Mechan. Prop., 27)

[2003Pan] Pandey, B., Nambissan, P.M.G., Suwas, S., Verma, H.C., "Mössbauer and Positron Annihilation Studies in Plastically Deformed $Fe_{72-x}Al_{28}Ti_x$ (x = 0, 2, 9) Alloys", *J. Mag. Magn. Mater.*, **263**, 307–314 (2003) (Crys. Structure, Experimental, 29)

[2003Ste] Stein, F., Schneider, A., Frommeyer, G., "Flow Stress Anomaly and Order-Disorder Transition in Fe_3Al-Based Fe-Al-Ti-X Allos with X = V, Cr, Nb, or Mo", *Intermetallics*, **11**(1), 71–82 (2003) (Crys. Structure, Experimental, Mechan. Prop., 53)

[2003Ter] Terashita, N., Nose, Y., Ikeda, T., Nakajima, H., Inui, H., Yamaguchi, M., "Diffusion of ^{59}Fe in γ-TiAl Single Crystals", *Mater. Lett.*, **57**, 3357–3360 (2003) (Experimental, Transport Phenomena, 9)

[2004Gua] Guan, X., Iwasaki, K., Kishi, K., Yamamoto, M., Tanaka, R., "Dry Sliding Wear Behavior of Fe-28Al and Fe-28Al-10Ti Alloys", *Mater. Sci. Eng. A*, **366**, 127–134 (2004) (Experimental, Kinetics, Mechan. Prop., Morphology, 19)

[2004Her] Herrman, J., Inden, G., Sauthoff, G., "Deformation Behaviour of Iron-rich Iron-Aluminium Alloys with Ternary Transition Metal Additions", *Steel Res. Int.*, **75**, 339–342 (2004) (Experimental, Mechan. Prop., 38)

[2004Nay] Nayak, S.S., Murty, B.S., "Synthesis and Stability of $L1_2$-Al_3Ti by Mechanical Alloying", *Mater. Sci. Eng. A*, **367**, 218–224 (2004) (Crys. Structure, Experimental, Morphology, Phase Relations, 25)

DOI: 10.1007/978-3-540-69761-9_13

[2004Pal] Palm, M., Sauthoff, G., "Deformation Behaviour and Oxidation Resistance of Single-phase and Two-phase $L2_1$-Ordered Fe-Al-Ti Alloys", *Intermetallics*, **12**, 1245–1259 (2004) (Experimental, Mechan. Prop., 89)

[2004Sch] Schmid-Fetzer, R, "Al-Ti (Aluminum-Titanium)", MSIT Binary Evaluation Program, in *MSIT Workplace*, Effenberg, G. (Ed.), MSI, Materials Science International Services GmbH, Stuttgart; Document ID: 20.15634.1.20 (2004) (Phase Diagram, Phase Relations, Review, #, *, 85)

[2005Gho] Ghosh, G., "Aluminium-Iron-Titanium", in "*Landolt-Boernstein, Numerical Data and Functional Relationships in Science and Technology (New Series). Group IV: Physical Chemistry*", Martienssen, W. (Ed.), "*Ternary Alloy Systems. Phase Diagrams, Crystallographic and Thermodynamic Data*", Vol. 11A2, Effenberg, G., Ilyenko, S. (Eds.), Springer-Verlag, Berlin, Heidelberg, 426–452 (2005) (Phase Diagram, Phase Relations, Assessment, Crys. Structure, 96)

[2005Gol] Golovin, I.S., Divinski, S.V., Cizek, J., Prochazka, I., Stein, F., "Study of Atom Diffusivity and Related Relaxation Phenomena in Fe_3Al-(Ti,Nb)-C Alloys", *Acta Mater.*, **53**, 2581–2594 (2005) (Experimental, Interface Phenomena, Transport Phenomena, 40)

[2005Pal] Palm, M., "Concepts Derived from Phase Diagram Studies for the Strengthening of Fe-Al-Based Alloys", *Intermetallics*, **13**, 1286–1295 (2005) (Review, Phase Relations, Phys. Prop., 81)

[2005Ste] Stein, F., Palm, M., Sauthoff, G., "Structure and Stability of Laves Phases Part II - Structure Type Variations in Binary and Ternary Systems", *Intermetallics*, **13**, 1056–1074 (2005) (Review, 249)

[2006Gry] Grytsiv, A., Rogl, P., Pomjakushin, V., "Structural Transition with Loss of Symmetry in Ti-M-Al Based G-phases (M = Fe and Co)", *Intermetallics*, **14**, 784–791 (2006) (Crys. Structure, Experimental, Phase Relations, *, 15)

[2006MSIT] "Al-Fe (Aluminum-Iron)", Diagrams as Published, in *MSIT Workplace*, Effenberg, G. (Ed.), Materials Science International Services, GmbH, Stuttgart; Document ID: 30.10236.1.20, (2006) (Crys. Structure, Phase Diagram, Phase Relations, 11)

[2006Pal] Palm, M., Lacaze, J., "Assessment of the Al-Fe-Ti System", *Intermetallics*, **14**, 1291–1303 (2006) (Phase Diagram, Phase Relations, Review, 126)

[2006Yan] Yan, X., Chen, X.-Q., Grytsiv, A., Witusiewicz, V.T., Rogl, P., Podloucky, R., Pomjakushin, V., Giesterd, G., "Site Preference, Thermodynamic, and Magnetic Properties of the Ternary Laves Phase $Ti(Fe_{1-x}Al_x)_2$ with the Crystal Structure of the $MgZn_2$-type", *Int. J. Mater. Res. (Z. Metallkd.)*, **97**, 450–460 (2006) (Crys. Structure, Experimental, Phase Relations, Thermodyn., *, 41)

[Mas2] Massalski, T.B. (Ed.), *Binary Alloy Phase Diagrams*, 2nd edition, ASM International, Metals Park, Ohio (1990)

[V-C] Villars, P. and Calvert, L.D., *Pearson's Handbook of Crystallographic Data for Intermetallic Phases*, ASM, Metals Park, Ohio (1985)

DOI: 10.1007/978-3-540-69761-9_13

Aluminium – Iron – Zinc

Gautam Ghosh

Introduction

Constitutional equilibria in the Al-Fe-Zn system is very important for the production of high quality Zn-coatings in steels by a process commonly known as hot-dip galvanizing. As a result, a large number of experimental studies have been carried out to determine the phase equilibria. The earlier results [1922Fue, 1934Fue, 1945May, 1947May, 1953Geb, 1953Ray, 1961Ren] on the phase equilibria were reviewed several times [1943Mon, 1952Han, 1961Phi, 1969Wat, 1976Mon]. [1953Ray] studied the solidification using about 150 ternary alloys, and also reported isothermal sections at 350 and 370°C. [1961Ren] investigated the phase equilibria in alloys containing up to 20 mass% Al and 20 mass% Fe. They reported isothermal sections at 600, 400°C and at room temperature. The most comprehensive study was carried out by [1970Koe] and [1971Koe]. They investigated a large number of alloys containing up to 60 mass% (Fe+Zn). The alloys were prepared using Armco-grade Fe and 99.99 mass% Al and Zn. The ternary alloys were prepared by adding either Fe or Zn to a master alloy of Fe:Al 50:50 or to pure Al. The solidification path and the isothermal sections were determined by means of thermal analysis, X-ray diffraction and microstructural investigations. They presented a reaction scheme, liquidus surface, nine isothermal sections in the temperature range of 250 to 700°C, and four temperature-composition sections. [1973Ure1] investigated the partial isothermal section at 450°C by means of metallography and electron microprobe analysis. They carried out equilibration experiments using solid Al-Fe intermetallic (FeAl, $FeAl_2$, Fe_2Al_5, or Fe_4Al_{13}) and either liquid Zn or Zn-1.71Al (mass%) alloy. Prepared samples in evacuated capsules were held at 450°C for 800 h followed by quenching in iced water. These results were critically assessed by [1992Gho] and [1992Rag].

Recently, there has been a renewed interest in the phase equilibria, particularly the Zn corner around 450°C, due to very stringent quality control requirements of galvanized steel sheets for the automotive industry. As a result, recent studies are focused primarily in experimental determination [1990Che, 1992Per, 1994Tan, 1995Tan2, 1996Tan, 1997Gyu, 1997Uwa1, 1999Tan] and CALPHAD modeling [1991Bel, 1992Per, 1999Cos, 2001Gio, 2002Bai] of phase equilibria of the Zn corner in the temperature range of 450 to 470°C. Due to rapid interfacial reaction between steel and liquid Al-Zn alloys, the importance of metastable equilibria [1991Bel, 1992Per, 2002Bai], diffusion path [1992Per, 1998Ada, 1998Uch1, 1998Uch2, 2002Bai], and the mechanism of phase transformations [1994Lin, 1995Lin1, 1995Lin2, 1995Tan1, 1995Yam2, 1997Mcd, 1997Mor, 1997Ser, 1998Ada, 1998Uch1, 1998Uch2, 1998Yam, 2002Bai] during interfacial reaction have also been elucidated.

[1990Che] prepared three ternary alloys using Al, Fe and Zn powders of unspecified purity. The final heat treatment of the alloys was annealing at 450°C for about 10 h. The phase equilibria were determined by XRD and SEM/EDX techniques. [1991Bel] determined the stable and metastable solubility limits of Fe in liquid (Zn) 447 to 480°C. [1992Per] determined the metastable and stable isothermal sections at 450°C based on the interfacial reaction studies between solid Al-Fe and liquid Al-Zn alloys. They used Al-Fe alloys containing 5, 29 and 36 at.% Al, and liquid Al-Zn alloys containing 0.12, 0.22, 0.39 and 11.2 at.% Al. Both short time (less than 30 min) and long time (1000 h) experiments were carried out. The phase compositions were determined by SEM/EDX technique. [1994Tan] reported an isothermal section of Zn corner at 470°C. Tang [1995Tan2, 1996Tan] reported the phase equilibria at 450°C by combining the results of [1990Che] and his experimental data of the Zn-corner. [1997Uwa1] prepared four ternary alloys by dry ball milling. They used elemental powders of following purity: 99.5% Al, 99.9+% Fe and 99.9% Zn. The ball milled powders were annealed at 300, 400 and 570°C for 3 h. They used DSC to study phase transformations, and XRD to identify the phases. Some of the controversial results of [1997Uwa1] have been the subject of extensive discussions [1997Tan, 1997Uwa2, 1998Tan, 1998Uwa]. [2000Tan] determined the Fe solubilities in dilute liquid Al-Zn alloys in the temperature range of 450 to 480°C. He prepared 16 ternary alloys containing up to 0.1 mass% Fe and up to 0.23 mass% Al using 99.5% pure Fe

DOI: 10.1007/978-3-540-69761-9_14

and Al, and special high grade Zn. The final equilibrations of encapsulated samples were carried out at 450, 465 and 485°C for 40 h followed by water quenching. The phase equilibria information were extracted from SEM/EDX analysis. [2002Tan] re-investigated the phase equilibria of the Zn corner at 435°C using six ternary alloys. They were annealed at 450°C for 15 days, and composition of phases were determined by SEM-EDS analysis. [2002Bai] reported a calculated isothermal section at 450°C.
These recent results have been reviewed by [2003Rag].

Binary Systems

The Al-Fe, Al-Zn and Fe-Zn binary phase diagrams are accepted from [2006MSIT], [2003Per] and [1982Kub], respectively.
There are some differences between the presently accepted binary phase diagrams and those accepted by the previous investigators [1953Ray, 1970Koe, 1971Koe]. For example, [1970Koe] and [1971Koe] accepted an Al-Fe phase diagram in which all the order-disorder transitions involving (αFe), α_1 and α_2 phases were considered to be first order, whereas in this assessment, (αFe) ⇌ α_2 and α_1 ⇌ α_2 reactions have been considered to be second order [1982Kub] reflected by the absence of the corresponding two-phase fields. Furthermore, the Al-Fe phase diagram has undergone slight modification due to recently established congruent melting behavior of the Fe_4Al_{13} phase [1986Len].
In the case of the Fe-Zn phase diagram, [1953Ray, 1970Koe] and [1971Koe] considered the δ phase to be stable between 672 and 620°C and the δ_1 phase to be stable below 640°C [1953Ray, 1970Koe, 1971Koe, 1973Ure1]. However, according to [1982Kub] the δ phase (which is the δ_1 phase as designated by the above authors) is stable below 665°C. It is worth mentioning that [1970Koe] and [1971Koe] convincingly established the δ phase at temperatures above the δ_1 phase field near the Zn corner, but later on [1973Ure1] failed to identify the δ phase above the δ_1 phase field. Also, according to [1982Kub], the Γ and δ phases react to form the Γ_1 phase at 550°C. This feature was also absent in the Fe-Zn phase diagram accepted by the previous studies [1953Ray, 1970Koe, 1971Koe, 1973Ure1]. Very recent study of solid-state equilibria of Zn rich alloys [2001Mit], and thermodynamic modeling of phase equilibria [2000Reu, 2001Su] are consistent with the Fe-Zn phase diagram assessed by [1982Kub].
In the Al-Zn phase diagram, the β phase designated by [1953Ray, 1970Koe, 1971Koe, 1973Ure1] is identical to (Al) in the phase diagram given by [1983Mur]. All these features are taken into account in this critical assessment of phase equilibria.

Solid Phases

Available data suggest that the solubility of Zn in α(Fe, Al) is a function of time of heat treatment at 450°C, with less Zn after shorter time compared to longer time. For example, [1990Che] gives 2 mass% Zn after 10 h at 450°C, while [1992Per] gives 2.26 mass% Zn after less than 30 min at 450°C and 4.85 mass% Zn after 1000 h at 450°C.
The equilibrium solubility of Zn in Fe_4Al_{13} at 450°C are 7 mass% [1973Ure1], 5.5 mass% [1990Che], 7.61 mass% [1992Per], while under metastable equilibrium Fe_4Al_{13} can dissolve up to 13.92 mass% [1992Per] and 15.2 mass% [1997Gyu]. [1953Ray] noted that the X-ray diffraction pattern of Zn containing Fe_4Al_{13} is slightly different from that of pure Fe_4Al_{13} which might be due to the slight structural alteration caused by the non-random occupation of the Zn atoms. [1992Per] reported that the presence of Zn in $FeAl_2$ is hardly detectable.
The solubility of Zn in Fe_2Al_5 (η) has been determined several times by reacting Fe with liquid Al-Zn bath containing varying amounts of Al [1971Ghu, 1973Har, 1973Ure1, 1973Ure2, 1984Nit, 1990Che, 1991Sai, 1992Per, 1997Gyu]. Available data fall in the range of 11 to 23 mass% Zn, and also show a systematic trend that the Zn-content in Fe_2Al_5 (η) is a function of reaction time. Due to rapid interdiffusion, the data after short time reaction show higher solubility of Zn in Fe_2Al_5 compared to long time experiments. For example, [1992Per] found 22.87 mass% Zn in Fe_2Al_5 after reaction at 450°C for less than 30 min compared to 18.7 mass% Zn after reaction at 450°C for 1000 h. [1971Ghu] noted a scatter of 14 to 17 mass% Zn in Fe_2Al_5 after reaction at 600°C for 10s. It is important to note that while short time reaction data is relevant to industrial galvanizing process, long time data is appropriate to construct the equilibrium phase diagram.

DOI: 10.1007/978-3-540-69761-9_14

Accordingly, we have accepted the solubility of 18.7 mass% Zn (11 at.%) at 450°C [1992Per] as equilibrium value. X-ray diffraction and density measurement show that Zn atoms reside on the Fe site for up to 6.7 at.% Zn giving the formula $Fe_4Zn_{10}Al$, and beyond this composition Zn atoms also reside on the Al sites giving the formula $Fe_4Zn_9Zn_2$ [2001Koe].
[1973Ure1] reported a solid solubility of 3.6 mass% Al in the δ phase ($FeZn_{10}$) at 450°C, which is in qualitative agreement with that of [1956Hor]. On the other hand, [1990Che] and [1992Per] reported solid solubilities of 2.8, 3.71, and 1.84 mass% Al at 450°C. Since the latter value was obtained after long time (1000 h) heat treatment, it is considered as equilibrium solid solubility while other values correspond to metastable equilibria. The ζ phase ($FeZn_{13}$) dissolves 0.78 mass% Al at 450°C [1992Per], but [1961Ren] gives a much lower value of 0.2 mass%. The solid solubilities of Al in Γ and Γ_1 phase at 450°C are similar to that in ζ phase [1992Per]. On the other hand, Tang's [1996Tan] isothermal section at 450°C show much higher solubility of Al in these two phases which may correspond to industrial galvanizing conditions.
[1992Per] reported two Γ Phases, Γ_1 (denoted as Γ_2 by [1992Per]) and Γ_2 (denoted as Γ_3 by [1992Per]), after equilibration for 1000 h at 450°C. However, [1973Ure1] did not detect any Γ_2 after 800 h equilibration at 450°C. On the hand, [1995Yam2] reported continuous solid solubility (Γ_1) and [1996Tan] reported continuous solid solubility (Γ′) in the isothermal sections at 440 and 450°C, respectively. It is possible that these conditions are realized during galvanizing process, and may not represent equilibrium. Later, [1998Yam] synthesized single phase alloys corresponding to Γ_2 and Γ_3 compositions of [1992Per], and diffusion annealing (conditions are not specified) of mechanically pressed Γ_2 and Γ_3 did not show any evidence of continuous solid solubility. Even though the crystallographic data of Γ_2 is lacking, available results suggest that it may be a ternary phase.
The details of the crystal structures and lattice parameters of the solid phases are listed in Table 1.

Invariant Equilibria

Based on the results of [1970Koe] and [1971Koe], the reaction scheme is summarized in Fig. 1. A number of changes have been made to comply with the binary phase diagrams accepted here. The reaction scheme proposed by [1970Koe] contained fourteen invariant reactions. However, three invariant reactions proposed to occur at 485, 440 and 320°C [1970Koe, 1971Koe] are not considered in Fig. 1 as they are not compatible with the presently accepted binary phase diagrams. The assessed reaction scheme is consistent with all the phase diagram information available until now. [1961Ren] proposed a ternary U type invariant reaction $L+FeAl_2 \rightleftharpoons \delta+Fe_2Al_5$ at 592°C; however, subsequent detailed investigations by [1970Koe, 1971Koe] and [1973Ure1] failed to detect this reaction.

Liquidus Surface

Figure 2 shows the liquidus surface from 20 to 70 mass% Al and 0 to 40 mass% Zn and Fig. 3 shows the liquidus surface of the Zn corner, both according to [1970Koe] and [1971Koe]. Results of solidification studies of Zn rich ternary alloys by [1945May, 11947May] and [1962May] and of Al/Zn rich alloys [1953Geb] agree quantitatively with those of [1970Koe] and [1971Koe].

Isothermal Sections

Figures 4, 5 and 6 show the isothermal sections at 700, 575 and 500°C, respectively, after [1970Koe] and [1971Koe]. Figure 7 shows the isothermal section of the Zn corner at 500°C [1970Koe, 1971Koe]. Figures 8 and 9 show partial isothermal section at 470 [1994Tan] and 460°C [2000Tan], respectively, depicting the solubility limits of Fe in liquid-Zn with respect to ζ ($FeZn_{13}$), δ ($FeZn_{10}$), and η (Fe_2Al_5) phases.
The isothermal section at 450°C has been investigated several times. There is substantial agreement between the earlier results of [1970Koe], [1971Koe] and [1973Ure1]. Recent significant results are due to [1990Che, 1992Per, 1995Tan2, 1996Tan]. Except for [1992Per] and [1996Tan], others did not consider Γ_1 phase in the 450°C isothermal section. Figure 10 shows the isothermal section at 450°C [1992Per]. Figure 11 shows the isothermal section of Zn corner depicting the phase fields involving liquid, ζ, δ, Γ_1

DOI: 10.1007/978-3-540-69761-9_14

and Γ_2 [1992Per]. [2002Tan] labelled as Γ_2 phase T. Despite qualitative agreement between the results of [1992Per], [1996Tan] and [2002Tan] at 450°C, the isothermal section of [1992Per] is preferred because the authors used much longer annealing time. Figure 12 shows the isothermal section at 450°C depicting the saturation limits of Fe with respect to ζ, δ, Γ_2 and η phase in liquid Zn [1996Tan]. Contrary to the suggestion of [1962Cam] that the solubility of Fe should decrease with Al content in liquid Zn, [1973Ure1] proposed that the solubility of Fe in liquid Zn at 450°C is 0.029 mass%, irrespective of the Al content. In fact, [1991Bel] showed that when η phase is in equilibrium with liquid Zn, indeed the Fe solubility decreases with increasing Al content in liquid Zn which is seen in Figs. 8, 9 and 12. Thermodynamic calculations also predict a similar behavior [2002Bai].
The isothermal section of the Zn-corner at 400°C [1970Koe, 1971Koe] is shown in Fig. 13. The Fe_4Al_{13}-Al-Zn partial isothermal sections at 350, 330, 300 and 250°C are shown in Figs. 14, 15, 16, 17, respectively according to [1970Koe] and [1971Koe]. A number of adjustments have been made in the isothermal sections in order to comply with the binary phase diagrams.
[1961Ren] studied the isothermal sections of the Zn corner with up to about 20 mass% (Fe+Al) at 600°C, 450°C and room temperature. At 600°C, [1961Ren] observed three-phase fields L+δ+$FeAl_2$ and L+Fe_2Al_5+$FeAl_2$, and proposed a ternary U type invariant reaction L+$FeAl_2$⇌δ+Fe_2Al_5 at 592°C. However, more detailed investigations by [1970Koe, 1971Koe] and [1973Ure1] failed to observe these features. The partial isothermal section at 450°C given by [1961Ren] agrees qualitatively with that of [1973Ure1], but the exact locations of the phase boundaries differ significantly. Because of these reasons, the results of [1961Ren] are not accepted here.

Temperature – Composition Sections

Figures 18, 19, 20 and 21 show isopleths at 30, 90, 95 and 98 mass% Zn, respectively [1970Koe, 1971Koe]. In Fig. 18, several changes have been made to comply with the accepted Al-Zn phase diagram.

Thermodynamics

[1995Yam1] reported the activity coefficient of Al in liquid Al-Zn alloys containing up to 10 mass% Zn, and in liquid Al-Fe-Zn alloys containing up to 1 mass% Al at 480°C. [1995Yam2] determined the chemical potential of Al in liquid Zn, in equilibrium with Fe_4Al_{13}, η (Fe_2Al_5), Γ_2, δ ($FeZn_{10}$), and ζ ($FeZn_{13}$) in the temperature range of 432 to 510°C. [1971Ghu] reported that the heat formation of Fe $(Al, Zn)_3$ is much more negative compared to the heat of formation of Fe_4Al_{13} and Fe_2Al_5 phases; however, the actual values reported by [1971Ghu] are very doubtful.
[2000Tan] reported that the solubility product of Fe_2Al_5 in liquid Zn can be expressed as
$\ln (\text{mass\% Al})^5(\text{mass\% Fe})^2 = 28.1 - 33066/T$
where T is the temperature in Kelvin. Besides, [2000Tan] has also discussed a procedure to calculate the solubility limits of Fe in liquid Zn with respect to saturation of ζ, δ and η phase. [1991Bel] reported solubility products of Fe_4Al_{13}, Fe_2Al_5, $FeAl_2$, FeAl and $FeZn_{13}$ in liquid Zn. Using the experimental solubility data, [2001Gio] has derived the Gibbs energy of formation of $Fe_2Al_5Zn_x$ (η). [2002Feu] measured the standard enthalpy of formation of ζ phase at $Fe_{0.07}Zn_{0.93}$ using solution calorimetry technique.
Several attempts have been made to calculate phase diagrams by CALPHAD method [1991Bel, 1992Per, 1999Cos, 2001Gio, 2002Bai]. Of particular interest is the prediction of solubility of Fe and Al in liquid Zn around 450°C, and also the diffusion path during hot-dip galvanizing process. [1991Bel] calculated metastable solubilities in liquid-Zn with respect to ζ+Fe_2Al_5, ζ+FeAl, ζ+Fe_4Al_{13} and ζ+$FeAl_2$ saturations at 447 and 477°C, and did not consider the δ phase. On the other hand [1992Per] calculated the solubility of Fe in liquid-Zn at 450°C considering all binary phases, and found a slightly higher solubility of Fe in liquid-Zn compared to [1991Bel] due to participation of the δ phase.
[1999Cos] calculated the 465°C isothermal section, but only the Zn-corner to understand the limiting factor controlling solubility of Fe in liquid Zn. They did not consider any ternary interaction parameter in the liquid phase and also the ternary solubility of Fe-Zn intermetallics. Nonetheless, the calculated activity coefficients of Al in liquid Zn-0.01 mass% Fe-*x*Al alloys are in good agreement with the experimental data of Yamaguchi *et al.* [1995Yam1, 1995Yam2]. Even though their calculated solubility limit of Fe_2Al_5 is in good

DOI: 10.1007/978-3-540-69761-9_14

agreement with experiment, the calculated three phase equilibrium L+Fe_2Al_5+Fe_4Al_{13} differs significantly from the experimental data [1995Yam2, 1998Yam].
[2002Bai] calculated the entire isothermal section at 450°C, and it appears that they overestimated the solid solubility of Al in ζ, Γ and Γ_1 phase compared to the experimental data of [1992Per]. Also, they did not consider the Γ_2 phase. Nonetheless, their calculation clearly shows a decrease in solubility of Fe in liquid Zn when it is in equilibrium with the η phase (Fe_2Al_5).

Miscellaneous

The solubility of Fe in a liquid Zn-4Al (mass%) alloy, in the temperature range of 400 to 675°C, was determined by [1963Fri]. The solubility can be expressed as
log (mass% Fe) = 3.6359 – 5149/T
log (at.% Fe) = 3.6825 – 5150/T
where T is the temperature in K.
Additions of Al to a liquid Zn bath inhibit the reaction between solid Fe and liquid Zn during the normal galvanizing process. It is believed that Al causes the formation of an inhibition layer, consisting of Fe_2Al_5, at the substrate/coating interface [1995Tan1]. However, detailed experiments using TEM/SEM/XRD techniques clearly show that the inhibition layer actually consists of Fe_2Al_5 and Fe_4Al_{13}. The details of the reactions and the formation sequences of the different binary intermetallic phases during the hot dip galvanizing process have been reported by [1965Sou, 1971Ghu, 1973Har, 1973Ure2, 1975Gut, 1984Nit, 1991Sag, 1995Lin1, 1995Lin2, 1995Tan1, 1997Mcd, 1997Ser, 1998Uch1, 1998Uch2]. Addition of Si also suppresses the rapid exothermic reaction between liquid Al-Zn and Fe by forming a solid reaction layer [1989Sel] which acts as a diffusion barrier. A comprehensive review of physical metallurgy of the galvanizing process has been presented by Marder [2000Mar].
[1998Akd] proposed that the value of activity coefficient of Al in α (Fe, Al, Zn) alloys has a strong influence on the formation and growth kinetics of interfacial diffusion layer. Besides, [2002Bai] compiled the diffusion data in ζ, δ, Γ and Γ_1 phases which were then used to model the mobility of components in these phases within CALPHAD formalism.
[1977Sho] investigated the effect of pressure on the reaction kinetics between solid Fe and liquid Zn-1.5Al (mass%) at 501°C. An applied pressure was found to cause the intermetallic compounds to become unstable and change the overall reaction rate from linear to non-linear. The stability of ζ phase, compared to other phases, under pressure is markedly affected by the presence of the Al in the melt.

Table 1. Crystallographic Data of Solid Phases

Phase/ Temperature Range [°C]	Pearson Symbol/ Space Group/ Prototype	Lattice Parameters [pm]	Comments/References
(Al)	*cF*4 $Fm\bar{3}m$ Cu	a = 404.88 a = 403.52 a = 403.29 a = 403.14	pure Al at 24°C [V-C] at 63.0 at.% Zn and 360°C [1983Mur] at 64.8 at.% Zn and 360°C [1983Mur] at 70.1 at.% Zn and 360°C [1983Mur]
(αFe)	*cI*2 $Im\bar{3}m$ W	a = 286.65	pure Fe at 20°C [V-C]
(Zn)	*hP*2 $P6_3/mmc$ Mg	a = 266.46 c = 494.61	pure Zn at 22°C [V-C]

(*continued*)

DOI: 10.1007/978-3-540-69761-9_14

Phase/ Temperature Range [°C]	Pearson Symbol/ Space Group/ Prototype	Lattice Parameters [pm]	Comments/References
α_1, Fe_3Al ≤ 552.5	*cF*16 $Fm\bar{3}m$ BiF_3	*a* = 578.86 to 579.3	[2006MSIT], solid solubility ranges from 22.5 to 36.5 at.% Al
α_2, FeAl ≤ 1310	*cP*2 $Pm\bar{3}m$ CsCl	*a* = 289.76 to 290.78	[2006MSIT], at room temperature solid solubility ranges from 22.0 to 54.5 at.% Al
ε, Fe_2Al_3 1232 - 1102	*cI*16?	*a* = 598.0	[2006MSIT], solid solubility ranges from 54.5 to 62.5 at.% Al
$FeAl_2$ ≤ 1156	*aP*18 *P*1 $FeAl_2$	*a* = 487.8 *b* = 646.1 *c* = 880.0 α = 91.75° β = 73.27° γ = 96.89°	[2006MSIT], at 66.9 at.% Al solid solubility ranges from 65.5 to 67.0 at.% Al
η, Fe_2Al_5 ≤ 1169	*oC*24 *Cmcm*	*a* = 765.59 *b* = 641.54 *c* = 421.84 *a* = 764.14 *b* = 642.76 *c* = 421.87 *a* = 762.23 *b* = 646.25 *c* = 423.00	[2006MSIT], at 71.5 at.% Al solid solubility ranges from 71.0 to 72.5 at.% Al. Equilibrium solubility is up to 11 at.% Zn at 450°C [1992Per]. [2001Koe], at $Fe_4Al_{10}Zn$ [2001Koe], at $Fe_4Al_9Zn_2$
Fe_4Al_{13} ≤ 1160	*mC*102 *C*2/*m* Fe_4Al_{13}	*a* = 1552.7 to 1548.7 *b* = 803.5 to 808.4 *c* = 1244.9 to 1248.8 β = 107.7 to 107.99° *a* = 1549.2 *b* = 807.8 *c* = 1247.1 β = 107.69	[2006MSIT], 74.16 to 76.7 at.% Al solid solubility ranges from 74.5 to 75.5 at.% Al [2006MSIT], at 76.0 at.% Al sometimes called $FeAl_3$ in the literature
Γ, Fe_3Zn_{10} ≤ 782	*cI*52 $I\bar{4}3m$ Fe_3Zn_{10} ? Cu_5Zn_8	*a* = 897.41 *a* = 901.8	[V-C], solid solubility ranges from 68.0 to 82.5 at.% Zn
Γ_1, $Fe_{11}Zn_{39}$ ≤ 550	*cF*408 $F\bar{4}3m$ $Fe_{11}Zn_{39}$	*a* = 1796.3	[V-C2], solid solubility ranges from 75.5 to 81.0 at.% Zn
δ, $FeZn_{10}$ ≤ 665	*hP*555 $P6_3mc$	*a* = 1283.0 *b* = 5770.0	[V-C], solid solubility ranges from 86.5 to 92.0 at.% Zn. Equilibrium solubility

(*continued*)

DOI: 10.1007/978-3-540-69761-9_14

Phase/ Temperature Range [°C]	Pearson Symbol/ Space Group/ Prototype	Lattice Parameters [pm]	Comments/References
	$FeZn_{10}$		is up to 4.3 at.% Al at 450°C [1992Per].
ζ, $FeZn_{13}$ ≤ 530	*mC*28 *C*2/*m* $CoZn_{13}$	*a* = 1342.4 *b* = 760.8 *c* = 506.1 β = 127.3°	[V-C], solid solubility ranges from 92.5 to 94.0 at.% Zn. Equilibrium solubility is up to 1.85 at.% Al at 450°C [1992Per].
Γ_2, $AlFe_{14}Zn_{1.5}$ ≤ 450 (?)	-	-	[1992Per, 1998Yam]

DOI: 10.1007/978-3-540-69761-9_14

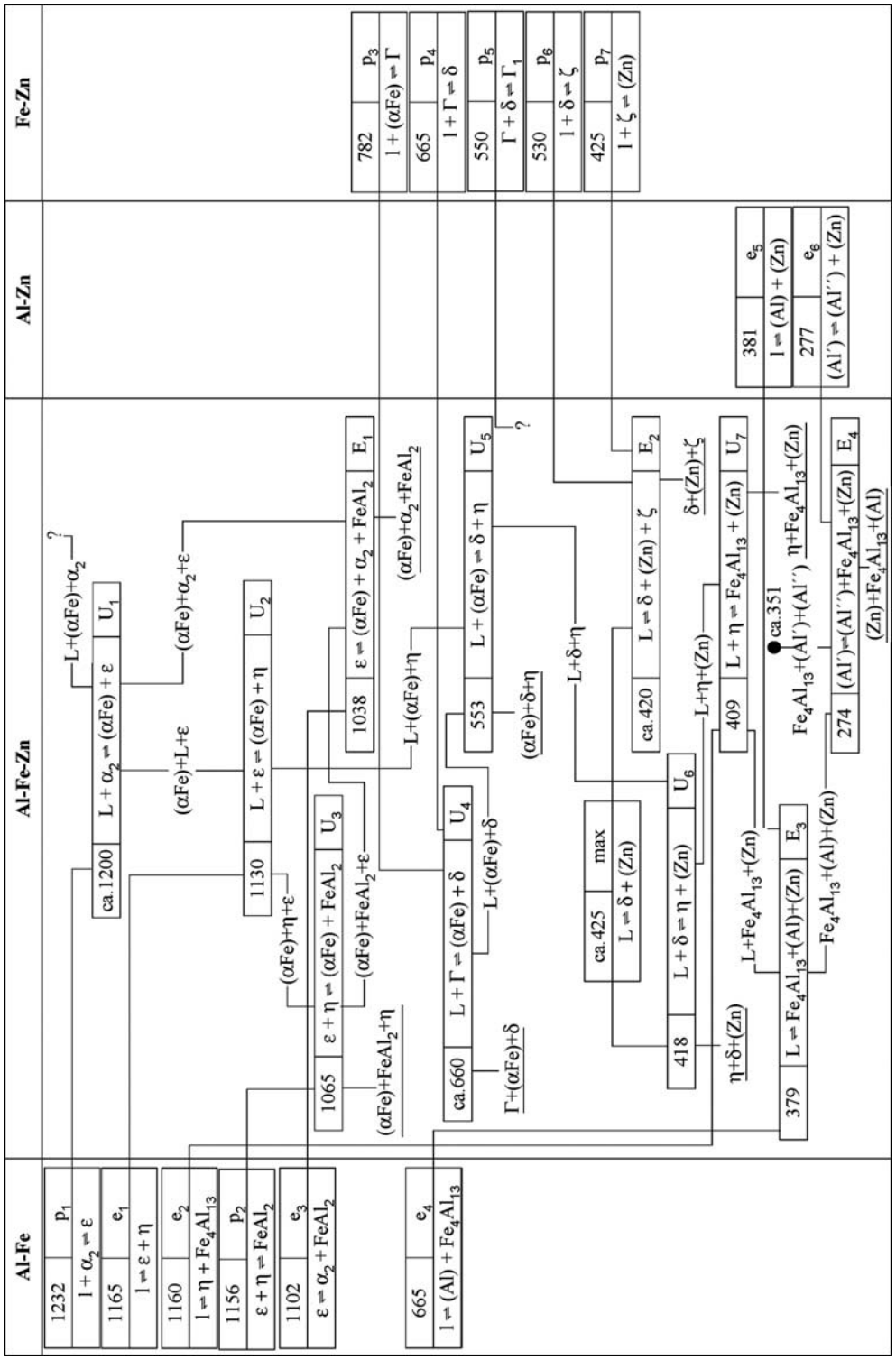

Fig. 1. Al-Fe-Zn. Reaction scheme

DOI: 10.1007/978-3-540-69761-9_14

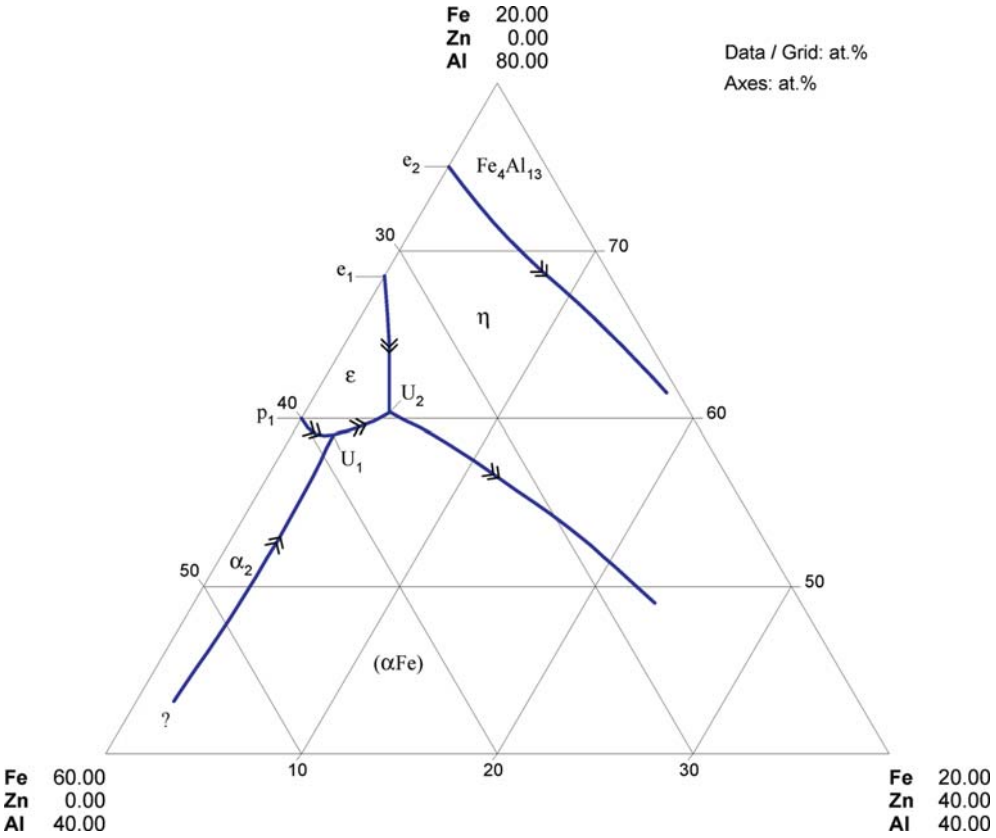

Fig. 2. Al-Fe-Zn. Partial liquidus surface

DOI: 10.1007/978-3-540-69761-9_14

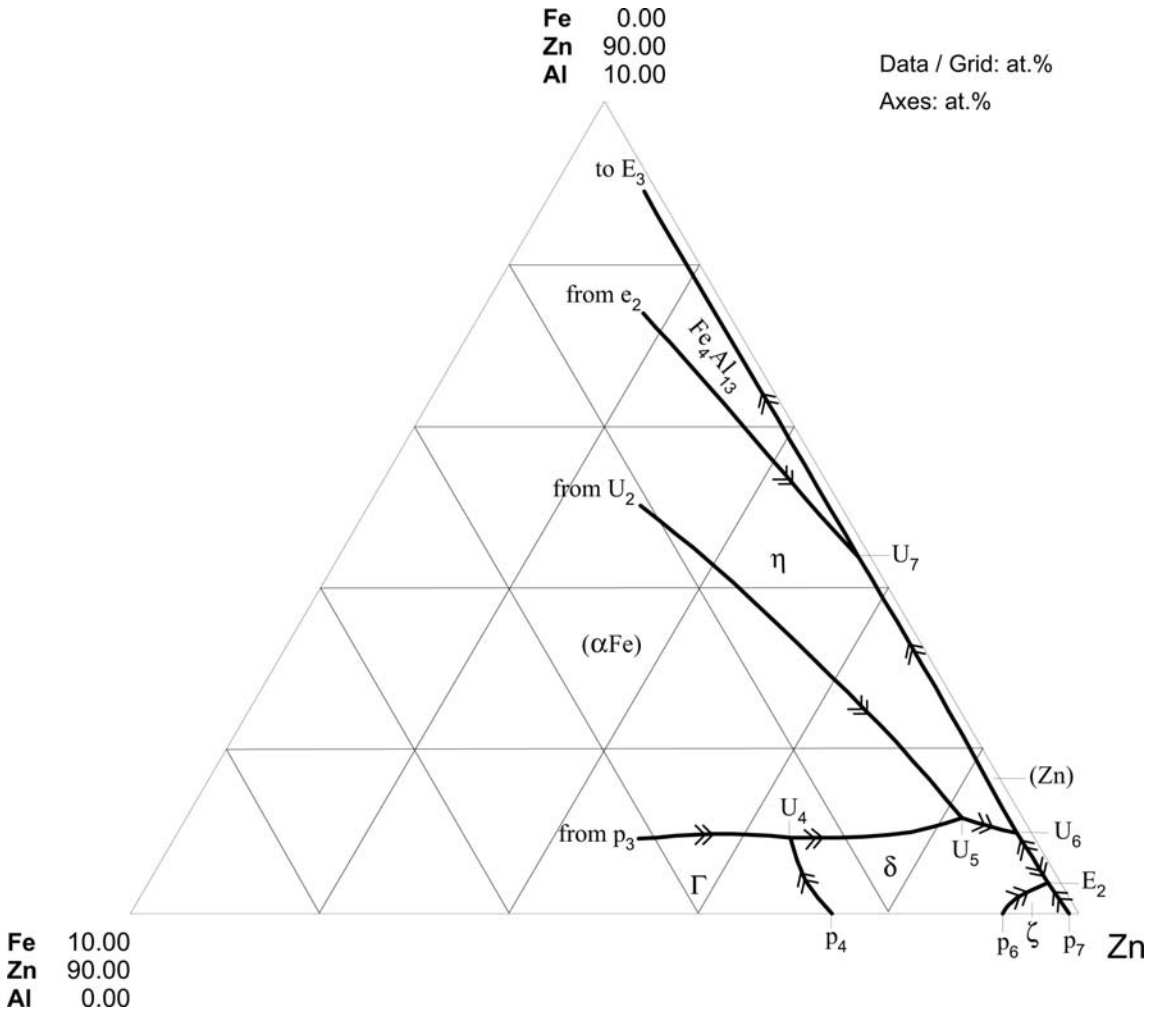

Fig. 3. Al-Fe-Zn. Liquidus surface of the Zn corner

DOI: 10.1007/978-3-540-69761-9_14

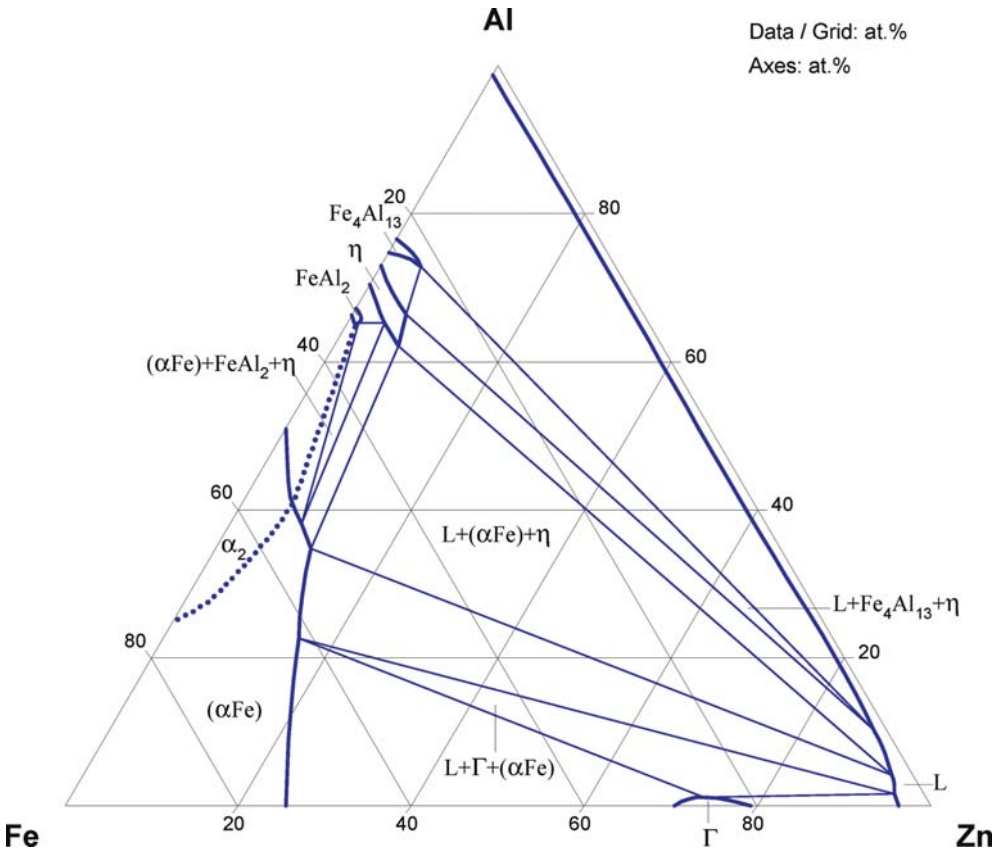

Fig. 4. Al-Fe-Zn. Isothermal section at 700°C

DOI: 10.1007/978-3-540-69761-9_14

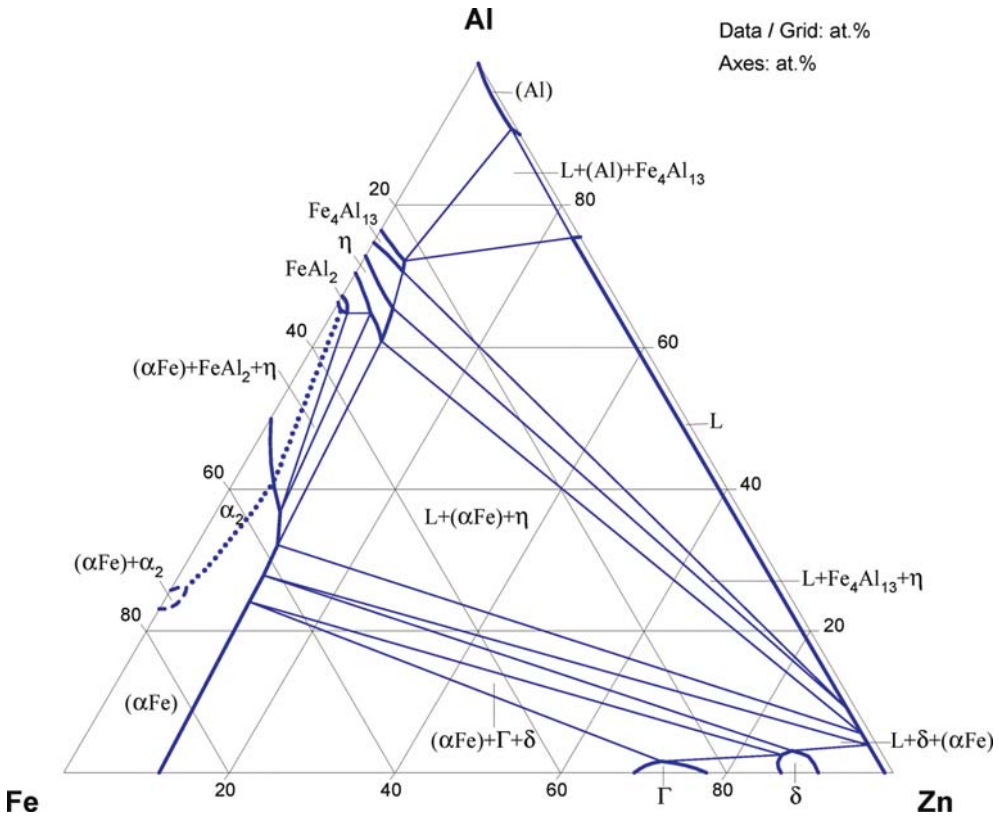

Fig. 5. Al-Fe-Zn. Isothermal section at 575°C

DOI: 10.1007/978-3-540-69761-9_14

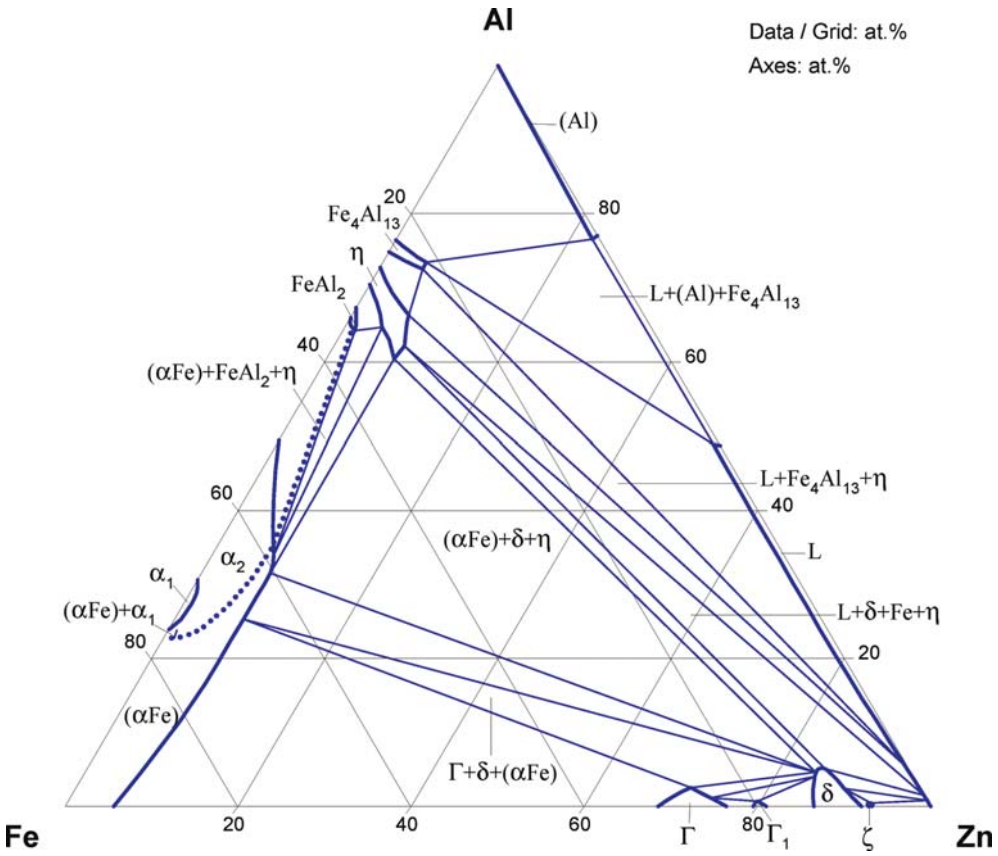

Fig. 6. Al-Fe-Zn. Isothermal section at 500°C

DOI: 10.1007/978-3-540-69761-9_14

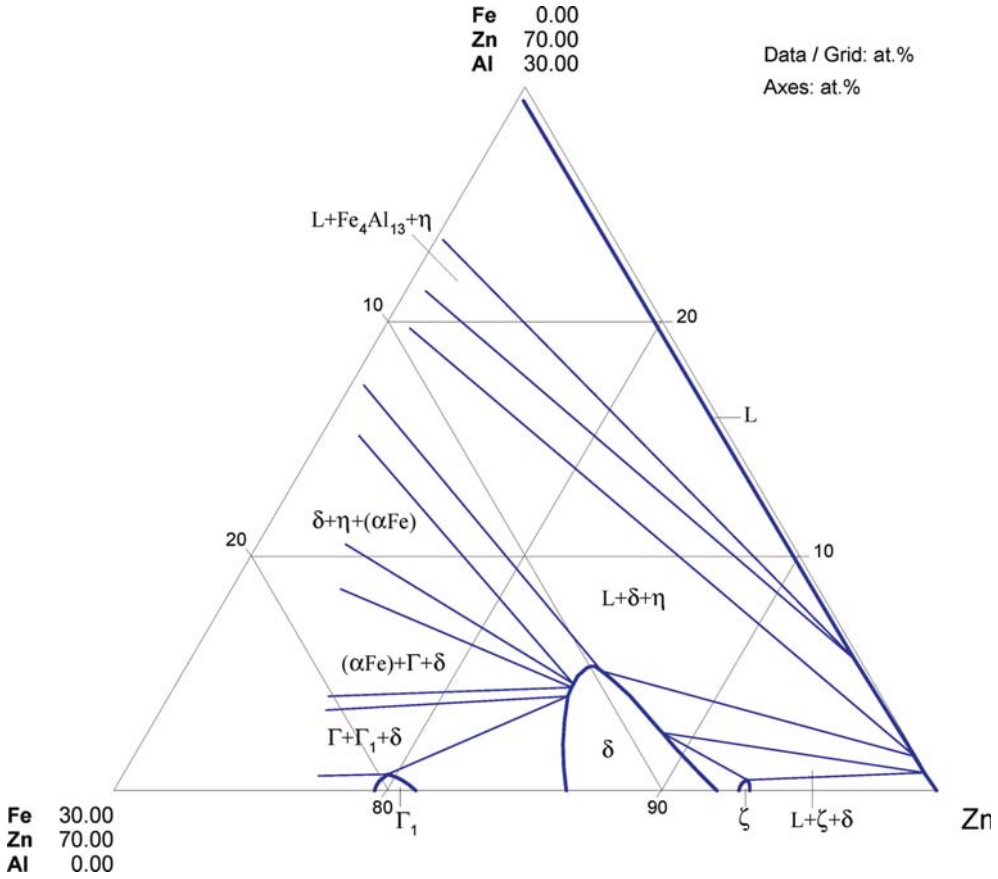

Fig. 7. Al-Fe-Zn. Partial isothermal section at 500°C

DOI: 10.1007/978-3-540-69761-9_14

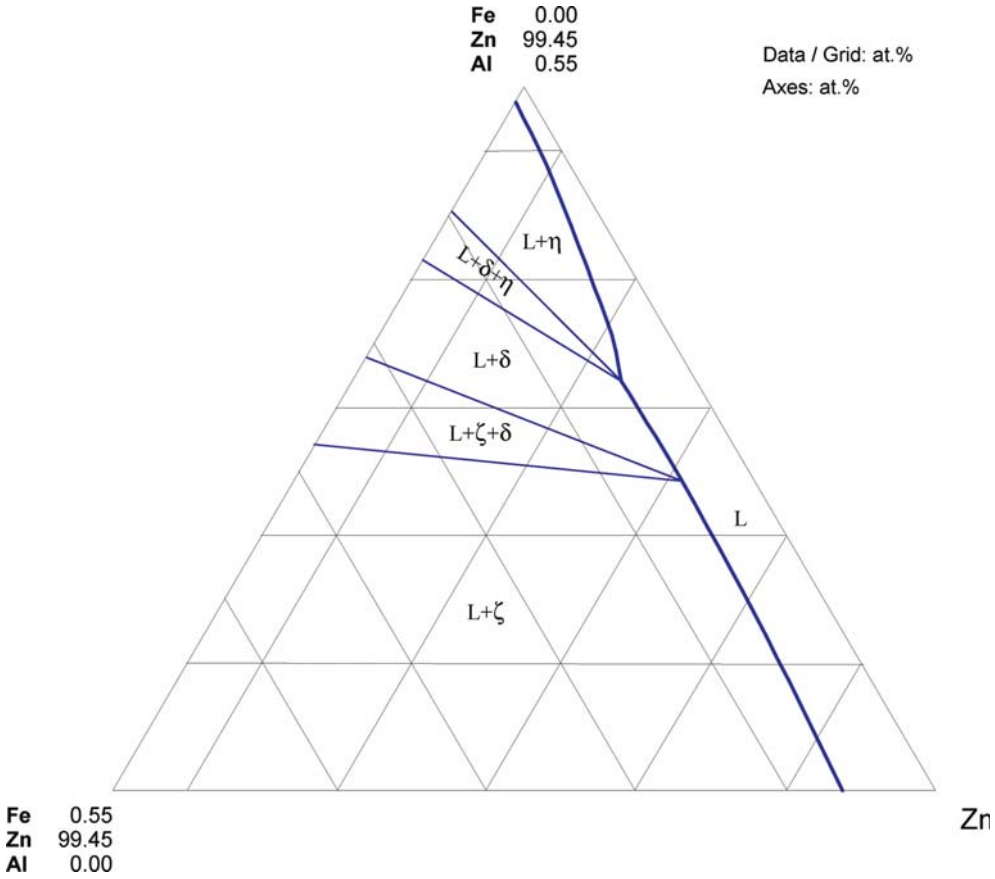

Fig. 8. Al-Fe-Zn. Partial isothermal section at 470°C

DOI: 10.1007/978-3-540-69761-9_14

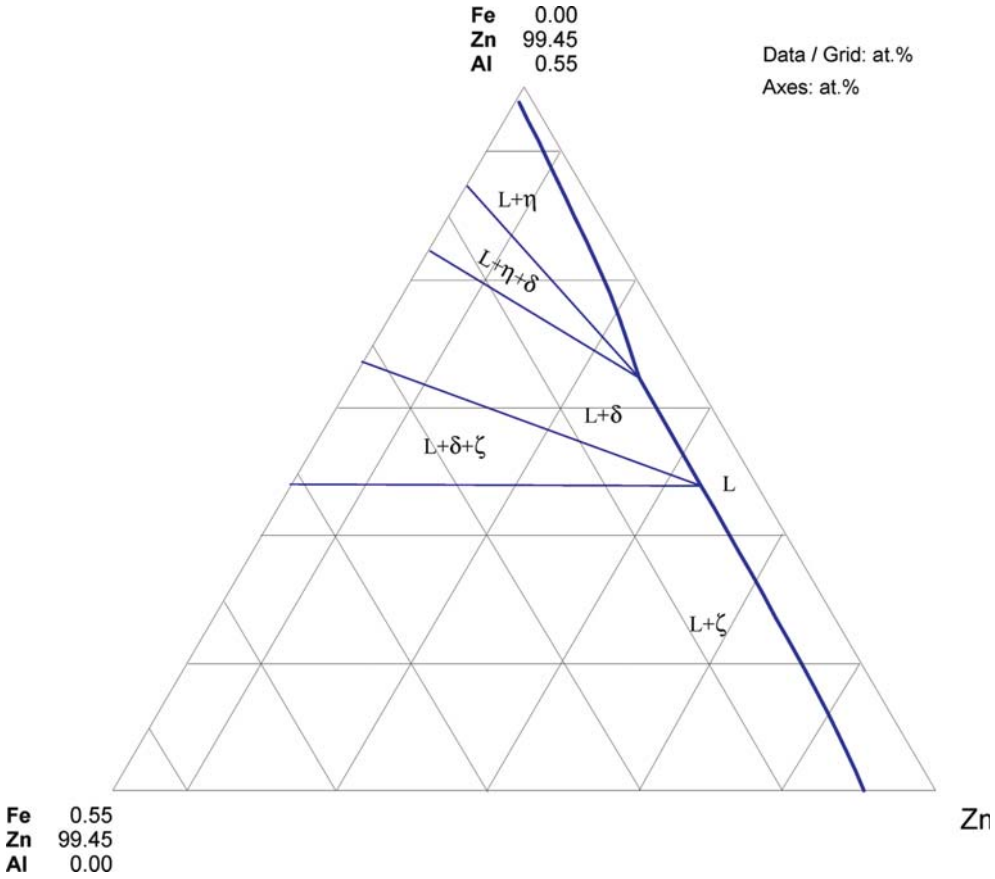

Fig. 9. Al-Fe-Zn. Partial isothermal section at 460°C

DOI: 10.1007/978-3-540-69761-9_14

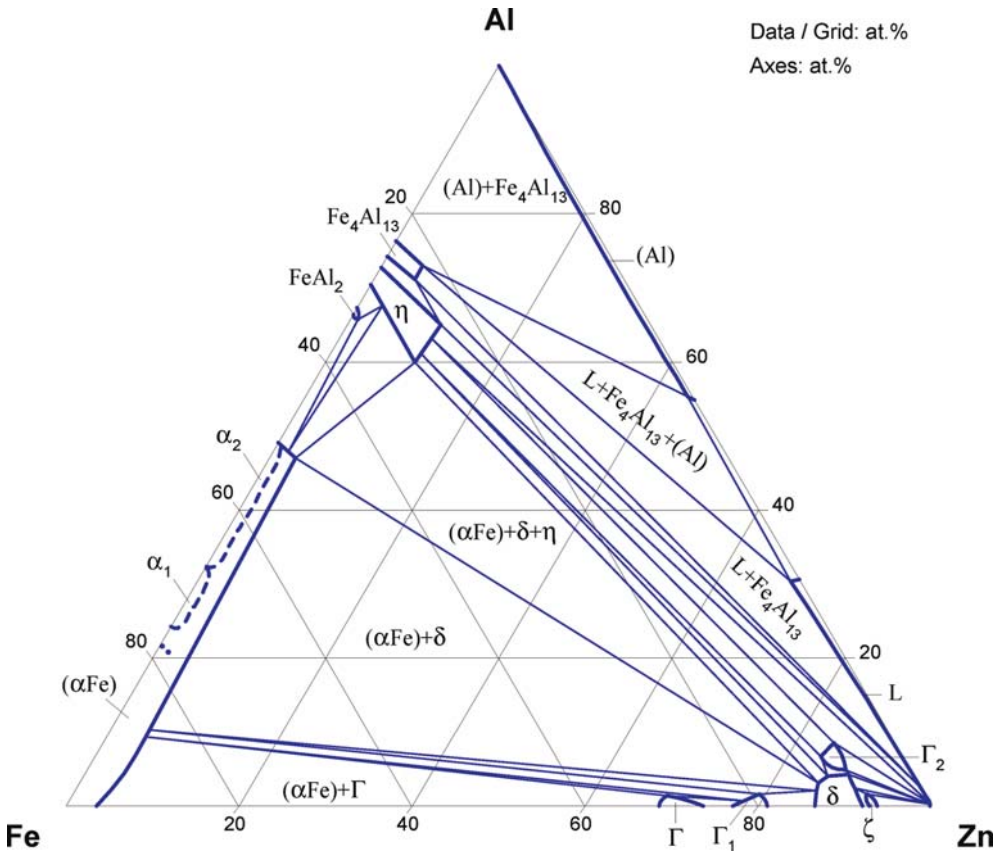

Fig. 10. Al-Fe-Zn. Isothermal section at 450°C

DOI: 10.1007/978-3-540-69761-9_14

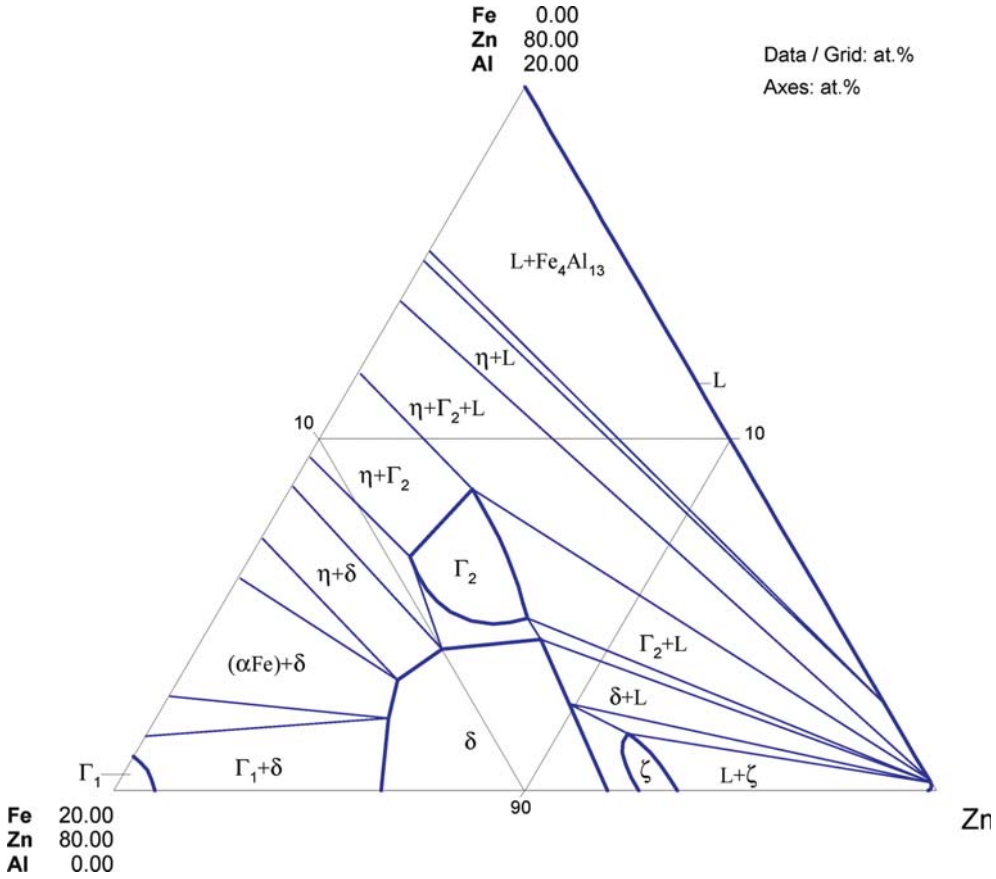

Fig. 11. Al-Fe-Zn. Partial isothermal section at 450°C

DOI: 10.1007/978-3-540-69761-9_14

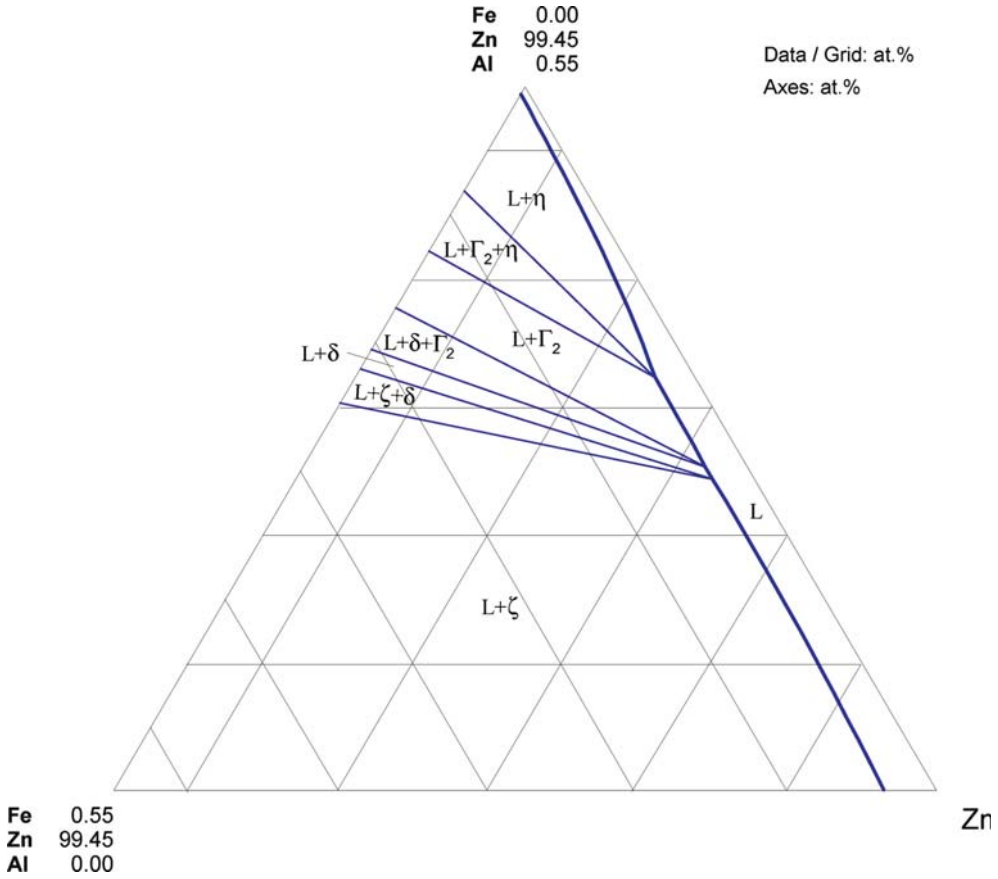

Fig. 12. Al-Fe-Zn. Partial isothermal section at 450°C

DOI: 10.1007/978-3-540-69761-9_14

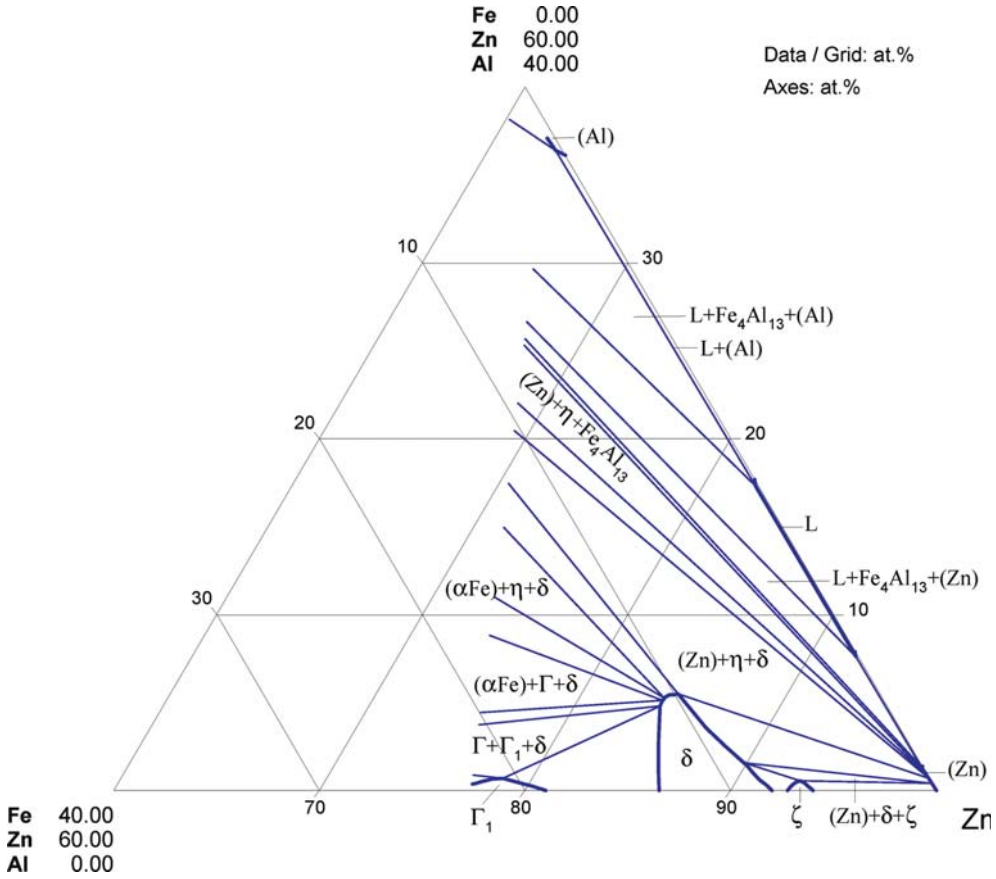

Fig. 13. Al-Fe-Zn. Partial isothermal section at 400°C

DOI: 10.1007/978-3-540-69761-9_14

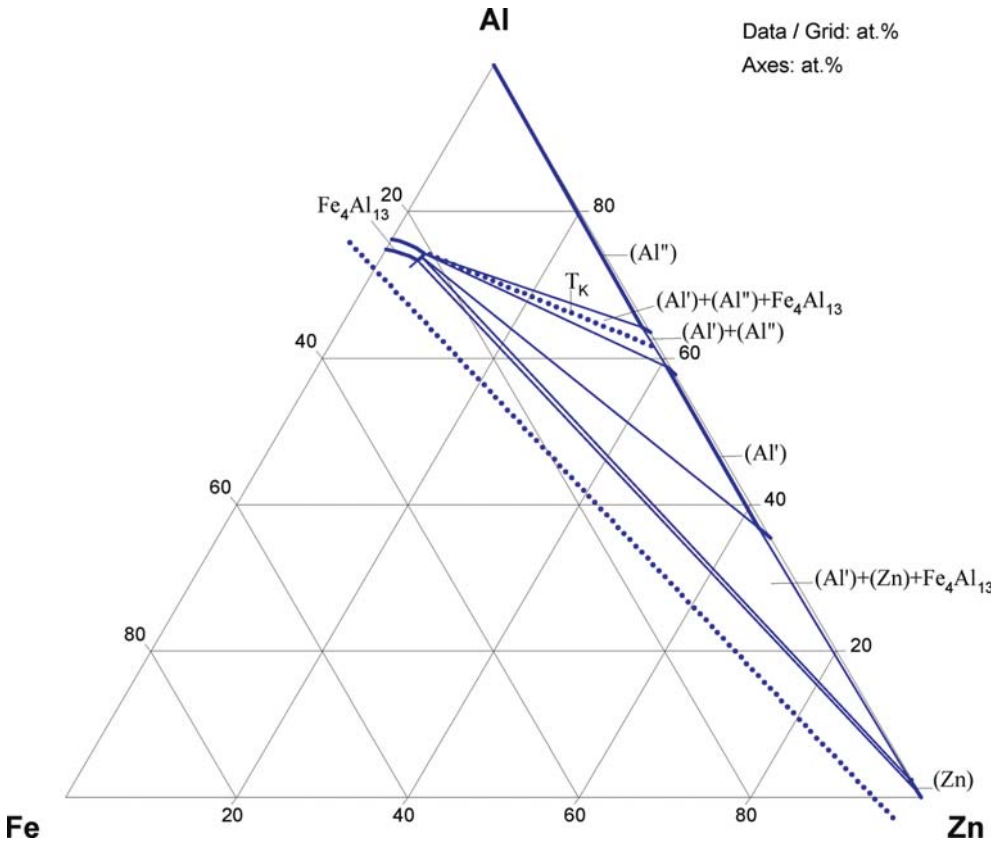

Fig. 14. Al-Fe-Zn. Partial isothermal section at 350°C

DOI: 10.1007/978-3-540-69761-9_14

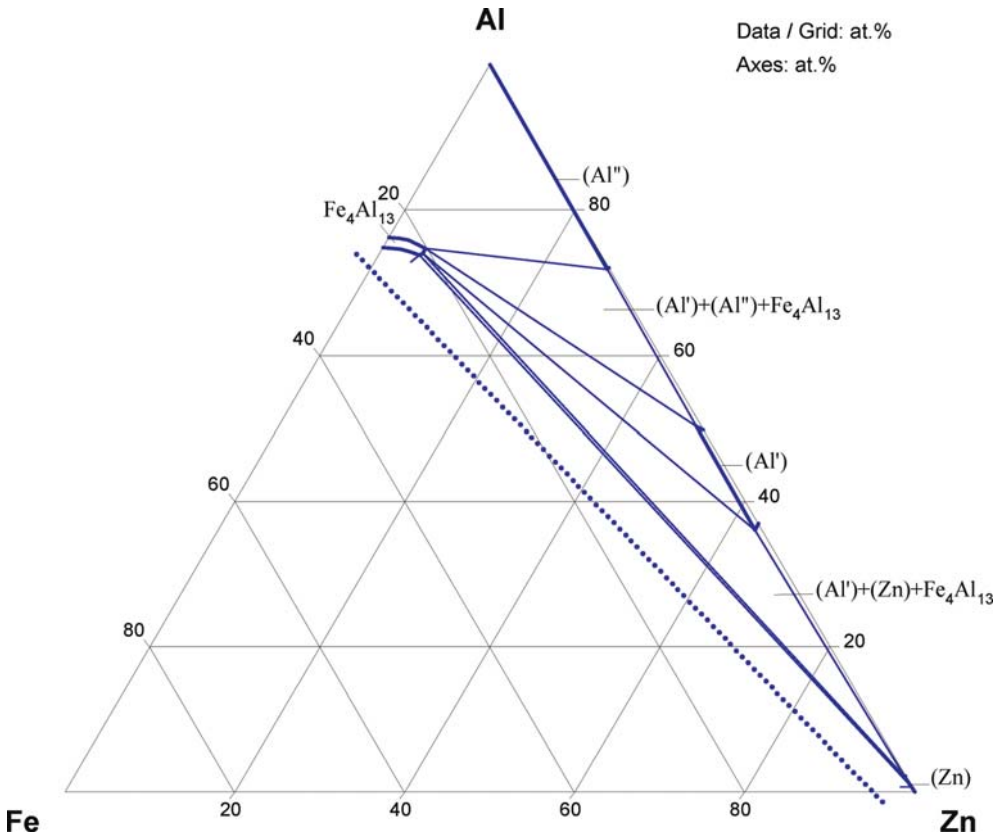

Fig. 15. Al-Fe-Zn. Partial isothermal section at 330°C

DOI: 10.1007/978-3-540-69761-9_14

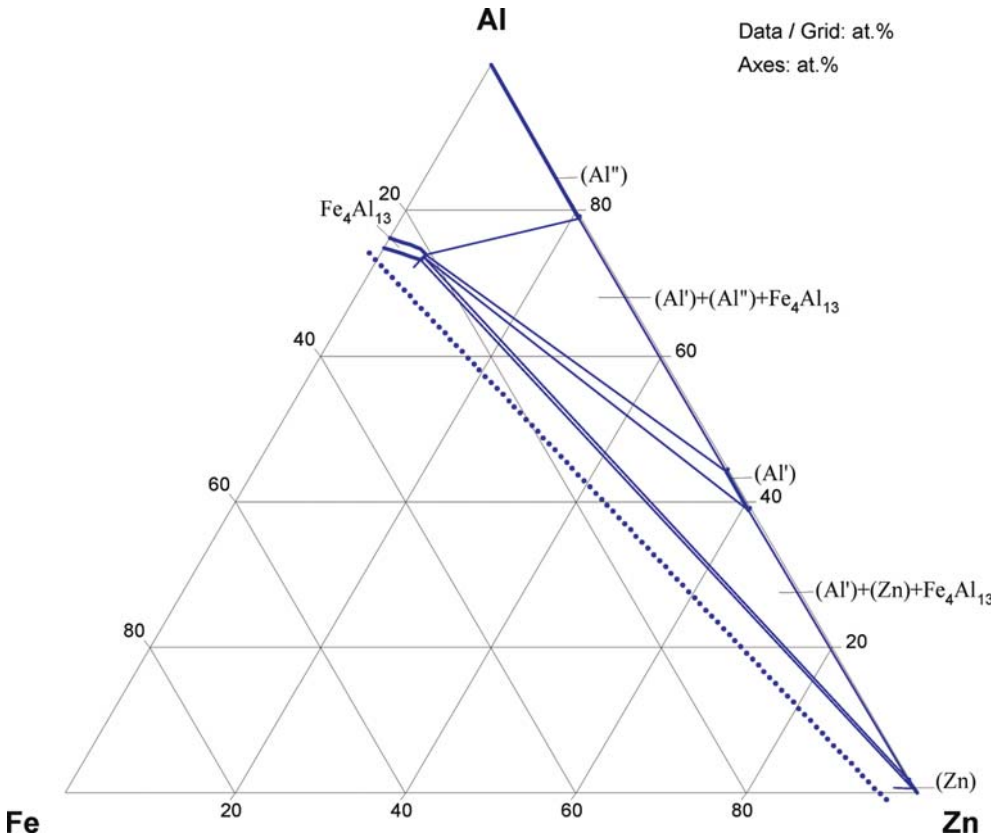

Fig. 16. Al-Fe-Zn. Partial isothermal section at 300°C

DOI: 10.1007/978-3-540-69761-9_14

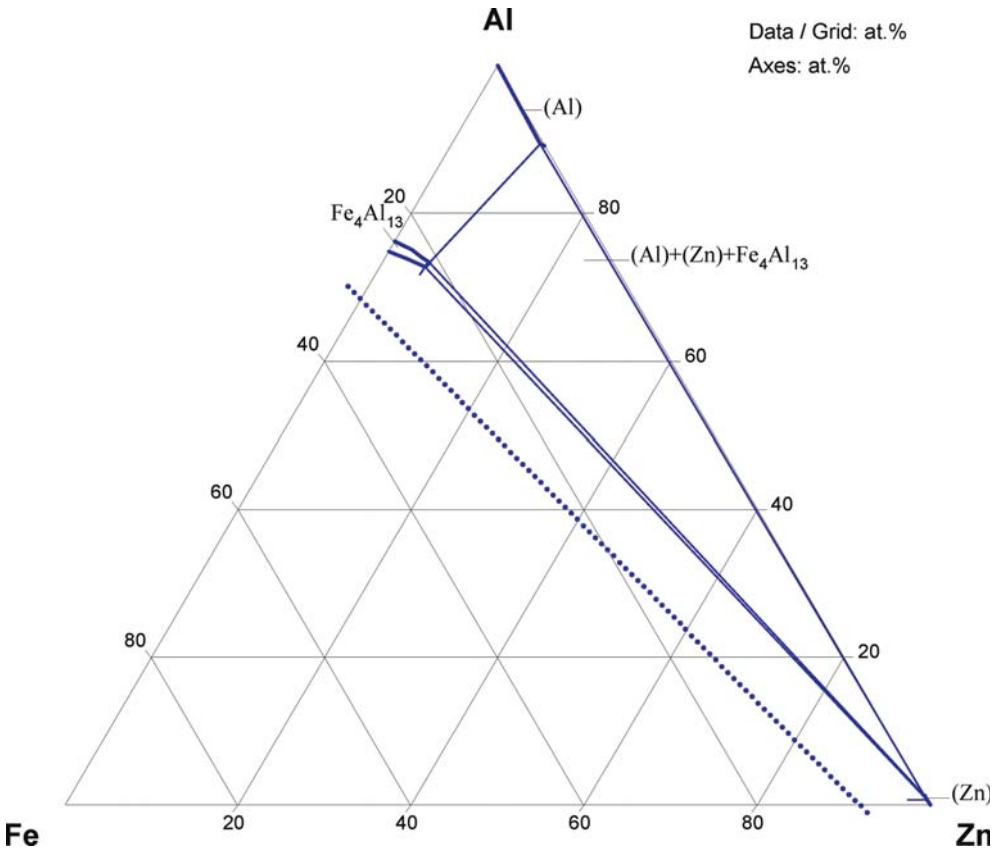

Fig. 17. Al-Fe-Zn. Partial isothermal section at 250°C

DOI: 10.1007/978-3-540-69761-9_14

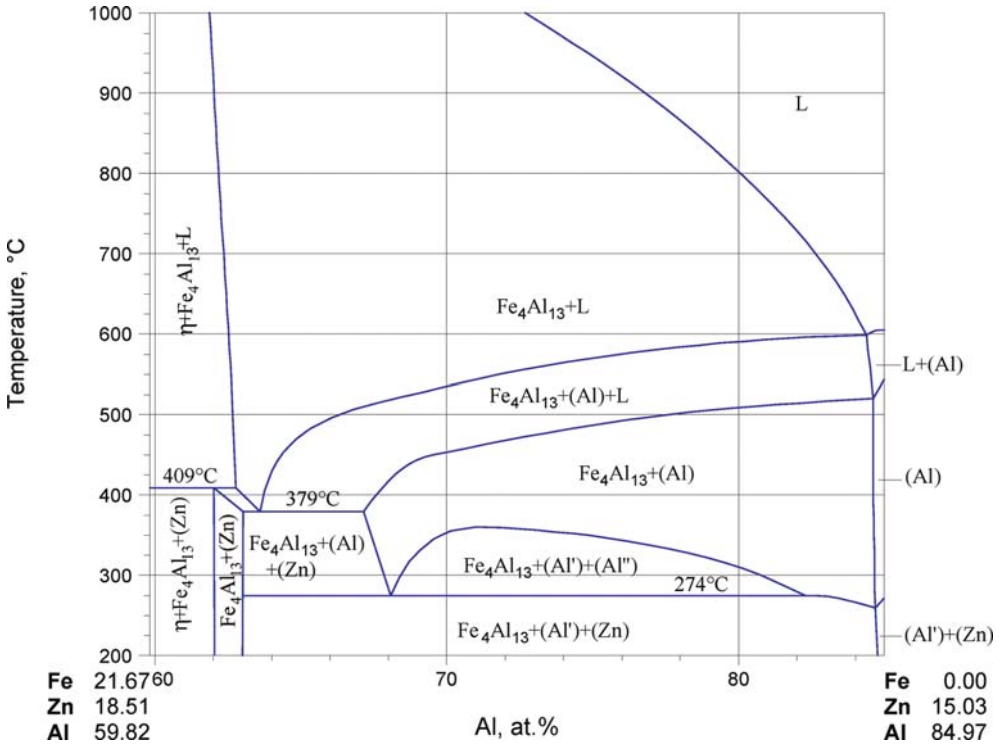

Fig. 18. Al-Fe-Zn. Section at a constant Zn-content of 30 mass%

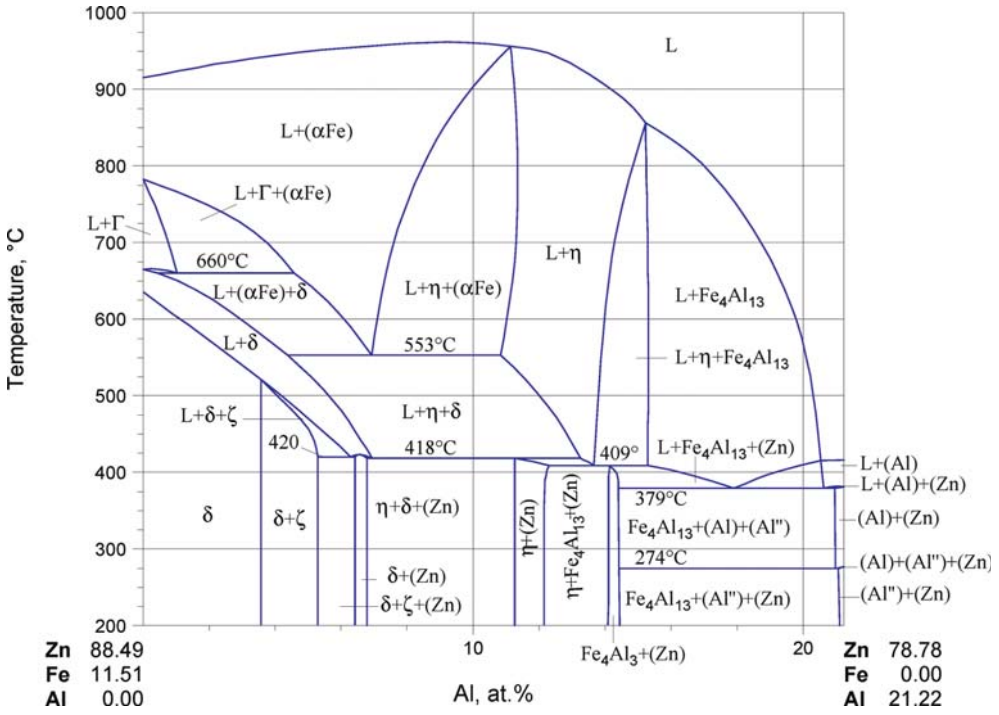

Fig. 19. Al-Fe-Zn. Vertical section at a constant Zn-content of 90 mass%

DOI: 10.1007/978-3-540-69761-9_14

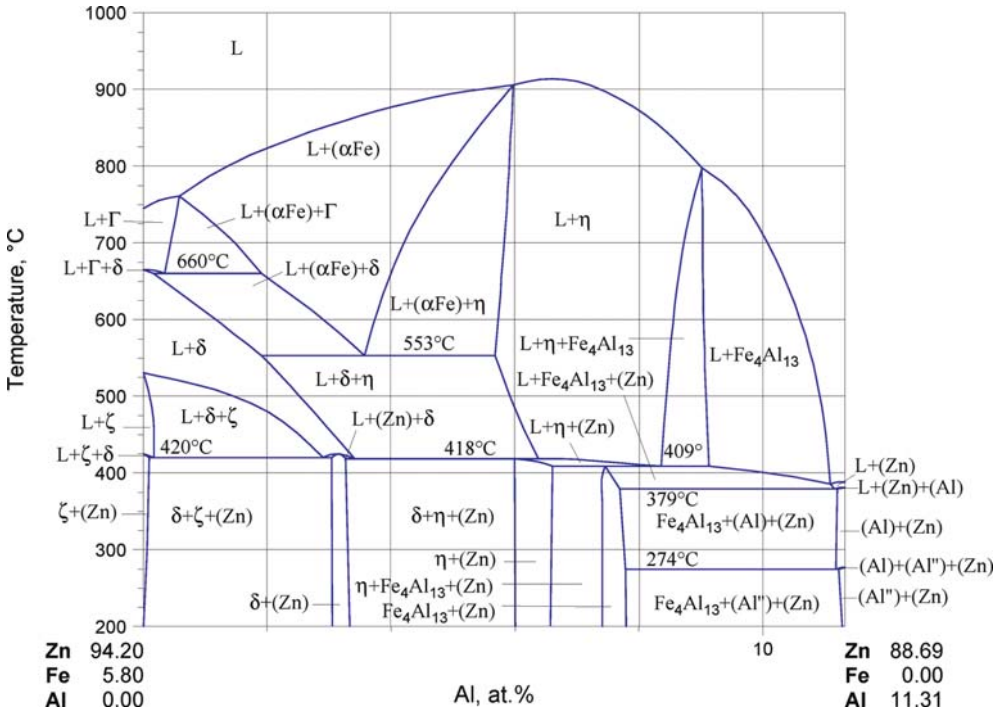

Fig. 20. Al-Fe-Zn. Vertical section at a constant Zn-content of 95 mass%

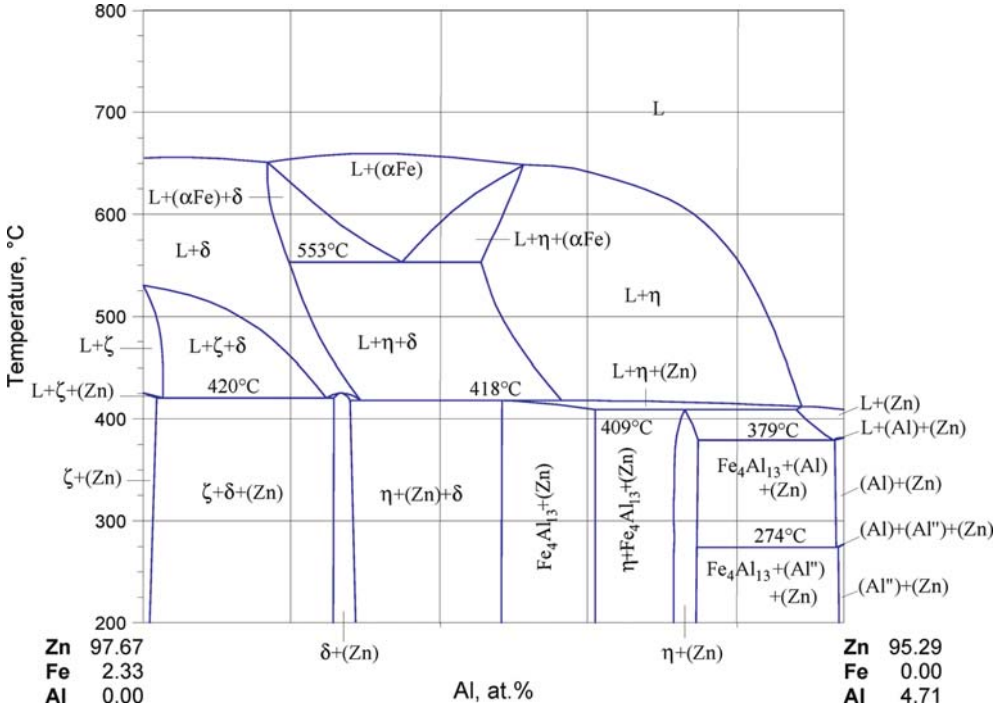

Fig. 21. Al-Fe-Zn. Vertical section at a constant Zn-content of 98 mass%

DOI: 10.1007/978-3-540-69761-9_14

References

[1922Fue] Fuess, V., "Aluminium-Zinc-Iron" in *Metallography of Aluminium and its Alloys* (in German), 157–159 (1922) (Phase Diagram, Phase Relations, Review, 2)

[1924Fus] Fuss, V., "On the Constitution of Ternary Alloys of Aluminium" (in German) *Z. Metallkd.*, **16**, 24–25 (1924) (Phase Diagram, Phase Relations, Experimental, 5)

[1934Fue] Fuess, V., "Aluminium-Zinc-Iron" in "*Metallography of Aluminium and its Alloy*" (in German), 157–159 (1934) (Phase Diagram, Phase Relations, Review, 1)

[1943Mon] Mondolfo, L.F., "Aluminium-Iron-Zinc", in "*Metallography of Aluminum Alloys*", John Wiley and Sons, Inc., New York (1943) 98–99 (Phase Diagram, Review, 1)

[1945May] Mayer, A., "Investigation of the Ternary Zinc-Aluminium-Iron System" (in Italian), *Metallurgia Italiana*, **37**, 95–98 (1945) (Phase Diagram, Phase Relations, Experimental, 33)

[1947May] Mayer, A., "The Ternary System: Zinc-Aluminium-Iron"(in Italian), *Gazz. Chim. Ital.*, **77**, 55–66 (1947) (Phase Diagram, Phase Relations, Experimental)

[1952Han] Hanemann, H., Schrader, A., "Aluminium-Zinc-Iron" in " *Ternary Alloys of Aluminium*" (in German), Atlas Metallographicus, Verlag Stahleisen, Düsseldorf, **3**(2), 157–159 (1952) (Review, 1)

[1953Geb] Gebhardt, E., "Investigation on the Ternary Aluminium-Iron-Zinc" (in German). *Z. Metallkd.*, **44**, 206–211 (1953) (Phase Diagram, Phase Relations, Experimental, 18)

[1953Ray] Raynor, G.V., Faulkner, C.R., Noden, J.D., Harding, A.R., "Ternary Alloys Formed by Aluminium, Transitional Metals and Divalent Metals", *Acta Met.*, **1**, 629–648 (1953) (Phase Diagram, Phase Relations, Experimental, *, 32)

[1956Hor] Horstmann, D., Malissa, H., "Electrolytic Isolation of Intermetallic Fe-Zn Compounds and Determination of the Solubility of Several Metals in These Compounds" (in German), *Arch. Eisenhüttenwesen*, **27**, 423–428 (1956) (Experimental, 4)

[1961Phi] Phillips, H.W.L., "Al-Fe-Zn" in "*Equilibrium Diagrams of Aluminium Alloy Systems*", The Aluminium Development Association, London, **97**, (1961) (Phase Diagram, Phase Relations, Review, 1)

[1961Ren] Rennhack, E.H., "Zinc-Rich Corner of the Zn-Fe-Al System", *Trans. AIME*, **221**, 775–779 (1961) (Phase Diagram, Phase Relations, Experimental, *, 13)

[1962Cam] Cameron, D.I., Ormay, M.K., "The Effect of Agitation, Cooling, and Al on the Alloying in Hot-Dipping in Zn", *6th Int. Conf. on Hot Dip Galvanizing, Interlaken*, Zinc Development Association, London, 276–311 (1962) (Experimental)

[1962May] Mayer, A., Morandi, F., "Investigation of Zn-Al-Fe Alloys" (in Italian), *Gazz. Chim. Ital.*, **92**, 1005–1020 (1962) (Experimental, 15)

[1963Fri] Friebel, V.R., Lantz, W.J., Roe, W.P., "Liquid Solubilities of Selected Metals in Zinc-4% Aluminium", *Trans. ASM*, **56**, 90–100 (1963) (Experimental, 12)

[1965Sou] Southin, R.T., Wright, D.A., "Fe2Al5 and FeSi in Zinc Alloys", *J. Inst. Metals*, **93**, 357–358 (1965) (Experimental, 12)

[1969Wat] Watanabe, H., Sato, E., "Phase Diagrams of Aluminum-Base Systems" (in Japanese) *Keikinzoku*, **19**(11), 499–535 (1969) (Phase Diagram, Phase Relations, Review, 232)

[1970Koe] Koester, W., Goedecke, T., "The Fe-Al-Zn Ternary System" (in German), *Z. Metallkd.*, **61**, 649–658 (1970) (Phase Diagram, Phase Relations, Experimental, #, *, 13)

[1971Ghu] Ghuman, A.R.P., Goldstein, J.I., "Reaction Mechanisms for the Coatings Formed During Hot Dipping of Fe in 0-10% Al-Zn Baths at 450-700°C", *Metall. Trans.*, **2**, 2903–2914 (1971) (Experimental, 18)

[1971Koe] Köster, W., Gödecke, T., "The Iron-Aluminium-Zinc Ternary System", *Proc. 9th Int. Conf. Hot Dip Galvanizing*, 128-139 (1971) (Phase Diagram, Phase Relations, Experimental, #, *, 13)

[1973Har] Harvey, G.J., Mercer, P.D., "Aluminium-rich Alloy Layers Formed During the Hot Dip Galvanizing of Low Carbon Steel", *Metall. Trans.*, **4**, 619–621 (1973) (Experimental, 8)

[1973Ure1] Urednicek, M., Kirkaldy, J.S., "An Investigation of the Phase Constitution of Iron-Zinc-Aluminium at 450°C", *Z. Metallkd.*, **64**, 419–427 (1973) (Phase Diagram, Phase Relations, Experimental, #, *, 21)

DOI: 10.1007/978-3-540-69761-9_14

[1973Ure2] Kirkaldy, J.S., "Mechanism of Iron Attack Inhibition Arising from Additions of Aluminium to Liquid Zn (Fe) during Galvanizing at 450°C", *Z. Metallkd.*, **64**, 899–910 (1973) (Experimental, 26)

[1975Gut] Guttman, H., Niessen, P., "Galvanizing Si Steels in Al-containing Baths", *Proc. Seminar Galvanizing Si-containing Steels, Int.*, Lead Zinc Research Organisation, Inc. New York, USA (1975) 198–218 (Experimental, 10)

[1976Mon] Mondolfo, L.F., "Aluminium-Iron-Zinc" in *Metallography of ALuminium Alloys*, John Wiley and Sons, Inc. New York (1976) 98–99 (Review, 1)

[1977Sho] Short, N.R., Mackowiak, J., "The Effect of Pressure on the Reactions between Fe (s)-Zn: 1.5% Al (l) at 501°C", *Corrosion Science*, **17**, 397–404 (1977) (Experimental, 13)

[1982Kub] Kubaschewski, O., "Iron-Aluminium" and "Iron-Zinc", in "*Iron-Binary Phase Diagrams*", Springer Verlag, Berlin, 5-9 and 172-175 (1982) (Phase Diagram, Review, #, 26, 13)

[1983Mur] Murray, J.L., "The Al-Zn (Aluminum-Zinc)", *Bull. Alloy Phase Diagrams*, **4**, 155–73 (1983) (Phase Diagram, Phase Relations, Review, #, 194)

[1984Nit] Nitto, H., Yamazaki, T., Morita, N., Yabe, K., Bandooo, S., "Effect of Aluminium in Zinc on Alloying of Zinc Coating of Galvanized Steel" (in Japanese), *Jetsu-to-Hagane*, **70**, 1719–1726 (1984) (Experimental, 20)

[1986Len] Lendvai, A., "Phase Diagram of Al-Fe Sytem up to 45 mass% Iron", *J. Mater. Sci. Lett.*, **5**, 1219–1220 (1986) (Phase Diagram, Phase Relations, Experimental, #, *, 7)

[1989Sel] Selverian, J.H., Marder, A.R., Notis, M.R., "The Effects of Silicon on the Reaction Between Solid Iron and Liquid 55 wt.% Al-Zn Baths", *Metall. Trans. A*, **20A**(3), 3543–555 (1989) (Experimental, 16)

[1990Che] Chen, Z.W., Sharp, R.M., Gregory, J.T., "Fe-Al-Zn Ternary Phase Diagram at 450°C", *Mater. Sci. Technol.*, **6**(12), 1173–1176 (1990) (Assessment, Phase Diagram, Phase Relations, Experimental, #, *, 16)

[1991Bel] Belisle, S., Leson, V., Gagne, M., "The Solubility of Iron in Continuous Hot-Dip Galvanizing Baths", *J. Phase Equilib.*, **12**(3), 259–265 (1991) (Phase Diagram, Phase Relations, Experimental, Thermodyn., 7)

[1991Sag] Sagiyama, M., Inagaki, J.-I., Morita, M., "Fe-Zn Alloying Behavior and the Coating Microctructure of Galvannealed Steel Sheets", *NKK Technical Review (Japan)*, **(63)**, 38–45 (1991) (Abstract, Experimental, 14)

[1991Sai] Saito, M., Uchida, Y., Kittaka, T., Hirose, Y., Hisamatsu, Y., "Formation Behavior of Alloy Layer in Initial-Stages of Galvanizing" (in Japanese), *Jetsu to Hagane*, **77**(7), 947–954 (1991) (Experimental, 7)

[1992Gho] Ghosh, G., "Aluminium-Iron-Zinc", MSIT Ternary Evaluation Program, in *MSIT Workplace*, Effenberg, G. (Ed.), MSI, Materials Science International Services GmbH, Stuttgart; Document ID: 10.17658.1.20, (1992) (Crys. Structure, Phase Diagram, Phase Relations, Assessment, 27)

[1992Per] Perrot, P., Tissier, J.C., Dauphin, J.Y., "Stable and Metastable Equilibria in the Fe-Zn-Al System at 450°C", *Z. Metallkd.*, **83**, 786–790 (1992) (Calculation, Phase Diagram, Phase Relations, Experimental, #, *, 12)

[1992Rag] Raghavan, V., "The Al-Fe-Zn (Aluminium-Iron-Zinc) System", in *Phase Diagrams of Ternary Iron Alloys*, Part 6A, Indian Institute of Metals, Calcutta, 215-223 (1992) (Phase Diagram, Phase Relations, Review, 24)

[1994Lin] Lin, C.S., Meshii, M., "The Effect of Steel Chemistry on The Formation of Fe-Zn Intermetallic Compounds of Galvanneal-Coated Steel Sheets", *Metall. Mater. Trans. B*, **25B**(5) 721–730 (1994) (Experimental, Kinetics, 31)

[1994Tan] Tang, N., "Comment on Fe-Al-Zn (Iron-Aluminium-Zinc)", *J. Phase Equilib.*, **15**, 3237–238 (1994) (Theory, #, *, 10)

[1995Lin1] Lin, C.S., Meshii, M., Cheng, C.C., "Microstructural Characterization of Galvanneal Coatings by Transmission Electron-Microscopy", *SIJ Int.*, **35**(5), 494–502 (1995) (Experimental, Kinetics, 43)

DOI: 10.1007/978-3-540-69761-9_14

[1995Lin2] Lin, C.S., Meshii, M., Cheng, C.C., "Phase Evolution in Galvanneal Coatings on Steel Sheets", *SIJ Int.*, **35**(5) 503–511 (1995) (Experimental, Kinetics, 28)

[1995Tan1] Tang, N., "Modeling Al Enrichment in Galvanized Coatings", *Metall. Mater. Trans. A*, **26A**(7), 1699–1704 (1995) (Theory, Kinetics, 23)

[1995Tan2] Tang, N., "Refined 450°C Isotherm of Zn-Fe-Al Phase Diagram", *Mater. Sci. Technol.*, **11**(9) 870–873 (1995) (Phase Diagram, Phase Relations, Experimental, *, 23)

[1995Yam1] Yamaguchi, S., Fukatsu, N., Kimura, H., Kawamura, K, Iguchi, Y., O-Hashi, T., "Development of Al Sensor in Zn Bath for Continuous Galvanizing Processes" in *Proc. Galvatech'95*, ISS-AIME, Warrendale, Pa, 647-655 (1995) (Experimental, Thermodyn., *, 12)

[1995Yam2] Yamaguchi, S., Makino, H., Sakatoku, A., Iguchi, Y., "Phase Stability of Dross Phases in Equilibrium with Liquid Zn Measured by Al Sensor" in *Proc. Galvatech'95*, ISS-AIME, Warrendale, Pa, 787-794 (1995) (Experimental, Thermodyn., *, 11)

[1996Tan] Tang, N.-Y., "450°C Isotherm of Zn-Fe-Al Phase Diagram Update", *J. Phase Equilib.*, **17**(5), 396–398 (1996) (Phase Diagram, Phase Relations, Experimental, #, *, 13)

[1997Gyu] Gyurov, S., "The Reaction Between Solid Iron and Liquid Zn-Al Baths", *Z. Metallkd.*, **88**(4), 346–352 (1997) (Phase Diagram, Phase Relations, Experimental, Kinetics, 33)

[1997Mcd] McDevitt, E., Morimoto, Y., Meshii, M., "Characterization of the Fe-Al Interfacial Layer in a Commercial Hot-Dip Galvanized Coating", *SIJ Int.*, **37**(8), 776–782 (1997) (Experimental, 24)

[1997Mor] Morimoto, Y., McDevitt, E., Meshii, M., "Characterization of the Fe-Al Inhibition Layer Formed in the Initial Stages of Hot-Dip Galvannealing", *SIJ Int.*, **37**(9), 906–913 (1997) (Experimental, 28)

[1997Ser] Sere, P.R., Culcasi, J.D., Elsner, C.J, Di Sarli, A.R., "Factors Affecting the Hot-dip Zinc Coatings Structure" (in Spanish), *Rev. de Metall.*, **33**(6), 376–381 (1997) (Experimental, Kinetics, 11)

[1997Tan] Tang, N.-Y., "Discussion of "Kinetics and Phase Transformation Evaluation of Fe-Zn-Al Mechanically Alloyed Phases", *Metall. Mater. Trans. A*, **28A**(11), 2433–2434 (1997) (Theory, 11)

[1997Uwa1] Uwakwen, O.N.C., Liu, Z., "Kinetics and Phase Transformation Evaluation of Fe-Zn-Al Mechanically Alloyed Phases", *Metall. Mater. Trans. A*, **28A**(3), 517–525 (1997) (Phase Diagram, Phase Relations, Experimental, *, 26)

[1997Uwa2] Uwakwen, O.N.C., Liu, Z., "Authors' Reply", *Metall. Mater. Trans. A*, **28A**(11), 2434–2435 (1997) (Theory, 7)

[1998Ada] Adachi, Y., Arai, M., "Transformation of Fe-Al Phase to Fe-Zn Phase on Pure Iron During Galvanizing Layer", *Mater. Sci. Eng. A*, **254**(1-2), 305–310 (1998) (Crys. Structure, Experimental, 8)

[1998Akd] Akdeniz, M.V., Mekhrabon, A.O., "The Effect of Substitutional Impurities on the Evolution of Fe-Al Diffusion Layer", *Acta Mater.*, **46**(4), 1185–1192 (1998) (Calculation, Thermodyn., 55)

[1998Tan] Tang, N.-Y., "Discussion of "Kinetics and Phase Transformation Evaluation of Fe-Zn-Al Mechanically Alloyed Phases", *Metall. Mater. Trans. A*, **29A**(10), 2643–2644 (1998) (Phase Diagram, Phase Relations, Theory, 9)

[1998Uch1] Uchida, Y., Andoh, A., Komatsu, A., Yamakawa, K., "Changing Process from ζ Center Dot Fe-Zn Phase to Al-Fe Intermetallic Compounds in Molten Zn-5mass%Al Alloy Bath" (in Japanese), *Tetsu to Hagane*, **84**(9), 632–636 (1998) (Experimental, 6)

[1998Uch2] Uchida, Y., Andoh, A., Komatsu, A., Yamakawa, K., "Changing Process from ζ Center Dot Fe-Zn Phase to Al-Fe Intermetallic Compounds in Molten Zn-5mass%Al Alloy Bath" (in Japanese), *Tetsu to Hagane*, **84**(9), 637–642 (1998) (Experimental, 4)

[1998Uwa] Uwakwen, O.N.C., Liu, Z., "Authors' Reply", *Metall. Mater. Trans. A*, **29A**(10), 2644–2645 (1998) (Phase Diagram, Phase Relations, Theory, 5)

[1998Yam] Yamaguchi, S., "Thermochemical Stability and Precipitation Behavior of Dross Phases in CGL Bath" in *Proc. Galvatech'98*, Chiba, Japan, The Iron and Steel Institute of Japan, 84-88 (1998) (Experimental, Thermodyn., *, 8)

DOI: 10.1007/978-3-540-69761-9_14

[1999Cos] Costa e Silva, A., Avillez, R.R., Marques, K., "A Preliminary Assessment of the Zn-rich Corner of the Al-Fe-Zn System and Its Implications in Steel Coating", *Z. Metallkd.*, **90**(1), 38–43 (1999) (Calculation, Phase Diagram, Phase Relations, Thermodyn., *, 25)

[1999Tan] Tang, N.-Y., "Characteristics of Continuous-Galvanizing Baths", *Metall. Mater. Trans. B.*, **30**(1), 144–148 (1999) (Phase Diagram, Phase Relations, *, 26)

[2000Mar] Marder, A.R., "The Metallurgy of Zinc-Coated Steel", *Prog. Mater. Sci.*, **45**, 191–271 (2000) (Phase Diagram, Phase Relations, Phys. Prop., Review, 188)

[2000Reu] Reumont, G., Perrot, P., Fiorani, J.M., Hertz, J., "Thermodynamic Assessment of the Fe-Zn System", *J. Phase Equilib.*, **21**(4), 371–378 (2000) (Thermodyn., *, 26)

[2000Tan] Tang, N.-Y., "Determination of Liquid-Phase Boundaries in Zn-Fe-Mx Systems", *J. Phase Equilib.*, **21**(1), 70–77 (2000) (Phase Diagram, Phase Relations, Experimental, Thermodyn., #, *, 29)

[2001Gio] Giorgi, M.-Y., Guillot, J.-B., Nicolle, R., "Assessment of the Zinc-Aluminium-Iron Phase Diagrams in the Zinc-Rich Corner", *Calphad*, **25**(3), 461–474 (2001) (Phase Diagram, Phase Relations, Thermodyn., *, 36).

[2001Koe] Koester, M., Schuhmacher, B., Sommer, D., "The Influence of the Zinc Content on the Lattice Constants and Structure of the Intermetallic Compound Fe2Al5", *Steel Res.*, **72**(9), 371–375 (2001) (Crys. Structure, Experimental, 29)

[2001Mit] Mita, K., Ikeda, T., Maeda, M., "Phase Diagram Study of Fe-Zn Intermetallics", *J. Phase Equilib.*, **22**(2), 122–125 (2001) (Experiment, Phase Diagram, Phase Relations, #, *, 14)

[2001Su] Su, X., Tang, N.-Y., Toguri, J.M., "Thermodynamic Evaluation of the Fe-Zn System", *J. Alloys Compd.*, **325**(9), 129–136 (2001) (Thermodyn., *, 49)

[2002Bai] Bai, K., Wu, P., "Assessment of the Zn-Fe-Al System for Kinetic Study of Galvanizing", *J. Alloys Compd.*, **347**, 156–164 (2002) (Phase Diagram, Phase Relations, Thermodyn., Kinetics, *, 40)

[2002Feu] Feutelais, Y., Legendre, B., de Avillez, R. R., "Standard Enthalpy of Formation of the ζ-Phase in the Fe-Zn System at 298 K", *J. Alloys Compd.*, **346**, 1–2 (2002) (Experimental, Thermodyn., Kinetics, *, 20)

[2002Tan] Tang, N.Y., Su, P., "Assessment of the Zn-Fe-Al System for Kinetic Study of Galvanizing", *J. Alloys Comp.*, **347** 156–164 (2002) (Phase Diagram, Phase Relations, Experimental, #, *, 16)

[2003Per] Perrot, P., "Al-Zn (Aluminium-Zinc)", MSIT Binary Evaluation Program, in *MSIT Workplace*, Effenberg, G. (Ed.), MSI, Materials Science International Services GmbH, Stuttgart; submitted for publication, (2003) (Phase Diagram, Phase Relations, Assessment, Crys. Structure, 41)

[2003Rag] Raghavan, V., "Al-Fe-Zn (Aluminum-Iron-Zinc)", *J. Phase Equilib.*, **24** 546–550 (2003) (Phase Diagram, Phase Relations, Review, *, 33).

[2006MSIT] "Al-Fe (Aluminum-Iron)", Diagrams as Published, in *MSIT Workplace*, Effenberg, G. (Ed.), Materials Science International Services, GmbH, Stuttgart; Document ID: 30.10236.1.20, (2006) (Crys. Structure, Phase Diagram, Phase Relations, 11)

[V-C] Villars, P. and Calvert, L.D., *Pearson's Handbook of Crystallographic Data for Intermetallic Phases*, ASM, Metals Park, Ohio (1985)

[V-C2] Villars, P. and Calvert, L.D., *Pearson's Handbook of Crystallographic Data for Intermetallic Phases*, 2nd edition, ASM, Metals Park, Ohio (1991)

DOI: 10.1007/978-3-540-69761-9_14

Boron – Carbon – Iron

Peter Rogl

Introduction

The hardening effect in borided steels and ferrous alloys motivated the investigation of phase relations in the Fe rich corner of the B-C-Fe system as early as 1922 [1922Vog]. An exploratory investigation of phase relations revealed compatibility of FeB with carbon and boron carbide at temperatures 1400 to 1500°C [1952Gla]. Boron solubility at 1000°C in Fe_3C was studied by [1957Nic], followed by systematic investigations of the solidification behavior, the liquidus surface and isothermal sections in the iron-rich corner by various research groups [1966Kan, 1963Sta, 1967Bor, 1968Bor, 1971Fom, 1974Fom1, 1974Fom2, 1976Fom, 1978Fom, 1981Fom]. Most studies were based on the existence of metastable Fe_3C, accordingly resulting in metastable phase diagrams. Similar techniques of alloy preparation and similar quenching rates naturally provided some agreement on the shape of the (metastable) liquidus surface 1922Vog, 1966Kan, 1968Bor], whilst different quenching rates [1963Sta, 1978Fom] arrived at a liquidus surface largely at variance to the findings of [1922Vog, 1966Kan, 1968Bor]. There is closer agreement among all the above mentioned research groups on the (metastable) isothermal sections and solubility limits for the ternary solid solutions $Fe_{23}(B_xC_{1-x})_6$ and $Fe_3(B_xC_{1-x})$: 700°C [1966Kan, 1967Bor], 800°C [1963Sta, 1967Bor], 950°C [1966Kan] and 1000°C [1967Bor, 1978Fom]. A detailed analysis of the true phase equilibria at temperatures above ca. 1000°C was performed by [1985Sch], providing a precisely established liquidus surface in the iron rich region ($\geq$ 66 at.% Fe) and an estimation for the rest of the diagram.
The topography of the B-C-Fe system was summarized by [1949Jae, 1986Rag, 1994McH, 1995Vil]. Thermodynamic calculations are due to [1974Has, 1981Nis, 1988Oht, 1995Rab].
A summary of experimental studies of phase equilibria is given in Table 1.

Binary Systems

For this assessment, stable and metastable equilibria in the C-Fe binary system are accepted in the version presented by [Mas2] amended by a small modification for the liquid composition (Fe82.27C17.73 at.%) in the eutectic reaction L $\rightleftharpoons$ (γFe) + (C) by [2001Fen]. Phase equilibria in the B-Fe system were reinvestigated by [1985Smi, 1986Smi] and were summarized in [1992Rog]. A thermodynamic assessment and calculation is from [1995Hal]. A metastable diagram including the metastable compounds Fe_3B (Fe_3C type) and $Fe_{23}B_6$ was presented by [1978Her]. Depending on the rate of quenching a liquid alloy $Fe_{76}B_{24}$, two modifications of Fe_3B, *i.e.* the Fe_3P type and the Ti_3P type, were obtained by [1982Kha] and were claimed to exist as high- and low-temperature compounds, respectively, within a small temperature window of the equilibrium diagram ($1140 < T < 1250$°C). Similarly, the τ phase ($Fe_{23}B_6$) was speculated by [1991Kha] to belong to the equilibrium diagram within a small temperature window $650 \leq T \leq 800$°C. A listing of the crystallographic information of all stable and metastable phases pertinent to the B-C-Fe system is presented in Table 2, including also the ternary solid solution phases.

Solid Phases

The B-C-Fe system is characterized by the formation of extended solid solutions $Fe_3(B,C)$ and $Fe_{23}(B,C)_6$. Whilst the experimental studies of [1957Nic, 1966Kan, 1963Sta, 1967Bor, 1968Bor, 1978Fom] reveal a continuous C/B substitution $Fe_3B_xC_{1-x}$ starting from (metastable) binary Fe_3C, [1985Sch] attempted to provide true equilibrium conditions and consequently showed a truly ternary solid solution $Fe_3B_xC_{1-x}$ entirely within the ternary system ($0.05 \leq x \leq 0.90$ at 1050°C). The boron rich limit is thereby in close agreement with the value of $x \leq 0.80$ at 1000°C reported by [1957Nic, 1967Bor, 1978Fom]. Unfortunately no investigations in true equilibrium were performed by [1985Sch] at lower temperatures. Therefore the boron rich limit in $Fe_3B_xC_{1-x}$ at 950°C ($x \leq 0.78$ [1966Kan]), at 900°C ($x \leq 0.78$ [1967Bor], $x \leq 0.72$ [1978Fom]), at 800°C ($x \leq 0.84$ [1963Sta]; $x \leq 0.77$ [1967Bor]) and at 700°C ($x \leq 0.59$ [1967Bor]) cannot be compared

DOI: 10.1007/978-3-540-69761-9_15

with its true equilibrium value, however, it is assumed to correspond quite closely. Although limits for the lattice parameter variation in the boron containing cementite were given by [1974Fom2], no compositional values were attributed; from chemical analyses, density and X-ray data a formula $Fe_{2.875}B_{0.625}C_{0.5}$ with Fe/B distribution in the Fe sites was claimed.
A similar situation, however, with poor agreement, exists for the so called τ phase, $Fe_{23}(B_xC_{1-x})_6$ [1954Car], for which limits of existence were reported as follows: at 700°C; $0.27 \leq x \leq 0.60$ [1967Bor] and $0.55 \leq x \leq 0.72$ [1966Kan]; at 800°C, $0.23 \leq x \leq 0.62$ [1967Bor] and $0.58 \leq x \leq 0.69$ [1963Sta], at 900°C, $0.27 \leq x \leq 0.64$ [1967Bor], and $0.23 \leq x \leq 0.52$ [1978Fom], at 1080°C $0.37 \leq x \leq 0.81$ [1978Fom]. Crystallographic data are collected in Table 2. The linear variation of the unit cell parameters as a function of the C/B exchange in line with Vegard's rule indicates ideal substitution behavior.

Quasibinary Systems

No quasibinary sections were experimentally established for the B-C-Fe system. From the design of the liquidus surface for the equilibrium diagram, [1985Sch] assumed the existence of two quasibinary sections FeB - C and FeB - $B_{4.5}C$, both with a eutectic maximum. Obviously [1985Sch] was unaware of the early data by [1952Gla] reporting on stable two-phase equilibria at 1500°C: FeB + (C) and FeB + 'B_4C'. No further details have been reported.

Invariant Equilibria

Invariant equilibria for the Fe rich part of the system B-C-Fe (≥ 65 at.% Fe) were carefully determined by [1985Sch]. The reaction scheme was extended to the rest of the diagram, to provide a consistent set (see Table 3). The reactions are summarized in terms of a Scheil diagram, presented in Fig. 1. According to the experimental data of [1985Sch], the solid solution $Fe_3(B,C)$ arises on cooling from a peritectic reaction P_1 at 1191°C: $L + Fe_2B + (C) \rightleftharpoons Fe_3(B_xC_{1-x})$ with $x = 0.76$. The metastable extensions of the lines of double saturation furthermore reveal a metastable equilibrium $L \rightleftharpoons (\gamma Fe) + (C) + Fe_2B$ at about $T_E \approx 1040$°C. A continuous line of metastable congruent melting points of $Fe_3(B,C)$ allows to define the metastable temperature of melting for Fe_3B at 1214°C [1985Sch].
Metastable reactions in the Fe rich corner were recorded by several research groups [1922Vog, 1966Kan, 1963Sta, 1967Bor, 1978Fom]. Whereas the findings of [1922Vog, 1966Kan, 1967Bor] show at least some resemblance, they are at significant variation to the version reported by [1963Sta] and [1978Fom], who both claimed a primary field of crystallization for $Fe_{23}(B,C)_6$. For comparison see Figs. 2a and 2b. A possible explanation may be found from the significantly different techniques of alloy preparation and particularly from the different quenching rates employed. For the metastable eutectic $L \rightleftharpoons (\gamma Fe) + Fe_2B + Fe_3(B,C)$ a value of 1097°C was assigned by [1968Bor], which is close to the corresponding temperature of 1100°C given by [1922Vog] (no temperature given by [1978Fom]) and by [1966Kan]. The latter author, however, determined a transition reaction instead with a minimum in one of the monovariant lines. Whilst [1963Sta] reported on three eutectic reactions and three corresponding maxima in the monovariant lines encircling the $Fe_{23}(B,C)_6$ region, [1978Fom] showed only one maximum and one eutectic ($L \rightleftharpoons (\gamma Fe) + Fe_{23}(B,C)_6 + Fe_3(B,C)$) but two transition reactions instead (labeled as "peritectic": $L + Fe_2B \rightleftharpoons Fe_{23}(B,C)_6 + (\gamma Fe)$; $L + Fe_2B \rightleftharpoons Fe_{23}(B,C)_6 + Fe_3(B,C)$; [1987Spi] demonstrated that an increase in cooling rate during solidification promotes an increase in the uniformity of primary phases, eutectic and "peritectic" structures, which may lead to a reduction in the tendency of B-C-Fe alloys towards brittle failure.
The absence of τ-$Fe_{23}(B,C)_6$ in the isothermal sections at 1050°C [1985Sch], 1000° [1957Nic, 1967Bor], 950°C [1966Kan] lead to the general conclusion on its instability at temperatures higher than about 900° C. [1967Bor] arrived at a maximum temperature of $T = 965$°C above which τ is supposed to decompose according to the reaction: $(\gamma Fe) + Fe_3(B,C) \rightleftharpoons Fe_{23}(B,C)_6$. These findings are in agreement with data by [1976Fom] who observed a decomposition temperature >950°C. [1963Sta] claimed instability of the τ phase at temperatures below 800°C according to the reaction $\tau + Fe_2B \rightleftharpoons Fe_3(B,C) + (\gamma Fe)$. Data of [1967Bor], however, still reveal τ phase with a considerable broad field of homogeneity at 700°C. But the temperature-dependent width of this field seems to contract at lower temperatures [1968Bor], suggesting indeed decomposition below about 600°C but according to a eutectoid reaction: $\tau \rightleftharpoons (\alpha Fe) + Fe_2B + Fe_3(B,C)$. All the reactions starting from the metastable decomposition of the liquid down to the

DOI: 10.1007/978-3-540-69761-9_15

decomposition of the τ phase are summarized in Fig. 3 essentially relying on the isothermal sections and isopleths derived by [1967Bor, 1968Bor].

Liquidus, Solidus and Solvus Surfaces

A detailed liquidus surface for the B-C-Fe equilibrium diagram was established by [1985Sch] in the iron-rich corner; it is shown in Fig. 4a. Assuming two quasibinary eutectic reactions, $L_1 \rightleftharpoons$ FeB + (C) and $L_2 \rightleftharpoons$ FeB + $B_{4.5}C$, the liquidus surface was completed for the entire diagram (see Fig. 4b), resulting in two ternary boron rich eutectic reactions, $L_1 \rightleftharpoons$ (βB) + 'B_4C' + FeB and $L_2 \rightleftharpoons$ (C) + 'B_4C' + FeB. As can be seen from Fig. 4a, boron significantly reduces the carbon solubility of the melt in the Fe rich region up to a minimum point at about 16.22 mass% B on the section FeB - C. The dashed lines in Fig. 4a denote the metastable extrapolations of the lines of double-saturation and reveal the corresponding metastable reactions. For a comparison of the experimentally observed metastable liquidus surfaces in the iron rich corner see Section "Invariant Equilibria" and Figs. 2a and 2b.
In slowly cooled alloys (5 K·min^{-1}) with less than 0.02 mass% B solidification ends with eutectic crystallization: the skeletal eutectic was said to consist of (γFe)+Fe_2B [1987Mal]; the eutectic with C content raising above 0.1 mass% C shows (γFe)+Fe_3(B,C). On further cooling boron-containing cementite precipitates from the supersaturated austenite phase resulting in an outer layer of cementite at the periphery of the eutectic columns [1987Mal]. A calculation of the precipitation behavior in a Fe-0.8C-0.1B (mass%) alloy is due to [1999Yam].

Isothermal Sections

Phase relations in the iron rich corner were investigated for several isothermal sections: 700°C [1967Bor, 1966Kan]; 800°C [1963Sta, 1967Bor]; 900°C [1967Bor, 1978Fom]; 950°C [1966Kan]; 1000°C [1967Bor, 1978Fom], 1050°C [1985Sch] and at 1080°C [1978Fom]. Except for the section at 1050°C [1985Sch] (Fig. 5), which covers the entire diagram in true equilibrium, all other sections constructed involve metastable binary Fe_3C and thus merely represent metastable conditions at least for the region adjacent to the C-Fe binary. The various authors usually agree on the type of phase field distribution, but agreement on the extent of the homogeneity region for the τ-Fe_{23}(B,C)$_6$ is rather poor (for discussion, see Section "Solid Phases"). We follow the experimental results of [1967Bor], which are consistent with the Scheil diagram for the (metastable) isothermal reactions in Fig. 3. Isothermal sections (metastable) are shown for 1000°C (Fig. 6), 900°C (Fig. 7), 800°C (Fig. 8) and 700°C (Fig. 9).

Temperature – Composition Sections

Two isopleths, $Fe_{23}B_6$ - $Fe_{23}C_6$ and Fe_3B - Fe_3C were established by [1968Bor]. As they are consistent with the isothermal sections, which involve binary metastable Fe_3C, these isopleths are again metastable at least in the vicinity of the C-Fe boundary. The isopleths are shown in Figs. 10 and 11 with small changes to conform to the congruent melting point of metastable Fe_3C at 1252°C. A series of isopleths in the Fe rich region was constructed by [1922Vog] - these results are not shown here, as the existence of Fe_3(B,C) and Fe_{23}(B,C)$_6$ was neglected.

Thermodynamics

Partial and integral enthalpies of mixing of liquid components in the Fe rich part of the system ($x_C < 0.2$, $x_{Fe} < 0.5$, $x_B < 0.2$) have been derived from isoperibolic high temperature calorimetry (Fig. 12a) [1994Wit]. The concentration dependencies of the enthalpies of mixing allowed to calculate the glass forming temperatures GFT in terms of a GFT surface (Fig. 12b) [1994Wit] in satisfactory agreement with metallic glasses obtained by splat cooling with a thickness of >50 μm [1987Sud]. The specific heat of ferromagnetic metallic glasses $Fe_{80}B_{20-x}C_x$ ($0 \le x \le 8$), measured in the temperature range from 1.5 to 10 K, revealed a gamma-value of 6.26 mJ·mol^{-1}K^{-2} independent on the carbon concentration [1984Maj].
The activity of boron in molten C-Fe alloys was measured at 1600°C [1965Bur]. The solubility of carbon in molten B-C-Fe alloys was determined in the temperature range from 1300 to 1450°C to determine the

DOI: 10.1007/978-3-540-69761-9_15

thermodynamic parameters of boron in liquid iron; employing an interstitial model, the activity coefficient of boron at infinite dilution and the interaction parameters in liquid iron have been derived [1995Hua].
A full set of thermodynamic data involving thermodynamic assessments and CALPHAD type modeling of the B-C-Fe system are due to several authors [1974Has, 1981Nis, 1988Oht, 1995Rab].

Notes on Materials Properties and Applications

The influence of boron on the hardness of steels was investigated by [1922Vog]. Saturation magnetization, Curie temperatures as a function of C/B substitution were measured by [1957Nic] for $Fe_3(B,C)$. Saturation moments as well as Curie temperatures change linearly with the boron content from T_C = 190°C, $\mu_s = 1.79\mu_B$/Fe-atom for Fe_3C to T_C = 578°C, $\mu_s = 2.0\mu_B$/Fe-atom for $Fe_3B_{0.8}C_{0.2}$. $Fe_{23}B_3C_3$ in as cast state is ferromagnetic (T_C = 742 K; $\mu_s = 1.98\mu_B$/Fe-atom; magnetization σ = 178.5 $Am^2 \cdot kg^{-1}$); the polar Kerr rotation angle (at room temperature and in an external field of 1280 $kA \cdot m^{-1}$) is $2\Phi_K$ = –0.75 (633 nm), $2\Phi_K$ = –0.86 (830 nm) and $2|\Phi_K|/\sigma$ = 0.0042 [1983Bus]

Miscellaneous

The technological advantage of boriding steel and ferrous alloys lies in the formation of a surface boron-containing layer of high abrasive wear resistance, good corrosion resistance and high hot-hardness. Consequently many research groups devoted their studies to tasks such as (i) investigation on surface properties of treated low carbon and alloyed steels (AISI and 5115 steels, boriding and carburizing) [2000Sel], (ii) mechanism of thermochemical growth of iron borides on iron [2004Mar], (iii) self-propagating eutectic boriding [2002Ge], (iv) interrupted boriding of medium-carbon steels [2002Gop], (v) boride-layer growth kinetics in boriding of Fe and C-Fe, Cr-Fe and Fe-Ni alloys [1989Bra]. The influence of carbon content in the borided Fe-alloys on the microstructure of iron borides was studied by [2006Kul]. Details on laser surface hardening of structural ferrous alloys may be found from [1998Bam]. [2003Abe] investigated the influence of carbon and aluminium additions on the Fe-10 mass% B system. [1989Tur] examined the processes of structure formation during sintering of powder compacts Fe + 3 mass% B_4C with 85 to 87% density. At temperatures $T \leq 1000$°C gas transport forms a layer of iron borides on B_4C. Above 1050°C the appearance of a liquid phase forms $Fe_3(B,C)$ and ensures densification of the sinter body. Chemical interaction and wetting were studied between boron carbide and liquid iron [1979Pan, 1994Ter]. Whereas [1979Pan] found an initial spreading of liquid Fe on B_4C according to $r^2 = f(t)$ slowing down to $r^5 = f(t)$ (the initial contact angle of 60° decreased to 36° and finally was 35° involving formation of compounds in the contact zone), rapid reaction between B_4C-powders with liquid Fe was said to lead to boron carbide dissolution and iron boride formation (Fe_2B, $Fe_{23}(B,C)_6$) [1994Ter]. [1991Kan] studied the wear mechanism of high wear-resistance materials (among them Fe-B-3C) for automotive valve trains. Thermo-activation analysis of amplitude-dependent internal friction was used by [1993Lev] to determine in Fe-0.04 mass% C and Fe-0.059 mass% C-0.003 mass% B alloys the energy of binding of a dislocation with a point defect and the length of free dislocation segment. Micro-alloying of low-carbon iron by boron decreases the density of impurity dislocations and subsequently reduces the microscopic yield point [1993Lev]. The growth of a boride needle in steel was investigated by [1987Isa] and it was found that growth in the axial direction and lateral growth are determined by the same parameters: decrease in the rate of axial growth leads to increase in the rate of lateral growth. The effect of B addition on strain aging properties of ferritic steels was examined for B-C-Fe alloys [2003Abe]. Structure and properties and deformation peculiarities of monoboride Fe(B,C) crystals in (B-C-Fe) alloys depending on the cooling rate were investigated by metallographic, X-ray, chemical, spectral, micro-X-ray, and thermal analyses [1996Spi]. Laser heating of Fe-rich eutectic B-C-Fe alloys resulted in a three-zone structure originating from heterogeneous nucleation at the original microstructure of an ultrafine eutectic reaction followed by massive crystallization of a zone of metastable $Fe_3(B,C)$. The third zone was a metallic glass when the massive reaction is frozen-in. A time-temperature crystallization diagram was given [1988Hor].
X-ray diffraction diagrams were recorded for Fe-B15to25 at.% as well as for FeC16B17 in the liquid and amorphous states. Measurement of the structural factor and radial distribution function revealed only small differences between the amorphous and liquid states [1981Mir].

DOI: 10.1007/978-3-540-69761-9_15

The neutron autoradiography technique, which was said to allow measuring boron concentrations 5±1 ppm in massive samples, was used to measure boron concentrations along the carbon gradient of a carburized B-Fe alloy [1978Cam]. A new analytical method based on the spectral lines was used for accurate determination of B in B-C-Fe alloys [1975Tve].
NMR hyperfine field distributions for ^{10}B, ^{11}B and ^{57}Fe were performed on $Fe_3B_{1-x}C_x$ ($0.1 \leq x \leq 0.4$) at 4.2 K and from 10 to 60 MHz [1987Zha]. An ^{11}B-NMR study was devoted to elucidate the development of short-range order (*bct*-Fe_3B and *o*-Fe_3B) in $Fe_{80}B_{20-x}C_x$ amorphous alloys with thermal treatment [1994Mao], whereas the effect of short-range order on the magnetic properties of B-C-Fe amorphous alloys (recorded by means of NMR and magnetization measurements was discussed by [1992Ge].
The well-defined minimum in the low-temperature electrical resistivity in $Fe_{80}B_{20-x}$ ($x = 0$, 2 and 8), which increases with x, was found to be insensitive to a magnetic field as high as 39 kOe and thus it was concluded that the origin of the resistivity minimum may be other than magnetic. The magnetoresistance data seem to suggest the presence of both localization and correlation effects [1988Roy]. Thin ribbons of amorphous alloys $Fe_{84}B_{16-x}C_x$ and $Fe_{86}B_{14-x}C_x$ were characterized with magnetic measurements (Curie temperature, magnetization, saturation moment) [1978Lub, 1979Lub, 1980Lub] as well as by Mössbauer spectroscopy [1981Lin]. The magnetic anisotropy was found to be independent of x for all $Fe_{84}B_{16x}C_x$ alloys [1981Lin]. Amorphous alloys of $Fe_{86}B_{14-x}C_x$ ($5 \leq x \leq 7$) were reported to have excellent soft-magnetic properties with the AC loss less than 0.5 $W \cdot kg^{-1}$ at 17 kG and 60 Hz: room-temperature saturation induction approached 18 kG after appropriate heat treatment [1979Hat1, 1979Hat2].

Table 1. Investigations of the B-C-Fe Phase Relations, Structures and Thermodynamics

Reference	Method/Experimental Technique	Temperature/Composition/Phase Range Studied
[1922Vog]	Melting in ceramic tubes of 20 g samples under hydrogen starting from electrolyte iron and carbon rods and adding ferrobor with 21.5 at.% B. The alloys were cooled from 1300 to 1150 at $2°C \cdot s^{-1}$; perlitic structures at $1°C \cdot s^{-1}$.	Metallography, hardness measurements and thermal analyses (from temperature *vs* time recordings at a quenching rate of 1 to 2 $K \cdot s^{-1}$) were employed to study the solidification in the region Fe-Fe_3C-FeB.
[1952Gla]	Hotpressing of powder mixtures (elemental powders and Fe_3C, FeB) in graphite dies at 1300 to 1500°C.	XPD on hotpressed samples (74.5Fe20B5.5C; 75Fe_3C25B; 71Fe_3C29B; 67FeB33B)
[1954Car]	Identification by X-ray powder diffractometry (XPD) of $Cr_{23}C_6$ type structure in samples prepared from master alloys of iron-4.4 mass% C and iron-5.7 or 8.9 mass% B.	Sample sintered from powders, annealed at 850°C sealed in Vycor-tubes for "extended periods". $Fe_{23}(B,C)_6$ type structure found in samples ranging from 1.5-2.5 mass% B and 2.5-4.5 mass% C
[1957Nic]	Quantitative metallography, XPD and magnetic measurements served to determine the boron solubility in Fe_3C as well as the influence on the magnetic properties of Fe_3C.	B-C-Fe alloys with a boron content varying from 0 to 5.4 mass% B were melted (50 g each) from elemental carbonyl Fe-ingot, C and B. Part of the alloy was powdered, annealed at 1000°C for 24 h in evacuated Vycor capsules, ground to a 300 mesh powder prior to XPD. The second part of the

(*continued*)

DOI: 10.1007/978-3-540-69761-9_15

Reference	Method/Experimental Technique	Temperature/Composition/Phase Range Studied
		alloy was metallographically examined in as cast condition and after anneal at 1000°C, 170 h.
[1963Sta]	From metallographic and XPD analyses liquidus projection and phase equilibria for the isothermal sections at 800°C were determined.	Alloys (2 g each) in the Fe rich corner were melted in sinter Al_2O_3-crucibles in a high frequency furnace in air and waterquenched. Starting materials were electrolyte Fe (99.5 mass%), graphite (99.94%), crystalline B (98.5%) and a master alloy of Fe with 4.72 mass% C. A part of each alloy was annealed at 800°C for 200 h in vacuum sealed quartz capsules. The carbon content was determined via gas-volumetry.
[1966Kan]	Metallography, XPD were employed to derive phase equilibria in the isothermal sections at 700 and 950°C.	Alloys prepared from binary master alloys.
[1967Bor] [1968Bor]	Metallography, thermal analyses (<5 $K \cdot s^{-1}$) and XPD were used to determine the liquidus projection, phase equilibria in the isothermal sections at 700, 800, 900, and 1000°C, as well as two isopleths Fe_3B-Fe_3C and $Fe_{23}B_6$-$Fe_{23}C_6$.	About 40 alloys (100 g each) in the Fe rich part (<30 at.% B, <25 at.% C) were melted under argon in a high-frequency furnace starting from graphite and master alloys of Fe-4.48 mass% C and ferrobor with 13.51% B. After solidifying from ca 1700°C the alloys were quenched in water. Annealing conditions vary between 100 h at 1000°C and 2 months at 700°C. The composition of the alloys was controlled by gas-volumetry (carbon) and by alkaline titration for boron. Some alloys were powderized and compacted for long term anneal in evacuated quartz ampoules.
[1974Fom1] [1974Fom2] [1976Fom] [1978Fom] [1981Fom]	Solidification studies at fast (150-200°C·min^{-1}) and slow (50-100°C·min^{-1}) and very slow (10-20°C·min^{-1}) cooling of alloys in the region Fe, Fe_2B, Fe_3C. Determination of the solid solution range of $Fe_3B_{1-x}C_x$ in solidified alloys. Determination of isothermal sections at 900, 1000, 1080°C and of the liquidus surface for the Fe rich part. Conditions for stability/metastability of the $Fe_{23}(B,C)_6$ phase. Techniques used were XPD and metallography.	Alloys in the range 1-4 mass% B, 1-5 mass% C were melted at 1250°C in an arc furnace in Al_2O_3 crucibles in vacuum of 10^{-2} to 10^{-3} mm Hg. Starting materials were ingots of iron, graphite and crystallized boron (99.5%). Samples were cooled from 1100 to 700°C ion steps of 50°C holding for 2 to 15 min. For isothermal sections the alloys were sealed in quartz capsules and annealed at 900°C for 200 h

(*continued*)

DOI: 10.1007/978-3-540-69761-9_15

Reference	Method/Experimental Technique	Temperature/Composition/Phase Range Studied
[1985Sch]	Liquidus surface, isothermal equilibria at 1250°C and a series of isopleths were determined from thermal analyses.	Starting materials were electrolyte Fe (99.998%), graphite (99.94%) and crystallized boron (99.8%). Alloys were melted in a high frequency or Tammann furnace. The B and C content of the alloys was controlled by wet chemical methods. Isothermal reactions were determined on alloys (50 g each) heated in a Mo-wire furnace to preset temperature under argon in Fe- or C-crucibles. (2 K·min^{-1}). Fast quenching was achieved by casting the liquid alloys on a cooled Cu plate.
[1987Mal]	Electron microprobe analysis (EMPA) and XPD on quenched and slowly cooled Fe rich B-C-Fe alloys were used to study solidification. Thermal and chemical etching was used for phase contrast.	Samples containing 0.02-0.10 mass% B, 0.08-0.66 mass% C were melted in a vacuum electrofurnace and cooled at 5°C·min^{-1}. A second set of samples was annealed at various temperatures in the range from 800 to 1160° and quenched.
[1989Tur]	Processes of structure formation during sintering of powder compacts Fe + 3 mass% B_4C with 85 to 87% density. XPD, EMPA, LOM.	Powder compacts (Fe, B_4C, 50-100 μm) were heated to 1050°C at 10-12°C·s^{-1} and sintered at 1050°C for 2 h.

Table 2. Crystallographic Data of Solid Phases

Phase/ Temperature Range [°C]	Pearson Symbol/ Space Group/ Prototype	Lattice Parameters [pm]	Comments/References
(γFe) 1394 - 912	*cF*4 $Fm\bar{3}m$ Cu	a = 364.67 a = 357.3	[Mas2] at 25°C [V-C2] dissolves up to 9.06 at.% C at 1153°C [Mas2]
$Fe_{1-x}C_x$		a = 361.8	at 25°C [V-C2]
		a = 363.0	at 200°C [V-C2]
		a = 366.0	at 400°C [V-C2]
		a = 369.3	at 1000°C [V-C2]
(αδFe) (αFe)(r) ≤ 912	*cI*2 $Im\bar{3}m$ W	a = 286.65	[Mas2]

(*continued*)

DOI: 10.1007/978-3-540-69761-9_15

Phase/ Temperature Range [°C]	Pearson Symbol/ Space Group/ Prototype	Lattice Parameters [pm]	Comments/References
$Fe_{1-x}B_x$		a = 286.0	at x = 0.09 [V-C2]
(δFe)(h2) 1538 - 1394		a = 293.15	[Mas2]
(βB) < 2092	*hR*333 $R\bar{3}m$ βB	a = 1093.30 c = 2382.52	[1993Wer]
		a = 1092.2 c = 2381.1	at 1.1 at.% C [1993Wer] linear da/dx; dc/dx
		a = 1095.14 c = 2386.1	at $FeB_{\sim 49}$ [V-C2]
		a = 1097.18 c = 2387.05	at $FeB_{\sim 20}$ [V-C2]
(C)gr < 3827 (S.P.)	*hP*4 $P6_3/mmc$ C (graphite)	a = 246.12 c = 670.90	[Mas2]
		a = 246.023 c = 671.163	[1967Low]
		a = 246.75 c = 669.78	at 2.35 at.% B_{max} (2350°C) linear da/dx, dc/dx, [1967Low]
(C)d	*cF*8 $Fd\bar{3}m$ C (diamond)	a = 356.69	at 25°C, 60 GPa [Mas2]
'B_4C' < 2450	*hR*45 $R\bar{3}m$ $B_{13}C_2$	a = 565.1 to 560.7 c = 1219.6 to 1209.5	9 to 20 at.% C [1990Ase]
$B_{25}C$	*tP*52 $P\bar{4}2m$	a = 872.2 c = 508.0	[V-C2] also $B_{51}C_1$, $B_{49}C_3$; all metastable?
FeB < 1588	*oP*8 *Pnma* FeB	a = 550.6 b = 295.2 c = 406.1	[1992Rog]
Fe_2B < 1407	*tI*12 *I*4/*mcm* $CuAl_2$	a = 510.9 c = 424.9	[1992Rog]
$Fe_3B(h_1)$ ~1250 - ~1150	*tI*32 $I\bar{4}$ Fe_3P	a = 865.5 c = 429.7	metastable [1992Rog]

(*continued*)

DOI: 10.1007/978-3-540-69761-9_15

Phase/ Temperature Range [°C]	Pearson Symbol/ Space Group/ Prototype	Lattice Parameters [pm]	Comments/References
$Fe_3B(h_2)$ ~1220 - ~1140	*tP*32 $P4_2/n$ Ti_3P	*a* = 864.8 *c* = 431.4	metastable [1992Rog]
Fe_3B < 1214	*oP*16 *Pnma* Fe_3C	*a* = 542.8 *b* = 666.9 *c* = 443.9	metastable, [1985Sch] [1992Rog]
$Fe_{23}B_6$ ~800 - ~650	*cF*116 $Fm\bar{3}m$ $Cr_{23}C_6$	*a* = 1076	[1991Kha] metastable
$Fe_{23}(B_xC_{1-x})_6$ < 965		*a* = 1058.1	at *x* = 0.23 [1967Bor]
		a = 1063.4	at *x* = 0.63 [1967Bor] linear d*a*/d*x*
		a = 1059.4	C rich [1963Sta]
		a = 1062	B rich [1963Sta], [1954Car]
		a = 1061	at $Fe_{23}B_5C$ [1974Fom1, 1976Fom] $\rho_{exp.}$= 7.5 (3) Mgm^{-3}
Fe_4C	*cP*5 $P\bar{4}3m$ Fe_4C	*a* = 387.8	[V-C2] thin films, metastable
Fe_5C_2	*mC*28 *C*2/*c* Mn_5C_2	*a* = 1156.2 *b* = 457.27 *c* = 505.95 β = 97.74°	[V-C2] metastable
Fe_7C_3	*oP*40 *Pnma* Mn_7C_3 or *hP*20 $P6_3mc$ Th_7Fe_3	*a* = 454.0 *b* = 687.9 *c* = 1194.2 *a* = 688.2 *c* = 454.0	[V-C2] metastable [V-C2] metastable
$Fe_{20}C_9$	*o**116	*a* = 906 *b* = 1569 *c* = 794	[V-C2] metastable
Fe_2C	*oP*6 *Pnnm* Fe_2C	*a* = 470.4 *b* = 431.8 *c* = 283.0	[V-C2], metastable

(*continued*)

DOI: 10.1007/978-3-540-69761-9_15

Phase/ Temperature Range [°C]	Pearson Symbol/ Space Group/ Prototype	Lattice Parameters [pm]	Comments/References
Fe_3C	*hP*8 $P6_322$ Fe_3C	*a* = 476.7 *c* = 435.4	[V-C], metastable
Fe_3C < 1252	*oP*16 *Pnma* Fe_3C		[1985Sch] 0.05 ≤ *x* ≤ 0.90 at 1050°C; Metastable.
$Fe_3(B_xC_{1-x})$ < 1191		*a* = 507.87 *b* = 672.97 *c* = 451.44	[V-C2]
		a = 543 *b* = 665 *c* = 445	at *x* = 0 [1987Zha]
		a = 533 *b* = 666 *c* = 447	at *x* = 0.4 [1987Zha] linear d*a*/d*x*, d*b*/d*x*, d*c*/d*x*
		a = 508 *b* = 673 *c* = 452	at *x* = 0 [1967Bor]
		a = 537 *b* = 666 *c* = 445	at *x* = 0.8 [1967Bor] linear variation
		a = 507.90 *b* = 674.80 *c* = 451.50	at *x* = 0 [1957Nic] alloys quenched from 1000°C,
		a = 540.52 *b* = 666.85 *c* = 445.00	at *x* = 0.8 [1957Nic] alloys quenched from 1000°C, practically linear variation
		a = 519.9 *b* = 662.6 *c* = 446.8	[1974Fom2] $\rho_{exp.}$ = 7.43 (3) Mgm^{-3} $Fe_{2.875}B_{0.625}C_{0.5}$
		a = 508.8 *b* = 674.3 *c* = 452.3	[1974Fom2]

DOI: 10.1007/978-3-540-69761-9_15

Table 3. Invariant Equilibria

Reaction	T [°C]	Type	Phase	Composition (at.%)		
				Fe	B	C
$L \rightleftharpoons FeB + B_4C$	?	e (max_1)	-	-	-	-
$L \rightleftharpoons (\beta B) + FeB + B_4C$	?	E_1	-	-	-	-
$L \rightleftharpoons FeB + (C)$	?	e (max_2)	-	-	-	-
$L \rightleftharpoons FeB + B_4C + (C)$	?	E_2	-	-	-	-
$L + FeB \rightleftharpoons Fe_2B + (C)$	1350	U_1	Fe_2B FeB	66.7 50	33.3 50	≈0 ≈0
$L + Fe_2B + (C) \rightleftharpoons Fe_3(B,C)$	1191	P_1	Fe_2B (C)	66.7 ≈0	33.3 ≈0	≈0 ≈100
$L + Fe_2B \rightleftharpoons (\gamma Fe) + Fe_3(B,C)$	1148	U_2	Fe_2B (γFe)	66.7 ≈100	33.3 ≈0	≈0 ≈0
$L + (C) \rightleftharpoons (\gamma Fe) + Fe_3(B,C)$	1145	U_3	(γFe) (C)	≈100 ≈0	≈0 ≈0	≈0 ≈100
$L \rightleftharpoons (\gamma Fe) + Fe_3(B,C)$	1029	e (min)	(γFe)	≈100	≈0	≈0

DOI: 10.1007/978-3-540-69761-9_15

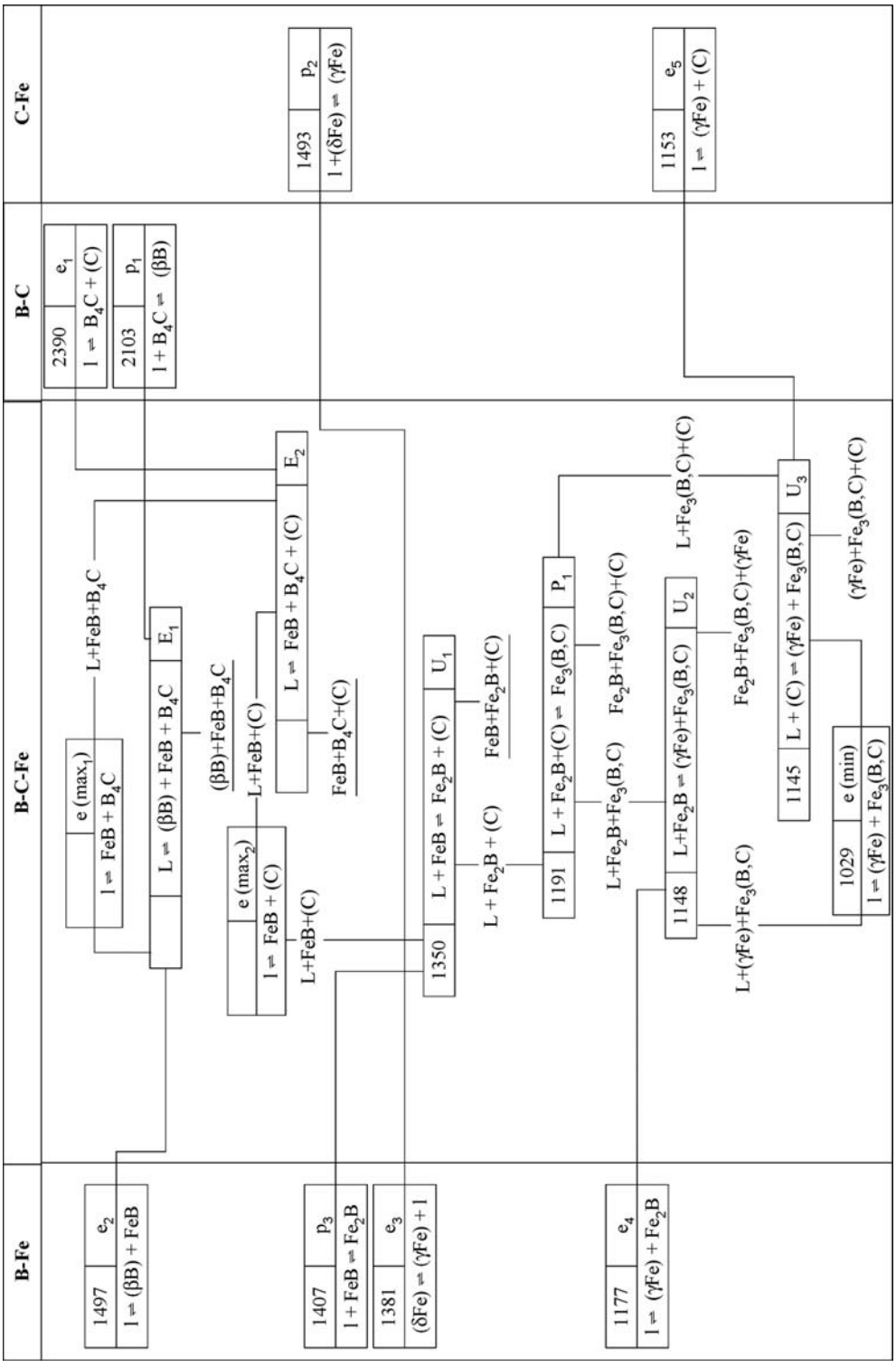

Fig. 1. B-C-Fe. Reaction scheme of the equilibrium diagram for $T > 1000°C$

DOI: 10.1007/978-3-540-69761-9_15

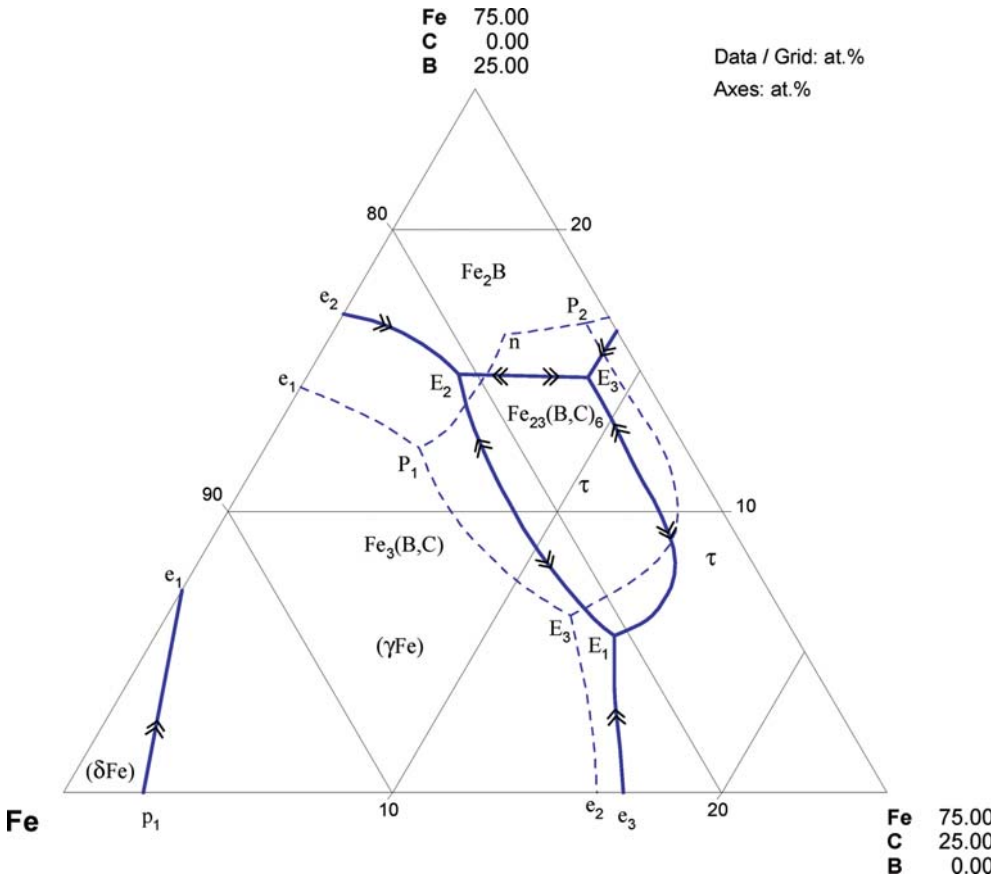

Fig. 2a. B-C-Fe. Partial liquidus projection (metastable); solid line after [1963Sta] from alloys cast on a copper plate and quenched in water; dashed line [1978Fom] from alloys quenched at 50°C·min^{-1}

DOI: 10.1007/978-3-540-69761-9_15

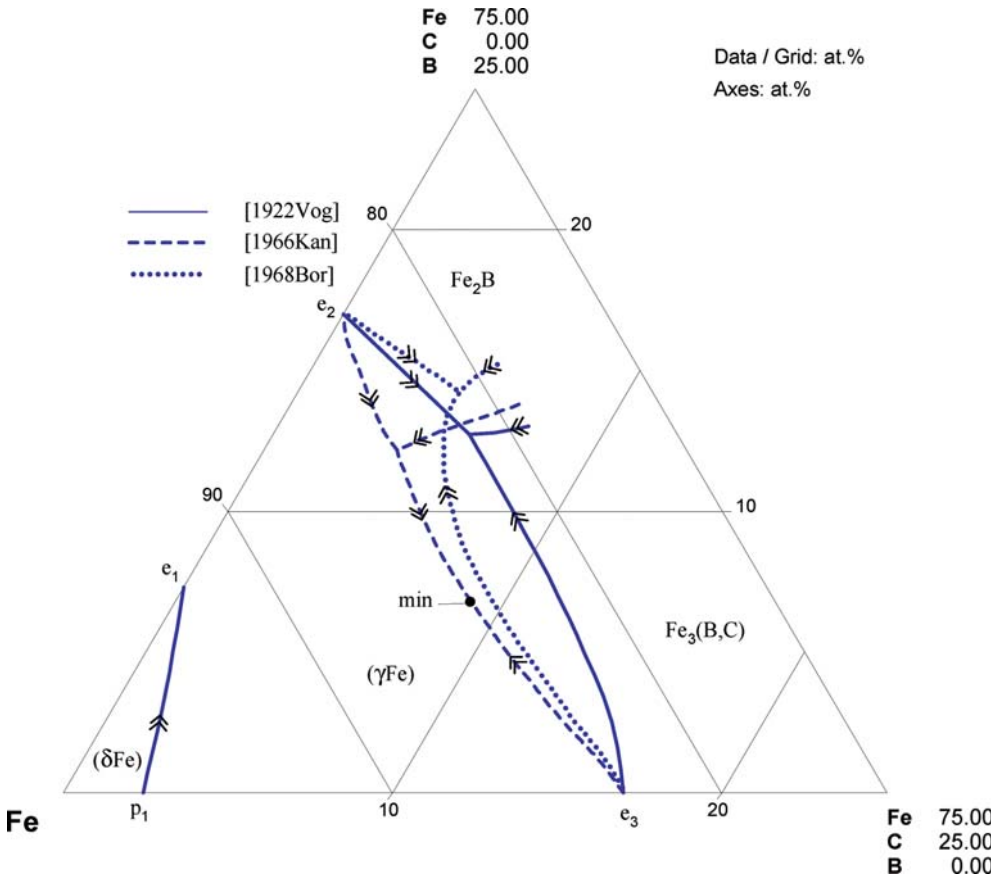

Fig. 2b. B-C-Fe. Partial liquidus projection (metastable): Comparison of results on alloys cooled at a rate of 1-2 $K \cdot s^{-1}$ [1922Vog], cooled at ~ 5 $K \cdot s^{-1}$ [1966Kan], [1968Bor]

DOI: 10.1007/978-3-540-69761-9_15

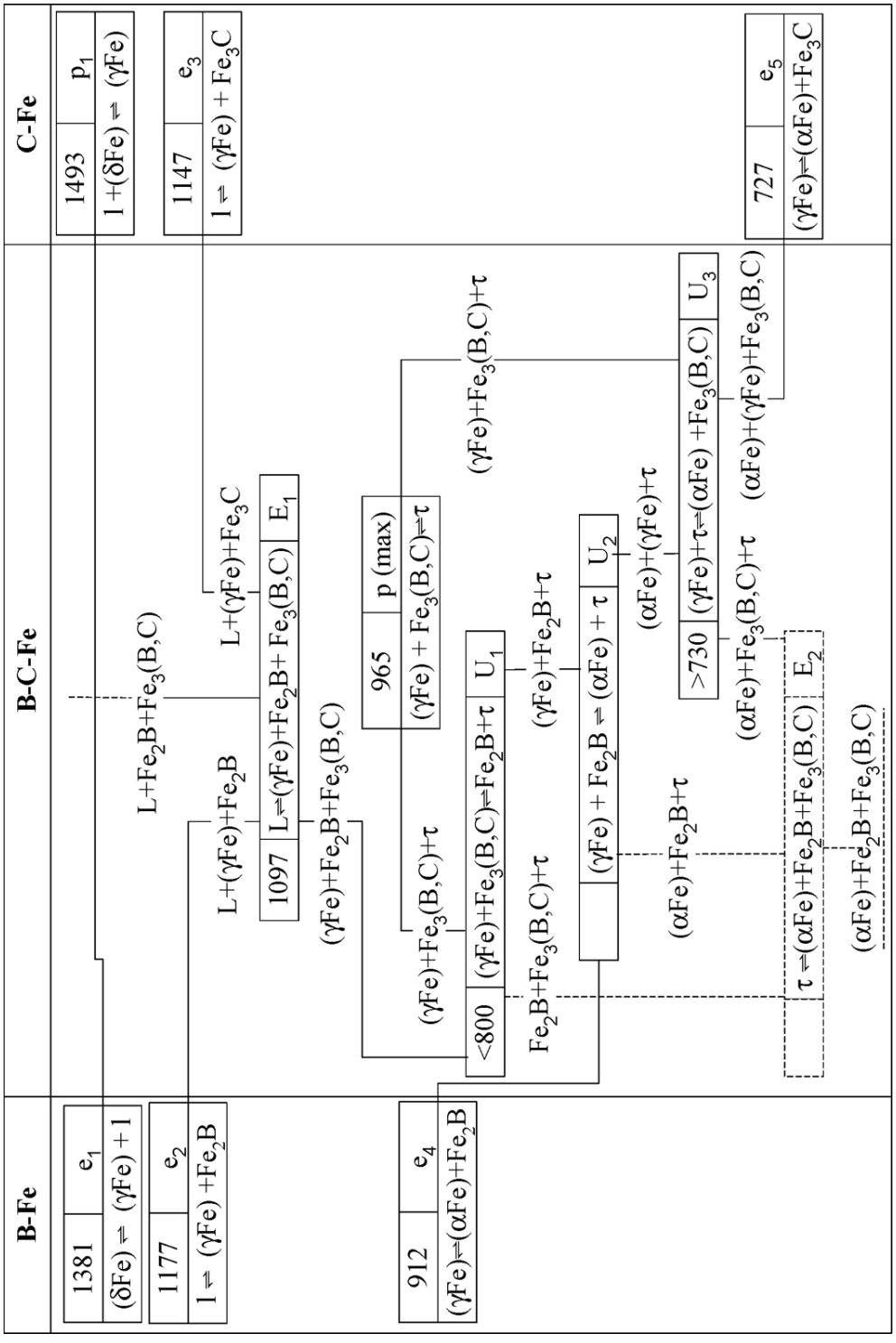

Fig. 3. B-C-Fe. Partial reaction scheme; metastable

DOI: 10.1007/978-3-540-69761-9_15

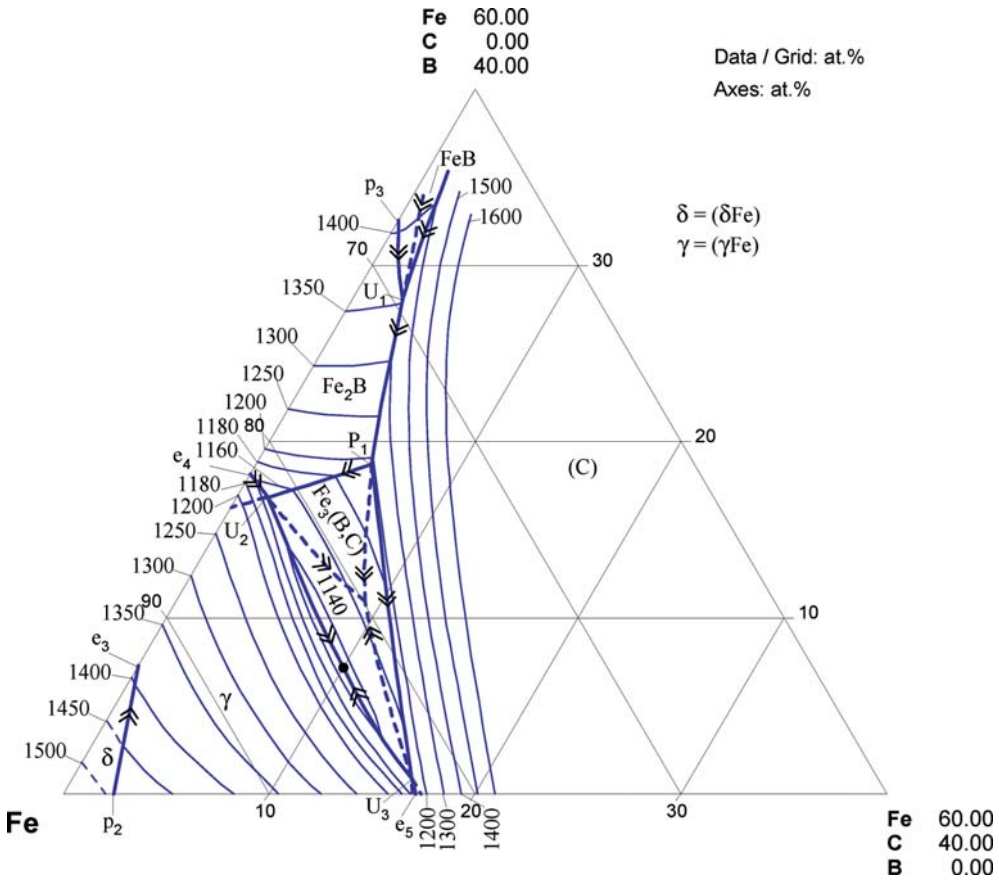

Fig. 4a. B-C-Fe. Liquidus surface for the Fe rich part; dashed lines are metastable extrapolation of the monovariant lines

DOI: 10.1007/978-3-540-69761-9_15

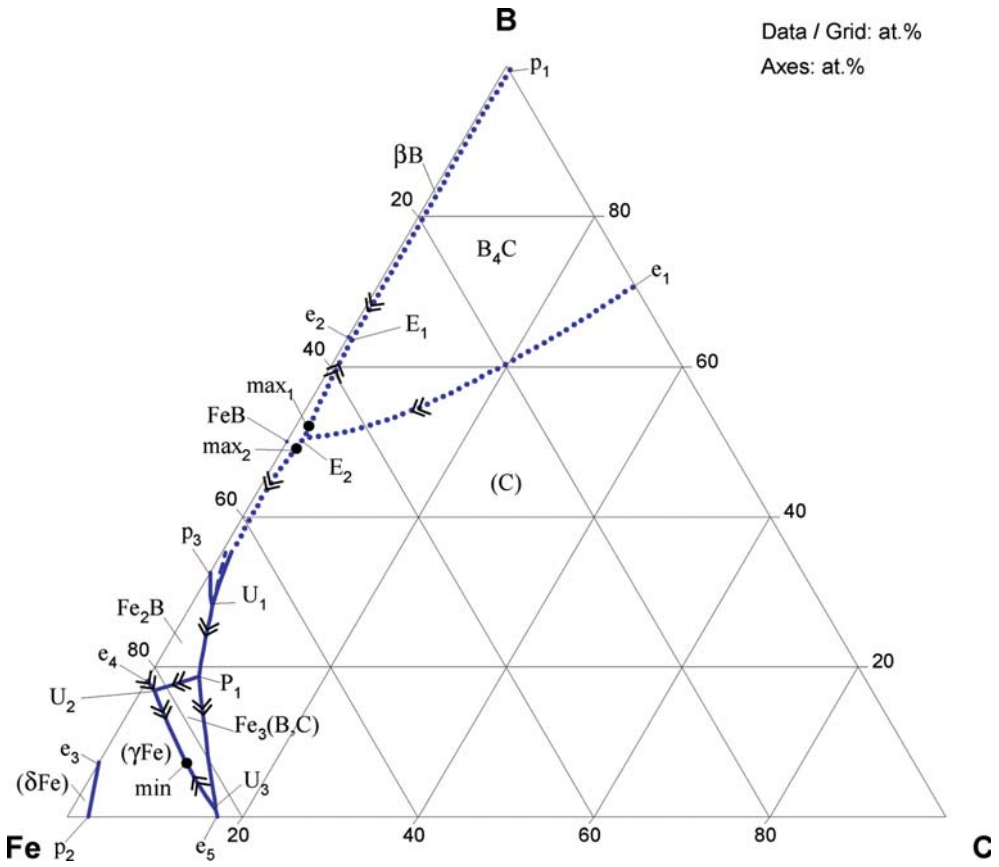

Fig. 4b. B-C-Fe. Liquidus surface; dotted lines are proposed

DOI: 10.1007/978-3-540-69761-9_15

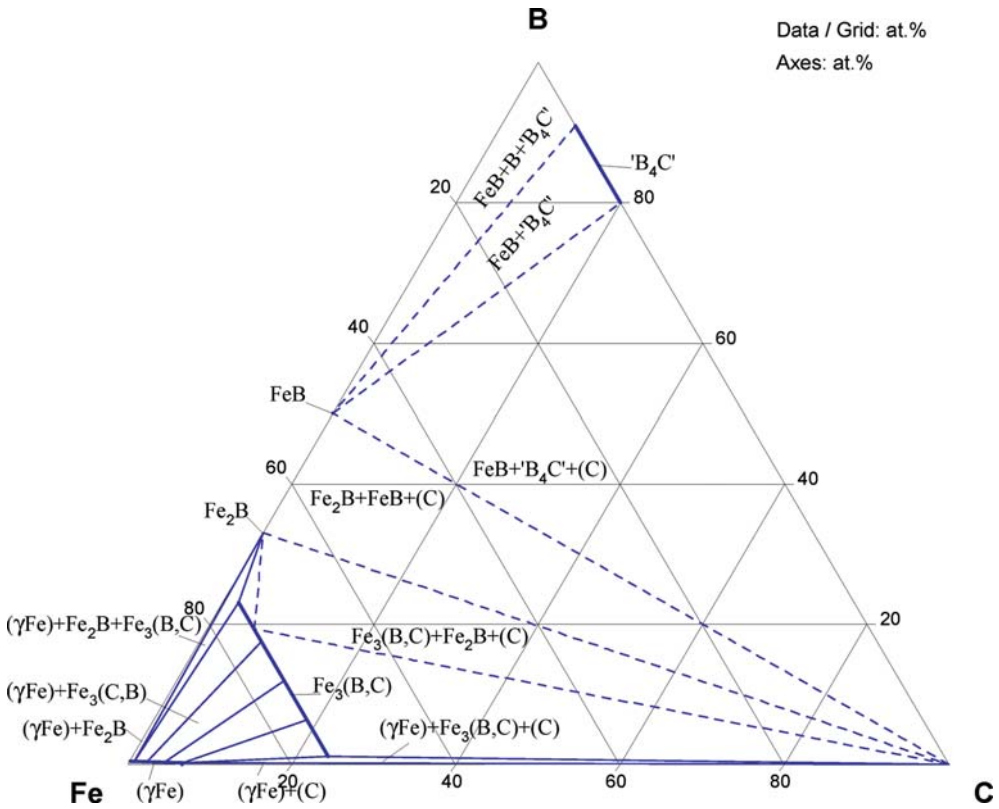

Fig. 5. B-C-Fe. Isothermal section at 1050°C; stable equilibria

DOI: 10.1007/978-3-540-69761-9_15

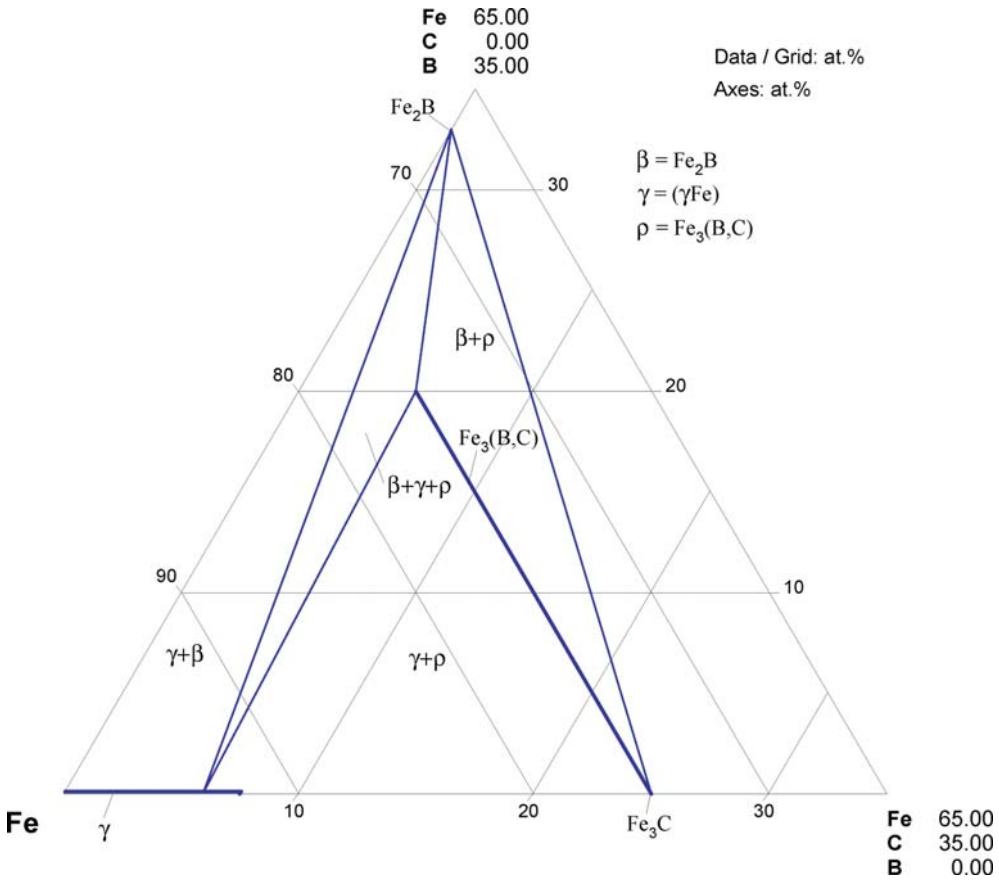

Fig. 6. B-C-Fe. Partial isothermal section at 1000°C; metastable

DOI: 10.1007/978-3-540-69761-9_15

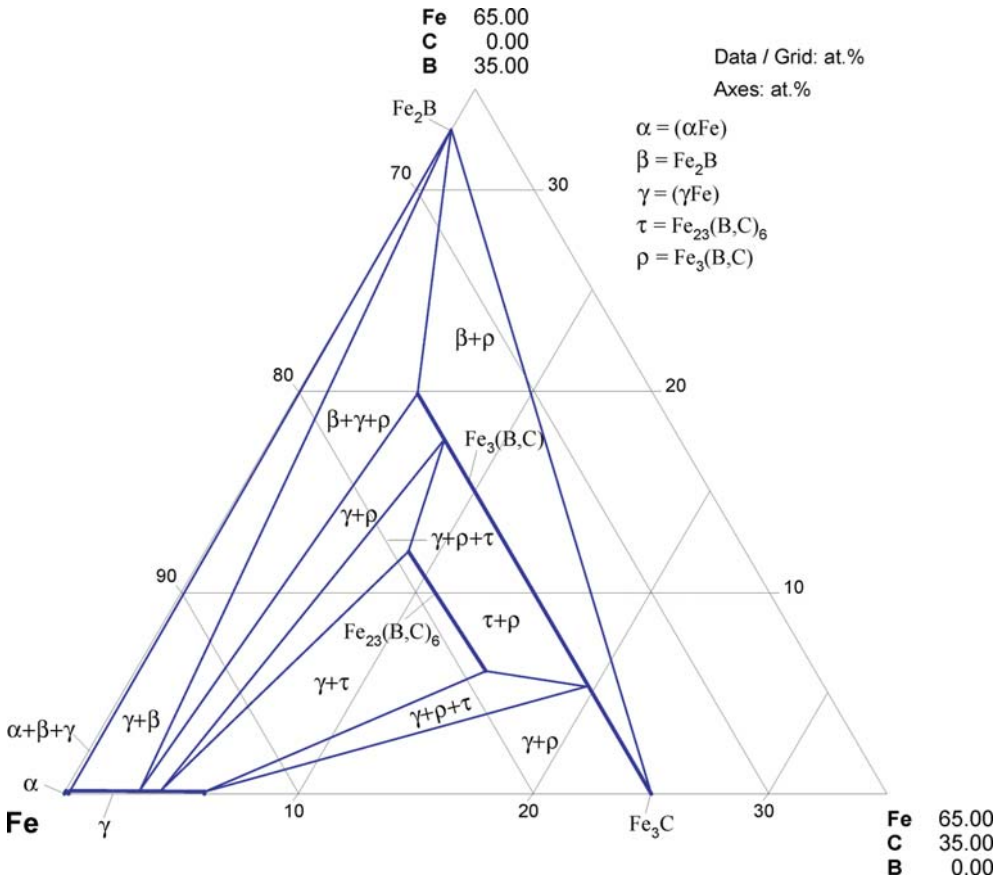

Fig. 7. B-C-Fe. Partial isothermal section at 900°C; metastable

DOI: 10.1007/978-3-540-69761-9_15

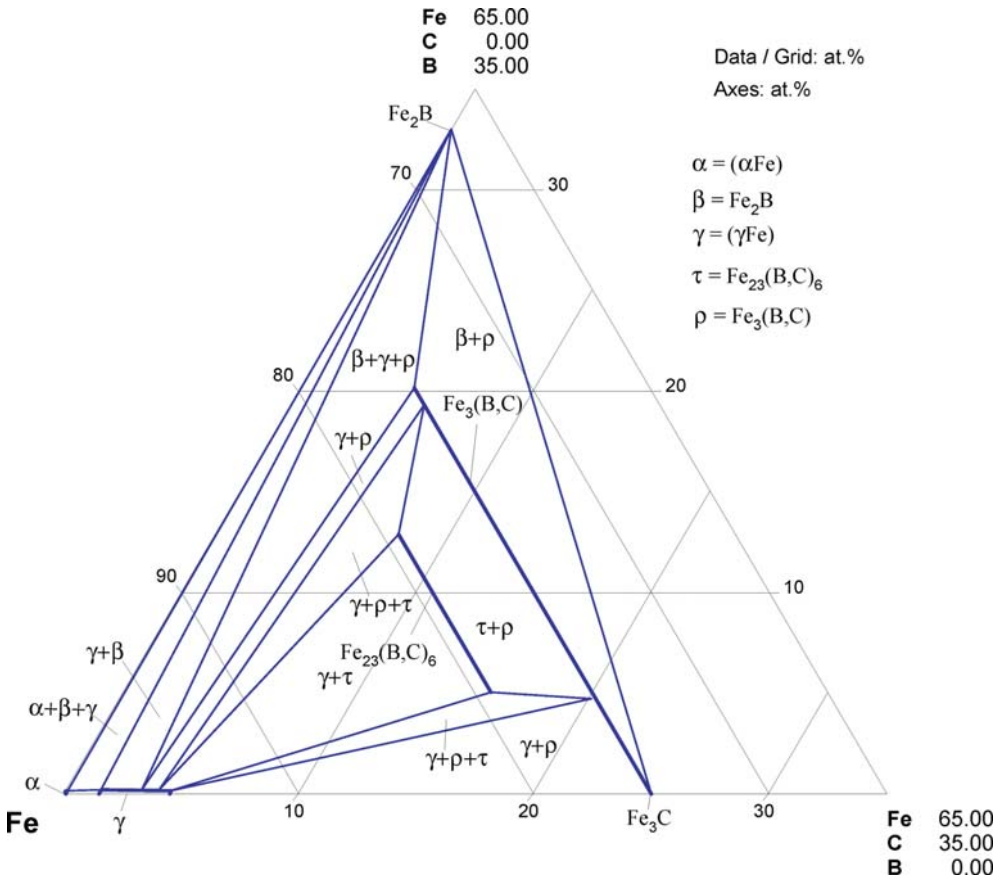

Fig. 8. B-C-Fe. Partial isothermal section at 800°C; metastable

DOI: 10.1007/978-3-540-69761-9_15

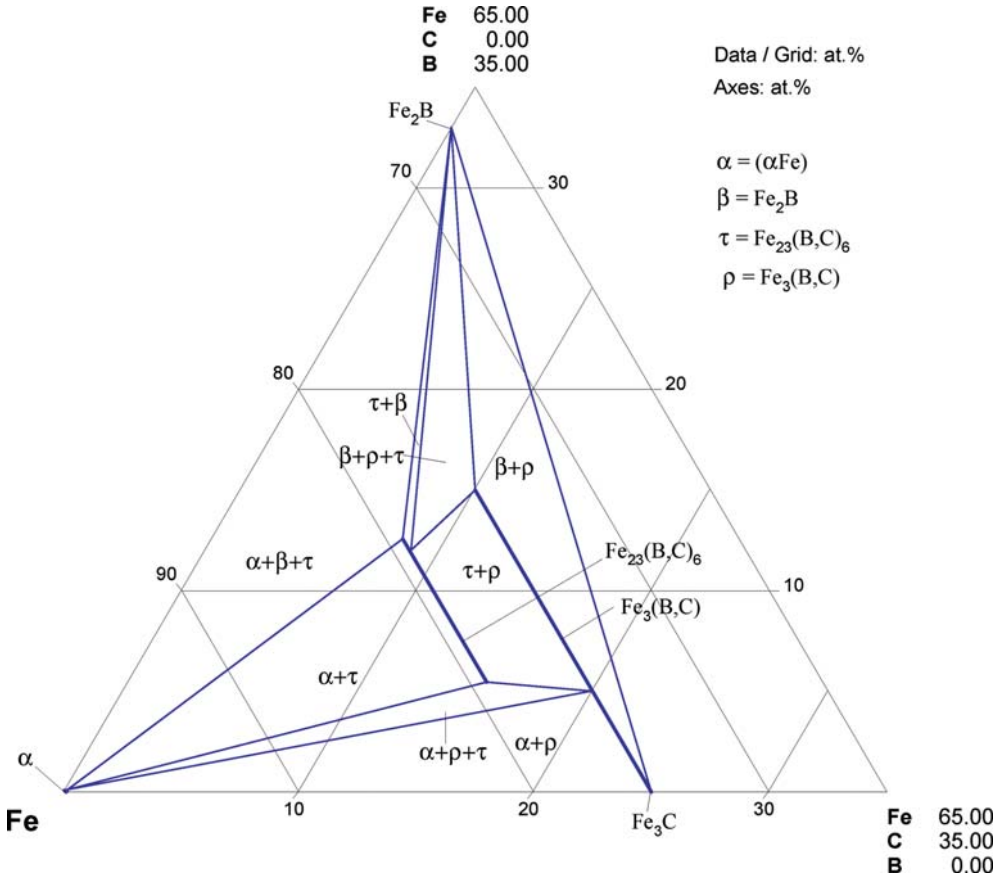

Fig. 9. B-C-Fe. Partial isothermal section at 700°C; metastable

DOI: 10.1007/978-3-540-69761-9_15

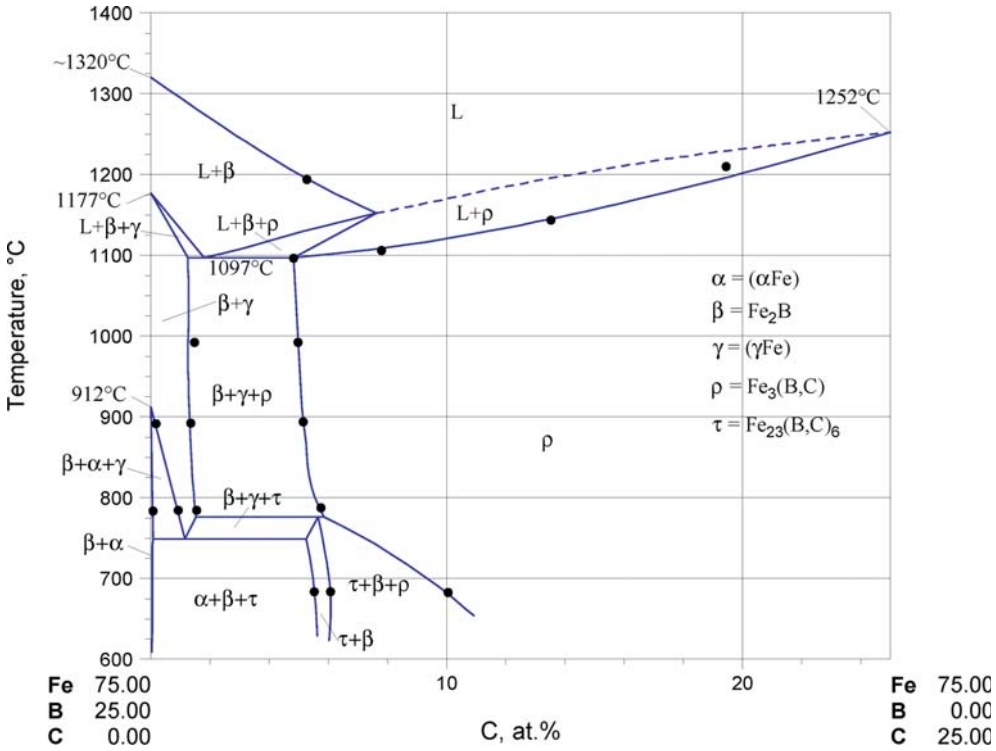

Fig. 10. B-C-Fe. Isopleth Fe_3B - Fe_3C; metastable

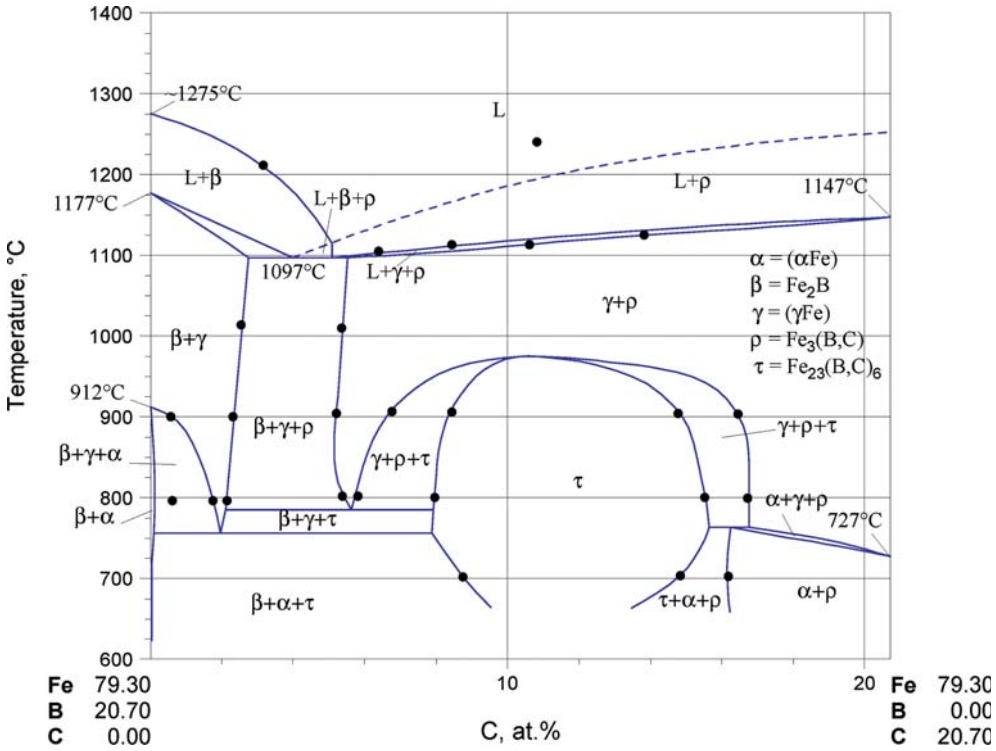

Fig. 11. B-C-Fe. Isopleth $Fe_{23}B_6$ - $Fe_{23}C_6$; metastable

DOI: 10.1007/978-3-540-69761-9_15

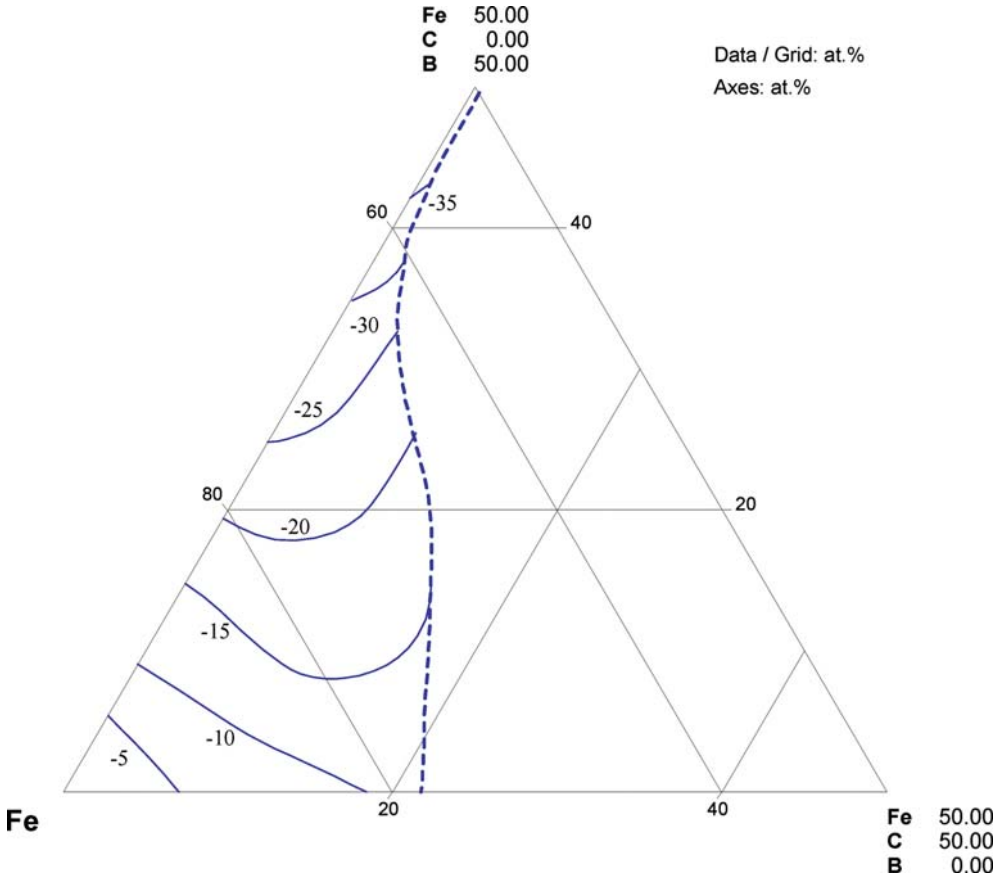

Fig. 12a. B-C-Fe. Integral enthalpies of mixing ($kJ \cdot mol^{-1}$) of liquid components

DOI: 10.1007/978-3-540-69761-9_15

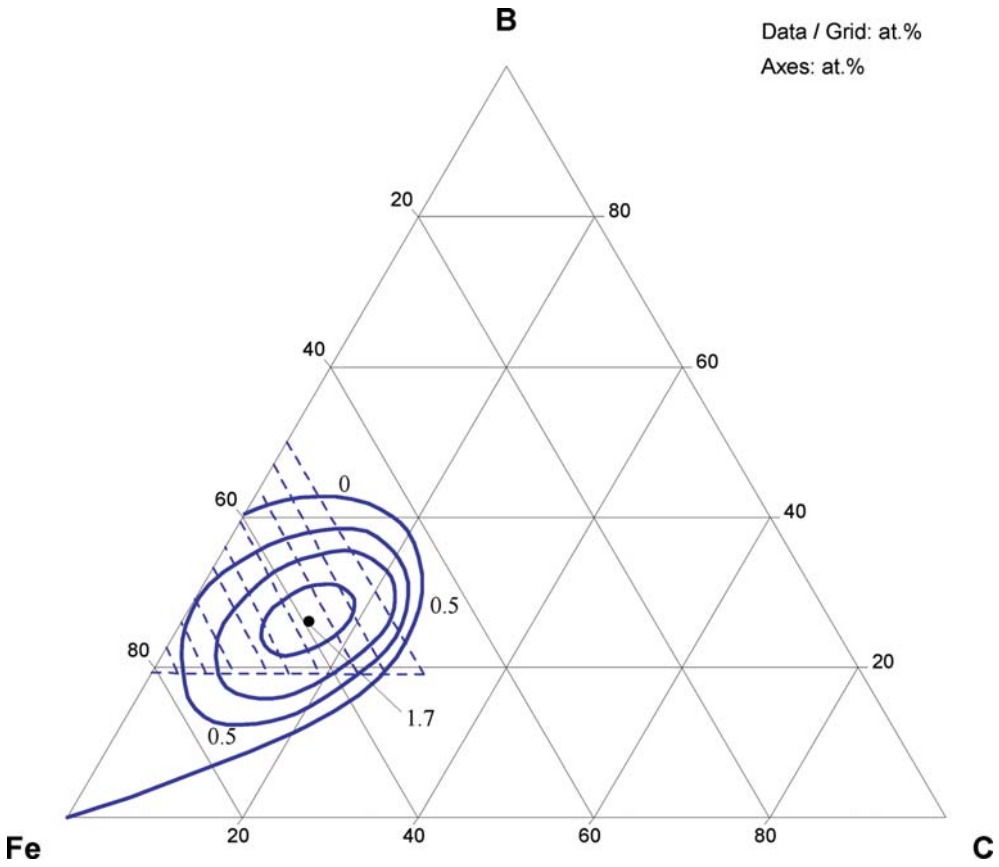

Fig. 12b. B-C-Fe. Glass forming tendency of B-C-Fe melts. In the shaded regions glasses were obtained by splat cooling

DOI: 10.1007/978-3-540-69761-9_15

References

[1922Vog] Vogel, R., Tammann, G., "On the Ternary System Fe-B-C" (in German), *Z. Anorg. Allgem. Chemie*, **123**, 225–275 (1922) (Experimental, Phase Diagram, Phase Relations, Mechan. Prop., 3)

[1949Jae] Jänecke, E., "C-Fe-B" (in German), *Kurzgefasstes Handbuch Aller Legierungen*, 679–680 (1949) (Review, 0)

[1952Gla] Glaser, F.W., "Contribution to the Metal Carbon-Boron System", *Trans. Amer. Inst. Min. Met. Eng.*, **194**(4), 391–396 (1952) (Experimental, 0).

[1954Car] Carroll, K.G., Darken, L.S., Filer, E.W., Zwell, L., "A New Iron Boro-Carbide", *Nature*, **174**, 978–979 (1954) (Experimental, Crys. Structure, 3).

[1957Nic] Nicholson, M.E., "Solubility of Boron in Fe_3C and Variation of Saturation Magnetization, Curie Temperature, and Lattice Parameter of $Fe_3(B,C)$ with Composition", *Trans-AIME (J. Metals)*, **209**, 1–6 (1957)

[1963Sta] Stadelmaier, H.H., Gregg, R.A., "The Ternary Compound $Fe_{23}B_3C_3$ in the System Fe-B-C", *(in German), Metall. (Berlin)*, **17**, 412–414 (1963) (Phase Relations, Experimental, 7)

[1965Bur] Burylev, B.P., "Activity of B, Mg, and As in Molten Fe-C Alloys", *(in Russian), Izv. Vysh. Uchebn. Zaved., Chern. Metall.*, **6**, 5–9 (1965) (Experimental, Thermodyn., 13)

[1966Kan] Kaneko, H, Nishizawa, T., Chiba, A., "Borides and Carbides in the System Fe-B-C" (in Japanese), *Nippon Kinzoku Gakkaishi*, **30**, 263–269 (1966) (Experimental, Phase Relations, 11)

[1967Bor] Borlera, M.L., Pradelli, G., "Solid State Equilibria in the System Fe-B-C" (in Italian), *Metall. Ital.*, **59**, 907 (1967) (Experimental, Morphology, Crys. Structure, Phase Diagram, Phase Relations, 31)

[1967Low] Lowell, C.E., "Solid Solution of Boron in Graphite", *J. Am. Ceram. Soc.*, **50**, 142–144 (1967) (Crys. Structure, Experimental, 5)

[1968Bor] Borlera, M.L., Pradelli, G., "On the System Fe-B-C" (in Italian), *La Metallurgia Italiana*, **60**(3), 140–146 (1968) (Experimental, Crys. Structure, Phase Diagram, Phase Relations, 4)

[1971Fom] Fomichev, O.I., Zhluktenko, E.I., Katkov, V.F., Spiridonova, I.M., "The Ternary Diagram $Fe\text{-}Fe_2B\text{-}Fe_3C$" (in Russian), VINITI Document N. 3163-71, Zh. Fiz. Khim., **45**, 2688–2689 (1971) (Abstract, 0)

[1974Fom1] Fomichev, O.I., Katkov, V.F., Kushnereva, A.K., "On the Complex cubic Fe Borocarbide in the Ternary B-C-Fe System", *Zh. Fiz. Khim.*, **48**, 2580 (1974) (Experimental, Crys. Structure, 5)

[1974Fom2] Fomichev, O.I., Katkov, V.E., Kushnereva, A.K, "Study of the Carbide Phase in Ternary B-C-Fe Alloys", *Izv. Vyssh. Ucheb. Zaved., Chern. Met.*, (3), 119-121 (1974) (Experimental, Crys. Structure, 6)

[1974Has] Hasebe, M., Nishizawa, T., "Thermodynamic Analysis of the B-C-Fe Ternary Equilibrium System", *Nihon Kinzoku Gakkaishi*, **38**(1), 46–54 (1974) (Thermodyn., Calculation, Phase Diagram, Phase Relations, 33)

[1975Tve] Tverdokhlebova, S.V., Tsikora, I.L., Spiridonova, I.M., "Spectral Analysis of Iron-Boron-Carbon Alloys", *Industrial Laboratory*, **41**(11), 1657–9 (1975) (Experimental, 4)

[1976Fom] Fomichev, O.I., Katkov, V.F., Kushnereva, A.K., "Phase Composition of Alloys Fe-B-C", *Inorg. Mater. (Engl. Trans.)*, **12**(1), 111–112 (1976), translated from *Izv. Akad. Nauk SSSR, Neorg. Mater.*, 12 (1), 128-129 (1976) (Experimental, Crys. Structure, 4)

[1978Cam] Cameron, T.B., Morral, J.F., "Studies of the Fe-C-B Phase Diagram by Autoradiography", *Applications of Phase Diagrams in Metallurgy and Ceramics*, Nat. Bur. Standards Washington, DC, USA, Part I, pp. 566 (1978) (Experimental, 0)

[1978Fom] Fomichev, O.I., Katkov, V.F., Kushnereva, A.K.: *Russ. J. Phys. Chem. (Engl. Transl.)*, **52**(9), 1294–1296 (1978), translated from *Zh. Fiz. Khim.*, 52(9), 2240–2243 (1978)(Experimental, Phase Diagram, 6)

DOI: 10.1007/978-3-540-69761-9_15

[1978Her] Herold, U., Köster, U., "Metastable Phases in Extremly Fast Solidified Iron-Boron Aloys" (in German), *Z. Metallkd.*, **69**(5), 326–332 (1978) (Experimental, Phase Diagram, Crys. Structure, 27)

[1978Lub] Luborsky, F.E., Becker, J.J., Liebermann, H.H., "Replacement of Boron by Carbon in B-C-Fe Amorphous Alloys", *Rapidly Quenched Metals III. Metals Soc*. **Part II**, 249–52 (1978) (Experimental, 3)

[1979Pan] Panasiuk, A.D., Oreshkin, V.D., Maslennikova, V.R., "Investigation of Kinetics of Boron Carbide Interaction with Liquid Aluminium, Silicon, Nickel and Iron" (in Russian), *Poroshkov. Metall. (Kiev)*, **199**(7), 79–83 (1979) (Experimental, Kinetics, Morphology, Mechan. Prop., 9)

[1979Hat1] Hatta, S., Egami, T., Graham, C.D. Jr., "Fe-B-C Amorphous Alloys with Room-Temperature Saturation Induction Over 17.5 kG", *Appl. Phys. Lett.*, **34**(1), 113–115 (1979) (Experimental, Magn. Prop., 12)

[1979Hat2] Hatta, S., Egami, T., "Temperature-Dependence of Magnetization of Amorphous Fe-B-C Alloys", *J. Appl. Phys.*, **50**(3), 1589–1591 (1979) (Experimental, Magn. Prop., 16)

[1979Lub] Lubovsky, F.E., Flanders, P.J., Liebermann, H.H., Walter, J.L.: 'Effect of Metalloid on Magnetostriction of Fe-B-C and Fe-B-Si Amorphous Alloys", *IEEE Trans. Magn.*, **15**(6), 1961–1962 (1979) (Experimental, Magn. Prop., 13)

[1980Lub] Lubovsky, F.E., Becker, J.J., Walter, J.L., Martin, D.L., "The Fe-B-C Ternary Amorphous Alloys", *IEEE Trans. Magn.*, **16**(3), 521–525 (1980) (Experimental, Phase Relations, Magn. Prop., 21)

[1981Fom] Fomichev, O.I., Katkov, V.F., Kushnereva, A.K., Brekharya, G.P., "Study of the Ternary Phase in the System Fe-B-C", *(in Russian) Inorg. Mater. (Engl. Trans.)*, **12**(1), 111–112 (1976) *Izv. Vyssh. Ucheb. Zaved., Chern. Met.*, (1), 101-103 (1981)(Experimental, Crys. Structure, 4).

[1981Lin] Lin, S.T., Jang, L.Y., Chou, L.S., "Mössbauer Study of Fe-B-C and Fe-B-Si Amorphous Alloys", *Solid State Commun.*, **38**(9), 853–857 (1981) (Experimental, Magn. Prop., 10)

[1981Mir] Miroshnichenko, I.S., Spektor, E.Z., Bashev, V.F., "Structure of Fe-B and Fe-C-B Alloys in Liquid and Amorphous States" (in Russian), *Metallofizika*, **3**(4), 111–131, (1981) (Experimental, 10)

[1981Nis] Nishizawa, T., Hasebe, M., "Computer Calculation of Phase Diagrams of Iron Alloys" (in Japanese), *Tetsu to Hagane*, **67**(1), 2086–2097 (1981) (Review, Thermodyn., Phase Diagram, 110)

[1982Kha] Khan, Y., Kneller, E., Sostarich, M., "The Phase Fe3B", *Z. Metallkd.*, **73**(10), 624–626 (1982) (Experimental, Crys. Structure, Phase Diagram, 13)

[1983Bus] Buschow, K.H.J., van Engen, P.G., Jongebreur, R., "Magneto-Optical Properties of Metallic Ferromagnetic Materials", *J. Magn. Magn. Mater.*, **38**, 1–22 (1983) (Magn. Prop., Optical Prop., 23)

[1984Maj] Majumdar, A.K., Üffinger, G., "Effect of Carbon Substitution on the Specific Heat of $Fe_{80}B_{20-x}C_x$ ($0 \leq x \leq 8$)", *Solid State Commun.*, **51**(12), 967–969 (1984) (Experimental, Thermodyn., 11)

[1985Smi] Smid, I., Rogl, P., "Phase Equilibria and Structural Chemistry in Ternary Systems: Transition Metal - Boron - Nitrogen", *Proceedings of the 11th Intl. Plansee Seminar*, **Vol. 2,** Bildstein, H., Ortner, H., (Eds.), Verlag Tyrolia, Innsbruck, Austria, 1029–1035 (1985) (Experimental, Phase Relations, 17)

[1985Sch] Schürmann, E., Shao-Xiong,, Li, "Investigation of the Liquid Equilibria in the Ternary System Fe-B-C" (in German), *Giessereiforschung*, **37**(4), 121–129 (1985) (Experimental, Phase Diagram, 18)

[1986Rag] Raghavan, V., Ghosh, G., "The Boron-Carbon-Iron System", *J. Alloy Phase Diagrams*, **2**(2), 77–92 (1986) (Review, Phase Diagram, Crys. Structure, 41)

DOI: 10.1007/978-3-540-69761-9_15

[1986Smi] Smid, I., Rogl, P., "Phase Equilibria and Structural Chemistry in Ternary Systems: Transition Metal - Boron - Nitrogen", *Inst. Phys. Conf.* Ser. No. 75, Ch. 4, Adam Hilger Ltd., 249-257 (1986) (Experimental, Phase Diagram, Crys. Structure, 17)

[1987Isa] Isakov, M.G., Prusakov, G.M., Shcherbedinskii, G.V., "Kinetics of Boride Growth in Fe-B and Fe-B-C Systems", *Russ. Metall.*, (1), 182-189 (1987) (Experimental, Kinetics, 8)

[1987Mal] Malinochka, Y.N., Koval'chuk, G.Z., Yarmosh, V.N., Shmelev, Yu.S., Garmash, L.I., "Structure and Phase Composition of Eutectic in Fe-C-B and Fe-C-B-Cu Alloys with a Low Boron Content", *Russ. Metall.*, **6**,178–181 (1987) translated from *Izv. Akad. Nauk SSSR, Met.*, **6**, 174-177 (1987) (Experimental, 4)

[1987Sud] Sudzuki, K., Fujimori, H., Mosumoto, K., "Amorphous Metals" (in Russian), *Metallurgiya*, Moscow, (1987) as quoted by [1994Wit]

[1987Spi] Spiridonova, I.M., "Effect of Cooling Rate on the Structure and Properties of Fe-B-C Alloys", *Metal Science and Heat Treatment*, **29**(9–10), 699–671 (1987) (Experimental, 3)

[1987Zha] Zhang, Y.D., Budnick, J.I., Sanchez, F.H., Hines, W.A., Yang, D.P., Livingston, J.D., "NMR-studies in Orthorhombic $Fe_3B_{1-x}C_x$ ($0.1 \beta \leq x \beta \leq 0.4$)", *J. Appl. Phys.*, **61**(8), 4358–4360 (1987) (Experimental, Crys. Structure, 17)

[1988Hor] Hornbogen, E, Staniek, S, "The Origin of the 3-Zone Structure at the Surface of Laser Melted Eutectic Fe-B-C Alloys", *Z. Metallkd.*, **79**(6), 375–380 (1988) (Experimental, 6)

[1988Oht] Ohtani, H., Hasche, M., Ishida, K., Nishizawa, T., "Calculation of Fe-B-C Ternary Phase Diagram", *Trans. Iron Steel Inst. Japn.*, **28**, 1043–1050 (1988) (Thermodyn., Phase Diagram, Phase Relations, 30)

[1988Roy] Roy, S.B., Nigam, A.K., Chandra, G., Majumdar, A.K., "Electrical Resistivity and Magnetoresistance in Fe-B-C Amorphous Alloys", *J. Phys. F (Metal Physics)*, **18**(12), 2625–2633 (1988) (Experimental, Magn. Prop., Electr. Prop., 30)

[1989Bra] Brakman, C.M., Gommers, A.W.J., Mittemeijer, E.J., "Boriding of Fe and Fe-C, Fe-Cr and Fe-Ni Alloys: Boride-Layer Growth Kinetics", *J. Mater. Res.*, **4**(6), 1354–1370 (1989) (Experimental, Kinetics, Morphology, Phase Relations, Thermodyn., 25)

[1989Tur] Turov, Y.V., Khusid, B.M., Voroshin, L.G., Khina, B.B., Kozlovskii, I.L., "Structure Formation in Sintering Iron-Boron Carbide Powder Composite", translated from *Poroshkov. Metall. (Kiev)*, **6**, 25–31 (1991) (Experimental, 6)

[1990Ase] Aselage, T.L., Tallant, D.R., Gieske, J.H., "Preparation and Properties of Icosahedral Borides", in "*The Physics and Chemistry of Carbides, Nitrides and Borides*", Freer, R. (Ed.) Proc. NATO Advanced Research Workshop, Manchester, U.K. Sept. 1989, published as *ASI-Series, Series E: Applied Sciences*, **Vol. 185**, Kluwer Acad. Publ., Dordrecht (1990) 97–111 (Crys. Structure, Review, Experimental, 14)

[1991Kha] Khan, Y., Wibbeke, H., "Formation of the τ-Phase in the Fe-B Alloys", *Z. Metallkd.*, **82**(9), 703–705 (1991) (Experimental, Crys. Structure, 6)

[1991Kan] Kano, M., Tanimoto, I., "Wear Mechanism of High Wear-Resistana Materials for Automotive Valve Trains", *Wear*, **151**(2), 229–243 (1991) (Abstract, Mechan. Prop., 14)

[1992Ge] Ge, S.H., Mao, M.X., Chen, G.L., Chen, Z.H., Zhang, C.L., Zhang, Y.D., Hines, W.A., Budnick, J.I., "Effect of Short-range Order on the Magnetic Properties of Fe-B-C Amorphous Alloys: NMR and Magnetization Measurements", *Phys. Rev. B: Condens. Matter*, **45**(9), 4695–4699 (1992) (Experimental, Magn. Prop., 16)

[1992Rog] Rogl, P., "The System B-N-Fe" in"*Phase Diagrams of Ternary Boron Nitride and Silicon Nitride Systems*,", Rogl, P. Schuster, J.C., (Eds.), ASM, Materials Park, OH 1992, 33–36 (Crys. Structure, Thermodyn., Phase Diagram, Phase Relations, Experimental, Review, 9)

[1993Lev] Levin, D.M., Kanunnikova, I.Yu., "Influence of Boron on Parameters of Impurity Pinning for Dislocations in Low-Carbon Iron", *Bull. Russ. Acad. Sci. Physics*, **57**(11), 1937–1940 (1993) (Experimental, 11)

DOI: 10.1007/978-3-540-69761-9_15

[1993Wer] Werheit, H., Kuhlmann, U., Laux, M., Lundstrm, T., "Structural and Electronic Properties of Carbon-Doped β-Rhombohedral Boron", *Phys. Stat. Sol.*, **B179** 489–511 (1993) (Crys. Structure, Experimental, 51)

[1994Mao] Mao, M.X., Ge, S.H., Chen, Z.H., Chen, G.L., Zhang, C.L., Zhang, Y.D., Hines, W.A., Budnick, J.I., "Development of Short-range Order in Fe-B-C Amorphous Alloys With Thermal Treatment - an NMR Study", *J. Magn. Magn. Mater.*, **138**(3), 301–306 (1994) (Crys. Structure, Experimental, 20)

[1994McH] McHale, A.E., "B-C-Fe"in "*Phase Equilibria Diagrams, Phase Diagrams for Ceramists*," **10**, 181–182 (1994) (Phase Diagram, Phase Relations, 2)

[1994Wit] Witusiewisz, V.T., "Thermodynamic Properties of Liquid Alloys of 3d Transition Metals with Metalloids (Silicon, Carbon and Boron)", *J. Alloys Compd.*, **203**, 103–116 (1994) (Thermodyn., 89)

[1994Ter] Terry, B.S., Chinyamakobvu, O.S., "Assessment of B_4C Reaction with Liquid Iron Alloys", *J. Mater. Sci.*, **29**, 464–467 (1994) (Experimental, 6)

[1995Hal] Hallemans, B., Wollants, P., Roos, J.R., "Thermodynamic Assessment of the Fe-Nd-B Phase Diagram", *J. Phase Equilib.*, **16**(2), 137–149 (1995) (Calculation, Phase Relations, Thermodyn., 41)

[1995Rab] Rabitsch, K., Sitte, R., Ebner, R., Jeglitsch, F., "Solidification Behavior in Extremely Fast Solidified Fe-Cr-B-C Alloys", *Prakt. Metallographie, Sonderband*, **26**, 545–556 (1995) (Experimental, Theory, 15)

[1995Hua] Huang, X.M., Ischak, W.G., Fukuyama, H., Fujisawa, T., Yamauchi, C., "Activities of Fe-B-N and Fe-C-B Systems by Interstitial Solution Theory" (in Japanese), *Tetsu to Hagane (J. Iron Steel Inst. Jpn.)*, **81**(11), 1049–1054 (1995) (Experimental, Thermodyn., 23)

[1995Vil] Villars, P., Prince, A., Okamoto, H., "Handbook of Ternary Alloys Phase Diagrams", **Vol. 5**, ASM International, Materials Park, Ohio, USA (1995) (Phase Diagam, Crys. Structure, Review, 7).

[1996Spi] Spiridonova, I.M., Sukhovaya, E.V., Balakin, V.F., "Structure and Deformation Peculiarities of Fe(B,C) Crystals", *Metallurgiya*, **35**(2), 65–67 (1996) (Experimental, Crys. Structure, 8)

[1998Bam] Bamberger, M., "Laser Surface Hardening of Structural Ferrous Alloys", *Int. Mater. Rev.*, **43**(5), 189–203 (1998) (Review, 66)

[1999Yam] Yamashita, T., Matsuzaki, A., Takajo, S., Hasebe, M., "Precipitation Behaviours of Cementite in Fe-0.8 mass% C-0.1 mass% B Alloy" (in Japanese), *J. Jpn. Inst. Met.*, **63**(6), 708–716 (1999) (Calculation, Phase Relations, 9)

[2000Sel] Selcuk, B., Ipek, R., Karamis, M.B., Kuzucu, V., "An Investigation on Surface Properties of Treated Low Carbon and Alloyed Steels (Boriding and Carburizing)", *J. Mat. Proc. Tech.*, **103**(2), 310–317 (2000) (Experimental, Mechan. Prop., Morphology, 13)

[2001Fen] Fenstad, J., Tuset, J.Kr., "The Binary Diagrams within the System Fe-Mn-C-O, and the Thermal Properties of Elemental Manganese", *INFACON 9: Proceedings of the International Ferro-Alloys Congress*, June 2001, Quebec, Canada, **9**, (2001) (Experimental, Phase Relations, Thermodyn., 25)

[2002Ge] Ge, C.L., Ye, R.C., "Research on Self-propagating Eutectic Boriding", *J. Mat. Proc. Tech.*, **124**(1–2), 14–18 (2002) (Crys. Structure, Experimental, Mechan. Prop., Phase Diagram, Phase Relations, 9)

[2002Gop] Gopalakrishnan, P., Snankar, P., Palaniappa, M., Ramakrishnan, S.S., "Interrupted Boriding of Medium-Carbon Steels", *Metall. Mater. Trans. A*, **33**(5), 1475–1485 (2002) (Phase Diagram, 34).

[2003Abe] Abenojar, J., Velasco, F., Martinez, M.A., "Influence of Carbon and Aluminium Additions on the Fe-10% B (wt.) System", *J. Mat. Proc. Tech.*, **143–144**, 28–23 (2003) (Crys. Structure, Experimental, Morphology, Phase Relations, 10)

[2003Abe] Abe, T., Onodera, H., "Effect of Boron Addition on Strain Aging Properties of Ferritic Steels", *Tetsu to Hagane (J. Iron Steel Inst. Jpn.)*, **89**(3), 357–361 (2003) (Experimental, Mechan. Prop., 29)

DOI: 10.1007/978-3-540-69761-9_15

[2004Mar] Martini, C., Palombarini, G., Carbuciccio, M., "Mechanism of Thermochemical Growth of Iron Borides on Iron", *J. Mater. Sci.*, **39**(3), 933–937 (2004) (Crys. Structure, Experimental, Kinetics, Morphology, Phase Relations, 19)

[2006Kul] Kulka, M., Pertek, A., Klimek, L., "The Influence of Carbon Content in the Borided Fe-alloys on the Microstructure of Iron Borides", *Mater. Charact.*, **56**(3), 232–240 (2006) (Crys. Structure, Experimental, Morphology, Phase Relations, 12)

[Mas2] Massalski, T.B. (Ed.), *Binary Alloy Phase Diagrams*, 2nd edition, ASM International, Metals Park, Ohio (1990)

[V-C] Villars, P. and Calvert, L.D., *Pearson's Handbook of Crystallographic Data for Intermetallic Phases*, ASM, Metals Park, Ohio (1985)

[V-C2] Villars, P. and Calvert, L.D., *Pearson's Handbook of Crystallographic Data for Intermetallic Phases*, 2nd edition, ASM, Metals Park, Ohio (1991)

DOI: 10.1007/978-3-540-69761-9_15

Boron – Cobalt – Iron

Olga Fabrichnaya

Introduction

Phase relations and thermodynamic properties of the B-Co-Fe system are of interest because metallic amorphous materials with high magnetic permeability form from melts using rapid quenching. Phase relations in the B-Co-Fe system were studied experimentally by [1952Hae, 1980Gia, 1980Rog, 1981Pra]. An isothermal section at 1000°C, quasibinary and vertical sections as well as a liquidus surface were constructed by [1981Pra]. An isothermal section at 900°C was constructed based on diffusion couple experiments by [1989Van]. These data were used to explain diffusion paths for Co/Fe_2B and $Co_{0.8}Fe_{0.2}$/Fe_2B and to present a schematic representation of boron activity in the system. Ushi and Ogawa [1991Ush] performed emf measurements at 1300°C and derived boron activity in melts. Witusievicz [1995Wit] measured partial enthalpies of formation of the B-Co-Fe liquid alloys by isoperibolic calorimetry at 1627°C. The crystallization behavior of $(Fe_xCo_{100-x})_{100-y}B_y$ amorphous alloys was studied by [1980Lat, 1982Ber, 1987Mat, 1989Zem, 1990Zem2, 1991Ste, 1991Zem, 2001Gup]. Experimental studies in the B-Co-Fe system are summarized in Table 1.
[1999McH] presented a review of synthesis, structural characterization, properties and applications of amorphous and nanocrystalline soft magnetic materials.

Binary Systems

The binary phase diagrams are accepted from [Mas2].

Solid Phases

The (γFe) and (αCo) form continuous solid solutions. The Co_2B and Fe_2B phases form continuous solid solutions $(Fe,Co)_2B$, and CoB and FeB form continuous solutions (Fe,Co)B. The phase Co_3B is stable only in the B-Co binary system; in the B-Fe this phase is metastable. However, Fe can substitute a quite remarkable amount of Co and solid solutions are formed from pure Co_3B up to 60 mol% of Fe_3B. Crystallographic information related to the solid phases is presented in Table 2.

Quasibinary Systems

The CoB-FeB system is quasibinary. The phase diagram of this quasibinary system presented in Fig. 1 is taken from [1981Pra].

Invariant Equilibria

Information relating to the ternary eutectic as determined by [1981Pra] is presented in Table 3.

Liquidus, Solidus and Solvus Surfaces

The liquidus surface constructed by [1981Pra] is presented in Fig. 2. The reaction scheme constructed from the liquidus surface is presented in Fig. 3.

Isothermal Sections

Isothermal sections of the B-Co-Fe system at 900 and 1000°C are presented in Figs. 4 and 5, based on the experimental data of [1989Van] and [1981Pra], respectively. It should be mentioned that there is a

DOI: 10.1007/978-3-540-69761-9_16

remarkable difference in the phase composition of the $(Fe,Co)_2B$ and (Fe,Co) metallic alloys in equilibrium with $(Fe,Co)_3B$ presented by [1980Rog] and [1981Pra]. The distribution of Co and Fe between (Fe,Co)B and $(Fe,Co)_2B$ was studied by [1952Hae] at 1100°C, by [1980Rog] at 1000°C and by [1980Gia] at 800, 1000 and 1200°C. The distribution of Co and Fe between $(Fe,Co)_3B$ and $(Fe,Co)_2B$ at 1000°C was studied by [1980Gia] and [1980Rog]. It should be mentioned that the data of [1980Rog] for Co/Fe distribution between (Fe,Co)B and $(Fe,Co)_2B$ phases are in a good agreement with the data of [1980Gia]. However, according to [1980Gia] the $(Fe,Co)_2B$ phase is substantially more enriched with Fe than $(Fe,Co)_3B$ is, than obtained by [1980Rog]. The investigation of [1980Gia] confirmed the conclusion of [1952Hae] that metal with the lower atomic number concentrated in the phase enriched with boron. It was also shown that this tendency decreases with increasing temperature. The distribution of Co/Fe between (Fe,Co)B and $(Fe,Co)_2B$ is shown in Fig. 6, between $(Fe,Co)_2B$ and $(Fe,Co)_3B$ in Fig. 7.

Temperature – Composition Sections

The system Co_2B-Fe_2B is not quasibinary. The Co_2B compound melts congruently, while the Fe_2B melts peritectically forming liquid and FeB. The Co_2B-Fe_2B vertical section from [1981Pra] is presented in Fig. 8. The alloy with 80 mol% of CoB_2 melts congruently at a temperature of 1200°C.

Thermodynamics

The activity of boron in the liquid phase at 1300°C derived by [1991Ush] from emf measurement is presented in Fig. 9.

[1995Wit] determined partial enthalpies of formation of B-Co-Fe melts using high-temperature isoperibolic calorimetry. The partial enthalpies of the components were determined for Fe/(Fe+Co) ratios of ¼, ½ and ¾ and B concentration from 0 to 40 at.% at a temperature of 1627°C. The results obtained are presented in Figs. 10a-10c. The limiting partial mixing enthalpy of B in the B-Co-Fe melt is presented in Fig. 11. The integral enthalpies of mixing at 1627°C are presented in Fig. 12. It can be seen that the system possesses significantly negative values of the integral enthalpies of mixing. This fact confirms that there are strong attractive interactions between unlike particles and is consistent with the presence of several binary and ternary associates in the liquid.

A calculation of the isothermal section of the B-Co-Fe system at 1000°C was performed by [1980Rog] based on thermodynamic data and using the regular solution model for the phases. Agreement of the calculated section with other data is discussed above, under the section Isothermal Sections.

[1982Ber] studied the crystallization behavior of the amorphous $Fe_{83-x}Co_xB_{17}$ alloys. The melting point and the heat of fusion/crystallization were measured by combined DSC-DTA. The results are presented in Fig. 13.

Notes on Materials Properties and Applications

Transition metal borides form an interesting class of compounds which are characterized by high melting points and metallic-like properties. Several of the borides are ferromagnetic and in many ways their magnetic behavior resemble that of the transition series. The low temperature heat capacity from 1.5 to 15 K was measured by [1971Han] for FeB and $Fe_{0.75}Co_{0.25}B$. The low temperature heat capacity was measured for the FeB-CoB system especially near the critical concentration for ferromagnetism [1970Kue]. It was found that in the critical concentration range, the linear term γT of C_p is largely increased and the heat capacity curves reveal anomalies at low temperatures. Magnetic properties of $(Fe_xCo_{1-x})B$ at 4.2 K were derived from magnetic measurements and NMR investigations [1980Lem]. The composition dependence of the ferromagnetic Curie temperature and saturation magnetization were presented. It was concluded that Co atoms do not carry any magnetic moment in the $(F_xCo_{1-x})B$ borides.

Iron-based amorphous alloys have been found to be of great technological importance due to a unique combination of their properties, such as high strength and good soft ferromagnetic properties. These alloys are, however, thermodynamically metastable and transform to the more stable crystalline phases on thermal treatment. The useful mechanical and physical properties alter significantly during the crystallization process. The influence of Cr additives on the crystallization of the amorphous $Fe_{74}Co_{10-x}Cr_xB_{16}$ alloys

DOI: 10.1007/978-3-540-69761-9_16

was studied by [1987Mat]. For $Fe_{74}Co_{10}B_{16}$ alloys, two well-defined exotherms are obtained. On the addition of Cr, the separation between the exotherms decreases leading to a single exothermic stage at 7.5 and 10 at.% Cr. The XRD study demonstrated that the first peak corresponds to the appearance of (αFe), while the second peak corresponds to the crystallization of the Co_2B and Fe_3B phases. [1982Ber] studied the crystallization behavior of an amorphous glass of composition $(Fe_{1-x}Co_x)_{83}B_{17}$ for $0 < x < 0.75$ and found the formation of (αFe) and $(Fe,Co)_2B$ phases. In addition, hardness, embrittlement and oxidation behavior were reported. The thermal stability of the amorphous Co rich alloys $Fe_{6.2}Co_{76.8}B_{17}$, $Fe_6Co_{74}B_{20}$ and $Fe_{5.8}Co_{71.2}B_{23}$ was studied by [1980Lat] using calorimetry (DSC). XRD indicated the formation of (αCo) solid solutions and Co_2B. [1991Ste] studied non-isothermal crystallization in as quenched and pre-annealed amorphous $Fe_{85-x}Co_xB_{15}$ alloys at $12 < x < 25$ by means of DSC, XRD and transmission electron microscopy. Crystallization takes place with continuous heating in two steps at peak temperatures of about 412 and 501°C, respectively, according to Fe/Co ratio. According to [1991Ste], precipitation of (αFe) occurs by dendritic growth in the first stage followed by the metastable Fe_3B phase, and cubic and hexagonal Co while the stable boride phases are formed during the second stage. Prolonged annealing drastically lowers the first step crystallization temperature. [1990Ste] studied the crystallization process of amorphous $Fe_{85-x}Co_xB_{15}$ ($12 < x < 25$) subjected to both heat treatment and electron beam irradiation. The heat treatment and electron beam irradiation, taking place during TEM observations lead to an induced crystallization, which starts at temperatures some hundred degrees lower than without this treatment. A recent study [2001Gup] of the crystallization behavior of $(Fe_{1-x}Co_x)_{85}B_{15}$ confirmed that primary phase of precipitation was the bcc Co-Fe alloy, while during the second step the $(Fe_{1-y}Co_y)_2B$ compound was formed. At compositions of $x = 0.25$, the amorphous alloys exhibit an increase in magnetization, magnetostriction and hyperfine magnetic field that were attributed to short-range order of the Fe_3Co type in the amorphous alloy. A much weaker anomaly was also found at $x = 0.471$, which corresponds to the intermetallic compound FeCo. The DSC measurements of [2001Gup] indicated an anomaly in the crystallization temperature at $x = 0.247$.

[1992Dol] measured the Curie temperatures (T_C) of the $Fe_yCo_{80-y}B_{20}$ alloys for five compositions at $y = 6$, 24, 40, 56, 72. It was demonstrated that T_C increases, attains a maximum, and then decreases with y increasing. The permeability was measured using a method based on the reflection pulse technique. The physical constants of the energetic model of ferromagnetic hysteresis were derived from anisotropy energy constants, initial susceptibility, coercivity and saturation magnetization measured for the $Fe_{64}Co_{21}B_{15}$ alloy in the temperature range 25-300 K by [1999Hau]. [1987Vas measured magnetic properties of the amorphous alloy $Fe_9Co_{66}B_{25}$. For three kinds of samples, untreated, field annealed and stress-field annealed, the induced anisotropy and room temperature magnetization curves were obtained, and the low-field susceptibility was measured from 20 to 400°C. The calculated hysteresis loop for the FeCoB alloy demonstrated good agreement with the experimental data. [1988Vla] measured the compositional dependence of the linear saturation magnetostriction, spontaneous volume magnetostriction and the magnetic saturation polarization for amorphous $Fe_xCo_{80-x}B_{20}$ ($0 \le x \le 20$) at room temperature. [1990Mis] measured saturation magnetization at 77 K for the amorphous alloy $(Fe_yCo_{1-y})_{80}B_{20}$ at $0 < y < 0.3$. The mean magnetic moment of the transition reaction was calculated from this value. The amorphous $Fe_{21}Co_{64}B_{15}$ alloy was subjected to a Joule heating treatment by [2004Coi] in order to study the effect on magnetoimpedance. Electrical resistance during the thermal treatment, hysteresis loop measurements, XRD and Mössbauer spectroscopy were monitored in order to study structural changes induced by the current annealing technique.

Polyphase sintering is an effective technique of particulate-reinforced and dispersion-strengthened metal matrix composite production. B-Co-Fe cermets are the new metal matrix composites. [2006Now] studied Fe-Fe_2B mixtures, Fe-Co-$(FeCo)_2B$ and the addition of Mo and Cu to the Fe-Co-$(FeCo)_2B$ system. The cermets produced were subjected to metallographic tests, XRD, microanalysis, hardness and microhardness examination, as well as sliding dry friction wear tests. Dilatometry was used to monitor the basic phenomena taking place during polyphase sintering of the investigated system of B-Co-Fe.

Thermoelectric power measurements were carried out in liquid quenched amorphous alloys of the composition $Fe_{83-x}Co_xB_{17}$ at $x = 93$, 75, 10 and temperatures in the range 77-300 K. Thermoelectric power of the $(Fe_xCo_{1-x})B$ solid solution was measured by [2004Ued] in the temperature range 177-677°C at $x = 0$, 0.01, 0.1, 0.5 and 1.

Property investigations of Co-Fe borides and amorphous alloys are summarized in Table 4.

DOI: 10.1007/978-3-540-69761-9_16

Miscellaneous

The phase transition and microstructure of as-deposited B-Fe, B-Co and B-Co-Fe alloy films on copper, mica, glass and NaCl single crystals were examined using differential scanning calorimetry and transmission electron microscopy by [1986Cha]. The microstructure appears to be either in the amorphous state or partially crystallized, depending on the composition of the films.

Self-diffusion in amorphous $Fe_{35}Co_{50}B_{15}$ and $Fe_{68}Co_{17}B_{15}$ alloys was investigated using radioactive ^{59}Fe and ^{58}Co tracer atoms by [1994Pav]. It was found that the diffusivity of Fe equals to that of Co and it is independent of mutual concentration of the transition metal in alloys. The mean activation enthalpy was calculated.

The kinetics of crystallization of $(Fe_{1-x}Co_x)_{83}B_{17}$ and $(Fe_{1-x}Co_x)_{80}B_{20}$ $0.25 \leq x \leq 100$ amorphous alloys were studied by [1982Ber] and time-temperature-transformation diagrams were constructed. The kinetics of crystallization of $Fe_{70}Co_{10}B_{20}$ and $Fe_{85-x}Co_xB_{15}$ at x = 12, 15, 17, 19, 21, 23, 25 were studied by [1989Zem, 1990Zem1, 1990Zem2, 1991Zem] using Mössbauer spectroscopy, and the enthalpy of activation was estimated. According to [1991Zem], the crystallization proceeds in three stages; nucleation and primary crystallization of the metal alloy followed by the rather slow decay of metastable $(Fe,Co)_3B$. The Co rich amorphous alloys studied by [1980Lat] exhibited only one exothermic effect. The activation energy of crystallization was calculated by [1980Lat] from DSC measurements.

The NMR spectra of the amorphous alloys $Fe_{81}Co_3B_{16}$ and $Fe_{70}Co_{10}B_{20}$ were measured at 4.2 K by [1993Koh]. It was confirmed that the spin-lattice relaxation is independent of the external magnetic field in the magnetically saturated samples and it was found that it does not depend on the Co concentration. [1990Mis] studied the influence of Fe substitution on the ^{59}Co-hyperfine field in amorphous $(Fe_yCo_{1-y})_{80}B_{20}$ $(0 < y < 0.3)$ using NMR. It was found that amorphous alloys have atomic short range order similar to the corresponding crystalline alloys.

[1988Cor] and [1989Wel] described the preparation of B-Co-Fe amorphous alloys by the reduction of metal ions in an aqueous solution using KBH_4 and $NaBH_4$. [1987Miu] described a flame-spray quenching process for the production of amorphous powders of B-Co-Fe alloys. [1987Boc] studied boronizing of the iron substrate electroplated with cobalt using BCl_3 and H_2. Experimental data indicated that the sequence of phases was (Fe,Co)B, FeB, Fe_2B, substrate. The (Fe,Co)B phase may be transformed into $(Fe,Co)_2B$ by annealing.

Table 1. Investigations of the B-Co-Fe Phase Relations, Structures and Thermodynamics

Reference	Method/Experimental Technique	Temperature/Composition/Phase Range Studied
[1952Hae]	Phase equilibration, XRD	1100°C Co/Fe distribution between (Fe,Co)B and $(Fe,Co)_2B$
[1970Kue]	Adiabatic calorimetry	FeB-CoB 1.2-4.2 K
[1971Han]	XRD, adiabatic calorimetry	$Fe_{0.75}Co_{0.25}B$, FeB at T = 1.5-15 K
[1980Gia]	Phase equilibration, XRD	800, 1000, 1200°C Co/Fe distribution between (Fe,Co)B and $(Fe,Co)_2B$ 800 and 1000°C Co/Fe distribution between $(Fe,Co)_3B$ and $(Fe,Co)_2B$
[1980Lat]	DSC, XRD	427 - 627°C, $Fe_{6.2}Co_{76.8}B_{17}$, $Fe_6Co_{74}B_{20}$, $Fe_{5.8}Co_{71.2}B_{23}$
[1980Rog]	XRD	B-Co-Fe T = 1000°C
[1981Pra]	Phase equilibration, XRD, thermal analysis, optical microscopy	Isothermal section at 1000°C, vertical section Co_2B-Fe_2B, quasibinary

(*continued*)

DOI: 10.1007/978-3-540-69761-9_16

Reference	Method/Experimental Technique	Temperature/Composition/Phase Range Studied
		section CoB-FeB, liquidus surface at 1000-1600°C
[1982Ber]	Calorimetry, XRD electron diffraction	300 - 1400°C, $(Fe_{1-x}Co_x)_{83}B_{17}$ and $(Fe_{1-x}Co_x)_{80}B_{20}$ $25 \le x \le 100$
[1984Fru]	XRD, Mössbauer spectroscopy	$FeCo_2B$ and Co_3B
[1986Cha]	DSC, transmission electron microscopy (TEM)	B-Fe, B-Co and B-Co-Fe alloy films on Cu, glass, NaCl single crystal
[1987Boc]	XRD, optical microscopy, SEM, EPXMA	Co-Fe annealing in H_2 at 950°C, boronizing immediately after annealing with H_2+BCl_3
[1987Mat]	DSC, XRD	327 - 577°C, $Fe_{74}Co_{10-x}Cr_xB_{16}$, x = 0, 2.5, 5, 7.5, 10
[1988Cor]	XRD, EXAFS (X-ray absorption fine structure) spectra, XPS (X-ray photoelectron spectroscopy)	$Fe_{37}Co_{17}B_{15}O_{31}$, T = 200, 350, 450, 550°C
[1989Van]	Diffusion couple, XRD, optical microscopy, SEM, EPMA	Isothermal section at 900°C
[1989Zem]	Mössbauer spectroscopy	260 - 350°C, $Fe_{70}Co_{10}B_{20}$, $Fe_{64}Co_{21}B_{15}$
[1991Ste]	DSC, XRD, TEM	387 - 501°C, $Fe_{85-x}Co_xB_{15}$, $12 < x < 25$
[1991Ush]	EMF boron activity in melt	1300°C, x(B) up to 40 at.%
[1991Zem]	Mössbauer spectroscopy	300 - 350°C, $Fe_{64}Co_{21}B_{15}$
[1995Wit]	High-temperature isoperibolic calorimetry partial mixing enthalpy	1627°C, x(B) up to 50%
[2001Gup]	XRD, DSC, Mössbauer spectroscopy	T = 350 - 600°C $(Fe_{100-x}Co_x)_{85}B_{15}$ x = 14.1-58.8
[2006Now]	Metallography, XRD, microanalysis, dilatometry	1100 - 1160°C, $p = 10^{-3}$ Pa, Fe-Fe_2B, Fe-Co-$(FeCo)_2B$

Table 2. Crystallographic Data of Solid Phases

Phase/ Temperature Range [°C]	Pearson Symbol/ Space Group/ Prototype	Lattice Parameters [pm]	Comments/References
(αδFe)	*cI*2		
(αFe)(r) ≤ 912	$Im\bar{3}m$ W	a = 286.65	pure Fe at 25°C [Mas2]
(δFe)(h_2) 1538 - 1394		a = 293.15	pure Fe at 1480°C [Mas2]

(*continued*)

DOI: 10.1007/978-3-540-69761-9_16

Phase/ Temperature Range [°C]	Pearson Symbol/ Space Group/ Prototype	Lattice Parameters [pm]	Comments/References
(γFe,αCo)	*cF*4 $Fm\bar{3}m$		
(γFe)(h_1) 1394-912	Cu	a = 364.67	pure Fe at 915°C [V-C2, Mas2]
(αCo) 1495 - 422		a = 356.88 a = 354.47	pure Co at 520°C [V-C2] [Mas2]
(εFe)	*hP*2 $P6_3/mmc$ Mg	a = 246.8 c = 396.0	at 25°C, 13 GPa [Mas2]
(εCo) < 400	*hP*2 $P6_3/mmc$ Mg	a = 250.7 c = 406.9	at 25°C[V-C2]
$\alpha'(Fe_{1-x}Co_x)$ < 730	*cI*2 $Im\bar{3}m$ W	a = 286.7 to 284.2	$0.25 \le x \le 0.75$ [V-C2]
(βB)	*hR*333 $R\bar{3}m$ βB	a = 1093.30 c = 2382.52	[1993Wer]
(Fe_xCo_{1-x})B	*oP*8		$0 \le x \le 1$
FeB < 1650°C	*Pnma* FeB	a = 526 b = 304.2 c = 395.4	x = 0 [V-C2]
CoB < 1460°C		a = 550.3 b = 294.6 c = 406.4	x = 1 [V-C2]
		a = 539.2 b = 298.3 c = 400.6	x = 0.5 [1980Rog]
		a = 542.2 b = 296.3 c = 403.8	x = 0.75 [1971Han]
		a = 526 to 550 b = 304.2 to 295 c = 395.4 to 406	$0 \le x \le 1$ at 1000°C [1980Rog]
$(Fe_xCo_{1-x})_2$B	*tI*12 $I4/mcm$		$0 \le x \le 1$
Co_2B < 1280	$CuAl_2$	a = 501.5 c = 422.0	x = 0 [V-C2]

(*continued*)

DOI: 10.1007/978-3-540-69761-9_16

Phase/ Temperature Range [°C]	Pearson Symbol/ Space Group/ Prototype	Lattice Parameters [pm]	Comments/References
Fe_2B < 1389		a = 511 c = 424.9	x = 1 [V-C2]
		a = 507.0 c = 422.9	x = 0.5 [1980Rog]
		a = 501.2 to 510.8 c = 422 to 425.2	$0 \le x \le 1$ at 1000°C [1980Rog]
$(Fe_xCo_{1-x})_3B$	*oP*16		$0 \le x \le 0.6$
	Pnma	a = 522.1	x = 0 [1984Fru]
Co_3B < 1125	Fe_3C	b = 663.1 c = 440.8	
		a = 522.91 b = 663.44 c = 441.17	x = 0.09 [1984Fru]
		a = 530.7 b = 663.59 c = 442.55	x = 0.333 [1984Fru]
		a = 533 b = 663.5 c = 443	x = 0.4 [1980Rog]
		a = 533.7 b = 664.4 c = 442.8	x = 0.5 [1980Gia]
		a = 522.3 to 533 b = 662.2 to 663.5 c = 440.8 to 443	x = 0.04 at 1000°C [1980Rog]
Fe_3B (I)	*oP*16 *Pnma* Fe_3C	a = 542.8 b = 669.9 c = 443.9	metastable, [V-C2]
Fe_3B (II)	*tI*32 $I\bar{4}$ Ni_3P	a = 865.5 c = 429.7	metastable, [V-C2]

Table 3. Invariant Equilibria

Reaction	T [°C]	Type	Phase	Composition (at.%)		
				B	Co	Fe
L ⇌ α(Fe,Co) + $(Fe,Co)_3B$+$(Fe,Co)_2B$	1040	E	L	20	50	30

MSIT®
DOI: 10.1007/978-3-540-69761-9_16

Table 4. Investigations of the B-Co-Fe Materials Properties

Reference	Method / Experimental Technique	Type of Property
[1980Lem]	NMR	Curie temperature, saturation magnetization 4.2 K
[1987Vas]	Magnetic measurements	Magnetization curve at 25°C, susceptibility 30-400°C
[1988Vla]	Magnetic measurements	Linear saturation magnetostriction, spontaneous volume magnetostriction, magnetic saturation polarization at 25°C
[1989Wel]	Mössbauer spectra	Magnetic hyperfine field, isomer shift
[1990Zem1]	Mössbauer spectra	Hyperfine magnetic induction
[1990Zem2]	Mössbauer spectra	Hyperfine magnetic induction
[1990Mis]	Magnetic measurements, NMR	Saturation magnetization, magnetic moment, hyperfine field
[1992Dol]	Magnetic measurements	Curie temperature, magnetic moment, permeability
[1993Koh]	NMR	Nuclear spin-lattice relaxation of ^{59}Co in external magnetic field
[1994Pav]	Radioactive ^{59}Fe and ^{58}Co tracer atoms, ion beam sputtering for serial sectioning	Self-diffusion
[1999Hau]	Magnetic measurements	Hysteresis loops at applied stress
[1999Naq]	Voltage measurement	Thermoelectric power 77-300 K
[2004Coi]	Electric measurements, magnetic measurements	Electric resistance, hysteresis loop measurements, magnetoimpendance
[2004Ued]	Voltage measurement	Thermoelectric power 350-950°C

DOI: 10.1007/978-3-540-69761-9_16

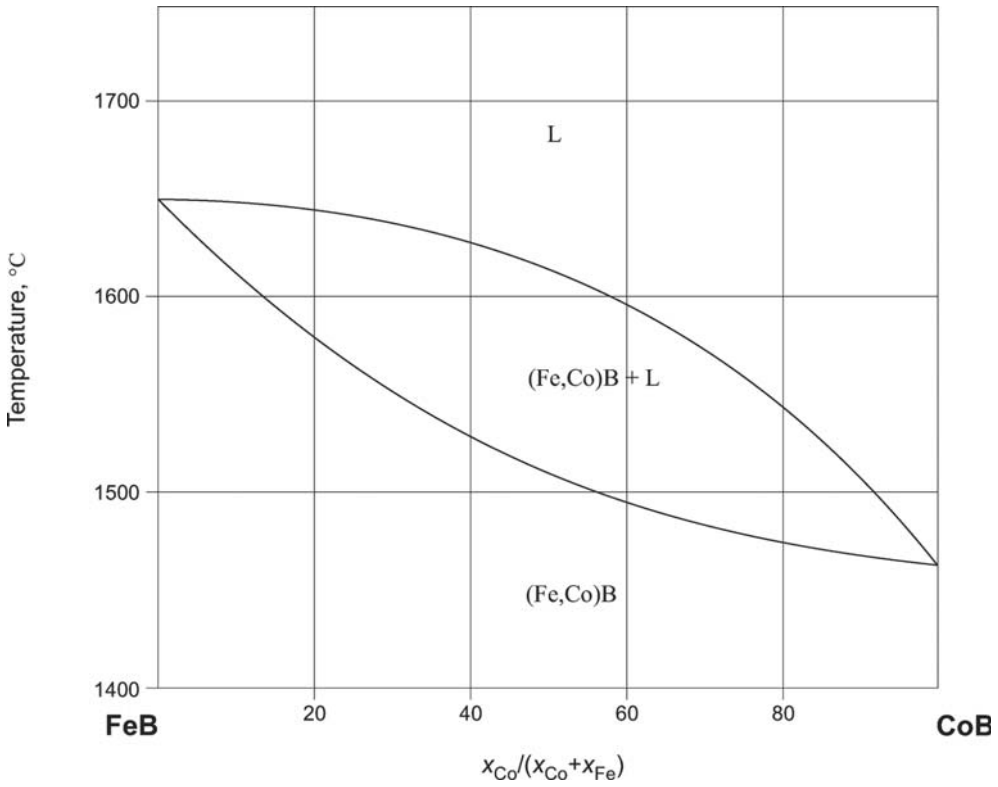

Fig. 1. B-Co-Fe. Phase diagram of the CoB-FeB quasibinary system

DOI: 10.1007/978-3-540-69761-9_16

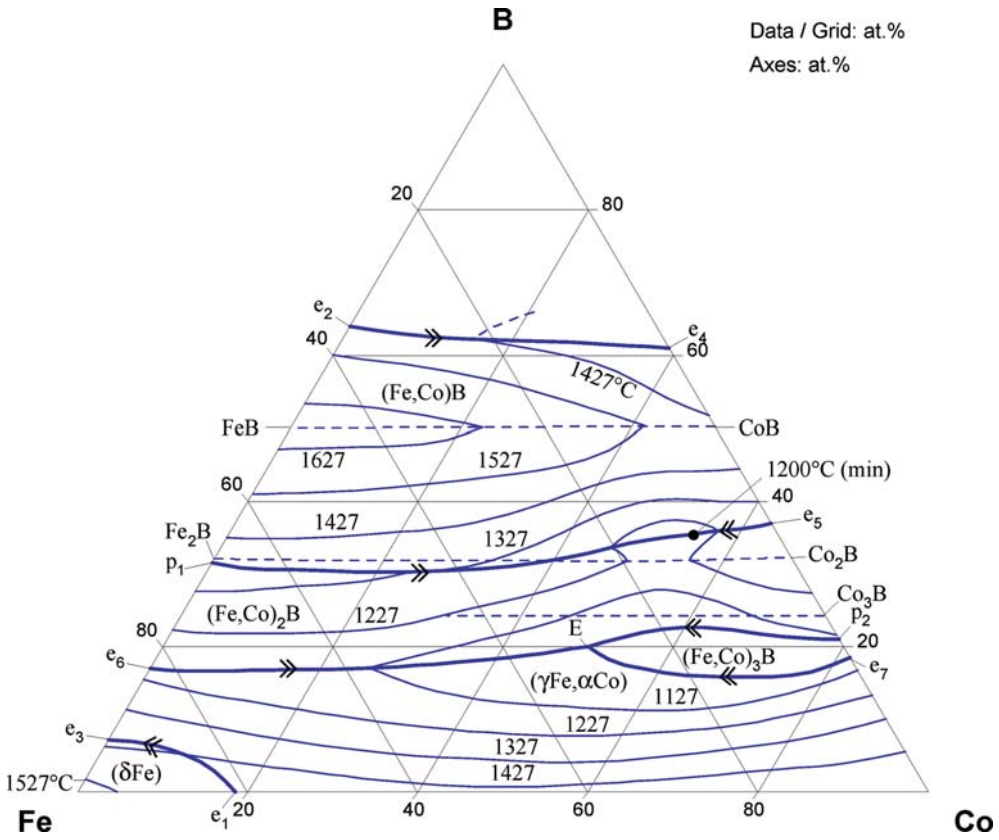

Fig. 2. B-Co-Fe. Liquidus surface projection

DOI: 10.1007/978-3-540-69761-9_16

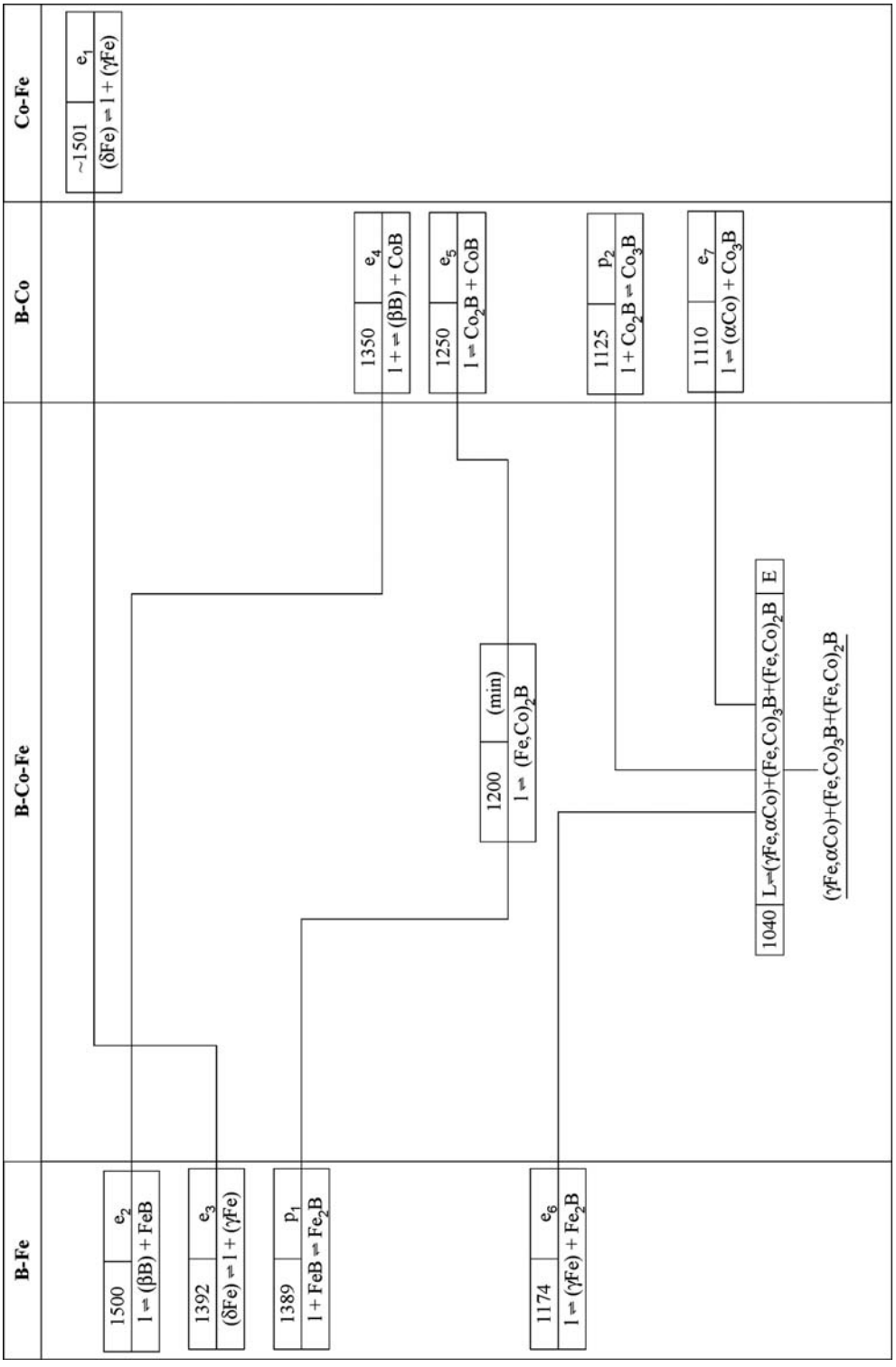

Fig. 3. B-Co-Fe. Reaction scheme

DOI: 10.1007/978-3-540-69761-9_16

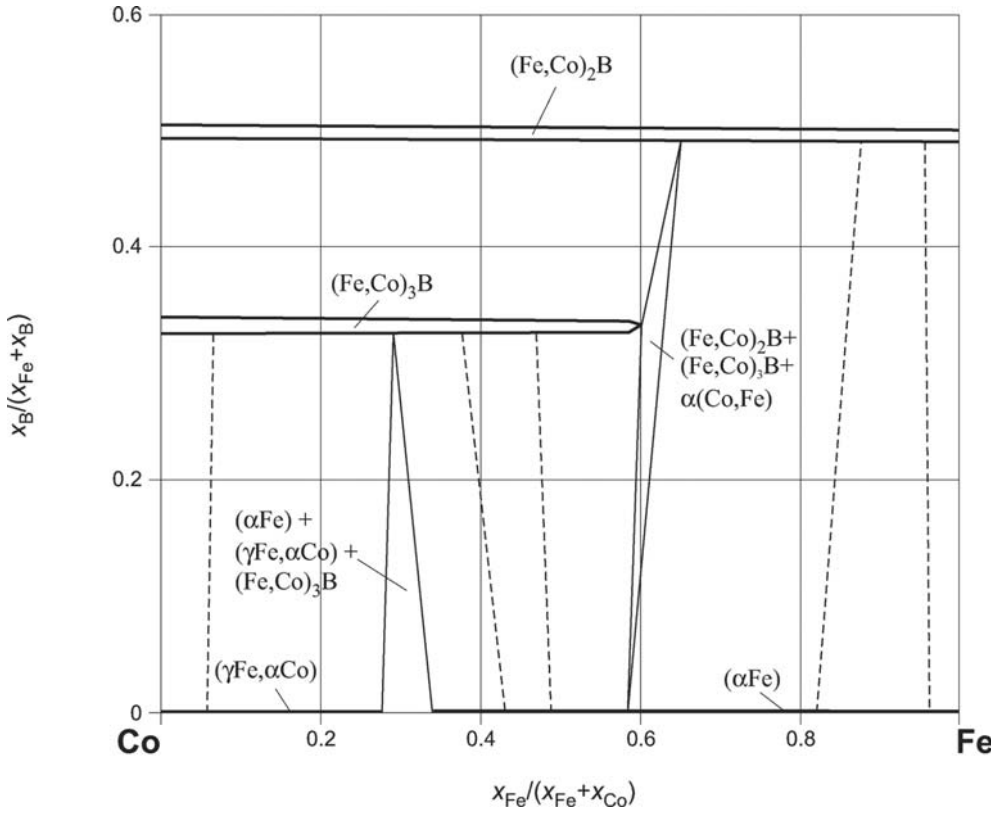

Fig. 4. B-Co-Fe. Isothermal section at 900°C

DOI: 10.1007/978-3-540-69761-9_16

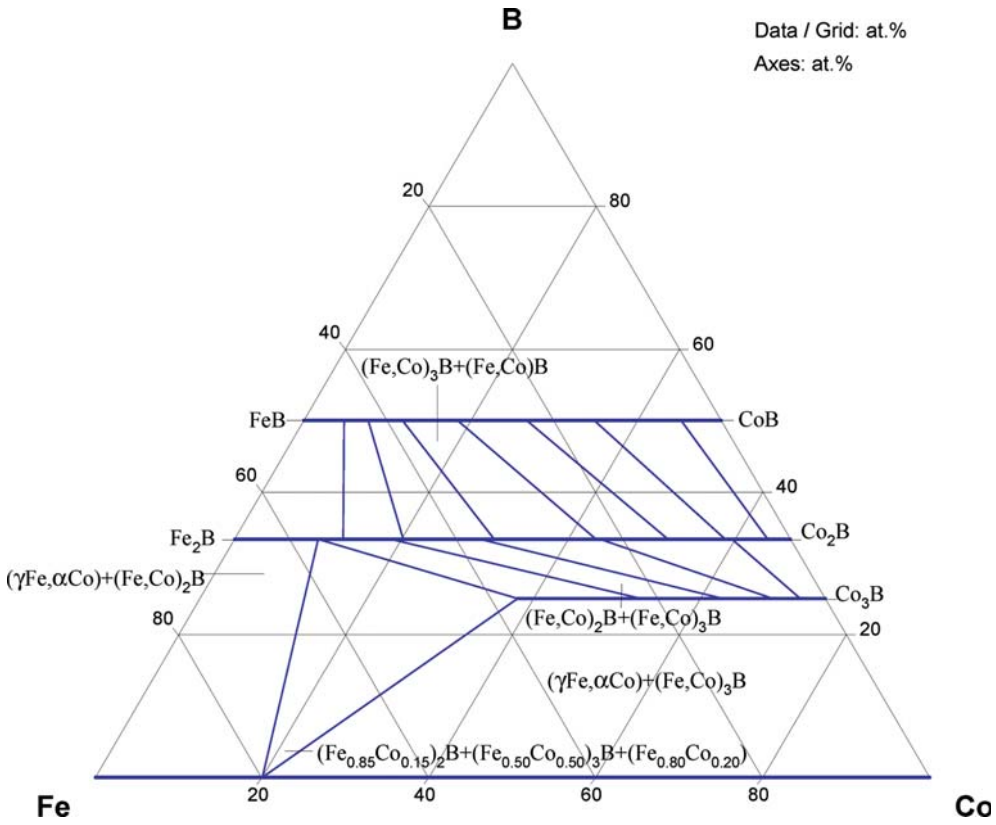

Fig. 5. B-Co-Fe. Isothermal section at 1000°C

DOI: 10.1007/978-3-540-69761-9_16

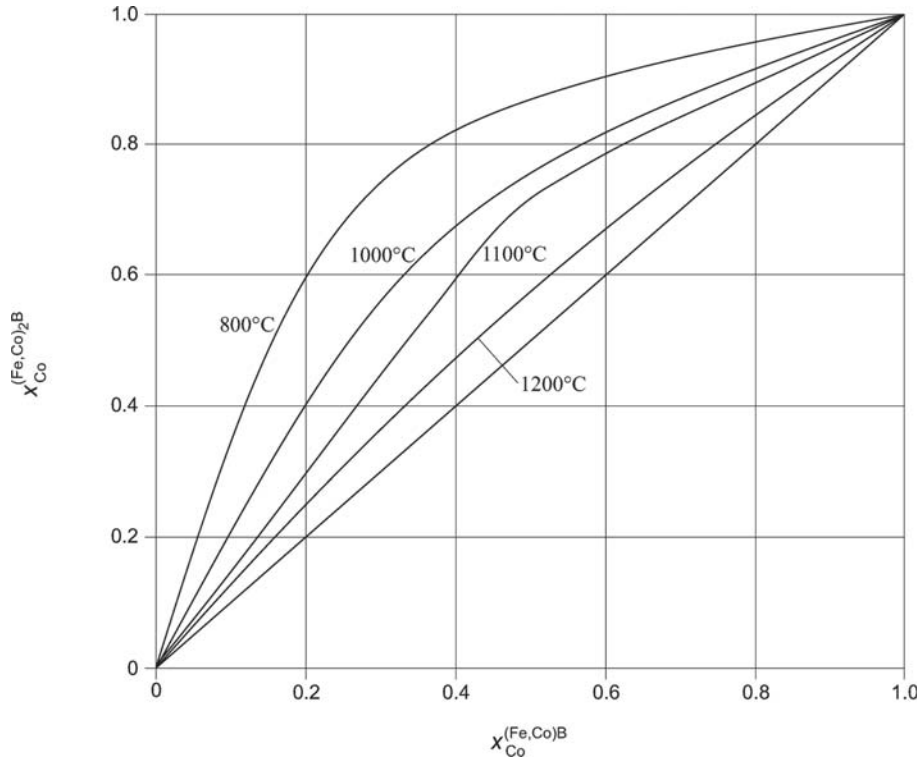

Fig. 6. B-Co-Fe. Distribution of Co/Fe between (Fe,Co)B and $(Fe,Co)_2B$

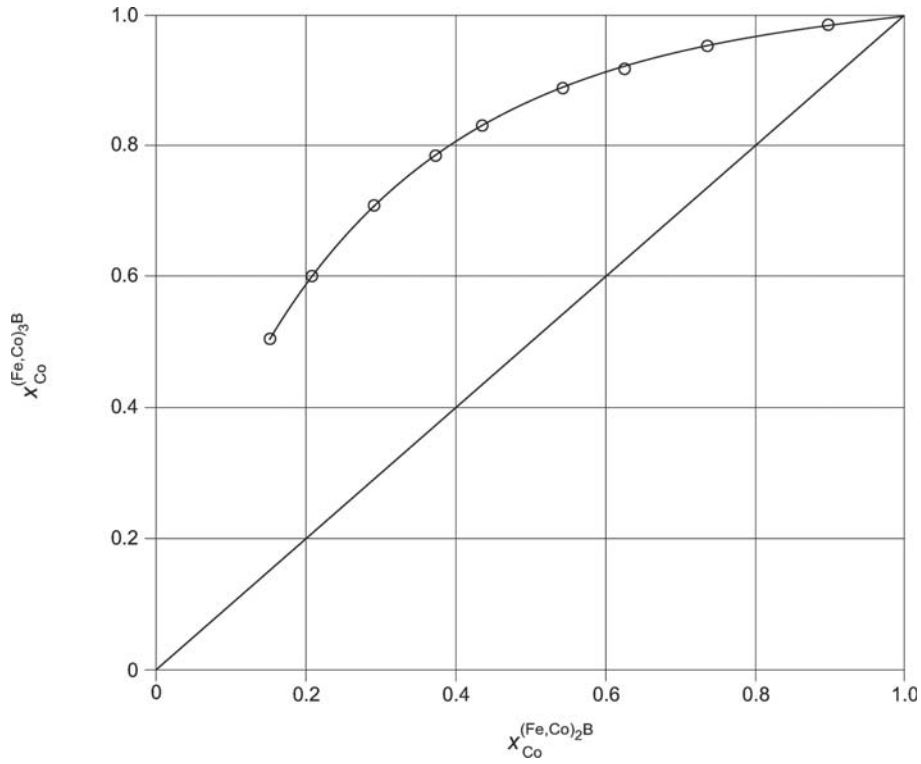

Fig. 7. B-Co-Fe. Distribution of Co/Fe between $(Fe,Co)_2B$ and $(Fe,Co)_3B$

DOI: 10.1007/978-3-540-69761-9_16

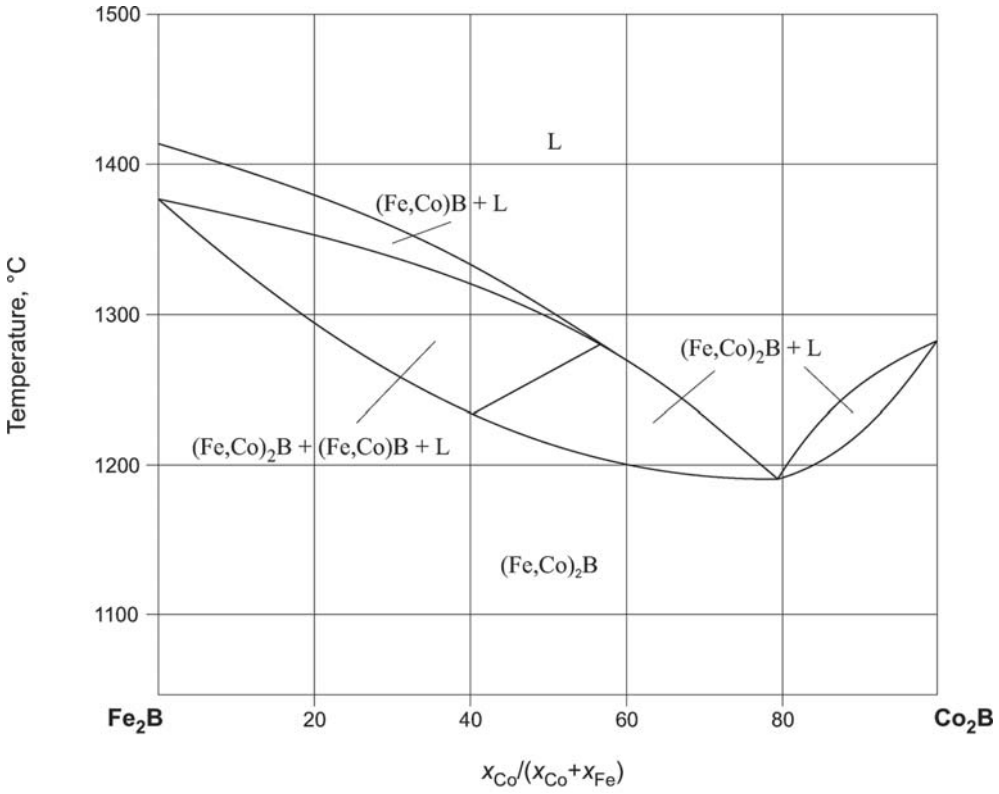

Fig. 8. B-Co-Fe. Vertical section Co_2B-Fe_2B

DOI: 10.1007/978-3-540-69761-9_16

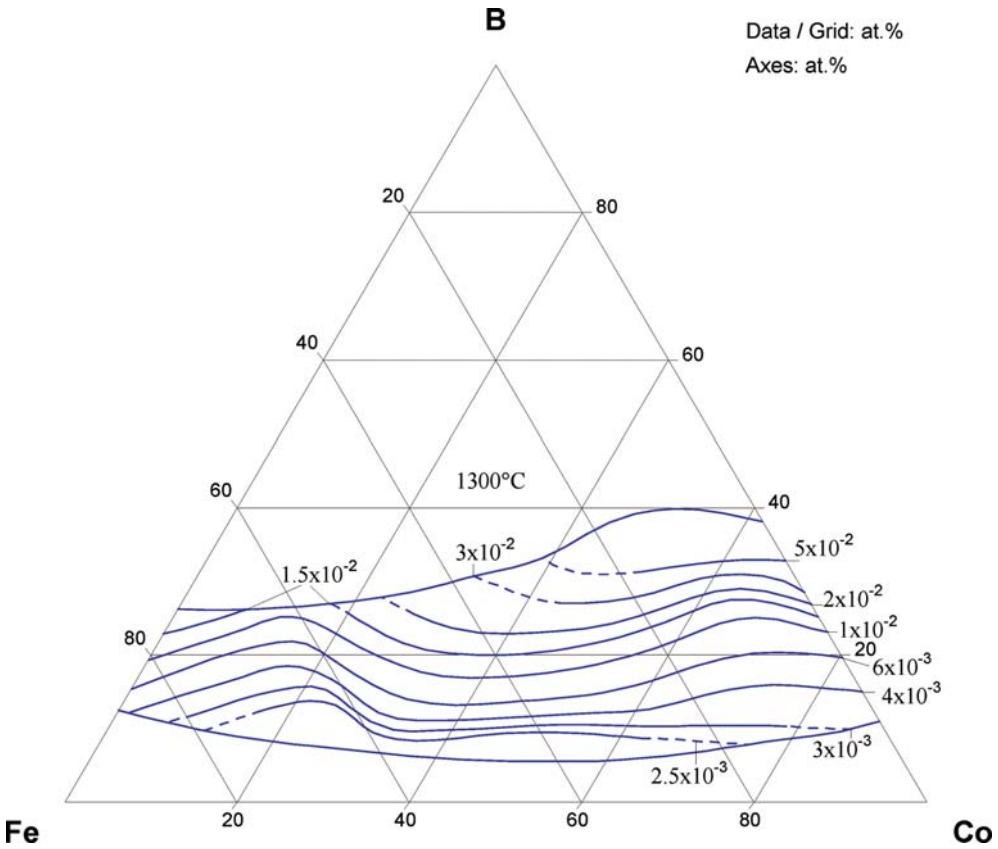

Fig. 9. B-Co-Fe. Isoactivity lines of boron in B-Co-Fe liquid at 1300°C with solid boron as reference state

DOI: 10.1007/978-3-540-69761-9_16

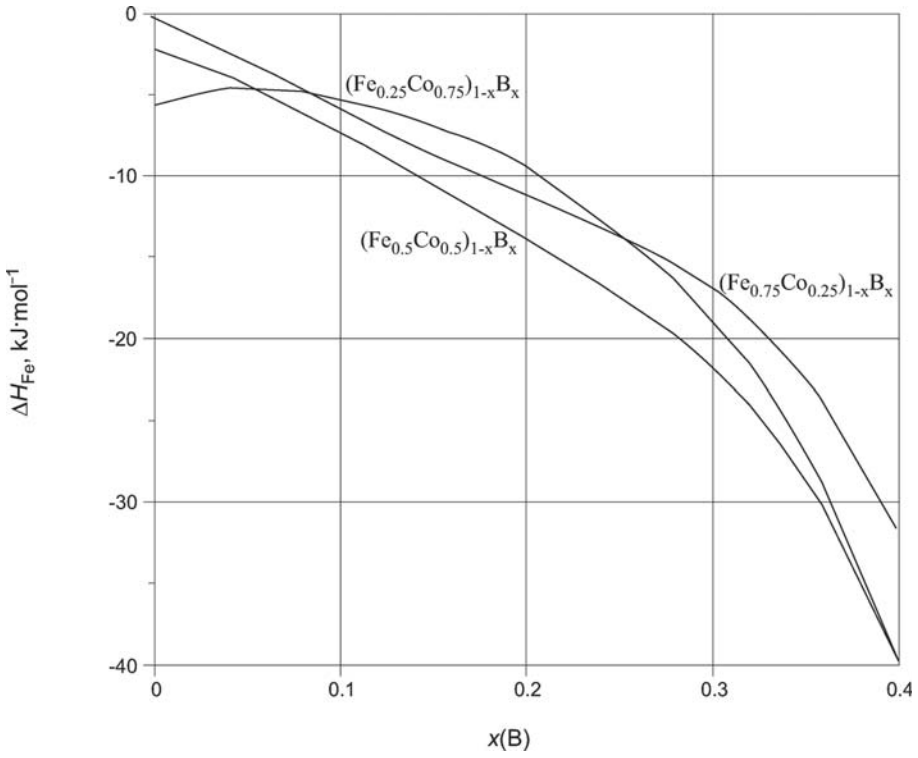

Fig. 10a. B-Co-Fe. Partial mixing enthalpy of Fe in B-Co-Fe melt at 1627°C

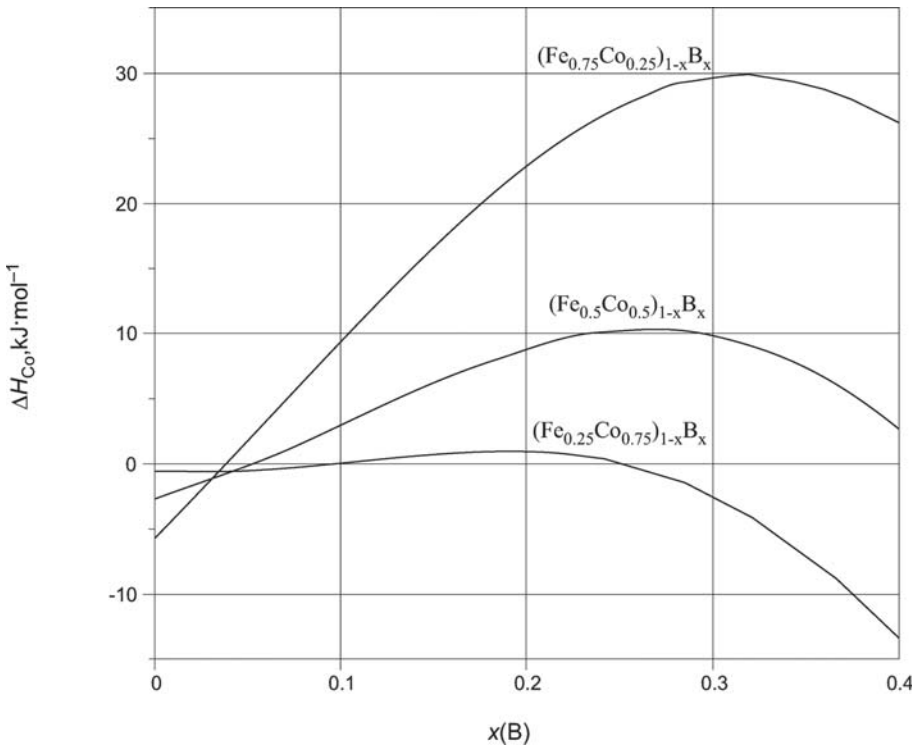

Fig. 10b. B-Co-Fe. Partial mixing enthalpy of Co in B-Co-Fe melt at 1627°C

DOI: 10.1007/978-3-540-69761-9_16

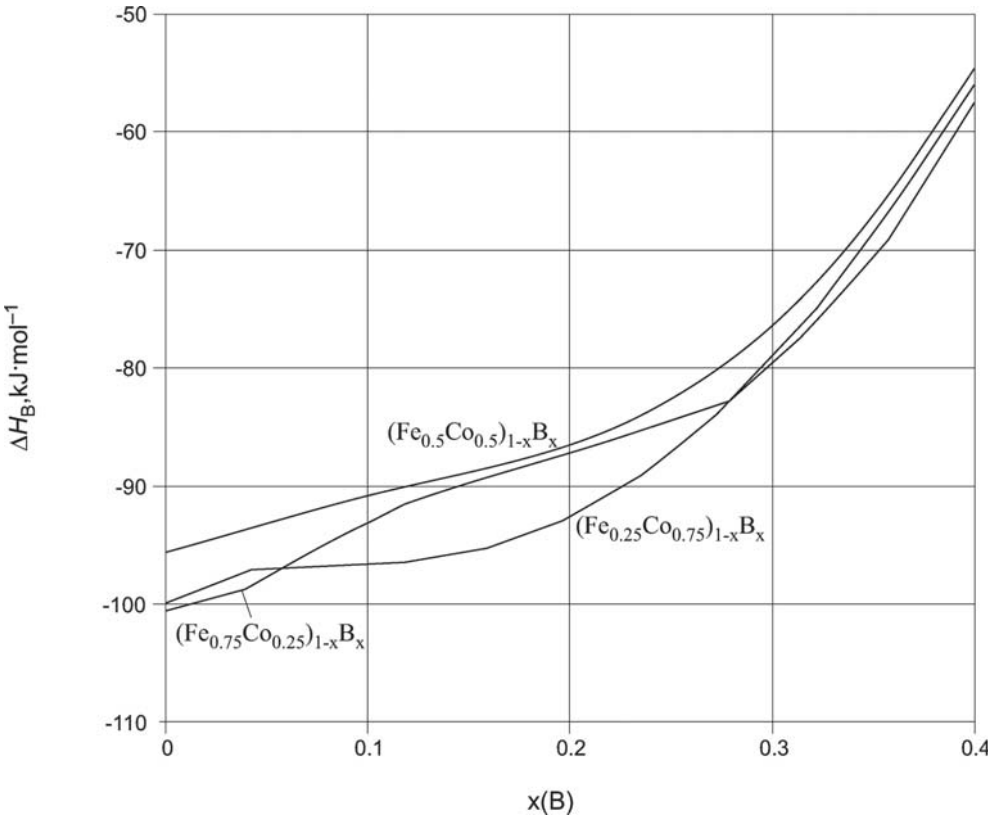

Fig. 10c. B-Co-Fe. Partial mixing enthalpy of B in B-Co-Fe melt at 1627°C

DOI: 10.1007/978-3-540-69761-9_16

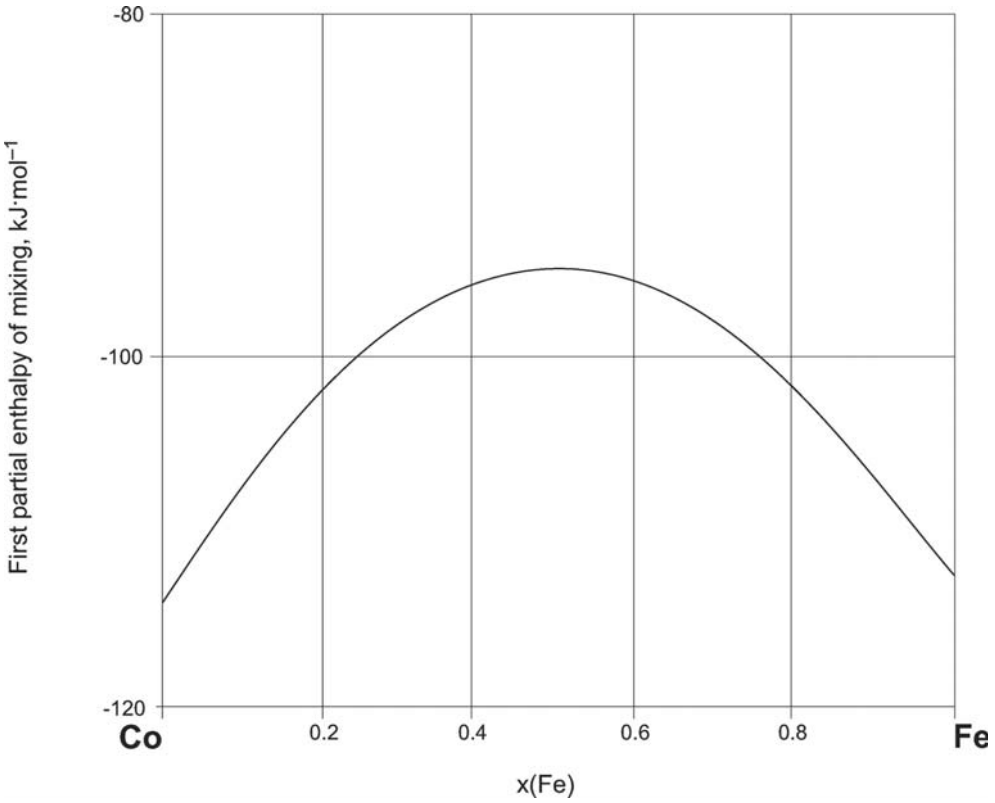

Fig. 11. B-Co-Fe. Limiting partial mixing enthalpy of B *vs* Fe concentration in ultimately dilute alloy B-Co-Fe at 1627°C

DOI: 10.1007/978-3-540-69761-9_16

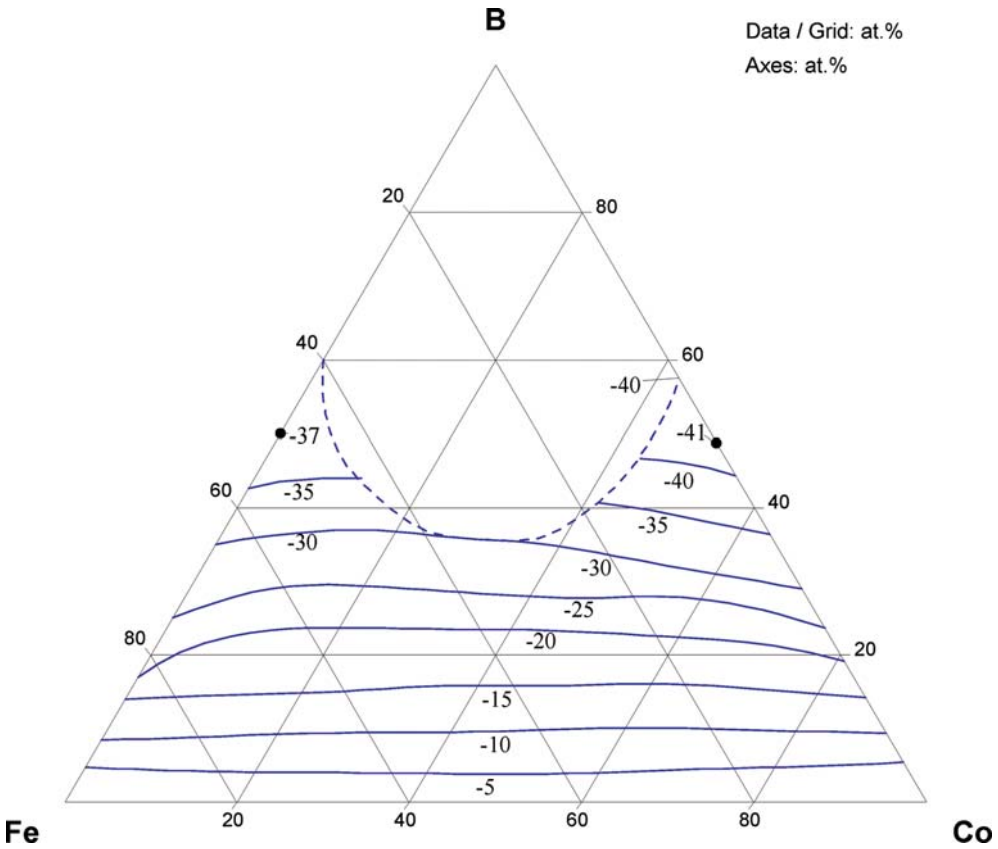

Fig. 12. B-Co-Fe. Integral enthalpy of mixing at 1627°C

DOI: 10.1007/978-3-540-69761-9_16

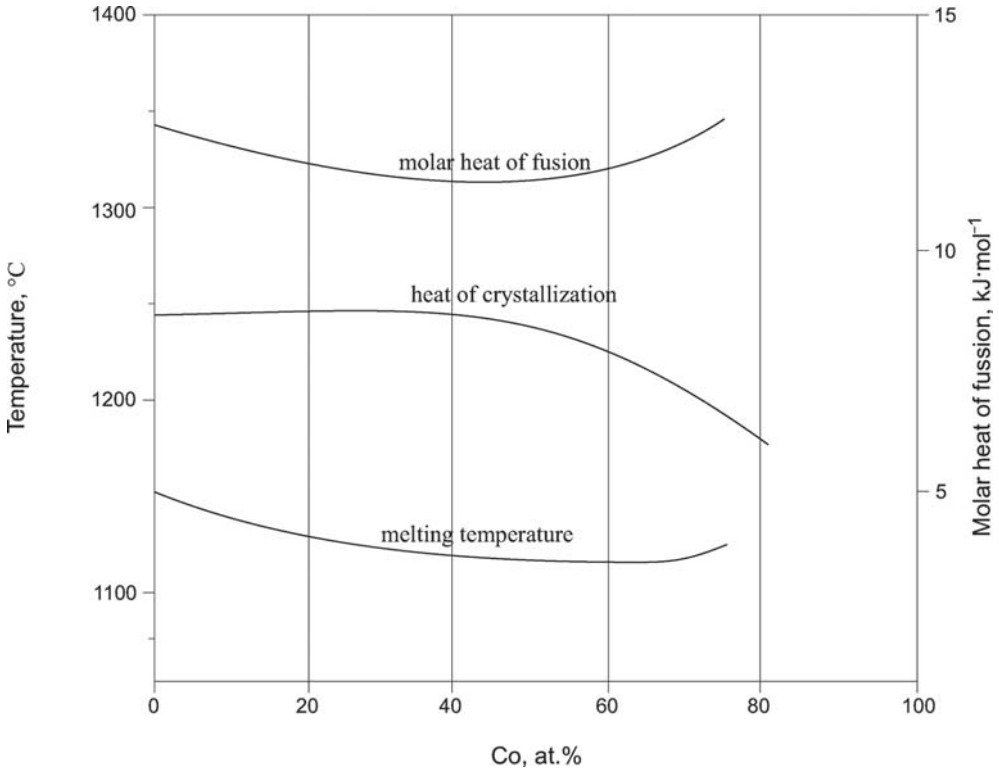

Fig. 13. B-Co-Fe. Melting point and heat of fusion/crystallization of $Fe_{83-x}Co_xB_{17}$ alloy

DOI: 10.1007/978-3-540-69761-9_16

References

[1952Hae] Haegg, G., Kiessling, R., "Distribution Equilibria in Some Ternary Systems Me1-Me2-B and the Relative Strength of the Transition-Metal-Boron Bond", *J. Inst. Met.*, **81**, 57–60 (1952) (Phase Relations, Experimental, 6)

[1970Kue] Kuentzler, R., "Specific Heat of Nearly Ferromagnetic Borides $(Co\text{-}Ni)_2B$ and (Fe-Co)B", *J. Appl. Phys.*, **41**(3), 908–909 (1970) (Crys. Structure, Experimental, Magn. Prop., 15)

[1971Han] Hanson, B.D., Mahnig, M., Toth, L.E., "Low Temperature Heat Capacities of Transition Metal Borides", *Z. Naturforschung A*, **26**(4), 739–746 (1971) (Crys. Structure, Experimental, Thermodyn., 28)

[1980Gia] Gianoglio, C., Quadrini, E., "Equilibrium Distribution of the Solid Solutions of the Cobalt-Iron-Boron System" (in Italian), *Atti Acad. Sci. Torino I. Classe Sci. Fis., Mathem. Natur.*, **114**(3–4), 319–327 (1980) (Experimental, Phase Diagram, 9)

[1980Lat] Latuszkiewicz, J., Kulic, T., Matyja, H., "Thermal-Stability of Amorphous Co-Fe-B, Co-Si-B and Co-Fe-Si-B Alloys", *J. Mater. Sci.*, **15**(9), 2396–2398 (1980) (Experimental, 9)

[1980Lem] Lemius, B., Kuentzler, R., "An NMR Investigation of the Intermetallic Borides $(Co_{1-x}Mn_x)B$ and $(Co_{1-x}Fe_x)B$. II. Ferromagnetic Alloys, *J. Phys. F (Metal Physics)*, **10**(1), 155–167 (1980) (Experimental, Magn. Prop., 9)

[1980Rog] Rogl, P., Schuster, J.C., Nowotny, H., "Phase Equilibrium And Compound Formation In Fe-M(metal)-B-X(nonmetal) Systems", Boron Steel, *Proc. Int. Symp.*, 1979 (Pub. 1980), 33–43., *Proc. Int. Symp*., Met. Soc. AIME, Milwaukee, 1979 (1980) (Phase Diagram, Phase Relations, 18)

[1981Pra] Pradelli, G., Gianoglio, C., Quadrini, E., "The Cobald-Iron-Boron System in the Presence of Liquid" (in Italian), *Metall. Ital.*, **73**(7–8), 351–355 (1981) (Experimental, Morphology, Phase Diagram, Phase Relations, 19)

[1982Ber] Bergmann, H.W., Brokmeier, U., "Crystallization Behaviour of Fe-B-Cr, Fe-B-Co, and Fe-B-Ni Alloys", *Met. Sci.*, **16**, 191–196 (1982) (Phase Relations, Experimental, 14)

[1984Fru] Fruchart, D., "Structural Studies of the Cementite-type Compositions: Effect of Hydrogen on Fe3C Using the Neutron Diffraction Method. Mössbauer Spectrometry of FeCo2B and Co3B:^{57}Fe", *J. Solid State Chem.*, **51**, 246–252 (1984) (Crys. Structure, Experimental, 35)

[1986Cha] Chang, Y.H., Yung, S.W., Chin, T.S., Hung, H.P: "The Phase Transition and Microstructure of Fe-Co-B Alloy Films", *J. Cryst. Growth*, **78**(2), 235–241 (1986) (Crys. Structure, Experimental, Magn. Prop., Morphology, Phase Relations, 11)

[1987Boc] Bochmann, G., Klaus, E., Fritsche, G., Wagnre, W., "Phase Structure of Boride Layers on Iron Substrates with Electroplated Cobalt Layers", *Cryst. Res. Techn.*, **22**(7), 961–967 (1987) (Experimental, Morphology, 14)

[1987Mat] Mathur, R.P., Murthy, V.N., Akhtar, D., Subrahmanian, P., Jagannathan, R., "Crystallization Process in Amorphous $Fe_{74}Co_{10\text{-}x}Cr_xB_{16}$ Alloys", *J. Mater. Sci. Lett.*, **6**(9), 1019–1022 (1987) (Experimental, Phase Relations, 12)

[1987Miu] Miura, H., Isa, S., Omuro, K., "A Flame-Spray Quenching Process for Continuous Production of Amorphous Powders of Fe-Ni-P-B, Ni-Si-B, and Co-Fe-B Alloys", *Trans. Jpn. Inst. Met*., **28**(1), 57–62 (Experimental, Morphology, 13)

[1987Vas] Vasquez, M., Ascasibar, E., Hernando, A., Nielsen, O.V., "Co-Si-B and Fe-Co-B Amorphous Alloys: Induced Anisotropy and Various Magnetic Properties", *J. Magn. Magn. Mater.*, **66**(1), 37–44 (1987) Magn. Prop., Experimental, 16)

[1988Cor] Corrias, A., Ennas, G., Licheri, G., Marongiu, G., Musinu, A., Paschina, G., Piccaluga, G., Pinna, G., Magini, M., "Fe-o-B Amorphous Alloy Powder by Chemical Reduction", *J. Mater. Sci. Lett.*, **7**, 407–409 (1988) (Expreimental, 14)

[1988Vla] Vlasak, G., Jergel, M., Duhaj, P., "Comopsitional Dependence of Magnetostriction of Amorphous Co-Fe-B and Co-Ni-B Alloys", *Mat. Sci. Eng.*, **99**, 109–112 (1988) (Magn. Prop., Experimental, 15)

[1989Van] Van Loo, F.J.J., van Beek, J.A., "Reactions and Phase Relations in the Systems Fe-Ni-B and Fe-Co-B", *Z. Metallkd.*, **80**(4), 245–250 (1989) (Electr. Prop., Phase Diagram, 12)

DOI: 10.1007/978-3-540-69761-9_16

[1989Wel] Wells, S., Charles, S.W., Morup, S., Linderoth, S., van Wontergheim, J., Larsen, J., Madsen, M. B., "A Study of Fe-B and Fe-Co-B Alloy Particles Produced by Reduction with Borohydride", *J. Phys.: Condens. Matter*, **1**(43), 8199–8208 (1989) (Experimental, Magn. Prop., 24)

[1989Zem] Zemcik, T., Havlicek, S., "Crystallization Kinetics of the Fe-Co-B Amorphous-Alloys by Mössbauer Scanning Experiments", *Hyperfine Interact.*, **51**, 1045–1050 (1989) (Experimental, 2)

[1990Mis] Misawa, M., Tanaka, Y., Nagai, H., Tsujimura, A., "Spin-Echo NMR Study of ^{59}Co-Hyperfine Field Distributions in Amorphous (C,T)-B Alloys (T = Fe, Ni, Mn)", *J. Non-Crystalline Solids*, **117/118**, 344–346 (1990) (Magn. Prop., Experimental, 6)

[1990Ste] Stergioudis, G.A., Polychroniadis, E.K., "Induced Crystallization in Fe-Co-B Amorphous Alloys by Heat-Treatment and Electron-Beam Irradiation", *Mater. Res. Bull.*, **25**(10) 1287–1290 (1990) (Experimental, 15)

[1990Zem1] Zemcik, T., "Hyperfine Field Relaxations in the Fe-Co-B Amorpous-Aloys", *Hyperfine Interact.*, **55**(1–4), 1099–1102 (1990) (Experimental, Magn. Prop., 8)

[1990Zem2] Zemcik, T., Havlicek, S., "Crystallization Kinetics of the Fe-Co-B Amorphous-Alloys", *Hyperfine Interact.*, **55**(1–4), 1103–1106 (1990) (Experimental, Kinetics, 7)

[1991Ste] Stergioudis, G., Ivanov, G., Polychroniadis, E.K., "Evolution of Crystallization of the FeCoB Amorphous Alloys", *Phys. Status Solidi A*, **124**, 393-399 (Experimental, 14)

[1991Ush] Ushio, R., Ogawa, O., "Activities of Boron in the Binary Ni-B and the Ternary Co-Fe-B Melts", *Metall. Trans. B*, **21B**, 47–52 (1991) (Experimental, Phase Diagram, 15)

[1991Zem] Zemcik, T., Havlicek, S., "Low-Temperature Crystallization of the Fe-Co-B Amorphous-Alloys", *Hyperfine Interact.*, **69**(1–4), 673–676 (1991) (Experimental, 4)

[1992Dol] Dolocan, V., Dolocan , E., "Curie Temperature Measurements in Amorphous Fe-Co-B Alloys", *J. Phys. III* (Applied Physics, Materials Science, Fluids, Plasma and Instrumentation), **2**(6), 915–920 (1992) (Experimental, Magn. Prop., 10)

[1993Koh] Kohout, J., Englich, J., Sedlak, B., Stepankova, H., Trhlik, M., Lutgemeier , H., "Nuclear Spin-Lattice Relaxation in Ferromagnetic Amorphous Alloys $Fe_{81}Co_3B_{16}$ and $Fe_{70}Co_{10}B_{20}$ Measured by NMR and Nuclear Orientation", *Hyperfine Interact.*, **78**(1–4), 511–514 (1993) (Magn. Prop., Experimental, 7)

[1993Wer] Werheit, H., Kuhlmann, U., Laux, M., Lundstrm, T., "Structural and Electronic Properties of Carbon-ped β-Rhombohedral Boron", *Phys. Stat. Sol.*, **B179**, 489–511 (1993) (Crys. Structure, Experimental, 51)

[1994Pav] Pavlovsky, J., "Diffusion of Fe and Co in Co-Fe-B Amorphous Alloys", *Metal. Mater.*, **32**(2), 87–90 (1994), translated from *Kovove Mater.*, **32**(2), 126–131 (1994) (Kinetics, Interface Phenomena, Thermodyn., Experimental, 9)

[1995Wit] Witusiewicz, V.T: "Thermodynamics of Binary and Ternary Melts of the 3d Transition Metals (Cr, Mn, Fe, Co and Ni) with Boron", *Thermochim. Acta*, **264**, 41–58 (1995) (Experimental, Thermodyn., 25)

[1999Hau] Hauser, H., Groessinger, R., "Isotropic Hysteresis Modeling of Fe-Co-B Alloys", *J. Appl. Phys.*, **85**(9), 5133–5135 (Magn. Prop., 9)

[1999McH] McHenry, M.E., Willard, M.A., Laughlin, D.E., "Amorphous and Nanocrystalline Materials for Applications as Soft Magnets", *Prog. Mater. Sci.*, **44**(4), 291–433 (1999) (Crys. Structure, Electr. Prop., Experimental, Magn. Prop., Phase Relations, Review, 302)

[1999Naq] Naqvi, S.M.M.R., Rizvi, S.D.H., Raza, S.M., Rizvi, S., Hussain, A., Rahman , F., "Thermoelectric Power Studies in Liquid Quenched Amorphous Alloys", *Solid State Commun.*, **110**(8), 463–468 (1999) (Electr. Prop., Experimental, 11)

[2001Gup] Gupta, A., Ruwali, K., Paul, N., Duhaj, P., "Crystallization Behavior of Amorphous $(Fe_{100-x}Co_x)_{85}B_{15}$", *Mater. Sci. Eng. A*, **304–306**, 371–374 (2001) (Experimental, Phase Relations, 7)

[2004Coi] Coisson, M., Kane, S.N., Tiberto, P., Vinai, F., "Influence of DC Joule-Heating Treatment on Magnetoimpedance Effect in Amorphous $Co_{64}Fe_{21}B_{15}$ Alloy", *J. Magn. Magn. Mater.,* **271**

DOI: 10.1007/978-3-540-69761-9_16

(2–3), 312–317 (2004) (Crys. Structure, Electr. Prop., Experimental, Magn. Prop., Morphology, Phase Relations, 11)

[2004Ued] Ueda, M., Hayakawa, H., Mukaida, M., Imai, Y., "Seebeck Coefficients of Iron Group Elements Borides", *Intermetallics*, **12**(1), 155–58 (2004) (Electr. Prop., Experimental, 8)

[2006Now] Nowacki, J., "Polyphase Sintering and Properties of Metal Matrix Composites", *J. Mat. Proc. Tech.*, **175**(1–3), 316–323 (2006) (Experimental, Morphology, Mechan. Prop

[Mas2] Massalski, T.B. (Ed.), *Binary Alloy Phase Diagrams*, 2nd edition, ASM International, Metals Park, Ohio (1990)

[V-C2] Villars, P. and Calvert, L.D., *Pearson's Handbook of Crystallographic Data for Intermetallic Phases*, 2nd edition, ASM, Metals Park, Ohio (1991)

DOI: 10.1007/978-3-540-69761-9_16

Boron – Chromium – Iron

Anatoliy Bondar

Introduction

The ternary system has gained attention of materials scientists due to its potential for the development of iron (steel) matrix composites, thermochemical boriding of Cr containing steels and chromium boride coating on steels, amorphous/nanocomposite and magnetic materials. Therefore phase equilibria were extensively studied. An overview of the results of these investigations are presented in Table 1.
The phase diagram is presented as isothermal sections from 700 to 1250°C [1970Che, 1973Bor, 1976Gor, 1983Gia, 1985Gia], partial liquidus surface in the Fe corner [1966Kan, 1998Mie, 2001Chr], and a CrB-FeB quasibinary section [1987Shi]. Crystal structures were studied in [1964Bro, 1995Gol, 2001Cal, 2003Guo], enthalpy of formation of melts was determined using calorimetric data by [1995Wit1, 1995Wit2] and thermodynamic computation of the liquidus surface in the Fe corner was reported in [1998Mie].

Binary Systems

The B-Cr phase diagram was taken from [2006Bon] mainly based on the experimental data of [1969Por, 1972Por] and supplemented with borides Cr_2B_3 and CrB_4 following [1987Oka, 1968And].
The B-Fe phase diagram used in the present evaluation is the same as for the B-Fe-Mo system in this issue. It is accepted after [1994Hal] and modified only by the noticeable homogeneity field of the B phase, as reported in [1976Cal, 1996Lya, 2002Tak]. So, the Fe_3B is considered as metastable, rather than high-temperature phase as in [1981Kha, 1982Kha, 1996Lya].
The Cr-Fe phase diagram is accepted after [1993Itk], where it is not so far from [Mas2].

Solid Phases

All the unary and binary phases are presented in Table 2. No stable ternary compound was found in the system. During crystallization of amorphous alloy $Fe_{70}Cr_{10}B_{20}$, a tetragonal $I\bar{4}$ $Fe_2Cr_4B_8$ ternary boride was identified, which transformed to another $I4/mcm$ $Fe_6Cr_2B_4$ at further heating [2005San].
Solubility of third element in the chromium and iron borides was found to be substantial, as it is presented in Fig. 1 for Cr_5B_3, Cr_2B and Fe_2B and in Fig. 2 for the monoborides CrB and FeB. At 1250°C the extension of Cr_2B reaches the composition $(Cr_{0.3}Fe_{0.7})_2B$, and for Fe_2B it is up to $(Cr_{0.25}Fe_{0.75})_2B$ [1973Bor]. The Cr_5B_3 boride dissolves 13 at.% Fe at this temperature [1973Bor]. The mutual solubility of CrB and FeB is rather large, reaching the compositions of $(Cr_{0.6}Fe_{0.4})B$ and $(Cr_{0.8}Fe_{0.2})B$, respectively (Fig. 2). The Fe solubility in Cr_3B_4 and CrB_2 is about 6 at.% at 1100°C [1976Gor], and for CrB_4 it may be estimated as about 2 at.% Fe. In the ternary alloys the Cr_2B_3 boride existence was not reported anywhere.
The boride based on Fe_3B was identified after rapid solidification as a constituent of metastable eutectic (Fe) + Fe_3B [1995Gol, 1982Ber]. However, no thermal arrest of M_3B separation was found in [1982Ber] before melting.
[2003Guo] determined the boron solubility in metal matrix of alloys contained about 12 mass% Cr, 1.4 mass% B, some other elements and Fe to balance as 0.185 to 0.515 mass% in as-cast martensite and 0.015 to 0.059 mass% after the 750°C tempering. According to [2001Cal] the indicated shifts in the phonon frequencies and identification of additional vibration modes of the melted Fe-8Cr-0.095B (mass%) alloy are the evidences for the interstitial nature of boron soluble in the alloy.

Quasibinary Systems

The CrB-FeB quasibinary section was reported in [1987Shi] and is presented in Fig. 2. At temperatures below 1200°C it is supplemented by data of [1970Che, 1973Bor, 1976Gor, 1983Gia], showing the retrograde solvus of CrB. In the section there is a peritectic invariant reaction L + CrB ⇌ FeB at ~1960°C.

DOI: 10.1007/978-3-540-69761-9_17

At ~1000°C and below the authors of [1987Shi] found two allotropic modifications of CrB, which were of the CrB and αMoB crystal structure types. Since the transformation was irreversible, the latter modification seems to be metastable.

Invariant Equilibria

Invariant equilibria in the composition range Cr-CrB-FeB-Fe are presented in Fig. 3 and Table 3, based on data for the CrB-FeB quasibinary section [1987Shi] and Fe corner [1966Kan, 1998Mie, 2001Chr]. A hypothetic consideration of [1992Rag1] was also used. As seen in Table 3, the data of [1966Kan] and [2001Chr] concerning points U_4 and U_5 differ in temperatures by 40 or 25°C and in composition by 5 or 2 at.% Cr, respectively (the difference in B does not exceed 1 at.%).

Liquidus Surface

For the first time, the liquidus surface was constructed based on experimental data by [1966Kan] in the Cr-Cr_2B-Fe_2B-Fe field. The partial liquidus surface projection up to 20 mass% Cr and 6 mass% B was reported in [2001Chr] referring to unpublished works of E. Graham. For the liquidus surface projection in Fig. 4, the version from [2001Chr] is preferred in the Fe rich part (up to 20 mass% Cr and 6 mass% B) as more detailed and better consistent with the B-Fe phase diagram. Beyond the range, it was combined with the hypothetic liquidus lines of [1992Rag1] who took into account data of [1966Kan, 1987Shi].

Isothermal Sections

Figures. 5 to 8 present isothermal sections at 1250 [1973Bor], 1100 [1976Gor, 1983Gia], 900 [1970Che] and 700°C [1970Che, 1966Kan]. As shown in Figs. 1 and 2, at these temperatures the extensions of boride homogeneity fields are in good agreement. For the 1100°C section the results of [1983Gia] were mainly preferred, except for the CrB homogeneity range. In the 1250°C isothermal section the liquid phase was not included by [1973Bor], although the temperature is higher than the U_4 and U_5 invariant points in the liquidus. The proper correction was made in Fig. 5 based on the liquidus isotherm from [2001Chr] (Fig. 4).

The main discrepancy is related to the equilibrium between (γFe) and Cr_2B. As seen in Fig. 4, the liquidus from [2001Chr] (as well as [1966Kan]) evidences that this equilibrium exists in the solidus surface, at 1201 to 1230°C. In the 1100°C sections of [1976Gor, 1983Gia] (Fig. 6) there is the alternative equilibrium (αFe) + Fe_2B, and [1992Rag1] has hypothesized that the solid-phase invariant reaction (γFe) + $Cr_2B \rightleftharpoons$ (αFe) + Fe_2B takes place at ~1150°C. However, the (γFe) + Cr_2B equilibrium was presented in the 900°C sections of [1970Che] (Fig. 7), contrary to [1976Gor, 1983Gia]. Since the data of each taken separately seem to be correct, it is impossible to make an unambiguous choice. Accepting the version of [1992Rag1] about the solid-phase invariant transformation at ~1150°C, the metal-boride equilibria in Fig. 7 is shown following [1970Che] by dashed lines.

In the range up to 50 at.% B the system was studied twice at 1100°C, in [1976Gor] and [1983Gia] (Fig. 6). The data are consistent, differences in composition do not exceed 5 at.% (Figs. 1 and 2). In Fig. 6 the isothermal section from [1983Gia] is preferred, where the phase compositions in three-phase equilibria were estimated by careful analysis of concentration dependences of lattice parameters. The only exception is made for the CrB phase, because the Fe solubility in this phase after [1983Gia] seems to be understated (Fig. 2). The same situation is at 700°C, where the range Cr-Cr_2B-Fe_2B-Fe was studied in both [1970Che] and [1966Kan]. The 700°C isothermal section is presented after [1970Che] (Fig. 2), except for the Cr solubility in Fe_2B, because the 8 at.% seems to be better than 11 at.%, as seen in Fig. 1.

It should be noted here that the region Cr_3B_4-B-FeB is insufficiently studied, as yet, and the authors of [1976Gor, 1970Che] reported that their XRD patterns contained unidentified reflexes. In Figs. 6 to 8 this region is shown mainly with dotted lines.

[1958Aro] studied alloys at Fe:Cr atomic ratio of 54:46 containing from 0 to 26 at.% B (arc melted alloys annealed at 700°C for 40 d) and found that the section passes throughout the single-phase σ-CrFe and two-phase (Cr,αFe) + Cr_2B fields.

DOI: 10.1007/978-3-540-69761-9_17

Temperature – Composition Sections

The only vertical section at 10 mass% Cr was schematically presented by [1966Kan].

Thermodynamics

Partial and integral enthalpies of formation of B-Cr-Fe melts were determined by means of isothermal calorimeter at 1880°C in [1995Wit1, 1995Wit2], where excess entropies and Gibbs energies were also estimated (Figs. 9a, 9b, 9c, 10a and 10b). Concentration dependencies of the partial enthalpies have complicated character, which relates to passing cluster types in liquid from M_3B at x_{Fe}:x_{Cr} 0:1 to 0.25:0.75 to M_2B at x_{Fe}:x_{Cr} 0.5:0.5 to 1:0. While, the integral enthalpy is continuously decreasing from ~0 to –37 kJ·mol^{-1}, passing from the metal corners to the B- and Fe rich part.
In [1998Mie] the ternary parameters for the liquid, (αFe) and (γFe) phases were optimized and a good agreement of calculated liquidus line e_1U_4 with experimental data of [1966Kan] was provided.

Notes on Materials Properties and Applications

Literature data concerning investigations of the boron-iron-molybdenum materials properties are listed in Table 4.
[2005Dyb] found that Fe_2B with 7 at.% Cr and FeB with 6 at.% Cr were formed between a Fe-10 mass% Cr and B at 850 to 950°C, and the boride layer yields about a 5-fold increase in the alloy wear resistance. The same two boride layers of Fe_2B and FeB were found at 0 to 4 mass% Cr and 750 to 1000°C in [1988Bad] and at 4.2 to 18 mass% Cr 1000°C [1989Bra] after boriding. Different boriding media were studied in [1985Car] at 850°C. Another technique to prepare boride coatings, laser alloying of Fe or steel plates with CrB_2 was examined in [1991Sha, 1994Sha].
A number of works was focused on preparation and investigation of amorphous ribbons consisting of B-Cr-Fe. In [1985Kal, 1985Kov, 1985Nov, 1985Pot, 1986Dro, 1986Zay, 1988Har, 1989Dro, 1999Cen] they were studied as magnetic materials. Mechanical properties of amorphous materials were examined in [1987Gle, 1990Mil, 1996Gle]. [1979Kik1, 1979Kik2, 1979Kik3] reported that the amorphous ribbons $(Cr_xFe_{1-x})_{85}B_{15}$ ($0 \le x \le 15$) exhibit Invar characteristics, which were studied in relation to temperature and Cr content.

Miscellaneous

[2005Kar, 2003Chr] determined the crystallization enthalpy for an amorphous alloy $Fe_{76}Cr_2B_{22}$ (DSC) as 2.1 eV. The alloy crystallized at 462°C (shifting it higher by 15°C comparing to the binary $Fe_{78}B_{22}$) to yield simultaneously αFe nanograins and Fe_3B boride. Close temperature, 450°C was obtained by [2005San] for the crystallization of amorphous alloy $Fe_{70}Cr_{10}B_{20}$. As shown in [1982Ber], Cr additions raise the crystallization temperature of amorphous ribbons from 380-420°C (binary B-Fe alloys) to 480-285°C (at 25 at.% Cr). [1979Kik1, 1979Kik3] had given quite close temperatures.
Interactions in cold-compacted powder samples Cr-FeB, Fe-CrB and CrB-FeB further annealed at 1000°C were studied by XRD and Mössbauer spectrum measurements in [2002Car, 1998Car].
As found in [2001Jin, 1999Jin, 1998Jin] (TEM, SEM and Auger analysis), as-sprayed coatings from a powder of 56.3Fe-24.2Cr-3.04B (mass%) with minor contents of Ni and Mo contained $Cr_{1.65}Fe_{0.35}B_{0.96}$ and Cr_2B boride particles in a matrix consisting of nanocrystalline (Cr,αFe) supersaturated with B (1.4 at.%).
Samples of fine particles $Cr_xFe_{80-x}B_{20}$ ($5 \le x \le 70$) were prepared via chemical reduction of salt solutions with KBH_4 or $NaBH_4$ and their magnetic and other properties were then examined in [1995Fio, 1995Sub, 1997Zha].

DOI: 10.1007/978-3-540-69761-9_17

Table 1. Investigations of the B-Cr-Fe Phase Relations, Structures and Thermodynamics

Reference	Method/Experimental Technique	Temperature/Composition/Phase Range Studied
[1958Aro]	Alloys from the metals of 99.7 mass% purity and 94% B, at Fe:Cr atomic ratio of 54:46 containing from 0 to 26 at.% B, were arc melted and annealed at 700°C 40 days, followed by XRD.	The section was found to pass form the single-phase σ-FeCr field to two-phase (Cr,αFe) + (Cr_2B) at 700°C.
[1964Bro]	The alloy $Cr_{0.9}Fe_{1.1}B_{0.9}$ (after wet chemical analysis) melted in zirconia crucible was examined using single crystal XRD.	The crystal structure was refined it to be of the Mn_4B type.
[1966Kan]	As-cast and annealed at 700°C alloys were studied by optical microscopy, XRD and DTA.	The liquidus surface projection and isothermal section at 700°C were presented for the field Cr-Cr_2B-Fe_2B-Fe.
[1970Che]	XRD and optic metallography were applied for samples from Cr of 99.5 mass% purity, Fe of 99.9 mass% and B of 99.5 mass%, which were melted in an arc furnace or (compositions above 50 at.% B) sintered at 1500°C for 10 h. At 900 and 700°C the samples were annealed for 400 and 750 h, respectively.	The isothermal sections at 700 and 900°C were presented for the whole concentration range.
[1973Bor]	Samples from Cr of 99.999 mass% purity, Armco Fe, B of 99.9 mass% and master-alloy Fe - 13.51 mass% B were sintered in Arat 1250°C. They were examined by metallography and XRD.	The 1250°C isothermal section was presented for the field Cr-CrB-FeB-Fe.
[1976Gor]	Samples were melted in an arc furnace or (compositions above 50 at.% B) sintered at 1500°C for 11 h from Cr of 99.87 mass% purity, carbonyl Fe and B of 99.1 mass% and then studied by optic metallography and XRD.	The isothermal section at 1100°C was presented for the whole concentration range.
[1982Ber]	Amorphous ribbons and crystallized samples of compositions $(Cr_xFe_{1-x})_{83}B_{17}$ and $(Cr_xFe_{1-x})_{80}B_{20}$ ($0 \le x \le 25$) were examined with DSC, XRD and measurements of microhardness.	Crystallization behaviour and microhardness were studied.
[1983Gia]	XRD and chemical analysis were applied for samples of research purity (99.9 mass% Cr, 99.5 mass% Fe and 98 mass% B), prepared by sintering at 800, 1000, 1100 and 1200°C for 100 to 1000 h.	The paper presents the 1100°C isothermal section for the Cr-CrB-FeB-Fe field and lattice parameters for the phases, as well as the data on mutual solubilities of boride phases at 800, 1000 and 1200°C.
[1985Gia]	Composition of phases and partition of the metals were considered in the range Cr_2B-CrB-FeB-Fe_2B basing on their previous results reported in [1983Gia].	

(*continued*)

DOI: 10.1007/978-3-540-69761-9_17

Reference	Method/Experimental Technique	Temperature/Composition/Phase Range Studied
[1987Shi]	Samples were prepared from the powder elements (Cr of 99 % purity, Fe of 99.9 %). They were mixed, pressed and annealed, at 1000°C 10 days, at 1200°C 4 days and at temperatures from 1300 to 2300°C using a high-pressure piston-cylinder apparatus (10 kb, cooling rate of 400°C·s^{-1}). The samples sintered at 900 to 2300°C were studied with XRD (at room temperature and up to 600°C for the (FeB) phase) and magnetization measurement (the latter from –196 to 800°C).	The CrB-FeB quasibinary section was presented.
[1995Gol]	Layers formed during laser surface alloying of AISI 1045 steel with CrB were examined with TEM, including selected-area electron diffraction and X-ray dispersive spectroscopy, and XRD.	It was found that the Cr_2B boride contains several polytypes originating from the transformation $Fe_2B \rightarrow Cr_2B$ and due to similarity and differences of the both borides.
[1995Wit1, 1995Wit2]	Isothermal calorimetry at 1880°C was carried out in three sections with x_{Fe}:x_{Cr} as 0.25:0.75, 0.50:0.50 and 0.75:0.25	The whole range of existence of homogeneous liquid phase, from Cr-Fe binary up to 32 at.% B, enthalpies of mixing were determined.
[1998Mie]	Equilibrium of liquid, ferrite and austenite was assessed using ThermoCalc package.	For the phases the thermodynamic parameters were optimized and the liquidus curve projection was presented
[2001Cal]	XRD, Neutron diffraction, inelastic neutron scattering spectra, internal friction measurement were applied to study the nature of boron soluble in the melted Fe-8Cr-0.095B (mass%) alloy of research purity.	Shifts in the phonon frequencies and identification of additional vibration modes support the interstitial nature of boron soluble in the alloy.
[2001Chr]	The partial liquidus surface projection up to 20 mass% Cr and 6 mass% B and solubility of Cr in Fe_2B were reported referring to unpublished works of E. Graham (The University of Queensland, Brisbane, Australia).	
[2003Guo]	XRD, SEM and TEM were used to determine constituents of alloys, as-cast and annealed at 750°C, and boron solubility in metal matrix. The alloys contained about 12 mass% Cr, 1.4 mass% B; together with 1 or 2 mass% Ni; 0.5, 0.6 or 1.2 mass% Si; 0.2, 0.8 or 1.1 mass% Mn; 0.4 or 0.55 mass% Cu; ~0.15 or 0.36 mass% C, as well as 0.7 mass% V and 0.9 mass% Mo sometimes.	The boron solubility was 0.185 to 0.515 mass% in as-cast martensite and 0.015 to 0.059 mass% after the 750°C tempering.
[2004Guo1]	Two B-Cr-Fe cast irons containing 11.3 and 13.5 mass % Cr, 1.4 and 1.6 mass % B and minor contaminants (additions) of C, Si,	The M_2B boride distribution was studied and modeled.

(*continued*)

DOI: 10.1007/978-3-540-69761-9_17

Reference	Method/Experimental Technique	Temperature/Composition/Phase Range Studied
	Mn, Mo, V, Ni, Cu were examined by SEM and microhardness measurements.	
[2005San]	DSC, Neutron thermodiffraction, resistivity, magnetization. Ribbons of $Fe_{70}Cr_{10}B_{20}$ composition were obtained by melt spinning	An amorphous alloy $Fe_{70}Cr_{10}B_{20}$ crystallized at 450°C

Table 2. Crystallographic Data of Solid Phases

Phase/ Temperature Range [°C]	Pearson Symbol/ Space Group/ Prototype	Lattice Parameters [pm]	Comments/References
(αCr) < 1863	*cI*2 *Im*$\bar{3}$*m* W	*a* = 288.48	at 25°C [Mas2]
(δFe) 1538 - 1394	*cI*2 *Im*$\bar{3}$*m* W	*a* = 293.15	[Mas2]
γ, (γFe) 1394 - 912	*cF*4 *Fm*$\bar{3}$*m* Cu	*a* = 352.3	at 915°C [V-C2, Mas2]
(αFe), α < 912	*cI*2 *Im*$\bar{3}$*m* W	*a* = 286.65	at 25°C [Mas2]
(βB) < 2092	*hR*315 or *hR*333 βB	*a* = 1093.02 *c* = 2381.66	pure B (99.9999%) [1976Lun]
		a = 1092.65 ± 0.04 *c* = 2380.96 ± 0.13	arc melted crystalline B [1981Cre]
		a = 1096.0 ± 0.4 *c* = 2388.4 ± 0.2	$Fe_{2.7}B_{97.3}$ [2002Tak]
$(Cr_{1-x}Fe_x)_2B$ < 1850	*oF*40 *Fddd* Mn_4B	*a* = 1469.2 *b* = 739.9 *c* = 426.6	[1974Lug] $0 \le x \le 0.7$ at 1250°C [1973Bor]
		a = 1441 *b* = 725 *c* = 421	*x* = 0.6 [1970Che]
Cr_5B_3 < 1890	*tI*32 *I*4/*mcm* Cr_5B_3	*a* = 546.8 *c* = 1008.9	[1974Lug], it dissolves 13 at.% Fe at 1250°C [1973Bor]

(*continued*)

DOI: 10.1007/978-3-540-69761-9_17

Phase/ Temperature Range [°C]	Pearson Symbol/ Space Group/ Prototype	Lattice Parameters [pm]	Comments/References
$(Cr_{1-x}Fe_x)$ B, < 2090	*oC*8 *Cmcm* CrB	a = 297.5 b = 786.6 c = 293.4	[1974Lug], $0 \le x \le 0.4$ at ~1100°C [1987Shi]
		a = 298.2 b = 787.2 c = 293.7	x = 0.30 [1983Gia]
Cr_3B_4 < 2080	*oI*14 *Immm* Ta_3B_4	a = 294.6 b =1301.8 c = 296.4	[1974Lug], it dissolves ~6 at.% Fe at 1100°C [1976Gor]
Cr_2B_3 ≤ 1500	*oC*20 *Cmcm* V_2B_3	a = 302.64 ± 0.05 b =1811.5 ± 0.4 c = 295.42 ± 0.04	[1987Oka]
CrB_2 < 2200	*hP*3 *P6/mmm* AlB_2	a = 297.3 c = 307.0	[1974Lug], it dissolves ~6 at.% Fe at 1100°C [1976Gor]
CrB_4 ≤ 1400	*oI*10 *Immm* CrB_4	a = 474.4 b = 547.7 c = 286.6	[1968And]
Fe_3B Metastable	Fe_3P	a = 865.5 c = 429.7	[1982Kha]
$(Fe_{1-x}Cr_x)_2B$ < 1408	*tI*12 *I4/mcm* $CuAl_2$	a = 510.9 c = 424.9	[1992Rag2] $0 \le x \le 0.25$ at 1250°C [1973Bor]
		a = 512.4 c = 422.6	x = 0.20 [1983Gia]
$(Fe_{1-x}Cr_x)$ B < 1633	*oC8* *Cmcm* FeB	a = 550.2 b = 294.8 c = 405.7	[1992Rag2], $0 \le x \le 0.8$ at ~1960°C [1987Shi]
		a = 556.0 b = 292.6 c = 413.5	x = 0.45 [1983Gia]

Table 3. Invariant Equilibria

Reaction	T [°C]	Type	Phase	Composition (at.%)			References
				Cr	Fe	B	
L + CrB ⇌ FeB	1960	p_1	L	33	17	50	[1987Shi]
			CrB	45.5	4.5	50	[1987Shi]
			FeB	40	10	50	[1987Shi]

(*continued*)

DOI: 10.1007/978-3-540-69761-9_17

Reaction	T [°C]	Type	Phase	Composition (at.%)			References
				Cr	Fe	B	
L + Cr_5B_3 ⇌ Cr_2B + CrB	~1850	U_1	L	60	6	34	[1992Rag1]
L + CrB ⇌ Cr_2B + FeB	~1700	U_2	L	28	29	43	[1992Rag1]
L + FeB ⇌ Cr_2B + Fe_2B	~1350	U_3	L	14	53,5	32,5	[1992Rag1]
L + (Cr,αFe) ⇌ (γFe) + Cr_2B	1270	U_4	L	17.3	71.1	11.6	[1966Kan]
	1270			14.7	73.8	11.5	[1998Mie]
	1230			11.9	75.7	12.4	[2001Chr]
L + Cr_2B ⇌ (γFe) + Fe_2B	1226	U_5	L	10.4	75.2	14.5	[1966Kan]
	1201			7.5	78.4	14.1	[2001Chr]
Cr_2B + (γFe) ⇌ (Cr,αFe) + Fe_2B	~1150	U_6	No data	-	-	-	[1992Rag1]

Table 4. Investigations of the B-Cr-Fe Materials Properties

Reference	Method/Experimental Technique	Type of Property
[1966Yas]	Wetting of CrB_2 by melted Fe.	The limiting wetting angle was found to be 25°.
[1979Kik1, 1979Kik3]	Amorphous ribbons $(Cr_xFe_{1-x})_{85}B_{15}$ ($0 \le x \le 15$) were examined with DSC, XRD and measurements of magnetic and other properties.	Curie and crystallization temperatures, magnetic moments, thermal expansion, Young's modulus (concentration and temperature dependences) and corrosion in 3% NaCl were studied. Invar characteristics depending on Cr content and temperature.
[1979Kik2]	Young's modulus with electrostatc driving technique at −100 to 500°C for amorphous ribbons $(Cr_xFe_{1-x})_{85}B_{15}$ ($0 \le x \le 15$).	Invar characteristics together with Δ E effect were reported.
[1985Car]	Plates of AISI 420 steel were subjected to boriding at 850°C for 15 h in different boriding media and then examined with metallography, XRD and Mössbauer spectroscopy.	Structure of surface, phase constituents and role of Cr in formation of coatings at boriding were reported.
[1985Kal]	Amorphous ribbons $Cr_{10}Fe_{76}B_{14}$, $Cr_{10}Fe_{75}B_{15}$ and $Cr_{15}Fe_{70}B_{15}$, prepared by spinning, were examined by DSC and then after different stages of crystallization with TEM and Mössbauer spectroscopy.	Partition of Cr between α metal phase and borides M_3B (on the first stage of crystallization) and between α metal phase and borides M_2B later was studied.
[1985Kov]	Magnetic properties were measured for amorphous ribbons $Cr_xFe_{85-x}B_{15}$ (x varied from 0 to 21.5), prepared by spinning.	Magnetic polarization was studied at 4.2 to 300 K.
[1985Nov]	Magnetic properties were measured from room temperature to 377°C for amorphous ribbons $Cr_xFe_{85-x}B_{15}$ (x varied from 0 to 10), prepared by spinning.	Curie temperature was lowered by 6.5 at.% Cr from 325 to 115°C

(*continued*)

DOI: 10.1007/978-3-540-69761-9_17

Reference	Method/Experimental Technique	Type of Property
[1985Pot]	Amorphous ribbons $Cr_3Fe_{80}B_{17}$, prepared by spinning, were examined by measuring magnetic properties in as-prepared and annealed at $0.8 \cdot T_C$ (T_C is Curie temperature) states.	Magnetic susceptibility was measured from room temperature to 177°C.
[1986Dro]	Amorphous ribbons were obtained by spinning and examined with DSC and Mössbauer spectroscopy.	Crystallization was shown to have two stages, formation of α metal phase and boride M_3B and transformation of latter to M_2B. Magnetic characteristics.
[1986Zay]	Amorphous ribbons $Cr_xFe_{85-x}B_{15}$ (x varied from 0 to 20), prepared by spinning, were examined after different stages of crystallization with TEM and XRD.	Structure and morphology of samples were studied for different stages of crystallization.
[1987Gle]	Ribbons prepared with spinning technique at various cooling rates were studied with TEM and microindentation.	Structural states of samples and their micro hardness and ductility were studied.
[1987Shi]	Samples were prepared from the powder elements by sintering at 900 to 2300°C and studied with XRD and magnetization measurement (the latter from –196 to 800°C).	It presents the magnetic moment and T_C for the FeB phase $Cr_{1-x}Fe_xB$ at x from 0.5 to 1.0, as well as the temperature dependence of its lattice parameters from room temperature to 600°C.
[1988Bad]	Samples from Cr-Fe alloys containing Fe-0.5 mass% Cr and Fe-4 mass% Cr were subjected to boriding at 1000°C.	Boride layers of Fe_2B and FeB were found and their texture was studied.
[1988Har]	XRD and magnetic susceptibility measurements were applied to amorphous ribbons $Cr_xFe_{80-x}B_{20}$ (x = 10, 12, 15, 18, 20), prepared by spinning.	The Curie temperatures and magnetic susceptibility were studied and discussed.
[1988Pus]	Amorphous ribbons $Cr_{10}Fe_{75}B_{15}$, as-prepared and annealed, were examined with Mössbauer and photoelectron spectroscopy, Auger analysis and DSC	Structural relaxations at 200 to 375°C were studied, which took place lower the temperature of crystallization, 447°C.
[1989Bra]	Samples from Fe, Fe-0.5 mass% Cr and Fe-4 mass% Cr were subjected to boriding at 750 to 1000°C.	Boride layers of Fe_2B and FeB were found and the kinetic of their growing was studied.
[1989Dro]	Amorphous ribbons $Cr_xFe_{85-x}B_{15}$ (x = 10, 12, 15, 18, 20), prepared by spinning, were examined with TEM and magnetization measurements after annealing at 400 to 900°C.	Magnetic properties were studied in relation the heat treatment and structure of samples.
[1989Kol]	TEM, XRD and DSC were applied to amorphous-to-crystalline ribbons $(Cr_xFe_{100-x})_{83}B_{17}$ (x = 1, 3, 5).	Crystallization of the amorphous samples was studied

(*continued*)

DOI: 10.1007/978-3-540-69761-9_17

Reference	Method/Experimental Technique	Type of Property
[1990Kuz]	Amorphous ribbons $Cr_{15}Fe_{70}B_{15}$, prepared by spinning, were examined with XRD and Mössbauer spectroscopy and magnetization measurements.	Mössbauer spectroscopy parameters were measured.
[1990Mil]	Amorphous ribbons $Cr_xFe_{85-x}B_{15}$ prepared by spinning and examined with XRD, DSC and microindentation.	Deformation mechanisms and microhardness of samples were studied in the temperature range from –196 to 600°C.
[1990Pus]	Amorphous ribbons B-Cr-Fe, 10 and 15 at.% Cr, 15 at.% B, after annealing in air at atmospheric and low pressure and temperatures from 300 to 350°C were examined with Mössbauer spectroscopy and Auger analysis.	Crystallization of the amorphous samples and formation of oxides were studied.
[1990Sch]	Plates of C45 steel were laser alloyed with CrB_2 were studied with Mössbauer spectroscopy, XRD, SEM/EPMA and microhardness.	The surface contains martensite, retained austenite and borides as orthorhombic $(Cr_{27}Fe_{73})_3B$ and undissolved CrB_2, not excluding Fe_2B.
[1991Kos]	Fine particles samples $Cr_xFe_{80-x}B_{20}$ ($5 \leq x \leq 70$) were prepared via chemical reduction of Cr and Fe chlorides solution with $NaBH_4$ and studied with Mössbauer spectroscopy and magnetization measurements after annealing at 600 to 1000°C.	As-prepared particles consist of mixture of one magnetic and two paramagnetic phases. Annealing higher ~800°C resulted in crystallization.
[1991Sha]	Plates of α iron laser alloyed with CrB_2 were studied with SEM/EDX, XRD, Auger analysis and microhardness.	Fe_2B was found to form in coating. Microhardness of the coating is about 13 GPa.
[1992Ono]	Amorphous ribbons $(Cr_{0.3}Fe_{0.7})_{100-x}B_x$ ($11.2 \leq x \leq 20.9$), prepared by spinning, were examined with Mössbauer spectroscopy and magnetization measurements.	From the angular dependences of spectrum, the structural isotropy is revealed at about $x = 16$.
[1994Car]	XRD and Mössbauer Spectroscopy were applied for samples Cr-Fe_2B and Cr-FeB prepared from powders by cold - compacting and further annealing at 1000°C for 200 h.	The atom diffusion and interaction were studied.
[1994Sha]	Plates of α iron were laser alloyed with CrB_2 and the samples were studied with SEM/EDX and Auger analysis.	The structure is characterized by residual CrB_2 particles enveloped in Fe-18Cr-30B layer on a surface and then $(Cr,Fe)_2B$ dendrites grown towards the Fe dendrites grown on the substrate.

(*continued*)

DOI: 10.1007/978-3-540-69761-9_17

Reference	Method/Experimental Technique	Type of Property
[1995Fio, 1995Sub]	Fine particles samples $Cr_xFe_{80-x}B_{20}$ ($5 \leq x \leq 70$) were prepared via chemical reduction of $CrCl_3$ and $FeSO_4$ solution with $NaBH_4$ and studied with TEM, SEM, XRD, Mössbauer spectroscopy and magnetization measurements.	Magnetic and structural characteristics were reported.
[1996Gle]	Spinning technique with various cooling rates was used to prepare B-Cr-Fe samples with amorphous-crystalline structure, which were studied with TEM and measurements of mechanical properties.	Structure and microhardness were examined in relation with the technique variation.
[1997Zha]	Nanometer particles samples B-Cr-Fe, contained 1 at.% Cr and ~3 to 7.5 at.% B, were prepared via chemical reduction of Cr and Fe chloride solution with KBH_4 and studied with TEM/EDS, XRD and magnetic measurements in as-prepared and annealed at 500°C states.	Magnetic characterization and structure of samples were examined in relation with the annealing and technique variation.
[1998Car]	XRD and Mössbauer spectroscopy were applied for samples CrB-FeB prepared from powders by cold-compacting and further annealing at 1000°C for 8 h.	The atom diffusion and interaction were studied.
[1998Zak]	Ribbons of $(Cr_{0.1}Fe_{0.9})_{85}B_{15}$ composition prepared with spinning and then laser treated were studied with angular ellipsometry.	Optical polarization characteristics were obtained.
[1999Cen]	Barkhausen noise power spectrum, the coercive force and Barkhausen impulse density were aplied for amorphous ribbons $Fe_{77.4}Cr_{6.5}B_{16.1}$.	Remagnetization process and amorphous structure were studied.
[1999Jin, 1998Jin]	TEM, SEM and Auger analysis were used to study a powder of 56.3Fe-24.2Cr-3.04B (mass%) with minor contents of Ni and Mo and spray coatings from it.	The powder and coatings consist of $Cr_{1.65}Fe_{0.35}B_{0.96}$ and Cr_2B borides in metal α-matrix.
[2001Jin]	TEM/EDS was used for as-sprayed coatings, which were also annealed at 400 and 527°C.	The coatings were from $Cr_{1.65}Fe_{0.35}B_{0.96}$ and Cr_2B borides in metal α-matrix supersaturated with B.
[2002Car]	XRD and Mössbauer spectroscopy. Samples Cr-FeB and Fe-CrB were prepared from powders by cold-compacting and further annealing at 1000°C for 16 and 116 h.	The atom diffusion and interaction were studied.
[2003Chr]	XRD and HREM. Amorphous ribbons $Fe_{76}Cr_2B_{22}$ and $Fe_{78}B_{22}$ were obtained by melt spinning, followed by annealing for 1 h at 27 to 627°C with the step of 25°C.	For an amorphous alloy $Fe_{76}Cr_2B_{22}$, the crystallization enthalpy was determined as 2.0 eV and were examined.

(*continued*)

DOI: 10.1007/978-3-540-69761-9_17

Reference	Method/Experimental Technique	Type of Property
[2004Guo2]	An alloy containing 1.4 mass% B was studied by SEM/microanalysis.	The non-equilibrium segregation of boron was studied in relation with regimes of thermal treatments.
[2005Dyb]	SEM/EPMA, XRD, abrasive wear resistance test, microhardness. Samples from a melted alloy Fe-10 mass% Cr and mixture of B and KBF_4 were annealed at 850, 900 and 950°C	Boride layers of Fe_2B and FeB were found to form between a Fe-10 mass% Cr and B at 850 to 950°C. The kinetic of their growing was studied.
[2005Kar]	DSC, XRD, resistivity, magnetic permeability. Amorphous ribbons $Fe_{76}Cr_2B_{22}$ and $Fe_{78}B_{22}$ were obtained by melt spinning, followed by annealing for 1 h at 300 to 900 K with the step of 25 K.	The amorphous alloy $Fe_{76}Cr_2B_{22}$ crystallized at 462°C

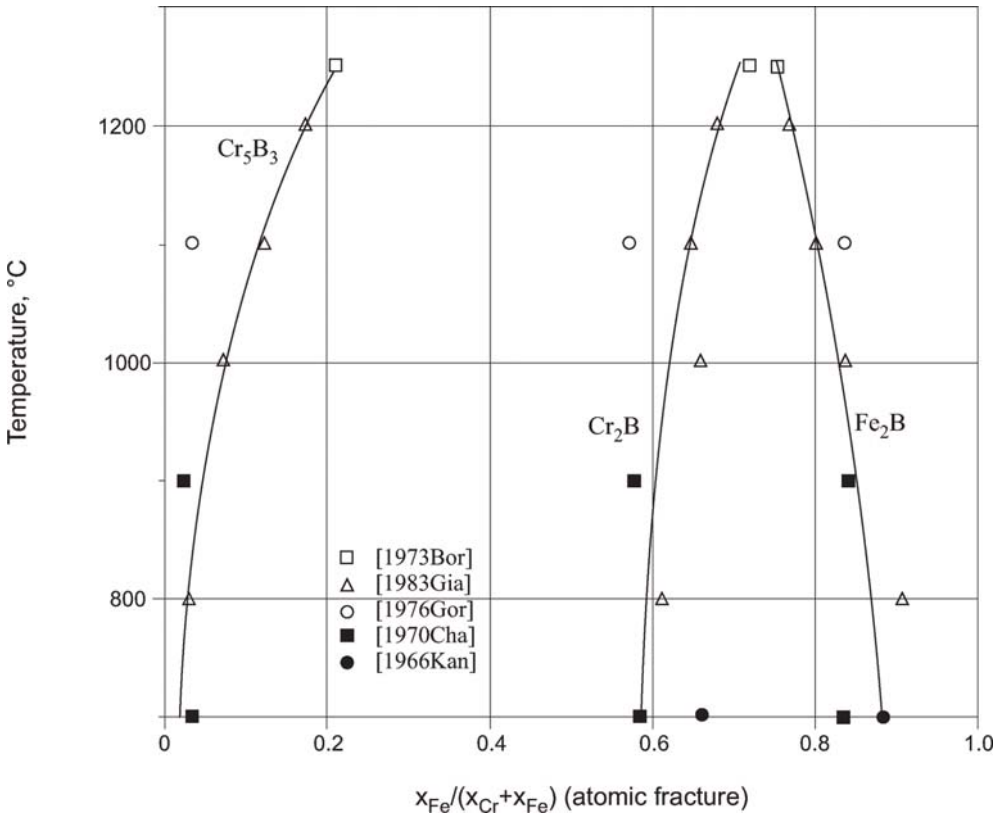

Fig. 1. B-Cr-Fe. Composition of boride phases with the maximal solubility, Cr_5B_3, Cr_2B and Fe_2B

DOI: 10.1007/978-3-540-69761-9_17

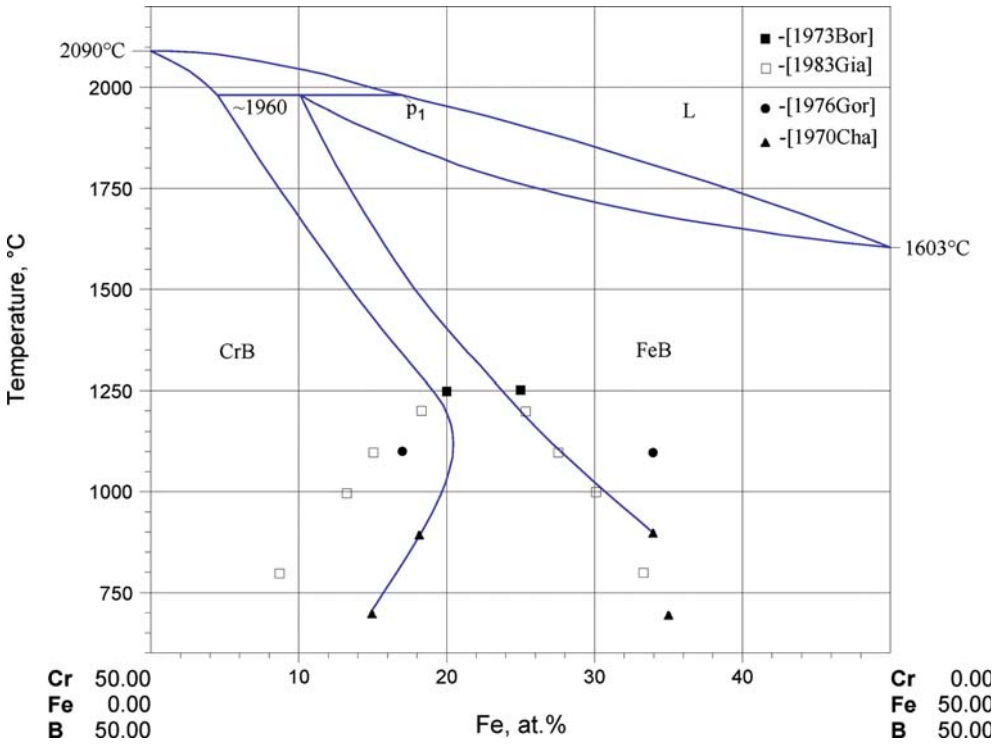

Fig. 2. B-Cr-Fe. Quasibinary section CrB-FeB. Points denote data on the maximal solubility. The phase diagram above 1200°C is presented after [1987Shi]

DOI: 10.1007/978-3-540-69761-9_17

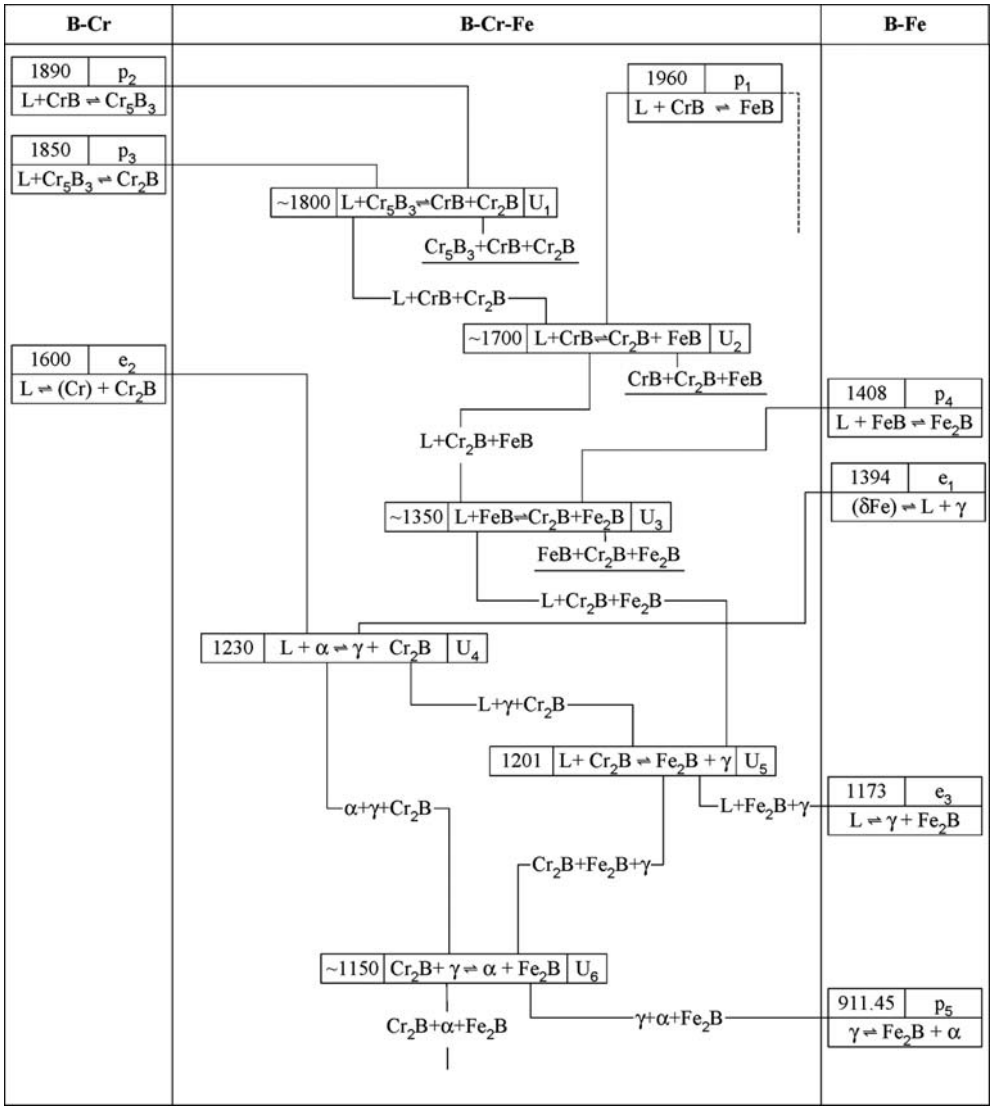

Fig. 3. B-Cr-Fe. Partial reaction scheme

DOI: 10.1007/978-3-540-69761-9_17

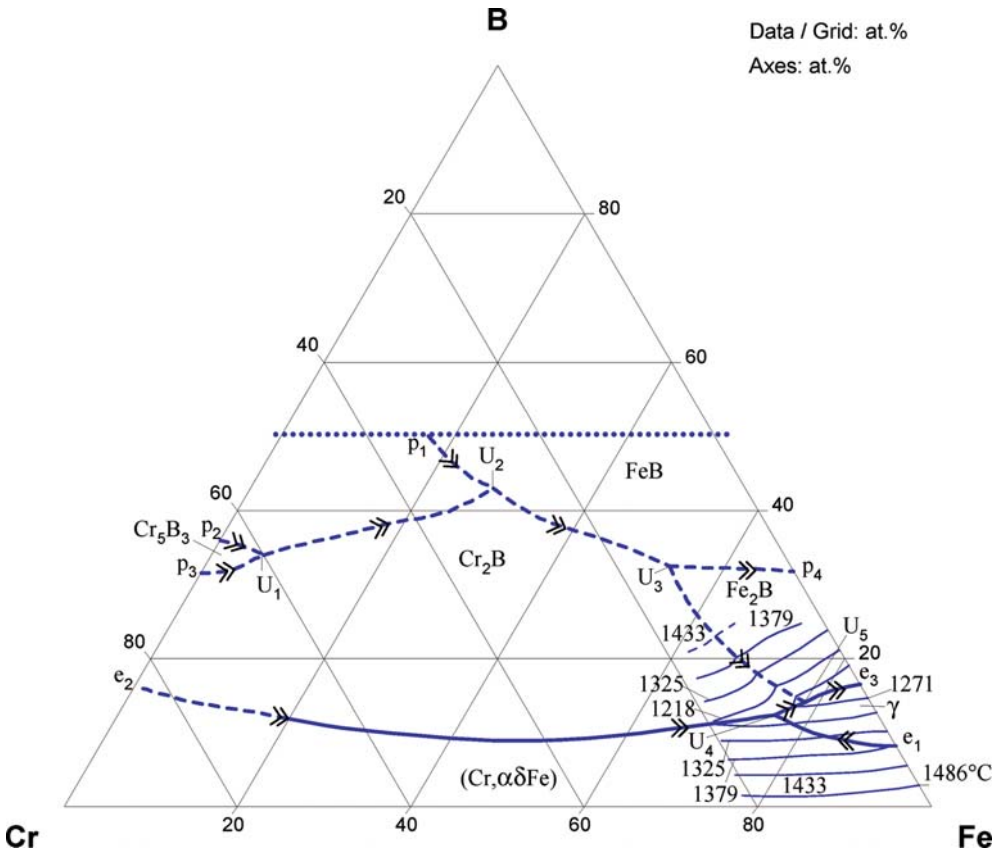

Fig. 4. B-Cr-Fe. Partial liquidus projection

DOI: 10.1007/978-3-540-69761-9_17

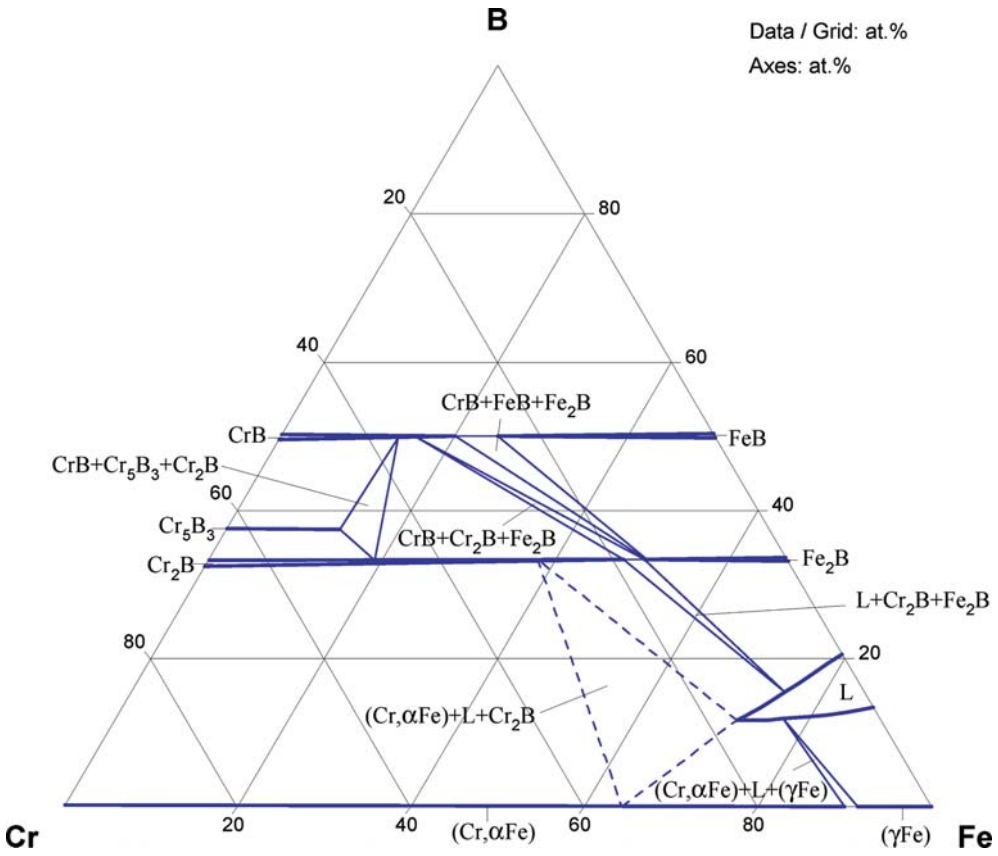

Fig. 5. B-Cr-Fe. Partial isothermal section at 1250°C

DOI: 10.1007/978-3-540-69761-9_17

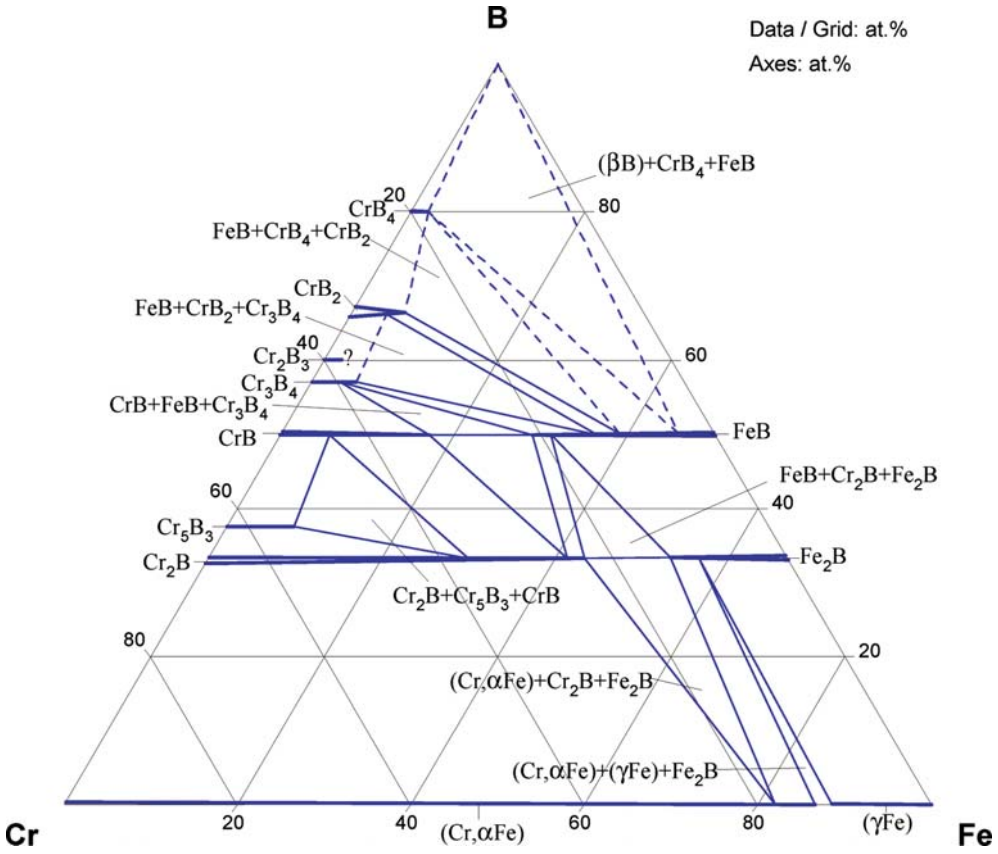

Fig. 6. B-Cr-Fe. Isothermal section at 1100°C

DOI: 10.1007/978-3-540-69761-9_17

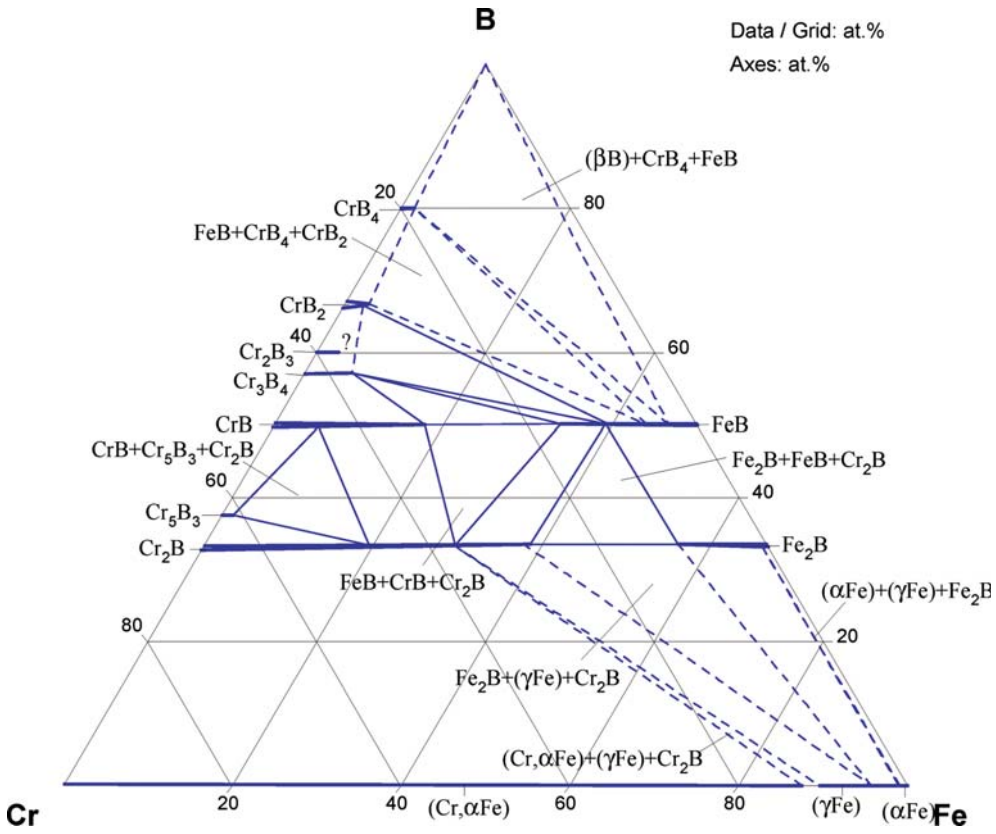

Fig. 7. B-Cr-Fe. Isothermal section at 900°C

DOI: 10.1007/978-3-540-69761-9_17

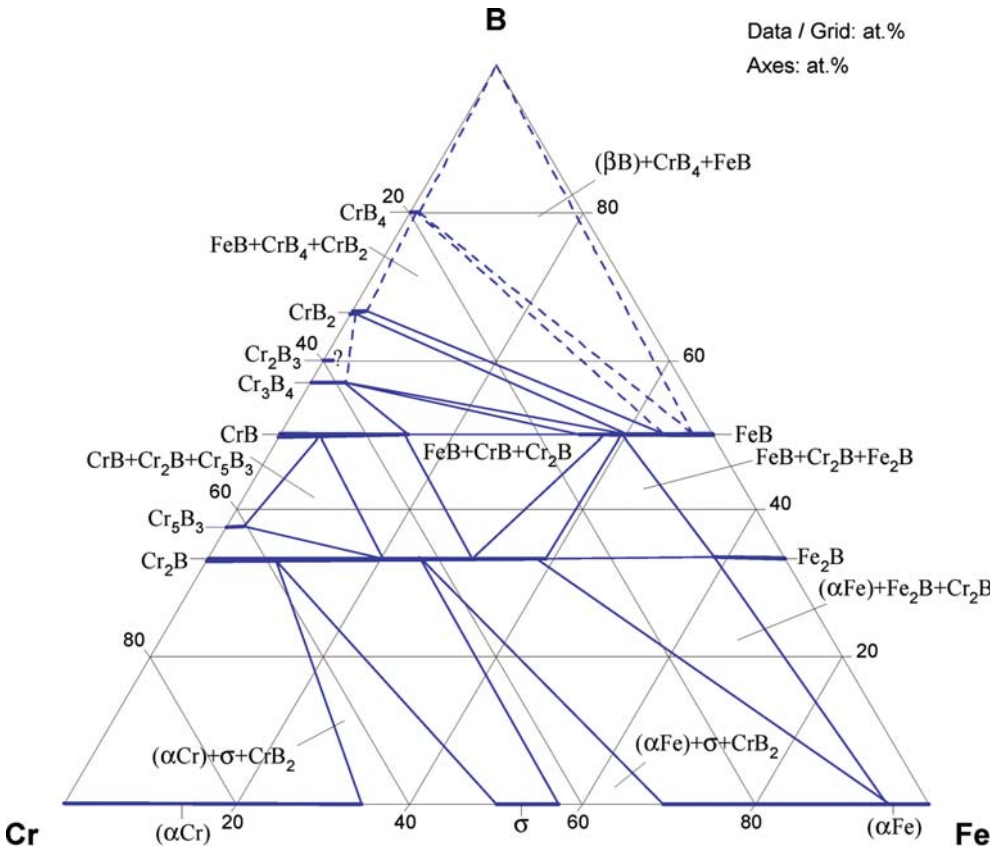

Fig. 8. B-Cr-Fe. Isothermal section at 700°C

DOI: 10.1007/978-3-540-69761-9_17

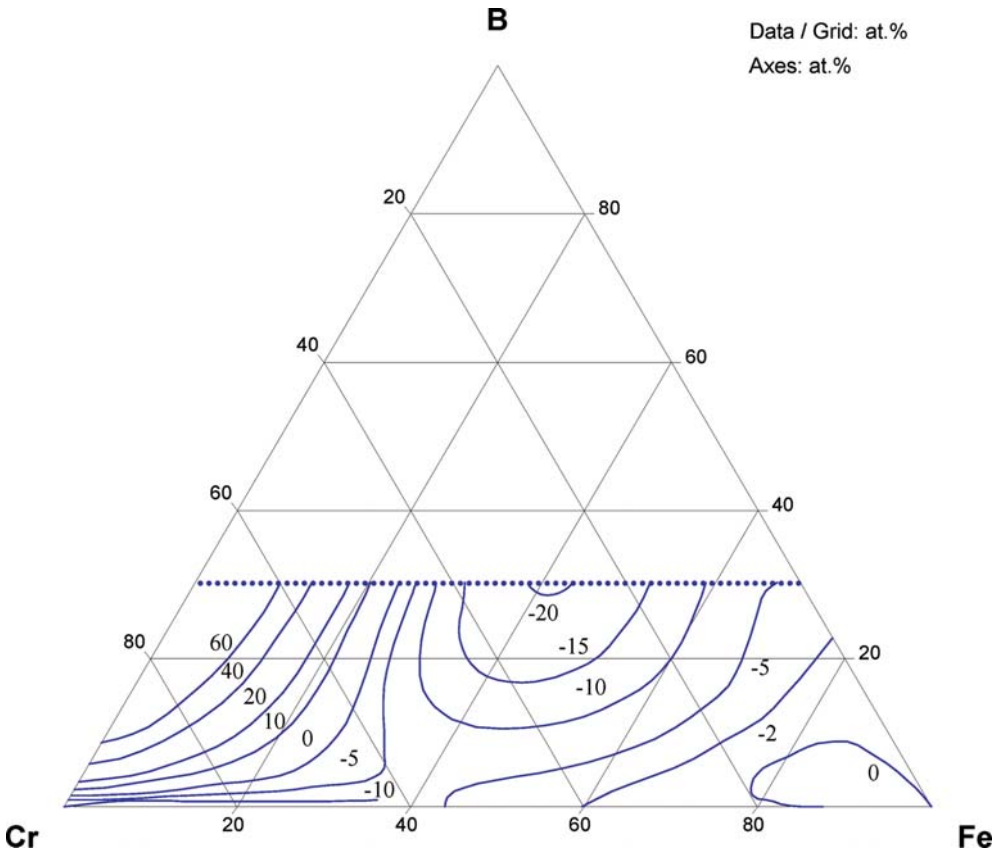

Fig. 9a. B-Cr-Fe. Partial enthalpies ($kJ \cdot mol^{-1}$) of formation of ternary B-Cr-Fe melts for iron in the system at 1880°C

DOI: 10.1007/978-3-540-69761-9_17

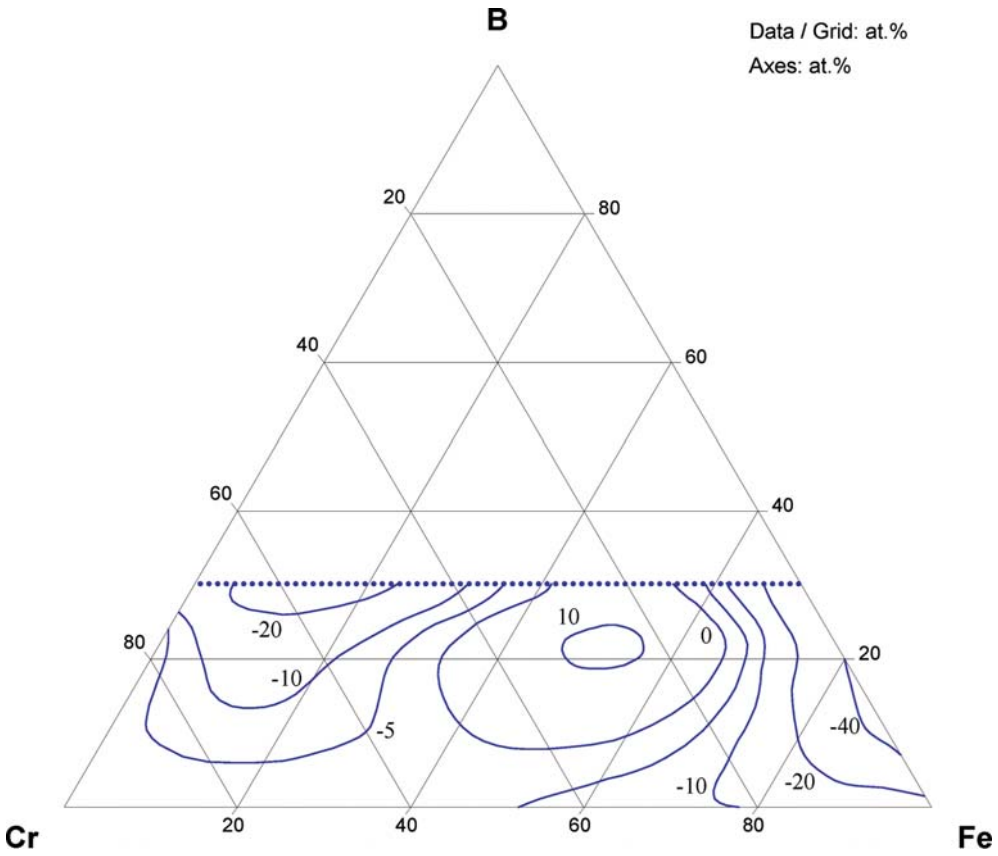

Fig. 9b. B-Cr-Fe. Partial enthalpies ($kJ \cdot mol^{-1}$) of formation of ternary B-Cr-Fe melts for chromium at 1880°C

DOI: 10.1007/978-3-540-69761-9_17

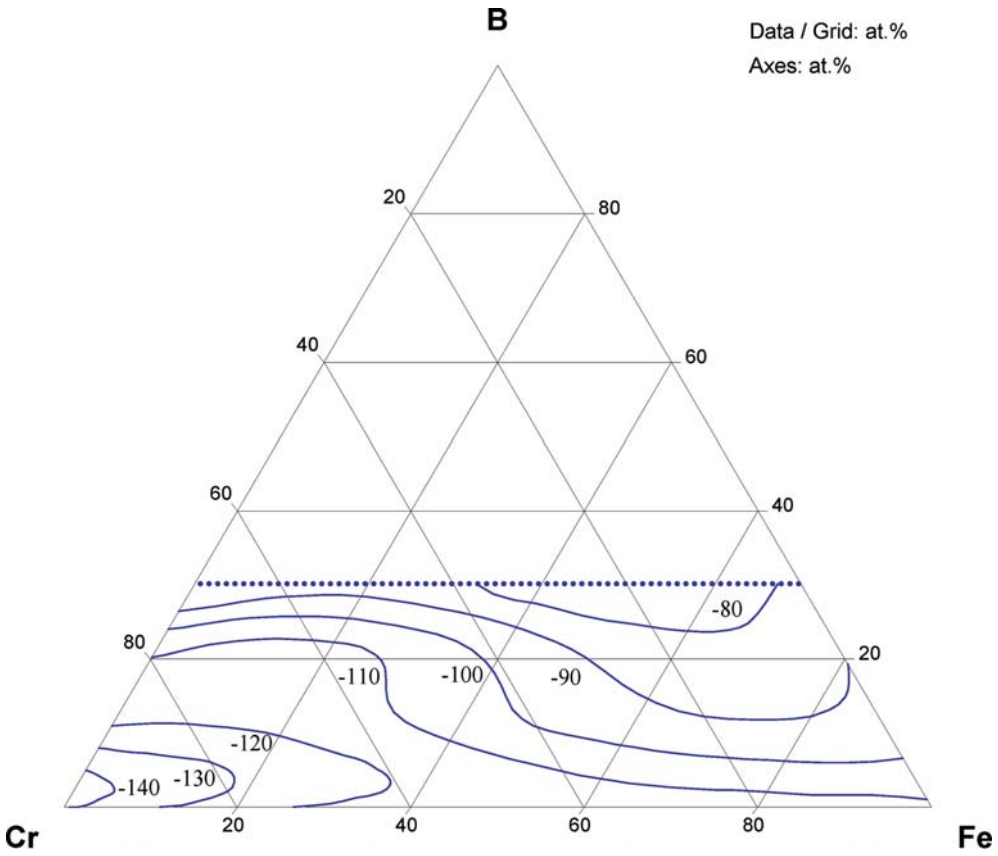

Fig. 9c. B-Cr-Fe. Partial enthalpies ($kJ \cdot mol^{-1}$) of formation of ternary B-Cr-Fe melts for boron at 1880°C

DOI: 10.1007/978-3-540-69761-9_17

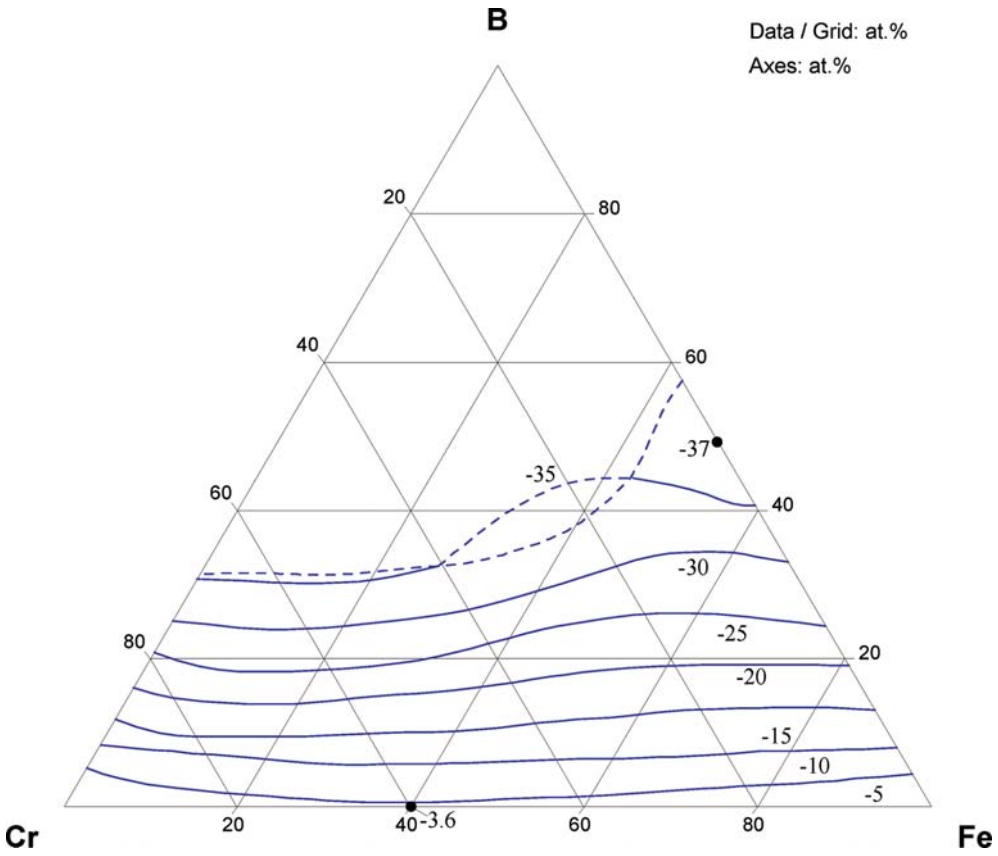

Fig. 10a. B-Cr-Fe. Integral enthalpies of formation of ternary B-Cr-Fe melts at 1880°C

DOI: 10.1007/978-3-540-69761-9_17

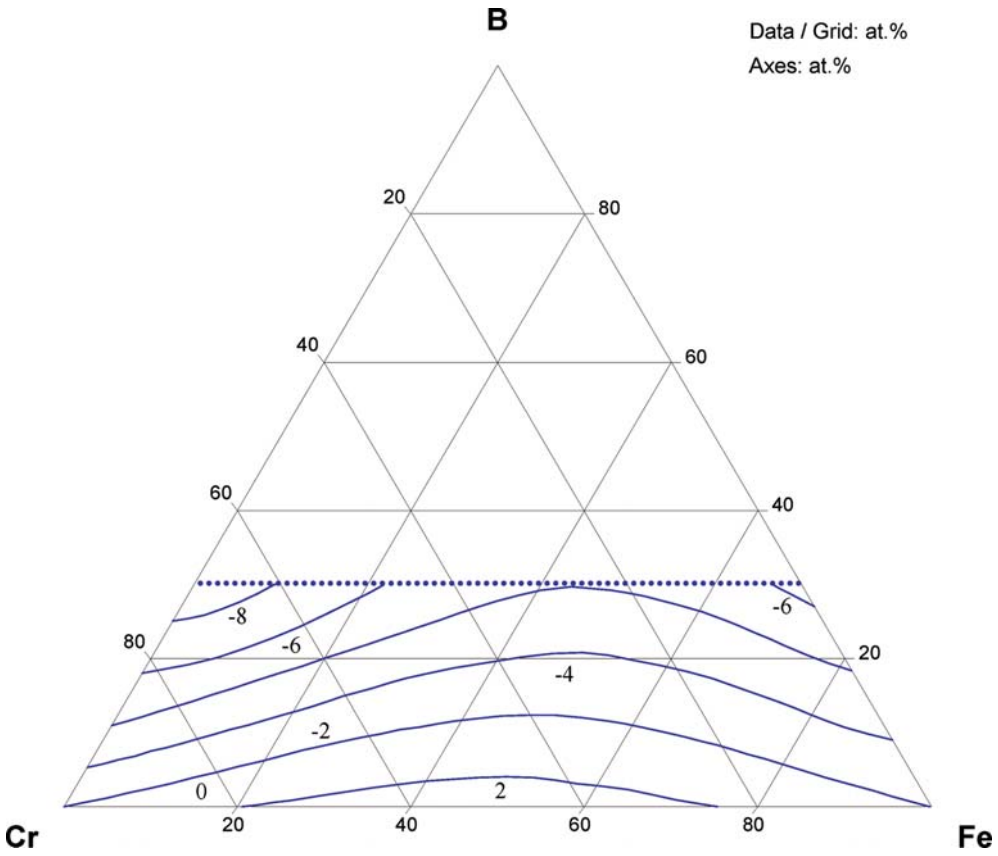

Fig. 10b. B-Cr-Fe. Integral entropies of formation of ternary B-Cr-Fe melts at 1880°C

DOI: 10.1007/978-3-540-69761-9_17

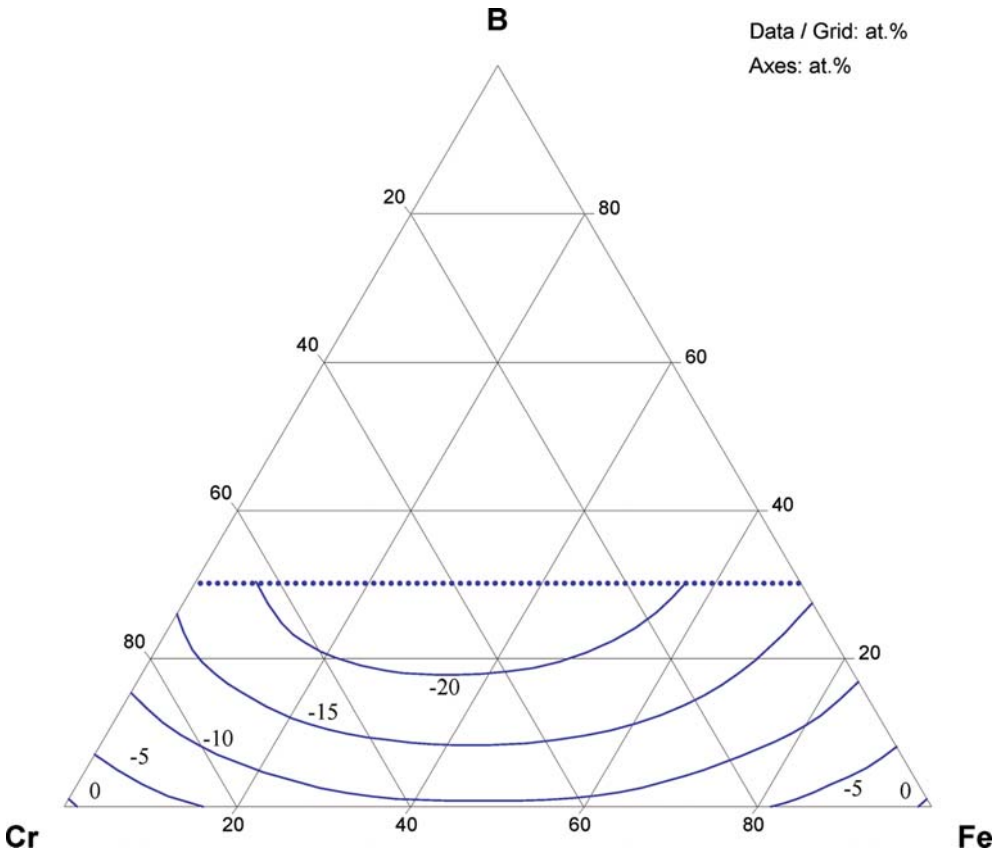

Fig. 10c. B-Cr-Fe. Integral Gibbs energy of formation of ternary B-Cr-Fe melts at 1880°C

DOI: 10.1007/978-3-540-69761-9_17

References

[1958Aro] Aronsson, B., Åselius, J., "The Efect of the Boron on the Formation of σ-FeCr at 700°C", *Acta Chem. Scand.*, **12**(7), 1476–1480 (1858) (Crys. Structure, Phase Relations, Experimental, 15)

[1964Bro] Brown, B.E., Beerntsen, D.J., "Refinement of an Iron Chromium Boride with the Mn_4B Structure", *Acta Crystallogr.*, **17**, 448–450 (1964) (Crys. Structure, Experimental, 12)

[1966Kan] Kaneko, H., Nishizawa, T., Chiba, A., "Borides in Stainless Steel" (in Japanese), *Nippon Kinzoku Gakkai-Si (J. Jpn. Inst. Met.)*, **30**(2), 157–163 (1966) (Crys. Structure, Morphology, Phase Diagram, Experimental, #, *, 17)

[1966Yas] Yasinskaya, G.A., "The Wetting of Refractory Carbides, Borides and Nitrides by Molten Metals", *Sov. Powder Metall Met. Ceram.*, **43**(7), 557–569 (1966), translated from *Poroshk. Metall.*, (7), 53–56 (1966) (Experimental, Interface Phenomena, 5)

[1968And] Andersson, S., Lundström, T., "The Crystal Structure of CrB_4", *Acta Chem. Scand.*, **22**, 3103–3110 (1968) (Crys. Structure, Experimental, 8)

[1969Por] Portnoy, K.I., Romashov, V.M., Romanovich, I.V., "The Phase Diagram of the System Chromium-Boron" (in Russian), *Poroshk. Metall*, (4), 51–57 (1969) (Phase Diagram, Experimental, #, 19)

[1970Che] Chepiga, M.V., Kuz'ma, Yu.B., "Phase Equilibria in the Chromium-Iron-Boron System" (in Russian), *Izv. VUZ Chern. Metall.*, (3), 127–130 (1970) (Crys. Structure, Morphology, Phase Diagram, Experimental, #, *, 8)

[1972Por] Portnoy, K.I., Romashov, V.M., "Binary Phase Diagrams of Some Elements with Boron (Review)" (in Russian), *Poroshk. Metall.*, (5), 48–56 (1972) (Phase Diagram, Phase Relations, Review, #, 44)

[1973Bor] Borlera, M.L., Pradelli, G., "On the System Iron-Chromium-Boron. Reports About Solid State Equilibria in the System at 1250°C" (in Italian), *Metall. Ital.*, **65**(7–8), 421–424 (1973) (Crys. Structure, Morphology, Phase Diagram, Experimental, #, *, 5)

[1974Lug] Lugscheider, E., Knotek, O., Reimann, H., "The Ternary System Nickel-Chrom-Bor" (in German), *Monatsh. Chem.*, **105**(1), 80–90 (1974) (Phase Diagram, Crys. Structure, Experimental, #, 32)

[1976Cal] Callmer, B., Lundstroem, T., "A Single-Crystal Diffractometry Investigation of Iron in β-Rhombohedral Boron", *J. Solid State Chem.*, **17**, 165–170 (1976) (Crys. Structure, Experimental, 12)

[1976Gor] Gorbunov, A.E., Boduryan, F. M., "On Phase Equilibria in the Ternary System Chromium-Boron-Iron" (in Russian), Veprintsev, V.I. (Ed.), *Nauchnye Trudy No. 16: Tverdye Splavy i Tugoplavkie Metally, Vses. Nauchn.-Issled, i Proektn. Inst. Tugoplavk. Met. i Tverd. Splavov (VNIITS)*, Metallurgiya, Moscow, (16), 172–178 (1976) (Crys. Structure, Morphology, Phase Diagram, Experimental, #, *, 16)

[1976Lun] Lunström, T., Tergenius, L.E., "On the Solid Solution of Copper in ΔE-Rhombohedral Boron", *J. Less-Common Met.*, 47, 23–28 (1976) (Crys. Structure, Experimental, 10)

[1979Kik1] Kikuchi, M., Fukamichi, K., Masumoto, T., "The ΔE Effect in Iron-Boron and Iron-Chromium-Boron Amorphous Invar Aloys", *J. Magn. Magn. Mater.*, **10**(2–3), 300–302 (1979) (Experiment, Mechan. Prop., 12)

[1979Kik2] Kikuchi, M., Fukamichi, K., Masumoto, T., "Invar-Type and Elinvar-Type Amorphous Fe-Cr-B Alloys with High Corrosion-Resistance" (in Japanese), *J. Jpn. Inst. Met.*, **43**(10), 885–890 (1979) (Experiment, Magn. Prop., Mechan. Prop., 20)

[1979Kik3] Kikuchi, M., Fukamichi, K., Masumoto, T., "Invar- and Elinvar-Type Amorphous Fe-Cr-B Alloys with High Corrosion Resistance", *Sci. Rep. Res. Inst. Tohoku Univ. Ser. A - Phys. Chem. Metall.*, **27**(2), 210–219 (1979) (Experiment, Magn. Prop., Mechan. Prop., 23)

[1981Cre] Crespo, A.J., Tergenius, L.-E., Lundström, T., "The Solid Solution of 4d, 5d and Some p Elements in β Rhomhedral Boron", *J. Less-Common Met.*, 77, 147–150 (1981) (Crys. Structure, Experimental, 12)

DOI: 10.1007/978-3-540-69761-9_17

[1981Kha] Khan, Y., Kneller, E., Sostarich, M., "Stability and Crystallization of Amorphous Iron-Boron Alloys Obtained by Quenching from the Melt", *Z. Metallkd.*, **72**(8), 553–557 (1982) (Crys. Structure, Phase Diagrm, Experiment, #, 21)

[1982Ber] Bergmann, H.W., Brokmeier, U., "Crystallization Behaviour of Fe-B-Cr, Fe-B-Co, and Fe-B-Ni Alloys", *Met. Sci.*, **16**, 191–196 (1982) (Crys. Structure, Phase Relation, Experimental, Mechan. Prop., 14)

[1982Kha] Khan, Y., Kneller, E., Sostarich, M., "The Phase Fe_3B", *Z. Metallkd.*, **73**(10), 624–626 (1982) (Crys. Structure, Phase Diagrm, Experiment, #, 13)

[1983Gia] Gianoglio, C., Pradelli, G., Vallino, M., "Solid State Equilibria in the Cr-Fe-B System at the Temperature of 1373 K", *Metall. Sci. Technol.*, **1**(2), 51–57 (1983) (Crys. Structure, Phase Diagram, Experimental, Review, #, *, 14)

[1985Car] Carbucicchio, M., Sambogna, G., "Influence of Chromium on Boride Coatings Produced on Iron-Alloys", *Thin Solid Films*, **126**(3–4), 299–305 (1985) (Crys. Structure, Morphology, Experimental, 25)

[1985Gia] Gianoglio, C., Pradelli, G., "The Cr-Fe-B System: Distribution Equilibria of Metal Atoms in Biphasic Fields" (in Italian), *Atti Accad. Sci. Torino, Cl. Sci. Fis., Met. Nat.*, **117**(4–6), 391–402 (1985) (Crys. Structure, Phase Diagram, Experimental, #, 6)

[1985Kal] Kaloshkin, S.D., Alekseev, L.A., Tomilin, I.A., Dong, H.F., "Investigation of Cr Redistribution Between Phases During Crystallisation of Amorphous Fe-Cr-B Alloys by JGRS Methods" (in Russian), *Dokl. AN SSSR*, **284**(5), 1120–1124 (1985) (Crys. Structure, Phase Relations, Experimental, 11)

[1985Kov] Ková, J., Potocký, L., Kisdi-Koszó, E., Novák, L., "Low Temperature Magnetic Properties of Amorphous Fe-Cr-B Alloys", *Acta Phys. Slov*aca, **35**(4–5), 240–243 (1985) (Experimental, Magn. Prop., 8)

[1985Nov] Novák, L., Potocký, L., Kisdi-Koszó, E., Lovas, A., Daniel-Szabó, J., "Curie Temperature of Fe-Cr-B and Fe-W-B Metallic Glasses", *Acta Phys. Slovaca*, **35**(4–5), 244–247 (1985) (Experimental, Magn. Prop., 5)

[1985Pot] Potocký, L., Vojtaník, P., Kisdi-Koszó, E., Lovas, A., "Some Magnetic Properties and Magnetic After-Effect in Amorphous $Fe_{80}T_3B_{17}$ Alloys", *Acta Phys. Slovaca*, **35**(4–5), 279–284 (1985) (Experimental, Magn. Prop., 8)

[1986Dro] Drozdova, M.A., Batyrev, I.G., Prokoshin, A.F., Makhotkin, V.E., Korytov, V.V., "Magnetic and Electron Structure of Amorphous Fe-M-B Alloys (M = V, Cr, Mn)", *Sov. Phys. - Solid State*, **28**(8), 1390–1392 (1986), translated from *Fiz. Tverd. Tela*, **28**, 2486–2491 (1986) (Crys. Structure, Phase Relations, Experimental, Thermodyn., 7)

[1986Zay] Zaytsev, A.K., Kaloshkin, S.D., Kandyba, G.I., Tomilin, I.A., "Structural Pecularities of Crystallization of Amorphous Alloys $Fe_{85-x}Cr_xB_{15}$", *Phys. Met. Metallogr.*, **61**(5), 173–177 (1986), translated from *Fiz. Met. Metalloved.*, **61**(5), 1019–1022 (1986) (Crys. Structure, Experimental, Morphology, Thermodyn., 4)

[1987Gle] Glezer, A.M., Molotilov, B.V., Ovcharov, V.P., Utevskaya, O.L., Chicherin, Yu.Ye., "The Structure and Mechanical Properties of Fe-Cr-B Alloys During the Transition from Amorphous to Crystalline State", *Phys. Met. Metallogr.*, **64**(6), 59–62 (1987), translated from *Fiz. Met. Metalloved.*, **64**(6), 1106–1109 (1987) (Crys. Structure, Experimental, Mechan. Prop., 5)

[1987Oka] Okada, S., Atoda, T., Higashi, I., "Structural Investigation of Cr_2B_3, Cr_3B_4, and CrB by Single-Crystal Diffractometry", *J. Solid State Chem.*, **68**, 61–67 (1987) (Crys. Structure, Experimental, 9)

[1987Shi] Shirae, K., Ueda, Y., Kachi, S., Kosuge, K., "Phase Diagram and Magnetovolume Effect of Pseudobinary CrB-FeB System", *Mater. Res. Bull.*, **22**(4), 521–526 (1987) (Crys. Structure, Phase Diagram, Experimental, #, 10)

[1988Bad] Badini, C., Mazza, D., "The Texture of Borided Layers Grown on Fe-Ni and Fe-Cr Alloys", *J. Mater. Sci. Lett.*, **7**(6), 661–662 (1988) (Crys. Structure, Experimental, Kinetics, 10)

DOI: 10.1007/978-3-540-69761-9_17

[1988Har] Hargraves, P., Dunlap, R.A., "Magnetic Critical Properties of Amorphous Fe-Cr-B Alloys Measured by AC Susceptibility Techniques", *J. Magn. Magn. Mater.*, **75**(3), 378–382 (1988) (Experimental, Magn. Prop., 19)

[1988Pus] Pustov, Yu.A., Baldokhin, Yu.V., Opara, B.K., Kolotyrkin, P.Ya., Ovcharov, V.P., Kislogubov, I.A., "Thermal Stability of Amorphous Alloy Fe-Cr-B", *Phys. Met. Metallogr.*, **65**(1), 147–154 (1988), translated from *Fiz. Met. Metalloved*., **65**(1), 159–167 (1988) (Crys. Structure, Phase Relations, Experimental, Kinetics, 20)

[1989Bra] Brakman, C.M., Gommers, A.W.J., Mittemeijer, E.J., "Boriding of Fe and Fe-C, Fe-Cr and Fe-Ni Alloys: Boride-Layer Growth Kinetics", *J. Mater. Res.*, **4**(6), 1354–1370 (1989) (Phase Relations, Experimental, Kinetics, 25)

[1989Dro] Drozdova, M.A., Glezer, A.N., Krasavin, Y.I., Savvin, A.A., "Variations in the Magnetic Properties and Structure of Amorphous FeCrB Alloys in the Process of Crystallization", *Phys. Met. Metallogr. (Engl. Transl.)*, **67**(5), 63–68 (1989), translated from *Fiz. Met. Metalloved*., **67**(5), 896–901 (1989) (Crys. Structure, Experimental, Magn. Prop., 3)

[1989Kol] Kolb-Telieps, A., Luft, U., "Relations Between Structure and First-Step Crystallization of Iron-Metal-Boron Glasses", *J. Non-Cryst. Solids*, **109**, 59–63 (1989) (Crys. Structure, Experimental, Kinetics, 7)

[1990Kuz] Kuzmann, E., Vértes, A., Novochatskii, I.A., Pákozdi, A., Varga, I., Jaen, J., Ianov, L.A., Usatyuk, I.I., Kaverin, Yu. F., "Mössbauer Study of the Effect of Preparation Parameters in Rapidly Quenched Fe-Cr-P-C, Fe-Cr-B and Ni(^{57}Fe)P Amorphous Alloys", *Hyperfine Interact.*, **55**(1–4), 1013–1020 (1990) (Crys. Structure, Experimental, 5)

[1990Mil] Milman, Y.V., Pan, S.V., Postoi, S.V., Ivashchenko, P.K., "Microhardness of Amorphous Metallic Alloys Fe-Cr-B", *Sov. Powder Metall. Met. Ceram.*, **29**(8), 632–635 (1990), translated from *Poroshk. Metall.*, (8), 49–53 (1990) (Experimental, Mechan. Prop., 11)

[1990Pus] Pustov, Y.A., Baldokhin, Y.V., Labutin, V.Y., Nefedov, V.I., Kolotyrkin, P.Y., Ovcharov, V.P., Kislogubov, I.A., "Avalanche-Type Relaxation Processes in Fe-Cr-B System Alloys at Isothermal Annealing at Different Partial Oxygen Pressure" (in Russian), *Dokl. Akad. Nauk SSSR*, **311**(3), 654–658 (1990) (Experimental, Kinetics, 2)

[1990Sch] Schaaf, P., Biehl, V., Gonser, U., Bamberger, M., Langohr, M., Maisenhalder, F., "CXMS Study of Mild-Steel Laser Alloyed with CrB_2", *Ber. Bunsen-Ges. Phys. Chem. Chem. Phys.*, **87**(9), 757–761 (1983) (Crys. Structure, Experimental, Mechan. Prop., 17)

[1991Kos] Kostikas, A., Papaefthymiou, V., Simopoulos, A., Li, Y.P., Hadjipanayis, G.C., "Mössbauer Studies of Fine Particles of Fe-Cr-B", in "*Science and Technology of Nanostructured Magnetic Materials*", Hadjipanayis, G.C., Prinz, G.A. (Eds.), Proceedings of a NATO Advanced Study Institute, Plenum Press, NewYork, 551–557 (1991) (Crys. Structure, Experimental, Magn. Prop., 14)

[1991Sha] Shafirstien, G., Bamberger, M., Langohr, M., Maisenhalder, F., "Laser Surface Alloying of Carbon Steel and α-Fe with CrB_2 Particles", *Surf. Coat Technol.*, **45**, (1991) 417–423 (Crys. Structure, Experimental, Mechan. Prop., 6)

[1992Ono] Onodera, H., "Electric-Field Gradients and Structural Anisotropy in Amorphous Fe(Cr)-B and Fe(Cr)-P Alloys Studied by ^{57}Fe Mössbauer Spectroscopy", *Sci. Rep. Res. Inst. Tohoku Univ., Ser. A - Phys. Chem. Metall.*, **36**(2), 200–212 (1992) (Crys. Structure, Experimental, 34)

[1992Rag1] Raghavan, V., "The B-Cr-Fe (Boron-Chromium-Iron) System", in "*Phase Diagrams of Ternary Iron Alloys*", Raghavan, V. (Ed.), Ind. Inst. Met., Calcutta, **6A**, 309–317 (1992) (Crys. Structure, Phase Relations, Review, #, 9)

[1992Rag2] Raghavan, V., "The Fe-B (Iron-Boron) System" in "*Phase Diagrams of Ternary Iron Alloys"*, Indian Institut of Metals, Calcutta, **6A**, 12–13 (1992) (Crys. Structure, Phase Diagram, Phase Relations, Review, 3)

[1993Itk] Itkin, V.P., "Cr-Fe" in "*Phase Diagrams of Binary Iron Alloys*" Okamoto, H. (Ed.), ASM International, Materials Park, OH (1993) (Crys. Structure, Phase Diagram, Thermodyn., Review, #)

DOI: 10.1007/978-3-540-69761-9_17

[1994Car] Carbucicchio, M., Palombarini, G., Sambogna, G., "Alloying of Fe-B Compounds with Cr: Effects of Fe Liberation and Comparison with Ni Alloying", *Hyperfine Interact.*, **92**(1–4), 993–999 (1994) (Phase Relations, Experimental, Kinetics, 9)

[1994Hal] Hallemans, B., Wollants, P., Roos, J.R., "Thermodynamic Reassessment and Calculation of the Fe-B Phase Diagram", *Z. Metallkd.*, **85**(10), 676–682 (1994) (Crys. Structure, Phase Diagram, Thermodyn., Assessment, #, 36)

[1994Sha] Shafirstein, G., Ariely, S., Bamberger, M., Maisenhalder, F., Langohr, M., "Modeling of Solidification Behavior During Laser-Surface Alloing of Ferrous-Alloys with CrB_2", *Mater. Sci. Technol.*, **10**(9), 837–840 (1994) (Morphology, Experimental, 7)

[1995Fio] Fiorani, D., Romero, H., Suber, L., Testa, A.M., Vittori, M., Montone, A., Dormann, J.L., Maknani, J., "Synthesis and Characterization of Amorphous $Fe_{80-x}Cr_xB_{20}$ Nanoparticles", *Mater. Sci. Eng. A*, **A204**(1–2), 165–168 (1995) (Experimental, Magn. Prop., 9)

[1995Gol] Goldfarb, I., Kaplan, W.D., Ariely, S., Bamberger, M., "Fault-Induced Polytypism in $(Cr,Fe)_2B$", *Philos. Mag. A*, **72**(4), 963–979 (1995) (Crys. Structure, Experimental, 21)

[1995Sub] Suber, L., Fiorani, D., Romero, H., De Pamphilis, A., Vittori, M., Montone, A., Dormann, J.L., Maknani, J., "Sysnthesis, Characterization and Magnetic Properties of Fine Fe-Cr-B Amorphous Particles", *Mater. Sci. Forum*, **195**, 209–214 (1995) (Experimental, Magn. Prop., 8)

[1995Wit1] Witusiewicz, V.T., "Thermodynamics of Binary and Ternary Melts of the 3d Transition Metals (Cr, Mn, Fe, Co and Ni) with Boron", *Thermochim. Acta*, **264**, 41–58 (1995) (Experimental, Thermodyn., 25)

[1995Wit2] Witusiewicz, V.T., "Thermodynamics of Formation of Binary and Ternary Melts of the 3d Transition Metals with Metalloid" (in Ukrainian), Summary of Thesis, National Academy of Science of Ukraine, Kiev, pp. 55 (1995) (Experimental, Thermodyn., 0)

[1996Gle] Glezer, A.M., Pozdnyakov, V.A., Kirienko, V.I., Zhigalina, O.M., "Structure and Mechanical Properties of Liquid-Quenched Nanocrystals", *Mater. Sci. Forum*, **225–227**, 781–786 (1996) (Crys. Structure, Experimental, Mechan. Prop., 4)

[1996Lya] Lyakishev, N.P., "B-Fe" in "*Phase Diagrams of Binary Metal Systems*" (in Russian), Mashinostriyeniye, Moscow, **1**, 442–444 (1996) (Crys. Structure, Phase Diagram, Review, #, 10).

[1997Zha] Zhang, L., Manthiram, A., "Synthesis and Characterization of Chains Composed of Nanometer Size Fe-Cr-B Particles", *J. Magn. Magn. Mater.*, **168**(1–2), 85–93 (1997) (Experimental, Magn. Prop., 15)

[1998Car] Carbucicchio, M., Palombarini, G., Rateo, M., Sambogna, G., "High Temperature Solid State Reactivity between Iron and Chromium Monoborides", *Hyperfine Interact.*, **116**, 143–148 (1998) (Phase Relations, Experimental, Kinetics, 10)

[1998Jin] Jin, H.W., Rhyim, Y.M., Park, C.G., Kim, M.C., "Microstructural Development of Nanocrystalline Fe-Cr-B Alloy During the Thermal Spray Coating Process" (in Korean), *J. Korean Inst. Met.*, **36**(11), 1909–1914 (1998) (Crys. Structure, Experimental, 11)

[1998Mie] Miettinen, J., "Approximate Thermodynamic Solution Phase Data for Steels", *Calphad*, **22**(2), 275–300 (1998) (Phase Diagrams, Assessment, Calculation, #, 83)

[1998Zak] Zakharenko, N.I., Poperenko, L.V., Yurgelevich, I.V., "Ellipsometric Study of Rapidly Quenched Fe-Cr-B Ribbons Subjected to Laser Treatment", *Phys. Met. Metallogr.*, **85**(5), 28–31 (1998), translated from *Fiz. Metal. Metalloved.*, **85**(5), 517–519 (1998) (Experimental, Optical Prop., 5)

[1999Cen] Ceniga, L., Novak, L., Kisdi-Koszo, E., "The Influence of Heat Treatment on the Barkhausen Effect in the Fe-Cr-B Amorphous Alloy", *J. Magn. Magn. Mater.*, **196–197**, 154–155 (1999) (Crys. Structure, Experimental, Magn. Prop., 2)

[1999Jin] Jin, H.W., Park, C.G., Kim, M.C., "Microstructure and Amorphization Induced by Frictional Work in Fe-Cr-B Alloy Thermal Spray Coatings", *Surf. Coat. Technol.*, **113**, 103–112 (1999) (Crys. Structure, Experimental, 25)

DOI: 10.1007/978-3-540-69761-9_17

[2001Cal] Calos, N.J., Graham, E., Cousens, D.R., Christodoulou, P., Kennard, C.H.L., Bekessy, L.K., Parker, S.F., "Mode of Boron Solubility in Ferrous Alloys", *Mater. Trans*., **42**(3), 496–501 (2001) (Crys. Structure, Experimental, 31)

[2001Chr] Christodoulou, P., Calos, N., "A Step Towards Designing Fe-Cr-B-C Cast Alloys", *Mater. Sci. Eng. A*, **A301**, 103–117 (2001) (Crys. Structure, Phase Diagrams, Experimental, #, 12)

[2001Jin] Jin, H.W., Park, C.G., Kim, M.C., "In Situ TEM Heating Studies on the Phase Transformation of Metastable Phases in Fe-Cr-B Alloy Spray Coatings", *Mater. Sci. Eng. A*, **A304–306**, 321–326 (2001) (Crys. Structure, Experimental, Kinetics, 12)

[2002Car] Carbucicchio, M., Grazzi, C., Palombarini, G., Rateo, M., Sambogna, G., "On the Phase Transformations in Cr-FeB and Fe-CrB Systems at High Temperature", *Hyperfine Interact*., **139/140**, 393–398 (2002) (Phase Relations, Experimental, Kinetics, 10)

[2002Tak] Takizava, H., Haze, N., Okamoto, K., Uheda, K., Endo, T., "Microwave Synthesis of Fe-Doped β-Rhombohedral Boron", *Mater. Res. Bull.*, **37**, 113–121 (2002) (Crys. Structure, Experimental, 18)

[2003Chr] Chrobak, A., Haneczok, G., Stokosa, Z., Kwapuliski, P., Rasek, J., Chekowska, G., "Magnetic Properties of $Fe_{76}X_2B_{22}$ (X = Cr, Zr, Nb) Amorphous Alloys", *Phys. Status Solidi A*, **A196**, 248–251 (2003) (Crys. Structure, Experimental, Magn. Prop., 7)

[2003Guo] Guo, C., Kelly, P.M., "Boron Solubility in Fe-Cr-B Cast Irons", *Mater. Sci. Eng. A*, **A352**, 40–45 (2003) (Crys. Structure, Morphology, Experimental, 8)

[2004Guo1] Guo, C., Kelly, P.M., "Modeling of Spatial Distribution of the Eutectic M_2B Borides in Fe-Cr-B Cast Irons", *J. Mater. Sci*., **39**(9), 1109–1111 (2004) (Morphology, Experimental, Calculation, Mechanical Properties, 2)

[2004Guo2] Guo, C., Kelly, P.M., "The Non-Equilibrium Segregation of Boron in Matrix Grains in Fe-Cr-B Alloys" (in Chinese), *J. Baotou Univ. Iron Steel Techn*., **23**(2), 134–140 (2004) (Morphology, Experimental, 11)

[2005Dyb] Dybkov, V.I., Lengauer, W., Barmak, K., "Formation of Boride Layers at the Fe-10 % Cr Alloy-Boron Interface", *J. Alloys Compd*., **398**(1–2), 113–122 (2005) (Interface Phenomena, Kinetics, Experimental, Mechan. Prop., 15)

[2005Kar] Karolus, M., Kwapulinski, P., Chrobak, D., Haneczok, G., Chrobak, A., "Crystallization in $Fe_{76}X_2B_{22}$ (X = Cr, Zr, Nb) Amorphous Alloys", *J. Mat. Proc. Tech*., **162–163**, 203–208 (2005) (Crys. Structure, Kinetics, Experimental, Magn. Prop., Phase Relations, 11)

[2005San] Santos, J.D., Olivera, J., Gorria, P., Perez, M.J., Sanchez, M.L., Hernando, B., Prida, V.M., Fernandez-Martinez, A., Cuello, G., "Structural Evolution and Magnetic Properties in $Fe_{70}Cr_{10}B_{20}$ Ribbons", *J. Magn. Magn. Mater*., **294**(2), e155-e158 (2005) (Crys. Structure, Kinetics, Experimental, Magn. Prop., Phase Relations, 4)

[2006Bon] Bondar, A., "Boron-Chromium-Nickel", in "*Landolt-Boernstein, Numerical Data and Functional Relationships in Science and Technology (New Series). Group IV: Physical Chemistry*", Martienssen, W. (Ed.), "Ternary Alloy Systems. Phase Diagrams, Crystallographic and Thermodynamic Data", Vol. 11C3, Effenberg, G., Ilyenko, S. (Eds.), Springer-Verlag, Berlin, Heidelberg, 153–167 (2006) (Crys. Structure, Phase Diagram, Review, #, 28)

[V-C2] Villars, P. and Calvert, L.D., *Pearson's Handbook of Crystallographic Data for Intermetallic Phases*, 2nd edition, ASM, Metals Park, Ohio (1991)

[Mas2] Massalski, T.B. (Ed.), *Binary Alloy Phase Diagrams*, 2nd edition, ASM International, Metals Park, Ohio (1990)

DOI: 10.1007/978-3-540-69761-9_17

Boron – Iron – Manganese

Yong Du, Honghui Xu, Chao Zhang

Introduction

The phase equilibria in the B-Fe-Mn ternary system have been investigated by several groups of authors [1952Hae, 1958Kot, 1966Kuz, 1975Pra2, 1976Pra]. The existence of the continuous solid solutions between Fe_2B and Mn_2B was reported by [1952Hae, 1958Kot] and that between FeB and MnB by [1952Hae]. This feature was confirmed by [1966Kuz], who presented an isothermal section at 800°C. [1966Kuz] prepared the samples from electrolytic Mn (99.5%), carbonyl Fe (99.99%), and B (99.5%). Carefully-mixed powders were pressed into briquettes and sintered at temperatures of 1300 to 1500°C for 3 h in an electric vacuum furnace. Some of the samples containing up to 20 at.% B were prepared by fusing in an electric resistance furnace using Al_2O_3 crucibles under a pure argon atmosphere. After annealing in quartz ampoules at 800°C for 300 to 500 h, the samples were quenched into cold water. Both the sintered and annealed samples were examined by X-ray diffraction (XRD) analysis. The experimental results suggested that the solubilities of Fe in Mn_4B, Mn_3B_4, and MnB_2 are negligible. Two partial isothermal sections at 850 and 1000°C with the B content up to 50 at.% were constructed by [1975Pra2]. Their experimental results indicated that in the temperature range of 850-1150°C two continuous solid solutions, $(Mn_{1-x}Fe_x)_2B$ and $(Mn_{1-x}Fe_x)B$, are in equilibrium. [1975Pra3] confirmed the tetragonal structure of $(Mn_{1-x}Fe_x)_2B$ and the rhombic structure of $(Mn_{1-x}Fe_x)B$ and measured their lattice parameters as a function of composition. Using XRD, thermal analysis, and microstructure observation, [1976Pra] determined the liquidus projection below 60 at.% B and established two vertical sections at 33 at.% B and 50 at.% B. The experimental results due to [1976Pra] were reviewed by [1980Bra].
Effect of the Mn addition on the peritectoid reaction temperature of the Fe-0.2B (mass%) alloy was investigated by [1966Has] employing differential thermal analysis (DTA).

Binary Systems

The binary B-Fe, B-Mn and Fe-Mn phase diagrams are accepted from [Mas2].

Solid Phases

Table 1 lists the crystal structure data for the solid phases in the ternary B-Fe-Mn system. The ternary phase $(Mn,Fe)_{23}B_6$ with a cubic structure was discovered by [1975Pra1] and determined by [1975Pra2] to show a homogeneity range of $(Mn_{0.78\sim0.40}Fe_{0.22\sim0.60})_{23}B_6$. According to [1975Pra1] this phase exists in the temperature range from 850 to 920°C. The stability range of this ternary phase needs to be further investigated.

Quasibinary Systems

The quasibinary MnB-FeB system was measured by [1976Pra] using DTA method, supplemented with XRD technique. It is shown in Fig. 1.

Invariant Equilibria

A four-phase equilibrium, $L \rightleftharpoons (\delta Mn,\delta Fe) + (\gamma Mn,\gamma Fe) + (Mn_{1-x}Fe_x)_2B$ occurs at 1085°C, and 10 at.% B, 10 at.% Fe, 80 at.% Mn [1976Pra].
Partial reaction scheme is drawn in Fig. 2 according to the liquidus surface from [1976Pra].

Liquidus Surface

An experimental liquidus projection below 60 at.% B [1976Pra] is shown in Fig. 3.

DOI: 10.1007/978-3-540-69761-9_18

Isothermal Sections

Figure 4 shows the whole isothermal section at 800°C measured by [1966Kuz], who found the existence of a continuous series of solid solutions between the isostructural compounds Mn_2B-Fe_2B and MnB-FeB. The phase relation close to the B-Mn system is amended to bring it into agreement with the currently accepted B-Mn phase diagram. It should be noted that there is disagreement with the accepted B-Mn binary diagram [Mas2] for both the isothermal sections presented by [1975Pra2] and that at 800°C by [1966Kuz]. The stoichiometric phase Mn_4B [Mas2] was incorrectly shown on the isothermal sections at 850 and 1000°C as the phase with a large homogeneity range of about 20-29 at.% B [1975Pra2]. [1966Kuz] reported the appearance of MnB_2 at 800°C. While according to [Mas2], this phase decomposes into Mn_3B_4 and MnB_4 at 1100°C. The ternary phase τ_1 reported by [1975Pra2] does not occur at 800°C.
Figures 5 and 6 show the partial isothermal sections at 850°C and 1000°C [1975Pra2], respectively. Minor modification to the Mn-rich corners was made in order to get the phase equilibria into agreement with the currently accepted B-Mn phase diagram [Mas2].

Temperature – Composition Sections

Using DTA method, [1976Pra] established the vertical sections from Mn_2B to Fe_2B. This vertical sections is reproduced in Fig. 7.

Thermodynamics

The partial and integral enthalpies of formation for the B-Fe-Mn system at 1557°C were measured by [1995Wit] using a high-temperature isoperibolic calorimeter.
The low temperature heat capacity of $(Fe_xMn_{1-x})B$ (x = 0.25, 0.5, and 0.8) from 1.5 to 15 K was measured by [1971Han] using a standard adiabatic calorimeter in liquid helium cryostat.

Notes on Materials Properties and Applications

The melts of the B-Fe-Mn system are used for the production of high-magnetic-permeability metallic amorphous materials by means of rapid quenching. Mössbauer spectra in the temperature range of 4 to 300 K for the continuous solid solution and the thermal expansion of $(Fe_{0.65}Mn_{0.35})_2B$ are measured by [1975Shi]. No thermal expansion anomaly is observed. The influence of various 3d transition elements on the magnetic and electron structure of amorphous alloy B-Fe was studied by [1986Dro] using a vibration magnetometer and Mössbauer spectroscopy. The pressure induced changes of the magnetization curves of the amorphous B-Fe-Mn alloys were investigated by [1989Wis] within the pressure range up to 2.5 GPa at temperatures close to room temperature. [1984She] measured the electrical resistivity of $(Fe_xMn_{1-x})_{80}B_{20}$ (x = 0.75-1) as a function of temperature between 4.2 to 300 K.

Miscellaneous

Using XRD technique, [1966Kuz] determined the variation of the lattice parameters of the continuous solid solution $(Fe_xMn_{1-x})_2B$. Following the same technique, [1975Shi measured the lattice parameters of this solid solution. Their experimental data are shown in Figs. 8a and 8b, showing a good agreement with each other within estimated experimental errors.

DOI: 10.1007/978-3-540-69761-9_18

Table 1. Crystallographic Data of Solid Phases

Phase/ Temperature Range [°C]	Pearson Symbol/ Space Group/ Prototype	Lattice Parameters [pm]	Comments/References
(βB) < 2092	*hR*333 $R\bar{3}m$ βB	*a* = 1093.30 *c* = 2382.52	[1993Wer]
(εFe)	*hP*2 $P6_3/mmc$ Mg	*a* = 246.8 *c* = 396.0	at 25°C, 13 GPa [Mas2]
(δFe) 1538 - 1394	*cI*2 $Im\bar{3}m$ W	*a* = 293.78 *a* = 293.15	[V-C2, Mas2] [V-C2]
(γFe,γMn) (γFe) 1394 - 912 (γMn) 1138 - 1100	*cF*4 $Fm\bar{3}m$ Cu	 *a* = 364.67 *a* = 386.0	continuous solid solution, pure Fe at 915°C [V-C2, Mas2], pure Mn [Mas2]
(αFe) < 912	*cI*2 $Im\bar{3}m$ W	*a* = 286.65	pure Fe at 25°C [Mas2]
(δMn) 1246 - 1138	*cI*2 $Im\bar{3}m$ W	*a* = 308.0	pure Mn [Mas2]
(βMn) 1100 - 727	*cP*20 $P4_132$ βMn	*a* = 631.52	pure Mn [Mas2] dissolves up to 30 at.% Fe at 700°C [Mas2]
(αMn) < 727	*cI*58 $I\bar{4}3m$ αMn	*a* = 891.26	pure Mn at 25°C [Mas2] dissolves up to 30 at.% Fe at 700°C [Mas2]
$(Mn_{1-x}Fe_x)B$ FeB < 1650 MnB < 1890	*oP*8 *Pnma* FeB 	 *a* = 550.6 *b* = 295.2 *c* = 406.1 *a* = 556.0 *b* = 297.7 *c* = 414.5	 *x* = 1 [V-C2, Mas2] *x* = 0 [V-C2, Mas2]
$(Mn_{1-x}Fe_x)_2B$ Fe_2B < 1389 Mn_2B < 1580	*tI*12 *I*4/*mcm* Al_2Cu 	 *a* = 511.0 *c* = 424.9 *a* = 514.9 *c* = 420.9	 *x* = 1 [V-C2, Mas2] *x* = 0 [V-C2, Mas2]

(*continued*)

DOI: 10.1007/978-3-540-69761-9_18

Phase/ Temperature Range [°C]	Pearson Symbol/ Space Group/ Prototype	Lattice Parameters [pm]	Comments/References
MnB_4 < 1375	*mC*10 *C*2/*m* MnB_4	*a* = 550.3 *b* = 536.7 *c* = 294.9	[V-C2, Mas2]
MnB_2 1827 - 1100	*hP*3 *P*6/*mmm* AlB_2	*a* = 300.9 *c* = 303.9	[V-C2, Mas2]
Mn_3B_4 < 1827	*oI*14 *Immm* Ta_3B_4	*a* = 303.6 *b* = 1284.2 *c* = 296.4	[V-C2, Mas2]
Mn_4B < 1120	*oF*48 *Fddd*	*a* = 1453.95 *b* = 729.14 *c* = 420.82	[V-C2, Mas2]
*$(Mn,Fe)_{23}B_6$ 920 - > 800	Cubic	*a* = 1069.7 *a* = 1064.0	for $(Mn_{0.78}Fe_{0.22})_{23}B_6$ [1975Pra2] for $(Mn_{0.40}Fe_{0.60})_{23}B_6$ [1975Pra2]

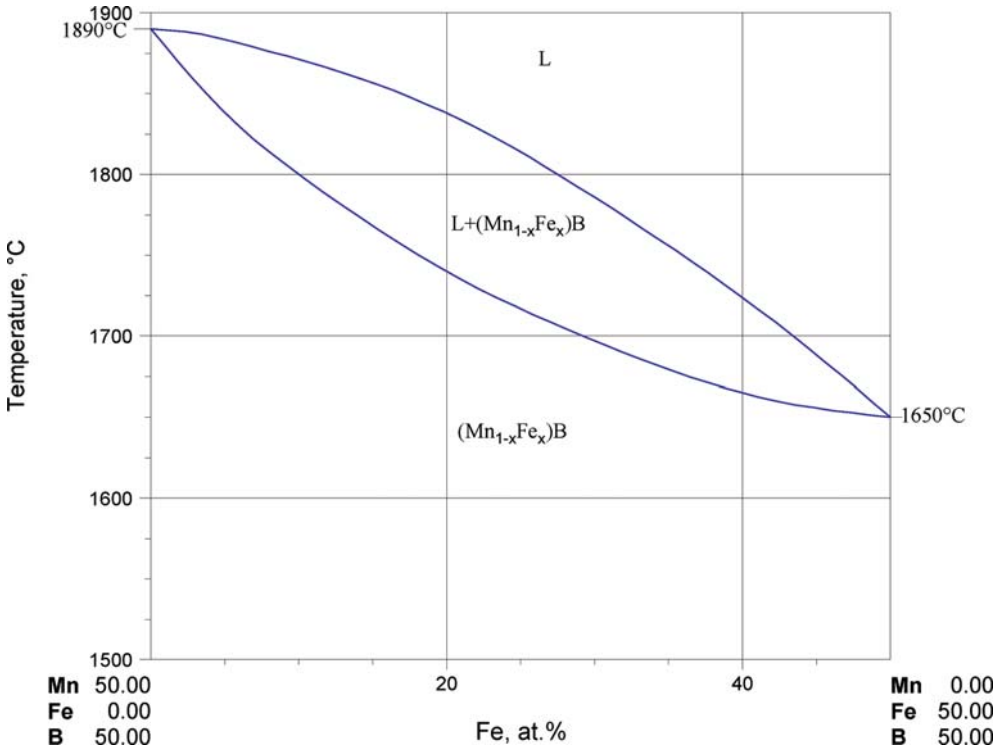

Fig. 1. B-Fe-Mn. Quasibinary section MnB - FeB

DOI: 10.1007/978-3-540-69761-9_18

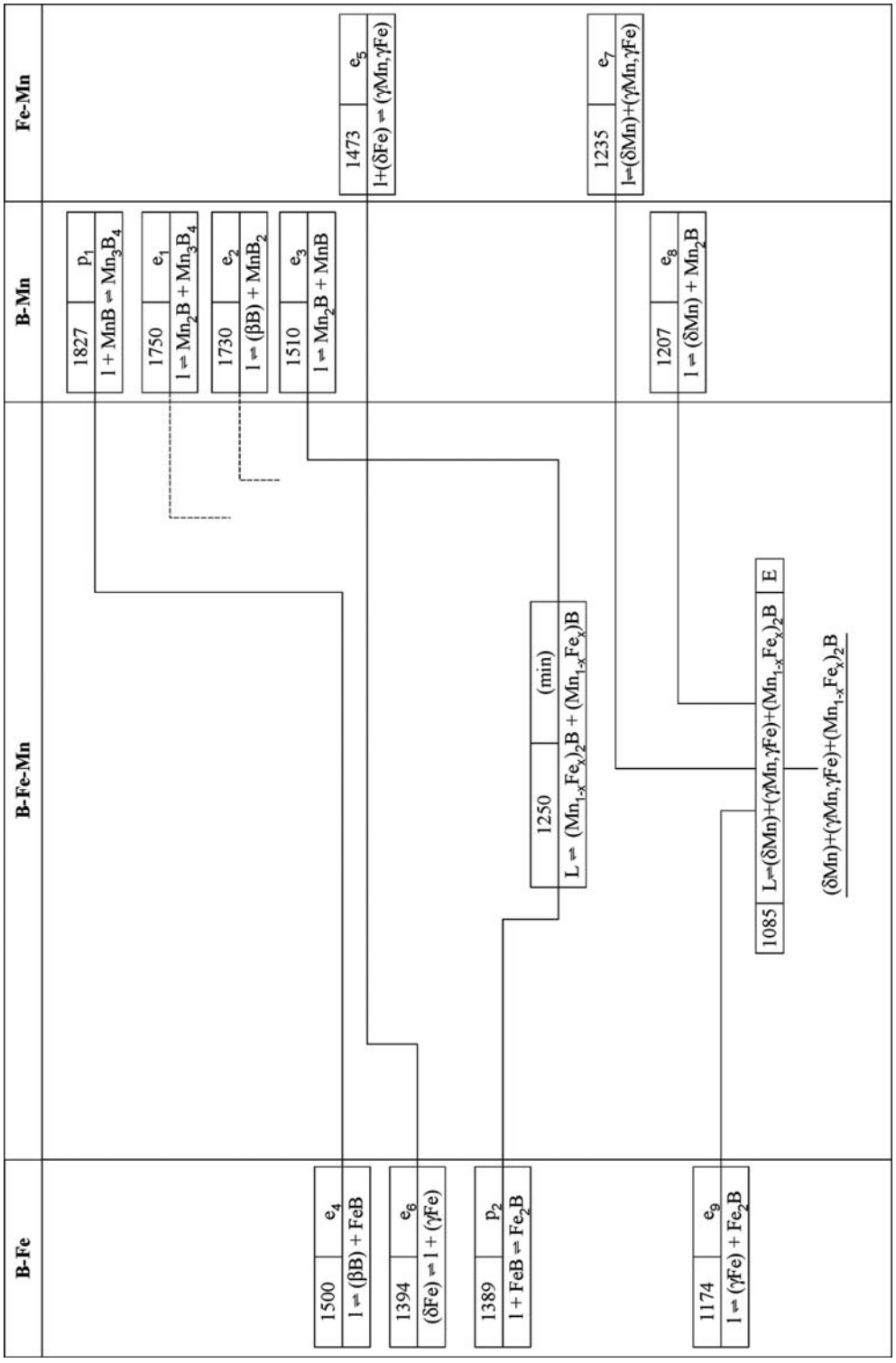

Fig. 2. B-Fe-Mn. Partial reaction scheme

DOI: 10.1007/978-3-540-69761-9_18

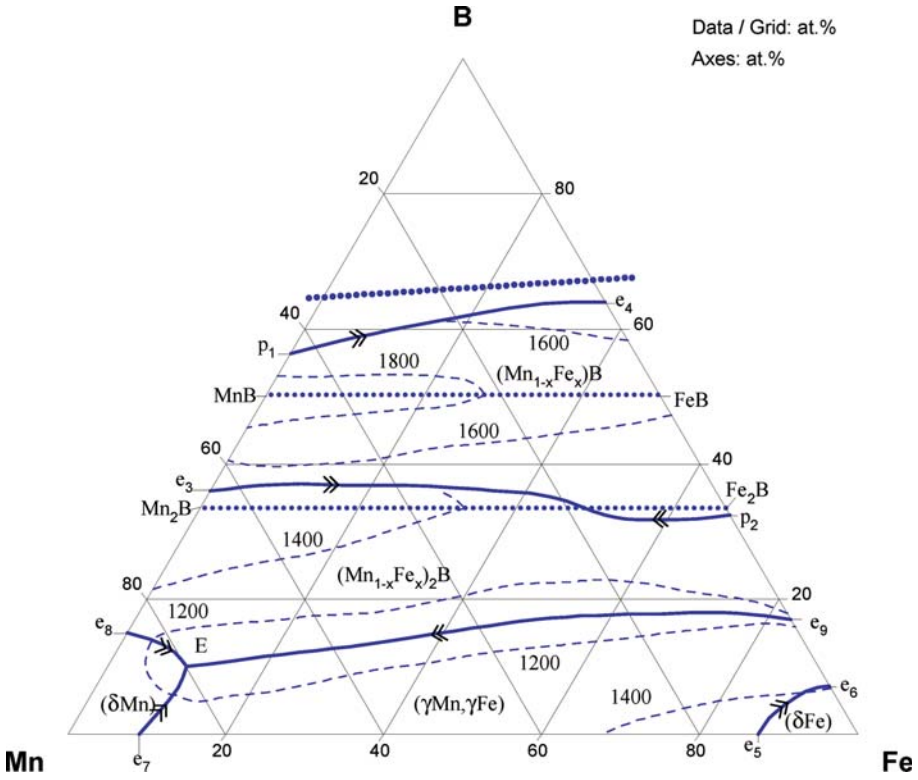

Fig. 3. B-Fe-Mn. Partial liquidus surface projection

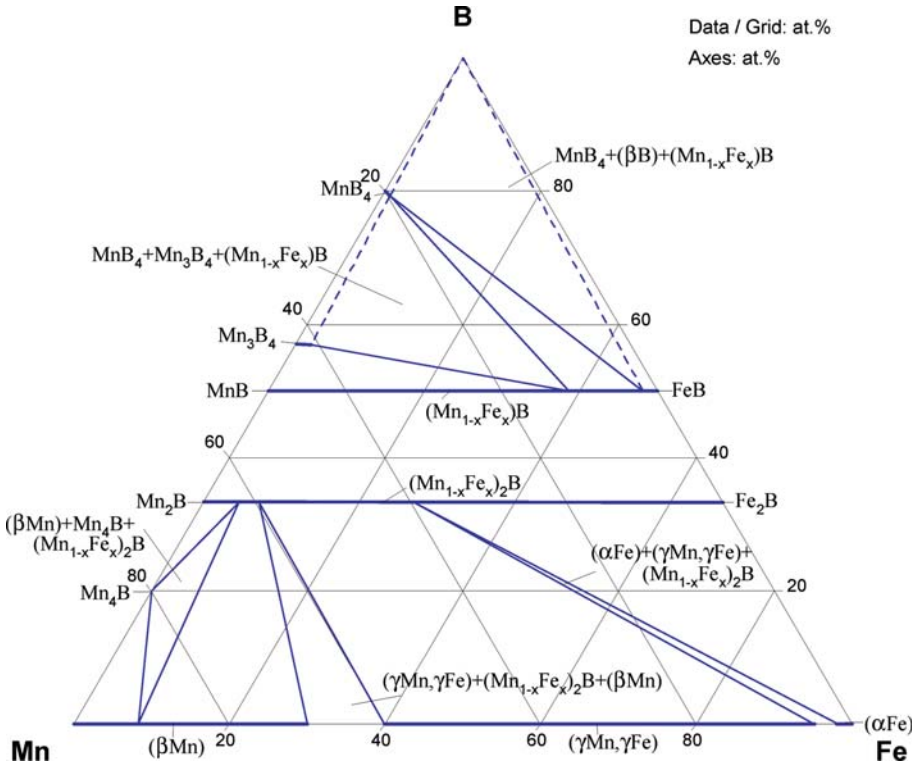

Fig. 4. B-Fe-Mn. Isothermal section at 800°C

DOI: 10.1007/978-3-540-69761-9_18

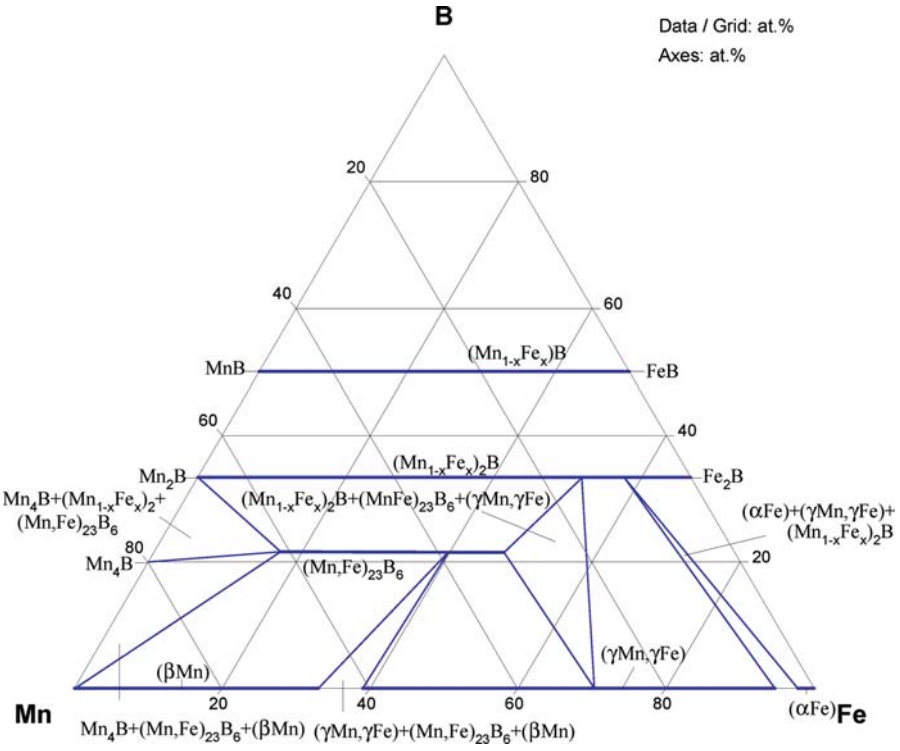

Fig. 5. B-Fe-Mn. Partial isothermal section at 850°C

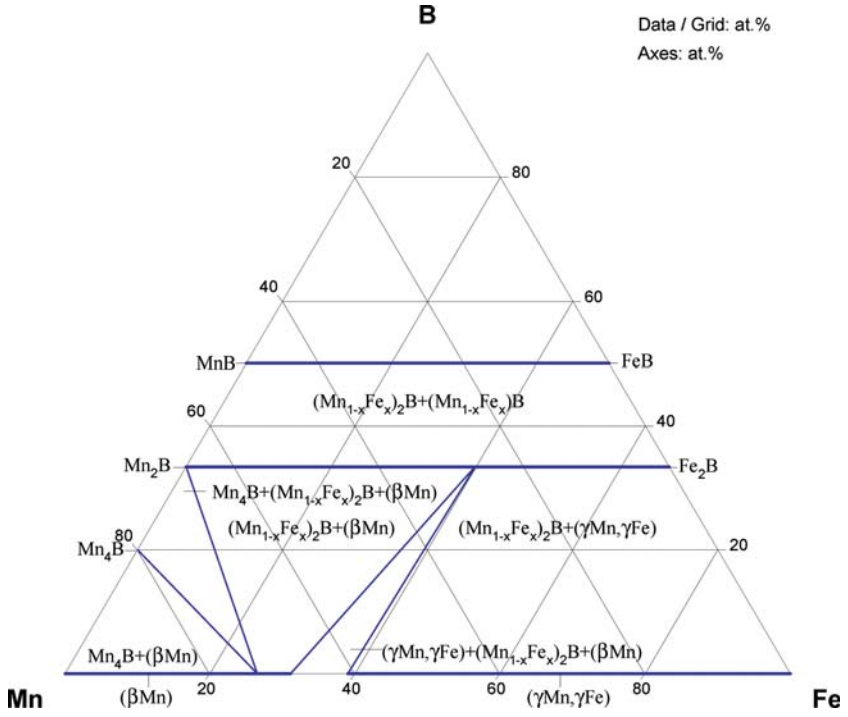

Fig. 6. B-Fe-Mn. Isothermal section at 1000°C

DOI: 10.1007/978-3-540-69761-9_18

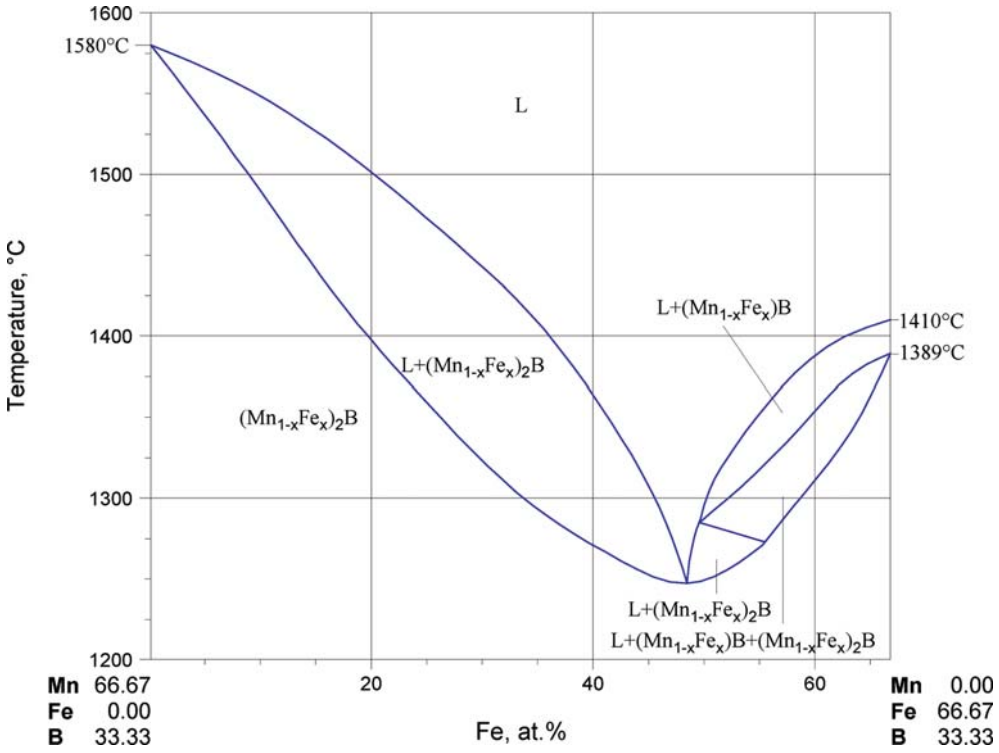

Fig. 7. B-Fe-Mn. Vertical section Mn_2B - Fe_2B

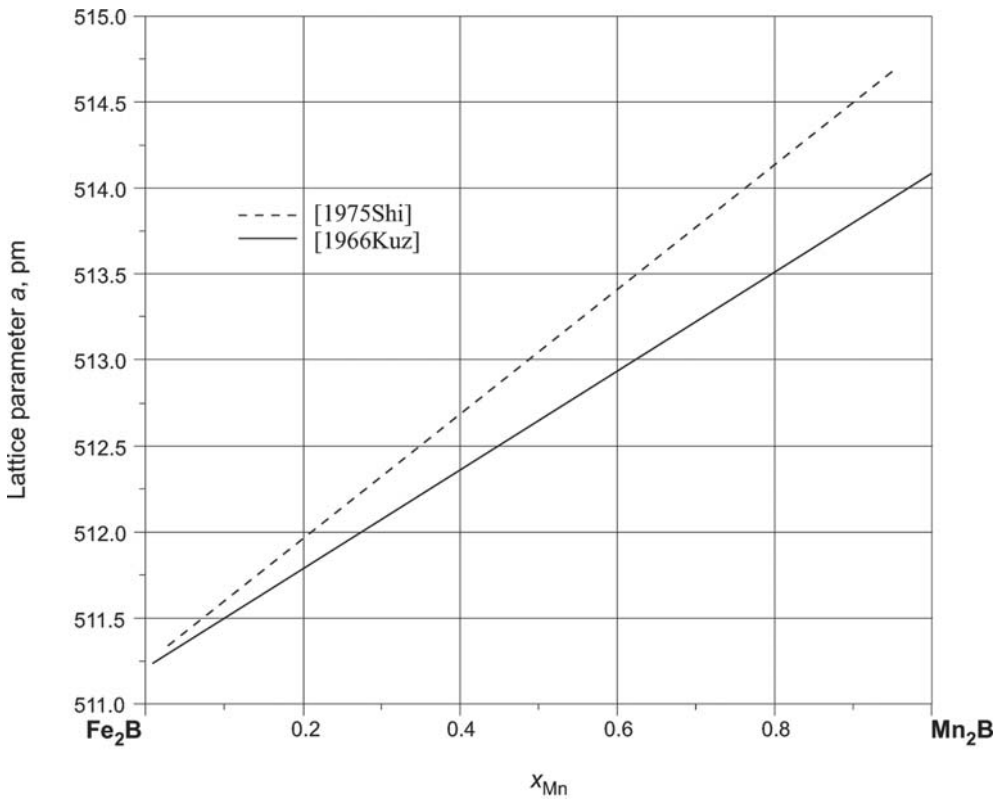

Fig. 8a. B-Fe-Mn. Effect of B on lattice parameters of $(Fe_xMn_{1-x})_2B$. *a*-lattice parameter

DOI: 10.1007/978-3-540-69761-9_18

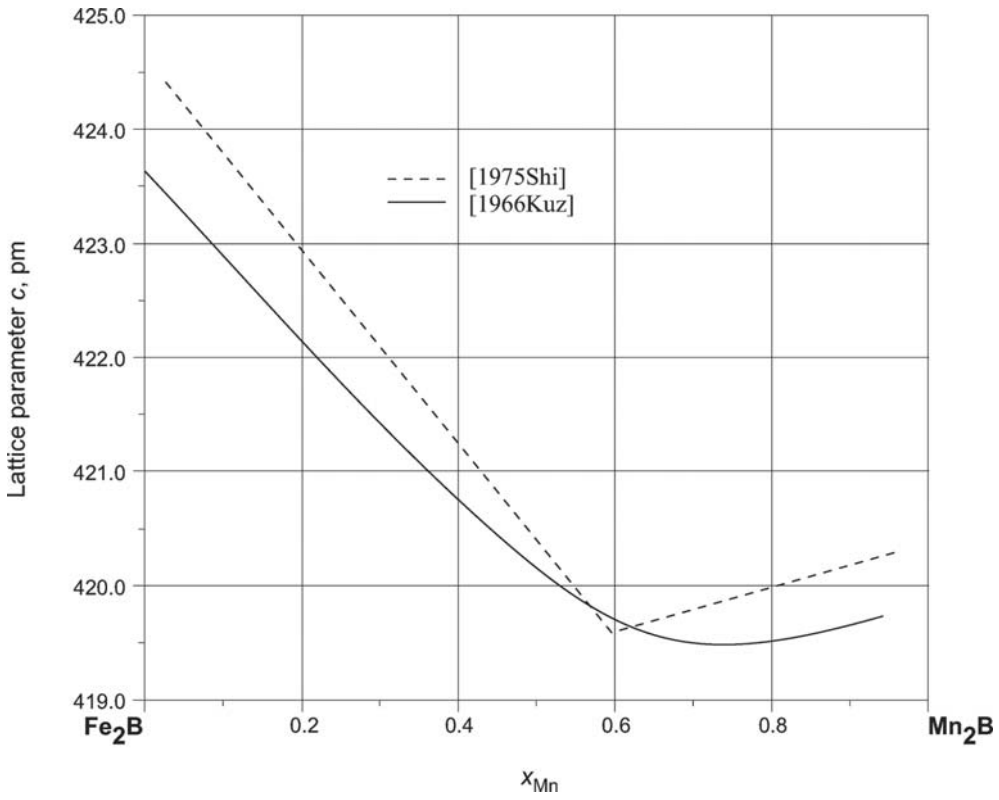

Fig. 8b. B-Fe-Mn. Effect of B on lattice parameters of $(Fe_xMn_{1-x})_2B$. *c*-lattice parameter

DOI: 10.1007/978-3-540-69761-9_18

References

[1952Hae] Haegg, G., Kiessling, R., "Distribution Equilibria in Some Ternary Systems Me_1-Me_2-B and the Relative Strength of the Transition-Metal-Boron Bond", *J. Inst. Met.*, **81**, 57–60 (1952) (Experimental, Phase Relations, 6)

[1958Kot] Kotel'nikov, R.B., *Sbornik Nauch. Trudov Nauch. Tech. Obshchestva Tsvetnoi Met.*, Moscow, Inst. Tsvetn. Metal. i Zolota, **29**, 315–322 (1958) as quoted by [1976Pra2]

[1966Has] Hasegawa, M., Okamoto, M., "A Study on the Ternary Alloys of iron and Boron" (in Japanese), *Nippon Kinzoku Gakkai-Shi*, **30**(6), 533–540 (1966) (Experimental, Mechan. Prop., (Phase Diagram, 12)

[1966Kuz] Kuzma, Yu.B., Chepiga, M.V., Plakhina, A.M., "Phase Equilibria in the Cr-Co-B, Mn-Fe-B, and Mn-Co-B Systems", *Russ. Metall.*, **2**(7), 1038–1043 (1966), translated from *Izv. Akad. Nauk. SSSR, Neorg. Mater.*, **2**, 1218–1224 (1966) (Phase Relations, Phase Diagram, Experimental, #, *, 14)

[1971Han] Hanson, B.D., Mahnig, M., Toth, L.E., "Low Temperature Heat Capacities of Transition Metal Borides", *Z. Naturforsch. A*, **26**(4), 739–746 (1971) (Crys. Structure, Experimental, Thermodyn., 29)

[1975Pra1] Pradelli, G., Gianoglio, C., "The τ Phase in the Fe-Mn-B System" (in Italian), *Met. Ital.*, **67**(1), 21–23 (1975) (Crys. Structure, Experimental, 7)

[1975Pra2] Pradelli, G., Gianoglio, C., "Solid State Equilibrium of Fe-Mn-B System" (in Italian), *Atti. Accad. Sci. Tor., C. Sci. Fis. Mat. Nat.*, **58**(1), 29–36 (1975) (Phase Relations, Experimental, 11)

[1975Pra3] Pradelli, G., Gianoglio, C., "Solid Solutions of the Type $(Fe,Mn)_2B$ and (Fe,Mn)B" (in Italian), *Atti Accad. Sci. Tor., C. Sci. Fis. Mat. Nat.*, **109**(3–4), 279–286 (1975) (Phase Relations, Experimental, 5)

[1975Shi] Shigematsu, T., "Mössbauer and Structural Studies on $(Fe_{1-x}Mn_x)_2B$", *J. Phys. Soc. Jpn.*, **39**, 1233–1238 (1975) (Crys. Structure, Experimental, 19)

[1976Pra] Pradelli, G., Gianoglio, C., "The Fe-Mn-B System" (in Italian), *Met. Ital.*, **68**(1), 19–23 (1976) (Phase Relations, Experimental, 6)

[1980Bra] Brandes, E.A., Flint, R.F., "Manganese Phase Diagrams", in "*Manganese Phase Diagrams*", Manganese Centre, Paris, France, **162**, 89 (1980) (Phase Diagram, Phase Relations, Review, 1)

[1984She] Shen, B.G., Zhan, W.S., Zhang Z.Y., Wu, Z.L., "Temperature (4.2–300K) Dependence of Electrical Resistivity of FeMB (M = Mn, Mo) Amorphous Alloys" (in Chinese), *Acta Metall. Sin.*, **20**(3), B164–170 (1984) (Experimental, Elect. Prop., 18)

[1986Dro] Drozdova, M.A., Batyrev, I.G., Prokoshin, A.F., Makhotkin, V.E., Korytov, V.V., "Magnetic and Electron Structure of Amorphous Fe-M-B Alloys (M = V, Cr, Mn)", *Sov. Phys. - Solid State*, **28**(8), 1390–1392 (1986) (Experimental, Magn. Prop., Electronic Structure, 7)

[1989Wis] Wisniewski, R., Rostocki, A.J., Magiera, A., Zych, W., "Pressure Changes of B(H) Curves of Fe-Mn-B Amorphous Alloys", *J. Magn. Magn. Mater.*, **81**(1–2), 121–124 (1989) (Experimental, Magn. Prop., 7)

[1993Wer] Werheit, H., Kuhlmann, U., Laux, M., Lundstroem, T., "Structural and Electronic Properties of Carbon-Doped β-Rhombohedral Boron", *Phys. Stat. Sol.*, **B179**, 489–511 (1993) (Crys. Structure, Experimental, 51)

[1995Wit] Witusiewicz, V.T., "Thermodynamics of Binary and Ternary Melts of the 3d Transition Metals (Cr, Mn, Fe, Co and Ni) with Boron", *Thermochim. Acta*, **264**, 41–58 (1995) (Experimental, Calculation, Thermodyn., 25)

[V-C2] Villars, P. and Calvert, L.D., *Pearson's Handbook of Crystallographic Data for Intermetallic Phases*, 2nd edition, ASM, Metals Park, Ohio (1991)

[Mas2] Massalski, T.B. (Ed.), *Binary Alloy Phase Diagrams*, 2nd edition, ASM International, Metals Park, Ohio (1990)

DOI: 10.1007/978-3-540-69761-9_18

Boron – Iron – Molybdenum

Kostyantyn Korniyenko, Anatoliy Bondar

Introduction

Boron-iron-molybdenum alloys gained scientific and practical interest due to a positive effect that boron additions have on the microstructure and physical properties of alloyed sintered steels, applied in automotive industry and in wear resistant structural components. On the other hand, by studying the influence of molybdenum additions to the iron borides new applications of B-Fe-Mo alloys were found, in particular for cutting tools. For systematic optimization of alloy compositions of such materials and components it is of great importance to know the phase relations in the corresponding B-Fe-Mo system. However, up to now, this information is relatively poor. It is presented in literature by a series of isothermal sections [1966Has1, 1966Gla, 2000Lei, 2004Sar, 2005Sar] and phase configurations and crystal structures of intermediate phases reported by a number of papers: [1953Ste, 1964Col1, 1964Col2, 1964Rie, 1965Kuz, 1965Rie, 1966Gla, 1966Has1, 1966Has2, 1969Bis, 1973Dey, 1973Rog, 1980Vin, 1983Ber, 1984Dun, 1986Muk, 1986Tak, 1987Ger, 1987Tak, 1988Efi, 1988Ide, 1989Ide, 1989Kol, 1995Dud, 1997Dud, 1997Wan, 2000Lei, 2000Mol, 2001Kar1, 2001Kar2, 2004Sar, 2005Sar]. Thermodynamic properties were obtained experimentally by [1983Ber, 1997Wan]. The experimental methods used and the temperature and composition ranges studied are shown in Table 1. The B-Fe-Mo system was reviewed in [1992Rag, 2003Rag], and reviews of crystal structures of the phases were presented in [1979Run, 2003Luk]. Further research on the nature of the phase equilibria in this system is needed, in particular with respect to the liquidus, solidus and solvus surfaces but also with respect to the alloy's thermodynamics and targeted studies to be able to complete the reaction scheme for the whole range of compositions.

Binary Systems

As edge binary phase diagrams those reported by [Mas2] are accepted, where the Fe-Mo phase diagram is the result of thermodynamic assessment by [1982Gui] using the CALPHAD method. It should be mentioned that the existence of Mo_3B_2 is rejected in the present evaluation following reviews of [1996Pov] and [1998Rog].

Solid Phases

Crystallographic data of the unary, binary and ternary phases are listed in Table 2. The solubilities of the third component in each of the binary B-Fe, B-Mo and Fe-Mo phases were found to be small. Two ternary phases with the crystal structures different from any of the unary and binary phases were found, namely τ_2-Mo_2FeB_2 and τ_4-$Mo_{1+x}Fe_{2-x}B_4$. The τ_1-$Mo_2Fe_{13}B_5$ phase forms from the melt at ~1100°C and decomposes below 1000°C [1966Has1].

It was reported by [2000Lei] that additions of molybdenum stabilize the metastable Fe_3B phase (with the same Ti_3P type structure) at the composition $MoFe_{14}B_5$, stable only in an extremely narrow temperature range of 1110-1080°C. The τ_3-$Mo_{1-x}Fe_xB$ possesses the same crystal structure as the βMoB and can be considered as a βMoB phase stabilized by iron.

Invariant Equilibria

Analyzing experimental data of [1966Gla] at 1000°C and of [1966Has1] at 1050°C Raghavan suggested in his review [1992Rag] that a transition reaction (Mo) + τ_2 ⇌ (Mo_2B) + μ occurs at the temperature between 1000 and 1050°C, because the two-phase equilibrium (Mo_2B) + μ found at 1000°C by [1966Gla] changed to (Mo) + τ_2 at 1050°C, according to the data of [1966Has1]. It was found by [1966Has2] that

DOI: 10.1007/978-3-540-69761-9_19

addition of 0.43 at.% (0.73 mass%) Mo to B-Fe alloys increases the temperature of peritectoid reaction $\alpha + Fe_2B \rightleftharpoons \gamma$ from ~ 913°C to 947°C.

Isothermal Sections

Isothermal sections at 1050°C were constructed by [1966Has1] and [2000Lei] based on experimental investigations in the whole range of compositions. The isothermal section at 1050°C is presented in Fig. 1 according to the experimental data of [2000Lei] with amendments to maintain consistency with the accepted binary phase diagrams. The homogeneity range of the Mo_2B_5 phase in the B-Mo system is enlarged according to the accepted binary diagram. Extensions of the Fe_2B and FeB phases into the ternary system are slightly increased based on the EMPA data of [2000Lei]. The results of the investigation by [2000Lei] indicated that three ternary phases are stable at 1050°C, namely, τ_2, τ_3 and τ_4 phases. The isothermal section constructed by [1966Has1] at 1050°C is similar to the one obtained by [2000Lei] excepting composition and the homogeneity ranges of ternary phases and stability of τ_1 phase ($Fe_{13}Mo_2B_5$) found by [1966Has1]. Isothermal section at 1000°C was constructed by [1966Gla]. It is similar to the isothermal section at 1050°C constructed by [2000Lei]. Several differences should be mentioned. The homogeneity ranges of the ternary phase are essentially different in [1966Gla] and [2000Lei]. Equilibria involving the MoB_4 phase were not shown by [1966Gla]. According to the data of [1966Gla], the two-phase equilibrium (Mo_2B) + μ exists at 1000°C, while [1966Has1] and [2000Lei] indicated another two-phase equilibrium, (Mo) + τ_2, at 1050°C.

Thermodynamics

Isothermal sections of the B-Fe-Mo system in the range of boron content up to 34 at.% at the temperatures of 1200°C and 1280°C were calculated by [2004Sar, 2005Sar] with the Thermo-Calc program using published thermodynamic databases of the binary boundary systems: B-Fe [1994Hal], B-Mo [2001Mor] and Fe-Mo [1982Gui]. Four phases were considered in calculations, namely: liquid, iron based solid solutions γ and α, hypothetical continuous series of solid solutions between Mo_2B and Fe_2B, as well as the μ, Mo_6Fe_7 phase. However, it should be mentioned that the existence of a continuous series of solid solutions between Mo_2B and Fe_2B was not confirmed by any experimental investigation.

Notes on Materials Properties and Applications

Applications of the B-Fe-Mo alloys are related, in the first place, with positive effect of boron additions on microstructures and physical properties of alloyed sintered steels, in particular, based on the Astalloy Mo powder (Fe-1.5 mass% Mo *i.e.* Fe-0.88 at.% Mo). These steels have many applications in the automotive industry and as structural wear resistant materials. However, their applications are limited by the particular porosity values. To reduce the porosity and to increase the consolidation of sintered alloy steels, miscellaneous techniques within powder metallurgy technologies are utilized, as well as an activated sintering process, including some boron additions. Experimental studies revealed that boron activates the sintering process and increases in the degree of densification and in result improves the mechanical properties [2001Kar2]. On the other hand, additions of molybdenum to the iron borides allow to design properties that make them suitable cutting tool materials. The development of metallic glasses is another area of application for the B-Fe-Mo system.

Literature data concerning investigations of the boron-iron-molybdenum materials properties are listed in Table 3. Factors affecting the strength properties of the Fe rich vacuum-induction melted B-Fe-Mo alloys were studied by [1964Col2] (abstract of this article was also presented in [1964Col1]). The approximate molybdenum contents were 2, 4, 9 and 19 mass% and approximate boron contents were 0.0005, 0.0014, 0.005 and 0.063 mass%. The phases extracted from the annealed specimens and identified by X-ray diffraction analysis included the *R*, Mo_2Fe_3 phase, the τ_2-Mo_2FeB_2 phase as well as an oxide having a diffraction pattern practically identical to that of $MnFe_2O_4$. Three types of alloy strengthening were observed. Alloys with 2 mass% of Mo seem to be hardenable by a bainitic type transformation of austenite to ferrite;

DOI: 10.1007/978-3-540-69761-9_19

alloys with 4 mass% of Mo were hardened by the solid solution mechanism; those containing 9 or 19 mass% Mo were strengthened by precipitation of the *R*, Mo_2Fe_3 phase. No dispersion reinforcement by borides was recognized in any of the alloys. [1986Muk] have reported that cyclic tempering of the $Mo_{10.5}Fe_{70.5}B_{19}$ alloy at the temperatures of 550 to 650°C leads to decrease of the alloy hardness. The Mixtures containing up to 1.1 mass% B and up to 5 mass% Mo, compacted and sintered at 1200°C, demonstrated negative effects on the densification and ductility by forming the τ_2-Mo_2FeB_2 phase, although strength and hardness were improved [1987Ger]. The change of mechanical properties of rapidly quenched alloys in the range of B or Mo content 10 to 20 at.% during cooling and heat-treatment cycles (550 to 650°C) was demonstrated by [1988Efi]. The ternary B-Fe-Mo alloys annealed in the temperature range of 1077-1327°C and containing 6 mass% Mo have a composite microstructure consisting mainly of a complex boride τ_2-Mo_2FeB_2 as a hard phase and a ferritic binder [1988Ide, 1989Ide]. The mechanism of liquid phase sintering of the $Mo_{26.6}Fe_{43.9}B_{29.5}$ alloy was presented by [1988Ide, 1989Ide]. The microstructure formation of sintered materials based on the prealloyed Fe-1.5 mass% Mo powder with 0.2 to 0.6 mass% of boron addition was investigated by [1995Dud, 1997Dud, 2000Mol, 2001Kar1, 2001Kar2]. A eutectic liquid phase Fe + Fe_2B activating the sintering of Fe-1.5 mass% Mo + B powder system was formed [1995Dud, 1997Dud]. The sintering behavior of Fe and Fe-Mo prealloyed powder compacts containing from 0.5 to 3.5 mass% Mo and fixed boron additions has been studied by [2004Sar, 2005Sar] with special emphasis on the microstructural development, the formation of the liquid phase and the liquid phase sintering mechanisms involved during the densification process. The interaction processes between boron and molybdenum are related to extinction/or decrease of the liquid eutectic phase portion and to the strengthening of the alloyed Fe-Mo matrix by formed boride particles. The Fe-1.5Mo-0.4B (mass%, corresponds to the Fe-0.9Mo-2B in at.%) alloy sintered at 1200°C reached the tensile strength of 487 to 550 MPa, elongation of 2.5 to 4.8%, hardness H_V above 2 GPa, and the density of 7150 $kg \cdot m^{-3}$. The sintering behavior of Fe and Fe-Mo prealloyed powder compacts containing from 0.5 to 3.5 mass% Mo and fixed boron addition has been studied by [2004Sar, 2005Sar] with special emphasis on the microstructural development, the formation of the liquid phase and the liquid phase sintering mechanisms involved during the densification process. Magnetic properties of the B-Fe-Mo amorphous alloys were reported by [1980Vin, 1984Dun, 1992Kis, 1999Wan]. The electrical resistivity of $(Mo_xFe_{1-x})_{80}B_{20}$ (x = 0.05 to 0.18) amorphous alloys as a function of temperature between 4.2 and 300 K has been studied by [1984She].

Miscellaneous

Thermal stability of the $(Mo_5Fe_{95})_{83}B_{17}$ metallic glass was studied by [1983Ber]. A two-step process of crystallization of this metallic glass was carried out. Good agreement was likewise observed for three various applied types of calorimetric techniques (peak shift, temperature change as well as isothermal) with a view to determine the activation energy after first cycle of crystallization. The thermal behavior of the amorphous alloys with the boron content from 6.4 to 30.0 at.% prepared by electrolytic plating were investigated by [1997Wan] using differential scanning calorimetry. A two-step process of crystallization was observed for the amorphous $Mo_{13.3}Fe_{63.4}B_{23.3}$, $Mo_{11.3}Fe_{58.7}B_{30.0}$, $Mo_{16.3}Fe_{73.6}B_{10.1}$ and $Mo_{18.9}Fe_{74.7}B_{6.4}$ alloys. The crystallization temperature ranges from 745 to 771 K (472 to 498°C) for B contents between 6.4 and 30.0 at.% at a heating rate of 10 $K \cdot min^{-1}$. A minimum value of the enthalpy change upon crystallization, H_x, was observed at 6.4 at.% B (27.5 $kJ \cdot mol^{-1}$) while the maximum value was found at 23.3 at.% B (39.0 $kJ \cdot mol^{-1}$).
Positron studies of the crystallization kinetics of the metallic glass $Mo_2Fe_{78}B_{20}$ were performed by [1980Car] using a zero-angle 2γ-spectrometer. The isotope ^{64}Cu was used as a position source. Since the activation energies at the start and the end of crystallization were practically equal, the authors have concluded that the transition from the glassy to the crystalline state is a thermally activated first order process. [2001Kar1, 2001Kar2] studied the mechanism of sintering of the Astaloy Mo powder with elemental boron powder (0.2, 0.4 or 0.8 mass%) using the addition of 0.8 mass% lubricant in the form of zinc stearate. It was concluded that the sintering temperature plays a very important role in these processes. So, at 1120°C the sintering mechanism of the Astalloy Mo sample with boron is solid state sintering, while at 1200°C, as a result of the eutectic reaction between ferrite and complex borides, a permanent liquid phase occurs. In the last case the sintering mechanism is liquid phase sintering.

DOI: 10.1007/978-3-540-69761-9_19

Table 1. Investigations of the B-Fe-Mo Phase Relations, Structures and Thermodynamics

Reference	Method/Experimental Technique	Temperature/Composition/Phase Range Studied
[1953Ste]	X-ray diffraction	Mo_2FeB_4
[1964Col2]	X-ray diffraction, metallography (optical and electron microscopies)	2-19 mass% Mo
[1964Rie]	X-ray diffraction	Mo_2FeB_2
[1965Kuz]	X-ray diffraction	800°C; $Mo_2Fe_{21}B_6$
[1965Rie]	X-ray diffraction	Mo_2FeB_2
[1966Gla]	X-ray diffraction, optical microscopy	1000°C; whole range of compositions
[1966Has1]	X-ray diffraction	950 - 1100°C; whole range of compositions
[1966Has2]	Chemical analysis, optical and electron microscopy, X-ray diffraction	≤ 1100°C; 0.02 at.% B, 0.2 at.% B
[1969Bis]	Thermal analysis	≤ 1040°C; ~$Mo_{1.91}Fe_{98.024}B_{0.066}$ (mass%)
[1973Dey]	Mössbauer spectroscopy	Mo_2FeB_2
[1973Rog]	X-ray diffraction	$Mo_{0.4}Fe_{2.6}B$
[1980Vin]	X-ray diffraction (Debye-Scherrer technique)	$Mo_5Fe_{95-x}B_x$ ($15 \le x \le 25$)
[1983Ber]	Differential scanning calorimetry (DSC). Types of it are as following: peak shift, temperature change, isothermal	$(Mo_5Fe_{95})_{83}B_{17}$
[1984Dun]	^{57}Fe Mössbauer spectroscopy	4.2 K; 20 at.% B, 0 to 14 at.% Mo
[1986Muk]	X-ray diffraction, optical microscopy	≤ 1600°C, $Mo_{10.5}Fe_{70.5}B_{19}$
[1986Tak]	X-ray diffraction, chemical analysis (Leco automatic analyzer)	1127 - 1327°C; $Mo_{22.4}Fe_{52.8}B_{24.8}$, $Mo_{25.3}Fe_{49.5}B_{25.2}$, $Mo_{25.7}Fe_{50.9}B_{23.4}$
[1987Ger]	Optical microscopy, scanning electron microscopy (SEM), X-ray diffraction	1200°C; the Fe rich corner
[1987Tak]	X-ray diffraction, SEM, Auge spectroscopy	1200 - 1300°C; 5 mass% B, Mo/B atomic ratios 0.7 to 1.1
[1988Efi]	Metallography, X-ray diffraction	550 - 650°C, 1500-1600°C; 10 to 20 at.% B, 10 to 20 at.% Mo
[1988Ide]	Metallography	1077 - 1327°C; 6 mass% Mo
[1989Ide]	DTA, X-ray diffraction, SEM	$Mo_{26.6}Fe_{43.9}B_{29.5}$
[1989Kol]	X-ray diffraction, TEM	$(Mo_xFe_{100-x})_{83}B_{17}$ (x = 3, 15, 25)

(*continued*)

DOI: 10.1007/978-3-540-69761-9_19

Reference	Method/Experimental Technique	Temperature/Composition/Phase Range Studied
[1995Dud]	Optical microscopy, SEM, TEM	1100 - 1220°C; Fe-1.5 mass% Mo + (0.2 - 0.6) mass% B
[1997Dud]	Optical microscopy, SEM, TEM	1100 - 1220°C; Fe-1.5 mass% Mo + (0.2 - 0.6) mass% B
[1997Wan]	X-ray diffractometer, SEM, DSC	(6.4 - 30.0) at.% B
[2000Lei]	X-ray powder diffraction, electron microprobe analysis	1050°C; whole range of compositions
[2000Mol]	Optical microscopy, SEM, energy dispersive X-ray spectroscopy (EDXS)	1200°C; Fe-1.5 mass% Mo + (0.2 - 0.6) mass% B
[2001Kar1]	X-ray diffraction, optical microscopy	1200°C; Fe-1.5 mass% Mo + (0.2 - 0.6) mass% B
[2001Kar2]	X-ray diffraction, optical microscopy	1200°C; Fe-1.5 mass% Mo + (0.2 - 0.6) mass% B
[2004Sar]	Optical microscopy, SEM	800-1280°C; $Mo_{2.0}Fe_{96.4}B_{1.6}$, $Mo_{0.9}Fe_{97.6}B_{1.5}$ $Mo_{0.3}Fe_{98.2}B_{1.5}$
[2005Sar]	Optical microscopy, SEM	1000-1280°C; $Mo_{2.0}Fe_{96.4}B_{1.6}$, $Mo_{0.9}Fe_{97.6}B_{1.5}$ $Mo_{0.3}Fe_{98.2}B_{1.5}$

Table 2. Crystallographic Data of Solid Phases

Phase/Temperature Range [°C]	Pearson Symbol/ Space Group/ Prototype	Lattice Parameters [pm]	Comments/References
(βB) < 2092	*hR*333 $R\bar{3}m$ βB	a = 1093.30 c = 2382.52	1993Wer] dissolves ~ 2.5 at.% Fe at 1500°C [Mas2] dissolves < 1 at.% Mo at 1920 ± 25°C [Mas2]
(δFe) (h_2) 1538 - 1394, 1.013 bar	*cI*2 $Im\bar{3}m$ W	a = 293.15	[Mas2] in the Fe-Mo binary system joins with the (αFe), dissolves 24.4 at.% Mo at 1449°C [Mas2]
γ, (γFe) (h_1) 1394 - 912	*cF*4 $Fm\bar{3}m$ Cu	a = 364.67	at 915°C [V-C2, Mas2] dissolves 1.7 at.% Mo at ~ 1140°C [Mas2]
α, (αFe) (r) < 912	*cI*2 $Im\bar{3}m$	a = 286.65	at 25°C [Mas2]

(*continued*)

DOI: 10.1007/978-3-540-69761-9_19

Phase/Temperature Range [°C]	Pearson Symbol/ Space Group/ Prototype	Lattice Parameters [pm]	Comments/References
	W		in the Fe-Mo binary system joins with the (δFe) [Mas2]
		a = 286.69	in the $Mo_{10}Fe_{65}B_{25}$ alloy sintered at 1050°C [2000Lei]
(εFe)	*hP*2 $P6_3/mmc$ Mg	a = 246.8 c = 396.0	at 25°C, $1.3 \cdot 10^5$ bar [Mas2] high-pressure modification
(Mo) < 2623	cI2 $Im\bar{3}m$ W	a = 314.70	at 25°C [Mas2] dissolves < 1 at.% B at 2175 ± 6°C and 31.3 at.% Fe at 1611°C [Mas2]
		a = 314.51	in the $Mo_{55}Fe_{25}B_{20}$ and $Mo_{60}Fe_{10}B_{30}$ alloys sintered at 1050°C [2000Lei]
Fe_2B < 1399	*tI*12 *I*4/*mcm* $CuAl_2$	a = 511.0 c = 424.9	33.3 at.% B [V-C2]
		a = 511.35 c = 425.56	in the $Mo_{30}Fe_{30}B_{40}$ arc-melted alloy annealed at 1050°C [2000Lei]
FeB < 1603	*oP*8 *Pnma* FeB	 a = 550.6 b = 295.2 c = 406.1	50 at.% B [V-C2]
		a = 559.09 b = 295.80 c = 408.13	in the $Mo_{18}Fe_{27}B_{55}$ arc-melted alloy annealed at 1050°C [2000Lei]
Fe_3B			metastable produced by quenching of liquid $Fe_{76}B_{24}$, exists in the approximate temperature interval 1150 to 1250°C [1981Kha, 1982Kha]
	*tI** Fe_3P	a = 865.5 c = 429.7	disordered high-temperature modification [1982Kha]
	*t*** $Fe_3B_{0.63}P_{0.37}$	a = 864.8 c = 431.4	ordered low-temperature modification [1982Kha]
	*oP*16 *Pnma* Fe_3C	a = 443.9 b = 542.8 c = 669.9	orthorhombic modification coexists in a small amount with high-temperature modification [1982Kha]
	*tP** $P4_2/n$ Ti_3P	a = 863.2 c = 431.1 a = 863.16	in the rapid-quenched alloys [1992Rog]

(*continued*)

DOI: 10.1007/978-3-540-69761-9_19

Phase/Temperature Range [°C]	Pearson Symbol/ Space Group/ Prototype	Lattice Parameters [pm]	Comments/References
		c = 431.29	in the arc-melted $Mo_5Fe_{70}B_{25}$ alloy [2000Lei]
Mo_2B	*tI*12		33 to 34 at.% B [Mas2]
< 2280	*I*4/*mcm*	a = 554.7	[V-C2]
	$CuAl_2$	c = 473.9	
		a = 554.87	in the $Mo_{60}Fe_{10}B_{30}$ alloy sintered at
		c = 473.47	1050°C [2000Lei]
βMoB	*oC*8		48 to 51 at.% B [Mas2]
2600 - 1800	*Cmcm*	a = 315.1	[1992Rag]
	CrB	b = 847.0	
		c = 308.2	
αMoB	*tI*16		48 to 50 at.% B [Mas2]
< 2180	$I4_1/amd$	a = 311.0	[V-C2]
	αMoB	c = 1695	dissolves 0.5 at.% Fe at 1050°C [2000Lei]
		a = 311.62	in the $Mo_{45}Fe_5B_{50}$ arc-melted alloy
		c = 1693.5	annealed at 1050°C [2000Lei]
MoB_2	*hP*3		62 to 66 at.% B [Mas2]
2375 - 1517	*P*6/*mmm*	a = 304	[1992Rag]
	AlB_2	c = 306	
Mo_2B_5	*hR*21		67 to 69 at.% B [Mas2]
< 2140	$R\bar{3}m$	a = 301.1	[V-C2]
	Mo_2B_5	c = 2093.0	dissolves 2.3 at.% Fe at 1050°C [2000Lei]
		a = 300.83	in the $Mo_{15}Fe_{15}B_{70}$ arc-melted alloy
		c = 2091.47	annealed at 1050°C [2000Lei]
MoB_4	*hP*20		~ 79 at.% B [Mas2]
< 1807	$P6_3/mmc$	a = 520.33	Mo rich [1973Lun]
	WB_4	c = 634.98	
		a = 520.26	B rich [1973Lun]
		c = 634.99	
		a = 520.42	in the $Mo_2Fe_{73}B_{75}$ alloy sintered at
		c = 635.05	1050°C [2000Lei]
σ, MoFe	*tP*30		43.3 to 57.1 at.% Fe [Mas2]
1611 - 1235	$P4_2/mnm$	a = 918.8	[H]
	σCrFe	c = 481.2	
μ, Mo_6Fe_7	*hR*39		56 to 61 at.% Fe [Mas2]
< 1370	$R\bar{3}m$	a = 475.46	[V-C2]
	W_6Fe_7	c = 2571.6	

(*continued*)

DOI: 10.1007/978-3-540-69761-9_19

Phase/Temperature Range [°C]	Pearson Symbol/ Space Group/ Prototype	Lattice Parameters [pm]	Comments/References
		a = 475.91 c = 2571.52	in the $Mo_{30}Fe_{50}B_{20}$ and $Mo_{55}Fe_{25}B_{20}$ alloys sintered at 1050°C [2000Lei]
R, Mo_2Fe_3 1488-1200	hR159 $R\bar{3}$ $Co_5Cr_2Mo_3$	 a = 1091.0 c = 1935.4	61.5 to 66.1 at.% Fe [Mas2] $Mo_{1.9}Fe_{3.1}$, at 1250 to 1490°C [V-C2]
		a = 1095.6 c = 1935.3	annealed at 1250°C [V-C2]
λ, $MoFe_2$ < 927	hP12 $P6_3/mmc$ $MgZn_2$	 a = 475.5 c = 776.7	66.7 at.% Fe [Mas2] [V-C2]
*τ_1, $Mo_2Fe_{13}B_5$ ~1100 - < 1000	tP32 $P4_2/n$ Ti_3P	a = 863.4 c = 428.1	annealed at 1050°C [1966Has1]
*τ_2, Mo_2FeB_2	tP10 $P4/mbm$ U_3Si_2	a = 578.2 c = 314.8	[1964Rie]
		a = 580.7 c = 314.2	annealed at 1000°C [1966Gla]
		a = 577.26 c = 314.61	in the $Mo_{30}Fe_{30}B_{40}$ arc-melted alloy annealed at 1050°C [2000Lei]
*τ_3, $Mo_{1-x}Fe_xB$	oC8 $Cmcm$ CrB	 a = 315.7 b = 839.7 c = 306.3	6.5 to 9 at.% Mo at 50 at.% B, T = 1050°C [2000Lei] annealed at 1050°C [1966Has1]
		a = 315.26 b = 841.86 c = 306.62	in the $Mo_{45}Fe_5B_{50}$ arc-melted alloy annealed at 1050°C [2000Lei]
*τ_4, $Mo_{1+x}Fe_{2-x}B_4$	oI14 $Immm$ Ta_3B_4	 a = 312.8 b = 1270 c = 298.4	13 to 25 at.% Mo at 57 at.% B, T = 1050°C [2000Lei] x = 0, annealed at 1000°C [1966Gla]
		a = 311 b = 1427 c = 319	x = 1, annealed at 1050°C [1966Has1]
		a = 299.6 b = 1279 c = 309.9	x = 0.06, annealed at 1050°C [2000Lei]
		a = 301 b = 1300 c = 310.5	x = 0.43, annealed at 1050°C [2000Lei]

(*continued*)

DOI: 10.1007/978-3-540-69761-9_19

Phase/Temperature Range [°C]	Pearson Symbol/ Space Group/ Prototype	Lattice Parameters [pm]	Comments/References
		a = 304 b = 1340 c = 312.8	x = 1, annealed at 1050°C [2000Lei]

Table 3. Investigations of the B-Fe-Mo Materials Properties

Reference	Method/Experimental Technique	Type of Property
[1964Col2]	Vickers hardness measurements, tensile tests, creep-rupture tests	Hardness, stress, tensile strength
[1966Has2]	Vickers hardness measurements, tensile and impacts tests	Hardness, tensile strength, impact properties
[1973Dey]	Mössbauer spectroscopy	Magnetic hyperfine structure, atomic magnetic ordering
[1980Vin]	Inductance bridge method, four-point method	Curie temperature, electrical resistivity, coercive field
[1983Ber]	Thermomechanical system (TMS), thermogravimetric system (TGS) studies	Magnetization, electrical resistance, hardness
[1984Dun]	Magnetization measurements, ^{57}Fe Mössbauer spectroscopy (constant acceleration spectrometer)	Magnetization, magnetic moment, Fe hyperfine field distribution
[1984She]	Electrical resistivity-temperature dependence measurements	Electrical resistivity
[1986Muk]	Vickers microhardness tests (PMT-3 apparatus); yield stress, elongation, tensile strength tests (“Instron” apparatus)	Microhardness, tensile strength, yield point
[1986Tak]	Density, strength, Rockwell hardness tests	Transverse rupture strength (TRS), density, hardness
[1987Ger]	Dilatometry, density, hardness (Brinell), stress and ductility tests	Tensile elongation, density, hardness, porosity, ductility
[1987Tak]	Density, strength, Rockwell hardness tests	TRS, hardness, density
[1988Efi]	Stress, strength, Vickers microhardness tests (PMT-3 apparatus)	Ultimate tensile strength, yield stress, microhardness
[1988Ide]	Density, strength, Rockwell hardness tests	TRS, hardness, density
[1989Ide]	Thermal dilatometry, Rockwell hardness tests	TRS, elongation
[1992Kis]	Magnetic measurements	Magnetic moment, Curie temperature
[1995Dud]	Static tensile, three-point bend tests (“Instron 1302” equipment), Vickers hardness and microhardness tests, dilatometry	Density, microhardness, hardness, tensile and bending strength, elongation

(*continued*)

DOI: 10.1007/978-3-540-69761-9_19

Reference	Method/Experimental Technique	Type of Property
[1997Dud]	Static tensile, three-point bend tests ("Instron 1302" equipment), Vickers hardness and microhardness tests, dilatometry	Density, microhardness, hardness, tensile and bending strength, elongation
[1998Wan]	Microhardness tests	Microhardness
[1999Wan]	Magnetic measurements, microhardness tests	Magnetic losses, microhardness
[2000Mol]	Dilatometry, water displacement technique, Vickers microhardness tests	Density, porosity, elongation, microhardness
[2001Kar1]	Water displacement, Brinell hardness tests; tensile strength and elongation ("Instron 1302" equipment) tests	Density, hardness, strength, elongation
[2001Kar2]	Water displacement, Brinell hardness tests; tensile strength and elongation ("Instron" equipment) tests	Density, hardness, strength, elongation

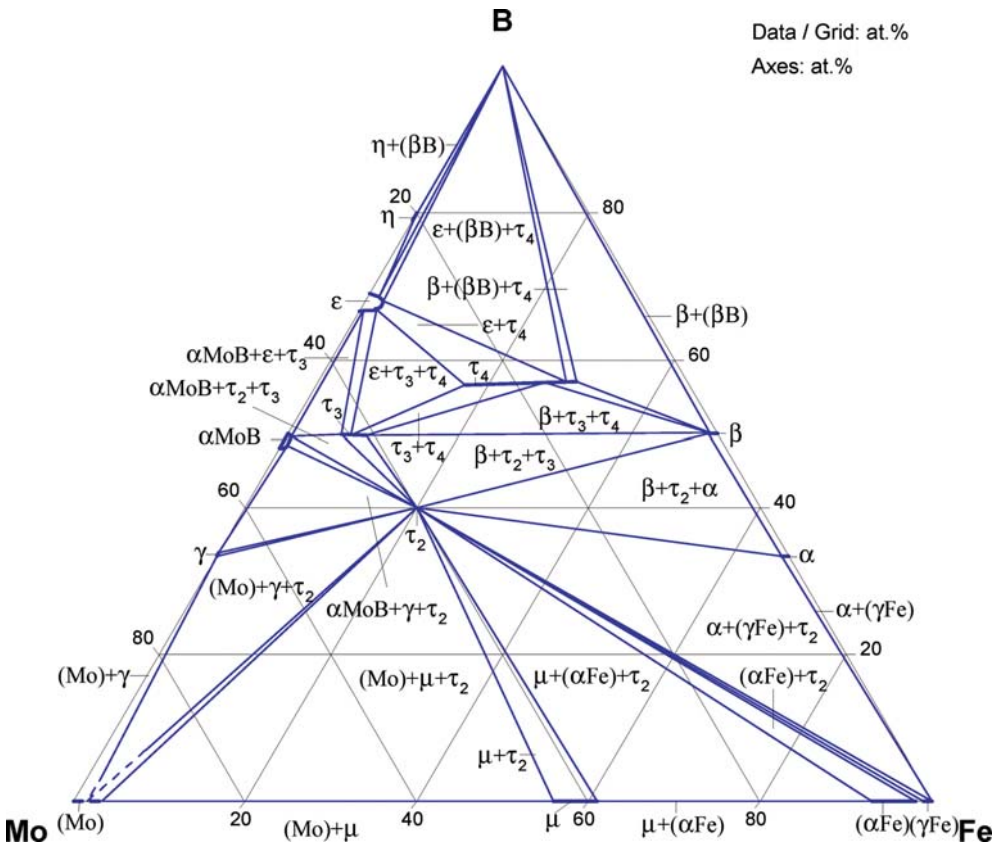

Fig. 1. B-Fe-Mo. Isothermal section at 1050°C

DOI: 10.1007/978-3-540-69761-9_19

References

[1953Ste] Steinitz, R., Binder, I., "New Ternary Boride Compounds", *Powder Met. Bull.*, **6**(4), 123–125 (1953) (Crys. Structure, Phase Relations, Experimental, 6)

[1964Col1] Coldren, A.P., Semchyshen, M., "Factors Affecting the High-Temperature Strength of Iron-Rich Fe-Mo-B Alloys", *J. Met.*, **16**(1), 101 (1964) (Crys. Structure, Morphology, Abstract, Mechan. Prop., 1)

[1964Col2] Coldren, A.P., Semchyshen, M., Scholz, W.G., "Factors Affecting the Strength of Iron-Rich Iron-Molybdenum-Boron Alloys", *Trans. Metall. Soc. AIME*, **230**, 1236–1250 (1964) (Crys. Structure, Morphology, Experimenta1, Mechan. Prop., 10)

[1964Rie] Rieger, W., Nowotny, H., Benesovsky, F., "The Crystal Structure of Mo_2FeB_2" (in German), *Monatsh. Chem.*, **95**, 1502–1503 (1964) (Crys. Structure, Experimental, 3)

[1965Kuz] Kuz'ma, Yu.B., Voroshilov, Yu.V., Cherkashin, E.E., "New Ternary Compounds with $W_2Cr_{21}C_6$ Type Structure", *Inorg. Mater. (Engl. Trans.)*, **1**(7), 1017–1019 (1965), translated from *Izv. Akad. Nauk SSSR, Neorg. Mater.*, **1**(7), 1109–1111 (1965) (Crys. Structure, Experimental, 3)

[1965Rie] Rieger, W., Nowotny, H., Benesovksy, F., "About Some Complex Borides of the Transition Metals" (in German), *Monatsh. Chem.*, **96**(3), 844–851 (1965) (Crys. Structure, Phase Diagram, Experimental, 10)

[1966Gla] Gladyshevskii, E.I., Fedorov, T.F., Kuz'ma, Yu.B., Skolozdra, R.V., "Isothermal Section of the System Molybdenum-Iron-Boron" (in Russian), *Poroshk. Metall.*, (4), 55–60 (1966) (Crys. Structure, Morphology, Phase Diagram, Experimental, *, 6)

[1966Has1] Haschke, H., Nowotny, H., Benesovsky, F., "Investigations in the Ternary Systems {Mo, W}-{Fe, Co, Ni}-B" (in German), *Monatsh. Chem.*, **97**, 1459–1468 (1966) (Crys. Structure, Phase Diagram, Experimental, *, 6)

[1966Has2] Hasegawa, M., Okamoto, M., "A Study on the Ternary Alloys of Iron and Boron" (in Japanese), *Nippon Kinzoku Gakkai-Si*, **30**(6), 533–540 (1966) (Morphology, Phase Relations, Experimental, Mechan. Prop., 12)

[1969Bis] Biss, V., Coldren, A.P., "Continuous Cooling Transformation of an Fe-1.91 % Mo-0.066 % B-0.002 % C Alloys", *Trans. Metall. Soc. AIME*, **245**, 884–886 (1969) (Morphology, Phase Diagram, Experimental, 3)

[1973Dey] De Young, D.B., Barnes, R.G., "^{57}Fe Moessbauer Study of Some $M_2(M')B_2$ Borides", *J. Phys. Chem. Solids*, **34**, 139 (1973) (Crys. Structure, Experimental, Electronic Structure, Magn. Prop., 5)

[1973Lun] Lundstroem, T., Rosenberg, I., "The Crystal Structure of the Molybdenum Boride $Mo_{(1-x)}B_3$", *J. Solid State Chem.*, (6), 299–305 (1973) (Crys. Structure, Experimental, 5)

[1973Rog] Rogl, P., Nowotny, H., "New Complex Borides" (in German), *Monatsch. Chem.*, **104**(4), 943–952 (1973) (Crys. Structure, Experimental, 25)

[1979Run] Rundqvist, S., Andersson, Y., Pramatus, S., "Coordination and Bonding in Represantatives of the Fe_3P-, Ti_3P-, α-V_3S-, and β-V_3S Type Structures", *J. Solid State Chem.*, **28**, 41–49 (1979) (Crys. Structure, Review, 42)

[1980Car] Cartier, E., Heinrich, F., "Positron Studies of the Crystallization Kinetics in the Metallic Glass $Fe_{78}Mo_2B_{20}$", *Helv. Phys. Acta*, **53**, 266–269 (1980) (Morphology, Experimental, Kinetics, 8)

[1980Vin] Vind Nielsen, H.J., "Magnetic Properties of Fe-Cr-B and Fe-Mo-B Metallic Glasses", *J. Magn. Magn. Mater.*, **19**(1–3), 138–140 (1980) (Crys. Structure, Experimental, Electr. Prop., Magn. Prop., 24)

[1981Kha] Khan, Y., Kneller, E., Sostarich, M., "Stability and Crystallization of Amorphous Iron-Boron Alloys Obtained by Quenching from the Melt", *Z. Metallkd.*, **72**(8), 553–557 (1982) (Crys. Structure, Phase Diagram, Experimental, 21)

[1982Gui] Guillermet, A.F., "The Fe-Mo (Iron-Molybdenum) System", *Bull. Alloy Phase Diagrams*, **3**(3), 359–367 (1982) (Crys. Structure, Phase Diagram, Phase Relations, Thermodyn., Review, *, 40)

DOI: 10.1007/978-3-540-69761-9_19

[1982Kha] Khan, Y., Kneller, E., Sostarich, M., "The Phase Fe_3B", *Z. Metallkd.*, **73**(10), 624–626 (1982) (Crys. Structure, Phase Diagram, Experimental, 13)

[1983Ber] Bergmann, H.W., Brokmeier, U., Fritsch, H.U., "Experimental Investigation on the Thermal Stability of Metallic Glasses", *Ber. Bunsen-Ges. Phys. Chem.*, **87**, 757–761 (1983) (Crys. Structure, Morphology, Thermodyn., Experimental, Mechan. Prop., 15)

[1984Dun] Dunlap, R.A., Stroink, G., "Magnetic Properties of Amorphous Fe-Mo-B Alloys", *Canad. J. Phys.*, **62**, 714–719 (1984) (Crys. Structure, Experimental, Morphology, Magn. Prop., 21)

[1984She] Shen, B., Zhan, W., Zhang, Zh., Wu, Z., "Temperature (4.2–300 K) Dependence of Electrical Resistivity of FeMB (M = Mn, Mo) Amorphous Alloys" (in Chinese), *Acta Metall. Sin.*, **20**(3), B164-B170 (1984) (Morphology, Experimental, Electr. Prop., 18)

[1986Muk] Mukhin, G.G., Efimov, Yu.V., Dmitriev, V.N., Buravleva, I.S., "Influence of Cyclic Tempering on Mechanical Properties of Rapid-Quenched Alloys" (in Russian), *Metalloved. i Term. Obrabotka Metallov*, (11), 51–53 (1986) (Crys. Structure, Morphology, Experimental, Mechan. Prop., 8)

[1986Tak] Takagi, K., Watanabe, T., Ando, T., Kondo, Y., "Effect of Molybdenum and Carbon on the Properties of Iron Molybdenum Boride Hard Alloys", *Inter. J. Powder Metallurgy*, **22**(2), 91–96 (1986) (Morphology, Phase Relations, Experimental, Mechan. Prop., Phys. Prop., 7)

[1987Ger] German, R.M., Hwang, K.-S., Madan, D.S., "Analysis of Fe-Mo-B Sintered Alloys", *Powder Metallurgy International*, **19**(2), 15–18 (1987) (Crys. Structure, Morphology, Experimental, Phys. Prop., 18)

[1987Tak] Takagi, K., Komai, M., Ide, T., Watanabe, T., Kondo, Y., "Effects of Mo and Cr Contents on the Properties and Phase Formation of Iron Molybdenum Boride Base Hard Alloys", *Powder Metallurgy International*, **19**(5), 30–33 (1987) (Crys. Structure, Morphology, Phase Relations, Experimental, Mechan. Prop., 13)

[1988Efi] Efimov, Yu.V., Mukhin, G.G., Fridman, Z.G., Bouravleva, I.S., Myasnikova, E.A., "The Change of the Amorphous State of Fe-Mo-B Alloys on Heating", *J. Non-Cryst. Solids*, **103**, 45–48 (1988) (Phase Relations, Experimental, Mechan. Prop., 6)

[1988Ide] Ide, T., Nakano, K., Ando, T., "Effects of Mo Content and Sintering Temperature on the Strength, Hardness and Density of Fe-6 mass% B-*x* mass% Mo Alloys", *Powder Metallurgy International*, **20**(3), 21–24 (1988) (Crys. Structure, Morphology, Phase Relations, Experimental, Mechan. Prop., 17)

[1989Ide] Ide, T., Ando, T., "Reaction Sintering of an Fe-6 wt% B-48 wt% Mo Alloy in the Presence of Liquid Phases", *Metall. Trans. A*, **20A**, 17–24 (1989) (Morphology, Phase Relations, Phys. Prop., 16)

[1989Kol] Kolb-Telieps, A., Luft, U., "Relations Between Structure and First-Step Crystallization of Iron-Metal-Boron Glasses", *J. Non-Cryst. Solids*, **109**, 59–63 (1989) (Crys. Structure, Morphology, Experimental, 7)

[1992Kis] Kisdi-Koszó, E., Lovas, A., Kovác, J., Varga, L.K., Zsoldos, E., "Inhomogeneous Atomic Distribution and Its Effect on Magnetic Properties of Diluted Fe-TM-B Metallic Glasses", *J. Magn. Magn. Mater.*, **112**, 39–40 (1992) (Morphology, Experimental, Magn. Prop., 4)

[1992Rag] Raghavan, V., "The B-Fe-Mo (Boron-Iron-Molybdenum) System", in "*Phase Diagrams of Ternary Iron Alloys"*, Indian Institute of Metals, Calcutta, **6A**, 365–369 (1992) (Crys. Structure, Phase Diagram, Phase Relations, Review, 8)

[1992Rog] Rogl, P., in "*Phase Diagrams of Ternary Boron Nitride and Silicon Nitride Systems*", Rogl, P., Schuster, J.C. (Eds.), ASM, Materials Park, OH, 33–36 (1992) (Crys. Structure, Phase Diagram, Thermodyn., Review)

[1993Wer] Werheit, H., Kuhlmann, U., Laux, M., Lundstrm, T., "Structural and Electronic Properties of Carbon-Doped β-Rhombohedral Boron", *Phys. Stat. Sol.*, **B179**, 489–511(1993) (Crys. Structure, Experimental, 51)

[1994Hal] Hallemans, B., Wollants, P., Roos, J.R., "Thermodynamic Reassessment and Calculation of the Fe-B Phase Diagram", *Z. Metallkd.*, **85**(10), 676–682 (1994) (Crys. Structure, Phase Diagram, Thermodyn., Assessment, #, 36)

DOI: 10.1007/978-3-540-69761-9_19

[1995Dud] Dudrová, E., Salak, A., Selecká, M., Bure, R., "Properties and Microstructure of Fe-1.5 Mo Powder Steel Sintered with a Boron-Based Liquid Phase", *Metal. Mater.*, **33**(2), 60–65 (1995), *transl. from Kovove Mater.*, **33**(2), 82–93 (1995) (Morphology, Phase Relations, Experimental, Mechan. Prop., Phys. Prop., 11)

[1996Pov] Povarova, K.B., "B-Mo. Boron-Molybdenum", in "*Phase Diagrams of Binary Metallic Systems*" (in Russian), Lyakishev, N.P. (Ed.), Vol. **1**, Mashinostroenie, Moscow, 461–464 (1996) (Crys. Structure, Phase Diagram, Review, *, 14)

[1997Dud] Dudrová, E., Selecká, M., Bure, R., Kabátova, M., "Effect of Boron Addition on Microstructure and Properties of Sintered Fe-1.5Mo Powder Materials", *ISIJ Int.*, **37**(1), 59–64 (1997) (Morphology, Phase Relations, Experimental, Phys. Prop., 11)

[1997Wan] Wang, L.L., Zhang, B.W., Yi, G., Ouyang, Y.F., Hu, W.Y., "Structure and Crystallization of Amorphous Fe-Mo-B Alloys Obtained by Electroless Plating", *J. Alloys Compd.*, **255**(1–2), 231–235 (1997) (Crys. Structure, Morphology, Phase Relations, Thermodyn., Experimental, 5)

[1998Rog] Rogl, P., "Metal-Boron-Carbon Ternary Systems", Effenberg, G. (Ed.), MSIT-ASM International, OH, USA, 1–480 (1998) (Crys. Structure, Phase Diagram, Thermodyn., Review, *)

[1998Wan] Wang, L.L., Zhao, L.H., Zhang, B.W., Ouyang, Y.F., Liao, S.Z., Hu, W.Y., "Composition Dependence of Some Physical Properties of Fe-TM-B (TM = Mo, W, Mo-W) Alloys Obtained by Electroless Plating", *Plating & Surface Finishing*, **85**(12), 96–98 (1998) (Morphology, Experimental, Mechan. Prop., 9)

[1999Wan] Wang, L.L., Zhao, L.H., Zhang, B.W., Liao, S.Z., Ouyang, Y.F., Hu, W.Y., Shu, X.L., Yuan, X.J., "Annealing Temperature Dependence of A-C Magnetic Losses and Microhardness in Fe-TM-B (TM = Fe, Mo, W, Mo-W) Alloys Obtained by Electroless Plating", *Plating & Surface Finishing*, **86**(12), 84–86 (1999) (Morphology, Experimental, Magn. Prop., Mechan. Prop., 5)

[2000Lei] Leithe-Jasper, A., Klesnar, H., Rogl, P., Komai, M., Takagi, K.-I., "Reinvestigation of Isothermal Section in M (M = Mo, W)-Fe-B Ternary Systems at 1323K" (in Japanese), *J. Jpn. Inst. Met.*, **64**(2), 154–162 (2000) (Crys. Structure, Morphology, Phase Diagram, Phase Relations, Experimental, #, 30)

[2000Mol] Molinari, A., Pieczonka, T., Kazior, J., Gialanella, S., Straffelini, G., "Dilatometry Study of the Sintering Behavior of Boron-Alloyed Fe-1.5 % Mo Powder", *Metall. Trans. A*, **31A**(6), 1497–1506 (2000) (Crys. Structure, Morphology, Phase Relations, Experimental, Phys. Prop., 19)

[2001Kar1] Karwan-Baczewska, J., "The Properties and Structure of Boron Modified P/M Iron-Molybdenum Alloys", *Arch. Metall.*, **46**(4), 439–445 (2001) (Crys. Structure, Morphology, Experimental, Kinetics, Mechan. Prop., Phys. Prop., 14)

[2001Kar2] Karwan-Baczewska, J., Rosso, M., "Effect of Boron on Microstructure and Mechanical Properties of PM Sintered and Nitrided Steels", *Powder Metall.*, **44**(3), 221–227 (2001) (Crys. Structure, Morphology, Experimental, Kinetics, Mechan. Prop., Phys. Prop., 14)

[2001Mor] Morishita, M., Koyama, K., Yagi, S., Zhang, G., "Calculated Phase Diagram of the Ni-Mo-B Ternary System", *J. Alloys Compd.*, **314**, 212–218 (2001) (Phase Diagram, Thermodyn., Calculation, Review, *)

[2003Luk] Lukachuk, M., Poettgen, R., "Intermetallic Compounds with Ordered U_3Si_2 or Zr_3Al_2 Type Structure - Crystal Chemistry, Chemical Bonding and Physical Properties", *Z. Kristallogr.*, **218**, 767–787 (2003) (Crys. Structure, Thermodyn., Review, Electronic Structure, Electr. Prop., Magn. Prop., 197)

[2003Rag] Raghavan, V., "B-Fe-Mo (Boron-Iron-Molybdenum)", *J. Phase Equilib.*, **24**(5), 449–450 (2003) (Crys. Structure, Phase Diagram, Phase Relations, Assessment, 8)

[2004Sar] Sarasola, M., Gómez-Acebo, T., Castro, F., "Liquid Generation During Sintering of Fe-3.5 % Mo Powder Compacts with Elemental Boron Additions", *Acta Mater.*, **52**,

DOI: 10.1007/978-3-540-69761-9_19

4615–4622 (2004) (Morphology, Phase Diagram, Phase Relations, Thermodyn., Calculation, Experimental, 33)

[2005Sar] Sarasola, M., Gómez-Acebo, T., Castro, F., "Microstructural Development During Liquid Phase Sintering of Fe and Fe-Mo Alloys Containing Elemental Boron Additions", *Powder Met.*, **48**(1), 59–67 (2005) (Morphology, Phase Diagram, Phase Relations, Thermodyn., Calculation, Experimental, 22)

[H] Hansen, M. and Anderko, K., *Constitution of Binary Alloys*, McGraw-Hill, New York (1958)

[V-C2] Villars, P. and Calvert, L.D., *Pearson's Handbook of Crystallographic Data for Intermetallic Phases*, 2nd edition, ASM, Metals Park, Ohio (1991)

[Mas2] Massalski, T.B. (Ed.), *Binary Alloy Phase Diagrams*, 2nd edition, ASM International, Metals Park, Ohio (1990)

DOI: 10.1007/978-3-540-69761-9_19

Boron – Iron – Nitrogen

Vasyl Tomashik

Introduction

A brief review of the experimental data for the B-Fe-N system was carried out by [1987Rag]. The first experimental data concerning this system were published in 1951 by [1951Kie], who showed that the products of the Fe_2B and FeB chemical interaction with NH_3 are BN and those Fe nitrides which are stable in streaming ammonia at the reaction temperature [1951Kie]. The solubility of nitrogen in solid B-Fe alloys has been studied by [1962Fou] and its solubility in liquid B-Fe alloys has been measured to the solubility limit for the BN formation in [1964Eva, 1964Isa]. The phase equilibria at 900°C have been established by [1986Smi] (these data were included in the short review of [1993Rag]). The obtained results confirmed the data of [1951Kie] and [1962Fou]. It was indicated in the review of [1987Mor] that BN is in equilibrium with B-Fe-N liquid alloys. The equilibria between solid BN and the Fe melts dissolving nitrogen and boron at 1600°C were established by [1968Sch].
The interaction of the carbon steel with various modifications of BN was studied by [1978Vis], the interaction of *h*BN with Fe at high temperatures and pressures was investigated in [1982Vas, 2003Fed, 2003Sue, 2004Bok, 2004Tao] and the interaction of FeB nanoparticles with the nitrogen plasma was studied by [2004Loh].
Thermodynamic properties of B-Fe-N alloys were investigated in [1962Fou, 1964Eva, 1968Sch, 1974Sig, 2001War].
A summary of experimental studies of phase equilibria is given in Table 1.

Binary Systems

The B-Fe and Fe-N phase diagrams are accepted from [Mas2]. The congruently melting FeB and incongruently melting Fe_2B compounds exist in the B-Fe system. The metastable Fe_3B phase was also found in this system. Fe_4N, Fe_2N and ε phase exist in the Fe-N system.
The B-N system is accepted from [2003Rec]. Only one intermediate phase BN exists in this system. Boron nitride has four crystalline structural modifications: cubic (*c*BN), wurtzite (*w*BN), hexagonal (*h*BN) and rhombohedral (*r*BN). Except for that, there are two other ordered BN phases: EBN, obtained by explosion (E) of a mixture of *h*BN and *a*BN, compressed *h*BN attributable to a monoclinic lattice distortion of *h*BN and two disordered BN phases: turbostratic BN (*t*BN) and amorphous BN (*a*BN).

Solid Phases

Solubilities of N in the boron containing γFe alloys were determined in [1962Fou] at 950-1150°C in the range 0.001-0.9 mass% B. It was demonstrated that solubility of nitrogen decreases with increasing boron content.
Crystallographic data of all unary and binary phases are listed in Table 2. Ternary phases were not found in this system.

Quasibinary Systems

According to the data of [1986Smi] one can assume that BN-Fe and BN-FeB could be the quasibinary sections but their phase diagrams are not investigated.

Liquidus Surface

The solubility of boron and nitrogen in Fe melts in equilibrium with solid BN at 1600°C and various N_2 pressures is shown in Fig. 1 [1968Sch].

DOI: 10.1007/978-3-540-69761-9_20

The solubility data indicated that B decreases the solubility of nitrogen in liquid Fe (Fig. 2) [1964Eva]. These data were confirmed by [1964Eva] and [1964Isa]. Within the limits of experimental accuracy the data indicated that Sieverts' law was observed below the BN solubility limit at all B concentration studied [1964Eva].

Isothermal Sections

A part of the isothermal section at 900°C is shown in Fig. 3 [1986Smi]. The mutual solubilities of the components were found to be rather small and no ternary compounds formed under high purity conditions.
From the data for the solubility of BN in (γFe) and the nitrogen amount in the solid solution with BN and Fe_2B the isothermal sections of the Fe corner of the B-Fe-N ternary system at 950, 1050 and 1150°C were constructed by [1962Fou] (Figs. 4a, 4b, 4c).

Thermodynamics

The equilibrium between solid BN and liquid Fe-B-N alloy was studied by [1964Eva, 1964Isa, 1968Sch]. The data agree within experimental uncertainty. Data on the solubility of B and N in liquid alloys were treated by Wagner's model and mixing parameters and equilibrium constants were derived. It was showed by [1974Sig, 1987Mor] that temperature dependent first-order interaction parameters are sufficient to describe the experimental data. It should be mentioned that [1964Eva] measured log K using both Sievert's method and the sampling method. Hence, the calculations of [1987Mor] based on experimental data of Evans *et al.* [1964Eva] are recommended in the present evaluation: $\log K = -10000/T + 4.64$ $e^B_N = 1000/T - 0.437$ $e^B_B = 0.038$ in the temperature range 1550-1750°C.
It was estimated by [1962Fou] that the activity coefficient of nitrogen in the solid B-Fe-N alloys is decreased by B addition. According to the data of [1964Eva] the activity coefficient of nitrogen in liquid B-Fe-N alloys increases with increasing B content in the investigated range 0 to 7 mass% B. The effect of boron on the nitrogen activity coefficient in liquid Fe at 1550, 1600, 1650, 1700 and 1750°C is shown in Fig. 5 according to [1964Eva]. The activity coefficients of boron and nitrogen in the B-Fe-N melts were calculated by [1964Isa] from experimental data on B and N solubility in the liquid phase and it was shown that both activity coefficients increase with increasing boron content.
Thermodynamic data for some reactions in the B-Fe-N system are given in Table 3. Thermodynamic data for reactions involving amorphous BN are compiled in [2001War].

Notes on Materials Properties and Applications

Boron is widely used in the ferrous metallurgy for the steels microalloying. The small additions of B should be effective in reducing the soluble nitrogen content in steels to a level low enough to remove the danger of strain aging [1962Fou]. The forming BN paralyzes the B positive influence on the dead melting steel and *vice versa* gives the nonaging properties for the unkilled steel [1964Isa]. The increase of surface hardness and wear resistance is often associated with *c*BN formation [1999Ugl].
It was shown that the synthesis of *c*BN with the Fe additions at the stationary heating leads to the forming of the polycrystals containing FeB and Fe_2B and at the pulse heating the impurity of γFe is included [1982Vas]. The samples with γFe inclusions have higher cutting properties compare to the samples with Fe borides. Therefore to obtain *c*BN polycrystals from *h*BN with Fe addition with high mechanical properties it is necessary to use the pulse heating which excludes the Fe borides formation [1982Vas].
The internal friction of *h*BN-dispersed composite steel reaches a maximum at 4 mass% *h*BN [2003Sue]. This is because the internal friction of the composite steel depends upon both the internal friction due to the magnetic domain wall movement of ferrite and this one due to the deformation of *h*BN. Mechanical properties are practically unaffected by dispersion of 4 mass% *h*BN. Experimental results suggest that a composite steel showing promise as an advanced damping material can be attained by appropriate control of the microstructures of the steel part and the sintered core [2003Sue].

Miscellaneous

The stability of Fe borides in ammonia increases with increasing B content [1951Kie].

DOI: 10.1007/978-3-540-69761-9_20

Process and resulting products of solid-state reaction between Fe and *h*BN were studied by ball milling a mixture with a Fe to *h*BN volume ratio of 1:12.5 and/or heat treating under normal or high pressure [2004Tao]. A small amount of Fe_4N was observed in the mixture annealed at 500°C and a little inclusions of γFe(N) was obtained at 900°C. All Fe atoms in the mixture reacted with nitrogen in the BN to form a single ε (Fe_xN) phase when the mixture was milled for 60 h or annealed for 1 h under 4 GPa at 420-530°C. However no B-Fe phases were observed [2004Tao].

The solid BN films are formed on the B-Fe melt surfaces at the nitrogen contact within certain conditions [1964Isa]. According to the data of [1978Vis] the interaction of the carbon steel with *c*BN, *h*BN and *w*BN is absent at 1130°C and Fe_2B is formed at the interaction at 1230-1330°C. The interaction of *c*BN with this steel is the most active.

The wetting angle of Fe on *h*-BN, as measured by the sessile drop method at the temperature above the iron melting temperature was given as $\Theta = 112°$ [1966Yas].

A nanocomposite of nanometer-sized granular ε (Fe_xN) embedded in a nonmagnetic amorphous BN matrix was prepared by ball milling mixture of αFe and *h*BN in Ar atmosphere [1998Liu]. The grain size of the ε (Fe_xN) alloy was about 10-20 nm and the nitrogen concentration increases with extending milling time. It was found that a critical grain size of the αFe reacting with nitrogen in the amorphous BN is about 8 nm.

According to the data of [2004Bok] the particles of Fe and *h*BN after mechanical activation form aggregates with a size of 300-1000 nm. The Fe particles exhibit a rather broad size distribution (from 3-7 to 100 nm) while the minimal size of the BN particles is several tens of nanometers. Annealing of Fe samples with BN after preliminary mechanical activation at 860°C caused the formation of nanosized encapsulated particles of Fe_2B. Their surface was coated with a shell of *h*BN with the thickness from 5 to 15 nm. The size of the encapsulated particles varies within a rather broad range from 30 to 50 nm to several hundred nanometers [2004Bok].

The growth of *h*BN nanotubes and nanocages has been achieved by the nitrogen plasma treatment of FeB nanoparticles at temperature close to the eutectic melting point of the alloy (<1000°C) [2004Loh]. In addition to BN nanotubes (5-10 nm diameter), BN nanotubulus (100-200 nm diameter) created by interconnected chains of BN nanocages, as well as BN hollow microspheres can be grown. The recrystallization of Fe from smaller FeB particles results in crystalline Fe nanowires encapsulated by BN. The nanostructure formation can be controlled by the liquid flow of nanoparticles where interfacial wetting behavior and surface tension play a key mechanistic role [2004Loh]. Fe fine particles coated with BN nanolayers have been synthesized by annealing mixtures of αFe_2O_3 and B powders at 1100°C for 2 h in N_2 atmosphere [2004Tok]. The Fe particles had diameters of ~300 nm with BN nanolayers coating of 1-10 nm, which improved oxidation resistance of Fe particles. BN nanotubes with diameter of ~100 nm are also synthesized besides the BN nanolayers. A Curie temperature of the particles showed approximately 780°C [2004Tok]. The Fe films were amorphized by B implantation and these films were then implanted with nitrogen ions [1999Ugl]. It was found that multienergy implantation results in almost flat nitrogen and boron distribution. Investigations have shown that for low nitrogen doses an amorphous magnetic $(Fe\text{-}B,N)_m$ phase dominates. When the nitrogen concentration exceeds the B one paramagnetic $(Fe\text{-}B,N)_p$ and Fe_2N at the expense of the crystalline αFe were formed. Annealing at 500°C leads to crystallization $(Fe\text{-}B,N)_m$ through Fe_2B and Fe_4N formation [1999Ugl].

The results obtained by [2001War] showed that complete nitridation of ferroboron precursor in a mixture of $NH_3 + H_2$ under ambient pressure with BN formation can be achieved at 400°C with 20 vol.% NH_3. The nitrided product consists of amorphous BN, Fe and metastable Fe nitrides. An alternative route using 100 vol.% N_2 is also possible, but a higher reaction temperature (≥1430°C) is needed. The product from the high temperature route contains partially crystallized *h*BN, Fe and virtually no metastable Fe nitrides [2001War].

The interaction of *h*BN with carbonyl iron at a noncatalytic synthesis leads to the formation of the magnetically ordered phase ε (Fe_3N) and amorphous (B-Fe) which decomposes at elevated temperatures to metallic Fe precipitates [2003Fed]. In samples prepared by catalytic synthesis the dominating stable fraction of Fe is paramagnetic Fe^{3+} in low symmetry surrounding. These results may give some hints for the degradation in the mechanical properties of *c*BN cutting edges.

DOI: 10.1007/978-3-540-69761-9_20

Table 1. Investigations of the B-Fe-N Phase Relations, Structures and Thermodynamics

Reference	Method/Experimental Technique	Temperature/Composition/Phase Range Studied
[1951Kie]	XRD	352-768°C / Fe_2B or FeB + NH_3
[1962Fou]	Sieverts' method	950-1150°C / B-Fe-N alloys containing 0.001 to 0.91 mass% B
[1964Eva]	Sieverts' method, quenching method	1550-1750°C / B-Fe-N alloys containing 0 to 7.06 mass% B
[1964Isa]	Sieverts' method	1540 and 1590°C / B-Fe-N alloys containing 0 to 4.75 mass% B
[1966Yas]	Sessile drop method, metallography, chemical analysis	BN + Fe melt
[1968Sch]	Sieverts' method	1600°C / B-Fe-N alloys containing up to 10 mass% B
[1974Sig]	Calculation	1600°C / B-Fe-N
[1978Vis]	XRD, metallography,	1130-1330°C / *c*BN, *h*BN and *w*BN + steel
[1982Vas]	Mössbauer spectroscopy, microhardness	up to 2230°C and up to 7 GPa / *h*BN + Fe
[1986Smi]	XRD	900°C / B-Fe-N
[1998Liu]	XRD, TEM, Mössbauer spectroscopy, mechanical alloying	room temperature / *h*BN + αFe
[1999Ugl]	AES, XPS, conversion electron Mössbauer spectroscopy	200, 350 and 500°C / B-Fe-N
[2001War]	XRD, SEM with EDX	up to 1430°C / B-Fe-N
[2003Fed]	Mössbauer spectroscopy, XRD, X-ray energy-dispersive microanalysis	2000-2500°C and 7-7.5 GPa / *h*BN + Fe
[2003Sue]	SEM, transversal vibration method	650°C / *h*BN + Fe
[2004Bok]	XRD, electron microscopy	up to 860°C / *h*BN + Fe
[2004Loh]	XRD, TEM	up to 1000°C / FeB + N_2
[2004Tao]	XRD, DSC	420-900°C / *h*BN + Fe
[2004Tok]	XRD, SEM, HRTEM, EDX, Fourier transform infrared and Raman spectroscopy	1100°C / αFe_2O_3 + B + N_2

DOI: 10.1007/978-3-540-69761-9_20

Table 2. Crystallographic Data of Solid Phases

Phase/ Temperature Range [°C]	Pearson Symbol/Space Group/Prototype	Lattice Parameters [pm]	Comments/References
(βB) < 2092	*hR*333 $R\bar{3}m$ βB	*a* = 1093.30 *c* = 2382.52	[Mas2, 1993Wer]
(δFe) 1538 - 1394	*cI*2 $Im\bar{3}m$ W	*a* = 293.15	[Mas2]
(γFe) 1394 - 912	*cF*4 $Fm\bar{3}m$ Cu	*a* = 364.67	at 915°C [V-C2, Mas2]
(αFe) < 912	*cI*2 $Im\bar{3}m$ W	*a* = 286.65	at 25°C [Mas2]
(αN) < –237.54	*cP*8 *Pa*3 αN	*a* = 566.1	[Mas2]
*h*BN < 2397	*hP*4 $P6_3mc$ BN	*a* = 250.4 *c* = 666.1	[2003Rec]
*c*BN	*cF*8 $F\bar{4}3m$ ZnS	*a* = 361.53 ± 0.04	[2003Rec]
*w*BN	*hP*4 $P6_3/mmc$ ZnS	*a* = 255.0 ± 0.5 *c* = 423 ± 1	[2003Rec]
*r*BN	*hR*6	*a* = 250.4 *c* = 999.1	[2003Rec]
Compressed *h*BN	*mC*4 *C*2/*c* or *Cc*	*a* = 433 *b* = 250 *c* = 310 to 330 β = 92 to 95°	[2003Rec]
Fe_4N < 680	*cF*8 $Fm\bar{3}m$ NaCl	*a* = 379.0 ± 0.1	19.3 to 20.0 at.% N [V-C2, Mas2]
Fe_4N	*cP*5 $Pm\bar{3}m$ $CaTiO_3$	*a* = 389.6 ± 0.2	mineral Roaldite [V-C2]
ε phase	*hP*4 $P6_3/mmc$		~15 to ~33 at.% N [V-C2, Mas2];

(*continued*)

DOI: 10.1007/978-3-540-69761-9_20

Phase/ Temperature Range [°C]	Pearson Symbol/Space Group/Prototype	Lattice Parameters [pm]	Comments/References
$Fe_{4.96}N_2$	NiAs	a = 274.42 ± 0.04 c = 440.25 ± 0.11	[V-C2];
Fe_3N		a = 270.5 c = 437.6	mineral Siderazote [V-C2]
Fe_2N < 500	*hP*9 $P\bar{3}1m$ V_2N	a = 478.7 c = 441.8	[V-C2, Mas2]
FeB < 1650	*oP*8 *Pnma* FeB	a = 550.3 b = 294.6 c = 406.4	49.5 to 40.0 at.% Fe [V-C2, Mas2]
Fe_2B < 1389	*tI*12 *I4/mcm* Al_2Cu	a = 511.0 ± 0.3 c = 424.9 ± 0.3	[V-C2, Mas2]
Fe_3B(I)	*oP*16 *Pnma* Fe_3C	a = 542.8 b = 669.9 c = 443.9	metastable phase [V-C2, Mas2]
Fe_3B(II)	*tI*32 $I\bar{4}$ Ni_3P	a = 865.5 c = 429.7	high-temperature phase [V-C2, Mas2]

Table 3. Thermodynamic Data of Reaction or Transformation

Reaction or Transformation	Temperature [°C]	Quantity, per mol of atoms [kJ, mole, K]	Comments
$2Fe + BN \rightleftharpoons Fe_2B + 1/2N_2$	950-1150	$\Delta G^0_T = 108.84 - 0.055\ T$	[1962Fou]
$2Fe + BN \rightleftharpoons Fe_2B + N_\gamma$		$\Delta G^0_T = 100.59 - 0.018\ T$	
$BN \rightleftharpoons B_\gamma + 1/2N_2$		$\Delta G^0_T = 275.86 - 0.138\ T$	
$BN \rightleftharpoons B_\gamma + N_\gamma$		$\Delta G^0_T = 267.61 - 0.100\ T$	
$BN \rightleftharpoons B_L + N_L$	1550-1750	$\Delta G^0_T = 192.14 - 0.089\ T$	[1964Eva]
$FeB + 1/2\ N_2 \rightleftharpoons Fe + a$BN	25-727°C	$\Delta G^0_T = -198.75 + 0.097495\ T$	[2001War]
xFeB +1/2 $(1+x)$ $N_2 \rightleftharpoons Fe_xN + x(a$BN)		$\Delta G^0_T = -200.54 + 0.012148\ T$	

DOI: 10.1007/978-3-540-69761-9_20

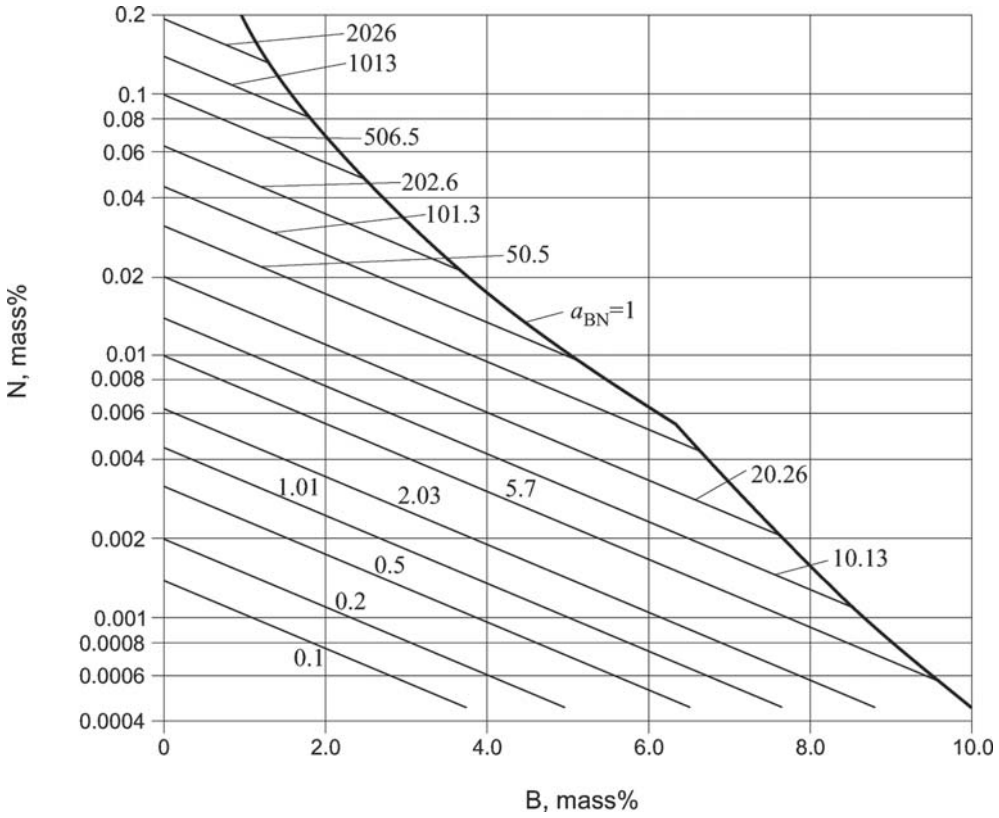

Fig. 1. B-Fe-N. Equilibria between liquid B-Fe-N alloys and BN at 1600°C and various N_2 pressure (in kPa)

DOI: 10.1007/978-3-540-69761-9_20

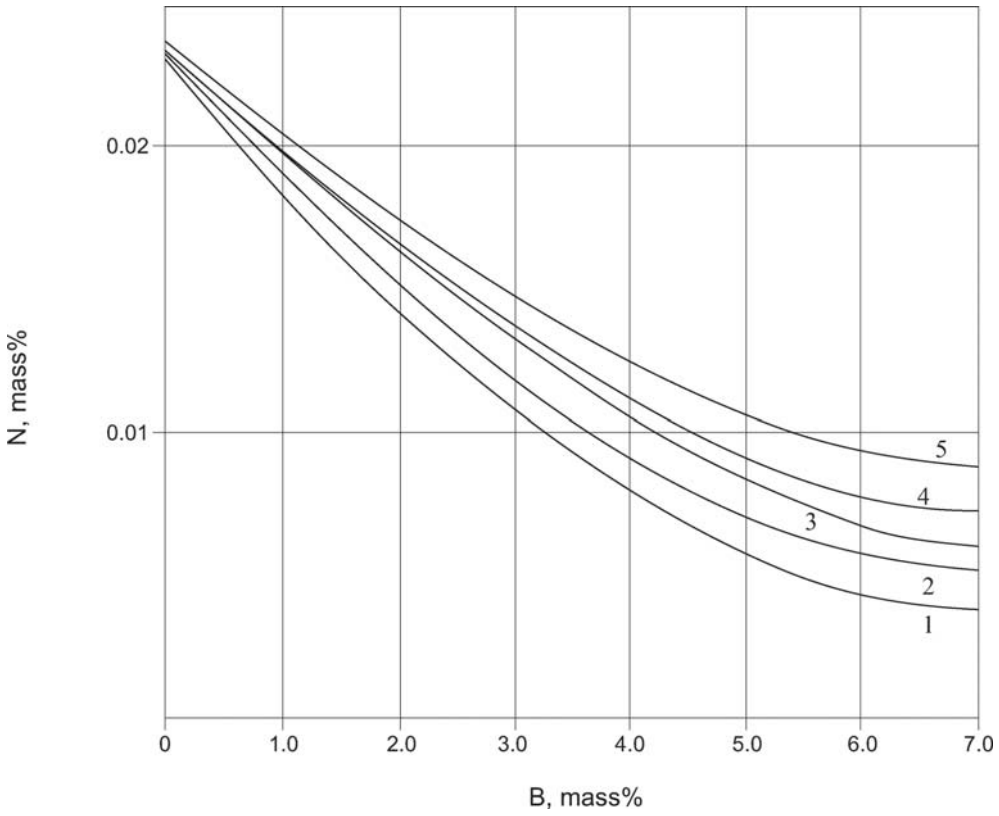

Fig. 2. B-Fe-N. Effect of boron on the nitrogen solubility at 1550 (1), 1600 (2), 1650 (3), 1700 (4) and 1750°C (5)

DOI: 10.1007/978-3-540-69761-9_20

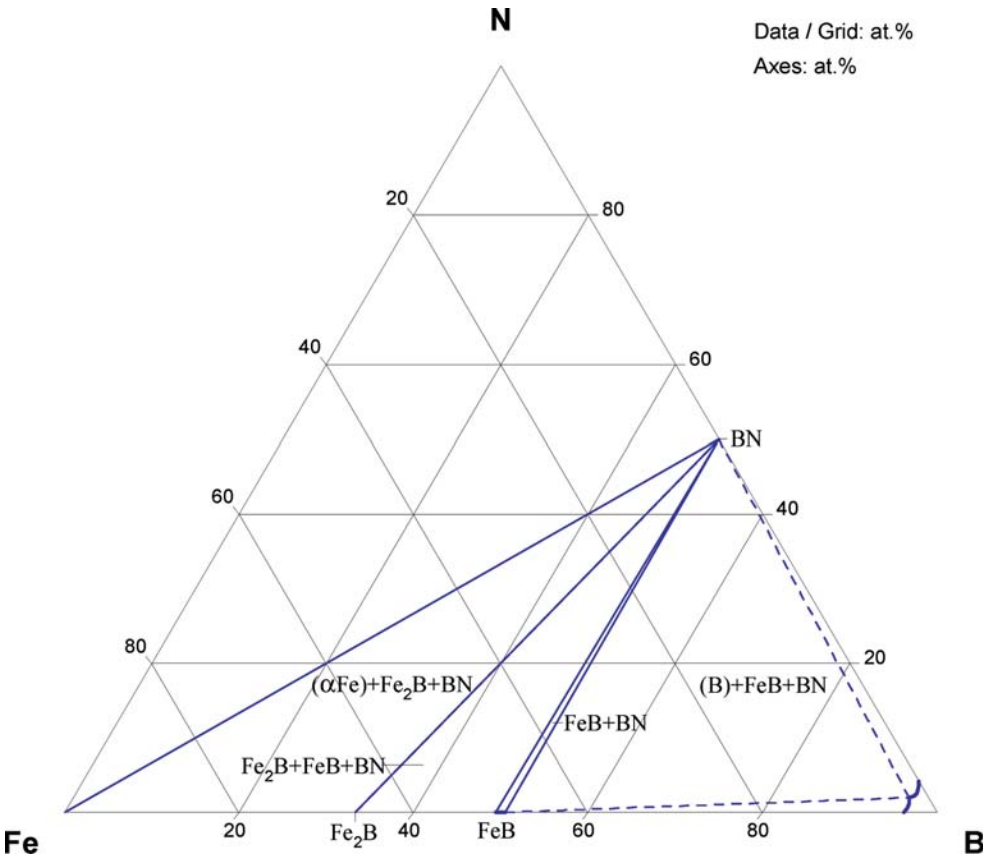

Fig. 3. B-Fe-N. Isothermal section at 900°C and 101.3 kPa argon

DOI: 10.1007/978-3-540-69761-9_20

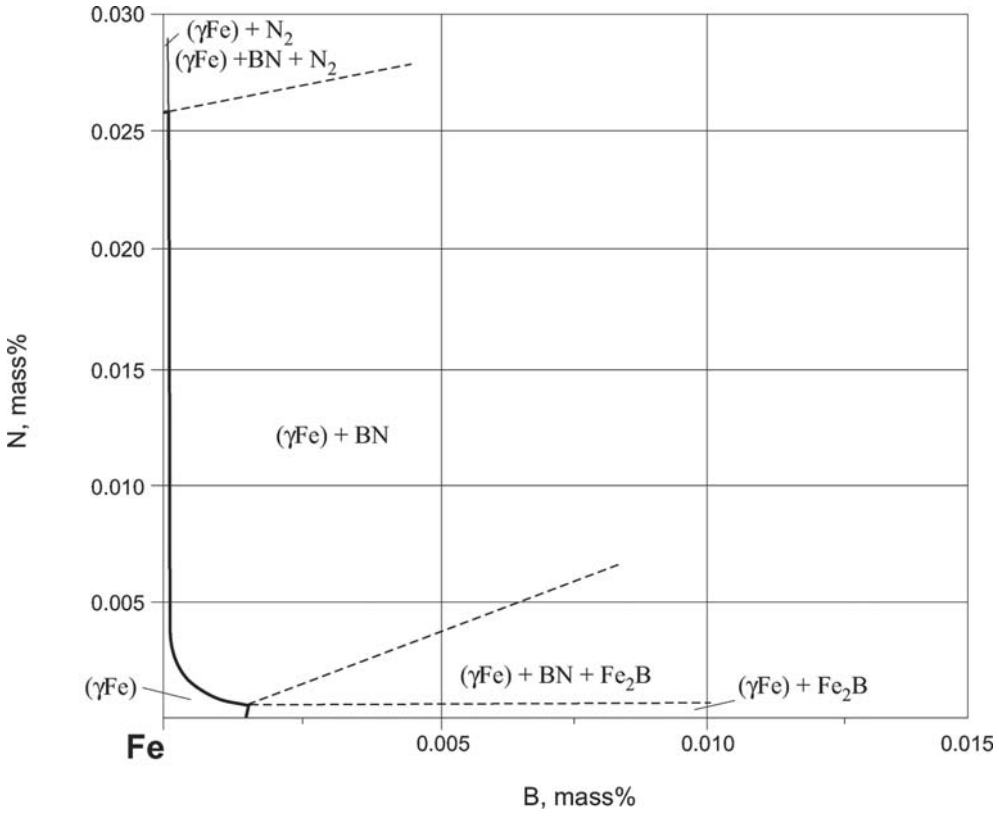

Fig. 4a. B-Fe-N. Isothermal section of the Fe corner at 950°C and 101.3 kPa nitrogen

DOI: 10.1007/978-3-540-69761-9_20

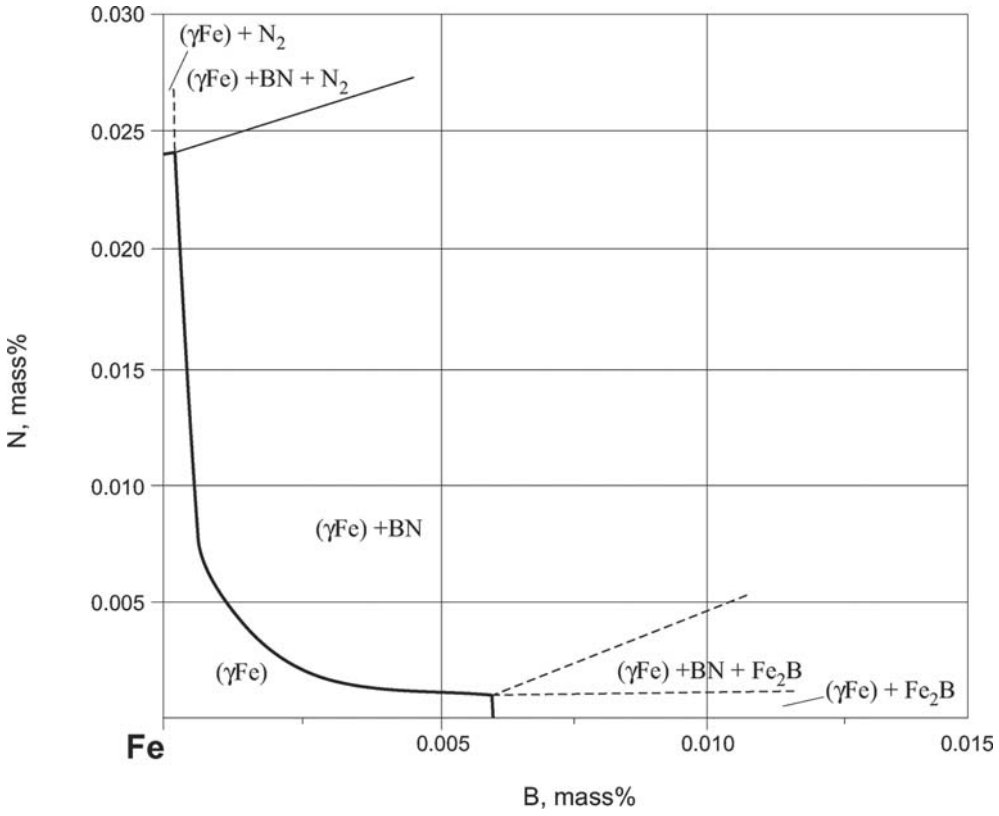

Fig. 4b. B-Fe-N. Isothermal section of the Fe corner at 1050°C and 101.3 kPa nitrogen

DOI: 10.1007/978-3-540-69761-9_20

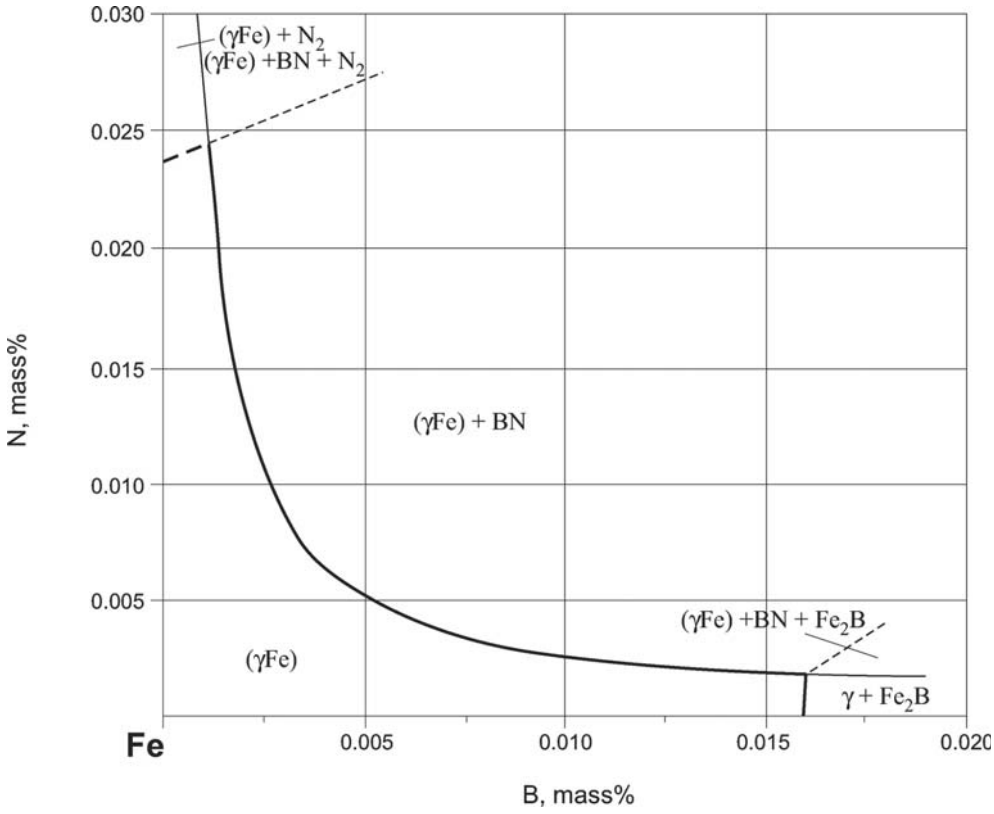

Fig. 4c. B-Fe-N. Isothermal section of the Fe corner at 1150°C and 101.3 kPa nitrogen

DOI: 10.1007/978-3-540-69761-9_20

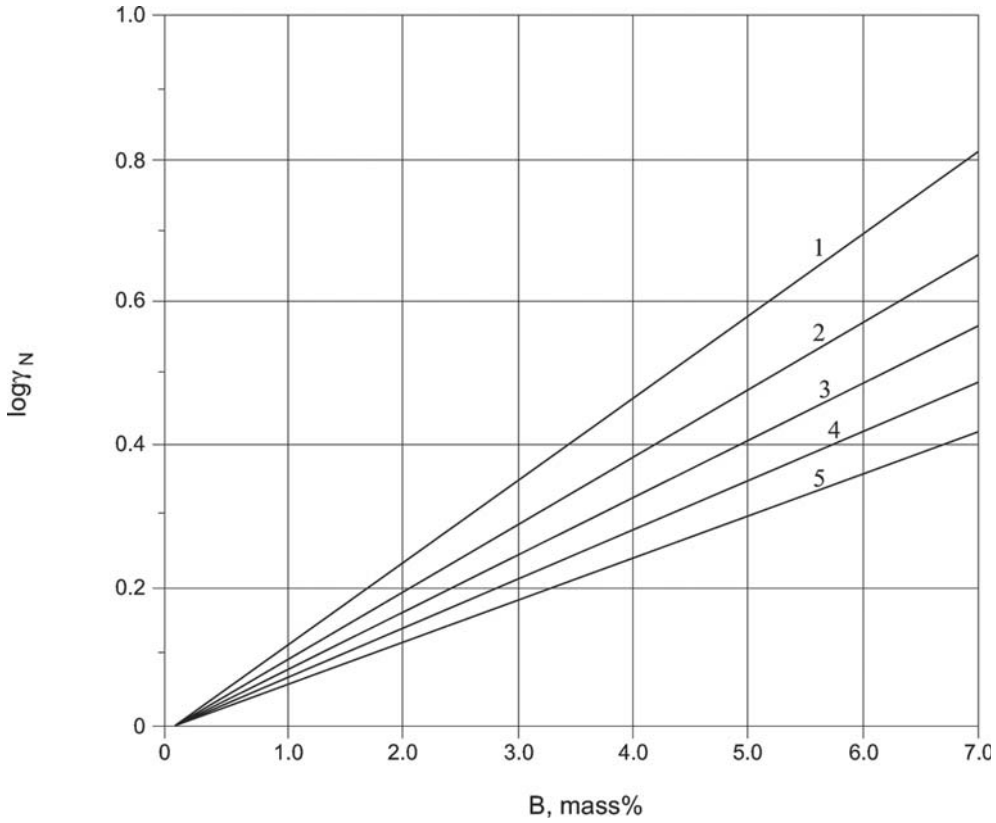

Fig. 5. B-Fe-N. Effect of boron on the nitrogen activity coefficient at 1550 (1), 1600 (2), 1650 (3), 1700 (4) and 1750°C (5)

DOI: 10.1007/978-3-540-69761-9_20

References

[1951Kie] Kiessling, R., Liu, Y.H., "Thermal Stability of the Chromium, Iron, and Tungsten Borides in Streaming Ammonia and the Existence of a New Tungsten Nitride", *Trans. Met. Soc. AIME*, **191**(8), 639–642 (1951) (Experimental, Phase Relations, 11)

[1962Fou] Fountain, R.W., Chipman, J., "Solubility and Precipitation of Boron Nitride in Iron-Boron Alloys", *Trans. Met. Soc. AIME*, **224**, 599–606 (1962) (Experimental, Mechan. Prop., Phase Relations, Thermodyn., 18)

[1964Eva] Evans, D.B., Pehlke, R.D., "The Boron-Nitrogen Equilibrium in Liquid Iron", *Trans. Met. Soc. AIME*, **230**, 1657–1662 (1964) (Experimental, Phase Relations, Thermodyn., 8)

[1964Isa] Isayev, V.F., Morozov, A.N., "Nitrogen Solubility and Nitrides Formation in the Iron-Boron Melts" (in Russian), *Izv. Akad. Nauk SSSR. Metall. i Gorn. Delo*, (2), 13–16 (1964) (Experimental, Phase Relations, Thermodyn., 9)

[1966Yas] Yasinskaya, G.A., "The Wetting of Refractory Carbides, Borides and Nitrides by the Molten Metals", *Sov. Powder Metall. Met. Ceram.*, (7), 557–559 (1966), translated from *Poroshk. Metall.*, (7), 53–56 (1966) (Experimental, Phase Relations, 5)

[1968Sch] Schenck, H., Steinmetz, E., "Chemical Activities of Boron and Nitrogen in the Liquid Phase of the System Iron-Boron-Nitrogen at 1600°C" (in German), *Arch. Eisenhuettenwes.*, **39**(4), 255–257 (1968) (Experimental, Phase Relations, Thermodyn., 12)

[1974Sig] Sigworth, G.K., Elliott, J.F., "The Thermodynamics of Liquid Dilute Iron Alloys", *Met. Sci.*, **8**, 298–310 (1974) (Review, Thermodyn., 249)

[1978Vis] Vishnevskiy, A.S., Delevi, V.G., Mukovoz, Yu.A., Ositinskaya, T.D., Chapalyuk, V.P., "Interaction of the Boron Nitride with Steels and Titanium" (in Russian), *Sintetich. Almazy*, (4), 17–22 (1978) (Experimental, Phase Relations, 4)

[1982Vas] Vasilyev, E.A., Leusenko, A.A., Mazurenko, A.M., Rakitskiy, E.B., Shablovskiy, A.V., "Investigation of the *c*BN Polycrystals Sinthesized from α-BN with Iron Addition Using NMR Method" (in Russian), *Sverkhtverd. Mater.*, (6), 5–7 (1982) (Experimental, Phase Relations, Mechan. Prop., 6)

[1986Smi] Smid, I., Rogl, P., "Phase Equilibria and Structure Chemistry in Ternary Systems: Transition Metal-Boron-Nitrogen", *Inst. Phys. Conf. Series*, **75**(4), 249–259 (1986) (Experimental, Phase Diagram, 17)

[1987Mor] Morita, Z., Tanaka, T., Yanai, T., "Equilibria of Nitride Forming Reactions in Liquid Iron Alloys", *Metall. Trans. B*, **18B**(3), 195–202 (1987) (Review, Phase Relations, Thermodyn., 29)

[1987Rag] Raghavan, V., "The B-Fe-N (Boron-Iron-Nitrogen) System", in "*Phase Diagrams of Ternary Iron Alloys*", **1**, 149–151 (1988) (Review, Phase Diagram, Crys. Structure, Thermodyn., 7)

[1993Rag] Raghavan, V., "B-Fe-N (Boron-Iron-Nitrogen)", *J. Phase Equilib.*, **14**(5), 619–620 (1993) (Review, Phase Diagram, 2)

[1993Wer] Werheit, H., Kuhlmann, U., Laux, M., Lundstrm, T., "Structural and Electronic Properties of Carbon-Doped β-Rhombohedral Boron", *Phys. Status Sol.*, **B179**, 489–511(1993) (Crys. Structure, Experimental, 51)

[1998Liu] Liu, L., Yao, B., Wang, H., Li, F., Ding, B., Su, W., "Formation of ε-Fe_xN/BN Magnetic Nanocomposite and Its Thermodynamic and Kinetic Analyses", *Chin. Sci. Bull.*, **43**(6), 467–470 (1998) (Experimental, Phase Relations, Thermodyn., Kinetics, 10)

[1999Ugl] Uglov, V.V., Fedotova, J.A., Jagielski, J., Gawlik, G., Stanek, J., "Transformation of Amorphous *a*-(Fe-B) Phase During Nitrogen Implantation", *Nucl. Instrum. Methods Phys. Res. B*, **159B**(4), 218–226 (1999) (Experimental, Phase Relations, 12)

[2001War] Warner, T., Liu, C., Fray, D.J., "Synthesis of Boron Nitride from Ferroboron Part I - Nitriding", *Mater. Sci. Technol.*, **17**(9), 1039–1044 (2001) (Experimental, Calculation, Phase Relations, 17)

[2003Fed] Fedotova, J.A., Stanek, J., Shishonok, N.A., Uglov, V.V., "Mössbauer Study of Iron Impurities in Cubic Boron Nitride", *J. Alloys Compd.*, **352**(1–2), 296–303 (2003) (Experimental, Crys. Structure, Phase Relations, Kinetics, 24)

DOI: 10.1007/978-3-540-69761-9_20

[2003Rec] Record, M.Ch., Tedenac, J.-C., "B-N (Boron-Nitrogen)", MSIT Binary Evaluation Program, in *MSIT Workplace*, Effenberg, G. (Ed.), Materials Science International Services, GmbH, Stuttgart; submitted for publication (2003) (Crys. Structure, Phase Diagram, Assessment, 50)

[2003Sue] Sueyoshi, H., Rochman, N.T., Kawano, S., "Damping Capacity and Mechanical Property of Hexagonal Boron Nitride-Dispersed Composite Steel", *J. Alloys Compd.*, **355**, 120–125 (2003) (Experimental, Mechan. Prop., Phys. Prop., 10)

[2004Bok] Bokhonov, B., Korchagin, M., Borisova, Yu., "Formation of Nanosized Particles Encapsulated in Boron Nitride During Low-temperature Annealing of Mechanochemically Treated Fe-BN Mixtures", *J. Alloys Compd.*, **372**(1–2), 141–147 (2004) (Experimental, Phase Relations, Morphology, 24)

[2004Loh] Loh, K.P., Lin, M., Yeadon, M., Boothroyd, C., Hu, Z., "Growth of Boron Nitride Nanotubes and Iron Nanowires from the Liquid Flow of FeB Nanoparticles", *Chem. Phys. Lett.*, **387**(1–3), 40–46 (2004) (Experimental, Phase Relations, Morphology, 22)

[2004Tao] Tao, J.G., Yao, B., Yang, J.H., Zhang, S.J., Zhang, K., Bai, S.Z., Ding, Z.H., Wang, W.R., "Mechanism of Formation of Fe-N Alloy in the Solid-State Reaction Process Between Iron and Boron Nitride", *J. Alloys Compd.*, **384**(1–2), 268–273 (2004) (Experimental, Phase Relations, 20)

[2004Tok] Tokoro, H., Fujii, S., Oku, T., "Iron Fine Particles Coated With Boron Nitride Nanolayers Synthesized by a Solid Phase Reaction", *Diamond Related Mater.*, **13**(4–8), 1139–1143 (2004) (Experimental, Phase Relations, Morphology, 21)

[V-C2] Villars, P. and Calvert, L.D., *Pearson's Handbook of Crystallographic Data for Intermetallic Phases*, 2nd edition, ASM, Metals Park, Ohio (1991)

[Mas2] Massalski, T.B. (Ed.), *Binary Alloy Phase Diagrams*, 2nd edition, ASM International, Metals Park, Ohio (1990)

DOI: 10.1007/978-3-540-69761-9_20

Boron – Iron – Niobium

Peter Rogl

Introduction

The excellent soft-magnetic behavior of nanocrystalline materials "NANOPERM" have attracted interest in B-Fe-Nb base alloys. Information on the B-Fe-Nb system in general is rather scarce, although phase relations have been elucidated for an isothermal section at 800°C revealing the existence of two ternary compounds, $Nb_3Fe_3B_4$ and NbFeB [1967Kuz, 1968Kuz]. Phase relations in the B-Fe-Nb system were reviewed by [1990Kuz].

Binary Systems

Phase equilibria in the B-Fe system were reinvestigated by [1985Smi, 1986Smi] and were summarized in [1992Rog]. A thermodynamic assessment and calculation is from [1994Hal]. A metastable diagram including the metastable compounds Fe_3B (Fe_3C type) and $Fe_{23}B_6$ was presented by [1978Her]. Depending on the rate of quenching a liquid alloy $Fe_{76}B_{24}$, two modifications of Fe_3B, *i.e.* the Fe_3P type and the Ti_3P type, were obtained by [1982Kha] and were claimed to exist as high- and low-temperature compounds, respectively, within a small temperature window of the equilibrium diagram ($1140 < T < 1250$°C). Similarly, the τ phase ($Fe_{23}B_6$) was speculated by [1991Kha] to belong to the equilibrium diagram within a small temperature region $650 \leq T \leq 800$°C. The Fe-Nb system was accepted in the version of [1991Bej, 1993Bej], who proved the Nb_3Fe_2 phase to be metastable. A thermodynamic evaluation of the Fe-Nb system is from [2000Tof]. B-Nb is in the version of [2005Nun, 1998Rog]. A listing of the crystallographic information of all stable and metastable phases pertinent to the B-Fe-Nb system is presented in Table 1, including also ternary solid solution phases.

Solid Phases

From the two hitherto known ternary compounds in the B-Fe-Nb system, $Nb_3Fe_3B_4$ and NbFeB, only the structure of the latter has been evaluated and was found to be isotypic with the ordered ZiNiAl type [1967Kuz, 1968Kuz]. No homogeneity regions were observed for the ternary compounds at 800°C [1968Kuz]. Mutual solid solubilities of iron and niobium borides were indicated to be very small (at least < 1 at.%, [1968Kuz]) except for a large solubility of iron in Nb_3B_2 reaching at 800°C a maximum of 20 at.% Fe [1968Kuz]. In analogy to the B-Fe-Mo system full atom order was postulated for the end point of the solid solution Nb_2FeB_2 in terms of the Mo_2FeB_2 type (ordered U_3Si_2 type) structure [1968Kuz]. For a general discussion of the crystal chemistry of U_3Si_2 type compounds see [2003Luk]. Crystallographic data of all solid phases are collected in Table 2.

Isothermal Sections

Phase relations established by [1968Kuz] at 800°C (see Fig. 1) are characterized by the formation of two ternary compounds, $Nb_3Fe_3B_4$ and NbFeB, and a large solid solution $(Nb_{1-x}Fe_x)_3B_2$ for $0 < x < 0.333$.

Notes on Materials Properties and Applications

Niobium additions are a key constituent in iron-boron based amorphous soft magnets, although Nb reduces somewhat the magnetic ordering temperature. The development of soft magnetic nanocrystalline alloys consisting of fine crystallites (bcc Fe) embedded in an amorphous matrix lead to soft magnetic behavior superior to amorphous alloys in terms of higher magnetization and higher long-term stability of properties. Particularly the nanocrystalline alloy $B_9Fe_{84}Nb_7$ (under the brand NANOPERM") exhibits excellent magnetic behavior (B_s = 1.52 Tesla, H_C = 4.8 $A \cdot m^{-1}$, μ_e = 51000) and is widely used in telecommunication,

DOI: 10.1007/978-3-540-69761-9_21

micro-devices, power electronics, *etc*. As these alloys are in metastable condition their properties are dependent on composition and processing conditions. Therefore many papers deal with the nanocrystallization process of Nb containing metallic glasses as well as with the magnetic behavior [1991Haw, 1991Leu, 1993Suz, 1994Koj, 1994Mak1, 1994Mak2, 1995Mak, 1994Lee, 1995Suz, 1996Yav, 1999McH, 1997Ino, 1997Mak1, 1997Mak2, 1997Mak3, 1997Nai, 1998Nai, 1999Hu, 2000Sko, 2001Caa, 2001Suz, 2002Sko, 2003Chr, 2003Gao, 2004Bit, 2004Sko, 2004Sun, 2004Zhi, 2005Sha, 2005Kar, 2006Lu].
TEM analyses on melt spun B-Fe-Nb ribbons showed nanoscale phase separation into bcc-Fe clusters, boride clusters with prism structure and Fe-Nb polyhedra [2004Hir]. Employing DSC and X-ray diffraction [2001Ima] observed a distinct phase transformation sequence in amorphous ribbons of $B_xFe_{90-x}Nb_{10}$: for $x = 10$ the sequence led from amorphous to αMn type to αFe type to (αFe type + o-Fe_3B + Fe_2B), whilst for $x = 20$, 30 the sequence was: amorphous to supercooled liquid to $Fe_{23}B_6$ type to (αFe type + o-Fe_3B + Fe_2B). A hypothetical free energy diagram was presented.
Niobium additions were furthermore said to markedly increase hardness and tensile strength of B-Fe alloys air-cooled from 950 or 1100°C and water quenched; ductility and toughness of the alloy, however, decreased with Nb additions [1966Has]. A general survey of the effect of concentration and transition metals on crystallization of Fe based amorphous alloys was given by [1987She]. [1980Che] evaluated some key physico-mechanical properties of iron-boride materials alloyed with Nb, Mo, and W.

Miscellaneous

In $B_{24-x}Fe_{76}Nb_x$ alloys a $Cr_{23}C_6$ type phase was identified for $4 \leq x \leq 8$. The phase was observed during heat treatment of the amorphous alloys or by rapid quenching the melts. On heating of the amorphous alloys, this phase crystallizes at about 853 K, prior to decomposition into Fe_2B and a yet unknown phase. From X-ray data one Nb atom per formula unit was said to be randomly sharing the B sites creating an equivalent number of vacancies on the Fe sites. The $Cr_{23}C_6$ type phase is magnetically soft with a coercive field of 2.23 $kA \cdot m^{-1}$ and a saturation magnetization of about 0.16 $Am^2 \cdot g^{-1}$; $T_C = 823$ K. The heat of crystallization is found to be about 3.43 $kJ \cdot (g\text{-atom})^{-1}$ [1991Haw].

Table 1. Investigations of the B-Fe-Nb Phase Relations, Structures and Thermodynamics

Reference	Method/Experimental Technique	Temperature/Composition/ Phase Range Studied
[1967Kuz]	XPD on powder compacts arc melted under argon (< 50at.% B) or sintered in vacuum at 1500°C for 10 h (> 50 at.% B). The arc melted samples were annealed in vacuum at 1300°C for 5 h followed by slow cooling (50°C·h^{-1}) to 1000°C. All specimens were sealed in quartz capsules and annealed at 800°C for 40 h and quenched. Microscopic analyses.	Phase equilibria in an isothermal section at 800°C
[1968Kuz]	Single crystal study of NbFeB. Single crystals were obtained by mechanical fragmentation from alloy $Nb_{25}Fe_{55}B_{20}$	Determination of the structure of NbFeB

DOI: 10.1007/978-3-540-69761-9_21

Table 2. Crystallographic Data of Solid Phases

Phase/ Temperature Range [°C]	Pearson Symbol/ Space Group/ Prototype	Lattice Parameters [pm]	Comments/References
(δFe) 1538 - 1394	*cI*2 $Im\bar{3}m$ W	a = 293.15	[Mas2] dissolves 3.27 at.% Nb at 1370°C [1993Bej]
(γFe) 1394 - 912	*cF*4 $Fm\bar{3}m$ Cu	a = 364.67 a = 357.3	[Mas2] at 25°C [V-C2]
(αFe) < 912 $Fe_{1-x}B_x$	*cI*2 $Im\bar{3}m$ W	a = 286.65 a = 286.0	[Mas2] at x = 0.09 [V-C2]
(Nb) < 3422	*cI*2 $Im\bar{3}m$ W	a = 316.552	[Mas2] dissolves 7 at.% Fe at 1500°C [1993Bej]
(βB) < 2092	*hR*333 $R\bar{3}m$ βB	a = 1093.30 c = 2382.52 a = 1095.14 c = 2386.1 a = 1097.18 c = 2387.05	[1993Wer] at $FeB_{\sim 49}$ [V-C2] at $FeB_{\sim 20}$ [V-C2]
$NbFe_2$ < 1630	*hR*12 $P6_3/mmc$ $MgZn_2$	 a = 484.5 c = 789.3	32 to 37 at.% Nb [1993Bej] [V-C2]
$Nb_{19}Fe_{21}$ < 1520	*hR*39 $R\bar{3}m$ W_6Fe_7	a = 492.6 c = 2680	48 to 52 at.% Nb [1993Bej] [V-C2]
FeB < 1588	*oP*8 *Pnma* FeB	a = 550.6 b = 295.2 c = 406.1	[1992Rog]
Fe_2B < 1407	*tI*12 *I*4/*mcm* $CuAl_2$	a = 510.9 c = 424.9	[1992Rog]
$Fe_3B(h_1)$ ~1250 - ~1150	*tI*32 $I\bar{4}$ Fe_3P	a = 865.5 c = 429.7	metastable [1992Rog]
$Fe_3B(h_2)$ ~1220 - ~1140	*tP*32 $P4_2/n$ Ti_3P	a = 864.8 c = 431.4	metastable [1992Rog]

(*continued*)

DOI: 10.1007/978-3-540-69761-9_21

Phase/ Temperature Range [°C]	Pearson Symbol/ Space Group/ Prototype	Lattice Parameters [pm]	Comments/References
Fe_3B < 1214	*oP*16 *Pnma* Fe_3C	*a* = 542.8 *b* = 666.9 *c* = 443.9	metastable [1992Rog]
$Fe_{23}B_6$ ~ 800 - ~ 650 B-Fe-Nb	*cF*116 $Fm\bar{3}m$ $Cr_{23}C_6$	*a* = 1076 *a* = 10819	[1991Kha] metastable in amorphous alloys $Nb_xFe_{76}B_{24-x}$ ($4 < x < 8$) [1991Haw]
Nb_3B_2 < 2080	*tP*10 *P4/mbm*	*a* = 619.79 *c* = 329.26	[1992Rog] oxygen stabilized? [1985Zak]
$(Nb_{1-x}Fe_x)_3B_2$	? U_3Si_2	-	$0 < x < 0.333$ at 800°C [1968Kuz]
NbB < 2917	*oC*8 *Cmcm* CrB	*a* = 329.74 *b* = 872.38 *c* = 316.69	[1992Rog]
		a = 330.2 *b* = 875.5 *c* = 316.8	as cast, at 32.9 at.% B [1985Zak]
		a = 330.0 *b* = 873.3 *c* = 316.6	at 32.9 at.% B, 25 h at 1950°C [1985Zak]
		a = 329.61 *b* = 872.24 *c* = 316.53	[1991Oka]
Nb_5B_6 < 2870	*oC*22 *Cmmm* V_5B_6	*a* = 315.30 *b* = 2274.4 *c* = 330.49	[1992Rog]
		a = 315.67 *b* = 2276.7 *c* = 330.34	[1991Oka]
Nb_3B_4 < 2935	*oI*14 *Immm* Ta_3B_4	*a* = 314.51 *b* = 1410.62 *c* = 330.19	[1992Rog]
		a = 314.28 *b* = 1407.6 *c* = 330.33	[1991Oka]
Nb_2B_3	*oC*20 *Cmcm* V_2B_3	*a* = 330.58 *b* = 1948.1 *c* = 312.93	[1991Oka]

(*continued*)

DOI: 10.1007/978-3-540-69761-9_21

Phase/ Temperature Range [°C]	Pearson Symbol/ Space Group/ Prototype	Lattice Parameters [pm]	Comments/References
NbB_2 < 3036	*hP*3 *P6/mmm* AlB_2	*a* = 311.11 *a* = 326.27	65 to 70 at.% B Nb rich at 1800°C [2005Nun]
		a = 308.53 *c* = 330.72	B rich at 1800°C [2005Nun]
		a = 311.15 *c* = 326.57	Nb rich [1991Oka]
		a = 310.37 *c* = 332.37	B rich [1991Oka]
		a = 311.2 *c* = 327.0	at 227°C [V-C2]
		a = 312.3 *c* = 329.0	at 727°C [V-C2]
		a = 314.0 *c* = 331.5	at 1227°C [V-C2]
		a = 309.5 *c* = 330.0	NbB_2, quenched from 3000°C See [1992Rog]
*τ_1, NbFeB	*hP*9 $P\bar{6}2m$ ordered Fe_2P (ZrNiAl-type)	*a* = 601.5 *c* = 322.2	[1967Kuz] $\rho_{exp.}$ = 7.84 $Mg \cdot m^{-3}$
*τ_2, $Nb_3Fe_3B_4$	unknown	-	[1968Kuz]

DOI: 10.1007/978-3-540-69761-9_21

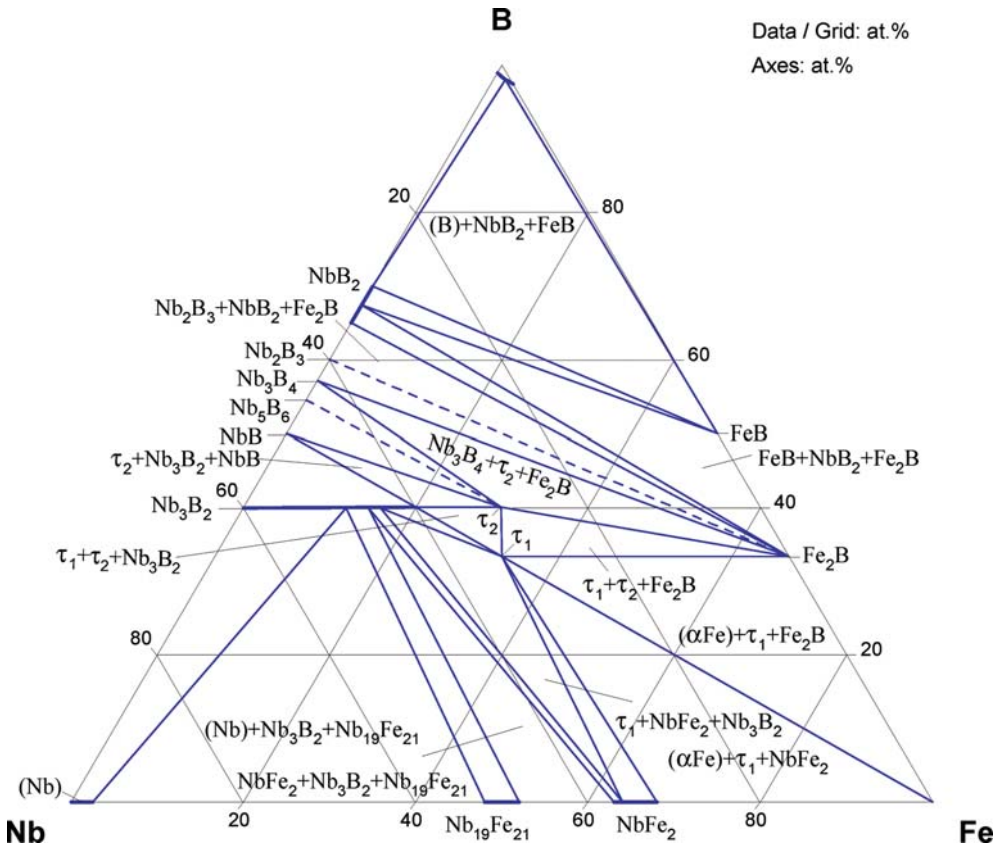

Fig. 1. B-Fe-Nb. Isothermal section at 800°C

DOI: 10.1007/978-3-540-69761-9_21

References

[1966Has] Hasegawa, M., Okamoto, M., "A Study on the Ternary Alloys of Iron and Boron" (in Japanese), *Nippon Kinzoku Gakkai-Si*, **30**(6), 533–540 (1966) (Experimental, Mechan. Prop., Morphology, Phase Relations, 12)

[1967Kuz] Kuzma, Y.B., "Crystal Structures of NbFeB and TaFeB Compounds", *Dop. Akad. Nauk Ukr. RSR, A.*, **A10**, 939–940 (1967) (Crys. Structure, 3)

[1968Kuz] Kuz'ma, Yu.B., Ts'olkovskii, T.I., Baburova, O.P., "The Systems Nb-Fe-B and Nb-Co-B", *Inorg. Mater. (Engl. Trans.)*, **4**(7), 950–953 (1968), translated *from Izv. Akad. Nauk SSSR, Neorg. Mater.*, **4**(7), 1081–1085 (1968) (Crys. Structure, Phase Relations, 19)

[1978Her] Herold, U., Köster, U., "Metastable Phases in Extremly Fast Solidified Iron-Boron Alloys" (in German), *Z. Metallkd.*, **69**(5), 326–332 (1978) (Experimental, Phase Diagram, Crys. Structure, 27)

[1980Che] Chernienko, V.V., Martyukhin, I.D., "Effect of Niobium, Molybdenum, and Tungsten on Some Properties of Iron-Boride Materials", *Sov. Powder Metall. Met.Ceram.*, **19**(2), 135–138 (1980) (Experimental, 5)

[1982Kha] Khan, Y., Kneller, E., Sostarich, M., "The Phase Fe_3B", *Z. Metallkd.*, **73**(10), 624–626 (1982) (Experimental, Crys. Structure, Phase Diagram, 13)

[1985Smi] Smid, I., Rogl, P., "Phase Equilibria and Structural Chemistry in Ternary Systems: Transition Metal - Boron - Nitrogen", *Proceedings of the 11th Intl. Plansee Seminar*, **Vol. 2**, Bildstein, H., Ortner, H., (Eds.), Verlag Tyrolia, Innsbruck, Austria, 1029–1035 (1985) (Experimental, Crys. Structure, Phase Diagram, 17)

[1985Zak] Zakharov, A.M., Pshokin, V.P., Ivanova, E.I., "Niobium Corner of the System Nb-B-C", *Russ. Metall*, **5**, 192–195 (1985) (Experimental, Crys. Structure, Phase Relations, 10)

[1986Smi] Smid, I., Rogl, P., "Phase Equilibria and Structural Chemistry in Ternary Systems: Transition Metal - Boron - Nitrogen", *Inst. Phys. Conf. Ser.* No. 75, Ch. 4, Adam Hilger Ltd., 249–257 (1986) (Experimental, Crys. Structure, Phase Relations, 17)

[1987She] Shen Bao Gen, Zhan Wen Shan, Zhao Jian Gao, Chen Jinchang, Pan Xiao Shuo, "Effect of Concentration and Transition Metals on Crystallization of Fe-based Amorphous Alloys", *Acta Metall. Sin.*, **23**(5) 220–226 (1987) (Experimental, Magn. Prop., 12)

[1990Kuz] Kuz'ma, Yu.B., Chaban, N.F., "Binary and Ternary Systems which Contain Boron" (in Russian), *Metallurgia*, Moscow, 316 (1990) (Review, Crys. Structure, Phase Relations, 5)

[1991Bej] Bejarano, J.M.Z., Gama, S., Ribeiro, C.A., Effenberg, G., Santos, G., "On the Existence of the Fe_2Nb_3 Phase in the Fe-Nb System", *Z. Metallkd.*, **82**, 615–620 (1991) (Experimental, Phase Diagram, Phase Relations, 7)

[1991Haw] Hawig, R., Khan, Y., Wibbeke, H., "Magnetic, Electrical Properties and Crystallization Behaviour of Amorphous $Nb_xFe_{76}B_{24-x}$ Alloys", *Z. Metallkd.*, **82**(8), 646–649 (1991) (Experimental, Kinetics, 8)

[1991Kha] Khan, Y., Wibbeke, H., "Formation of the τ-Phase in Fe-B Alloys", *Z. Metallkd.*, **82**(9), 703–705 (1991) (Experimental, Crys. Structure, 6)

[1991Leu] Leu, M.S., Lin, C.S., Lin, S.T., "The Determination of Curie-temperature of Amorphous Fe-Nb-B Alloys by DSC under Magnetic-Field", *Scr. Metall. Mater.*, **25**(3), 637–640 (1991) (Experimental, Magn. Prop., 6)

[1991Oka] Okada, S., Hamano, K., Lundstrom, T., Higashi, I., "Crystal Growth of the New Compound Nb_2B_3, and the Borides NbB, Nb_5B_6, Nb_3B_4, and NbB_2, Using the Copper-Flux Method", *AIP Conference Proceedings 231 on Boron-Rich Solids*, Emin, D., *et al.* (Eds.), Albuquerque, USA, 1990, New York (NY) AIP, 456–459 (1991) (Experimntal, Crys. Structure, 12)

[1992Rog] Rogl, P., "The System B-N-Fe" in "*Phase Diagrams of Ternary Boron Nitride and Silicon Nitride Systems*", Rogl, P., Schuster, J.C., (Eds.), ASM, Materials Park, OH 33–36 (1992) (Crys. Structure, Thermodyn., Phase Relations, Experimental, Review, 9)

[1993Bej] Bejarano, J.M.Z., Gama, S., Ribeiro, C.A., Effenberg, G., "The Fe-Nb Phase Diagram", *Z. Metallkd.*, **84**, 160–164 (1993) (Experimental, Phase Diagram, Phase Relations, 6)

DOI: 10.1007/978-3-540-69761-9_21

[1993Suz] Suzuki, K., Makino, A., Inoue, A., Masumoto, T., "Low Core Losses of Nanocrystalline Fe-M-B (M = Zr, Hf, or Nb) Alloys", *J. Appl. Phys*., **74**(5), 3316–22 (1993) (Experimental, Magn. Prop., 12)

[1993Wer] Werheit, H., Kuhlmann, U., Laux, M., Lundstroem, T., "Structural and Electronic Properties of Carbon-Doped β-Rhombohedral Boron", *Phys. Stat. Sol*., **B179**, 489–511 (1993) (Crys. Structure, Experimental, 51)

[1994Hal] Hallemans, B., Wollants, P., Roos, J.R., "Thermodynamic Reassessment and Calculation of the Fe-B Phase Diagram", *Z. Metallkd.*, **85**(10), 676–82 (1994) (Calculation, Phase Relations, Thermodyn., Phase Diagram, 21)

[1994Koj] Kojima, A., Horikiri, H., Kawamura, Y., Makino, A., Inoue, A., Masumoto, T., "Magnetic Properties of Extruded Nanocrystalline Fe-Nb-B Alloys", *IEEE Trans. J. Magn. Japan*, **9**(6), 47–54 (1994) (Experimental, Magn. Prop., 13)

[1994Koj] Kojima, A., Horikiri, H., Kawamura, Y., Makino, A., Inoue, A., Masumoto, T., "Production of Nanocrystalline bcc Fe-Nb-B Bulk Alloys by Warm Extrusion and Their Magnetic Properties", *Mater. Sci. Eng. A - Stuctural Materials properties Microstructure & Processing*, **179**, 511–515 (1994) (Experimental, Magn. prop., 12)

[1994Lee] Joong Seon Lee, Kwang Youn Kim, Tae-Hwan Noh, Il Koo Kang, Yeon Chul Yoo., "The Crystallization Behavior and Magnetic Properties of Fe-B-Nb Amorphous Alloys", *J. Korean Inst. Met. Mater.*, **32**(8), 999–1005 (1994) (Experimental, Magn. Prop., 11)

[1994Mak1] Makino, A., Yoshida, S., "Microstructure and Magnetic Properties of Nanocrystalline bcc Fe-Nb-B Soft Magnetic Alloys", *IEEE Trans. Magn*., **30**(6 Part 1) 4848–4850 (1994) (Experimental, Magn. Prop., 10)

[1994Mak2] Makino, A., Suzuki, K., Inoue, A., Masumoto, T., "Magnetic Properties and Core Losses of Nanocrystalline Fe-M-B (M-Equivalent-to-Zr, Hf or Nb) Alloys", *Mater. Sci. Eng. A-Struct. Mater. Prop. Microstruct. Proces.*, **179**, 127–131 (1994) (Experimental, Magn. Prop., 9)

[1995Mak] Makino, A., Inoue, A., Masumoto, T., "Soft Magnetic Properties of Nanocrystalline Fe-M-B (M = Zr, Hf, Nb) Alloys With High Magnetization", *Nanostruct. Mater.*, **6**(5–8), 985–988 (1995) (Experimental, Magn. Prop., 8)

[1995Suz] Suzuki, K., Cadogan, J.M., Dunlop, J.B., Sahajwalla, V., "Two-Stage Nanostructural Formation Process in Fe-Nb-B Soft Magnetic Alloys", *Appl. Phys. Lett*., **67**(10), 1369–1371 (1995) (Experimental, Magn. Prop., 11)

[1996Yav] Yavari, A.R., Drbohlav, O., "Mechanisms of Nanocrystallization of Fe- and Al-Based Amorphous Precursors", *Mater. Sci. Forum*, **225–227**, 295–304 (1996) (Crys. Structure, Experimental, Mechan. Prop., 40)

[1997Ino] Inoue, A., Makino, A., "Improvement of Soft Magnetic Properties of Nanocrystalline Fe-M-B (M = Zr and Nb) Alloys and Their Applications", *Nanostruct. Mater.*, **9**(1–8), 403–412 (1997) (Experimental, Magn. Prop., 11)

[1997Mak1] Makino, A., Hatanai, T., Naitoh, Y., Bitoh, T., Inoue, A., Masumoto, T., "Applications of Nanocrystalline Soft Magnetic Fe-M-B (M = Zr, Nb) Alloys, NANOPERM(R)", *IEEE Trans. Magn*., **33**(5), pt.2, 3793–3798 (1997) (Experimental, Magn. Prop., 10)

[1997Mak2] Makino, A., Hatanai, T., Inoue, A., Masumoto, T., "Nanocrystalline Soft Magnetic Fe-M-B (M = Zr, Hf, Nb) Alloys and Their Applications", *Mater. Sci. Eng. A*, **A226–228**, 594–602 (1997) (Experimental, Magn. Prop., 31)

[1997Mak3] Makino, A., Yoshida, S., Inoue, A., Masumoto, T., "Magnetic Properties and Low Core Losses of Nanocrystalline Fe-M-B (M = Zr, Hf or Nb) Alloys", *New Horizons for Materials*, Proc. General Sect. Forum New Mater. 8th CIMTEC-World Ceramics Congress and Forum on New Materials, TECHNA, Faenza, Italy, 377–384 (1995) (Experimental, Magn. Prop., 11)

[1997Nai] Naitoh, Y., Bitoh, T., Hatanai, T., Makino, A., Inoue, A., Masumoto, T., "Applications of Nanocrystalline Soft Magnetic Fe-M-B (M = Zr, Nb) Alloys", *Nanostruct. Mater.*, **8**(8), 987–995 (1997) (Experimental, Magn. Prop., 7)

DOI: 10.1007/978-3-540-69761-9_21

[1998Nai] Naitoh, Y., Bitoh, T., Hatanai, T., Makino, A., Inoue, A., "Application of Nanocrystalline Soft Magnetic Fe-M-B (M = Zr, Nb) Alloys to Choke Coils", *J. Appl. Phys*., **83**(11), 6332–6334 (1998) (Experimental, Magn. Prop., 6)

[1998Rog] Rogl, P., "Niobium-Boron-Carbon", in "*Phase Diagrams of Ternary Metal-Boron-Carbon Systems*", Effenberg, G., (Ed.), ASM-Intl, MSI, 197–213 (1998) (Review, Crys. Structure, Experimental, Phase Diagram, 25)

[1999Hu] Hu, J.F., Zhou, S.X., Chen, W.Z., Wang, Y.Z., "Giant Magnetoimpedance Effect in Fe-Nb-B Ribbon", *Solid State Communications*, **109**(10), 661–664 (1999) (Experimental, Magn. Prop., 8)

[1999McH] McHenry, M.E., Willard, M.A., Laughlin, D.E., "Amorphous and Nanocrystalline Materials for Applications as Soft Magnets", *Prog. Mater. Sci.*, **44**(4), 291–433 (1999) (Crys. Structure, Electr. Prop., Experimental, Magn. Prop., Phase Relations, Review, 302)

[2000Sko] Skorvanek, I., Duhaj, P., Groessinger, R., "Low-temperature Magnetic Behaviour in Amorphous and Nanocrystalline Fe-Nb-B Alloys", *J. Magn. Magn. Mater.*, **215–216**, 431–433 (2000) (Experimental, Magn. Prop., 12)

[2000Tof] Toffolon, C., Servant C., "Thermodynamic Assessment of the Fe-Nb System", *Calphad*, **24**(2), 97–112 (2000) (Thermodyn., Phase Diagram, Review, 40)

[2001Caa] Caamano, Z., Dolidze, T., Surinach, S., Baro, M.D., Munoz, J.S., "Nanocrystallization Behaviour of $Fe_{82}Nb_6B_{12}$ Alloy", *Mater. Sci. Eng. A*, **304–306**, 296–299 (2001) (Crys. Structure, Experimental, 17)

[2001Ima] Imafuku, M., Sato, S., Koshiba, H., Matsubara, E., Inoue, A., "Structural Variation of Fe-Nb-B Metallic Glasses During Crystallization Process", *Scr. Mater.*, **44**(8–9), 2369–2372 (2001) (Crys. Structure, Experimental, Phase Relations, 6)

[2001Suz] Suzuki, K., Cadogan, J.M., Aoki, K., Tsai, A.P., Inoue, A., Masumoto, T., "Nanocrystallization and Glass Transition in Cu-free Fe-Nb-B Soft Magnetic Alloys", *Scr. Mater.*, **44**(8–9), 1417–1420 (2001) (Experimental, Thermodyn., 7)

[2002Sko] Skorvanek, I., Svec, P., Greneche, J.-M., Kovac, J., Marcin, J., Gerling, R., "Influence of Microstructure on the Magnetic and Machanical Behaviour of Amorphous and Nanocrystalline FeNbB Alloy", *J. Phys.: Condens. Matter*, **14**(18), 4717–4736 (2002) (Crys. Structure, Experimental, Magn. Prop., Mechan. Prop., Morphology, Phys. Prop., 42)

[2003Gao] Gao, Y., Shindo, D., Bitoh, T., Makino, A., "Mediated Exchange Interaction in Fe-Nb-B Nanocrystalline Soft Magnetic Materials", *Phys. Rev. B: Condens. Matter*, **67**, 172409 (2003) (Experimental, Magn. Prop., Morphology, 21)

[2003Chr] Chrobak, A., Haneczok, G., Stoklosa, Z., Kwapulinski, P., Rasek, J., Chelkowska, G., "Magnetic Properties of $Fe_{76}X_2B_{22}$ (X = Cr, Zr, Nb) Amorphous Alloys", *Phys. Status Solidi A*, **196**(1), 248–251 (2003) (Experimental, Magn. Prop., 7)

[2003Luk] Lukachuk, M., Poettgen, R., "Intermetallic Compounds with Ordered U_3Si_2 or Zr_3Al_2 Type Structure - Crystal Chemistry, Chemical Bonding and Physical Properties", *Z. Kristallogr.*, **218**, 767–787 (2003) (Crys. Structure, Electr. Prop., Magn. Prop., Review, Thermodyn., 197)

[2004Bit] Bitoh, T., Makino, A., Inoue, A., "The Effect of Grain-size Distribution on Coercivity in Nanocrystalline Soft Magnetic Alloys", *J. Magn. Magn. Mater.*, **272–276**(2), 1445–1446 (2004) (Calculation, Morphology, 7)

[2004Hir] Hirotsu, Y., Hanada, T., Ohkubo, T., Makino, A., Yoshizawa, Y., Nieh, T.G., "Nanoscale Phase Separation in Metallic Glasses Studied by Advanced Electron Microscopy Techniques", *Intermetallics*, **12**(10–11), 1081–1088 (2004) (Calculation, Crys. Structure, Experimental, Morphology, 18)

[2004Sko] Skorvanek, I., Kovac, J., Koetzler, J.J., "Temperature Evolution of Coercive Field and Thermal Relaxation Effects in Nanocrystalline FeNbB Alloys", *J. Magn. Magn. Mater.*, **272–276**(2), 1503–1505 (2004) (Experimental, Kinetics, Magn. Prop., Morphology, Phase Relations, 6)

[2004Sun] Sunol, J.J., Gonzalez, A., Saurina, J., Escoda, L., Bruna, P., "Thermal and Structural Characterization of Fe-Nb-B Alloys Prepared by Mechanical Alloying", *Mater. Sci. Eng. A*, **375–377**, 874–880 (2004) (Crys. Structure, Experimental, Magn. Prop., Phase Relations, 29)

DOI: 10.1007/978-3-540-69761-9_21

[2004Zhi] Zhi Qi-Zheng, Wang Ji-Jie, Chen Wen-Zhi, He Kai-Yuan., "Structure and Magnetic Properties of Nanocrystalline Fe-Nb-B Alloys", *J. Northeastern Univ. Technol. (Natur. Sci.)*, **25**(11), 1072–1075 (2004) (Experimental, Magn. Prop., 10)

[2005Kar] Karolus, M., Kwapulinski, P., Chrobak, D., Haneczok, G., Chrobak, A., "Crystallization in $Fe_{76}X_2B_{22}$ (X = Cr, Zr, Nb) Amorphous Alloys", *J. Mat. Proc. Tech.*, **162–163**, 203–208 (2005) (Crys. Structure, Electr. Prop., Experimental, Phase Relations, 11)

[2005Nun] Nunes, C.A., Kaczorowski, D., Rogl, P., Baldissera, M.R., Suzuki, P.A., Coelho, G.C., Grytsiv, A., André, G., Boureé, F., Okada, S., "The NbB_2-phase Revisited: Homogeneity Range, Defect Structure, Superconductivity", *Acta Mater.*, **53**, 3679–3687 (2005) (Phase Relations, Crys. Structure, Magn. Prop., Experimental, 33)

[2005Sha] Shalyguina, E.E., Molokanov, V.V., Komarova, M.A., Melnikov, V.A., Abrosimova, N.M., "Inverted Near-Surface Hysteresis Loops in Annealed $Fe_{80.5}Nb_7B_{12.5}$ Ribbons", *J. Magn. Magn. Mater.*, **290–291**(2), 1438–1441 (2005) (Experimental, Magn. Prop., Morphology, Phase Relations, 24)

[2006Lu] Lu, W., Yang, L., Yan, B., Huang, W.-h., Lu, B., "Nanocrystalline $Fe_{84}Nb_7B_9$ Alloys Prepared by Mechanical Alloying and Ultra-High-Pressure Consolidation", *J. Alloys Compd.*, **413**(1–2), 85–89 (2006) (Crys. Structure, Experimental, Magn. Prop., Morphology, 21)

[V-C2] Villars, P. and Calvert, L.D., *Pearson's Handbook of Crystallographic Data for Intermetallic Phases*, 2nd edition, ASM, Metals Park, Ohio (1991)

[Mas2] Massalski, T.B. (Ed.), *Binary Alloy Phase Diagrams*, 2nd edition, ASM International, Metals Park, Ohio (1990)

DOI: 10.1007/978-3-540-69761-9_21

Boron – Iron – Neodymium

Annelies Malfliet, Gabriele Cacciamani, Nathalie Lebrun, Peter Rogl

Introduction

Partial liquidus surfaces have been extensively studied up to 40 at.% B [1985Mat, 1987Tsa, 1992Rag, 1994Kno], in the Fe [1986Sch, 1987Hen] and in the Nd [1991Lan1, 1991Lan2] rich corners. Discrepancies were observed on the sequence of the ternary reactions as well as on the compositions and the homogeneity ranges of the τ_1, Nd_2B_5, NdB_4, τ_2 and τ_3 phases.
Several experimental investigations have been carried out on isothermal and polythermal B-Fe-Nd sections [1986Bus1, 1986Bus2, 1986Che, 1986Sch, 1987Tsa, 1990Hao, 1991Lan3, 1994Kno]. Samples were generally prepared by arc melting the pure elements and/or a B-Fe master alloy under an inert atmosphere. After annealing in Ta containers at an appropriate temperature samples were investigated by classical methods (DTA, LOM, SEM). In a few cases diffusion couples technique was used.
A thermodynamic modelling and assessment of the system was performed by [1995Hal]: this was very helpful in discussing discrepancies and contradictions present between the different experimental results.
[1992Rag] first reviewed the ternary system B-Fe-Nd. Later, due to the new data of [1994Kno] and [1995Hal] a reassessment has been done in [2003Rag].
Table 1 included all experimental data on phase equilibria, crystal structure and thermodynamics.

Binary Systems

The Fe-Nd system is taken from a thermodynamic calculation done by [1993Hen].
After [Mas2], two thermodynamic optimizations of the B-Fe system were carried out by [1994Hal] and [2002Rom]. Agreements were observed except for the temperature of the eutectic reaction L $\rightleftharpoons$ (γFe) + Fe_2B which was found to be 20°C lower in the CALPHAD assessment of [2002Rom]. Recent thermodynamic experimental work of [2003Zai] confirmed the eutectic temperature found by [1994Hal] using a least-square optimization. The equilibrium phase diagram was then accepted from [1994Hal] with slight modification concerning the melting temperature of pure boron. It has been estimated to be 2092°C instead of 2075°C.
The B-Nd system was reassessed by [1996Lia, 1995Hal]. Disagreements were observed concerning the peritectic reaction L + NdB_4 $\rightleftharpoons$ Nd_2B_5. The assessed temperature of [1996Lia] has been lower (1350°C) than the experimental one (2000°C) measured by [1976Spe] whereas the calculated temperature reported by [1995Hal] was found higher (2113°C). Moreover, these two new phase diagrams proposed after [Mas2] suggest a strange shape of the liquidus curve. [1996Lia] estimated the liquidus curve from results on the B-Sm system. The liquidus curve proposed by [1995Hal] led to a non reliable miscibility gap. Consequently, these two new phase diagrams were not retained and the one suggested by [Mas2] was accepted in this assessment.

Solid Phases

Ternary phase equilibria show three ternary compounds, which all seem to exist at fixed compositions without significant homogeneity regions: τ_1-$Nd_2Fe_{14}B$, τ_2-$Nd_{1.11}Fe_4B_4$ and τ_3-$Nd_5Fe_2B_6$. The crystal structures of these three phases have all been carefully elucidated (see Table 2). Detailed investigation of the crystal and magnetic structure of τ_1-$Nd_2Fe_{14}B$ by means of single crystal X-ray and neutron diffraction [1996Wol, 1996Obb, 2001Wol] showed that the diffraction data at room temperature (RT) were essentially compatible with the tetragonal symmetry $P4_2/mnm$ as a good approximation: at RT the magnetic structure is collinear with the resulting magnetization parallel to the *c*-axis. Below T_{SR} = 140 K a spin reorientation occurs tilting the easy axis from the *c*-axis, the neodymium moments no longer being confined to the (110) plane and at 20 K the resulting magnetism deviates by 32.3° from the pseudo-tetragonal axis. With respect to the high magnetostrictive forces observed, the crystal symmetry lowers from tetragonal $P4_2/mnm$ to monoclinic *Cm*: this crystal and magnetic symmetry lowering is accompanied with a change

DOI: 10.1007/978-3-540-69761-9_22

in the systematic extinctions already observable at RT but becomes severe below T_{SR} = 140 K. From a high-energy synchrotron powder diffraction study, the magnetostriction effect in $Nd_2Fe_{14}B$ was monitored via the unit cell parameters as a function of temperature (10 < T < 1000 K): a large Invar effect is visible on both lattice parameters at about 10-15 K above T_C [2005Yan].
The incommensurate crystal structure of τ_2 $Nd_{1.11}Fe_4B_4$ as an interpenetration of two substructures consisting of (i) a three-dimensional framework of edge-sharing Fe-tetrahedra and B-B pairs and (ii) infinite chains of rare earth atoms along the c-axis, has been also treated in terms of a four-dimensional superspace group P^{Cmma} [1999Zha].
Besides these equilibrium compounds, the occurrence of a series of metastable phases during diversified solidification techniques was reported by various authors; an attempt to cover all these phases is made in Table 2. Although no doubt exists on the peritectic formation of the hard magnetic phase τ_1-$Nd_2Fe_{14}B$, DTA experiments on the solidification of τ_1 revealed the existence of a presumably metastable phase in the temperature range of about 1100 to 1130°C, for which an approximate formula of $Nd_2Fe_{17}B_{\sim1}$ was attributed and which on cooling was said to decompose in (γFe) + τ_1 [1987Sch, 2002Sta]. Metastable $Nd_2Fe_{17}B_{\sim1}$ was confirmed via in situ synchrotron diffraction during solidification of an electromagnetically levitated $Nd_{14}Fe_{79}B_7$ alloy [2001Gao1, 2001Gao2, 2002Vol, 2003Gao, 2004Vol1, 2004Vol2]. The diffraction spectra were indexed on a rhombohedral lattice (a = 864.7, c = 1255.5 pm) and isotypism with the Th_2Zn_{17} type structure ($Nd_2Fe_{17}B_{\sim1}$ similar to $Nd_2Fe_{17}C_x$) was proposed [1987Sch, 2004Vol1, 2004Vol2]. Undercooling and solidification of bulk $Nd_{15.5}Fe_{77.5}B_{7.5}$ alloy droplets showed that the primary phase for solidification changed from (γFe) to $Nd_2Fe_{14}B$ to metastable $Nd_2Fe_{17}B_x$ with increasing undercooling level: the critical undercoolings were determined to be 40 K and 50 K for $Nd_2Fe_{14}B$ and $Nd_2Fe_{17}B_x$ respectively [2002Gao]. However, the X-ray spectra of the small particles were indexed on a hexagonal lattice (a = 496, c = 416 pm) different from the Th_2Zn_{17} type [2001Gao1, 2001Gao2]. It shall be noted that the X-ray pattern of another metastable hexagonal phase found in melt-spun alloys shows the $TbCu_7$ type as a disordered version of the Th_2Zn_{17} type structure [1996Gab, 2004Vol1, 2004Vol2]. The $TbCu_7$ type phase containing boron was also observed in melt spun ribbons $Nd_9Fe_{91-x}B_x$ (0 < x < 9), annealed for 10 min at temperatures from 500 to 780°C [1996Gab].
τ_4 $Nd_2Fe_{23}B_3$ was prepared from melt-spun ribbons and characterized by X-ray powder diffraction (unique structure type, R_F = 0.10) [1986DeM]. Differential scanning calorimetry data for this composition showed a strong exothermic effect on heating (20 $K \cdot s^{-1}$) at 908 K, which was attributed to the crystallization of the amorphous alloy. The characteristic X-ray peaks of this phase disappear on heating the alloy to temperatures T > 1013 K under decomposition of the phase into mainly (αFe) and τ_2-$Nd_{1.11}Fe_4B_4$. These observations were confirmed by [1994Gu], who isolated a single phase labelled "$Nd_6Fe_{77}B_{17}$" after recrystallization of rapidly quenched alloys (DTA peak at 904 K) and claimed isotypism from a simple comparison of the X-ray spectrum with the one of τ_4-$Nd_2Fe_{23}B_3$ (no lattice parameter given!). The τ_4 phase was also reported in rapidly quenched alloys $Nd_6Fe_{74}B_{20}$, which were reheated at 10°C·min^{-1} up to 920 K [1991Kim]. Differential scanning calorimetry (DSC) for an alloy slightly richer in boron, $Nd_2Fe_{23}B_5$, revealed a second exothermic peak on heating (20 $K \cdot s^{-1}$) at 968 K, which was attributed to the crystallization of the a second phase (not specified) [1986DeM]. The authors of [1986Bus1, 1986Bus2] made it likely, that the crystal structure of this second phase corresponds to the $SrNi_{12}B_6$ type. Close to the phase τ_4-$Nd_2Fe_{23}B_3$ a so-called M phase (τ_5) was identified upon crystallization of melt-spun alloys in a single-phase region with 82.8-85.5 at.% Fe and a B/Nd ratio between 2.3 and 3 [1988Alt]. All diffraction peaks were indexed on the basis of a cubic body centred cell (a = 1237.7 pm), the absence of extinctions for reflections (hkl), however, indicates that there is no isotypism with bcc-τ_4 [1988Alt]. A DSC-scan (40 $K \cdot s^{-1}$) for amorphous "$Nd_{4.4}Fe_{84.4}B_{11}$" revealed a (ferro)-magnetic ordering temperature T_C = 466 K (the true ordering temperature T_C = 584 K was found from a second DSC-run), a first crystallization at 852 K (formation of the τ_5 phase with ΔE = 3.3 kJ·mol^{-1}) and a second exothermic peak on heating at 975 K, which was attributed to the decomposition of the τ_5 phase into mainly (αFe) and τ_2-$Nd_2Fe_{14}B$, $NdFe_{12}B_6$ [1988Alt].
Two bcc superstructures to a simple A_2 type structure ($a = n \cdot a_0$, n = 2,4) were obtained either by quenching melts (moderate cooling rates, 30m·s^{-1})) or by crystallizing melt spun ribbons of composition $Nd_{2-x}Fe_{14}B$ (0 < x < 1) at 875 K for 10 min [1993Kha]. These materials were soft magnetic with Curie temperatures 400 to 600 K. The phases were said to decompose above 900-1000 K [1993Kha] into (αFe) and τ_1 $Nd_2Fe_{14}B$. At higher temperatures, the products of decomposition were (αFe) and a new tetragonal phase was found

DOI: 10.1007/978-3-540-69761-9_22

with a = 615.1 and c = 675.6 pm. In this context fit the spherulites, observed in melt spun amorphous ribbons $Nd_7Fe_{89}B_4$, which after anneal at 625°C for 10 min reveal a BiF_3 type phase based on a W type subunit: the phase exhibits long range order, characterized by the splitting of superspots in selected area diffraction patterns [1999Kon].

Invariant Equilibria

The data on the invariant equilibria are given in Table 3. A reaction scheme is given in Figs. 1a, 1b. In the Fe rich part the experimental compositions were selected from data of [1986Sch, 1994Kno]. The compositions of the other ternary reactions were deduced from the well done thermodynamic assessment done by [1995Hal] who proposed a calculated liquidus surface in agreement with experimental data [1986Sch, 1994Kno]. Most of the ternary reaction temperatures were taken from [1994Hal]. The reaction scheme was redrawn from the one proposed by [1995Hal] with some slight modifications on the binary edges.

Liquidus, Solidus and Solvus Surfaces

[2003Rag] noted discrepancies in the various experimental data available in the literature concerning the liquidus surface.

At the Fe rich corner, the four-phase invariant reaction L + Fe_2B ⇌ (γFe) + τ_2 reported by [1985Mat, 1987Tsa] is not in agreement with the one suggested by [1986Sch]. [1986Sch] pointed out that this U reaction was probably due to a manifestation of metastability. [1987Hen] confirmed this result and proposed a Fe rich corner liquidus surface in agreement with the one suggested by [1986Sch].

At the Nd rich compositions, two different type reactions L ⇌ (βNd) + τ_1 + τ_2 and L + τ_3 ⇌ (βNd) + τ_2 were reported by [1985Mat, 1987Tsa]. The eutectic reaction was not confirmed by [1991Lan1, 1991Lan2, 1994Kno] and was replaced by a U type reaction L + τ_2 ⇌ (βNd) + τ_1. The same authors also reported a region of the primary crystallization for τ_1 narrower than the one found in [1985Mat]. The more recent and precise experimental work done by [1994Kno] was retained. Nevertheless, some modifications should be done since [1994Kno] did not observed the binary phase Nd_5Fe_{17} in the solidification reactions due to kinetic effects. As this binary phase was well established by [1990Lan], this new phases has to be added.

[1995Hal] made for the first time a thermodynamic assessment of this system. It was found a very small primary crystallization of the phase Nd_5Fe_{17}. The sequence of the ternary reactions proposed by [1995Hal] is in general good agreement with the experimental ones with nevertheless some discrepancies on compositions. Two news ternary reactions were suggested by the calculation: L + NdB_4 ⇌ τ_2 + τ_3 and L + NdB_4 + Nd_2B_5 ⇌ τ_3. This leads to larger homogeneity ranges for the Nd_2B_5 and NdB_4 phases which were never observed. The calculated liquidus surface reported by [1995Hal] confirms all experimental results for the composition regions where the solidification behavior has been well established. Nevertheless, the calculated regions of primary crystallization of τ_2 and τ_3 are found lower than those reported in [1985Mat, 1986Sch, 1991Lan3, 1994Kno]. However, the final solidification regions of τ_1, τ_2 and τ_3 are closer, results in accordance with most of the limited available experimental data concerning these regions. Consequently, the calculated liquidus surface proposed by [1995Hal] has been retained in this assessment with some slight modifications concerning the composition of the ternary reactions for which the experimental data were well determined. The corresponding liquidus surface is reproduced on Fig. 2. The position of p_3 binary reaction has been modified to be in agreement with the accepted binary. More experimental investigations are necessary in order to confirm the different ternary reactions.

Isothermal Sections

Several isothermal sections have been studied in this system: at 1000°C in the Fe rich corner by [1986Sch] and in the low boron side by [1990Hao], at 900°C (700°C in the Nd richer part) in the whole composition range by [1986Bus1, 1986Bus2], at room temperature and in the $0 < x(B) < 0.5$ composition range by [1986Che].

The 1000°C sections are in poor agreement. Isothermal solid-liquid equilibria, were not directly investigated by [1986Sch], but they suggest that liquid phase substantially extends into the ternary from the Fe-Nd side and it contains about 10 at.% B when in equilibrium with τ_1 and τ_2. According to [1990Hao], however, the

DOI: 10.1007/978-3-540-69761-9_22

liquid phase has a narrow composition range close to the Fe-Nd side. As for solid state equilibria different triangulations are presented in the Fe rich corner: according to [1986Sch] the Fe_2B-τ_1 two phase equilibrium is stable at this temperature while the equilibrium Fe-τ_2 is reported by [1990Hao]. The result by [1986Sch] is here preferred (Fig. 3) because it is based on a more extensive investigation including the liquidus surface and several temperature-composition sections.
The two-phase equilibrium Fe-τ_2 is reported in the 900°C section investigated by [1986Bus1, 1986Bus2] (Fig. 4). It is then supposed, in agreement with the thermodynamic assessment by [1995Hal], that a U type invariant equilibrium $Fe_2B + \tau_1 \rightleftharpoons Fe + \tau_2$ occurs at an intermediate temperature. It could not be recognized in the vertical sections studied by [1986Sch] due to the occurrence, in the same temperature range, of the (γFe)-(αFe) transition.
The room temperature section by [1986Che] is in substantial agreement with [1986Bus1, 1986Bus2]: it is here accepted (Fig. 5) with the addition of the Nd_5Fe_{17} binary phase.

Temperature – Composition Sections

Several B-Fe-Nd temperature-composition sections have been studied in literature, mainly limited to the low boron side of the system. [1986Che] investigated two sections crossing at the τ_1 composition: one at 6 at.% B and 0 to 35 at.% Nd and the other from Nd_2Fe_{17} to $Nd_8Fe_{27}B_{24}$. [1986Sch] investigated four sections: at 73.3 and 80 at.% Fe, at 4 at.% B (0 to 35 at.% Nd) and at 1:2 B/Nd ratio (for $1 > x(Fe) > 0.7$). [1994Kno] extended the investigation of the section at 4 at.% B up to about 60 at.% Nd, and investigated the sections at 30 at.% Nd (up to about 15 at.% B) and between $Nd_{73}Fe_{27}$ and $Fe_{77}B_{23}$. [1987Tsa] determined the sections from pure Nd to $Fe_{14}B$ and to Fe_4B. Finally [1991Lan3] studied the section at 60 at.% Nd up to 20 at.% B.
The sections proposed by the different authors are not completely consistent to each other. According to [1986Che] τ_1 is congruent melting while according to [1986Sch] and other authors it undergoes an incongruent formation. This conclusion is here accepted because it is supported by a larger number of results. Sections by [1986Sch] and [1994Kno] are self consistent and in good agreement with the accepted liquidus surface but in some of them experimental data points appear which are not related to any phase boundary. Sections by [1987Tsa] seem less accurate than those by [1994Kno], but not in evident contradiction with them. Finally, the section by [1991Lan3] seems wrong at high temperature: the highest thermal effect reported close to the Fe-Nd binary is at about 950°C while the corresponding accepted binary liquidus temperature is more than 1200°C. Even on the boron rich side of the section the liquidus curve suggests an extrapolated binary B-Nd liquidus which does not agree with the accepted B-Nd phase diagram.
[1995Hal] undertook a thermodynamic assessment. The calculated isopleths Fe-τ_1, at 4 at.% B, 30 at.% Nd are in remarkable agreement with the experimental data.
A few representative temperature - composition sections are reported in Figs. 6 to 9 taken from [1986Sch] and [1995Hal] without correction according accepted liquidus surface.

Thermodynamics

No experimental thermodynamic investigation has been carried out on the B-Fe-Nd system, but it has been thermodynamically modelled by [1995Hal]. Experimental isothermal and polythermal sections are reproduced reasonably well, especially considering the large uncertainties affecting part of the ternary system and even the binary sub-systems (B-Nd in particular). The calculation generally supports our previous remarks and choices about the reliability of the experimental sections.

Notes on Materials Properties and Applications

$Nd_2Fe_{14}B$

Although the phase τ_1-$Nd_2Fe_{14}B$ has been identified already in 1979 by Chaban *et al.* [1979Cha] (labelled "$Nd_3Fe_{16}B$"), Sagawa *et al.* [1984Sag2] and Croat *et al.* [1984Cro] discovered the exceptional magnetic

DOI: 10.1007/978-3-540-69761-9_22

properties of this compound with high positive uniaxial anisotropy yielding an extremely high energy product $(BH)_{max}$ ≈450 kJ·m^{-3}, the highest known among magnetic materials. A chronology of the discovery of the high performance magnet $Nd_2Fe_{14}B$ can be found from [1991Sta]. A summary on the magnetic properties is due to [1986Bus1, 1986Bus2, 1991Bus, 1998Bur].

$Nd_2Fe_{14}B$ is a hard magnetic phase with high anisotropy field and large saturation magnetization. The large saturation magnetization is the result of ferromagnetic coupling between the relatively high Nd and Fe moments from 6 inequivalent Fe sites [1984Her, 1985Giv, 1987Fru, 1987Ono, 1989Zha, 1992Ge]. Measurements of the Nd magnetic moments identify 2 inequivalent Nd sites [1984Her, 1985Giv, 1992Jed, 1993Kap]. [1993Min] used a self-consistent linearized muffin-tin-orbital band method to study the electronic and magnetic structure of $Nd_2Fe_{14}B$ and compared it with Photo Emission Spectroscopy measurements. The PES spectra suggest Nd 4f and Fe 3d hybridization. The high magnetic anisotropy of $Nd_2Fe_{14}B$ is mainly provided by the Nd sublattice. The anisotropy fields and constants have been determined [1984Giv, 1985Koo, 1986Yam, 1986And, 1987Ota, 1988Cad, 2005Pas]. The anisotropy energy is described by a phenomenological relation, similar to the expression of [1988Cad]: $E_A = K_1\sin^2\theta + (K_2+K_2'\cos4\varphi)\sin^4\theta + (K_3+K_3'\cos4\varphi)\sin^6\theta$, with θ and φ the polar angles between the rare earth sublattice magnetization and the crystallographic axes. K_1 changes from negative to positive values around the spin reorientation temperature T_{sr}. At T_{sr} there is a transition from a collinear magnetic structure where the magnetization is parallel to the *c*-axis to a low temperature structure with a non-zero angle between the magnetization and the *c*-axis. The easy axis of magnetization and spin reorientation temperature are investigated by [1984Sag2] for $Nd_xB_yFe_{100-x-y}$ (x = 13-19, y = 4-17), by [1985And], by [1985Koo] for $Nd_{16}Fe_{77}B_7$, by [1986Hir] for $Nd_2Fe_{14}B$ single crystals, by [1986Yam] and by [1995Cha1]. There results agree well, leading to an easy axis of magnetization at an angle of ~30° with respect to the *c*-axis at 4.2 K and a spin reorientation temperature of 135-138 K. The temperature dependence of the spontaneous magnetization has been investigated by several researchers [1985Bur, 1986Hir, 1991Koh, 1992Rie, 1987Nag]. At the Curie temperature T_C a transition from the low temperature ferromagnetic state to the high temperature paramagnetic state is observed. According to the results of [1986Hir], the Curie temperature T_C is 586 K. [1985Bur] analyzed the magnetic phase transition in $Nd_2Fe_{14}B$ polycrystals, while [1991Koh, 1992Rie] did the same for single crystals. The pressure dependence of T_C is reported by [1987Nag].

$Nd_2Fe_{14}B$ compounds absorb a significant amount of hydrogen forming stable hydrides. [1984Oes2, 1986And, 1995Isn] obtain respectively the compounds $Nd_2Fe_{14}BH_{2.7}$, $Nd_2Fe_{14}BH_{3.8}$ $Nd_2Fe_{14}BH_5$. Hydrogen absorption influences the magnetic moment, exchange interactions, magnetocrystalline anisotropy and magnetostriction of $Nd_2Fe_{14}B$. Loading τ_1 $Nd_2Fe_{14}B$ with hydrogen showed a strong increase of magnetization and Curie temperature: for maximal hydrogen uptake, $Nd_2Fe_{14}BH_5$, the saturation magnetization at 300 K increased by 5.6%, T_C = 403°C [1984Her], while the magnetic anisotropy decreases. [1984Oes2, 1986And, 1995Isn]., [1995Sou] determined the effect of H, C and N on the magnetization and the spin reorientation of $Nd_2Fe_{14}B$.

$Nd_2Fe_{14}B$-based magnets exhibit excellent permanent magnetic properties resulting from the large saturation magnetization and the high anisotropy field. Three types of NdFeB magnets may be distinguished according to the Nd content: (a) alloys with low Nd content containing a soft magnetic phase (αFe) or Fe_3B; (b) near-stoichiometric Nd alloys with single phase $Nd_2Fe_{14}B$; (c) high Nd alloys with a Nd rich phase. The used composition is related to the production of NdFeB magnets, for which two major commercial routes are developed: (i) the powder metallurgical route and (ii) rapid solidification techniques [1998Bur]. For the powder metallurgical route, bulk alloys are obtained by casting, melt-spinning or reduction-diffusion processes. These alloys are consequently powdered by different procedures, such as mechanical grinding, hydrogen decrepitation (HR) or hydrogen-decrepitation-desorption-recombination (HDDR) processes, inert gas atomization and spark erosion methods. Traditionally, microcrystalline magnets tend to be produced by the sintering process, where powder is aligned in a magnetic field and subsequently pressed and sintered to a full dense magnet material. Commonly, high-Nd alloys are used as starting material to avoid undissolved primary Fe dendrites from the peritectic formation of $Nd_2Fe_{14}B$ and to enhance the sintering process by low melting grain boundary phases. Nevertheless, the presence of these boundary phases reduces the proportion of $Nd_2Fe_{14}B$ phase, thereby limiting the remanence to lower values than the maximum value of single

DOI: 10.1007/978-3-540-69761-9_22

$Nd_2Fe_{14}B$. Improvements of the casting process facilitate faster cooling rates, more homogeneity and finer microstructures; consequently, lower Nd contents are needed. For bonded or hot-deformed magnets, melt spinning ribbons with a near-stoichiometric $Nd_2Fe_{14}B$ composition are used. Although the content of nonmagnetic phases in bonded magnets is low, the remanence is lower than expected as a result of binder content, pores and internal shear losses. On the other hand, rapid solidification techniques, such as melt-spinning or atomization, are developed to enhance the microstructure, and hence the magnetic properties of NdFeB magnets [1984Cro]. Through careful control of the melt-spinning process, nanocrystalline structures are possible, which leads to enhanced values of the remanence, above the theoretical Stoner-Wohlfarth value ($B_s/2$) for randomly oriented noninteracting crystals. The effect of solidification kinetics on the microstructure, and hence magnetic properties, has been investigated for several Fe-B-Nd compositions, for example $Nd_{11.8}Fe_{82.3}B_{5.9}$/$Nd_{11}Fe_{83.5}B_{5.5}$ [1999Her], $Nd_2Fe_{14}B$ [2001Oza, 2004Oza1], $Nd_{14}Fe_{79}B_7$ [2004Oza2] and $Nd_{12.5}Fe_{82}B_{5.5}$ [2004Tia]. The magnetic properties of melt-spun ribbons of low Nd two-phase alloys are studied by [1995Cha2, 2000Liu, 2001Sai, 2002Kim1, 2002Kim2, 2002Gu, 2002Li, 2003Shi, 2004Har]. The remanence, coercivity and energy product lie in the range 0.7-1.5T, 207-504 $kA \cdot m^{-1}$ and 40-158 $kJ \cdot m^{-3}$, respectively. Near-stoichiometric single phase melt-spun ribbons have a remanence of 0.90-0.97 T, an intrinsic coercivity of 546-840 $kA \cdot m^{-1}$ and an energy product of 130-150 $kJ \cdot m^{-3}$ [1995Cha2, 2004Har]. High Nd alloys produced by melt spinning are examined by [1995Cha2, 1997Sun, 2001Gir1, 2001Gir2, 2001Woo, 2001Kon, 2001Alk, 2002Cre, 2002Kim1, 2002Kim2]. Their measurements reveal a coercivity of 1000-2150 $kA \cdot m^{-1}$, while the energy product is around 90 $kJ \cdot m^{-3}$.

Insufficient temperature stability and corrosion resistance are the main factors limiting the applications of NdFeB magnets. The oxidation and corrosion behavior of NdFeB powders has been studied by different groups [1990LeB, 1993Tur, 1996Ste]. Powder oxidizes in air via two different routes, namely a relatively quick, total oxidation of the intergranular Nd rich phase and the oxidation of $Nd_2Fe_{14}B$. Under certain conditions, the latter phase disproportionates into (αFe) and Nd and B oxides, as observed by [1997Edg] on $Nd_{16.4}Fe_{75.7}B_{7.9}$. Although sintered magnets are stable in dry air at room temperature, the chemical stability in more aggressive media is low. Oxidation tests in humid environments on commercial magnets reveal intergranular corrosion with a preferential corrosion of the Nd rich intergranular phase [1995Cyg]. NdFeB magnets degrade faster when in magnetized state as reported by [1991Bal] and [2001Cos] for $Nd_{15}Fe_{77}B_8$ and a commercial magnet, respectively. Two methods are investigated to diminish the corrosion and oxidation behavior of NdFeB magnets, namely the addition of alloying elements like Al, Nb or Cu [1991LeB, 1993Szy], and the application of protective surface coatings.

Other stable and metastable phases

Ternary compounds of the type $Nd_{1+\varepsilon}Fe_4B_4$ are often observed as an impurity phase in NdFeB magnets, for example in an alloy with composition Nd = 6-8 % and Fe/B = 6 by [1997Fan]. $NdFe_4B_4$ is nonmagnetic in the temperature interval from room temperature down to 77 K [1984Oes1]. $Nd_5Fe_2B_6$ is never reported as an impurity phase in NdFeB magnets. The ternary metastable phases $Nd_2Fe_{23}B_6$ and $Nd_2F_{17}B_x$ (x~1.1) are observed in magnets prepared by rapid solidification processes. The first phase is found by [1997Fan] in an alloy with composition Nd = 6% and Fe/B = 6, while the latter is observed by [2001Gao1, 2003Gao] for $Nd_xFe_{100-1.5x}B_{0.5x}$ (x = 11.8-15) and $Nd_{16}Fe_{76}B_8$/ $Nd_{18}Fe_{73}B_9$/ $Nd_{22}Fe_{67}B_{11}$, respectively.

Differential scanning calorimetry for a melt-spun alloy with composition $Nd_2Fe_{23}B_3$ showed a weak endothermic effect on heating (20 $K \cdot s^{-1}$) at about 660 K, which was attributed to ferromagnetic ordering. The Curie temperature changed from T_C=525 for the melt-spun condition to 655 K after crystallization [1986DeM]. ^{57}Fe-Mössbauer data for $Nd_2Fe_{23}B_3$ revealed details of the Fe-moments for the five independent Fe-sites [1986Bus1, 1986Bus2]. The activation energy for the crystallization of $Nd_2Fe_{23}B_3$ was determined to be ΔE = 447 $kJ \cdot mol^{-1}$ [1986DeM]. $NdFe_{12}B_6$ was reported to be ferromagnetic with T_C = 230 K [1986Bus1, 1986Bus2].

[2005Shi] studied the crystal structure and morphology of the Nd rich grain boundary phase in post-annealed B-Fe-Nd magnets by Transition Electron Microscopy (TEM): when the Nd rich phase was thinner than 2 nm it was amorphous, but when growing in thickness it became cubic face centered ($a \approx \subsetneq$540 pm) in a simple orientation relationship $(111)_{Nd2Fe14B}$ (111) Nd and $(010)_{Nd2Fe14B}$ (1-11) Nd. At a sufficiently large supply of oxygen, the Nd rich phase transforms to a phase, which was supposed to be isostructural with

DOI: 10.1007/978-3-540-69761-9_22

Nd_2O_3 [2005Shi]. TEM analyses on a melt spun $Nd_{18}Fe_{76}B_6$ alloy identified the τ_1 phase, a fcc phase $Nd_{73}Fe_{27}$ and a tetragonal Nd rich phase (a = 380, c = 540 pm, $I\bar{4}2m$), which contained oxygen in solution (ratio Nd/Fe = 13) [2001Alk].
Details on experimental methods are reported on Table 4

Table 1. Investigations of the B-Fe-Nd Phase Relations, Structures and Thermodynamics

Reference	Method/Experimental Technique	Temperature/Composition/Phase Range Studied
[1985Mat]	Microstructure analysis, X-ray diffraction, calorimetry	Up to 4 at.% B
[1986Bus1]	XRD, DTA	700 and 900°C / Fe-Nd-B
[1986Bus2]	XRD, metallography	$Nd_2Fe_{14}B$, annealed 3 weeks at 900°C
[1986Che]	XRD, DTA	25 - 1600°C / Nd-Fe-B with B ≤ 50 at.% B
[1986Sch]	Microstructure analysis, X-ray diffraction, calorimetry	600 - 1400°C / Up to 40 at.% B and 40 at.% Nd
[1987Hen]	Microstructure analysis, calorimetry	Up to 30 at.% B and 20 at.% Nd
[1987Tsa]	DTA, LOM, SEM+EPMA (EDX), XRD	500 - 1500°C / Up to 30 at.% B
[1988Alt]	XRD, DTA	127 - 727°C / 3.5-8 at.% Nd, 7-17 at.% B, 88-76 Fe
[1990Hao]	Diffusion couples, XRD, SEM +EPMA	1000°C / Fe-Nd alloys with less than 80 at.% B
[1991Kim]	DTA, XRD	647°C / $Fe_{74}Nd_6B_{20}$
[1991Lan1]	Microstructure analysis, calorimetry	600 - 1150°C / Up to 40 at.% Fe and 20 at.% B
[1991Lan2]	Microstructure analysis, calorimetry	600 - 1150°C / Up to 40 at.% Fe and 20 at.% B
[1993Kha]	XRD	602°C / $Nd_{2-x}Fe_{14}B$ ($0 \le x \le 1$)
[1994Gu]	DTA, XRD	427 - 727°C / $Nd_6Fe_{77}B_{17}$
[1994Kno]	DTA, light optical, microscopie	327 - 1227°C / Up to 40 at.% B
[1995Hal]	Thermodynamic calculations	B-Fe-Nd
[1996Gab]	XRD	0 - 800°C / $Nd_9Fe_{91-x}B_x$ ($0 \le x \le 9$)
[1996Obb]	XRD	–253 and 17°C / $Nd_2Fe_{14}B$
[1996Wol]	Neutron diffraction	17°C / $Nd_2Fe_{14}B$
[1999Kon]	SAD, DTA, SEM	Nd_7 $Fe_{89}B_4$
[2001Gao1]	XRD, SEM, EDX	$Nd_xFe_{100-1.5x}B_{0.5x}$ (x = 11.8-15)
[2001Wol]	Neutron diffraction	–253°C / $Nd_2Fe_{14}B$

DOI: 10.1007/978-3-540-69761-9_22

Table 2. Crystallographic Data of Solid Phases

Phase/ Temperature Range [°C]	Pearson Symbol/ Space Group/ Prototype	Lattice Parameters [pm]	Comments/References
(δFe) 1538 - 1394	*cI*2 $Im\bar{3}m$ W	a = 293.15	[Mas2]
(γFe) 1394 - 912	*cF*4 $Fm\bar{3}m$ Cu	a = 364.67 a = 357.3	[Mas2] at 25°C [V-C2]
(αFe) < 912 $Fe_{1-x}B_x$	*cI*2 $Im\bar{3}m$ W	a = 286.65 a = 286.0	[Mas2] at x = 0.09 [V-C2]
(βB) < 2092	*hR*333 $R\bar{3}m$ βB	a = 1093.30 c = 2382.52 a = 1095.14 c = 2386.1 a = 1097.18 c = 2387.05	[1993Wer] at $FeB_{\sim 49}$ [V-C2] at $FeB_{\sim 20}$ [V-C2]
(βNd) 1021 - 863	*cI*2 $Im\bar{3}m$ W	a = 413	[Mas2]
(αNd) < 863	*hP*4 $P6_3/mmc$ αLa	a = 365.82 c = 1179.66	[Mas2]
FeB < 1588	*oP*8 *Pnma* FeB	a = 550.6 b = 295.2 c = 406.1	[1992Rog]
Fe_2B < 1407	*tI*12 *I*4/*mcm* $CuAl_2$	a = 510.9 c = 424.9	[1992Rog]
$Fe_3B(h_1)$ ~1250 - ~ 1150	*tI*32 $I\bar{4}$ Fe_3P	a = 865.5 c = 429.7	metastable [1992Rog]
$Fe_3B(h_2)$ ~1220 - ~ 1140	*tP*32 $P4_2/n$ Ti_3P	a = 864.8 c = 431.4	metastable [1992Rog]
Fe_3B < 1214	*oP*16 *Pnma* Fe_3C	a = 542.8 b = 666.9 c = 443.9	metastable, [1992Rog]

(*continued*)

DOI: 10.1007/978-3-540-69761-9_22

Phase/ Temperature Range [°C]	Pearson Symbol/ Space Group/ Prototype	Lattice Parameters [pm]	Comments/References
$Fe_{23}B_6$ ~800 - ~ 650	*cF*116 $Fm\bar{3}m$ $Cr_{23}C_6$	a = 1076	[1991Kha] metastable
Nd_2B_5 ≅ 2000	*mP*28 $P2_1/c$ Gd_2B_5	a = 730.5 b = 727.3 c = 742.65 β = 102.16°	Boron rich [Mas2]
NdB_4 < 2350	*tP*20 *P*4/*mbm* ThB_4		[Mas2]
		a = 721.22 c = 410.71	Boron rich 1000°C, [1993Gal]
		a = 721.99 c = 410.27	Nd rich, 1000°C, [1993Gal]
NdB_6 < 2610	*cP*7 $Pm\bar{3}m$ CaB_6		[Mas2]
		a = 412.74	NdB_4-saturated [1996Lia]
		a = 412.8	NdB_{66}-saturated, at 89.7 at.% B [1996Lia]
		a = 412.66	at 25°C [1993Gal]
		a = 414.2	at 323°C [V-C2]
		a = 415.2	at 623°C [V-C2]
		a = 412.8	at 78 K [V-C2]
NdB_{66} < 2150	*cF*1608 $Fm\bar{3}c$	a = 2350.8 a = 2350.6	[Mas2] from rapidly quenched parts of as cast alloy [1993Gal]
Nd_2Fe_{17}(r) < 1208	*hR*57 $R\bar{3}m$ Th_2Zn_{17}	a = 857 to 859 c = 1244 to 1248	[V-C2]
$Nd_2Fe_{17}B_{\sim 1}$		a = 864.7 c = 1255.5	appears as metastable phase when solidifying an $Nd_{14}Fe_{79}B_7$ alloy [2004Vol1, 2004Vol2]; for a metastable B-Fe-Nd phase with disordered Th_2Zn_{17} structure ($TbCu_7$ type) see [1996Gab]
Nd_5Fe_{17} <780	*hP*228 $P6_3/mcm$ Nd_5Fe_{17}	a = 2021.4 c = 1232.9	[1991Lan3]
$NdFe_5$ metastable?	*hP*6 *P*6/*mmm* $CaCu_5$	a = 494.6 c = 417.0	[1986Sta] from splat-cooled alloy
* τ_1, $Nd_2Fe_{14}B$	*tP*68 $P4_2/mnm$ $Nd_2Fe_{14}B$	a = 880.4 c = 1220.5	[1984Sho] R_F = 0.066 (all reflections); called ''$Nd_3Fe_{16}B$'' by [1979Cha]

(*continued*)

DOI: 10.1007/978-3-540-69761-9_22

Phase/ Temperature Range [°C]	Pearson Symbol/ Space Group/ Prototype	Lattice Parameters [pm]	Comments/References
	* true symmetry monoclinic *Cm*		true symmetry of crystal and magnetic structure below T_C = 588 K [1996Wol, 1996Obb, 2001Wol] for dependency of lattice parameters as f(T), 10 < T < 1000 K see [2005Yan]
* τ_2, $Nd_{1.11}Fe_4B_4$	*tP*162+18ε *Pccn* $RE_{1+\varepsilon}Fe_4B_4$ incommensurate	a = 711.7 c = 3507	[1986Giv] R_F = 0.081 $c_{Fe}/c_{Nd} = 1 + \varepsilon = 10/9$; c_{Fe} = 389.7, c_{Nd} = 350.2 labelled "$Nd_2Fe_7B_6$" by [1984Sag1]
* τ_3, $Nd_5Fe_2B_6$	*hR*39 $R\bar{3}m$ $Pr_5Co_2B_6$	a = 546.4 c = 2417	[1997Yar] $Nd_{5-x}Fe_{2+x}B_6$; called "Nd_2FeB_3" by [1979Cha]
* τ_4, $Nd_2Fe_{23}B_3$ metastable < 750°C	*cI*224 $I\bar{4}3d$ $Nd_2Fe_{23}B_3$	a = 1419	[1986DeM] from rapidly quenched alloys; labelled "$Nd_6Fe_{77}B_{17}$" [1994Gu]
* τ_5, "$Nd_{4.4}Fe_{84.4}B_{11}$" metastable < 700°C	*cI*146-156? $Im\bar{3}m$ or subgroups $Nd_{4.4}Fe_{84.4}B_{11}$ type	a = 1237.7	[1988Alt] from rapidly quenched alloys
* τ_6, $NdFe_{12}B_6$ metastable < 750°C	*hP*57 $R\bar{3}m$ $SrNi_{12}B_6$	a = 960.5 c = 754.9	[1986Bus1, 1986Bus2] from rapidly quenched alloys
* τ_7, $Nd_{2-x}Fe_{14}B$ metastable < 750°C	*cI*? Superstructure of W type	a = 601.4 ($a = 2a_o$)	0 < x < 1 [1993Kha] from rapidly quenched alloys Nd2Fe20B
* τ_8, $Nd_2Fe_{34}B_5$ metastable < 750°C	*cI*? Superstructure of W type	a = 1240 ($a = 4a_o$)	0 < x < 1 [1993Kha] from rapidly quenched alloys
* τ_9 metastable	tetragonal ?	a = 615.1 c = 675.6	decomposition product of τ_7 or τ_8 on heating above 1000 K [1993Kha]

Table 3. Invariant Equilibria

Reaction	T [°C]	Type	Phase	Composition (at.%)		
				B	Fe	Nd
L + NdB_6 + NdB_4 ⇌ FeB	1628	P_1	L	47.74	51.76	0.50
			NdB_6	85.72	0.00	14.28
			NdB_4	80.00	0.00	20.00
			FeB	50.00	50.00	0.00

(*continued*)

DOI: 10.1007/978-3-540-69761-9_22

Reaction	T [°C]	Type	Phase	Composition (at.%)		
				B	Fe	Nd
$L + NdB_6 \rightleftharpoons FeB + NdB_{66}$	1533	U_1	L	?	?	?
			NdB_6	85.72	0.00	14.28
			FeB	50.00	50.00	0.00
			NdB_{66}	98.51	0.00	1.49
$L \rightleftharpoons NdB_{66} + (\beta B) + FeB$	1509	D_1	L	?	?	?
			NdB_{66}	98.51	0.00	1.49
			(βB)	100.00	0.00	0.00
			FeB	50.00	50.00	50.00
$l + NdB_4 \rightleftharpoons \tau_2$	1411	p_4	l	40.00	45.00	15.00
			NdB_4	80.00	0.00	20.00
			τ_2	20.94	20.94	58.12
$L + FeB \rightleftharpoons NdB_4 + Fe_2B$	1388	U_2	L	39.00	57.00	4.00
			FeB	50.00	50.00	0.00
			NdB_4	80.00	0.00	20.00
			Fe_2B	33.33	66.67	0.00
$L + NdB_4 \rightleftharpoons Fe_2B + \tau_2$	1375	U_3	L	39.00	54.00	7.00
			NdB_4	80.00	0.00	20.00
			Fe_2B	33.33	66.67	0.00
			τ_2	20.94	20.94	58.12
$L + NdB_4 + Nd_2B_5 \rightleftharpoons \tau_3$	1237	P_2	L	13.00	34.23	52.77
			NdB_4	80.00	0.00	20.00
			Nd_2B_5	71.43	0.00	28.57
			τ_3	46.16	15.38	38.46
$L + NdB_4 \rightleftharpoons \tau_2 + \tau_3$	1192	U_4	L	15.87	42.60	41.67
			NdB_4	80.00	0.00	20.00
			τ_2	20.94	20.94	58.12
			τ_3	46.16	15.38	38.46
$l + (\gamma Fe) \rightleftharpoons \tau_1$	1180	p_7	l	8.00	76.00	16.00
			(γFe)	0.00	100.00	0.00
			τ_1	5.89	82.35	11.76
$L + (\gamma Fe) \rightleftharpoons \tau_1 + Nd_2Fe_{17}$	1130	U_5	L	2.00	66.00	32.00
			(γFe)	0.00	100.00	0.00
			τ_1	5.89	82.35	11.76
			Nd_2Fe_{17}	0.00	89.47	10.53
$l \rightleftharpoons \tau_1 + \tau_2$	1115	e_6	l	17.00	73.00	10.00
			τ_1	5.89	82.35	11.76
			τ_2	20.94	20.94	58.12
$l \rightleftharpoons Fe_2B + \tau_1$	1110	e_7	l	18.00	75.00	7.00
			Fe_2B	33.33	66.67	0.00
			τ_1	5.89	82.35	11.76
$L \rightleftharpoons Fe_2B + \tau_1 + (\gamma Fe)$	1105	E_1	L	17.00	76.00	7.00
			Fe_2B	33.33	66.67	0.00

(*continued*)

DOI: 10.1007/978-3-540-69761-9_22

Reaction	T [°C]	Type	Phase	Composition (at.%)		
				B	Fe	Nd
			τ_1	5.89	82.35	11.76
			(γFe)	0.00	100.00	0.00
$L \rightleftharpoons \tau_1 + \tau_2 + Fe_2B$	1095	E_2	L	20.00	72.00	8.00
			τ_1	5.89	82.35	11.76
			τ_2	20.94	20.94	58.12
			Fe_2B	33.33	66.67	0.00
$Fe_2B + \tau_1 \rightleftharpoons (\gamma Fe) + \tau_2$	981	U_6	Fe_2B	33.33	66.67	0.00
			τ_1	5.89	82.35	11.76
			(γFe)	0.00	100.00	0.00
			τ_2	20.94	20.94	58.12
$(\gamma Fe) + Nd_2Fe_{17} + \tau_1 \rightleftharpoons (\alpha Fe)$	934	P_3	(γFe)	0.00	100.00	0.00
			Nd_2Fe_{17}	0.00	89.47	10.53
			(αFe)	0.00	100.00	0.00
			τ_1	5.89	82.35	11.76
$(\gamma Fe) + \tau_1 \rightleftharpoons (\alpha Fe) + \tau_2$	922	U_7	(γFe)	0.00	100.00	0.00
			τ_1	5.89	82.35	11.76
			(αFe)	0.00	100.00	0.00
			τ_2	20.94	20.94	58.12
$(\gamma Fe) + \tau_2 \rightleftharpoons (\alpha Fe) + Fe_2B$	921	U_8	(γFe)	0.00	100.00	0.00
			τ_2	20.94	20.94	58.12
			(αFe)	0.00	100.00	0.00
			Fe_2B	33.33	66.67	0.00
$L + Nd_2B_5 \rightleftharpoons \tau_3 + (\beta Nd)$	894	U_9	L	1.00	6.20	92.80
			Nd_2B_5	71.43	0.00	28.57
			τ_3	46.16	15.38	38.46
			(βNd)	0.00	0.00	100.00
$(\beta Nd) \rightleftharpoons L + \tau_3 + (\alpha Nd)$	854	D_2	(βNd)	0.00	0.00	100.00
			L	?	?	?
			τ_3	46.16	15.38	38.46
			(αNd)	0.00	0.00	100.00
$(\beta Nd) + Nd_2B_5 \rightleftharpoons (\alpha Nd) + \tau_3$	854	D_3	(βNd)	0.00	100.00	0.00
			Nd_2B_5	71.43	0.00	28.57
			(αNd)	0.00	100.00	0.00
			τ_3	46.16	15.38	38.46
$L + Nd_2Fe_{17} \rightleftharpoons Nd_5Fe_{17} + \tau_1$	768	U_{10}	L	0.60	30.40	69.00
			Nd_2Fe_{17}	0.00	89.47	10.53
			Nd_5Fe_{17}	0.00	77.27	22.73
			τ_1	5.89	82.35	11.76
$L + \tau_3 \rightleftharpoons (\alpha Nd) + \tau_2$	702	U_{11}	L	1.00	22.00	77.00
			τ_3	46.16	15.38	38.46
			(αNd)	0.00	0.00	100.00
			τ_2	20.94	20.94	58.12

(*continued*)

DOI: 10.1007/978-3-540-69761-9_22

Reaction	T [°C]	Type	Phase	Composition (at.%)		
				B	Fe	Nd
$L + \tau_2 \rightleftharpoons (\alpha Nd) + \tau_1$	685	U_{12}	L	1.00	23.00	76.00
			τ_2	20.94	20.94	58.12
			(αNd)	0.00	0.00	100.00
			τ_1	5.89	82.35	11.76
$L \rightleftharpoons \tau_1 + Nd_5Fe_{17} + (\alpha Nd)$	678	E_3	L	0.50	23.50	76.00
			τ_1	5.89	82.35	11.76
			Nd_5Fe_{17}	0.00	77.27	22.73
			(αNd)	0.00	100.00	0.00

Table 4. Investigations of the B-Fe-Nd Materials Properties

Reference	Method/experimental technique	Type of property
[1984Her]	Neutron diffraction	Magnetic moments in $Nd_2Fe_{14}B$
[1984Giv]	High temperature translation balance, bitter-coil type magnetometer	Ordering temperature, magnetic anisotropy
[1984Oes1]	XRD	Microstructure
[1984Oes2]	Magnetisation curves	H absorption
[1984Sag2]	XRD, vibrating sample magnetometer	Magnetic anisotropy
[1985And]	Vibrating sample magnetometer	Magnetic anisotropy
[1985Bur]	Faraday type balance	Magnetic phase transition
[1985Giv]	Neutron diffraction	Magnetic moments in $Nd_2Fe_{14}B$
[1985Koo]	Vibrating sample magnetometer	Magnetic anisotropy
[1986And]	Induction in pulsed magnetic field, vibrating magnetometer, quartz piezoelectric gage	Magnetic anisotropy, magnetostriction
[1986Hir]	Vibrating sample magnetometer, torque magnetometer	Temperature dependence of magnetization
[1986Yam]	Torque magnetometer	Magnetic anisotropy
[1987Fru]	^{57}Fe Mössbauer spectroscopy	Magnetic moments in $Nd_2Fe_{14}B$
[1987Nag]		Pressure dependence of magnetization
[1987Ono]	^{57}Fe Mössbauer spectroscopy	Magnetic moments in $Nd_2Fe_{14}B$
[1987Ota]	Torque magnetometer	Magnetic anisotropy
[1988Cad]	Bitter-coil type magnetometer	Magnetic anisotropy
[1989Zha]	Mössbauer spectroscopy, ^{11}B and ^{57}Fe NMR	Magnetic moments in $Nd_2Fe_{14}B$

(*continued*)

MSIT®
DOI: 10.1007/978-3-540-69761-9_22

Reference	Method/experimental technique	Type of property
[1991Bal]	Acid corrosion test	Corrosion of FeNdB magnets
[1991Koh]	Magnetization isotherms, modified Arrott plots, the method of Kouvel and Fisher, scaling plots and ln(J) *versus* ln ($>H_0$) plots	Magnetic phase transition
[1991LeB]	Mössbauer spectroscopy, XRD	Corrosion of NdFeB magnets
[1992Ge]	Fe hyperfine field nuclear magnetic resonance (NMR) and Mössbauer effect (ME)	Magnetic moments in $Nd_2Fe_{14}B$
[1992Jed]	^{145}Nd NMR	Magnetic moments in $Nd_2Fe_{14}B$
[1992Rie]	Magnetization data	Magnetic phase transition
[1993Kap]	Spin-echo nuclear magnetic resonance spectra of ^{143}Nd, ^{145}Nd	Magnetic moments in $Nd_2Fe_{14}B$
[1993Min]	Photo Emission Spectroscopy	Electronic structure
[1993Szy]	Acid corrosion test and atmospheric corrosion test	Corrosion of NdFeB magnets
[1995Cha1]	X-Ray circular magnetic dichroism (XCMD)	Magnetic anisotropy
[1995Cyg]	Oxygen-water vapour corrosion test	Corrosion of NdFeB magnets
[1995Isn]	Neutron diffraction	H absorption
[1995Sou]	Magnetic susceptibility measurements by extraction technique and Bitter-coil type magnetometer, thermomagnetic torquemeter	Effect of H, C and N on the magnetization and the spin reorientation of $Nd_2Fe_{14}B$
[1996Ste]	Mössbauer spectroscopy	
[1997Edg]	DSC, XRD, EPMA, TEM, Mössbauer spectroscopy	Oxidation of NdFeB magnets
[1997Fan]	TG/DTA, TEM, XRD, vibrating sample magnetometer	Magnetic properties, microstructure
[1997Sun]	Pulse magnetometer	Magnetic properties
[1998Mia]	Vibrating sample magnetometer	Magnetic properties
[1999Her]	Cooling under electromagnetic levitation	Solidification, microstructure
[2000Liu]	Pulse magnetometer	Magnetic properties
[2001Alk]	Vibrating sample magnetometer	Magnetic properties
[2001Cos]	3.5% NaCl immersion test, permeameter	Corrosion, magnetic properties
[2001Gao1]	SEM, EPMA, XRD	Solidification, microstructure

(*continued*)

DOI: 10.1007/978-3-540-69761-9_22

Reference	Method/experimental technique	Type of property
[2001Gir2]	Superconducting quantum interference device, vibrating sample magnetometer	Magnetic properties
[2001Kon]	Vibrating sample magnetometer	Magnetic properties
[2001Oza]	SEM, EPMA, XRD	Solidification, microstructure
[2001Sai]	Recording fluxmeter	Magnetic properties
[2001Woo]	Vibrating sample magnetometer	Magnetic properties
[2002Gu]	Vibrating sample magnetometer	Magnetic properties
[2002Kim1 2002Kim2]	Vibrating sample magnetometer	Magnetic properties
[2002Li]	Pulse magnetometer	Magnetic properties
[2003Gao]	SEM, EPMA, XRD	Solidification, microstructure
[2003Shi]	Electron holography	Magnetic properties
[2004Har]	Superconducting quantum interference device, vibrating sample magnetometer	Magnetic properties
[2004Oza2, 2004Oza1]	XRD, SEM, DSC, vibrating sample magnetometer	Microstructure
[2004Tia]	XRD, TEM, vibrating sample magnetometer, DTA	Microstructure, magnetization, thermal properties
[2005Pas]	Magnetization and torque curves	Magnetic anisotropy

DOI: 10.1007/978-3-540-69761-9_22

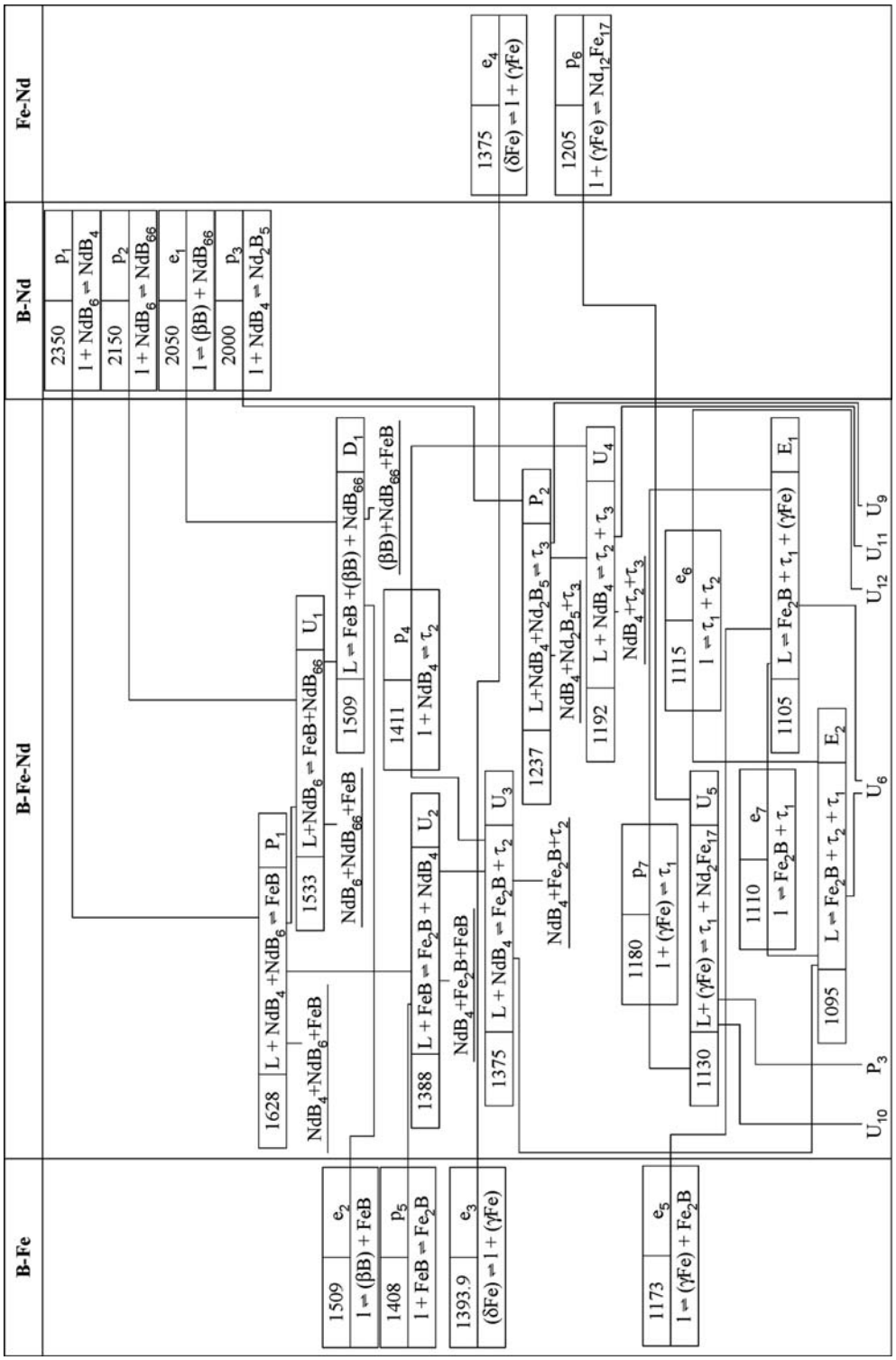

Fig. 1a. B-Fe-Nb. Reaction scheme, part 1

DOI: 10.1007/978-3-540-69761-9_22

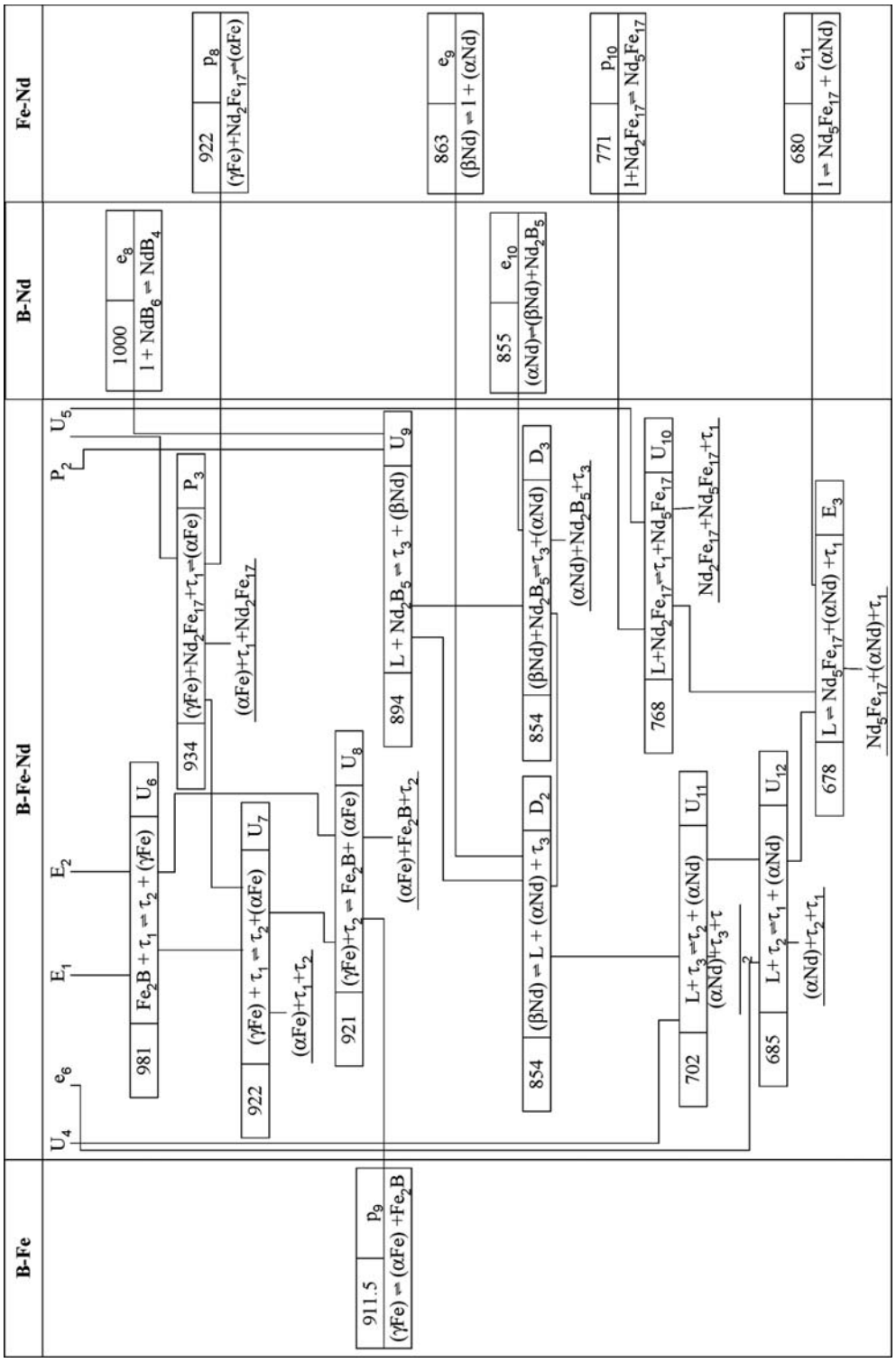

Fig. 1b. B-Fe-Nd. Reaction scheme, part 2

DOI: 10.1007/978-3-540-69761-9_22

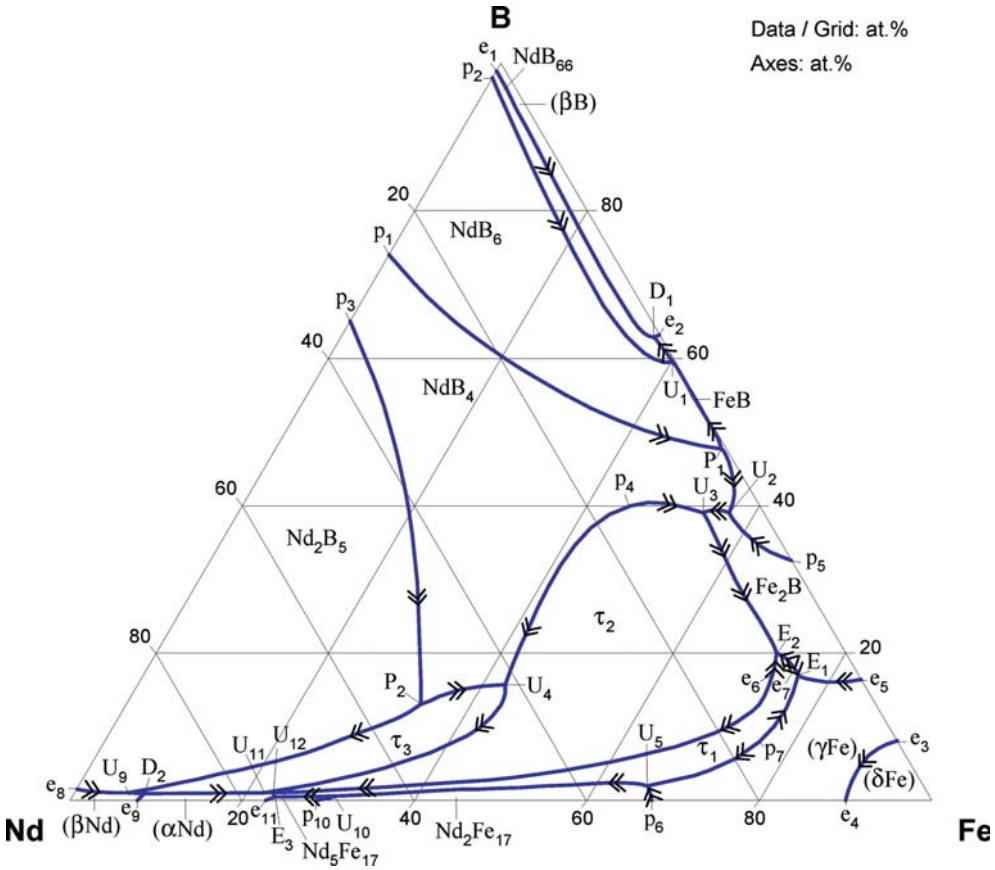

Fig. 2. B-Fe-Nd. Liquidus surface projection

DOI: 10.1007/978-3-540-69761-9_22

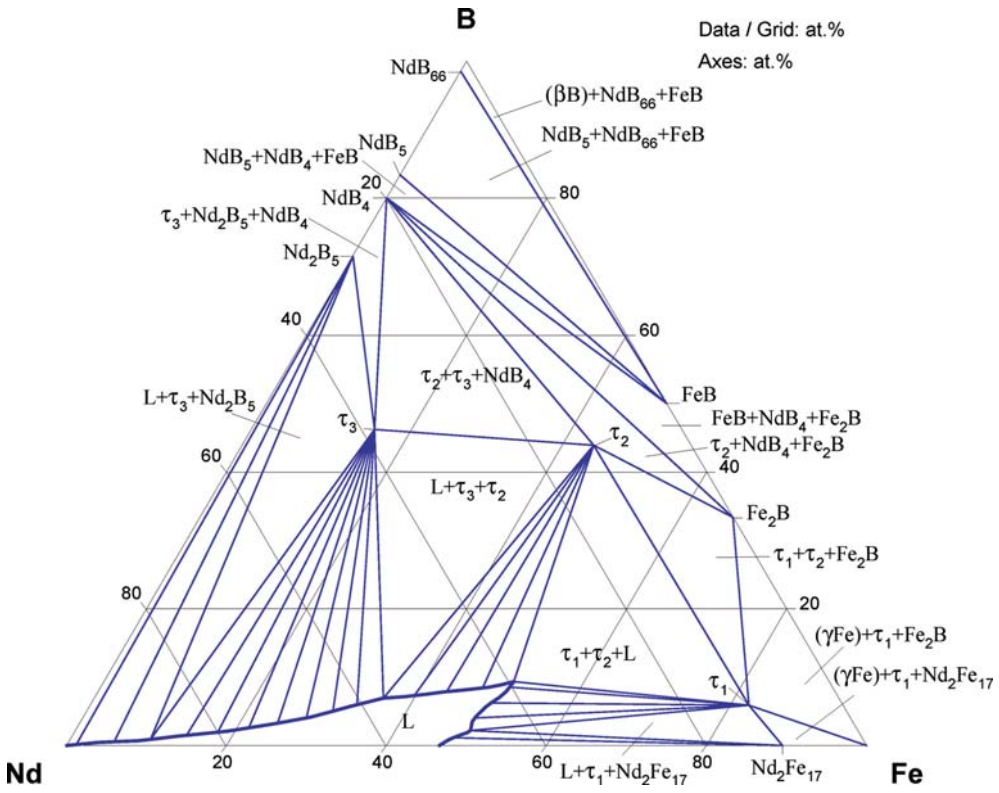

Fig. 3. B-Fe-Nd. Isothermal section at 1000°C

DOI: 10.1007/978-3-540-69761-9_22

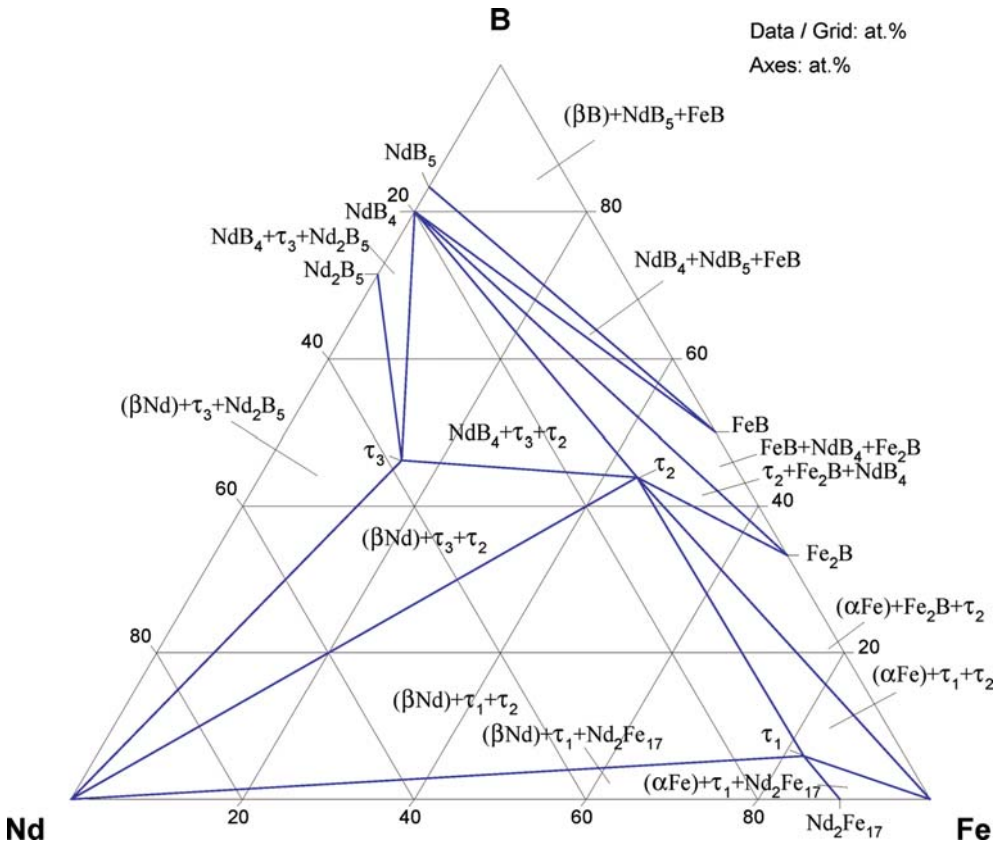

Fig. 4. B-Fe-Nd. Isothermal section at 900°C

DOI: 10.1007/978-3-540-69761-9_22

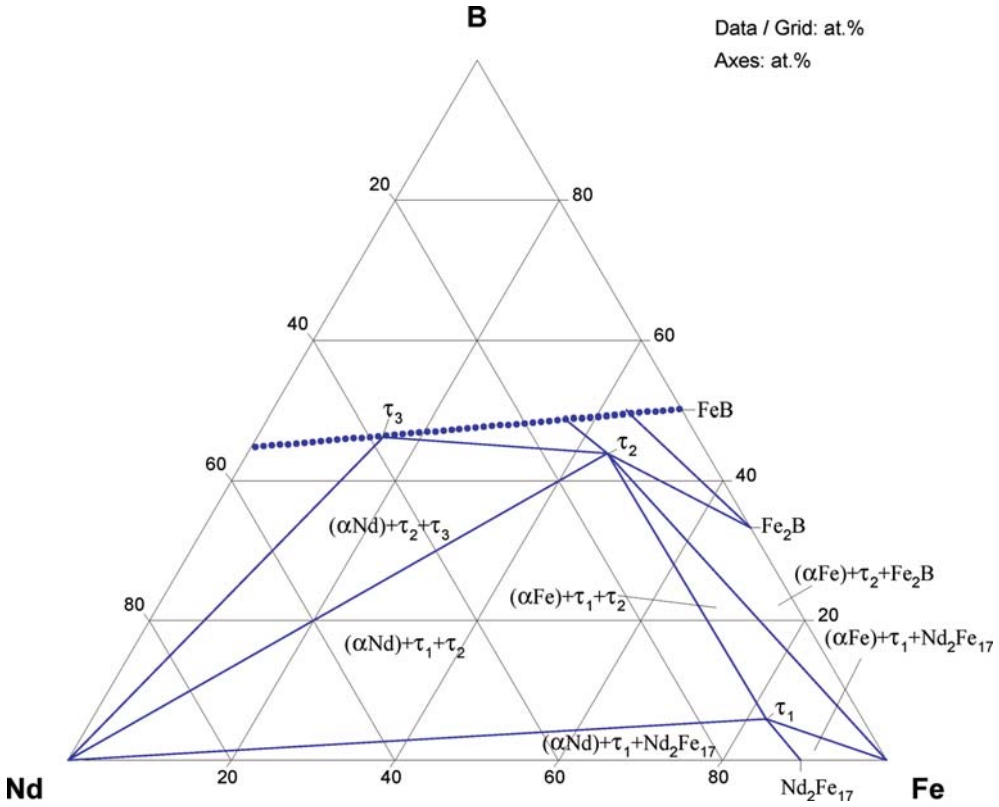

Fig. 5. B-Fe-Nd. Partial isothermal section at room temperature

DOI: 10.1007/978-3-540-69761-9_22

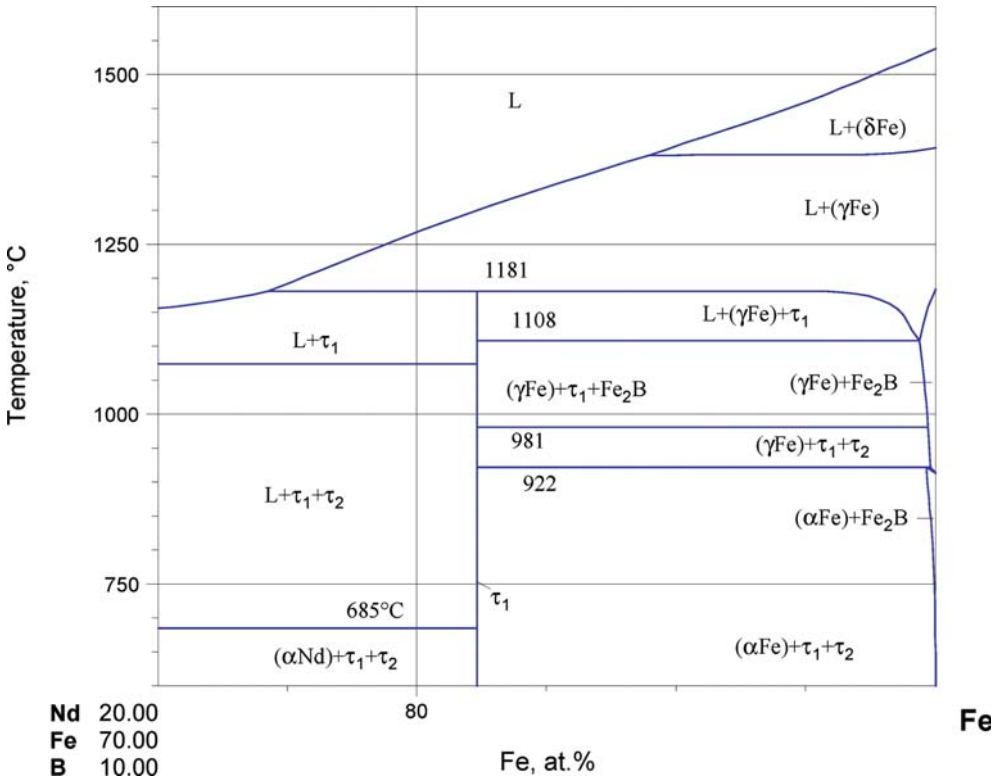

Fig. 6. B-Fe-Nd. Fe rich part of the temperature - composition section at Nd:B = 2:1

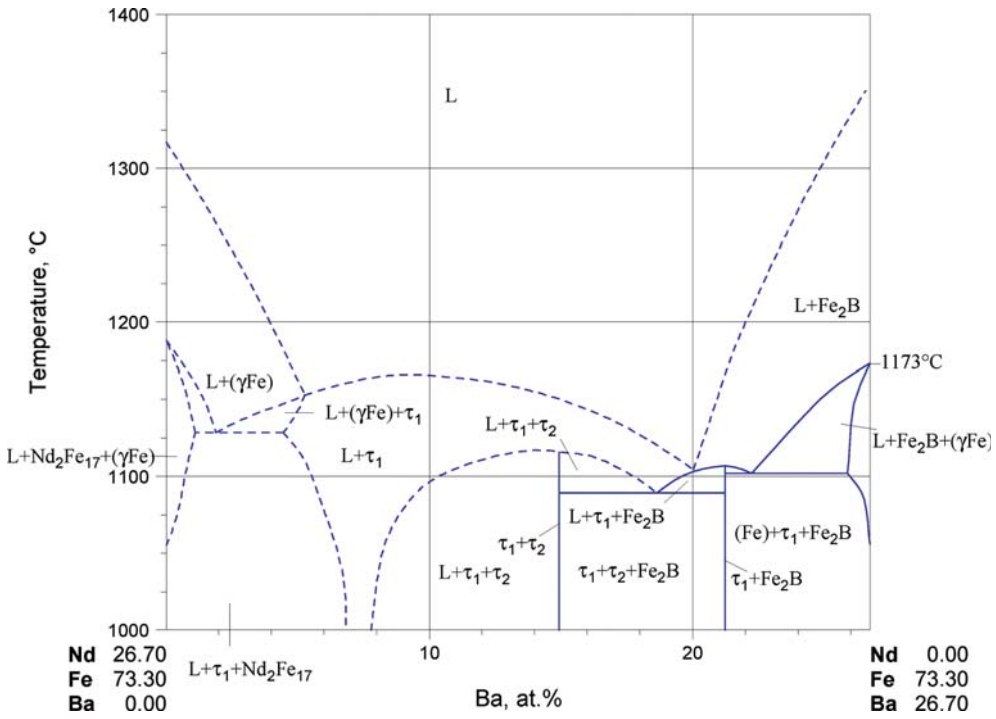

Fig. 7. B-Fe-Nd. Temperature - composition section at 73.3 at.% Fe

DOI: 10.1007/978-3-540-69761-9_22

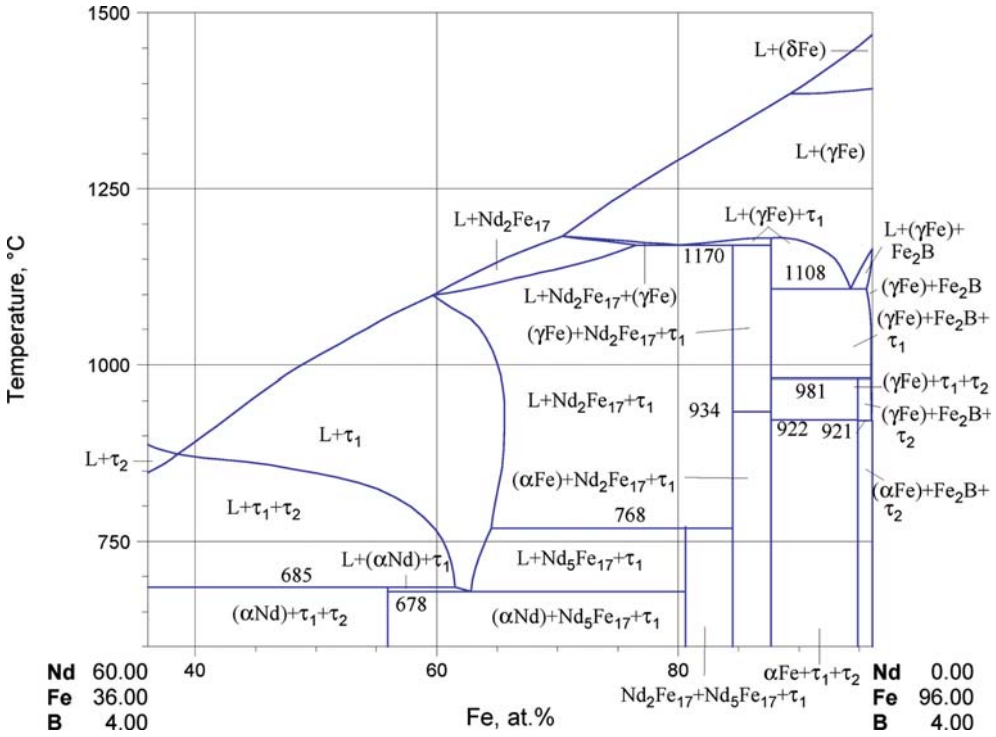

Fig. 8. B-Fe-Nd. Temperature - composition section at 4 at.% B

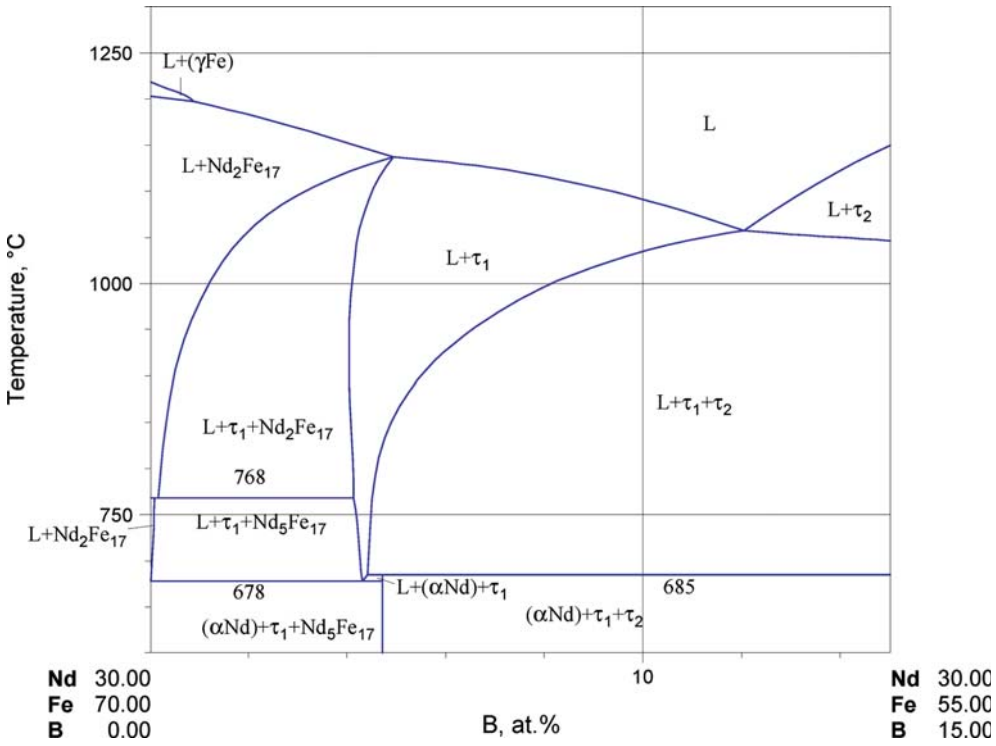

Fig. 9. B-Fe-Nd. Partial temperature - composition section at 30 at.% Nd

DOI: 10.1007/978-3-540-69761-9_22

References

[1976Spe] Spear, K.E., "Phase Behavior and Related Properties of Rare-Earth Borides", *Mater. Sci. Technol*., **4**, 91–159 (1976) (Phase Relations)

[1979Cha] Chaban, N.F., Kuz'ma, Yu.B., Bilonizhko, N.S., Kachmar, O.O., Petriv, N.V., "Ternary Systems {Nd, Sm, Gd} - Fe - B", *Dop. Akad. Nauk Ukrain. RSR, Ser. A, Fiz-Mat. Tekh. Nauki*, (10), 873–876 (1979) (Crys. Structure, Experimental, Phase Diagram, Phase Relations, 13)

[1984Cro] Croat, J.J., Herbst, J.F., Lee, R.W., Pinkerton, F.E., "Pr-Fe and Nd-Fe-based Materials: A New Class of High-Performance Permanent Magnets", *J. Appl. Phys*., **55**, 2078–2082 (1984) (Experimental, Crys. Structure, Magn. Prop., 9)

[1984Giv] Givord, D., Li, H.S., Perrier de la Bathie, R., "Magnetic Properties of $Y_2Fe_{14}B$ and $Nd_2Fe_{14}B$ Single Crystals", *Solid State Commun.*, **51**(11), 857–860 (1984) (Crys. Structure, Experimental, Magn. Prop., 7)

[1984Her] Herbst, J.F., Croat,.J.J., Pinkerton, F.E., Yelon, W.B., "Relationships Between Crystal-Structure and Magnetic Properties in $Nd_2Fe_{14}B$", *Phys. Rev. B*, **29**, 4176–4178 (1984) (Crys. Structure, Experimental, Magn. Prop., 17)

[1984Oes1] Oesterreicher, K., Oesterreicher, H., "On the Phase $NdFe_4B_4$ and its Implication in the Magnetic Hardening of $Nd_2Fe_{14}B$ Permanent Magnets", *J. Less-Common Met.*, **104**, L19-L21 (1984) (Crys. Structure, Experimental, 3)

[1984Oes2] Oesterreicher, K., Oesterreicher, H., "Structure and Magnetic Properties of $Nd_2Fe_{14}BH_{2.7}$", *Phys. Status Solidi A, Appl. Res.*, **85**(1), K61-K64 (1984) as quoted by [1998Bur]

[1984Sag1] Sagawa, M., Fujimura, S., Yamamoto, H., Matsuura, Y., Hiraga, K., "Permanent Magnet Materials based on the Rare Earth-Iron-Boron Tetragonal Compounds", *IEEE Trans. Magn. Vol. Mag.*,**20**(5), 1584–1589 (1984) (Experimental, Crys. Structure, Phase Realtions, Magn. Prop., 19)

[1984Sag2] Sagawa, M., Fujimura, S.,Togawa, M., Yamamoto, H., Matsuura, Y., "New Material for Permanent Magnets on the Base of Nd and Fe", *J. Appl. Phys.*, **55**, 2083–2087 (1984) (Experimental, Crys. Structure, Magn. Prop., 8)

[1984Sho] Shoemaker, C.B., Shoemaker, D.P., Fruchart, R., "The Structure of a New Magnetic Phase Related to the Sigma Phase - Iron Neodymium Boride $Nd_2Fe_{14}B$", *Acta Crystallogr., Sect. C: Cryst. Struct. Commun.*, **40**, 1665–1668 (1984) (Crys. Structure, Experimental, 10)

[1985And] Andreev, A.V., Bartashevich, M.I., Deryagin, A.V., Zadvorkin, S.M., Tarasov, E.N., Terentyev, S.V., "Crystal Structure and Magnetic Properties of the Compounds $R_2Fe_{14}B$" (in Russian), *Dokl. Akad. Nauk SSSR*, **283**(6), 1369–1371 (1985) (Crys. Structure, Experimental, 3)

[1985Bur] Burzo, E., Boltich, E.B., Huang, M.Q., Wallace, W.E., *Proc. 8th Int. Workshop on Rare-Earth Magnets and Their Applications*, Dayton (OH), 771–782 (1985) as quoted by [1998Bur]

[1985Giv] Givord, D., Moreau, J.M., Tenaud, P., "$Nd_5Fe_{18}B_{18}$ ($Nd_{1.11}Fe_4B_4$), a New Nowotny-Like Phase - Structural and Magnetic Properties", *Solid State Commun.*, **55**(4), 303–306 (1985) (Crys. Structure, Experimental, Magn. Prop., 11)

[1985Koo] Koon, N.C., Das, B.N., Rubinstein, M., Tyson, J., "Magnetic Properties of $R_2Fe_{14}B$ Single Crystals", *J. Appl. Phys.*, **57**(8), 4091–4093 (1985) (Experimental, Magn. Prop., 10)

[1985Mat] Matsuura, Y., Hirosawa, S., Yamamoto, H., Fujimura, S., Sagawa, M., Osamura, K., "Phase Diagram of the Nd-Fe-B Ternary System", *Japan. J. Appl. Phys.*, **24**(8), L635–L637 (1985) (Experimental, Phase Diagram, Phase Relations, 11)

[1986And] Andreev, A.V., Deryagin, A.V., Kudrevatykh, N.V., Mushnikov, N.V., Reimer, V.A., Terent'ev, S.V., "Magnetic Properties of $Y_2Fe_{14}B$ and $Nd_2Fe_{14}B$ and Their Hydrides", *Sov. Phys.- JETP (Engl. Transl.)*, **63**(3), 608–612 (1986), translated from *Zh. Eksp. Teor. Fiz*., **90**, 1042–1050 (1986) (Crys. Structure, Experimental, 17)

[1986Bus1] Buschow, K.H.J., de Mooij, D.B., Daams, J.L.C., van Noort, H.M., "Phase Relationships, Magnetic and Crystallographic Properties of Nd-Fe-B Alloys", *J. Less-Common Met.*, **115**, 357–366 (1986) (Crys. Structure, Phase Diagram, 16)

DOI: 10.1007/978-3-540-69761-9_22

[1986Bus2] Buschow, K.H.J., "New Permanent Magnet Materials", *Mater. Sci. Rep.***1**, 1–64 (1986) (Review, 210)

[1986Che] Che, G., Liang, J., Wang, X., "Phase Diagram of Nd-Fe-B Ternary", *Sci. Sini. A*, **29**(11), 1172–1185 (1986) (Phase Diagram, 8)

[1986Dem] De Mooij, D.B., Buschow, K.H.J., "A novel ternary Nd-Fe-B compound", *Philips Journal of Research*, **41**(4), 400–409 (1986) (Experimental, Crys. Structure, 10)

[1986Giv] Givord, D., Tenaud, P., Moreau, J.M., "Refinement of the Crystal Structure of $R_{1+\varepsilon}Fe_4B_4$ Compounds (R = Nd, Gd)", *J. Less Common Met.*, **123**, 109–116 (1986) (Experimental, Crys. Structure, 5)

[1986Hir] Hirosawa, S., Matsuura, Y., Yamamoto, H., Fujimura, S., Sagawa, M., Yamauchi, H., "Magnetization and Magnetic Anisotropy of $R_2Fe_{14}B$ Measured on Single Crystals", *J. Appl. Phys.*, **59**, 873–879 (1986) (Crys. Structure, Experimental, Magn. Prop., 15)

[1986Sch] Schneider, G., Henig, E.-T., Petzow, G., Stadelmaier, H., "Phase Relations in the System Fe-Nd-B", *Z. Metallkd.*, **77**(11), 755–761 (1986) (Experimental, Phase Diagram, Morphology, 26)

[1986Sta] Stadelmaier, H.H., Schneider, G., Ellner, M., "A $CaCu_5$ Type Iron-Neodymium Phase Stabilized by Rapid Solidification", *J. Less Common Met*., **115**, L11-L14 (1986) (Experimental, Crys. Structure, 8)

[1986Yam] Yamada, O., Tokuhara, H., Ono, F., Sagawa, M., Matsuura, Y., "Magnetocrystalline Anisotropy in $Nd_2Fe_{14}B$ Intermetallic Compound", *J. Magn. Magn. Mater.*, **54–57**, 585–586 (1986) (Experimental, Magn. Prop., 7)

[1987Fru] Fruchart, R., L'Heritier, P., Dalmas de Réotier, P., Fruchart, D., Wolfers, P., Coey, J.M.D, Ferriera, L.P., Guillen, R., Vuillet, P., Yaouanc, A., "Mössbauer Spectroscopy of $R_2Fe_{14}B$", *J. Phys. F: Met.Phys.*, **17**(2), 483–501 (1987) (Experimental, Magn. Prop., 58)

[1987Hen] Henig, E.-T., Schneider, G., Stadelmaier, H., "Metastable Solidification of Fe Rich Iron-Neodymium-Boron Alloys", *Z. Metallkd.*, **78**(11), 818–820 (1987) (Experimental, Phase Diagram, Morphology, 7)

[1987Nag] Nagata, H., Hirosawa, S., Sagawa, M., Ishibashi, A, Endo, S., "Pressure Dependence of the Curie Temperature of Intermetallic Compounds $Y_2Fe_{14}B$, $Ce_2Fe_{14}B$, $Nd_2Fe_{14}B$", *J. Magn. Magn. Mater.*, **70**(1–3), 334–336 (1987) (Experimental, Magn. Prop., 9)

[1987Ono] Onodera, H., Yamauchi, Y., Yamada, M., Yamamoto, H., Sagawa, M., Hirosawa, S., "Mossbauer Study of the Intermetallic Compound $Nd_2Fe_{14}B$. II. Temperature Dependence and Spin Reorientation", *J. Magn. Magn. Mater.*, **68**(1), 15–27 (1987) (Experimental, Magn. Prop., 36)

[1987Ota] Otani, Y., Miyajima, H., Chikazumi, S., "Magnetocrystalline Anisotropy in Nd-Fe-B Magnet", *J. Appl. Phys.*, **61**(8), 3436–3438 (1987) (Experimental, Magn. Prop., 5)

[1987Sch] Schneider, G., Henig, E.T., Petzow, G., Stadelmaier, H.H., "Phase Relations in the System Fe-Nd-B", *Z. Metallkd.*, **77**, 755 (1987) (Experimental, Crys. Structure, Phase Realtions, 26)

[1987Tsa] Tsai, D.S., Chin, T.S., Hsu, S.E., "The Phase Diagrams of the Pseudobinary Nd-($Fe_{14}B$) and the Fe-Nd-B Ternary System", *IEEE Trans. Magn.*, **23**(5), 3607–3609 (1987) (Experimental, Phase Diagram, Phase Relations, 7)

[1988Alt] Altounian, Z., Ryan, D.H., Tu, G.H., "A New Metastable Phase in the Nd-Fe-B System", *J. Appl. Phys.*, **64**(10), 5723–5725 (1988) (Experimental, Phase Relations, 4)

[1988Cad] Cadogan, J.M., Gavigan, J.P., Givord, D., Li, H.S., "A New Approach to the Analysis of Magnetization Measurements in Rare-Earth Transition-Metal Compounds - Application to $Nd_2Fe_{14}B$", *J. Phys. F: Met. Phys.*, **18**(4), 779–787 (1988) (Crys. Structure, Experimental, Magn. Prop., 17)

[1989Zha] Zhang, Y.D., Budnick, J.I., Yang, D.P., Potenziani, E., Pedziwiatr, A.T., Wallace, W.E., Sagawa, M., "Magnetic Field Dependence of ^{11}B and ^{57}Fe NMR in $Nd_2Fe_{14}B$ Compounds", *J. Magn. Magn. Mater.*, **79**(1), 136–142 (1989) (Experimental, Magn. Prop., 16)

[1990Hao] Hao, S., Xu, W., "An Isobar-Isothermal Phase Diagram of the Nd-Fe-B System at Atmospheric Pressure and 1000°C", *Zhongguo Xitu Xuebao (J. Chin. Rare Earth Soc.)*, **8**(3), 200–205 (1990) (Phase Diagram, Phase Relations, 5)

DOI: 10.1007/978-3-540-69761-9_22

[1990Lan] Landgraf, F.J.G., Schnaider, G.S., Villas-Boas, V., Missell, F.P., "Solidification and Solid State Ttransformations in Fe-Nd : a Revised Phase Diagram", *J. Less-Common Met.*, **163**, 209–218 (1990) (Experimental, Morphology, Magn. Prop., Phase Diagram, Phase Relations, 28)

[1990LeB] Le Breton, J.M., Teillet, J., "Oxidation of (Nd,Dy)FeB Permanent-Magnets Investigated by Fe-57 Mössbauer-Spectroscopy", *IEEE Trans. Magn*, **26**, 2652–2654 (1990) (Phase Relations, Experimental, Interface Phenomena, 9)

[1991Bal] Bala, H., Szymura, S., "An Electrochemical Investigation of Dissolution of Nd-Fe-B Magnets in Acid-Solution under Cathodic Polarization", *Corros. Sci.*, **32**(9), 953–963 (1991) (Experimental, Electrochemistry, Magn. Prop., 21)

[1991Bus] Buschow, K.H.J., "New Developments in Hard Magnetic-Materials", *Rep. Prog. Phys.*, **54**(9), 1123–1213 (1991) (Crys. Structure, Electronic Structure, Magn. Prop., Phase Diagram, Phase Relations, Review, 370)

[1991Kha] Khan, Y, Wibbeke, H., "Formation of the τ Phase in the Fe-B Alloys", *Z. Metallkd.*, **82**(9), 703–705 (1991) (Experimental, Crys. Structure, 6)

[1991Kim] Kim, J.-K., Saitoh, H., Hirano, K.-I., "Formation of Metastable Crystalline Phases in Amorphous $Fe_{74}R_6B_{20}$ Alloys (R = Ce, Nd, Sm, Gd, Tb, Dy, Er)", *J. Non-Cryst. Solids*, **128**(2), 162–165 (1991) (Phase Relations, Crys. Structure, Experimental, 15)

[1991Koh] Köhler, D., Kronmüller, H., "The Magnetic Phase-Transition in $Fe_{14}Nd_2B$ Single-Crystals", *J. Magn. Magn. Mater.*, **92**(3), 344–352 (1991) (Phase Relations, Experimental, Magn. Prop., 17)

[1991Lan1] Landgraf F.J.G., Missell F.P., "Ternary Iron-Neodymium-Boron Diagram" (in Portugese), *Congr. Anu.-Assoc. Bras. Met., 46th*, **3**, 401–419 (1991) (Experimental, Phase Diagram, Morphology, 28)

[1991Lan2] Landgraf, F.J.G., Missell, F.P., Knoch, G., Grieb, B., Henig, E.-T., "Binary Fe-Nd Metastable Phases in the Solidification of Fe-Nd-B Alloys", *J. Appl. Phys.*, **70**(10-II), 6107–6109 (1991) (Experimental, Morphology, Phase Diagram, Phase Relations, 12)

[1991Lan3] Landgraf, F.J.G., Schneider, G., Villas-Boas, V., Missel, F.P., "Solidification and Solid Phase Transformations in Fe-Nd: A Revised Phase Diagram", *J. Less-Common Met.*, **163**, 209–218 (1990) (Experimental, Crys. Structure, Phase Realtions, #, 28)

[1991LeB] Le Breton, J.M., Teillet, J., "Mössbauer and X-ray Study of NdFeB Type Permanent-Magnets Oxidation - Effect of Al and Nb Addition", *J. Magn. Magn. Mater.*, **101**(1–3), 347–348 (1991) (Experimental, Interface Phenomena, 7)

[1991Sta] Stadelmaier, H.H., Henig, E-T., Ptzow, G., "A Chronic of the Development of Iron Based Rare Earth High-Performance Magnets", *Z. Metallkd.*, **82**, 163–168 (1991) (Review, 73)

[1992Ge] Ge, S.H., Zhang, Y.D., Li, F.S., Budnick, J.I., Panissod P., "Hyperfine Fields and Magnetism in the $Nd_2Fe_{14}B$ Compound: a Combined Mössbauer and NMR Study", *J. Magn. Magn. Mater.*, **116**(1–2), 211–219 (1992) (Crys. Structure, Experimental, Magn. Prop., 27)

[1992Jed] Jedryka, E., Wojcik, M., Panissod, P., "2 Magnetic States of Nd in $Nd_2(CoFe)_{14}B$ – ^{145}Nd NMR-Study", *J. Magn. Magn. Mater.*, **104**, 1405–1406 (1992) (Crys. Structure, Experimental, Magn. Prop., 8)

[1992Rag] Raghavan, V., "The B-Fe-Nd (Boron-Iron-Neodymium) System", in "*Phase Diagrams of Ternary Iron Alloys"*, Part 6, Indian Institute of Metals, Calcutta, **6A**, 374–386 (1992) (Phase Diagram, Review, 35)

[1992Rie] Ried, K., Köhler, D., Kronmüller, H., "Experimental Hints for Crossover-Behavior in the Ferromagnetic Phase-Transition of $Fe_{14}Nd_2B$", *J. Magn. Magn. Mater.*, **116**, 259–266 (1992) (Phase relations, Experimental, Magn. Prop., 33)

[1992Rog] Rogl, P., Schuster, J.C., "System Iron-Boron-Nitrogen", in "*Ternary Boronnitrides and Siliconnitrides*", ASM, Oh., USA, 1–128 p.p., 1992

[1992Zha] Zhao, Z.B., Hong, S.Y., "A Group Theoretical Consideration of the Diffraction Patterns of $Nd_{1+\varepsilon}$ -Fe_4B_4 Compounds", *J. Phys.: Condens. Matter*, **4**(47), 9221–9234 (1992) (Calculation, Crys. Structure, Electronic Structure, Experimental, 32)

DOI: 10.1007/978-3-540-69761-9_22

[1993Gal] Galpin, D., "Investigation of the Ternary System Neodymium-Boron-Carbon" (in French), Stage de Fin d'Etudes, Genie Physique, INSA Rennes, France, 1–42 (1993) (Experimental, Crys. Structure, Phase Diagram, 50)

[1993Hen] Hennemann, K., Lukas, H.L., Schaller, H.J., "Constitution and Thermodynamics of Fe-Nd Alloys", *Z. Metallkd.*, **84**, 668–674 (1993) (Experimental, Calculation, Thermodyn., Phase Diagram, Phase Relations, 34)

[1993Kap] Kapusta, C., Figiel, H., Stoch, G., Lord, J.S., Riedi, P.C., "NMR of Nd and Sm in $Nd_2Fe_{14}B$ and $Sm_2Fe_{14}B$", *IEEE Trans. Magn.*, **29**(6), 2893–2895 (1993) (Crys. Structure, Experimental, Magn. Prop.)

[1993Kha] Khan, Y., Wang, R.-J., Kneller, E., "Structure and Magnetic Properties of New bcc *A*2 Type Based Superstructures in R-Fe-B Systems", *Z. Metallkd.*, **84**(12), 881–885 (1993) (Crys. Structure, Experimental, Magn. Prop., 9)

[1993Min] Min, B.I., Kang, J.S., Hong, J.H., Jeong, J.I., Lee, Y.P., Choi, S.D., Lee, W.Y., Yang, C.J., Olson, C.G., "Electronic and Magnetic-Structures of the Rare-Earth Permanent-Magnet $Nd_2Fe_{14}B$", *Phys. Rev. B*, **48**(9), 6217–6224 (1993) (Calculation, Crys. Structure, Electronic Structure, Experimental, Magn. Prop., 32)

[1993Szy] Szymura, S., Bala, H., Stoklosa, H., Sergeev, V.V., "Microstructure, Magnetic Properties and Corrosion Behavior of the Copper-Doped Nd-Fe-B Sintered Magnets", *Phys. Status Solidi A*, **137**(1), 179–188 (1993) (Magn. Prop., Morphology, Kinetics, Experimental, 23)

[1993Tur] Turek, K., Liszkowski, P., Figiel, H., "The Kinetics of Oxidation of Nd-Fe-B Powders", *IEEE Trans. Magn.*, **29**(6), 2782–2784 (1993) (Kinetics, Experimental, Magn. Prop., 13)

[1993Wer] Werheit, H., Kuhlmann, U., Laux, M., Lundström, T., "Structural and Electronic Properties of Carbon-Doped ß-Rhombohedral Boron", *Phys. Status Solidi*, **B179**, 489–511 (1993) (Crys. Structure, Phys. Prop., Experimental, 51)

[1994Gu] Gu, B.X., Shen, B.G., Zhai, H.R., "A Metastable Ternary Nd-Fe-B Compound", *J. Appl. Phys.*, **75**(10), 6955–6957 (1994) (Crys. Structure, Experimental, Magn. Prop., Phase Relations, 5)

[1994Hal] Hallemans, B., Wollants, P., Roos, J.R., "Thermodynamic Reassessment and Calculation of the Fe-B Phase Diagram", *Z. Metallkd.*, **85**(10), 676–682 (1994) (Thermodyn., Calculation, Phase Diagram, 36)

[1994Kno] Knoch, K.G., Reinsch, B., Petzow, G., "$Nd_2Fe_{14}B$ - Its Region of Primary Solidification", *Z. Metallkd.*, **85**(5), 350–353 (1994) (Experimental, Phase Diagram, Phase Relations, Morphology, 18)

[1995Cha1] Chaboy, J., Marcelli, A., García, L.M., Bartolomé, J., Kuz'min, M.D., Maruyama, H., Kobayashi, K., Kawata, H., Iwazumi, T., "X-ray Circular Magnetic Dichroism as a Probe of Spin Reorientation Transitions in $Nd_2Fe_{14}B$ and $Er_2Fe_{14}B$ Systems", *J. Magn. Magn. Mater.*, **140–144**, 1051–1052 (1995) (Phase Relations, Experimental, Magn. Prop., 9)

[1995Cha2] Chapman, J.N., Heyderman, L.J., Young, S., Donnet, D.M., Zhang, P.Z., Davies, H.A., "Micromagnetic and Microstructural Studies of NdFeB by TEM", *Scr. Metall.*, **33**(10–11), 1804–1816 (1995) (Morphology, Experimental, Magn. Prop., 10)

[1995Cyg] Cygan, D.F., McNallan, M.J. "Corrosion of NdFeB Permanent Magnets in Humid Environments at Temperatures up to 150°C", *J. Magn. Magn. Mater.*, **139**, 131–138 (1995) (Morphology, Experimental, Kinetics, 19)

[1995Hal] Hallemans, B., Wollants, P., Roos, J.R., "Thermodynamic Assessment of the Fe-Nd-B Phase Diagram", *J. Phase Equilib.*, **16**(2), 137–149 (1995) (Calculation, Phase Relations, Thermodyn., Phase Diagram, 41)

[1995Isn] Isnard, O., Yelon, W.B., Miraglia, S., Fruchart, D., "Neutron-Diffraction Study of the Insertion Scheme of Hydrogen in $Nd_2Fe_{14}B$", *J. Appl. Phys.*, **78**(3), 1892–1898 (1995) (Crys. Structure, Magn. Prop., Experimental, 26)

[1995Sou] Soubeyroux, J.L., Fruchart. D., Isnard, O., Miraglia, S., Tomey, E., "Role of the (H,C,N) Iinterstitial Elements on the Magnetic Properties of Iron-Rare Earth Permanent Magnet Alloys", *J. Alloys Compd.*, **219**, 16–24 (1995) (Crys. Structure, Experimental, Magn. Prop., 37)

DOI: 10.1007/978-3-540-69761-9_22

[1996Gab] Gabay, A.M., Popov, A.G., Gaviko, V.S., Belozerov, Ye.V., Yermolenko, A.S., "The Structure and Magnetic Properties of Rapidly Quenched and Annelaed Multiphase Nanocrystalline $Nd_9Fe_{91-x}B_x$ Ribbons", *J. Alloys Compd.*, **245**, 119–124 (1996) (Crys. Structure, Experimental, 9)

[1996Lia] Liao, P.K., Spear, K.E., "The B-Nd (Boron-Neodymium) System", *J. Phase Equilib.*, **17**(4), 335–339 (1996) (Phase Diagram, Phase Relations, Crys. Structure, Thermodyn., Assessment, 29)

[1996Obb] Obbade, S., Wolfers, P., Fruchart, D., Argoud, R., Muller, J., Palacios, E., "A Precise Crystal Structure Determination. Part II: an X-Ray Four-Circle Study of $Nd_2Fe_{14}B$ at 20 and 290 K", *J. Alloys Compd.*, **242**, 80–84 (1996) (Crys. Structure, Experimental, 11)

[1996Ste] Steyaert, S., LeBreton, J.M., Teillet, J., "Kinetic Parameters of the Dissociation of $Nd_2Fe_{14}B$ during Oxidation Determined by Mossbauer Spectrometry", *J. Phys.Condens. Matter*, **8**(49), 10721–10736 (1996) (Morphology, Experimental, Kinetics, 22)

[1996Wol] Wolfers, P., Obbade, S., Fruchart, D., Verhoef, R., "Precise Crystal and Magnetic Structure Determinations. Part I. A Neutron Diffraction Study of $Nd_2Fe_{14}B$ at 20 K", *J. Alloys Compd.*, **242**, 74–79 (1996) (Crys. Structure, Experimental, 31)

[1997Edg] Edgley, D.S., Le Breton, J.M., Steyaert, S., Ahmed, F.M., Harris, I.R., Teillet J., "Characterisation of High Temperature Oxidation of Nd-Fe-B Magnets", *J. Magn. Magn. Mater.*, **173**, 29–42 (1997) (Phase Relations, Experimental, Magn. Prop., 33)

[1997Fan] Fang, J.S., Hsieh, M.F., Chen, S.K., Chin, T.S., "Magnetic Properties and Structure of Nd-(Fe,B) Nanocomposite Alloys With Fixed Fe/B Ratios at 4–14", *Japan. J. Appl. Phys.*, **36**(10), 6316–6324 (1997) (Crys. Structure, Experimental, Magn. Prop., Morphology, Phase Relations, 19)

[1997Sun] Sun, W.-S., Li, S-D., Quan, M-X., "The Effect of Phase Constituent on the Magnetic Properties for Melt-Spun $Nd_{15}Fe_{77}B_8$ Ribbons", *J. Magn. Magn. Mater.*, **176**, 307–312 (1997) (Experimental, Magn. Prop., 16)

[1997Yar] Yartys, V.A., Wiesinger, G., Harris, I.R., "Hydrogenation Behaviour and Structure of $R_2Fe_2B_6$ (R = Ce, Pr, Nd, Sm, Gd, Tb) Borides", *J. Alloys Compd.*, **252**, 201–208 (1997) (Crys. Structure, Experimental, 14)

[1998Bur] Burzo, E., "Permanent Magnets Based on R-Fe-B and R-Fe-C Alloys", *Rep. Prog. Phys.*, **61**(9), 1099-1266 (1998) (Crys. Structure, Electronic Structure, Interface Phenomena, Magn. Prop., Phase Diagram, Phase Relations, Review, 1151)

[1998Mia] Miao, W.F., Ding, J., McCormicck, P.G., Street, R., "Remanence-Enhanced $Nd_8Fe_{87}M_1B_4$ (M = Fe, V, Si, Ga, Cr) Alloys", *J. Magn. Magn. Mater.*, **177–181**, 976–977 (1998) (Experimental, 5)

[1999Her] Hermann, R., Bächer, I., Löser, W., Schultz, L., "Primary Solidification of $Nd_2Fe_{14}B$ by Levitation and Quenching of Undercooled Melts", *J. Magn. Magn. Mater.*, 196–197, 737–739 (1999) (Morphology, Experimental, 4)

[1999Kon] Konno, T.J., Uehara, M., Hirosawa, S., Sumiyama, K., Suzuki, K., "Electron Diffraction Study on the Long-Range-Ordered Metastable Fe-Nd-B Phase", *Philos. Mag. A*, **79**(10), 2413–2436 (1999) (Crys. Structure, Experimental, 20)

[2000Liu] Liu, W., Zhang, Z.D., Liu, J.P., Sun, X.K., Sellmyer, D.J., Zhao, X.G., "Phase Constitution and Magnetic Properties of $Nd_{10}Fe_{76}B4M_{10}$ and $Nd_{10}Fe_{76}B_2M_{12}$ (M = Fe, Ti, V, Cr, Mn, Co, and Al) Alloys Prepared by Mechanical Alloying", *J. Magn. Magn. Mater.*, **221**, 278–284 (2000) (Experimental, Magn. Prop., 15)

[2001Alk] Al-Khafaji, M.A., Ahmad, I., Rainforth, W.M., Davies, H.A., Buckley, R.A., "Investigation of the Phase Constitution and Structure of Rapidly Solified Hard Magnetic $Nd_{18}Fe_{76}B_6$ Ribbons by Transmission Electron Microscopy", *Philos. Mag. A*, **81**(1), 11–24 (2001) (Crys. Structure, Experimental, Magn. Prop., 27)

[2001Cos] Costa, I., Oliveira, M.C.L., Takiishi, H., Saiki, M., Faria, R.N., "Corrosion Behaviour of Commercial $NdFe_B$ Magnets - The Effect of Magnetization", *Key Eng. Mater.*, **189–191**, 340–345 (2001) (Experimental, Interface Phenomena, Magn. Prop., 15)

DOI: 10.1007/978-3-540-69761-9_22

[2001Gao1] Gao, J., Volkmann, T., Roth, S., Loeser, W., Herlach, D.M., "Phase Formation in Undercooled NdFeB Alloy Droplets", *J. Magn. Magn. Mater.*, **234**, 313–319 (2001) (Crys. Structure, Experimental, Magn. Prop., 14)

[2001Gao2] Gao, J., Vollmann, Th., Herlach, D.M., "Metastable Solidification of NdFeB Alloys by Drop-Tube Processing", *J. Mater. Res.*, **16**(9), 2562–2567 (2001) (Crys. Structure, Experimental, Phase Relations, 17)

[2001Gir1] Girt, E., Krishnan, K.M., Thomas, G., "Optimization of Magnetic Properties of Nanostructured Nd-Fe-B: Approaching Ideal Stoner-Wohlfarth Behaviour", *Scr. Mater.*, **44**(8–9), 1431–1435 (2001) (Experimental, Magn. Prop., Phase Relations, 10)

[2001Gir2] Girt, E., Krishnan, K.M., Thomas, G., Girt, E., Altounian, Z., "Coercivity Limits and Mechanism in Nanocomposite Nd-Fe-B Alloys", *J. Magn. Magn. Mater.*, **231**(2–3), 219–230 (2001) (Crys. Structure, Experimental, Magn. Prop., Morphology, Phase Relations, 24)

[2001Kon] Kong, H.Z., Ding, J, Wang, L., Li, Y., "Bulk Hard Magnetic Alloys in Nd-Fe-B System Prepared by Casting and Melt Spinning", *Mater. Trans.*, **42**(4), 674–677 (2001) (Experimental, Magn. Prop., 18)

[2001Oza] Ozawa, S., Saito, T., Yu, J., Motegi, T., "Solidification Behavior in Undercooled Nd-Fe-B Alloys", *J. Alloys Compd.*, **322**(1–2), 276–280 (2001) (Crys. Structure, Experimental, Morphology, Phase Relations, 15)

[2001Sai] Saito, T., "Production of Bulk Materials of an $Nd_4Fe_{77.5}B_{18.5}$ Alloy and Their Magnetic Properties", *IEEE Trans. Magn.*, **37**(4), 2561–2563 (2001) (Experimental, Magn. Prop., 12)

[2001Wol] Wolfers, P., Bacmann, M., Fruchart, D., "Single Crystal Neutron Diffraction Investigations of the Crystal and Magnetic Structures of $R_2Fe_{14}B$ (R = Y, Nd, Ho, Er)", *J. Alloys Compd.*, **317–318**, 39–43 (2001) (Crys. Structure, Experimental, Magn. Prop., 14)

[2001Woo] Woodward, R.C., Gorham, N.T., Street, R., Crew, D.C., Girt, E., Krishnan, K.M., "Coercivity, Time Dependence and Reversible Magnetization in Nd Rich Nd-Fe-B Alloys", *IEEE Trans. Magn.*, **37**(4), 2493–2496 (2001) (Experimental, Magn. Prop., 13)

[2002Cre] Crew, D.C., Girt, Er., Suess, D., Schrefl, T., Krishnan, K.M., Thomas, G., Guilot, M., "Magnetic Interactions and Reversal Behavior of $Nd_2Fe_{14}B$ Particles Diluted in a Nd Matrix", *Phys. Rev. B*, **66**(18), 184418_1–184418_13 (2002) (Experimental, Magn. Prop., Morphology, 33)

[2002Gao] Gao, J., Volkmann, T., Herlach, D.M., "Critical Undercoolings for Different Primary Phase Formation in $Nd_{15}Fe_{77.5}B_{7.5}$ Alloy", *IEEE Trans. Magn.*, **38**(5), 2910–2912 (2002) (Experimental, Phase Relations, 10)

[2002Gu] Gu, B.X., "Exchenge Coupling in Nanocomposite $(Fe, Nd)_3B/\alpha$-Fe Hard Magnetic Materials", *Phys. Status Solidi A*, **191**(2), 571–576 (2002) (Crys. Structure, Experimental, Magn. Prop., 13)

[2002Kim1] Kim, H.-T., Kim, Y.B., Park, W.S., "Magnetic Contour of Nano-Composite Nd-Fe-B Melt-Spun Alloys", *J. Magn. Magn. Mater.*, **239**, 430–432 (2002) (Experimental, Magn. Prop., Phase Relations, 5)

[2002Kim2] Kim, H.T., Park, W.S., Kim, Y.B., "Temperature Dependence on the Magnetic Properties of Nano-Crystalline Nd-Fe-B Melt-Spun Alloys", *J. Magn. Magn. Mater.*, **239**(1–3), 441–443 (2002) (Experimental, Magn. Prop., Phase Relations, 7)

[2002Li] Li, S., Gu, B., Bi, H., Tian, Z., Xie, G., Zhu, Y., Du, Y., "Role of Amorphous Grain Boundaries in Nanocomposite NdFeB Permanent Magnets", *J. Appl. Phys.*, **92**(12), 7514–7518 (2002) (Crys. Structure, Experimental, Interface Phenomena, Magn. Prop., Morphology, 24)

[2002Rom] Rompaey, T.V., Hari Kumar, K.C., Wollants, P., "Thermodynamic Optimization of the B-Fe System", *J. Alloys Compd.*, **334**, 173–181 (2002) (Calculation, Thermodyn., Phase Diagram, Phase Relations, 45)

[2002Sta] Stadelmaier, H.H., Petzow, G., "Metastable Alloys at Moderate Cooling Rates", *Z. Metallkd.*, **93**(10), 1019–1023 (2002) (Experimental, Magn. Prop., Phase Relations, Review, 42)

DOI: 10.1007/978-3-540-69761-9_22

[2002Vol] Volkmann, T., Gao, J., Herlach, D.M., "Direct Crystallization of the Peritectic $Nd_2Fe_{14}B_1$ Phase by Undercooling of Bulk Alloy Melts", *Appl. Phys. Lett.*, **80**(11), 1915–1917 (2002) (Crys. Structure, Experimental, Morphology, Phase Relations, 12)

[2003Gao] Gao, J., Volkmann, T., Herlach, D.M., "Solidification of Levitated Nd-Fe-B Alloy Droplets at Significant Bulk Undercoolings", *J. Alloys Compd.*, **350**(1–2), 344–350 (2003) (Crys. Structure, Experimental, Morphology, Phase Relations, 20)

[2003Rag] Raghavan, V., "B-Fe-Nd (Boron-Iron-Neodymium)", *J. Phase Equilib.*, **24**(5), 451–454 (2003) (Phase Diagram, Assesssment, 17)

[2003Shi] Shindo, D., Park, Y.-G., Murakami, Y., Gao, Y., Kanekiyo, H., Hirosawa, S., "Electron Holography of Nd-Fe-B Nanocomposite Magnets", *Scr. Mater.*, **48**(7), 851–856 (2003) (Experimental, Magn. Prop., Morphology, Phase Relations, 13)

[2003Zai] Zaitsev, A., Zaitseva, N., Kodentsov, A., "Thermodynamic Properties and Phase Equilibria in the Iron-Boron System. Transition of the Fe-B Melt into the Amorphous State", *J. Mater. Chem.*, **13**, 943–950 (2003) (Experimental, Thermodyn., Phase Relations, Calculation, 65)

[2004Har] Harland, C.L., Lewis, L.H., Chen, Z., Ma, B.-M., "Exchange Coupling and Recoil Loop Area in $Nd_2Fe_{14}B$ Nanocrystalline Allos", *J. Magn. Magn. Mater.*, **271**(1), 53–62 (2004) (Experimental, Magn. Prop., Morphology, 27)

[2004Oza1] Ozawa, S., Saito, T., Motegi, T., "Effects of Cooling Rate on Microstructures and Magnetic Properties of Nd-Fe-B Alloys", *J. Alloys Compd.*, **363**(1–2), 263–270 (2004) (Experimental, Kinetics, Magn. Prop., Morphology, 22)

[2004Oza2] Ozawa, S., Li, M., Sugiyama, S., Jimbo, I., Hirosawa, S., Kuribayashi, K., "Microstructual Evolution and Magnetic Properties of the Nd-Fe-B Alloys Solidified from Undercooled Melt by Containerless Solidification", *Mater. Sci. Eng. A*, **382**(1–2), 295–300 (2004) (Crys. Structure, Experimental, Magn. Prop., Morphology, Phase Relations, 22)

[2004Tia] Tian, Z., Li, S., Peng, K., Gu, B., Zhang, J., Lu, M., Du, Y., "The Microstructure and Magnetic Properties of NdFeB Magnets Directly Solidified at a Low Cooling Rate", *Mater. Sci. Eng. A*, **380**, 143–146 (2004) (Morphology, Experimental, Magn. Prop., 18)

[2004Vol1] Volkmann, T., Strohmenger, J., Gao, J., Herlach, D.M., "Observation of a Metastable Phase During Solidification of Undercooled Nd-Fe-B Alloy Melts by in Situ Diffraction Experiments Using Synchrotron Radiation", *Appl. Phys. Lett.*, **85**(12), 2232–2234 (2004) (Crys. Structure, Experimental, 10)

[2004Vol2] Volkmann, T., Gao, J., Strohmenger, J., Herlach, D.M., "Direct Crystallization of the Peritectic $Nd_2Fe_{14}B_1$ Phase by Undercooling of the Melt", *Mater. Sci. Eng. A*, **375–377**, 1153–1156 (2004) (Crys. Structure, Experimental, Morphology, Phase Diagram, Phase Relations, 8)

[2005Pas] Pastusbenkov, Y.G., Skokov, K.P., Suponev, N.P., Stakhovski, D., "Low-Temperature Magnetization Distribution and Magnetization Reversal in Fe-Nd-B Permanent Magnets", *J. Magn. Magn. Mater.*, **290–291**, 644–646 (2005) (Crys. Structure, Experimental, Magn. Prop., 8)

[2005Shi] Shinba, Y., Konno, T.J., Ishikawa, K., Hiraga, K., Sagawa, M., "Transmission Electron Microscopy Study on Nd Rich Phase and Grain Boundary Structure of Nd-Fe-B Sintered Magnets", *J. Appl. Phys.*, **97**(5), 053504 (2005) (Crys. Structure, Experimental, Morphology, 32)

[2005Yan] Yang, N, Dennis, K.W., McCallum, R.W., Kramer, M.J., Zhang, Y, Lee, P.L., "Spontaneous Magnetostriction in $R_2Fe_{14}B$ (R = Y, Nd, Gd, Tb, Er)", *J. Magn. Magn. Mater.*, **295**(1), 65–76 (2005) (Crys. Structure, Experimental, Magn. Prop., 42)

[V-C2] Villars, P. and Calvert, L.D., *Pearson's Handbook of Crystallographic Data for Intermetallic Phases*, 2nd edition, ASM, Metals Park, Ohio (1991)

[Mas2] Massalski, T.B. (Ed.), *Binary Alloy Phase Diagrams*, 2nd edition, ASM International, Metals Park, Ohio (1990)

DOI: 10.1007/978-3-540-69761-9_22

Boron – Iron – Nickel

Annelies Malfliet, Jozefien De Keyzer

Introduction

B-Fe-Ni alloys, in particular around a composition of $Fe_{40}Ni_{40}B_{20}$, are important for their soft magnetic properties. Especially amorphous alloys are widely investigated.
The system was reviewed by Raghavan in 1992 [1992Rag], mainly based on the research of [1968Kuz] and [1989Loo]. A ternary compound of the $Cr_{23}C_6$ type is metastable [1967Aye, 1969Sta]. Main features of the system are the complete solid solubility between Fe_2B and Ni_2B [1966Kan] and a large solubility of Fe in Ni_3B [1967Mon].
Isothermal sections in this system are known at 700°C [1966Kan], 800°C [1968Kuz] and 925°C [1989Loo]. [1966Kan] also determined a partial liquidus surface. Temperature-composition sections were established at 26 at.% B [2005Tok] and 33 at.% B [1972Tav]. Enthalpies of mixing for several isopleths were measured by [1995Wit] and a thermodynamic assessment was made by [2005Tok]. Investigations on phase relations, structures and thermodynamics are summarized in Table 1.

Binary Systems

After the review by [Mas2], two thermodynamic optimizations of the B-Fe system were carried out by [1994Hal] and [2002Rom]. Agreements were observed except for the temperature of the eutectic reaction $L \rightleftharpoons (Fe) + Fe_2B$ which was found to be 20°C lower in the CALPHAD assessment of [2002Rom]. Recent thermodynamic experimental work of [2003Zai] confirmed the eutectic temperature found by [1994Hal] using a least-square optimization. The equilibrium phase diagram was then accepted from [1994Hal] (Fig. 1). The B-Ni phase diagram as accepted in [Mas2] was mainly based on the original work of [1965Sch]. The thermodynamic assessment done by [1993Tep] was revised by [1999Cam]. The latter was then accepted here (Fig. 2). The Fe-Ni phase diagram is accepted from [2006Kuz], which is essentially the same as the recent review by [2006Cac].

Solid Phases

Crystallographic data of all unary and binary phases are listed in Table 2. A ternary phase of the $Cr_{23}C_6$ type was mentioned by [1967Aye]. This phase was not found by [1968Kuz] and was concluded to be metastable [1969Sta]. It is formed when the formation of Ni_3B is suppressed [2002Sta].
A continuous solid solution between Fe_2B and Ni_2B was found by [1966Kan] and confirmed by [1967Mon, 1969Sta, 1986Gia]. Ni_3B solves up to 45 at.% Fe [1967Mon, 1968Kuz, 1969Sta, 1989Loo].
[1967Mon] measured the lattice parameters of the solid solution $(Fe_xNi_{1-x})_2B$ and $(Fe_xNi_{1-x})_3B$ in function of x. For $(Fe_xNi_{1-x})_2B$, the parameter a increases in a nonlinear manner, while c attains a minimum at $x = 0.6$. For the orthorhombic phase $(Fe_xNi_{1-x})_3B$ from $x = 0$ to $x = 0.7$ all three parameters a, b and c increase. The lattice parameters are shown in Figs. 3a-b. [1972Tav] also measured the lattice parameters for the system $(Fe_xNi_{1-x})_2B$, which deviate little from the curve of [1967Mon]. Measurements of [1969Ruh] show that the alloys 1.8B-Fe-13Ni, 2.0B-Fe-13Ni and 2.0B-Fe-24Ni (mass%) exhibit a lattice contraction in comparison to the corresponding binary Fe-Ni alloys.

Quasibinary Systems

The sections NiB-FeB and Ni_2B-Fe_2B show a quasibinary behavior, but are not completely quasibinary due to the peritectic formation of NiB and Fe_2B.

Invariant Equilibria

A eutectic reaction $L \rightleftharpoons Ni_3B + Fe_2B + \gamma$ at 1057°C nearby a composition of 18 at.% B and 40 at.% Ni is proposed by [1962Bre]. [1966Kan] finds a minimum at 1032°C in the liquidus line starting from the binary

DOI: 10.1007/978-3-540-69761-9_23

eutectic L ⇌ Fe_2B + γ and going downwards into the ternary at a composition of 20 at.% B and 40 at.% Ni. The conclusion of [1992Reg] that a ternary eutectic exists at this composition and a temperature of ~1040°C is accepted here (see Table 3).

Liquidus, Solidus and Solvus Surfaces

Information about the reactions with liquid is limited to a partial liquidus surface from the experimental investigation of [1966Kan], which is redrawn in Fig. 4. The monovariant line coming from the binary eutectic between γ(Fe,Ni) and Fe_2B reaches a minimum in the ternary system for the composition $B_{20}Fe_{40}Ni_{40}$ (at.%) at ~1040°C according to [1992Reg], which corresponds to the invariant reaction E.

Isothermal Sections

Three isothermal sections are shown in Figs. 5, 6 and 7 at respectively 700°C, 800°C and 925°C. [1966Kan] equilibrated samples with 1 at.% B at 700°C and extracted the borides from the austenite phase with a HCl solution. After chemical and X-ray diffraction investigation, they found only $(Fe,Ni)_2B$ and could not identify Ni_3B. Tie-lines were determined between the Fe_2B phase and the (γFe,Ni) phase (Fig. 5). [1968Kuz] prepared 40 alloys in the whole composition range to establish a section at 800°C. It is however not clear whether the used techniques are sufficient to determine the phase composition accurately. A NiB_{12} phase was observed, which was also found in the binary B-Ni system by [1966Por], but this phase is metastable and probably due to carbon impurities. A second isothermal section was determined by [1986Gia]. A solubility of 35 at.% Ni in FeB is found, which is in contradiction with [1968Kuz]. Since the samples of [1968Kuz] were equilibrated for 600 h whereas the samples of [1986Gia] only 4 to 20 h, it can be assumed that the latter ones did not reach full equilibrium. Therefore, the section at 800°C of [1968Kuz], adapted to the accepted binaries is given here (Fig. 6). The section at 925°C by [1989Loo], shown in Fig. 7, includes tie-lines but is limited to < 33 at.% B. A qualitatively good agreement with [1968Kuz] is observed.
However when the boundaries of the three-phase fields are drawn on an isopleth through the eutectic composition together with the experimental values for the composition at the eutectic temperature [1966Kan], it can be seen that the proposed sections are hard to combine. Since the study of [1989Loo] includes EPMA measurements, it is expected to be more reliable than [1968Kuz].

Temperature – Composition Sections

Figure 8 gives an isopleth at 33 at.% B from the experimental work of [1972Tav]. This section was slightly modified according to the accepted binary systems. An isopleth at 26 at.% B based on DSC measurements [2005Tok] and data of [1966Kan, 1968Kuz, 1989Loo] is shown in Fig. 9.

Thermodynamics

[1995Wit] determined the partial enthalpies of mixing for 0 - 0.4 at.% B along 4 lines with constant ratios of Fe and Ni: $(Fe_{0.75},Ni_{0.25})_{100-x}B_x$, $(Fe_{0.5},Ni_{0.5})_{100-x}B_x$, $(Fe_{0.25},Ni_{0.75})_{100-x}B_x$, $(Fe_{0.10},Ni_{0.90})_{100-x}B_x$ (Figs. 10a-d).
Two CALPHAD type assessments were made by [1998Mie] and [2005Tok]. [1998Mie] extrapolated from the binaries and introduced 3 ternary parameters to get a reasonable agreement for the eutectic reaction L ⇌ Ni_3B + Fe_2B + γ. Since he did not take into account any other experimental data, this description should be considered approximate. [2005Tok] based their assessment on their own DSC measurements and on literature data of [1969Sta], [1968Kuz] and [1989Loo]. Although the agreement with experiments is quantitatively correct, phase compositions and tie-lines are not reproduced very good. Moreover, no ternary thermodynamic data were used for the optimization. The agreement with the experimental data of [1995Wit] is rather poor.

Notes on Materials Properties and Applications

The materials properties that have been investigated are mostly magnetic properties. The Curie point and magnetic moment of crystalline $(Fe_{1-x}Ni_x)_2B$ alloys are measured by [1962Cad, 1970Iga]. Both the Curie

DOI: 10.1007/978-3-540-69761-9_23

point and the magnetic moment per transition atom decrease non-linearly with increasing x. At $x \sim 0.8$ the Curie point is ~100 K and the magnetic moment becomes very small. Accordingly, [1979Tra] observed at this composition a variation in the lattice parameters and attributed it to the ferromagnetic to paramagnetic transition. B-Fe-Ni based amorphous alloys by rapid solidification techniques exhibit soft ferromagnetic properties. Several studies are dedicated to reveal the influence of heat treatment [1979Lub, 1988Kun, 1988Mit] and mechanical pressure [1988Kun, 1992Man] on the magnetic properties of these amorphous alloys, but their effect is highly dependent on the experimental conditions. The ferromagnetic to paramagnetic transition in amorphous $(Fe_{1-x}Ni_x)_{100-y}B_y$ alloys has been studied by [1988Ilo, 2001Kis] for respectively $y = 20$ and 18.5 at.%. Other studies deal with more specific topics. [1980Tea] studied the relation between inhomogeneity on atomic scale and the resonance line width in $(Fe_{1-x}Ni_x)_{83}B_{17}$ alloys, but found no clear relation. [1983Jag] measured the disaccommodation of the permeability of amorphous $(Fe_{1-x}Ni_x)_{80}B_{20}$ with $0 \leq x \leq 0.5$. He states that the disaccommodation is a decreasing function of x in the as-quenched state, while an increasing function is observed in the annealed state. [2005Du] found that the addition of boron to Fe-Ni alloys enhances the milling and magnetic properties of nanocrystalline and amorphous Fe-Ni alloys, but that a subsequent heat treatment leads to a deterioration of the magnetic properties.

The influence of Ni on the mechanical properties of Fe-0.2B (mass%) is investigated by [1966Has]. The addition of Ni (≤1.02 mass%) leads to an increase in Vickers hardness in water-quenched and annealed state. [1983Hun] investigated the influence of heat treatment and composition on the strength and ductility of $(Fe_{1-x}Ni_x)_{100-y}B_y$ alloys with $x = 0$ - 0.93 and $y = 9$ - 25 at.%. By increasing the boron concentration, a marked increase in strength and a strong decrease in ductility is observed. Fracture toughness measurements indicated a reduction in ductility after annealing at short times.

The tracer diffusivity of ^{59}Fe in amorphous $Fe_{40}Ni_{40}B_{20}$ and $Fe_{41}Ni_{41}B_{18}$ decreases with relaxation until it reaches a plateau which is dependent of temperature and follows an Arhenius law: $D_0^T \exp(-H^T/kt)$ with D_0^T the pre-exponential factor and H^T the tracer diffusion enthalpy [1987Pfa, 1985Hor]. [1989Bra] found that the activation energy for diffusion of B in FeB and FeB_2 increases on alloying with Ni.

Main experimental investigations are gathered in Table 4.

Miscellaneous

Amorphous alloys were prepared by melt-spinning [1983Ber, 1983Kha], by chemical reduction [1991Gha, 1993Hu, 2001Zys] and by flame sprayed coating [1987Bor].

Several studies on the structure and crystallization of amorphous B-Fe-Ni alloys were performed. [1980Was] states that the replacement of Fe by Ni has little to no effect on the structure, whereas crystallization temperature and Curie temperature are strongly affected by this replacement. [1982Ber] investigated the crystallization behavior of $(Fe_{1-x}Ni_x)_{83}B_{17}$ alloys. Up to 25 at.% Ni, the crystallization to eutectic Fe and $(Fe,Ni)_3B$ occurs in two stages, depending on temperature and annealing time. A Ni content of 25 at.% lowers the start temperature of the eutectic crystallization and above 30 at.% Ni, the formation of (γFe,Ni) is observed. Mössbauer studies on the crystallization behavior of $(Fe_{0.5}Ni_{0.5})_{100-y}B_y$ with $y = 16$, 18, 20, 22, 25 at.% and $(Fe_{1-x}Ni_x)_{80}B_{20}$ with $x = 0.75$, 0.6875, 0.5, 0.25 were done by [1990Kon, 1991Kon1, 1991Kon2].

[1983Kha, 1983Gor] studied the composition dependence of the glass-forming ability. [1988Cun] introduced the concept of effective temperature and time to predict the anisothermal onset of crystallization in B-Fe-Ni alloys. He used the experimental TTT curves of [1983Gor] to compare his results.

[1984Kro] modelled the relaxation phenomena in amorphous alloys and used his model to quantitatively describe the time and temperature dependence of experimental relaxation spectra of $Fe_{80-x}Ni_xB_{20}$. Calculations of [1995Zou] suggest that magnetic after effects are related to local rearrangements of atom pairs B-Fe and B-Ni.

Calculated enthalpies of formation of M_3B [1987Rez] suggest that the increase in crystallization temperature of $Fe_{80}M_5B_{15}$ alloys is linearly related to the difference in enthalpy of formation between M_3B and Fe_3B. For Ni, this results in a small decrease of 0.5 K.

The use of 20B-Fe-10Ni (mass%) alloys activates the sintering process of iron powder compacts [1989Nis] through the formation of eutectic liquid.

DOI: 10.1007/978-3-540-69761-9_23

The addition of boron to austenitic Fe-Ni alloys causes grain boundary hardening through grain boundary segregation [1991She].
Assuming saturation was reached after 5 minutes of firing between 1100 and 1250°C, [1992Efi] found solubilities of iron in a Ni-B melt (2.0-6.7 mass% B). The diffusion coefficient of iron in the melt is estimated to be larger than $8 \cdot 10^{-6}$ $cm^2 \cdot s^{-1}$.

Table 1. Investigations of the B-Fe-Ni Phase Relations, Structures and Thermodynamics

Reference	Method/Experimental Technique	Temperature/Composition/Phase Range
[1962Bre]	Thermal analysis	18B-Fe-40Ni (at.%)
[1966Has]	Thermal differential analysis, electron microscopy, X-ray measurements, Vickers hardness	0.2B-Fe-1.02Ni (mass%), 0.02B-Fe-0.09Ni (mass%) and 0.02B-Fe-0.34Ni (mass%) up to 1100°C
[1966Kan]	Thermal differential analysis, X-ray measurements, microstructural analysis	*x*B-Fe-*y*Ni (x = 2-6 mass% $y \leq 40$ mass%)
[1967Mon]	X-ray measurements	$(Fe,Ni)_2B$, $(Ni,Fe)_3B$ at 850°C
[1967Aye]	X-ray measurements	$(Fe,Ni)_{23}B_6$ at 850°C
[1968Kuz]	Phase diagram investigation by X-ray measurements and microstructure analysis	800°C, 40 alloys in whole composition range
[1969Ruh]	X-ray measurements	1.8B-Fe-13Ni, 2.0B-Fe-13Ni and 2.0B-Fe-24Ni (mass%)
[1969Sta]	Phase diagram investigation by X-ray measurements and microstructure analysis	800°C, $x_B < 0.4$
[1972Tav]	X-ray measurements and chemical analysis	$(Fe,Ni)_2B$ at 1100°C
[1980Was]	X-ray diffraction	amorphous $(Fe_{0.6}Ni_{0.4})_{100-y}B_y$ for y = 14 to 24 at.%, amorphous $(Fe_{1-x}Ni_x)_{80}B_{20}$ for x = 0.3 to 0.7
[1986Gia]	X-ray diffraction and atomic absorption analysis	(Fe, Ni)-*x*B with x = 11-12 mass%
[1989Bra]	Penetration depth measurements	Borided Fe-*x*Ni with x = 0, 4 and 10 mass% at 752-1002°C
[1989Loo]	Diffusion couple measurements	925°C, $x_B < 0.33$
[1995Wit]	Enthalpies of mixing by calorimetry	$(Fe_xNi_{1-x})_{100-y}B_y$ with x = 0.1, 0.25, 0.5, 0.75 and $y < 40$ at.% at 1600°C
[1998Mie]	Calculation	entire system
[2005Du]	Thermal differential analysis, electron microscopy, X-ray diffraction	25-650°C, Fe-40Ni-18B (at.%)
[2005Tok]	DSC measurements	< 1400°C, 26 at.% B

DOI: 10.1007/978-3-540-69761-9_23

Table 2. Crystallographic Data of Solid Phases

Phase/ Temperature Range [°C]	Pearson Symbol/ Space Group/ Prototype	Lattice Parameters [pm]	Comments/References
(βB) < 2092	*hR*333 $R\bar{3}m$ βB	*a* = 1093.30 *c* = 2382.52	[1993Wer]
(αFe) < 912	*cI*2 $Im\bar{3}m$ W	*a* = 286.65	at 25°C, [Mas2]
γ, (γFe,Ni)	*cF*4 $Fm\bar{3}m$	*a* = 357.5	(FeNi 50-50 at.%) [V-C2]
(Ni), < 1455	Cu	*a* = 352.32	at 100% Ni [2006Cac]
(γFe) 1394 - 912		*a* = 364.67	at 100% Fe, at 25°C [Mas2]
(δFe) 1538 - 1394	*cI*2 $Im\bar{3}m$ W	*a* = 293.15	pure Fe at 1480°C [Mas2]
FeB < 1588	*oP*8 *Pnma* BFe	a = 550.6 b = 295.2 c = 406.1	[1992Rog], dissolves up to 5 at.% Ni [1968Kuz]
NiB < 1035	*oC*8 *Cmcm* BCr	*a* = 292.9 *b* = 739.2 *c* = 296.1	[V-C2, Mas2]
m-Ni_4B_3 < 1018	*mC*28 *C*2/*c* B_3Ni_4	*a* = 642.83 *b* = 487.95 *c* = 781.91	[V-C2, Mas2]
o-Ni_4B_3 < 1025	*oP*28 *Pnma* B_3Ni_4	*a* = 1195.41 *b* = 298.15 *c* = 656.84	[V-C2, Mas2]
$(Ni,Fe)_3B$ < 1214	*oP*16 *Pnma* Fe_3C	*a* = 542.8 *b* = 666.9 *c* = 443.9	dissolves up to 45 at.% Fe [1967Mon, 1968Kuz, 1969Sta, 1989Loo] Fe_3B, metastable [1992Rog]
$FeNi_3$ < 517	*cP*4 $Pm\bar{3}m$ $AuCu_3$	*a* = 355.23	Fe-Ni: 63 - ~85 at.% Ni [2006Cac]
$(Fe,Ni)_2B$ < 1407 Fe_2B	*tI*12 *I*4/*mcm* $CuAl_2$	*a* = 510.9 *c* = 424.9	Fe_2B [1992Rog]

(*continued*)

DOI: 10.1007/978-3-540-69761-9_23

Phase/ Temperature Range [°C]	Pearson Symbol/ Space Group/ Prototype	Lattice Parameters [pm]	Comments/References
Ni_2B		a = 499.1 c = 424.6	Ni_2B [V-C2]
* $Ni_{20}Fe_3B_6$ ($Ni_{18.5}Fe_{4.5}B_6$)	$cF116$ $Fm\bar{3}m$ $Cr_{23}C_6$	a = 1050.1 to 1052	[1967Aye], [1969Sta], [2002Sta], metastable
NiB_n	-	-	[1993Tep], [1972Por], metastable

Table 3. Invariant Equilibria

Reaction	T [°C]	Type	Phase	Composition (at.%)		
				B	Fe	Ni
L ⇌ Ni_3B + Ni_2B + (γFe,Ni)	~1040	E	L	20	40	40

Table 4. Investigations of the B-Fe-Ni Materials Properties

Reference	Method/Experimental Technique	Type of Property
[1962Cad]	Thermomagnetic measurements	Curie point and magnetic moment
[1966Has]	Hardness measurements	Vickers hardness
[1970Iga]	Magnetic torque measurements and X-ray single crystal diffraction	Magnetocrystalline anisotropy constants
[1979Lub]	Hysteresis loops with integrating flux meter	Coercive field, saturation magnetization, remanence, core loss, permeability
[1979Tra]	X-ray measurements	Magnetic transition
[1980Tea]	Ferromagnetic resonance measurements	Resonance linewidth
[1983Hun]	Hardness, tensile and low cycle fatigue measurements	Mechanical properties
[1983Jag]	Magnetic measurements	Disaccomodation of magnetic permeability
[1985Hor]	Radiotracer technique	Self-diffusion of Fe in B-Fe-Ni
[1987Pfa]	Radiotracer technique	Self-diffusion of Fe in B-Fe-Ni
[1988Kun]	Magnetic measurements with a magnetooptical laser hysteriograph	Magnetic properties (H_c, J_s, J_r)
[1988Ilo]	Magnetic measurements using the standard Faraday technique	Magnetization, magnetic susceptibility

(*continued*)

DOI: 10.1007/978-3-540-69761-9_23

Reference	Method/Experimental Technique	Type of Property
[1988Mit]	Magnetic measurements with an integrating fluxmeter under applied stress	Magnetic properties (M_r, anisotropy constants)
[1989Bra]	Penetration depth measurements	Boride layer growth kinetics
[1991Gha]	Mössbauer measurements	Hyperfine interactions
[1992Man]	Magnetic measurements with a fluxmeter	Magnetization, spin-wave stiffness coefficient and interaction range
[2001Kis]	XRD, vibrating sample magnetometer	Magnetic transition
[2005Du]	XRD, DSC, SEM, TEM, magnetization measurements with a vibrating sample magnetometer	Magnetic properties (M_s, H_c)

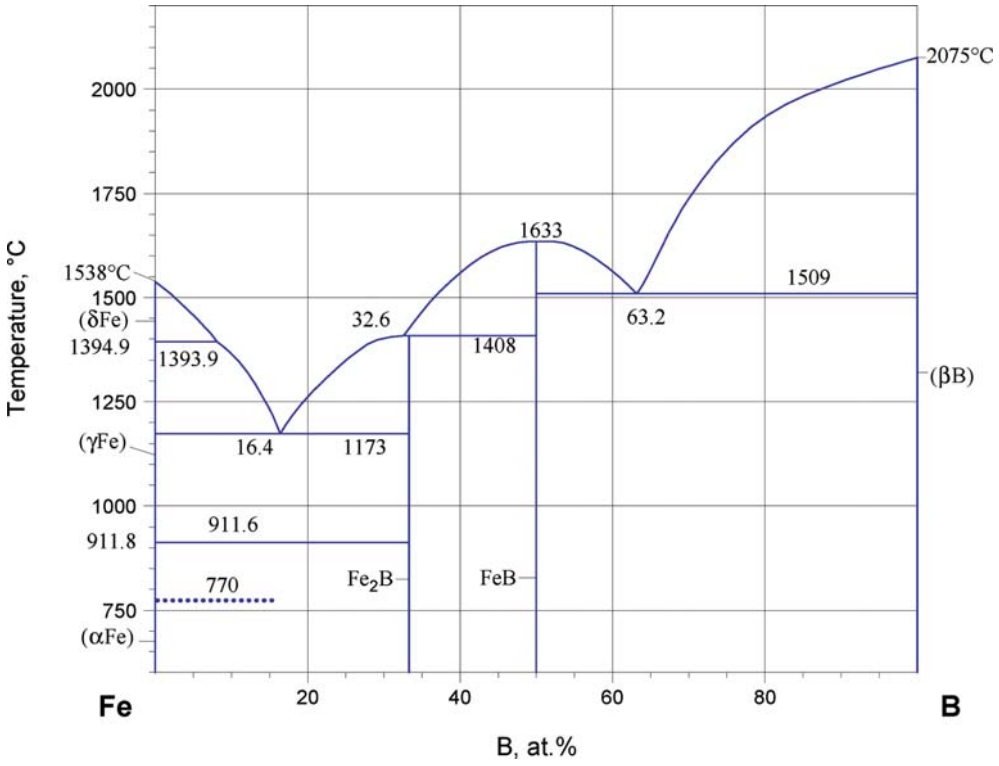

Fig. 1. B-Fe-Ni. B-Fe phase diagram

DOI: 10.1007/978-3-540-69761-9_23

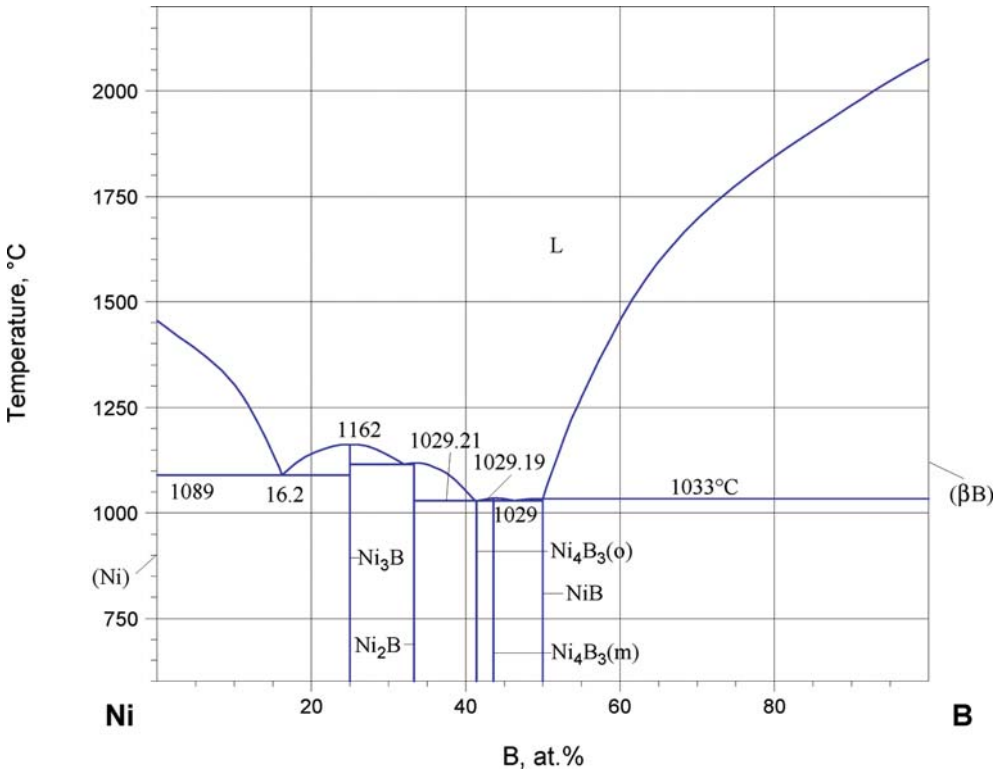

Fig. 2. B-Fe-Ni. B-Ni phase diagram

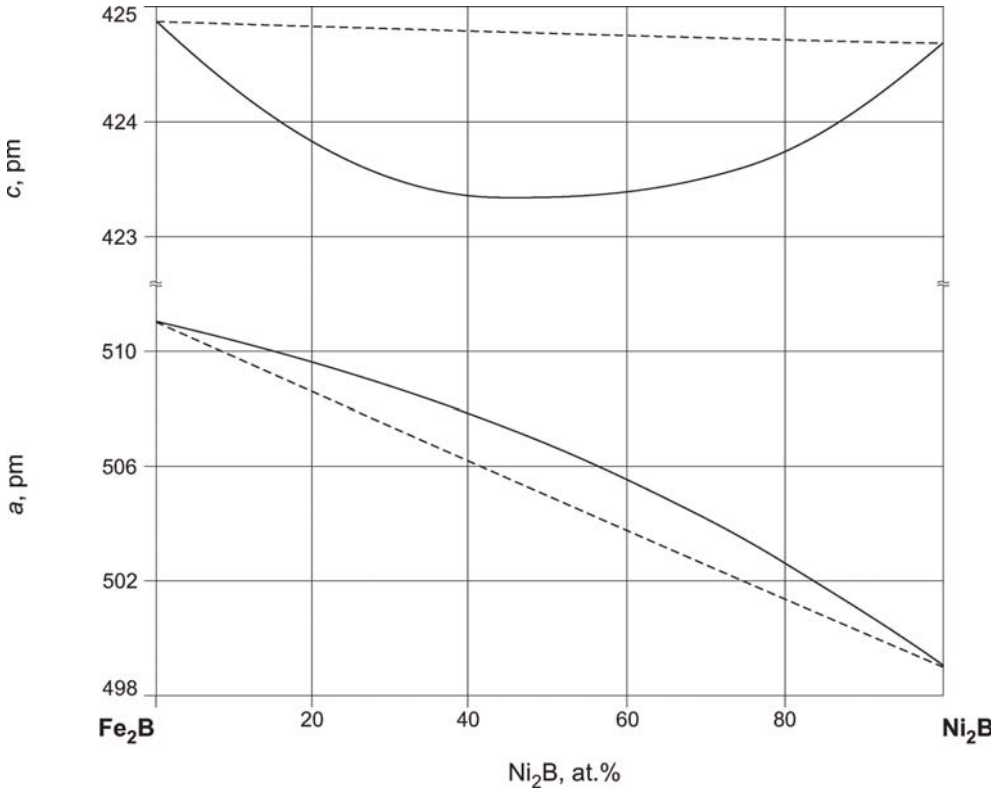

Fig. 3a. B-Fe-Ni. Lattice parameters of $(Fe,Ni)_2B$

DOI: 10.1007/978-3-540-69761-9_23

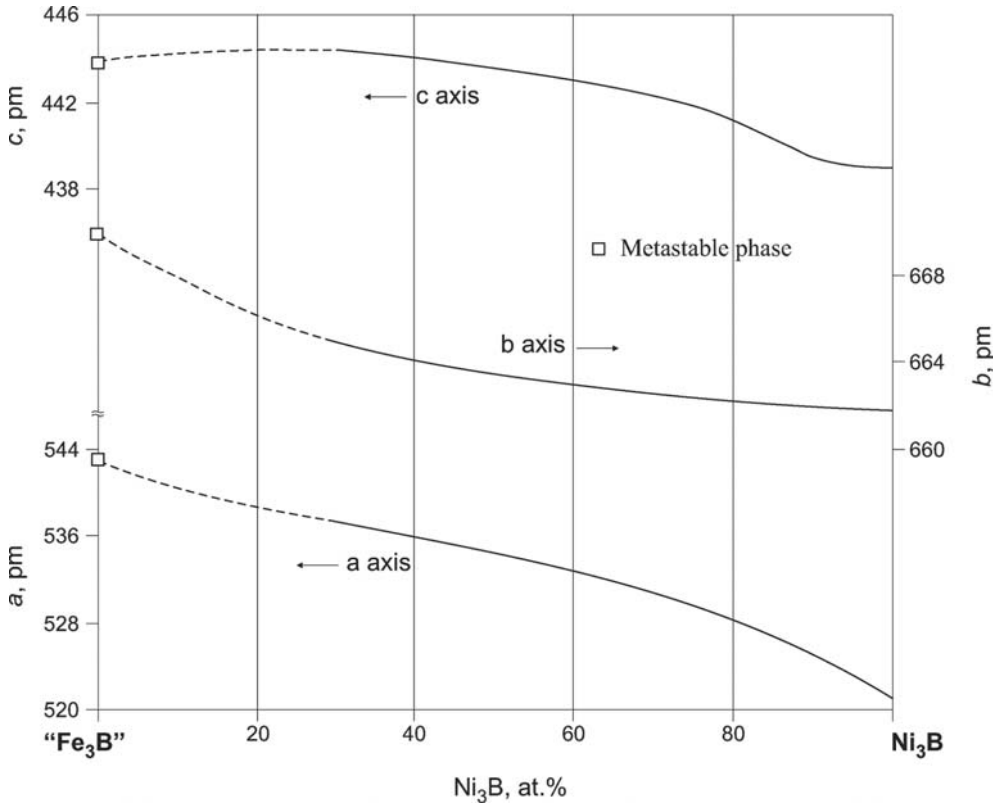

Fig. 3b. B-Fe-Ni. Lattice parameters of $(Fe,Ni)_3B$

DOI: 10.1007/978-3-540-69761-9_23

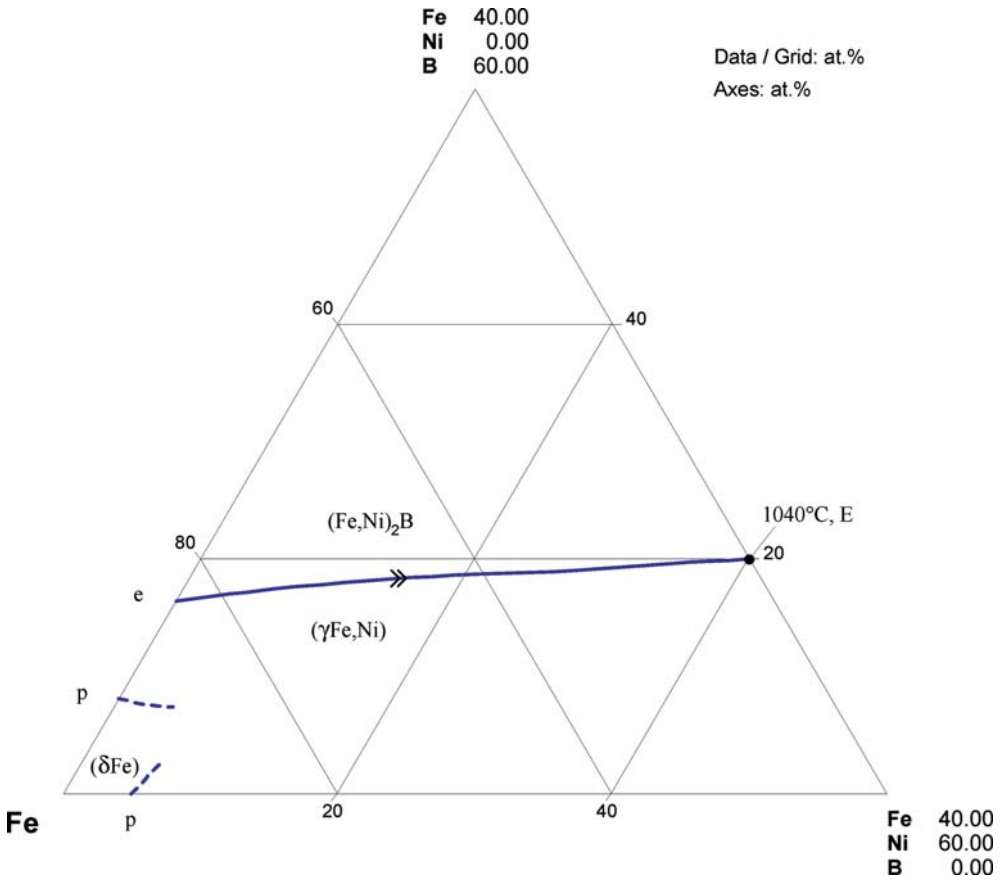

Fig. 4. B-Fe-Ni. Partial liquidus surface, with univariant line and primary phases for $0 < xB < 0.33$ and $0 < xNi < 0.5$

DOI: 10.1007/978-3-540-69761-9_23

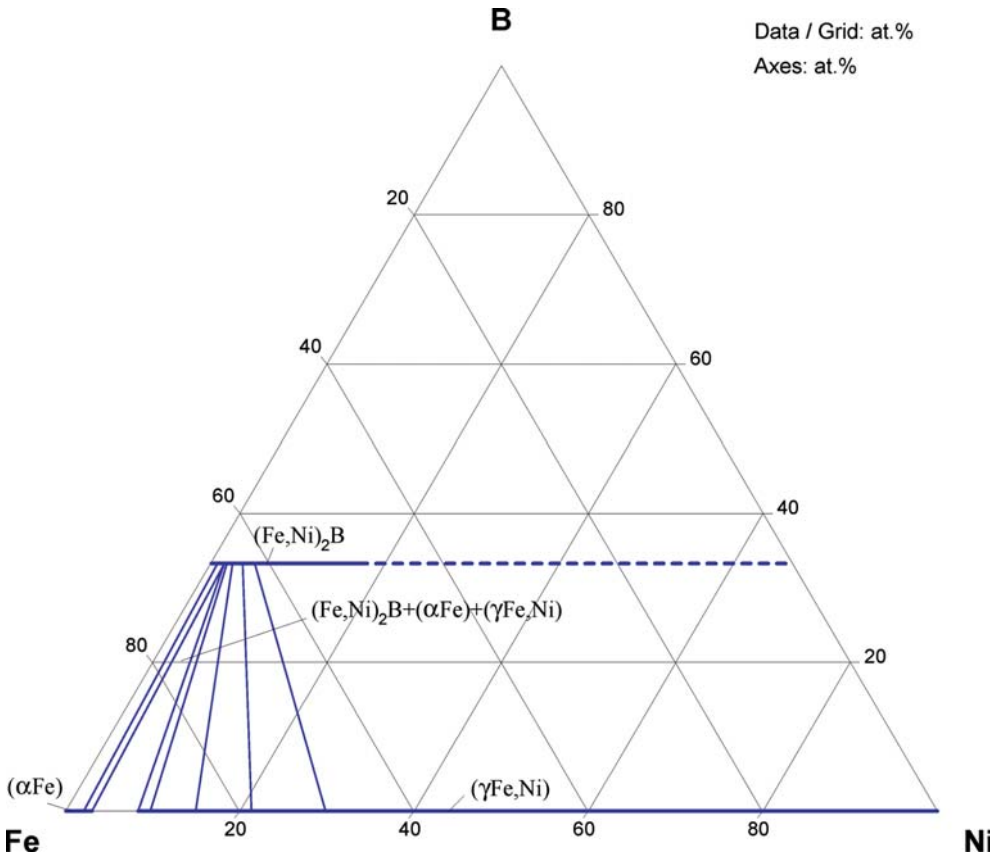

Fig. 5. B-Fe-Ni. Partial isothermal section at 700°C

DOI: 10.1007/978-3-540-69761-9_23

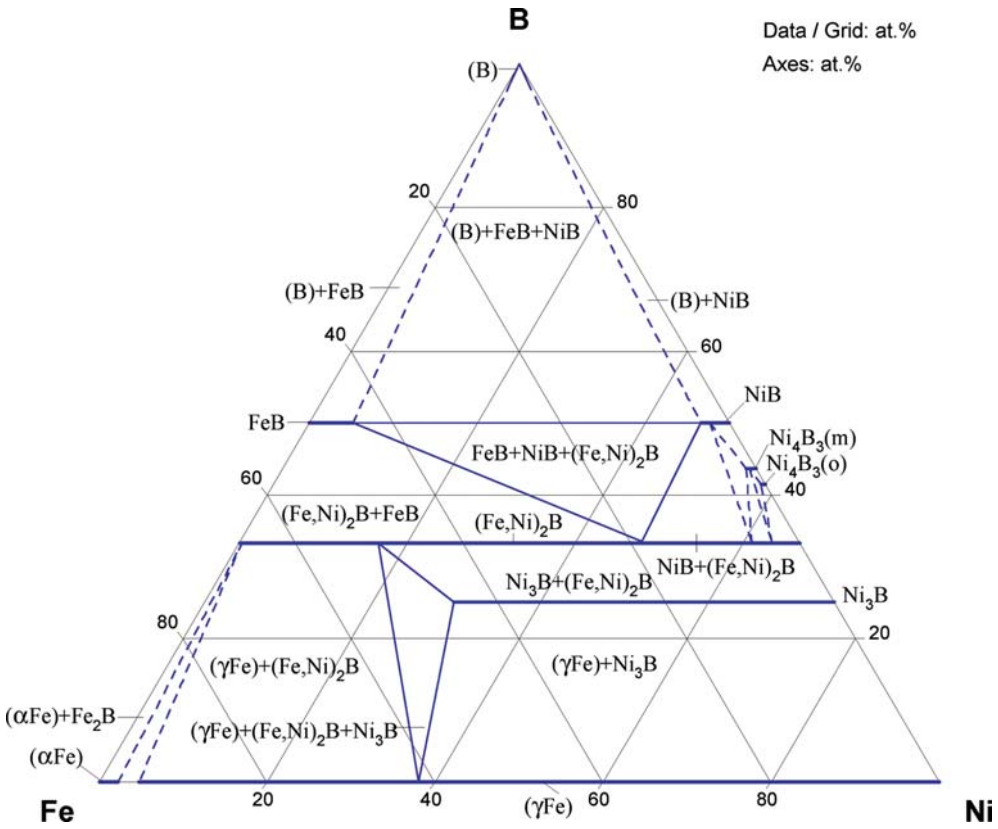

Fig. 6. B-Fe-Ni. Isothermal section at 800°C

DOI: 10.1007/978-3-540-69761-9_23

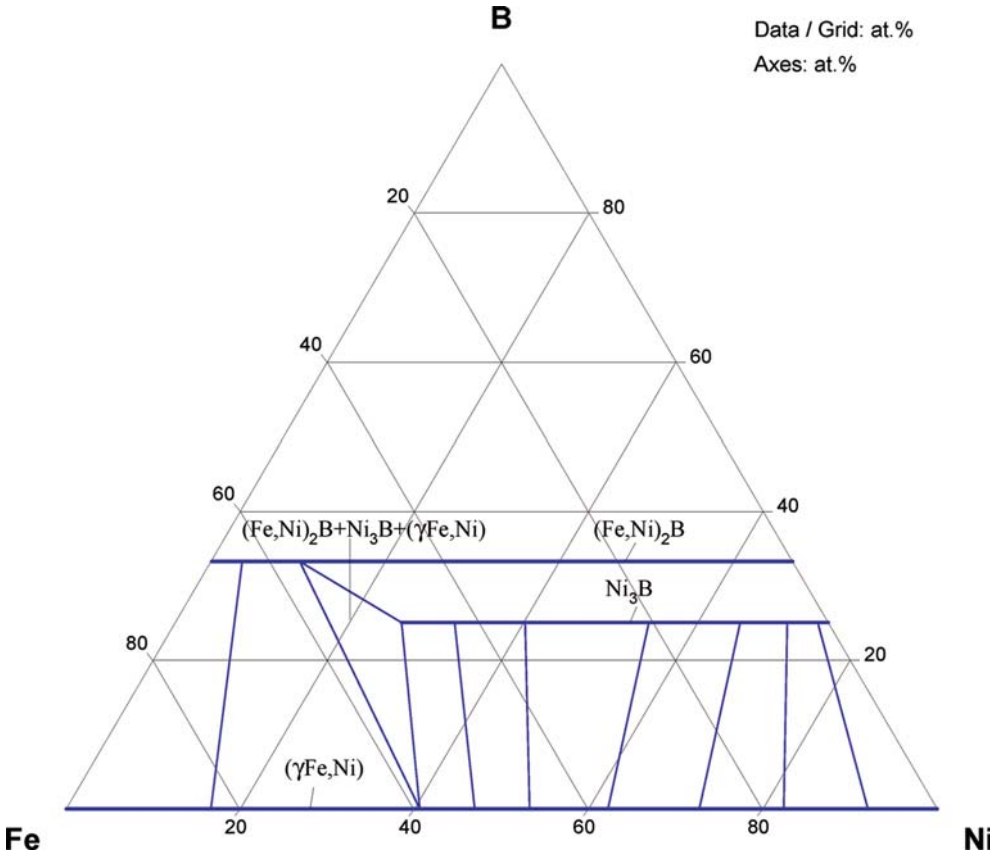

Fig. 7. B-Fe-Ni. Partial isothermal section at 925°C

DOI: 10.1007/978-3-540-69761-9_23

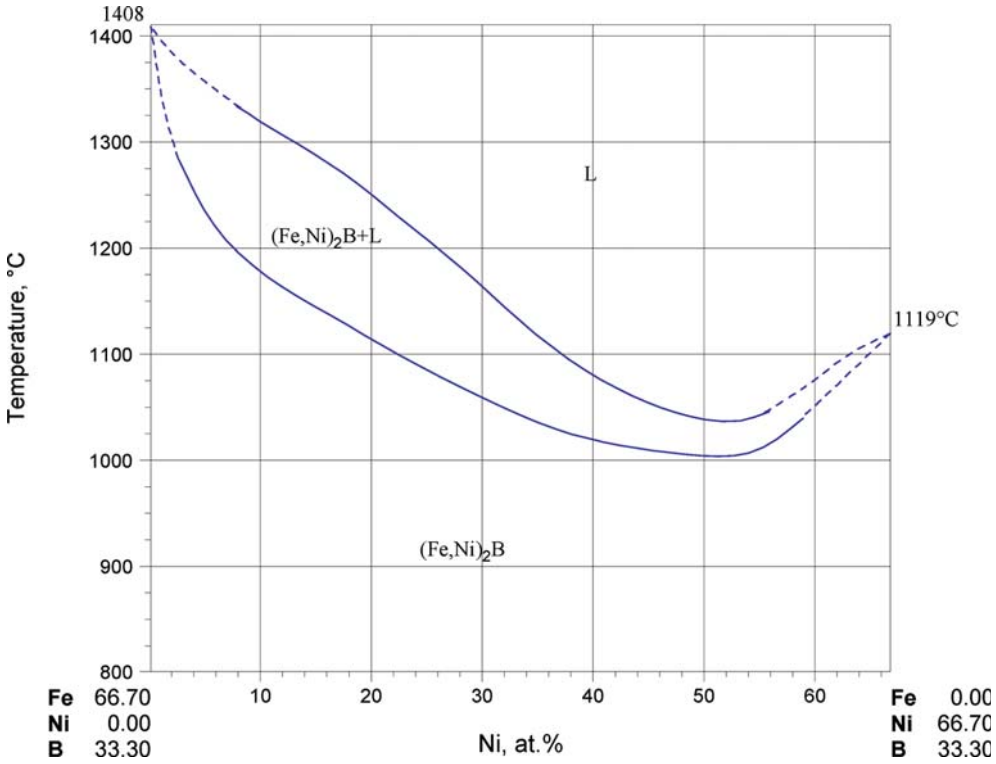

Fig. 8. B-Fe-Ni. Isopleth at 33 at.% B

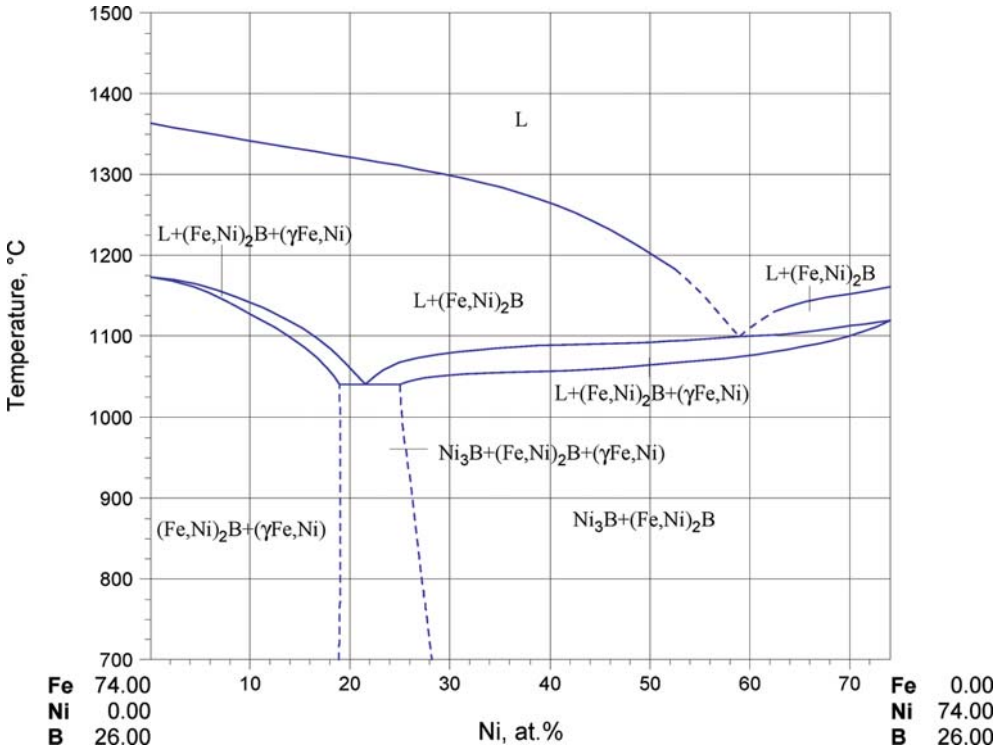

Fig. 9. B-Fe-Ni. Isopleth at 26 at.% B

DOI: 10.1007/978-3-540-69761-9_23

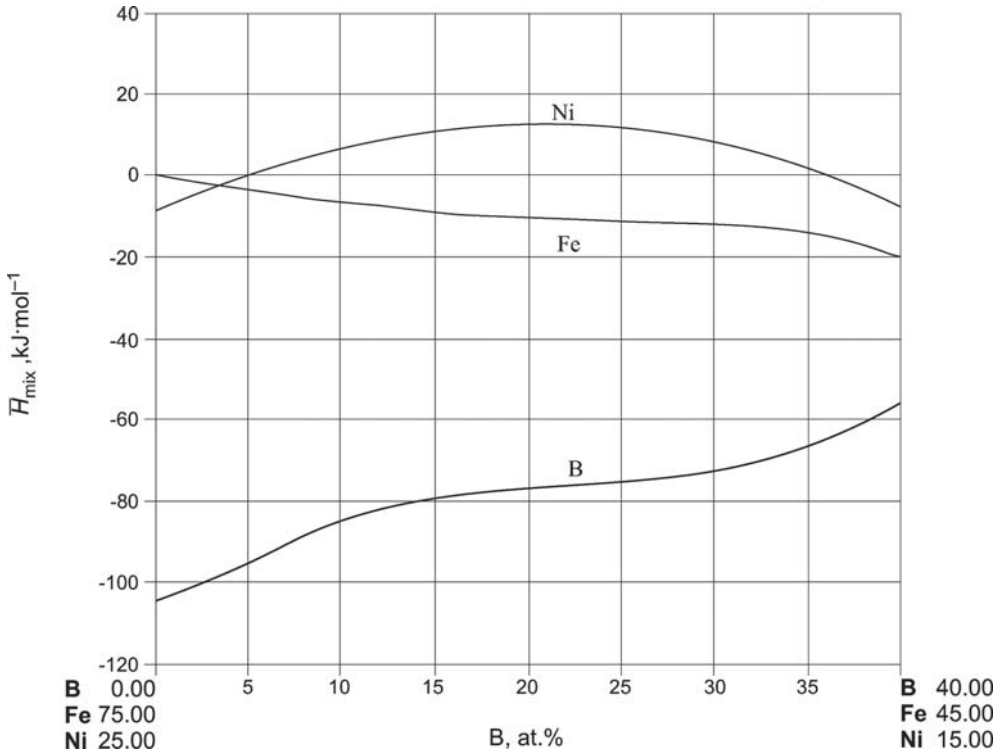

Fig. 10a. B-Fe-Ni. Partial enthalpies of mixing of liquid at 1600°C for Fe:Ni=3:1

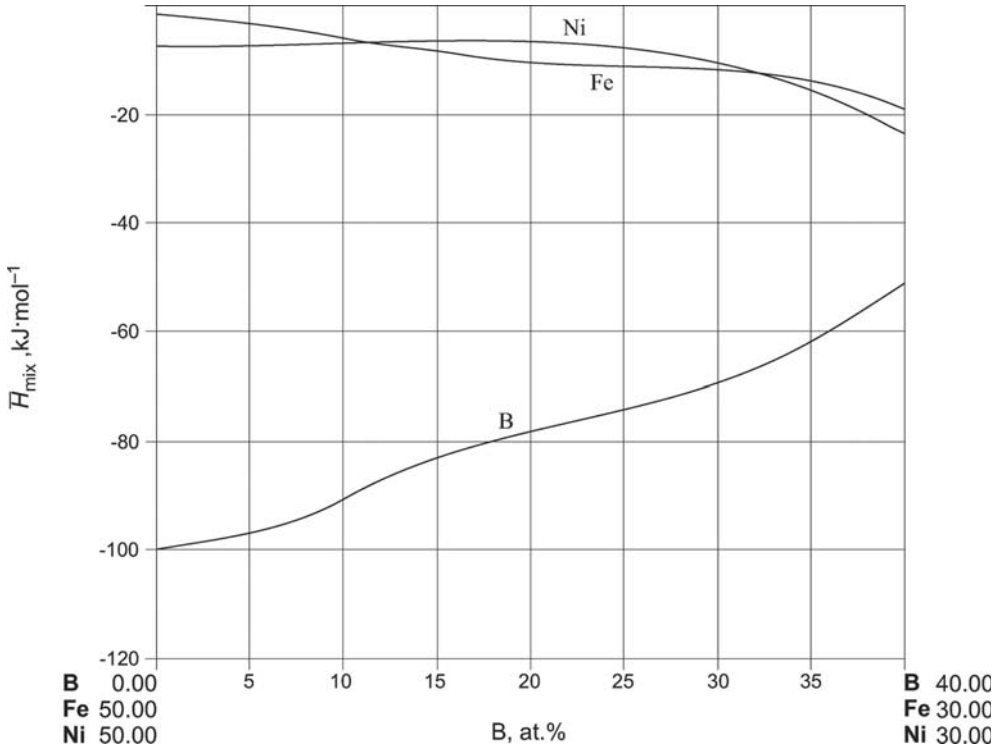

Fig. 10b. B-Fe-Ni. Partial enthalpies of mixing of liquid at 1600°C for Fe:Ni=1:1

DOI: 10.1007/978-3-540-69761-9_23

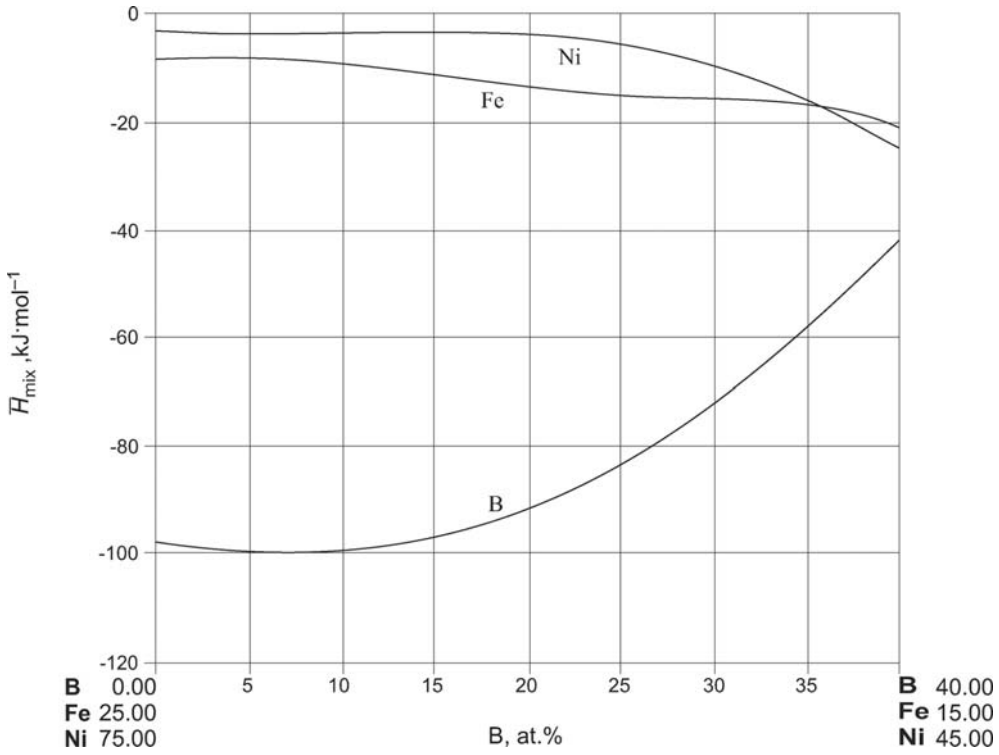

Fig. 10c. B-Fe-Ni. Partial enthalpies of mixing of liquid at 1600°C for Fe:Ni=1:3

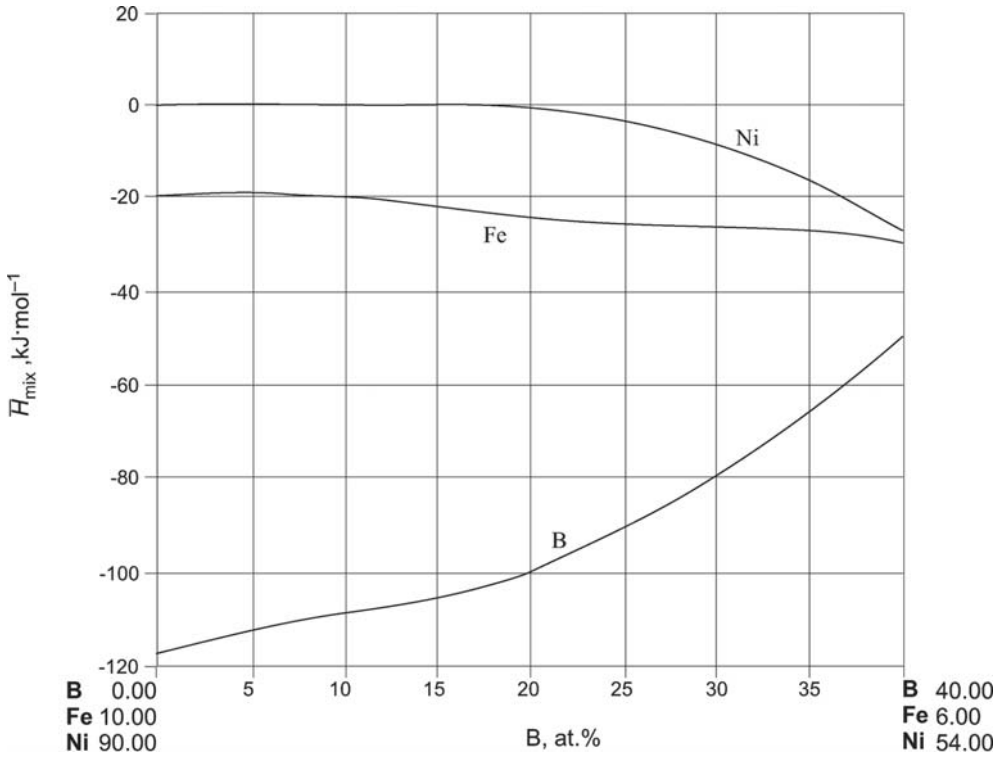

Fig. 10d. B-Fe-Ni. Partial enthalpies of mixing of liquid at 1600°C for Fe:Ni=1:9

DOI: 10.1007/978-3-540-69761-9_23

References

[1962Bre] Bredzs, N., Schwartzbart, H., "Grain-Boundary Penetration and Base Metal Erosion in High-Temperature Brazing", *Welding*, **41**, 129–144 (1962) (Electronic Structure, Experimental, Morphology, Phase Diagram, Phase Relations, 15)

[1962Cad] Cadeville, M.-C., Meyer, J.-P., "Curie Points and Ferromagnetic Moments of the Irons Group Borides of the Type M_2B, MB, $(M_1,M_2)_2B$ and $(M_1,M_2)B$" (in French), *Compt. Rend. Acad. Sci. Paris, Ser. 2*, **255**, 3391–3393 (1962) (Experimental, Magn. Prop., 8)

[1965Sch] Schoebel, J.-D., Stadelmaier, H.H., "The Binary System Nickel-Boron" (in German), *Z. Metallkd.*, **56**(12), 856–859 (1965) (Phase Diagram, Experimental, 14)

[1966Has] Hasegawa, M., Okamoto, M., "A Study on the Ternary Alloys of Iron and Boron" (in Japanese), *Nippon Kinzoku Gakkai-Si*, **30**(6), 533–540 (1966) (Experimental, Mechan. Prop., Morphology, Phase Relations, 12)

[1966Kan] Kaneko, H., Nishizawa, T., Chiba, A., "Borides in Stainless Steel" (in Japanese), *Nippon Kinzoku Gakkai-Si*, **30**(2), 157–163 (1966) (Crys. Structure, Experimental, Morphology, Phase Diagram, Phase Relations, 17)

[1966Por] Portnoi K.I., Chubarov V.M., Romashov V.M., Levinskaya M.K., Salibekov S.E., "Investigation of Equilibrium Diagram of Nickel-Boron Alloys" (in Russian), *Dokl. Akad. Nauk SSSR*, **169**, 1104–1106 (1966) (Crys. Structure, Phase Diagram, Phase Relations, Experimental, 10)

[1967Mon] Monnier, G., Riviere, R., Ayel, M., "Variations of Crystal Parameters of $(FeNi)_2B$ and $(FeNi)_3B$ Solid Solutions" (in French), *Compt. Rend. Acad. Sci. Paris, Ser. C*, **264C**, 862–865 (1967) (Crys. Structure, Experimental, 8)

[1967Aye] Ayel, M., Riviere, R., Monnier, G., "On the Existence of a New Complex Boride $(Fe, Ni)_{23}B_6$ of the $Cr_{23}C_6$ Structure Type" (in French), *Compt. Rend. Acad. Sci. Paris, Ser. C*, **264C**, 1756–1757 (1967) (Crys. Structure, Experimental, 6)

[1968Kuz] Kuzma, Yu.B., Koval, V. P., "Phase Equilibria in the Fe-Ni-B System", *Inorg. Mater. (Engl. Trans.)*, **4**(3), 381–383 (1968), translated from *Izv. Akad. Nauk SSSR, Neorg. Mater.*, **4**, 450–452 (1968) (Phase Diagram, Phase Relations, Morphology, Crys. Structure, Experimental, 8)

[1969Ruh] Ruhl, R.C., Cohen, M., "Splat Quenching of Iron-Nickel-Boron Alloys", *Trans. Metall. Soc. AIME*, **245**, 253–257 (1969) (Crys. Structure, Experimental, Phase Relations, 23)

[1969Sta] Stadelmaier, H.H., Pollock, C.B., "The Metastable τ-Phase in the Fe-Ni-B System" (in German), *Z. Metallkd.*, **60**(12), 960–961 (1969) (Crys. Structure, Experimental, Phase Diagram, Phase Relations, 4)

[1970Iga] Iga, A., "Magnetocrystalline Anisotropy in $(Fe_{1-x}Ni_x)_2B$ System", *Japan. J. Appl. Phys.*, **9**, 414–415 (1970) (Crys. Structure, Experimental, Magn. Prop., 5)

[1972Por] Portnoy, K.I., Chubarov, V.M., Romashov, V.M., Levinskaya, M.Kh., Salibekov, S.E., "Investigation of the Phase Diagram of the Ni-B System" (in Russian), *Dokl. Akad. Nauk SSSR*, **169**(5), 1104–1106 (1966) (Crys. Structure, Experimental, Phase Diagram, Phase Relations, 10)

[1972Tav] Tavadze, F.N., Doliashvili, K.A., Lomiya, T.P; Avlokhashvili, D.V., *Voprosy Metallovedeniya i Korrozii Metallov*, (3), Metniereva, Tbilisi, 12–19, (1972)

[1979Lub] Luborsky, F.E., Walter, J.L., Liebermann, H.H., "Engineering Magnetic Properties of Fe-Ni-B Amorphous Alloys", *IEEE Trans. Magn.*, **15**(1), 909–911 (1979) (Magn. Prop., Experimental, 14)

[1979Tra] Traore, K., Kappler, J.P., "Study of the Variation of the Crystalline Parameters of Solid Solutions of Manganese, Cobalt, Nickel and Iron Borides, as a Function of their Composition" (in French), *Bull. Soc. Chim. Fr.*, (9–10), 419–425 (1979) (Crys. Structure, Experimental, 16)

[1980Tea] Teale, R.W., Wild, R., "Ferromagnetic Resonance in Amorphous Iron-Nickel-Boron Alloys", *J. Phys. F: Met. Phys.*, **10**, 2055–2058 (1980) (Experimental, Magn. Prop., 4)

[1980Was] Waseda, Y., Aust, K.T., Walter, J.L., "Structural Investigation of Amorphous Iron-Nickel-Boron Alloys", *J. Mater. Sci.*, **15**, 1252–1258 (1980) (Crys. Structure, Experimental, 26)

DOI: 10.1007/978-3-540-69761-9_23

[1982Ber] Bergmann, H.W., Brokmeier, U., "Crystallization Behaviour of Fe-B-Cr, Fe-B-Co, and Fe-B-Ni Alloys", *Met. Sci.*, **16**, 191–196 (1982) (Experimental, Mechan. Properties, Phase Relations, Thermodyn., 14)

[1983Ber] Bergmann, H.W., Brokmeier, U., Fritsch, H.U., "Experimental Investigation on the Thermal Stability of Metallic Glasses", *Ber. Bunsen-Ges. Phys. Chem.*, **87**, 757–761 (1983) (Crys. Structure, Experimental, Mechan. Prop., Phase Relations, Thermodyn., 15)

[1983Gor] Gordelik, P., "Variation of Structure Dependendent Properties of Amorphous Fe-Ni-B Alloys with Concetration" (in German), Diss., Uni. Stuttgart, pp.145 (1983)

[1983Hun] Hunger, G., Mordike, B.L., "Mechanical Properties of Metallic Glasses", *J. Non-Cryst. Solids*, **56**, 213–236 (1983) (Experimental, Mechan. Prop., 11)

[1983Jag] Jagielinski, T., "Disaccommodation of Magnetic Permeability at Amorphous Fe-Ni-B Alloys", *IEEE Trans. Magn.*, **19**(5), 1934–1936 (1983) (Magn. Prop., Experimental, 9)

[1983Kha] Khan, Y., Geiss, V., "Glass-Forming Ability of the Melt-Quenched $(Fe_{1-y}Ni_y)_3B$ Alloys", *Z. Metallkd.*, **74**(5), 317–318 (1983) (Phase Relations, Experimental, 4)

[1984Kro] Kronmueller, H., "Magnetic Aftereffects, Induced Anisotropies, and the Role of Two-Level Systems in Amorphous Alloys", *J. Magn. Magn. Mater.*, **41**, 366–375 (1984) (Magn. Prop., Experimental, 31)

[1985Hor] Horvath, J., Pfahler, K., Ulfert, W., Frank, W., Mehrer, H., "^{59}Fe Tracer Self-Diffusion in Amorphous Fe-Ni-B Alloys", *J. Phys., Colloq.*, **46**(12), C8-645-C8-649 (1985) (Experimental, 12)

[1986Gia] Gianoglio, C., Badini, C., "Distribution Equilibria of Iron and Nickel in Two Phase Fields of the Fe-Ni-B System", *J. Mater. Sci.*, **21**, 4331–4334 (1986) (Crys. Structure, Phase Relations, 16)

[1987Bor] Borisov, Yu.S., Oliker, V.E., Korzhik, V.N., Kunitskii, Yu.A., Krasyuk, A.D., Revo, S.L., "Structural Characteristics of Flame-Sprayed Fe-Ni-B Alloy Coating", *Sov. Powder Metall. Met. Ceram. (Engl. Transl.)*, **26**(11), 885–888 (1987) (Crys. Structure, Morphology, Experimental, 9)

[1987Pfa] Pfahler, K., Horvath, J., Frank, W., "^{59}Fe-Tracer-Diffusion and Coercive-Field Investigations on Amoprhous Fe-Ni-B Alloys", *Cryst. Lattice Defects (Amorph. Mater.)*, **17**, 249–264 (1987) (Morphology, Thermodyn., Experimental, Calculation, 20)

[1987Rez] Reznitskii, L.A., "Thermochenical Model of the Bond in Transition Metal Borides", *Russ. J. Phys. Chem. (Engl. Transl.)*, **61**(7), 938–941 (1987) (Calculation, Thermodyn., 20)

[1988Cun] Cunat, Ch., "A New Concept of Effective Temperature to Correlate Isothermal and Anisothermal Continuous Temperature-Time-Transformation Curves-Application to Crystallization of Fe-Ni-B Amorphous Alloys", *Mater. Sci. Eng.*, **97**, 297–300 (1988) (Theory, Phase Diagram, 6)

[1988Ilo] Ilonca, G., Florescu, V., "Magnetic Phase Transition in Amorphous Fe-Ni-B and Fe-B-Si Alloys", *Mater. Sci. Eng.*, **99**, 43–45 (1988) (Magn. Prop., Phase Diagram, Phase Realtions, Experimental, 9)

[1988Kun] Kunitskiy, Yu.A., Nemirovskiy, A.V., Korzhik, V.N., "Variation of the Local Magnetic Parameters in Cast Amorphous and Sputtered Alloys $Fe_{40}Ni_{40}B_{20}$ after Mechanical and Heat Treatment", *Phys. Met. Metall.*, **65**(2), 78–84 (1988), translated from *Fiz. Metal. Metalloved.*, **65**(2), 295–301, (1988) (Crys. Structure, Experimental, Magn. Prop., Thermodyn., 14)

[1988Mit] Mitra, A., Ghatak, S.K., "Magnetic Properties of Amorphous Fe-Ni-B Alloy Under Heat-Pulse Annealing and Stress", *J. Magn. Magn. Mater.*, **74**, 285–290 (1988) (Magn. Prop., Mechan. Prop., Experimental, 15)

[1989Bra] Brakman, C.M., Gommers, A.W.J., Mittemeijer, E.J., "Boriding of Fe and Fe-C, Fe-Cr and Fe-Ni Alloys: Boride-Layer Growth Kinetics", *J. Mater. Res.*, **4**(6), 1354–1370 (1989) (Experimental, Kinetics, Morphology, Phase Relations, Thermodyn., 25)

[1989Loo] Van Loo, F.J.J., van Beek, J.A., "Reactions and Phase Relations in the Systems Fe-Ni-B and Fe-Co-B", *Z. Metallkd.*, **80**(4), 245–250 (1989) (Electr. Prop., Phase Diagram, Phase Relations, Experimental, 12)

[1989Nis] Nishida, T., Yamamiya, M., Chida, S., "Densification of Iron Powder Compacts by Liquid Phase Sintering Using Fe-Ni-B Master Alloy Powder and Improvement of Their Mechanical

DOI: 10.1007/978-3-540-69761-9_23

Properties" (in Japanese), *J. Jpn. Inst. Met.*, **53**(7), 716–722 (1989) (Mechan. Prop., Experimental, 11)

[1990Kon] Kondoro, J.W., Campbell, S.J., "Crystallisation of Fe-Ni-B Amorphous Alloys", *Hyperfine Interact.*, **55**, 993–1000 (1990) (Experimental, Phase Relations, Crys. Structure, 11)

[1991Kon1] Kondoro, J.W., Campbell, S.J., Gonser, U., "A Mössbauer Study of Crystallization in Amorphous $Fe_xNi_{80-x}B_{20}$ ($20 \leq x \leq 60$)", *Phys. Status Solidi A*, **125**(1), 67–77 (1991) (Experimental, Morphology, 21)

[1991Kon2] Kondoro, J.W., Gonser, U., "Characterizing Structure in the Fe-Ni-B Amoprhous System", *Hyperfine Interact.*, **69**, 615–618 (1991) (Phase Relations, Thermodyn., Experimental, 8)

[1991Gha] Ghafari, M., Saida, J., Brand, R.A., Nakamura, Y., "Hyperfine Interactions in Ultrafine Amorphous Fe-M-B (M = Ni, Co) Alloys", *Hyperfine Interact.*, **69**, 599–602 (1991) (Crys. Structure, Experimental, 4)

[1991She] Shenhua, S., Tingdong, X., Zhexi, Y., Zongsen, Y., "Equilibrium Grain-Boundary Segregation and the Effect of Boron in B-Doped Fe-30 wt.% Ni Austenitic Alloys", *Acta Metall. Mat.*, **39**(5), 909–914 (1991) (Phase Relations, Interface Phenomena, Experimental, Morphology, 30)

[1992Efi] Efimenko, L.P., "Solution of Iron in Ni-B System", *Russ. Metall. (Engl. Transl.)*, **2**, 185–188 (1992), translated from *Izv. Ross. Akad. Nauk, Met.*, **2**, 216–219 (1992) (Phase Relations, Experimental, 9)

[1992Man] Mandal, K., Ghatak, S.K., "Stress Dependence of Magnetic Properties of a Fe-Ni-B Alloy", *Solid State Commun.*, **84**(7), 743–747 (1992) (Experinemtal, Magn. Prop., Mechan. Prop., 13)

[1992Rag] Raghavan, V., "The B-Fe-Ni (Boron-Iron-Nickel) System", in "*Phase Diagrams of Ternary Iron Alloys"*, Indian Institute of Metals, Calcutta, **6A**, 387–394 (1992) (Phase Diagram, Phase Relations, Review, 10)

[1992Rog] Rogl, P., Schuster, J.C., "System Iron-Boron-Nitrogen", in "*Ternary Boronnitrides and Siliconnitrides*", ASM, OH, 1–128 (1992) (Crys. Structure, Phase Diagrams, Phase Relations, Review)

[1993Hu] Hu, Z., Chen, Y., Hsia, Y.F., "Ultrafine Amorphous Fe-Ni-B and Fe-P-B Particles", *Nucl. Instrum. Methods Phys. Res. B*, **76**(1–4), 121–123 (1993) (Experimental, Morphology, 17)

[1993Tep] Teppo, O., Taskinen, P., "Thermodynamic Assessment of Nickel-Boron Phase Diagram" (in English), *Mater. Sci. Technol.*, **9**(3), 205–212 (1993) (Assessment, Phase Diagram, Thermodyn., 41)

[1993Wer] Werheit, H., Kuhlmann, U., Laux, M., Lundstrm, T., "Structural and Electronic Properties of Carbon-Doped β-Rhombohedral Boron", *Phys. Stat. Sol.*,**B179**, 489–511(1993) (Crys. Structure, Experimental, 51)

[1994Hal] Hallemans, B., Wollants, P., Roos, J., "Thermodynamic Reassessment and Calculation of the Fe-B Phase Diagram", *Z. Metallkd.*,**85**, 676–682 (1994) (Thermodyn., Calculation, Phase Diagram, 36)

[1995Wit] Witusiewicz, V.T., "Thermodynamics of Binary and Ternary Melts of the 3d Transition Metals (Cr, Mn, Fe, Co and Ni) with Boron", *Thermochim. Acta*, **264**, 41–58 (1995) (Experimental, Thermodyn., 25)

[1995Zou] Zou, X.W., Jin, Z.Z., Zhuang, H.Z., Tang, C.H., "Study of the Magnetic Relaxation for Amorphous $Fe_{50}Ni_{30}B_{20}$ by Low Energy Excitations", *Physica B*, **212**(1), 39–42 (1995) (Magn. Prop., Experimental, 10)

[1998Mie] Miettinen, J., "Approximate Thermodynamic Solution Phase Data for Steels", *Calphad*, **22**(2), 275–300 (1998) (Assessment, Calculation, Phase Relations, Phase Diagram, Thermodyn., 98)

[1999Cam] Campbell, C.E., Kattner, U.R., "A Thermodynamic Assessment of the Ni-Al-B System", *J. Phase Equilibr.*, **20**(5), 485–496 (1999) (Assessment, Phase Relations, Thremody., Calculation, 50)

DOI: 10.1007/978-3-540-69761-9_23

[2001Kis] Kiss, L.F., Bakonyi, I., Lovas, A., Baran, M., Kadlecova, J., "Magnetic Properties of Amorphous $Ni_{81.5-x}Fe_xB_{18.5}$ Alloys (x = 1, 2, 3): A Further Key to Understand the Magnetism of Amorphous $Ni_{81.5}B_{18.5}$", *Phys. Rev. B*, **64**(6), 064417_1–064417_7 (2001) (Experimental, Magn. Prop., 29)

[2001Zys] Zysler, R.D., Ramos, C.A., Romero, H., Ortega, A., "Chemical Synthesis and Characterization of Amorphous Fe-Ni-B Magnetic Nanoparticles", *J. Mater. Sci.*, **36**(9), 2291–2294 (2001) (Experimental, Morphology, 19)

[2002Rom] Van Rompaey, T., Hari Kumar, K.C., Wollants, P., "Thermodynamic Optimization of the B-Fe System", *J. Alloys Compd.*, **334**, 173–181 (2002) (Calculation, Thermodyn., Phase Diagram, Phase Relations, 45)

[2002Sta] Stadelmaier, H.H., Petzow, G., "Metastable Alloys at Moderate Cooling Rates", *Z. Metallkd.*, **93**(10), 1019–1023 (2002) (Experimental, Magn. Prop., Phase Relations, Review, 42)

[2003Zai] Zaitsev, A., Zaitseva, N., Kodentsov, A., "Thermodynamic Properties and Phase Equilibria in the Iron-Boron System. Transition of the Fe-B Melt into the Amorphous State", *J. Mater. Chem.*, **13**, 943–950 (2003) (Experimental, Thermodyn., 65)

[2005Du] Du, S.W., Ramanujan, R.V., "Mechanical Alloying of Fe-Ni Based Nanostructured Magnetic Materials", *J. Magn. Magn. Mater.*, **292**, 286–298 (2005) (Crys. Structure, Experimental, Magn. Properties, Morphology, Phase Relations, 27)

[2005Tok] Tokunaga, T., Ohtani, H., Hasebe, M., "Thermodynamic Study of Phase Equilibria in the Ni-Fe-B System", *Mater. Trans.*, **46**(6), 1193–1198 (2005) (Calculation, Experimental, Phase Diagram, Phase Relations, Thermodyn., 24)

[2006Cac] Cacciamani, G., De Keyzer, J., Ferro, R., Klotz, U.E., Lacaze, J., Wollants, P., "Critical Evaluation of the Fe-Ni, Fe-Ti and Fe-Ni-Ti Alloy Systems", *Intermetallics*, **14**, 1312–1325 (2006) (Phase Diagram, Thermodyn., Assessment, 161)

[2006Kuz] Kuznetsov, V, "Fe-Ni (Iron-Nickel)", MSIT Binary Evaluation Program, in *MSIT Workplace*, Effenberg, G. (Ed.), MSI, Materials Science International Services, GmbH, Stuttgart; to be published, (2006) (Crys. Structure, Phase Diagram, Phase Relations, Assessment, 41)

[Mas2] Massalski, T.B. (Ed.), *Binary Alloy Phase Diagrams*, 2nd edition, ASM International, Metals Park, Ohio (1990)

[V-C2] Villars, P. and Calvert, L.D., *Pearson's Handbook of Crystallographic Data for Intermetallic Phases*, 2nd edition, ASM, Metals Park, Ohio (1991)

DOI: 10.1007/978-3-540-69761-9_23

Boron – Iron – Phosphorus

Vasyl Tomashik

Introduction

The B-Fe-P ternary system has been under investigation since 1958 when it was shown that despite the binary boride Fe_3B being a metastable phase, solid solutions of $Fe_3B_xP_{1-x}$ are present at $0.5 < x < 1$ [1958Run]. These data were confirmed by subsequent investigations [1962Fru, 1962Run, 1964Fru] (these four articles were included in the review of [1988Rag]). Experimental studies have also been devoted to a second ternary phase, Fe_5B_2P, which is stable in this system [1962Fru, 1962Run, 1967Bla, 1975Hae]. The characteristics of the $Fe_2B_xP_{1-x}$ solid solutions have been studied by [1980Cha]. The only isothermal section available is for 1000°C. It has been constructed by [1962Run]. The alloys were melted under argon and annealed at 1000°C for 1-2 weeks. XRD and chemical analyses were performed on quenched alloys.
Amorphous alloys occurred in some of the samples studied [1971Yam, 1976Dur, 1979Ama, 1981Nak, 1988Abr, 1989Abr, 1991Aro1, 1991Aro2, 1993Hu, 1995Hu, 1996Xia, 1997Hu].
P_2 vapor pressure measurements over liquid alloys of the ternary system and thermodynamic property calculations were carried out by [1983Ban]. The mixing parameter of the B-Fe-P liquid was calculated by [1993Din] using Miedema's method.
The equilibrium grain boundary segregation of P was investigated in B-Fe-P alloys after austenitizing at temperatures ranging from 825-1100°C [1988Paj]. The effect of B on the grain boundary P segregation in a high-purity Fe + 2 mass% P alloy was investigated in [1992Liu].
Table 1 lists the numerous experimental studies of phase equilibria, crystal structure and thermodynamics.

Binary Systems

The binary systems B-Fe, B-P and Fe-P are accepted from [Mas2]. It should be mentioned that the phase diagram of the B-P system is not available owing to a lack of experimental data. The phase diagram of Fe-P system is available only for Fe rich compositions.

Solid Phases

Two ternary phases, $Fe_3B_xP_{1-x}$ (τ_1) and Fe_5B_2P (τ_2), have been identified in the B-Fe-P ternary system [1958Run, 1962Fru, 1962Run, 1964Fru]. According to [1962Run], the τ_1 phase is stable at 1000°C in the composition range $0.48 < x < 0.99$. The upper limit of B content in these solid solutions has not been clearly established, but it is close to $x = 1$. According to the data of [1958Run, 1962Run], a three-phase equilibrium (αFe) + τ_1 + Fe_2B was not seen; probably owing to kinetic constraints or experimental difficulties in determining small phase amounts by XRD. It was assumed in [1962Run] that τ_1 is stable up to P contents of less than 1 at.%. A linear change in the lattice parameters over the composition range from $Fe_3B_{0.48}P_{0.52}$ to $Fe_3B_{0.94}P_{0.06}$ was given by [1962Run]. According to [1962Run], Fe_3P forms solid solutions up to a composition of $Fe_3B_{0.3}P_{0.7}$ with a linear change in the tetragonal lattice parameters. A break in solubility was observed by [1962Run] for x values between 0.3 and 0.48. The results of [1964Fru], who determined the break in the solubility for x values in the range 0.330 and 0.494, are in good agreement with [1962Run].
According to the data of [1962Run], the solubility of B in the Fe_2P phase reaches 3.3 at.% at 1000°C but the solubility of P in iron borides and the solubility of B in FeP and FeP_2 is negligible.
Fe_5B_2P has a small range of homogeneity [1962Fru, 1962Run, 1975Hae]. The unit cell dimensions of this compound decreases with decreasing P/B atomic ratio [1975Hae]. The deviations from the ideal composition are most likely associated with P/B substitution at the phosphorus positions. The simultaneous solubility of P and B in (αFe) is very restricted [1962Run].
The details of the atom occupancy in the structures of Fe_3P solid solutions, τ_1 and Fe_5B_2P (τ_2) are discussed in [1962Fru].
Crystallographic data of all unary, binary and ternary phases are listed in Table 2.

DOI: 10.1007/978-3-540-69761-9_24

Quasibinary Systems

According to the literature data, it is possible to assume that the BP-FeB, BP- Fe_2P and FeB-Fe_2P sections are quasibinary but their phase diagrams have not been constructed.

Isothermal Sections

The isothermal section of the B-Fe-P ternary system in the region Fe-FeP_2-BP-FeB is shown in Fig. 1 following experimental study by [1962Run] at 1000°C. No distinction was made between the γ and α forms of iron. The τ_2 phase is shown having a small range of homogeneity. It displays two-phase equilibria with the $Fe_3B_xP_{1-x}$ solid solution, Fe_2P, FeB and Fe_2B phases. The B_6P phase is not stable at this temperature.

Thermodynamics

The P vapor pressure over liquid B-Fe-P alloys has been measured at 1400°C by [1983Ban]. The experimental results obtained are presented in Table 3. The derived activity coefficient of P in liquid B-Fe-P alloys at 1400°C is presented in Fig. 2 [1983Ban].

The experimental data were described by Wagner's formalism with a first order interaction parameter ε^B_P equal to 1.49 ± 0.16 (e^B_P = 0.015 ± 0.004). According to the thermodynamic calculations based on Miedema's method, the value of ε^B_P parameter is equal to 17.29 [1993Din].

Notes on Materials Properties and Applications

The Curie point for the compositions $Fe_3B_{0.36}P_{0.64}$ and $Fe_3B_{0.82}P_{0.18}$ (τ_1) is equal 493 and 527°C, respectively and that for the compound Fe_5B_2P is within the interval 342 to 366°C (the substitution of B by P leads to an increase in the Curie point) [1962Fru, 1967Bla]. The concentration dependence of the Curie point for $Fe_3B_xP_{1-x}$ and τ_1 solid solutions is shown in Fig. 3a. All of these phases are ferromagnetic. The average magnetic moment of the Fe atoms in the compound Fe_5B_2P is 1.73μ_B [1967Bla].

The magnetic ordering temperature of $Fe_2B_xP_{1-x}$ ($x < 0.15$) solid solutions increases rapidly with increasing B content (Fig. 3b) [1980Cha]. The first-order transition in pure Fe_2P was found to be suppressed when B was added and a transition region of about 10°C was observed in which the paramagnetic and ferromagnetic phases coexist.

Phosphorus is one of several elements which segregate at grain boundaries in iron and steels and cause intergranular fracture [1992Liu]. On the other hand, it has several beneficial effects: it improves the deep drawability of low-carbon steel at room temperature and the ductility of some steels at high temperatures. Boron is generally used to improve the hardenability of some steels.

Boron alloying strongly decreases the segregation level of P in the B-Fe-P alloys and could thus effectively reduce the grain boundary embrittlement induced by phosphorus enrichment [1988Paj]. [1992Liu] indicated that the addition of 12.5 ppm B to a high-purity Fe + 2 mass% P alloy completely suppresses the intergranular fracture induced by the P segregation and decreases the ductile-brittle transition temperature by about 170°C when quenched from 800°C.

Nonmonotonic dependence of giant ΔE-effect *vs* magnetic field has been observed in amorphous B-Fe-P alloys after thermal annealing at temperatures above 300°C [1991Aro1, 1993Kis]. The results obtained showed that such behavior of the ΔE-effect was due to thermostimulation perpendicular to the ribbon plane magnetic anisotropy. It was supposed that the induced magnetic anisotropy is caused by changing the chemical composition of the near-surface layer [1993Kis].

Table 4 lists the methods and experimental techniques used for the investigation of the material properties of B-Fe-P alloys.

Miscellaneous

Amorphous alloys of compositions $Fe_{79}B_{21-x}P_x$ ($3 < x < 17$) and $Fe_{94-x}B_xP_6$ ($11 < x < 19$) have been obtained by means of splat cooling techniques [1971Yam, 1976Dur, 1979Ama, 1988Abr]. The glasses of about 2 mm in width and 20 μm thick were prepared by rapid quenching from the melt [1981Nak] and ultra

DOI: 10.1007/978-3-540-69761-9_24

fine amorphous alloys particles have been obtained by a chemical reduction method [1993Hu, 1995Hu, 1997Hu]. The composition and size of the ultra fine amorphous alloy particles have been effectively regulated over a wide range by altering the reaction conditions such as reaction procedure and the pH value of the reactant solutions, which in turn can be used to regulate the properties of the particles. The Fe-containing crystallization products for the high-P-content samples are (αFe), Fe_2P and Fe_3P and no iron borides are observed [1997Hu]. According to thermodynamic calculations, amorphous B-Fe-P alloys can be more stable than B-Fe and Fe-P alloys [1996Xia].

The crystallization temperature of the $Fe_{80}B_7P_{17}$ alloy is 410°C and the ferromagnetic Curie point for the amorphous state is around 360°C. It was established that the crystalline state is composed of at least two ferromagnetic phases, the Curie points of which are about 500 and 750°C, respectively [1971Yam]. For a given Fe content in the amorphous B-Fe-P alloys, the magnetic moment μ and the Curie point T_C both increase with substitution of B for P, and μ was found to decrease when the P (or B) content is increased on Fe substitution, and for the same concentration, T_C increases [1976Dur]. On thermocycling of the $Fe_{83}B_7P_{10}$ amorphous alloy, a monotonic decrease in the magnetization takes place [1988Abr]. Increasing the temperature up to 400-460°C leads to the formation of the (αFe) and the $Fe_3B_{0.63}P_{0.37}$ phase [1988Abr, 1989Abr]. (αFe) and $Fe_3B_{0.49}P_{0.51}$ are formed on heating the $Fe_{80}B_{11}P_9$ amorphous alloy to 400°C [1989Abr]. According to [1991Aro2], the surface zone of the amorphous ribbon with the composition $Fe_{83}B_{10}P_7$ is most thermally stable at a depth of 100 nm and the composition of this zone was determined to be $Fe_{66}B_{19}P_{15}$. The activation energy of crystallization of this amorphous alloy is equal to 170 $kJ \cdot mol^{-1}$.

The segregation of P in austenite occurs at equilibrium but some additional segregation takes place during quenching [1988Paj]. Boron was found to decrease the grain boundary concentration of phosphorus. Grain boundary B concentration does not show any clear dependence on austenitizing temperature, on intergranular P concentration nor on B content of the sample. This suggests that B also segregates during cooling [1988Paj]. According to [1992Liu], the segregation of P in a high-purity Fe + 2 mass% P alloy decreases markedly with the B segregation: P atoms are replaced by B atoms at grain boundaries. The free energy of B segregation at 800°C is determined to be 100 $kJ \cdot mol^{-1}$.

$Fe_3B_xP_{1-x}$ solid solutions have been obtained by the simultaneous diffusion of B and Fe in Fe_3P at 950°C [1964Fru].

Table 1. Investigations of the B-Fe-P Phase Relations, Structures and Thermodynamics

Reference	Method/Experimental Technique	Temperature/Composition/ Phase Range Studied
[1958Run]	XRD	Room temperature / $Fe_3B_xP_{1-x}$ ($0.48 < x < 1.0$)
[1962Fru]	XRD	< 600°C / B-Fe-P
[1962Run]	XRD, chemical analysis	1000°C / Fe-FeP_2-BP-FeB-Fe
[1964Fru]	XRD	< 600°C / $Fe_3B_xP_{1-x}$
[1967Bla]	XRD	< 400°C / Fe_5B_2P
[1971Yam]	XRD	< 800°C / $Fe_{80}B_7P_{17}$
[1975Hae]	XRD, Moessbauer spectroscopy	80-900 K / Fe_5B_2P
[1979Ama]	Mössbauer spectroscopy	Room temperature / $Fe_{79}B_xP_{21-x}$ ($5 < x < 16$); $Fe_{94-x}B_xP_6$ ($11 < x < 19$)
[1980Cha]	XRD, Mössbauer spectroscopy	< 80-530 K / $Fe_2B_xP_{1-x}$ ($x < 0.15$)

(*continued*)

DOI: 10.1007/978-3-540-69761-9_24

Reference	Method/Experimental Technique	Temperature/Composition/ Phase Range Studied
[1983Ban]	Vapor pressure measuring by the transportation method	1400°C / B-Fe-P
[1988Abr]	XRD, DTA, TGA, magnetization measurements	250-460°C / $Fe_{83}B_7P_{10}$
[1988Paj]	AES	825-1100°C / B-Fe-P
[1989Abr]	XRD, TEM	320-500°C / $Fe_{80}B_{11}P_9$ and $Fe_{83}B_{10}P_7$
[1991Aro2]	AES, electron microscopy	360-450°C / $Fe_{83}B_{10}P_7$
[1992Liu]	AES, SEM, optical microscopy	0-800°C / (Fe + 2 mass% P) + B
[1993Din]	Calculation	1600°C / B-Fe-P
[1993Hu]	TEM, Mössbauer spectroscopy	100-500°C / $Fe_{82}B_7P_{11}$
[1995Hu]	TEM, Mössbauer spectroscopy, XRD, inductive coupled plasma method, DSC	up to 700°C / $Fe_{100-x-y}B_yP_x$ ($3.6 < x < 10.5$ and $6.6 < y < 32.0$)
[1997Hu]	Mössbauer spectroscopy, TEM, XRD, XPS, DSC	up to 700°C / $Fe_{75}B_{17}P_8$

Table 2. Crystallographic Data of Solid Phases

Phase/ Temperature Range [°C]	Pearson Symbol/ Space Group/ Prototype	Lattice Parameters [pm]	Comments/References
(βB) < 2092	*hR*333 $R\bar{3}m$ βB	a = 1093.30 c = 2382.52	[Mas2, 1993Wer]
(δFe) 1538 - 1394	*cI*2 $Im\bar{3}m$ W	a = 293.15	[Mas2]
(γFe) 1394 - 912	*cF*4 $Fm\bar{3}m$ Cu	a = 364.67	at 915°C [V-C2, Mas2]
(αFe) < 912	*cI*2 $Im\bar{3}m$ W	a = 286.65	at 25°C [Mas2]

(*continued*)

DOI: 10.1007/978-3-540-69761-9_24

Phase/ Temperature Range [°C]	Pearson Symbol/ Space Group/ Prototype	Lattice Parameters [pm]	Comments/References
(P) (red) < 417	*c**66		sublimation at 1 bar triple point at 576°C, > 36.3 bar; triple point at 589.6 at 1 atm [Mas2]
		a = 1131	[V-C2]
(P) (white) < 44.14	*c***	*a* = 718	at 25°C [Mas2]
	?		common form of elemental P, probably less stable than P (red) at 25°C [Mas2]
	P (white)		
(P) (black)	*oC*8	*a* = 31.36	at 25°C [Mas2]
	Cmca	*b* = 1047.8	
	P (black)	*c* = 437.63	
βBP > 825	*hP*4	*a* = 365.2	[V-C2, Mas2]
	$P6_3mc$	*c* = 590.0	
	ZnS		
αBP < 825	*cF*8	*a* = 453.4	[V-C2, Mas2]
	$F\bar{4}3m$		
	ZnS		
B_6P < 2120	*hR*42	*a* = 598.4	[V-C2, Mas2]
	$R\bar{3}m$	*c* = 1185.0	
	B_6P		
$Fe_3B_xP_{1-x}$ < 1166	*tI*32		$0 \le x \le 0.3$
	$I\bar{4}$		
	Ni_3P	*a* = 910.0	at 22°C; *x* = 0 [V-C2, Mas2]
		c = 445.92	
		a = 913.7	at 414°C; *x* = 0 [V-C2, Mas2]
		c = 450.62	
		a = 917.4	at 678°C, *x* = 0 [V-C2, Mas2]
		c = 452.99	mineral Schreibersite
		a = 896.8	*x* = 0.3 [1962Run]
		c = 441.4	
Fe_2P < 1370	*hP*9	*a* = 586.75 ± 0.02	33.3 to 34 at.% P, mineral Barringerite
	$P\bar{6}2m$	*c* = 345.81 ± 0.02	[V-C2, Mas2]
	Fe_2P		
$Fe_2P_{0.96}B_{0.04}$		*a* = 589.74 ± 0.02	[1980Cha]
		c = 340.99 ± 0.03	
$Fe_2P_{0.92}B_{0.08}$		*a* = 591.63 ± 0.02	[1980Cha]
		c = 336.95 ± 0.03	
$Fe_2P_{0.85}B_{0.15}$		*a* = 593.56 ± 0.03	[1980Cha]
		c = 332.51 ± 0.03	
Fe_2P	*oP*12	*a* = 577.5	high-pressure phase
	Pnma	*b* = 357.1	[V-C2, Mas2]
	Co_2Si	*c* = 664.1	

(*continued*)

DOI: 10.1007/978-3-540-69761-9_24

Phase/ Temperature Range [°C]	Pearson Symbol/ Space Group/ Prototype	Lattice Parameters [pm]	Comments/References
FeP	*oP*8 *Pmna* MnP	a = 519.10 b = 309.83 c = 579.09	[V-C2, Mas2]
FeP_2	*oP*6 *Pnnm* FeS_2	a = 497.29 ± 0.07 b = 565.68 ± 0.08 c = 272.30 ± 0.04	66 to 67 at.% P [V-C2, Mas2]
FeP_4 (I)	*mP*30 $P2_1c$ FeP_4	a = 461.9 ± 0.1 b = 1367.0 ± 0.2 c = 700.2 ± 0.1 β = 101.48°	[V-C2, Mas2]
FeP_4 (II)	*mC*40 *C*2/*c* FeP_4	a = 505.43 ± 0.07 b = 1040.7 ± 0.2 c = 1106.9 ± 0.2 β = 91.14 ± 0.01°	at 20°C [V-C2, Mas2]
FeP_4 (HP)	*oC*12 $C222_1$ FeP_4	a = 500.5 ± 0.1 b = 1021.3 ± 0.3 c = 553.0 ± 0.1	high-pressure phase [V-C2, Mas2]
FeB < 1650	*oP*8 *Pnma* FeB	a = 550.3 b = 294.6 c = 406.4	49.5 to 40.0 at.% Fe [V-C2, Mas2]
Fe_2B < 1389	*tI*12 *I*4/*mcm* Al_2Cu	a = 511.0 ± 0.3 c = 424.9 ± 0.3	[V-C2, Mas2]
Fe_3B(I)	*oP*16 *Pnma* Fe_3C	a = 542.8 b = 669.9 c = 443.9	metastable phase [V-C2, Mas2]
Fe_3B(II)	*tI*32 $I\bar{4}$ Ni_3P	a = 865.5 c = 429.7	metastable, [V-C2]
* τ_1, $Fe_3B_xP_{1-x}$	*tP*32 $P4_2$/n	a = 888.8 c = 440.1	x = 0.48 [1962Run]
		a = 864.9 c = 431.4	x = 0.06 [1962Run]
		a = 872.7 c = 431.6	x = 0.18 [1962Fru]
* τ_2, Fe_5PB_2	*tI*32 *I*4/*mcm* Cr_3B_5	a = 548.7 c = 1035.8	[1962Fru]
		a = 549.2 c = 1071.3	[1962Fru]

(*continued*)

DOI: 10.1007/978-3-540-69761-9_24

Phase/ Temperature Range [°C]	Pearson Symbol/ Space Group/ Prototype	Lattice Parameters [pm]	Comments/References
		a = 548.2 c = 1033.2	[1962Run, 1975Hae]
		a = 548.8 c = 1036.4	[1967Bla]

Table 3. Vapor Pressure Measurements

Phase(s)	Temperature [°C]	Pressure P_2 (bar)	Comments
Liquid B-Fe-P	1400	$3.88 \cdot 10^{-4}$	mass% P 11.5, mass% B 0.79
		$1.72 \cdot 10^{-4}$	mass% P 8.62, mass% B 2.0
		$5.24 \cdot 10^{-4}$	mass% P 11.4, mass% B 2.78
		$1.71 \cdot 10^{-4}$	mass% P 7.70, mass% B 3.69

Table 4. Investigations of the B-Fe-P Materials Properties

Reference	Method/Experimental Technique	Type of Property
[1962Fru]	Magnetic metering	Curie point
[1967Bla]	Magnetothermal analysis	Curie point
[1971Yam]	Magnetization and electrical resistance measurements	Curie point
[1976Dur]	Faraday method, magnetic permeability measurements	Magnetic permeability, Curie point
[1981Nak]	Magnetoresistance measurements	Magnetoresistivity
[1991Aro1]	Magnetoinductive method	Giant ΔE-effect
[1993Kis]	Vibrating reed method, magnetoinductive method	Giant ΔE-effect

DOI: 10.1007/978-3-540-69761-9_24

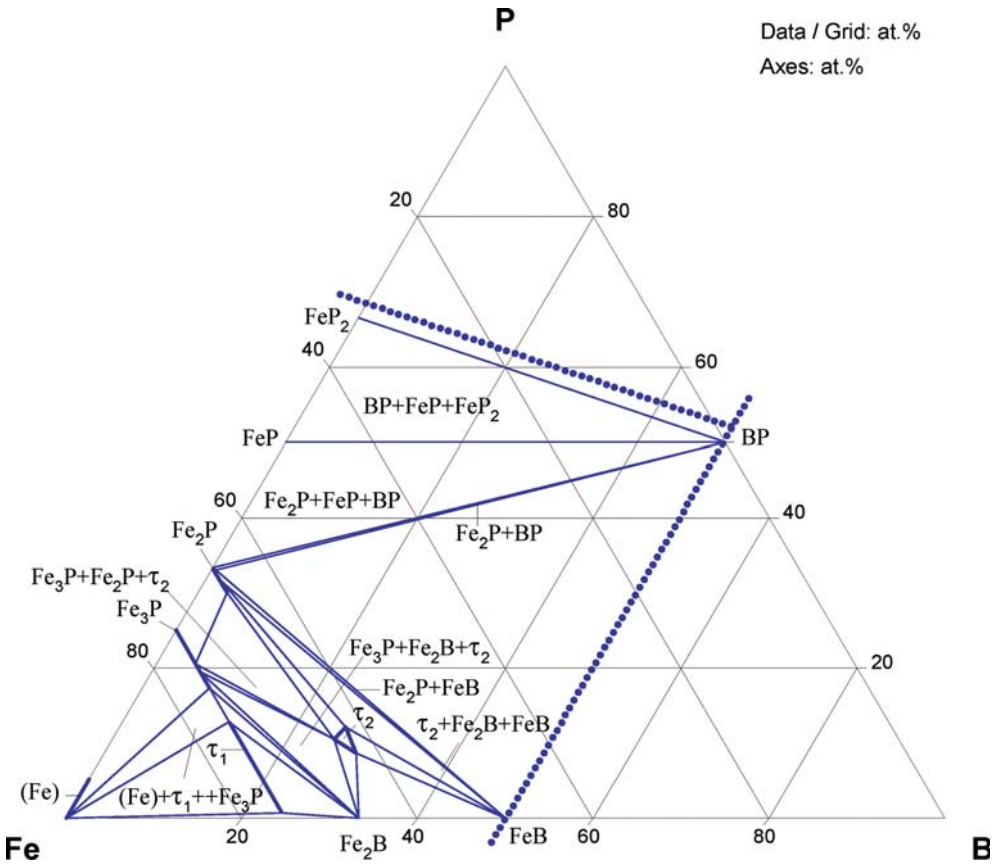

Fig. 1. B-Fe-P. Isothermal section at 1000°C

DOI: 10.1007/978-3-540-69761-9_24

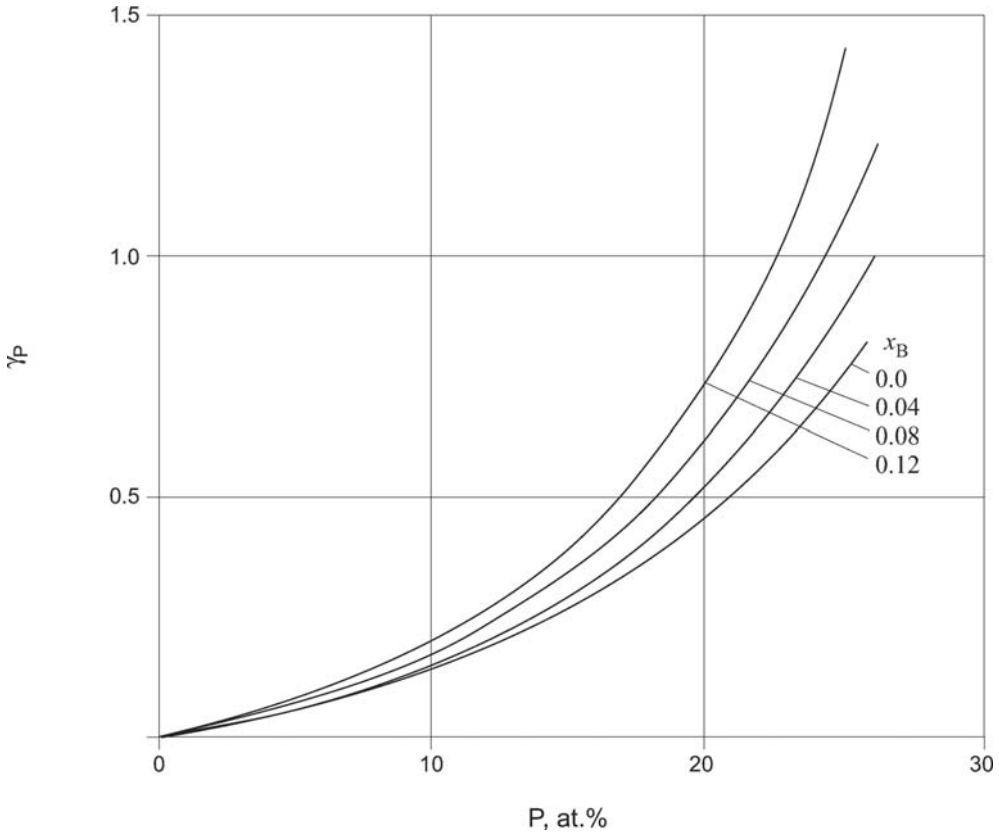

Fig. 2. B-Fe-P. Activity coefficient of P in liquid B-Fe-P alloys at 1400°C

DOI: 10.1007/978-3-540-69761-9_24

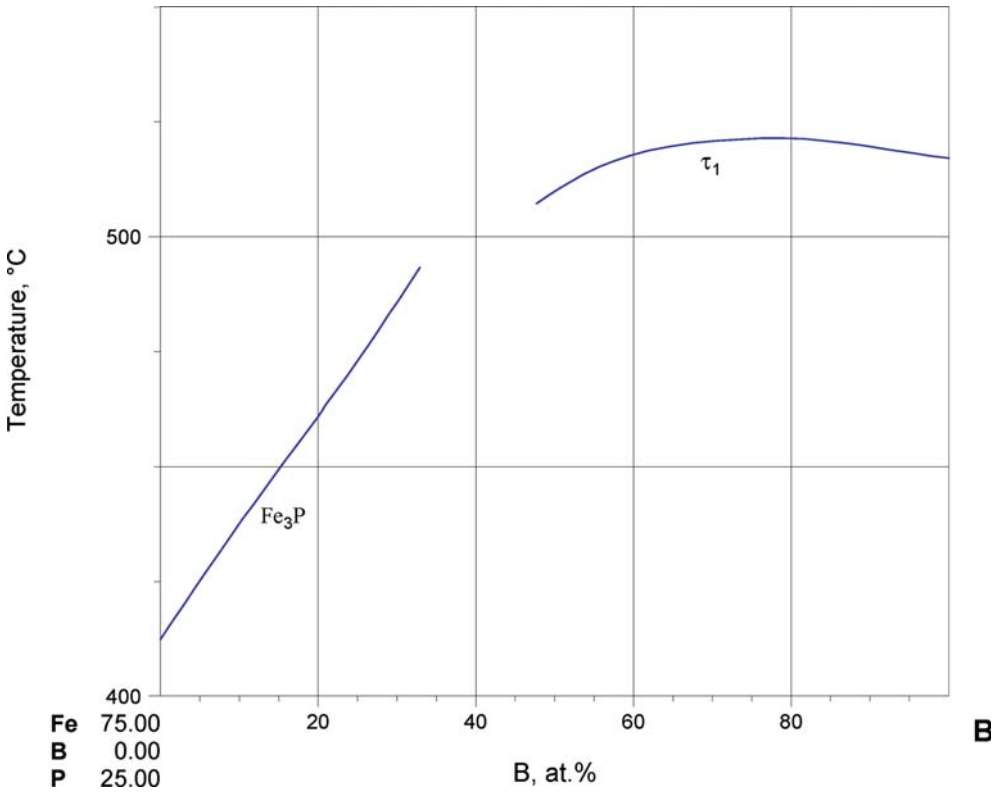

Fig. 3a. B-Fe-P. Concentration dependence of the Curie point for Fe_3P and τ_1 solid solutions

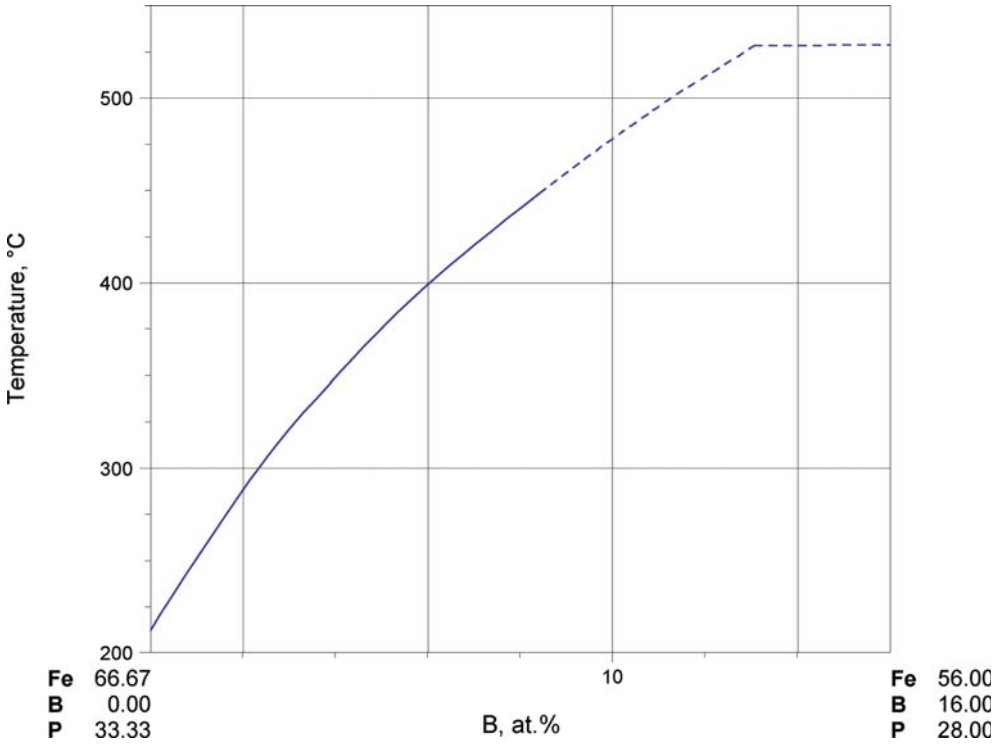

Fig. 3b. B-Fe-P. Concentration dependence of the Curie point of the $Fe_2B_xP_{1-x}$ solid solutions

DOI: 10.1007/978-3-540-69761-9_24

References

[1958Run] Rundqvist, S., "Two Borides with the Cementite Structure", *Nature*, **181**, 259–260 (1958) (Experimental, Phase Relations, Crys. Structure, 3)

[1962Fru] Fruchart, E., Triquet, A.-M., Fruchart, R., Michel, A., "Two New Ferromagnetic Compounds in the Ternary System Iron - Phosphorus - Boron" (in French), *Compt. Rend. Acad. Sci. Paris*, **255**(5), 931–933 (1962) (Crys. Structure, Experimental, 5)

[1962Run] Rundqvist, S., "X-Ray Investigations of the Ternary System Fe-P-B. Some Features of the Systems Cr-P-B, Mn-P-B, Co-P-B and Ni-P-B", *Acta Chem. Scand.*, **16**(1), 1–19 (1962) (Experimental, Phase Relations, Crys. Structure, 37)

[1964Fru] Fruchart, E., Triquet, A.-M., Fruchart, R., "Magnetic Studies of Borophosphides of Iron, $Fe_3B_xP_{1-x}$ ε and ε_1. Notes on the Metal Bonds of the Metal Transitive - Metalloid in These Compounds" (in French), *Ann. Chim. (Paris)*, **9**(7–8), 323–332 (1964) (Experimental, Crys. Structure, Magn. Prop., 47)

[1967Bla] Blanc, A.-M., Fruchart, E., Fruchart, R., "Magnetic and Crystallographic Studies of the $(Fe_{1-x}Cr_x)_3P$ Solution Solids and the Ferromagnetic Phase Fe_5B_2P" (in French), *Ann. Chim. (Paris)*, **2**(5), 251–254 (1967) (Experimental, Phase Relations, Crys. Structure, Magn. Prop., 6)

[1971Yam] Yamauchi, K., Nakagawa, Y., "Amorphous Ferromagnetic Fe-P-B Alloys Prepared by a New Technique of Splat Cooling", *J. Appl. Phys.*, **10**(12), 1730 (1971) (Experimental, Phase Relations, Magn. Prop., 4)

[1975Hae] Haeggstroem, L., Waeppling, R., Ericsson, T., Andersson, Y., Rundqvist, S., "Mössbauer and X-Ray Studies of Fe_5PB_2", *J. Solid State Chem.*, **13**, 84–91 (1975) (Experimental, Crys. Structure, Electronic Structure, Magn. Prop., 5)

[1976Dur] Durand, J., "Concentration Dependence of the Magnetic Properties in Amorphous Fe-P-B Alloys", *IEEE Trans. Magn.*, **12**(6), 945–947 (1976) (Experimental, Crys. Structure, Magn. Prop., 17)

[1979Ama] Amamou, A., "Mössbauer Effect and Short-Range Order in Fe-P-B and Fe-P-C Amorphous Alloys" *Phys. Status Solidi. A*, **54**(2), 565–572 (1979) (Experimental, Phase Relations, Magn. Prop., 31)

[1980Cha] Chandra, R., Bjarman, S., Ericsson, T., Haeggstroem, L., Wilkinson, C., Waeppling, R., Andersson, Y., Rundqvist, S., "A Mössbauer and X-Ray Study of $Fe_2P_{1-x}B_x$ Compounds ($x < 0.15$)", *J. Solid State Chem.*, **34**, 389–396 (1980) (Experimental, Crys. Structure, Electronic Structure, Magn. Prop., 32)

[1981Nak] Naka, M., Kern, R., Gonser, U., "Magnetoresistance of Fe-B-P Glasses", *J. Appl. Phys.*, **52**(3), Pt. 1, 1448–1450 (1981) (Experimental, Phase Relations, Magn. Prop., 11)

[1983Ban] Ban-ya, S., Maruyama, N., Fujino, "The Effect of C, Si, Sn and B on the Activity of Phosphorus in Liquid Iron" (in Japanese), *Tetsu to Hagane*, **69**, 921–928 (1983) (Experimental, Thermodyn., 32)

[1988Abr] Abrosimova, G.E., Serebryakov, A.V., Sokolovskaya, Zh.D., "Change of Structure and Magnetic Properties of Amorphous Iron Base Metal - Metalloid Alloys" (in Russian), *Fiz. Met. Metalloved.*, **66**(4), 727–730 (1988) (Experimental, Phase Relations, Magn. Prop., 11)

[1988Paj] Paju, M., Viefhaus, H., Grabke, H.J., "Phosphorus Segregation in Austenite in Fe-P-C, Fe-P-B and Fe-P-C-B Alloys", *Steel Res.*, **59**(8), 336–343 (1988) (Experimental, Morphology, 32)

[1988Rag] Raghavan, V., "The B-Fe-P (Boron-Iron-Phosphorus) System", in "*Phase Diagrams of Ternary Iron Alloys*", **3**, 19–23 (1988) (Review, Phase Diagram, Crys. Structure, Thermodyn., 5)

[1989Abr] Abrosimova, G.E., Aronin, A.S., Voropayeva, L.V., "Structural Changes in the Amorphous Alloys at the Heating" (in Russian), *Metallofizika*, **11**(3), 102–105 (1989) (Experimental, Phase Relations, Morphology, Crys. Structure, 8)

[1991Aro1] Aronin, A.S., Kislov, V.A., Kobelev, N.P., Soyfer, Ya.M., "Manifestation of the Giant ΔE-Effect in Amorphous Fe-B-P Alloys" (in Russian), *Fiz. Tverd. Tela*, **33**(4), 1001–1005 (1991) (Experimental, Magn. Prop., 8)

DOI: 10.1007/978-3-540-69761-9_24

[1991Aro2] Aronin, A.S., Ivanov, S.A., Yakshin, A.E., "Increasing of the Near-Surface Crystallization Temperature in Fe-B-P Amorphous Alloys" (in Russian), *Fiz. Tverd. Tela*, **33**(9), 2527–2532 (1991) (Experimental, Phase Relations, Thermodyn., 7)

[1992Liu] Liu, C.M., Nagoya, T., Abiko, K., Kimura, H., "Effect of Boron on the Grain Boundary Segregation of Phosphorus and Intergranular Fracture in High-Purity Fe-0.2% P-B Alloys", *Metall. Trans. A*, **23A**, 263–269 (1992) (Experimental, Morphology, Mechan. Prop, Thermodyn., 18)

[1993Din] Ding, X., Wang, W., Han, Q., "Thermodynamic Calculation of Fe-P-B System Melt", *Acta Metall. Sin. (China)*, **29**(12), B527–B532 (1993) (Calculation, Phase Relations, Theory, Thermodyn., 7)

[1993Hu] Hu, Z., Chen, Y., Hsia, Y.F., "Ultrafine Amorphous Fe-Ni-B and Fe-P-B Particles", *Nucl. Instrum. Methods Phys. Res. B*, **76**(1–4), 121–123 (1993) (Experimental, Morphology, Phase Relations, 17)

[1993Kis] Kislov, V.A., Kobelev, N.P., Soifer, Ya.M., "Thermostimulated Perpendicular Magnetic Anisotropy and Giant ΔE-Effect in Amorphous Fe-B-P Alloys", *Mater. Sci. Forum*, **119–121**, 579–584 (1993) (Experimental, Magn. Prop., 8)

[1993Wer] Werheit, H., Kuhlmann, U., Laux, M., Lundström, T., "Structural and Electronic Properties of Carbon-Doped β-Rhombohedral Boron", *Phys. Stat. Sol.*, **B179**, 489–511(1993) (Crys. Structure, Experimental, 51)

[1995Hu] Hu, Z., Fan, Y., Wu, Y., Yan, Q., Chen, Y., "A Study on Fe-P-B Ultrafine Amorphous Alloy Particles", *J. Magn. Magn. Mater.*, **144**(1), 413–414 (1995) (Experimental, Morphology, Phase Relations, 5)

[1996Xia] Xia, W.S., Hu, Z., Jiang, Y.S., Chen, Y., "A Theoretical Study on Interactions Between the Components of Amorphous Alloy Fe (or Ni)-P-B Systems", *J. Mol. Struct.*, **366**(3), 259–263 (1996) (Theory, Phase Relations, 15)

[1997Hu] Hu, Zh., Wu, Y., Fan, Y., Yan, Q., Chen, Y., "Chemical Preparation and Investigation of Fe-P-B Ultrafine Amorphous Alloy Particles", *Sci. China, Ser. B*, **40**(3), 261–269 (1997) (Experimental, Morphology, 14)

[Mas2] Massalski, T.B. (Ed.), *Binary Alloy Phase Diagrams*, 2nd edition, ASM International, Metals Park, Ohio (1990)

[V-C2] Villars, P. and Calvert, L.D., *Pearson's Handbook of Crystallographic Data for Intermetallic Phases*, 2nd edition, ASM, Metals Park, Ohio (1991)

DOI: 10.1007/978-3-540-69761-9_24

Boron – Iron – Titanium

Volodymyr Ivanchenko, Tatiana Pryadko

Introduction

The study of B-Fe-Ti alloys was triggered by the development of Fe based alloys with high wear resistance that can be used as coating materials, TiB_2-reinforced high modulus steels, cutting materials and titanium based metal-matrix composites. [1974Shu] reported a quasibinary section along the Fe-TiB_2 join. A eutectic temperature of 1340°C and the eutectic composition of about 7 mol% TiB_2 have been proposed. These results were consistent with an isothermal section for 1000°C presented by [1967Fed] who showed that TiB_2 formed two-phase regions with all phases existing in the Fe-Ti and B-Fe binary border systems. Phase equilibria and solidification of B-Fe-Ti alloys in the region close to Fe-TiB_2 have been studied by [1992Ott]. [1999Tan] performed thermodynamic calculations of the Fe-TiB_2 equilibrium, supplemented with a limited experimental study. The calculations were carried out with and without considering the effect of the typical impurities found in the starting materials used in their powder metallurgical processing route. The isothermal section for 1000°C computed by [1999Tan] without including impurities shows that the (Fe)+TiB_2 two-phase equilibrium is shifted to the Fe-Ti border. This feature coincides with the experimental results of [1992Ott]. These investigations [1992Ott, 1999Tan] were reviewed by [2003Rag].

As mentioned above, B-Fe-Ti alloys may be used as material for the manufacture of cutting instruments. [1961Fun] studied Vickers hardness, the transverse strength and wear resistance of Fe-TiB_2 alloys produced by pressing and high temperature sintering as a function of composition and technological route. [1966Yas] studied the wetting of TiB_2 by liquid Fe. [1966Has] studied the influence of alloying with 0.2 mass% Ti on the peritectoid reaction temperature, Vickers hardness, and UTS of Fe-0.2 mass% B. It was shown, that alloying with Ti raises the peritectoid reaction temperature from 912 to 923°C, but this result was obtained on an alloy contaminated by 0.15 mass% Si and 0.2 mass% Mn.

[1972Tic] presented results of wear resistance studies of Fe-TiB_2 alloys with different volume fractions of the boride. It was shown that the best wear resistance is exhibited by the eutectic composition alloy, which has a regular structure. The presence of primary crystals of the soft α(Fe) in hypoeutectic alloys leads to a increase in the total wear owing to high wear of specimen. If the tested specimen has the hypereutectic composition and coarse TiB_2 primary are present in structure, the increase in the total wear is caused by wear of the counterpart. Mechanical properties of the eutectic alloy with Fe-6.3 mass% TiB_2 has been studied by [1977Shu]. Structure and mechanical properties of some B-Fe-Ti alloys have been studied by [2005Lou].

[1982Yur] studied the changes taking place in the fine structure of TiB_2 during vibratory milling and subsequent liquid-phase sintering of the TiB_2-Fe(Mo) cermet. Mo was added to improve the wetting of TiB_2 grains by the melt formed during sintering.

[1985Mak] presented the possibility of producing Fe-TiB_2 cermets using a self-propagation high-temperature synthesis (SHS) route. [1995Ras] studied the dependencies of TiB_2 formation under SHS and the hardness of cermets produced on using different Fe:TiB_2 ratios. It was shown that irregularities in the plots of the amount of TiB_2 and hardness with respect to green composition corresponded to the Ti/Fe ratio in the eutectic β(Ti)+TiFe and the B/Fe ratio in the eutectic FeB+FeB_n. The mechanism of phase changes in the B-Fe-Ti system following a combustion wave during SHS processing for a mixture of Ti, B, and Fe powders and a ferroboron alloy-titanium mixture with the same proportion of elements has been studied by [2000Lep, 2004Lep].

The kinetics of phase transformation and wear resistance of in-situ processed titanium matrix composites based on B-Fe-Ti has been studied by [1999Bra]. The sintering parameters employed when using the powder metallurgical route were improved with the aim of increasing wear resistance.

[1991Dud] presented magnetic properties and crystallization temperatures of magnetic glasses of $Fe_{80-x}Ti_xB_{20}$ (x = 6, 10, and 20 at.%).

DOI: 10.1007/978-3-540-69761-9_25

Isothermal grain growth in mechanically alloyed nanostructured $Fe_{80}Ti_8B_{12}$ at 642-712°C has been investigated by [2003Kra].
[1987Res] proposed a thermochemical model of the bonds in transition metal borides and tried to calculate the enthalpies of formation of the hypothetical borides M_3B and Ti_3B. The increase in the crystallization temperature of an amorphous $Fe_{80}Ti_5B_{15}$ alloy resulting from doping with Ti has been estimated.
Table 1 includes experimental data on phase equilibria, crystal structure and thermodynamics.

Binary Systems

The B-Fe and B-Ti phase diagrams are taken from [Mas2]. The Fe-Ti phase diagram is taken from the assessment of [1982Kub2].

Solid Phases

No ternary phases are formed in the B-Fe-Ti system.
[1995Rep] reported the formation of new boride phases: Ti_2B_5, TiB_{12}, $TiB_{\sim 25}$, $TiB_{\sim 55}$, and $TiB_{\sim 100}$ in the combustion products for B-Fe-Ti, B-Ni-Ti, B-Cu-Ti, and B-Si-Ti reaction powder mixtures. The new titanium borides revealed in the B-Ti system may result from stabilization by oxygen. Crystal structures of equilibrium and nonequilibrium phases are presented in Table 2.

Quasibinary Systems

[1974Shu] presented a eutectic quasibinary section from Fe to TiB_2. The measured eutectic temperature was 1340°C. The eutectic composition was reported as Fe-6.3 mol% TiB_2. The results presented by [1992Ott] confirm the general feature of the phase equilibria previously published by [1974Shu]. However, they provided evidence for the existence of a quasibinary section, not along the line Fe-TiB_2, as proposed by [1974Shu], but along the line (98 at.% Fe, 2 at.% Ti)-TiB_2. The eutectic temperature was found to be approximately 1320°C, which is very close to the value presented by [1974Shu]. The quasibinary section from [1992Ott] has not been included in the present evaluation.

Invariant Equilibria

Invariant equilibria are presented in Table 3 in accordance with the experimental results of [1992Ott].

Liquidus, Solidus and Solvus Surfaces

[1992Ott] found that the solubility of TiB_2 in liquid at 1450°C was about 8 at.% Ti and 16 at.% B. The partial liquidus surface in the Fe rich corner of the phase diagram is presented in Fig. 1 in accordance with [1992Ott].

Isothermal Sections

A partial isothermal section at 1050°C constructed following experimental studies is presented in Fig. 2 after [1992Ott]. It is in very close agreement with the computed isothermal section at 1000°C given by [1999Tan]. The isothermal section at 1000°C presented in Fig. 3 is a compilation of the isothermal section presented by [1967Fed] and the results of calculations performed [1999Tan]. The intermetallic compound Ti_2Fe presented in the isothermal section at 1000°C by [1967Fed] is omitted because it is not present in the accepted Fe-Ti binary system.

Temperature – Composition Sections

The Fe-TiB_2 vertical section was constructed by [1992Ott] based only on two experimental points. It is in contradiction with results presented by [1974Shu] and their own results. It is difficult to imagine that a reduction in the Ti content of the (Fe) solid solution can lead to lowering of the eutectic temperature of 1320°C [1992Ott] or 1340°C [1974Shu] to 1240°C [1992Ott]. The last temperature is very close to the

DOI: 10.1007/978-3-540-69761-9_25

value of 1260°C presented by [1974Shu], but for the temperature of the eutectoid reaction (δFe) ⇌ δ̂(γFe) + TiB_2. For this reason, this section was omitted in the present evaluation. The Fe-TiB_2 polythermal section presented in Fig. 4 has been calculated by [1999Tan], who used modified thermodynamic parameters for TiB_2 to match the eutectic temperature and composition to the experimental values. No FeB_2 is predicted, which basically agrees with the diagrams of [1974Shu].

Notes on Materials Properties and Applications

The hardness of TiB_2-Fe alloys varies considerably with composition. Thus, the hardness of the alloy with 8.22 mass% Fe is 17.6 GPa, and an increase in the Fe content to 48 mass% results in a decrease in the hardness to 8.2 GPa [1961Fun]. The transverse strength of TiB_2-Fe alloys is almost independent of the iron content. Increasing the test temperature to 1100°C does not lead to a fall in the transverse strength; on the contrary, the strength increases over the temperature range from 20 to 800°C. There is some decrease in the transverse strength when the test temperature is raised from 800 to 1100°C, but even in this case, the alloys are sometimes stronger that at room temperature. For example, the transverse strength of an alloy with 8.22 mass% Fe rises from 441 MPa to 461 MPa when the temperature is raised from 20 to 1100°C, but for an alloy with 48 mass% Fe, it decreases from 539 MPa to 392 MPa [1961Fun]. An SHS composite of Fe-50 mass% TiB_2 produced by combining the SHS process with rolling has a density of ~98% of the limiting value, the HRA hardness was ~91, strength limit on bending ~1200 MPa and wear resistance at the bend level of tungsten-coating hard alloy WC-Co (15 mass% Co) [2000Lep, 2004Lep].

A composite TiB_2-Fe powder obtained by a SHS technique may be recommended for the production of machine parts for construction and instrumental purposes by powder metallurgy methods, as well as for the deposition of protective coatings [2004Lep].

Eutectic and near-eutectic Fe-TiB_2 alloys were recommended as wear resistant and corrosion resistant coatings [1972Tic, 1974Shu, 1977Shu]. The mechanical properties of the near-eutectic alloy Fe-6.3 mass % TiB_2 are presented in Table 4 after [1977Shu].

The wear resistance of the titanium based metal matrix composites was measured by [1999Bra]. Under constant wear conditions (F = 2 N, s – 1000 m, v = 0,1 m/s), the samples show a wear resistant behavior of a 100Cr6 steel counterpart, if the TiB content exceeds 20 vol%. At lower TiB contents, the matrix substantially influences the wear resistance.

Mechanical properties of some ternary alloys obtained under compressive tests by [2005Lou] are presented in Table 5.

Metallic glasses of $Fe_{70}Ti_{10}B_{20}$ and $Fe_{60}Ti_{20}B_{20}$ have been crystallized at 167 and 527°C, respectively [1991Dud]. The Curie temperatures of $Fe_{80-x}Ti_xB_{20}$ metal glasses are equal to 327, 197, and 67°C at x = 6, 10, and 20 at.%, respectively [1991Dud].

Miscellaneous

Thermodynamic considerations led [1999Bra] to the conclusion that commercially pure titanium and B-Fe are appropriate for the production of a titanium based metal matrix composite reinforced by an in-situ reaction technique. In the case of arc melting, a complete phase transformation of the B-Fe alloys is observed during the cooling of the melt. Sintering parameters were optimized, and B-Fe was found to be completely consumed after 6 h at 950°C. Independent of the processing route, Fe atoms stabilize the (βTi) phase at room temperature. Subsequent annealing below the eutectoid temperature in the Fe-Ti system (595°C) is thought to transform the β phase towards (αTi) and TiFe. Regarding the low diffusion rates at such low temperatures, the β phase is still present after 12 h at 550°C.

The mechanism of structure production in composites produced by SHS depends significantly on the type of contact between the initial components due to contact eutectic formation [2000Lep, 2004Lep]. In the case when the mixture consists from Ti, B, and Fe powders, the high-melting compound TiB_2 forms as a result of the interaction between two melts. In the case of a ferroboron alloy-titanium mixture, TiB_2 forms as a result of the interaction between the ferrotitanium melt and solid ferroboron. The highly disperse and more homogeneous structure of the products forms after combustion of the second type mixture. The use of industrial

DOI: 10.1007/978-3-540-69761-9_25

ferroboron as an initial reagent allows the production of a high-quality material by combining the SHS process with rolling. Preliminary mechanoactivating of SHS Fe-TiB_2 powder results in a reduction in the sintering temperature of 30-70°C and decreases the isothermal holding time from 60 to 40 min. It was also found, that activation in gasoline leads to a charge in the phase composition of the sintered products [2004Lep].

The grain growth kinetics in nanocrystalline mechanically alloyed $Fe_{80}Ti_8B_{12}$ alloy in the temperature range of 642-712°C may be described as a two-stage process. The first stage, corresponding to the crystallization of the amorphous phase, may be described well by a model that takes into account pinning forces on grain boundaries. Grain coarsening in the second stage may be successfully described by a model of the normal grain growth. The activation energy values for each stage, were 300±10 and 280±10 $kJ \cdot mol^{-1}$, respectively, which is comparable with lattice self-diffusion in Fe [2003Kra].

Table 1. Investigations of the B-Fe-Ti Phase Relations, Structures and Thermodynamics

Reference	Method/Experimental Technique	Temperature/Composition/Phase Range Studied
[1966Has]	DTA	Up to 950°C, Fe-0.2Ti-0.2 B (mass%)
[1967Fed]	X-ray diffraction	1000°C, alloy compositions were located on the isopleths: 10 at.% B, 20 at.% B, 25 at.% B, 33.3 at.% B, 50 at.% B, 66.7 at.% B, 80 at.% B; (αFe)+TiB_2, Fe+TiB_2+$TiFe_2$, TiB_2+$TiFe_2$, TiB_2+TiFe +$TiFe_2$, TiB_2+TiFe, TiFe+Ti_2Fe+TiB_2, Ti_2Fe+(βTi) +TiB, TiB_2+FeB+Fe_2B, TiB_2+B+FeB, (γFe)+TiB_2 +Fe_2B
[1974Shu]	Optical microscopy, SEM, DTA	Up to 1540°C, from 0.5 to 14.16 mol% TiB_2, polythermal section Fe-TiB_2
[1985Mak]	Optical metallography, X-ray diffraction, microhardness measurements	Up to 2530°C, Molar ratio: Ti:2B:2Fe, Ti:2B:Fe, 3Ti:4B:Fe, 3Ti:6B:Fe
[1992Ott]	DTA, SEM, EPMA, decantation experiments	1450-1050°C, alloys located in the Fe corner of the phase diagram; L+TiB_2, L+(αFe), (αFe)+TiB_2+Fe_2B, (αFe)+TiB_2
[1995Ras]	Optical metallography, X-ray diffraction, SEM, EDX	Ratio components Fe:TiB_2 in final products from 14.71:85.9 to 73.37:26.63
[1999Bra]	X-ray diffraction, Mössbauer spectroscopy, SEM, EDX	Cast alloys and sintered at 850 and 1050°C + HIP for 3 h at 950°C and 100 MPa, Ti+5 mass% TiB, Ti+10 mass% TiB, Ti+15 mass% TiB, Ti+20 mass% TiB, Ti+25 mass% TiB, Ti+30 mass% TiB
[2000Lep] [2004Lep]	Optical microscopy, local X-ray spectrum analysis, X-ray diffractometry, microhardness, wear resistance	Fe-TiB_2, 50 mass% Fe
[2005Lou]	X-ray diffraction, SEM	$Ti_{64.7}Fe_{34.8}B_{0.5}$, $Ti_{64.4}Fe_{34.6}B_1$, $Ti_{74}Fe_{24}B_2$, (βTi)+TiFe

DOI: 10.1007/978-3-540-69761-9_25

Table 2. Crystallographic Data of Solid Phases

Phase/Temperature Range [°C]	Pearson Symbol/ Space Group/ Prototype	Lattice Parameters[pm]	Comments/References
(βB) < 2092	*hR*333 $R\bar{3}m$ βB	*a* = 1093.30 *c* = 2382.52	[1993Wer]
		a = 1092.2 *c* = 2381.1	at 1.1 at.% C [1993Wer] linear d*a*/d*x*; d*c*/d*x*
		a = 1095.14 *c* = 2386.1	at $FeB_{\sim 49}$ [V-C2]
		a = 1097.18 *c* = 2387.05	at $FeB_{\sim 20}$ [V-C2]
(αδFe)	*cI*2 $Im\bar{3}m$ W		
(αδFe) 1538 - 1394		*a* = 293.15	[Mas2]
(αFe) < 912		*a* = 286.65	at 25°C [Mas2]
(γFe) 1394 - 912	*cF*4 $Fm\bar{3}m$ Cu	*a* = 364.67	[Mas2]
(εFe)	*hP*2 $P6_3/mmc$ Mg	*a* = 246.8 *c* = 396.0	at 25°C, >25 GPa [Mas2]
(βTi) 1670 - 595	*cI*2 $Im\bar{3}m$ W	*a* = 330.65	[Mas2]
(αTi) < 882	*hP*2 $P6_3/mmc$ Mg	*a* = 295.06 *c* = 468.35	at 25°C [Mas2]
(ωTi)HP	*hP*3 *P*6/*mmm* ωTi	*a* = 462.5 *c* = 281.3	at 25°C [Mas2]
Fe_2B < 1389	*tI*12 *I*4/*mcm* Al_2Cu	*a* = 510.9 *c* = 424.9	[1982Kub1]
FeB < 1650	*oP*8 *Pbmn* FeB	*a* = 551.0 *b* = 295.0 *c* = 406.0	49.5-50 at.% B [1982Kub1]

(*continued*)

DOI: 10.1007/978-3-540-69761-9_25

Phase/Temperature Range [°C]	Pearson Symbol/ Space Group/ Prototype	Lattice Parameters[pm]	Comments/References
Fe_3B (m)	*oP*16 *Pnma* Fe_3C	*a* = 543 *b* = 666 *c* = 445	~25 at.% B [Mas2] metastable
TiFe < 1317	*cP*2 $Pm\bar{3}m$ CsCl	*a* = 298.8 to 297.7	48-50.2 at.% Fe [1981Mur]
$TiFe_2$ < 1424	*hP*12 $P6_3/mmc$ $MgZn_2$	*a* = 480.4 to 477.7 *c* = 784.9 to 780.7	65.2-72.8 at.% Fe, annealing at 1000°C [1981Mur]
TiB < 2180	*oP*8 *Pnma* FeB	*a* = 610.5 *b* = 304.8 *c* = 454.2	[1986Mur]
TiB (m)	*oC*8 *Cmcm* CrB	*a* = 323 *b* = 856 *c* = 305	[1992Gra] metastable
Ti_3B_4 < 2200	*oI*14 *Immm* Ta_3B_4	*a* = 325.9 *b* = 1373 *c* = 304.2	56.1 at.% B [1986Spe]
TiB_2 < 3225	*hP*3 $P6_3/mmm$ AlB_2	*a* = 302.8 to 304.0 *c* = 322.8 to 323.4	[1986Mur]

Table 3. Invariant Equilibria

Reaction	*T* [°C]	Type	Phase	Composition (at.%)		
				Ti	Fe	B
l ⇌ (αδFe) + TiB_2	1320	E	l	~6.7	~83.2	~10.1
			(αδFe)	>97.9	2.0	< 0.1
			TiB_2	33.3	0	66.7
l ⇌ (γFe) + TiB_2 + Fe_2B	1170	E	L	~0.3	~82.7	~17
			(γFe)	~0.5	~99.5	~0
			TiB_2	33.3	~0	66.7
			Fe_2B	~0	66.7	33.3

Table 4. Dependence of Mechanical Properties of Fe-50 mass% TiB_2 Alloy *vs* Temperature [1977Shu]

Temperature [°C]	UTS [MPa]	YS [MPa]	Ductility [%]
25	900	810	2
200	-	-	3

(*continued*)

DOI: 10.1007/978-3-540-69761-9_25

Temperature [°C]	UTS [MPa]	YS [MPa]	Ductility [%]
400	800	590	3
600	610	470	7
800	150	140	16
900	100	80	17
1000	120	115	34
1100	70	65	35

Table 5. Mechanical Properties, Density and Phase Composition Fe-Ti Alloys with B [2005Lou]

Alloy	E [GPa]	σ_{true} [MPa]	$\sigma_{0.2}$ [MPa]	ε [%]	ρ [Mg·m^{-3}]	Phase composition
$Ti_{64.7}Fe_{34.8}B_{0.5}$	150	2470	1840	4.3	4.475	(βTi)+TiFe
$Ti_{64.4}Fe_{34.6}B_1$	157	2050	1750	4.5	4.448	(βTi)+TiFe
$Ti_{74}Fe_{24}B_2$	169	1500	1500	0.2	5.377	(βTi)+TiFe

Table 6. Investigations of the B-Fe-Ti Materials Properties

Reference	Method/Experimental Technique	Type of Property
[1961Fun]	Measurements of Vickers hardness at 98 N load, transverse strength at 30 mm distance between supports	Vickers hardness, transverse strength at temperatures from 20 to 1100°C, wear strength on cutting
[1966Has]	Vickers method, tensile testing	H_V, UTS
[1966Yas]	Measurements of limiting wetting angle	Wetting of TiB_2 by liquid Fe
[1977Shu]	High-temperature tensile tests	Mechanical properties from room temperature to 1000°C, (UTS, YS, ductility)
[1985Mak]	SEM	Porosity
[1991Dud]	Weiss-Farrer magnetic balance, derivative thermo-magnetic-gravimetry, DTA	Magnetic moment, Curie temperature, crystallization temperature
[1999Bra]	A pin-on-disc type machine	Wear resistance of B-Fe-Ti cermets
[2001Wan] [2003Wan]	Hardness	Cracking resistance, hardness of the B-Fe-Ti composite coating developed by laser cladding
[2005Lou]	Compressive mechanical testing, instron - type machine at a strain rate $5 \cdot 10^{-4} \cdot s^{-1}$, Archimedean method using tetrabromoethane	Mechanical properties and density at room temperature.

DOI: 10.1007/978-3-540-69761-9_25

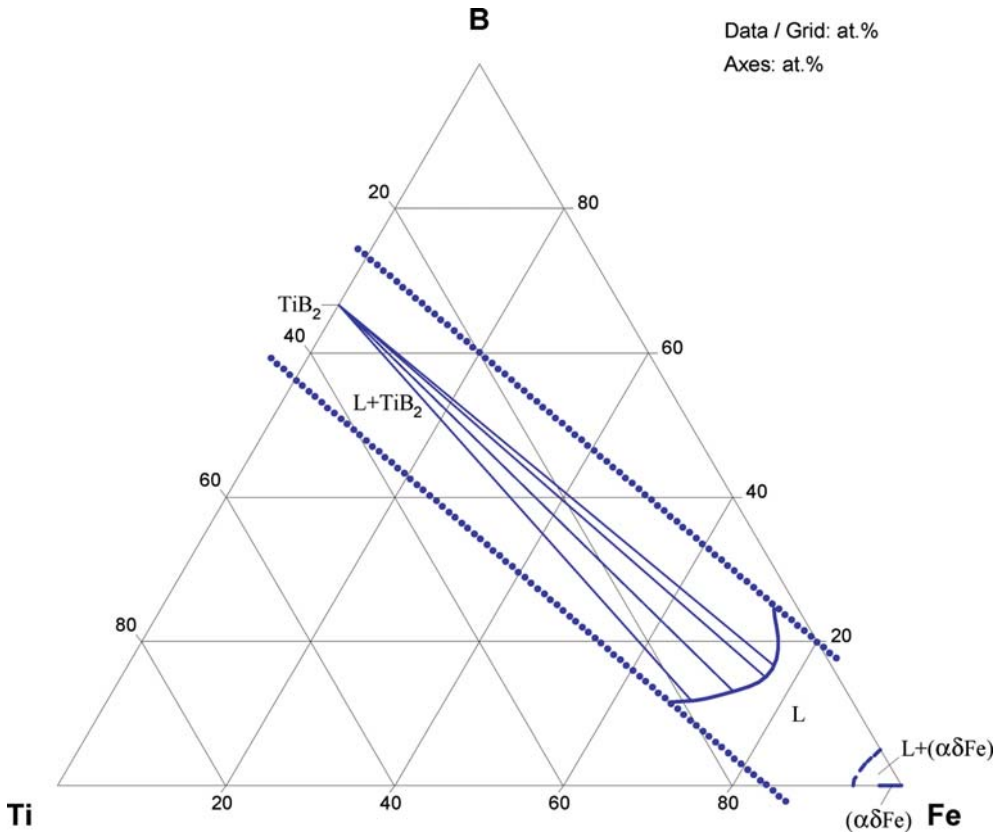

Fig. 1. B-Fe-Ti. Composition of the liquid phase in equilibrium with TiB_2 or Fe at 1450°C

DOI: 10.1007/978-3-540-69761-9_25

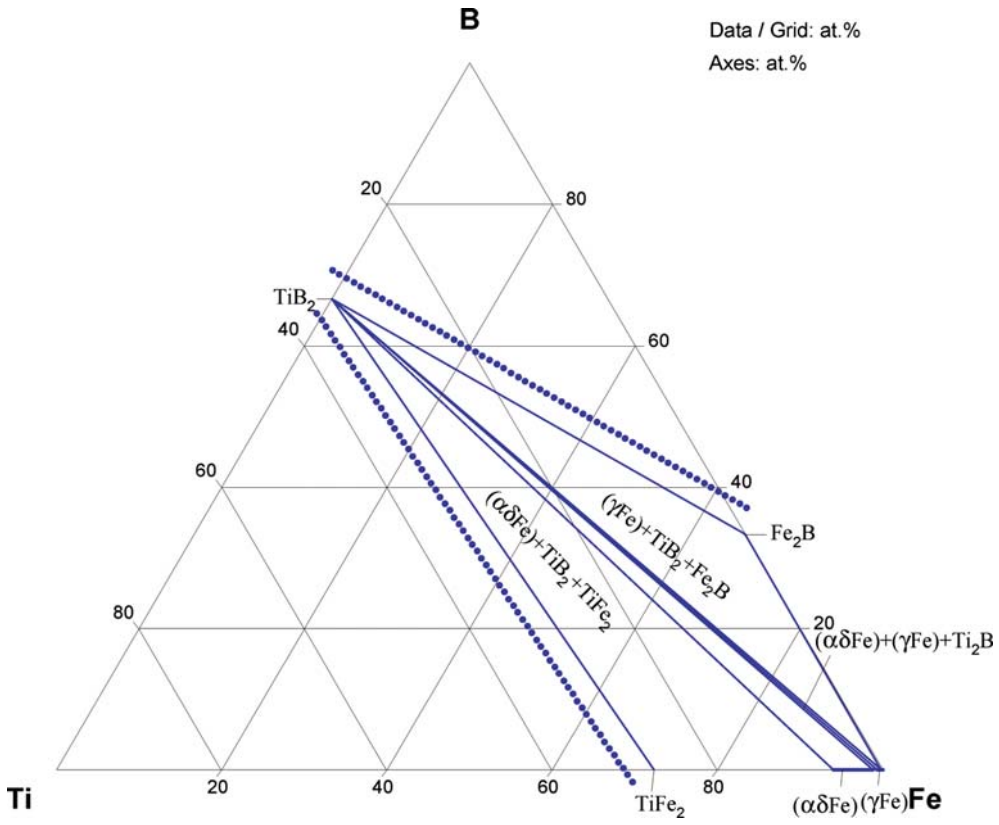

Fig. 2. B-Fe-Ti. Partial isothermal section at 1050°C

DOI: 10.1007/978-3-540-69761-9_25

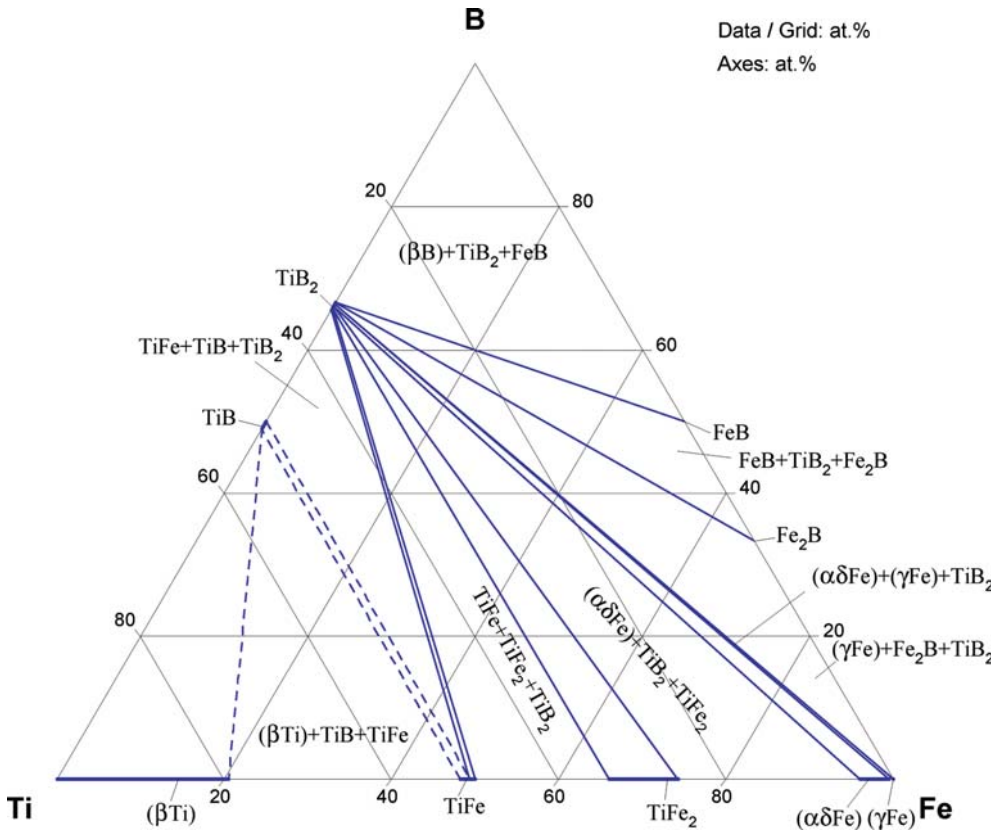

Fig. 3. B-Fe-Ti. Isothermal section at 1000°C

DOI: 10.1007/978-3-540-69761-9_25

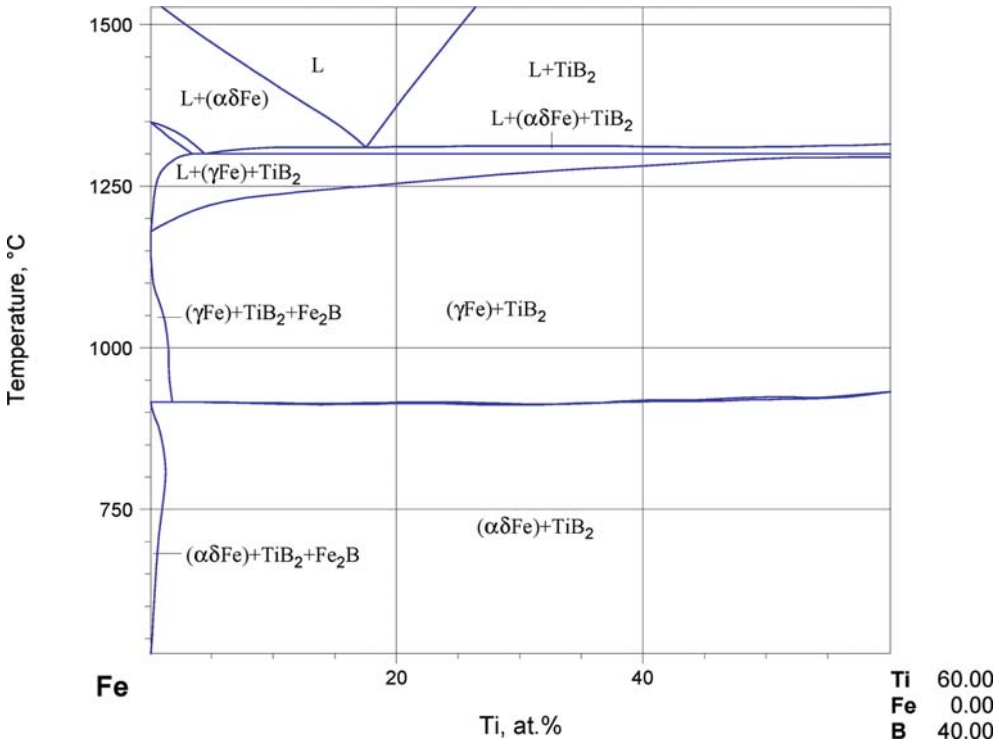

Fig. 4. B-Fe-Ti. Fe - TiB_2 vertical section

DOI: 10.1007/978-3-540-69761-9_25

References

[1961Fun] Funke, V.F., Samsonov, G.V., Yudkovsky, S.I., "Alloys of the System Ti-B-Fe", *J. Appl. Chem. USSR*, **34**(5), 973–978 (1961), translated from *Zh. Prikl. Khim.*, **34**(5), 1013–1020 (Crys. Structure, Morphology, Phase Relations, Experimental, Interface Phenomena, Mechan. Prop., 11)

[1966Has] Hasegawa, M., Okamoto, M., "A Study on the Ternary Alloys of Iron and Boron" (in Japanese), *Nippon Kinzoku Gakkai-Si*, **30**(6), 533–540 (1966) (Phase Relations, Morphology, Experimental, Mechan. Prop., 12)

[1966Yas] Yasinskaya, G.A., "Wetting of Refractory Carbides, Borides and Nitrides by Molten Metals", (in Russian), *Poroshk. Metall. (Kiev)*, **43**(7), 53–55 (1966) (Phase Relations, Experimental, Interface Phanomena, 5)

[1967Fed] Fedorov, T.F., Kuzma, Yu.B., "The Ti-Fe-B System" (in Russian), *Izv. Akad. Nauk SSSR, Neorg. Mater.*, **3**, 1498–1499 (1967) (Crys. Structure, Experimental, Phase Diagram, Phase Relations, *, 5)

[1972Tic] Tikhonovich, V.I., Shurin, A.K., Loktionov, V.A., Panarin, V.,E., "Structure and Wear Resistance of Fe Alloys with TiB_2" (in Russian), *Litye Iznosostoikie Mater.*, Institute of Casting, Kiev, 70–75 (1972) (Morphology, Phase Diagram, Experimental, Mechan. Prop., 13)

[1974Shu] Shurin, A.K., Panarin, V.E., "Phase Equilibria and Structure of Alloys of Fe with TiB_2, ZrB_2, and HfB_2" (in Russian), *Izv. Akad. Nauk SSSR, Met.*, **5**, 235–239 (1974) (Morphology, Phase Diagram, Phase Relations, Experimental, *, 6)

[1977Shu] Shurin, A.K., Panarin, V.E., Sul'zhenko, V.K., Kozyrskiy, G.Ya., "Properties of Eutectic Alloys with TiB_2 at High Temperatures" (in Russian), *Metalloved. Term. Obrab. Met.*, (8) 53–55 (1977) (Phse Diagram, Experimental, Mech. Prop., 4)

[1979Shu] Shurin, A.K., Dmitrieva, G.P., Panarin, V.E., "Hardness of Qusibinary Eutectic Alloys with Interstitial Phases" (in Russian), *Metallofizika*, **76**, 81–85 (1979) (Phase Relations, Experimental, Mechan. Prop., 6)

[1981Mur] Murray, J.L., "The Fe-Ti (Iron-Titanium) System", *Bull. Alloy Phase Diagrams*, **2**(3), 320–324 (1981) (Crys. Structure, Phase Diagram, Review, Thermodyn., 81)

[1982Kub1] Kubaschewski, O., "Iron-Boron", *Iron Binary Phase Diagrams*, Springer-Verlag, Berlin, 15–18 (1982) (Review, Phase Diagram, 31)

[1982Kub2] Kubaschewski, O., "Iron-Titanium", *Iron Binary Phase Diagrams*, Springer-Verlag, Berlin, 152–156 (1982) (Review, Phase Diagram, 26)

[1982Yur] Yuriditskii, B.Yu., Pesin, V.A., Ordan'yan, S.S., "Change in the Fine Structure of Titanium Diboride Occurring During the Sintering of a Ti-B_2-Fe(Mo) Cermet", *Sov. Powder Metall. Met. Ceram.*, **232**(4), 280–282 (1982), translated from *Poroshk. Metall.*, **232**(4), 32–35 (1982) (Crys. Structure, Morphology, Experimental, 7)

[1985Mak] Maksimov, Yu.M., Merzhanov, A.G., Pak, A.T., Raskolenko, L.G., Braverman, B.Sh., "High Temperature Synthesis of the Ti-B-Fe System" (in Russian), *Metally*, (2) 219–223 (1985) (Morphology, Phase Relations, 11)

[1986Mur] Murray, J.L., Liao, P.K., Spear, K.E., "The B-Ti System", *Bull. Alloy Phase Diagrams*, **7**, 550–555 (1986) (Phase Diagram, Review, Thermodyn., 48)

[1986Spe] Spear, K.E., McDowell, P., McMahon, F., "Experimental Evidence for the Existence of the Ti_3B_4 Phase", *J. Am. Ceram. Soc.*, **69**(1), C4–C5 (1986) (Crys. Structure, Experimental, Phase Diagram, 13)

[1987Res] Reznitskii, L.A., "Thermochenical Model of the Bond in Transition Metal Borides", *Russ. J. Phys. Chem.*, **61**(7), 938–941 (1987) (Calculation, Thermodyn., 20)

[1991Dud] Dudek, W., Gwiazda, J., Marianska, E., Moskalewicz, R., Oleniacz, J., Zych, W., "Magnetic Moment, Curie Temperature and Crystallization Temperature of Amorphous Alloys of the Type Fe-TM-B", *J. Magn. Magn. Mater.*, **94**(3), 243–246 (1991) (Phase Relations, Magn. Prop. Experimental, 15)

DOI: 10.1007/978-3-540-69761-9_25

[1992Gra] De Graef, M., Lofvander, J.P.A., McCollough, C., Levi, C.G., "The Evolution of Metastable B(f) Borides in a Ti-Al-B Alloy", *Acta Metall.*, **40**(12), 3395–3406 (1992) (Crys. Structure, Experimental, Phase Diagram, 22)

[1992Ott] Ottavi, L., Saint-Yours, C., Valignant, N., Allibert, C.H., "Phase Equilibria and Solidification of Fe-Ti-B Alloys in the Region Close to Fe-TiB_2", *Z. Metallkd.*, **83**(2), 80–83 (1992) (Morphology, Phase Diagram, Experimental, #, 8)

[1993Wer] Werheit, H., Kuhlmann, U., Laux, M., Lundström, T., "Structural and Electronic Properties of Carbon-Doped β-Rhombohedral Boron", *Phys. Stat. Sol.*, **B179**, 489–511 (1993) (Crys. Structure, Experimental, 51)

[1995Ras] Werheit, H., Kuhlmann, U., Laux, M., Lundström, T., "Structural and Electronic Properties of Carbon-Doped β-Rhombohedral Boron", *Phys. Stat. Sol.*, **B179**, 489–511 (1993) (Crys. Structure, Experimental, 51)

[1999Bra] Bram, M., Aubertin, F., Venskutonis, A., Breme, J., "Kinetics of the Phase Transformation and Wear Resistance of In-situ Processed Titanium Matrix Composites Based on Ti-Fe-B", *Mater. Sci. Eng. A*, **264**(1–2), 74–80 (1999) (Morphology, Phase Relations, Thermodyn., Experimental, Kinetics, 20)

[1999Tan] Tanaka, K., Saito, T., "Phase Equilibria in TiB_2-Reinforced Hidh Modulus Steel", *J. Phase Equilib.*, **20**(3), 207–214 (1999) (Calculation, Phase Relations, 22)

[2000Lep] Lepakova, O.K., Raskolenko, L.G., Maksimov, Y.M., "The Mechanism of Phase and Structure Formation of the Ti-B-Fe System in a Combustion Wave", *Combustion Explosion & Shock Waves*, **36**(5), 575–581 (2000) (Morphology, Phase Relations, Experimental, Mechan. Prop., 8)

[2003Kra] Krakhmalev, P.V., Yi, D., Nyborg, L., Yao, Y., "Isothermal Grain Growth in Mechanically Alloyed Nanostructured $Fe_{80}Ti_8B_{12}$ Alloy", *Mater. Lett.*, **57**(22–23), 3671–3675 (2003) (Crys. Structure, Morphology, Phase Relations, Experimental, Kinetics, 22)

[2003Rag] Raghavan, V., "B-Fe-Ti (Boron-Iron-Titanium)", *J. Phase Equilib.*, **24**(5), 455–456 (2003) (Phase Diagram, Review, *, 9)

[2004Lep] Lepakova, O.K., Raskolenko, L.G., Maksimov, Y.M., "Self-Propagating High - Temperature Synthesis of Composite Material TiB_2-Fe", *J. Mater. Sci.*, **39**(11), 3723–3732 (2004) (Crys. Structure, Morphology, Optical Prop., Phase Relations, Experimental, Kinetics, Mechan. Prop. 10)

[2005Lou] Louzguine-Luzgin, D.V., Louzguina-Luzgina, L.V., Inoue, A., "Investigation of the Structure and Properties of Hypereutectic Ti-based Bulk Alloys" in "*Integrative and Interdisciplinary Aspects of Intermetallics Symposium*", Materials Research Society Symposium Proceedings, Vol. **842**, Materials Research Society, Warrendale, PA, USA, 133–138 (2005) (Crys. Structure, Phase Relations, Experimental, Mechan., Prop., 16)

[V-C2] Villars, P. and Calvert, L.D., *Pearson's Handbook of Crystallographic Data for Intermetallic Phases*, 2nd edition, ASM, Metals Park, Ohio (1991)

[Mas2] Massalski, T.B. (Ed.), *Binary Alloy Phase Diagrams*, 2nd edition, ASM International, Metals Park, Ohio (1990)

DOI: 10.1007/978-3-540-69761-9_25

Boron – Iron – Tungsten

Peter Rogl

Introduction

Several research groups have dealt with the B-Fe-W system to elucidate formation of compounds, their crystal structure and phase relations. A first investigation by [1966Rie] established the structure of W_2FeB_2 (isotypic with W_2CoB_2) and was later recognized as low-temperature form stable below about 1300°C [1968Jed, 1969Kuz] with a U_3Si_2 type high temperature modification [1968Jed, 1969Kuz]. Investigation of an isothermal section at 1000°C revealed the existence of WFeB, W_2FeB_2, $W_{0.7}Fe_{0.15}B$ (CrB type) besides a low-temperature phase W_2FeB_4 with Ta_3B_4 type (< 850°C) [1966Has1]. The crystal structure of WFeB was found to be isotypic with TiNiSi [1968Jei, 1968Kuz]. Whilst there is no doubt on the existence of W_2FeB_4 [1966Has1, 1969Kuz] at temperatures below 800°C, the CrB type phase, $W_{0.7}Fe_{0.15}B$, [1966Has1] has not been verified by [1969Kuz, 2000Lei] and may be a simple solid solution of Fe in βWB. A reinvestigation of the ternary system by [2000Lei] established the phase relations at 1050°C with only two ternary compounds, WFeB and W_2FeB_2. In addition $(W_xFe_{1-x})_3B$ with the Ti_3P type was observed at $x \approx 0.2$ in a limited temperature range $1080 < T < 1100$°C. Phase relations in the B-Fe-W system were summarized by [1992Rag, 2003Rag].

Binary Systems

Phase equilibria in the B-Fe system were reinvestigated by [1985Smi, 1986Smi] and were summarized in [1992Rog]. A thermodynamic assessment and calculation is from [1994Hal]. A metastable diagram including the metastable compounds Fe_3B (Fe_3C type) and $Fe_{23}B_6$ was presented by [1978Her]. Depending on the rate of quenching a liquid alloy $Fe_{76}B_{24}$, two modifications of Fe_3B, *i.e.* the Fe_3P type and the Ti_3P type, were obtained by [1982Kha] and were claimed to exist as high- and low-temperature compounds, respectively, within a small temperature window of the equilibrium diagram ($1140 < T < 1250$°C). Similarly, the τ phase ($Fe_{23}B_6$) was speculated by [1991Kha] to belong to the equilibrium diagram within a small temperature region $650 \leq T \leq 800$°C. The Fe-W system was accepted in the version of [1986Nag] although [2000Lei] found no indications for the existence of the phases, WFe_2 ($MgZn_2$ type) and WFe (WNi type), but found at 1050°C the W_6Fe_7 phase, which does not exist at this temperature in [1986Nag]. A thermodynamic evaluation of the Fe-W system is from [1987Gus]. B-W is in the version of [1998Rog]. A listing of the crystallographic information of all stable and metastable phases pertinent to the B-Fe-W system is presented in Table 1, including also ternary solid solution phases.

Solid Phases

Five ternary phases were reported to form in the B-Fe-W system: WFeB [1966Has1, 1968Jei, 1968Kuz, 2000Lei], W_2FeB_2 [1966Rie, 1966Has1, 1968Jed, 1969Kuz, 2000Lei], $W_{0.7}Fe_{0.15}B$ [1966Has1], W_2FeB_4 [1966Has1] and $(W,Fe)_3B$ [2000Lei]. Whilst investigations by [1969Kuz] and [2000Lei] confirmed the existence of WFeB and W_2FeB_2 at 800°C and at 1050°C, the compound, $W_{0.7}Fe_{0.15}B$, reported by [1966Has1] with CrB type was not confirmed at 800°C by [1969Kuz, 2000Lei]. Neither was W_2FeB_4 [1966Has1], which was concluded by [1969Kuz, 2000Lei] to be stable only below 800°C. $(W_xFe_{1-x})_3B$ with the Ti_3P type was observed at $x \approx 0.2$ in a limited temperature range $1080 < T < 1100$°C and may be conceived as a ternary stabilization of metastable binary Fe_3B by Fe/W substitution [2000Lei]. Although, [1966Has1] - without giving any further details - indicated small mutual solid solubility among iron and tungsten borides, the reinvestigation of [2000Lei] employing EMPA did not reveal any metal exchange.

Some controversy particularly exists on the solid solubility of W in Fe_2B: whereas [1969Kuz] reports on a solubility of about 5 at.% W raising the lattice parameters from $a = 510.9$, $c = 424.9$ for binary Fe_2B to $a = 512.5$, $c = 423.4$ pm in ternary alloys at 800°C (?), no significant solubility was observed at

DOI: 10.1007/978-3-540-69761-9_26

1050°C by [2000Lei]. Furthermore, no homogeneity regions were observed for the ternary compounds at 1050°C [2000Lei].
The ternary compound W_2FeB_2 exhibits two structural modifications: W_2FeB_2 (h) with U_3Si_2 type was reported from as cast alloys [1968Jed, 1969Kuz] as well as in alloys annealed at 1500°C for 20 h [1969Kuz]. A homogeneity region was suggested by both research groups from the variation of lattice parameters. Whilst [1968Jed] suggested a formula W_2FeB_2 (W, $x_W = 0.183$ in 4h, B, $x_B = 0.394$ in 4g), X-ray model calculations by [1969Kuz] revealed partial metal order: 3.5W + 0.5Fe in 4h ($x_W = 0.18$), 2Fe on 2a, and 4B in 4g ($x_B = 0.39$) for a formula $W_{1.75}Fe_{1.25}B$. $W_{1.75}Fe_{1.25}B$ was said to decompose into WFeB, W_2FeB_2 (r), Fe_2B (and FeB ?) after anneal for 20 h at 1300°C [1969Kuz].
Crystallographic data of all ternary phases are collected in Table 2.

Isothermal Sections

Phase relations established by [2000Lei] at 1050°C (see Fig. 1) correspond to some extent to the isothermal section at 1000°C given by [1966Has1]. In contradiction to [1966Has1], however, no boron-rich W_2FeB_4 and $W_{0.7}Fe_{0.15}B$ phases were encountered thus reducing the amount of ternary phases to two: WFeB and W_2FeB_2. The region in the isothermal section with boron contents higher than 50 at.% B is dominated by three-phase fields depicting the equilibria FeB + $WB_{2+x}(W_2B_{5-x})$ + αWB, FeB + $WB_{2+x}(W_2B_{5-x})$ + $W_{1-x}B_3$ and FeB + (βB) + $W_{1-x}B_3$ (see Fig. 1) [2000Lei]. The $W_{1-x}B_3$ phase was not observed by [1966Has1]. The region with boron contents lower than 50 at.% B is governed by the two ternary phases WFeB and W_2FeB_2. WFeB represents the ternary phase with the lowest boron content at 1050°C being in equilibrium with (Fe). Equilibria determined by [2000Lei] in the Fe-W rich part are at variance to those in the accepted binary of [1986Nag] (see binary systems). Similarly the homogeneity regions observed for binary W-borides are slightly different from the data calculated.

Notes on Materials Properties and Applications

Tungsten is one of the constituents of a Mo_2FeB_2 based cermet where high hardness in combination with good corrosion and wear resistance defines the use for injection molding machine parts, for hot copper extruding dies [1997Tak], or for gas turbine engines [1991Sau].

Miscellaneous

Tungsten additions were said to markedly increase hardness and tensile strength of B-Fe alloys air-cooled from 950 or 1100°C and water quenched; ductility and toughness of the alloy, however, decreased with W additions [1966Has2].
Attempts to describe the thermal stability of metallic glasses $(Fe_{95}W_5)_{83}B_{17}$ as a function of temperature, pressure and composition were made by [1983Ber] employing calorimetric and hardness measurements. Relations between structure and first steps in crystallization were investigated on $(Fe_{100-x}W_x)_{83}B_{17}$ glasses ($x = 3, 15, 25$) by means of TEM and X-ray diffraction [1989Kol]. As a first step crystallization of (αFe,W) was observed followed by $(Fe,W)_3B$. A similar crystallization scheme was reported from amorphous soft magnet $Fe_{91-x}W_xB_9$ [2002Sul]. A general survey of the effect of concentration and transition metals on crystallization of Fe based amorphous alloys was given by [1987She]. [1998Guo] reported on the crystallization temperature and activation energy of crystallization in amorphous B-Fe-W nano-powders (30-100 nm with nearly spherical morphology).
[1985Nov, 1986Che] studied the decrease of the Curie temperature and change of resistivity of $Fe_{85-x}W_xB_{15}$ and $(Fe_{1-x}W_{x)\ 84.5}B_{15.5}$ glasses ($x < 10$) with increasing Fe/W substitution. Correlation between magnetic properties and density of Fe-T-B (T = W, Cr) glassy alloys was discussed by [1984Kon]. Soft magnetic properties of amorphous $Fe_{81.4}W_{2.6}B_{16}$ and the influence of hydrogenation-dehydrogenation were characterized by [2002Cen, 2002Nov]. Magnetic properties on various Fe-TM-B diluted alloys were also recorded by [1992Kis]. The effect of pressure on the Curie temperature of B-Cr-Fe and B-Fe-W amorphous alloys was elucidated by [1990Mih].

DOI: 10.1007/978-3-540-69761-9_26

^{57}Fe Mössbauer spectroscopy (4.2 to 300 K) of W_2FeB_2 (W_2CoB_2 type) suggested spontaneous magnetic order with a small saturation field of 1.8-2.5 Tesla [1973You].
Technical parameters for electrodeposition of boron-containing Fe-W and Fe-Mo alloys on copper cathode from baths containing ferrous sulfate, sodium tungstate (or molybdate), boron phosphate, ammonium citrate, 1-dodecylsulfate-Na and ammonia or sulfuric acid for pH adjustments have been determined [2000Pra]. Magnetic properties and micro-hardness of 1 to 3 μm thick layers of Fe-TM-B (TM = Sn, TN, Mo-W) alloys prepared by electroless plating were studied by [1998Wan, 1999Wan].
[1980Che] evaluated some key physicomechanical properties of iron-boride materials alloyed with Nb, Mo, and W. The greatest strengthening effect (σ_t = 62-75 kgf·mm^{-2} at 30-33 HRC) is achieved with iron-tungsten matrices infiltrated.

Table 1. Investigations of the B-Fe-W Phase Relations, Structures and Thermodynamics

Reference	Method/Experimental Technique	Temperature/Composition/Phase Range Studied
[1966Has1]	XPD on powder compacts arc melted under argon, wrapped in Mo-foil, sealed in quartz capsules and annealed at 1000°C for 3 weeks. Some alloys were annealed at 1600°C; some alloys were prepared via hot-pressing in graphite dies.	Phase equilibria in an isothermal section at 1000°C. Determination of the crystal structure of four ternary compounds: WFeB, W_2FeB_2, $W_{0.7}Fe_{0.15}B$ and the low-temperature phase W_2FeB_4 (< 850°C).
[1966Rie]	XPD on arc-melted alloys.	Determination of the structure of W_2FeB_2
[1968Jed]	XPD on arc-melted alloys 20-25 at.% W; 30 at.% Fe, 45-50 at.% B.	Determination of the high temperature form of W_2FeB_2
[1968Jei]	XPD on powder compacts induction melted under argon, sealed in quartz capsules and annealed at 950°C for 3 weeks.	Determination of the structure of WFeB.
[1968Kuz]	XPD on powder compacts sintered in evacuated quartz capsules at 900°C for 480 h.	Determination of the structure of WFeB
[1969Kuz]	XPD on argon arc-melted powder compacts, annealed for 20 h at 1300°C in vacuum on a Mo-boat. Samples rich in Fe were heated in Al_2O_3 crucibles to 1300°C and slowly cooled (15°C·h^{-1}) to 800°C. All alloys were annealed for 500 h in evacuated quartz capsules.	Determination of the structure of $W_{1.75}Fe_{1.25}B$ from alloys 30-35 at.% W, 30-25 at.% Fe, 40 at.% B.
[2000Lei]	Samples were prepared from powder compacts, prereacted at 600 to 900°C prior to repowdering and recompacting and finally were arc melted. Annealing was performed in a high vacuum furnace on arc melted alloys at 1400°C for 4 d, cooled to 1250°C (50°C·d^{-1}) and 1050°C for one week. Sintered compacts in Al_2O_3 crucibles were annealed at 1250°C for 4 d followed by 1050°C for one week. XPD (Fe-radiation) and EMPA (W, Fe, B).	Phase equilibria in an isothermal section at 1050°C. Existence and confirmation of the crystal structure of two ternary compounds: WFeB, W_2FeB_2. Formation of $(W_xFe_{1-x})_3B$ at x = 0.2 in a limited temperature range 1080 < T < 1100°C.

DOI: 10.1007/978-3-540-69761-9_26

Table 2. Crystallographic Data of Solid Phases

Phase/ Temperature Range [°C]	Pearson Symbol/ Space Group/ Prototype	Lattice Parameters [pm]	Comments/References
(δFe) 1538 - 1394	*cI*2 $Im\bar{3}m$ W	a = 293.15	[Mas2]
(γFe) 1394 - 912	*cF*4 $Fm\bar{3}m$ Cu	a = 364.67 a = 357.3	[Mas2] at 25°C [V-C2]
(αFe) < 912 $Fe_{1-x}B_x$	*cI*2 $Im\bar{3}m$ W	a = 286.65 a = 286.0	[Mas2] at x = 0.09 [V-C2]
(W) < 3422	*cI*2 $Im\bar{3}m$ W	a = 316.552	[Mas2]
(βB) < 2092	*hR*333 $R\bar{3}m$ B	a = 1093.30 c = 2382.52 a = 1095.14 c = 2386.1 a = 1097.18 c = 2387.05	[1993Wer] at $FeB_{\sim 49}$ [V-C2] at $FeB_{\sim 20}$ [V-C2]
FeB < 1588	*oP*8 *Pnma* FeB	a = 550.6 b = 295.2 c = 406.1	[1992Rog]
Fe_2B < 1407	*tI*12 *I*4/*mcm* $CuAl_2$	a = 510.9 c = 424.9	[1992Rog]
$Fe_3B(h_1)$ ~1250 - ~1150	*tI*32 $I\bar{4}$ Fe_3P	a = 865.5 c = 429.7	metastable [1992Rog]
$Fe_3B(h_2)$ ~1220 - ~1140	*tP*32 $P4_2/n$ Ti_3P	a = 864.8 c = 431.4	metastable [1992Rog]
Fe_3B < 1214	*oP*16 *Pnma* Fe_3C	a = 542.8 b = 666.9 c = 443.9	metastable [1992Rog]
$Fe_{23}B_6$ ~800 - ~650	*cF*116 $Fm\bar{3}m$ $Cr_{23}C_6$	a = 1076	[1991Kha] metastable
W_2B < 2670	*tI*12 *I*4/*mcm* $CuAl_2$	a = 556.7 c = 474.4 a = 557.0 c = 474.4	[V-C2] W rich [1998Rog]

(*continued*)

DOI: 10.1007/978-3-540-69761-9_26

Phase/ Temperature Range [°C]	Pearson Symbol/ Space Group/ Prototype	Lattice Parameters [pm]	Comments/References
		a = 557.2 c = 474.6	B rich [1998Rog]
αWB < 2170	$tI16$ $I4_1/amd$ αMoB	a = 309.73 c = 1695.67 a = 312.18 c = 1691.88 a = 310.1 c = 1695.5 a = 312.8 c =1690.3	W rich [V-C2] B rich [V-C2] W rich [1998Rog] B rich [1998Rog]
βWB < 2665	$oC8$ $Cmcm$ CrB	a = 312.4 b = 844.5 c = 306.0 a = 314.2 b = 850.6 c = 306.5	[1998Rog] W rich [1998Rog]
W_2B_{5-x}(h) or WB_{2+x}(h) 2365 - ~900	$hP12$ $P6_3/mmc$ W_2B_{5-x}	a = 298.2 c = 1387.3 a = 298.35 c =1388.12 a = 298.76 c =1389.70	at $WB_{\sim 1.80}$ [1998Rog] W rich [V-C2] for $WB_{1.97}$ [1998Rog] B rich [V-C2]
W_2B_{5-x}(r) or WB_{2+x} (r) < 900	$hR21$ $R\bar{3}m$ Mo_2B_{5-x}	a = 301.1 c = 2093	[V-C2] metastable?
$W_{1-x}B_3$ < 2020	$hP20$ $P6_3/mmc$ $W_{1-x}B_3$	a = 520.04 c = 633.48 a = 520.05 c = 633.56	W rich [V-C2] B rich [V-C2]
W_6Fe_7	$hR39$ $R\bar{3}m$ W_6Fe_7	a = 475.63 b = 2572.8	[V-C2]
* τ_1, WFeB	$oP12$ $Pnma$ TiNiSi	a = 582.3 b = 316.1 c = 681.0 a = 583.2 b = 316.3 c = 681.1	at 1000°C [1968Jei] at 900°C [1968Kuz]

(*continued*)

DOI: 10.1007/978-3-540-69761-9_26

Phase/ Temperature Range [°C]	Pearson Symbol/ Space Group/ Prototype	Lattice Parameters [pm]	Comments/References
		a = 582.78 b = 316.63 c = 682.06	at 1050°C, [2000Lei] in equilibrium with (αFe) and W_6Fe_7
		a = 582.37 b = 316.42 c = 681.85	at 1050°C, [2000Lei] in equilibrium with W_2FeB_2
* τ_2, $(W_xFe_{1-x})_3B_2$(h) > 1300	*tP*12 *P*4/*mbm* U_3Si_2	a = 569.0 c = 316.2	high temperature form W_2FeB_2 [1968Jed]
		a = 575.3 to 573.9 c = 316.1 to 315.9	for $x \approx 0.58$, [1969Kuz] stable above ca 1300°C.
* τ_2, W_2FeB_2(r) < 1300°C	*oI*10 *Immm* W_2CoB_2	b = 711 a = 465 c = 322	low temperature form at 800°C [1969Kuz]
		b = 712.4 a = 461.0 c = 314.8	[1966Rie]
		a = 712.14 b = 461.38 c = 314.93	at 1050°C, [2000Lei] in equilibrium with WFeB
		a = 712.52 b = 461.06 c = 315.29	at 1050°C, [2000Lei] in equilibrium with αWB
* τ_3, $W_{0.7}Fe_{0.15}B$	*oC*8 *Cmcm* CrB	a = 315.5 b = 834.5 c = 305.4	at 1000°C [1966Has1]
* τ_4, W_2FeB_4	*oI*12 *Immm* Ta_3B_4	a = 311.0 b = 1441 c = 317.6	at 1000°C [1966Has1]
* τ_5, $(W_xFe_{1-x})_3B$ 1110 - 1080	*tP*14 $P4_2/n$ Ti_3P	a = 863.53 c = 431.60	at $x \approx 0.2$ [2000Lei]

DOI: 10.1007/978-3-540-69761-9_26

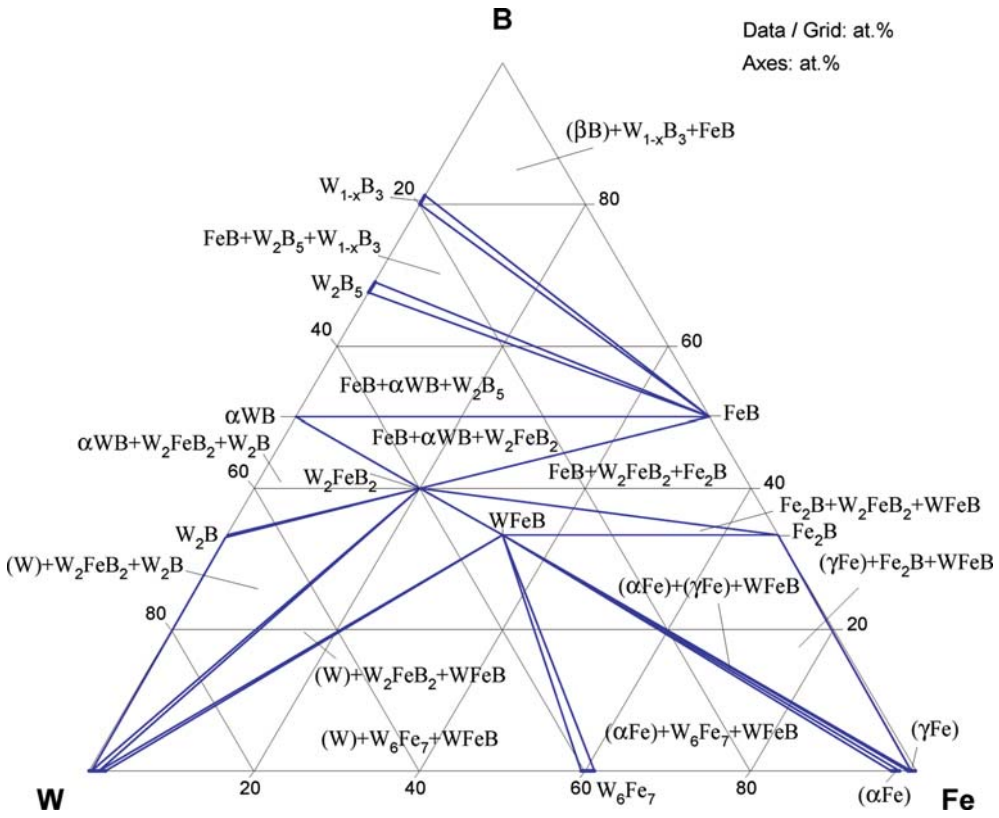

Fig. 1. B-Fe-W. Isothermal section at 1050°C

DOI: 10.1007/978-3-540-69761-9_26

References

[1966Has1] Haschke, H., Nowotny, H., Benesovsky, F., "Investigations in the Systems (Mo, W)-(Fe, Co, Ni)-B" (in German), *Monatsh. Chem.*, **97**, 1459–1468 (1966) (Crys. Structure, Experimental, Phase Diagram, 6)

[1966Has2] Hasegawa, M., Okamoto, M., "A Study on the Ternary Alloys of Iron and Boron" (in Japanese), *Nippon Kinzoku Gakkai-Si*, **30**(6), 533–540 (1966) (Experimental, Mechan. Prop., Morphology, Phase Relations, 12)

[1966Rie] Rieger, W., Nowotny, H., Benesovsky, F., "The Crystal Structure of W_2CoB_2 and Isotypic Phases" (in German), *Monatsh. Chem.*, **97**(2), 378–382 (1966) (Crys. Structure, Experimental, 3)

[1968Jed] Jedlicka, H., Nowotny, H., Benesovsky, P., "The Crystal Structure of the High-Temperature Form of W_2FeB_2" (in German), *Monatsh. Chem.*, **99**, 1068–1069 (1968) (Crys. Structure, Experimental, 2)

[1968Jei] Jeitschko, W., "The Crystal Structure of MoCoB and Related Compounds", *Acta Crystallogr.*, **24B**, 930–934 (1968) (Experimental, Crys. Structure, 37)

[1968Kuz] Kuz'ma, Yu.B., Kripyakevich, P.I., Chepiga, M.V., "Crystal Structure of the Compounds MoCoB, WCoB, and WFeB", *J. Struct. Chem.*, **9**(2), 268–269 (1968), translated from *Zh. Strukt. Khim.*, **9**(2), 327–329 (1968) (Crys. Structure, Experimental, 6)

[1969Kuz] Kuzma, Yu.B., Chepiga, M.V., "X-Ray Investigation of the Tungsten-Iron-Boron and Tungsten-Cobalt-Boron Systems", *Inorg. Mater.*, **5**(1), 40–43 (1969), translated from *Izv. Akad. Nauk SSSR, Neorg. Mater.*, **5**(1), 49–53 (1969) (Crys. Structure, Experimental, 19)

[1973You] De Young, D.B., Barnes, R.G., "^{57}Fe Moessbauer Study of Some $M_2(M')B_2$ Borides", *J. Phys. Chem. Solids*, **34**, 139 (1973) (Crys. Structure, Electronic Structure, Experimental, 5)

[1978Her] Herold, U., Koester, U., "Metastable Phases in Extremly Fast Solidified Iron-Boron Alloys" (in German), *Z. Metallkd.*, **69**(5), 326–332 (1978) (Experimental, Phase Diagram, Crys. Structure, 27)

[1980Che] Chernienko, V.V., Martyukhin, I.D., "Effect of Niobium, Molybdenum, and Tungsten on Some Properties of Iron-Boride Materials", *Sov. Powder Metall. Met. Ceram.*, **19**(2), 135–138 (1980) (Experimental, 5)

[1982Kha] Khan, Y., Kneller, E., Sostarich, M., "The Phase Fe_3B", *Z. Metallkd.*, **73**(10), 624–626 (1982) (Experimental, Crys. Structure, Phase Diagram, 13)

[1983Ber] Bergmann, H.W., Brokmeier, U., Fritsch, H.U., "Experimental Investigation on the Thermal Stability of Metallic Glasses", *Ber. Bunsen-Ges. Phys. Chem.*, **87**, 757–761 (1983) (Experimental, 15)

[1984Kon] Konczos, G., Kisdi-Koszo, E., Lovas, A., Kajcsos, Z., Potocky, L., Daniel-Szabo, J., Kovac, J., Novak, L., "Correlation Between Magnetic Properties and Density of Fe-T-B (T = W, Cr) Glassy Alloys", *J. Magn. Magn. Mater.*, **41**(1–3), 122–124 (1984) (Experimental, Magn. Prop., 7)

[1985Nov] Novak, L., Potocky, L., Kisdi-Koszo, E., Lovas, A., Daniel-Szabo, J., "Curie Temperature of Fe-Cr-B and Fe-W-B Metallic Glasses", *Acta Phys. Slovaca*, **35**(4–5), 244–247 (1985) (Experimental, Magn. Prop., 5)

[1985Smi] Smid, I., Rogl, P., "Phase Equilibria and Structural Chemistry in Ternary Systems: Transition Metal - Boron - Nitrogen", *Proceedings of the 11th Intl. Plansee Seminar*, **Vol. 2**. Bildstein, H., Ortner, H. (Eds.), Verlag Tyrolia, Innsbruck, Austria, 1029–1035 (1985) (Experimental, Crys. Structure, Phase Diagram, 17)

[1986Che] Chen, Jin-Chang., Shen, Bao-Gen., Zhan, Wen-Shan., Zhao, Jian-Gao., "Effect of W Addition on Magnetic, Electric Properties and Thermal Stability of Amorphous Fe-B Alloys", *Acta Phys.,Sin.*, **35**(8) 979–88 (1986) (Experimental, Magn. Prop., Electr. Prop., 20)

[1986Nag] Nagender Naidu, S.V., Sriramamurthy, A.M., Rama Rao, P., "The System W-Fe", *J. Alloy Phase Diagrams*, **2**(3), 176–188 (1986) (Experimental, Crys. Structure, Phase Diagram, Review, 81)

DOI: 10.1007/978-3-540-69761-9_26

[1986Smi] Smid, I., Rogl, P., "Phase Equilibria and Structural Chemistry in Ternary Systems: Transition Metal - Boron - Nitrogen", *Inst. Phys. Conf. Ser. No. 75*, Ch. 4, Adam Hilger Ltd., 249–257 (1986) (Experimental, Crys. Structure, Phase Relations, 17)

[1987She] Shen, Bao Gen., Zhan, Wen Shan., Zhao, Jian Gao., Chen, Jinchang., Pan, Xiao Shuo, "Effect of Concentration and Transition Metals on Crystallization of Fe-based Amorphous Alloys", *Acta Metall. Sin.*, **23**(5), 220–226 (1987) (Experimental, 12)

[1987Gus] Gustafson, P., "A Thermodynamic Evaluation of the C-Fe-W System", *Metall. Trans*., **18A**, 175–188 (1987) (Experimental, Thermodyn., 28)

[1989Kol] Kolb-Telieps, A., Luft, U., "Relations Between Structure and First-Step Crystallization of Iron-Metal-Boron Glasses", *J. Non-Cryst. Solids*, **109**, 59–63 (1989) (Experimental, 7)

[1990Mih] Mihalik, M., Zentko, A., "Effect of Pressure on the Curie Temperature of Fe-Cr-B and Fe-W-B Amorphous Alloys", *Acta Phys. Slovaca*, **40**(4), 268–71 (1990) (Experimental, Magn. Prop., 8)

[1991Kha] Khan, Y., Wibbeke, H., "Formation of the τ-Phase in Fe-B Alloys", *Z. Metallkd.*, **82**(9), 703–705 (1991) (Experimental, Crys. Structure, 6)

[1991Sau] Saunders, N., Pan, L.M., Clay, K., Small, C., Miodownik, A.P., "Microstructure and Properties of a Rapidly Solidified Fe-Cr-Mo-Alloy", in "*User Aspects of Phase Diagrams*", Proc. Petten Conf., The Institut of Metals (1991) (Experimental, Thermodyn., 22)

[1992Kis] Kisdi-Koszo, E., Lovas, A., Kovac, J., Varga, L.K., Zsoldos, E., "Inhomogeneous Atomic Distribution and its Effect on Magnetic Properties of Diluted Fe-TM-B Metallic Glasses", *J. Magn. Magn. Mater*., **112**(1–3), 39–40 (1992) (Experimental, Magn. Prop., 4)

[1992Rag] Raghavan, V., "B-Fe-W (Boron-Iron-Tungsten)" in "*Phase Diagrams of Ternary Iron Alloys"*, Part 6, Ind. Inst. Metals, Calcutta, India, 444–448 (1992) (Experimental, Review, Phase Diagram, 16)

[1992Rog] Rogl, P., "The System B-N-Fe" in "*Phase Diagrams of Ternary Boron Nitride and Silicon Nitride Systems*", Rogl, P., Schuster, J.C. (Eds.), ASM, Materials Park, OH, p. 33–36 (1992) (Crys. Structure, Thermodyn., Phase Diagram, Experimental, Review, 9)

[1993Wer] Werheit, H., Kuhlmann, U., Laux, M., Lundstroem, T., "Structural and Electronic Properties of Carbon-Doped β-Rhombohedral Boron", *Phys. Stat. Sol.*, **B179**, 489–511 (1993) (Crys. Structure, Experimental, 51)

[1994Hal] Hallemans, B., Wollants, P., Roos, J.R., "Thermodynamic Reassessment and Calculation of the Fe-B Phase Diagram", *Z. Metallkd.*, **85**(10), 676–82 (1994) (Calculation, Phase Relations, Thermodyn., Phase Diagram, 21)

[1997Tak] Takagi, K., Yamasaki,-Y., Komai, M., "High-strength Boride Base Hard Materials", *J. Solid State Chem.*, **133**(1), 243–248 (1997) (Experimental, 4)

[1998Guo] Guo, Y.G., Zhang, Y.B.W., Wang, L.L., Ouyang, Y.F., Liao, S.Z., "Preparation and Thermal Properties of Amorphous B-Fe-W Alloy Nano-Powders", *J. Mater.Proc. Techn*., **74**(1–3), 10–13 (1998) (Experimental, 19)

[1998Rog] Rogl, P., "Tungsten-Boron-Carbon", in "*Phase Diagrams of Ternary Metal-Boron-Carbon Systems*", Effenberg, G., (Ed.), ASM-Intl, MSI, 372–427 (1998) (Review, Crys. Structure, Experimental, Phase Diagram, 32)

[1998Wan] Wang, L.L., Zhao, L.H., Zhang, B.W., OuYang, Y.F., Liao, S.Z., Hu, W.Y., "Composition Dependence of Some Physical Properties of Fe-TM-B (TM = Mo, W, Mo-W) Alloys Obtained by Electroless Plating", *Plating and Surface Finishing*, **85**(12), 96–98 (1998) (Experimental, 9)

[1999Wan] Wang, L.L., Zhao, L.H., Zhang, B.W., Hu, W.Y., Shu, X.L., Sheng, X., "Magnetic Properties of Fe-TM-B (TM = Sn, W, Mo-W) Alloys Prepared by Electroless Plating", *Z. Metallkd*., **90**(5), 338–341 (1999) (Experimental, Magn. Prop., 13)

[2000Lei] Leithe-Jasper, A., Klesnar, H., Rogl, P., Komai, M., Takagi, K.-I., "Reinvestigation of Isothermal Section in M (M = Mo, W)-Fe-B Ternary Systems at 1323 K" (in Japanese), *J. Jpn. Inst. Met.*, **64**(2), 154–162 (2000) (Crys. Structure, Experimental, Phase Relations, Phase Diagram, 30)

DOI: 10.1007/978-3-540-69761-9_26

[2000Pra] Prasad, S., Marinho, F.A., Silva, L.B., "A Comparative Study on Electrodeposition of Fe-W-B and Fe-Mo-B Alloys", *J. Indian Chem. Soc.*, **77**(6), 311–313 (2000) (Experimental, 22)

[2002Cen] Ceniga, L., Kovac, F., "Influence of Annealing Process on Magnetic Properties and Barkhausen Noise of the Fe-W-B Amorphous Alloy", *Czech. J. Phys*. **52**(Suppl A), A73-A76, (2002) (Experimental, Magn. Prop., 9)

[2002Nov] Novak, L., Ceniga, L., Kovac, F., "Influence of Hydrogenation-Dehydrogenation Process on Magnetic Properties and Barkhausen Noise of the Fe-W-B Amorphous Alloy", *Czech. J. Phys*., **52**(Suppl A), A77-A80, (2002) (Experimental, Magn. Prop., 6)

[2002Sul] Sulitanu, N., "Nanostructure Formation and Soft Magnetic Properties Evolution in $Fe_{91-x}W_xB_9$ Amorphous Alloys", *Mater. Sci. Eng. B-Solid State Mater. Adv. Technol*., **90** (1–2), 163–170 (2002) (Experimental, Magn. Prop., 32)

[2003Rag] Raghavan, V., "B-Fe-W (Boron-Iron-Tungsten)", *J. Phase Equilib.*, **24**(5), 457–458 (2003) (Assessment, Crys. Structure, Phase Diagram, Phase Relations, 7)

[V-C2] Villars, P. and Calvert, L.D., *Pearson's Handbook of Crystallographic Data for Intermetallic Phases*, 2nd edition, ASM, Metals Park, Ohio (1991)

[Mas2] Massalski, T.B. (Ed.), *Binary Alloy Phase Diagrams*, 2nd edition, ASM International, Metals Park, Ohio (1990)

DOI: 10.1007/978-3-540-69761-9_26

Barium – Iron – Oxygen

Jozefiende Keyzer, Pierre Perrot, Myriam Sacerdote, Andy Watson

Introduction

The first barium ferrite investigated was $BaFe_{12}O_{19}$ by [1938Ade] who recognized the similarity of its structure with that of the so-called β alumina ($Na_2O{\cdot}11Al_20_3$) and its isotypy with the mineral known as magnetoplumbite $PbFe_{12}O_{19}$. The structure of this compound was determined for the first time by [1967Tow] and is in good agreement with more recent studies of [1985Obr, 1992Shi].
The investigation of the Ba-Fe-O ternary system is concerned mainly with the study of $BaFe_{12}O_{19}$ and related compounds, which have magnetic properties of significant practical importance (Table 1). Barium oxide is also known to stabilize the higher oxidation states of iron, for instance in $BaFeO_3$ in which iron has the valence IV [1970Bel, 1971Zan].

Binary Systems

Ba and Fe have no mutual solubility in the solid or the liquid state [Mas2]. The Fe-O system accepted by [Mas2], mainly from the fundamental work of [1945Dar, 1946Dar] has been carefully assessed by [1991Sun]. The Ba-O system is accepted from the thermodynamic assessment of [1995Zim] reproduced by [1997Oka]. A continuous Ba-O liquid solution exists up to the ratio O/Ba = 2. The oxygen pressure above liquid BaO at the melting temperature of BaO (2013°C) is 0.322 Pa; the oxygen pressure at the invariant point BaO-BaO_2-liquid at 1077°C is 1.92 MPa. The thermodynamic assessment of the Ba-O system carried out by [1998Lys] agrees with that of [1995Zim]. The gaseous species above liquid BaO are mainly BaO and Ba_2O_2. The decomposition of BaO_2 has been investigated by [2001Jor] which gives a peritectic decomposition of BaO_2 under 0.1 MPa of oxygen pressure of 807°C.

Solid Phases

Crystallographic data for all unary phases and binary and ternary oxides are listed in Table 2. The mixed oxides of Ba and Fe lie mainly on the BaO-Fe_2O_3 join. All these phases are easily synthesized by solid-state reaction between Fe_2O_3 and a barium salt such as $BaCO_3$ or $BaNO_3$. The compound $BaFe_{12}O_{19}$ whose structure is the "magnetoplumbite" type is easily reduced and gives the mixed compounds $BaFe_{15}O_{23}$ (or $BaFe_{12}O_{19}{\cdot}Fe_3O_4$) and $BaFe_{18}O_{27}$ (or $BaFe_{12}O_{19}{\cdot}2Fe_3O_4$) in which a proportion of the iron has the valence state II [1975Man, 1976Bat]. Nanoparticles of $BaFe_{12}O_{19}$ were prepared by [1995Cho], who confirmed the parameters. The compound $BaFe_7O_{11}$ (or $BaFe_4O_7{\cdot}Fe_3O_4$) whose existence has been proposed by [1975And] has not been confirmed. In these compounds, clusters of $BaFe_{12}O_{19}$ alternate with clusters of Fe_3O_4. The compounds richest in BaO are harder to reduce when the BaO content increases but on the other hand, they are easier to oxidize. The compound $BaFeO_{2.5}$ (or $Ba_2Fe_2O_5$), in which the iron has a valency of III may be oxidized up to the composition $BaFeO_3$ in which all of the iron is in the valence state of IV.
It seems probable that there is not a continuous solid solution at low temperatures between $BaFeO_{2.5}$ and $BaFeO_3$ because $BaFeO_{2.5}$ has a structure of the brownmillerite type whereas $BaFeO_3$ has a structure of the perovskite type. Another problem comes from the fact than x in $BaFeO_{3-x}$ is also strongly dependent on the oxygen pressure imposed on the system and this parameter is never taken into account by crystallographers. The structure of $BaFeO_{3-x}$ is dependent on x with much disagreement amongst different authors. On the other hand, [2004Del] showed that the observed structure is also a function of the synthesis conditions. It is probable that some structures are metastable. [1964Hoo] gives two different phases between $BaFeO_{2.47}$ and $BaFeO_{2.92}$; [1965McC] proposes an orthorhombic structure for $BaFeO_{2.5}$ and a hexagonal structure for $BaFeO_{2.82-2.95}$; [1966Mor] detects seven phases between $BaFeO_{2.5}$ and $BaFeO_{2.92}$, namely, two triclinic, two rhombohedral, one cubic, one tetragonal and one hexagonal. [1970Bel] found hexagonal, cubic, rhombohedral and monoclinic phases! The first structures proposed for $Ba_2Fe_2O_5$ [1965McC, 1971Zan, 1973Luc] were orthorhombic of the brownmillerite ($Ca_2Fe_2O_5$) type. Actually

DOI: 10.1007/978-3-540-69761-9_27

[1990Par], the structure is more complex due to ordering of oxygen vacancies. Electron diffraction shows this phase to be monoclinic [1993Par]. The same author showed by using high temperature X-ray diffraction, that, above 880-900°C, $Ba_2Fe_2O_5$ undergoes a magnetic transition and becomes cubic with the perovskite type. This structure has already been observed by [1946Erc, 1961Der] for the $BaFeO_{2.625}$ compound. The accepted structures are given in Table 2.
The solid solution between $Ba_3Fe_2O_6$ and $Ba_7Fe_4O_{13}$ has been confirmed by [1990Shi]. Compounds in which a portion of the iron or the whole of the iron has an oxidation state of IV are observed when the Ba/Fe ratio in the compound is higher than 1. For instance, the orthorhombic phase $Ba_{10}Fe_2O_{13}$ containing only Fe(III) may be oxidized in $Ba_{10}Fe_2O_{14}$ containing only Fe(IV) [1979Mon]. The first structure of the compound Ba_3FeO_5 determined by [1965Man] using powdered material was not confirmed by the more recent determination of [2002Del]. The compound $Ba_3Fe_2O_6$ is stable under an air atmosphere at temperatures higher than 800°C. Below 800°C, compounds containing Fe(IV) are obtained [1972Mon]. $BaFe_2O_4$ undergoes polymorphic transitions [1972Mer, 2003Mue]. The structure of the $\beta BaFe_2O_4$ and $\gamma BaFe_2O_4$ phases should be considered as an orthorhombic deformation of the hexagonal structure. [1972Mer] proposes the existence of a $\beta' BaFe_2O_4$ metastable phase obtained by quenching the β phase to room temperature; however, the crystal structure parameters of β' are close to those of β, so that, the existence of β' seems doubtful. The compound $BaFeO_4$ in which the whole Fe is in a state of oxidation VI has been prepared [1973Ich] by ion exchange between K_2FeO_4 and Ba acetate in an aqueous solution of KOH below 0°C to avoid the reduction of ferrates VI ions. By heating under oxygen pressure up to 150 MPa and 1200°C, $BaFeO_4$ looses its oxygen to give a triclinic form of $BaFeO_3$ above 950°C, an hexagonal form between 750 and 900°C and a tetragonal form below 520°C. The transition between these phases seems irreversible and these phases are not observed by heating $BaFeO_{2.5}$ under oxygen pressure.

Quasibinary Systems

Figure 1 shows the $BaO\text{-}Fe_2O_3$ quasibinary section for temperatures between 800 and 1200°C taken from [1981Pou].

Isothermal Sections

Figure 2 shows the isothermal section for the Ba-Fe-O system for temperatures between 700 and 1000°C and ambient partial pressures of oxygen taken from [1994Li2]. As Ba is liquid at these temperatures it was necessary to add a tentative liquid phase boundary based on the Ba-O and Ba-Fe binary systems. This figure had also been modified to take into account the existence of high oxygen compounds (BaO_2, $BaFeO_3$), stable under 0.1 MPa of oxygen pressure.

Thermodynamics

Three different studies have been carried out to determine the Gibbs energies of formation for some of the most stable compounds in the $BaO\text{-}Fe_2O_3$ system. [1976Deo] performed emf measurements using barium fluoride as solid electrolyte and determined the Gibbs energy of formation for $BaFe_{12}O_{19}$, $BaFe_2O_4$, $Ba_2Fe_2O_5$ from the oxides as well as the Gibbs free energy for the reaction $1/2\ Ba_2Fe_2O_5 \rightarrow BaFe_2O_{5+x}$ (Table 3). By measuring the carbon dioxide pressure in equilibrium with $BaCO_3$ and ferrites, [1981Pou] calculated the energies of formation from the oxides for $BaFe_{12}O_{19}$, $BaFe_2O_4$, $Ba_2Fe_2O_5$, $Ba_3Fe_2O_6$ and $Ba_5Fe_2O_8$. Most recently, [2004Rak] measured Gibbs energies of formation for the same five compounds by emf measurement using CaF_2 as electrolyte. Although the latter author gives the most complete elaboration, it should be noted that agreement with [1976Deo] is stated wrongly in the text of the article and values from this reference as well as from [1981Pou] and [1994Li2] are quoted incorrectly. Disagreement between the different measurements for the formation energies is significant, particularly for the $BaFe_{12}O_{19}$ compound. At the moment it is not clear which value is more accurate and therefore the values of the different studies are given in Table 3. Calculation of the enthalpy of formation of $BaFeO_3$ was carried out by [1990Rez], and of $BaFe_{12}O_{19}$, $Ba_3Fe_2O_6$ and $Ba_7Fe_4O_{13}$ by [1992Rez]. These data are also listed in Table 3. [2004Rak] also measured the emf of a solid oxide galvanic cell in order to obtain the oxygen potential difference over the three-phase mixture $BaFe_{12}O_{19} + BaFe_2O_4 + Fe_3O_4$ (Table 3). Based on their

DOI: 10.1007/978-3-540-69761-9_27

measurements and the formation energies for the binary compounds, they computed an oxygen potential diagram for 827°C (Fig. 3). A fourth thermodynamic study was carried out by [1994Li1, 1994Li2] who determined the Gibbs energy for the reaction $BaFe_{12}O_{19} \rightleftharpoons BaFe_2O_4 + 10/3\ Fe_3O_4 + 5/6\ O_2$ and the oxygen pressure over the three-phase equilibrium $BaFe_{12}O_{19} + BaFe_2O_4 + Fe_3O_4$ using oxygen coulometry (Table 4). It can be seen that also these data do not agree with data from the other references. [1984Iwa] measured the activities of Fe_xO in $BaO + Fe_xO$ slags at 1400°C (Fig. 4). Interaction parameters (e^{Ba}_O) between Ba and oxygen in liquid iron determined by [1992Kat] and [1993Wan] to be equal to −52 at 1600°C, −50 at 1650°C and −48 at 1600°C according to the first author and −46 at 1600°C according to the latter. This last value lies within the experimental scatter of the value obtained by the first author.

Notes on Materials Properties and Applications

$BaFe_{12}O_{19}$ is one of the most widely used materials for permanent magnet applications with more than 70,000 metric tons being produced annually [1997Par, 1993Alc]. It is also used in recording media where it is necessary to withstand high demagnetizing forces [1999Cro]. The material has high coercivity, high saturation magnetization, excellent stability and resistance to corrosion. Most importantly, it is very cheap to produce. Coercivity values of between 1-5 kOe can be achieved, depending in the method of manufacture. Investigation of materials properties are listed in Table 5.

Miscellaneous

The standard preparation method is to mix the component oxides or carbonates and fire at temperatures higher than 1200°C for between 6 and 24 h [1997Par]. The process can be carried out in a number of steps (~12).

Alternative production routes can result in a change in properties. Self-propagation high-temperature synthesis (SHS) has been employed to improve production and properties [1997Par, 2001Par2, 2002Mar]. A mixture of Fe_2O_3, Fe and BaO_2 (internal oxidizing reagent) or $BaCO_3$ is ignited by a hot nichrome wire at around 800°C, either under pure oxygen or air [2002Mar]. The reaction occurs by the propagation of a reaction front throughout the mixture, moving at approximately 2 $mm \cdot s^{-1}$ [2001Par1, 2001Par2] resulting in very high temperatures; typically in the region of 1200°C. The result is a multiphase product; when the SHS is carried out a mixture of Fe_2O_3, Fe, $BaFe_2O_4$, Fe_3O_4 and FeO is produced. The mixture is then sintered at around 1150°C for 6 h giving a material with comparable properties of the commercial product. Further research into SHS production of the material has involved applying a magnetic field to the mixture as the reaction proceeds [2000Agu, 2001Par2]. It was found that on increasing the field the velocity of the propagation wave increased accompanied by a change in the magnetic properties. An applied field of 1.1 T resulted in the alignment of the presyntered grains increasing the interfacial contact resulting in a increased reaction rate from 2 - 5 $mm \cdot s^{-1}$ [1997Par] and a 20% reduction in the coercivity [2000Agu]. The SHS product was a two-phase material; a shiny fibrous fused solid with large grains with a low H_c and high σ_{max}, and a red-black matt solid with low H_c and low σ_{max}. The latter phases are the relatively low magnetization phases; Fe_2O_3 and $Fe_{1-x}O$.

High-energy ball milling has been used to produce small particles, < 1μm - smaller than a single domain size, in order to increase coercivity. [1995Bar] milled commercial hexaferrite in air to produce material with a smaller particle size. Short milling times were accompanied by a rapid reduction in magnetization owing to the formation of a paramagnetic phase. Earlier, [1994Kac] found that annealing following a milling treatment could also have an effect on properties. Milling (1000 h) followed by annealing in air at 1000°C raised the H_c from 74.4 $kA \cdot m^{-1}$ to 445.6 $kA \cdot m^{-1}$. Particle sizes in the region of 3 μm were produced.

[2001Men] investigated the effect of varying the Fe/Ba ratio in the starting material. The maximum M_s was achieved with Fe/Ba = 12, but increasing to 15 gave a higher value of H_c. They also found that milling time was important with a time of 40 h giving the best results.

[1998Gol] studied the effect of particle size on macroscopic magnetic properties. A critical particle volume exists, which is determined as when the energy of magnetic anisotropy is equal to the thermal energy. At this point, the magnetic moment of the particle ceases to be along the direction of easy magnetization and fluctuates in space. This is the superparamagnetic state. The magnetic field ($H \leq 17$ kOe) and temperature dependence (300K – T_c) of the magnetization was studied using single domain particles with a size between 20 and 140 nm.

DOI: 10.1007/978-3-540-69761-9_27

Other methods have been employed to produce nanometer sized particles. [2000Gon] produced particles of $BaFe_{12}O_{19}$ with a size of 10 nm in diameter by pyrolysis of an aerosol produced by ultrasonic frequency spraying of a barium iron citrate solution in a tube furnace at 1000°C. The hexaferrite phase was found to form at lower temeratures than other methods as a consequence of the nature of the precursor aerosol solution. The particle size could be increased by further heat treatment of the particles.
Growth of single crystal ferrites was studied by [1966Vos].

Table 1. Investigations of the Ba-Fe-O Phase Relations, Structures and Thermodynamics

Reference	Method/Experimental Technique	Temperature/Composition/Phase Range
[1938Ade]	X-ray powder diffraction	$BaFe_{12}O_{19}$
[1946Erc]	Solid phase reactions, X-ray diffraction	Fe_2O_3-$Ba_2Fe_2O_5$-$Ba_8Fe_8O_{21}$, 500-1100°C, 0.1 MPa of oxygen pressure
[1954Bra, 1957Bra]	Solid phase reactions, X-ray diffraction	$BaFe_{12}O_{19}$ - Fe_3O_4
[1960Bat]	Phase diagram investigation by X-ray, thermographic and micrographic methods	BaO-Fe_2O_3, 1300-1550°C
[1960Got]	Phase diagram investigation by X-ray, thermographic and micrographic methods	$Ba_2Fe_2O_5$-Fe_2O_3, 800-1500°C
[1961Oka]	Magnetic susceptibility measurements	$BaFe_2O_4$
[1962Zio]	Phase diagram investigation by X-ray, thermographic and spectroscopic methods	$BaFe_{12}O_{19}$-$BaFe_2O_4$, 900-1500°C
[1964Hoo]	Phase equilibrium under controlled oxygen pressure	Fe_2O_3-$Ba_2Fe_2O_5$-Fe_3O_4, 1300-1550°C, 1 kPa to 10 MPa of oxygen pressure
[1965McC]	X-ray powder diffraction	$BaFeO_{2.5}$-$BaFeO_{2.95}$, 325-915°C
[1965Man]	X-ray powder diffraction	Ba_3FeO_5
[1965Mor, 1966Mor]	Solid-state reactions, X-ray powder diffraction	$BaFeO_{2.5}$-$BaFeO_3$, 300-1100°C
[1967Tow]	X-ray single crystal diffraction	$BaFe_{12}O_{19}$
[1968Ber]	Solid-state reactions, X-ray analysis	Fe_2O_3-$Ba_2Fe_2O_5$, 250-1000°C
[1970Bel]	X-ray powder diffraction	$BaFeO_{2.5}$-$BaFeO_3$, 1100-1250°C under air
[1971Mit]	X-ray single crystal diffraction	$BaFe_2O_4$, 1300-1470°C under oxygen
[1971Zan]	X-ray powder diffraction, infra-red and Mössbauer spectrometry	$BaFeO_{2.5}$-$BaFeO_{2.93}$, 700-1000°C
[1972Mer]	X-ray powder diffraction	$BaFe_2O_4$, 25-1100°C
[1972Mon]	X-ray powder diffraction	$Ba_3Fe_2O_6$, 1000-1200°C under air
[1973Ich]	Mössbauer investigation	$BaFeO_4$, $T < 1200$°C, $P < 150$ MPa
[1973Luc]	X-ray powder diffraction	$BaFeO_{2.5}$-$BaFeO_3$, 950-1300 under air

(*continued*)

DOI: 10.1007/978-3-540-69761-9_27

Reference	Method/Experimental Technique	Temperature/Composition/Phase Range
[1973Oka, 1975Oka]	X-ray powder diffraction	$BaFe_4O_7$, hydrothermal synthesis, 200-300°C
[1973Slo]	Solid-state reactions, X-ray powder diffraction	$BaFe_{12}O_{19}$-$BaFe_2O_4$, 800-1200°C
[1974Ale]	Calculation	Heats of formation of $BaFe_2O_4$ from component oxides.
[1975Man]	Solid-state reactions, X-ray powder diffraction	$Ba_2Fe_2O_5$-$BaFeO_3$-BaO, 800-1150°C
[1979Boi]	X-ray single crystal diffraction	$Ba_2Fe_6O_{11}$, 1200°C under air atmosphere
[1979Mon]	Solid-state reactions, X-ray powder diffraction	$Ba_4Fe_2O_7$-$Ba_4Fe_2O_{7.32}$, $Ba_5Fe_2O_8$-$Ba_5Fe_2O_{8.2}$, $Ba_{10}Fe_2O_{13}$-$Ba_{10}Fe_2O_{14}$, 800-1100°C
[1979Pou]	X-ray powder diffraction, infra-red spectroscopy	$Ba_2Fe_6O_{11}$, 850-1200°C under air atmosphere
[1979Vul]	Microscopic and X-ray examination	$BaFe_2O_4$-$Ba_7Fe_4O_{13}$, 1300-1400°C
[1981Neu]	Progressive reduction under H_2-H_2O atmospheres and X-ray analysis	$Ba_2Fe_2O_5$-$Ba_7Fe_4O_{13}$-Fe, 1000°C
[1981Pou]	Solid-state reactions, measurements of CO_2 pressure at equilibrium	BaO-Fe_2O_3 800-1200°C, Gibbs energy of formation measured at 1000°C
[1985Igu]	Behavior of defects in wustite under Co-CO_2 atmospheres	FeO-BaO, 1000-1200°C
[1985Obr]	X-ray single crystal diffraction	$BaFe_{12}O_{19}$
[1986Sha]	X-ray powder diffraction, infra-red spectroscopy	$BaFeO_{2.5}$-$BaFeO_3$, 1100°C under air, then 700°C, 10 MPa
[1987Par]	X-ray powder diffraction, transmission electron microscopy	$Ba_2Fe_2O_5$, 1100°C, under 0.1 MPa nitrogen
[1990Che]	Mössbauer spectrometry	$BaFe_{12}O_{19}$, 12 to 723 K
[1990Par]	X-ray single crystal diffraction, transmission electron microscopy, Mössbauer spectrometry	$Ba_2Fe_2O_5$, 1100°C
[1990Shi]	X-ray powder diffraction, Mössbauer	BaO-Fe_2O_3, 800-1250°C
[1990Rez] [1992Rez]	Calculation	Enthalpies of formation of $BaFeO_3$, $BaFe_{12}O_{19}$, $Ba_3Fe_2O_6$ and $Ba_7Fe_4O_{13}$
[1993Par]	High temperature X-ray powder diffraction, transmission electron microscopy	$BaFeO_{2.5}$-$BaFeO_{2.93}$, 25-1100°C
[1994Li2]	Gibbs energy of formation, solid-state electrochemical cell	$BaFe_{12}O_{19}$, $BaFe_2O_4$, 700-1000°C
[1995Cho]	X-ray structure by Rietveld refinement, magnetic coercivity	$BaFe_{12}O_{19}$

(*continued*)

DOI: 10.1007/978-3-540-69761-9_27

Reference	Method/Experimental Technique	Temperature/Composition/Phase Range
[2001Gom]	X-ray structure by Rietveld refinement, high resolution synchrotron	$BaFeO_{2.5}$-$BaFeO_{2.8}$, 850°C under oxygen
[2002Del]	X-ray single crystal diffraction, magnetic measurements, Mössbauer spectrometry	Ba_2FeO_4, Ba_3FeO_5, 750°C under air atmosphere
[2003Gao]	Mössbauer spectroscopy	$BaFe_{12}O_{19}$
[2004Del]	X-ray single crystal diffraction,	$BaFeO_{2.8}$

Table 2. Crystallographic Data of Solid Phases

Phase/ Temperature Range [°C]	Pearson Symbol/ Space Group/ Prototype	Lattice Parameters [pm]	Comments/References
(Ba) < 727	*cI*2 $Im\bar{3}m$ W	a = 502.27	at 25°C [Mas2]
(δFe)(h_2) 1538 - 1394	*cI*2 $Im\bar{3}m$ W	a = 293.15	pure Fe at 1480°C [Mas2]
(γFe)(h_1) 1394 - 912	*cF*4 $Fm\bar{3}m$ Cu	a = 364.67	pure Fe at 915°C [Mas2]
(αFe)(r) ≤ 912	*cI*2 $Im\bar{3}m$ W	a = 286.65	pure Fe at 25°C [Mas2]
BaO_{1+x} < 2013	*cF*8 $Fm\bar{3}m$ NaCl	 a = 553.9 a = 559.0	$0 < x < 0.076$ [1997Oka] at 25°C [V-C2] at 852°C [2001Jor]
BaO_{2-x} < 1077	*tI*6 *I4/mmm* CaC_2	a = 380.83 c = 672.39	$0 < x < 0.53$ [1995Zim, 2001Jor] decomposes at 807°C under 0.1 MPa of oxygen pressure
$Fe_{1-x}O$ (Wustite) 1422 - 569	*cF*8 $Fm\bar{3}m$ NaCl	 a = 431.0 a = 429.3	$0.05\ x < 0.12$ [1991Sun] x = 0.05 x = 0.12
Fe_3O_4 (r) < 580	*oP*56 *Pbcm* Fe_3O_4 (r)	a = 1186.8 b = 1185.1 c = 1675.2	[V-C2]
Fe_3O_4 (h) (Magnetite) 1597 - 580	*cF*56 $Fd\bar{3}m$ $MgAl_2O_4$	a = 839.6 a = 854.5	at 25°C at 1000°C [V-C2]

(*continued*)

DOI: 10.1007/978-3-540-69761-9_27

Phase/ Temperature Range [°C]	Pearson Symbol/ Space Group/ Prototype	Lattice Parameters [pm]	Comments/References
αFe_2O_3 (Hematite) < 1451	*hR*30 $R\bar{3}c$ Al_2O_3	*a* = 503.42 *c* = 1374.83	at 600°C [Mas2, V-C2]
βFe_2O_3	*cI*80 $Ia\bar{3}$ Mn_2O_3	*a* = 939.3	metastable phase [V-C2]
γFe_2O_3 (Maghemite)	*cF*56 $Fd\bar{3}m$ $MgAl_2O_4$	*a* = 834	metastable phase [1989Rag]
* $BaFe_{12}O_{19}$ < 1600	*hP*64 $P6_3/mmc$ $PbFe_{12}O_{19}$ (magnetoplumbite)	*a* = 589.20 ± 0.01 *c* = 2318.3 ± 0.1 *a* = 589.28 ± 0.03 *c* = 2320.1 ± 0.3	[1985Obr] [1992Shi]
* $BaFe_{15}O_{23}$	*hR*234 $R\bar{3}m$	*a* = 588.0 *c* = 8411	[1954Bra] Structure related to $BaFe_{12}O_{19}$
* $BaFe_{18}O_{27}$	*hP*92 $P6_3/mmc$	*a* = 588.0 *c* = 3284.5	[1954Bra] Structure related to $BaFe_{12}O_{19}$
* $BaFe_4O_7$	*hP*24 $P6_3/m$ $BaFe_4O_7$	*a* = 516.0 ± 0.3 *c* = 1381.1 ± 0.9	[1973Oka, 1975Oka]
* $Ba_2Fe_6O_{11}$	*oP*76 *Pnmn* $Ba_2Fe_6O_{11}$	*a* = 2302.4 ± 1.0 *b* = 518.1 ± 0.3 *c* = 890.0 ± 0.4	[1979Boi, 1979Pou]
* $\gamma BaFe_2O_4$ (r) < 800	*oB*56 $Bb2_1m$ $\gamma BaFe_2O_4$	*a* = 538.7 ± 0.2 *b* = 1905.6 ± 0.6 *c* = 845.8 ± 0.3	[1971Mit, 1972Mer] Cannot be compared with $BaAl_2O_4$
* $\beta BaFe_2O_4$ (h_1) 800 - 1000	*o**28	*a* = 546.3 ± 0.3 *b* = 946.1 ± 0.5 *c* = 871.0 ± 0.5	[1961Oka, 1972Mer]
* $\alpha BaFe_2O_4$ (h_2) 1450 - 1000	*hP*14 $P6_3/mmc$ $BaAl_2O_4$	*a* = 545.8 ± 0.1 *c* = 901.6 ± 0.2	[1972Mer]
* $Ba_2Fe_2O_5$ (r) < 900	*mP** $P2_1/c$ $Ba_2Fe_2O_5$	*a* = 2343.1 ± 0.5 *b* = 1172.4 ± 0.1 *c* = 696.9 ± 0.1 β = 98.74 ± 0.01°	[1987Par, 1990Par], supercell of a cubic perowskite cell
* $BaFeO_{3-x}$ (r)	*hP*24 $P6_3/mmc$	 *a* = 568.3 ± 0.2 *c* = 1391.6 ± 0.5	$0.35 \geq x \geq 0.07$ *x* = 0.33 [1973Luc]

(*continued*)

DOI: 10.1007/978-3-540-69761-9_27

Phase/ Temperature Range [°C]	Pearson Symbol/ Space Group/ Prototype	Lattice Parameters [pm]	Comments/References
		a = 568.6 c = 1392.2	x = 0.22 [1986Sha]
		a = 566.8 ± 0.5 c = 1389 ± 1	x = 0.075 [1971Zan]
* $BaFeO_{3-x}$ (h)	*cP*5 $Pm\bar{3}m$ $CaTiO_3$ (perovskite)	a = 0.41	0.5 ≥ x ≥ 0.07 > 900°C for $BaFeO_{2.5}$ [1993Par]
* $Ba_3Fe_2O_6$	*cP*264	a = 1674.4	[1972Mon, 1975Man]
$Ba_7Fe_4O_{13}$		a = 1677	[1981Neu]
* Ba_2FeO_4	*mP*28 $P2_1/n$ Ba_2FeO_4	a = 603.4 ± 0.2 b = 764.7 ± 0.2 c = 1016.2 ± 0.3 β = 92.931 ± 0.006	[2002Del]
* $Ba_5Fe_2O_8$	*c***	a = 1497.5	[1975Man, 1990Shi]
* Ba_3FeO_5	*oP*36 *Pnma* Ba_3FeO_5	a = 1030.1 ± 0.1 b = 815.1 ± 0.1 c = 761.1 ± 0.1	[2002Del]

Table 3. Thermodynamic Data of Reaction or Transformation

Reaction or Transformation	T [°C]	Quantity, per mol of atoms [kJ, mol, K]	Comments
Ba + 12 Fe + 19/2 O_2 ⇌ $BaFe_{12}O_{19}$	697 - 878	$\Delta_f G°$ = –5431.3 +1.5317 T (± 0.6)	[2004Rak] derived from emf measurements
BaO + 6 Fe_2O_3 ⇌ $BaFe_{12}O_{19}$	587 - 741	$\Delta_f G°$ = –70.040 – 0.0311 T (± 0.800)	[1981Pou] derived from carbon dioxide pressure measurements
	690 - 850	$\Delta_f G°$ = –89.244 +0.01139 T (± 0.250)	[1976Deo] derived from emf measurements
	25	$\Delta_f H°$ = –56	[1992Rez] calculated
$BaFe_{12}O_{19}$ ⇌ $BaFe_2O_4$ + 10/3 Fe_3O_4 + 5/6 O_2?	700 - 1000	ΔG = 723 – 0.480 T	[1994Li2] derived from oxygen coulometric titration
$BaFe_{12}O_{19}$ ⇌ $BaFe_2O_4$ + 10/3 Fe_3O_4 + 5/6 O_2	775 - 948	$\Delta\mu(O_2)$ = 355.33 – 0.18225 T	[2004Rak] derived from emf measurements
Ba + 2 Fe + 2 O_2 ⇌ $BaFe_2O_4$	697 - 878	$\Delta_f G°$ = –1461.4 +0.3745 T (± 1.3)	[2004Rak] derived from emf measurements

(*continued*)

DOI: 10.1007/978-3-540-69761-9_27

Reaction or Transformation	T [°C]	Quantity, per mol of atoms [kJ, mol, K]	Comments
$BaO + Fe_2O_3 \rightleftharpoons BaFe_2O_4$	652 - 823	$\Delta_f G° = -93.800 + 0.0027\ T\ (\pm 0.500)$	[1981Pou] derived from carbon dioxide pressure measurements
	752 - 1017	$\Delta_f G° = -87.948 + 0.01621\ T\ (\pm 0.435)$	[1976Deo] derived from emf measurements
$2\ Ba + 2\ Fe + 5\ O_2 \rightleftharpoons Ba_2Fe_2O_5$	697 - 876	$\Delta_f G° = -2038.3 + 0.4433\ T\ (\pm 1.4)$	[2004Rak] derived from emf measurements
$2\ BaO + Fe_2O_3 \rightleftharpoons Ba_2Fe_2O_5$	957 - 1077	$\Delta_f G° = -169.220 + 0.0234\ T\ (\pm 0.310)$	[1981Pou] derived from carbon dioxide pressure measurements
	927 - 1027	$\Delta_f G° = -168.465 + 0.0127\ T\ (\pm 2.275)$	[1976Deo] derived from emf measurements
$1/2\ Ba_2Fe_2O_5 \rightleftharpoons Ba_2Fe_2O_5 + \xi$	777 - 927	$\Delta G = -58.116 + 0.04816\ T\ (\pm 1.110)$	[1976Deo], derived from emf measurements
$3\ Ba + 2\ Fe + 3\ O_2 \rightleftharpoons ?Ba_3Fe_2O_6$	696 - 877	$\Delta_f G° = -2700.1 + 0.6090\ T\ (\pm 1.5)$	[2004Rak] derived from emf measurements
$3\ BaO + Fe_2O_3 \rightleftharpoons Ba_3Fe_2O_6$	927 - 1077	$\Delta_f G° = -307.000 - 0.1022\ T\ (\pm 0.680)$	[1981Pou] derived from carbon dioxide pressure measurements
	25	$\Delta_f H° = -176$	[1992Rez] calculated
$5\ Ba + 2\ Fe + 3\ O_2 \rightleftharpoons ? Ba_5Fe_2O_8$	700 - 877	$\Delta_f G° = -3984.1 + 0.9300\ T\ (\pm 1.6)$	[2004Rak] derived from emf measurements
$5\ BaO + Fe_2O_3 \rightleftharpoons Ba_5Fe_2O_8$	823 - 1095	$\Delta_f G° = -465.260 - 0.1848\ T\ (\pm 0.900)$	[1981Pou] derived from carbon dioxide pressure measurements
$5\ BaO + Fe_2O_3 \rightleftharpoons Ba_7Fe_4O_{13}$	25	$\Delta_f H° = -410$	[1992Rez] calculated
$BaO + FeO_2 \rightleftharpoons BaFeO_3$	25	$\Delta_f H° = -1087$	[1990Rez] calculated based on the change in the coordination number of Ba and Fe. Note, FeO_2 is a hypothetical compound having the rutile structure

Table 4. Vapor Pressure Measurements

Phase(s)	Temperature [°C]	Pressure [bar]	Comments
$BaFe_{12}O_{19} + BaFe_2O_4 + Fe_3O_4$	700 - 1000	$\ln(p_{O2}) = 69.37 - 1.04 \cdot 10^5 \cdot T^{-1}$	[1994Li2], derived from oxygen coulometric titration

DOI: 10.1007/978-3-540-69761-9_27

Table 5. Investigations of the Ba-Fe-O Materials Properties

Reference	Method/Experimental Technique	Type of Property
[1953Gal]	Calculation of molecular magnetic moments	Magnetic properties
[1961Oka]	Autorecording magnetic balance	Measurement of susceptibility with respect to temperature for $BaO{\cdot}Fe_2O_3$
[1965McC]	Pendulum magnetometry	Variation in magnetization with respect to oxygen stoichiometry and temperature $BaFeO_{2.83}$-$BaFeO_{2.95}$
[1975Oka]	Mössbauer spectroscopy	Magnetic properties and antiferromagnetic ordering of $BaO{\cdot}2Fe_2O_3$.
[1990Che], [2003Gao]	Mössbauer spectroscopy	$BaFe_{12}O_{19}$
[1994Kac]	Vibrating sample magnetometry	Thermally activated transformation of nanostructured $BaFe_{12}O_{19}$.
[1995Bar]	Mössbauer, thermomagnetic measurement by vibrating sample magnetometer	Effect of grinding on the magnetization of $BaFe_{12}O_{19}$ samples.
[1997Par]	Vibrating sample magnetometry	Magnetization of $BaFe_{12}O_{19}$ produced by SHS reaction.
[1998Gol], [2000Li]	Mössbauer spectroscopy	Magnetic properties of $BaFe_{12}O_{19}$ nanoparticles
[1998Kre]	Raman spectroscopy	Electronic structure
[1999Cro]	Vibrating sample magnetometry	Magnetic properties of $BaFe_2O_4$ prepared by SHS reaction.
[2000Agu]	Bulk magnetometry	Magnetic properties of $BaFe_{12}O_{19}$ of material produced by SHS in large magnetic fields
[2000Aff], [2001Par2]	Vibrating sample magnetometry	Magnetic properties of $BaFe_{12}O_{19}$ of material produced by SHS.
[2001Jan]	Vibrating sample magnetometry	Magnetic properties of $BaFe_{12}O_{19}$ produced by microwave processing.
[2001Mar], [2005Mal]	Vibrating sample magnetometry	Magnetic properties of material produced via sol-gel.
[2001Men]	Vibrating sample magnetometry	Magnetic properties as a function of milling an heat treatment.
[2002Del]	SQUID magnetometry	Magnetic properties of $BaFe_2O_4$ and Ba_3FeO_5.
[2002Teh]	SQUID magnetometry	Magnetic properties of Co-doped $BaFe_{12}O_{19}$.
[2003Fu]	Vibrating sample magnetometry	Magnetic properties of ferrites produced via microwave combustion

(*continued*)

DOI: 10.1007/978-3-540-69761-9_27

Reference	Method/Experimental Technique	Type of Property
[2004Lic]	Inductively coupled plasma and Fourier transform infra-red spectroscopy	Electrical properties
[2005Dho]	SQUID magnetometry	Effects of grain boundaries on magnetic properties of $BaFe_{12}O_{19}$.
[2005Sin]	Vibrating sample magnetometry	Effects of dopant on magnetic properties of $BaM_{11}O_{19}$ produced by an aerosol route.

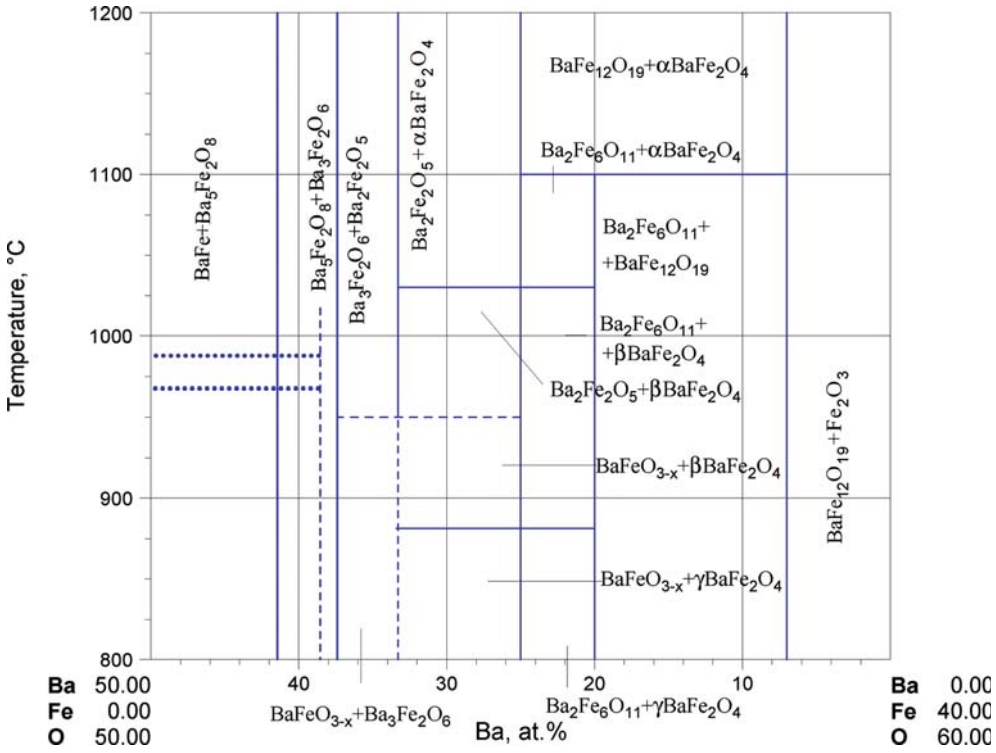

Fig. 1. Ba-Fe-O. BaO-Fe_2O_3 quasibinary section

DOI: 10.1007/978-3-540-69761-9_27

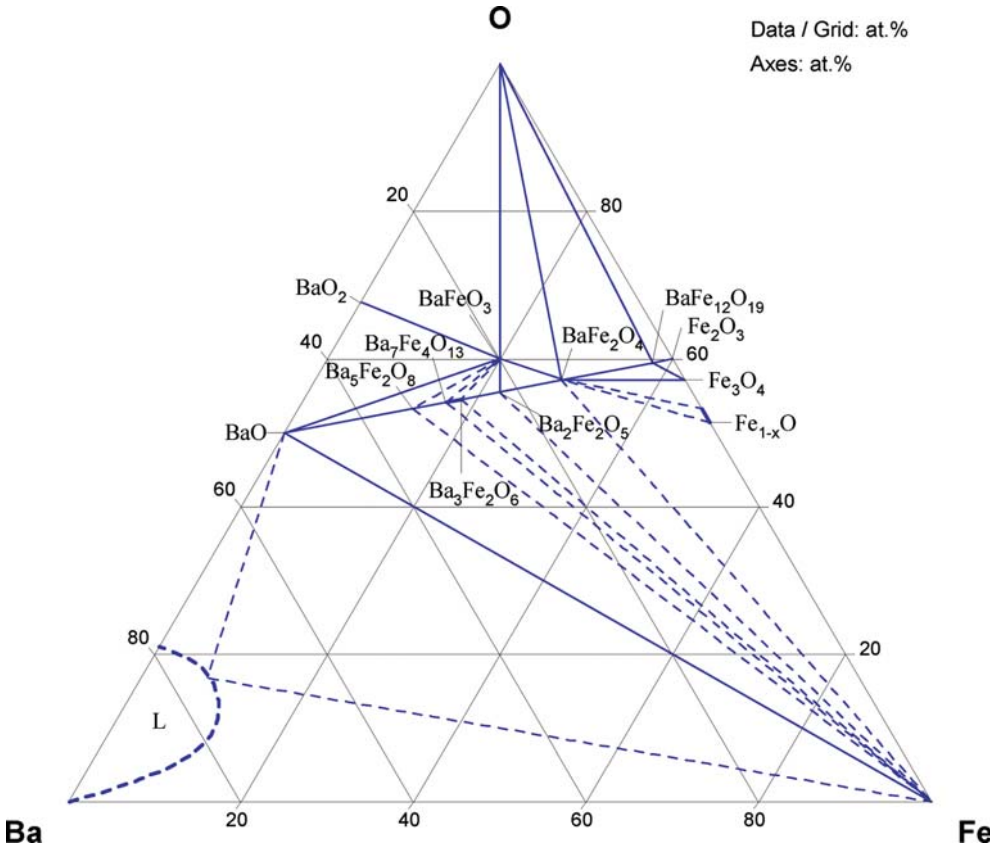

Fig. 2. Ba-Fe-O. Isothermal section, valid for 700 - 1000°C. Tentative line of equilibrium with the liquid drawn from the Ba-O and Ba-Fe binary systems for 900°C

DOI: 10.1007/978-3-540-69761-9_27

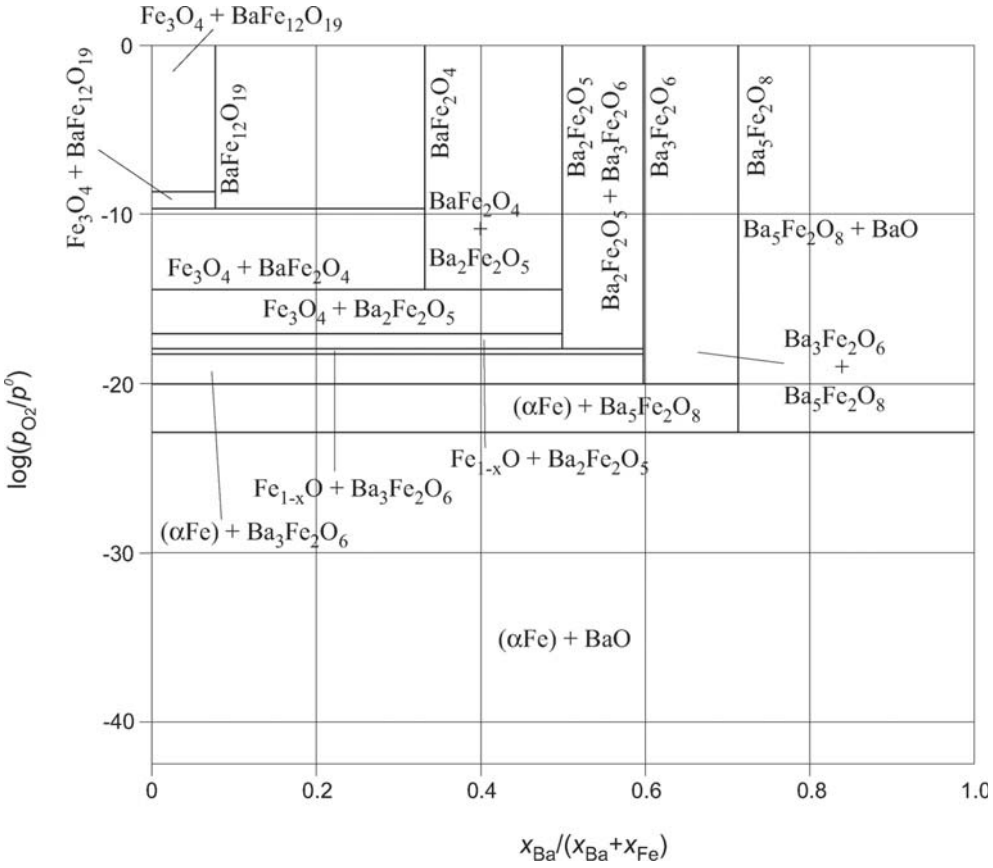

Fig. 3. Ba-Fe-O. Oxygen potential diagram at 827°C

DOI: 10.1007/978-3-540-69761-9_27

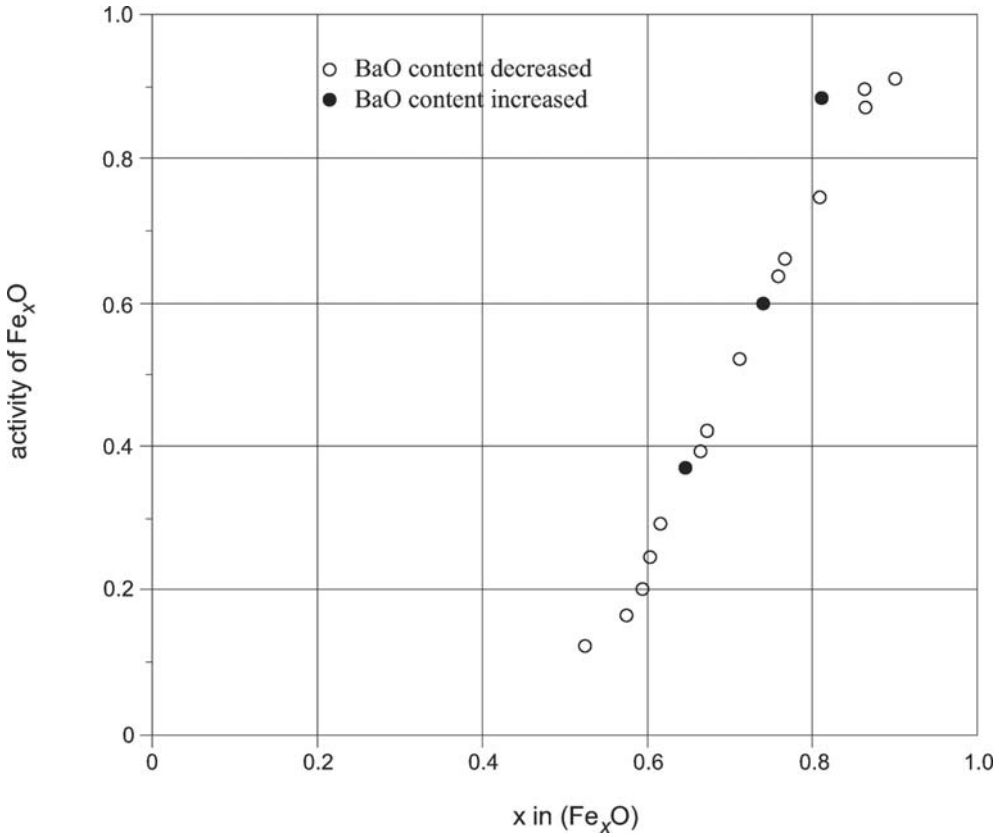

Fig. 4. Ba-Fe-O. Activity of Fe_xO in liquid BaO + Fe_xO at 1400°C; the standard state for Fe_xO is pure liquid Fe_xO in equilibrium with pure (δFe) at 1400°C, for BaO it is pure super-cooled liquid BaO at 1400°C

DOI: 10.1007/978-3-540-69761-9_27

References

[1938Ade] Adelskoeld, V., "X-ray Studies on Magneto-Plumbite, $PbO.6Fe_2O_3$ and Other Substances Resembling "β-Alumina", $NaO.11Al_2O_3$", *Arkiv Kemi, Mineral. Geol.*, **12A**(29), 1–9 (1938) (Crys. Structure, Experimental, 11)

[1945Dar] Darken, L.S., Gurry, G.W., "The System Iron-Oxygen - I - The Wuestite Field and Related Equilibria", *J. Am. Chem. Soc.*, **67**, 1398–1412 (1945) (Experimental, Thermodyn., Phase Diagram, *, 26)

[1946Dar] Darken, L.S., Gurry, G.W., "The System Iron-Oxygen - II - Equilibrium and Thermodynamics of Liquid Oxides and other Phases", *J. Am. Chem. Soc.*, **68**, 798–816 (1946) (Experimental, Thermodyn., Phase Diagram, *, 24)

[1946Erc] Erchak, M., Fankuchen, I., Ward, R., "Reaction Between Ferric Oxide and Barium Carbonate in the Solid Phase. Identification of Phases by X-Ray Diffraction", *J. Am. Chem. Soc.*, **68**(10), 2085–2093 (1946) (Crys. Structure, Experimental, 13)

[1953Gal] Gal'perin, F., "Magnetic Moments and the Crystal Structure of Ferromagnetic Metals and Alloys" (in Russian), *Dokl. Akad. Nauk SSSR*, **88**, 643–644 (1953) (Crys. Structure, Experimental, Magn. Prop., 11)

[1954Bra] Braun, P.B., "Structure Determinations of Barium Iron Oxides", *Acta Crystallogr.*, **7**(10), 640 (1954) (Crys. Structure, Experimental, Abstract)

[1957Bra] Braun, P.B., "Crystal Structures of a New Group of Ferromagnetic Compounds", *Philips Res. Rep.*, **12**(6), 491–548 (1957) (Crys. Structure, Experimental, 17)

[1960Bat] Batti, P., "Equilibrium Diagram of the System $BaO-Fe_2O_3$" (in Italian), *Ann. Chim. (Rome)*, **50**, 1461–1478 (1960) (Phase Diagram, Experimental, 6)

[1960Got] Goto, Y., Takada, T., "Phase Diagram of the System $BaO-Fe_2O_3$", *J. Am. Ceram. Soc.*, **43**(3), 150–153 (1960) (Phase Diagram, Experimental, 11)

[1961Der] Derbyshire, S.W., Fraker, A.C., Stadelmaier, H.H., "A Barium-Iron-Oxide with Perovskite Structure", *Acta Crystallogr.*, **14**(12), 1293 (1961) (Crys. Structure, Experimental, 6)

[1961Oka] Okazaki, C., Mori, S., Kanamaru, F., "Magnetic and Crystallographical Properties of Hexagonal Barium Mono-Ferrite, $BaO{\cdot}Fe_2O_3$", *J. Phys. Soc. Jpn.*, **16**(1), 119 (1961) (Crys. Structure, Experimental, Magn. Prop., 4)

[1962Zio] Ziolowski, Z., "The Pseudobinary System $Ba_{0.6}Fe_2O_3$-$BaO{\cdot}Fe_2O_3$" (in Polish), *Prace Inst. Hutnic.*, **14**(2), 155–163 (1962) (Experimental, Phase Diagram, 8)

[1964Hoo] Van Hook, H.J., "Thermal Stability of Barium Ferrite ($BaFe_{12}O_{19}$)", *J. Am. Ceram. Soc.*, **47**(11), 579–581 (1964) (Experimental, Phase Diagram, 8)

[1965McC] MacChesney, J.B., Potter, J.F., Sherwood, R.C., Williams, H.J., "Oxygen Stoichiometry in the Barium Ferrates, Its Effect on Magnetization and Resistivity", *J. Chem. Phys.*, **43**(9), 3317–3322 (1965) (Experimental, 19)

[1965Man] Von Mansmann, M., "Crystal Structure of the Pentaoxometallates(IV) of Barium and Isotype of These Compounds" (in German), *Z. Anorg. Allg. Chem.*, **339**, 52–56 (1965) (Crys. Structure, Experimental, 11)

[1965Mor] Mori, S., "Preparation of Various Phases of $BaFeO_{3-x}$", *J. Am. Ceram. Soc.*, **48**(3), 165 (1965) (Abstract, Experimental, 5)

[1966Mor] Mori, S., "Phase Transformation in Barium Orthoferrate $BaFeO_{3-x}$", *J. Am. Ceram. Soc.*, **49**(11), 600–605 (1966) (Experimental, 17)

[1966Vos] Voskanyan, R.A., "Growth of Barium Ferrite Single Crystals from Solution in Melts", *Sov. Phys.-Crystallogr. (Engl. Transl.)*, **10**(5), 628–629 (1966), translated from *Kristallografiya*, **10**(5), 748–750 (1965) (Crys. Structure, Experimental, 5)

[1967Tow] Townes, W.D., Fang, J.H., Perrotta, A.J., "The Crystal Structure and Refinement of Ferrimagnetic Barium Ferrite, $BaFe_{12}O_{19}$", *Z. Kristallogr.*, **125**(1–6), 437–449 (1967) (Crys. Structure, Experimental, 13)

[1968Ber] Beretka, J., Ridge, M.J., "The Reaction Between Iron(III) Oxide and Barium Carbonate in Vacuo", *J. Chem. Soc.*, **A**(10), 2463–2465 (1968) (Experimental, 14)

DOI: 10.1007/978-3-540-69761-9_27

[1970Bel] Belyaev, I.N., Fesenko, E.G., Filip'ev, V.S., Kokarovtseva, I.G., "The Crystal Structure of Barium Iron (IV) Oxides in the System $BaFeO_3$-$BaFeO_{2.5}$", *Sov. Phys.-Crystallogr.*, **14**(5), 782–784 (1970), translated from *Kristallografiya*, **14**(5), 910–913 (1969) (Crys. Structure, Experimental, 12)

[1971Mit] Mitsuda, H., Mori, S., Okazaki, C., "The Crystal Structure of Barium Monoferrite, $BaFe_2O_4$", *Acta Crystallogr., Sect. B: Struct. Crystallogr. Crys. Chem.*, **27B**(6), 1263–1269 (1971) (Crys. Structure, Experimental, 18)

[1971Zan] Zanne, M., Gleitzer, C., Aubry, J., "Barium Ferrates(III-IV) at Ba/Fe=1: Phase Diagram and Property Diagram", (in French), *Bull. Soc. Chim. Fr.*, (7), 2451–2455 (1971) (Phase Relations, Phase Diagram, Electr. Prop., Magn. Prop., Experimental" 20)

[1972Mer] Meriani, S., "Polymorphism of Barium Monoferrite, $BaFe_2O_4$", *Acta Crystallogr., Sect. B: Struct. Crystallogr. Crys. Chem.*, **28B**, 1241–1243 (1972) (Crys. Structure, Experimental, 7)

[1972Mon] Montorsi, M., Brisi, C., "A New Compound Related to the BaO-Fe_2O_3" (in Italian), *Ann. Chim. (Rome)*, **62**(9), 641–645 (1972) (Crys. Structure, Experimental, 4)

[1973Ich] Ichida, T., "Mössbauer Study of the Thermal Decomposition Products of $BaFeO_4$", *J. Solid State Chem.*, **7**, 308–315 (1973) (Crys. Structure, Experimental, 27)

[1973Luc] Lucchini, E., Meriani, S., Minichelli, D., "X-Ray Study of Two Phases of $BaFeO_{3-x}$", *Acta Crystallogr., Sect. B: Struct. Crystallogr. Crys. Chem.*, **29B**(6), 1217–1219 (1973) (Crys. Structure, Experimental, 8)

[1973Oka] Okamoto, S., Okamoto, S.I., Ito, T., "The Crystal Structure of Barium Diferrite", *Acta Crystallogr., Sect. B: Struct. Crystallogr. Crys. Chem.*, **29B**(4), 832–838 (1973) (Crys. Structure, Experimental, 22)

[1973Slo] Sloccari, G., "Phase Equilibria in the Subsystem $BaO{\cdot}Fe_2O_3$-$BaO{\cdot}6Fe_2O_3$", *J. Am. Ceram. Soc.*, **56**(9), 489–490 (1973) (Experimental, 14)

[1974Ale] Alekseev, V.I., Strigunov, F.I., Nekrich, M.I., "Calculation of Heats and Gibbs Energies of Formation of Some Barium Silicates, Aluminates and Ferrites from Oxides", *Vestn. Khark. Politekh. Inst.*, **97**, 53–61 (1974) (Calculation, Thermodyn., 6)

[1975And] Anderson, J.S., Hutchison, J.L., "The Study of Long Range Order in Hexagonal Barium Ferrite Layer Structures", *Cont. Phys.*, **16**(5), 443–467 (1975) (Crys. Structure, Experimental, 34)

[1975Man] Mansour, N.A., Gadalla, A.M., Hennicke, H.W., "Redox-Reactions of the Oxygen of Barium and Iron in Air" (in German), *Ber. Deut. Keram. Ges.*, **52**(7), 201–204 (1975) (Crys. Structure, Experimental, 24)

[1975Oka] Okamoto, S., Sekizawa, H., Okamoto, S.I., "Hydrothermal Synthesis, Structure and Magnetic Properties of Barium Diferrite", *J. Phys. Chem. Solids*, **36**(6), 591–595 (1975) (Experimental, Magn. Prop., 16)

[1976Bat] Batti, P., "Phase Diagrams, Structure and Magnetic Behaviour of Hexagonal Ferrites" (in Italian), *Ceramurgia Int.*, **6**(1), 11–16 (1976) (Phase Diagram, Magn. Prop., Review, 12)

[1976Deo] Deo, B., Kachhawaha, J.S., Tare, V.B., "Free Energy of Formation of Barium Ferrites", *Met. Trans. B*, **7B**(3), 405–409 (1976) (Thermodyn., Experimental, 13)

[1979Boi] Boivin, J.-C., Thomas, D., Pouillard, G., Perrot, P., "Crystal Structure Determination of Barium Ferrite $Ba_2Fe_6O_{11}$" (in French), *J. Solid State Chem.*, **29**, 101–108 (1979) (Crys. Structure, Experimental, 15)

[1979Mon] Montorsi, M., Appendino, P., "Studies on the Basic Zone of Barium-Iron-Oxygen System" (in Italian), *Atti Accad. Sci. Tor., C. Sci. Fis. Mat. Nat.*, **113**(5–6), 479–490 (1979) (Phase Diagram, Crys. Structure, Experimental, 29)

[1979Pou] Pouillard, G., Alam, M.S., Trinel-Dufour, M.-C., Perrot, P., "Some Structural Characteristics of Barium Ferrite $Ba_2Fe_6O_{11}$" (in French), *Compt. Rend. Sec. C*, **288**(21), 517–520 (1979) (Experimental, Crys. Structure, 9)

[1979Vul] Vulkov, V., Deneva, A., Stavraka, D., "Phase Studies of Barium Ferrites in a Highly Basic Part of the BaO-Fe_2O_3 System", *Stroit. Mater. Silik. Prom-st.*, **20**(2), 3–5 (1979) (Experimental, Phase Relations, 2)

DOI: 10.1007/978-3-540-69761-9_27

[1981Neu] Neu, P., Zanne, M., Gerardin, R., Gleitzer, C., "Progressive Reduction of Baryum Ferrite $Ba_2Fe_2O_5$ and Study of Appearing Phases $Ba_2Fe_2O_{5-2x}$ of Brownmillerite-Type Structure and $Ba_7Fe_4O_{13}$" (in French), *Ann. Chim. (Paris)*, **6**(6), 525–534 (1981) (Crys. Structure, Experimental, 14)

[1981Pou] Pouillard G., Shamsul A.M., Trinel-Dufour M.C., Perrot P., "The Binary System Barium Oxide-Iron(iii) Oxide (BaO-Fe_2O_3): Phase Diagram and Thermodynamic Properties", *J. Chem. Res.*, (*S*), (5), 136–137, (M), 1720–1747 (1981) (Phase Diagram, Thermodyn., Experimental, #, *, 40)

[1984Iwa] Iwase, M., Yamada, N., Ichise, E., Akizuki, H., "A Thermodynamic Study of SrO+Fe_xO and BaO+Fe_xO Liquid Slags by Disposable Electrochemical Oxygen Probes", *Arch. Eisenhuettenwes.*, **55**(9), 415–420 (1984) (Thermodyn., Experimental, 12)

[1985Igu] Iguchi, Y., Kubokoya, R., Hirao, J., "Redox Equilibria in Wustite Doped with CaO, SrO, and BaO" (in Japanese), *Nippon Kinzoku Gakkai-shi*, **49**(4), 279–284 (1985) (Phase Relations, Experimental, 27)

[1985Obr] Obradors, X., Collomb, A., Pernet, M., Samaras, D., Joubert, J.C., "X-Ray Analysis of the Structural and Dynamic Properties of $BaFe_{12}O_{19}$ Hexagonal Ferrite at Room Temperature", *J. Solid State Chem.*, **56**, 171–181 (1985) (Crys. Structure, Experimental, 30)

[1986Sha] Shaplygin, I.S., Shubrt, Ya., Zakharov, A.A., "Preparation and Proprietes of the Hexagonal Phases $BaFeO_{3-x}$, Formed at High Pressures", *Russ. J. Inorg. Chem.*, **31**(7), 1074–1076 (1986), translated from *Zh. Neorg. Khim.*, **31**, 1869–1873 (1986) (Crys. Structure, Experimental, 9)

[1987Par] Parras M., Vallet-Regi, M., Gonzalez-Calbet, J.M., Alario-Franco, M.A., Grenier, J.C., Hagenmuller, P., "A Reassessment of $Ba_2Fe_2O_5$", *Mater. Res. Bull.*, **22**(10), 1413–1419 (1987) (Crys. Structure, Experimental, 8)

[1989Rag] Raghavan, V., "The Fe-O System", in "*Phase Diagrams of Ternary Iron Alloys"*, Indian Inst. of Metals, Calcutta, **5**, 5–8 (1989) (Phase Diagram, Crys. Structure, Review, 3)

[1990Che] Chen, Y.L., Li, X.D., Xu, B.F., "A Mössbauer Study of the Bipyramidal Lattice Site (2b) in $BaFe_{12}O_{19}$", *Hyperfine Interact.*, **62**, 219–224 (1990) (Crys. Structure, Magn. Prop, Experimental, 9)

[1990Par] Parras, M., Fournes, L., Grenier, J.C., Pouchard, M., Vallet, M., Calbet, J.M., Hagenmuller, P., "Structural Aspects and Mössbauer Resonance Investigation of $Ba_2Fe_2O_5$", *J. Solid State Chem.*, **88**, 261–268 (1990) (Crys. Structure, 19)

[1990Rez] Reznitskii, L.A., "Thermochemistry of Anion-Deficient Perovskites and Compounds with Brownmillerite Structure", *Russ. J. Phys. Chem.*, **64**(8), 1197–1199 (1990), translated from *Zh. Fiz. Khim*., **64**, 2228–2231 (1990) (Thermodyn., Calculation, 14)

[1990Shi] Shipko, M.N., Letyuk, L.M., Aksel'rod, N.L., Fedorov, A.N., Tkachenko, E.V., "Structure of Phases in the System BaO-Fe_2O_3", *Inorg. Mater. (Engl. Trans.)*, **26**(12), 2196–2199 (1990), translated from *Izv. Akad. Nauk SSSR, Neorg. Mater*., **26**(12), 2551–2555, (1990) (Crys. Structure, Experimental, 9)

[1991Sun] Sundman, B., "An Assessment of the Fe-O System", *J. Phase Equilib.*, **12**(1), 127–140 (1991) (Phase Diagram, Thermodyn., Assessment, 53)

[1992Kat] Kato, S., Iguchi, Y., Ban-Ya, S., "Deoxidation Equilibrium of Liquid Iron with Barium" (in Japanese), *Tetsu to Hagane*, **78**(2), 253–259 (1992) (Phase Relations, Experimental, 17)

[1992Rez] Reznitskii, L.A., "Estimation of the Enthalpies of Formation of Compounds with the Magnetoplumbite Structure $MFe_{12}O_{19}$ (M = Pb, Sr, Ba) and of Barium Ferrites", *Russ. J. Phys. Chem. (Engl. Transl.)*, **66**(7), 1027–1028 (1992), translated from *Zh. Fiz. Khim.*, **66**, 1931–1932, (1992) (Thermodyn., Calculation, 8)

[1992Shi] Shin, H.S., Kwon, S.-J., "A Suggestion on the Standard X-ray Powder Diffraction Pattern of Barium Ferrite", *Powder Diffr.*, **7**(4), 212–214 (1992) (Crys. Structure, Experimental, 9)

[1993Alc] Alcock, C.B., "Thermodynamic and Transport Properties of Electroceramic Oxide Systems", *J. Alloys Compd.*, **197**, 217–227 (1993) (Experimental, Phys. Prop., Review, Thermodyn., 28)

DOI: 10.1007/978-3-540-69761-9_27

[1993Par] Parras, M., Gonzalez-Calbet, J.M., Vallet-Regi, M., Grenier, J.C., "A High Temperature Study of the $BaFeO_{3-y}$ System", *Solid State Ionics*, **63–65**, 714–718 (1993) (Crys. Structure, Experimental, 14)

[1993Wan] Wang, J., Han, Q., Wei, S., Song, B., "Equilibrium of Ba-O, Ba-S and Ba-P in Molten Fe" (in Japanese), *Jinshu Xuebao*, **29**(2), B64-B69 (1993) (Experimental, Phase Relations, 12)

[1994Kac] Kaczmarek, W.A., Ninham, B.W., "Preparation of High-Coercivity Fine Barium Ferrite Powder", *J. Appl. Phys.*, **78**(15), 6065–6067 (1994) (Crys. Structure, Experimental, Magn. Prop., 8)

[1994Li1] Li, J.S., Guer, T.M., Sinclair, R., Rosenblum, S.S., Hayashi, H., "Oxygen Coulometric Titration Study of M Ba-Ferrite", *Solid State Ionics*, **73**(3–4), 185–188 (1994) (Experimental, Phase Relations, Thermodyn., 6)

[1994Li2] Li, J., Guer, T.M., Sinclair, R., Rosenblum, S.S., Hayashi, H., "Thermochemical Stability of $BaFe_{12}O_{19}$ and $BaFe_2O_4$ and Phase Relations in the Ba-Fe-O Ternary System", *J. Mater. Res.*, **9**(6), 1499–1512 (1994) (Experimental, Phase Diagram, Thermodyn., #, 40)

[1995Bar] Barinov, V.A., Tsurin, V.A., Gaviko, V.S., Yermakov, A.Ye., Teytel, Ye.I., Shegoleva, N.I., Leccabue, F., Watts, B.E., Panizzieri, R., Bocelli, G., Diaz Castafi, S., "Effects of Mechanical Grinding on Magneto-Structural Properties of $BaFe_{12}O_{19}$ Powders", *J. Magn. Magn. Mater.*, **139**, 143–150 (1995) (Crys. Structure, Experimental, Magn. Prop., 24)

[1995Cho] Choy, J.H, Song, S.W., Han, Y.S., "Xanes Study and Rietveld Refinement for the Nanometer-Sized Polycrystalline Ferrite, $AFe_{12}O_{19}$ (A = Sr, Ba)", *Synth. Met.*, **71**(1–3), 2057–2058 (1995) (Crys. Structure, Experimental, 6)

[1995Zim] Zimmermann, E., Hack, K., Neuschutz, D., "Thermochemical Assessment of the System Ba-O", *Calphad*, **19**(1), 119–127 (1995) (Phase Diagram, Thermodyn., Assessment, 55)

[1997Oka] Okamoto, H., "Ba-O (Barium - Oxygen)", *J. Phase Equilib.*, **18**(4), 400 (1997) (Phase Diagram, Review, 3)

[1997Par] Parkin, I.P., Elwin, G., Fernadez Barquin, L., Bui, Q.T., Pankhurst, Q.A., Komarov, A.V., Morozov, Y.G., "Self-Propagating High Temperature Synthesis of Hexagonal Ferrites $MFe_{12}O_{19}$ (M = Sr, Ba)", *Adv. Mater.*, **9**(8), 643–645 (1997) (Crys. Structure, Experimental, Magn. Prop., 7)

[1998Gol] Golubenko, Z.V., Olkhovik, L.P., Sizova, Z.I., Kamzin, A.S., "Study of the Magnetic State of a Highly Dispersed $BaO{\cdot}6Fe_2O_3$ System With Near Critical Particle Size", *Phys. Solid State*, **40**(7), 1178–1181 (1998) (Experimental, Magn. Prop., Phase Relations, 14)

[1998Kre] Kreisel, J., Lucazeau, G., Vincent, H., "Raman Spectra and Vibrational Analysis of $BaFe_{12}O_{19}$ Hexagonal Ferrite", *J. Solid State Chem.*, **137**(1), 127–137 (1998) (Crys. Structure, Electronic Structure, Experimental, 51)

[1998Lys] Lysenko, V.A., "Thermodynamic Calculation of the Barium-Oxygen Phase Diagram", *Inorg. Mater. (Engl. Trans.)*, **34**(9), 910–914 (1998) (Calculation, Phase Relations, Thermodyn.)

[1999Cro] Cross, W.B., Affleck, L., Kuznetsov, M.V., Parkin, I.P., Pankhurst, Q.A., "Self-Propagating High-Temperatire Synthesis of Ferrites MFe_2O_4 (M = Mg, Ba, Co, Ni, Cu, Zn), Reactions in an External Magnetic Field", *J. Mater. Chem.*, **9**, 2545–2552 (1999) (Crys. Structure, Experimental, Magn. Prop., 26)

[2000Aff] Affleck, L., Aguas, M.D., Pankhurst, Q.A., Parkin, I.P., Steer, W.A., "Combustion Synthesis of $BaFe_{12}O_{19}$ in an External Magnetic Field: Time-Resolved X-Ray Diffraction (TRXRD) Studies", *Adv. Mater.*, **12**(18), 1359–1362 (2000) (Magn. Prop., Experimental, 10)

[2000Agu] Aguas, M.D., Affleck, L., Parkin, I.P., Kuznetsov, M.V., Steer, W.A., Pankhurst, Q.A., Barquin, L.F., Roberts, M.A., Boamfa, M.L., Perenboom, J.A.A.J., "The Effect of Large Magnetic Fields on Solid State Combustion Reactions: Novel Microstructure, Lattice Contraction and Reduced Coercivity in Barium Hexaferrite", *J. Mater. Chem.*, **10**, 235–237 (2000) (Crys. Structure, Experimental, Magn. Prop., 13)

[2000Gon] Gonzalez-Carreno, T., Morales, M.P., Serna C.J., "Barium Ferrite Nanoparticles Prepared Directly by Aerosol Pyrolysis", *Mater. Lett.*, **43**(3), 97–101 (2000) (Magn. Prop., Experimental, Crys. Structure, 19)

DOI: 10.1007/978-3-540-69761-9_27

[2000Li] Li, Z.W., Ong, C.K., Yang, Z., Wei, F.L., Zhou, X.Z., Zhao, J.H., Morrish, A.H., "Site Preference and Magnetic Properties for a Perpendicular Recording Material: $BaFe_{12-x}Zn_{x/2}Zr_{x/2}O_{19}$ Nanoparticles", *Phys. Rev. B*, **62**(10), 6530–6537 (2000) (Crys. Structure, Experimental, Magn. Prop., 31)

[2001Gom] Gomez, M.I., Lucotti, G., de Moran, J.A., Aymonino, P.J., Pagola, S., Stephens, P., Carbonio, R.E., "Ab Initio Structure Solution of $BaFeO_{2.8-\delta}$, a New Polytype in the System $BaFeO_y$ ($2.5<y<3.0$) Prepared from the Oxidative Thermal Decomposition of $BaFe[(CN)_5NO]_3H_2O$", *J. Solid State Chem.*, **160**, 17–24 (2001) (Crys. Structure, Experimental, 48)

[2001Jan] Janasi, S.R., Rodrigues, D., Landgraf, F.J.G., Emura, M., "Magnetic Properties of Barium Ferrite Powders Obtained by Coprecipitation", *Key Eng. Mater.*, **189–191**, 661–666 (2001) (Experimental, Magn. Prop., 20)

[2001Jor] Jorda, J.L., Jondo, T.K., "Barium Oxides: Equilibrium and Decomposition of BaO_2", *J. Alloys Compd.*, **327**, 167–177 (2001) (Crys. Structure, Experimental, Phase Relations, 28)

[2001Mar] Martinez Garcia, R., Reguera Ruiz, E., Estevez Rams, E., Martinez Sanchez, R., "Effect of Precursor Milling on Magnetic and Structural Properties of $BaFe_{12}O_9$ M-Ferrite", *J. Magn. Magn. Mater.*, **223**, 133–137 (2001) (Experimental, Magn. Prop., 9)

[2001Men] Mendoza-Suarez, G., Matutes-Aquino, J.A., Escalante.Garcia, J.I., Mancha-Molinar, H., Rios-Jara, D., Johal, K.K, "Magnetic Properties and Microstructure of Ba-Ferrite Powders Prepared by Ball Milling", *J. Magn. Magn. Mater.*, **223**, 55–62 (2001) (Experimental, Magn. Prop., 7)

[2001Par1] Parkin, I.P., Pankhurst, Q.A., Affleck, L., Aguas, M.D., Kuznetsov, M.V., "Self-Propagating High Temperatire Synthesis of $BaFe_{12}O_{19}$, $Mg_{0.5}Zn_{0.5}Fe_2O_4$ and $Li_{0.5}Fe_{2.5}O_4$, Time Resolved X-ray Diffraction Studies (TRXRD)", *J. Mater. Chem.*, **11**, 193–199 (2001) (Crys. Structure, Experimental, 31)

[2001Par2] Parkin, I.P., Elwin, G., Kuznetsov, M.V., Pankhurst, Q.A., Bui, Q.T., Forster, G.D., Barquin, L.F., Komarov, A.V., Morozov, Y.G., "Self-Propagating High Temperature Synthesis of $MFe_{12}O_{19}$ (M = Sr, Ba) from the Reactions of Metal Superoxides and Iron Metal", *J. Mat. Proc. Tech.*, **110**(2), 239–243 (2001) (Crys. Structure, Experimental, Magn. Prop., 20)

[2002Del] Delattre, J.L., Stacy, A.M., Young, V.G., Long, G.J., Hermann, R., Grandjean, F., "Study of the Structural, Electronic, and Magnetic Properties of the Barium-Rich Iron(IV) Oxides, Ba_2FeO_4 and Ba_3FeO_5", *Inorg. Chem.*, **41**(11), 2834–2838 (2002) (Crys. Structure, Experimental, Magn. Prop., 28)

[2002Mar] Martirosyan, K.S., Avakyan, P.B., Nersesyan, M.D., "Phase Formation During Self-Propagation High-Tempetature Synthesis of Ferrites", *Inorg. Mater. (Engl. Trans.)*, **38**, 400–403 (2002) (Crys. Structure, Experimental, 11)

[2002Teh] Teh, G.B., Jefferson, D.A., "High-Resolution Transmission Electron Microscopy Studies of Sol-Gel-Derived Cobalt-Substituted Barium Ferrite", *J. Solid State Chem.*, **167**, 254–257 (2002) (Crys. Structure, Experimental, Magn. Prop., 12)

[2003Fu] Fu, Y.P., Lin, C.H., Pan, K.Y., "Fe/Ba Ratio Effect on Magnetic Properties of Barium Ferrite Powders Prepared by Microwave-Induced Combustion", *Japan. J. Appl. Phys.*, **42**(5A), 2681–2684 (2003) (Experimental, Magn. Prop., Phase Relations, 13)

[2003Gao] Gao, F.M., Li, D.C., Zhang, S.Y., "Mössbauer Spectroscopy and Chemical Bonds in $BaFe_{12}O_{19}$ Hexaferrite", *J. Phys.: Condens. Matter*, **15**(29), 5079–5084 (2003) (Crys. Structure, Electronic Structure, Experimental, Magn. Prop., 19)

[2003Mue] Mueller-Buschbaum, H., "The Crystal Chemistry of AM_2O_4 Oxometallates", *J. Alloys Compd.*, **349**(1–2), 49–104 (2003) (Crys. Structure, Review, 476)

[2004Del] Delattre, J.L., Stacy, A.M., Siegrist, T., "Structure of Ten-Layer Orthorhombic $Ba_5Fe_5O_{14}$ ($BaFeO_{2.8}$) Determined from Single Crystal X-Ray Diffraction", *J. Solid State Chem.*, **177**(3), 928–935 (2004) (Crys. Structure, Experimental, 31)

[2004Lic] Licht, S., Naschitz, V., Rozen, D., Halperin, N., "Cathodic Charge Transfer and Analysis of Cs_2FeO_4, K_2FeO_4 and Mixed Alkali Fe (VI) Ferrate Super-Irons", *J. Electrochem. Soc.*, **151**(8), A1147-A1151 (2004) (Crys. Structure, Electr. Prop., Experimental, 15)

DOI: 10.1007/978-3-540-69761-9_27

[2004Rak] Rakshit, S.K., Parida, S.C., Singh, Z., Prasad, R., Venugopal, V., "Thermodynamic Properties of Ternary Oxides in the System Ba-Fe-O Using Solid-State Electrochemical Cell with Oxide and Fluoride ion Conducting Electrolytes", *J. Solid State Chem.*, **177**(4–5), 1146–1156 (2004) (Experimental, Phase Diagram, Thermodyn., 22)

[2005Dho] Dho, J., Lee, E.K., Park, J.Y., Hur, N.H., "Effects of the Grain Boundary on the Coercivity of Barium Ferrite $BaFe_{12}O_{19}$", *J. Magn. Magn. Mater.*, **285**(1–2), 164–168 (2005) (Experimental, Magn. Prop., Phase Relations, Transport Phenomena, 23)

[2005Mal] Mali, A., Ataie, A., "Influence of Fe/Ba Molar Ratio on the Characteristics of Ba-Hexaferrite Particles Prepared by Sol-Gel Combustion Method", *J. Alloys Compd.*, **399**(1–2), 245–250 (2005) (Crys. Structure, Experimental, Magn. Prop., Phase Relations, 26)

[2005Sin] Singhal, S., Garg, A.N., Chandra, K., "Evolution of the Magnetic Properties During the Thermal Treatment of Nanosize $BaMFe_{11}O_{19}$ (M = Fe, Co, Ni, and Al) Obtained Through Aerosol Route", *J. Magn. Magn. Mater.*, **285**(1–2), 193–198 (2005) (Crys. Structure, Experimental, Magn. Prop., Optical Prop., 21)

[V-C2] Villars, P. and Calvert, L.D., *Pearson's Handbook of Crystallographic Data for Intermetallic Phases*, 2nd edition, ASM, Metals Park, Ohio (1991)

[Mas2] Massalski, T.B. (Ed.), *Binary Alloy Phase Diagrams*, 2nd edition, ASM International, Metals Park, Ohio (1990)

DOI: 10.1007/978-3-540-69761-9_27

Carbon – Cobalt – Iron

Andy Watson and Lesley Cornish

Introduction

Interest in the C-Co-Fe system is related mainly to steel production. An early study of the phase equilibria in the system was provided by [1932Vog]. Using thermal analysis and microscopical techniques, they determined 6 isoplethal sections at Fe:Co ratios of 49:1, 29:1, 9:1, 7:3, 1:1 and 3:7 (by mass) in the Fe rich corner of the system. Subsequently, work has focused on the effects of Co on C levels in Fe solutions. The solubility of C in liquid Fe with Co was studied at 1550 and 1350°C by [1956Tur, 1969Sch], 1450°C by [1960Fuw], 1600°C by [1963Sch] and at 1375°C by [1964Dai]. [1983Jan1, 1983Jan2] determined the solubility at 1600, 1550 and 1500°C. The experimental technique employed was virtually the same in each case. Mixtures of Fe and Co were melted in a graphite crucible under argon gas, and after equilibrium was reached, the melt was quenched. The C content was then determined by combustion analysis. The solubility of C in γFe was studied by [1969Fra]. Rod samples of induction melted master Co-Fe alloys were packed in graphite crucibles with graphite powder and pure Fe foil. The crucible was heated to 1000°C for 72 h under flowing dried hydrogen before quenching by moving to the water cooled end of the furnace. The C levels in the samples were then determined.

Much of the research into the system, however, was focused on the C activity in solid alloys. A number of researchers have studied the effects of Co on the C activity in solid [1960Pet, 1963Bro, 1965Smi, 1972Wil] and liquid [1959Fuw] ternary alloys. Known CO/CO_2 mixtures were passed over a charge of the three components, held in a high-frequency induction furnace at different temperatures. After equilibration (~5 h) the alloys were solidified for chemical analysis leading to C activities. Because of concerns in the experimental technique relating to gas mixture inhomogeneity owing to thermal diffusion and carbon deposition in cold parts of the apparatus, [1972Foo] employed a closed chamber where the gas employed acts purely as a transport medium. The affect of Co content on the activity of C was also determined by measuring the C solubility [1959Fuw]. The melt was continually stirred with a carbon rod until equilibrium was achieved. The melt was sampled for analysis, and further Co additions made and the stirring and sampling process repeated. These data were reviewed by [1963Ell]. A similar gas equilibration technique was used by [1963Bro]. The effect of Co on the carbon activity in austenite alloys was studied by [1972Wil]. Spiral specimens of alloy, pure Fe and a source of C in the form of cast Fe particles were heated at temperatures of 850, 925 and 1050°C. After equilibration, the carbon activity was determined from the amount of C in the pure Fe specimen. They found that Co increased the carbon activity of austenite. [1968Chi] reviewed the experimental data for the activity of carbon in alloyed austenite at 1000°C. The Phase equilibrium data were critically reviewed by [1984Riv, 1988Ray, 1994Rag, 2002Rag].

The enthalpies of mixing of the ternary liquid were determined calorimetrically at 1900°C by [1993Wit, 1994Wit]. Partial and integral enthalpies were presented and also, they suggested that repulsive forces take place between the like and unlike atoms.

In addition to the experimental studies of phase equilibria and thermodynamics, many researchers took a theoretical approach. [1965Bur] extrapolated the thermodynamic properties of the binary systems in order to calculate isotherms in the ternary system. [1966Aar] took three different statistical thermodynamic approaches to the thermodynamics of interstitial solid solutions. They found that that based on the Lacher-Fowler-Guggenheim model best fit the experimental activity data available in the literature. [1968Zup] employed an extension of the Langmuir lattice gas model to calculate the carbon activity, and [1971Ale] used a quasi-chemical approach to calculate the thermodynamics of the ternary liquid. More recently however, Calphad modelling techniques have been employed. [1977Uhr] used experimental carbon activity data from the literature [1965Smi, 1968Bod] to determine a temperature independent interaction parameter. [1988Hoc] calculated metal-carbon interactions for solid ternary alloys, and in the same year, a full Calphad assessment of all available experimental phase equilibrium and thermodynamic information was carried out by [1988Gui]. [1985Eno] used a central atom model to calculate ortho and paraequilibria between ferrite and

DOI: 10.1007/978-3-540-69761-9_28

austenite in the C-Co-Fe ternary system. More recently, [2004Tao] has used a new method to calculate ternary solution thermodynamics from those in the associated binary systems. The method involved a combination of free volume theory and the lattice model. Good agreement between calculated and observed activity coefficients was found, which the authors attributed to the physical basis of the model.
Through an interest in the production of industrial diamonds, work has been carried out on the effects of pressure on the phase equilibria in the C-Co-Fe system. [1990Put] performed XRD studies on materials that had been prepared at 827°C and applied pressures of up to 6 hPa. They found that the equilibrium structure of the C at 5 hPa was graphite, whereas at the higher pressure it was diamond. However, these pressures seem to be low when compared with the work of [1991Pav, 1993Koc, 1993Tur, 1995Tur, 1996Koc], who conducted phase equilibrium studies at pressures up to 6 GPa. They used thermal analysis, metallography, XRD and EPMA, and by applying the assessment of [1988Gui] as a starting point, they modeled the ternary system at high pressures producing melting diagrams for pressures of 0.1 MPa, 4.7 GPa and 6 GPa.
Experimental phase diagram and thermodynamic studies are listed in Table 1.

Binary Systems

The C-Co binary system is accepted from [Mas2]. The phase diagram is of the simple eutectic type with an invariant temperature 1320°C. Analogous to the C-Fe system, the CoC_3 phase is metastable giving a metastable eutectic temperature of 1192°C. However, this phase becomes stable at pressures higher than 4.5 MPa [1996Koc]. In the assessment of the C-Co system given by [1987Gui], the metastable eutectic is given as 1235°C.
The C-Fe system is accepted from [2006MSIT]. The Co-Fe system is accepted from a Calphad assessment given by [2002Ohn]. The phase diagram is essentially the same as given in [Mas2], but it extends to lower temperatures following phase equilibrium studies using thin films.

Solid Phases

No ternary phases are found in this system. The solid phases are essentially solutions based on Fe and Co, although the bcc phase in the Co-Fe system orders with decreasing temperature. There seems to be no indication how this may extrapolate into the ternary system. As in the C-Fe system, the Co_3C phase is metastable in the C-Co binary system. At high pressures, a number of other Fe-carbides can become stable, most notably Fe_7C_3 which has been observed in high pressure work on this ternary system [1993Koc, 1996Koc]. According to [V-C2], there are two possible crystal structures for this phase, but [1993Koc, 1996Koc] did not specify the structure of the phase they observed. Crystallographic data relating to the binary phases are given in Table 2.

Invariant Equilibria

No ternary invariant equilibria are observed in the system at atmospheric pressures. [1993Koc] used derivative thermal analysis, metallography and XRD to investigate the eutectic univariant line in the ternary system. The observed that it rises monotonically from the C-Fe to the C-Co binary system, contradicting earlier work [1988Ray] suggesting that it possesses a minimum; although this minimum was found by [1988Gui] as a result of their assessment. However, [1993Koc, 1996Koc] report the presence of a ternary eutectic $L \rightleftharpoons \gamma + (Fe,Co)_3C + (C)gr$ appearing at 4.7 GPa and 1077°C. They also report the presence of a crystallization field for Diamond, and if this is the case, it would be expected that two other invariant equilibria would be present. In fact, these seem to appear on the liquidus surface presented, but they are not annotated. At higher pressures, a ternary transition reaction appears, $L + (Co,Fe)_7C_3 \rightleftharpoons (Co,Fe)_3C + (C)d$ at 1312°C. At the higher pressure, the temperature of the ternary eutectic is reduced to 1057°C. According to [1991Pav], the ternary eutectic lies at a composition of 39 at.% Fe 48 at.% Co 13 at.% C at 5.7 GPa.

Liquidus, Solidus and Solvus Surfaces

Figure 1 shows a projection of the liquidus isotherms of the ternary system, taken from the assessment of [1988Gui]. The direction of the arrows on the univariant line suggests a minimum in agreement with the

DOI: 10.1007/978-3-540-69761-9_28

review of [1988Ray]. Figures 2 and 3 show the solubility of graphite in the liquid phase, taken from the assessment of [1988Gui]. In Fig. 2, graphite solubility is plotted against Co concentration for temperatures 1350, 1450 and 1650°C based on the experimental observations of [1956Tur, 1969Sch]. Figure 3 shows the graphite solubility with respect to Fe content at temperatures of 1370 and 1600°C. The calculated solubility lines are in very good agreement with the experimental data of [1963Sch, 1964Dai, 1969Sch]. Figure 4 shows the assessed solubility of graphite in the γ phase at 1000°C taken from [1988Gui], based on the work of [1969Fra]. Again, the agreement between the experimental and assessed curve is very good. Figures 5 and 6 show the liquidus projection for pressures of 4.7 and 6 GPa, respectively, taken from [1993Koc, 1996Koc]. As cementite is stabilized owing to the high pressure, a eutectic reaction appears in the ternary system. At higher pressures, the Fe_7C_3 phase is stabilized which in turn results in a transition reaction. Figure 5 shows a small primary solidification region for diamond which expands considerably at 6 GPa. However, neither diagrams show a primary solidification region associated with the Co_3C phase which appears at higher pressures, as indicated by the authors. This region of both of these diagrams should be taken as tentative.

Temperature – Composition Sections

Figures 7-12 show calculated temperature-composition sections for stable and metastable equilibria taken from the assessment produced by [1988Gui]. The stable diagram phase boundaries are given as solid lines; the metastable diagram is given with dotted lines. The liquidus lines are in good agreement with the experimental work of [1932Vog]. Slight changes have been made to the diagrams to ensure agreement with the accepted binary systems.

Thermodynamics

Figure 13 shows the calculated solubility of C in austenite at 1000°C, taken from the assessment of [1988Gui]. The solubilities are calculated for different carbon activities. The calculated data agree very well with experimental values that were given by [1965Smi] for this temperature. A similar plot is shown in Fig. 14. Figure 15 shows the calculated carbon activity at 850, 925 and 1050°C. Figure 16 shows isoenthalpy of mixing contours for the liquid phase for 1627°C, taken from [1994Wit].

Notes on Materials Properties and Applications

The magnetic properties of C-Co-Fe alloys have come under scrutiny, particularly with respect to the effects of Co substitution, and more recently, in applications related to aviation. [1953Dra] prepared Co containing cementites by carburizing Co-Fe alloys. They found that the Curie temperature of the cementite increased with increasing Co content. Fe-Co alloys are very useful for high temperature applications in aviation where soft magnetic materials are required. Whilst having high saturation and high Curie temperature, they are very brittle, particularly at low temperatures [2004Sun]. The addition of C induces the precipitation of carbides at grain boundaries, particularly if a carbide former is also added, which helps to increase the strength of the material. An FeCo alloy with 0.5 mass% C has a yield strength of 458 MPa with 15% elongation. Increasing the C level to 2 mass% increases the yield strength to 1050 MPa, with a corresponding reduction in the ductility to 9%. The saturation magnetization is only marginally affected (2.36 increases to 2.37 T) [2004Sun, 2005Sun].

C-Co-Fe alloys have been used as magnetic bearing materials [2000Li]. Hiperco® Alloy 27 (Co-27Fe), has been strengthened with C giving a material with high induction (B = 20 and 21 kG at H = 100 and 150 Oe, respectively) and high yield stress (517-586 MPa) with good ductility (21%). A post-forge treatment is necessary to achieve the required combination of properties.

Recently, the development of nanocrystalline materials and thin films has been of interest. [2001Zha] prepared Fe-Co(C) nanocapsules by an arc discharge process using a mixture of methane and helium. HRTEM revealed that the magnetic cores of the nanocapsules were protected by graphite shells, and that the saturation magnetization of these nanocapsules decreases monotonically, while the coercivity decreases significantly with increasing temperature.

[2005Kiy] fabricated carbon-doped (0-9 at.%) Co-Fe thin films and found that adding 2.5 at.% carbon decreased coercivity. Further additions of carbon did not influence the soft magnetic properties, whereas

DOI: 10.1007/978-3-540-69761-9_28

the saturation flux density was decreased down to 2 T. [2005Kit] used a similar fabrication technique, and in microstructural analyses of the films, discovered nanocrystals with a higher magnetic moment and lower carbon content than the amorphous matrix in which they were dispersed. The sputtering conditions strongly influenced the internal stress in the films, which strongly influenced the magnetic properties. They concluded that it was necessary to fabricate stress-free films to order to obtain appropriate soft magnetic properties, such as low coercivity and appropriate uniaxial anisotropy.
[2005Miy] prepared C-Co-Fe alloy coatings by electrodeposition from a sulfate solution containing citric acid and L-ascorbic acid. The crystal structure and mechanical properties of the coatings were examined by using XRD and Vickers hardness measurements. It was found that the microstructure of C-Co-Fe alloy coatings with 30.0 to 83.8 mass% Co contained an intermediate phase having the same crystal structure as the cubic cobalt phase that is produced by the evaporation of Co on a cold substrate under a He atmosphere. However, this cubic structure changes to tetragonal by the incorporation of carbon. This intermediate phase is quite unstable and transforms to *bcc*-Fe and *hcp*-Co phases during pulverization. The hardness of Co-Fe alloy coatings was improved by the codeposition of carbon, and maximum hardness (H_v = 800) was obtained for the Fe-10.9Co-1.1C (mass%) alloy.
The material property studies are listed in Table 3.

Miscellaneous

As Co is an important alloying element in steels, much research effort has been spent on the study of diffusion and phase transformations. [1964App, 1964Bro, 1964Smi] carried out much of the early work on measurement of the diffusivity of C in austenite. [1964App] used an autoradiographic technique to study the effects of Co additions on the diffusivity of C at three different temperatures. With alloys containing up to 12 at.% Co, they found that initially, the diffusivity decreases with added Co but then increases with more Co addition. This effect is paralleled by variations in the activation energy and the constant for diffusion. [1964Smi] studied the variation of the diffusion constant of C with varying temperature (850-1100°C) for two alloys with Co contents of 89.7 and 79.3 mass% Co. They found a linear relationship between the log of the diffusion coefficient and inverse temperature in the region of the Curie point, suggesting that it is not affected by electronic spin disorder.
The effects of the addition of 3 at.% Co on the kinetics of grain boundary ferrite allotriomorph formation relative to those in C-Fe alloys of comparable carbon content were evaluated by [1973Kin]. It was found that the TTT curve for the initiation of the transformation was displaced to shorter times at higher reaction temperatures by the addition of the Co. This, or course will affect the hardenability. In subsequent work by [1986Eno1, 1986Eno2], further measurements were analyzed using classical nucleation theory in conjunction with 'the pillbox model' and free energy changes calculated for the reaction using a standard sublattice model and the central atoms model. Auger microprobe studies of the grain boundary compositions and results of the analysis suggest that the effect of Co on the proeutectoid ferrite kinetics stems from changes in the volume free energy. The nucleation and growth of ferrite allotriomorphs has been reviewed by [2004Aar].
[1976Ko] studied the effects of magnetism on the partition of Co between ferrite and cementite. They found that the temperature dependence of the partition coefficient deviated from normal Arrhenius behavior in the region of the Curie temperature. As the equilibration temperature was reduced, it was found that the partition coefficient was lower than would be expected, and this was attributed to magnetic effects from the Fe. [2003Zab, 2004Zab] have prepared active cobalt alloy cathodes for hydrogen evolution in hot concentrated sodium hydroxide solutions by electrodeposition. It was found that the cathodic activity of cobalt was enhanced by alloying with Fe and C. The carbon additions help to prevent open circuit corrosion.
The effect of Co on the Snoek peak height was investigated by [2004Sai]. They found that Co decreased the height of the peak owing to strain fields generated by the difference in the atomic size of the Fe and Co atoms on the ferrite lattice.
Synthetic diamonds have been grown at pressures of around 5.5 GPa and 1527°C from a C-Co-Fe alloy melt by [1990Pav]. EXAFS, XRD, SEM and optical microscopy revealed metallic inclusions in the diamond, consisting of a mixture of $(Fe_{1-x}Co_x)_3C$ and ledeburite eutectic.
C-Co-Fe alloys were splat quenched by [1969Ruh]. At high carbon contents, a new hcp phase (designated epsilon, but different from epsilon carbide) was retained.

DOI: 10.1007/978-3-540-69761-9_28

Table 1. Investigations of the C-Co-Fe Phase Relations, Structures and Thermodynamics

Reference	Method/Experimental Technique	Temperature/Composition/Phase Range Studied
[1932Vog]	Thermal analysis, optical microscopy	Vertical sections at Fe:Co ratios 49:1, 29:1, 9:1, 7:3, 1:1 and 3:7 (by mass)
[1953Dra]	XRD	Crystal structures of Co containing cementites
[1956Tur] [1960Fuw] [1963Sch]	Equilibration and quenching	Solubility of C in Fe-Co melts
[1959Fuw]	Equilibration with CO/CO_2 mixtures	Graphite solubility in Fe-Co melts. Activity of C
[1960Pet] [1963Bro] [1965Smi]	Equilibration with CO/CO_2 mixture	Activity of C in solid alloys
[1964Dai]	Equilibration of the melt followed by sampling	Solubility of graphite in liquid Fe-Co alloys
[1965Bur]	Calculation	Determination of ternary isotherms using thermodynamic properties of the binary systems
[1966Aar]	Calculation	Thermodynamics of austenite to proeutectoid reaction
[1968Bod]	Calculation	Prediction of C activities in austenite
[1968Chi]	Calculation	Modeling of C activity in austenite at 1000°C
[1968Zup]	Calculation	Statistical thermodynamic treatment of austenite
[1969Fra]	Equilibration and quenching	Solubility of graphite in austenite at 1000°C
[1969Ruh]	EXAFS, XRD, SEM, optical microscopy	Inclusions in synthetic diamonds
[1969Sch]	Equilibration of melt	Liquidus, 1350-1570°C, $3.6 < C < 5$, $5 <$ at.% Co < 70
[1971Ale]	Calculation	Application of quasichemical model predict activity of C in solid solutions
[1972Foo]	Equilibration with CO/CO_2	Measurement of C activity in ternary melts at 1550°C. Carbon solubility for $0 < x_{Co} < 0.35$
[1972Wil]	Equilibration of alloy strip specimens with C	Determination of C activity with respect to C content at 850, 925 and 1000°C
[1983Jan1] [1983Jan2]	Equilibration of melt	C solubility in ternary melts with respect to Co content $0 < x_{Co} < 0.4$, $T = 1500$, 1550 and 1600°C
[1985Eno]	Calculation (central atoms model)	Ferrite and austenite phase boundaries
[1988Gui]	Assessment	Complete system
[1988Hoc]	Calculation	Interaction parameter for the liquid phase

(*continued*)

DOI: 10.1007/978-3-540-69761-9_28

Reference	Method/Experimental Technique	Temperature/Composition/Phase Range Studied
[1990Put]	Annealing under high pressure	C rich equilibria at 827°C
[1991Pav] [1991Pav] [1996Koc]	DTA, derivative thermal analysis at high pressures	Liquidus surface at pressures up to 5.7 GPa
[1993Tur] [1995Tur]	Calculation	Liquidus surface at pressures up to 6 GPa
[1993Wit] [1994Wit]	Adiabatic calorimetry	Enthalpies of mixing of liquid alloys
[2004Tao]	Calculation	Modeling of C activity coefficient in solid solutions
[2005Miy]	XRD, Vickers hardness	Crystal structure and mechanical properties of C-Co-Fe coatings electrodeposited from aqueous solution

Table 2. Crystallographic Data of Solid Phases

Phase/Temperature Range [°C]	Pearson Symbol/ Space Group/ Prototype	Lattice Parameters [pm]	Comments/References
(C)d	*cF*8 $Fd\bar{3}m$ C (diamond)	a = 356.69	at 25°C, 60 GPa [Mas2]
(C)gr < 3827	*hP*4 $P6_3/mmc$ C (graphite)	a = 246.12 c = 670.90	at 25°C [Mas2] sublimation point
(δFe)(h_2) 1538 - 1394	*cI*2 $Im\bar{3}m$ W	a = 293.15	pure Fe at 1480°C [Mas2]
γ, $Fe_{1-x}Co_x$	*cF*4 $Fm\bar{3}m$		
(γFe) 1394 - 912	Cu	a = 364.67	at 915°C [V-C2, Mas2]
(αCo) 1495 - 422		a = 356.88 a = 354.47	at 520°C [V-C2] [Mas2] austenite
(εCo) < 422	*hP*2 $P6_3/mmc$ Mg	a = 250.71 c = 406.86	at 25°C [Mas2]
(αFe) < 912	*cI*2 $Im\bar{3}m$ W	a = 286.65	at 25°C [Mas2] ferrite

(*continued*)

DOI: 10.1007/978-3-540-69761-9_28

Phase/Temperature Range [°C]	Pearson Symbol/ Space Group/ Prototype	Lattice Parameters [pm]	Comments/References
$(Fe_{1-x},Co_x)_3C(\theta)$	*oP*16 *Pnma*		[V-C2]
Fe_3C	Fe_3C	$a = 507.87$ $b = 672.97$ $c = 451.44$	metastable
Co_3C			metastable
$(Fe_{1-x},Co_x)_7C_3$			at 6 GPa [1993Koc, 1996Koc]
Fe_7C_3	*hP*20 $P6_3mc$ Fe_3Th_7	$a = 688.2$ $c = 454.0$	[V-C2]
	*oP*40 *Pnma* Cr_7C_3	$a = 454.0$ $b = 687.9$ $c = 1194.2$	[V-C2]

Table 3. Investigations of the C-Co-Fe Materials Properties

Reference	Method / Experimental Technique	Type of Property
[1953Dra]	Thermomagnetic measurement	Variation in Curie temperature with Co content
[1964App]	Autoradiography	C diffusion in austenite
[1964Bro]	Transient equilibrium method	C diffusion in austenite
[1964Smi]	Decarburization method	C diffusion in austenite with respect to temperature
[2000Li]	Tensile and magnetic property measurement	Yield strength, magnetization of soft magnetic alloys.
[2001Zha]	Magnetic property measurement	Study of magnetic properties of nanocapsules
[2004Sai]	Internal friction measurement	Effect of Co on Snoek peak
[2005Kit]	Vibrating sample magnetometry, Mössbauer spectrometry	Magnetic properties of nanocrystals in thin films produced by sputtering
[2005Kiy]	Magnetization	Magnetic properties of thin films of composition $(Fe_{65}Co_{35})_{97.5}C_{2.5}$

DOI: 10.1007/978-3-540-69761-9_28

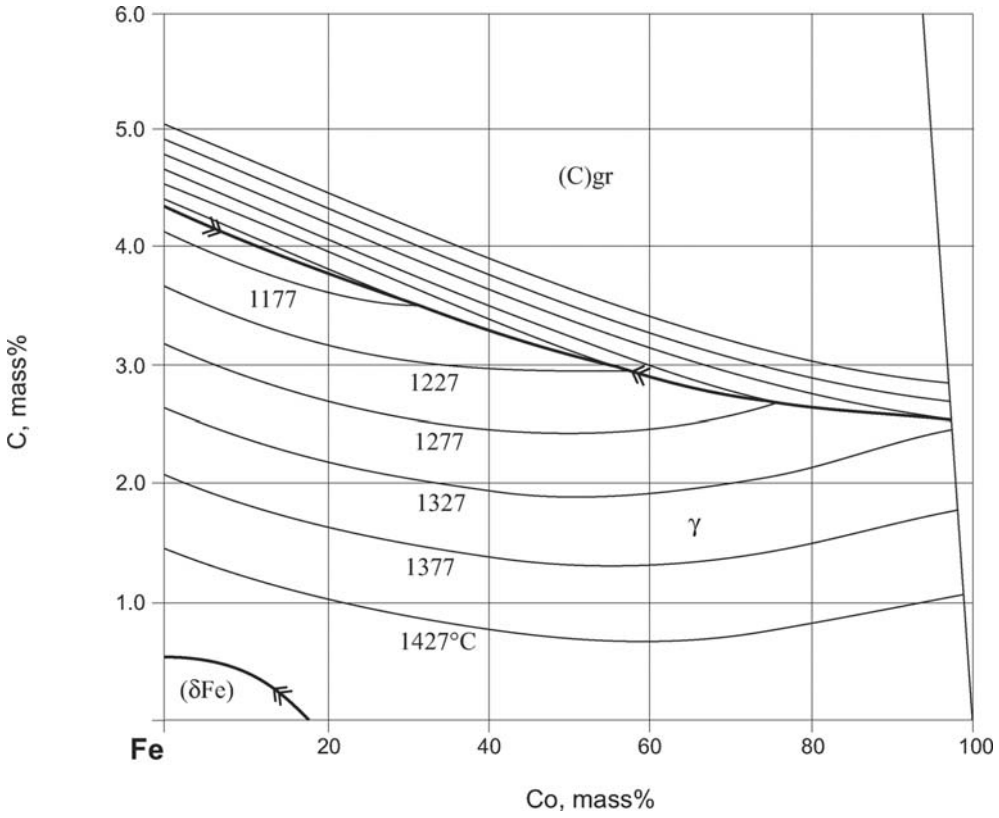

Fig. 1. C-Co-Fe. Projection of the liquidus isotherms of the ternary system

DOI: 10.1007/978-3-540-69761-9_28

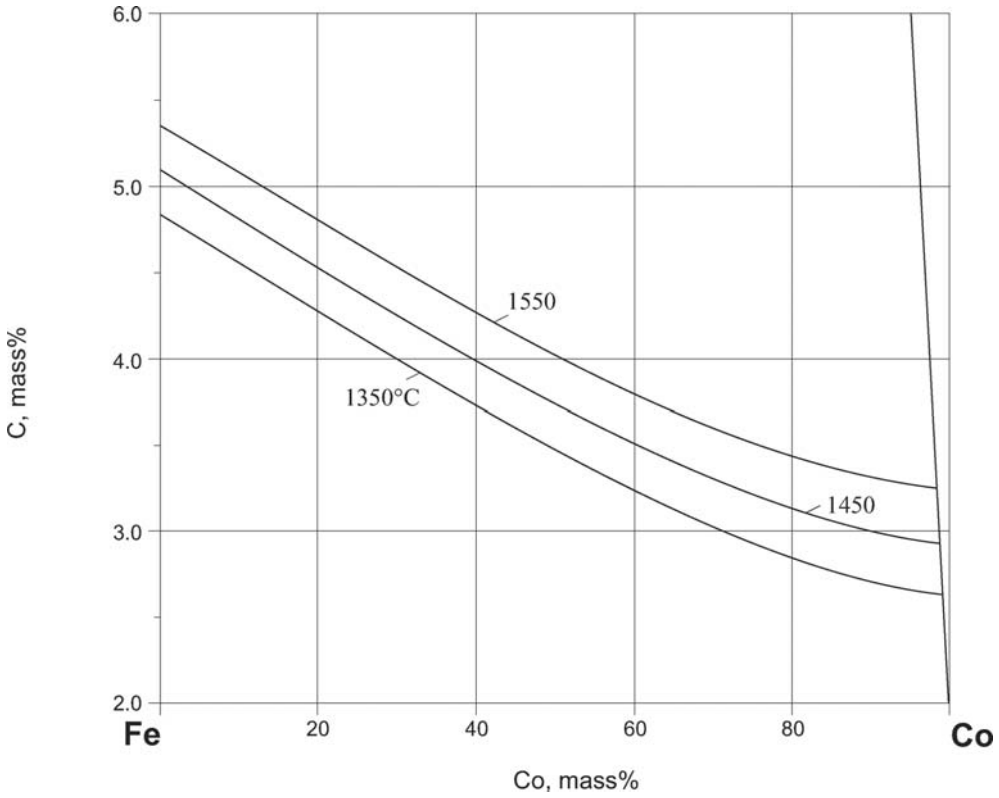

Fig. 2. C-Co-Fe. Solubility of graphite in the liquid phase at 1350, 1450 and 1550°C

DOI: 10.1007/978-3-540-69761-9_28

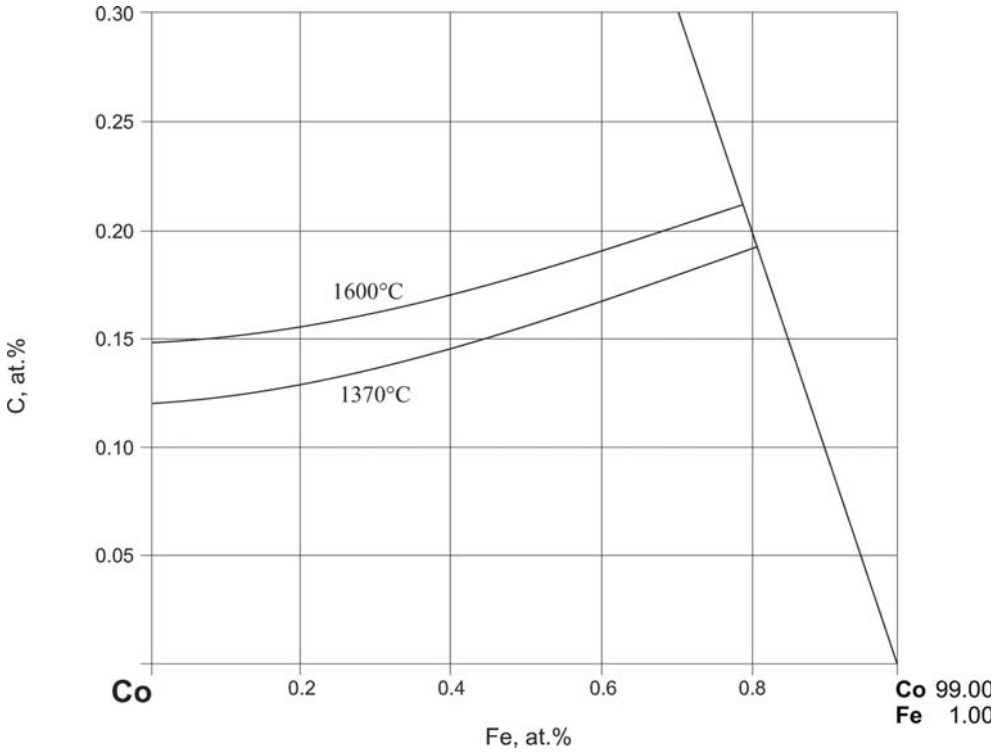

Fig. 3. C-Co-Fe. Solubility of graphite in the liquid phase at 1370, 1600°C

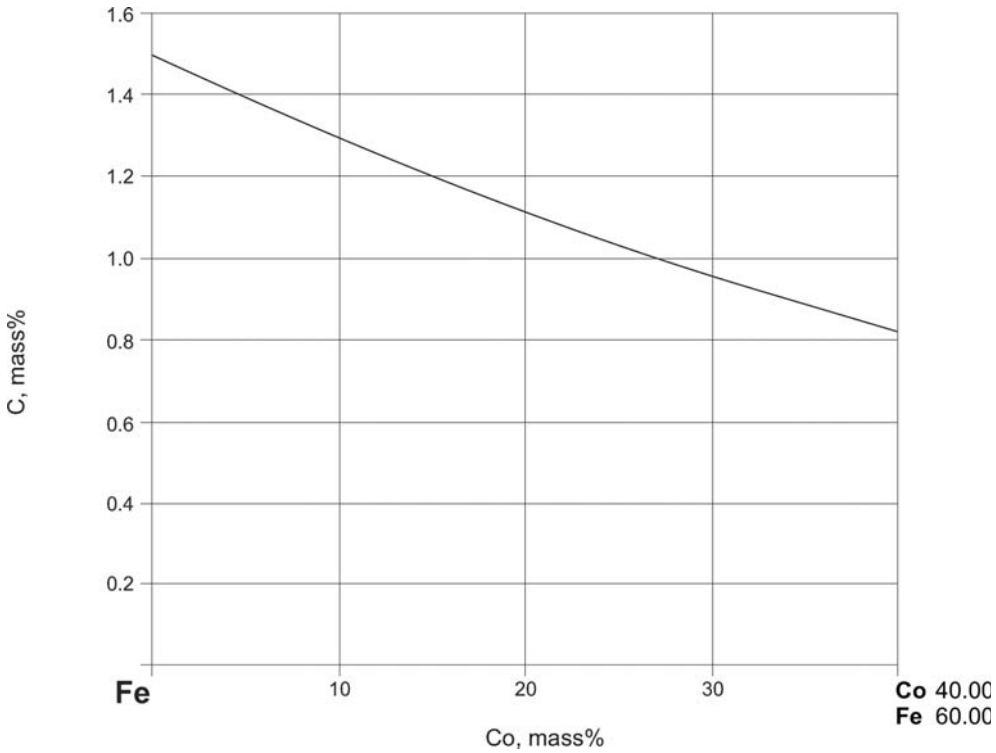

Fig. 4. C-Co-Fe. The solubility of carbon in austenite at 1000°C

DOI: 10.1007/978-3-540-69761-9_28

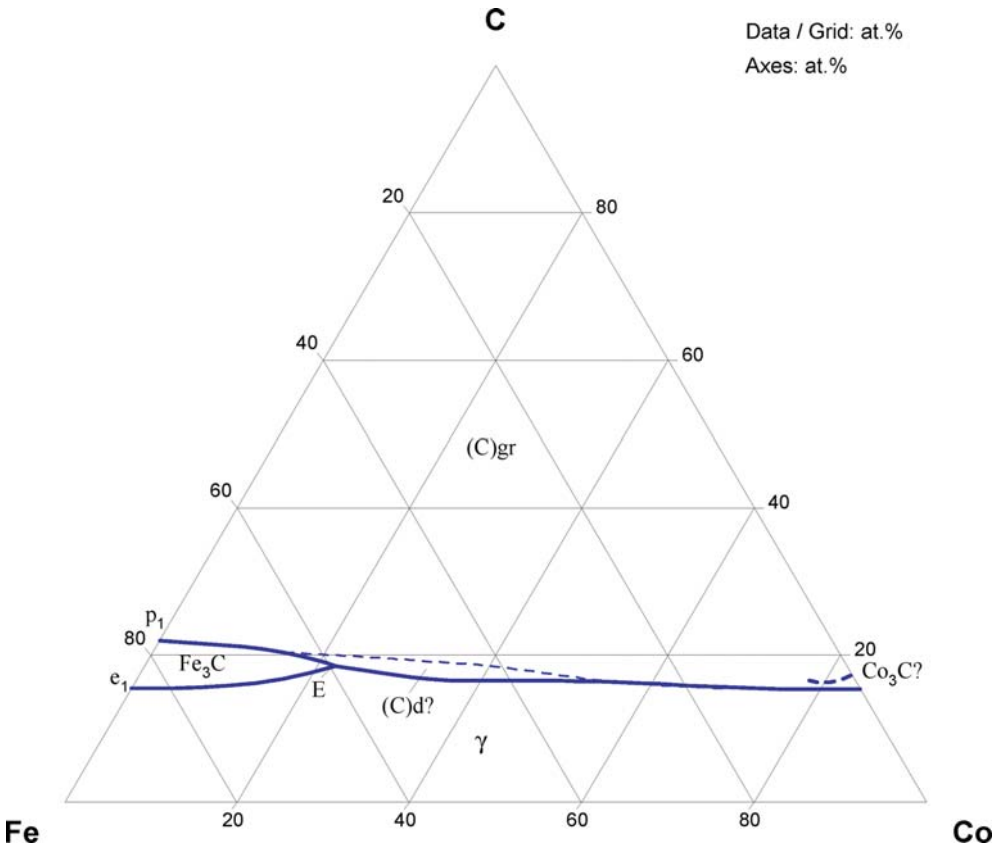

Fig. 5. C-Co-Fe. Liquidus projection at 4.7 GPa

DOI: 10.1007/978-3-540-69761-9_28

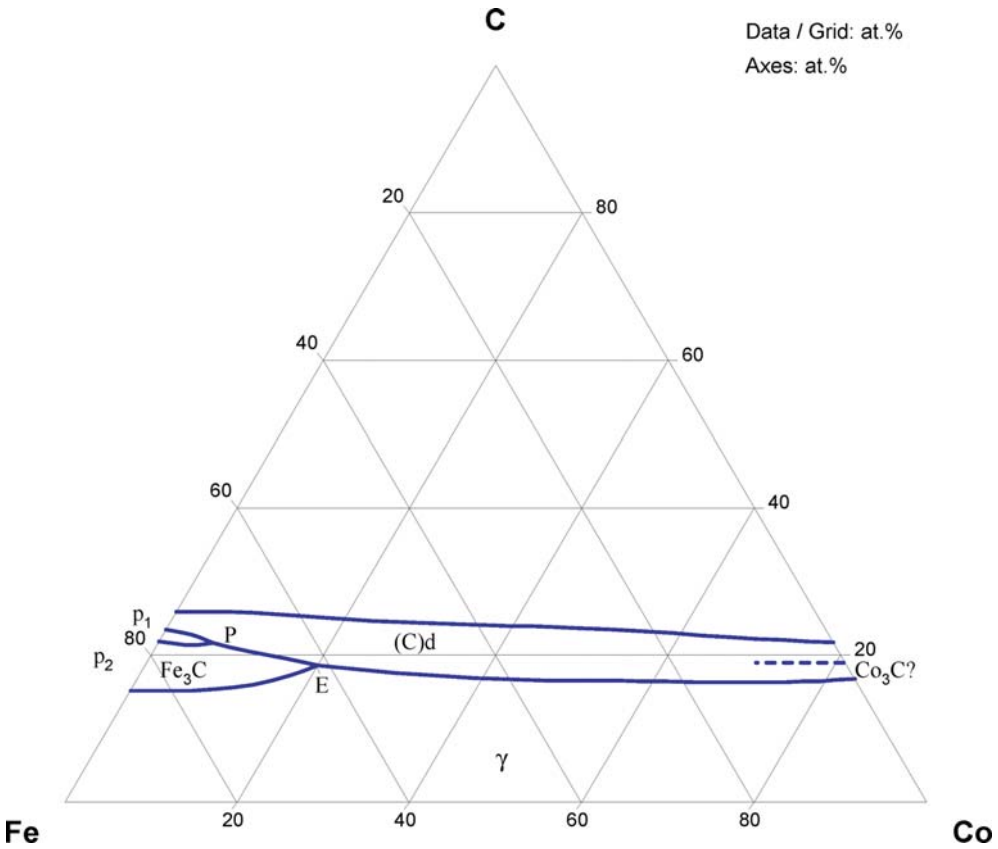

Fig. 6. C-Co-Fe. Liquidus projection at 6 GPa

DOI: 10.1007/978-3-540-69761-9_28

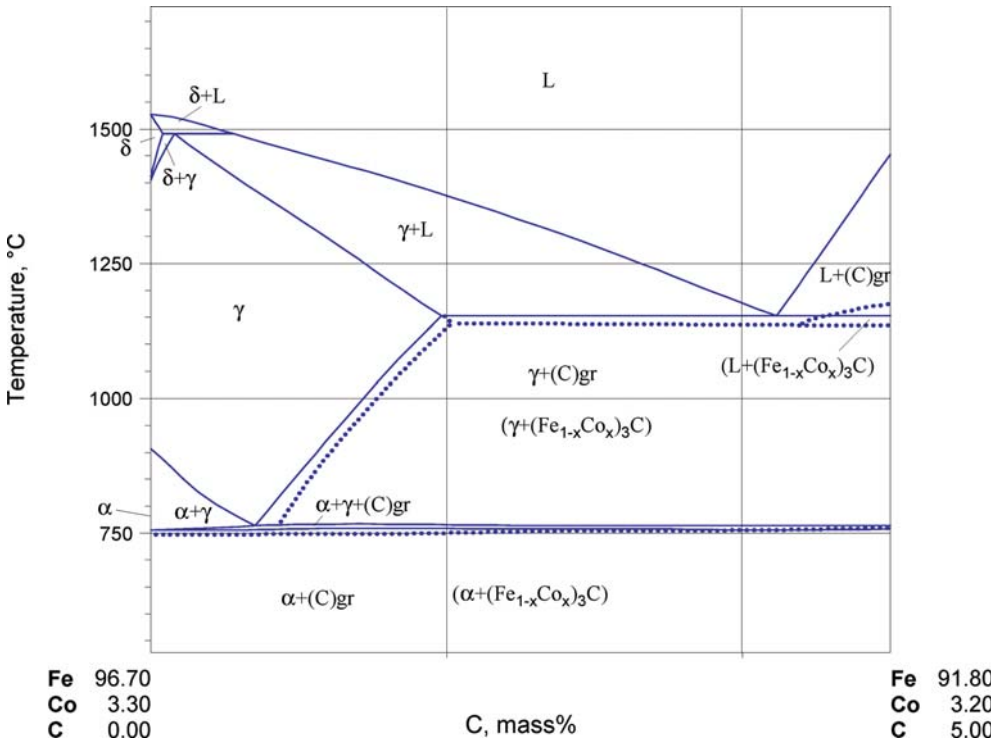

Fig. 7. C-Co-Fe. Vertical section at Fe:Co = 29:1 (mass%)

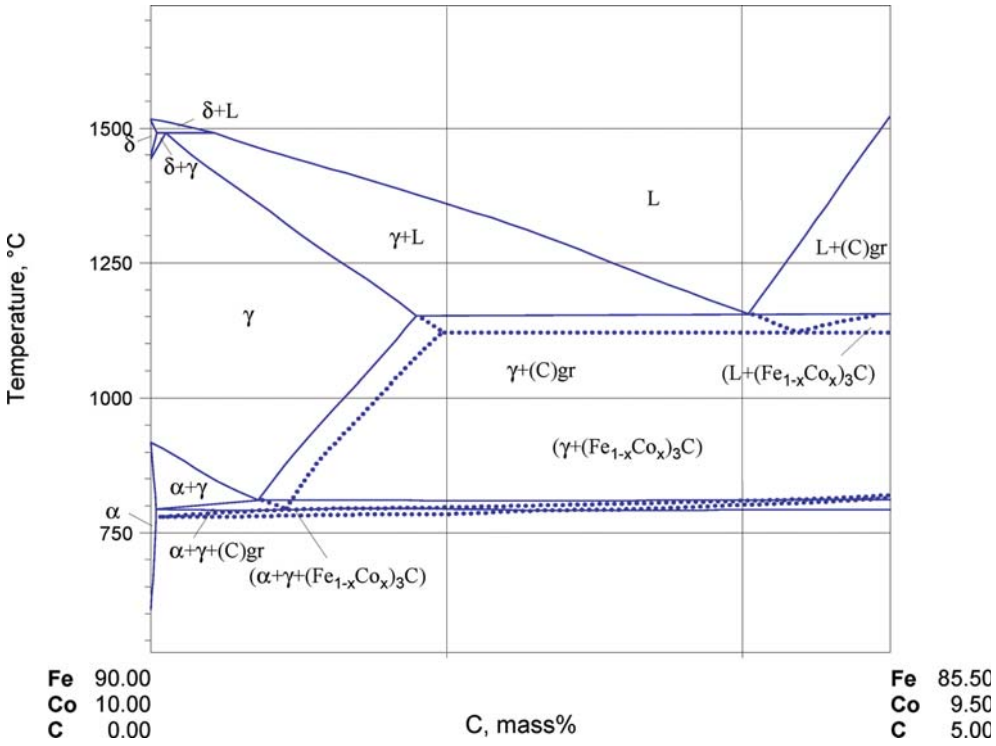

Fig. 8. C-Co-Fe. Vertical section at Fe:Co = 9:1 (mass%)

DOI: 10.1007/978-3-540-69761-9_28

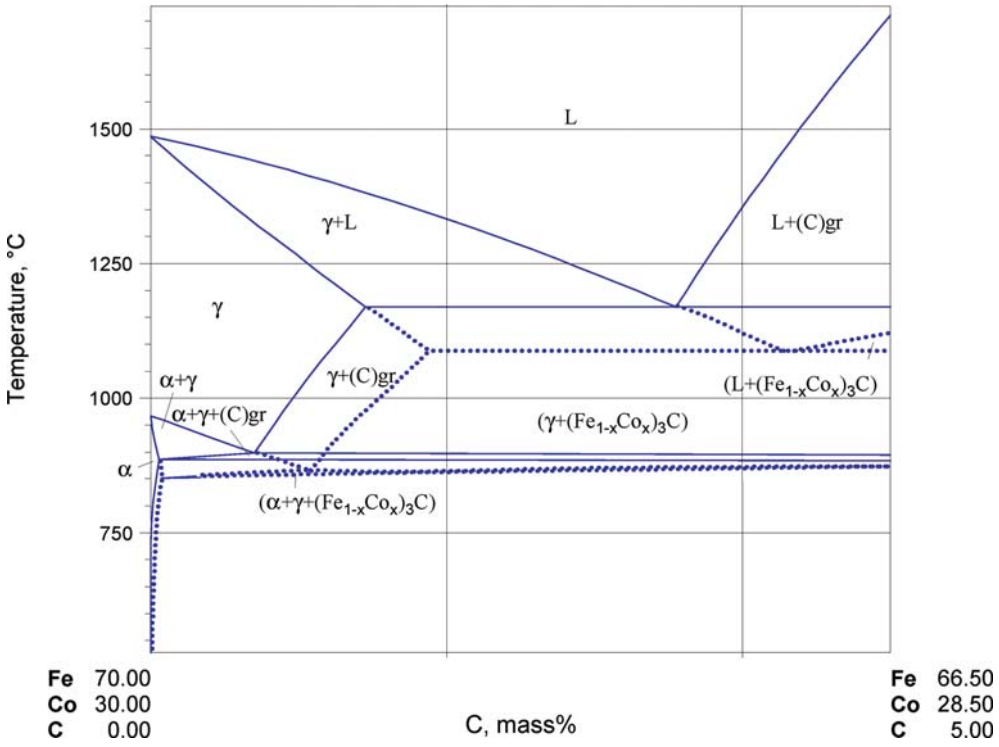

Fig. 9. C-Co-Fe. Vertical section at Fe:Co = 7:3 (mass%)

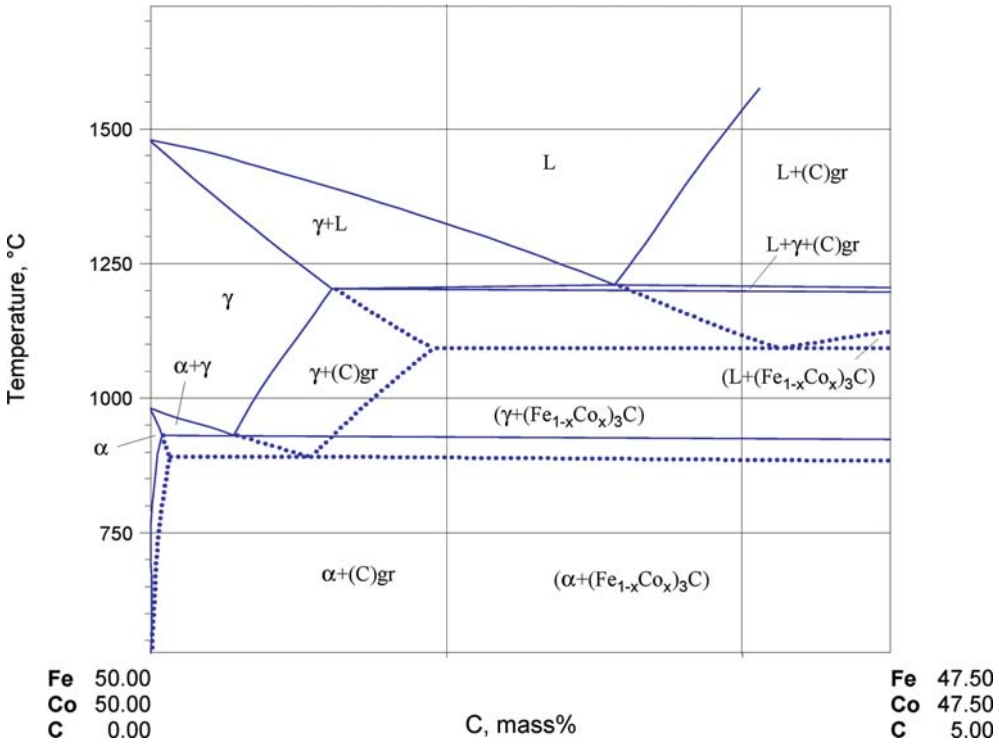

Fig. 10. C-Co-Fe. Vertical section at Fe:Co = 1:1 (mass%)

DOI: 10.1007/978-3-540-69761-9_28

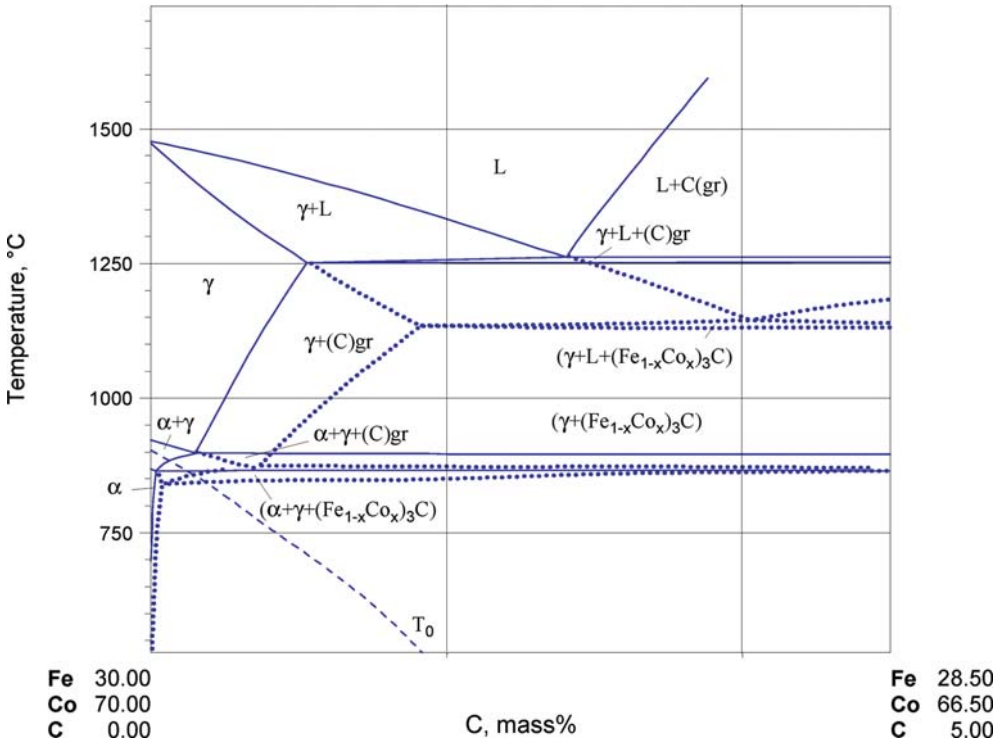

Fig. 11. C-Co-Fe. Vertical section at Fe:Co = 3:7 (mass%)

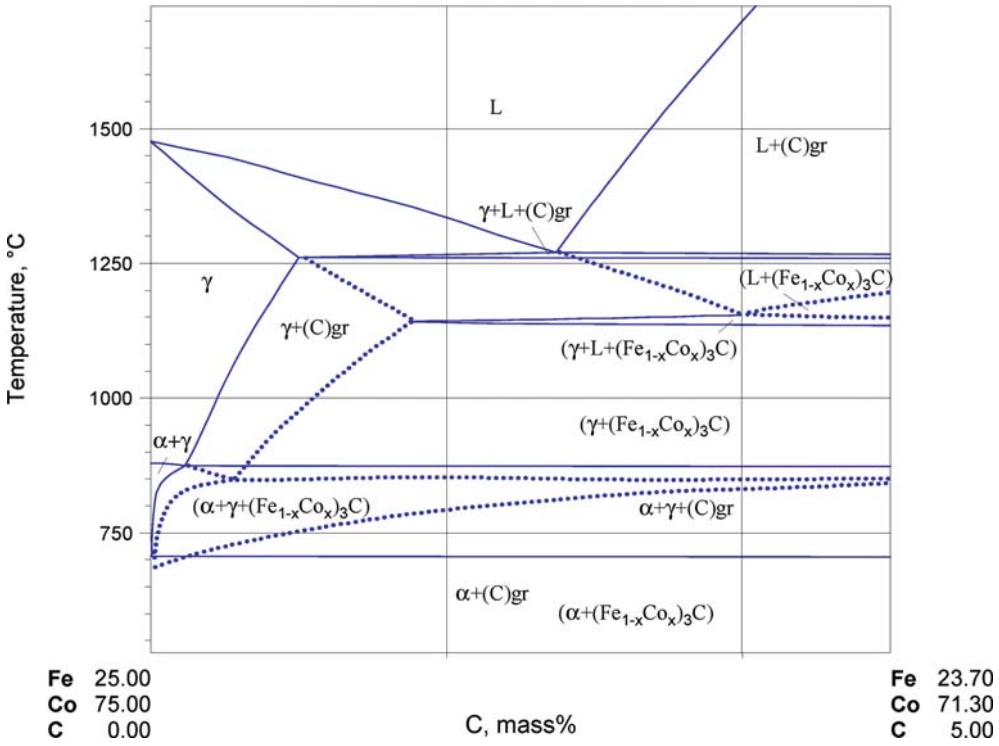

Fig. 12. C-Co-Fe. Vertical section at Fe:Co = 3:9 (mass%)

DOI: 10.1007/978-3-540-69761-9_28

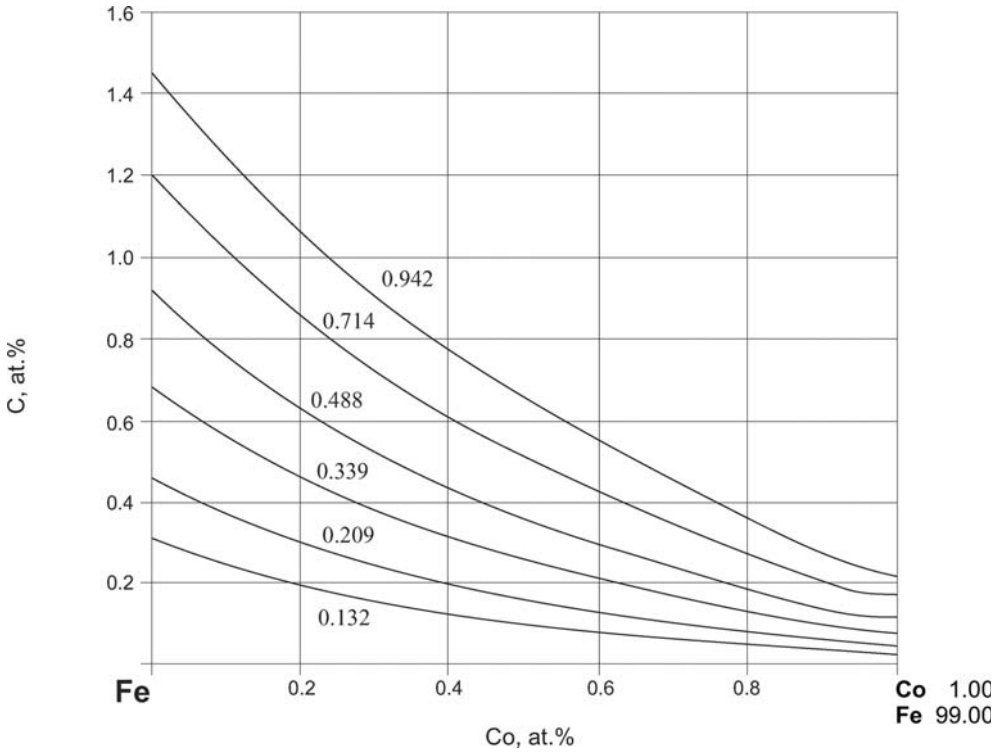

Fig. 13. C-Co-Fe. Solubility of carbon in austenite for various carbon activities, at 1000°C

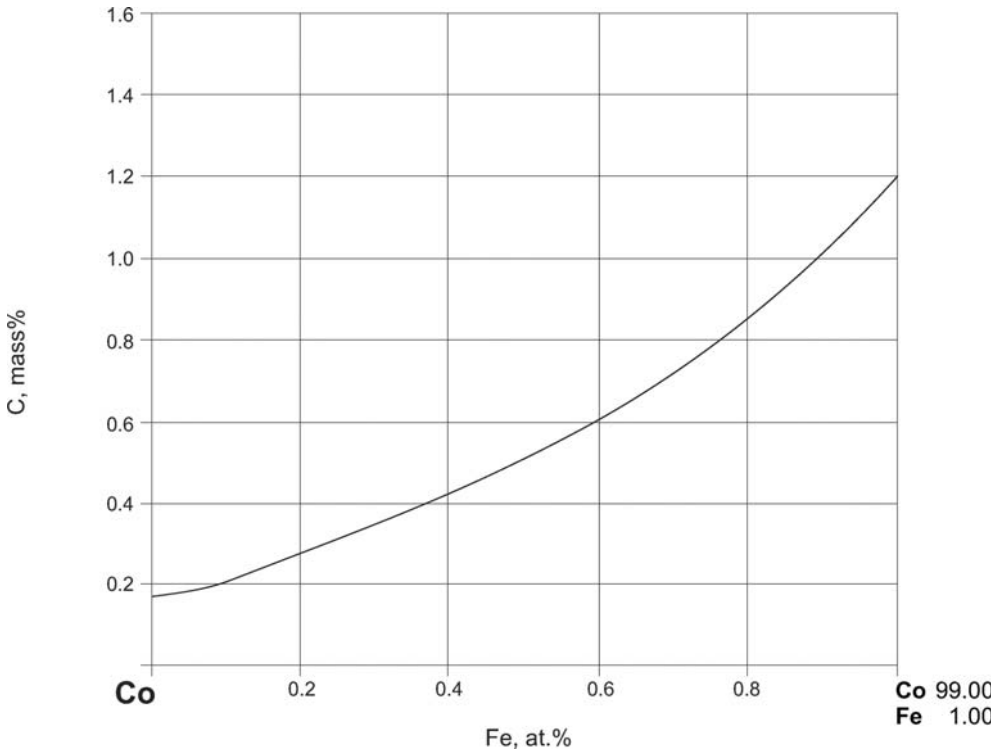

Fig. 14. C-Co-Fe. Solubility of carbon in austenite at 1000°C and carbon activity of 0.71

DOI: 10.1007/978-3-540-69761-9_28

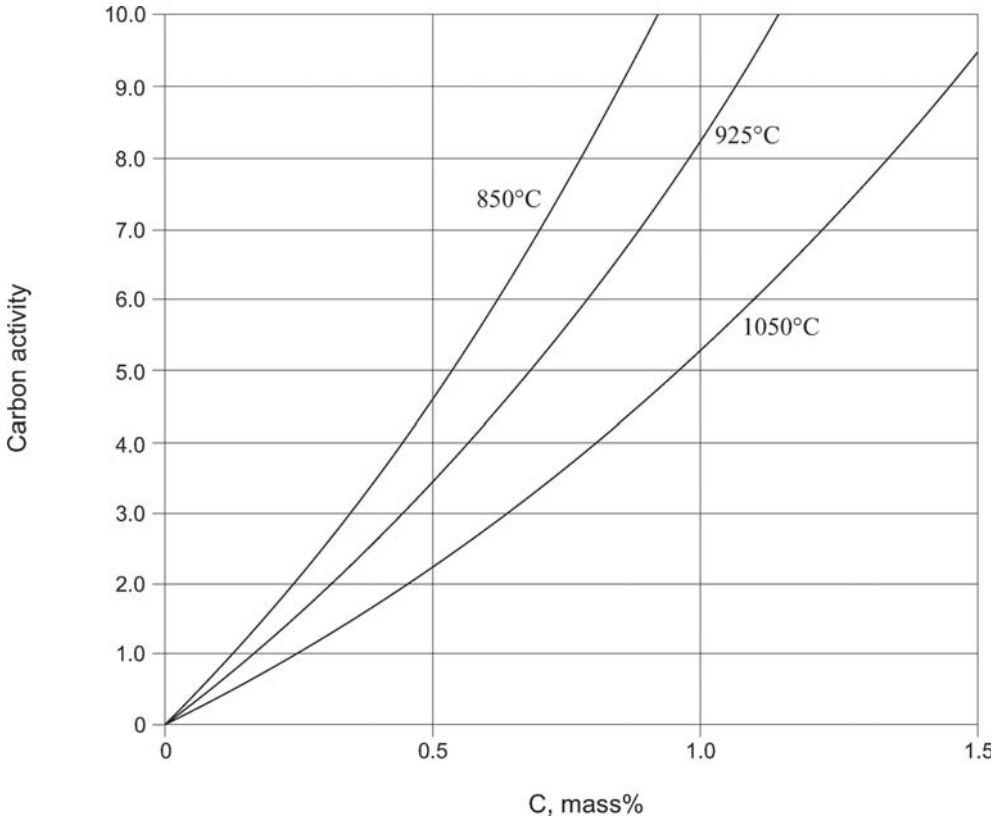

Fig. 15. C-Co-Fe. Carbon activity in C-Co-Fe solutions at 850, 925 and 1050°C

DOI: 10.1007/978-3-540-69761-9_28

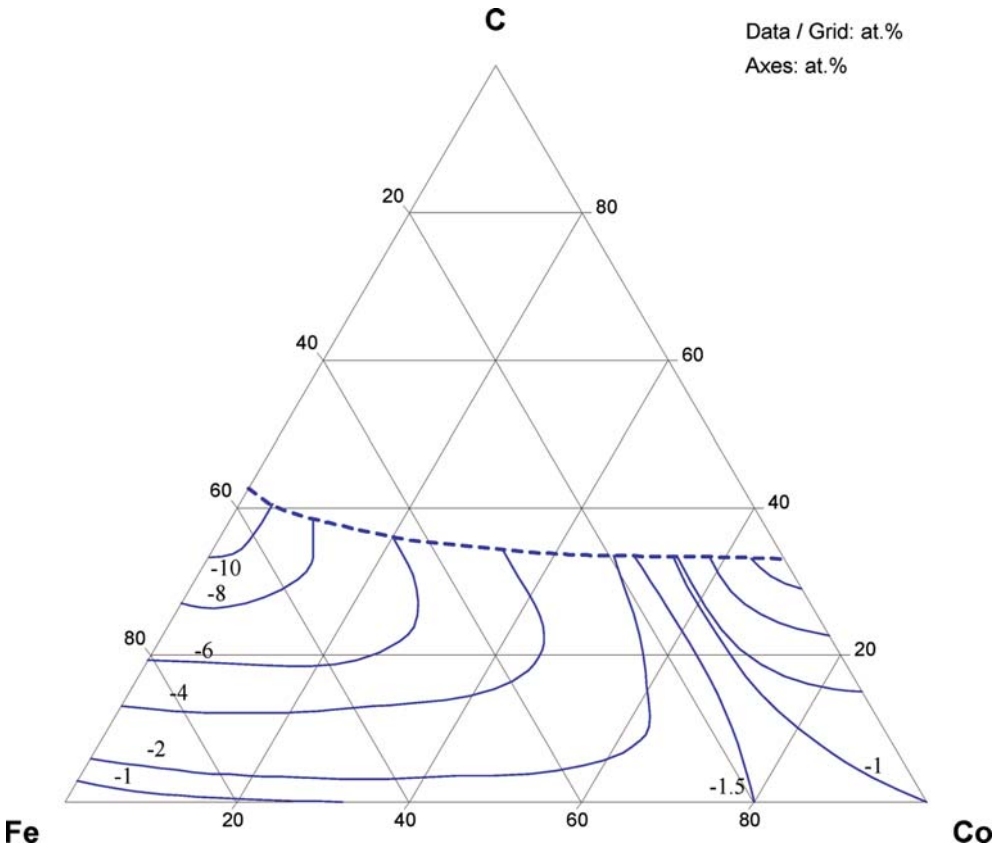

Fig. 16. C-Co-Fe. Isoenthalpy of mixing contours for the liquid phase for 1627°C

DOI: 10.1007/978-3-540-69761-9_28

References

[1932Vog] Vogel, R., Sundermann, W., "The Iron-Cobalt-Carbon System" (in German), *Arch. Eisenhuettenwes.*, **6**(1), 35–38 (1932) (Experimental, Morphology, Phase Diagram, 8)

[1953Dra] Drain, J., "A Physico-Chemical Study of the Carbide" (in French), *Ann. Chim. (Paris)*, **8**(12), 900–953 (1953) (Crys. Structure, Experimental, Magn. Prop., 40)

[1956Tur] Turkdogan, E.T., Hancock, R.A., Herlitz, S.I., Dentan, J., "Thermodynamics of Carbon Dissolved in Iron Alloys. Part V: Solubility of Graphite in Iron-Manganese, Iron-Cobalt, and Iron-Nickel Melts", *J. Iron Steel Inst., London*, **183**, 69–72 (1956) (Experimental, Phase Relations, Thermodyn., 17)

[1959Fuw] Fuwa, T., Chipman, J., "Activity of Carbon in Liquid Iron Alloys", *Trans. Metall. Soc. AIME*, **215**, 708–716 (1959) (Calculation, Experimental, Phase Relations, Thermodyn., 22)

[1960Fuw] Fuwa, T., Fujikura, M., Matoba, S., "Effect of Elements on the Solubility of Graphite in Liquid Iron" (in Japanese), *Tetsu to Hagane* (*J. Iron Steel Inst. Jpn.*), **46**, 235–237 (1960) (Experimental, Phase Relations, 8)

[1960Pet] Petrova, E.F., Lapshina, M.I., Shvartsman, L.A., "Influence of the Alloying Elements on the Thermodynamic Activity and Carbon Solubility in α-Iron" (in Russian), *Metalloved. Term. Obrab. Met.*, (4), 22–25 (1960) (Experimental, Phase Relations, Thermodyn., 2)

[1963Bro] Brown, L.C., Kirkaldy, J.S., "The Interaction Parameter for Solutions of Carbon and Cobalt in Austenite at 1000°C", *Trans. Metall. Soc. AIME*, **227**, 1461 (1963) (Thermodyn., Experimental, 5)

[1963Ell] Elliott, J.F., Gleiser, M., Ramakrishna, V., "Iron-Carbon-j Alloys", *Thermochemistry for Steelmaking*, Addision Wesley, Reading, MA, **2**, 531 (1963) (Thermodyn., Review)

[1963Sch] Schenck, H., Frohberg, M.G., Steinmetz, E., "Investigations on the Mutual Activities Influence in Homogeneous Metallic Substances Solubility. Part I. Experimental Investigations of Manganese-Carbon-X, Cobalt-Carbon-X, Nickel-Carbon-X Systems in Liquid State" (in German), *Arch. Eisenhuettenwes.*, **34**(1), 37–42 (1963) (Phase Diagram, Thermodyn., Experimental, Review, 30)

[1964App] Appleton, A.S., "The Diffusion of Carbon in Iron-Cobalt-Carbon Austenites", *Trans. Metall. Soc. AIME*, **230**, 893–898 (1964) (Experimental, Kinetics, Phase Relations, Thermodyn., 16)

[1964Bro] Brown, L.C., Kirkaldy, J.S., "Carbon Diffusion in Dilute Ternary Austenites", *Trans. Metall. Soc. AIME*, **239**, 223–226 (1964) (Experimental, Kinetics, 15)

[1964Smi] Smith, R.P., "The Diffusivity of Carbon in γ Iron-Cobalt Alloys", *Trans. Metall. Soc. AIME*, **230**, 476–480 (1964) (Experimental, Kinetics, Thermodyn., 18)

[1964Dai] Daines, W.L., Pehlke, R.D., "The Influence of Temperature and Alloying Elements on the Solubility of Graphite in Liquid Cobalt", *Trans. ASM*, **57**, 1011–1015 (1964) (Experimental, Phase Relations, 9)

[1965Bur] Burylev, B.P., "Determination of the Solubility Isotherms in the Ternary System Using Thermodynamic Properties of the Binary Alloys" (in Russian), *Izv. Vyss. Uchebn. Zaved., Khim., Khim. Tekhnol.*, **6**, 910–914 (1965) (Phase Relations, Thermodyn., Calculation, 17)

[1965Smi] Smith, R.P., "The Activity of Carbon in Iron-Cobalt Alloys at 1000°C", *Trans. Metall. Soc. AIME*, **233**, 397–401 (1965) (Thermodyn., Experimental, 14)

[1966Aar] Aaronson, H.I., Domian, H.A., Pound, G.M., "Thermodynamics of the Austenite: Proeuctoid Ferrite Transformation. I, Fe-C Alloys", *Trans. AIME*, **236**, 753–767 (1966) (Thermodyn., Calculation, 43)

[1968Bod] Bodsworth, C., Davidson, I.M., Atkinson, D. "Thermodynamic Properties of Interstitial Solutions of Iron-Base Alloys" *Trans. AIME*, **242**(6), 1135–1143 (1968) (Thermodyn., Calculation, 26)

[1968Chi] Chipman, J., Brush, E.F., "The Activity of Carbon in Alloyed Austentite at 1000°C", *Trans. AIME*, **242**, 35–41 (1968) (Thermodyn., Calculation, Review, 21)

[1968Zup] Zupp, R.R., Stevenson, D.A., "Statistical Thermodynamics of Carbon in Ternary Austenitic Iron-Base Alloys", *Trans. AIME*, **242**, 862–869 (1968) (Thermodyn., Calculation, 35)

DOI: 10.1007/978-3-540-69761-9_28

[1969Fra] Fray, D.J., Chipman, J., "The Solubility of Graphite in Fe-Ni and Fe-Co Alloys at 1000°C", *Trans. Metall. Soc. AIME*, **245**, 1143–1144 (1969) (Phase Relations, Experimental, 4)

[1969Ruh] Ruhl, R.C., Cohen, M., "Splat Quenching of Iron-Carbon Alloys", *Trans. AIME*, **245**, 241–251 (1969) (Crys. Structure, Experimental, Phase Relations, 50)

[1969Sch] Schuermann, E., Kramer, D., "Investigations on the Influence of Temperature and on the Equivalent Effect of the Alloy Elements on the Solubility of Carbon in Iron-Rich Carbon-Saturated Ternary and Multi-component Meltings" (in German), *Giessereiforschung*, **21**(1), 29–42 (1969) (Phase Relations, Experimental, 35)

[1971Ale] Alex, K., Mclellan, R.B., "A Quasi-Chemical Approach to the Thermodynamics of Ternary Solid Solutions Containing Both Substitutional and Interstitial Solute Atoms", *J. Phys. Chem. Solids*, **32**(2), 449–451 (1971) (Thermodyn., Calculation, 24)

[1972Foo] Foo, E.H., Lupis, C.H.P., "Activity of Carbon in Liquid Iron Alloys at 1550°C", *Metall. Trans.*, **3**, 2125–2131 (1972) (Phase Relations, Thermodyn., Experimental, 18)

[1972Wil] Williams, R., Bodsworth, C., "Effect of Cobalt, Copper and Manganese on the Thermodynamic Activity of Carbon in Iron-Base Austenites", *J. Iron Steel Inst., London*, **210**, 106–110 (1972) (Phase Relations, Phase Diagram, Thermodyn., Experimental, 11)

[1973Kin] Kinsman K.R., Aaronson H.I., "Influence of Al, Co, and Si upon the Kinetics of the Proeutectoid Ferrite Reaction", *Metall. Trans. A*, **4**(4), 959–967 (1973) (Experimental, Phase Relations, Mechan. Prop., 51)

[1976Ko] Ko, M., Sakuma, T., Nishizawa, T., "Effect of Magnetism on the Partition of Alloying Elements Between Cementite and Ferrite" (in Japanese), *J. Jpn. Inst. Met.*, **40**(6), 593–601 (1976) (Phase Relations, Experimental, Magn. Prop., 37)

[1977Uhr] Uhrenius, B., "Optimization of Parameters Describing the Interaction Between Carbon and Alloying Elements in Ternary Austenite", *Scand. J. Metall.*, **6**(2), 83–89 (1977) (Thermodyn., Calculation, 24)

[1983Jan1] Janas, M., Mamro, K., Ludwikowski, S., Jowsa, J., "Carbon Solubility in Fe-C(max)-Al, Fe-C(max)-Co, Fe-C(max)-Cu Alloys", *Metal. Odlew.*, **9**(2), 99–118 (1983) (Phase Relations, Thermodyn., Experimental, 7)

[1983Jan2] Janas, M., Mamro, K., Jowsa, J., Ludwikowski, S., "Assessment of Ferrous Alloy Component Influence on Carbon Solubility" (in Polish), *Metal. Odlew.*, **9**(3), 213–228 (1983) (Phase Relations, Thermodyn., Experimental, 28)

[1984Riv] Rivlin,V.G., "Phase Equilibria in Iron Ternary Alloys. 13: Critical Evaluation of the Constitution of Ternary Systems C-Fe-X (X = Co, Ni, Cu)", *Int. Met. Rev.*, **29**(2), 96–121 (1984) (Phase Diagram, Phase Relations, Review, 76)

[1985Eno] Enomoto, M., Aaronson H.I., "Calculation of α+γ Phase Boundaries in Fe-C-X Systems from the Central Atoms Model", *Calphad*, **9**(1), 43–58 (1985) (Phase Relations, Thermodyn., Calculation, 31)

[1986Eno1] Enomoto, M., Aaronson H.I., "Nucleation Kinetics of Proeutectoid Ferrite at Austenite Grain Boundaries in Fe-C-X Alloys", *Metall. Trans. A*, **17A**(8), 1385–1397, (1986) (Phase Relations, Thermodyn., Calculation, Experimental, Kinetics, 53)

[1986Eno2] Enomoto, M., Lange, W.F., III, Aaronson, H.I., "The Kinetics of Ferrite Nucleation at Austenite Grain Edges in Fe-C and Fe-C-X Alloys", *Metall. Trans. A*, **17A**(8), 1399–1407 (1986) (Phase Relations, Thermodyn., Calculation, Experimental, Kinetics, 19)

[1987Gui] Guillermet, A.F., "Thermodynamic Analysis of the Co-C System", *Z. Metallkd.*, **78**, 700–709 (1987) (Phase Diagram, Thermodyn., Assessment, #, *, 47)

[1988Gui] Guillermet, A.F., "Thermodynamic Properties of the Fe-Co-C System", *Z. Metallkd.*, **79**(5), 317–329 (1988) (Phase Diagram, Thermodyn., Assessment, 52)

[1988Hoc] Hoch, M., "Phase Stability of Carbon in FCC and BCC Metals", *Calphad*, **12**(1), 83–88 (1988) (Thermodyn., Calculation, Theory, 15)

[1988Ray] Raynor, G.V., Rivlin, V.G., "C-Co-Fe", in "*Phase Equilibria in Iron Ternary Alloys"*, Institute of Metals, London, 140–142 (1988) (Phase Diagram, Phase Relations, Review, 9)

DOI: 10.1007/978-3-540-69761-9_28

[1990Put] Putyatin, A.A., Kozlovskii, V.F., "Pressure Effect on the Phase Equilibrium in the Alloys of the Iron-Manganese-Cobalt-Carbon System", *Vestn. Mosk. Univ., Ser. 2: Khim*., **31**(4), 367–369 (1990) (Experimental, Phase Relations, Phase Diagram, 8)

[1990Pav] Pavel, E., Baluta, Gh., Barb, D., Gheorghe, L., Ilie, Gh., Lazar, D.P., Morariu, M., Giurgiu, C., "$(Fe_{1-x}Me_x)_3C$ Carbide Identification in Synthetic Diamond Crystals Produced at High Pressure and High Temperature in Fe-Me-C Systems, where Me = Ni, Co.", *Mater. Lett.***10(**1–2), 62–65 (1990) (Morphology, Phase Relations, Experimental, 9)

[1991Pav] Pavel, E., Pintiliescu, L., Baluta, Gh., Giurgiu, C., Barb, D., Lazar, D.P., Morariu, M., "The Ternary Constitution Diagrams for the Fe-Ni-C and Fe-Co-C Systems at 5.7 GPa", *Physica B*, **175**(4), 354–360 (1991) (Morphology, Phase Diagram, Phase Relations, Thermodyn., Experimental, Calculation, 21)

[1993Koc] Kocherzhinskii, Y.A., Kulik, O.G., Turkevich, V.Z., "Phase Equilibria in the Fe-Ni-C and Fe-Co-C Systems under High Temperatures and High Pressures", *High Temp. - High Pressures*, **25**, 113–116 (1993) (Phase Diagram, Calculation, Experimental, 9)

[1993Tur] Turkevich, V.Z., Kulik, O.G., "Calculation of Melt-Solid Equilibrium in the Fe-Co-C and Fe-Ni-C Systems Under Pressures Up To 6 GPa", *Dop. Akad. Nauk Ukr.*, (7), 75–80 (1993) (Calculation, Phase Diagram, Phase Relations, Thermodyn., 15)

[1993Wit] Witusievich, V.T., Shumikhin, V.S., "Enthalpy of Formation of Molten Fe-Mn(Co, Ni)-C Systems" (in Russian), *Rasplavy*, **5**, 78–80 (1993) (Thermodyn., Experimental, 13)

[1994Rag] Raghavan, V., "The C-Co-Fe System", *J. Phase Equilib.*, **15**(4), 416–417 (1994) (Phase Diagram, Review, 7)

[1994Wit] Witusiewicz, V.T., "Thermodynamic Properties of Liquid Alloys of 3d Transition Metals with Metalloids (Silicon, Carbon and Boron)", *J. Alloys Compd.*, **203**, 103–116 (1994) (Thermodyn., Experimental, 89)

[1995Tur] Turkevich, V.Z., Kulik, O.G., "High Pressure Influence on the Phase Diagram Construction of 3-d Transition Metals with Carbon Systems", *High Press. Res.*, **14**(1–3), 175–180 (1995) (Experimental, Calculation, Phase Relations, 8)

[1996Koc] Kocherzhinski, Yu.A., Kulik, O.G., "Equilibrium Phase Diagrams and Manufacture of Synthetic Diamond", *Powder Metall. Met. Cer.*, **35**(7–8), 470–483 (1996) (Experimental, Phase Relations, 37)

[2000Li] Li, L., "High Strength and High Induction Co-27-Fe-Co-0.23 Soft Magnetic Alloy for Forge Application", *J. Appl. Phys*., **87**(9), 6523–6524 (2000) (Experimental, Magn. Prop., Mechan. Prop., 3)

[2001Zha] Zhang, Z.D., Zheng, J.G., Skorvanek, I., Wen, G.H., Kovac, J., Wang, F.W., Yu, J.L., Li, Z.J., Dong, X.L., Jin, S.R., Liu, W., Zhang, X.X., "Shell/Core Structure and Magnetic Properties of Carbon-Coated Fe-Co(C) Nanocapsules", *J. Phys.-Condes. Matter.* **13**(9), 1921–1929 (2001) (Experimental, Magn. Prop., 12).

[2002Ohn] Ohnuma, I., Enoki, H., Ikeda, O., Kainuma, R., Ohtani, H., Sundman, B., Ishida, K., "Phase Equilibria in the Fe-Co Binary System", *Acta Mater.*, **50**, 379–393 (2002) (Assessment, Calculation, Experimental, Phase Relations, Thermodyn., 50)

[2002Ohn] Ohnuma, I., Enoki, H., Ikeda, O., Kainuma, R., Ohtani, H., Sundman, B., Ishida, K., "Phase Equilibria in the Fe-Co Binary System", *Acta Mater.*, **50**, 379–393 (2002) (Assessment, Calculation, Experimental, Phase Relations, Thermodyn., 50)

[2003Zab] Zabinski, P.R., Meguro, S., Asami, K., Hashimoto, K., "Electrodeposited Co-Fe and Co-Fe-C Alloys for Hydrogen Evolution in a hot 8 kmol m(-3) NaOH Solution", *Mater. Trans.*, **44**(11), 2350–2355 (2003) (Experimental, Phase Relation, Electrochemistry, 15)

[2004Aar] Aaronson, H.I., Reynolds, W.T., Purdy, G.R., "Coupled-Solute Drag Effect on Ferrite Formation in Fe-C-X Systems", *Metall. Mater. Trans. A*, **35A**(4), 1187–1210 (2004) (Experimental, Interface Phenomena, Kinetics, Morphology, Phase Relations, 148)

[2004Sai] Saitoh, H., Yoshinaga, N., Ushioda, K., "Influence of Substitutional Atoms on the Snoek Peak of Carbon in b.c.c. Iron", *Acta Mater.*, **52**(5), 1255–1261 (2004) (Experimental, Review, Interface Phenomena, Kinetics, Morphology, Phase Relations, 148)

DOI: 10.1007/978-3-540-69761-9_28

[2004Sun] Sundar, R.S., Deevi, S.C., "Influence of Alloying Elements on the Mechanical Properties of FeCo-V Alloys", *Intermetallics*, **12**(7–9), 921–927 (2004) (Magn. Prop., Mechan. Prop., Morphology, Review, 32)

[2004Tao] Tao, D.P., "A Thermodynamic Model for Solid Solutions and Its Application to the C-Fe-Co, C-Fe-Ni and Mn-Cr-Pt Solid Dilutions", *Mater. Sci. Eng. A*, **366**(2), 239–274 (2004) (Calculation, Theory, Thermodyn., 26)

[2004Zab] Zabinski, P.R., Meguro, S., Asami, K., Hashimoto, K., "Electrodeposited Co-Fe and Co-Fe-C Alloys for Hydrogen Evolution in a hot 8 kmol m(-3) NaOH Solution", *J. Jpn. Inst. Met*., **68**(7), 456–461 (2004) (Experimental, Phase Relation, Electrochemistry, 15)

[2005Kit] Kitamoto, Y., Tagami, H., Kiyota G., "Microstructural and Magnetic Study of Nanocrystalline Soft Magnetic Thin Films of Fe-C and Fe-Co-C Deposited with Sputtering", *IEEE Trans. Magn*., **41**(10), 3295–3297 (2005) (Experimental, Magn. Prop., 4)

[2005Kiy] Kiyota, G., Kitamoto, Y., Yamazaki, Y., "Fabrication of Fe-Co-C Thin Films Using Facing Targets Sputtering Method", *Electrochim. Acta*., **51**(5 Special Issue SI), 921–923 (2005) (Experimental, Magn. Prop., 5).

[2005Miy] Miyamoto, N., Sakamoto, S., Tamura, H., Matsuoka, M., Tamaki, J., "Effect of Carbon Content on Structural and Mechanical Properties of Fe-Co-C Alloy Electrodeposited from Aqueous Solutions", *J. Electrochem. Soc*., **152**(7), C488–C492 (2005) (Crys. Structure, Experimental, Mechan. Prop., 16).

[2005Sun] Sundar, R.S., Deevi, S.C., "Soft Magnetic Fe-Co Alloys: Alloy Development, Processing, and Properties", *Int. Mater. Rev.*, **50**(3), 157–192 (2005) (Crys. Structure, Phase Diagram, Phase Relations, Magn. Prop., Electr. Prop., Mechan. Prop., Review, 258)

[2006MSIT] "C-Fe (Iron-Carbon)", Diagrams as Published, in *MSIT Workplace*, Effenberg, G. (Ed.), Materials Science International Services, GmbH, Stuttgart; Document ID: 30.13598.1.20 (2006) (Crys. Structure, Phase Diagram, Phase Relations, 2)

[V-C2] Villars, P., Calvert, L.D., *Pearson's Handbook of Crystallographic Data for Intermetallic Phases*, 2nd edition, ASM, Metals Park, Ohio (1991)

[Mas2] Massalski, T.B. (Ed.), *Binary Alloy Phase Diagrams*, 2nd edition, ASM International, Metals Park, Ohio (1990)

DOI: 10.1007/978-3-540-69761-9_28